

UNCLASSIFIED

AD 429971

DEFENSE DOCUMENTATION CENTER

FOR

SCIENTIFIC AND TECHNICAL INFORMATION

CAMERON STATION, ALEXANDRIA, VIRGINIA



UNCLASSIFIED

NOTICE: When government or other drawings, specifications or other data are used for any purpose other than in connection with a definitely related government procurement operation, the U. S. Government thereby incurs no responsibility, nor any obligation whatsoever; and the fact that the Government may have formulated, furnished, or in any way supplied the said drawings, specifications, or other data is not to be regarded by implication or otherwise as in any manner licensing the holder or any other person or corporation, or conveying any rights or permission to manufacture, use or sell any patented invention that may in any way be related thereto.

64-7

429971

ASD-TR-61-579

429971

CATALOGED BY DDC

AS AD NO. _____

**PERFORMANCE OF AND DESIGN CRITERIA FOR DEPLOYABLE
AERODYNAMIC DECELERATORS**

TECHNICAL REPORT No. ASD-TR-61-579

DECEMBER 1963

AF FLIGHT DYNAMICS LABORATORY
RESEARCH AND TECHNOLOGY DIVISION
AIR FORCE SYSTEMS COMMAND
WRIGHT-PATTERSON AIR FORCE BASE, OHIO

Project No. 6065, Task No. 606503

FEB 10 1964

Prepared under Contract No. AF 33(616)-8112 by the
American Power Jet Co., Ridgefield, New Jersey.

NOTICES

When Government drawings, specifications, or other data are used for any purpose other than in connection with a definitely related Government procurement operation, the United States Government thereby incurs no responsibility nor any obligation whatsoever; and the fact that the Government may have formulated, furnished, or in any way supplied the said drawings, specifications, or other data, is not to be regarded by implication or otherwise as in any manner licensing the holder or any other person or corporation, or conveying any rights or permission to manufacture, use, or sell any patented invention that may in any way be related thereto.

Qualified requesters may obtain copies of this report from the Defense Documentation Center (DDC), (formerly ASTIA), Cameron Station, Bldg. 5, 5010 Duke Street, Alexandria, Virginia, 22314.

This report has been released to the Office of Technical Services, U.S. Department of Commerce, Washington 25, D. C., in stock quantities for sale to the general public.

Copies of this report should not be returned to the Research and Technology Division, Wright-Patterson Air Force Base, Ohio, unless return is required by security considerations, contractual obligations, or notice on a specific document.

FOREWORD

The scope of deployable aerodynamic decelerator requirements, techniques, and applicable technology has developed to the point at which an up-to-date guide is required for decelerator system selection, detail design, and performance prediction. It is increasingly clear that a system point of view must be adopted in which all pertinent aspects of mission, state-of-the-art, and technology are taken into account.

This report, therefore, brings together information and insights on all major factors that must be considered in designing and developing successful aerodynamic decelerator systems. Each subject is systematically developed, both individually and as it relates to other pertinent aspects. Theory, experience and judgment go hand-in-hand in the design of decelerators. The value of applying sound engineering principles from the very outset of the design consideration cannot be overemphasized. The decelerator is increasingly essential for successful mission performance, and its optimization should begin with the initial conception and design of the system.

This is the second major revision of the USAF Parachute Handbook. It represents an increase over its predecessors of approximately two-thirds in technical scope and content -- a point which underscores the progress and development experienced in this field. A cut-off date of approximately mid-1962 was applied to the data collection and references.

Prepared under Contract No. AF 33(616)-8112, Project No. 6065, Task No. 606503, this report is the product of a joint effort by the staffs of the Retardation and Recovery Branch, Flight Accessories Laboratory, Aeronautical Systems Division*, Mr. James H. DeWeese, Project Engineer, and of the American Power Jet Company, Ridgefield, New Jersey, under the supervision of Mr. George Chernowitz.

Special thanks for their individual contributions are due to Mr. Rudi J. Berndt of the Retardation and Recovery Branch, Flight Accessories Laboratory, Aeronautical Systems Division, and to Dr. Helmut J. Heinrich, of the University of Minnesota. The cooperation of Governmental Agencies and Industry in numerous regards is also gratefully acknowledged.

Recommendations with respect to corrections, deletions, additions, or any other changes to improve the format or contents of this report should be forwarded to the AF Flight Dynamics Laboratory, Research and Technology Division, Air Force Systems Command, Wright-Patterson Air Force Base, Ohio, Attn: FDFR.

*Now Recovery and Crew Station Branch, Vehicle Equipment Division, AF Flight Dynamics Laboratory, Research and Technology Division.

ABSTRACT

The present state-of-the-art, technology, and theory applicable to deployable aerodynamic decelerators, especially textile parachute canopies, are presented. Major types of decelerators are described, and their aerodynamic and operational characteristics, as well as applications, are discussed. Detailed coverage is given to decelerator materials, design and construction, hardware, test methods and vehicles, and test instrumentation. Decelerator design procedures and performance prediction techniques are demonstrated by sample calculations.

This report has been reviewed and is approved.



George L. Solt, Jr.
Chief, Recovery and Crew Station Branch
Vehicle Equipment Division
AF Flight Dynamics Laboratory

TABLE OF CONTENTS

	<i>Page</i>
INTRODUCTION	1
Chapter 1. STANDARD SYMBOLS AND GLOSSARY OF AERODYNAMIC DECELERATOR TERMS	13
Chapter 2. DESIGN REFERENCE DATA	33
Chapter 3. DEPLOYABLE AERODYNAMIC DECELERATORS, GENERAL	63
Chapter 4. AERODYNAMIC AND OPERATIONAL CHARACTERISTICS OF DEPLOYABLE AERODYNAMIC DECELERATORS	113
Chapter 5. APPLICATIONS	275
Chapter 6. MATERIALS FOR DEPLOYABLE AERODYNAMIC DECELERATORS	337
Chapter 7. DESIGN OF DEPLOYABLE AERODYNAMIC DECELERATORS AND DEPLOYABLE AERODYNAMIC DECELERATOR SYSTEMS	359
Chapter 8. DEPLOYABLE AERODYNAMIC DECELERATOR SYSTEM CONSTRUCTION DETAILS	395
Chapter 9. PARACHUTE HARDWARE AND AUXILIARY DEVICES	405
Chapter 10. PARACHUTE SUPPORT EQUIPMENT AND FACILITIES	437
Chapter 11. DEPLOYABLE AERODYNAMIC DECELERATOR TESTING	443
Chapter 12. SAMPLE CALCULATION FOR A DEPLOYABLE AERODYNAMIC DECELERATOR SYSTEM	501
Chapter 13. SPECIFICATIONS	529
INDEX	531

INTRODUCTION

Table of Contents

	<i>Page</i>
Early History	2
First Design Concepts	4
Deployment Origins	5
Military Development	5
Paratroops	7
Air Drop	7
Materials	7
The Scientific Approach	7
Recent History	8
Outlook	9

Illustrations

<i>Number</i>		<i>Page</i>
1	Leonardo Da Vinci's Parachute, 1452-1519	2
2	Fausto Veranzio's "Homo Volans", 1595	3
3	Sebastian Lenormand Jumps from Rooftops, Montpelier, France, 1783	3
4	Design for a Parachute, c. 1802 (Garnerin)	4
5	Cocking's Parachute, 1837	5
6	Mach No. - Altitude Flight Spectrum	10

Manuscript released by the author June 1963 for publication as an ASD Technical Report.

INTRODUCTION

Deployable aerodynamic decelerators are devices which, by virtue of their design configuration and performance characteristics, augment the basic drag, and in some cases the stability, of flight vehicles to which they are attached. In all aerodynamic drag devices, the retarding force is generated by changing the momentum of the air through which the device passes. This action brings about the desired change in flight-vehicle velocity and provides for a constant or programmed rate of descent of the suspended load. Although deployable aerodynamic decelerators are used with flight vehicles, they do not specifically form a part of the flight-vehicle structure.

Among deployable aerodynamic decelerators, the self-inflating textile parachute canopy is undoubtedly the best known, and is the most widely utilized because of its high drag efficiency and its relative simplicity of system and component design. Consequently, primary emphasis is given in the following chapters to the design considerations and performance characteristics of textile parachute canopies of various configurations.

The word *parachute* is derived from the French words *parare*, "to shield or defend," and *chute*, "a fall." By definition, a parachute is a folding umbrella-like device used for making a safe descent through the air. Although the parachute was initially conceived for use by human beings, devices for making safe descents are used today not only for premeditated and emergency escape of crew members from aero-space vehicles, or for the air drop of equipment, but they have also become one of the most important components in many types of flight vehicles. In fact, the changes in "parachute" configuration which have taken place during the last twenty years have led to defining drag devices in somewhat broader terminology as "deployable aerodynamic decelerators."

Early History. The history of parachutes dates back to medieval days. Evidence found in the historical archives at Peking, China, and translated by the French monk, Vasson, indicates that parachute-like devices were used as early as the 12th Century. Stories relate that some form of parachute was used during circus-type stunts arranged to entertain guests at Chinese court ceremonies. The relation between the umbrella, known to have been invented by the

Chinese, and this early device appears obvious.

The first known pictorial evidence of the drag principle appeared in the sketchbook of Leonardo da Vinci in 1514 (Fig.1). The device pictured was a pyramid-shaped structure by means of which, the sketch implied, a man might leap from a tower without greatly endangering his life. However, as far as is known,

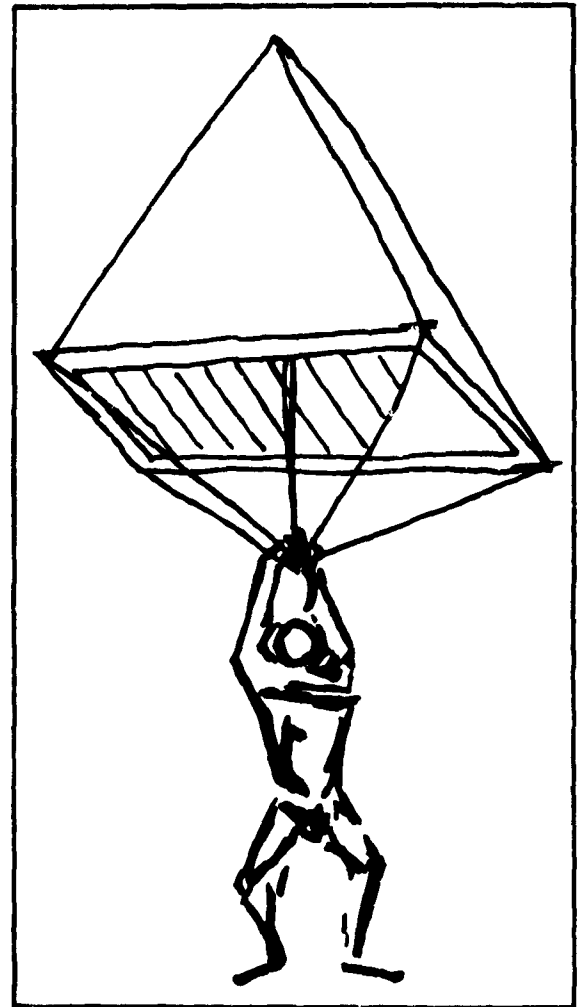


Fig. 1 Leonardo Da Vinci's Parachute, 1452-1519

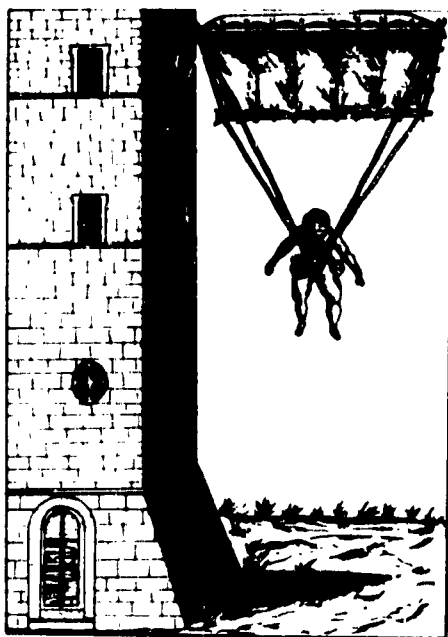


Fig. 2 Fausto Veranzio's "Homo Volans", 1595

da Vinci did not reduce his sketch to practice. Almost one hundred years lapsed before the concept of the parachute was again recorded in the annals of history. In 1595, Fausto Veranzio (Fig. 2), Hungarian mathematician living in Italy, published the idea of a parachute as a "fall breaker", and described several successful trial jumps which he claimed to have made from a tower in Venice; however, his claims to successful jumps have not really been substantiated.

More authority can be attached to the experiments of the Frenchman, Joseph Montgolfier, who, late in the 18th Century, began to put some of the then current scientific findings to practical use. Concurrent with his experiments on hot-air balloons, he became interested in the concept of parachute-like devices, and tested the invention he evolved by dropping a number of animals from towers. Subsequently, he himself test-jumped from the roof of his house at Annonay and later from "greater heights", presumably from one of his balloon gondolas. A French contemporary of Montgolfier, Sebastian Lenormand, successfully attempted a demonstration of the parachute concept by descending with the aid of a parachute-like device from the top of the Montpellier Observatory in Paris. It is not certain how far Montgolfier actually pursued his parachute experiments; however, it can be said that his balloons gave parachute jumping a sudden and practical impetus.

(Up to this time, professional exhibitionists and stuntmen had been jumping from towers or high build-

ings (Fig. 3). After Montgolfier had demonstrated balloon flying as practical, a more suitable platform was available, and an increase in parachute jumping, although still for stunt purposes, is recorded.)

The number of balloon accidents which occurred during this period led to the consideration of the parachute as a possible means of saving lives. This trend was accelerated late in the 18th century when Jean Pierre Blanchard, one of the most famous balloonists of the day and the first man to soar out over the English Channel, became interested in the parachute. After trying it successfully on animals, including his own dog, Blanchard personally made several successful jumps. At the turn of the century, between 1797 and 1802, Andrew Jacques Garnerin, who achieved fame by the number, daring, and success of his jumps, made a series of parachute drops both in England and in France, culminating in a jump from an altitude of ap-



Fig. 3 Sebastian Lenormand Jumps from Rooftops, Montpellier, France, 1783

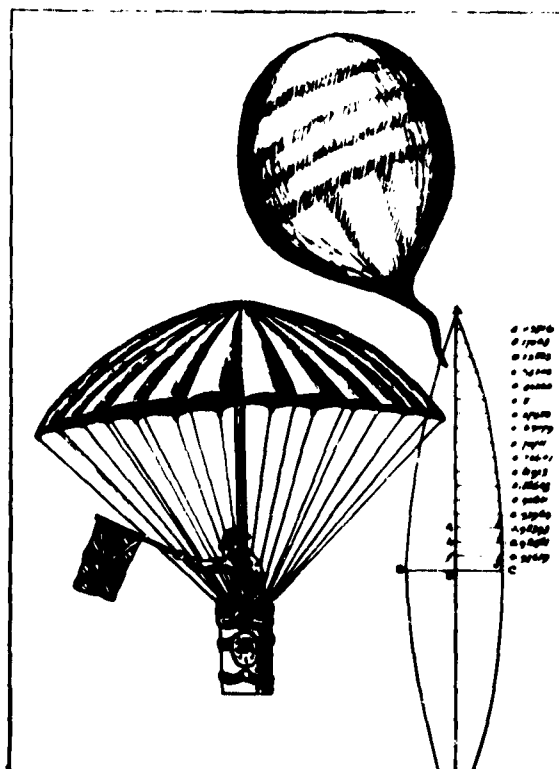


Fig. 4 Design for a Parachute, c. 1802 (Garnerin)

proximately 2400 meters in a cylindrical basket suspended from a parachute. All of the recorded parachute jumps up to this time had been of a premeditated nature. The first recorded emergency landing by parachute was not made until 24 July 1808 when the Polish aeronaut Jorđaki Kuparento descended safely from his burning balloon over the city of Warsaw.

The years of experimentation with parachutes until the turn of the 20th century had produced very little more than crude and sometimes unreliable devices for the purpose of performing stunts and providing entertainment. Inevitably, some parachutists were killed, with a consequent dampening of the enthusiasm of other jumpers. The advent of the airplane, however, changed this situation quickly. Partly because of the new thrill found in jumping from a moving aerial platform, and partly owing to the necessity of providing escape from disabled airplanes (considering their added complexities of operation), further development of the parachute accelerated. Besides changes to the parachute itself, changes in techniques of use became necessary. Thus, the advent of the airplane caused the launching of a series of scientific experiments to make the parachute more airworthy and led to the deployable aerodynamic decelerator of today.

First Design Concepts. One can safely assume that the first Chinese parachute was umbrella-shaped. Da Vinci's parachute (Fig. 1), however, consisted of four triangular pieces of cloth joined to form a pyramid from which the jumper was suspended by means of ropes. Da Vinci, in the *Codex Atlanticus*, 1493, added the following details: "If a man have a tent roof of calked linen, twelve braccia broad and twelve braccia high, he will be able to let himself fall from any height without danger to himself." Presumably, this parachute would have worked, at least to a degree. The parachute conceived by Veranzio (Fig. 2) consisted of a square of linen held rigid on a wooden frame. The jumper held on to four cords, one attached at each corner. Veranzio claimed that his design proved successful, and there is no reason to believe that it would not have worked.

The parachute with which Garnerin conducted his experiments was again umbrella-shaped, and like the umbrella, was reinforced by a central stem (see Fig. 4). This, at the time, was a revolutionary departure from having the parachute held open permanently by a rigid framework. However, Garnerin encountered serious oscillatory problems during his experiments, and initiated efforts to find the causes and possible remedies for these discouraging gyrations. Some of his contemporaries also concerned themselves with finding a solution to the oscillatory problem. The English scholar, Sir George Cayley, proposed as a remedy a cone-shaped parachute which would be used with the apex pointing downwards. Cayley developed this idea, and according to his report, it was used with success by the German, Lorenz Hengler. Hengler, in fact, made several jumps with this cone-shaped parachute from heights of from 30 to 120 meters "without experiencing the least discomfort."

A number of additional jumps were made, and experience proved that the inverted cone-shaped parachute was essentially sound in theory, but consistent success in practice was another matter. Consequently, more accidents inevitably happened. An English artist, Robert Cocking, experimented in 1837 with a parachute design (Fig. 5) based on Hengler's concept and was killed when his cone-shaped parachute disintegrated during a jump from 1700 meters altitude, probably because its construction was not sufficiently strong to support the 200 lb of suspended weight. Since Cocking's parachute had been widely publicized as the solution to the strange behavior of Garnerin's parachute, his death caused even wider public disbelief in and disapproval of the parachute concept. However, efforts were continued by others to solve the oscillation problem.

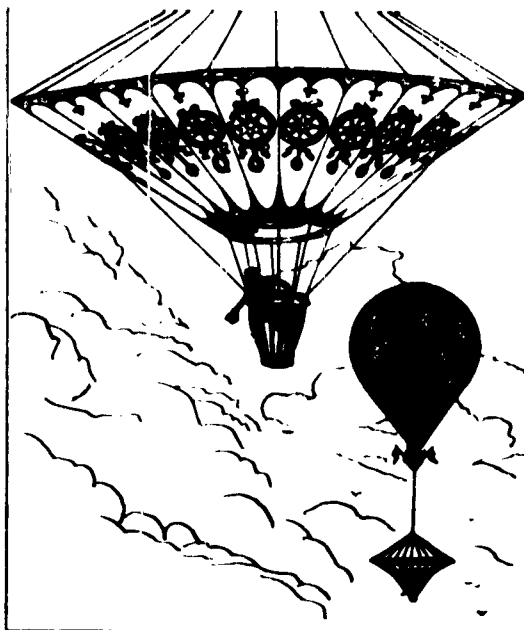


Fig. 5 Cocking's Parachute, 1837

The French astronomer Lelande theorized that the cause of the oscillatory motions of the parachute was the air trapped under the drag-producing surface and spilling out, first under one side and then the other. He alleviated the problem by permitting a constant and steadying flow of air to escape upward through a hole provided in the apex of the drag-producing surface. This was the first vent; and it worked.

Deployment Origins. A solution to the oscillatory problem had now been found and stunts with parachutes continued. Up to now, however, all parachutes used had been of the rigid or semi-rigid type, held open by a wooden frame. Early in 1804, a Frenchman named Bourget proved during a parachute jump in Germany that a completely collapsible parachute was not only practical, but was much more convenient to carry around. It could be folded when not in use, and it relied on air pressure alone to hold it open. Experiments with foldable parachutes continued, and in 1887 Captain Thomas Baldwin, an American jumper of much renown, introduced a collapsible silk parachute with vent opening in this country.

In 1890, Paul Letteman and Kaethe Paulus, German exhibition jumpers, demonstrated the first use of parachutes folded and packed in bags. Their innovation grew out of a special act, a double parachute jump, in which both performers left a balloon by means of one parachute; then one made a second jump with the other parachute. A bag-like container was used in

this exhibition to keep the entire parachute assembly intact until the very moment it was to be used. This container or bag idea, however, did not take hold immediately, and was not even utilized during the first jumps from the moving platform of the airplane.

Grant Morton, some believe, was the first man to jump by parachute from an airplane, although Captain Albert Berry, who had previously jumped from balloons, is another claimant for that honor. Morton, late in 1911, is reported to have jumped from a Wright Model B airplane flying over Venice Beach, California. Morton carried his folded parachute in his arms; as he jumped he threw the parachute canopy into the air. The parachute opened, and Morton landed safely. Captain Albert Berry, who like his father John, was somewhat experienced with balloons and parachutes, completed a successful parachute jump from a two-seated pusher plane near St. Louis. His 36-ft-diameter parachute was packed in a cone-shaped container fastened underneath the fuselage. Instead of being strapped in a harness, Berry was sitting on a trapeze bar attached to the suspension lines.

These parachutes and all others used before, were of the "automatic" type, meaning that they were either inflated prior to the jump or were pulled into the airstream from a container fastened to the aerial platform. This type of parachute, however, soon proved to be inadequate for safe escape from moving aerial platforms. In 1908, Leo Stevens devised the first parachute which could be opened by the jumper with a ripcord, although the "free" type parachute was not utilized substantially until 1920.

A patent granted early in 1911 to an Italian inventor named Pino for a flexible parachute, including a pilot chute, must be considered as one of the major milestones in parachute history. As claimed in the patent, the jumper using this new device would wear his parachute in a pack like a knapsack. On his head would be a hat-like device fashioned into a leather cap, which would blossom out into a smaller open parachute. During the jump, the small pilot chute would pull off the hat and deploy the larger parachute from the knapsack.

Military Development. When World War I began in 1914, very few crew members of balloons or airplanes carried parachutes. The Germans were probably the first to appreciate that a pilot's or crew member's life must be saved in case of emergency, and that the parachute was the means to accomplish this. Within a year, the Germans had equipped their balloon crews with a parachute developed by the woman parachutist, Kaethe Paulus. The British and French followed this example, equipping their balloons with parachutes packed in conical containers positioned

outside the gondola, and the Americans adopted the French balloon parachute. The heavy loss of aviators in balloon and airplane accidents, and downings caused by enemy actions, brought the parachute into its own.

An Austrian pilot made the first escape by parachute from a disabled plane, on the Russian front in 1916. Three months later, another Austrian pilot made a safe escape from another disabled plane. By 1917, the parachute had proven itself, and both Germans and English were equipping their air forces with these life-saving devices. By the summer of 1918, parachutes were in wide use on all fronts.

These early life-saving parachutes were basically of the bag type and operated "automatically". The German version was the Heinicke Sack parachute; the English, the Calthorp or "Guardian Angel" parachute. They were attached to the flier by means of a harness, and the bag-type parachute became, when not in use, a sort of cushion. From within its bag, the canopy was attached by a static line to the plane. When the pilot jumped, the tightening static line pulled the parachute from its container ready for action.

Improvements continued to be made to both parachutes during the following year to increase their operational reliability. The Germans successfully incorporated a principle first published by Pino, that of utilizing a smaller pilot parachute to deploy the large parachute, although the pilot parachute continued to be deployed by a static line. Further modifications were made also to the "Guardian Angel."

Still, the parachutes used during World War I were, by modern standards, makeshift contraptions. They had proven their worth, however, and formed the basis for experiments in design which were initiated immediately after the war and have continued since.

General William Mitchell, Commander of the U.S. Air Force in France, was primarily instrumental in getting an organized parachute test and development program started in the United States. As a result of his pleas for more and better parachutes for his pilots, a parachute facility was established at McCook Field, Dayton, Ohio, and began functioning in the summer of 1918. In December 1918, Major E. J. Hoffman was put in charge of the project, which had now become of considerable importance. Major changes in parachute design can be attributed to the collective and individual efforts of the members of this group.

Initially, experiments at McCook Field were conducted on automatic parachutes of two general types. In one, the parachute and its container were attached to the airplane, and the parachute was connected

with a rope to a harness worn by the jumper; in the second, the parachute was packed in a bag, worn by the jumper, and the rope connected the parachute directly to the airplane. In either case, the pilot or jumper had only to jump, and when he reached the end of the rope, the parachute was automatically pulled out of its container and into the airstream. Great difficulties were experienced during attempts to perfect this type of parachute deployment, and although hundreds of tests were conducted with these models, none met the rigorous requirements which had been established.

Thought was again given to a "free" parachute to be released from the pack by the operator after he jumped. The first model, known as Model A, was 38 ft in diameter, a flat circular parachute canopy made of straight-cut silk. It was composed of 40 gores with 40 braided suspension lines and had a vent 40 in. in diameter controlled by thick rubber bands. It was packed in a back-type pack. This model was later altered to a 24-ft-diameter canopy in a seat-type pack.

Considerable effort was expended on the development of the free parachute; on 28 April 1919, after a number of successful dummy tests, the new parachute was life-tested by jumping from an altitude of 1500 ft. Other tests followed, and the free parachute was accepted.

Testing of this parachute type, and further experimentation with other types, continued in this country and abroad. The first parachute which was standardized by the U. S. Army Air Corps, after considerable development effort and experimental testing, was of the seat type, for use by pilots and crew members. It consisted of a pack containing a flat circular solid-cloth canopy, 24 ft in diameter, incorporating a three-point harness release. It was given the designation S-1, and became standard in 1926. One year later, a second seat-type parachute was standardized under the designation S-2. It retained all the features of the S-1 parachute, except that it used a flat circular solid-cloth canopy 28 ft in diameter, to insure the safe descent of somewhat heavier crew members. By this time, several other applications for the parachute, aside from insuring the safe escape of crew members, became apparent, and parachutes for such specific applications as premeditated escape (paratroops) and air drop of supplies had to be developed.

Major Hoffman, who was in charge of the Parachute Unit at Wilbur Wright Field, Dayton, Ohio, started the development of a radically new type of parachute canopy, the triangular type, in 1929. In 1932, the triangular canopy was standardized and adapted to a seat-type parachute (S-3). It also found application in the first training parachute (C-1), which was a

combination of seat and back type, and in the first quick-attachable chest parachute (A-1) for insuring the maneuverability of gunners, observers, and photographers within aircraft.

Paratroops. Undoubtedly the largest impetus given the further development of the parachute was the concept of "Vertical Envelopment." The paratroop training program in the United States was launched, unofficially, as far back as the fall of 1928. At the instigation of General Mitchell, six armed parachutists jumped from a Martin bomber over Kelly Field, Texas. This demonstration, however, was regarded as merely another stunt. Although limited experimentation continued, it was not until the spring of 1940 that the United States established an official paratroop training program at Ft. Benning, Georgia. The first troop-type parachute (T-1) consisted of two ripcord-opened packs attached permanently to a single harness with two sets of risers; a back pack containing a 28-ft flat circular solid-cloth canopy; and a chest pack containing a 22-ft flat circular canopy. During subsequent modifications, harness webbing of a lighter weight was substituted (T-3), and initiation of deployment was changed from ripcord actuation to static-line actuation (T-4).

Probably one of the most important improvements in the efficient utilization of the parachute at that time was made by the introduction of the quick-release harness. The quick-release mechanism was patented in 1929 in Great Britain, and manufactured in the United States by the Irving Air Chute Co., Buffalo, N. Y. In 1944, the quick-release device became standard equipment in the U. S. Army Air Corps, and was incorporated in the seat-type parachute (S-5), the troop-type parachute (T-7), the chest-type parachute (A-4), and the back-type parachute (B-9).

Abroad, actual establishment of paratroop units and their training was initiated somewhat earlier than in the United States. France, for example, organized its first battalion of air troops in 1938, but abandoned the idea in 1939. Both Russia and Germany were training paratroopers long before this time. The first recorded jump, made by the national hero Gromov, occurred in Russia in 1927, and at her Sports Festival in 1930, Russia demonstrated the concept of "Vertical Invasion" by having armed men jump from an airplane by parachute to occupy the "headquarters of an enemy." Germany's paratroop program was under way as early as 1935, and further experiments were launched that led to the exploitation of parachutes for other than personnel applications.

Air Drop. Parallel with the development of parachutes for personnel applications, in particular to develop fully the concept of "Vertical Invasion,"

went the development of parachutes for the air dropping of military equipment. Although the air dropping of food, medicine, mail, and other essentials by means of parachutes over areas inaccessible to ordinary means of transportation was practiced in both Russia and the United States during the late 1920's and early 1930's, it was not until shortly before the start of World War II that concerted attempts were made in the United States to air-drop military equipment of significant weight. Naturally, in order to deliver these heavier loads successfully, either larger parachute canopies or the use of canopies in clusters had to be developed.

The first successful test in which parachute canopies were used in clustered configurations was accomplished in 1941 at Ft. Bragg, North Carolina. A mountain gun weighing 840 lb was delivered by means of three silk parachutes 22 ft in diameter, and following this a 75mm howitzer, separated into two bundles of 840 lb and 670 lb, was air dropped by means of clustered parachutes. By 1943, an entire series of cargo parachutes was standardized, starting with a 24-ft-diameter rayon canopy (G-1) for the air drop of supplies. Parachute canopies with diameters of 28 ft and 48 ft followed, and canopies with diameters up to 100 ft (G-11) are today in standard use.

Materials. For many years silk had been the favored material for the fabrication of parachutes. However, as early as 1940, experiments were made with man-made fibers as a substitute for silk. A large number of canopies, particularly cargo types, were fabricated of rayon. Nylon first perfected in 1938 soon came into its own, and has found extensive use in the manufacture of parachutes. By 1940, an extensive testing program with nylon canopies had been instituted, and by the end of 1943, nylon canopies were in wide use.

The Scientific Approach. It must be noted that, in general, steps taken up to about 1940 toward the development of parachutes were rather crude and arbitrary. The cut-and-try method was the most widely utilized, and the only prerequisites for parachute design and construction appeared to be a knowledge of the tailor's trade. It was not until the beginning of World War II that sufficient emphasis was placed upon the "science" of parachute design and performance prediction. The Germans and the British must be given credit as the first to appreciate the need for, and actually embark upon, scientific investigations to determine the more fundamental aspects of parachute design and operation. Most of the major developments in parachutes to satisfy the diversity of applications have occurred during and since the days of World War II.

The primary center for parachute research and de-

velopment in Germany was the Research Institute "Graf Zeppelin" near Stuttgart. Here, under the direction of Professor Dr. G. Madelung, Mr. Theodore Knacke, and Dr. Helmut G. Heinrich, significant advancements in parachute technology were accomplished. As a result of increasing requirements for parachutes to decelerate and stabilize bombs, mines, torpedoes, missile components, etc., and to decelerate aircraft and gliders during the landing phases, two radically different types of parachute canopies were evolved at this institute: the ribbon canopy (Dr. Madelung, Mr. Knacke) and the guide-surface canopy (Dr. Heinrich). Both types were developed to a high degree of excellence after considerable theoretical study and experimental effort.

The ribbon parachute found its first operational application for in-flight and landing deceleration of manned gliders. The capture of Fort Eben-Emael, Belgium, in 1940 by German paratroops and glider units demonstrated the effectiveness of the ribbon parachute as an aircraft decelerator and as a device to assist landing. In further modifications of the ribbon canopy, reefing systems were developed and added, and the parachute was employed not only to decelerate gliders, conventional aircraft, and later the first jet aircraft (such as the Arado 234 (1945), and the Messerschmitt 163 and 262), but also to decelerate mines and deliver military supplies safely from high- or low-flying aircraft with pinpoint accuracy. Indeed, the Natter (1944-45) was developed as an interceptor without landing gear, which was launched vertically. After completion of a mission, the pilot would fly to safe territory, where he actuated a mechanism that separated the aircraft into major subassemblies and deployed parachutes for the safe descent of both pilot and subassemblies.

The guide-surface parachute was first employed operationally for the trajectory control of bombs because of its excellent stability characteristics. First attempts to recover guided missiles or missile components (V-1 and V-2) were successfully accomplished in 1944 utilizing ribbon parachute canopies. These were also employed successfully for the stabilization and deceleration of the first ejection seat in early 1945. In addition, extensive theoretical efforts were carried on to analyze the operation of parachute canopies and to obtain fundamental knowledge about the aerodynamic characteristics of parachute canopies.

Research and development efforts also continued in the United States during the war years; however, a sizeable increase in the scope and extent of the overall program was not realized until after the war.

Recent History. The advancement of supersonic operations of military equipment, and the emphasis

on the development of ballistic missiles, brought about the requirement for an accelerated research and development program for parachutes and other deployable aerodynamic decelerators, and consequent further advancements in the state of the art. The primary center for research and development in the area of parachute technology has been and still is at Wright Field.

Under the direction and guidance of Capt. R. Barnes (1948-1951), Maj. W. McComb (1951), Maj. R. Wheeler (1953), and Mr. Warren P. Shepardson (1952 and since 1955), the Parachute Branch at Wright Field has conducted or sponsored a considerable number of projects designed to develop operational parachute systems for a variety of applications, ranging from premeditated or emergency escape of aircraft crew members to the delivery of military equipment and weapons, and including the in-flight and landing deceleration of jet aircraft and the recovery of drones and missile components. In addition, applied research has been emphasized to increase fundamental knowledge in the field of aerodynamic deceleration.

In the course of this extensive program, the first aircraft-deceleration parachute system for bomber aircraft (B-47) utilizing a ribbon canopy, was developed and standardized in 1949. Subsequently, all operational jet combat aircraft in the U. S. Air Force were equipped with parachute in-flight or landing deceleration systems, or both. The first live ejection-seat test was made late in 1945, recovering the subject successfully by parachute. The ring-slot canopy was developed during 1949 and 1950, and replaced the ribbon canopy in some applications.

In the area of parachute systems for premeditated and emergency escape, important advancements were also realized. A new personnel parachute canopy became available in the extended-skirt type, which was standardized for paratroop use in 1952 under the designation T-10. In search of a parachute canopy which would develop a lower opening shock and be highly stable, the personnel guide-surface canopy, conceived by Dr. H. G. Heinrich, was developed during the middle 1950's as a personnel parachute canopy for aircraft crew members.

Probably the most important single device which was incorporated into the personnel parachute is the automatic ripcord release device. As early as 1938, the Doronin brothers in Russia introduced an automatic parachute incorporating a device for opening the parachute pack mechanically rather than by means of a ripcord. Personnel parachutes incorporating automatic ripcord releases were introduced in the United States during the early 1950's, although considerable

testing with experimental devices had been accomplished earlier.

As the altitude ceiling of aircraft increased, new concepts of emergency escape for crew members had to be explored. The Russian parachutist Kharkohonov demonstrated in August 1940 that emergency escape from high altitudes is possible, by jumping from an aircraft flying at an altitude of 40,813 ft. In the United States, Arthur H. Starnes made a high altitude jump in the summer of 1942 from 30,800 ft, followed by Lt. Col. Randolph Lovelace who, in 1943, descended safely from an altitude of 40,200 ft. Previous high-altitude parachuting records were broken when U. S. Air Force Captains Mazza and Wheeler jumped from altitudes of 42,176 ft. and 42,048 ft., respectively. The current record is held by U. S. Air Force Capt. J. Kittinger who, in 1960, descended from an open balloon gondola floating at an altitude of 97,200 ft. Initially free-falling, and stabilized by a smaller parachute, his main parachute opened automatically at approximately 15,000 ft altitude and provided for a safe descent.

Concurrent with these advances in parachutes for emergency-escape applications, the development of parachutes for the air drop of very heavy military equipment, the recovery of target drones, and the initial deceleration and stabilization of flight vehicles from transonic and supersonic velocities was vigorously pursued.

The clustering of parachute canopies of all sizes and nearly all types became standard operational procedure, primarily for final-stage recovery applications of heavy equipment or vehicles. Major emphasis, however, was placed upon efforts to extend the operational capabilities of textile parachute canopies into the higher supersonic and high dynamic-pressure flight regimes, where parachute canopies of relatively small size are required initially to decelerate and then to stabilize flight vehicles to a velocity and altitude where the safe deployment of larger recovery-parachutes can be accomplished. As a result of continuing state-of-the-art advances, a ribbon canopy was successfully utilized in 1957 to recover the first ballistic missile nose cone after having re-entered the earth's atmosphere. Space travel had become a reality and the potential for the application of parachute canopies suddenly seemed unlimited.

Outlook. In considering the types of applications for deployable aerodynamic decelerators, specific boundaries of the regime concerned with Mach number and altitude for potential drag-device operations can be drawn. The resulting operational flight spectrum can then be further divided (Fig. 6) to define the operational functions which may be required of the aerodynamic decelerator.

The major area of textile parachute applications, naturally, is the subsonic-speed, low-altitude regime in which recovery or terminal deceleration operations of flight vehicles are initiated and accomplished. In general, it can be assumed that reliable self-inflation of textile parachute canopies can be achieved under dynamic pressure conditions greater than 1 lb per sq ft. At dynamic pressures below this value, utilization of inflation aids should be considered. The second broad area of textile-parachute application is the supersonic flight regime. It is bounded by a constant dynamic pressure line of 1 lb per sq ft (below which reliable self-inflation of flexible drag devices cannot be expected, and pressure-inflated or rigid aerodynamic-deceleration devices may be required); by a line above which disassociation effects become noticeable; and by a line of constant dynamic pressure of 10,000 lb per sq ft, above which the structural problems associated with flexible drag-devices may become insurmountable. A stagnation temperature line of 1000 F is shown in Fig. 6, which may be the limit for the use of currently known organic fibers such as HT-1, so far as the effects of aerodynamic heating are concerned.

With the initiation of space travel, however, there has been a broadening of perspectives, and the realization that the utilization of textile self-inflating parachutes was not quite so limitless as it first appeared. Out of this realization, an entirely new technical field was born, that of aerodynamic decelerator technology. The third area of aerodynamic decelerator application, lies in the hypersonic speed, low dynamic-pressure regime, in which augmenting drag-devices may be effectively utilized to minimize and limit aerodynamic heating and deceleration values on re-entering vehicles, as well as to control the final vehicle landing point. Since these devices will be required to operate at relatively low dynamic pressure, they must be either pressure-inflated or mechanically inflated. This flight regime, for the purpose of defining aerodynamic decelerator operations, is bounded by a line of equilibrium temperature (2000 F), above which materials selection are a severe problem, and by a line of constant dynamic pressure, 10 lb per sq ft, below which trajectory control by means of aerodynamic drag variation becomes generally ineffective, although some re-entry trajectory control may be achieved at lower dynamic pressures under certain conditions.

New concepts, new techniques, and entirely new shapes of aerodynamic decelerators are coming into being. Different problems are awaiting their solution. However, research in the specialized field of parachute technology must continue, to increase the drag efficiency and operational reliability, and to further

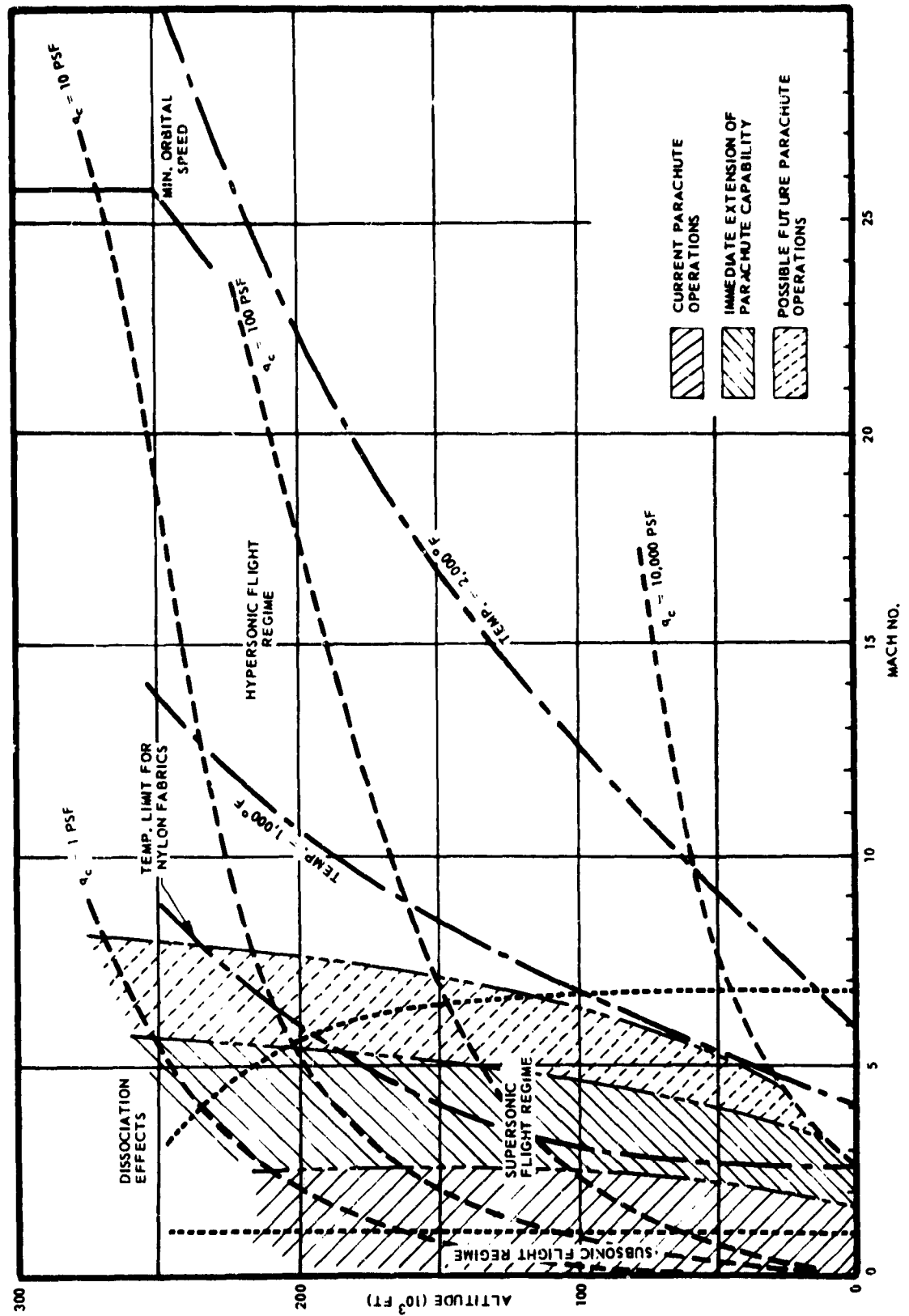


Fig. 6 Mach No. - Altitude Flight Spectrum

the understanding of the aerodynamic and operational characteristics of the most efficient aerodynamic decelerator presently known: the conventional textile parachute canopy. To this end, the cooperative efforts of both government agencies and industry are required.

The information and technical data presented in the following chapters represent the present state of the art of parachute technology. This information will be revised as new knowledge becomes available through tests and experience.

CHAPTER 1
STANDARD SYMBOLS AND GLOSSARY OF
DEPLOYABLE AERODYNAMIC DECELERATOR TERMS

Table of Contents

<i>Section</i>	<i>Page</i>
1 LIST OF SYMBOLS	14
2 GLOSSARY OF AERODYNAMIC DECELERATOR TERMS	20

CHAPTER 1

STANDARD SYMBOLS AND GLOSSARY OF DEPLOYABLE AERODYNAMIC DECELERATOR TERMS

SEC. 1 LIST OF SYMBOLS

The symbols listed below are a compilation of all standard symbols utilized throughout this report. This listing does not include some of the symbols which are defined as they are used in the text.

1.1 Primary Concepts

A	Area, general (other than reference area of the aerodynamic decelerator) (ft^2 or in.^2)
a	Acceleration (ft per sec^2)
a_s	Speed of sound in air (knots or ft/sec)
a	Arc which defines the gore width of a shaped-gore canopy ($= 2\pi r/n$) (ft or in.)
$a_{\max r}$	Region where additional local widening of the gore produces a lobe at the periphery
a	Constant, used in obtaining an approximate weight value for a parachute canopy
B	Number of blades in a rotary-type aerodynamic decelerator
B_{HR}	Horizontal ribbon width (in.)
B_{RR}	Radial ribbon width (in.)
B_{VL}	Vent line width (in.)
B_{VR}	Vertical ribbon width (in.)
b	Constant, used in obtaining an approximate weight value for a parachute canopy
C	Effective porosity (ratio of outflow velocity to inflow velocity through a porous fabric canopy)
c	Factor related to suspension line convergence angle
C_D	Drag coefficient, general
C_{D_o}	Drag coefficient related to the surface area, S_o (equivalent to C_{T_o} at $\alpha = 0$)
$C_{D_o(\text{eff})}$	Effective drag coefficient related to the surface area, S_o (a function of the angle of attack)
C_{D_p}	Drag coefficient related to the projected (inflated) surface area, S_p (equivalent to C_{T_p} at $\alpha = 0$)
C_{D^A}	Drag area of a body, general (ft^2)
$(C_D S)_{o,p}$	Drag area of the aerodynamic decelerator, based on either total surface (nominal) or projected (inflated) area (ft^2)
$(C_D S)_R$	Drag area of a reefed canopy (ft^2)
C_L	Lift coefficient, general
C_m	Moment coefficient, general

C_P	Pressure coefficient, general
C_Y	Normal force coefficient, general
C_T	Tangent force coefficient, general
D	Drag (lb) or Diameter (ft), general
D_c	Diameter, constructed (ft)
D_o	Nominal diameter of the aerodynamic decelerator $\sqrt{4 S_o \pi}$ (ft)
$D_{o,p}$	Diameter of the aerodynamic decelerator (either nominal or projected, as applicable) (ft)
D_p	Projected or inflated diameter of the aerodynamic decelerator (ft)
D_{R_1}	Skirt diameter of reefed canopy (ft)
D_{R_o}	Diameter of reefing line of fully inflated canopy (equivalent to D_S) (ft)
D_S	Canopy skirt diameter (ft)
d	Diameter of primary body (ft)
d_v	Vent diameter (ft)
E	Modulus of elasticity of canopy material (lb per in. ²)
E_k	Kinetic energy (ft lb)
e	Factor related to strength loss by abrasion
e_g	Base width of gore (in.)
e_{g_v}	Gore width at vent (in.)
e_{g_2}	Gore width at the skirt of the extension (in.)
F	Total retarding force (lb)
F_{b_1}	Aircraft retarding force immediately before brakes are applied (lb)
F_{b_2}	Aircraft retarding force immediately after brakes are applied (lb)
F_c	Constant retarding force (lb)
F_f	Aircraft frictional force (lb)
F_o	Maximum opening force (lb)
F_s	Line snatch force (lb)
f	Frequency of the periodic motion of the aerodynamic decelerator (sec ⁻¹)
g	Acceleration due to gravity (ft per sec ²) (32.2 at sea level)
h	Height or altitude (ft)
h_a	Actual constructed height of gore (in.)
h_e	Height of gore extension measured along centerline (in.)
h_g	Height of gore (in.)
I	Mass moment of inertia (slug-ft ²)

I_{sp}	Specific impulse (lb per sec per unit)
i	Safety factor
K_o	Factor related to orifice efficiency of inflatable bags
K_n	Knudsen number
k	Factor related to strength loss by fatigue
L	Lift force (lb)
L_a	Free length of pocket band (in.)
L_b	Length of intercept in the skirt (pocket band) (in.)
L_o	Length of gore (in.)
L_R	Length of reefing line (ft or in.)
L_S, l_s	Length of suspension lines (ft or in.)
l	Distance, general (ft or in.)
M	Mach number
M	Moment (ft lb)
m	Mass, general (slugs)
N, n	Number of gores (used interchangeably)
N	Normal force (lb)
n_{HR}	Number of horizontal ribbons
n_{VL}	Number of vent lines
σ	Factor related to strength loss in material from water and water vapor absorption
P	Pressure, general (lb per in. ² or lb per ft ²)
P	Tractive force, general (lb)
P_r	Prandtl number
P_h	Required hovering power (horsepower)
P	Static pressure (lb per in. ² or lb per ft ²)
q	Dynamic pressure ($= 0.5 \rho v^2$) (lb per ft ²)
q_s	Impact pressure corresponding to the velocity at snatch force (lb per ft ²)
R_e	Reynolds number
R_N	Nose radius of primary body (ft)
R_s	Distance between adjacent horizontal ribbons (in.)
r	Radius, general (ft)
r_b	Bulge radius (in.)
S	Reference area, general (ft ² or in. ²)

S_g	Area of gore (in. ²)
S_h	Stress in canopy cloth
S_{HR}	Area covered by horizontal ribbons (in. ²)
S_L	Aircraft landing roll distance (ft)
S_o	Surface area of aerodynamic decelerator (ft ² or in. ²)
$S_{o,p}$	Characteristic canopy area (ft ² or in. ²)
S_p	Projected (inflated) area of aerodynamic decelerator (ft ² or in. ²)
S_{p_i}	Instantaneous projected canopy area (ft ²)
S_{RB}	Area of reinforcing bands (in. ²)
S_{RR}	Area covered by radial ribbons (in. ²)
S_{VR}	Area covered by vertical tapes (in. ²)
S_λ	Total slot area of Ringslot canopy (ft ²)
s_o	Vent area of canopy (ft ² or in. ²)
T	Temperature, general (°F or °R)
T	Tangential force (lb)
t	Time, general (sec)
t_f	Filling time of aerodynamic decelerator (sec)
u	Strength loss factor at the connection point of the suspension line and the drag-producing surface or riser
V	Volume, general (ft ³ or in. ³)
v	Velocity, general (knots or ft per sec)
v_d	Deployment velocity (knots or ft per sec)
v_e	Equilibrium velocity (ft per sec)
v_{e_o}	Equilibrium velocity at sea level density (ft per sec)
v_o	Launch velocity (knots or ft per sec)
v_s	Velocity at suspension line stretch (knots or ft per sec)
v_t	Terminal velocity (ft per sec)
v_v	Vertical descent velocity (ft per sec)
W	Weight, general (lb)
X	Opening-shock factor denoting the relationship between maximum opening force and constant drag force ($= F_o/F_c$)
x	Ordinate along X-axis
y	Ordinate along Y-axis
z	Ordinate along Z-axis

Z	Number of suspension lines
α	Angle of attack (deg)
β	Gore vertex angle (deg)
γ	Ratio of specific heats
γ_s	Suspension line confluence angle (deg)
Δ	Small increment (not used alone)
δ	Ratio of canopy skirt diameters
ϵ	Emissivity of material
λ	Wavelength
λ_g	Geometric canopy porosity (percent)
λ_m	Mechanical porosity (permeability of fabric)
λ_t	Total canopy porosity (percent)
μ	Coefficient of friction
η	Efficiency factor
ξ	Elongation of suspension lines (percent)
ν	Kinematic viscosity ($\text{ft}^2 \text{ sec}$)
π_o	Polygon shape factor
ρ	Density of air at given altitude (slugs per ft^3)
ρ_o	Density of air at sea level (0.00238 slugs per ft^3)
σ	Density ratio ($= \rho / \rho_o$)
Ω	Rotational speed of rotating aerodynamic decelerator (radians per sec)
ω	Angular velocity (radians per sec)
θ	Trajectory inclination angle (deg)
ϕ	Aspect angle (deg)

1.2 Secondary Concepts (Used as subscripts and secondary subscripts)

a	Added; additional; absolute; actual; apparent
av	Average
AW	Adiabatic wall
b	Body; bulge
c	Canopy; critical; constant; constructed; uninflated
d	Deployment
D	Drag
e	Equilibrium; exit; earth

<i>f</i>	Filling; fabric; friction
<i>g</i>	Geometric; gore
<i>h</i>	Horizontal; hoop; hovering
<i>i</i>	Inlet; instantaneous; included; arbitrary; initial
<i>L</i>	Load; local
<i>m</i>	Material; mass
<i>M</i>	Moment
<i>N</i>	Normal
<i>o</i>	Opening; reference condition; nominal
<i>p</i>	Projected; pressure; parachute
<i>R</i>	Riser; radius; reefing
<i>r</i>	Resultant; radial
<i>s</i>	Skirt; snatch; suspension lines; static
<i>sq</i>	Squidding
<i>SL</i>	Sea level
<i>t</i>	Tangential; total
<i>T</i>	Total
<i>th</i>	Theoretical
<i>v</i>	Vertical; vent
<i>w</i>	Wall; wind; wake; weight
<i>x</i>	X-direction
<i>y</i>	Y-direction
<i>z</i>	Z-direction
∞	Free stream

SEC. 2 GLOSSARY OF AERODYNAMIC DECELERATOR TERMS

Accordion Folding. See *folding, accordion*.

Adapter, Harness Strap. A rectangular metal fitting with a crossbar. It is incorporated in a parachute harness to permit proper adjustment of webbing.

Adapter, Harness, Quick-Fit. An adapter with the fixed crossbar replaced by a floating friction grip. The adapter is incorporated in a harness web to permit quick adjustment.

Air Bags. Flexible, gas-filled bags that are inflated during load descent and valved to release their pressure upon ground contact to absorb impact forces.

Air Drop. A method of air movement wherein personnel, supplies, and equipment are unloaded from aircraft in flight.

Anchor Cable. A cable in an aircraft to which the parachute static line or straps are attached.

Apex. The center and topmost point of a parachute canopy.

Awl. A small, sharp-pointed tool used to make holes in heavy fabric or webbings for hand sewing.

Backstitch. Used to anchor a row of stitching by turning material and sewing back over original stitching a short distance.

Backstrap. A part of the harness that extends across the small of the wearer's back. It may or may not be adjustable.

Bag, Deployment. A container, usually of fabric, in which a parachute canopy is stowed for deployment. There may or may not be provision for stowing suspension lines on the bag. Usually, either a static line or pilot chute lifts the deployment bag away or extracts it from a parachute pack or storage container. Normally, with this system the suspension lines are extended before the drag producing surface emerges from the deployment bag.

Band, Lower Lateral. A webbing band inserted in the skirt hem of the drag-producing surface to reinforce the skirt.

Band, Upper Lateral. A webbing band inserted in the vent hem of the drag-producing surface to reinforce the vent.

Band, Pocket. A piece of tape or line attached at the outside of the skirt, across radial seams, in a manner that causes the gores to be pulled outward at inflation, thus improving the opening characteristics of the canopy.

Band, Reinforcement. Reinforcing tape, webbing, or ribbon, inserted in varied positions to reinforce weak points of construction or design in a drag-producing surface.

Band, Retainer. A rubber band used to hold folded suspension lines or static lines to deployment bags or parachute packs.

Bar, Packing. A long, flat bar of metal, plastic or wood, used to fold the canopy of a parachute during the packing process, and to aid in closing the pack.

Bartack. A concentrated series of zigzag-like stitches used to reinforce points of stress.

Basting. Temporary stitching, usually with long, loose stitches.

Beeswax. A wax used with paraffin to prevent fraying of webbing.

Bond Test. A prescribed method of subjecting ripcord pins to a certain weight-pull in order to determine hardness and ductility.

Bias. A cut or seam running obliquely across the threads of a fabric.

Binding. A piece of tape or fabric folded over and stitched to a raw edge of the fabric to prevent raveling or fraying.

Blanketing. A result, caused by the relative air flow over a load or body, which opposes the intended action of a pilot chute or parachute canopy by reversal of flow and turbulence.

Block Seam. Any seam which runs parallel to the warp or filling threads of material used in canopy construction.

Board, Tension. A device that is usually hooked to the parachute connector links to place tension on the canopy during inspection and packing.

Bobbin. A small, metal spool used to hold thread, as in a sewing machine.

Bodkin. A large-eyed needle, flat or round, and usually blunt, used to draw tape, ribbon, elastic, or cord through a loop or hem.

Bolt. A compact package or roll of fabric of any standard width, used in the United States as the designation for a length of 40 yards of material.

Bottom, False. A piece of pack fabric stitched to the inside of a pack for the purpose of retaining the pack frame; it also may serve as a base for stitching of the suspension-line retaining-loops.

Breakcord. A thread or tape tied between parachute components that is intended to break under desired load during deployment. See *Thread, Break*.

Breathing, Canopy. The pulsating or pumping action of an inflated canopy during descent.

Bridle. The arrangement of cords or webbings attaching the pilot chute to the apex of one or more canopies, or to the deployment bag or bags containing those canopies.

Broken Pick. A broken filling-thread, usually appearing as a streak along the fabric.

Bunched Stitching. A defective seam resulting from stitches being too close together; more stitches per inch than required.

Bungees. See *Elastics, pack-opening*.

Burns, Friction. The result of rapid rubbing together of two textile surfaces, generating frictional heat, which reduces the tensile strength of the textile and causes deterioration of individual threads. It occurs primarily during parachute deployment and initial inflation.

Cabinet, Drying. A facility used for the accelerated drying of parachutes.

Cable, Ripcord. A flexible cable joining the locking pins and the ripcord grip. The ripcord cable usually is of carbon steel or corrosion-resistant flexible steel, normally 3/32 inch in diameter. It consists of seven strands with seven wires per strand.

Cannibalize. To remove serviceable parts from one item of equipment in order to install them on another item of equipment.

Canopy. The portion of a parachute consisting of the drag-producing surface and the suspension lines extended to one or more mutual confluence points.

Canopy-Release Assemblies. Devices which allow immediate detachment of the canopy. They connect the harness main web straps to the canopy risers.

Chain. Method of shortening suspension lines for storage by looping and interlocking lines.

Chainstitch. Ornamental, basting, or seam stitch in which thread or threads are not interlocked but are held by a loop of needle thread being passed through another loop of needle thread or through a loop of bobbin thread. May be single-, double-, or triple-thread chain stitching.

Channel, Canopy. The space or opening through which the suspension lines are passed. It is formed by the overlapping of the fabric in the main seams, or by the addition of cover tape to the drag-producing surface.

Cheststrap. One of the harness straps sewed across the chest with a snap and a V-ring to prevent the wearer from falling out of the harness.

Chute. A term used interchangeably with the word "parachute."

Clevis. A U-shaped metal fitting, with a hole in each end to receive a pin or bolt. It is used on cargo parachutes and heavy drop kits.

Clevis Pin. A metal rod, usually fitted with cotter pin or threaded to receive a nut, inserted through holes in the end of clevis to hold clevis shut.

Clip, Safety. A U-shaped metal fitting used to prevent the accidental opening of the parachute harness release.

Cluster. A group of two or more parachutes that are attached to a single load and are designed to open simultaneously.

Cone, Pack (Locking Cone). A small, cone-shaped metal post sewn to one of the side flaps of

the pack. A hole is drilled longitudinally through the cone a short distance from the top to admit the ripcord locking-pin. Grommets of the opposing flap and the end tabs are placed over the cones and are held tightly in place by the insertion of ripcord pins in the holes provided.

Construction, Bias. A type of construction for drag-producing surfaces in which the sections are cut and arranged in the gores so that the threads and section seams make an angle of other than 90 deg (usually 45 deg) to the centerlines of the gores. Bias construction is used for additional strength, and for the economy of material that can be achieved by cutting sections from standard-width materials.

Construction, Block. A type of construction for drag-producing surfaces in which the sections are cut and arranged in the gores so that the warp threads and section seams make an angle of 90 deg to the centerline of the gore and are parallel to the skirt hem.

Container, Air-Drop. A container designed for the purpose of dropping equipment and supplies by parachute from aircraft in flight. The container may be constructed of cotton, duck, metal, fiberglass, plywood, netting, or other suitable material, depending on the type, weight, and shape of the cargo to be delivered. The container may or may not incorporate a harness for transmitting forces developed during canopy opening, and it may be carried on external racks or inside the aircraft.

Controlled - Parachute Tower. Also called *Controlled Tower*. See *Tower, Controlled Parachute Cords*. See *Lines, Suspension*.

Cord, Arming. A cord that pulls the firing wire out of a reefing-line cutter, or other actuating device, thereby arming the device.

Critical Closing Speed. The speed during acceleration at which a normally inflated canopy will collapse into the squid form.

Critical Opening Speed. The speed during deceleration at which a canopy in the squid form assumes normal inflation, but above which it will not fully inflate.

Crown. Specifically, a fabric panel used to cover a closed apex-vent in certain types of canopies, such as the G-13 cargo parachute. In general, the part of a canopy around the apex.

Cushion, Back. A pad attached to the inside of the harness of personnel parachutes to provide comfort for the wearer, and to hold the harness in place.

Cutter, Reefing-Line. A device designed to cut through the reefing line of a canopy. It normally incorporates a delay device (mechanical or pyrotechnical), a power device (mechanical or pyrotechnical), and a knife-edged cutter.

Damping. The reduction of induced oscillation of a parachute during descent.

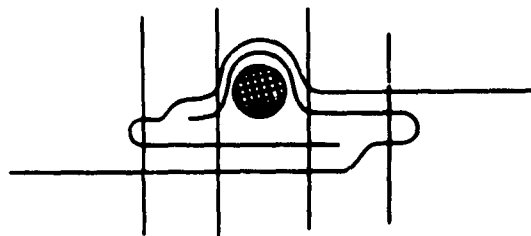
Dart. A short, tapered seam.

Deployment. That portion of a parachute's operation occurring from the initiation of ejection to the instant the lines are fully stretched, but prior to the initial inflation of the canopy.

Deployment, Bag. A method of canopy deployment utilizing a container, usually of fabric, for retaining the drag-producing surface of the canopy until the suspension lines are deployed. This reduces the snatch force by allowing the acceleration of the canopy mass in small increments only. The lines may or may not be stowed on the bag, depending on the intended use.

Deployment, Controlled Bag. A method of canopy deployment in which the deployment bag is attached to a static line and remains on the static line after the canopy is released.

Deployment, Free Bag. A method of canopy deployment in which the deployment bag is attached to a pilot chute. When a static line is used to open a pack, the bag remains in the pack until it is removed by the pilot chute.



Channel, Canopy

Development. That portion of a parachute's operation occurring from the moment of completion of suspension-line stretch to the moment of full inflation of the canopy. Used synonymously with "inflation".

Diameter, Constructed. A designation of the size of a canopy, based upon design dimensions.

Diameter, Nominal, (D_o). The computed diameter designation of any design of canopy, which equals the diameter of a circle having the same total area as the total area of the drag-producing surface, which includes all openings in the drag-producing surface, such as slots and vent. Since it refers to all canopies on a common basis, that is, in terms of surface area, this method of diameter designation is preferred for the comparison of drag efficiencies of different canopy designs. For canopies that have a vent area larger than one per cent of the total area, the vent area is deducted from the total area (for example, airfoil parachutes). This term is not used for canopies of the guide-surface type (ribbed and ribless).

Diameter, Projected, (D_p). The mean diameter of the inflated canopy, measured in the plane of the maximum cross-section area. On canopies where the fabric curves out between the suspension lines, the projected diameter is the mean diameter of the inner and outer diameters.

Disconnect, Ground. A device that instantaneously releases the canopy from the suspended load upon ground contact. This device may be actuated electrically, by the action of ground-contact switches or g-sensing devices; or it may be entirely mechanical and sensitive to canopy-load reduction.

Disreefing. The process of removing or changing the restrictive characteristics of a reefing system to increase the drag area of a canopy. This may be accomplished in one stage, in several stages, or continuously, until the canopy is fully inflated.

Double-W. A type of reinforcing stitch in which one W is offset approximately $\frac{1}{4}$ in. and superimposed upon another W.

Drift. The horizontal displacement of the canopy during descent. This may be caused by wind or gusts or by the inherent gliding tendencies of some canopy types.

D-Ring. A metal fitting shaped like a D into which snap connectors are hooked.

Drogue. A fabric surface shaped like a cone, usually used as tow target or wind sock, but sometimes used as a name for a small, first-stage canopy.

Drop Altitude. Actual altitude of an aircraft above the ground at the time of initiation of an air-drop operation.

Dropmaster. (1) An Air Force technician qualified to prepare, perform acceptance-inspection, load, lash, and eject material for air drop. (2) An air-crew member who during air drop operations will relay any required information between the pilot and jumpmaster.

Drop Test. See *Test, Drop*.

Dummy, Parachute. Torso-shaped dummy of variable weight used for testing personnel parachutes. It may be of rigid or articulated construction.

Elastics, Flap-Removing. See *Elastics, Pack-Opening*.

Elastics, Pack-Opening. Elastic cords, with a means of attachment at each end, installed on the pack under tension, used to separate the end flaps from the side flaps when the ripcord is pulled. These cords may be either rubber or metal springs.

Ends. Warp yarns in a woven fabric.

Eye. A small, steel-wire loop attached to the parachute pack, into which is fastened a hook on a pack-opening elastic.

Eyelet. A small, metal reinforcement for a hole in fabrics, similar to a grommet, but thinner and smaller,

and having no washer. The eyelet is used to reinforce lacing holes in small covers.

False Bottom. See *Bottom, False*.

Fastener, Glove. A small, metal fastener consisting of button with socket and stud with eyelet.

Fastener, Interlocking. A type of fastener made of two links of tape with a series of metal scoops which are interlocked by a pull-slide.

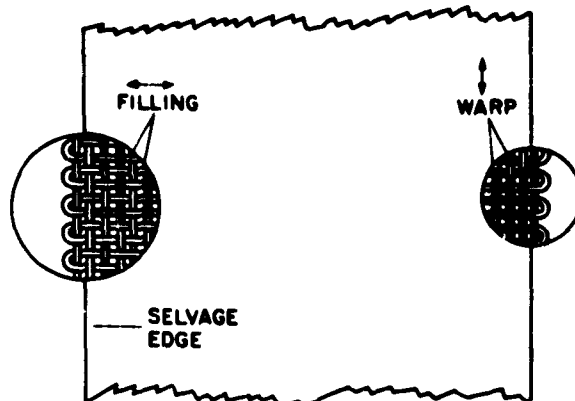
Fastener, "Lift-the-Dot". A small, metal device made of four parts: the stud, the washer, the socket, and the clinch plate. When the stud is manufactured with a screw base, the washer is eliminated. "Lift-the-Dot" fasteners are made in several types of metal, with different stud-lengths for use with the various weights of material. The term "Lift-the-Dot" indicates that the fastener is opened by lifting at one point only; that is, at a position beneath the small "dot" on the socket.

Fastener, Parachute-Pack. A metal fitting attached to a pack flap and designed to fit over a locking cone.

Fastener, "Tri-Lock". A button-type fastener that provides for release in only one quadrant. It serves the same purpose as a "Lift-the-Dot" fastener, but it provides a smoother surface.

Feed Dog. A mechanical device which feeds the material through a sewing machine.

Fid. A small, flat, tapered bar of metal or wood used during packing to insert the corner flaps into the pack.



Filling

Filling. Also called *woof*. These are the threads that run across the cloth as it comes from the loom. This term is not to be confused with "filling" in the sense of sizing, which means the addition of substances that give body or decreased porosity to the

material.

"Finite-Mass" Condition. A state of parachute operation. Use of this condition in calculation of filling time and opening shock of canopies stipulates that the velocity decay during the inflation is substantial and must, therefore, be considered in the calculation. Example: opening of personnel and cargo parachutes.

FIST. Abbreviated term used to designate flat circular ribbon canopies. These canopies are characterized by gores constructed of ribbons, usually 2 in. in width, placed parallel to the skirt, with slots of predetermined dimensions between the ribbons. These canopies were first designed in Germany by Flug-technisches Institut Der Technischen Hochschule Stuttgart. The use of this term is being discouraged.

Flap, Locking-Pin Protector. A flap that covers the locking pins and cones to prevent the pack from being opened by any means other than pulling the ripcord.

Flap, Pack. A fabric extension, on a side or end of the pack, designed to enclose and protect the canopy.

Flaring. Method of splitting, taping, and stitching the end of the webbing to widen it and prevent it from slipping through a fastener or adapter.

Folding, Accordion. Folding a canopy into folds of uniform length, accordion-fashion, before it is placed into the bag or pack. A folding bar can be used to help make neat and properly spaced folds.

Force, Snatch. A force of short duration that is imposed by the sudden acceleration of the canopy mass at the instant of complete extension of the suspension lines or similar components of a parachute system prior to inflation of the canopy.

Fortisan. A cellulose fabric that has great strength but very little elasticity.

Free-Drop. Delivery of supplies and equipment from aircraft in flight without use of parachutes.

French Serving. A form of whipping used on suspension lines of pilot parachutes to form a loop for the point of attachment of bridle cord or line. Also called French spiral-serving.

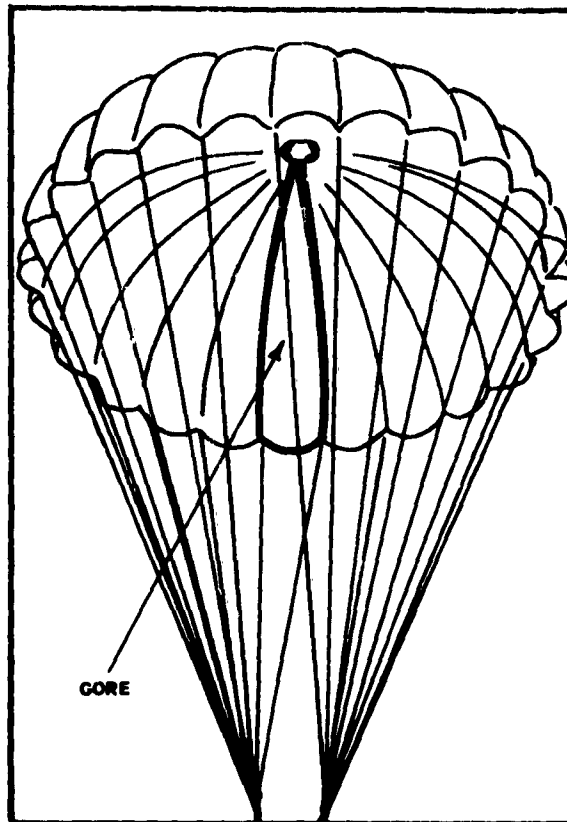
General-Purpose Bag. When used by the individual parachutist, it is an adjustable container designed for attachment to the parachute's harness to carry individual or team equipment that must accompany the parachutist during an airborne operation.

Gore. That portion of the drag producing surface contained between two adjacent suspension lines or radial seams.

Grip. See *Handle, Ripcord*.

Grommet. A metal eyelet and washer, used as a reinforcement around a hole in fabric. Grommets are used on pack flaps to fit over locking cones.

Handle, Ripcord. A metal loop designed to pro-



Gore

vide a grip for pulling locking pins from the locking cones of ripcord-actuated parachutes.

Hanger Line. A line or cord circling the skirt of a canopy within the skirt hem in place of the lower lateral band, and designed to distribute the load from the suspension lines, as on G-13 cargo parachute canopies.

Hardware. All metal fittings used on parachutes, parachute systems, and suspended loads.

Harness. An arrangement of webbing, with metal fittings, designed to conform to the shape of the load in order to secure it properly, and to properly distribute the stress from opening shock and the weight of the load.

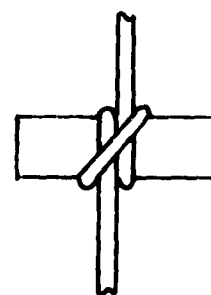
Harness Release. A manually operated device fixed to one end of harness webbing and equipped with three prongs to accommodate lugs on free ends of harness webbing; it is designed to permit rapid release of troop-type harness. Also used on the A-21 container.

Hem. Fabric folded back upon itself and sewed in this position to form both the peripheral edge and the vent of the canopy.

Hem-Rigged Canopy. A canopy whose suspension lines are attached to the skirt hem and do not pass over the drag-producing surface.

Hesitator, Skirt. A device that restricts the skirt of the drag-producing surface, thus preventing inflation until the expiration of the snatch force, at which time the hesitator line breaks and allows inflation of the canopy. This device reduces snatch force and possibility of canopy malfunctions.

High-Velocity Drop. The act or process of delivering supplies or equipment from an aircraft in flight where the rate of descent exceeds that obtained utilizing conventional cargo parachute methods (low-velocity drop) but less than terminal velocity (free-fall).



Hitch, Clove



Knot, Granny



Knot, Square

Hitch, Clove. A type of hitch used for attaching the suspension lines of a canopy to the connector links.

Hook, Apex. A hook placed at the end of the packing table that positions and holds the apex of the canopy to keep it under tension for packing or inspection.

Hook, Pack-Opening Elastic. Small, formed, steel-wire devices attached at both ends of pack-opening elastics. These are hooked in the eyes sewn on the pack.

Hook, Stow. A packing tool consisting of a handle and a bent-wire hook. It is used to pull the suspension lines into place in stow loops during packing of certain types of parachutes.

Horizontal Backstrap. That part of the backstrap which crosses the wearer's back horizontally.

Housing, Ripcord. A flexible metal tubing in which the ripcord cable is installed. The tubing protects the ripcord cable from snagging and provides a free path for it.

"Infinite-Mass" Condition. In the analysis of the dynamics of parachute opening, the approach which stipulates that the velocity of the parachute-load configuration does not change appreciably during

the period of canopy inflation, and can therefore be considered constant.

Inversion. A state in which the canopy has been turned inside out, identified by upper and lower lateral band folds and gore numbers appearing on the inside, and V-tabs appearing on outside.

Jumping Attitude. Steady, level flight of a troop-carrier aircraft at a speed necessary to permit parachutists to make a safe exit.

Keepers (Pack, Harness, Suspension-Line). Length of webbing sewed on a pack, or around suspension lines or risers, and adjusted to hold the pack firmly to the harness or load on which it is used, or to form a confluence point for suspension lines or risers to prevent relative movement of lines or risers.

Knot, Granny. A kind of readily made and insecure knot often made by the inexperienced in place of a square knot.

Knot, Overhand. A simple knot tied in each running end of a piece of cord above a square knot or surgeon's knot (which is similar to a square knot) to prevent the end from slipping back through the knot.

Knot, Square. A strong knot for joining two ropes or lines, which does not slip or loosen easily.

Knot, Surgeon's. A type of knot commonly used in place of a square knot to prevent mis-tying.

Legstrap. That part of the harness that passes under the wearer's leg and connects to the legstrap loop, or passes under the wearer's leg through the strap loop, and to the harness release.

Liftweb. That part of the harness comprising the main webbing support, extending from the connector links down through the saddle and up to the opposite connector links.

Line Burns. Burns caused by a suspension line passing over part of canopy.

Line, Guide or Control. One or more of the parachute lines that run from a slot or orifice in a steerable canopy to the harness providing a better facility to warp the canopy skirt for steerability. When such lines are under tension during parachute opening or descent, they are classed as suspension lines.

Line, Reefing. A length of cord or line passed through rings on the skirt of the drag-producing surface to delay or control the opening of the canopy.

Line, Static. A line, cable, or webbing, one end of which is fastened to the pack, canopy, or deployment bag, and the other to some part of the launching vehicle. It is used to open a pack or to deploy a canopy.

Line, Suspension. Cords or webbings of silk, nylon, cotton, rayon, or other textile materials, that con-

nect the drag-producing surface of the canopy to the harness or load. They provide the means for suspension of the person or load from the inflated drag-producing surface.

Line-Stowing. The process of drawing the suspension lines into suspension-line retaining-loops in the parachute pack to prevent entanglement of the lines during opening of the canopy. Stows may be held by retaining loops or rubber bands, or may be tied to stowing straps.

Lines, Twisted Suspension. A type of malfunction during canopy deployment caused by relative rotation of a suspended load, or pack, to the position of the canopy. One full twist is defined as a 360-degree rotation. This method is sometimes deliberately used to increase the opening time, and decrease the opening shock, of canopies.

Link, Connector. Usually identified as a small, rectangular metal fitting used to connect ends of risers or lift webs to suspension lines. The suspension lines are tied and sewn around one part of the link, and the webs are stitched around the other part. The design of the link may vary in size and shape, according to the intended use.

Link, Separable Connector. Any connector link comprised of readily separable elements, which may be used to facilitate assembly of canopies to a riser system.

Loading, Canopy. Parachute canopy loading is defined as the ratio of the force transmitted from canopy to suspended load to the drag area of the canopy.

Lockstitch. A sewing machine stitch in which two threads are interlocked by one thread being passed around the other.

Log Record, Army Parachute. (DA Form 10-42). A small booklet serving as a diary for a parachute with entries for station, inspections, packing, jumps or drops, modifications, and major repairs.

Loop, Retaining. Loop of webbing or tape, usually elastic, used to hold folded lines or excess webbing in position.

Loop, Stow. Webbing loop on deployment bag or pack to hold suspension lines in place on packed parachutes.

Lowering Strap. A webbing strap attached to parachutist's equipment-bag or weapon-case and to parachutist's harness to permit lowering of container below the jumper approximately 20 ft before landing.

Low-Velocity Drop. The act or process of delivering personnel, supplies, or equipment from aircraft in flight, utilizing sufficient parachute retardation to prevent any injury or damage upon ground impact.

(See *High-Velocity Drop*.)

Lug. A flat, metal fitting attached to the ends of harness webbing to provide attachment to the harness release.

Malfunction. The complete or partial failure of a canopy to achieve proper opening or descent. Some causes of malfunction are high porosity, canopy damage, twisted suspension lines, improper packing or rigging, and improper or blanketed deployment.

Mispick. A pick that failed to pass over or under the appropriate warp yarns during weaving.

Opening, Premature. Any accidental opening of the canopy before the desired time of opening.

Oscillation. The pendulum-like motion of a parachute-suspended load during descent.

Overedge. Long slanting stitches over raw edges of material to prevent raveling. Also called *whip-stitch*.

Pack (Pack Assembly). The term *pack* usually denotes the container alone. When so used, it is defined as a container that encloses the canopy or deployment bag and provides for a means of opening to allow deployment of the canopy. The canopy may or may not be placed in a deployment bag or sleeve.

Pack Cover. A piece of duck or canvas with static line attached, used to cover a packed canopy in some types of pack assemblies.

Pack End-Tab. A metal fitting secured to each end flap of a pack. The end tabs fit over locking cones and secure the end flaps in a closed position until the locking pins are pulled.

Pack Flap. A fabric extension on a side or end of the pack body designed to enclose and protect the canopy.

Pack Frame. A rigid or flexible frame used to maintain a desired pack shape.

Pack-Opening Spring-Band. A cloth-covered steel-spring assembly with a hook at each end, used to expedite opening of pack by rapidly pulling flaps away from canopy.

Paddle. A flat, narrow piece of wood used for dressing the parachute pack and for stowing certain webbings or flaps in retainers.

Palm, Sewing. A hand protector used in heavy hand-sewing to direct the needle through heavy material.

Parachute. An assembly consisting of canopy, risers, or bridles, deployment bag, and in some cases, a pilot chute. The pack and attaching webbings (harness) are considered a part of the parachute when they are not built into the suspended load as an integral part of the load.

Parachute, Air-Drop. A parachute designed to deliver equipment and supplies from an aircraft in flight. It is used synonymously with the term *cargo parachute*.

Parachute, Attached-Type. A parachute, the pack of which is so attached to an aircraft or other carrier that the canopy deploys from the pack as the load falls away.

Parachute, Back-Type. A parachute designed to be worn on a wearer's back and shoulders.

Parachute, Cargo. A parachute used to lower cargo from aircraft in flight.

Parachute, Chest-Type. A parachute designed for attachment to the wearer's chest.

Parachute, Extraction. A parachute used to extract cargo from aircraft in flight, and to deploy cargo parachutes.

Parachute, First-Stage. A parachute used for initial deceleration and stabilization of a falling object so that either the intermediate or the final-recovery parachute can be safely deployed. This term applies only to parachute recovery-systems. The terms *drogue* and *parabrake* may be used also; however, the use of these terms is being discouraged.

Parachute, Free-Type. A parachute, not attached to an aircraft or other carrier, that is operated by the jumper at his discretion.

Parachute, Intermediate. A parachute that has the purpose of further decelerating an object, after the first-stage parachute has been disconnected, to a speed at which it is safe to deploy the final-recovery parachute. This term applies only to parachute recovery-systems.

Parachute, Landing-Approach. A parachute used in flight to improve jet aircraft flight characteristics during normal landing approach, or in approach under marginal weather conditions.

Parachute, Landing-Deceleration. A parachute generally used on jet aircraft to decrease aircraft landing-roll distance. *Drag parachute* is used as an alternate term.

Parachute, Personnel. A parachute used to lower personnel from an aerospace vehicle in flight.

Parachute, Reserve. A second parachute, usually worn on the chest of personnel making a premeditated jump. It is used in the event of malfunction of the main parachute.

Parachute, Stabilization-Brake. A parachute used to maintain, or to make it possible to maintain, the attitude of a falling body, and to retard its fall.

Parachute, Static-Line. A parachute in which deployment of the canopy is initiated by means of a static line attached to an aircraft or other carrier. Both

"troop type" and some "air-drop type" parachutes may be placed in this category.

Parachute, Troop. A parachute used primarily by paratroopers for a premeditated jump over a designated area.

Parachute Rotation. The turning of a parachute canopy about its vertical axis during descent.

Partial Inversion. One or more suspension lines passing over the top of the canopy during deployment, preventing complete inflation of the canopy. Also called *Mac West*.

Peak. See *Apex*.

Permeability. A term used to designate the measured volume of air in cubic feet that will flow through one square foot of cloth in one minute at a given pressure. In the United States, permeability is measured by using a pressure of $\frac{1}{2}$ in. of water. In Great Britain, 10 in. of water pressure is used.

Pick. An individual filling yarn in webbing or fabric.

Pilot Chute. A small parachute used to aid and accelerate main-canopy deployment. Some types of pilot chutes are equipped with a spring-operated, quick-opening device. The frame is so compressed that it will open immediately when it is released from the pack.

Pin, Clevis. See *Clevis Pin*.

Pin, Locking. Short, metal prongs attached to a ripcord cable. Locking pins are inserted into locking cones to secure the pack flaps as a function of closing a parachute pack.

Pin, Ripcord. See *Pin, Locking*.

Platform. A base that serves as the support on which equipment may be loaded for air drop.

Pocket, Log Record. A small patch-pocket sewed to a part of the parachute, usually the pack or riser, for carrying the parachute record card.

Porosity, Effective. The ratio of the average velocity of air through a porous sheet to the free-stream velocity. It is utilized for performance calculations to relate cloth permeability to the pressure differential experienced across the cloth.

Porosity, Geometric. The ratio of the open area of a canopy drag-producing surface to the total canopy drag-producing surface area.

Porosity, Mechanical or Ribbon. The porosity expressed in per cent, of the material (ribbons) in ribbon or ring-slot type canopies. Mechanical porosity is obtained by dividing the ribbon permeability by 27.4 cu ft/sq ft/min.

Porosity, Total. The total porosity, expressed in per cent, of the canopy drag-producing surface. The total porosity is the sum of the geometric and mechanical porosities.

Rate of Descent. The vertical velocity, in feet per second, of a descending object.

Recovery System, Parachute. A parachute recovery system includes all items that are required to recover an object from flight and to land it safely on the ground or on water with a minimum of damage. In general, the following subsystems are included: first-stage, intermediate, and final-recovery parachutes; controlling devices; actuating devices; and landing or flotation devices, or both.

Reefing, Skirt. A restriction of the skirt of a drag-producing surface to a diameter less than its diameter when it is fully inflated. Reefing is used to decrease the opening shock, to decrease drag area, and to enhance stability.

Reefing, Vent. A means of altering the inflated shape of the canopy by pulling down the vent. This type of reefing may be used to change the drag area and to enhance stability.

Release, Canopy. A device that is designed to permit rapid separation of canopy and risers from the suspended load.

Release, Harness. A manually operated device incorporated in a harness. It is designed to permit the rapid release of the harness from the wearer.

Repairs, Minor. Any repairs required to return the parachute to perfect condition, but which, if not made, will not seriously affect its performance or airworthiness.

Rigger-Roll. To prepare an unpacked parachute for storage or movement by rolling the canopy into a ball and then rolling the suspension lines around the canopy. The canopy may be secured with a pack, if attached.

Rigger's Check. A routine inspection of a troop parachute, including check of harness adjustment, performed by a qualified parachute rigger immediately prior to enplaning of the paratrooper.

Rigging. The method of preparing a particular piece of equipment or load of supplies for heavy air-drop, as in "Rigging the 105mm Howitzer for Air Delivery."

Rings, Reefing. Metal rings attached to the skirt of a drag-producing surface at the suspension-line connection-points, through which a reefing line is passed. These rings are designed to eliminate any hinging action in the ring, which could mean consequent binding of the reefing line.

Ripcord. A locking device, consisting of cable, locking pins, and grip, that secures the pack in a closed condition. It permits the release of the canopy from the pack.

Ripstop, Nylon. Nylon fabric woven in intermittent box form with three or four additional closely picked yarns, designed to prevent travel of a rip or tear.

Riser. That portion of the suspension system between the confluence point of suspension lines and the point of attachment to the load. Since it must be as strong as the total strength of all suspension lines attached thereto, it usually is fabricated from high-strength material, such as textile webbing or, in some cases, steel cable.

Saddle. The part of the harness that is positioned in the main lift-web at the seat of wearer and widened and reinforced to provide a seat or sling for the wearer.

Safety. A thread or wire of specified breaking strength used to prevent accidental or premature release or separation of parts, as on the ripcord of the reserve parachute. Also used as a verb.

Safety Clip. See *Clip, Safety*.

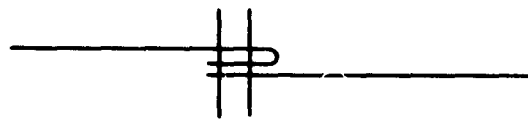
Sail. A term used to designate a condition noted in the deployment of a parachute canopy when the canopy, just after leaving its pack but still attached to a static line, is exposed broadside to the airstream and temporarily assumes a shape similar to a sail.

Seam. The fold or line formed by the sewing together of two pieces of material.

Seam, Bias. The radial or diametral seam of a bias-constructed drag-producing surface.

Seam, Block. A seam that runs parallel to the warp, or filling threads, of material used in block construction of drag-producing surfaces.

Seam, Diagonal. The diagonal or horizontal seams that join the sections of each gore of a bias-constructed drag-producing surface.

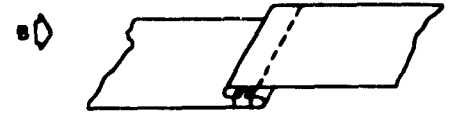
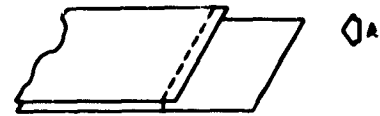


Seam, English Fell

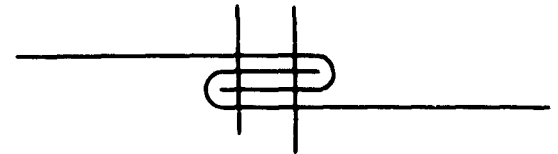
Seam, English-Fell. A type of seam in which one piece of material is folded back on itself and the other piece is a plain overlap.

Seam, Folded-Fell. In forming this type of seam, the plies of material are first joined as shown in (a). The one ply is then turned back, the edge of the other ply is turned, and the two plies are sewed with a second row of stitching, as shown in (b).

Seam, French-Fell. This type of seam is formed by turning the edges of both plies of the material,



Seam, Folded Fell



Seam, French Fell

lapping them as shown in the sketch, and sewing with two (or more) rows of stitches, which also secure the turned positions.

Seam, Radial. A seam that extends from the skirt to the vent and joins two gores. A portion of the suspension lines may be concealed in tubes formed by radial seams.

Searing. Method of sealing ends of nylon cord or webbing by melting them to prevent raveling.

Section. Any one of the pieces of cloth which, when assembled, form one gore of a drag-producing surface.

Selvage. The woven edge of cloth.

Separator, Line. A slotted metal or wood device used to hold suspension lines at the canopy skirt after separation into groups during packing.

Serving. A method of wrapping or binding the ends of cord or line so they will not unravel, or to provide protection for loops. It is also referred to as *whipping*. Served loops are sometimes used to replace connector links at the load end of the suspension lines. The latter construction, however, makes maintenance costly and difficult.

Shakeout. Method of suspending a canopy and shaking each gore in succession to free the canopy of loose dirt and debris.

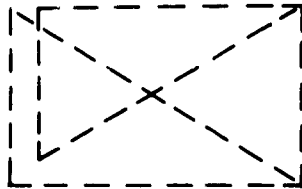
Shock, Deployment. See *Force, Snatch*.

Shock, Landing. The force imposed upon the suspended load at ground impact.

Shock, Opening. The maximum force developed during inflation of the canopy.

Shoulder Strap. That part of the harness which crosses the wearer's shoulder.

Shot Bag. A parachute packing tool. A rectangular duck bag is filled with sand or shot and used to hold folded gores in position during packing.



Single-X Stitch

Single-X. A stitch pattern representing an X-formation, usually used with a box-stitch.

Skirt. The reinforced hem forming the periphery of a drag-producing surface.

Sleeve. A tapered, fabric tube in which a canopy is placed to control the canopy's deployment.

Slipping, Controlled. A method of guiding an inflated canopy in a desired direction by manipulation of the suspension lines, spilling the air from one side of the skirt. This action causes an increased average rate of descent until the lines return to full length.

Slot. An opening within a gore of a drag-producing surface. The size and number of slots will determine or control the geometric porosity of certain canopy designs.

Snap, Friction Harness. A sliding-grip friction buckle with a metal snap attached to a parachute harness to secure two parts of the harness together, and also to permit quick fit adjustments on the wearer or load.

Snap, Harness. A hook-shaped spring-loaded metal fastener that snaps over a V- or D-ring to secure two parts of an assembly.

Snap, Static-Line. A metal device used to connect the free end of a static line to a cable or ring in an aircraft.

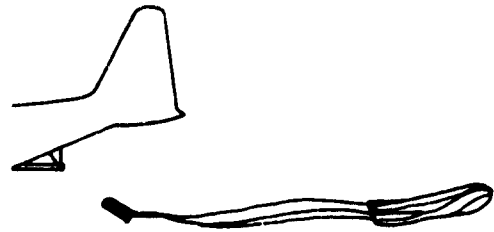
Speed, Critical Opening. See *Critical Opening Speed*.

Speed, Critical Closing. See *Critical Closing Speed*.

Speed, Sinking. See *Rate of Descent*.

Spike, Recovery. A pointed-beam extension on the nose of the load, which absorbs ground-impact energy by penetrating the ground.

Squidding. A state of incomplete canopy inflation in which the canopy has a pear-like or squid-like shape. Squidding occurs if the canopy is deployed above a critical speed.



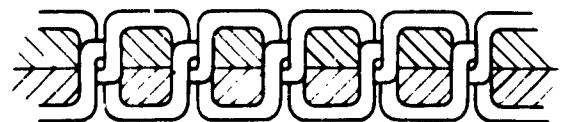
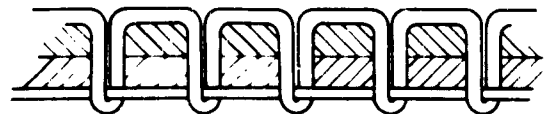
Squid Shape

Squid Shape. See illustration.

Stability, Dynamic. The tendency of a moving body to develop moments that act to damp motion.

Stability, Static. The tendency of a moving body to develop steady-state restoring moments when disturbed from a position of equilibrium.

Stiffener, Pack. Rectangular strips of metal or fiber placed in the pack flaps to stiffen the flaps. These strips are also used for shaping the sides and bottom of packs.



Stitch, Lock

Stitch, Box. A rectangular or square stitch pattern, generally used to enclose a single-X or triple-X stitch formation.

Stitch, Chain. Ornamental, basting, or seam stitch in which thread, or threads, is not interlocked but is held by a loop of needle thread or a loop of bobbin thread. There may be single-, double-, or triple-thread chain stitching.

Stitch, Double-Throw. Zigzag stitching in which the needle makes a center stitch between each left and right stitch.

Stitch, Four-Needle. A method of stitching that can be performed in one operation by a four-needle sewing machine. It is used in sewing the top hem, the circumferential hem, and the radial seams of a drag-producing surface.

Stitch, Luck. A nonraveling stitch used to form a seam.

Stitch, Single-Throw. Zigzag stitching in which the needles travel completely from one side to the other between stitches.

Stitching, Bunched. A defective seam resulting from a higher concentration of stitches per inch than is required.

Stitching, Zigzag. Stitching done by a sewing machine that makes stitches alternately on two or more parallel diagonal lines. It is used to reinforce and anchor the suspension lines to the drag-producing surface.

Stow. Any one loop of static line or suspension line compactly secured to the parachute pack.

Stow Hook. A packing tool consisting of a handle and a wire hook used to pull the suspension lines into place in stow loops during parachute packing.

Stow Loop. A webbing loop on the deployment bag, designed to hold suspension lines in place on a packed parachute.

Streamer. A malfunction in which a canopy stretches full-length during descent without reaching a squid shape.

Strength, Tear. The average force, measured in pounds, required for a continuous tear across either the filling or the warp of a fabric.

Strength, Tensile. The tension, measured in pounds, required to break a material. The tensile strength of a fabric is stated in pounds per inch width for warp and for filling. The tensile strength of webbing and tapes is stated for the full width, such as 250-lb tape.

Surface, Drag-Producing. That portion of a canopy consisting of the cloth area designed to produce the desired drag.

Swage. To join metal parts by pressure, such as in attaching ripcord locking pins to ripcord cable.

Tacking. A slight sewing, usually by hand, with long stitches as in basting, but usually concentrated in a certain area or around a certain point.

Tangle. The passing of one group of suspension lines through a second group, usually caused by pack or harness passing between two lines above connector

link.

Tape, Reinforcement. Tape or webbing sewed to the pack or canopy to strengthen the fabric at a weak spot or point of stress.

Tear Strength. See *Strength, Tear*.

Template. A pattern cut from durable material.

Terminal Velocity. The greatest velocity that a free-falling body, starting from rest, can attain against the resistance of air at any given altitude.

Test, Drop. A test to determine the working efficiency of a parachute and its systems by releasing it from an aircraft or from some height above the ground under conditions very similar to those found, or anticipated, in normal operation.

Thread, Break. A stitching intended to break easily under a relatively small stress. In certain types of packs, for example, a break-thread is used to fasten the lift webs inside the pack. This thread breaks during the deployment or opening of the canopy.

Thread, Marker. A colored thread woven into webbing to identify the breaking strength.

Tie-Down. A chain-and-binder assembly used to lash cargo to tie-down rings in aircraft or to heavy-drop platforms.

Time, Filling. The time elapsed between the full extension of the suspension lines (after canopy deployment) and the opening of the canopy to its fullest extent.

Time, Opening. The elapsed time between the initiation of canopy deployment and the opening of the canopy to its fullest extent.

Tower, Controlled-Parachute. A tower having the mechanism and equipment that allow a parachute to come straight down between cables. Such a tower is used for training in parachute jumping.

Tower, Drying. A facility where parachutes are suspended for drying and airing.

Triple-X. A stitch pattern resembling three adjoining X's. It is often used with a boxstitch.

Tuck. A shortening of material caused by pulling fabric up in folds and stitching across the gathered fabric.

Twist, Suspension-Lines. The twisting of each group of suspension lines separately, usually caused by rotation of the pack or harness between the two groups.

Underfold. A fold in which insufficient material has been folded inside the seam, usually resulting in exposed raw edges.

Velocity, Equilibrium. The velocity that a falling body can attain when the drag is equal to the weight; i.e., the acceleration equals zero.

Vent. An opening in the cloth surface of the canopy; specifically, the opening at the top, or apex of the drag-producing surface.

Vent, Puckered. A cloth sleeve or collar attached to and encircling the vent, puckered by the use of an elastic member that is tightly drawn at the apex of the vent.

V-Ring. A metal fitting in the form of a closed letter V that is used with snaps to secure or attach a load to a canopy.

V-Tap. A short length of tape or webbing wrapped

tightly around a suspension line and stitched to the skirt hem.

Warp. The threads that run parallel to the selvage edge of cloth; those threads that are crossed by the filling threads, also called *weft*. (For sketch, see *Threads, Filling*.)

Wax, Paraffin. Wax generally used with 50 per cent beeswax as a hot dip to prevent the fraying of cut ends of webbing, cord, and tape.

Web, Lift. See *Riser*.

Webbing. See *Harness*.

CHAPTER 2 DESIGN REFERENCE DATA

Table of Contents

<i>Section</i>	<i>Page</i>
1 CONVERSION FACTORS	34
2 PARAMETRIC TRAJECTORY CURVES AND NOMOGRAMS	35

Illustrations

<i>Number</i>		<i>Page</i>
2-1	Parametric Trajectory Plot, $\theta_o = 0^\circ$	37
2-2	Parametric Trajectory Plot, $\theta_o = 5^\circ$	39
2-3	Parametric Trajectory Plot, $\theta_o = 10^\circ$	41
2-4	Parametric Trajectory Plot, $\theta_o = 15^\circ$	43
2-5	Parametric Trajectory Plot, $\theta_o = 20^\circ$	45
2-6	Parametric Trajectory Plot, $\theta_o = 30^\circ$	47
2-7	Parametric Trajectory Plot, $\theta_o = 45^\circ$	49
2-8	Parametric Trajectory Plot, $\theta_o = 60^\circ$	51
2-9	Parametric Trajectory Plot, $\theta_o = 90^\circ$	53
2-10	True Airspeed vs Mach No. and Altitude	55
2-11	Altitude, Mach No. and Dynamic Pressure	57
2-12	Dynamic Pressure vs Velocity and Altitude	58
2-13	Equilibrium Velocity as a Function of C_{DS} , Altitude and Weight	59
2-14	Reliability Nomogram	61

CHAPTER 2

DESIGN REFERENCE DATA

SEC. 1 CONVERSION FACTORS

Multiply	By	To Obtain
atmospheres	76.0	cms of mercury
atmospheres	29.92	inches of mercury
atmospheres	33.90	feet of water
atmospheres	10,333	kg per sq meter
centimeters	0.3937	inches
cms of mercury	0.01316	atmospheres
cms of mercury	0.4461	feet of water
cms of mercury	136.0	kg per square meter
cms of mercury	0.1924	feet per second
cms per second	0.03281	feet per second
cms per second	0.02237	miles per hour
cm per sec per sec	0.03281	ft per sec per sec
cubic centimeters	3.531×10^{-5}	cubic feet
cubic feet	2.832×10^4	cubic cms
cubic inches	16.39	cubic centimeters
cubic meters	61,023	cubic inches
cubic yards	7.646×10^5	cubic centimeters
degrees (angle)	0.01745	radians
feet	30.48	centimeters
feet per sec	30.48	cms per sec
feet per sec	0.6818	miles per hour
ft per sec per sec	30.48	cm per sec per sec
grams	2.205×10^{-3}	pounds
Inches	10^3	mils
Inches of mercury	0.03342	atmospheres
Inches of mercury	1.133	feet of water
Inches of mercury	345.3	kg per square meter
Inches of mercury	70.73	pounds per square ft
Inches of mercury	0.4912	pounds per square in.
Inches of water	0.002458	atmospheres
Inches of water	0.07355	inches of mercury
Inches of water	25.40	kg per square meter
Inches of water	5.204	pounds per square ft
Inches of water	0.03613	pounds per square in.
Kilograms	2.2046	pounds
Knots	6080	feet per hr
knots	1.152	miles per hr
log ₁₀ N	2.303	log _e N or ln N

log _e N or ln N	0.4343	log ₁₀ N
meters	3.2808	feet
meters	39.37	Inches
meters per min	3.281	feet per minute
meters per min	0.05468	feet per second
meters per min	0.03728	miles per hour
meters per sec	3.284	feet per second
meters per sec	2.237	miles per hour
meters per sec per sec	3.281	feet per sec per sec
miles	1.609×10^5	centimeters
miles	1.6093	kilometers
miles per hr	44.70	centimeters per sec
miles per hour	88	feet per minute
miles per hour	1.467	feet per second
miles per hour	1.6093	kilometers per hour
miles per hour	0.8684	knots
pounds	453.6	grams
pounds per cu ft	0.01602	grams per cubic cm
pounds per cubic ft	16.02	kg per cubic meter
pounds per cu in.	27.68	grams per cubic cm
pounds per cu in.	1728	pounds per cu ft
pounds per foot	1.488	kg per meter
pounds per inch	178.6	grams per cm
pounds per sq ft	0.01602	feet of water
pounds per sq ft	4.882	kg per square meter
pounds per sq ft	6.944×10^{-3}	pounds per sq inch
pounds per sq in.	0.06804	atmospheres
pounds per sq inch	2.307	feet of water
pounds per sq in.	2.036	inches of mercury
sq centimeters	1.076×10^{-3}	square feet
sq centimeters	0.1550	square inches
sq feet	929.0	square centimeters
square feet	0.09290	square meters
square inches	6.452	square centimeters
square inches	6.944×10^{-3}	square feet
Temp (degs C)	1	abs temp (degs C)
+ 273		
Temp (degs C)	1.8	temp (degs Fahr)
+17.8		
temp (degs F)	1	abs temp (degs F)
+460		
temp (degs F)—32	5/9	temp (degs Cent)

SEC. 2 PARAMETRIC TRAJECTORY CURVES AND NOMOGRAMS

Derivation of Equations: The parametric trajectory curves shown in Fig. 2-1 through 2-9 have been extracted from a report prepared by Mr. T.A. Burns, General Electric Co., Missile and Space Vehicle Department, titled, "Parametric Trajectory Curves for the Preliminary Design of Parachute Recovery Systems," Aerodynamics Data Memo No. 4.64.

The assumptions used in deriving the working equations are as follows:

1. The vehicle may be considered a point mass.
2. The earth is assumed round and nonrotating.
3. Gravity is constant.
4. Drag is introduced as a step function.
5. $W/C_D S$ is constant for a given velocity vs. time plot.

The familiar equations of motion of a body falling through the atmosphere (See Sketch) are:

$$(1) \quad m \frac{dV}{dt} = W \sin \theta - \frac{\rho V^2}{2} C_D S$$

$$(2) \quad m \frac{d\theta}{dt} = W \cos \theta$$

$$(3) \quad \frac{dH}{dt} = -V \sin \theta$$

$$(4) \quad \frac{dR}{dt} = V \cos \theta$$

where θ = Path Angle of Vehicle

H = Altitude

R = Range

$$(5) \quad \sin \theta = \frac{\rho V^2}{(W/C_D S)t} = \frac{dV}{dtg}$$

The term $(W/C_D S)t$ is considered to be:

$$(6) \quad \frac{W_b + W_p}{(C_D S)_b + (C_D S)_p} = (W/C_D S)t$$

where the subscript "b" refers to the vehicle and the subscript "p" refers to the parachute.

Rewriting Equation (5) in terms of velocity ratios yields,

$$(7) \quad \sin \theta = \frac{\rho (V/V_o)^2}{2(W/C_D S)V_o^2} = \frac{d(V/V_o)}{d(tg/V_o)}$$

where the subscript "o" refers to initial conditions. Assume over the interval ΔH ,

$$(8) \quad \rho = \rho_{sl} e^{-\alpha H} \quad sl = \text{sea level}$$

then,

$$(9) \quad \rho/\rho_o = \frac{\rho_{sl} e^{-\alpha H}}{\rho_{sl} e^{-\alpha H_o}} = e^{-\alpha(H-H_o)}$$

Non dimensionalizing Equation (9),

$$(10) \quad \rho/\rho_o = \left[e^{-\frac{(H-H_o)g}{V_o^2}} \right] V_o^2 \alpha/g$$

where $V_o^2 \alpha/g$ is a parameter.

Substituting Equation (10), along with the relationship $V_o^2 = 2(W/C_D S)\rho_o$ into Equation (7) yields,

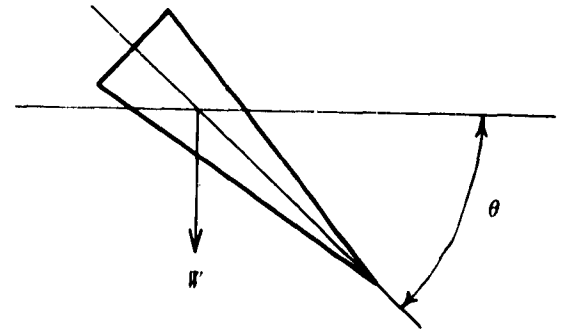
$$(11) \quad \frac{d(V/V_o)}{d(tg/V_o)} = \sin \theta = \frac{(V/V_o)^2}{(V_o/V_o)^2} \left[e^{-\frac{(H-H_o)g}{V_o^2}} \right] V_o^2 \alpha/g$$

The non-dimensional form of Equations (2), (3) and (4) is:

$$(12) \quad \frac{V}{V_o} \frac{d\theta}{d(tg/V_o)} = \cos \theta$$

$$(13) \quad \frac{d(Hg/V_o^2)}{d(tg/V_o)} = -\frac{V}{V_o} \sin \theta$$

$$(14) \quad \frac{d(Rg/V_o^2)}{d(tg/V_o)} = \frac{V}{V_o} \cos \theta$$



From Equations (11), (12), (13) and (14) the dimensionless variables and parameters are established as follows:

Variables

$$(a) V = V/V_o \quad (c) \Delta H = \frac{\Delta H g}{V_o^2}$$

$$(b) \Delta t = \frac{\Delta t g}{V_o} \quad (d) \Delta R = \frac{\Delta R g}{V_o^2}$$

Parameters

$$(e) \theta \quad (g) \frac{V_o^2 \alpha}{g}$$

$$(f) \frac{V_e}{V_o} \text{ or } \frac{V_o}{V_e}$$

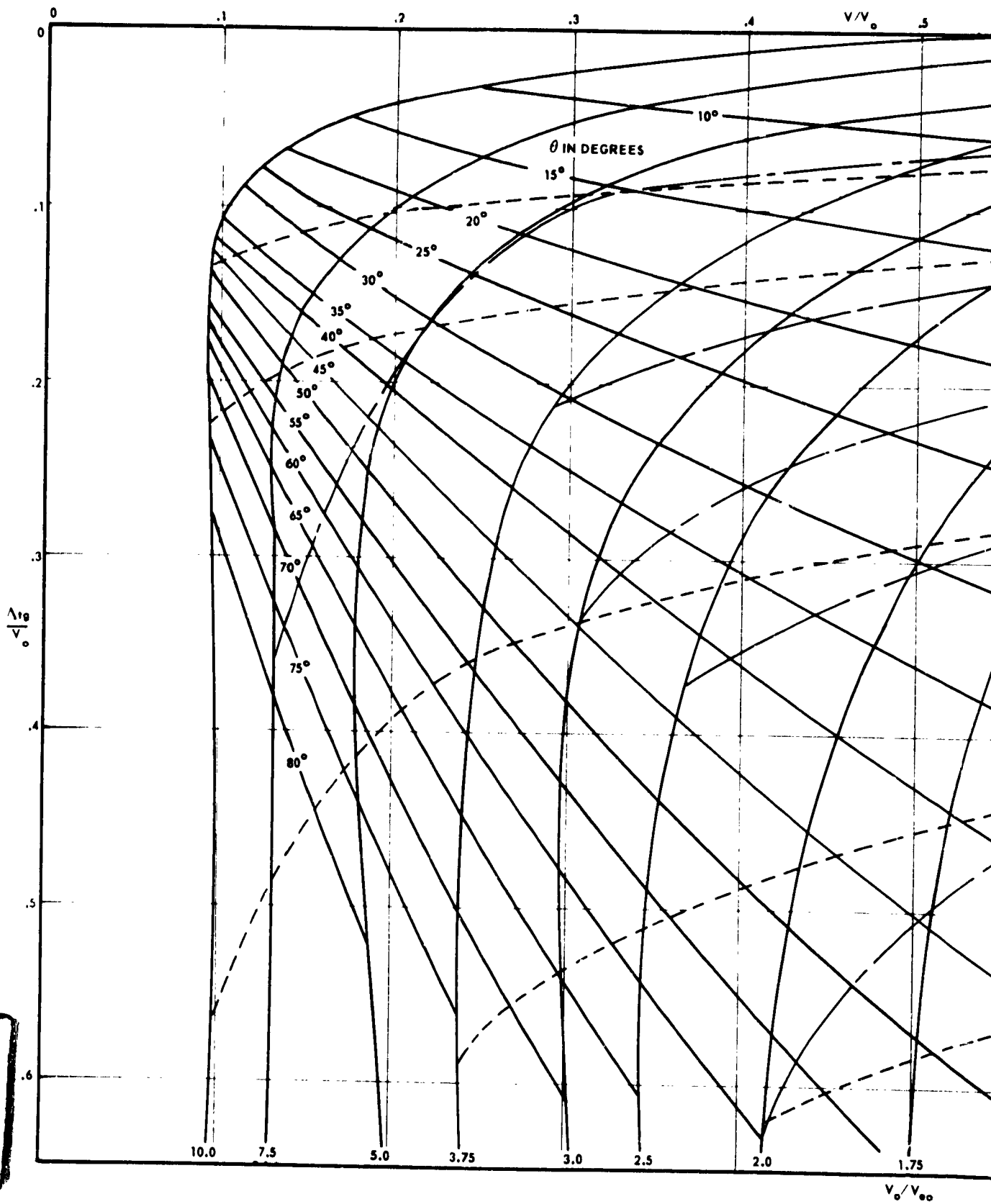
To define the curves V_e is considered as the equilibrium velocity at the initial altitude or V_{eo} . Parameter (f) then is expressed as V_o/V_{eo} .

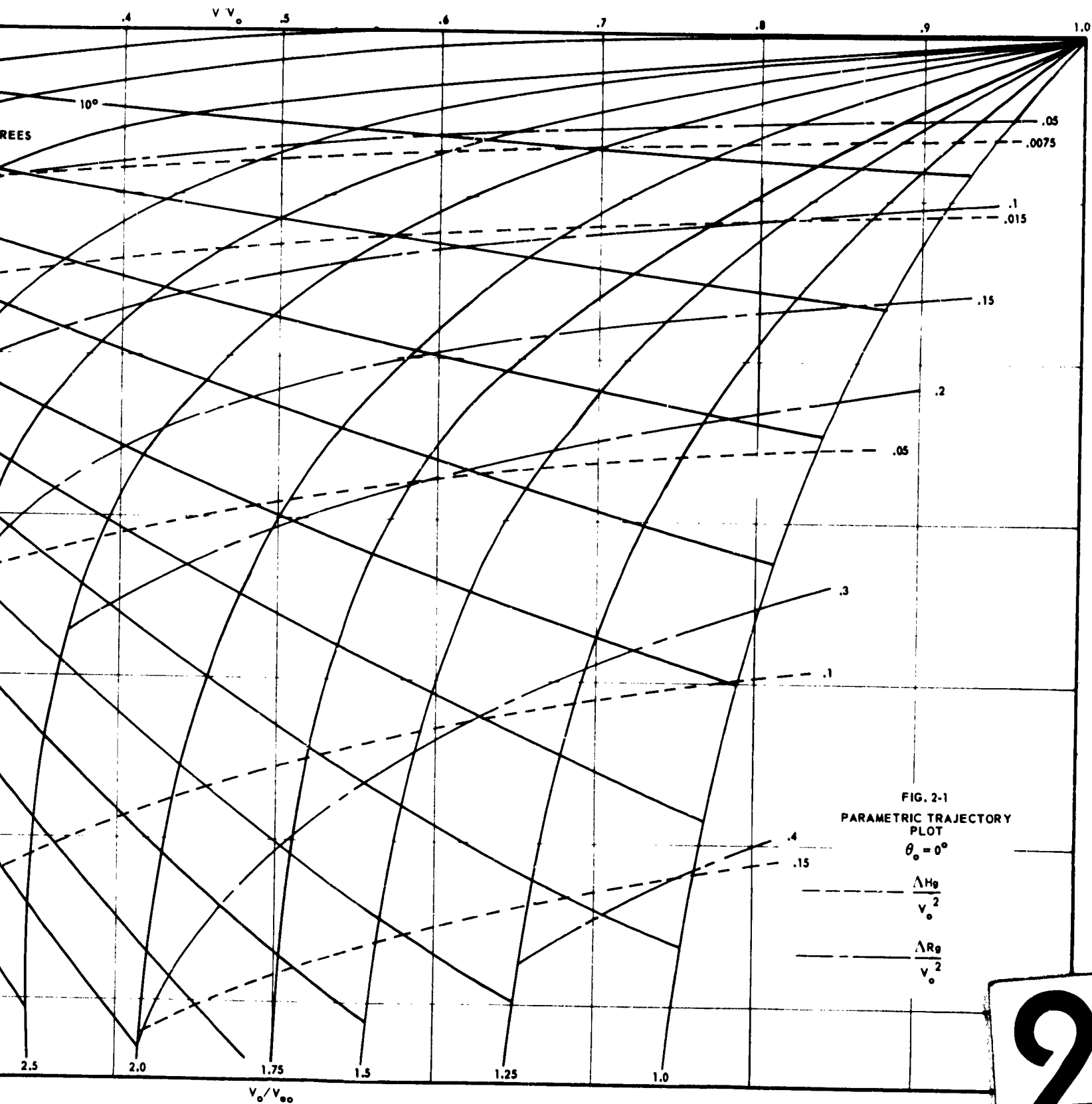
The following Table outlines the known values which are needed to enter the parametric trajectory curves shown in Figs. 2-1 through 2-9 and the values which may be read.

Known				Read			
θ_o	$\frac{V_o}{V_{eo}}$	$\frac{\Delta t g}{V_o}$		$\frac{\Delta H g}{V_o^2}$	$\frac{\Delta R g}{V_o^2}$	$\frac{V}{V_o}$	θ
θ_o	$\frac{V_o}{V_{eo}}$	$\frac{\Delta H g}{V_o^2}$		$\frac{\Delta t g}{V_o}$	$\frac{\Delta R g}{V_o^2}$	$\frac{V}{V_o}$	θ
θ_o	$\frac{V_o}{V_{eo}}$	$\frac{\Delta R g}{V_o^2}$		$\frac{\Delta t g}{V_o}$	$\frac{\Delta H g}{V_o^2}$	$\frac{V}{V_o}$	θ
θ_o	$\frac{V_o}{V_{eo}}$	$\frac{V}{V_o}$		$\frac{\Delta t g}{V_o}$	$\frac{\Delta H g}{V_o^2}$	$\frac{\Delta R g}{V_o^2}$	θ
θ_o	$\frac{V_o}{V_{eo}}$	θ		$\frac{\Delta t g}{V_o}$	$\frac{\Delta H g}{V_o^2}$	$\frac{\Delta R g}{V_o^2}$	$\frac{V}{V_o}$

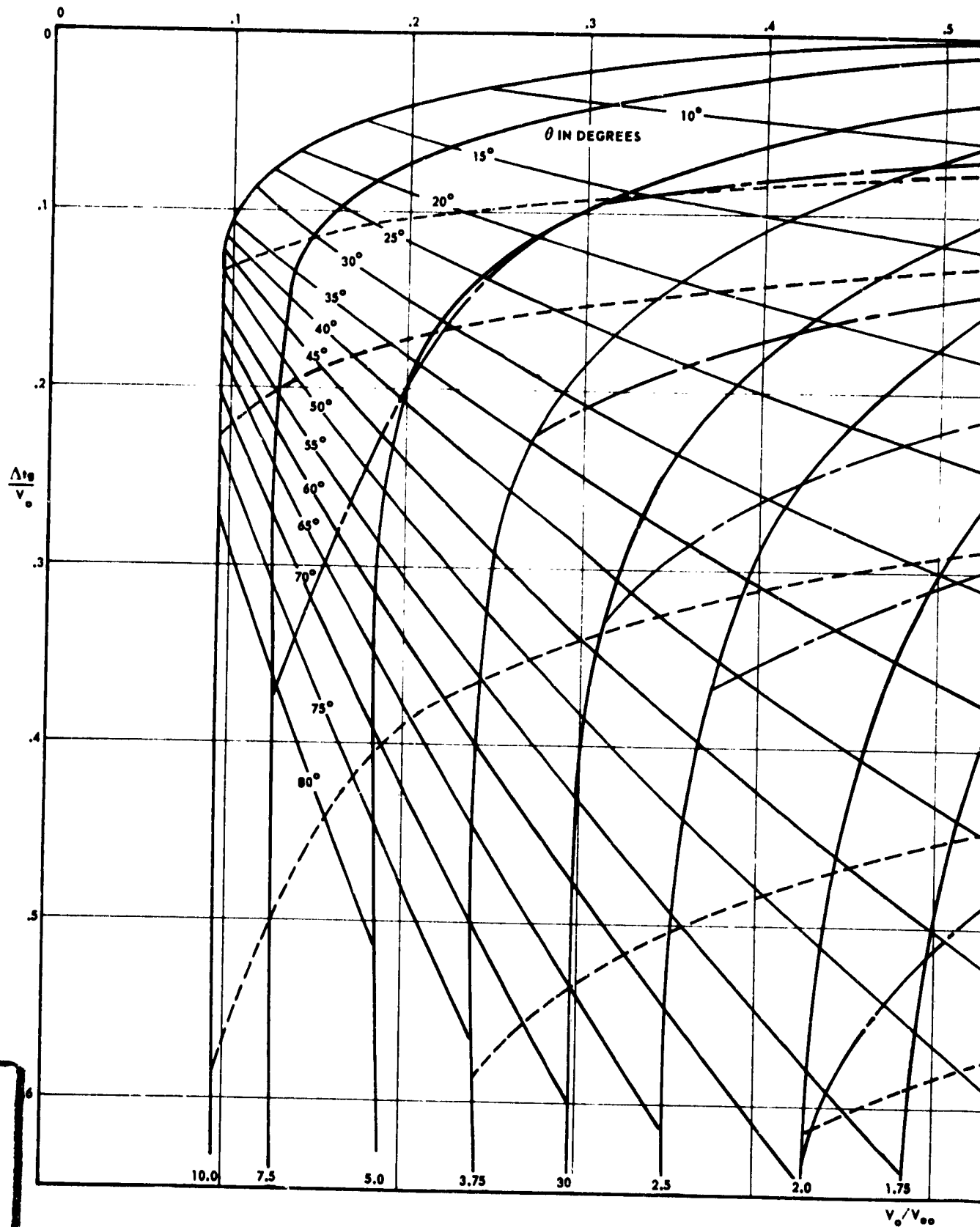
The approximate nature of these curves should be emphasized. They are for preliminary design only. A computer check using the point mass equations of motion should be made on all systems which are designed by the use of these data.

1





1



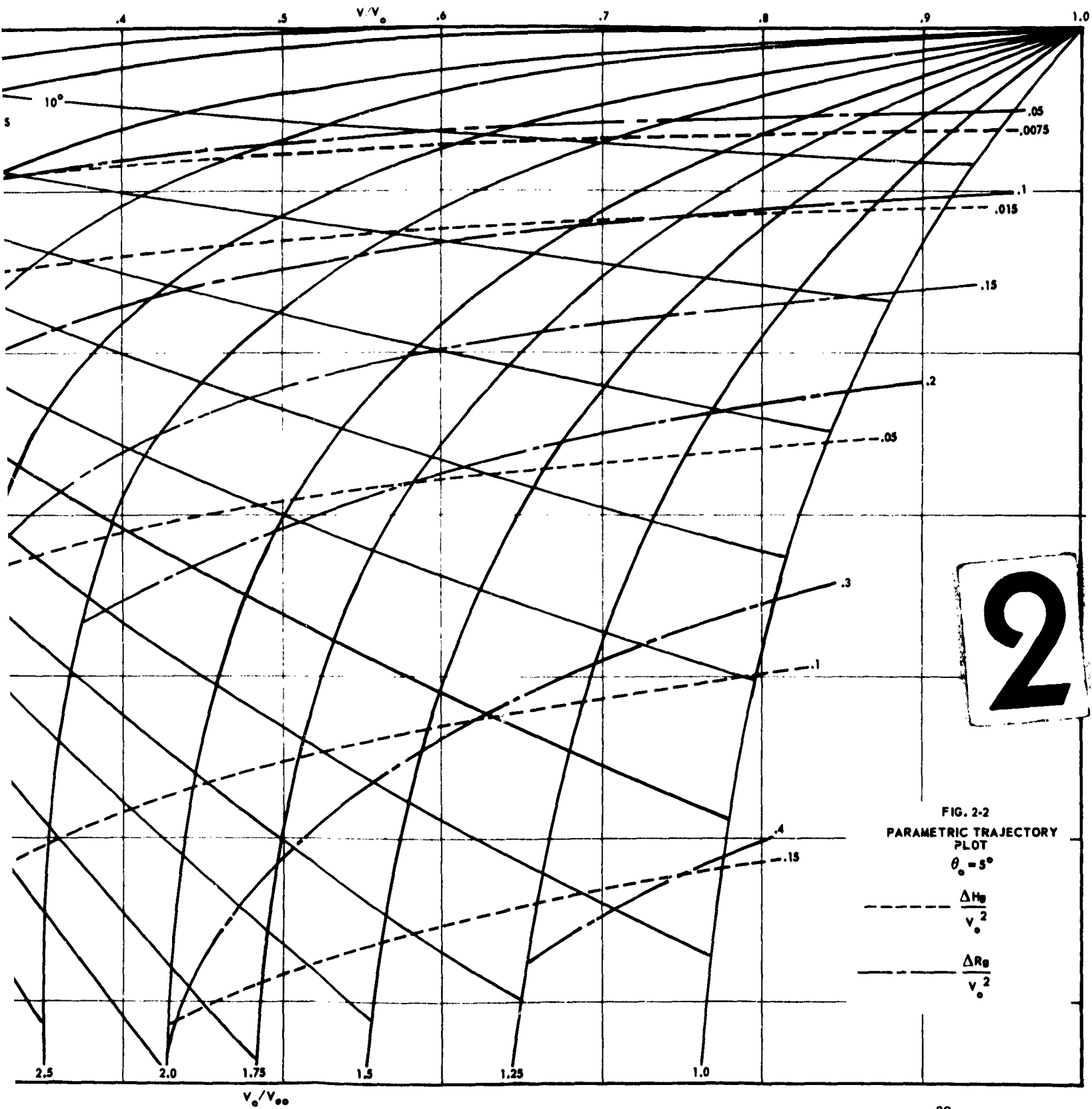
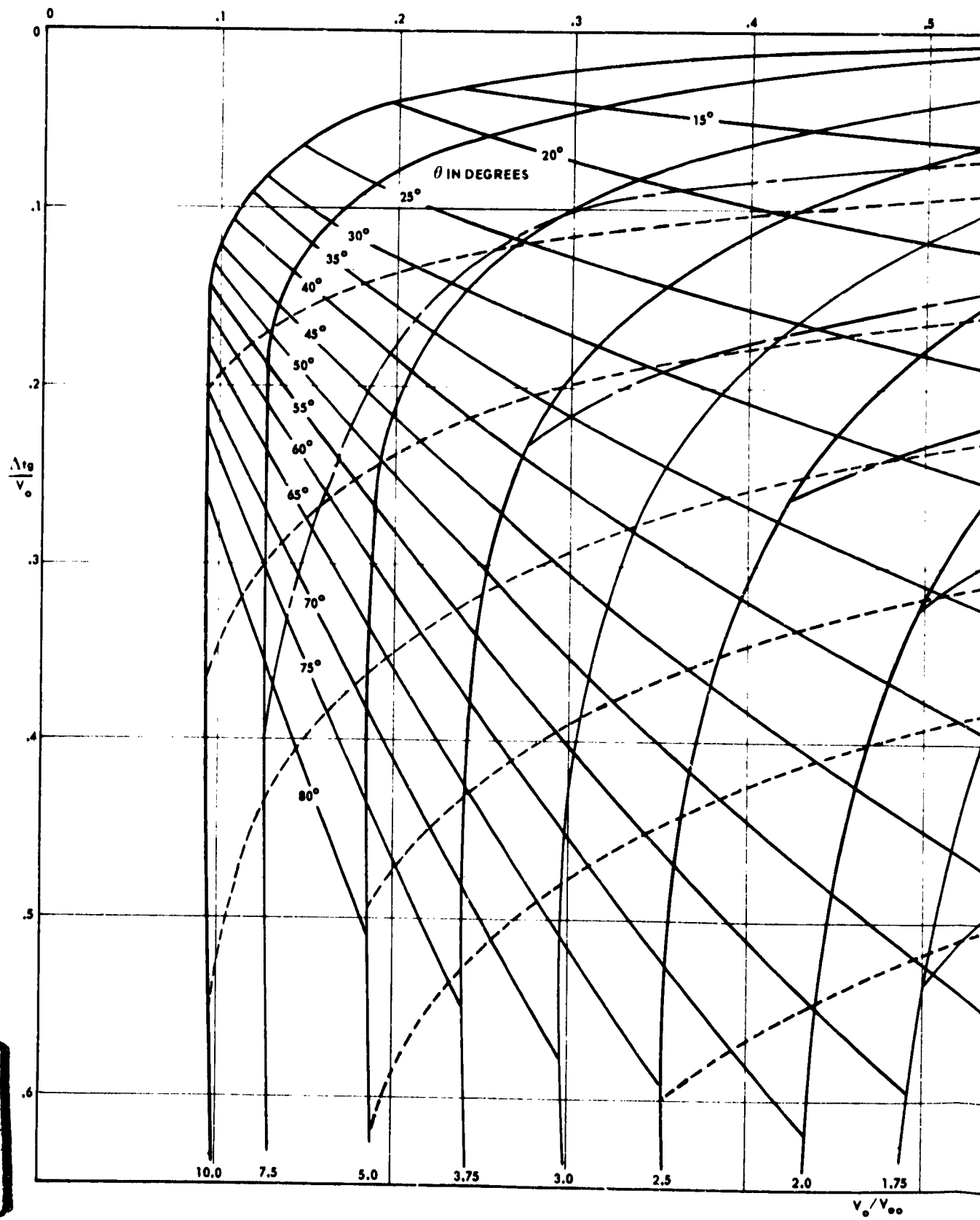
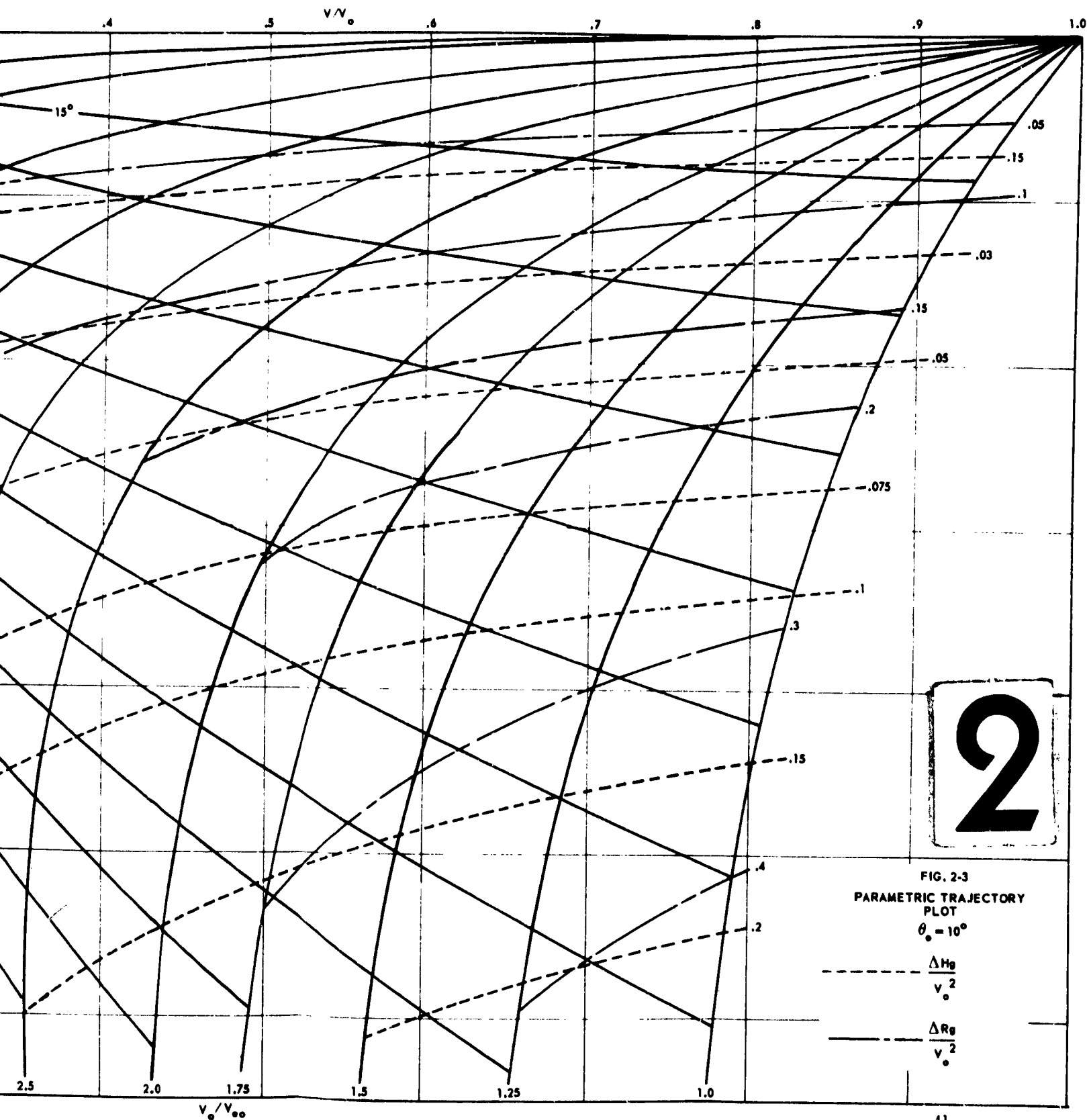


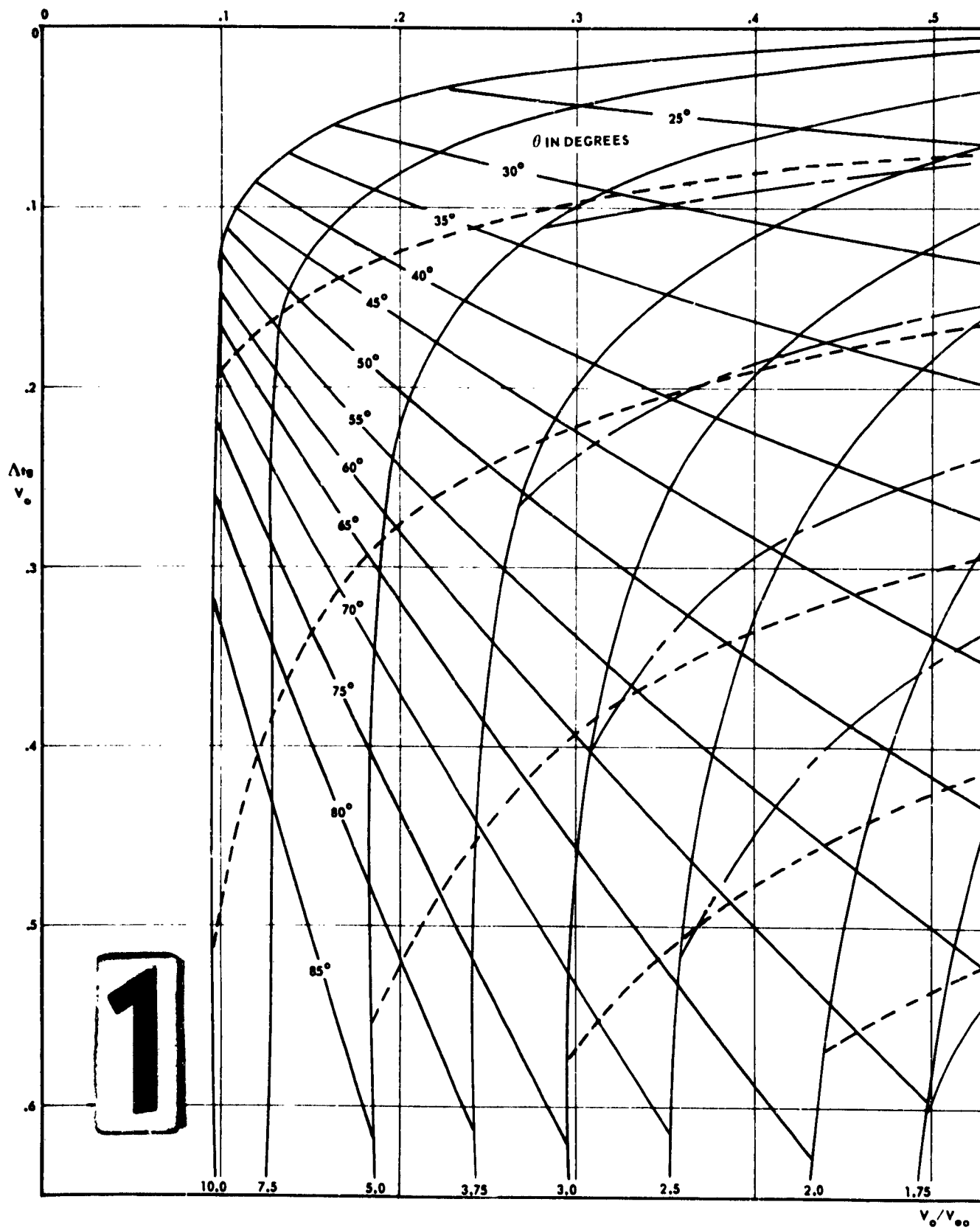
FIG. 2-2
 PARAMETRIC TRAJECTORY
 PLOT
 $\theta_0 = 3^\circ$

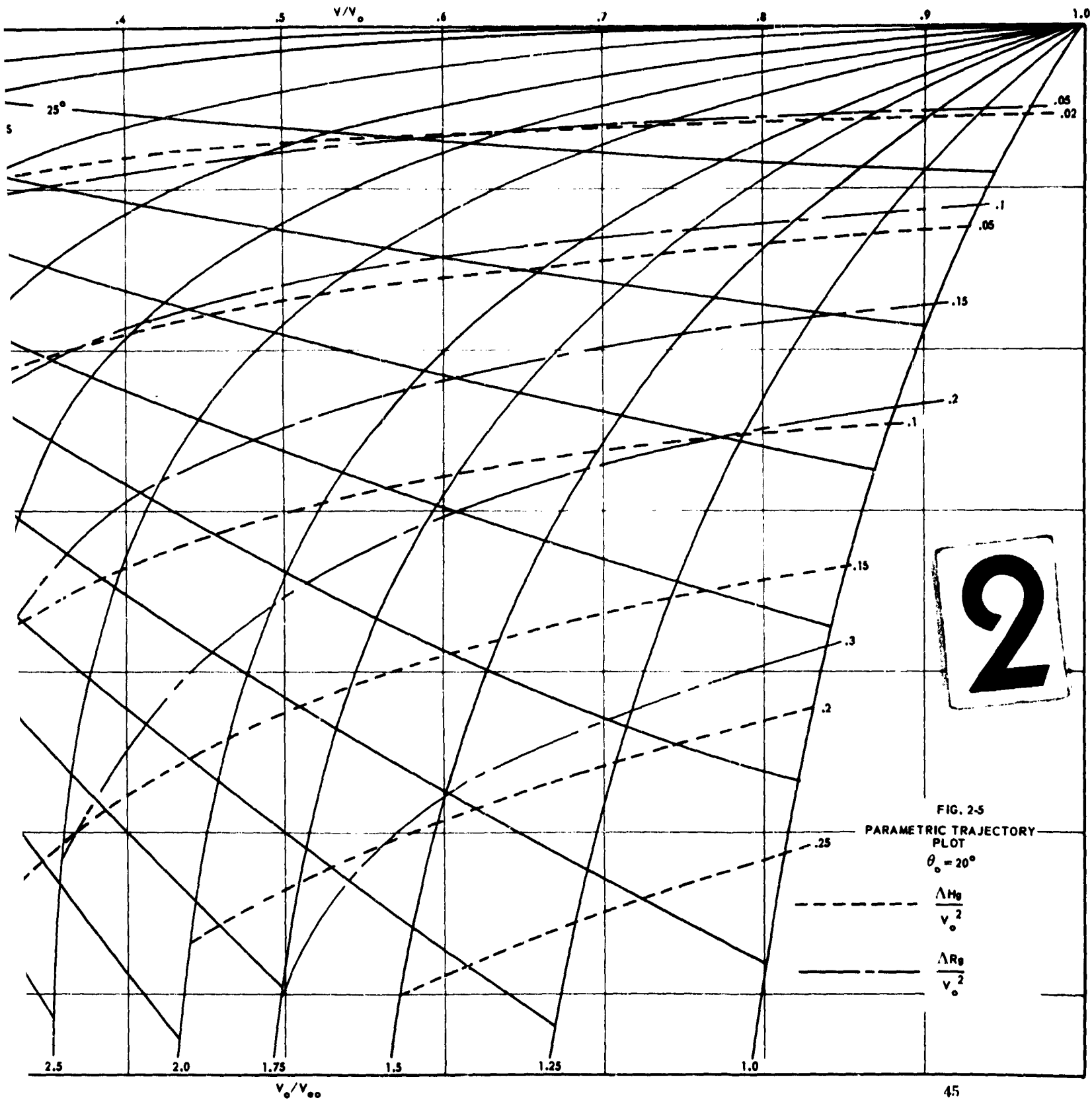
--- $\frac{\Delta H_0}{v_0^2}$
 — $\frac{\Delta R_0}{v_0^2}$

1

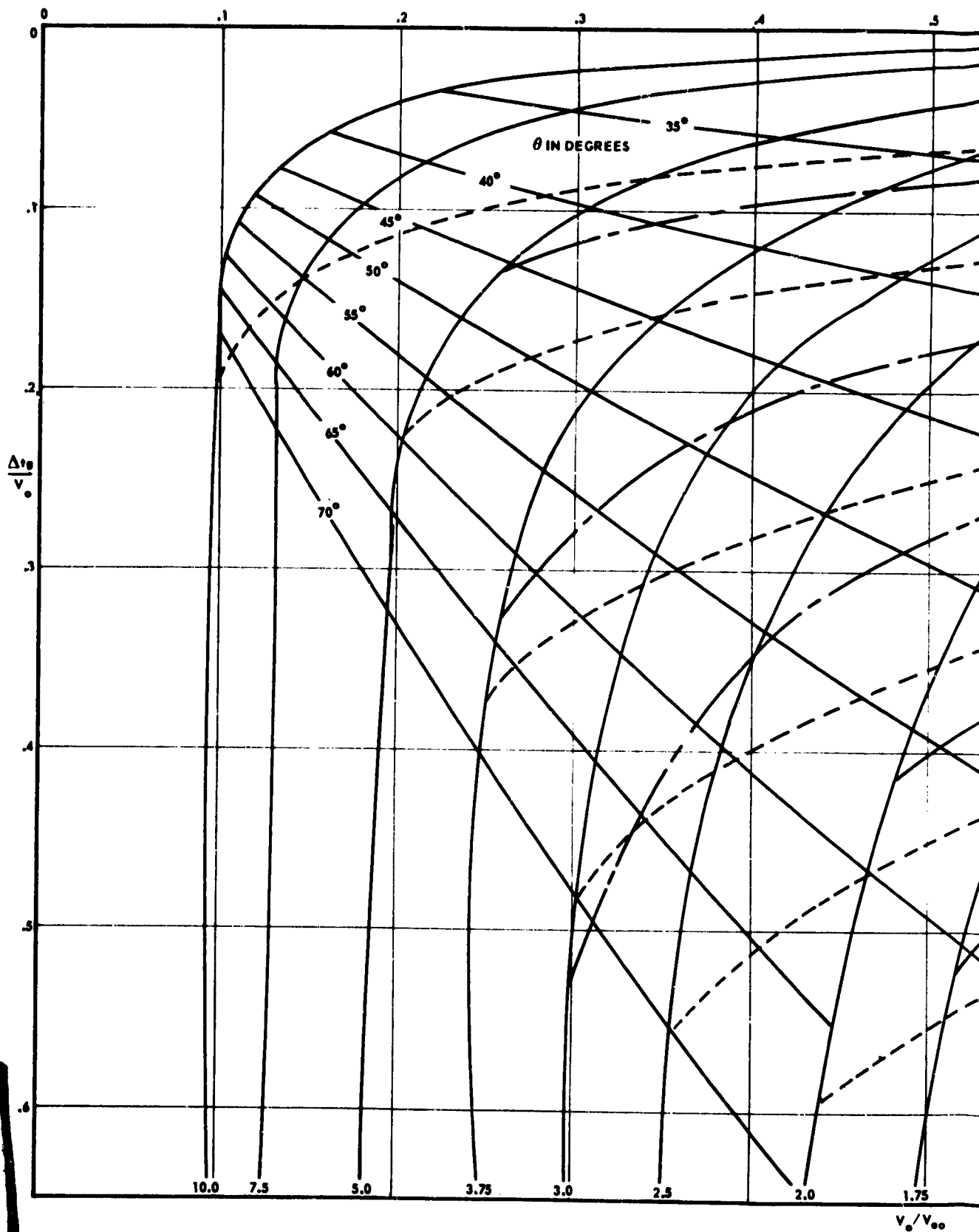


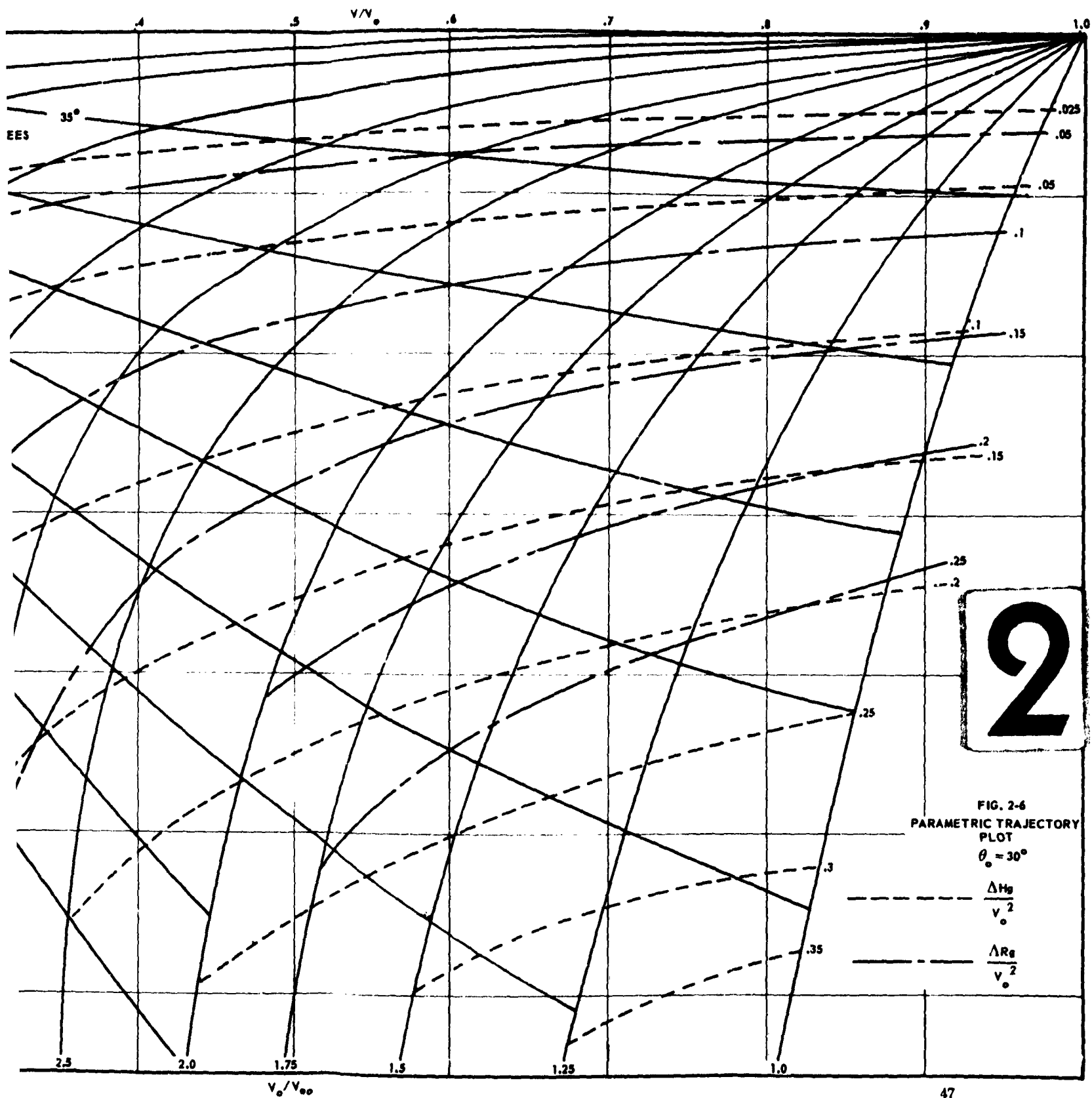


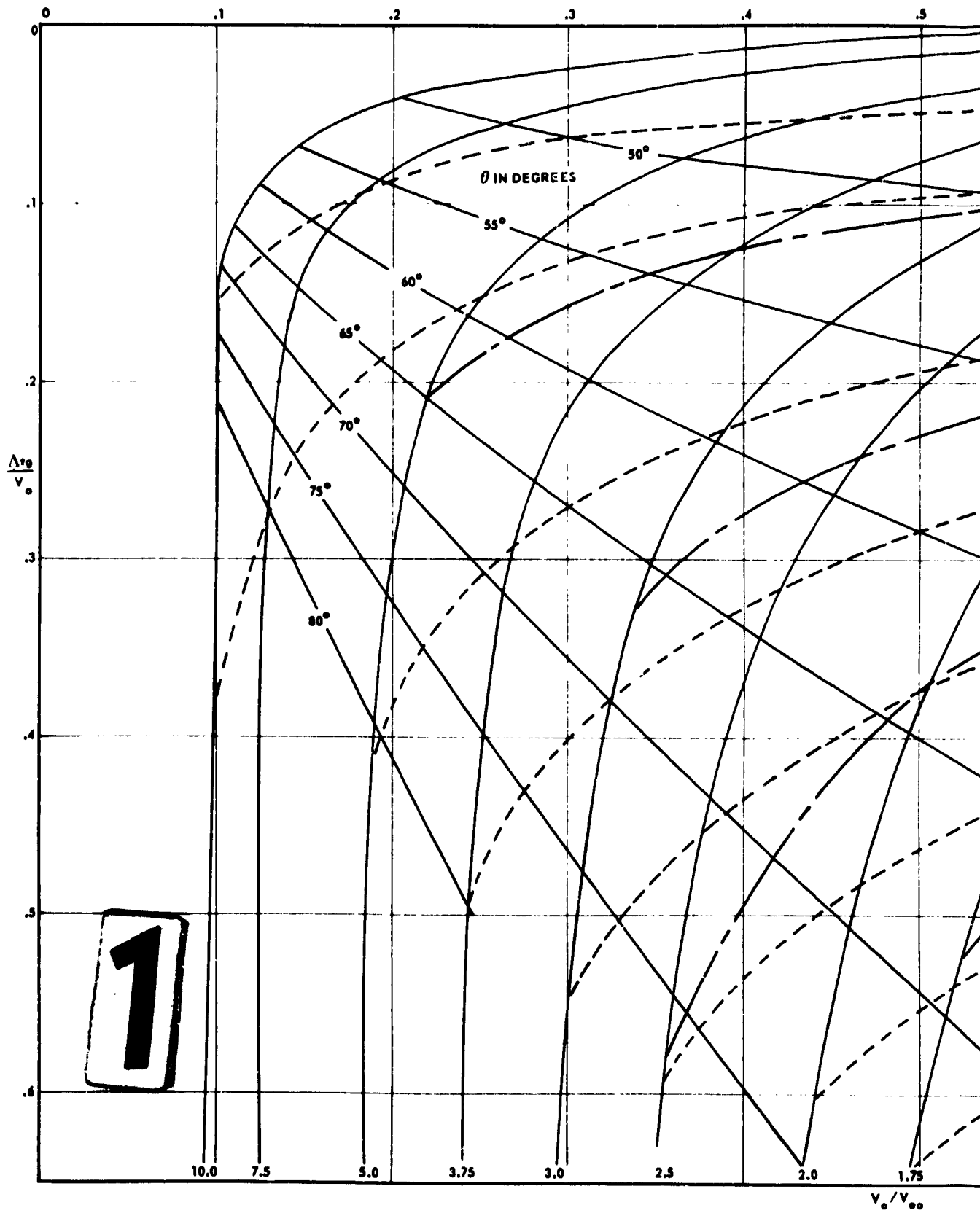




1







1

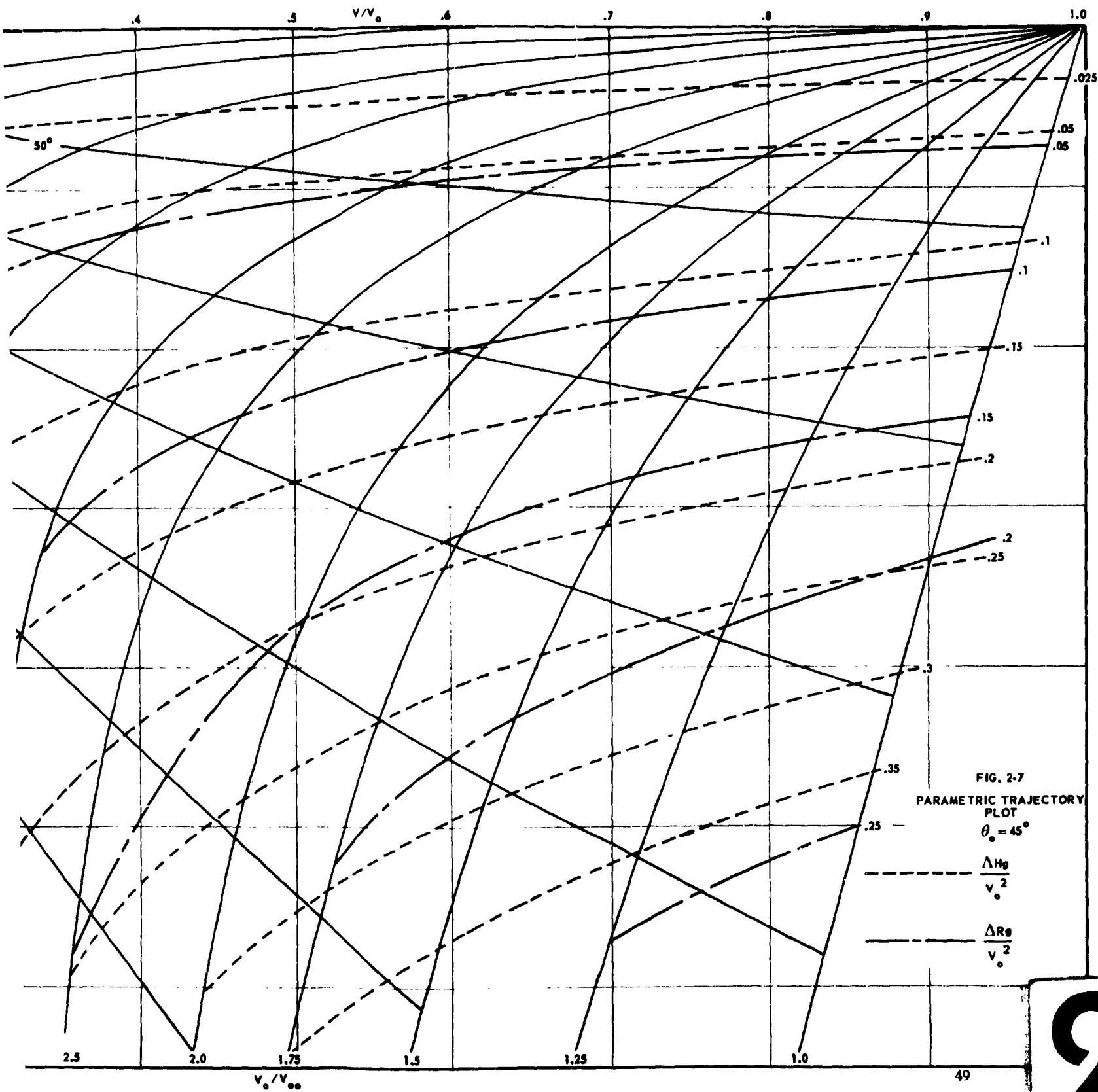
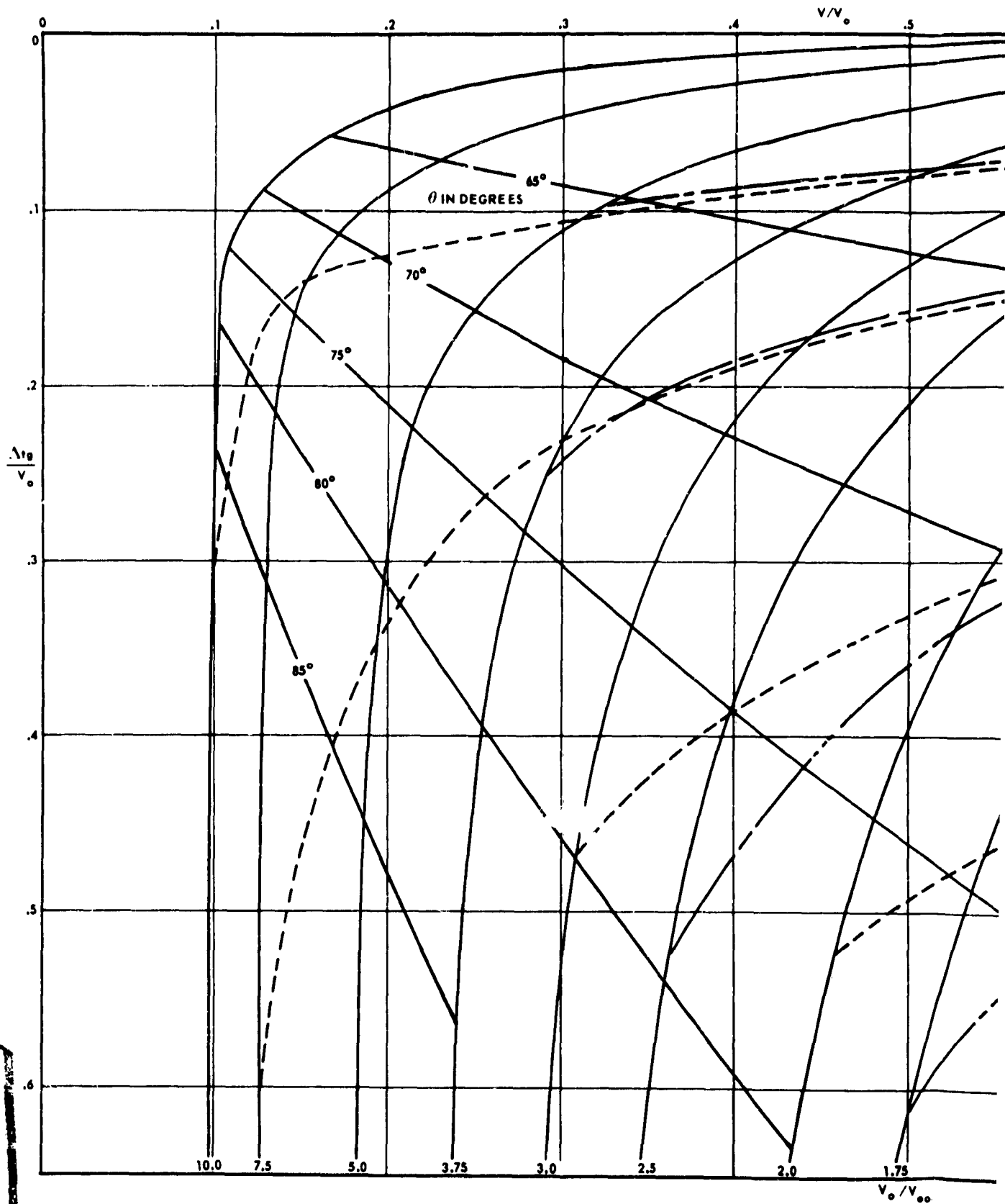
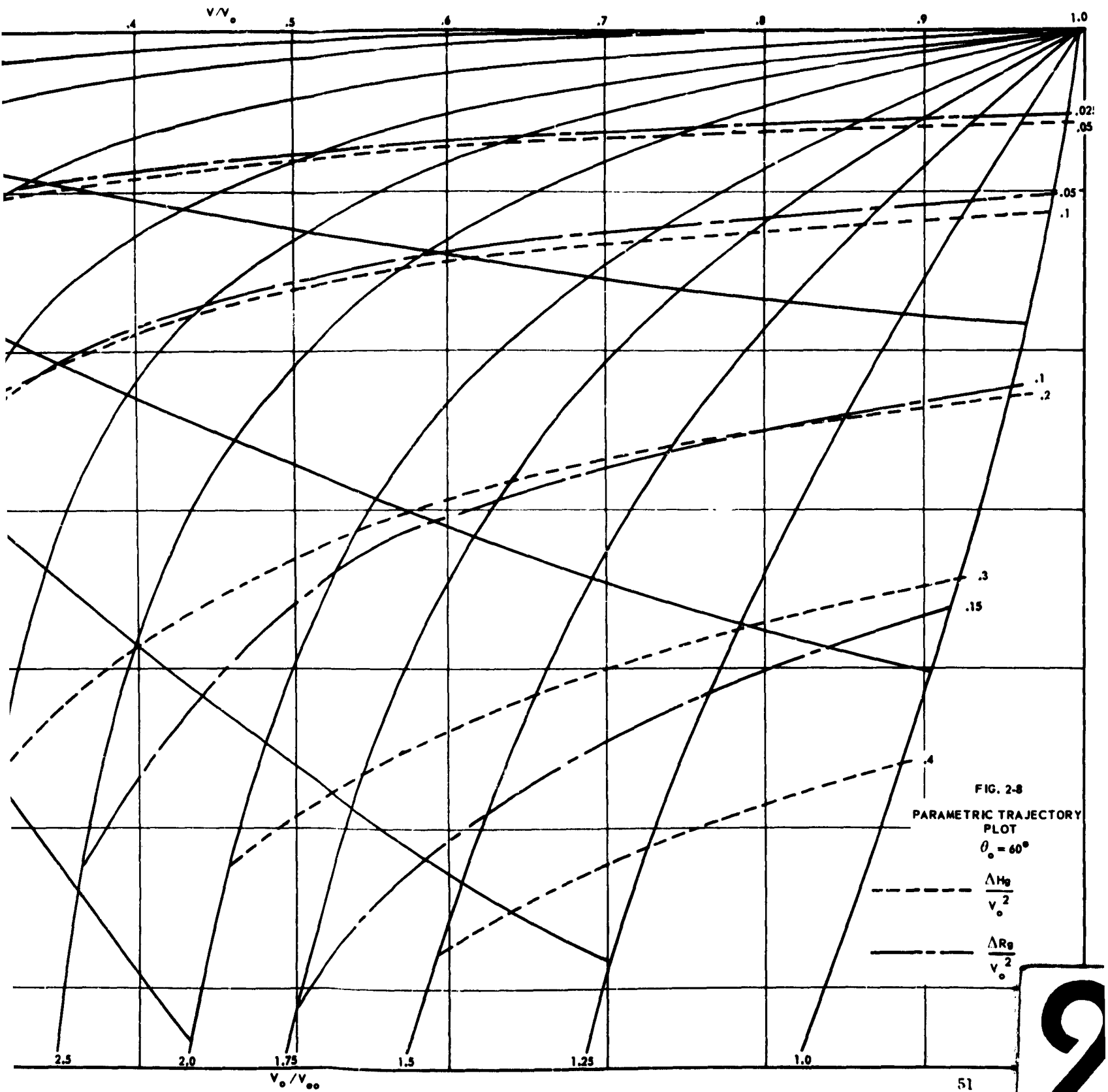
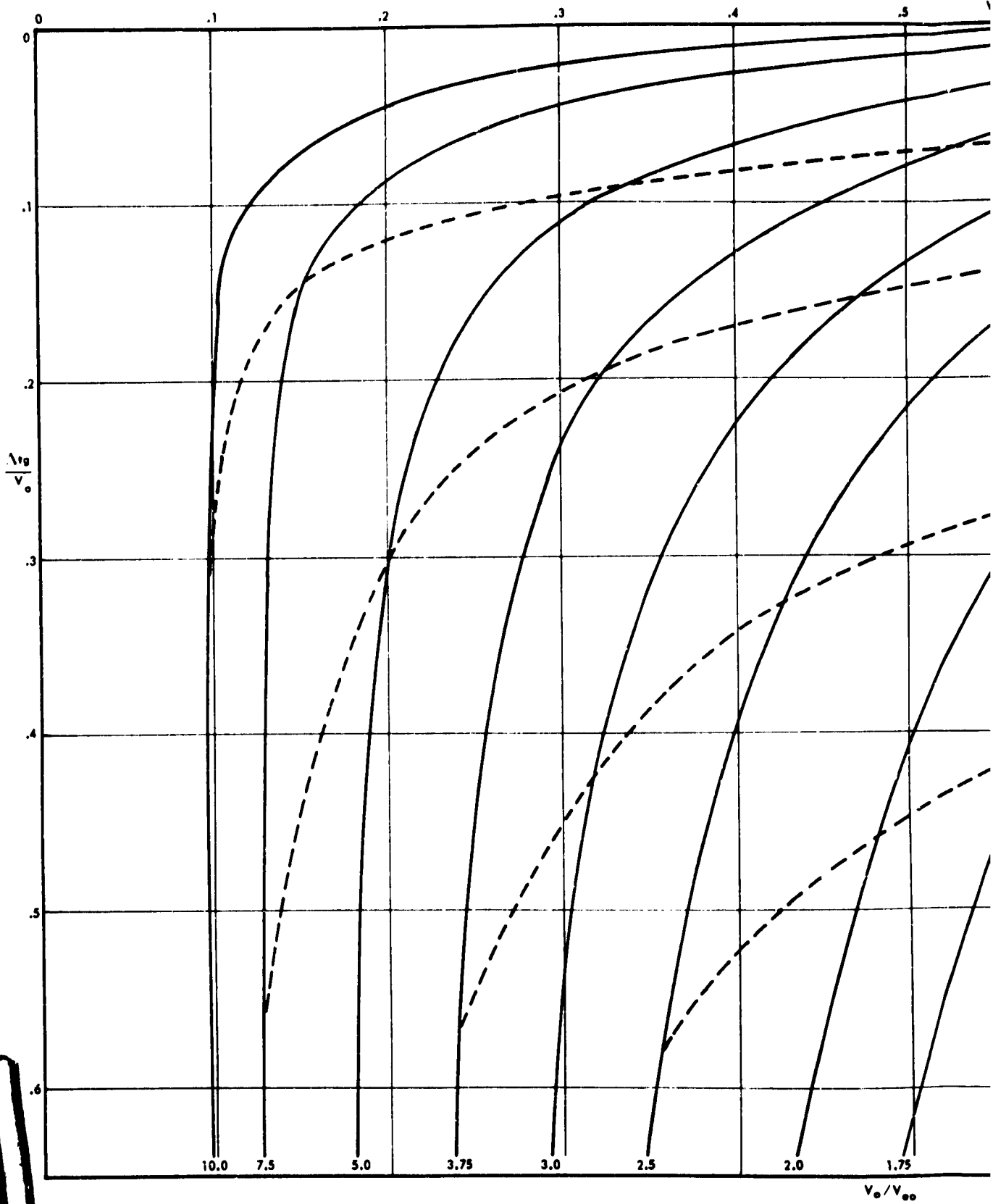


FIG. 2-7
PARAMETRIC TRAJECTORY
PLOT
 $\theta_0 = 45^\circ$

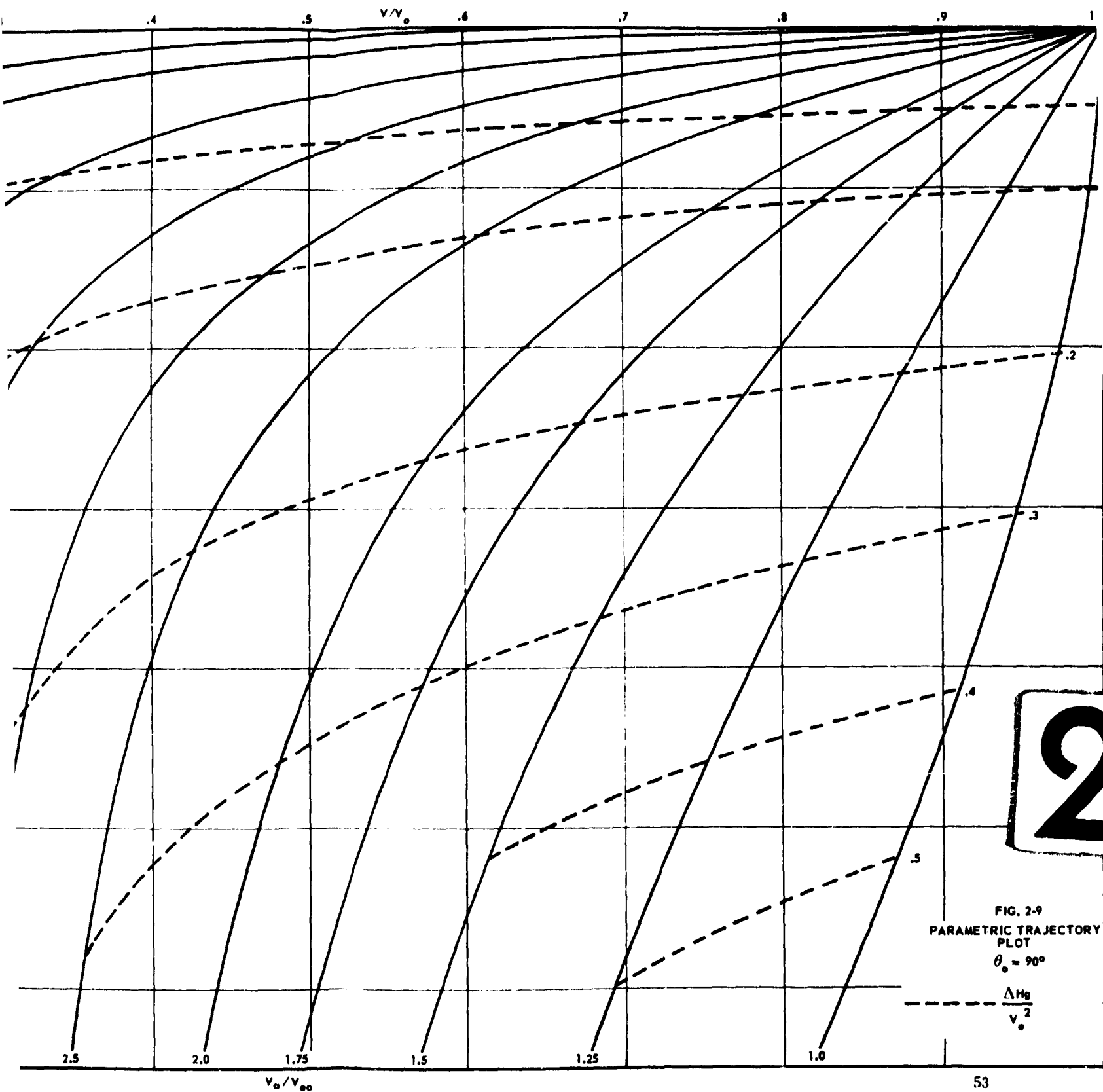


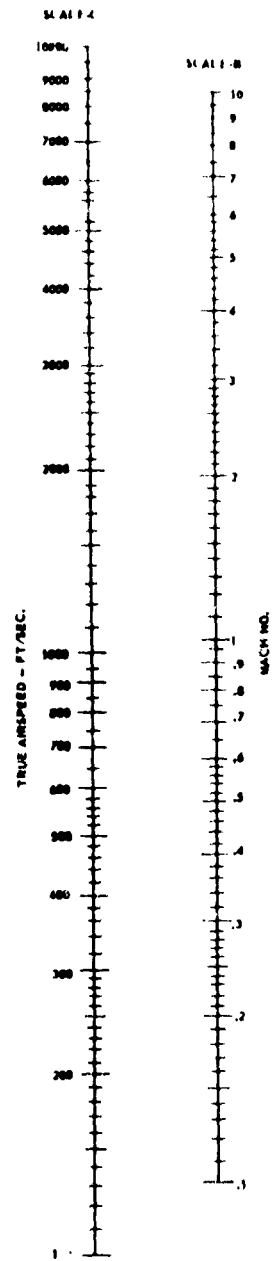
1



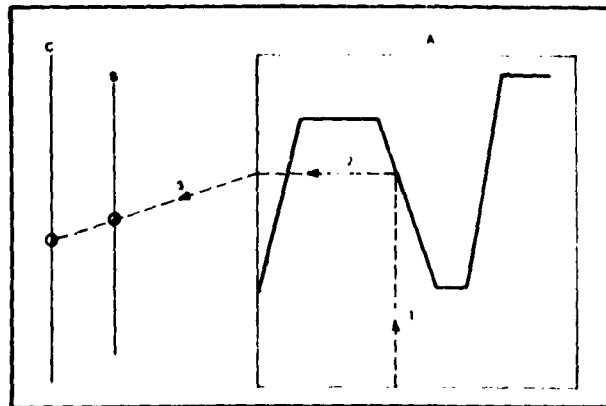


1

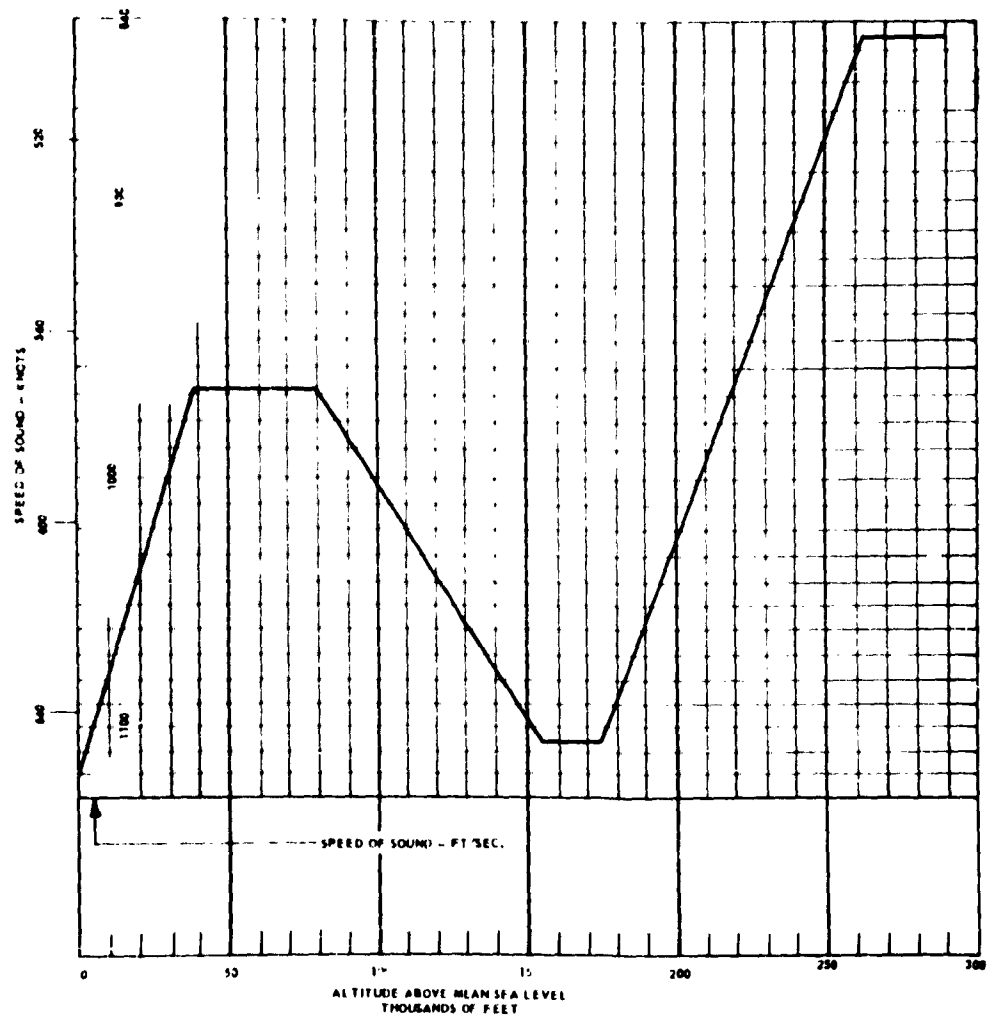




KEY



1



NOTE
SPEED OF SOUND VS ALTITUDE BASED ON
ARDC MODEL ATMOSPHERE, 1959

FIG. 2-10 TRUE AIRSPEED VS MACH NO. AND ALTITUDE

2

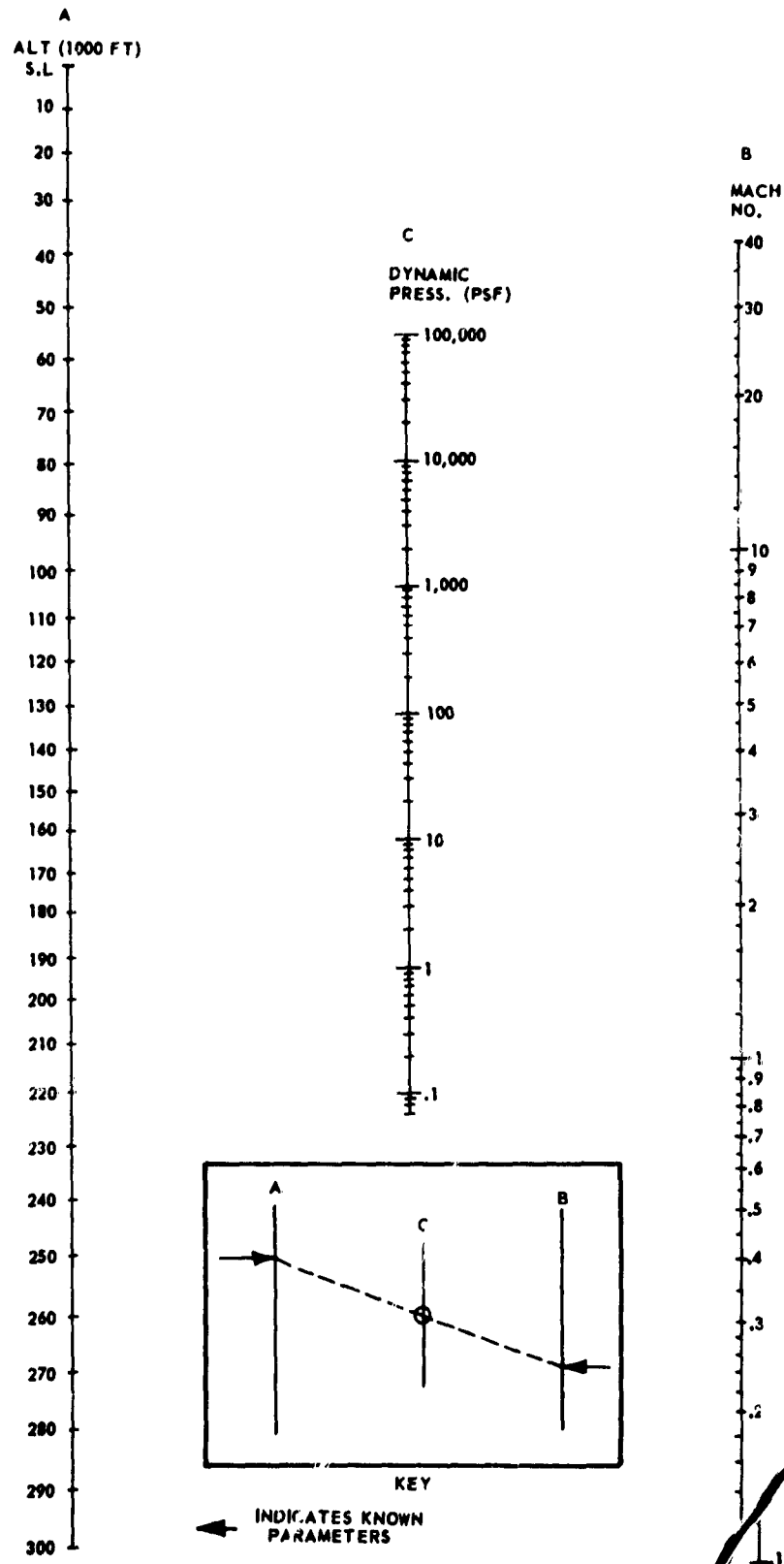


FIG. 2-11 ALTITUDE, MACH NO. AND DYNAMIC PRESSURE

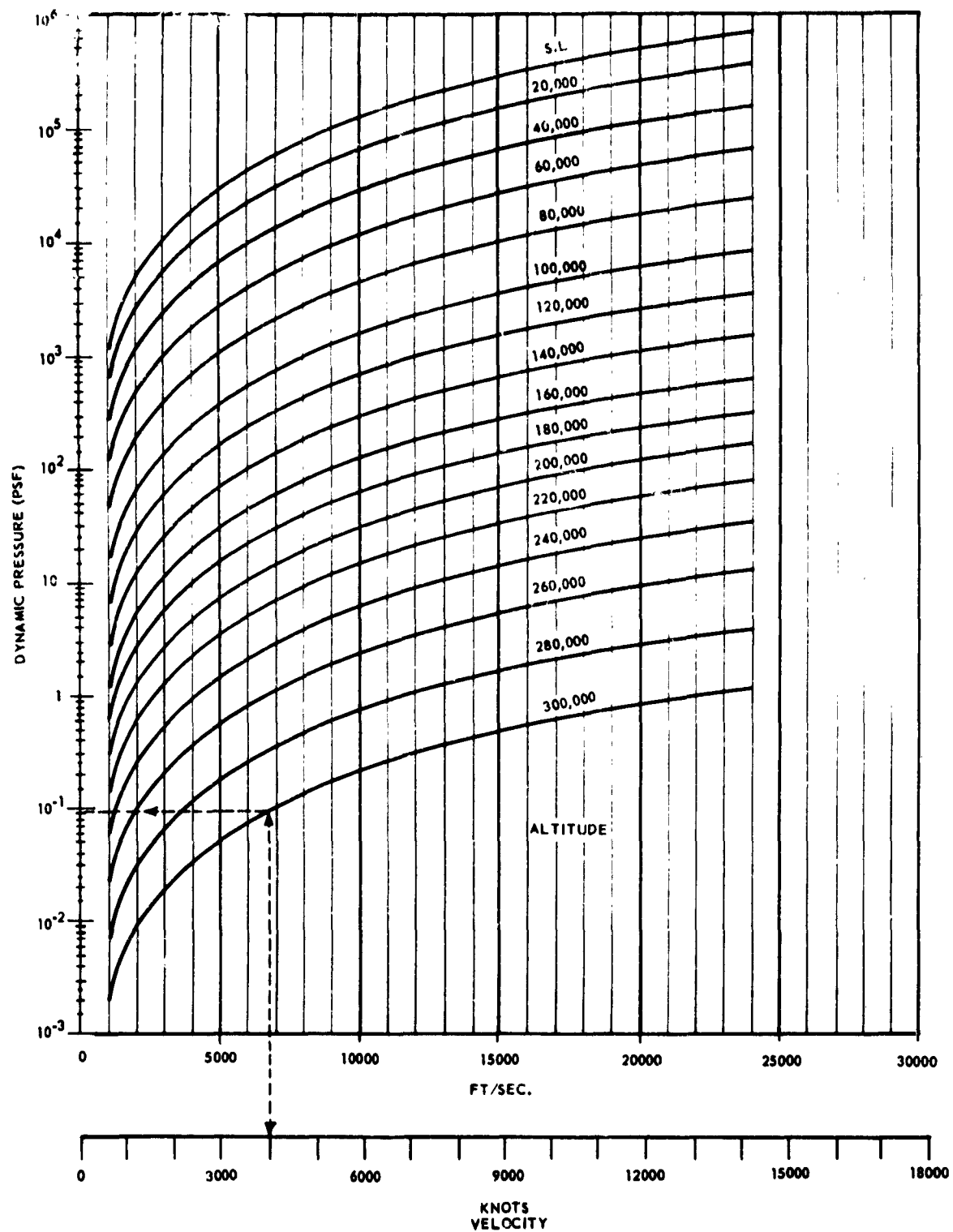
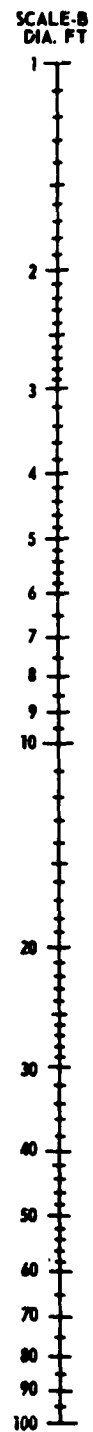
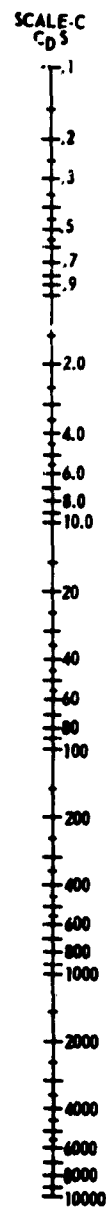
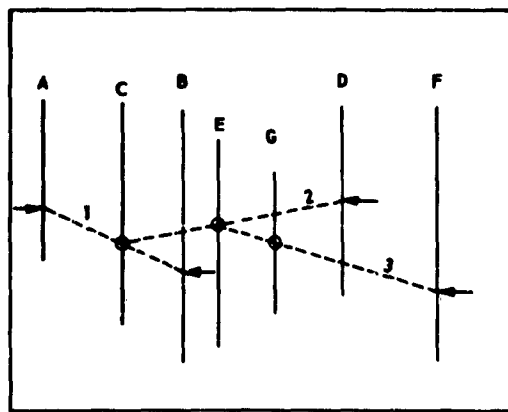


FIG. 2-12 DYNAMIC PRESSURE VS VELOCITY AND ALTITUDE



SCALE-E
INDEX

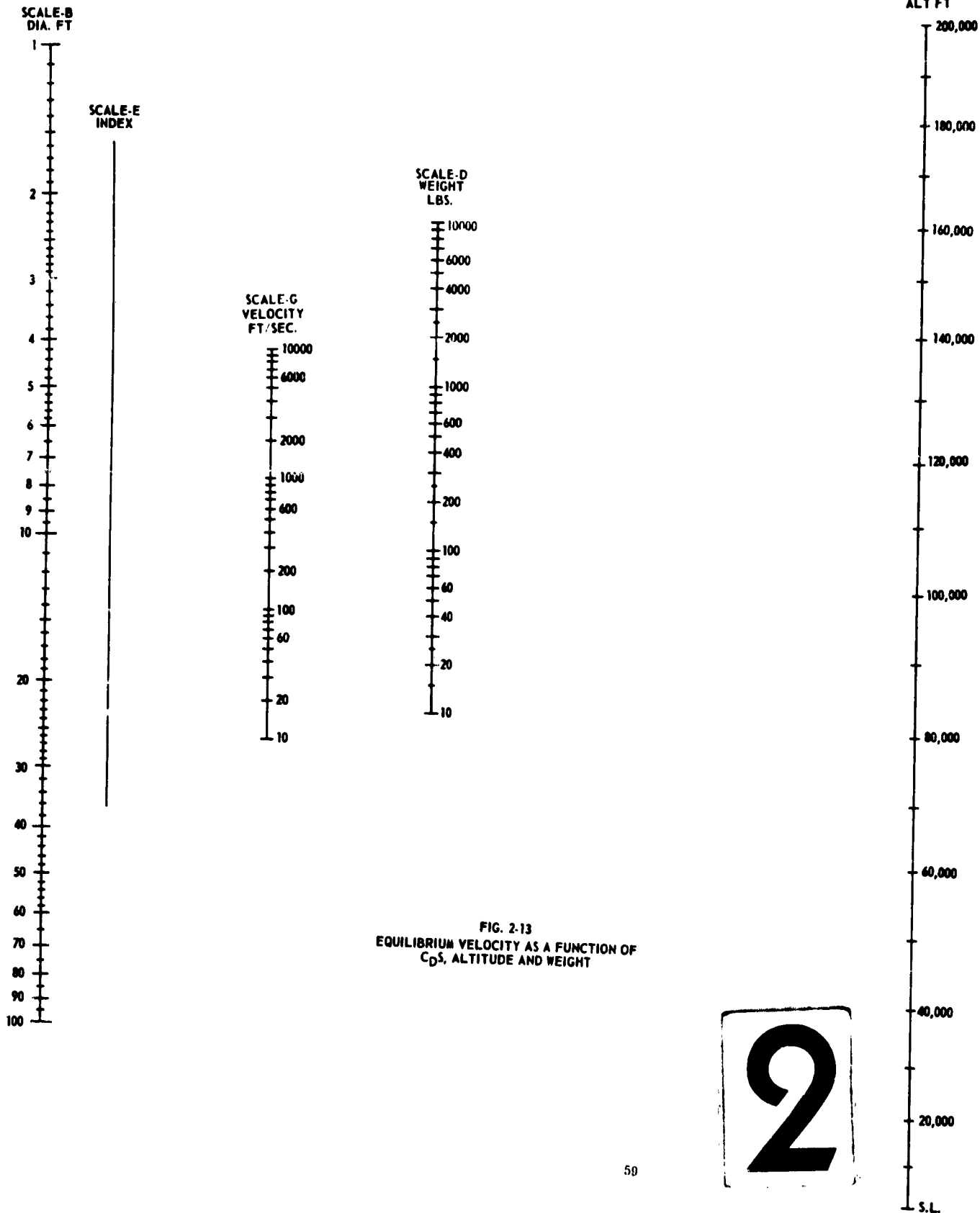
KEY



← INDICATES KNOWN PARAMETERS

1

E-C
3
.1
2
3
5
7
9
2.0
4.0
6.0
8.0
10.0
20
30
40
50
60
70
80
90
100
200
300
400
500
600
700
800
900
1000
2000
3000
4000
5000
6000
7000
8000
9000
10000



R = RELIABILITY
 $\lambda = \frac{1}{\theta}$ = FAILURE RATE
 θ = MEANTIME TO FAILURE
 $r = \lambda t = \frac{t}{\theta}$

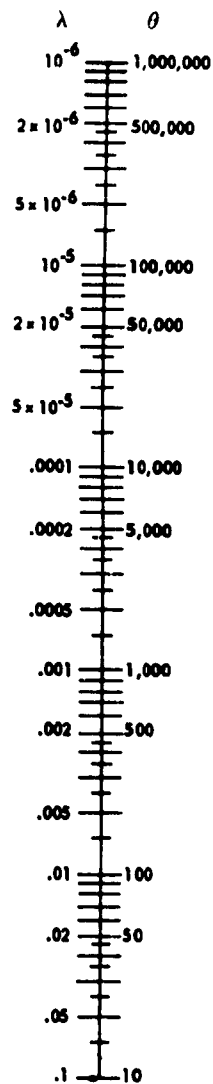
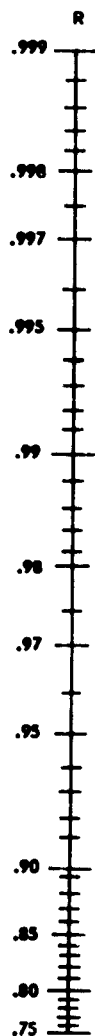


FIG. 2-14 RELIABILITY NOM

1

R = RELIABILITY
 $\lambda = \frac{1}{\theta}$ = FAILURE RATE
 θ = MEANTIME TO FAILURE
 $r = e^{-\lambda t} = e^{-\frac{t}{\theta}}$

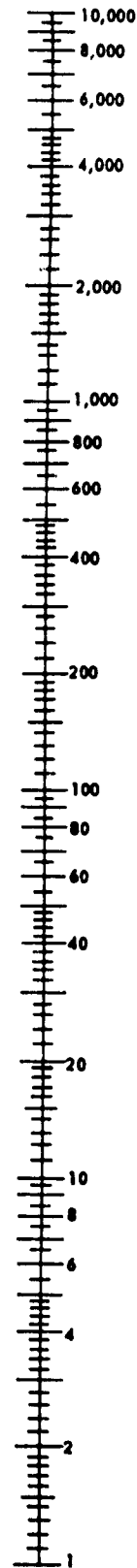
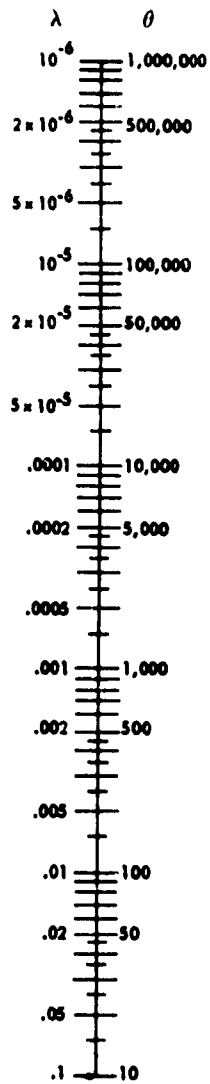


FIG. 2-14 RELIABILITY NOMOGRAM



CHAPTER 3 DEPLOYABLE AERODYNAMIC DECELERATORS, GENERAL

Table of Contents

<i>Section</i>	<i>Page</i>
1 TEXTILE PARACHUTE CANOPIES	65
1.1 Solid Textile Canopies	68
1.1.1 Flat Circular Canopy	68
1.1.2 Conical Canopy	70
1.1.3 Shaped-Gore Canopy	72
1.1.4 Extended-Skirt Parachute Canopy	74
1.1.5 Ribless Guide-Surface Canopy	77
1.1.6 Ribbed Guide-Surface Canopy	79
1.1.7 Personnel Guide-Surface Canopy	81
1.1.8 Modified Ribless Guide-Surface Canopy	83
1.2 Ribbon Parachute Canopies	85
1.2.1 Flat Circular Ribbon Canopy	85
1.2.2 Conical Ribbon Canopy	87
1.2.3 Shaped-Gore Ribbon Canopies	89
1.2.4 Ring-Slot Canopy	90
1.2.5 Ring-Sail Canopy (Sky-Sail)	93
1.3 Rotating Parachute Canopies	95
1.3.1 Rotafoil Canopy	95
1.3.2 Vortex Ring Canopy	97
1.4 Miscellaneous Canopies	99
1.4.1 General	99
1.4.2 Airfoil Canopy	99
1.4.3 Flat Noncircular Canopy	99
1.4.4 Wako Canopy	99
1.4.5 Steerable Parachute Canopies	99
2 DEPLOYABLE AERODYNAMIC DECELERATORS OTHER THAN TEXTILE PARACHUTE CANOPIES	99
2.1 Inflatable-Balloon Decelerators	99
2.1.1 Spherical Decelerators	99
2.2 Conical Decelerators	101
2.3 Spherical Segment Type	104
2.3.1 Analytical Investigation	104
2.3.2 Drag	105
2.3.3 Stability	105
2.3.4 Materials	105
2.3.5 Operational Method	106
2.4 Rotor Blades	106

References	Page
	111
Bibliography	112

Illustrations

Number		
3-1	Schematic of Spherical Decelerator	99
3-2	Drag Coefficient vs Mach No. for Spherical Drag Devices with Various Forebody Shapes at $1000 > 3$ and a 3% Bumble Fence	100
3-3	Spherical Decelerator Weight vs Diameter	100
3-4a	Spherical Decelerator with 3% Bumble Fence (Sections)	101
3-4b	Spherical Decelerator with 3% Bumble Fence	102
3-5	Drag Coefficient vs Mach No. for Spherical Decelerators	103
3-6	Schematic of 80 deg Ballute with 3.9% Fence (Side Inlets)	103
3-7	Supersonic Drag Coefficients of Inflatable Decelerators	103
3-8	Hypersonic Drag Data (Mach 10)	104
3-9	Estimated Inflatable Decelerator Weights	105
3-10	Preliminary Summary of Wind Tunnel Data C_D vs Mach No.	105
3-11	Representative Rotor-Type Decelerators	106
3-12	Typical Rotor-Blade Flight-Path	107
3-13	Possible Future Rotor Blade Application	108
3-14	Range vs L/D and Altitude	108
3-15	Rotor Drag Coefficient vs Mach Number	108
3-16	Rotor Drag vs Advance Ratio	108
3-17	Rate of Descent vs Altitude and Disk Loading	108
3-18	Disk Loading vs Hovering Time at Constant Energy Requirement	109
3-19	Typical Helicopter Rotor System Weights vs Diameter	109
3-20	Flexible Rotor Scaling Factor vs Tip Speed	110
3-21	Flexible Rotor Blade Weight vs Radius	110
3-22	Recovery System/Vehicle Weight Ratio vs Lift Coefficient	110
3-23	Lift-Drag Relationship, Flexible Airfoils	110

Tables

3-1	Typical Performance Characteristics of Parachute Canopies	66
3-2	Characteristics of Two Rene' 41 Cloths	104
3-3	Sample Flexible Blade Weights for 40-ft-Diameter Rotor	109

CHAPTER 3

DEPLOYABLE AERODYNAMIC DECELERATORS, GENERAL

The deployable aerodynamic decelerator system is made up of components which, functioning together, provide a means for the controlled descent, deceleration, or stabilization of a mass. Naturally, its most important component is the deployable aerodynamic decelerator. In addition, the system must provide means for the deployment of the aerodynamic decelerator, support for the suspended load, and, in some cases, the system must contain provisions for the automatic detachment of the aerodynamic decelerator from the suspended load.

Generally, the first considerations for the selection and design of the deployable aerodynamic deceleration device are those of the required drag and stability characteristics for the intended operational speed-and-altitude regime. Both drag and stability characteristics are determined almost entirely by the design configuration of the deployable aerodynamic decelerator.

A secondary consideration is the attainment of a high drag-efficiency in terms of weight or packed volume per aerodynamic decelerator drag area. This consideration may take on added significance if the available storage space is limited and the weight to be added to a given weapon system has to be held to a minimum.

A third consideration, but not necessarily third in importance, involves the selection and design of a deployment system for the aerodynamic decelerator, shock-attenuation systems, and associated hardware.

Many types of deployable aerodynamic decelerators have been investigated in the course of the Aerodynamic Decelerator Research and Development Program. Since many alternative shapes might be considered for the deceleration and/or stabilization of aerospace vehicles, it is virtually impossible to present a complete study of all possible variations. The designs and shapes discussed in the following sections represent those that have undergone sufficient investigation to establish some specific characteristics in performance, and are either most commonly used in general aerodynamic decelerator applications or have shown sufficient potential for future applications.

SEC. 1 TEXTILE PARACHUTE CANOPIES

Among the variety of deployable aerodynamic deceleration devices which may be considered for weapon system applications, conventional textile parachute canopies have the least weight and, in a majority of cases, the least bulk for a given drag area. Consequently, the textile parachute has found wide application for the deceleration, stabilization, and recovery of aerospace vehicles or their payloads. In view of its wide use and application, the parachute will be treated in much more detail than any othertype of aerodynamic decelerator in the following Chapters and Sections.

In all cases except the ribbed and ribless guide-surface canopies, canopy diameter as referred to hereafter is the "nominal diameter D_o ". For ribbed and ribless guide-surface canopies, the "constructed diameter D_c " is commonly used, which is equivalent, in these cases, to the "inflated diameter D_p ".

Drag coefficients as presented hereafter are based upon the area S_o (total area of the drag-producing surface), in all cases except for ribbed and ribless

type guide surface canopies. The symbol for the drag coefficient related to the area S_o is C_{D_o} . For ribbed and ribless type guide surface canopies, the drag coefficient is based upon the area S_p (projected area of the inflated canopy). For these canopy types, the symbol for the drag coefficient is C_{D_p} .

Data presented in the following table are intended only for purposes of comparison. The drag coefficients, ratios of force to the product of dynamic pressure and reference area, and values of average angle of oscillation values presented are peculiar only to the canopy size and operational conditions stated. At present, no accurate performance relationship between model and full-size parachute canopies can be established. For additional values of performance and design characteristics of larger-size canopies, refer to Chapter 4, Aerodynamic and Operational Characteristics of Canopies; Chapter 5, Deployable Aerodynamic Decelerator Applications; and Chapter 7, Design of Textile Canopies and Parachute Systems. Unless otherwise specified, all values listed in the following paragraphs refer to subsonic applications and sea-level density.

TABLE 3-1 TYPICAL PERFORMANCE CHARACTERISTICS OF PARACHUTE CANOPIES

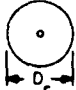


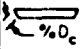












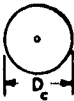
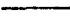


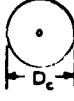



Canopy Type		Constructed Shape		Diameter Ratios		Drag Coefficient		Opening Shock Factor (Infinite Mass)	Stability	
		Plan View	Profile View	D_p/D_c	D_o/D_c	Range	Average (Prelim. Design)		$\partial C_M/\partial \alpha$ (about 0° angle of attack)	Average Angle of Oscill. (Free Descent)
SOLID TEXTILE	Flat Circular			-.70	1.00	C_{D_o} 0.65 to 0.90	C_{D_o} 0.75	-2.0	positive	$\pm 30^\circ$
	Extended Skirt			-.76	1.24	C_{D_o} 0.65 to 0.85	C_{D_o} 0.70 to 0.75	-1.8	positive	$\pm 20^\circ$
	Guide-Surface (Stabilization)			-1.0	1.60 for 10 gores	C_D 0.8 to 1.0	C_D 0.95	-1.1	negative	$\pm 2^\circ$
	Guide-Surface (Ribless)			-.95	1.51 for 10 gores	C_D 0.75 to 0.85	C_D 0.80	1.1 to 1.4	negative	$\pm 3^\circ$
	Guide-Surface (Modified Ribless)			-.95	1.5	C_{D_p} 0.75 to 0.85	C_{D_p} 0.78	1.1 to 1.4	negative	$\pm 5^\circ$
	Guide-Surface (Personnel)			-.73	1.15	C_{D_o} 0.68 to 0.80	C_{D_o} 0.72	-1.6	positive	$\pm 15^\circ$
	Shaped (Conical)			-.70	1.08	C_{D_o} 0.62 to 0.95	C_{D_o} 0.72	-1.8	positive	$\pm 20^\circ$
	Shaped-Gore (Hemispherical)			-1.0	1.41	C_{D_o} 0.65 to 0.85	C_{D_o} 0.75	-1.8	positive	$\pm 25^\circ$

TABLE 3-1 (Cont'd)

Canopy Type		Constructed Shape		Diameter Ratios		Drag Coefficient		Opening Shock Factor (Infinite Mass)	Stability	
		Plan View	Profile View	D_p/D_c	D_o/D_c	Range	Average (Prelim. Design)		$\partial C_M/\partial \alpha$ (about 0° angle of attack)	Average Angle of Oscill. (Free Descent)
RIBBON	Flat Circular			-.67	1.00	C_{D_o} 0.45 to 0.55	C_{D_o} 0.50	-1.05	negative	$\pm 5^\circ$
	Conical			-.70	1.08	C_{D_o} 0.45 to 0.55	C_{D_o} 0.50	-1.00	negative	$\pm 3^\circ$
	Ring Sail			-.70	1.16	C_{D_o} 0.70 to 0.95	C_{D_o} 0.78	-1.05	negative	$< \pm 10^\circ$
	Ring Slot			-.70	1.00	C_{D_o} 0.45 to 0.65	C_{D_o} 0.55	-1.05	negative	$\pm 10^\circ$

1.1 Solid Textile Canopies

1.1.1 FLAT CIRCULAR CANOPY

1.1.1.1 Canopy Design. This canopy is constructed as a flat circular surface with a center orifice (vent), and consists of a number of gores stitched together laterally, the joints forming the main radial seams.

1.1.1.2 Drag Coefficient. The drag coefficient CD_o of this canopy ranges from 0.65 to 0.90, depending upon canopy size, cloth permeability, and rate of descent. For preliminary calculations, an average CD_o of 0.75 is generally used.

1.1.1.3 Stability. For small canopies (below 32-ft diameter), oscillations of approximately ± 30 deg are common. On larger canopies, the average angle of oscillation generally decreases with increasing size.

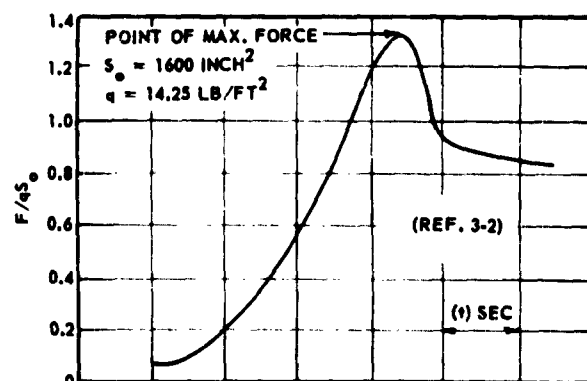
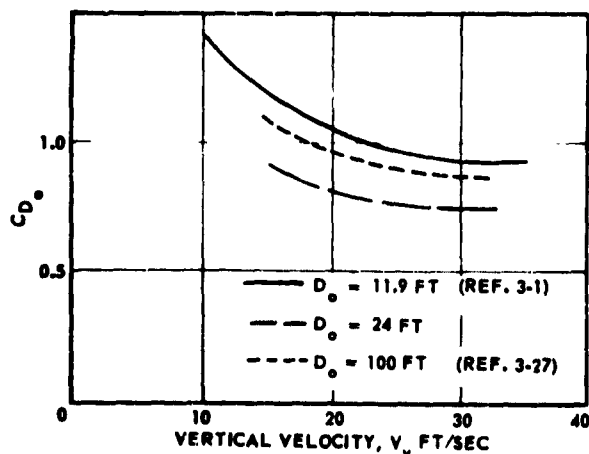
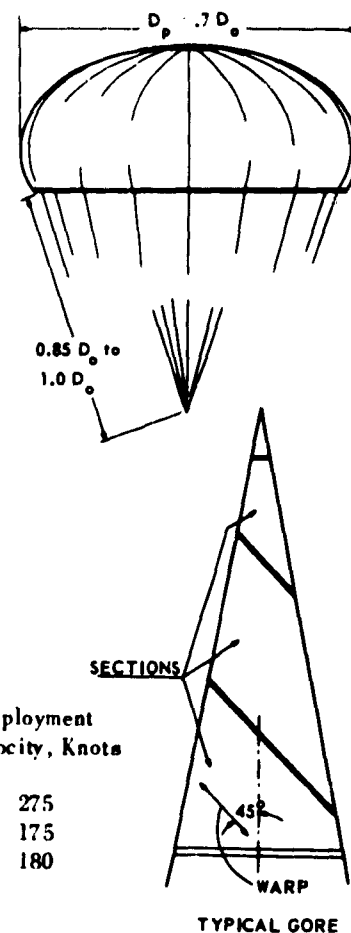
1.1.1.4 Opening-Shock. For "infinite mass" conditions, (see Glossary) the opening-shock factor approaches 2.0.

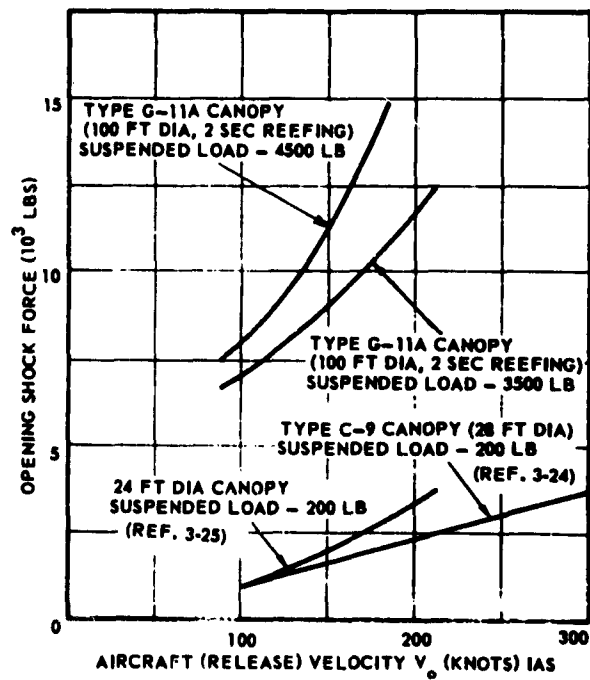
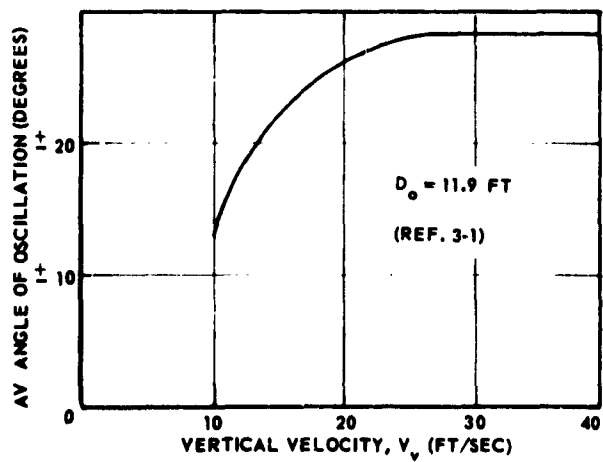
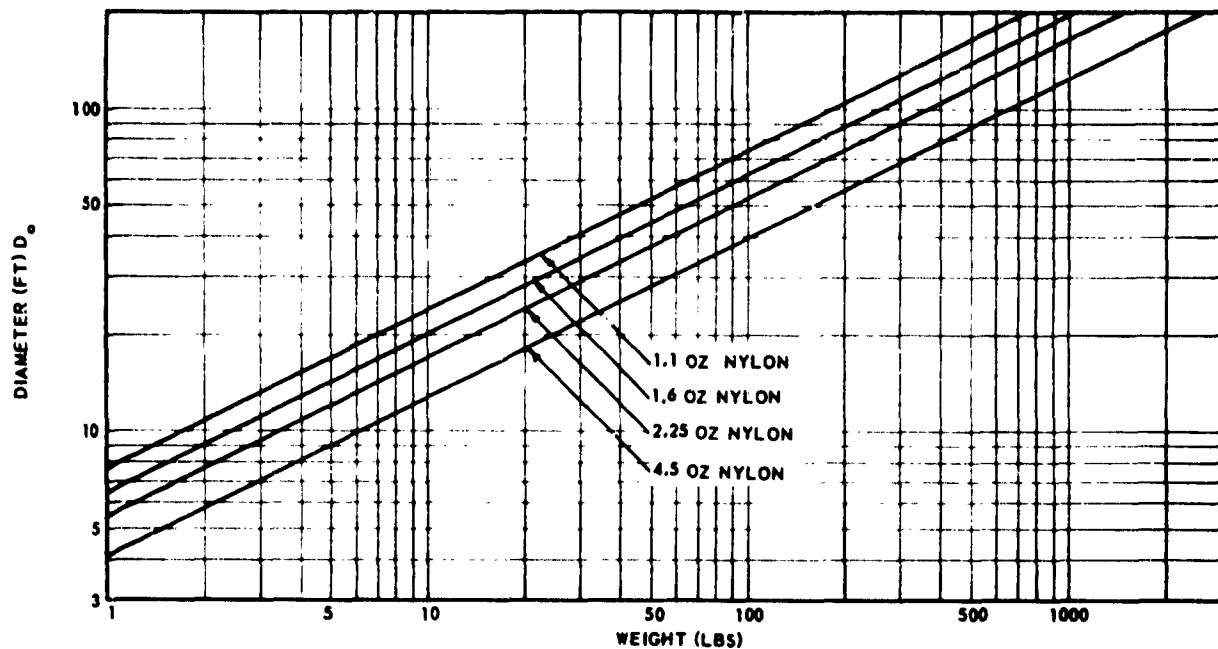
1.1.1.5 Application. Flat circular canopies are in wide use for personnel and air-drop applications.

1.1.1.6 Opening Reliability and Speed Limitations. This canopy is very reliable. However, it is generally limited to low-speed uses because, at higher speeds, it opens rapidly and has excessive opening-shock. Safe deployment-speed limitations for several specific canopy and load configurations are as follows:

Canopy Type and Diameter, ft	No. of Gores	Suspended Load, lb	Canopy Material	Line	Deployment Velocity, Knots
C-9 28	28	200	1.1 oz Nylon	550 lb	275
G-12 64	64	2200	2.25 oz Nylon	1000 lb	175
G-11A 100 (with 2 sec. reefing)	120	7000	1.6 oz Nylon	550 lb	180

1.1.1.7 Remarks. This canopy type is relatively easy to manufacture. Its stability characteristics and deployment speed limitations make it unsuitable for certain applications.





1.1.2 CONICAL CANOPY

1.1.2.1 *Canopy Design.* This canopy is constructed by joining gores having an included angle β of a value less than $360^\circ/V$ (depending on the desired cone angle of the canopy—see drawing). The value of this included angle is determined by equation:

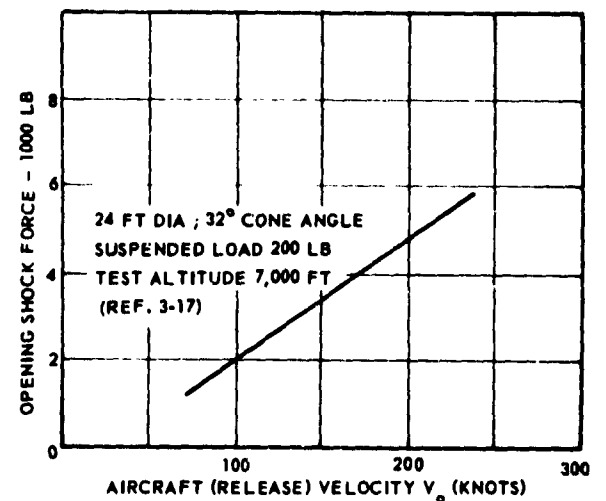
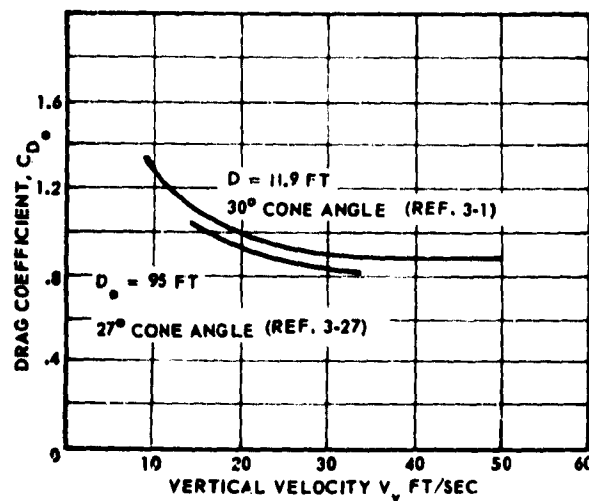
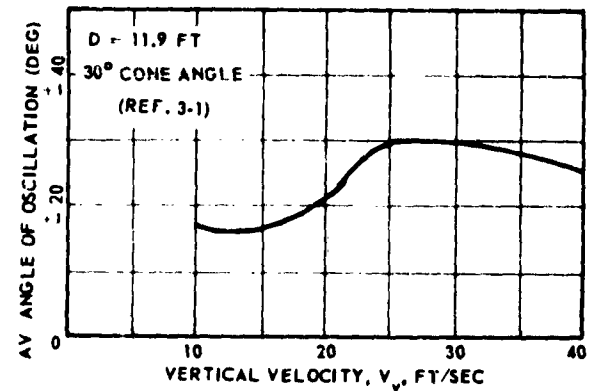
$$\beta = 2 \sin^{-1} \left[(\cos \alpha) \left(\sin \frac{180^\circ}{V} \right) \right]$$

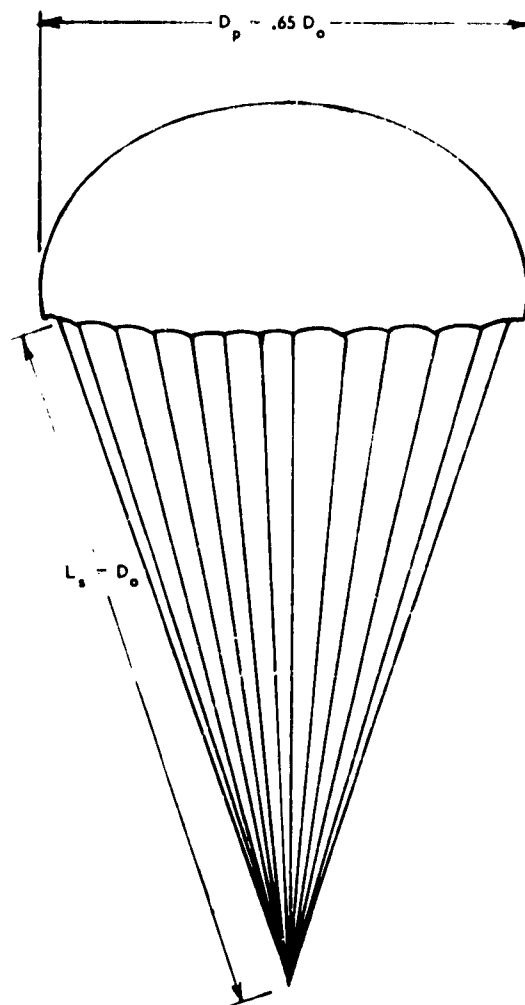
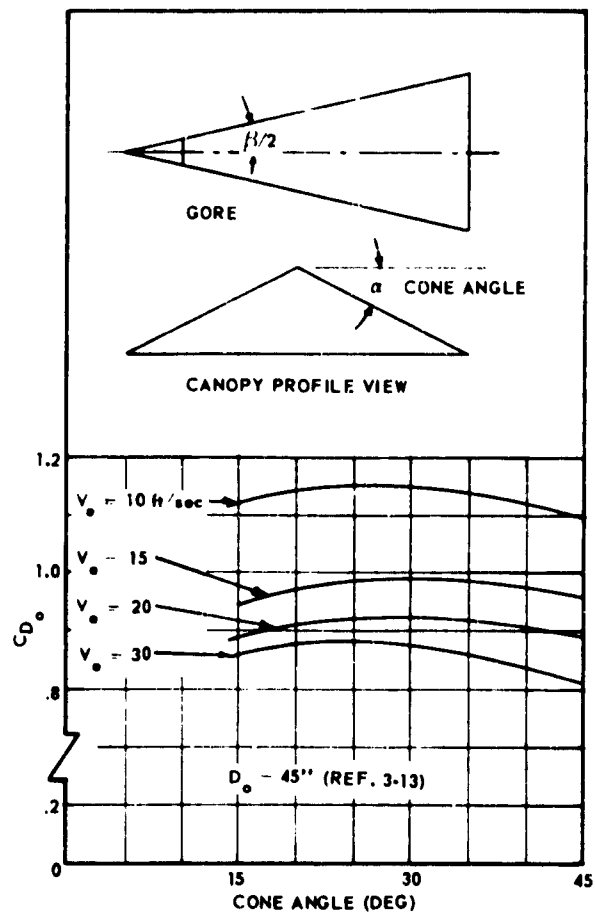
where β = Included angle of gore;
 α = Cone angle of canopy; and
 N = Number of gores in canopy.

1.1.2.2 *Drag Coefficient.* The drag coefficient: C_{D_0} of this canopy type ranges from 0.62 to 0.95, chiefly depending upon size, cone angle, and rate of descent. For preliminary calculations, a drag coefficient C_{D_0} of 0.72 is used.

1.1.2.3 *Stability.* Oscillation of the solid cloth conical canopy ranges between ± 30 and ± 10 deg depending on rate of descent, size, and cone angle.

1.1.2.4 *Opening Shock.* For infinite-mass conditions, the opening-shock factor is approximately 1.8.





1.1.3 SHAPED-GORE CANOPY

1.1.3.1 *Canopy Design.* This canopy design is similar to that of the solid flat type, with the exception that the gore design deviates from the triangular pattern. Because of the many variations of shaped gore canopy designs, it is impractical to cite specific performance figures.

1.1.3.2 *Drag Coefficient.* Many shaped gore canopy designs have been tested, and drag coefficients in the order of those for flat circular canopies have been obtained.

1.1.3.3 *Stability.* Stability varies with design. Some of the types tested have shown stability improvements over the flat circular type canopies.

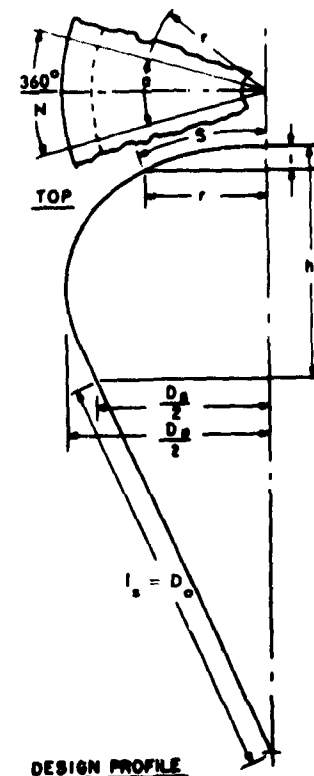
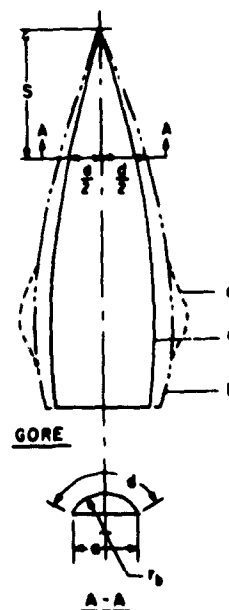
1.1.3.4 *Opening-Shock.* For infinite-mass conditions, the opening-shock factor is slightly less than those for flat circular canopy designs.

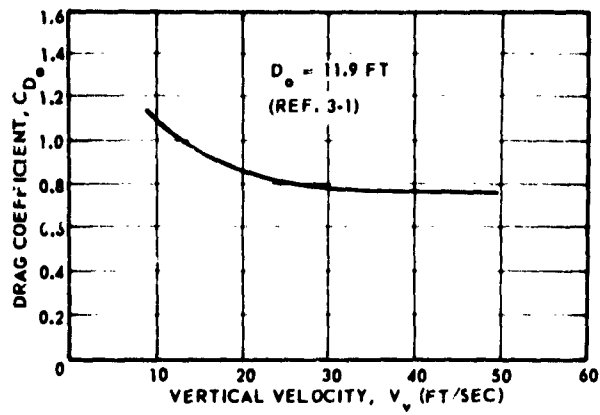
1.1.3.5 *Application.* These canopy types may be designed for applications that require reduced opening-shock or slightly better stability than is found in flat circular canopies, or both.

1.1.3.6 *Opening Reliability.* Reliability varies greatly with design. Hemispherical canopy designs have been found reliable for several applications.

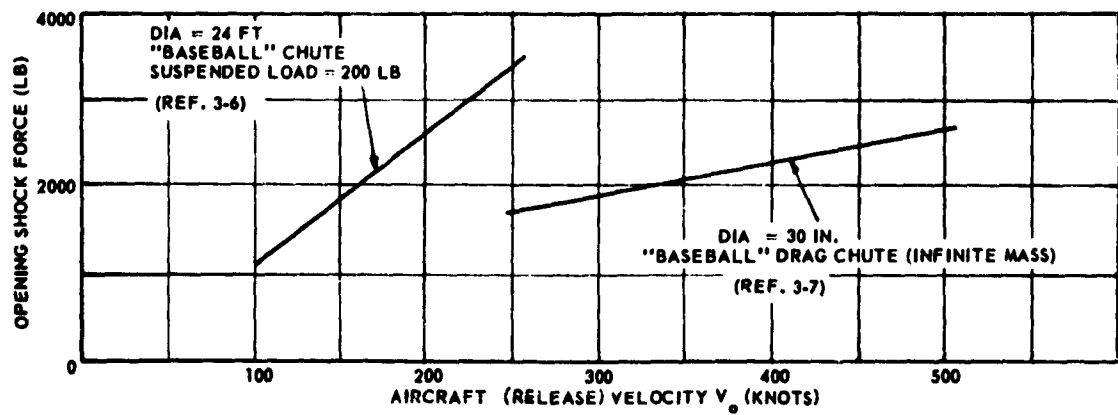
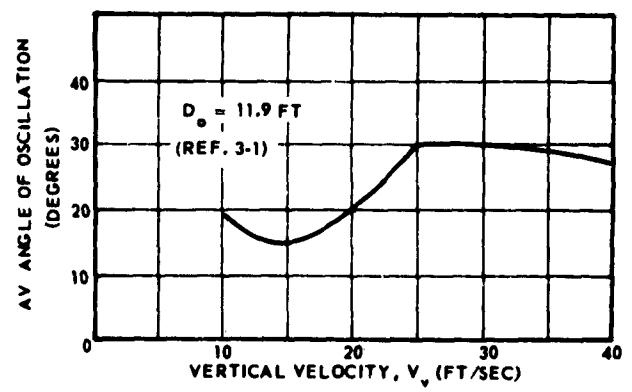
1.1.3.7 *Remarks.* Shaped-gore canopies generally have slightly more bulk and weight than others of comparable performance.

FLAT DEVELOPMENTS FOR
a SURFACE OF REVOLUTION
b FLUTED SURFACE
c PERIPHERAL LOBE





SHAPED-GORE,
HEMISPHERICAL



1.1.4 EXTENDED-SKIRT PARACHUTE CANOPY

1.1.4.1 *Canopy Design (Flat Extended-Skirt Canopy)*. This design is characterized by a flat circular center, to which is added an extension in the form of, an annular ring and of a width designated as a percent of flat circular diameter as shown in (1). The shape of the gore is shown in (2). The nomenclature for this type of canopy includes the size (nominal diameter D_o) and the percent of the extension, in addition to the full name. For example: 52-ft nominal diameter, 10 per cent flat extended-skirt parachute canopy.

1.1.4.2 *Canopy Design (Full Extended-Skirt Canopy)*. This design is characterized by a flat circular center, to which is added an extension in the form of an inverted truncated cone having a top diameter equal to the diameter of the flat circular center portion, as shown in (3). The cone angle is such that the cone formed by the suspension lines is a continuation of the inverted truncated cone extension. The shape of the gore is shown in (4). In this design, angle β is not equal to angle α , and must be determined in order to meet the requirement that the cone of the suspension lines be a continuation of the cone of the extension. The nomenclature for this canopy includes the size (nominal diameter D_o) and the percentage of the extension in addition to the full name. For example: 67.3-ft nominal diameter, 14.3 per cent full extended-skirt canopy.

1.1.4.3 *Drag Coefficient of the Canopy (Flat Extended-Skirt)*. The drag coefficient C_{D_o} averages 0.70; however, it will vary with rate of descent, size, and length of extension. For preliminary calculations, a

C_{D_o} of 0.70 is generally used.

1.1.4.4 *Drag Coefficient of the Canopy (Full Extended-Skirt)*. The drag coefficient C_{D_o} ranges between 0.70 and 0.85, depending on pressure, porosity, rate of descent, and size. For preliminary calculations, a C_{D_o} of 0.75 is generally used.

1.1.4.5 *Stability of the Canopy (Full Extended-Skirt)*. Oscillation of the full extended-skirt canopy generally ranges between ± 10 and ± 20 degrees, depending on design, size, and rate of descent.

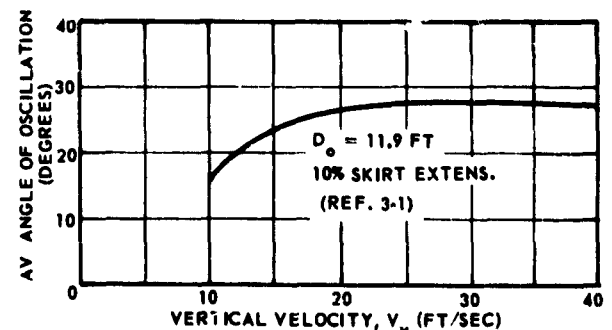
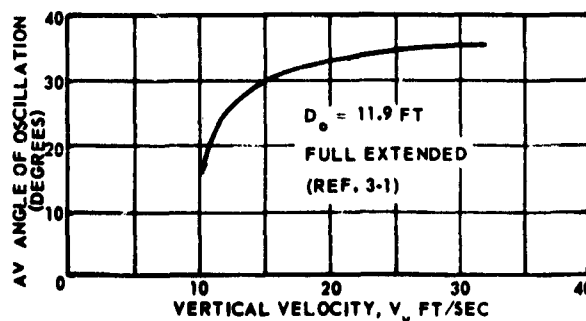
1.1.4.6 *Stability of the Canopy (Flat Extended-Skirt)*. Average oscillation angles for the flat extended-skirt canopy are slightly less than these for the full extended-skirt canopy.

1.1.4.7 *Opening-Shock*. For infinite-mass conditions, the opening-shock factor is approximately 1.8.

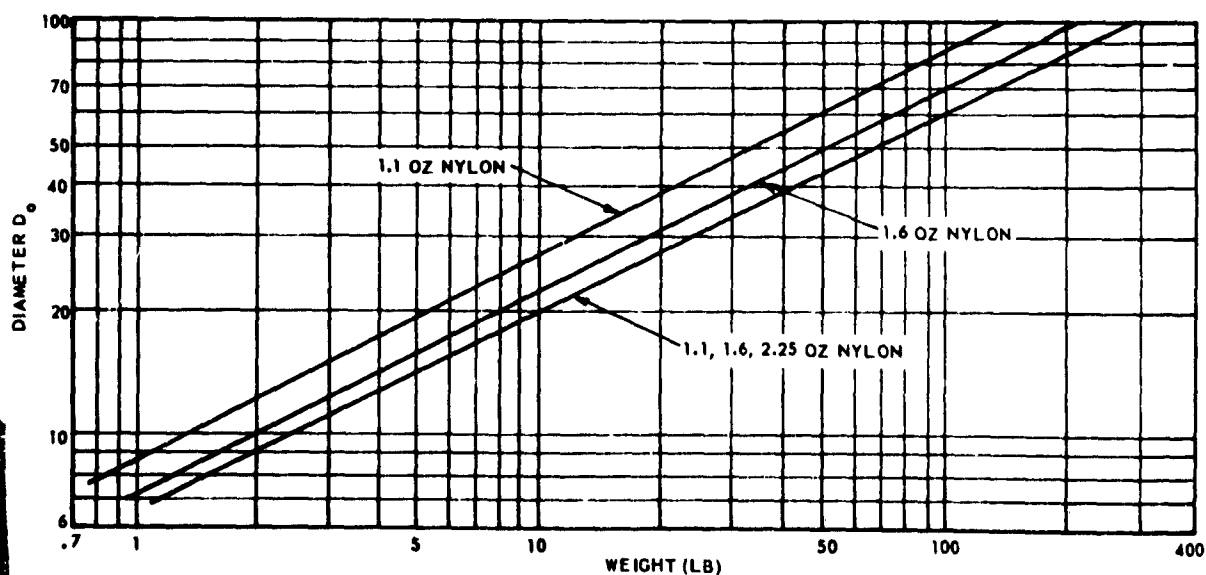
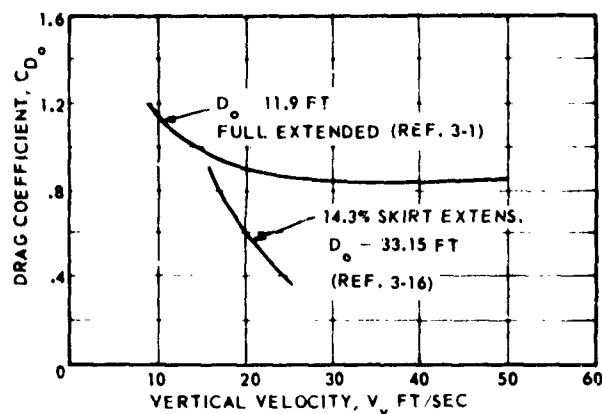
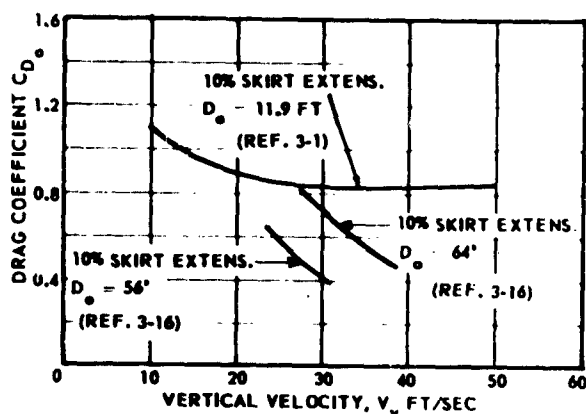
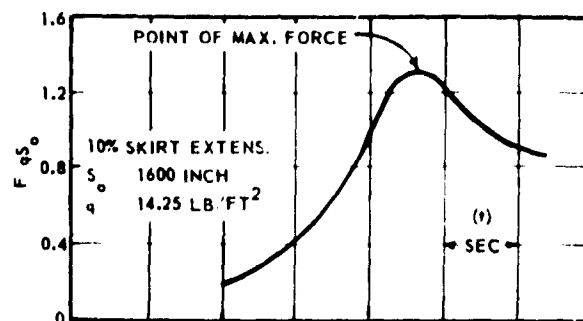
1.1.4.8 *Application*. At present, the full extended-skirt canopy is used only for air drop and for final-stage recovery of aerospace vehicles. The flat extended-skirt canopy is being used for both personnel and air-drop applications.

1.1.4.9 *Opening Reliability and Speed Limitations*. These canopies are considered to be sufficiently reliable for all air-drop applications. The flat extended-skirt canopy with pocket bands is considered to be as reliable as the flat circular canopy and is used for personnel applications. Because of reduced opening-shock forces, these canopies may be used at somewhat higher deployment velocities than those of the flat circular type. Safe deployment speed limitations for several specific canopy-and-load configurations are as follows:

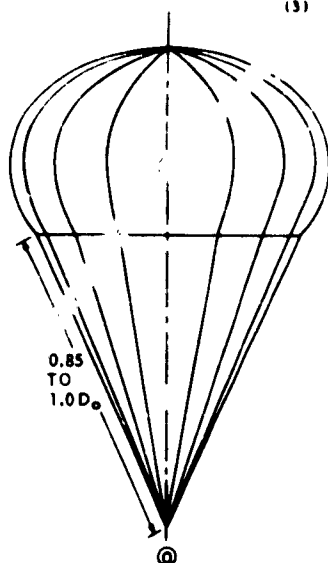
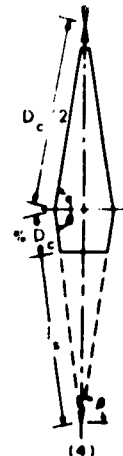
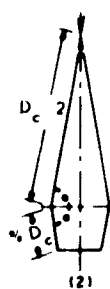
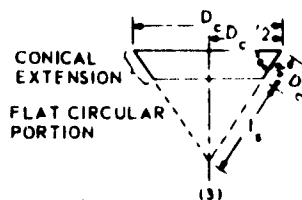
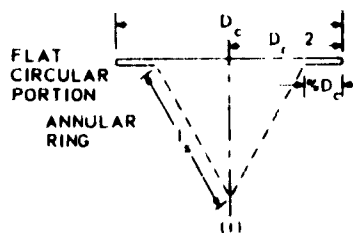
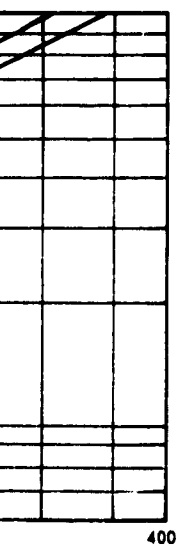
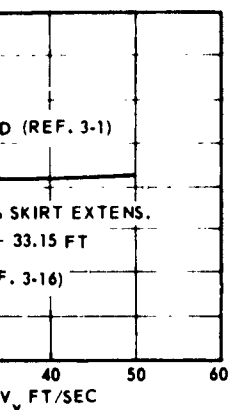
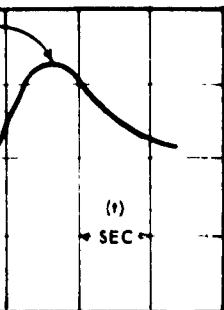
Canopy Type and Diameter	No. of Gores	Suspended Load, lb	Nylon Canopy Material	Lines, lb	Deployment Velocity, Knots
MC-1 35 ft 10% extended (nominal)	28	200	1.1 oz	375	300
67.3 14.3% extended	52	2300	1.1, 2.25 oz	550	275



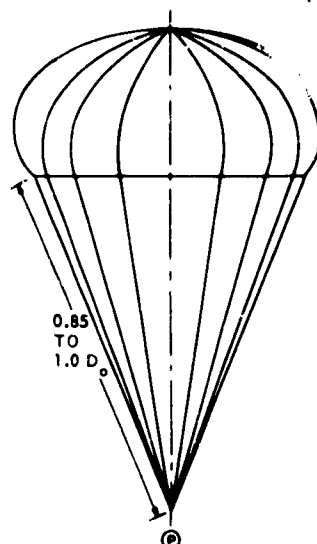
1.1.4.10 Remarks. Because of the lower drag-coefficient, these canopies are slightly more bulky than the flat circular type for identical rates of descent. In a similar respect, manufacturing costs are slightly higher than those for the flat circular type.



1

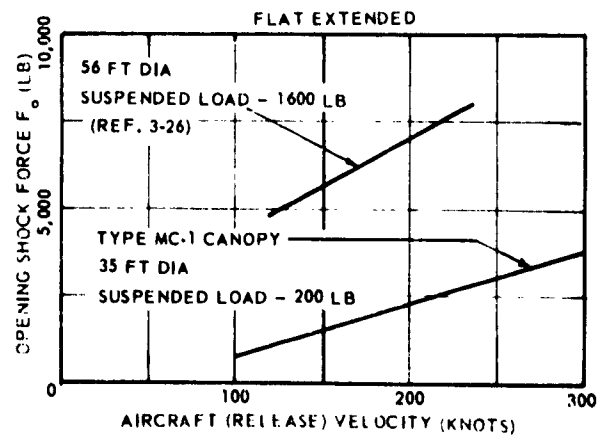
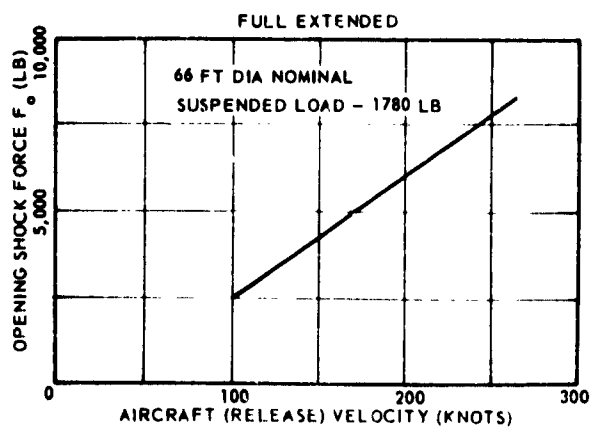


FLIGHT PROFILE
FULL EXTENDED-SKIRT



FLIGHT PROFILE
10% EXTENDED SKIRT

2



1.1.5 RIBLESS GUIDE-SURFACE CANOPY

1.1.5.1 *Canopy Design.* This type is constructed of bell-shaped roof panels and guide-surface panels, joined together to form the main seams.

1.1.5.2 *Drag Coefficient.* The drag coefficient C_{Dp} averages between 0.75 and 0.85. For preliminary calculations, C_{Dp} value of 0.80 is generally used.

1.1.5.3 *Stability.* This canopy is extremely stable and has excellent damping characteristics. Oscillation in free air is below ± 3 deg.

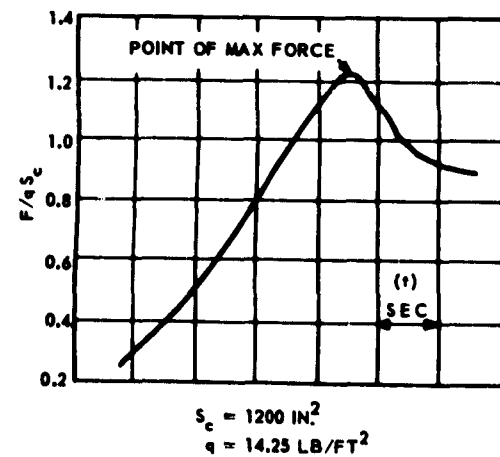
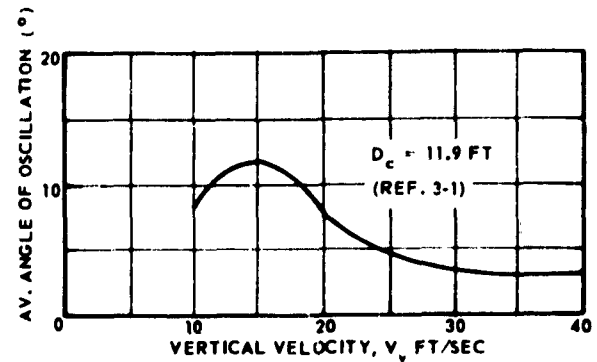
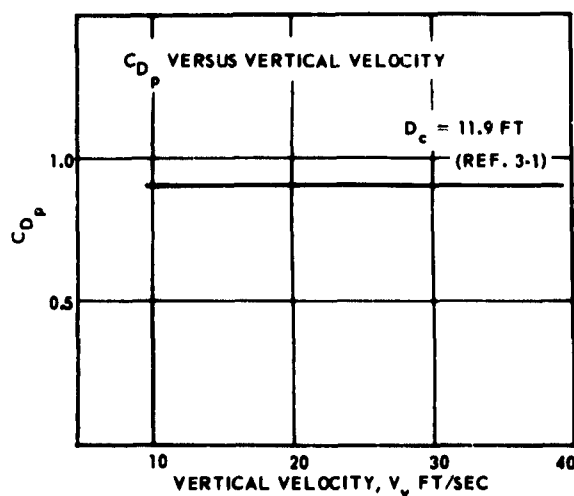
1.1.5.4 *Opening-Shock.* For infinite-mass conditions, the opening-shock factor ranges between 1.1 and 1.4, depending on specific design characteristics.

1.1.5.5 *Application.* This canopy may be used for stabilization, deceleration, or extraction applications, and for other applications requiring extreme stability, quick opening, and high reliability.

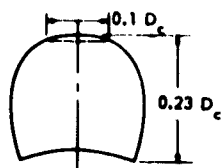
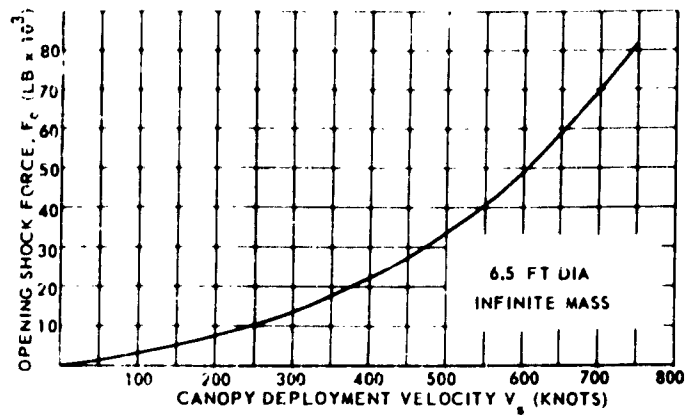
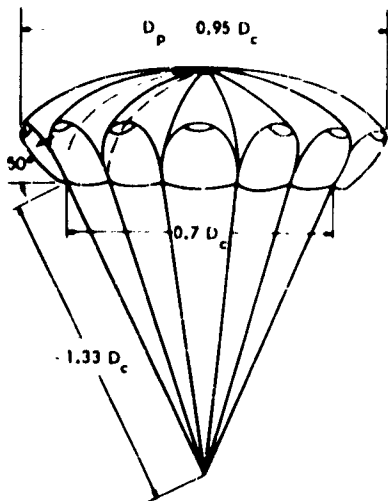
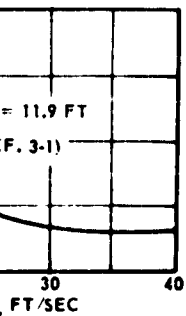
1.1.5.6 *Opening Reliability and Speed Limitations.* In most applications this canopy is highly reliable. Deployment speed limitations for specific canopy configurations and nearly infinite-mass conditions are as follows:

Canopy Diameter, ft	Suspended Load (Sled Test)	No. of Gores	Nylon Canopy Material, oz	Lines, lb	Deployment Velocity, Knots
6.5	Infinite mass	12	4.75	2250	360
6.5	Infinite mass	16	14	9000	720

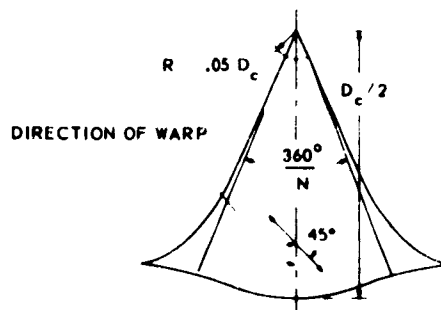
1.1.5.7 *Remarks.* The manufacturing cost of this canopy type is somewhat less than that of the ribbed type. For most applications it can replace the ribbed type.



1

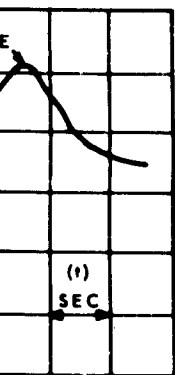


TYPICAL GUIDE SURFACE
PANEL

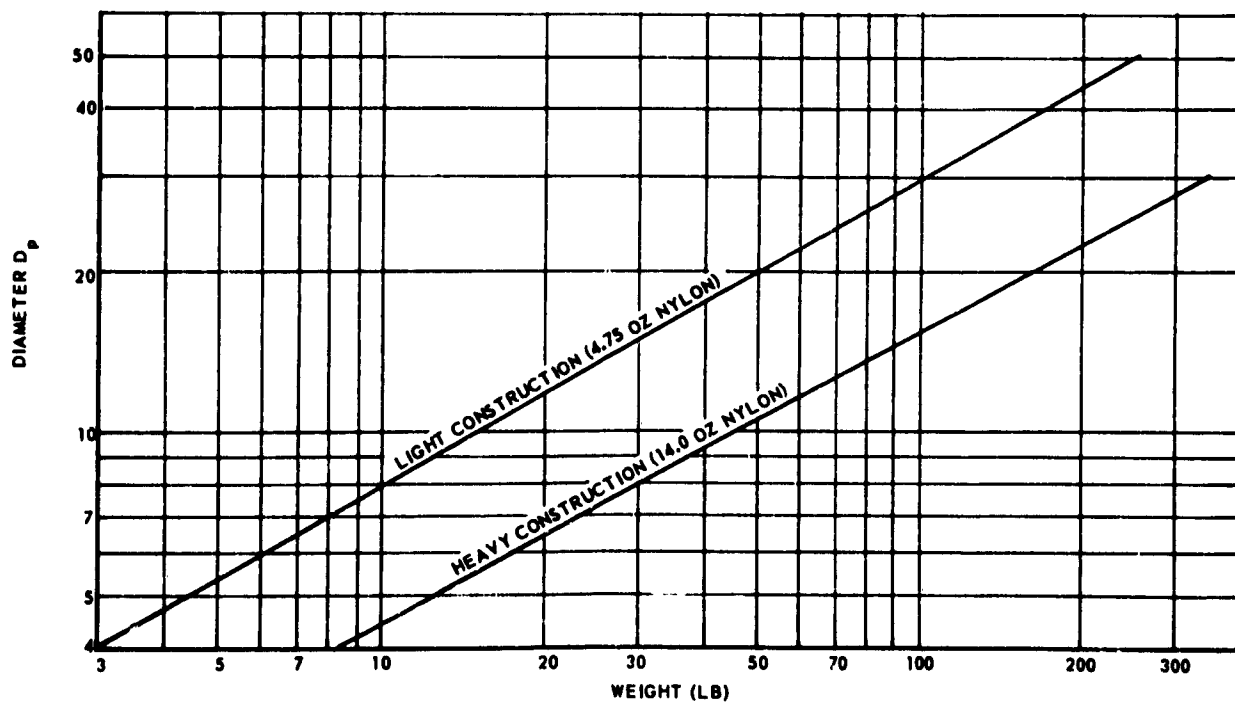


TYPICAL TOP PANEL

2



/FT²



1.1.6 RIBBED GUIDE-SURFACE CANOPY

1.1.6.1 *Canopy Design.* This canopy is intricate in shape. It is constructed of roof panels, guide-surface panels, and internal ribs joined together to form the main seams.

1.1.6.2 *Drag Coefficient.* The drag coefficient CD_p ranges upward from 0.8. For preliminary calculations, a CD_p value of 0.95 is generally used.

1.1.6.3 *Stability.* This parachute canopy is extremely stable. Oscillation in free stream averages below ± 2 deg.

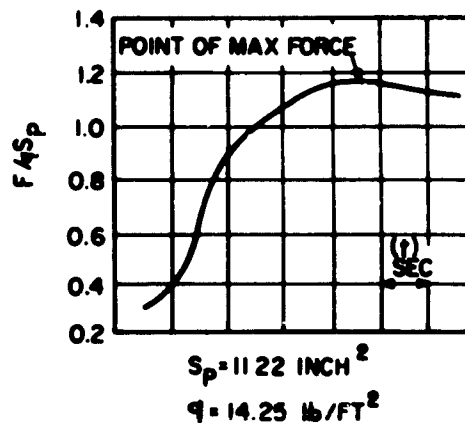
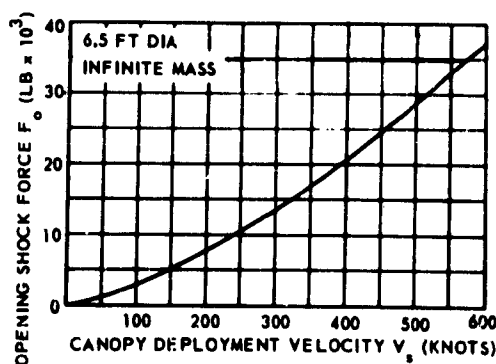
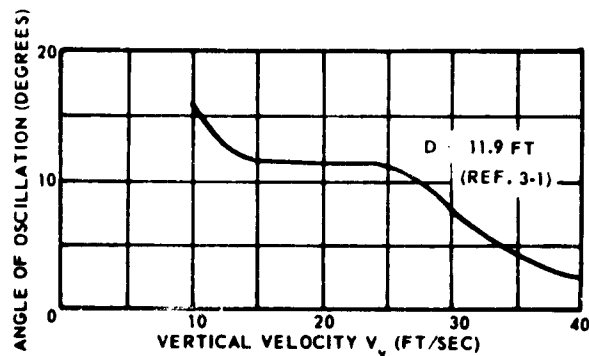
1.1.6.4 *Opening Shock.* For infinite-mass conditions, the opening-shock factor is approximately 1.1.

1.1.6.5 *Application.* This canopy may be used for stabilization and deceleration, or for other applications where extreme stability, reliability, and uniformity of the functional sequence are required.

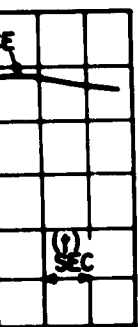
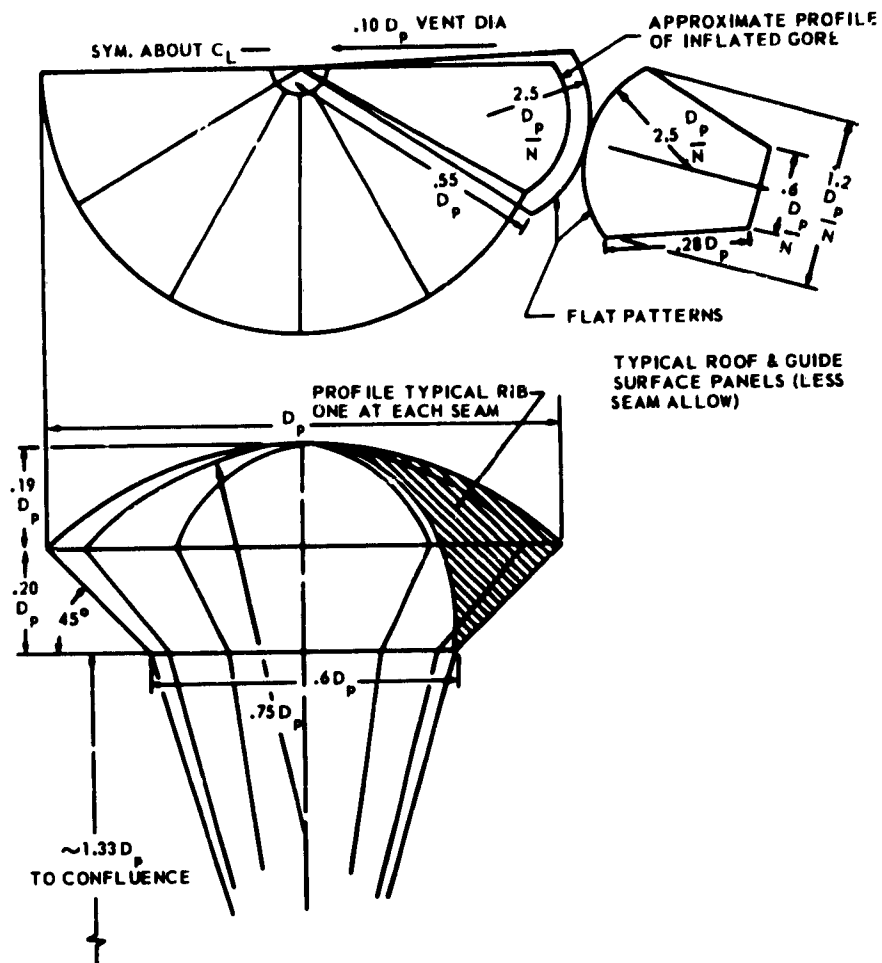
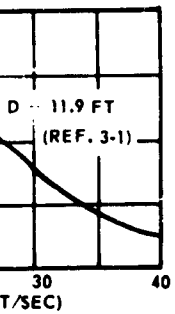
1.1.6.6 *Opening Reliability and Speed Limitations.* In most applications, this canopy is highly reliable. Safe deployment speed limitations for several specific canopy configurations and nearly infinite-mass conditions are as follows:

Canopy Diameter, ft	Suspended Load (Sled Test)	No. of Gores	Nylon Canopy Material, oz	Lines, lb	Deployment Velocity, Knots
6.5	Infinite mass	12	7	2250	405
6.5	Infinite mass	16	14	9000	650

1.1.6.7 *Remarks.* This canopy is somewhat difficult to manufacture, and manufacturing cost is relatively high. The ribless guide-surface canopy will replace the ribbed type in many applications.

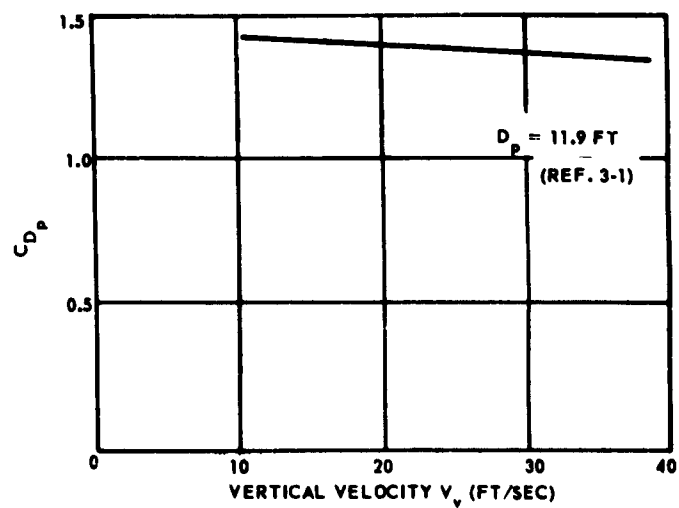


1



H^2
 FT^2

2



1.1.7 PERSONNEL GUIDE-SURFACE CANOPY

1.1.7.1 Canopy Design. The roof panels are identical in construction to those of the flat circular canopy. Alternate roof panels are extended to provide the guide surfaces. The guide surfaces somewhat resemble those found in ribless guide-surface canopies.

1.1.7.2 Drag Coefficient. The drag coefficient C_{D_0} of this canopy is only slightly less than that of the flat circular type. For preliminary calculations, a C_{D_0} value of 0.72 is generally used.

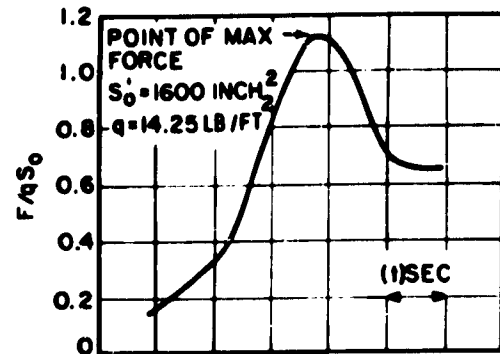
1.1.7.3 Stability. This canopy is considered to have marginal stability. Oscillations in free-stream are somewhat less than those for the extended-skirt canopies.

1.1.7.4 Opening-Shock. For infinite-mass conditions, the opening-shock factor approaches 1.6.

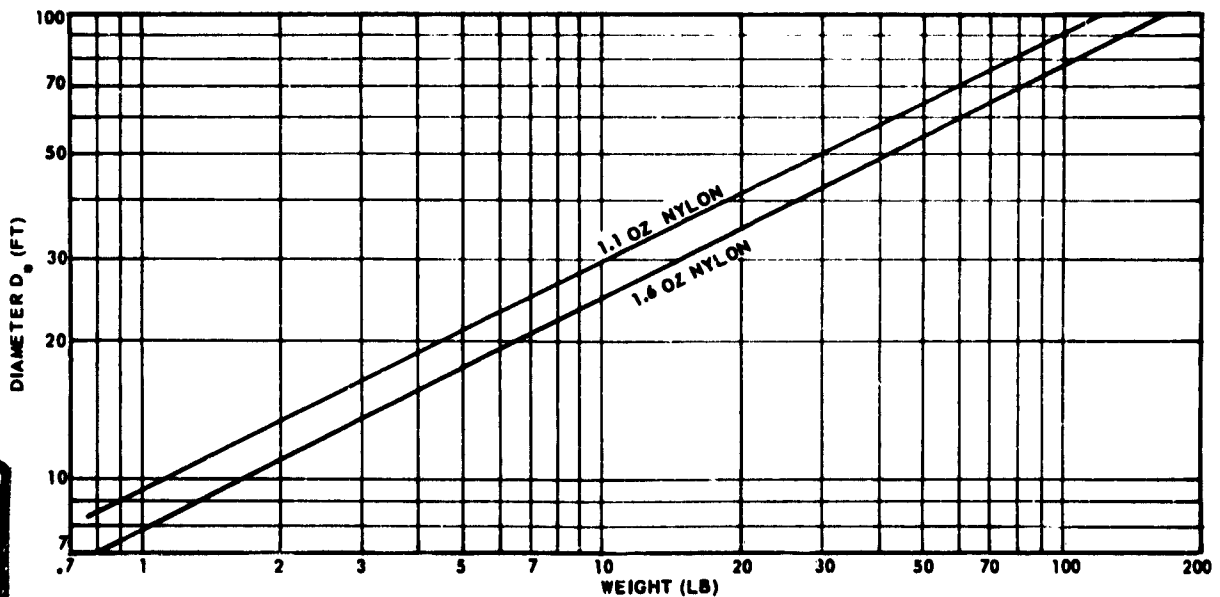
1.1.7.5 Application. This canopy has all the advantages of the flat circular canopy, plus improvements in maximum operational speed and stability, as well as in reduced opening-shock. However, opening time is longer compared to the flat circular or extended-skirt canopies.

1.1.7.6 Opening Reliability and Speed Limitations. For most applications, this canopy type is reliable, and can be used up to 375 knots bailout velocity for the following canopy and suspended-load configuration:

1.1.7.7 Remarks. The guide-surface extensions add only slightly to the manufacturing cost. The bulk, weight, and rate of descent are approximately the same as for a flat circular canopy of comparable performance.

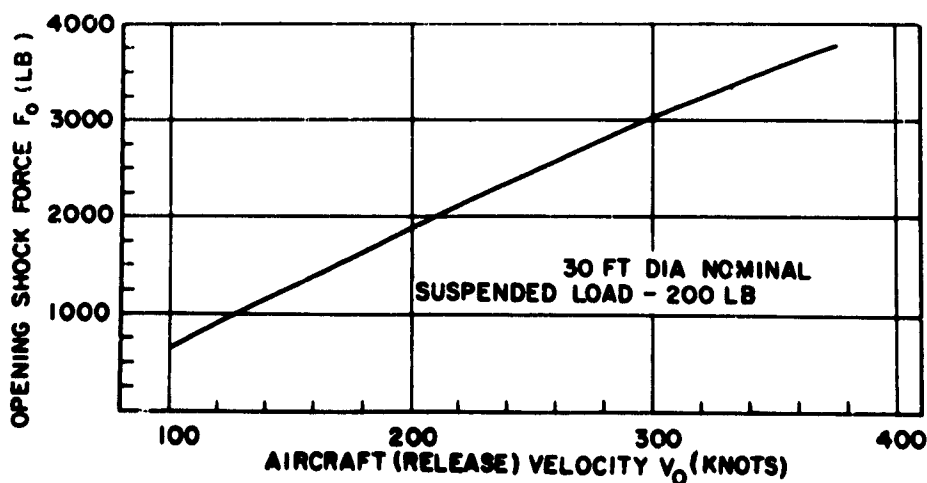
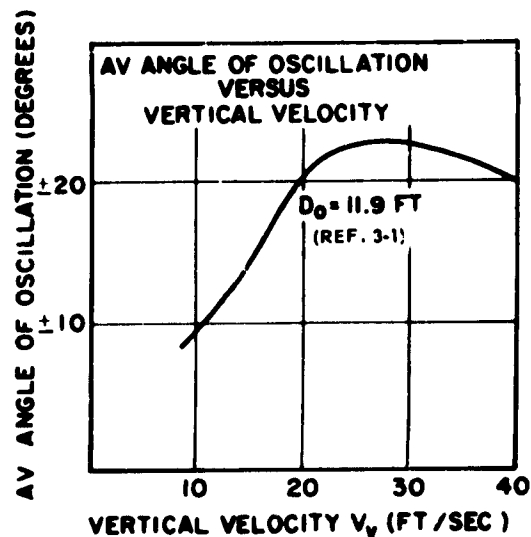
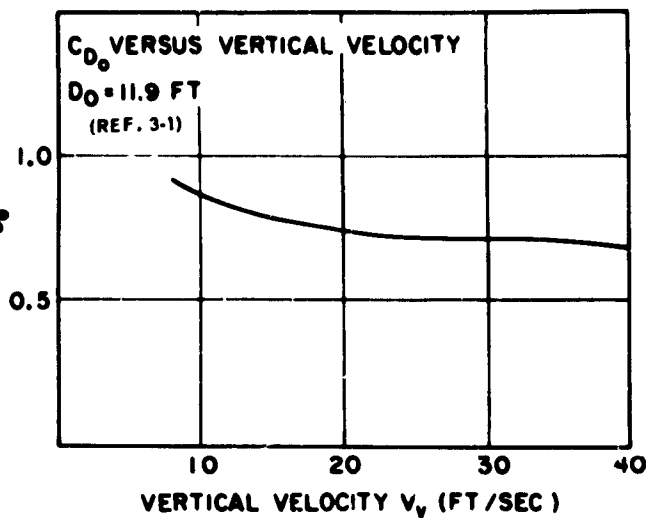
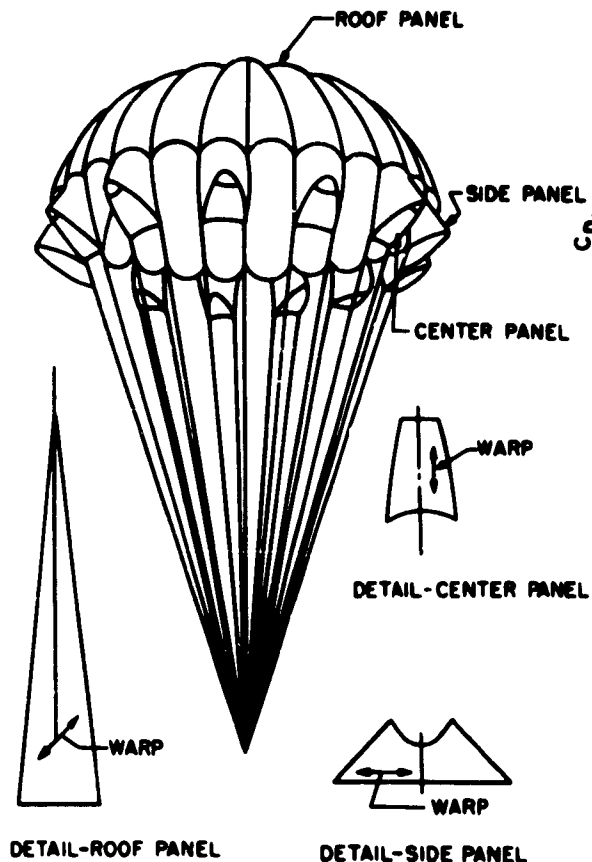
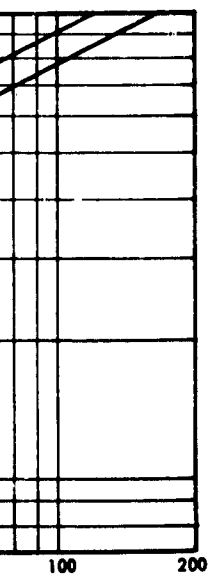
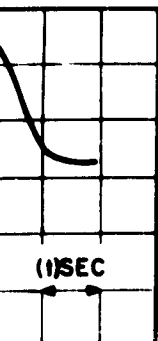


Canopy Nominal Diameter, Ft	No. of Gores	Suspended Load, lb	Nylon Canopy Material, oz	Lines, lb	Deployment Velocity, Knots
30	24	200	1.1	375	375



1

surface extensions
ing cost. The bulk,
oximately the same
arable performance.



1.1.8 MODIFIED RIBLESS GUIDE-SURFACE CANOPY

1.1.8.1 *Canopy Design.* This canopy is constructed by joining gore panels which have been formed from a single gore-pattern rather than the two required in constructing the ribless guide-surface canopy.

1.1.8.2 *Drag Coefficient.* The drag coefficient C_{Dp} varies between 0.75 and 0.85. For preliminary calculations, a C_{Dp} value of 0.78 is generally used.

1.1.8.3 *Stability.* This parachute canopy is not as stable as the ribless guide-surface canopy. Oscillation in free stream is less than ± 5 deg.

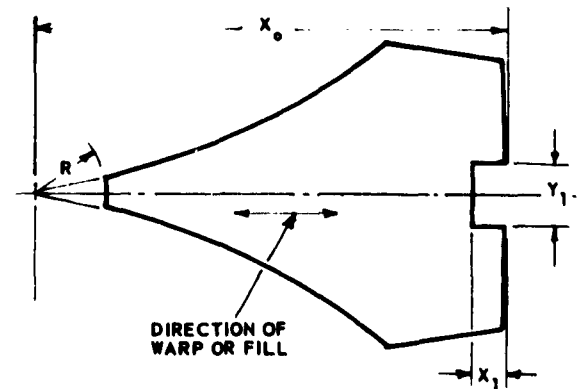
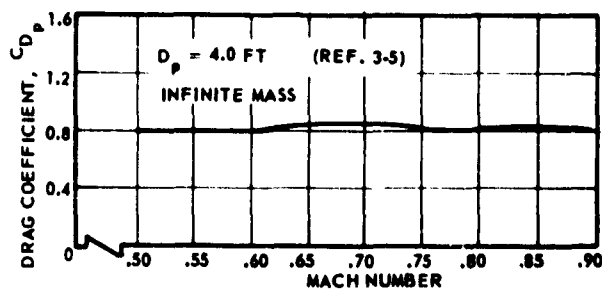
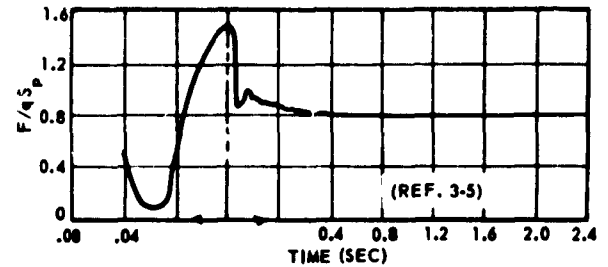
1.1.8.4 *Opening-Shock.* For infinite-mass conditions, the opening-shock factor ranges between 1.1 and 1.4, depending on specific design characteristics.

1.1.8.5 *Application.* This canopy may be used for stabilization, deceleration, or extraction, and for other first-stage applications requiring a high degree of stability and reliable functioning.

1.1.8.6 *Opening Reliability and Speed Limitations.* This canopy has good, reliable opening-characteristics. Deployment conditions for one specific canopy under infinite-mass conditions are as follows:

Canopy Diameter	Suspended Load, lb	No. of Gores	Nylon Canopy Material, oz
MC 14-75 30"	2200	6	7

1.1.8.7 *Remarks.* The manufacturing cost of this canopy is somewhat lower than that of the ribless type. For most extraction applications it can replace the ribless type.



$$X_0 = .55 D_{max}$$

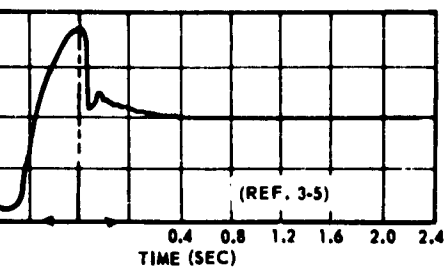
$$R = 0.1 D_{max}$$

$$X_1 = 0.5 Y_1$$

$$Y_1 = D_{max} / N \text{ WHERE } N = \text{NO. OF GOES}$$

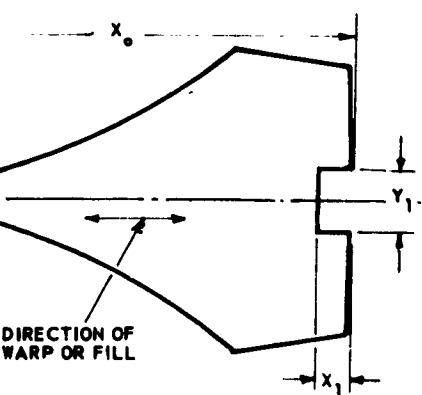


Remarks. The manufacturing cost of this is somewhat lower than that of the ribless type. In most extraction applications it can replace the type.

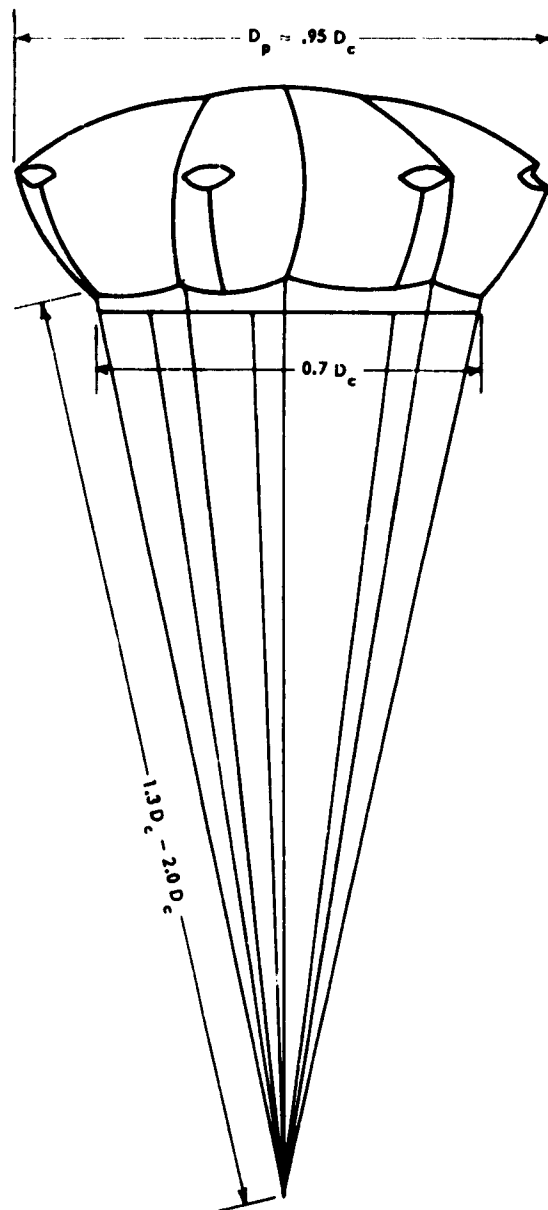


Deployment
Velocity, Knots

380



max
max
/N WHERE N = NO. OF GORES



2

1.2 Ribbon Parachute Canopies

1.2.1 FLAT CIRCULAR RIBBON CANOPY

1.2.1.1 *Canopy Design.* This canopy is of flat circular design and is composed of concentric ribbons, supported by a number of radial ribbons and smaller supporting tapes.

1.2.1.2 *Drag Coefficient.* The drag coefficient C_{D_0} ranges between 0.45 and 0.55, depending on design, size, and applications. For preliminary design purposes, a C_{D_0} value of 0.5 is generally used.

1.2.1.3 *Stability.* This canopy is very stable. Oscillations in free stream reach a maximum of ± 5 deg.

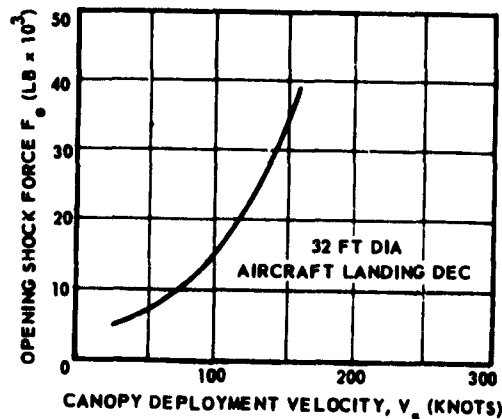
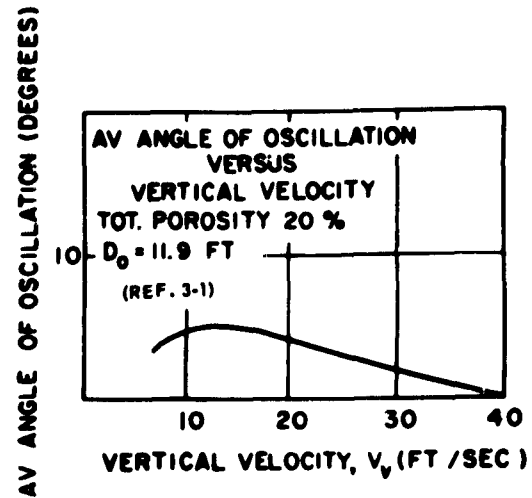
1.2.1.4 *Opening-Shock.* For infinite-mass conditions, the opening-shock is approximately 1.05.

1.2.1.5 *Application.* This canopy is especially adaptable for deceleration when good stability, drag, and high-speed deployment are required.

1.2.1.6 *Opening Reliability and Speed Limitations.* This canopy is relatively slow in opening. Opening reliability depends on specific design parameters. Safe deployment-speed limitations for specific canopy configurations and nearly infinite-mass conditions are as follows:

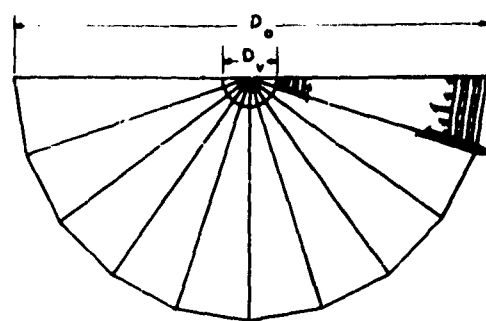
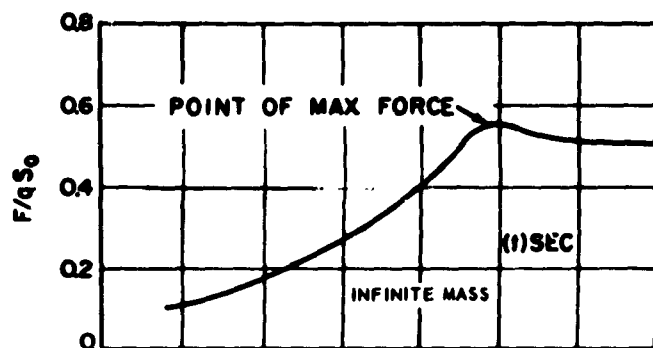
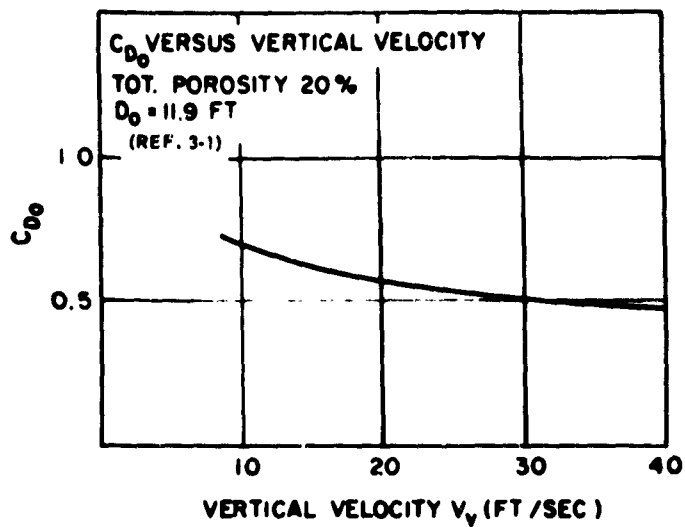
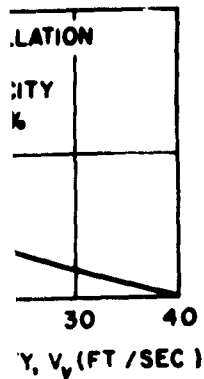
Canopy Diameter, ft	No. of Gores	Suspended Load	Nylon Canopy Ribbon	Lines, lb	Deployment Velocity, Knots
32	36	(Aircraft deceleration)	300 lb	2250	160
44	48	(Aircraft deceleration)	300 lb	4000	160

1.2.1.7 *Remarks.* This canopy is relatively easy to manufacture.

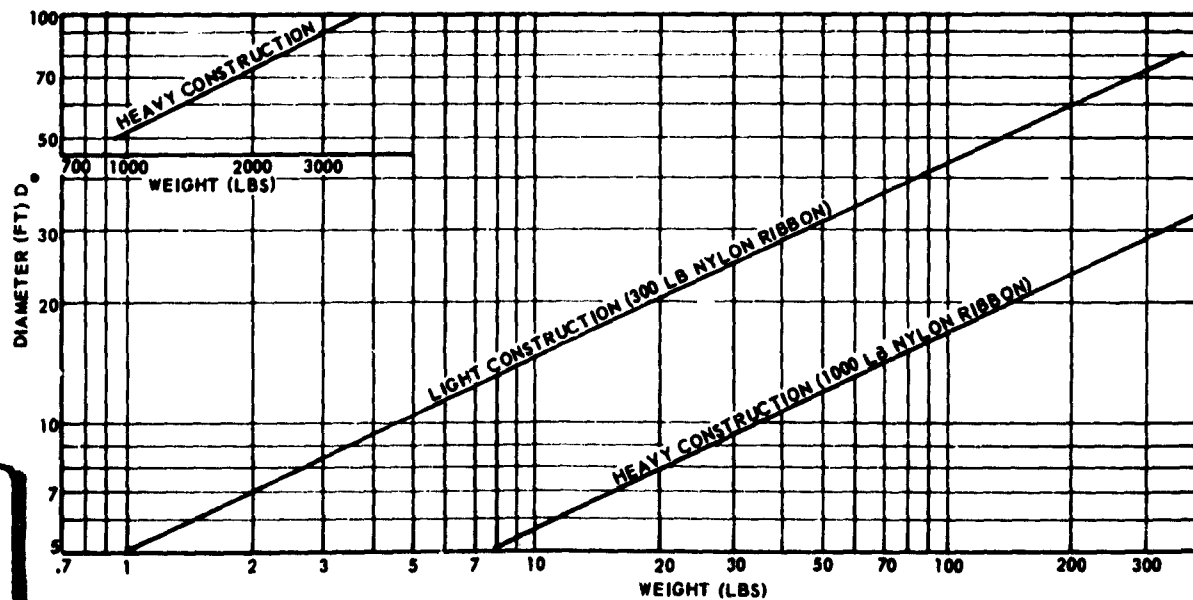
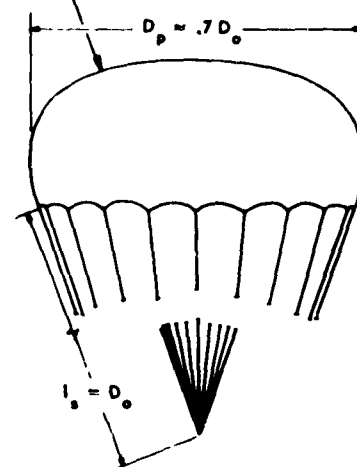


1

py is relatively easy



TYP. INFLATED PROFILE



2

1.2.2 CONICAL RIBBON CANOPY

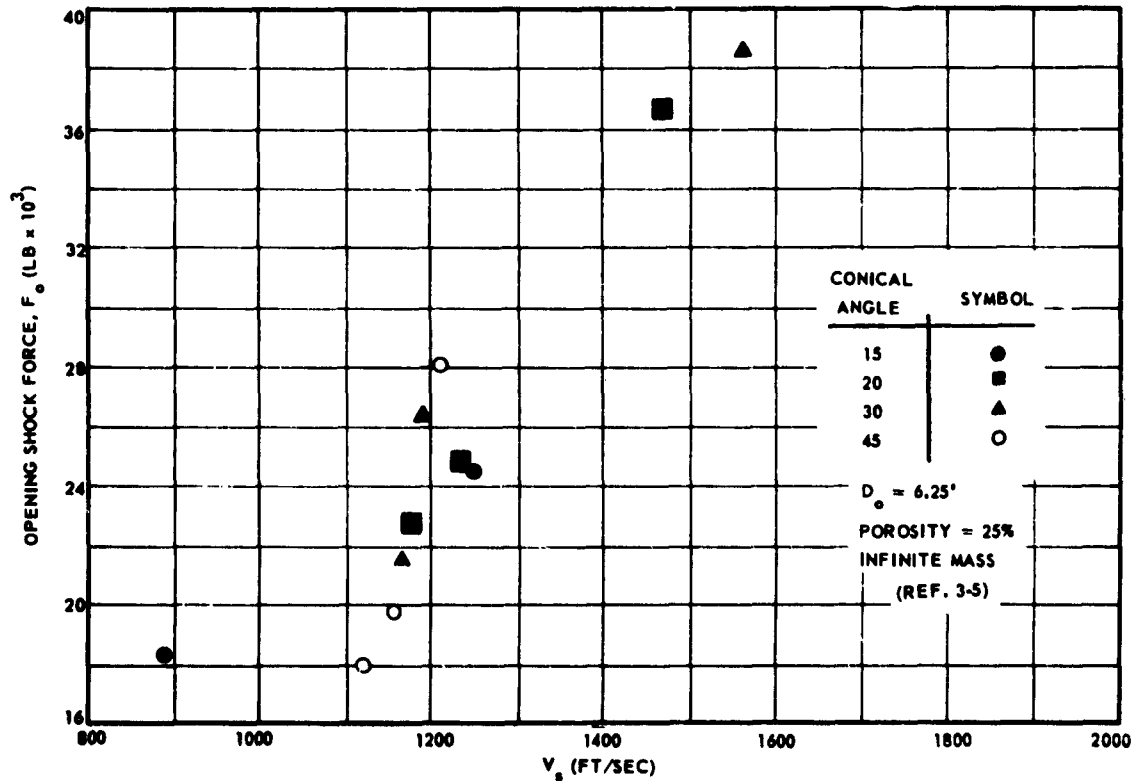
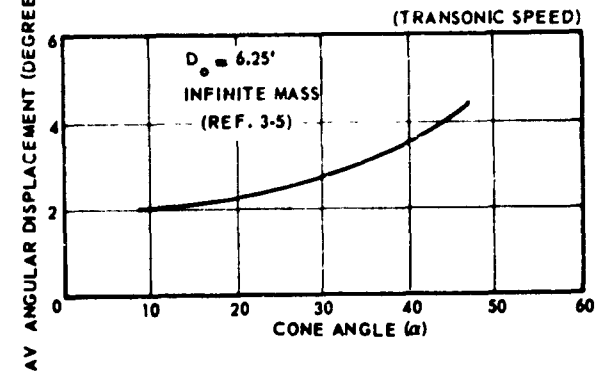
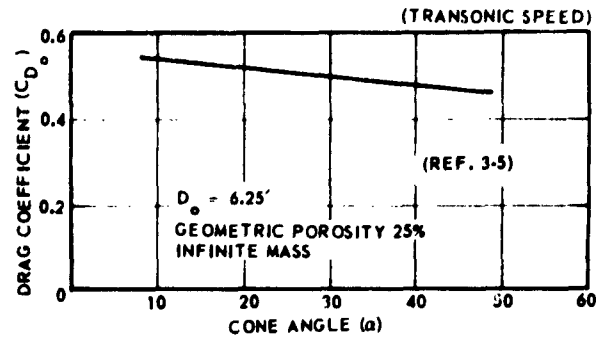
1.2.2.1 Canopy Design. The constructed shape of this canopy is obtained in the same manner as that described for the solid cloth conical canopy. The gores of this canopy, like the flat circular ribbon design, are composed of a grid of horizontal ribbons spaced and retained at close intervals by one or more vertical tapes. Radial bands extend from the vent to the skirt, joining adjacent gores.

1.2.2.2 Drag Coefficient. The drag coefficient, C_{D_0} , of this canopy ranges from 0.45 to 0.55, depending upon size, cone angle, and rate of descent. For preliminary calculations a drag coefficient C_{D_0} of 0.50 may be used.

1.2.2.3 Stability. This canopy is very stable. Oscillation in free stream, for a canopy with a 20-deg cone angle, reaches a maximum of ± 3 deg.

1.2.2.4 Opening Shock. For infinite-mass conditions, the opening shock is approximately 1.00.

1.2.2.5 Application. This canopy is adaptable where good stability and high-speed deployment are prime requirements.



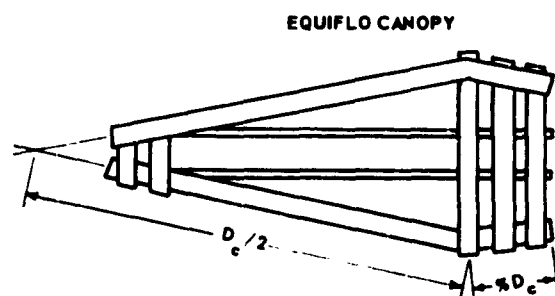
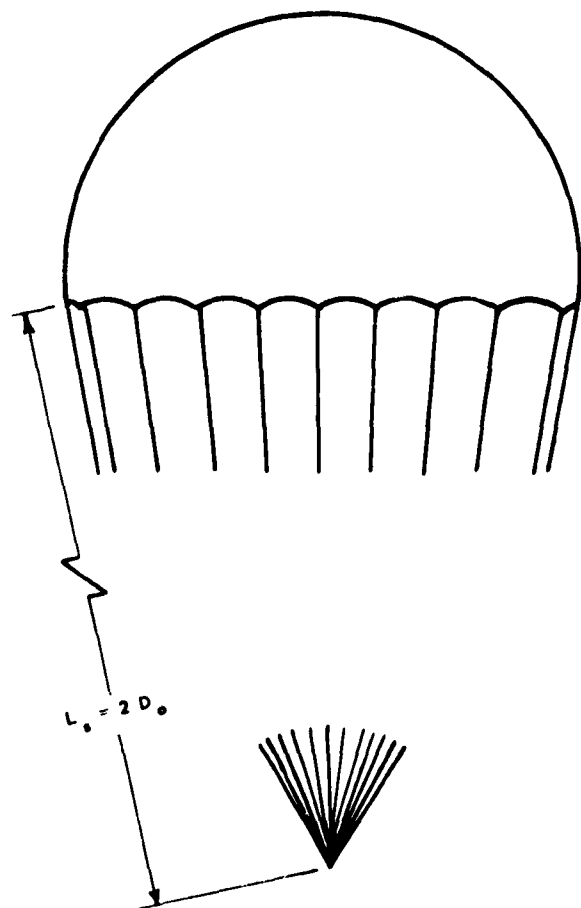
1.2.3 SHAPED-GORE RIBBON CANOPIES

Extension of the operational capabilities of ribbon canopies into the supersonic speed regime has led to the development of shaped-gore ribbon canopies. Of various canopy configurations investigated, two specific types have shown performance characteristics of superior nature: the Equiflo and the Hemisflo (Ref (3-5) and (3-9)).

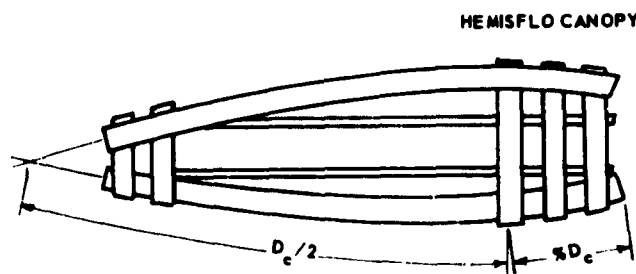
The upper portion of the Equiflo has a flat circular design, with a skirt extension added to the areas between adjacent suspension lines. The extension is expressed as a percentage of the constructed diameter. Standard ribbon-parachute construction is used.

The upper portion of the Hemisflo has a hemispherical design, with a skirt extension added to the areas between adjacent suspension lines. The constructed diameter is considered to be the circumferential distance of the hemispherical portion, measured from skirt edge to skirt edge over the apex of the canopy. Suspension-line length is related to this diameter.

Typical gore assemblies for these two canopies are shown below. Performance characteristics of the Equiflo and Hemisflo canopies in the supersonic flow regime are discussed in Chap. 4, Section 6.



EQUIFLO CANOPY



HEMISFLO CANOPY

Canopy Type & Nom Diam	Suspended Load	Ribbon Material	Lines	No. of Gores	Deployment Dyn Pressure, psf	Canopy Wt, lb
6.24 ft Hemisflo	Infinite mass (sled test)	2" 1500 lb	$2 D_o$ 6000 lb	16	794	19.4
4.12 ft Hemisflo	800 lb	1-1/4" 280 lb	$2 D_o$ 1000 lb	16	530	3.38
2.02 ft Hemisflo	230 lb	1-1/4" 650 lb	$2 D_o$ 550 lb	16	560	1.88
6.2 ft Equiflo	Infinite mass (sled test)	2" 1500 lb	$2 D_o$ 6000 lb	16	1500, 3340	20.7
4.03 ft Equiflo	800 lb	1-1/4" 120 lb	$2 D_o$ 350 lb	16	135	1.06

1.2.4 RING-SLOT CANOPY

1.2.4.1 Canopy Design. This canopy is of flat circular design. The canopy consists of wide, concentric, cloth strips with intervening air slots. The number of slots varies, depending upon canopy diameter.

1.2.4.2 Drag Coefficient. The drag coefficient C_{D_0} varies between 0.45 and 0.65, depending upon rate of descent and design. For preliminary calculations, a C_{D_0} value of 0.55 is generally used.

1.2.4.3 Stability. Most designs are very stable. Maximum oscillation angle is less than ± 10 degrees.

1.2.4.4 Opening-Shock. For infinite-mass con-

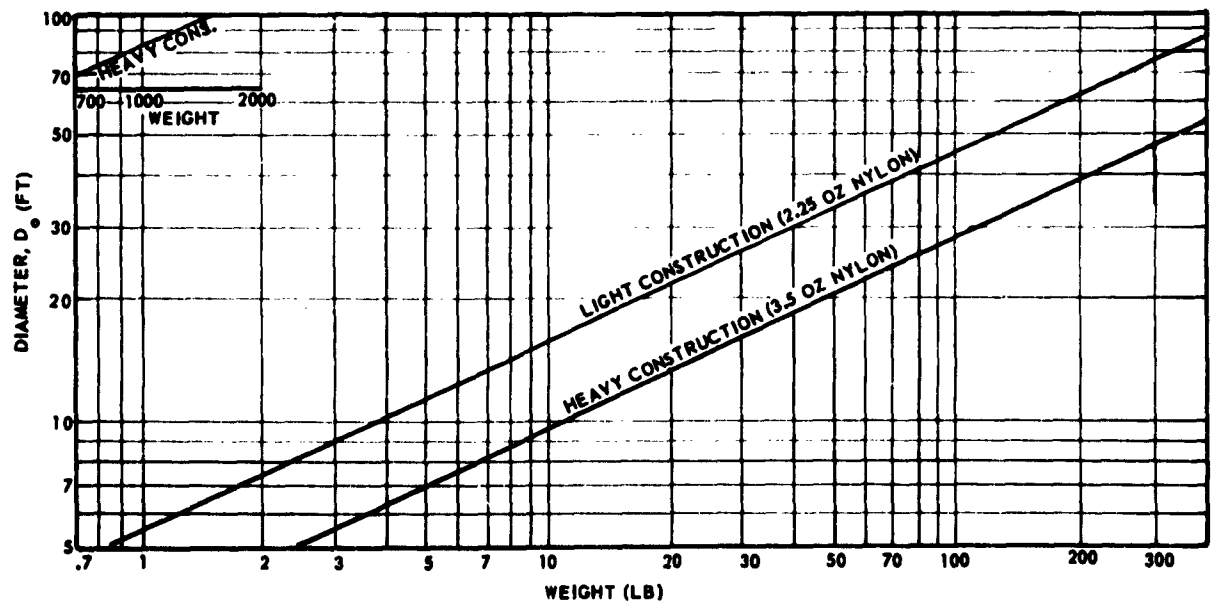
ditions, the opening-shock factor is approximately 1.05.

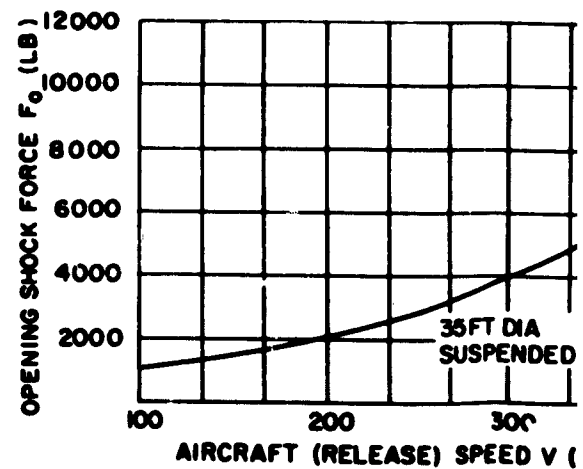
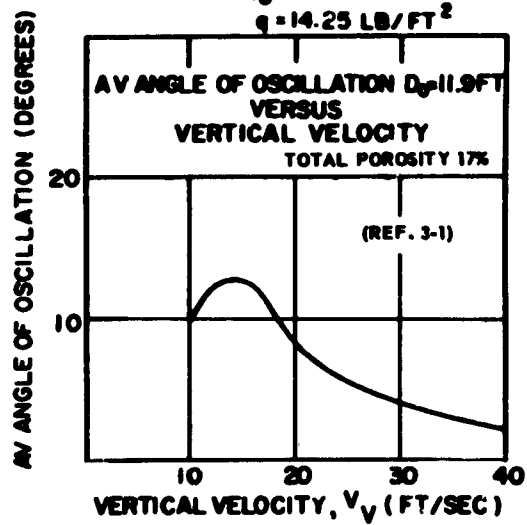
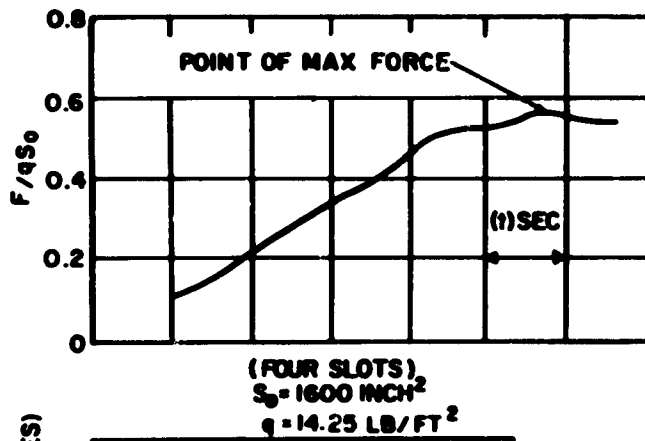
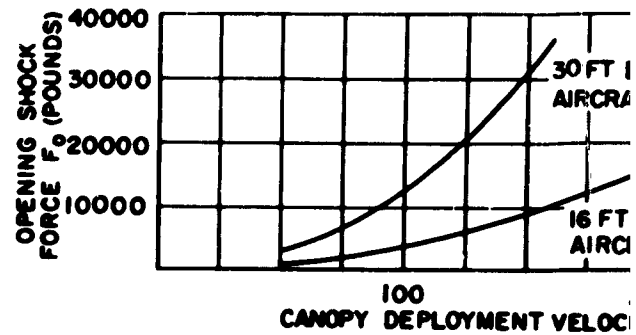
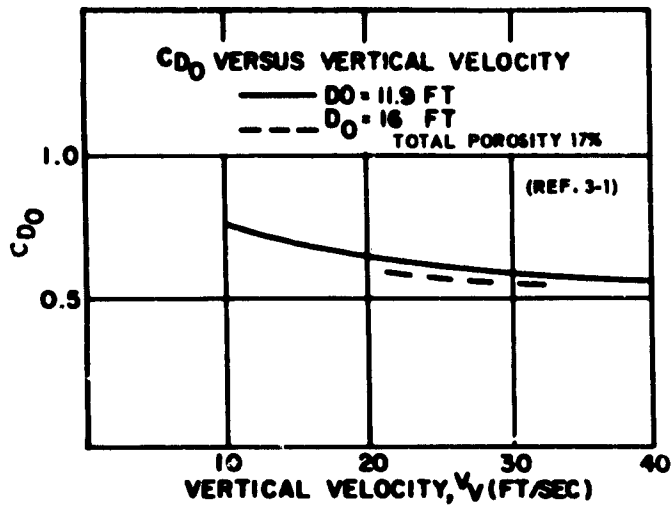
1.2.4.5 Application. These canopies may be used for deceleration or air-drop applications. They are also satisfactory as descent or recovery parachute canopies, when less oscillation and higher deployment speed than that found in the flat circular canopy is desired.

1.2.4.6 Opening Reliability and Speed Limitations. Opening reliability is comparable to that of flat circular ribbon canopy designs. Safe deployment velocities for some specific canopy and suspended-load configurations are as follows:

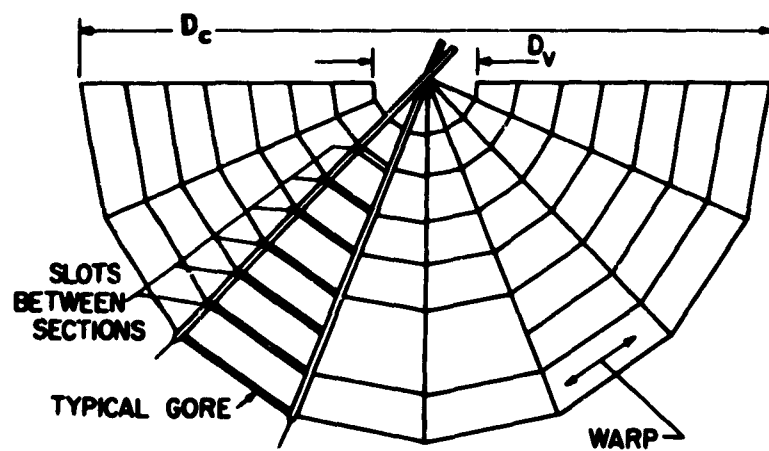
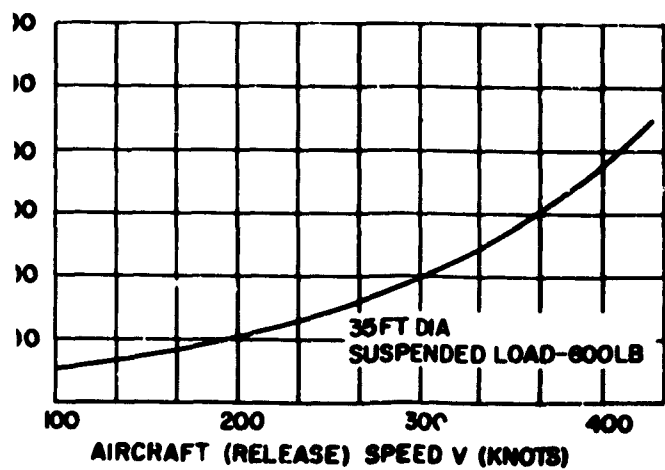
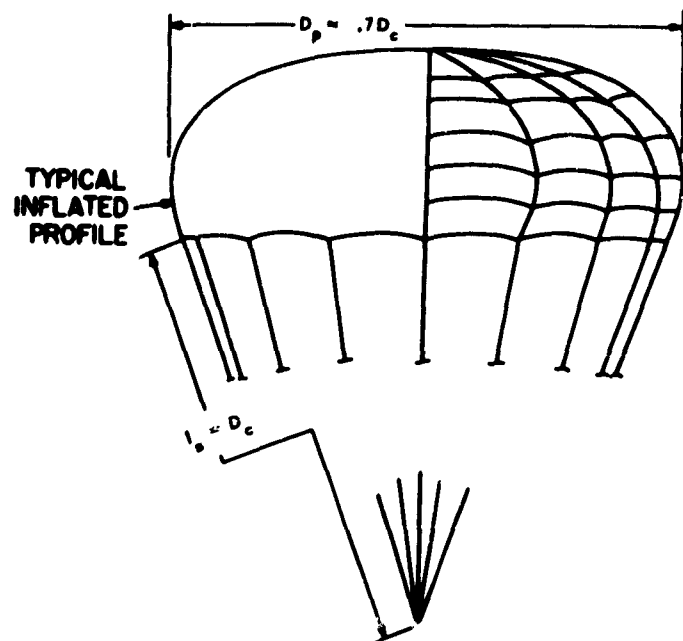
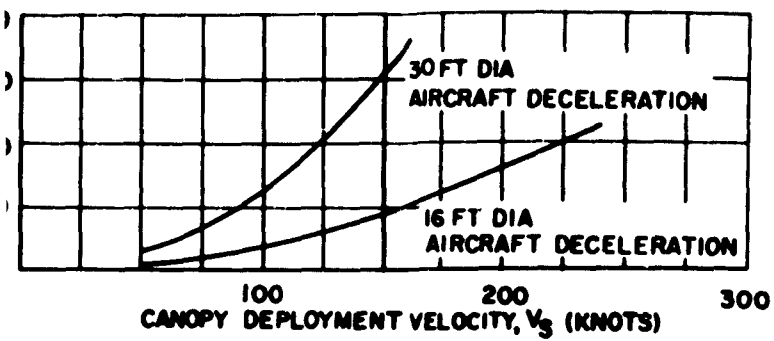
Canopy Diameter, ft	No. of Gores	Suspended Load, lb	Canopy Material & Lines Nylon, oz lb		Deployment Velocity, Knots
12	16	500	10	10,000	650
14.5	20	Aircraft Deceleration	2.25	1,500	160
16.0	20	500	2.25	1,500	195
16.0	20	Aircraft Deceleration	3.5	2,250	240
20	24	Aircraft Deceleration	2.25	1,500	200
24	28	Aircraft Deceleration	3.5	4,000	230
28	28	Aircraft Deceleration	2.25 & 3.5	2,250	175

1.2.4.7 Remarks. At the present time, this parachute canopy is more costly to manufacture than the flat circular canopy. It is less expensive to manufacture than the flat circular ribbon canopy, and is being substituted for the flat circular ribbon type for some applications.





1



2

1.2.5 RING-SAIL CANOPY (SKY-SAIL)

1.2.5.1 Canopy Design. This canopy was developed by Radioplane Company, Van Nuys, Calif. The ring-sail canopy is of the annular-ring type developed on a spherical surface by a unique system of gore coordinates. The basic shape is a quarter sphere. The slots in each gore are crescent-shaped rather than trapezoidal (except in the crown). The number of rings in the canopy is usually determined by the ratio of the canopy radius to the woven width of the cloth.

1.2.5.2 Drag Coefficient. The drag coefficient C_{D0} varies between 0.70 and 0.95, depending upon rate of descent and design. For preliminary calculations a C_{D0} value of 0.78 is generally used.

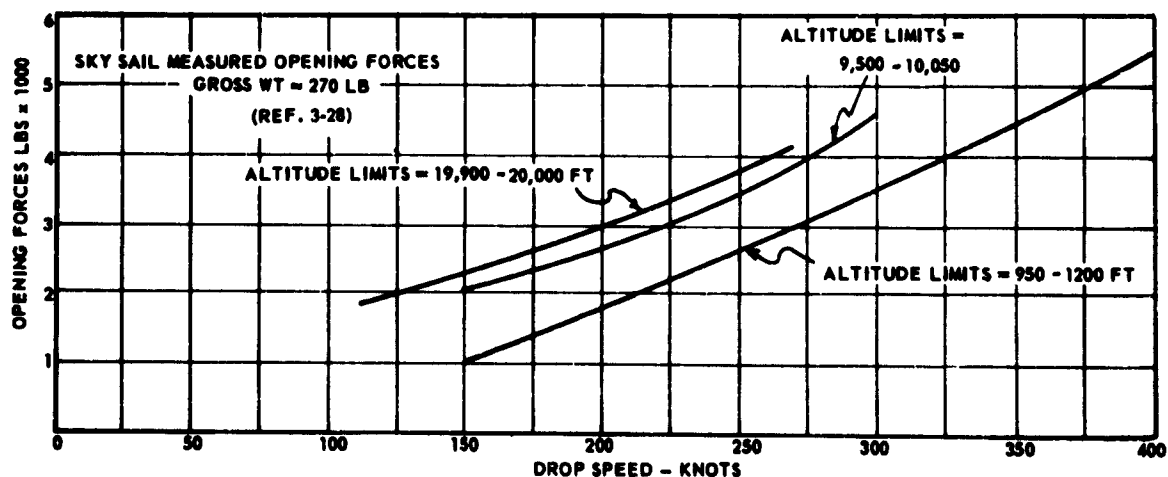
1.2.5.3 *Stability.* The average amplitude of oscillations of the ring-sail canopy is less than ± 10 deg.

1.2.5.4 Opening-Shock. For infinite-mass conditions, the opening-shock factor is approximately 1.05.

1.2.5.5 Application. These canopies may be used for recovery applications where excessive oscillation must be avoided and where the required speed is above the safe limits of solid cloth canopies.

1.2.5.6 Opening Reliability and Speed Limitations. The ring-sail canopy opens reliably, either reefed or non-reefed. Safe deployment velocities for some specific canopy and suspended-load configurations are as follows:

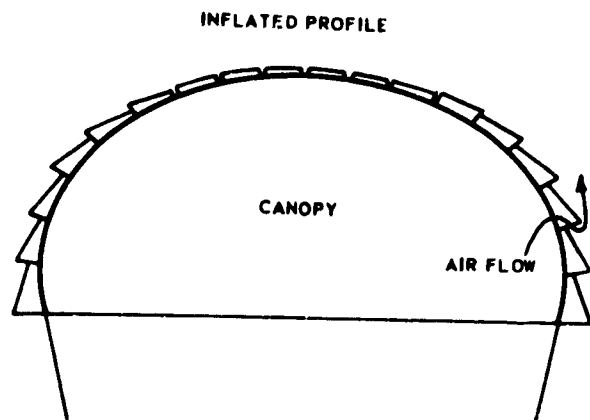
Canopy Diameter (ft)	No. of Gores	Suspended Load (lb)	Canopy Material, Lines	Assembly Wt (lb)	Vol (ft ³)	Deployment Velocity (knots)
63.1	48	Mercury Capsule (2300)	2.25 oz nylon 550 lb lines	57.2	2.26	150
74.2	60	Reentry Capsule (1700)	2.25 oz nylon 550 lb lines	76.9	2.76	139
63.0	48	Q-4 (1900 lbs)	2.25 oz nylon 550 lb lines	53.0	2.34	217
41.0	32	Escape Capsule (620)	2.25 oz nylon 550 lb lines	23.4	.765	351



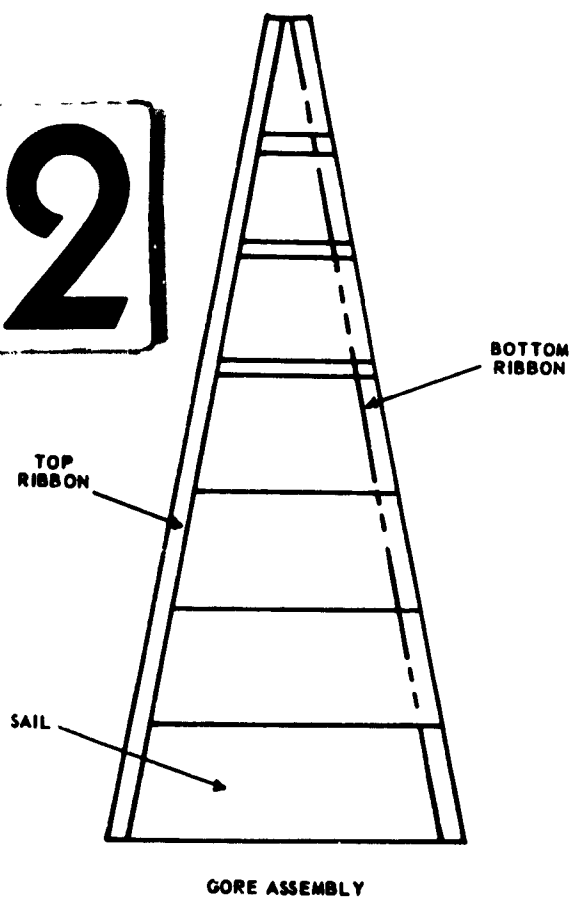
1

erally used.
 ange amplitude of os-
 is less than ± 10 deg.
 infinite-mass condi-
 approximately 1.05.
 canopies may be
 here excessive oscil-
 re the required speed
 olid cloth canopies.
 and Speed Limitations.
 ably, either reefed or
 cities for some speci-
 configurations are as

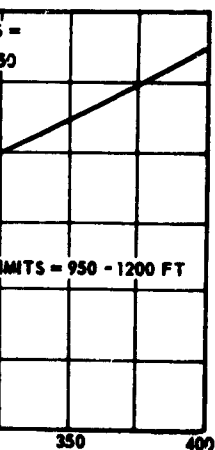
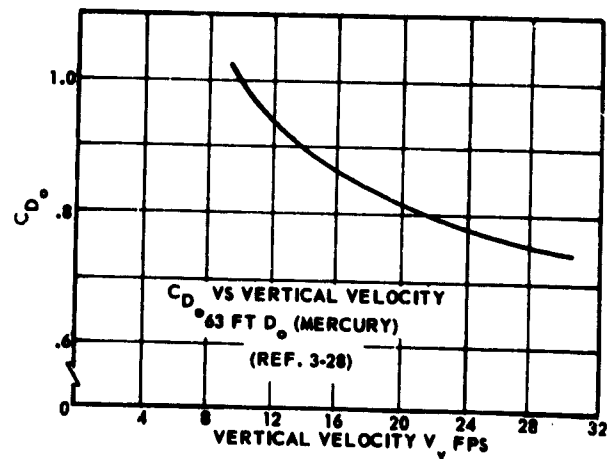
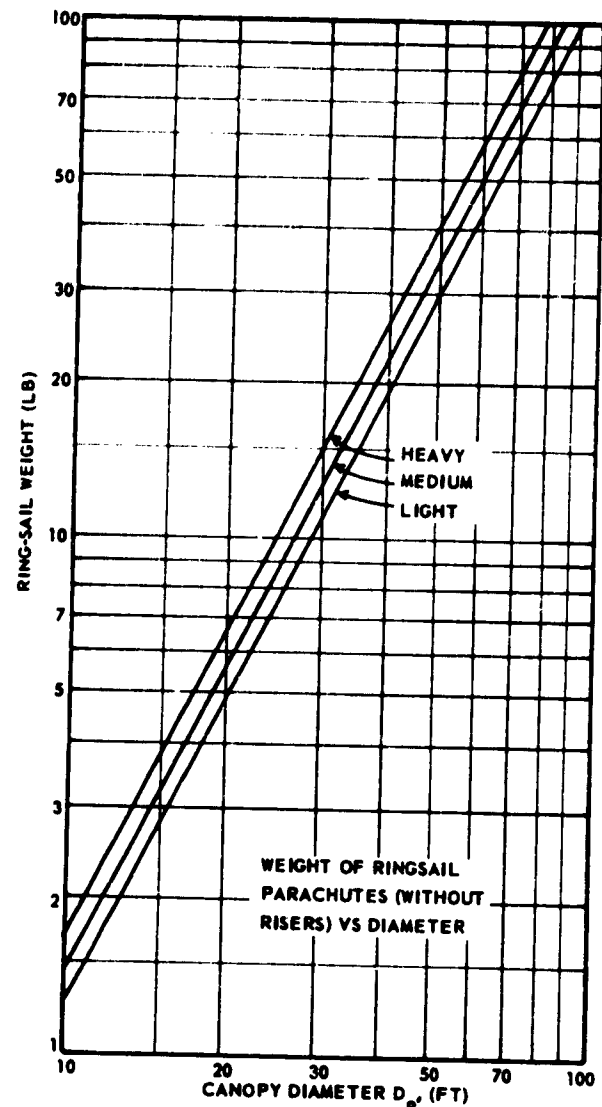
ent
 y
)



2



NOTE: C_D based on Surface Area of Quarter Sphere



1.3 Rotating Parachute Canopies

1.3.1 ROTAFOL CANOPY

1.3.1.1 Canopy Design. This parachute was developed by Radioplane Company, Van Nuys, Calif., under contract with the United States Government. Construction of the canopy is similar to that of the flat circular type. Openings in each gore transform each roof panel into a sail during operation, which causes rapid canopy rotation. A swivel has to be used to permit this rotation (relative to the suspended load), while transmitting minimum torque to the load.

1.3.1.2 Drag Coefficient. The drag coefficient C_{D_0} varies according to the design. On types tested it has ranged from 0.63 to 0.90. For preliminary calculations, a C_{D_0} value of 0.78 is generally used.

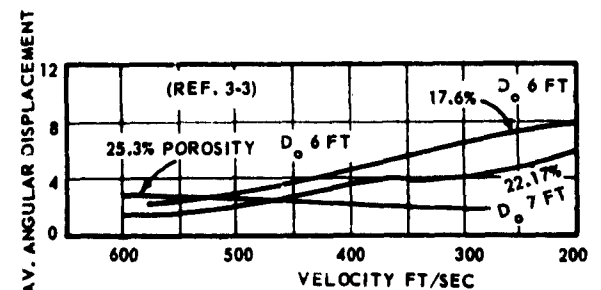
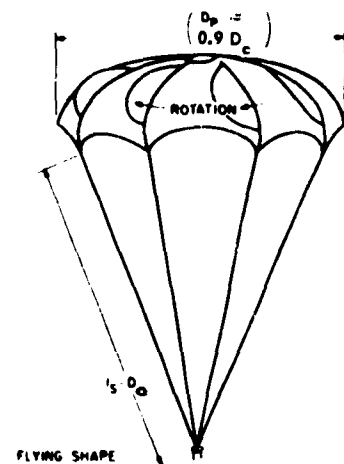
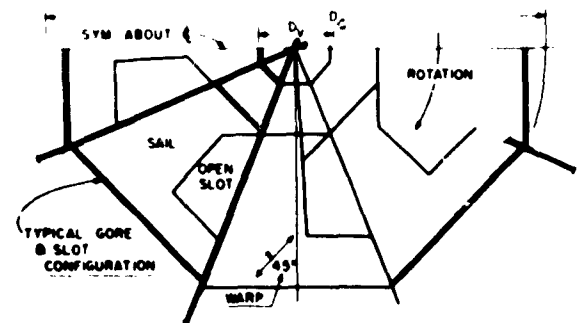
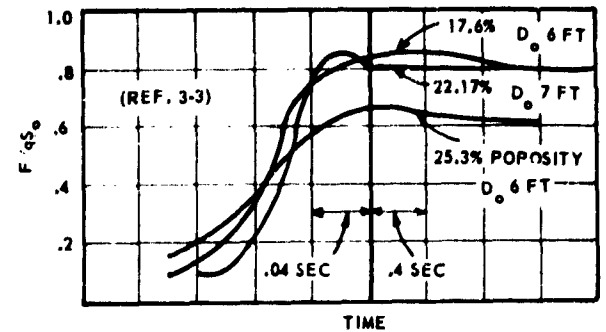
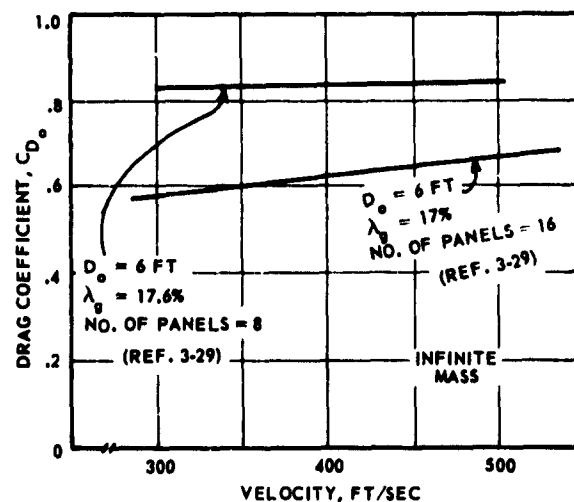
1.3.1.3 Stability. The stability of this canopy is very much a function of the design. Models range from stable to unstable, with a decrease in drag coefficient in the stable models.

1.3.1.4 Opening-Shock. For infinite-mass conditions, the opening-shock factor is approximately 1.06.

1.3.1.5 Application. This parachute canopy may be used for general deceleration applications.

1.3.1.6 Opening Reliability and Speed Limitations. Most designs are reliable in opening. Canopies (7-ft diameter) constructed of 7-oz Nylon and 3000-lb tensile-strength suspension lines have been deployed safely at a deployment velocity of 350 knots under nearly infinite-mass conditions.

1.3.1.7 Remarks. The parachute canopy itself is relatively low in bulk and weight, but because of the required swivel (and loading of the canopy skirt with weights for several types), this parachute becomes bulkier and weighs more than do comparable ribbon, ring-slot, or guide-surface parachutes.



1.3.2 VORTEX RING CANOPY

1.3.2.1 Canopy Design. This canopy was developed by Barish Associates of New York and licensed exclusively to Pioneer Parachute Co. for manufacture. The canopy consists of four sail-like panels that rotate about its apex in the manner of a helicopter rotor in autorotation. The gores are tailored and rigged with lines so as to produce a desired distribution of convexity. A swivel minimizes the torque transmitted to the suspended load.

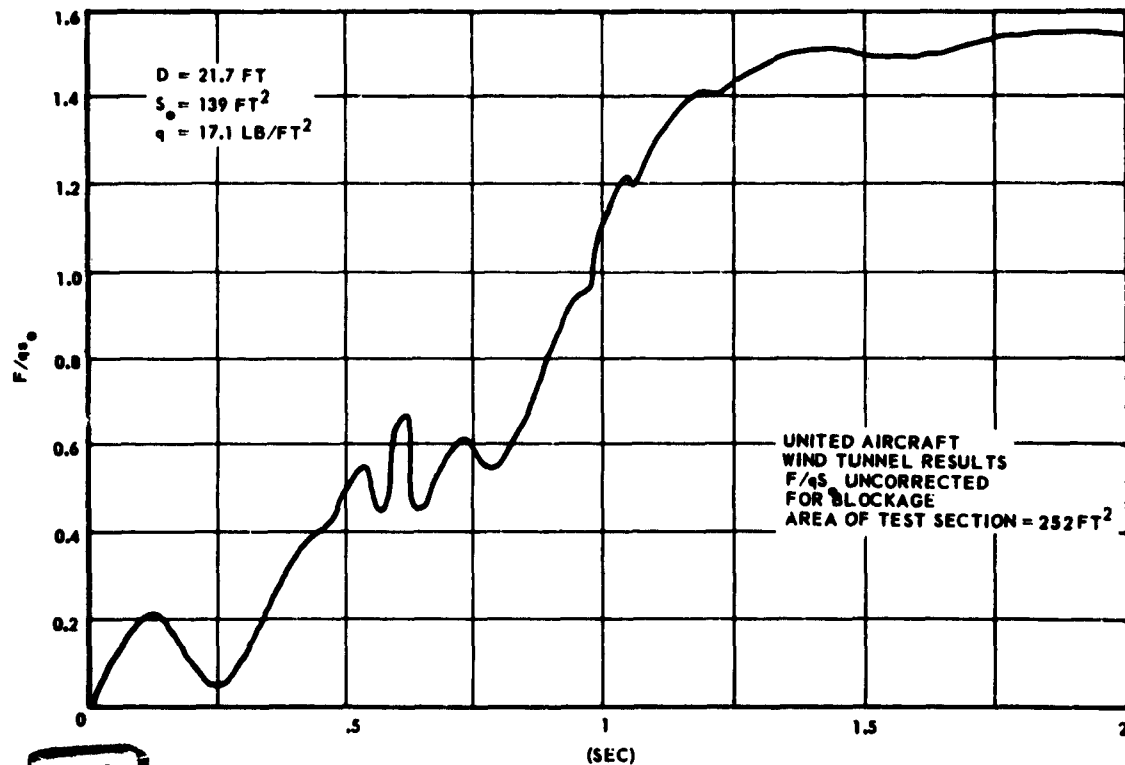
1.3.2.2 Drag Coefficient. The drag coefficient C_{D_0} varies according to the design. On types tested (Ref (3-8)), it ranged from 0.95 to 1.55. For preliminary calculations, a C_{D_0} value of 1.30 is recommended.

1.3.2.3 Stability. The vortex ring canopy has excellent stability characteristics.

1.3.2.4 Opening-Shock. The opening-shock factor (infinite-mass conditions) is approximately unity.

1.3.2.5 Remarks. Data from tests of this canopy are insufficient to establish opening reliability and speed limitation. Ref (3-8) presents wind-tunnel, aircraft tow, and aircraft drop test results utilized in the evaluation of two particular canopy designs. Representative weights for a 32-foot diameter nominal canopy are as follows:

Canopy weight - 9 lb; and
Swivel weight - 0.5 lb.

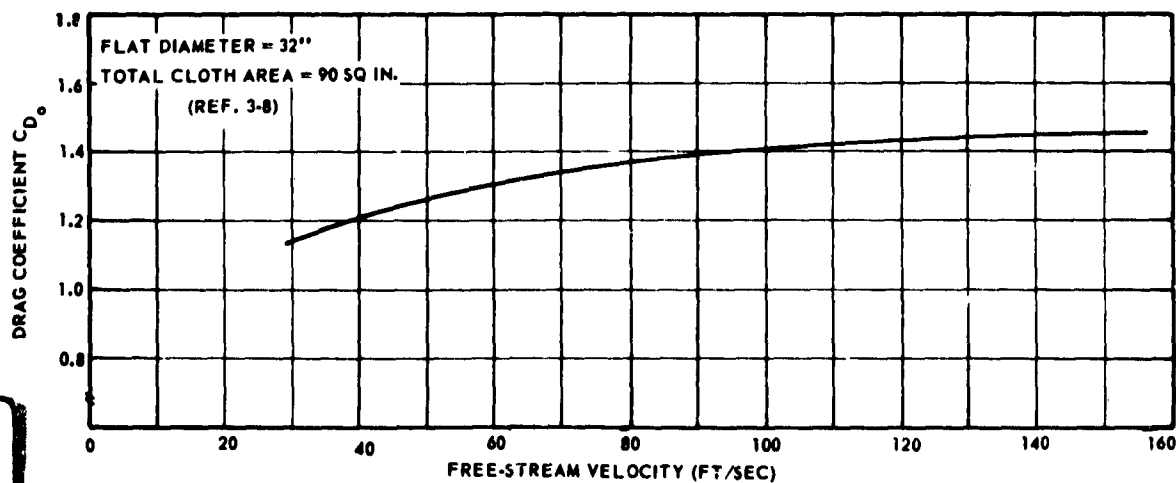
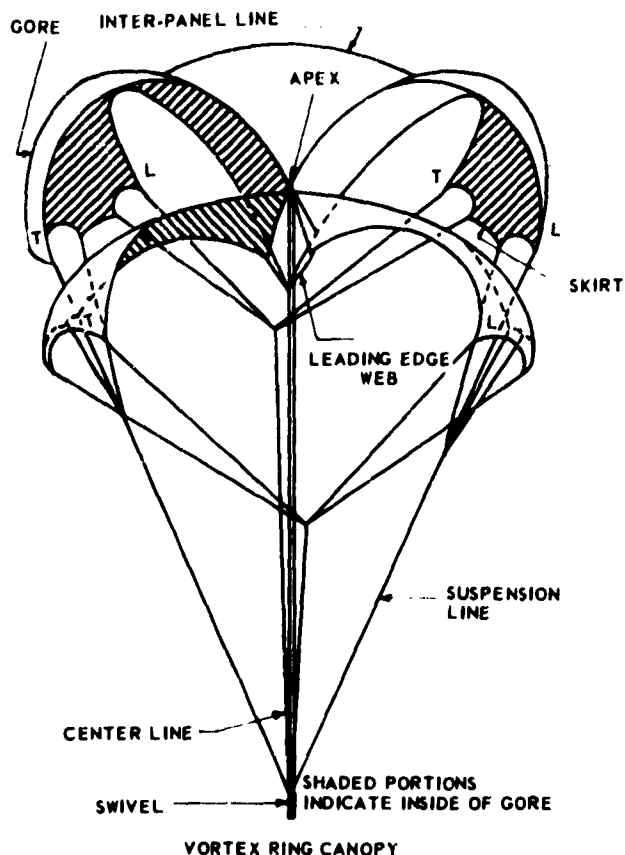


1

ring canopy has

pening-shock factor
approximately unity.
ests of this canopy
ing reliability and
ts wind-tunnel, air-
results utilized in
nopy designs. Re-
t diameter nominal

; and
lb.



2

1.4 Miscellaneous Canopies

1.4.1 GENERAL. Many model and full-size canopies of shapes other than those discussed, or variations of those shapes, have been built and tested. Some, such as the steerable canopies, compare reasonably in their performance characteristics with the type upon which the modification was based. On others, however, the data are not sufficient to draw any firm conclusions about their performance.

1.4.2 AIRFOIL CANOPY. This canopy is designed as a portion of a sphere cut by two parallel planes and, if projected, takes the form of a circular, annular ring, with the smaller diameter at the vent. It differs from a circular canopy with a vent in that the ratio of the area of the open vent in an airfoil canopy to the area of its fabric is significantly larger than the similar ratio for a regular circular canopy. The airfoil canopy's C_{D0} is approximately 0.85. The maximum deployment speed at which little or no damage occurs is low compared to those of other designs. In addition, the design of the suspension line system is very critical and, at present, can be determined only by drop-test. Its bulk and weight are slightly higher than those of a flat circular parachute with comparable performance.

1.4.3 FLAT NONCIRCULAR CANOPY. This is a general term to describe a flat canopy whose shape is a regular or irregular polygon. Coefficient of drag is sometimes higher than that of a flat circular canopy of the same area, but packing difficulties are numerous. Its opening-shock is usually as high, and its bulk and weight the same or slightly less, as those of a flat circular canopy with equivalent performance. Its reliability is the same or less. Some of these designs are remarkably stable. Manufacturing costs are higher.

1.4.4 WAKO CANOPY. As originally designed, this canopy is constructed as a hemisphere composed of a number of ribbons starting at the skirt, running tangent to the vent, then to the opposite skirt, in opposing pairs. This arrangement is repeated around the canopy as many times as required, and it results in a geodetic-type construction. Its bulk and weight are higher than those of the flat circular ribbon canopy. Like all ribbon canopies, it depends upon slow opening for its low opening-shock characteristics, and upon high geometrical porosity for its stability.

1.4.5 STEERABLE PARACHUTE CANOPIES. Steerable parachute canopies generally have been derived by modification of flat circular canopies. A discussion of steerable canopies may be found in Chap. 5, Sec. 7, Personnel Parachutes.

SECTION 2 DEPLOYABLE AERODYNAMIC DECELERATORS OTHER THAN TEXTILE PARACHUTE CANOPIES

2.1 Inflatable-Balloon Decelerators. The inflatable-balloon decelerator is a high-drag, blunt body fabricated from material with very low porosity. It is deployed and either self- or forced-inflated behind the payload that is to be recovered.

The requirement for inflatable-balloon decelerators resulted from the problems associated with the operation of parachutes at supersonic speeds. The erratic inflation and stability characteristics of parachutes at these speeds necessitated the investigation of other methods of aerodynamic deceleration.

The investigation of various configurations that could provide maximum stability and drag at minimum weight and bulk was conducted under two programs. The initial program was the investigation of a forced-inflated spherical decelerator capable of deployment from an altitude of 200,000 ft at Mach 4. The second effort extended the performance requirements to Mach 10 between 120,000 ft and 200,000 ft altitudes.

2.1.1 SPHERICAL DECELERATORS. The spherical configuration shown in Fig. 3-1 was investigated in wind-tunnel tests from low subsonic speeds up to Mach 3.96 (Ref (3-33)), and in free flight tests up to Mach 2.1 (Ref (3-35)). The flow separation, or "burble fence", was incorporated to provide subsonic stability.

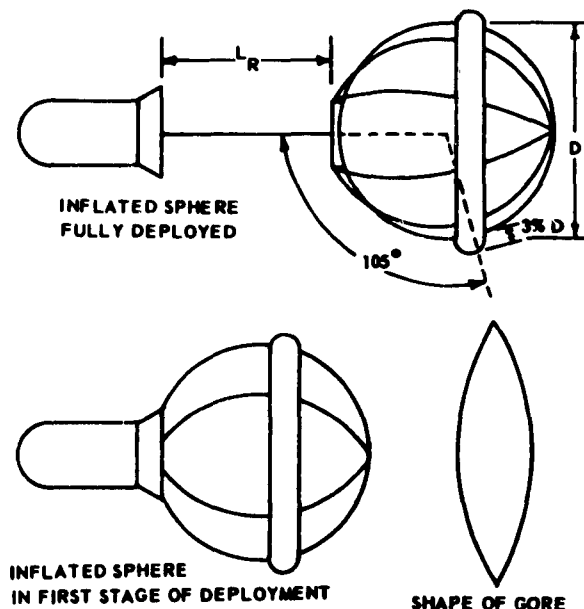


Fig. 3-1 Schematic of Spherical Decelerator

The subsonic instability, in the subcritical flow regime (Reynolds numbers less than 3.85×10^5), results from the unbalanced forces generated from the non-uniform pressure-distribution variation caused by the unsteady release of vortices into the wake of the decelerator. The burble fence positively trips the flow over the body from laminar to turbulent conditions. In the supercritical regime, at subsonic and transonic speeds, the flow separates evenly aft of the sphere, resulting in balanced forces and stability. Positive flow-separation occurs at supersonic and hypersonic speeds with-

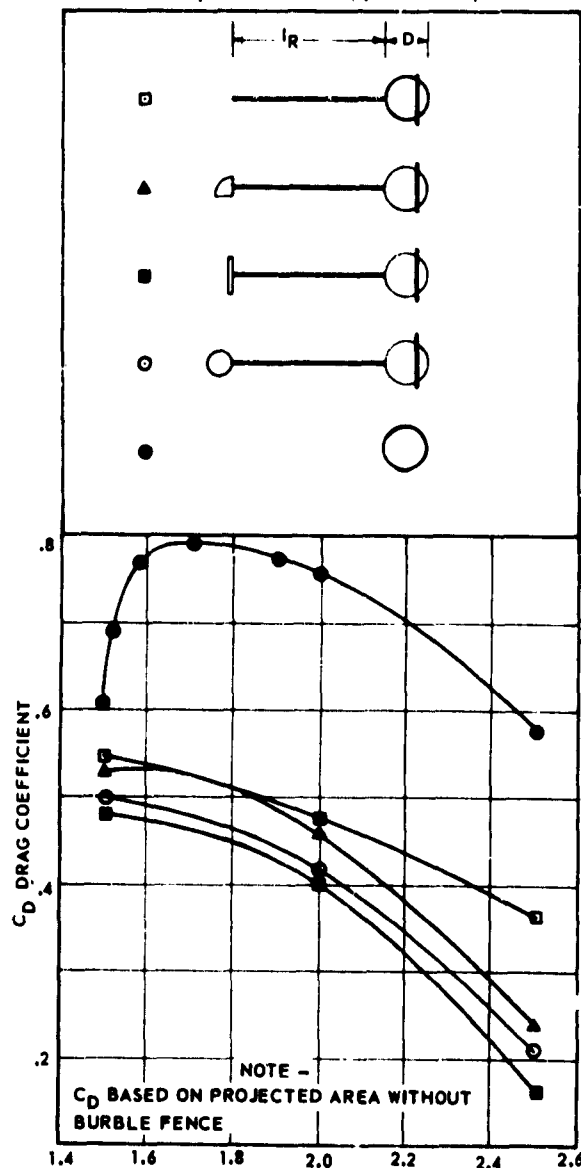


Fig. 3-2 Drag Coefficient vs Mach No. for Spherical Drag Devices with Various Forebody Shapes at $l_R/D = 3$ and a 3% Burble Fence

out Reynolds-number considerations.

The effects of the configuration of the primary body and trailing distances on the aerodynamic and thermodynamic characteristics of the spherical decelerator were investigated in the wind tunnel up to Mach 2.5. Fig. 3-2 shows the effect of forebody configuration (various sizes and shapes) on the decelerator drag coefficient (C_D is based on projected area without burble fence). A decelerator of 8.00 in. diameter was trailed at three decelerator diameters behind the forebody. The diameter of the burble fence was 0.25 in. (approximately 3 per cent of the sphere diameter) and was located 105 deg from the nose of the sphere.

Consideration was given to the variation in the system weight for various values of $W/C_D A$ (between 0.1 and 100) for high-speed recovery. Two representative fabric weights, 0.5 and 1.0 lb per sq yd (8 and 16 oz per sq yd) were used to determine system weights. Fiberglass pressure containers with compatible valving and hardware were used for inflation system-weights. A 500-lb payload plus hardware and fabric weights as well as a drag coefficient of 0.92 was used to calculate $W/C_D A$. Fig. 3-3 shows some calculated results of this analysis. It may be noted that decelerator system weights become impractical for $W/C_D A$ less than 10, with the test configuration.

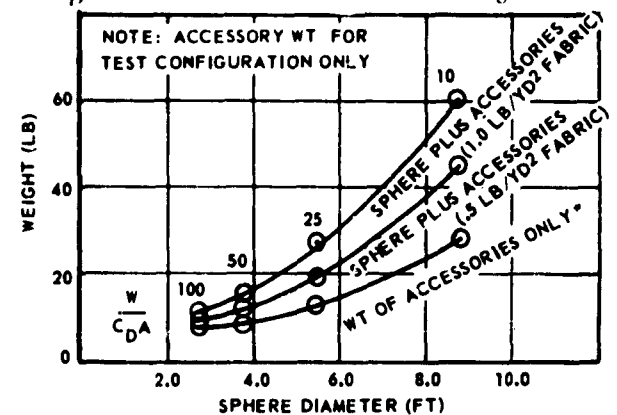


Fig. 3-3 Spherical Decelerator Weight vs Diameter

Fig. 3-4b shows the final free-flight test configuration. This sphere has an 8.9 ft diameter and uses 0.638 lb per sq yd (10.2 oz per sq yd) Dacron-Neoprene fabric. The total assembly weight is 47.5 lb. The decelerator is fabricated from 16 gores with a 3 per cent burble fence attached as shown in section A-A of Fig. 3-4a. The weight of the payload is distributed over the inflated sphere by 16 equally spaced, stranded steel cables extending over the top of the sphere, and taped over as shown in section C-C of Fig. 3-4a. The cables are attached to a metal flange, which in turn is attached to a single riser from the payload. Prior to deployment, the single riser is stored on a deployment

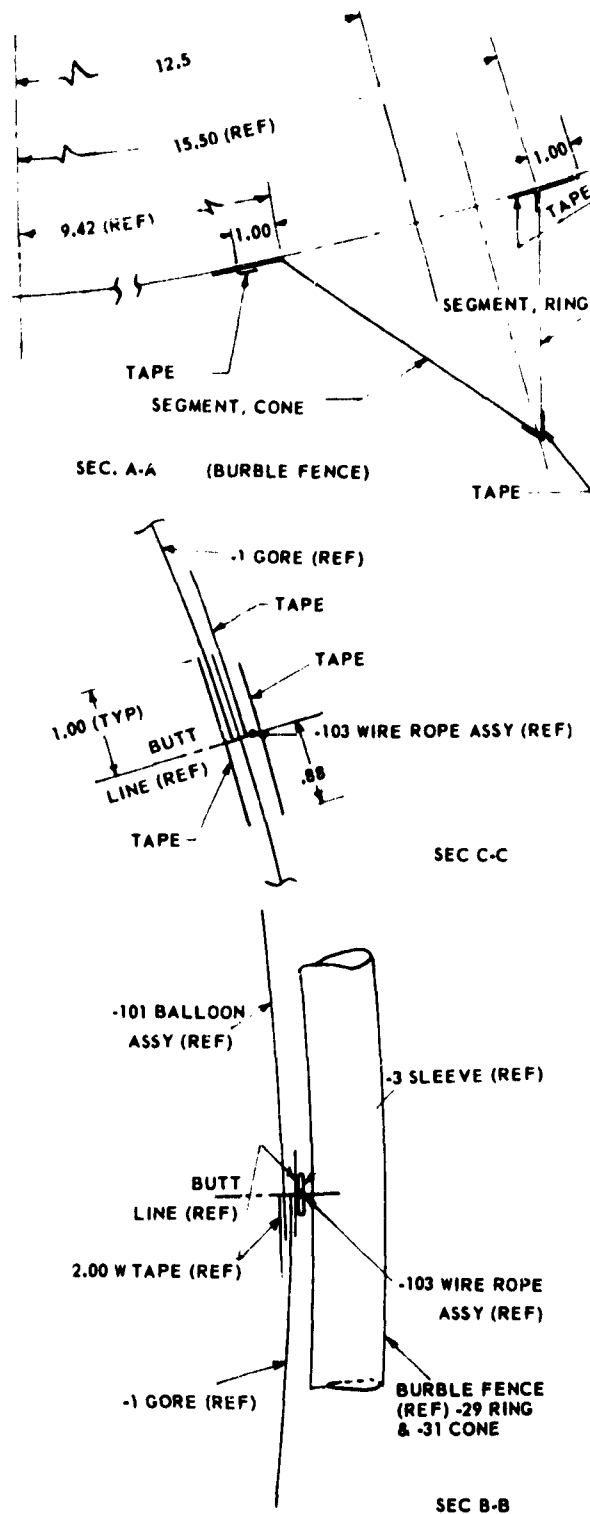


Fig. 3-4a Spherical Decelerator with 3% Burble Fence (Sections)

reel. This deployment reel allows the decelerator to deploy at a constant velocity, thereby reducing shock loads.

Inflation was accomplished with a 500 cu in. fiber-glass pressure bottle, charged with compressed nitrogen at 1950 psia. This results in a fully inflated decelerator internal pressure of 1.5 psia.

Fig. 3-5 shows drag coefficients obtained on a transonic and supersonic free flight test using the spherical configuration. In addition, the results of some wind-tunnel tests at higher Mach numbers on a sphere with a 6 per cent burble fence are presented for comparison.

2.2 Conical Decelerators. Blunt conical shapes were investigated for application as hypersonic decelerators because of their drag and stability characteristics. Solid cone models, with included nose angles of 60 deg, 100 deg, and 140 deg, were investigated in wind-tunnel tests at Mach 7 and 15 (Ref (3-30)). It was concluded that solid conical bodies with included nose-angles up to 140 deg were stable, in the regime and with the forebody configurations investigated. A program to investigate flexible inflatable trailing conical bodies showed that instability resulted with conical bodies with included nose angles greater than 80 deg (Ref (3-31)).

In the inflatable decelerator program, conical and decelerators with various other shapes were investigated supersonically (Mach 2.0 to 5.0). The initial series of tests were conducted with open-front inlet ram-air models and preinflated pressurized models. The pressurized models performed satisfactorily, but poor performance (due to air mass pulsation at the inlets) was found with the ram-air models. The ram-air models were modified with inlet valves (screen and reed type) for the second series of tests. A side-inlet screen-valved 80-deg conical Ballute (one type shown in Fig. 3-6) was considered the optimum configuration. Fig. 3-7 gives the drag results of these tests (C_D is based on projected diameter without burble fence).

The 80-deg conical ram and preinflated Ballutes, without burble fence, were tested at Mach 10 and temperatures up to 1500 F. The models were fabricated from Rene' 41 cloth, impregnated with a high-temperature silicone-glass frits coating to obtain a gas-tight cloth. The seams of the model were joined by spot welding. Fig. 3-8 shows the drag coefficients obtained on these tests (C_D based on projected diameter without burble fence). The ram-inflated tests resulted in a C_D discontinuity at an l/d of 6.5 which indicates a critical value of l/d for maximum drag. The increase in C_D for the preinflated test resulted at an l/d of 4.

The woven Rene' 41 cloths considered for the inflatable decelerator had to meet the general criteria

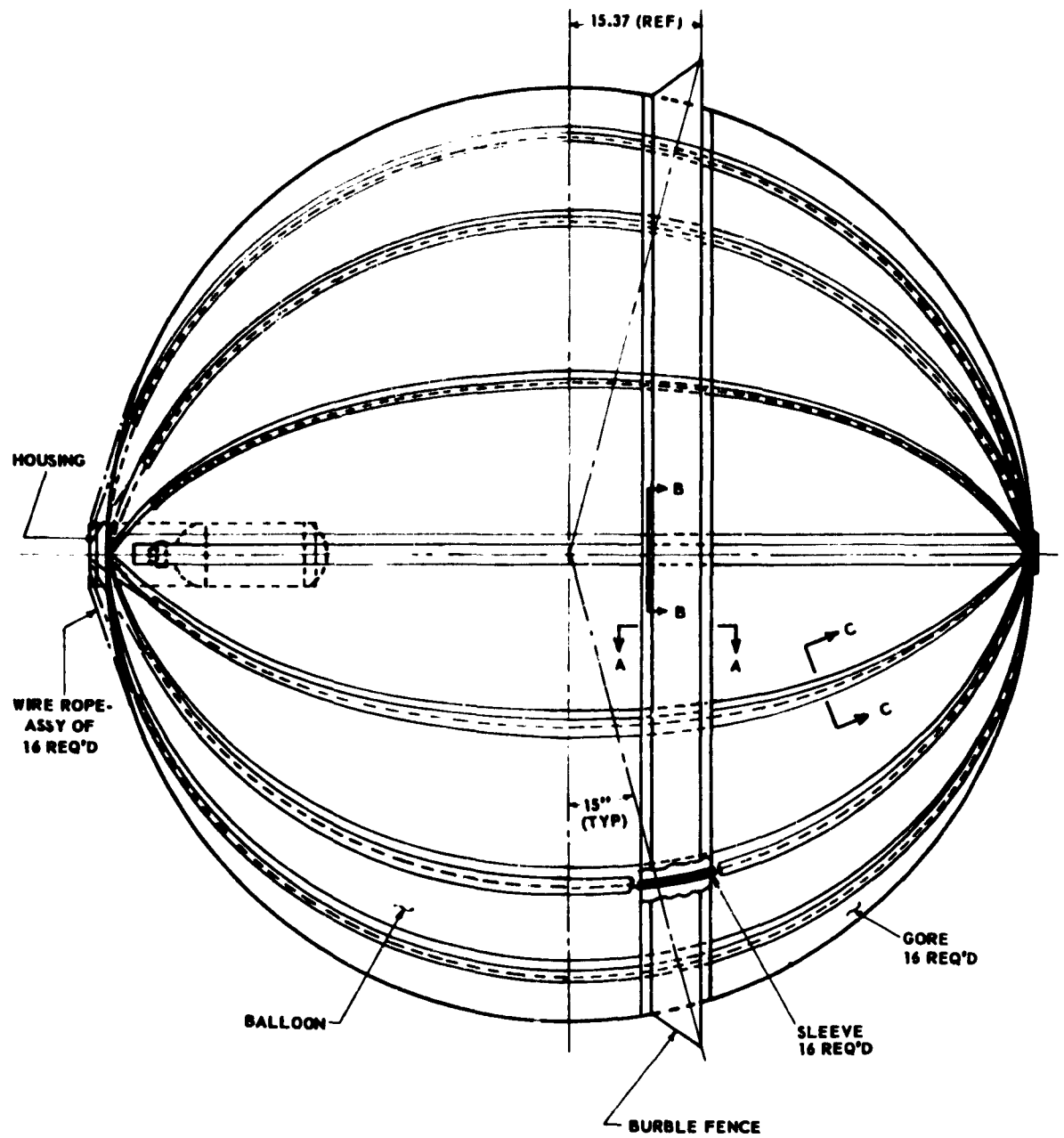


Fig. 3-4b Spherical Decelerator with 3% Burble Fence

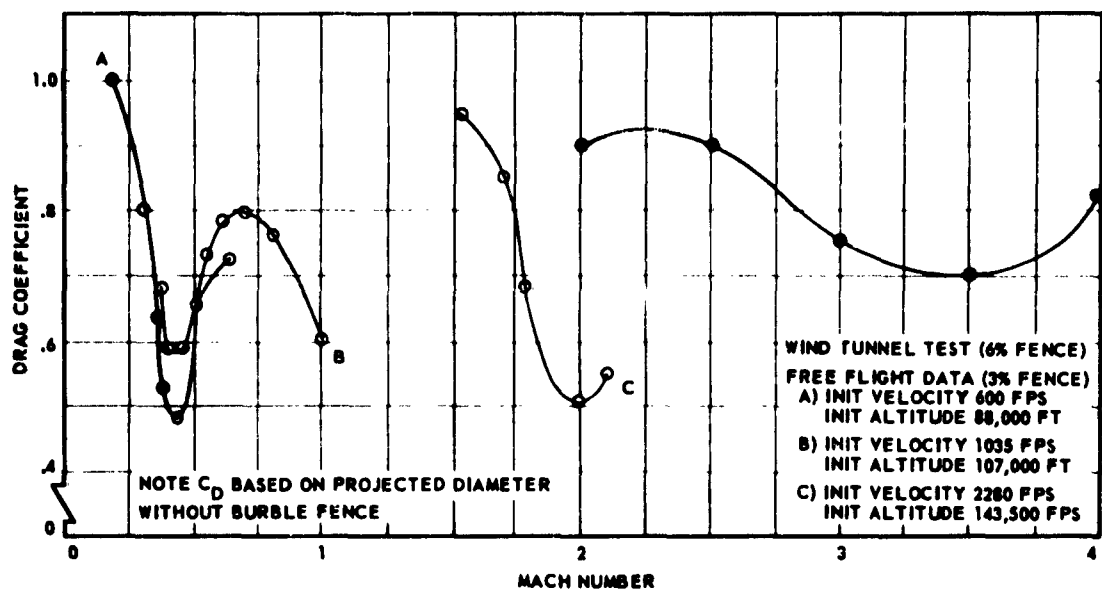


Fig. 3-5 Drag Coefficient vs Mach No. for Spherical Decelerators

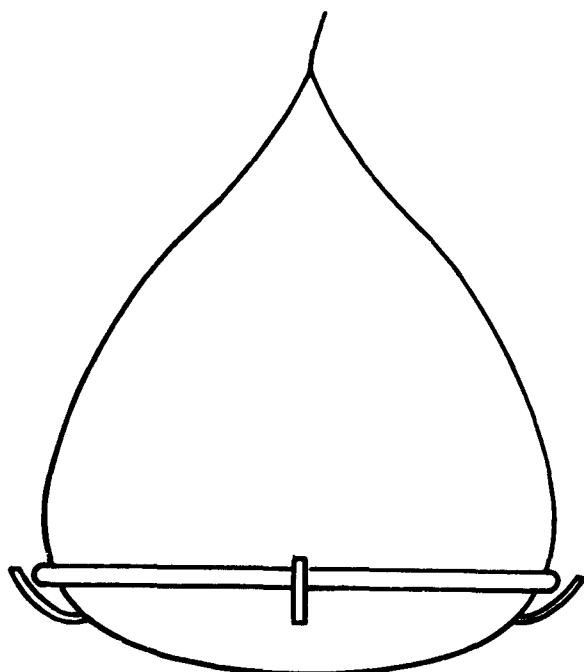


Fig. 3-6 Schematic of 80 deg Ballute with 3.9 percent Fence (Side Inlets)

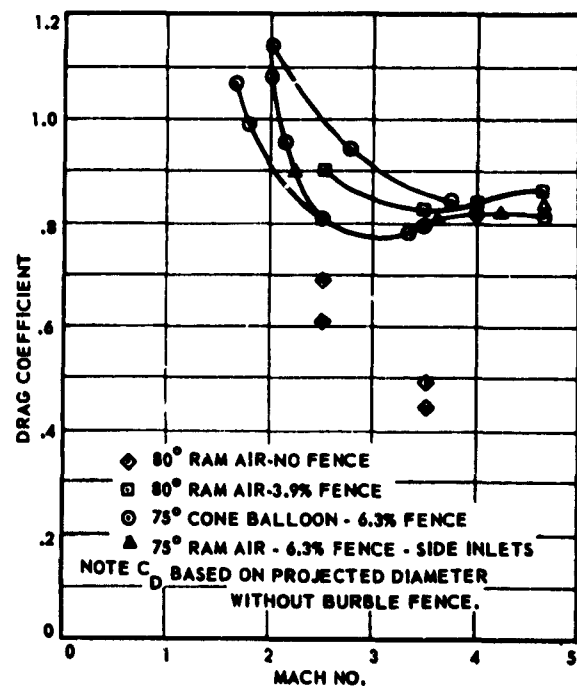


Fig. 3-7 Supersonic Drag Coefficients of Inflatable Decelerators

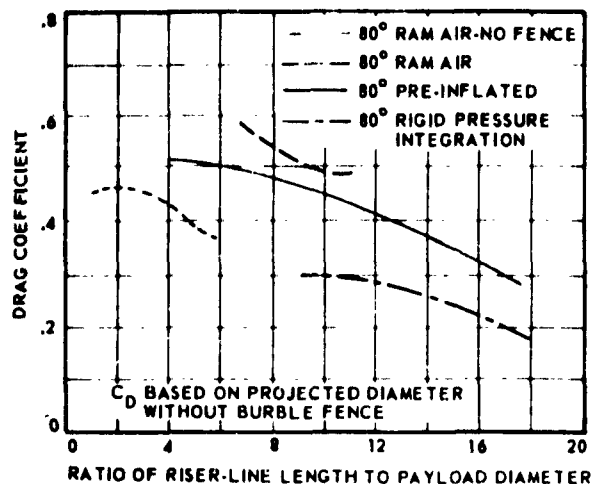


Fig. 3-8 Hypersonic Drag Data (Mach 10) of a flexible cloth capable of maintaining internal pressure to insure dimensional stability (shape) and withstanding temperatures up to 1500 F. An existing available cloth woven of 1.6 mil Rene' 41 wire (200 mesh) was found to be of insufficient strength. Two stronger cloths were woven and evaluated. The results and characteristics of these materials are presented in Table 3-2.

TABLE 3-2 CHARACTERISTICS OF TWO RENE' 41 CLOTHS

	CLOTH A	CLOTH B
Material	Rene' 41	Rene' 41
Wire Diameter (in.)	Single 0.0021	Seven wire strand Each wire 0.0015
Mesh	200 x 200	100 x 100
Ult Tensile (psi)		
Warp	68	183
Fill	96	193
Weld Results (% Efficiency)		
Warp	98	100
Fill	82	94
Cloth Weight (oz./yd ²)	8.75	17.50
Coating Required (oz./yd ²)	8.0	10.0
Total Weight (oz./yd ²)	17.0	27.0

The fabrication techniques for, and the joint efficiencies of, these materials were investigated. A two-row staggered spot-welded pattern was established to join the metallic cloth gores. This technique

was recommended since spot welding was preferable to seam welding and previous experience showed that every wire normal to the direction of loading must be welded and tear resistance is best when the spots are separated. A two-row staggered pattern of seven spots per in. per row, used with the Cloth B material, results in joint efficiencies equal to or greater than 90 per cent in both warp and fill.

An evaluation of the cloth weight versus inflation energy of various inflation methods applicable to the inflatable decelerator is presented in Ref (3-31). However, the success of the ram-air method in wind-tunnel tests, its obvious saving in weight, and its elimination of the requirement for zero-porosity cloth led to the recommendation that it be used for the decelerator inflation. In the flight regime where the dynamic pressure is insufficient to inflate the decelerator, a light internal bladder inflated by residual air may be incorporated. As the dynamic pressure increases, the ram-air inflation pressure increases and compresses the internal bladder.

The estimated weights and sizes of inflatable 80-deg ram-air conical decelerators are shown in Fig. 3-9 as related to dynamic pressure. Rene' 41 cloth at 1500°F is shown.

The following list of design requirements for inflatable-bulloon decelerators was based on the results of the analytical study, the experimental tests, and the subsequent final design study (Ref (3-31)).

- Use a ram-air, constant-stress configuration.
- Provide an apex nose angle of 80 deg.
- Provide a 7 per cent burble fence located on the decelerator "equator."
- Provide side ram-air inlets.
- Make the diameter of the Ballute greater than the payload diameter.
- Make the length of the tow line six to eight times the payload diameter.
- Design the fabric structure based on the more adverse of these two loading conditions:
 - Fabric differential-pressure load at peak temperature.
 - Fabric differential-pressure load at peak dynamic pressure.
- Provide pressure relief to control internal decelerator pressure, when required.

2.3 Spherical Segment Type

2.3.1 ANALYTICAL INVESTIGATION. A unique re-entry concept in orbiting the earth applications has been extensively investigated, both analytically and in wind-tunnel tests, under the direction of the Retardation and Recovery Branch of the Flight Accessories Laboratory. This decelerator concept has become

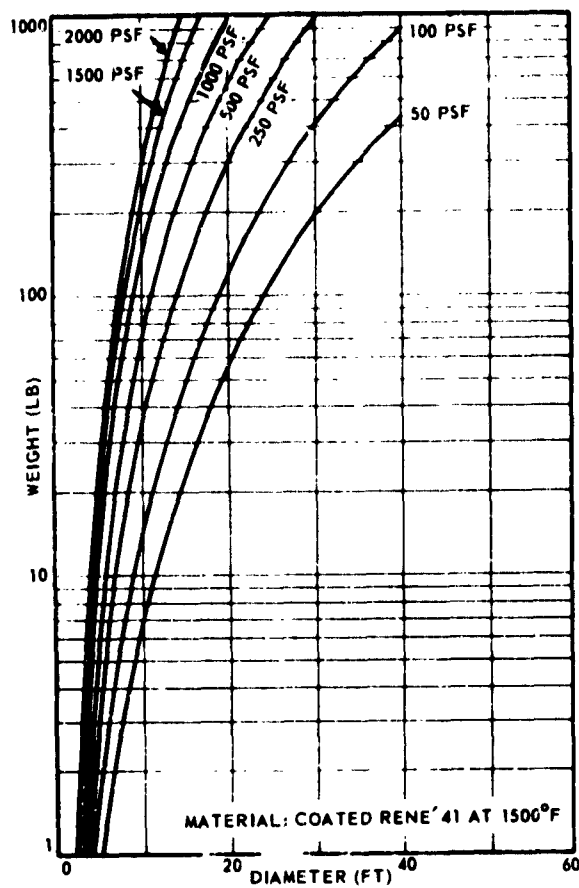


Fig. 3-9 Estimated Inflatable Decelerator Weights

known as the AVCO Drag Brake. The device utilizes extremely light metallic cloth-like skin to enclose a mechanically expandable structure which in appearance is very similar to an inverted umbrella. The concept

allows the payload container to be behind the basic structure, which protects the payload container from the extremely high temperatures associated with entering the atmosphere at orbital velocities (26,000 fps). The analytical investigation has shown that such a concept permits controlling of the maximum re-entry temperature and deceleration, and affords landing-point control within the orbital plane.

2.3.2 DRAG. The drag coefficient of the AVCO Drag Brake is slightly greater than unity in the speed regime above Mach 1. In the subsonic speed regime the drag-brake C_D is slightly less than for commonly used subsonic parachutes (Fig. 3-10). It should be noted that the same decelerator body is utilized in all flight regimes from orbital velocities to touch-down; therefore, maximum drag-generation must be balanced with other considerations such as heating rates, deceleration rates, and stability throughout the flight regime.

2.3.3 STABILITY. The decelerator design is such that the assembly is aerodynamically stable. The drag brake, which is essentially a spherical segment, has self-aligning aerodynamic moments, which lessen attitude-control problems. The control system and body dynamic investigations indicate that a three-axis on-off-rate damping system is required.

2.3.4 MATERIALS. A detailed analysis was carried out on a skin material. The success of the concept is dependent upon the availability of a lightweight, foldable non-porous material which could withstand the combined aerodynamic loading and the temperatures associated with re-entry heating. The skin material chosen is a 200x200-mesh 0.0016-in. diam Rene' 41 wire cloth coated with Pyromark. The coated wire cloth weighs approximately 0.05 psf. The Pyromark coating is required to reduce the porosity during the relatively short time-heat pulse. The cantilever arms or ribs are an open-truss triangular-shape design. The rib members are tubular Rene' 41 alloy and are

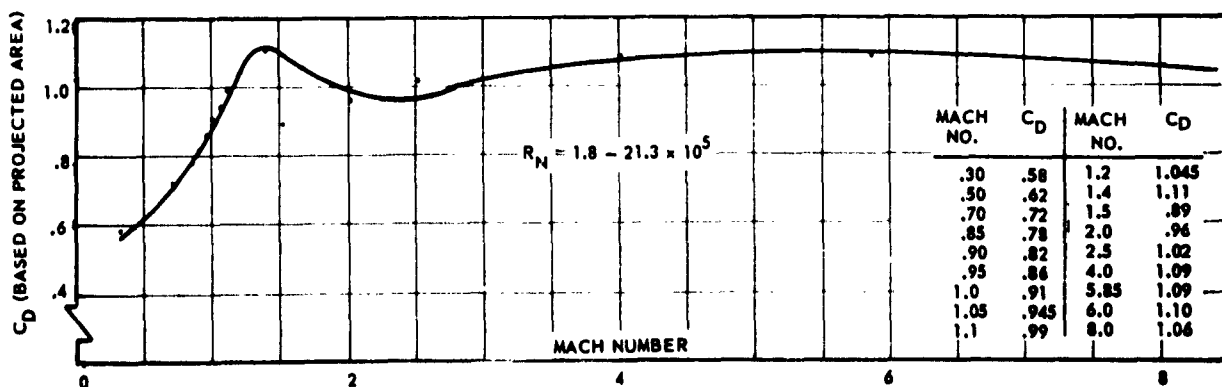


Fig. 3-10 Preliminary Summary of Wind Tunnel Data C_D vs Mach No.

joined by fusion-welding or brazed clusters.

2.3.5 OPERATIONAL METHOD. The drag brake is launched in the folded configuration with the stagnation plate facing the top of the booster. The complete drag-brake assembly is protected from the ascent heating and dynamic pressure by a cover which is jettisoned after leaving the perceptible atmosphere. The drag-brake remains closed during the orbiting phase. The descent is initiated by modulating the shape to control the drag required to give the desired trajectory. If the re-entry is initiated at approximately 100 n.m. (nautical miles), the drag modulation is discontinued about 1000 n.m. from the landing point and at an altitude above 300,000 ft. The drag brake remains in the fully open shape for the remainder of the re-entry. The landing speed is 40 fps, which is low enough for successful recovery on water.

2.4 Rotor Blades

Helicopter-type rotor blades are currently being investigated for use as aerodynamic decelerators. The advantage of rotor blades is their potential capability for controllable descent and soft (near-zero velocity) landing. The controlled descent is based upon the autorotative characteristics of rotors during the propeller braking-state during descent, at which time drag coefficients, based on projected disk area, are very similar to the maximum derived from parachutes (i.e., $C_{DR} = 1.15$), and lift-drag ratios developed give a significant gliding range. The kinetic energy stored in the rotating blades is converted to lift to give the flared soft-landing ability.

Successful operation of rotor-blade decelerators has been achieved repeatedly at speeds up to Mach 0.9 at sea-level conditions. Fig. 3-11 shows representative rotor-type decelerators. Controlled opening-shock was achieved, and the rate of descent was sufficiently low to enable the dropped system to be retrieved intact. A typical rotor-type decelerator flight-path is shown in Fig. 3-12.

Blade designs other than rigid are being explored as a means of reducing both weight and stowage requirements. Flexible rotor-blades appear attractive from the stand-point of attaining a high ratio of specific impulse to weight-volume $\frac{I_{sp}}{WT}$, comparable to the parachute.

A possible future application of manned space-capsule retardation is illustrated in Fig. 3-13.

From Fig. 3-14 it is seen that for a typical required overall L/D of 2.0, a rotor-recovered vehicle may be landed anywhere within a radius of approximately 19 miles if deployment is effected at 50,000 ft. The L/D of the rotor system less payload may be as high as five or six.

Typical drag-coefficients obtained during transonic

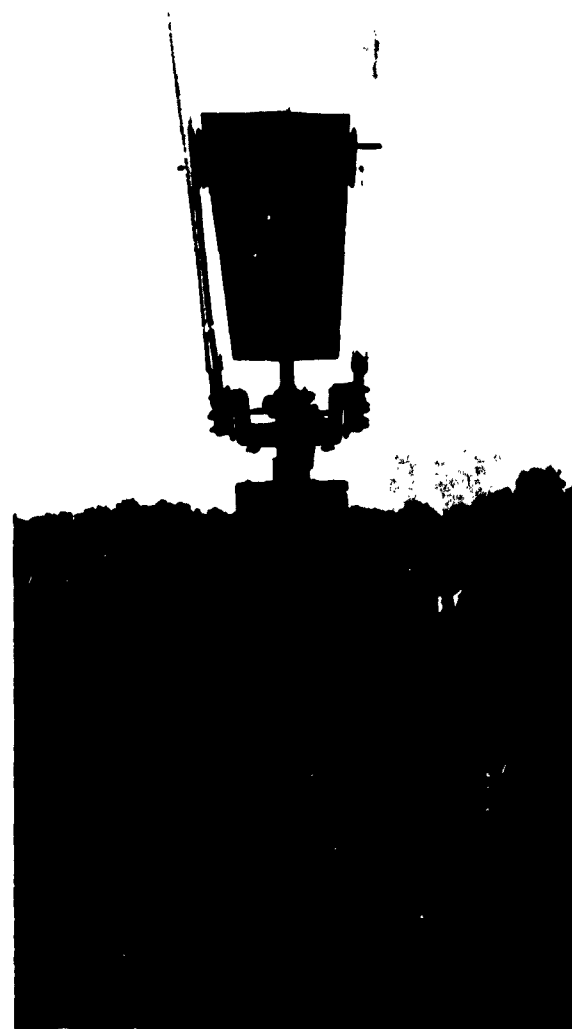


Fig. 3-11 Representative Rotor-Type Decelerators

wind tunnel tests of a rotor type decelerator at AEDC are shown in Fig. 3-15. Tip speed is relatively low (350 fps) for the plotted data. An increase of tip speed would have resulted in a decrease in advance ratio (i.e., axial flight velocity divided by rotor-tip speed) and consequently would have yielded higher drag-coefficients (see Fig. 3-16). Fig. 3-16 also illustrates the effect of varying "solidity," which is the ratio of total blade area to disk area, on the drag coefficient. Vertical descent rates (v_D) of rotary decelerators are chiefly dependent on rotor disk loading (ω) and altitude (see Fig. 3-17). Assuming the conditions (advance ratio, solidity, etc.) are such that they yield a drag coeffi-

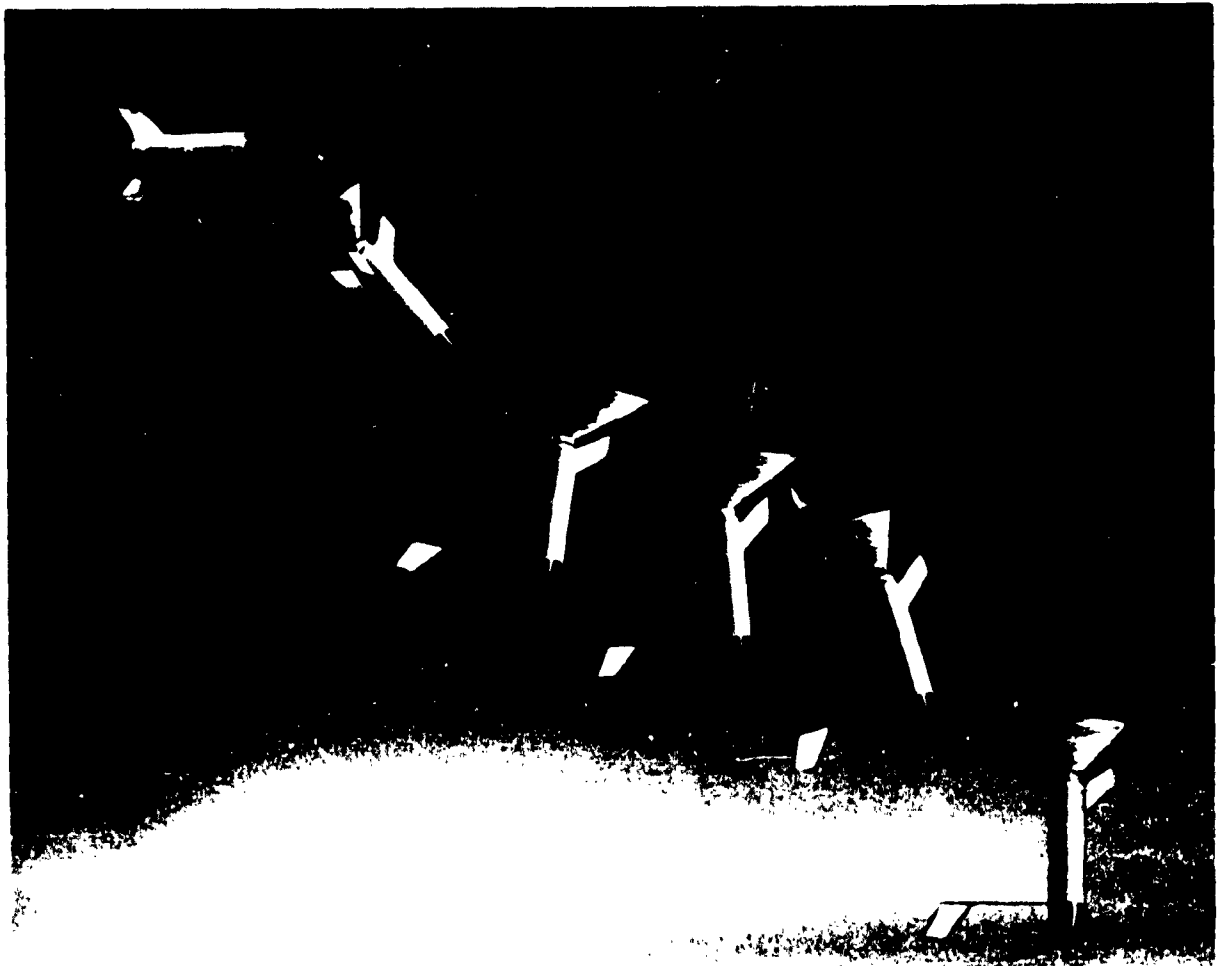


Fig. 3-12 Typical Rotor-Blade Flight-path

cient of 1.15, which is reasonable, let

$$C_{DR} = \frac{T}{1/2 \rho v_D^2 (\pi) (R)^2}$$

or,

$$1.15 = \frac{\omega}{\rho^{1/2} v_D^2}$$

then,

$$v_D \approx 27\sqrt{\omega(\rho_0/\rho)} = 1.315\sqrt{\omega/\rho}$$

Hovering time of rotary aerodynamic decelerators is of significance because it represents that time in which alternate landing-sites may be selected and maneuvers may be accomplished, and is directly de-

pendent upon energy-storing ability of the rotor blades. Energy availability varies directly with rotor diameter, rotating speed and weight, and indirectly with rotor disk-loading. Fig. 3-18 shows the variance of hovering time (Δt) with disk loading for a constant-energy requirement (E_H). This chart is actually a cross-plot of a curve of E_H vs Δt at constant loading, which results from the following equation:

$$E_H = (P_h) \Delta t = \left(T \cdot M \cdot \sqrt{\omega/2\rho} \right) \Delta t$$

Assuming $M = 0.7$ and thrust (T) = 2000 lb and

$$\rho = \rho_{s.l.} = 0.002377 \text{ lb-sec}^2/\text{ft}^4$$

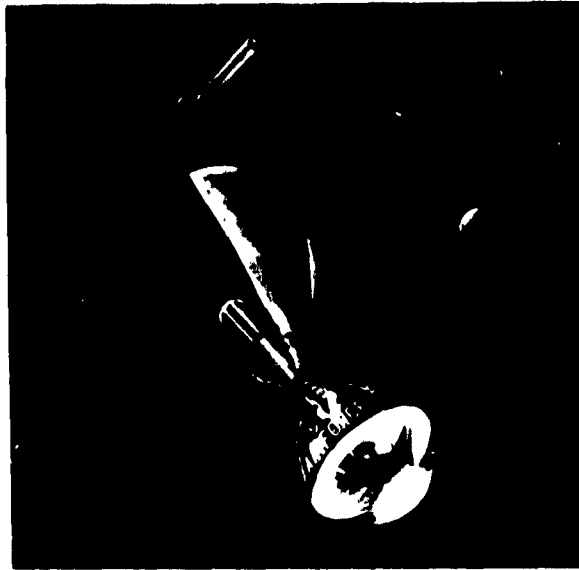


Fig. 3-13 Possible Future Rotor Blade Application

$$E_H = \left(\frac{2000}{0.7} \sqrt{\frac{\omega}{2 \times 0.002377}} \right) \Delta t$$

or, $E_H = 4.14 \times 10^4 \sqrt{\omega} \Delta t$

Recovery-system weight-volume relationship is considered very important, inasmuch as it directly affects the overall performance of a vehicle containing the recovery system. Typical weights of conventional helicopter (rigid) blades and hub (including the mechanical

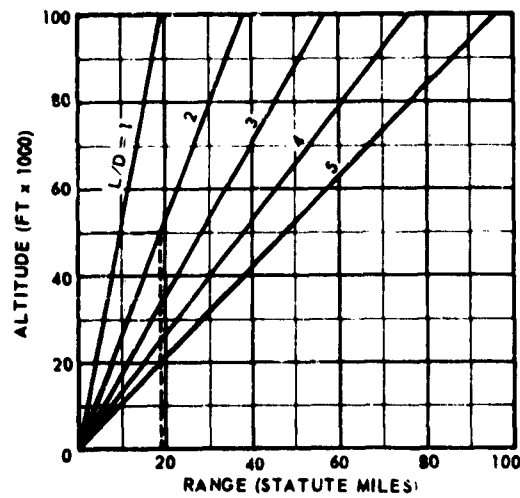


Fig. 3-14 Range vs L/D and Altitude

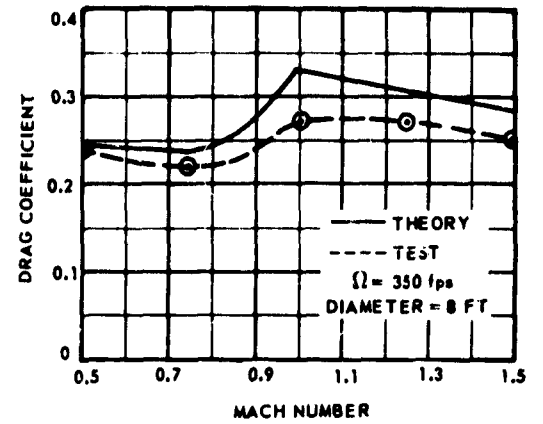


Fig. 3-15 Rotor Drag Coefficient vs Mach Number

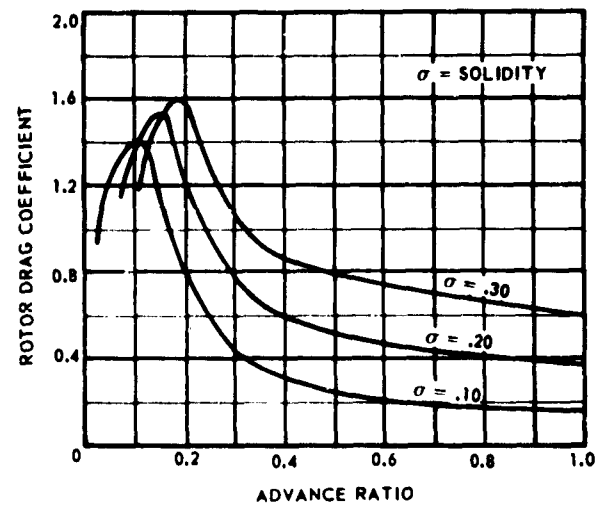


Fig. 3-16 Rotor Drag vs Advance Ratio

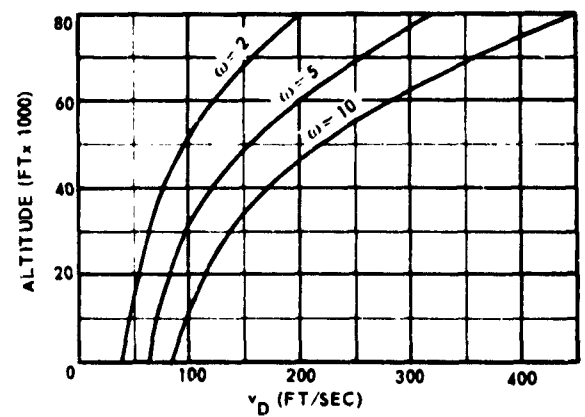


Fig. 3-17 Rate of Descent vs Altitude and Disk Loading

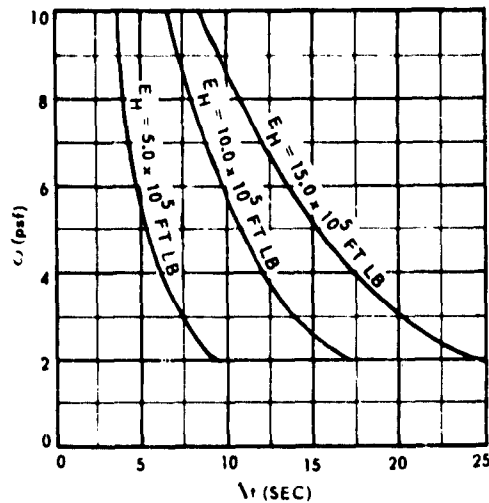


Fig. 3-18 Disk Loading vs Hovering Time at Constant Energy Requirement

control system) and the ratio of rotor-group weight to helicopter gross-weight are plotted as Fig. 3-19. However, the additional control and stabilization equipment required on a rotary-decelerated vehicle would tend to increase the weight of the total recovery-system by several percent of the gross weight. It should be remembered that the above chart represents *rigid* rotor-system weights. If a flexible rotor-system is utilized, a weight-saving of 40-50 per cent might be realized. However, the feasibility of using flexible rotors as

either lifting or decelerating devices is yet to be proven.

Two-dimensional theories of flexible airfoils at subsonic and supersonic airspeeds have been developed and are presented in Ref (3-34).

Findings to date indicate that flexible rotor-system weight varies in proportion to the cube of the rotor radius. Sample flexible-blade weights for a rotor with a 40-ft diameter are shown in Table 3-3; these weights have been calculated from the expression $W_B = KR^3$, where the factor K varies with rotor tip speed according to Fig. 3-20.

TABLE 3-3
SAMPLE FLEXIBLE BLADE WEIGHTS FOR
40-FT-DIAMETER ROTOR
($R = 20$ ft)

Tip Speed (V_T) fps	Blade Wt. (W_B) lb.
400	48.2
500	50.5
600	55.8

An example of flexible-rotor weight variance with blade radius at a constant tip speed is indicated in Fig. 3-21.

Typical weights for rigid blades of the H-21, H-37, H-16, and H-34 helicopters are superimposed on the curve in Fig. 3-21 (indicated by circled dots) to illustrate that flexible-rotor weights will equal or ex-

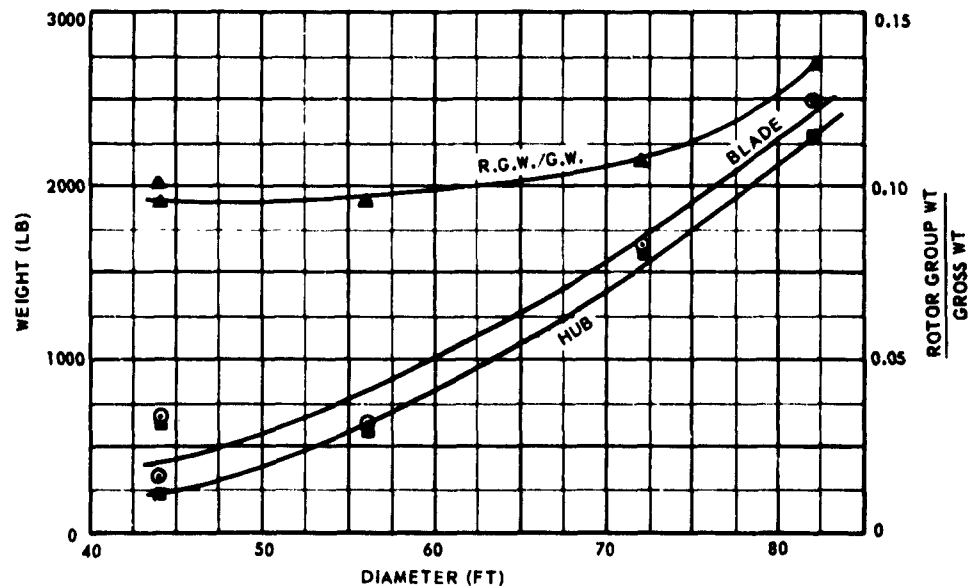


Fig. 3-19 Typical Helicopter Rotor System Weights vs Diameter

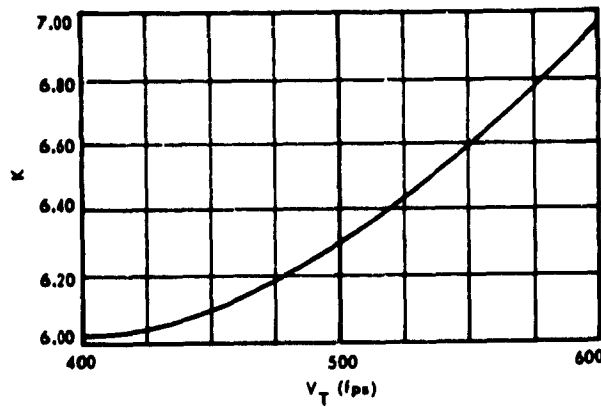


Fig. 3-20 Flexible Rotor Scaling Factor vs Tip Speed

ceed those of rigid-rotor weights after a specific rotor radius is attained. The weight-to-thrust ratio, which is approximately equivalent to the ratio of the flexible-rotor recovery-system weight to recoverable-vehicle gross weight (W_{rs}/W) is plotted against airfoil-section lift-coefficient for constant tip-speed in Fig. 3-22.

In the above plot, the rotor-system weight includes weights of hub, control system, deployment and retraction system, etc. The latter weight has been deter-

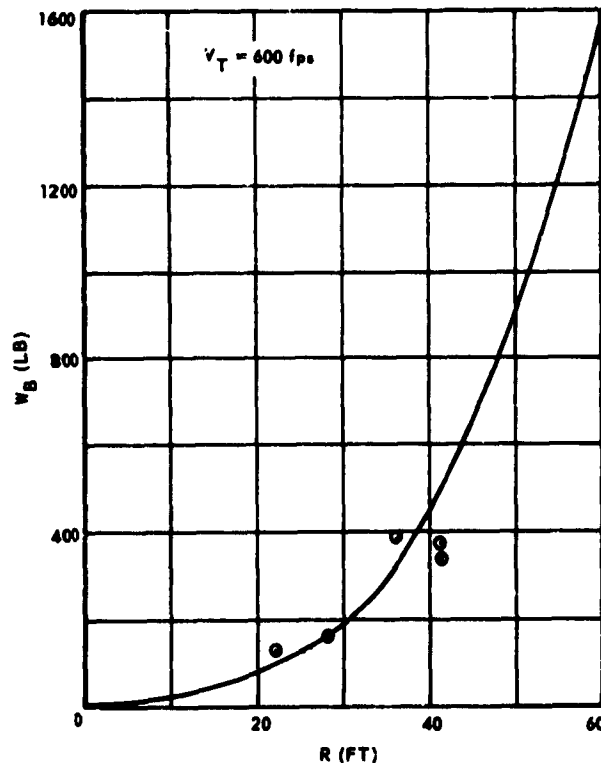


Fig. 3-21 Flexible Rotor Blade Weight vs Radius

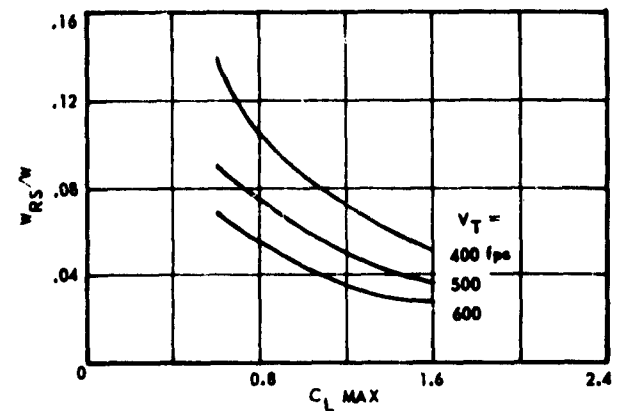


Fig. 3-22 Recovery System/Vehicle Weight Ratio vs Lift Coefficient

mined to be equivalent to approximately 20 per cent of the total rotor-tip weight.

Two-dimensional wind-tunnel tests of flexible, fabric airfoil sections were conducted May 1961 in the Brown University 9x9-in. transonic-supersonic wind tunnel throughout a Mach-number range from 0.3 to 0.75 and Reynolds-number range from 4.4×10^5 to 7.8×10^5 , to determine the aerodynamic characteristics of such sections. Based upon this experimental investigation and comparisons with theoretical predictions, it has been concluded that:

- (1) Flexible airfoils develop less lift due to camber than theoretically predicted, and their centers of pressure at zero angle-of-attack are generally toward the midchord;
- (2) Lift-curve slopes of the airfoils are in good accord with flexible-airfoil theory;
- (3) Separation exists over the rear of the airfoil sections at high cambers (i.e., 15 per cent);
- (4) Sections of 5 and 10 per cent camber develop maximum lift-drag ratios of 20; however, fabric per-

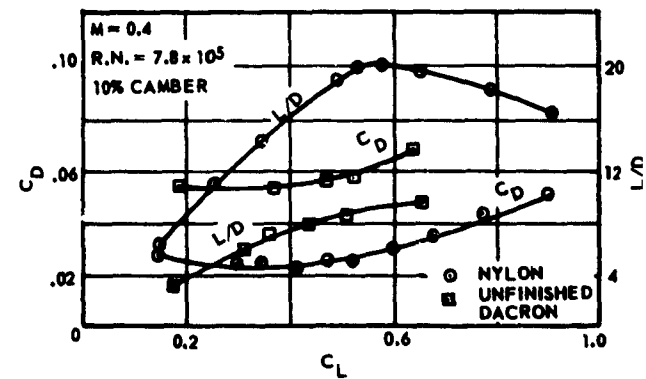


Fig. 3-23 Lift-Drag Relationship, Flexible Airfoils

meability can reduce these ratios to one-half of this figure, and has a significant effect on the aerodynamic efficiency of the overall section; and

(5) Airfoil-section fabrication techniques can significantly affect the performance derived.

It is believed that flexible-airfoil sections having a lower fabric permeability (e.g., less than 1.0 cfm, under 0.5 in. H_2O), and tested at substantially greater Reynolds numbers would display greater aerodynamic efficiency. Representative curves are displayed as Fig. 3-23.

The airfoil characteristics of the flexible sections have been compared with those derived from other solid, thin, cambered airfoils. The Eiffel and Gottingen airfoils have attained maximum L/D 's of 20 and 80 respectively. A comparison of the three types of airfoils, all having 10 per cent camber, is shown in the following table:

Type	$C_{D_{min}}$	C_{L_0}	L/D_{max}
Fabric Airfoils	0.0231	0.493	20.4
Gottingen Airfoils	0.026	0.96	41.7
Eiffel Airfoils	0.070	1.00	14.3

The material of which the flexible rotor-blade consists must be highly flexible. In addition, it should possess high tear-strength in both radial and tangential directions; ease of fabrication; low porosity; aerodynamic smoothness; resistance to abrasion, kinking, and aerodynamic oscillation; durability in the presence of heat and moisture; low weight; and dimensional stability. For extremely high-temperature application, a high-temperature-resistant metal cloth woven from multifilament yarn of metallic alloy such as Rene' 41 would be required.

REFERENCES

- (3-1) Stimler, F.S. and Ross, R.S., Drop Tests of 16,000 Square Inches. Model Parachutes, Volume VIII, AF TR 5867, May 1954.
- (3-2) Foote, Dr. J.R. and Giever, Dr. J.B., Study of Parachute Opening, Phase I, WADC TR 56-253, ASTIA NO. 110 675, September 1956.
- (3-3) Downing, Dr. J.R., Arenson, D.L., and McClow, Jr., J.H., Recovery Systems for Missiles and Target Aircraft, Subsonic Sled Test Phase, AF TR 5853, Part I, March 1954.
- (3-4) Engstrom, B.A. and Lang, R.P., Performance of Trailing Aerodynamic Decelerators at High Dynamic Pressures, Phase IV, WADD TR 58-284, Part IV, June 1961.
- (3-5) Pedersen, P.E., Study of Parachute Performance at Low Supersonic Deployment Speeds: Effects of Changing Scale and Clustering, ASD TR 61-186, May 1961.
- (3-6) Test and Evaluation of 24-Foot Hemispherical "Baseball" Parachute, Report No. 5028-49-2, U.S. Naval Parachute Experimental Unit, Naval Air Station, El Centro, Calif.
- (3-7) Test and Evaluation of Hemispherical "Baseball" Retarding Parachutes, Report No. 5018-49-4, U.S. Naval Parachute Experimental Unit, Naval Air Station, El Centro, Calif.
- (3-8) Gross, R.S., Riffle, A.B., Performance Evaluation of the Vortex Ring Parachute Canopy, ASD TR 61-410, June 1961.
- (3-9) Engstrom, B.H., Performance of Trailing Aerodynamic Decelerators at High Dynamic Pressures, Phases V and VI, WADD TR 58-284, Part V, May 1961.
- (3-10) Downing, Dr. J.R., McClow, Jr., J.H., Hawkins, Dr. H.V., and Fredette, R.O., Recovery Systems for Missiles and Target Aircraft, Subsonic Free Flight Validation Test Phase, AF TR 5853 Part II, March 1955.
- (3-11) Pounder, Edwin, Parachute Inflation Process Wind-Tunnel Study, Part 1. Infinite Mass Case, WADC TR 56-326, AD 97182, July 1956.
- (3-12) Pounder, Edwin, Parachute Inflation Process Wind-Tunnel Study, WADC TR 56-391, AD 97180, September 1956.
- (3-13) Knacke, T., and Hegele, A., Model Parachutes, Comparison Tests of Various Types, Memorandum Report MCREXE-672-12B, 12 January 1949.
- (3-14) Ewing, E.G., A Study to Establish a Parachute Research and Development Program, Vol. II, WADC TR 53-78, Vol. II, AD 110 452, August 1953.
- (3-15) Ewing, E.G., A Study to Establish a Parachute Research and Development Program, Vol. III, WADC TR 53-78, Vol. III, AD 110 453, August 1953.
- (3-16) Heinrich, H.G. and Scipio, L.A., Performance Characteristics of Extended Skirt Parachute, WADC TR 59-562, October 1959.
- (3-17) Freeman, H.F., and Rosenberg, C.W.O., I., High Altitude and High Airspeed Tests of Standard Parachute Canopies, AFFTC TR 58-32, AD 152 286, October 1958.
- (3-18) Giffen, A., and Swenson, W.A., Study and Development of Parachutes and Systems for In-Flight Landing Deceleration of Aircraft, Part II, Development and Test Evaluation of the Ring Slot Parachute, WADC TR 57-566, Part II, AD 155 707, January 1959.
- (3-19) Heinrich, H.G., Parachutes, Guide Surface, Memorandum Report No. MCREXE-672-25F, ATI

- No. 28935, February 1948.
- (3-20) Buhler, W.C., Parachute; Airfoil Type, Performance of, Memorandum Report No. MCREXE-672-19T, January 1949.
 - (3-21) Wilder, S.H., Model Parachute Test in Vertical Wind Tunnel at Wright Air Development Center, WADC TR 58-279, AD 204 424, September 1958.
 - (3-22) Knucke, T., FIST Type Parachute, Design, Use and Construction of, Memorandum Report No. MCREXE-672-19LJ, June 1948.
 - (3-23) Kiker, J.W., B-47 Approach Control Parachute, WADC TN 54-18, July 1954.
 - (3-24) Heinrich, H.G., Aerodynamics, Performance and Design of Personnel Guide Parachute, Memorandum Report No. WCEE-672-145-A-9-1, November 1951.
 - (3-25) Buhler, W.C., Porosity, Effect of, on Parachute Opening, MCREXE-672-2A, December, 1948.
 - (3-26) Graham, C.H., 56-ft. Nominal Diameter Parachute with 10% Extended Skirt, Technical Note FTL 54-17, August 1954.
 - (3-27) Gimalowski, E.A., Development of a Final Stage Recovery System for a 10,000 pound Weight, WADC TR 59-109, December 1958.
 - (3-28) Ewing, E.G., Ringsail Parachute Characteristics, Radioplane Report No. PTM-323-A, January 1961.
 - (3-29) Ciffrin, A., Aerodynamic Appraisal of the Rotofoil, Radioplane Report No. 633, March 1952.
 - (3-30) Champney, W.B., Athans, J.B., Mayerson, C.D., A Study of Hypersonic Aerodynamic Drag Devices, WADC TR 59-324 Part II, June 1961.
 - (3-31) Alexander, W.C., Investigation to Determine the Feasibility of Using Inflatable Balloon Type Drag Devices for Recovery Applications in the Transonic, Supersonic, and Hypersonic Flight Regime, Part II, ASD-TDR-62-702, (to be published).
 - (3-32) Penzand, J.A., Aerodynamic Force Characteristics of a Series of Lifting Cone and Cone-

Cylinder Configurations at a Mach Number of 6.83 and Angle of Attack up to 130-deg, NASA-TN-D-840, June, 1961.

- (3-33) Aebiker, F.R., Feasibility Study of an Inflatable Type Stabilization and Deceleration System for High-Altitude and High Speed Recovery, WADD TR 60-182, December 1961.
- (3-34) Nielsen, J.N., Burnell, J.A., and Sacks, A.H., Investigation of Flexible Rotor Systems, Results of Phases I and II, ASD-TR-61-600, Sept. 1961.
- (3-35) Aebisher, A.C., Investigation to Determine the Feasibility of Using Inflatable Balloon Type Drag Devices for Recovery Applications in the Transonic, Supersonic, and Hypersonic Flight Regime, Part I, ASD-TDR-62-702, (To be published).

BIBLIOGRAPHY

Kayser, L.D., Pressure Distribution, Heat Transfer, and Drag Tests on the Goodyear Ballute at Mach 10, ARDC-TDR-62-39, March 1962.

Kayser, L.D., Investigation of Landing Point Control of Re-Entry Vehicles Utilizing Variable Area Aerodynamic Decelerators Incorporating Lift, ASD-TDR-62-287, April 1962.

Penzand, J.A., Aerodynamic Force Characteristics of a Series of Lifting Cone and Cone-Cylinder Configurations at a Mach Number of 6.83 and Angle of Attack up to 130-Degrees, NASA-TN-D-840, June 1961.

Coats, J.D., Static and Dynamic Testing of Conical Trailing Decelerators for the Pershing Re-Entry Vehicle, ARDC-TD-60-188, October 1960.

Charzenkon, N., McShera, J.T., Aerodynamic Characteristics of Towed Cones Used as Decelerators at Mach Numbers 1.57 to 4.65, NASA-TN-D-994, December 1961.

Tyndall, R.R., Preliminary Qualitative Evaluation of a Stored Energy Recovery System, WADC TN 59-267, July 1959.

Tyndall, R.R., Analytical and Empirical Investigation of a Completely Flexible Rotor Blade, ASD Technical Memorandum ASRMP-TM-628, March 1962.

CHAPTER 4 **AERODYNAMIC AND OPERATIONAL CHARACTERISTICS OF** **DEPLOYABLE AERODYNAMIC DECELERATORS**

Table of Contents

<i>Section</i>	<i>Page</i>
1 GENERAL	122
2 THE ATMOSPHERE	122
2.1 Properties of the Earth's Atmosphere	123
2.1.1 Atmospheric Density	123
2.1.2 Ambient Temperature	125
2.1.3 Atmospheric Composition	125
2.1.4 Ionosphere	127
2.1.5 Winds and Turbulence	128
2.2 Earth Gravity	128
2.3 Environments of Other Planets	129
2.3.1 Venus	129
2.3.2 Mars	130
3 EFFECTIVE POROSITY OF TEXTILE MATERIALS	131
3.1 Definition of Effective Porosity	132
3.2 Measurements of Effective Porosity	133
3.3 Sample Calculation	140
4 SNATCH FORCE	141
4.1 Derivation of Energy Equation	141
4.2 Derivation of Velocity Equation	143
4.2.1 Equations for Velocity at Deployment Initiation	143
4.2.2 Equations for Velocity at Suspension-Line Stretch	144
4.2.3 Example of Snatch-Force Calculation	146
4.3 Measures to Reduce Snatch Force	148
5 FILLING-TIME AND OPENING-SHOCK OF CANOPIES	149
5.1 Opening-Shock of Canopies Under Finite-Mass Conditions	149
5.1.1 Solid Cloth Textile Canopies	149
5.1.2 Canopies with Inherent Geometric Porosity	162
5.2 Opening-Shock of Canopies Under Infinite-Mass Conditions	162
5.2.1 Filling Time	163
5.2.2 Opening-Shock	163
6 AERODYNAMIC DRAG	165
6.1 Introduction	165
6.2 Aerodynamic Drag of Canopies	165
6.2.1 Tangential-Force Coefficients of Canopies	165

<i>Section</i>	<i>Page</i>
6 AERODYNAMIC DRAG (Cont'd)	
6.2.2 Effects of Cloth Permeability	165
6.3 The Descending Canopy	170
6.3.1 The Gliding Parachute Canopy	172
6.3.2 The Oscillating Parachute Canopy	173
6.3.3 The Rate of Descent	173
6.4 Effects of Mach Number	174
6.5 Effects of Reynolds Number	179
6.6 Effects of Clustering	181
7 DRAG-AREA CONTROL	183
7.1 Application of Drag-Area Control	183
7.2 Reefing Methods Used for Controlling Drag Area	183
7.3 Reefing Lines	184
7.4 Multiple Reefing	185
7.5 Reefed Inflation Characteristics	185
7.6 Calculations for Skirt Reefing for Flat Circular Canopies	185
7.7 Skirt-Reefing of Extended-Skirt Canopies	186
7.8 Reefed Supersonic Parachutes	187
7.9 Reefing Rings	188
8 CANOPY PRESSURE DISTRIBUTION	188
8.1 Inflated Canopy – Pressure Distribution in Subsonic and Transonic Flow	188
8.2 Inflated Canopy – Pressure Distribution in Supersonic Flow	193
8.3 Inflating Canopy – Pressure Distribution in Subsonic Flow	196
9 CANOPY STRESS DISTRIBUTION	198
9.1 Definitions and Determination of Basic Working Equations for Cord-Line Profile	198
9.2 Cloth Stress as Function of the Gore Bulge and the Differential Pressure	201
9.3 The Method of Stress Analysis	203
10 PRIMARY-BODY WAKE EFFECTS	204
10.1 Subsonic Flow	204
10.1.1 Theoretical Approach for Determining Velocity and Pressure Distribution in Wake of Primary Bodies of Revolution	204
10.1.2 Drag Reduction on a Secondary Body Due to Wake of a Primary Body	210
10.2 Transonic and Supersonic Wake	211
10.2.1 Wake Behind Bodies of Revolution	211
10.2.2 Supersonic Wake Prediction	215
10.2.3 Drag Reduction of Secondary Bodies in the Wake of Primary Bodies	217
10.2.4 System Drag	218
11 PARACHUTE STABILITY	224
11.1 Static Stability	225
11.1.1 Normal-Force and Moment Coefficients of Various Canopy Types	226
11.1.2 Effects of Cloth Permeability (Effective Porosity)	226
11.1.3 Static Stability Determination Through Flow Visualization	227

<i>Section</i>	<i>Page</i>
11 PARACHUTE STABILITY (Cont'd)	
11.2 Dynamic Stability	228
11.2.1 Equation of Motion of a Parachute as a Rigid Body	229
11.2.2 Frequency Equation of the System of Equations of Motion	230
11.2.3 Sample Calculation for a Statically Stable Canopy	242
12 AERODYNAMIC HEATING	252
12.1 Energy Equations	252
12.1.1 Energy Flow Into Canopy by Convection	253
12.1.2 Convective Heat-Transfer Coefficient	253
12.1.3 Energy Flow into Canopy from Solar Radiation	254
12.1.4 Energy Loss from Canopy by Radiation to Space	254
12.1.5 Energy Loss from Canopy by Radiation to the Earth	257
12.1.6 Energy Stored by Canopy	257
12.1.7 Total Energy Balance	257
12.2 Sample Calculations	257
12.2.1 Case I	258
12.2.2 Case II	258
13 RELIABILITY	259
13.1 Reliability Requirements	259
13.2 Causes of Unreliability	260
13.3 Reliability Assessment	262
13.3.1 Definition of Reliability	262
13.3.2 Reliability Distributions	263
13.3.3 Single-Use vs Multiple-Use	263
13.3.4 Overall System Reliability	264
13.3.5 Component Reliability Analysis	266
13.4 Reliability-Assessment Interpretation	270
13.5 Reliability Improvement	271
References	271

Illustrations

<i>Number</i>		
4-1	Mean Molecular Weight vs Altitude	123
4-2	Pressure vs Altitude	125
4-3	Mass Density vs Altitude	125
4-4	Sound Speed vs Altitude	125
4-5	Kinematic Viscosity vs Altitude	126
4-6	Coefficient of Viscosity vs Altitude	126
4-7	Coefficient of Thermal Conductivity vs Altitude	126
4-8	Altitude vs Temperature	126

Illustrations (Cont'd)

<i>Number</i>	<i>Page</i>
4-9 Altitude vs Electron Density	127
4-10 Mean Wind Speed in Upper Atmosphere	127
4-11 Probability Occurrence of Extreme 3000-ft Shears with Height	127
4-12 Atmospheric Pressure on Mars	129
4-13 Atmospheric Temperature of Mars	129
4-14 Nominal Porosity of Parachute Cloth Materials vs Differential Pressure	131
4-15 Derivation of the Term Effective Porosity	132
4-16 Effective Porosity vs Differential Pressure	132
4-17 Microscopic Pictures of Four Generally-Used Parachute Cloth Materials	132
4-18 Effective Porosity vs Density Ratio (MIL-C-7020 B, Type I)	134
4-19 Effective Porosity vs Density Ratio (MIL-C-7350 B, Type I)	134
4-20 Effective Porosity vs Density Ratio (MIL-C-8021 A, Type I)	135
4-21 Effective Porosity vs Density Ratio (MIL-C-8021 A, Type II)	135
4-22 Effective Porosity vs Pressure Ratio (MIL-C-7020 B, Type I)	136
4-23 Effective Porosity vs Pressure Ratio (MIL-C-7350 B, Type I)	136
4-24 Effective Porosity vs Pressure Ratio (MIL-C-8021 A, Type I)	137
4-25 Effective Porosity vs Pressure Ratio (MIL-C-8021 A, Type II)	137
4-26 Effective Porosity of a Wire Screen vs Density Ratio	138
4-27 Effective Porosity of a Wire Screen vs Pressure Ratio	138
4-28 Density Exponent vs Pressure Ratio for MIL-C-7020 B, Type I, 40 lb/in. Nylon Cloth	139
4-29 Density Exponent vs Pressure Ratio for MIL-C-7350 B, Type I, 90 lb/in. Nylon Cloth	139
4-30 Density Exponent vs Pressure Ratio for MIL-C-8021 A, Type I, 200 lb/in. Nylon Cloth	140
4-31 Density Exponent vs Pressure Ratio for MIL-C-8021 A, Type II, 300 lb/in. Nylon Cloth	140
4-32 Force vs Time in the Opening of a Standard 28-ft Canopy, at 260 Knots	141
4-33 Force vs Time in the Opening of a Standard 28-ft Canopy with Reefing Rings, at 260 Knots	141
4-34 Representation of Length of Suspension Lines Behind Primary Body	142
4-35 Trial-and-Error Solution for t_1	145
4-36 Calculation Sheet to Determine t_2	147
4-37 Force vs Time of a 28-ft Flat Circular Canopy (No Bag Deployment)	148
4-38 Force vs Time of a 28-ft Flat Circular Canopy (Bag Deployment)	148
4-39 Shape of Fully Inflated Canopy	150

Illustrations (Cont'd)

Number	Page
4-40 Canopy Shape During Inflation	150
4-41 Diameter of Canopy Mouth During Inflation	151
4-42 Canopy Volume During Inflation	154
4-43 Approximation of Terms in Equation of Motion	156
4-44 Sample Calculation Sheet for Determining Instantaneous Canopy Volume	158
4-45 Instantaneous Volume of the Canopy as a Function of the Dimensionless Filling Time	160
4-46 V vs t_f and the Determination of Proper Filling Time	160
4-47 Sample Calculation Sheet for Maximum Force vs t_f	161
4-48 Values of the Parachute Force and Determination of the Opening-Shock	162
4-49 Variation of Ratio of Filling Time to Diameter with Snatch Velocity	163
4-50 Variation of Ratio of Filling Time to Diameter with Snatch Velocity	164
4-51 Tangent Force Coefficient vs Angle of Attack for Circular Flat Cloth Type Canopy	166
4-52 Tangent Force Coefficient vs Angle of Attack for 10% Flat Extended Skirt Cloth Type Canopy	166
4-53 Tangent Force Coefficient vs Angle of Attack for 14.3% Full Extended Skirt Cloth Type Canopy	167
4-54 Tangent Force Coefficient vs Angle of Attack for Conical Cloth Type Canopy	167
4-55 Tangent Force Coefficient vs Angle of Attack for Personnel Guide-Surface Cloth Type Canopy	168
4-56 Tangent Force Coefficient vs Angle of Attack for Ribbed Guide-Surface Cloth Type Canopy	168
4-57 Tangent Force Coefficient vs Angle of Attack for Ribless Guide-Surface Cloth Type Canopy	169
4-58 Tangent Force Coefficient vs Angle of Attack, Ring Slot Type Canopy of 20% Geometric Porosity	169
4-59 Tangent Force Coefficient vs Angle of Attack, Ribbon Parachute of 20% Geometric Porosity	169
4-60a Tangent Force Coefficient vs Angle of Attack of Various Canopies – Circular Flat	170
4-60b Tangent Force Coefficient vs Angle of Attack of Various Canopies – 10% Extended Skirt	170
4-60c Tangent Force Coefficient vs Angle of Attack of Various Canopies – Personnel Guide-Surface	171
4-61 Tangent Force Coefficient at Stable Angle of Attack as a Function of Effective Porosity for Several Canopy Types	171
4-62 Drag Coefficient at Zero Angle of Attack as a Function of Effective Porosity for Several Canopy Types	171
4-63 General Equilibrium Conditions	172
4-64 Variation of the Coefficient of Effective Drag, $C_{D_o} (eff)$, as a Function of Rate of Descent	173
4-65 Density and Gravity Ratios as a Function of Altitude	174
4-66 Comparative Performance Characteristics, Captive (Rocket Sled) Tests	175

Illustrations (Cont'd)

Number		Page
4-67	Drag Coefficient vs Mach Number, Rigid and Flexible Type Canopies	176
4-68	Required Theoretical Canopy Porosity to Achieve Stable Airflow Conditions (Canopy Diameters $D_0 < 6$ ft)	177
4-69	Comparative Drag Coefficients for Various Ribbon Type Canopy Designs	178
4-70	Drag Coefficient vs Mach Number, Hemisflo Ribbon Type Canopy (Free-Flight Test)	179
4-71	Area Ratio vs Mach Number, Hemisflo Ribbon Type Canopy (Free-Flight Test)	179
4-72	Drag Coefficient vs Area Ratio, Hemisflo Ribbon Type Canopy (Free-Flight Test)	179
4-73	C_D vs q , Hemisflo Ribbon Type Canopy (Free-Flight Test)	180
4-74	Effective Drag Coefficient vs Reynolds Number, Flat Circular Solid Cloth Type Canopy)	180
4-75	Drag Coefficient vs Reynolds Number, Hemisflo Ribbon Type Canopy (Free-Flight Test)	181
4-76	Area Ratio vs Reynolds Number, Hemisflo Ribbon Type Canopy (Free-Flight Test)	181
4-77	Average Decreasing Drag Coefficient Ratio for Flat Circular Solid Cloth Type Canopies in Clustered Configurations	181
4-78	Performance Characteristics of Flat Circular Ribbon Type Canopies in Triple Cluster Configuration	182
4-79	Reefing Methods – System I	183
4-80	Reefing Methods – System II	183
4-81	Reefing Methods – System III	183
4-82	Vent Reefing Forces in the Parachute, Suspension Lines and Control Lines	184
4-83	Skirt Reefing; Reefing Line, Control Line, and Skirt Opening Forces	184
4-84	C vs Number of Gores	185
4-85	Drag Area Ratio vs Reefing Line Diameter Ratio	186
4-86	Drag Area Ratio vs Reefing Line Diameter Ratio for Extended Skirt Canopies	187
4-87	Drag Coefficient Variation with Reefed Diameter Ratio	188
4-88	External Pressure Coefficients vs M_∞ for Flat Circular Ribbon Type Canopies	189
4-89	External and Internal Pressure Distribution for Flat Circular Ribbon Type Canopies	190
4-90	External and Internal Pressure Distribution for Guide-Surface Type Canopies	191
4-91	External Pressure Coefficients vs Mach Number for Guide-Surface Type Canopies	192
4-92	Schlieren Picture of a Ribbon-Type Drag-Producing Surface at a Free-Stream Mach Number of 0.897	193
4-93	Pressure Coefficient Distribution Curves of a 26%-Porosity Ribbon-Type Canopy Model With and Without Suspension Lines, No Forebody	194
4-94	Pressure Coefficient Distribution of a 26%-Porosity Ribbon-Type Canopy Model With Suspension Lines and Forebody	195

Illustrations (Cont'd)

Number	Page
4-95- Schematic Pressure Coefficient Distribution of Models 1 through 7 in Inflating Parachute 4-102 Canopy Series	197
4-103 Forces Acting on a Small Segment of a Flexible Shell in Equilibrium	199
4-104 Gore Pattern of T 10 Extended Skirt Parachute	199
4-105 Intersection of a Plane P_1 with Inflated Gore	200
4-106 Top View of Inflated Canopy	201
4-107 Profile of a Canopy Formed by the Gore Centerline	201
4-108 Equilibrium of a Strip of a Canopy Gore	202
4-109 Geometry of a Gore Section with Consideration of the Cloth Strain	202
4-110 Velocity Distribution for a Fluid at Rest and a Moving Body	205
4-111 Velocity Distribution for a Body at Rest and a Moving Fluid	206
4-112 Pressure Distribution in the Wake of a Body of Revolution ($C_D = 0.35$)	208
4-113 Velocity Distribution in Accordance with Analytical and Experimental Studies	210
4-114 κ vs x/D as Determined from Experimental Data	211
4-115 Data for a Body of Revolution (Based on $\kappa = 0.0633$ Related to C_p at $x/D = 8$)	212
4-116 Bodies of Revolution	213
4-117 κ vs x/D as Determined by Experiment	214
4-118a Wake Drag Coefficient Ratio	215
4-118b Wake Drag Coefficient Ratio	216
4-118c Wake Drag Coefficient Ratio	217
4-119a Wake Drag Coefficient Ratio	218
4-119b Wake Drag Coefficient Ratio	218
4-119c Wake Drag Coefficient Ratio	219
4-120 Schematic Diagram of Wake Structure	219
4-121 Sketch of Flow Patterns Around Primary Bodies Alone at Supersonic Speeds	220
4-122 Secondary Body Stagnation Pressure Coefficient vs M_∞ with Boundary Layer Bleed	220
4-123 Secondary Body Stagnation Pressure Coefficient vs Free-Stream Mach Number for a Flat Plate in the Wake of a Skirted Hemisphere	221
4-124 Total Drag Coefficient vs Free-Stream Mach Number for a Flat Plate in the Wake of a Semi-Infinite Cylinder with Boundary Layer Bleed	221
4-125 Pressure Relations of Body Combinations in Supersonic Flow	222
4-126 C_{pb} vs M_∞ for a Skirted Hemisphere with a Hollow Hemisphere in its Wake	222

Illustrations (Cont'd)

Number	Page
4-127 C_{Dh} vs M_∞ for a Semi-Infinite Cylinder with Boundary Layer Bleed and a Flat Plate in its Wake	223
4-128 Drag Coefficient vs Mach Number	223
4-129 C_{Df} vs M_∞ for a Hollow Hemisphere in the Wake of a Skirted Hemisphere	224
4-130 Parachute Coordinate System	225
4-131 Application of Forces on a Canopy	226
4-132 Determination of Normal Force Acting on Canopy	227
4-133 Results of Wind Tunnel Tests on Solid Flat, Slotted High Porosity, Ribbon and Guide-Surface Type Parachute Canopies (Rigid Models)	228
4-134 Moment Coefficients of Canopy Models	229
4-135 Normal Force and Moment Coefficient vs Angle of Attack for Circular Flat Cloth Canopy	230
4-136 Normal Force and Moment Coefficient vs Angle of Attack for 10% Flat Extended Skirt Cloth Canopy	230
4-137 Normal Force and Moment Coefficient vs Angle of Attack for 14.3% Full Extended Skirt Cloth Canopy	231
4-138 Normal Force and Moment Coefficient vs Angle of Attack for Conical Cloth Type Parachute Canopy	231
4-139 Normal Force and Moment Coefficient vs Angle of Attack for Personnel Guide-Surface Cloth Canopy	232
4-140 Normal Force and Moment Coefficient vs Angle of Attack for Ribbed Guide-Surface Cloth Canopy	232
4-141 Normal Force and Moment Coefficient vs Angle of Attack for Ribless Guide-Surface Cloth Canopy	233
4-142 Normal Force and Moment Coefficient vs Angle of Attack, Ring-Slot Canopy of 20% Geometric Porosity	233
4-143 Normal Force and Moment Coefficient vs Angle of Attack, Ribbon-Type Canopy of 20% Geometric Porosity	233
4-144 Normal Force Coefficient vs Angle of Attack of Various Parachutes	234
4-145 Moment Coefficient vs Angle of Attack of Various Parachutes	235
4-146 Flow Field Around Several Canopies at 15-Degree Angle of Attack	236
4-147 Parachute Canopy in Motion	237
4-148 Arrangement of Coordinates and Forces for Parachute System in Flight	238
4-149a Body of Revolution for $c/r = 0$ (Circular Disk)	239
4-149b Body of Revolution for $c/r = 1$ (Sphere)	239
4-150 Rotating Parachute System	240

Illustrations (Cont'd)

Number		Page
4-151	Graphical Representation of Apparent Moment of Inertia as a Function of c/r .	241
4-152	Apparent Mass Related to Enclosed Mass vs Porosity	243
4-153	Ribless Guide-Surface Parachute Canopy	244
4-154	Moment and Lift Coefficients vs Angle of Attack for Ribless Guide-Surface Canopy	245
4-155	Replacement of Ribless Guide-Surface Parachute by Rotational Ellipsoid	248
4-156	Graphical Presentation of Motion of Parachute System During Descent	250
4-157	Graphical Presentation of α and $\alpha + \beta$ vs Time	250
4-158	Reynolds Numbers for Various Altitudes	254
4-159	Average Heat Transfer Coefficients on Ribbon Grids at Supercritical Pressure Ratios	255
4-160	Reliability from a Series of Trials	265
4-161	Reliability Levels for a Series of Tests With and Without Failures	266
4-162	The Normal Distribution	268
4-163	Exaggerated Stress - Strength Distribution	270

Tables

4-1	Atmospheric Properties as a Function of Altitude, Temperature, Pressure and Density	124
4-2	Composition of the Lower (Dry) Atmosphere	127
4-3	Experimental Data for Ribless Guide-Surface Canopy Measured in Wind Tunnel at $Re \approx 6 \times 10^5$ and $v_\infty \approx 105$ ft/sec (Nominal Canopy Cloth Porosity = 120 cu ft per sq ft per min)	246
4-4	Coordinates of Parachute System During Descent	251
4-5	Angle of Attack (α) and Inclination Angle ($\alpha + \beta$)	251

CHAPTER 4

AERODYNAMIC AND OPERATIONAL CHARACTERISTICS OF DEPLOYABLE AERODYNAMIC DECELERATORS

SEC. 1 GENERAL

Knowledge of the aerodynamic and operational characteristics of deployable aerodynamic decelerators is one of the major prerequisites for the design and performance prediction of dependable aerodynamic deceleration and stabilization systems. In selecting a particular aerodynamic decelerator to perform a specific task, the characteristics of the decelerator itself must be known, so that its performance in combination with a primary body, i.e., as a system, can be predicted.

At the present time, sufficient knowledge is not available to provide accurate analytical approaches for the calculation of all performance and operational characteristics of deployable aerodynamic decelerators. This is particularly true with respect to those of textile parachute canopies because the dynamic behavior of textile parachute canopies is not adequately known or understood, particularly in the areas of canopy opening and descent. Consequently, experimental data must be relied upon primarily. However, in some areas analytical approaches have been developed which will yield reasonable approximations of the characteristics of actual decelerator performance.

In the following sections, an attempt is made to present performance characteristics for textile parachute canopies based on available data, and to compile analytical approaches for the calculation of textile parachute canopy performance and operation. It must be pointed out that these analytical approaches are initial attempts in developing calculation methods, and that these approaches are subject to revision as new knowledge becomes available. This knowledge will then be utilized to either verify, augment, or completely revise the method of analysis. However, the results obtainable by the analytical methods presented are, in most cases, reasonably accurate and may be utilized for the determination of textile parachute canopy and parachute systems performance and operation.

In order to obtain a comprehensive and yet easily distinguishable presentation of the complex area of

the aerodynamic and operational characteristics of textile parachute canopies and systems, this Chapter has been divided into a number of sections, each one dealing with a particular phenomenon associated with the performance and operation of parachute canopies.

Pertinent data about the atmospheric environment of our and other near planets are included since the existence of an atmosphere is the prerequisite for parachute or other aerodynamic decelerator operation. A discussion of the effective porosity of textile parachute materials is placed next, since major canopy performance and operational characteristics, such as opening force, drag, and stability are directly related to effective porosity. The remainder of the chapter is then divided into discussions of the various aspects of canopy operation and performance in a sequence normally occurring during parachute canopy operations.

A major portion of the material presented hereafter constitutes the current state-of-the-art of results or research studies conducted by the University of Minnesota under a Tri-Service sponsored program of basic aerodynamic decelerator investigations. Dr. Helmut G. Heinrich is the Principal Investigator on this program. Dr. Heinrich as well as members of his staff have contributed portions of the following sections.

As an aid to the practical application to the analytical approaches, some of the analytical methods presented in the following sections are used in the Sample Calculation, Chapter 12. This Chapter may be consulted for detailed calculation procedures.

SEC. 2 THE ATMOSPHERE

Aerodynamic deceleration devices may be expected to be deployed and operated in a wide range of altitudes and Mach numbers. Naturally, the effectiveness of drag devices is limited to the region wherein the density of the atmosphere creates a resistance force of sufficient magnitude to generate the required drag. This magnitude of the resistance or retarding force will vary according to the particular mission profile

desired; it is conceivable that, even at altitudes above 600,000 ft, the residual atmospheric density is still sufficient to decelerate a relatively large aerodynamic drag device and alter its trajectory. Consequently, in calculating or predicting the operational and performance characteristics of aerodynamic deceleration devices, properties of the atmosphere must be known for a considerable range of altitudes. Primary concern, of course, is with our own atmosphere; however, as the age of space travel advances added interest will focus upon the atmospheric properties of other planets, such as Mars and Venus. Therefore, pertinent information about these planets, to the extent known, is also included.

2.1 Properties of The Earth's Atmosphere

2.1.1 ATMOSPHERIC DENSITY. The best current estimates of the variation of mean atmospheric density with altitude are given by the 1959 ARDC Model Atmosphere (Ref (4-1)), as summarized in Table 4-1. These data represent an average of the overall relevant data, and in no way represent spatial or temporal variations. At lower altitudes, between sea level and approximately 250,000 ft, measurements are obtained by a variety of techniques and the accuracy of the data given in Ref (4-1) is estimated to be ± 10 per cent (Ref (4-2)). Between 250,000 and 750,000 ft, measurements are made by rockets and by satellite drag techniques, with accuracy probably between 30 and 100 per cent. Above 750,000 ft, satellite drag measurements yield accuracy roughly of a factor of two (Ref (4-2)). In general, the inaccuracy increases with increasing altitude; however, the ARDC mean densities are reasonably well confirmed by recent observations (Ref (4-3) through (4-7)).

Ref (4-2) considers the temporal variations of the atmospheric density and density variations with latitude. In the region between sea level and 600,000 ft altitude, the only major periodic variation is that of gravitation and thermal tides. Tides are observed principally as periodic variations in direction and magnitude of the upper atmospheric winds. Thermal tides are also observed as diurnal and semi-diurnal variations in the earth's magnetic field, caused by dynamo effects in the tidally perturbed ionosphere. The lunar semi-diurnal tide is smaller than the solar semi-diurnal tide by a factor of 15, although the moon's gravitational pull is significantly greater than the sun's. According to recent measurements, temporal variations in atmospheric density can be expected to be small at lower altitudes, reaching a peak of 20 per cent at approximately 350,000 ft and then damping out sharply. There will also be random fluctuations, confined largely to the altitude regime between 250,000

and 350,000 ft. It has been postulated that these variations consist of long-period gravity waves, generated by possible thermal instabilities or by meteorological disturbances in the lower atmosphere, propagating upwards with increasing amplitude and causing a maximum variation of approximately 10 per cent. Seasonal variations appear to be negligible except in high latitudes.

For altitudes above 600,000 ft, variations in density follow a different pattern. Here, the controlling factors are solar effects: diurnal, 27-day, 11-year cycle, and flare (not mechanical) effects. Ref (4-8) cites data reported at the Tenth International Astronautical Congress which show that at altitudes between 650,000 and 1,000,000 ft the effective air densities vary from day to day and month to month by up to 30 per cent, and by as much as a factor of three at higher altitudes. Between a latitude range of 35°S to 50°N, and at altitudes above 650,000 ft, air density does not vary with latitude by more than a factor of 1.5.

Changes in air density are relatively rapid. Diurnal variations of 2 per cent, 11 per cent, and 18 per cent have been reported at altitudes between 650,000 and 1,000,000 ft. The variation of air density is somewhat cyclic, with maximum and minimum values occurring about every 27 days at altitudes above 650,000 ft. Variation of atmospheric density from day to night in the upper atmosphere has not been sufficiently large to permit accurate measurement at altitudes up to

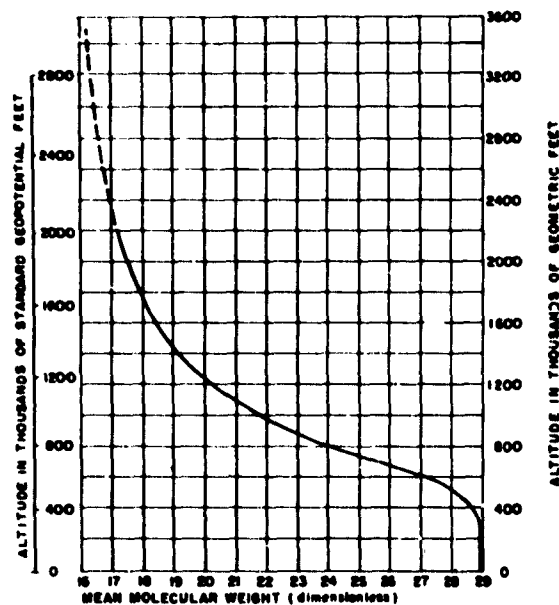
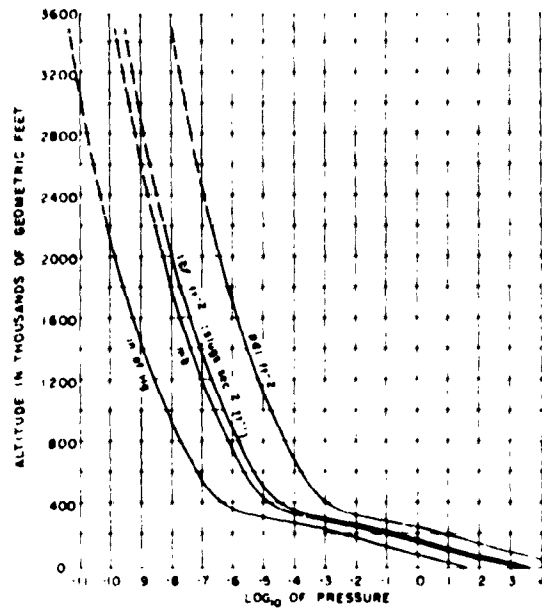


Fig. 4-1 Mean Molecular Weight vs Altitude

TABLE F. 4-1
ATMOSPHERIC PROPERTIES AS A FUNCTION OF
ALTITUDE, TEMPERATURE, PRESSURE & DENSITY

Altitude		Temp. T, °R	Pressure P, lb/ft ²	Density ρ , lb/ft ³	Altitude		Temp. T, °R	Pressure P, lb/ft ²	Density ρ , lb/ft ³
Z, ft	H, ft				Z, ft	H, ft			
0	0	518.69	2.1162 + 3	2.3769 - 3	96,000	95,560	412.27	2.7604	3.9007
3,000	3,000	507.99	1.8967	2.1752	99,000	98,582	417.16	2.4134	3.3704
5,000	5,998	497.30	1.6960	1.9869	102,000	101,504	422.05	2.1134	2.9172
9,000	8,996	486.61	1.5129	1.8113	105,000	104,474	426.94	1.8536	2.5293
12,000	11,993	475.92	1.3462	1.6480	108,000	107,444	431.83	1.6282	2.1967
15,000	14,989	465.23	1.1948	1.4962	111,000	110,412	436.72	1.4324	1.9109
18,000	17,984	454.55	1.0575	1.3553	114,000	113,380	441.60	1.2620	1.6649
21,000	20,979	443.87	9.3326 + 2	1.2249	117,000	116,347	446.49	1.1134	1.4528
24,000	23,972	433.20	8.2116	1.1043	120,000	119,313	451.37	9.8372 + 0	1.2697
27,000	26,965	422.53	7.2026	9.9311 - 4	123,000	122,279	456.25	8.7032	1.1113
30,000	29,957	411.86	6.2966	8.9068	126,000	125,243	461.13	7.7102	6.7410 - 6
33,000	32,948	401.19	5.4854	7.9656	129,000	128,207	466.01	6.8395	8.5505
36,000	35,938	390.53	4.7612	7.1028	132,000	131,170	470.88	6.0748 + 0	7.5159 - 6
39,000	38,927	389.99	4.1241	6.1608	135,000	134,132	475.76	5.4025	6.6156
42,000	41,916	389.99	3.5723	5.3365	138,000	137,093	480.63	4.8104	5.9309
45,000	44,903	389.99	3.0945	4.6227	141,000	140,053	485.50	4.2884	5.1460
48,000	47,890	389.99	2.6807	4.0045	144,000	143,013	490.38	2.8276	4.5473
51,000	50,876	389.99	2.3223	3.4692	147,000	145,971	495.24	3.4202	4.0234
54,000	53,861	389.99	2.0119	3.0055	150,000	148,929	500.11	3.0597	3.5642
57,000	56,845	389.99	1.7431	2.6039	153,000	151,886	504.98	2.7402	3.1613
60,000	59,828	389.99	1.5103	2.2561	156,000	154,842	508.79	2.4566	2.8130
63,000	62,810	389.99	1.3086	1.9548	159,000	157,797	508.79	2.2032	2.5228
66,000	65,792	389.99	1.1339	1.6938	162,000	160,751	508.79	1.9760 + 0	2.2626 - 6
69,000	68,772	389.99	9.8253 + 1	1.4678	165,000	163,705	508.79	1.7723	2.0294
72,000	71,752	389.99	8.5142	1.2719	168,000	166,657	508.79	1.5896	1.8202
75,000	74,731	389.99	7.3784	1.1022	171,000	169,609	508.79	1.4258	1.6326
78,000	77,709	389.99	6.3944	9.5523 - 5	174,000	172,560	508.79	1.2789	1.4644
81,000	80,687	389.99	5.5418	8.2787	177,000	175,510	504.77	1.1469	1.3238
84,000	83,663	392.69	4.8044	7.1277	180,000	178,460	497.49	1.0272	1.2028
87,000	86,639	397.59	4.1719	6.1132	183,000	181,408	490.21	0.1840 - 1	1.0915
90,000	89,613	402.48	3.6292	5.2531	186,000	184,356	482.94	8.1982	9.8898 - 7
93,000	92,587	407.38	3.1624	4.5225					



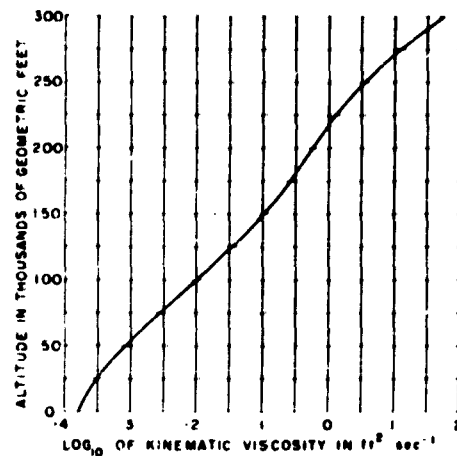


Fig. 4-5 Kinematic Viscosity vs Altitude

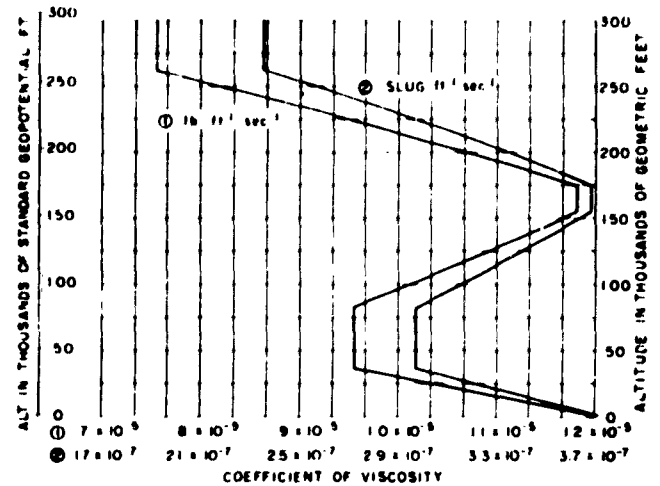


Fig. 4-6 Coefficient of Viscosity vs Altitude

ratio of $N_2/O_2 = 3.728$, and in a weight ratio of $N_2/O_2 = 3.2635$. Approximately one per cent of the dry atmosphere consists of trace gases, principally argon. Table 4-2 lists the composition of the lower dry atmosphere (Ref (4-8)).

Variables in the lower atmosphere are water vapor, ozone, and aeromols (particles of greater than molecular size suspended in the air). All of these constituents are distributed in a variety of ways, depending on latitude, longitude, altitude, and time, so that accurate prediction of their occurrences and quantities are difficult to make. Carbon dioxide is thought to vary slightly over long periods, owing to combustion of carbon fuels.

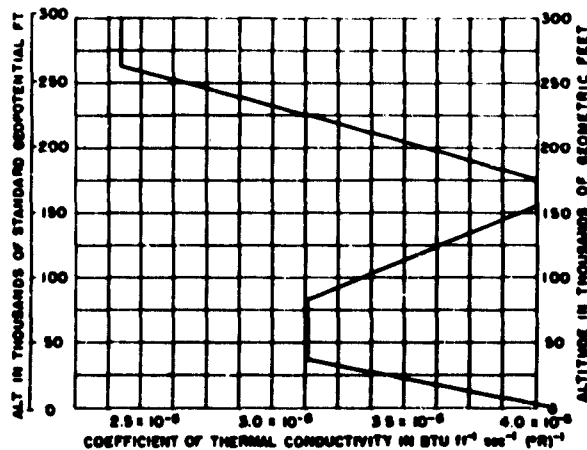


Fig. 4-7 Coefficient of Thermal Conductivity vs Altitude

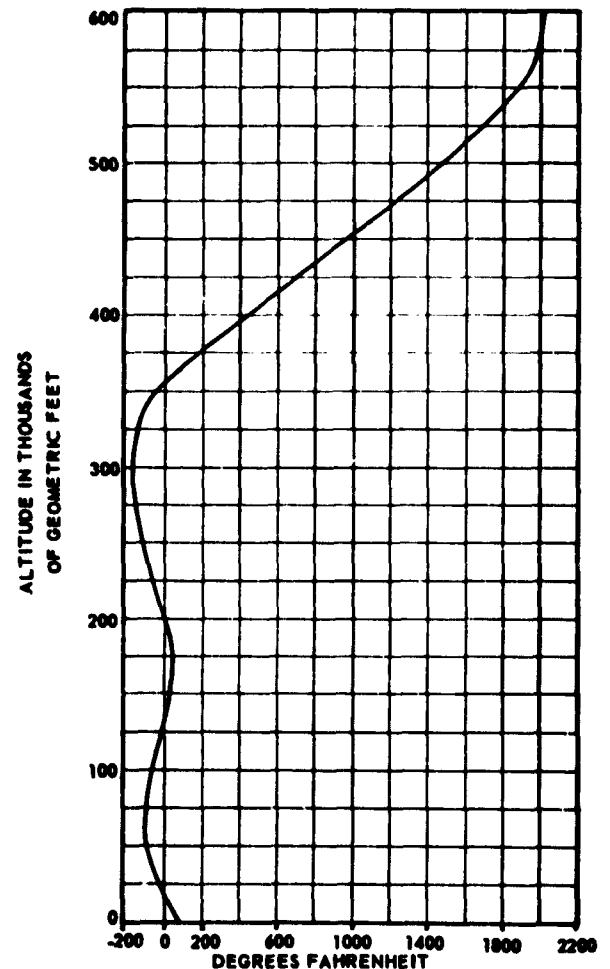


Fig. 4-8 Altitude vs Temperature

TABLE 4-2 COMPOSITION OF THE LOWER (DRY) ATMOSPHERE

Gas	Volume, %	Weight, %
Nitrogen (N ₂)	78.088	75.527
Oxygen (O ₂)	20.949	23.143
Argon (A)	9.3x10 ⁻¹	1.282
Carbon Dioxide (CO ₂)	3.0x10 ⁻²	4.6x10 ⁻²
Neon (Ne)	1.8x10 ⁻³	1.3x10 ⁻³
Helium (He)	5.2x10 ⁻⁴	7.2x10 ⁻⁵
Methane (CH ₄)	1.4x10 ⁻⁴	7.8x10 ⁻⁵
Krypton (Kr)	1.1x10 ⁻⁴	3.3x10 ⁻⁵
Nitrous Oxide (N ₂ O)	5.0x10 ⁻⁵	7.6x10 ⁻⁵
Hydrogen (H ₂)	5.0x10 ⁻⁵	3.5x10 ⁻⁶
Xenon (Xe)	8.6x10 ⁻⁶	3.9x10 ⁻⁵
Nitrogen Dioxide (NO ₂)	1.0x10 ⁻⁷	2.0x10 ⁻⁷

2.1.4 IONOSPHERE. The region of the atmosphere above 250,000 ft contains a series of layers of ions and electrons which comprise the ionosphere. These are commonly known as the D, E, F₁, and F₂ layers; each has individual properties. The ions and electrons in this region are not normally associated with aerodynamic considerations; however, the aerodynamic deceleration of vehicles based upon magneto-aerodynamic principles may be of major significance in this altitude regime.

The basic source of ionizing energy in the ionosphere is solar radiation, principally ultraviolet light; this

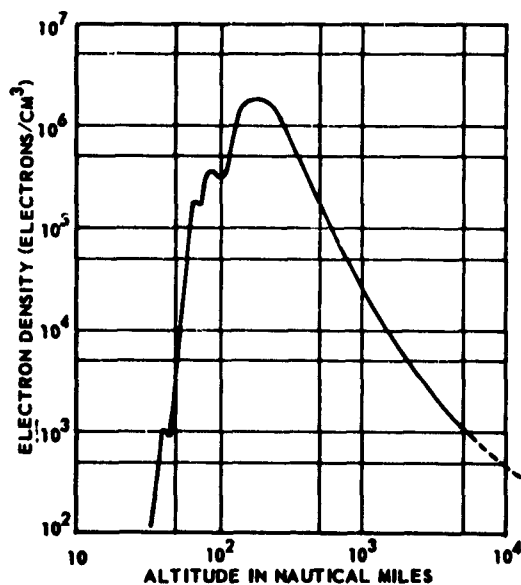


Fig. 4-9 Altitude vs Electron Density

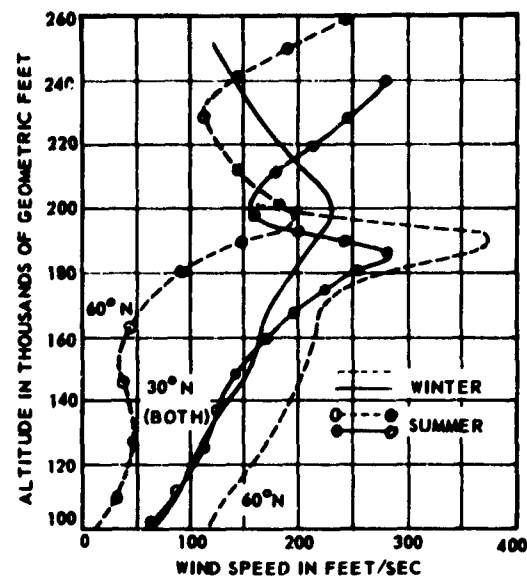


Fig. 4-10 Mean Wind Speed in Upper Atmosphere

explains the completely different conditions during day and night. Corpuscular radiation is also a contributing factor of importance. Constant changes occur in the ionosphere; as atoms and molecules are being converted to charged particles, the ions are recombining to form neutral gases.

For molecules or atoms which can be ionized by a particular wave-length of radiation, the production of

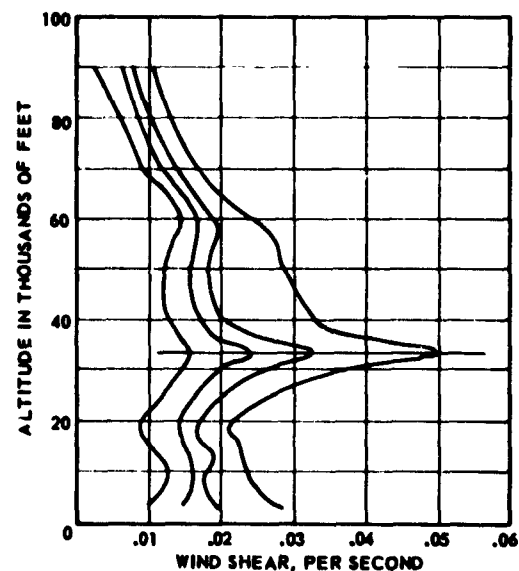


Fig. 4-11 Probability Occurrence of Extreme 3000-ft Shears with Height

charged particles is a function of the product of the incident radiation density, molecular density, and the molecule's effective cross-section. In the atmosphere, the density of molecules and atoms increases along the path of radiation, while the radiation intensity decreases as it is absorbed along the path. Thus, at some level, the product of radiation intensity and density of ionizable molecules reaches a maximum; this is the region of maximum electron production. At altitudes where the air begins to vary in composition with increasing height, there is a tendency for the ionization to become stratified, owing to differences in the solar-radiation absorptive characteristics of the gases. Curves of the variation of electron density with height show maxima which are the basis of the term "layers". Fig. 4-9 is a typical example of such a curve (Ref (4-8)); it is representative of conditions which exist at summer noon in mid-latitudes during periods of high sunspot numbers.

2.1.5 WINDS AND TURBULENCE. The probability of winds and gusts of a particular intensity is a factor that must be considered for the operation of any aerodynamic deceleration device. The study of winds may be divided into two phases: the wind structure, and the turbulence, i.e., gusts and wind shear.

A great deal of information has been accumulated on mean winds; the Handbook of Geophysics for Air Force Designers (Ref (4-21)) contains this type of data. For general operational planning applications, these data are very helpful; however, since variation at a specific location or time may be sizable, more specific information should be obtained for an immediate operational area. A study of all data collected for the higher altitude regime is presented in Ref (4-10). The mean winds determined in this study are shown in Fig. 4-10.

Superimposed on the general movement of the air are sudden changes, relatively abrupt discontinuities, and fluctuations. These fall under the general term "turbulence". Although fluctuations are always present in the atmosphere, their intensity and frequency vary with location, altitude, and with the days and seasons of the year. Gust factors for various mean and extreme wind speeds, particularly applicable for low altitudes, are given in the Handbook of Geophysics (Ref (4-21)).

Wind shear is defined as the vector difference between wind vectors at two relatively adjacent altitudes, divided by the altitude difference. The shear may be further resolved into a horizontal component and vertical component, or cross-component and a downwind component. The Handbook of Geophysics gives a maximum value of 45 fps per 1000 ft (0.045 per sec.) for the shear in the windiest area and season of the United States, based on wind speeds with a one per

cent probability. Fig. 4-11 shows the probability of occurrence of extreme 3000-ft shears with height, as taken from Ref (4-11).

2.2 Earth Gravity. The true nature of the gravity field has been a matter of intense speculation. Einstein's general theory of relativity is considered the most logical description at the present time.

The gravity field of the Earth consists of two parts, the principal part caused by mass, and a lesser part caused by the Earth's rotation. According to Ref (4-12), the rotational factor is small, being only about one-third of a per cent of the total field at sea level at the equator.

Both the centrifugal force and the effect of gravity are directed in a radial direction, their combined effect establishing the field. The work required to bring a unit mass from an infinite distance to any point in the field is defined as the potential. The first derivative of the gravity potential with respect to space coordinates is the force, or the equivalent acceleration of gravity for a unit mass. The acceleration of gravity varies over the surface of the Earth between the limits of 32.05 ft per sec² and 32.24 ft per sec². Based on its ellipsoid shape—equatorial radius: 3,444.054 n.m. (20,925,400 ft), polar radius: 3,432.458 n.m. (20,856,000 ft)—the variation of gravity with latitude at the Earth's surface is expressed by the International Gravity formula of 1930 (Ref (4-12)):

$$(4-1) \quad g = 978.049 (1 + 0.0052884 \sin^2 \phi - 0.0000059 \sin^2 2 \phi)$$

The value of g is given in cm per sec²; ϕ is the geographical latitude. The second term in the parenthesis covers both the geomagnetic flattening and the increase in centrifugal force as the poles are approached. The third term is a correction because of the earth's variation from a true spheroidal shape.

Variation of the acceleration of gravity with altitude is approximated by the inverse square law

$$(4-2a) \quad g = g_0 \left(\frac{R_1}{R_1 + h} \right)^2$$

where

R_1 = Effective radius of earth at latitude 45° 32' 33";
 h = Geometric altitude; and
 g_0 = Gravity at latitude 45° 32' 33" = 980.665 cm per sec².

Reference 4-13 gives the following formula for the calculation of values for the acceleration of gravity at any elevations above the Earth's surface:

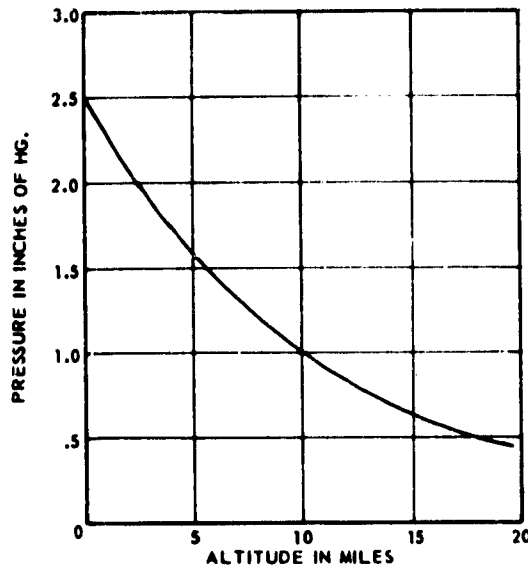


Fig. 4-12 Atmospheric Pressure on Mars

$$(4-2b) \quad g - g'_0 = (0.00030855 + 0.00000022 \cos 2\phi) h + 0.000072 \left(\frac{h}{1000} \right)^2$$

where

g = Acceleration of gravity in cm per sec²;

g'_0 = Value at sea level at the equator (978.04900 cm/sec²);

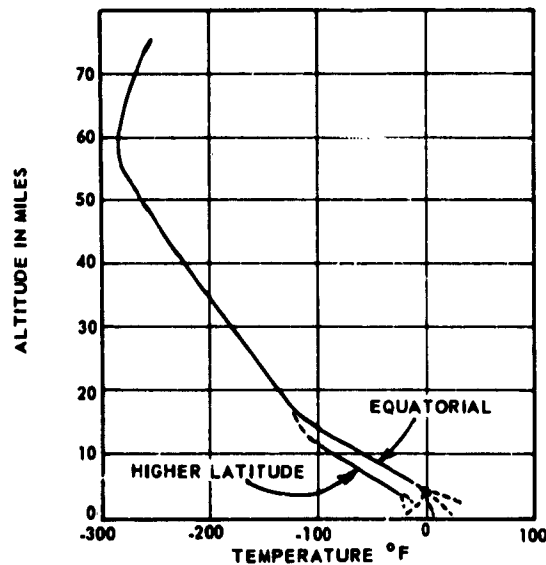


Fig. 4-13 Atmospheric Temperature of Mars

h = Altitude in meters; and

ϕ = Geodetic latitude (angle between the equatorial plane and the normal to the spheroid).

2.3 Environments of Other Planets. Aerodynamic deceleration devices may also be used to aid in the atmospheric entry and landing of space vehicles on other planets. Consequently, some knowledge of the atmosphere surrounding other planets will be required for decelerator design considerations. The two planets considered most likely to be the first targets of future space explorations are Venus and Mars.

2.3.1 VENUS. Venus is similar to Earth: its diameter of 6,680 n.m. is 0.97 that of our planet; its mass, volume, and surface gravity are 81 per cent, 92 per cent, and 85 per cent of the Earth's, respectively. Venus has a nearly circular orbit and is 0.72 of the Earth's distance from the sun; it is the closest planet to the Earth; at the nearest point it is 22.6×10^6 n.m. from the Earth. Earth and Venus both have extensive atmospheres.

The atmosphere of Venus is probably as deep as that of earth and possibly deeper. Ref (4-14) estimates the height of the visible cloud layer of Venus to be in excess of 80,000 ft. From occultations of stars by Venus, Ref (4-15) gives the atmospheric depth as between 250,000 and 400,000 ft. Calculations based on very tentative data indicate that the atmospheric pressure immediately above the cloud layer is between 1.6 and 4 Earth atmospheres. Based upon currently known data, Ref (4-16) cites the value of pressure at the surface of the planet Venus to be ten Earth atmospheres. If, however, the cloud tops are nearer to the surface, the entire atmospheric pressure could be less than Earth's.

Measurements of temperature in the upper atmosphere of Venus (Ref (4-17)) give both the day and night sides as nearly the same, approximately -40 F, with the night side slightly cooler.

One fact about the composition of the Venusian atmosphere stands out: there is definitely a considerable abundance of carbon dioxide. Ref (4-18) reported for the first time the presence of minute traces of water vapor, the total amount of which, if precipitated, would be 19 microns in thickness. Molecular oxygen has not been detected, but there is a possibility of the existence of atomic oxygen.

The cloud cover of Venus has been the object of many theories. From the sparse data available on the chemical processes which take place on Venus, there have been organic compounds suggested as cloud covering, but there is no observational evidence of the presence of any of these compounds as either gases, droplets, or particles. The belief that the

clouds consist of water is not unreasonable. The clouds of Venus are very likely some water with carbon compounds present. Dust can probably be ruled out as the main cloud constituent, but solid carbon dioxide is still a possibility (Ref (4-8)).

Physical Data of the Planet Venus:

Distance from the Sun	
Perihelion	57.4×10^6 n.m.
Mean	58.2×10^6 n.m.
Aphelion	59×10^6 n.m.
Closest approach to Earth	22.6×10^6 n.m.
Greatest distance from Earth	139×10^6 n.m.
Orbital eccentricity	0.007
Orbital inclination to ecliptic	$3^\circ 24'$
Mean orbital velocity	21.7 miles per sec
Mass, compared to Earth	0.82
Volume, compared to Earth	0.92
Diameter (including clouds)	6560 to 6800 n.m. (0.97 of Earth)
Oblateness	0.00
Density ($H_2O = 1$)	4.87
Density (Earth = 1)	0.89
Gravity, surface (Earth = 1)	0.86
Velocity of escape	6.3 miles per sec
Sidereal period	224.7 mean solar days
Rotational period	Several weeks (uncertain).
Axial inclination	24° (uncertain)
Temperature	
Upper atmosphere	-45 F (approx.)
Surface	Unknown, probably hot compared to Earth
Pressure, surface	Unknown; some very uncertain predictions give extremely high values, but low values are possible.

2.3.2 MARS. Mars is about half the diameter of the Earth, with a mass of about 0.10 and a gravity of about 0.33 that of Earth. Mars is about 1.5 times as far from the Sun as Earth, and takes almost two Earth years to complete its orbit about the Sun. The Martian day is close to an Earth day, being approximately 37 minutes longer. The tilt of the Martian axis with respect to its orbital plane is very similar to that of the Earth's, causing the same sort of seasonal variations in climate.

From visual and photographic evidence, and theoret-

ical considerations, the existence of an atmosphere on Mars is unquestioned, but knowledge about its properties is rather limited. Photographic evidence indicates that the Martian atmosphere is of considerable thickness. The pressure at the surface is estimated to be about 0.10 of the Earth's; and recent estimates (Ref (4-19)) indicate a surface pressure of 64 mm Hg (2.5 in.), the pressure at about 58,000 ft. in Earth's atmosphere. Atmospheric pressure is thought to decrease by a factor of ten for every 132,000 ft in elevation. Fig. 4-12 is a graph of pressure versus altitude based on data from Ref (4-19). At an altitude of about 90,000 ft, the pressure of approximately 0.5 in. Hg is identical to Earth's at that altitude. Above this level, the Martian atmosphere is thicker than the terrestrial. As a result, its braking resistance to a vehicle entering will be correspondingly larger.

The temperature profile of the Martian atmosphere is estimated in Ref (4-17) (see Fig. 4-13). The regions in the first few miles of altitude are expected to be in a state of turbulence because of convection currents arising from the warmer surface, and the temperature should be variable in this zone. Above 300,000 ft there are no data on which to judge temperature.

Frequent clouds are observed in the Martian atmosphere; they are usually quite thin, but sometimes obscure portions of the surface. In the lower atmosphere there are yellowish clouds, thought to be the result of vast dust storms which have been observed quite frequently. Some idea of winds on Mars can be inferred from the rate at which clouds have been observed quite frequently travelling across the planet's surface. These clouds are, of course, propelled by winds, and provides some indication of wind speeds. The average speed of the clouds, as reported in Ref (4-19), ranges between 15 and 40 mph.

The composition of the atmosphere is not known definitely, but the main constituent is probably molecular nitrogen (Ref (4-19)). A tentative composition for the Martian atmosphere, as reported in Ref (4-20), is 95 per cent nitrogen, 4 per cent argon, 1 per cent carbon dioxide, small amounts of water vapor and oxygen, and traces of gases such as neon, krypton, and xenon. Ionized and dissociated molecules are probably formed through the action of solar radiation on the upper atmosphere.

Physical Data of the Planet Mars:

Distance from the Sun	
Perihelion	112×10^6 n.m.
Mean	122.6×10^6 n.m.
Aphelion	133.6×10^6 n.m.
Closest approach to Earth	30×10^6 n.m.
Orbital eccentricity	0.0933

Orbital inclination to elliptic	1° 51'
Mean orbital velocity	15.0 miles per sec
Mass, compared to Earth	0.108
Diameter	3,640 m.m. (0.52 of Earth)
Oblateness	0.0052
Density ($H_2O = 1$)	3.96
Gravity, surface (Earth = 1)	0.39
Velocity of escape	3.2 miles per sec
Sidereal period	687.0 mean solar days
Rotational period	24 hr 37 min (mean solar)
Axial inclination	25° 12'
Temperature	
Upper atmosphere	Uncertain, about -150 F°
Surface	Uncertain, -140 F° to +85 F°
Pressure, surface	about 2.5 in. Hg

oscillations of basically unstable canopies also become more violent (Ref (4-22), (4-23)). Attempts have been made to explain the change in canopy inflation characteristics with altitude by the effect of the apparent mass and the mass of air included in the canopy (Ref (4-24)). The variation in the stability behavior of a canopy may also be attributed in part to the effect of apparent and included mass, because the motion of a freely descending parachute is a matter of dynamic stability in which the related air masses are significant terms (see Sec. 11 of this chapter).

However, it is also known that the stability behavior of a canopy depends on the porosity of its drag-producing surface (Ref (4-25), (4-26)). In combination with experience at higher altitudes, this leads to the conclusion that the porosity (or air permeability) of woven sheets is effectively reduced at higher altitudes. If this assumption is correct, it would also, at least in part, account for the increase of opening shock with altitude. Heinrich and Haak have discussed these aspects of porosity, and have also shown that the apparent mass of a canopy varies with the porosity of the drag-producing surface (Ref (4-27)). In view of this interaction of performance characteristics and porosity, studies were made in which the air flow through woven and porous sheets was measured, and correlated with air density and pressure. The results of these efforts are presented below.

SEC. 3 EFFECTIVE POROSITY OF TEXTILE MATERIALS

Several studies indicate that the opening-shock of solid cloth canopies increases with altitude and the

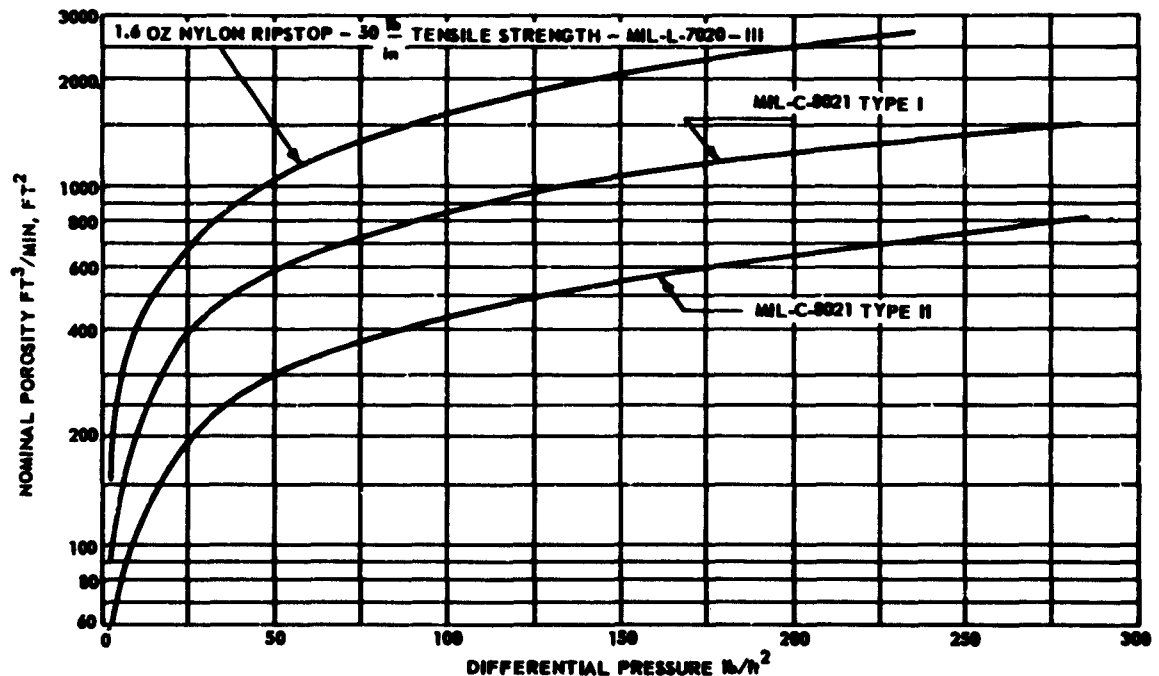
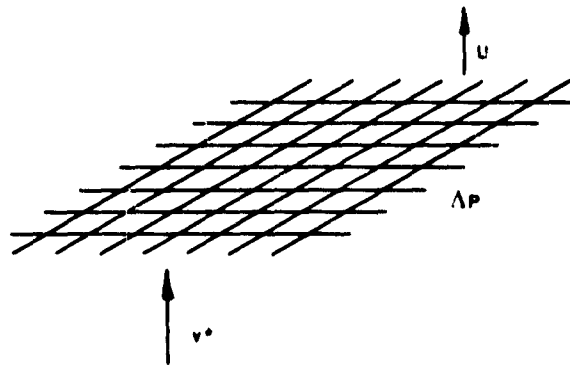


Fig. 4-14 Nominal Porosity of Parachute Cloth Materials vs Differential Pressure



$$\text{EFFECTIVE POROSITY } C = \frac{U}{v_*}$$

$$\text{WITH } \Delta P = \rho/2 v_*^2$$

$$C = \frac{U}{\sqrt{\frac{2\Delta P}{\rho}}}$$

$$\text{EFFECTIVE POROSITY AT SEA LEVEL } C_0 = \frac{U}{\sqrt{\frac{2\Delta P}{\rho}}}$$

Fig. 4-15 Derivation of the Term Effective Porosity

3.1 Definition of Effective Porosity. Porosity, considered as air permeability, is conventionally expressed as the volumetric flow rate of air per unit of cloth area under a certain differential pressure.

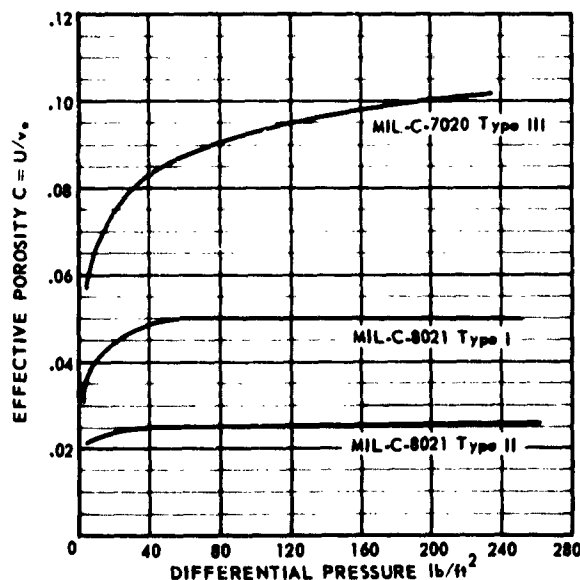


Fig. 4-16 Effective Porosity vs Differential Pressure

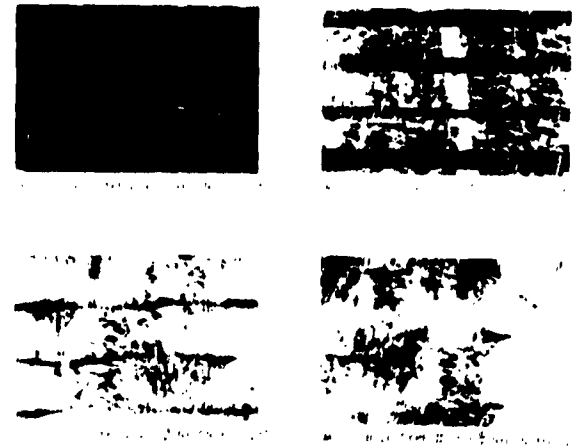


Fig. 4-17 Microscopic Pictures of Four Generally-Used Parachute Cloth Materials

Fig. 4-14 shows a typical diagram of this nominal porosity versus differential pressure for three commonly used parachute cloth materials.

For performance calculations, a dimensionless term is preferable, which would, for example, relate the average velocity, U , through the porous surface to the dynamic pressure of a fictitious velocity, v_* . Fig. 4-15 schematically shows the cloth as a grid in free air flow. The velocity in the free stream is v_* , and its related dynamic pressure, $0.5 \rho v_*^2$, is assumed to be identical to the differential pressure, Δp , across the cloth. The ratio U/v_* is called the effective porosity. Fig. 4-16 shows the effective porosity of the three parachute cloth materials of Fig. 4-14.

Considering the cloth as a porous screen leads to the idea of treating the flow through the cloth as a function of the ratio of the open to the solid area, and as a consequence, of the air resistance of the individual threads. If it were further assumed that the threads or yarns are circular cylinders, one may attempt to compute the air resistance of the woven sheet from the viscous drag of the individual cylinders. A number of investigations have been carried out in this manner (Ref (4-28), (4-29), (4-30)). However, the photographs of the four sample materials shown in Fig. 4-17 indicate that the assumption of a simple geometry for the cloth can be an over-simplification. The results of a purely analytical treatment of the drag problem could not encompass a large number of such very significant variables. Therefore, the actual mass flow through the cloth has been measured; the results of these experiments are reviewed below.

Fig. 4-14 indicates that the mass flow through the cloth increases with the differential pressure. It may

be assumed that this relationship will be monotone until the critical pressure differential is reached, at which the velocity through the orifices has reached the speed of sound. At this point, a further increase in the differential pressure will not increase the air velocity. Thus, it appears to be advisable to study the flow with respect to the incompressible and compressible flow regimes.

If one first considers incompressible flow, it may be assumed that the air flows through the fine orifices of a relatively thick cloth somewhat as through a pipe, in which the motion is neither completely laminar nor fully turbulent. Therefore, an analysis of the two border cases seems to be in order.

For fully developed laminar flow, Hagen-Poiseuille's law with the following relationship would be applicable.

$$(4-3) \quad \Delta p = \frac{128 \mu L Q}{\pi D^4}$$

where

μ = Viscosity;

L = Length of the tube;

Q = Flow rate; and

D = Diameter of the tube.

With $Q = U \pi D^2/4$, the average velocity in the pipe may be written

$$(4-4) \quad U = \frac{D^2}{32 \mu L} \Delta p$$

If the Hagen-Poiseuille relationship is applicable, the effective porosity may be presented as:

$$(4-5) \quad C = \frac{U}{v_*} = \frac{D^2}{32 \mu L} \sqrt{\frac{\rho \Delta p}{2}}$$

and specifically for sea-level density

$$(4-6) \quad C_0 = \left(\frac{U}{v_{*0}} \right) = \frac{D^2}{32 \mu_0 L} \sqrt{\frac{\rho_0 \Delta p}{2}}$$

For the first approximation, one may set $\mu = \mu_0$, and the effective porosity for any altitude, with $\rho/\rho_0 = \sigma$ and with the same differential pressure, may be written

$$(4-7) \quad C = C_0 \sigma^{1/2}$$

A similar analysis may be made for the assumption of

fully developed turbulent flow. With the Blasius formula (Ref (4-31))

$$(4-8) \quad \frac{\Delta p}{L} = \frac{\lambda}{D} \frac{\rho}{2} U^2$$

and

$$(4-9) \quad \lambda = 0.3164 \left(\frac{U \rho D}{\mu} \right)^{-1.4}$$

the velocity is

$$(4-10) \quad U = \left(\frac{2 \Delta p D^{5.4}}{0.3164 L} \right)^{1/7} (\mu \rho)^{-1/7}$$

Using $v_* = (2 \Delta p / \rho)^{1/2}$ and the subscript "zero" for sea-level density, the effective porosity, C , may be written

$$(4-11) \quad \frac{C}{C_0} = \left(\frac{\Delta p}{\Delta p_0} \right)^{1/4} \left(\frac{\mu_0}{\mu} \right)^{1/7} \left(\frac{\rho}{\rho_0} \right)^{1/14}$$

With $\mu = \mu_0$ and for the same differential pressure, for fully developed turbulent flow

$$(4-12) \quad C = C_0 \sigma^{1/4}$$

The assumption of laminar or turbulent flow in the region of incompressibility leads to a relationship of the form

$$(4-13) \quad C = C_0 \sigma^n$$

Experiments should now establish the value of the exponent n for various types of parachute material.

When the differential pressure, Δp , reaches or exceeds the critical value, flow through the orifices becomes sonic. Added pressure will not cause an increased flow velocity. At this point, effective porosity will decline with added pressure. For transonic and supersonic parachute operations, one should introduce, beside the density ratio ρ , the pressure ratio $\Delta p / \Delta p_{\text{crit}}$. If secondary effects are disregarded, one may expect that Eq 4-13 will be true for the compressible-flow regime. In the incompressible-flow regime, the value of n will probably be different.

3.2 Measurements of Effective Porosity.

In view of the analysis above, the effective porosity of four standard textile cloth materials was measured. Fig. 4-18 through 4-25 show their effective porosity C as function of the density ratio, σ , and the pressure ratio, $\Delta p / \Delta p_{\text{crit}}$, respectively.

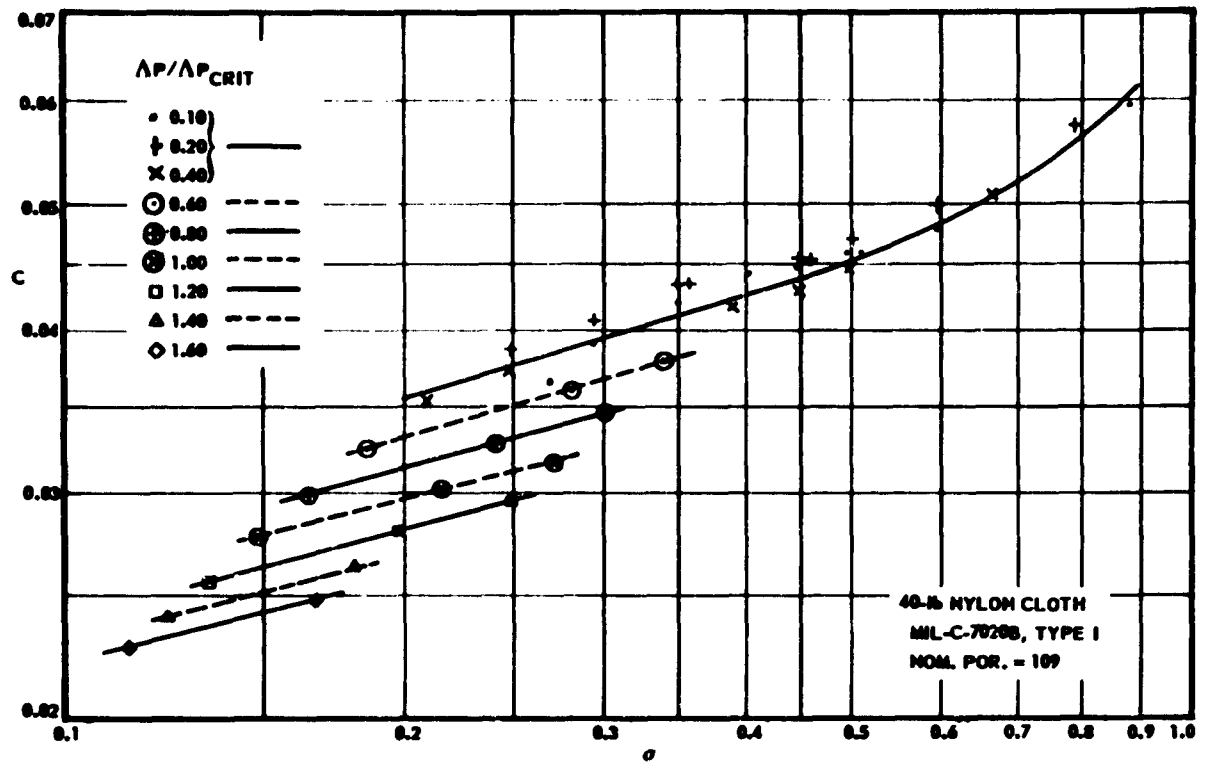


Fig. 4-18 Effective Porosity vs Density Ratio (MIL-C-7020B, Type I)

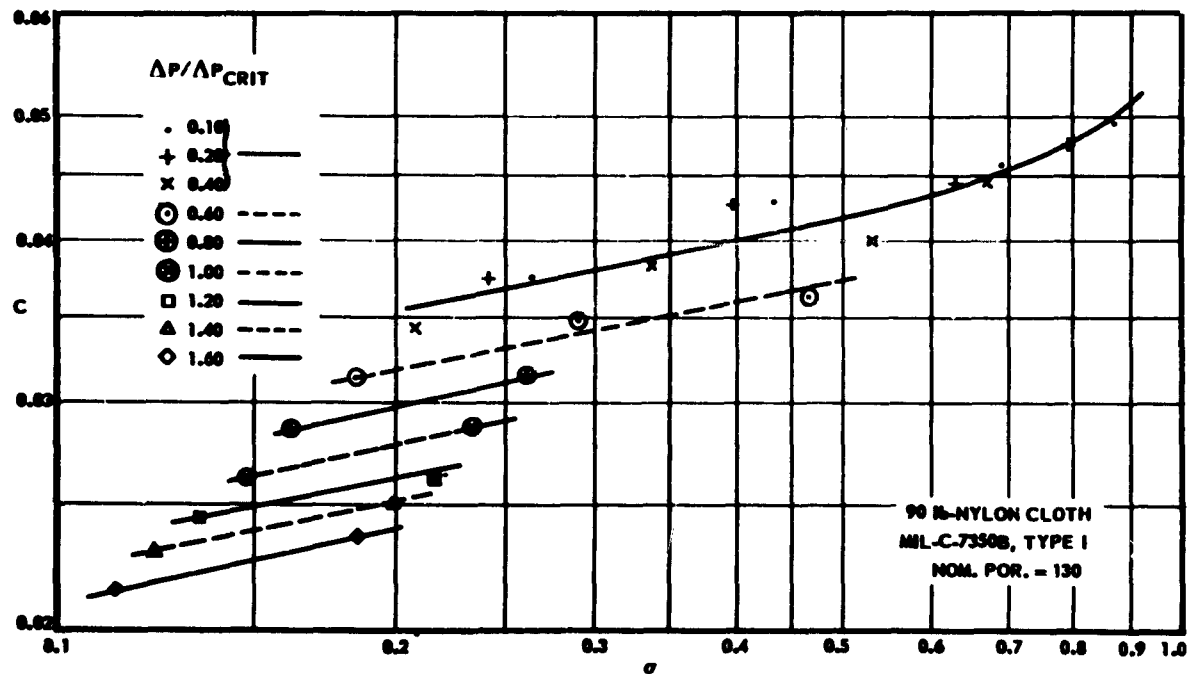


Fig. 4-19 Effective Porosity vs Density Ratio (MIL-C-7350B, Type I)

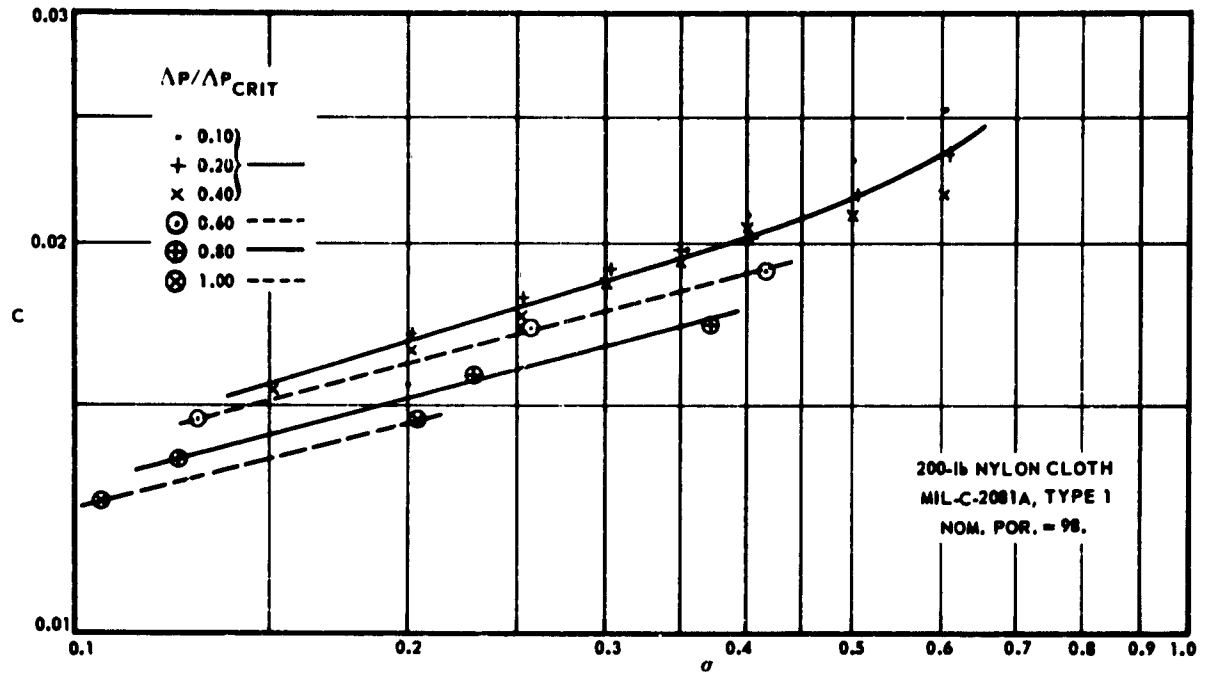


Fig. 4-20 Effective Porosity vs Density Ratio (MIL-C-8021A, Type I)

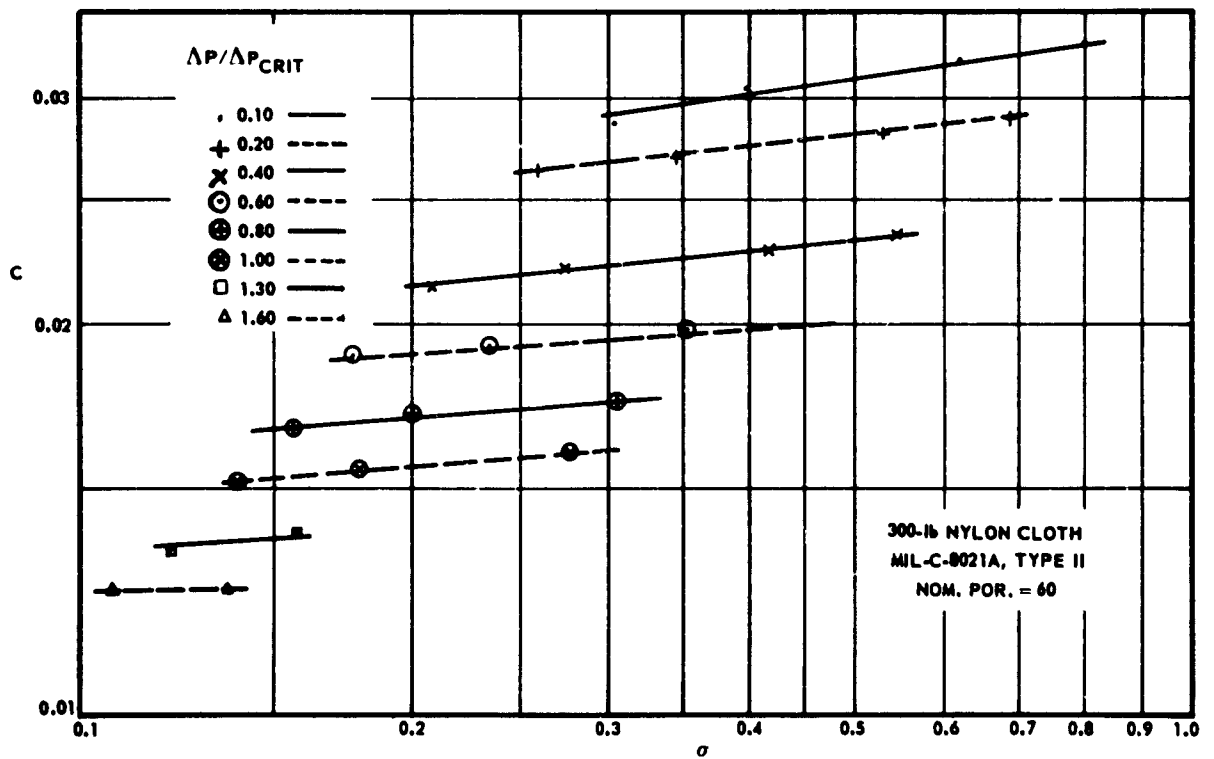


Fig. 4-21 Effective Porosity vs Density Ratio (MIL-C-8021A, Type II)

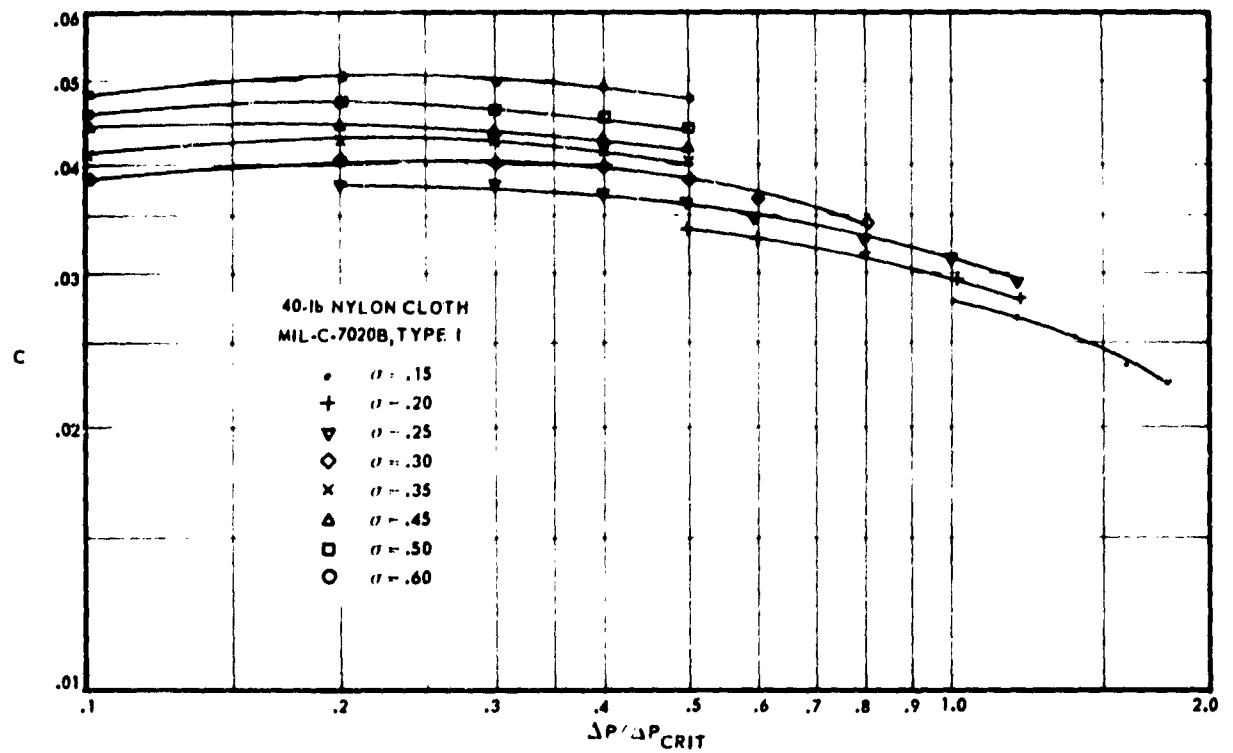


Fig. 4-22 Effective Porosity vs Pressure Ratio (MIL-C-7020B, Type I)

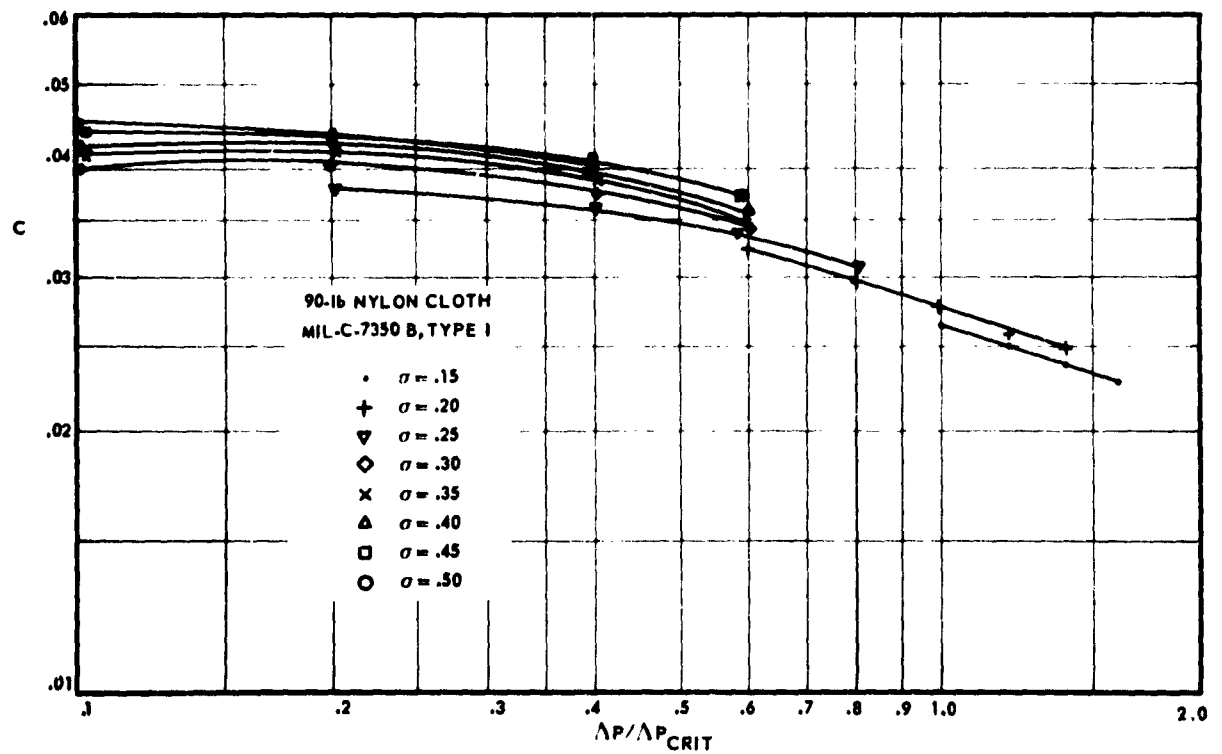


Fig. 4-23 Effective Porosity vs Pressure Ratio (MIL-C-7350B, Type I)

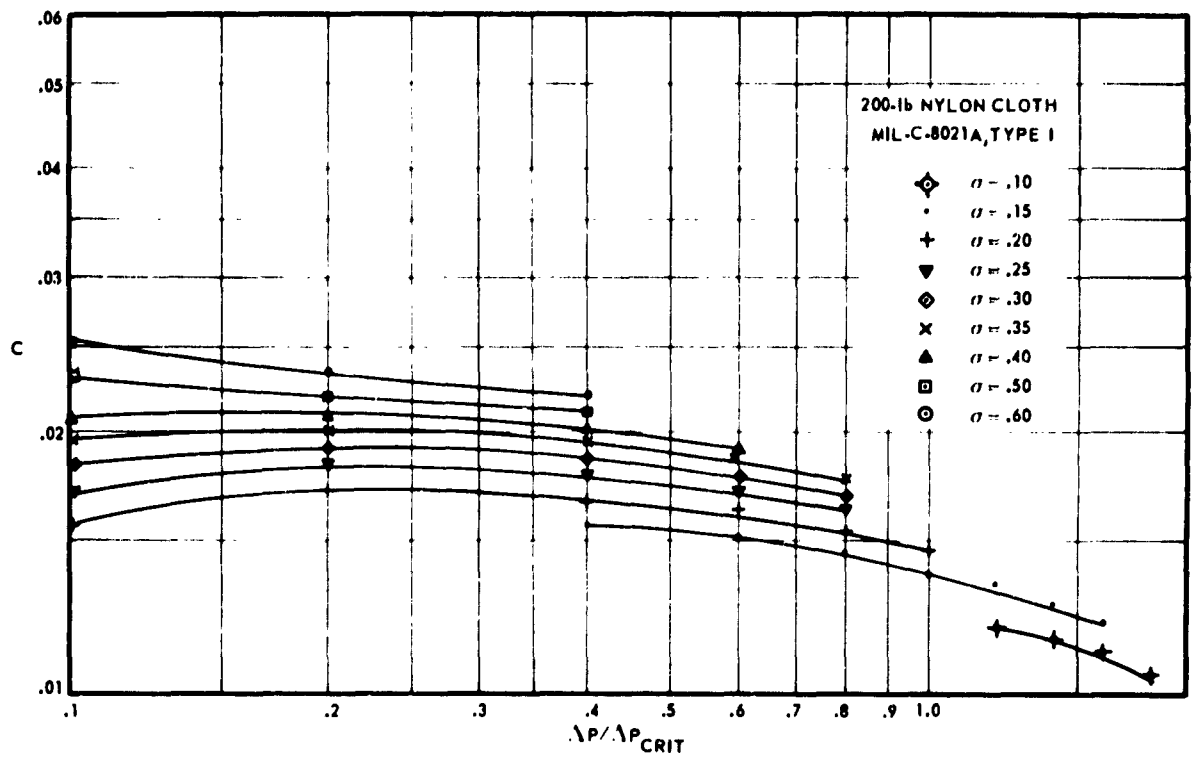


Fig. 4-24 Effective Porosity vs Pressure Ratio (MIL-C-8021A, Type I)

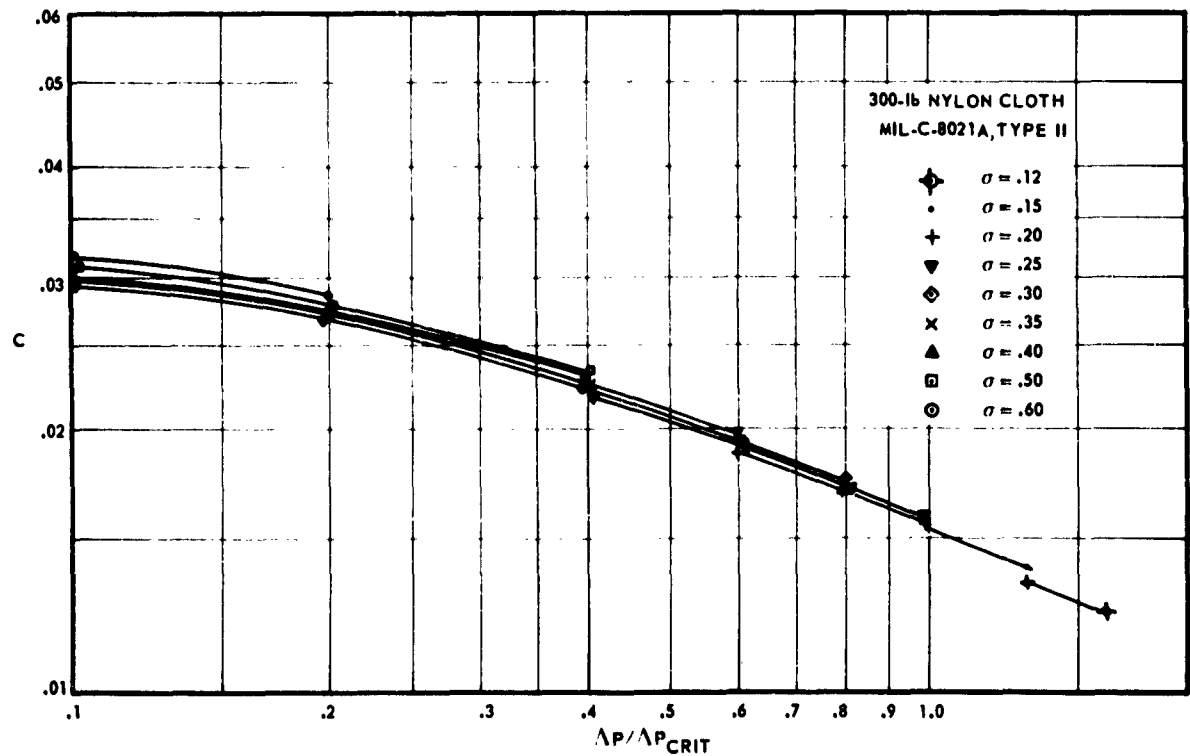


Fig. 4-25 Effective Porosity vs Pressure Ratio (MIL-C-8021A, Type II)

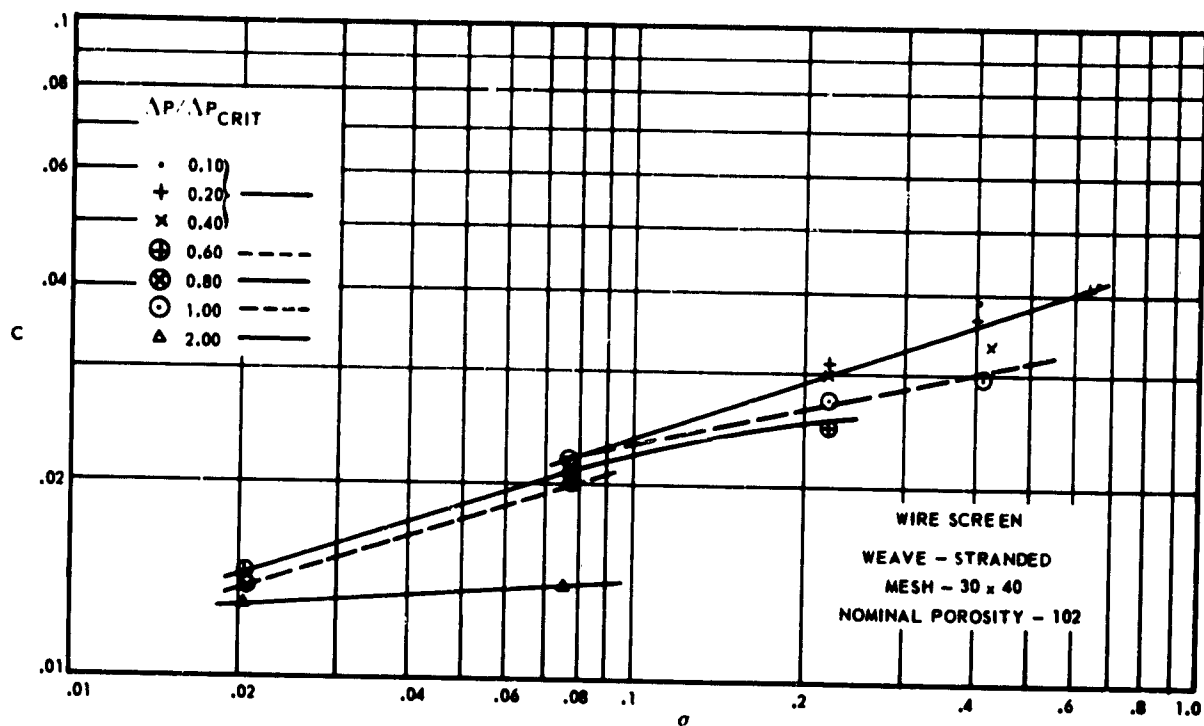


Fig. 4-26 Effective Porosity of a Wire Screen vs Density Ratio

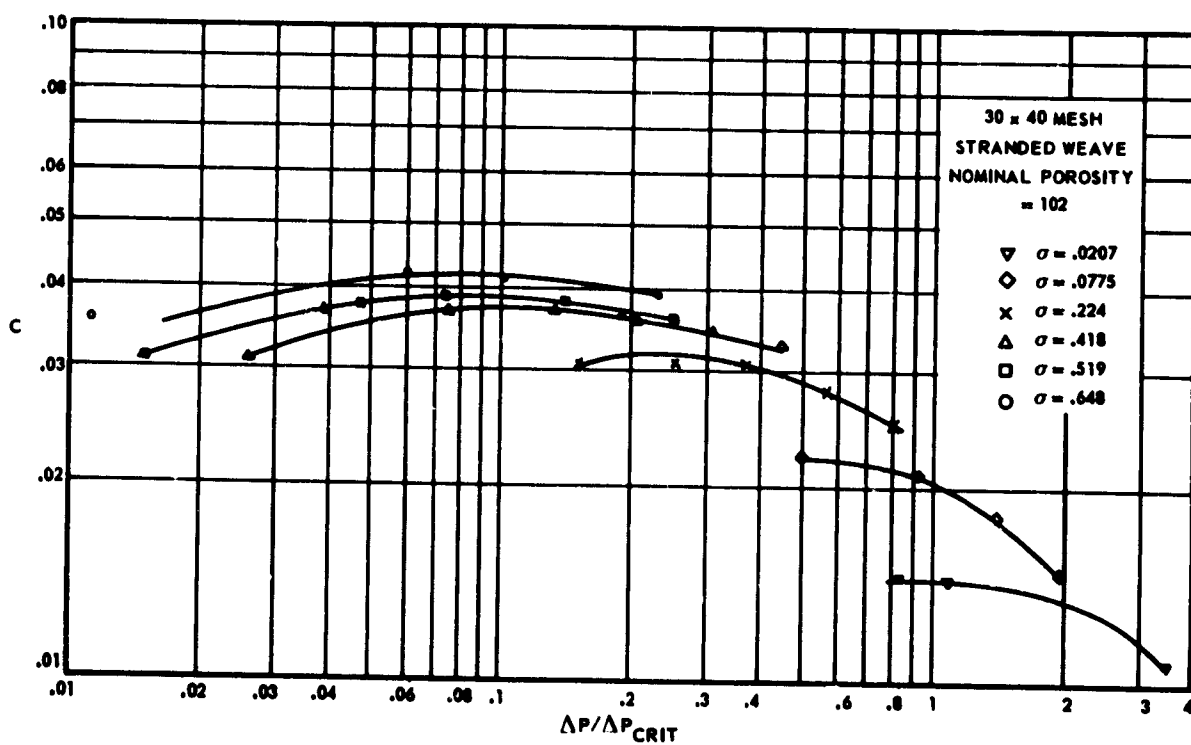


Fig. 4-27 Effective Porosity of a Wire Screen vs Pressure Ratio

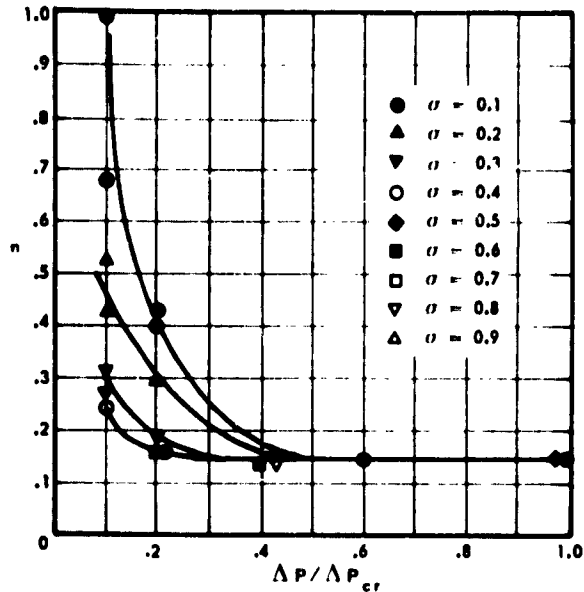


Fig. 4-28 Density Exponent vs. Pressure Ratio for MIL-C-7020B, Type I, 40 lb/in. Nylon Cloth

It may be pointed out that the density ratio is related to the free-stream conditions downstream of the porous screen. Fig. 4-26 and 4-27 are similar recordings of effective porosity for a wire screen with a nominal porosity of the order of magnitude of the cloth porosities. (The wire screen has been incorporated in the study because the textile screens may change their geometry under the pressure loading; thus, their porosity reflects not only Reynolds and Mach number effects, but also the unknown consequences of the elasticity of the cloth.) As can be seen, the wire screen shows the same characteristics as the

more elastic textile screens, and it appears justifiable to conclude that, for the parachute cloth materials tested, the elasticity is of secondary significance.

When the phenomenon which actually takes place is analyzed, it may be said that Fig. 4-18 through 4-25 reflect the influence of Reynolds as well as Mach number. For example, it can be seen that the effective porosity versus σ for pressure differentials $\Delta p/\Delta p_{crit}$ between 0.1 and 0.4 is essentially the same. These curves are related to the incompressible flow regime; the variation of the effective porosity is primarily a Reynolds number effect. In the region of higher pressure differentials, in which $\Delta p/\Delta p_{crit}$ approaches or exceeds unity, a certain change in the absolute value of the effective porosity as well as a change in slopes $\partial C/\partial \sigma$ and $\partial C/\partial (\Delta p/\Delta p_{crit})$ can be observed. This is understandable in view of the fact that the Mach number becomes generally more influential than the Reynolds number in the regime of compressible flow. Furthermore, it can be shown that the experimental results are in agreement with analytical predictions, based on the assumption that the flow through the orifices can be treated like sonic flow through converging nozzles.

Fig. 4-18 through 4-25 indicate that, at present, only a limited amount of data is available. However, the change of effective porosity is by its nature primarily important at higher altitudes, represented by lower values of σ . Therefore, it may be acceptable at this time to consider merely the effective porosities related to values of $\sigma < 0.5$. With this restriction, the slope, $\partial C/\partial \sigma$ versus $\Delta p/\Delta p_{crit}$, has been extracted from Fig. 4-18 through 4-21 and is presented in Fig. 4-28 through 4-31. It can be seen that the flow through the cloth varies significantly with the pressure

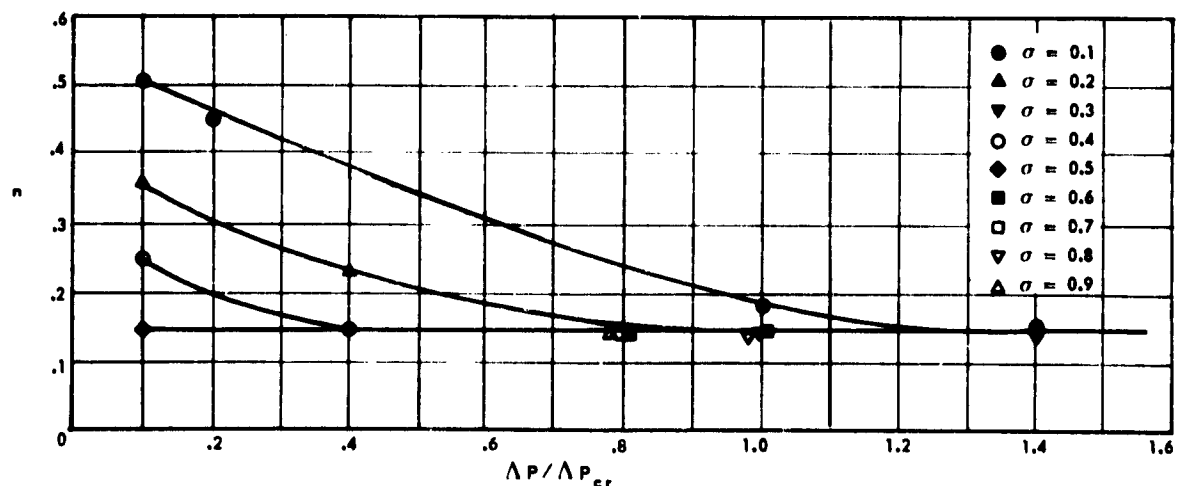


Fig. 4-29 Density Exponent vs. Pressure Ratio for MIL-C-7350R, Type I, 90 lb/in. Nylon Cloth

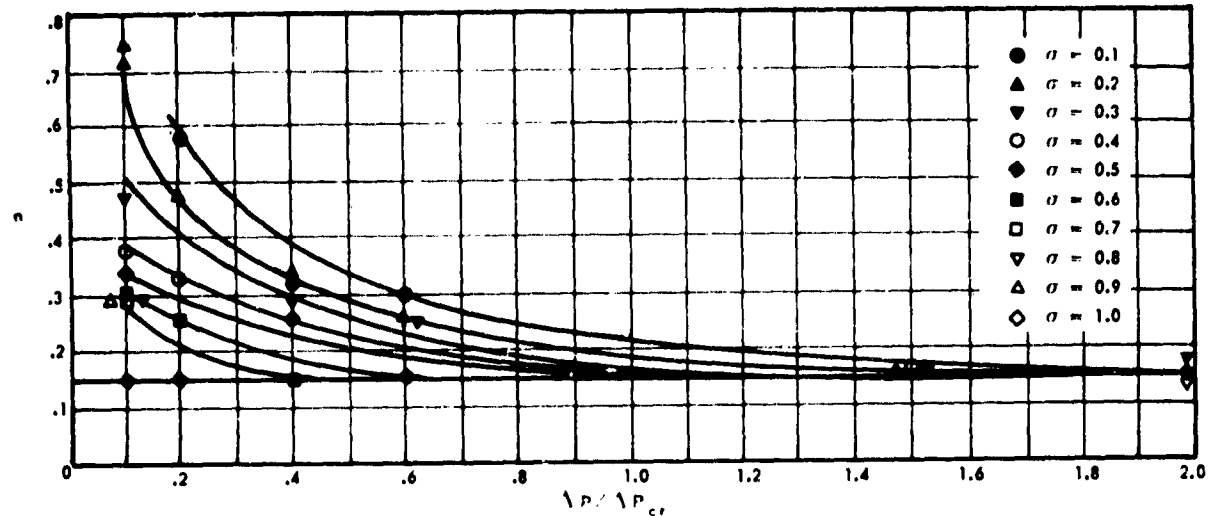


Fig. 4-30 Density Exponent vs Pressure Ratio for MIL-C-8021A, Type I, 200 lb. in. Nylon Cloth

differential.

In summary, this investigation shows that the effective porosity of woven sheets decreases with decreasing density or increasing pressure ratios. Fig. 4-18 through 4-25 can provide a direct reading of the effective porosity for specific conditions. Fig. 4-28 through 4-31, in connection with Eq 4-13, permits the calculation of the effective porosity, C , if the related porosity under sea level conditions, C_0 , is known.

3.3 Sample Calculation. The calculation of the opening shock of a solid cloth canopy that inflates at 20,000 ft altitude at a speed (v_s) = 265 fps requires knowledge of the effective porosity for the particular speed and altitude conditions given.

Standard atmosphere tables (Ref (4-1)) show (for 20,000-ft altitude) the density ratio $\sigma = 0.533$, the static pressure $p = 972.5$ psf, and the velocity of sound $a = 1037$ ft/sec. The Mach number for the opera-

tional speed is $v_s/a = 265/1037 = 0.256$; from NACA Report 1135 (Ref (4-40)), (for Mach No. 0.256) $p/p_t = 0.955$. Consequently the total pressure amounts to $p_t = 1018.3$ psf.

The pressure differential (Δp) is $p_t - p = 1018.3$ psf - 972.5 psf = 45.8 psf. The critical pressure ratio is $p/p_t = 0.5283$ or $p_{t \text{ crit}} = 972.5/0.5283 = 1840.8$ psf. Then, for this altitude, the critical pressure differential $\Delta p_{\text{crit}} = 1840.8 - 972.5 = 868.3$ psf. With these figures the pressure ratio at which the inflation begins is $\Delta p/\Delta p_{\text{crit}} = 45.8/868.3 = 0.0527$. Assuming the drag-producing surface of the parachute canopy is made from cloth MIL-C-7020, the effective porosity can then be obtained from Fig. 4-18. This figure shows an average curve for $\Delta p/\Delta p_{\text{crit}}$ between 0.1 and 0.4; it may be assumed that for a pressure ratio lower than 0.1 the same average curve would be valid. Thus, for $\sigma = 0.533$ the value of the effective porosity is $C = 0.046$. This figure should be used for the calcu-

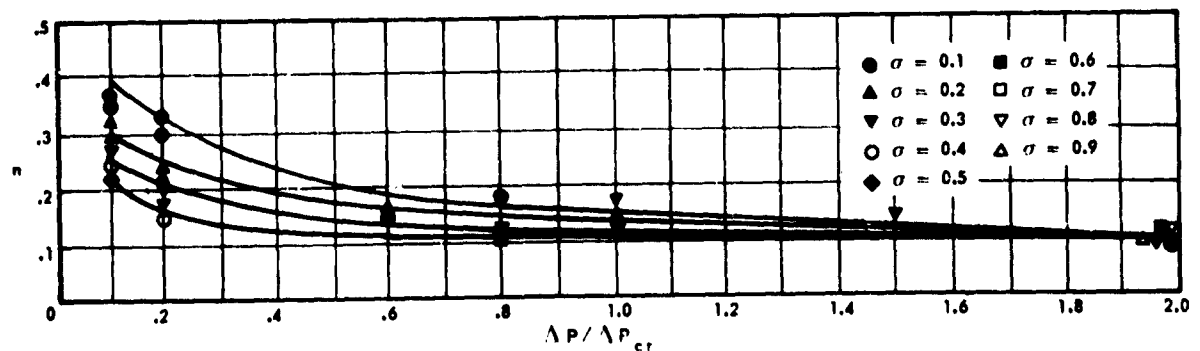


Fig. 4-31 Density Exponent vs Pressure Ratio for MIL-C-8021A, Type II, 300 lb. in. Nylon Cloth

lation of the opening shock, and also for considerations concerning the stability and the drag of the canopy at that altitude.

Another method which may be used to obtain the desired result involves calculating the effective porosity from Eq 4-13, using an n -value from Fig. 4-28 through 4-31.

SEC. 4 SNATCH FORCE

All deployments of trailing aerodynamic decelerators create a force known as "snatch force" which arises from the differential deceleration rates of the suspended load and the deploying decelerator. The rapid deceleration of the decelerator, in relation to the relatively slow deceleration of the suspended load, creates a sizable differential velocity which must be reduced to zero. Snatch force is defined as that force imposed upon the suspended load by the decelerator to accelerate the mass of the decelerator from its velocity at line extension (not stretch) to the velocity of the suspended load.

Fortunately, in the case of parachute operation, snatch forces are imposed at completion of suspension-line deployment, prior to actual inflation of the canopy. Thus, snatch force and opening-shock (Sec. 5) are not additive forces; rather, one follows closely after the other. (See Fig. 4-32 and 4-33.) At low speeds with present canopy designs and deployment methods, snatch forces do not exceed opening-shock values. With low-shock canopies now in use or under design, however, it is felt that the limiting factor on future parachute operation will be the snatch force, if means for its reduction are not provided for in the design of the parachute system. Opening-shocks can be reduced considerably by special reefing, venting, collapsing, or squidding canopy designs. Snatch forces, however, can be reduced only by controlled deployment (a very difficult process if the deployment system must be usable over a large range of speed), by reduction of parachute weight, by reduction of uninflated-canopy drag-area, and by reduction in pilot-chute drag-area. The latter two characteristics have a larger effect on proper deployment and opening, and cannot be reduced beyond a certain limit without adverse results on deployment and reliability.

Fig. 4-32 shows a record of force versus time in the opening of a standard flat circular 28-ft diameter canopy at 260 knots. Snatch force and opening shock are indicated. Fig. 4-33 is a record of force versus time in the opening of the same type of canopy with skirt reefing, at 260 knots. Here the snatch force exceeds the opening-shock considerably; the reefing

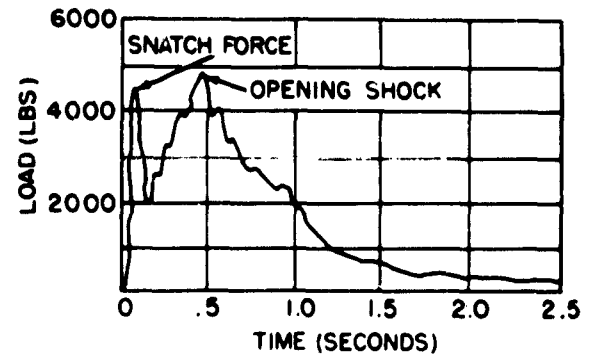


Fig. 4-32 Force vs Time in the Opening of a Standard 28-ft Canopy, at 260 Knots

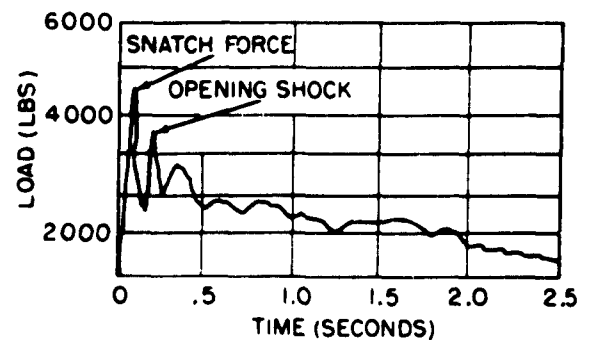


Fig. 4-33 Force vs Time in the Opening of a Standard 28-ft Canopy with Reefing Rings, at 260 Knots

system altered the canopy to a low-shock design. Since snatch force is the greater here, it must receive primary consideration.

4.1 Derivation of Energy Equation. Trailing aerodynamic deceleration devices, such as canopies, assume a relative velocity with respect to the primary body in the process of drifting aft of that body into their final position. Upon drifting aft a distance equal to length of the unstretched suspension-lines (L_s) (Fig. 4-34), the differential velocity between the primary and secondary bodies is at its maximum. After reaching L_s , the lines are stretched L_{max} , the secondary body is accelerated to the mutual speed of the primary and secondary bodies, and the differential velocity becomes zero. The inertia force, a consequence of this acceleration, is called snatch force.

The energy transmitted to the primary body upon full line-extension is

$$(4-14) \quad \Delta E = 1.2 m_c \left(V_{II, 2 (rel)}^2 - V_{II, 3 (rel)}^2 \right)$$

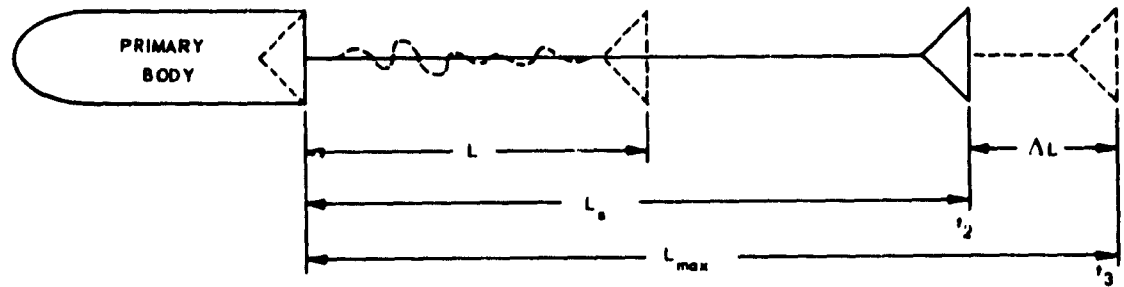


Fig. 4-34 Representation of Length of Suspension Lines Behind Primary Body

where

m_c = Mass of canopy cloth area and suspension lines across the cloth area;

$V_{II, 2} \text{ (rel)}$ = Velocity of secondary body relative to that of the primary body at time $t = t_2$; and

$V_{II, 3} \text{ (rel)}$ = Velocity of secondary body relative to that of the primary body at time $t = t_3$.

Relative velocities are used in the equation instead of actual velocities, because the distance through which the snatch force acts is measured relative to the primary body; thus, the velocities during this time must also be measured relative to the primary body. Substituting, since $V_{II, 3} \text{ (rel)} = 0$,

$$(4-15) \quad \Delta E = 1/2 m_c V_{II, 2}^2 \text{ (rel)}$$

If no special shock-absorbers are installed, the force must be transmitted through the suspension lines. Being elastic, the lines extend and transmit a tractive force on the drag-producing surface and the suspended load. Thus,

$$(4-16) \quad \Delta E = \int_{L_s}^{L_{\max}} P dL$$

where

P = Momentary tractive force in the suspension lines, lb; and

dL = Elongation of suspension lines, ft.

In order to integrate the above equation, the force (P) must be written as some function of the length (L). It may be possible to obtain such an equation

from the force-elongation curves of the various suspension line materials. However, if the force-elongation curve cannot be expressed in an equation, or if such a curve is not available, a first approximation of linearity may be assumed. The following equation may then be written

$$(4-17) \quad P = \frac{ZP'}{\xi'} \xi$$

where

Z = Number of suspension lines;

P' = Breaking strength of suspension lines, lb;

ξ' = Percent elongation of suspension lines at P' ;

ξ = Elongation of suspension lines, per cent.

From

$$(4-18) \quad L_{\max} = L_s + \Delta L = L_s + \xi L_s$$

It follows that

$$(4-19) \quad dL = L_s d\xi$$

and kinetic energy may be expressed as

$$(4-20) \quad \Delta E = L_s \frac{ZP'}{\xi'} \int \xi d\xi$$

which, after integration, becomes

$$(4-21) \quad E = (1/2) L_s \frac{ZP'}{\xi'} \xi^2 + C_1$$

From the initial conditions, when $E = 0$, $\Delta E = 0$, it follows that $C_1 = 0$ and the kinetic energy amounts to

$$(4-22) \quad E = (1/2) L_s \frac{ZP'}{\xi'} \xi^2$$

or

$$(4-23) \quad \xi = \sqrt{\frac{2 \Delta E \xi'}{Z L_s P'}}$$

Substituting this value for ξ into

$$(4-24) \quad P = \frac{Z P'}{\xi'} \xi$$

gives

$$(4-25) \quad P = \frac{Z P'}{\xi'} \sqrt{\frac{2 \Delta E \xi'}{Z L_s P'}} = \sqrt{\frac{2 \Delta E Z P'}{L_s \xi'}}$$

Substituting for ΔE from Eq 4-15

$$(4-26) \quad P = \sqrt{\frac{m_c V_{II, 2}^2 (rel) Z P'}{L_s \xi'}}$$

In this form, the force due to kinetic energy is now reduced to a function of the differential speed; the determination of this speed is the next objective in the calculation of snatch force.

4.2 Derivation of Velocity Equation. At the time of release, both bodies have the same actual velocity v_o . Upon separation, both bodies have the same actual velocity $V_{I, 1} = V_{II, 1} = v_d$. At the time $L = L_s$, the actual velocities of the primary and secondary bodies amount to $V_{I, 2}$ and $V_{II, 2}$ respectively. At the instant $L = L_{max}$, the primary and secondary bodies have the same actual speed $V_{I, 3} = V_{II, 3} = v_s$.

The actual velocity, v_s , is the velocity at the instant when the canopy is just starting to inflate and snatch force has already occurred. The mathematical calculations for converting launching velocity, v_o , to the velocity at the beginning of inflation, v_s , can be divided into several distinct steps.

If static-line deployment of the parachute is used, the time taken for the static-line to extend fully and initiate the separation of the parachute from the suspended mass must first be known. During this period, the suspended mass and parachute remain together and are assumed to be retarded only by the drag force generated by the suspended mass. It is also assumed that the launching vehicle maintains constant velocity and level flight. When this time has been found, the velocity of the system at the instant the static-line is fully extended must be calculated, taking into account the effect of gravity.

After separation of the parachute and suspended mass is initiated, it is necessary to find the time for the parachute and suspended mass to separate a distance equal to the length of the suspension lines, at

which instant the lines are straight but not stretched. During this period, the parachute and the suspended mass are retarded by their individual drag forces. It is necessary to find the individual velocities of the parachute and the suspended mass at the end of the time period of known length.

If it is assumed that the required time is negligible for the lines to stretch and snatch force to occur, the velocity of the system after snatch has occurred is the same as the velocity at the beginning of inflation, v_s , used in the calculations for opening-time and opening-forces of an inflating canopy.

4.2.1 EQUATIONS FOR VELOCITY AT DEPLOYMENT INITIATION. If the effect of gravity is neglected, the applicability of the equations derived is limited to the case of horizontal or near-horizontal deployment. The equation of motion for a body whose drag area is $C_D S$ can then be written as

$$(4-27) \quad m \frac{dv}{dt} = - \frac{1}{2} \rho C_D S v^2$$

Letting

$$(4-28) \quad J = \rho \frac{C_D S}{2m}$$

then

$$(4-29) \quad \frac{dv}{dt} = - J v^2$$

or

$$(4-30) \quad \frac{dv}{v^2} = - J dt$$

Integrating Eq 4-30

$$(4-31) \quad \frac{1}{v} = Jt + C_1$$

C_1 is the constant of integration. The initial conditions are $v = v_o$ at $t = 0$ which gives

$$(4-32) \quad C_1 = \frac{1}{v_o}$$

Substituting Eq 4-32 into Eq 4-31,

$$(4-33) \quad \frac{1}{v} = Jt + \frac{1}{v_o}$$

or

$$(4-34) \quad v = \frac{v_o}{Jv_o t + 1}$$

Eq 4-34 gives the velocity at any time t . It is also true that

$$(4-35) \quad v = \frac{dl}{dt}$$

or

$$(4-36) \quad \frac{dl}{dt} = \frac{v_o}{J_1 v_o t + 1}$$

which when integrated gives

$$(4-37) \quad l = \frac{1}{J_1} \ln(1 + J_1 v_o t) + C_{II}$$

C_{II} is again the constant of integration, which at $l=0$ and $t=0$ gives $C_{II}=0$.

Hence

$$(4-38) \quad l = \frac{1}{J_1} \ln(1 + J_1 v_o t)$$

where l is the distance traveled by the body in rectilinear motion.

It is necessary to know the time taken to extend the static-line before the velocity can be calculated. Assume that it takes t_1 seconds for the static line of length L_1 to extend fully. The horizontal distance traveled by the composite mass in this time is

$$(4-39) \quad l_1 = \frac{1}{J_1} \ln(1 + J_1 v_o t_1)$$

where

$$J_1 = \frac{\rho (C_D S)_b}{2 m_{b+c}}$$

m_{b+c} = Mass of suspended load plus complete parachute system;

$(C_D S)_b$ = Drag area of primary body; and

v_o = Velocity of launching vehicle.

The horizontal distance traveled in time t_1 by the launching vehicle is

$$(4-40) \quad l_2 = v_o t_1$$

After time, t_1 , the horizontal separation distance between the launching vehicle and mass m_{b+c} is given by

$$(4-41) \quad l_2 - l_1 = v_o t_1 - \frac{1}{J_1} \ln(1 + J_1 v_o t_1)$$

If the drag of the composite body in the vertical direc-

tion is neglected (since that velocity is small), the vertical distance traveled due to gravity is approximately $\frac{1}{2} g t_1^2$. The total displacement of the system with respect to the launching vehicle can now be determined from the Pythagorean Theorem.

$$(4-42) \quad L_1 = \sqrt{\frac{g^2 t_1^4}{4} + \left[v_o t_1 - \frac{1}{J_1} \ln(1 + J_1 v_o t_1) \right]^2}$$

This equation gives a relationship allowing the determination of time t_1 ; however, a trial-and-error solution is necessary (see Fig. 4-35). After t_1 has been determined by trial and error, the velocity at the instant the static-line is extended can be found from

$$(4-43) \quad V_{I,1} = \frac{v_o}{J_1 v_o t_1 + 1} = V_{II,1} = v_d$$

4.2.2 EQUATIONS FOR VELOCITY AT SUSPENSION-LINE STRETCH. Before the velocities of the primary and secondary bodies can be determined, it is necessary to find the time required to extend but not stretch the suspension lines.

Assuming that it takes t_2 seconds for the bodies to separate a distance L_s , the horizontal distance traveled by the primary bodies in time t_2 is

$$(4-44) \quad l_b = \frac{1}{J_b} \ln(1 + J_b v_d t_2)$$

where $J_b = \frac{\rho (C_D S)_b}{2 m_b}$;

$(C_D S)_b$ = Drag area of suspended load;

m_b = Mass of primary body (suspended load); and

$v_d = V_{I,1} = V_{II,1}$ = Velocity at static line extension or deployment velocity.

Similarly, the horizontal distance traveled by the secondary body, or canopy, in time t_2 is

$$(4-45) \quad l_c = \frac{1}{J_c} \ln(1 + J_c v_d t_2)$$

where

$$J_c = \frac{\rho (C_D S)_c}{2 m_c}$$

$(C_D S)_c$ = Drag area of uninflated parachute and pilot chute, when applicable; and

m_c = Mass of canopy, excluding suspension lines from canopy skirt to confluence point,

$$J_1 = \frac{\rho(C_0 S)_b}{2m_{b+c}} = 5.77 \times 10^{-4}$$

$$\frac{g^*}{4} = 259.2$$

$$L_1 = 15 \text{ ft.}$$

$$h = 7,500 \text{ ft.} \quad m_{b+c} = 6.57$$

$$v_0 = 220 \text{ in/sec.} \quad (C_0 S)_b = 4$$

$$\rho = 1.898 \times 10^{-3}$$

$$L_1 = \sqrt{\frac{g^2 t_1^4}{4} + \left[v_0 t_1 - \frac{1}{J_1} \ln(1 + J_1 v_0 t_1) \right]^2}$$

(1)	(2)	(3)	(4)	(5)	(6)	(7)	(8)	(9)	(10)	(11)	(12)
t_1	$v_0 t_1$	$J_1 v_0 t_1$	$1 + J_1 v_0 t_1$	$\ln(4)$	$(5) + J_1$	$(2) - (6)$	$(7)^2$	t_1^4	$(g^2/4) t_1^4$	$(9) + (8)$	$\sqrt{(11)} = L_1$
0.84	184.8	0.1068	1.1068	0.1015	175.7	9.1	82.81	0.498	129.08	211.89	14.56
0.85	187.0	0.1080	1.1080	0.1025	177.6	9.4	88.36	0.522	135.30	223.66	14.96
0.86	189.2	0.1093	1.1093	0.1037	179.5	9.7	94.09	0.547	141.78	235.87	15.36

Fig. 4-35 Trial-and-Error Solution for t_1

and pilot chute when applicable.

The separation between the bodies after time t_2 is

$$(4-46) \quad L_s = \frac{1}{J_b} \ln(1 + J_b v_d t_2) - \frac{1}{J_c} \ln(1 + J_c v_d t_2)$$

This gives a relationship to determine t_2 , but again a trial-and-error solution must be employed (see Fig. 4-36). Once t_2 is known, the velocities of the primary and secondary bodies may be found.

$$(4-47) \quad V_{I,2} = \frac{v_d}{J_b v_d t_2 + 1} \quad (\text{or the velocity of primary body})$$

$$(4-48) \quad V_{II,2} = \frac{v_d}{J_c v_d t_2 + 1} \quad (\text{or the velocity of secondary body})$$

It is assumed that the time taken for the suspension lines to stretch and snatch force to occur is small, so that deceleration of the primary body during this time due to its drag force is small and can be neglected. Therefore,

$$(4-49) \quad v_s = V_{I,2}$$

4.2.3 EXAMPLE OF SNATCH-FORCE CALCULATION. If it is assumed that the following conditions exist, the snatch force for those conditions can be calculated:

- $W_b = 200$ lb;
- $W_c = 11.5$ lb (for parachute canopy);
- $(C_D S)_b = 4$ sq ft (for suspended load);
- $(C_D S)_c = 3$ sq ft (for uninflated parachute canopy);
- $Z = 28$ suspension lines;
- $P' = 550$ lb, breaking strength, suspension lines;
- $L_s = 22.8$ ft, length of suspension lines;
- $L_1 = 15$ ft, static-line length;
- $\xi' = 36.7\%$ elongation of suspension lines (from load versus elongation curve);
- $v_o = 130$ knots launching speed = 220 fps;
- $\rho = 1.898 \times 10^{-3}$ slugs/ft³ (alt. 7500 ft)

Specific values, after solution, are as follows:

$$m_b = \frac{W_b}{g} = \frac{200}{32.2} = 6.21$$

$$m_c = \frac{W_c}{g} = \frac{11.5}{32.2} = 0.357$$

$$m_b + m_c = \frac{W_b + W_c}{g} = 6.57$$

$$J_1 = \frac{\rho (C_D S)_b}{2(m_b + m_c)} = \frac{(1.898 \times 10^{-3})(4)}{(2)(6.57)} = 5.778 \times 10^{-4}$$

$$J_b = \frac{\rho (C_D S)_b}{2m_b} = \frac{(1.898 \times 10^{-3})(4)}{(2)(6.21)} = 6.113 \times 10^{-4}$$

$$J_c = \frac{\rho (C_D S)_c}{2m_c} = \frac{(1.898 \times 10^{-3})(3)}{(2)(0.357)} = 7.975 \times 10^{-3}$$

By use of the calculation sheet, Fig. 4-35, it is found that $t_1 = 0.85$ sec. Hence

$$v_d = V_{I,1} = V_{II,1} = \frac{v_o}{J_1 v_o t_1 + 1} = \frac{220}{1.1080} = 198.6 \text{ fps}$$

Having obtained v_d , the velocity at static-line extension, the next objective is to find t_2 , the time required for separation of primary and secondary bodies for the distance L_s . Using calculation sheet Fig. 4-36, $t_2 = 0.49$ sec. Hence

$$V_{I,2} = \frac{v_d}{J_b v_d t_2 + 1} = \frac{198.6}{1.0594} = 187.5 \text{ fps} = V_{I,3} = V_{II,3}$$

$$\text{and} \quad V_{II,2} = \frac{v_d}{J_c v_d t_2 + 1} = \frac{198.6}{1.776} = 111.8 \text{ fps}$$

$$V_{II,2(\text{rel})} = V_{I,2} - V_{II,2} = 187.5 - 111.8 = 75.7 \text{ fps}$$

Substituting this velocity in the kinetic-energy equation

$$(4-50) \quad P = \sqrt{(m_c V_{II,2}^2 Z P') / (L_s \xi')}$$

$$\text{then} \quad P = \sqrt{[(0.357)(75.7)^2(28)(550)] / [(22.8)(0.367)]} = 1940 \text{ lb}$$

However, the snatch force in the suspension lines at

$$h = 7500 \text{ ft.} \quad (C.S)_c = 3$$

$$\rho = 1.898 \times 10^{-3} \quad (C.S)_h = 4$$

$$L_s = L_2 - L_c$$

$$J_c = \frac{\rho C_p S}{2 m_c} = 7.975 \times 10^{-3}$$

$$m_c = 0.357 \quad L_s = 22.8$$

$$L_s = \frac{1}{J_c} \ln(1 + J_c \gamma_d t_2) = \frac{1}{J_c} \ln(1 + J_c \gamma_d t_2)$$

$$m_h = 6.21 \quad \gamma_d = 198.6$$

$$J_c = \frac{\rho C_p S}{2 m_h} = 6.113 \times 10^{-4}$$

(1)	(2)	(3)	(4)	(5)	(6)	(7)	(8)	(9)	(10)	(11)
t_2	$\gamma_d t_2$	$J_c \gamma_d t_2$	$1 + J_c \gamma_d t_2$	$\ln(4)$	$(5) + J_c$	$J_c \gamma_d t_2$	$1 + J_c \gamma_d t_2$	$\ln(5)$	$(9) + J_c$	$(10) - J_c$
0.50	99.3	0.0607	1.0607	0.0589	96.35	0.7919	1.7919	0.5833	73.14	23.2
0.49	97.3	0.0595	1.0595	0.0578	94.55	0.7760	1.7760	0.5744	72.03	22.5
0.48	95.3	0.0583	1.0583	0.0567	92.75	0.7600	1.7600	0.5653	70.88	21.9

Fig. 4-36 Calculation Sheet to Determine t_2

L_{\max} is the sum of the force produced by the change in kinetic energy plus the average drag force or

(4-51)

$$F_s = P + F_c$$

where

$$(4-52) \quad F_c = \frac{P}{2} (C_D S)_c \left[\frac{V_{H,2}^2 + V_{H,3}^2}{2} \right]$$

which in this example turns out to be

$$F_s = 1940 + \frac{(0.001898)(3) [(111.8)^2 + (187.5)^2]}{(4)} =$$

2007.8 lb

The preceding sample calculation presents a method for determining the snatch force for a static-line deployment system, and shows the calculation of the time elapsed during static-line extension. If the snatch force is being calculated for a system which utilizes automatic deployment, where the time from release to deployment initiation is known, this step is eliminated. However, if a system is deployed by means of a pilot chute, the weight and drag area of the pilot chute must be added to the terms T_c and $(C_D S)_c$, respectively. See Chapter 12.

The assumption that there is an average drag-area of the uninflated canopy is not always reliable because normal canopies can be partially inflated during the period of line-stretch. The snatch force can thus be increased by a significant amount. In practice, the values of drag area measured will deviate considerably, both above and below the calculated values, if an uncontrolled deployment is employed. These possible errors in the assumption of average drag-area are reduced in magnitude when determining the snatch force for a parachute system which utilizes controlled deployment, using deployment bags, sleeves, or other devices which restrict the inflation of the canopy during deployment. These systems yield more consistent and predictable values of the drag area.

4.3 Measures to Reduce Snatch Force. The preceding discussion demonstrates that snatch force can be a significant factor for consideration in the design of parachute systems. In order to limit or reduce developed snatch forces, several methods can be employed:

(a) The drag area $(C_D S)$ of the uninflated canopy and pilot chute, when applicable, must be reduced to the minimum, and any tendency to inflate the canopy

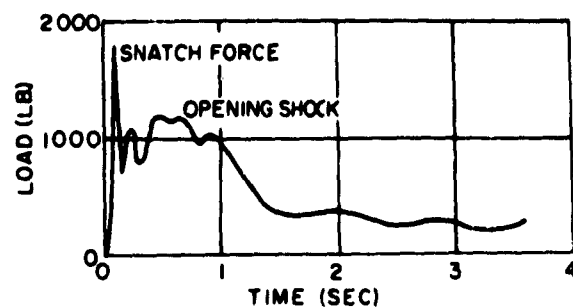


Fig. 4-37 Force vs Time of a 28-ft Flat Circular Canopy (No Bag Deployment)

partially prior to line stretch must be eliminated.

(b) Control of inflation tendencies may be accomplished by use of a device known as a skirt hesitator, which restricts the skirt of the canopy and prevents canopy inflation until the completion of line snatch. Tests show that hesitators have been successful at deployment speeds from 100 to 350 knots.

(c) Decrease of the distance, L_s (suspension-line length), will reduce snatch forces.

(d) Use of suspension lines with high elongation will decrease the peak force at snatch.

(e) Minimizing the canopy weight will reduce snatch force.

(f) Packing methods may also affect the development of snatch forces. When the canopy of a parachute is packed in a roll, rather than accordion folds, the mass of the canopy is not fully effective at the snatch. Only a fraction of the total mass is accelerated linearly with the suspension lines as a portion of the mass unrolls. The remainder of the canopy begins its rotating action which distributes the total force over a longer time base, reducing peak forces considerably.

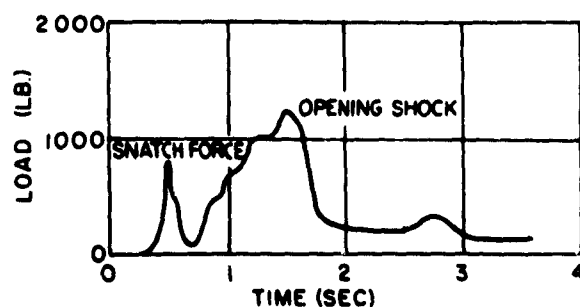


Fig. 4-38 Force vs Time of a 28-ft Flat Circular Canopy (Bag Deployment)

Experiments have shown that the maximum snatch-force is reduced by approximately 40 per cent if roll packing and deployment are used. Reduction of as much as 60 per cent has been accomplished by rolling a portion of the suspension lines also. This latter method, however, is unreliable.

(g) Bag deployment can be used. Experiments with man-carrying parachutes have shown that very high and undesirable snatch forces can be obtained at deployment speeds of 130 knots. A number of methods for reducing this force were employed, but none was as successful at speeds up to 350 knots, as bag deployment. Fig. 4-37 and 4-38 show comparative force (versus time) developed by a canopy with and without bag deployment. It should be noted that the recordings are average and typical, and are not isolated examples.

SEC. 5 FILLING-TIME AND OPENING-SHOCK OF CANOPIES

The determination of the filling-time and opening-shock of textile parachute canopies by mathematical processes, based upon an analysis of the physical process of canopy opening, has not yet been solved satisfactorily. Two different cases can be considered in the analysis of the dynamics of canopy opening. One, the "infinite mass" condition, stipulates that the velocity of the parachute-load configuration does not change appreciably during the period of canopy inflation, and can therefore be considered constant. The other case, the "finite mass" condition, stipulates that the velocity decay during the inflation is substantial and must, therefore, be considered. In general practice, the "infinite mass" condition can be assumed to exist if the canopy drag loading ($\frac{1}{2} \rho C_D S$) is larger than 30 psf, which means that the terminal velocity of the configuration at sea-level density will be greater than 150 fps.

A second differentiation should be made for the calculation of opening-shock forces developed by solid cloth textile parachute canopies and by canopies with inherent geometric porosity when the calculation is done under finite-mass conditions. In the development of opening-shock forces on solid cloth canopies, the effective porosity of the canopy cloth has been found to be a major factor and must be taken into consideration.

A much simpler approach can be taken in the calculation of opening-forces generated by canopies operating under infinite-mass conditions, since empirical values are known for various types of canopies which relate the maximum force developed to the

steady drag generated by the canopy under the same velocities conditions.

When a canopy is deployed downstream of the primary body, it is initially in an uninflated, elongated shape. The net gain of the air flowing in and out of the canopy alters the canopy's shape until the final shape of full inflation is reached. During this process, a retarding force acts upon the load connected to the canopy. The magnitude of this force is a function of the time of canopy inflation, usually called canopy filling-time. Since the filling-time of canopies considered operating under infinite-mass conditions is extremely short, by definition a velocity decay of the suspended load during canopy inflation will not occur. For canopy operations under finite-mass conditions, the canopy filling-time can be substantial, and throughout the process of filling a retarding force acts upon the suspended load. Therefore, the determination of the filling-time of a canopy is an essential part of the opening problem itself. The value of the filling-time must be known or be determined fairly accurately in order to calculate the resulting opening-shock; otherwise, if the filling-time has to be guessed or assumed, the success of the conventional methods depends upon the experience, related information, or successful estimation by the parachute designer.

5.1 Opening-Shock of Canopies Under Finite-Mass Conditions.

A number of methods for calculation of the opening-shock of canopies have been developed that provide generally satisfactory results if the approximate filling-time of the canopy is known. Several authors (Ref (4-34), (4-35), (4-36)) have proposed strictly analytical methods for the calculation of filling time and opening force. However, with attempts to make these methods as perfect and logical as possible, they have become cumbersome. Furthermore, a number of essential parameters are presently either not available or not well defined, and it appears to be very difficult to obtain results with any satisfactory degree of accuracy. The consequence is that these calculation methods have not checked out against experimental results, and have not been reduced to practice. A newer attempt is represented in Ref (4-37); however, this method was developed specifically for canopies with inherent geometric porosity, and so far has also not been reduced to general practice.

5.1.1 SOLID CLOTH TEXTILE CANOPIES. A new analytical method has been developed which adopts the concept initially proposed in Ref (4-34), but includes one primary and simplifying assumption: it is assumed that during the inflation process the drag area of the canopy increases with respect to time in a linear manner, and that this linearity is

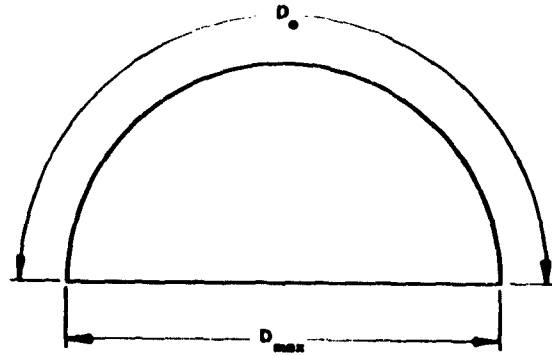


Fig. 4-39 Shape of Fully Inflated Canopy

determinate in the total filling-time. On the basis of this assumption, a number of governing relationships can be established. An analytical method has been devised which provides, with a reasonable amount of effort, numerical values for the filling-time as well as giving a force-time relationship.

5.1.1.1 Filling-Time. The time of inflation of a canopy depends upon the mass of air flowing into the canopy and the amount of air which is lost through the porous material of the canopy. The influx depends upon the instantaneous relative velocity; the loss of air depends on the differential pressure between both sides of the fabric. Consequently, the inflation of the drag-producing surface becomes a matter of a mass balance. The instantaneous velocity and the related pressure-differential follow from the equation of motion based on Newton's Second Law. Therefore, it may be said that the filling-time is a function of the mass balance and the equation of motion.

A drag force is associated with a canopy moving through air, based on the shape of the canopy. This drag is usually expressed in a form similar to other aerodynamic forces, and is the product of the dynamic pressure of the fluid and the drag area of the canopy. With the assumption that the drag area increases linearly with time during inflation, while the drag coefficient remains constant, a linear increase of projected canopy area is obtained. Thus, the projected canopy area, S_p , can be expressed as

$$(4-53) \quad S_p = \frac{\pi D_p^2}{4} = kt$$

The proportionality constant, k , is found from the condition $D_p = D_{\max}$ when $t = t_f$ which gives

$$(4-54) \quad k = \frac{\pi D_{\max}^2}{4 t_f}$$

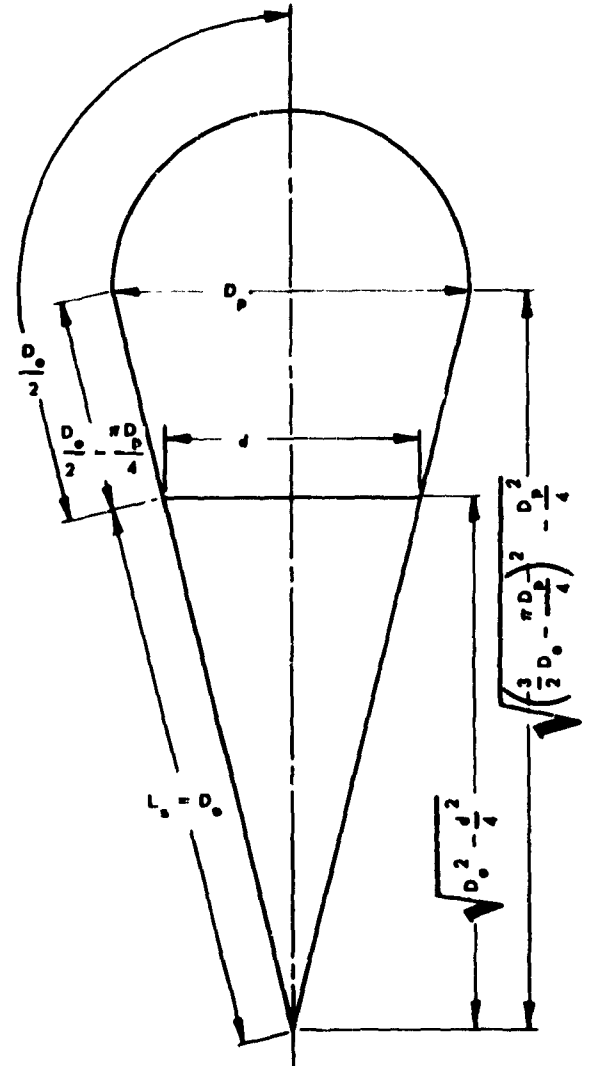


Fig. 4-40 Canopy Shape During Inflation

Considering only flat circular canopies with nominal diameters D_o , and considering the fully inflated canopy to be hemispherical (Fig. 4-39), D_{\max} can be expressed

$$(4-55) \quad D_{\max} = \frac{2 D_o}{\pi}$$

With this relationship, Eq 4-54 becomes

$$(4-56) \quad k = \frac{D_o^2}{\pi t_f}$$

Substituting this into Eq 4-53 given, for the projected

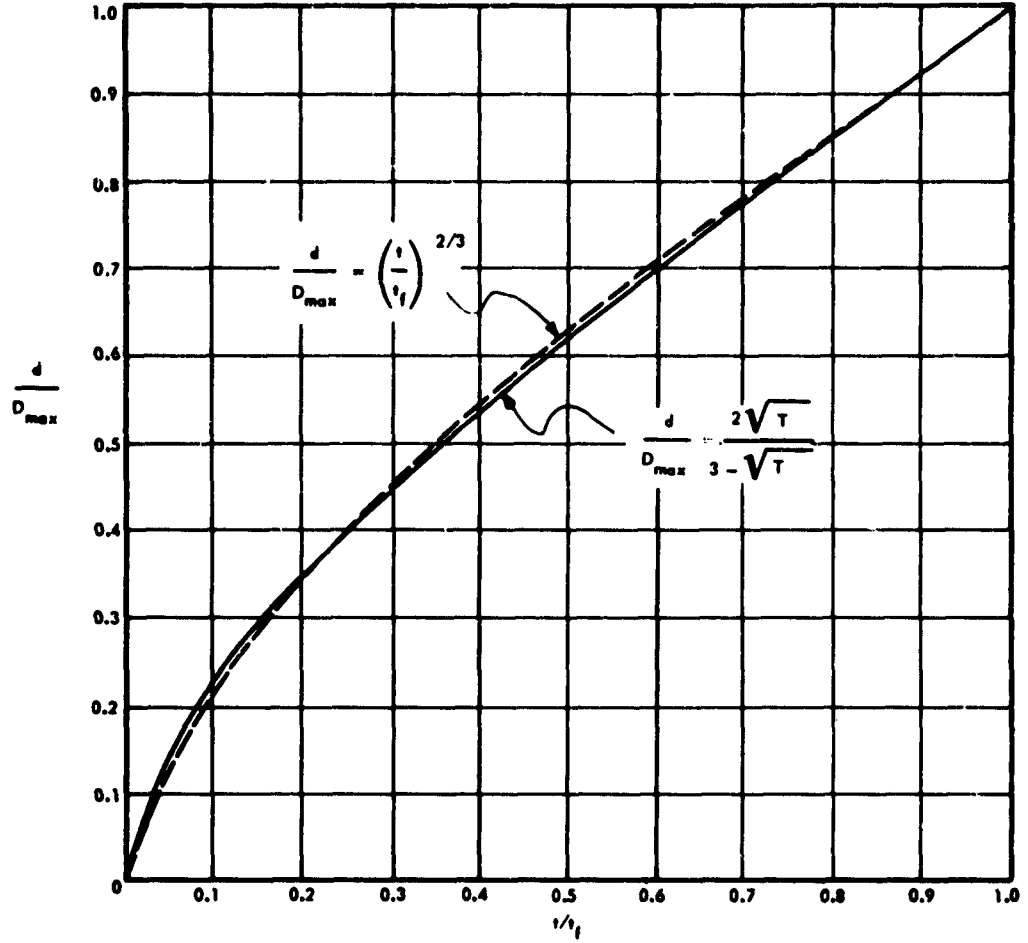


Fig. 4-41 Diameter of Canopy Mouth During Inflation

canopy area,

$$(4-57) \quad S_p = \frac{D_o^2}{\pi} \frac{t}{t_f}$$

or for the projected canopy diameter

$$(4-58) \quad D_p = \frac{2 D_o}{\pi} \left(\frac{t}{t_f} \right)^{1/2}$$

An idealized canopy shape during inflation was first proposed in Ref (4-34). It was assumed to consist of a hemisphere of diameter D_p and a truncated cone with lower base of diameter D_p and upper base of diameter d , as shown in Fig. 4-40. This assumption is not actually precise, since the spherical and conical surfaces will join tangentially, which would make the spherical portion slightly more than a hemisphere. This slight difference is neglected. Then, by similarity,

$$(4-59) \quad \frac{d}{L_s} = \frac{D_p}{L_s + \frac{D_o}{2} - \frac{\pi D_p}{4}}$$

Substituting the value of D_p from Eq 4-58 in Eq 4-59 and letting

$$(4-60) \quad \frac{t}{t_f} = T$$

gives the value of the instantaneous mouth diameter, d , of the canopy as

$$(4-61) \quad d = \frac{2 D_o}{\pi} \left[\frac{2 L_s T^{1/2}}{2 L_s + D_o - D_o T^{1/2}} \right]$$

Solid cloth canopies are constructed of porous fabrics which allow a certain portion of the air inflow to flow

through the drag-producing surface. It is the difference between the mass flow entering the mouth of the canopy and the mass flow through the drag-producing surface that causes the canopy to inflate. This may be expressed mathematically as

$$(4.62) \quad \frac{\pi d^2}{4} v_{in} \rho - \frac{\pi D_p^2}{2} U \rho = \frac{d}{dt} (\rho V)$$

Since the inflation of the canopy requires relatively little time, changes in altitude during the period of canopy inflation are negligible. Consequently, it can be assumed that the air density remains constant.

It is necessary to express the inflow and outflow velocities, v_{in} and U , as functions of the velocity of the load-parachute configuration, v . At the beginning of the inflation process the inflow velocity is nearly equal in magnitude to the free-stream velocity, whereas after complete inflation, a stagnation point is formed and the inflow velocity is negligible. As an approximation, it is assumed that the ratio of inflow velocity to free stream velocity decreases linearly with time, thus giving

$$(4.63) \quad \frac{v_{in}}{v} = 1 - T$$

The flow velocity through the drag-producing surface is then assumed to be proportional to the inflow velocity.

This gives

$$(4.64) \quad U = C v_{in}$$

where C is the "effective porosity" of the canopy fabric, defined as the ratio of the outflow velocity to the inflow velocity of the flow through a porous fabric (see Sec. 3). Thus, for Eq 4-64 to hold, the flow velocity just inside the drag-producing surface must be equal to the inflow velocity through the canopy mouth opening.

By substituting Eq 4-58, 4-61, 4-63, and 4-64 into Eq 4-62 and dividing by ρ ,

$$(4.65) \quad \frac{dV}{dt} = \frac{D_o^2}{\pi} v (1-T) T - \left[\left(\frac{2 L_s}{2 L_s + D_o - D_o T^{1/2}} \right)^2 - 2C \right]$$

By making the substitution

$$(4.66) \quad dt = t_f dT$$

Eq 4-65 becomes

$$(4.67) \quad \frac{dV}{dT} = \frac{D_o^2}{\pi} v t_f (1-T) T - \left[\left(\frac{2 L_s}{2 L_s + D_o - D_o T^{1/2}} \right)^2 - 2C \right]$$

This equation represents the basic working equation for finding the filling-time, t_f . By expressing v_s as a function of T and integrating the right side from $T=0$ to $T=1$, and the left side from $V=0$ to $V=V_{max}$, a solution for the filling-time can be obtained.

A further simplification of Eq 4-67 can be obtained by assuming that the length of parachute suspension lines, L_s , is equal to the nominal canopy diameter, D_o . Then from Eq 4-59

$$(4.68) \quad \frac{d}{D_o} = \frac{D_p}{\frac{3 D_o}{2} - \frac{\pi D_p}{4}}$$

With the expression for D_p given by Eq 4-58,

$$(4.69) \quad \frac{d}{D_o} = \frac{\frac{4}{\pi} T^{1/2}}{3 - T^{1/2}}$$

Since (Eq 4-55)

$$(4.70) \quad D_{max} = \frac{2 D_o}{\pi}$$

Eq 4-69 can be rewritten as

$$(4.71) \quad \frac{d}{D_{max}} = \frac{2 T^{1/2}}{3 - T^{1/2}}$$

For simplicity, this expression can be approximated, as shown in Fig. 4-41, by

$$(4.72) \quad \frac{d}{D_{max}} = T^{2/3}$$

or

$$(4.73) \quad d = \frac{2}{\pi} D_o T^{2/3}$$

With this simplification, the basic working equation for finding the filling time, t_f , becomes

$$(4.74) \quad \frac{dV}{dT} = \frac{D_o^2}{\pi} t_f v \left[(1-T) T^{4/3} - 2CT(1-T) \right]$$

Although the solution of the filling time for the infinite-mass case is relatively simple (see 5.2.1), a solution for the finite-mass case is much more com-

plicated, and Newton's Second Law of Motion must be used in the process. Newton's Second Law states that an unbalanced force which acts on a body produces a rate of change in the momentum of the body equal to the unbalanced force. It can be written as

$$(4.75) \quad \frac{d(mv)}{dt} = F$$

It should be pointed out that the filling-time and opening-shock equations are derived by neglecting the influence of gravity. This restricts the use of these equations to the case of horizontal or near-horizontal deployment. However, the equations can be modified to allow calculation of the filling time and opening-shock of a canopy under vertical deployment conditions (see Chapter 12). In the case of an inflating canopy, the force, F , is the aerodynamic drag force,

$$(4.76) \quad F = 0.5 \rho C_D S v^2$$

and the mass term, m , includes the mass of the suspended load, m_g , the mass of the air trapped inside the drag-producing surface of the canopy, m_i , and a term called apparent mass, m_a , which results from the transfer of energy to the surrounding air by a body moving through the air. The actual mass of the canopy itself is neglected.

(a) *Included Mass.* The included mass is the mass of the air trapped within the drag-producing surface of the canopy and can be expressed as $m_i = \rho V$. Assuming an idealized canopy shape during inflation (Fig. 4-40) and assuming $L_s = D_o$, the volume enclosed by the drag-producing surface is

$$(4.77a) \quad V = V_{\text{hemisphere}} + V_{\text{frustum}}$$

$$V = \frac{2}{3} \pi \left(\frac{D_p}{2} \right)^3 + \left[\frac{\pi}{3} \left(\frac{D_p}{2} \right)^2 \times \sqrt{\left(\frac{3}{2} D_o - \frac{\pi}{4} D_p \right)^2 - \frac{D_p^2}{4}} - \frac{\pi}{3} \left(\frac{d}{2} \right)^2 \sqrt{D_o^2 - \frac{d^2}{4}} \right]$$

or

$$(4.77b) \quad V = \frac{\pi D_p^3}{12} + \frac{\pi}{12} \left[D_p^2 \times \sqrt{\left(\frac{3}{2} D_o - \frac{\pi}{4} D_p \right)^2 - \frac{D_p^2}{4}} - d^2 \sqrt{D_o^2 - \frac{d^2}{4}} \right]$$

Substituting Eq 4-58 and 4-69 into Eq 4-77 gives

$$(4.78) \quad V = \frac{2 D_o^3}{3 \pi} T \left\{ \left[\frac{1}{4} - \frac{2}{(3 - T^{1/2})^3} \right] \times \sqrt{(3 - T^{1/2})^2 - \frac{4}{\pi^2} T} + \frac{1}{\pi} T^{1/2} \right\}$$

This equation is very complicated; a simplification by means of an appropriate approximation is desirable. Since

$$(4.79) \quad V_{\text{max}} = \frac{2 D_o^3}{3 \pi^2}$$

Eq 4-78 can be rewritten as

$$(4.80) \quad \frac{V}{V_{\text{max}}} = \pi T \left\{ \left[\frac{1}{4} - \frac{2}{(3 - T^{1/2})^3} \right] \times \sqrt{(3 - T^{1/2})^2 - \frac{4}{\pi^2} T} + \frac{1}{\pi} T^{1/2} \right\}$$

This equation is plotted in Fig. 4-42. A curve which very closely approximates Eq 4-80, also shown in Fig. 4-42, is given by

$$(4.81) \quad \frac{V}{V_{\text{max}}} = 1.058 - \frac{(T - 1.31)^2}{1.62}$$

From which

$$(4.82) \quad V = \frac{2 D_o^3}{3 \pi^2} \left(1.058 - \frac{(T - 1.31)^2}{1.62} \right)$$

The included mass is then

$$(4.83) \quad m_i = \rho V = \frac{2 \rho D_o^3}{3 \pi^2} \left(1.058 - \frac{(T - 1.31)^2}{1.62} \right)$$

The included mass may be an important item to be considered in the opening-shock analysis, and in each particular situation the effect of the included mass should be investigated to determine its significance. For example, the included mass at sea-level density for a fully inflated flat circular canopy with a nominal diameter, D_o , of 28 ft is 114 lb; for a canopy with a nominal diameter of 60 ft, the included mass is 1119 lb.

(b) *Apparent Mass.* During the inflation of a canopy, the flow pattern and the kinetic energy of the air surrounding the canopy undergo extreme changes due to the unsteadiness of motion and the changing shape of the canopy. This change of energy results in a force and is related to an increase in mass called

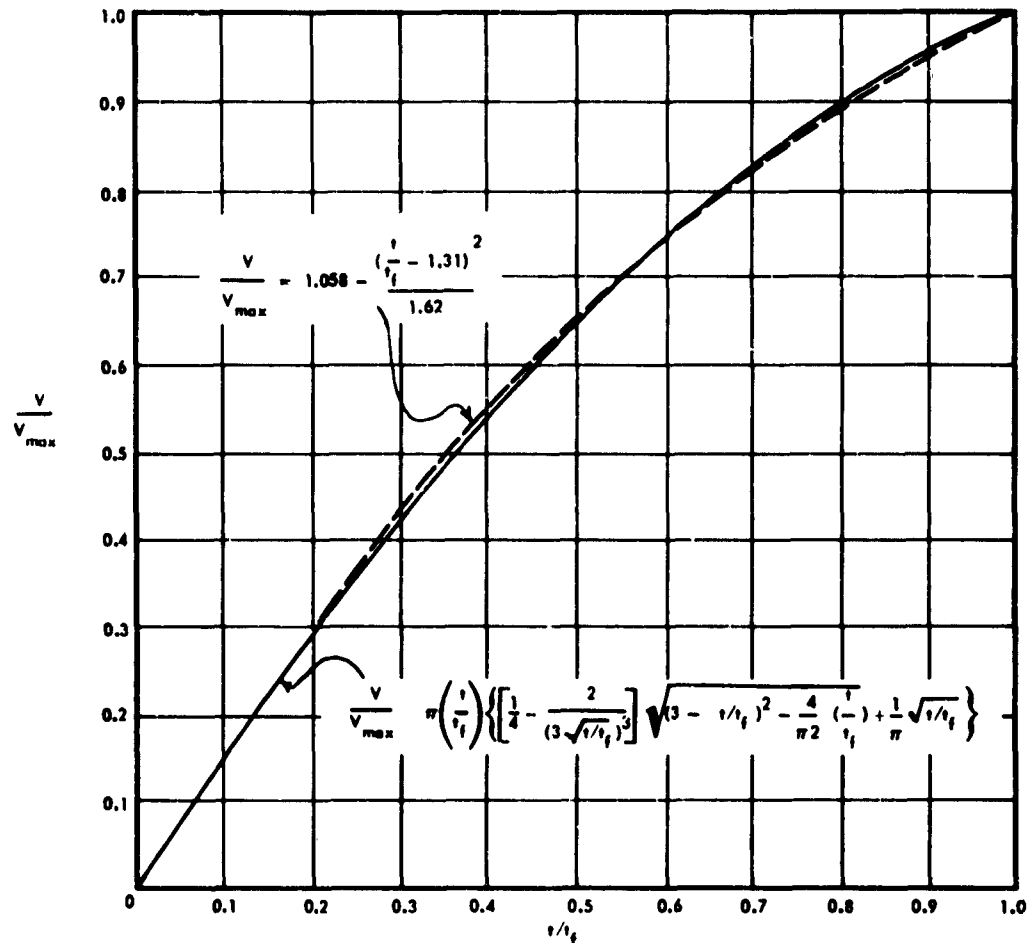


Fig. 4-42 Canopy Volume During Inflation

the "apparent" mass (Ref (4-24)). For regular solid bodies, such as spheres, in potential flow, the apparent mass can be determined exactly. It is possible to express the apparent mass of solid bodies of revolution as

$$(4-84) \quad m_a = K' \pi R^3 \rho$$

where R = Radius of the body; and

K' = Constant determined by the shape of the body.

For a solid sphere, $K' = 0.666$; for a solid flat disk, $K' = 0.849$ (Ref (4-17)).

Heinrich (Ref (4-25)) attempted to determine experimentally the apparent mass of inflated canopies of various types and of different porosities. He found that a value of $K' = 0.25$ gave a close approximation. This coefficient apparently changes in value during the period of inflation because, if the assumption

were made that it remained constant, the canopy would have an apparent mass equal to that of a fully inflated canopy with a projected diameter equal to the projected diameter of the inflating canopy. It is, therefore, a reasonable assumption that the apparent mass associated with intermediate inflated-canopy shapes is less than for the fully inflated canopy, and the approximation is made that the apparent-mass coefficient, K' , varies linearly with time during inflation, reaching a maximum value of 0.25 at full inflation. This is apparently the upper limit, and

$$(4-85) \quad K' = 0.25T$$

The apparent mass of a canopy can then be expressed as

$$(4-86) \quad m_a = 0.25 \pi R^3 \rho T$$

with

$$(4.87) \quad R = \frac{D_p}{2} = \frac{D_o T^{1/2}}{\pi}$$

and Eq 4-86 can be written as

$$(4.88) \quad m_a = \frac{\rho D_o^3}{4\pi^2} T^{5/2}$$

Under the stated assumptions, the apparent mass of the fully inflated canopy is equal in magnitude to 3/8 of the included mass; therefore, it cannot be neglected.

(c) *Total Mass.* The total mass, m , which was defined as the sum of the suspended mass, the included-air mass, and the apparent mass, can be expressed as

$$(4.89) \quad m = \frac{W}{g} + m_i + m_a$$

Substituting Eq 4-83 and 4-88 into Eq 4-89:

$$(4.90) \quad m = \frac{W}{g} + \frac{2\rho D_o^3}{3\pi^2} \left(1.058 - \frac{(T-1.31)^2}{1.62} \right) + \frac{\rho D_o^3}{4\pi^2} T^{5/2}$$

(d) *Instantaneous Velocity.* With the expression for the total mass given, a solution of Eq 4-75 can be attempted. Substituting the expression for the total mass (see Eq 4-89)

$$(4.91) \quad m = \frac{W}{g} + m_i + m_a$$

and the expression for the aerodynamic drag generated (see Eq 4-76),

$$(4.92) \quad F = \frac{\rho}{2} C_D S v^2$$

into Eq 4-75 yields

$$(4.93) \quad \frac{d}{dt} \left[\left(\frac{W}{g} + m_i + m_a \right) v \right] = - \frac{\rho}{2} C_D S v^2$$

or

$$(4.94) \quad \left(\frac{W}{g} + m_i + m_a \right) \frac{dv}{dt} + v \left(\frac{dm_i}{dt} + \frac{dm_a}{dt} \right) = - \frac{\rho}{2} C_D S v^2$$

By making the following substitutions

$$(4.95) \quad m_i = 99.1 \cdot 10^{-6} \sigma D_o^3 [1.71 - (T-1.31)^2] \quad \text{from Eq 4-83}$$

$$(4.96) \quad m_a = 60.075 \cdot 10^{-6} \sigma D_o^3 T^{5/2} \quad \text{from Eq 4-88}$$

$$(4.97) \quad \frac{dm_i}{dt} = -198.2 \cdot 10^{-6} \frac{\sigma D_o^3}{t_f} (T-1.31)$$

$$(4.98) \quad \frac{dm_a}{dt} = 150.2 \cdot 10^{-6} \frac{\sigma D_o^3}{t_f} T^{3/2}$$

$$(4.99) \quad \frac{\rho}{2} C_D S = \frac{\rho D_o}{2} (C_D S)_{\max} T$$

Eq 4-94 becomes

$$(4.100) \quad \left\{ \frac{W}{g \sigma D_o^3 \cdot 10^{-6}} + 60.075 T^{5/2} + 99.1 [1.71 - (T-1.31)^2] \right\} \left\{ \frac{dv}{dt} + \frac{v}{t_f} \right\} = [150.2 T^{3/2} - 198.2 (T-1.31)] - \frac{1189}{D_o^3} (C_D S)_{\max} T v^2$$

By rounding off the numerical coefficients and substituting

$$(4.101) \quad dt = t_f dT$$

Eq 4-100 becomes

$$(4.102) \quad 2 \left\{ \frac{W \cdot 10^6}{20 g \sigma D_o^3} + 3 T^{5/2} + 5 [1.71 - (T-1.31)^2] \right\} \left\{ \frac{dv}{dt} + 5v [3 T^{3/2} - 4 (T-1.31)] \right\} = - \frac{120 (C_D S)_{\max} t_f}{D_o^3} T v^2$$

In an attempt to simplify this equation, the expressions

$$(4.103) \quad 3 T^{5/2} + 5 [1.71 - (T-1.31)^2]$$

and

$$(4.104) \quad 3 T^{3/2} - 4 (T-1.31)$$

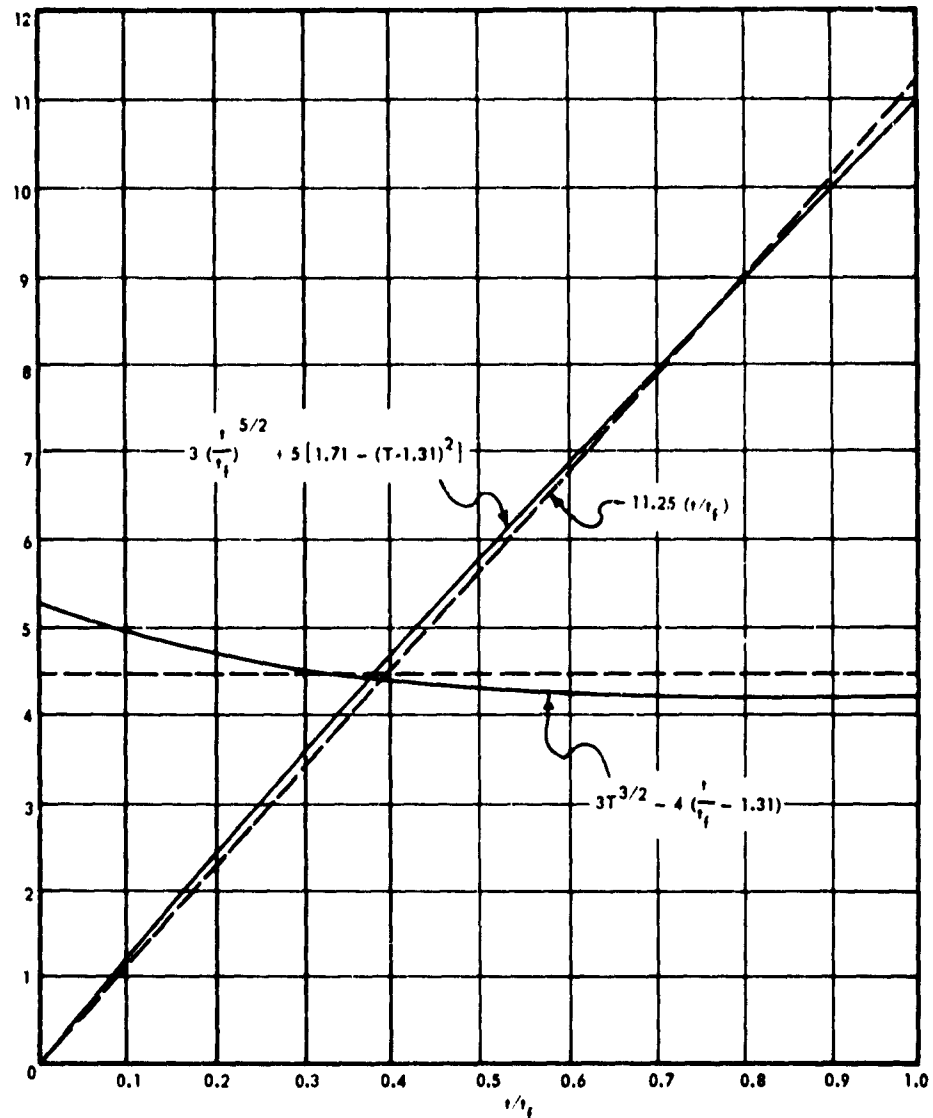


Fig. 4-43 Approximation of Terms in Equation of Motion

are plotted versus T in Fig. 4-43. From this plot it can be seen that the first expression, which represents the sum of the included and apparent masses, is very nearly linear and can be approximated by

$$(4-105) \quad 3T^{5/2} + 5 \left[1.71 - (T - 1.31)^2 \right] \approx 11.25T$$

The second expression also has a nearly constant value of

$$(4-106) \quad 3T^{3/2} - 4(T - 1.31) \approx 4.5$$

Since this last expression represents the rate of change of the sum of the included and apparent masses, and

since this sum is a nearly linear function of time, the constant value seems reasonable. Making these approximations, Eq 4-102 then becomes

$$(4-107) \quad 2 \left(\frac{W \cdot 10^6}{20 g \sigma D_o^3} + 11.25T \right) \frac{dv}{dt} + 22.5v \\ = - \frac{120 (C_D S)_{\max} t_f}{D_o^3} T v^2$$

This equation represents the instantaneous velocity of the load-parachute configuration during inflation and is in an integrable form. Letting

$$(4-108) \quad \frac{W \cdot 10^6}{20 g \sigma D_o^3} = 4$$

and

$$(4-109) \quad \frac{120 (C D S)_{\max} t_f}{D_o^3} = B$$

the solution for the instantaneous velocity, v , is

$$(4-110) \quad v = \left\{ \frac{B v_s}{2 (11.25)^2} \left[(11.25 T + 4) \ln \frac{11.25 T + 4}{4} - 11.25 T \right] + \frac{11.25 T + 4}{4} \right\}$$

(c) *Filling-Time Value.* Substituting into the basic working equation for finding the filling time (Eq 4-74) the value of v given by Eq 4-110, and writing the resultant equation in integral form, the following expression is obtained, from which the filling-time for the finite-mass case can be determined:

$$(4-111) \quad \int_0^{V_{\max}} dV = \int_0^1 \left\{ \frac{D_o^2 t_f v_s}{\pi} [(1-T) T^4 - 3 - 2CT(1-T)] \frac{dT}{dT} \right\} \div \left\{ \frac{B v_s}{2 (11.25)^2} \left[(11.25 T + 4) \ln \frac{11.25 T + 4}{4} - 11.25 T \right] + \frac{11.25 T + 4}{4} \right\}$$

The right-hand expression cannot be integrated directly without making broad assumptions and simplifications. Therefore, to determine the filling-time accurately, a numerical integration of the expression is necessary. This is further complicated by the fact that the integrand contains t_f , which necessitates the use of a trial and error solution.

From Eq 4-111 it can be seen that the value of the integral on the right-hand side remains the same for different velocities at the beginning of inflation, if the product $(v_s t_f)$ remains constant and the effective porosity, C , remains constant. The effective porosity actually varies slightly with v_s , but since this variation is small, it will be neglected. With this assumption, the filling-time becomes inversely proportional to the velocity at the beginning of canopy inflation.

Thus, if for the same operational altitude one determines the filling-time corresponding to one particular value of v_s , the filling-time corresponding to any other value of v_s can easily be determined from the relationship

$$(4-112) \quad t_f v_s = \text{constant}$$

The following numerical process is recommended to determine the filling time for any given case:

- (1) Calculate the volume of air enclosed by the fully inflated canopy drag-producing surface, V_{\max} , assuming it to be a perfect hemisphere:

$$(4-113) \quad V_{\max} = \frac{2D_o^3}{3\pi^2}$$

- (2) Calculate the corresponding value of the effective porosity, C , as outlined in Section 3.
- (3) Determine the velocity at the beginning of canopy inflation, v_s , or calculate in accordance with method outlined in Section 4.
- (4) Assume a value of the filling time, t_f , which appears to be in the right order and calculate the value of the integrand

$$(4-114) \quad f(T, t_f) = \left\{ \frac{D_o^2 t_f v_s}{\pi} [(1-T) T^4 - 3 - 2CT(1-T)] \right\} \div \left\{ \frac{B v_s}{2 (11.25)^2} \left[(11.25 T + 4) \ln \frac{11.25 T + 4}{4} - 11.25 T \right] + \frac{11.25 T + 4}{4} \right\}$$

for T varying from 0 to unity in intervals of 0.1. This calculation can be made conveniently on a calculation sheet, as shown in Fig. 4-44.

- (5) Plot the value of the integrand obtained under (4) above versus T , and measure the area under the curve with a planimeter. This area, which represents the right-hand side of Eq 4-111 is then compared with the integral on the left-hand side, which is equal to V_{\max} , the volume of the trapped or included air in the canopy drag-producing surface obtained under (1). If the values are equal or approximately equal, the assumed filling-time represents a satisfactory approximation of the actual filling-time of the canopy under consideration.
- (6) If the process under (5) does not show satisfac-

$$V_{max} = \int_0^1 f\left(\frac{z}{t_c}, t_c\right) dz$$

$$f\left(\frac{z}{t_c}, t_c\right) = \frac{D_0^2 t_c^2 \pi}{\pi} \left[\left(\frac{11.25}{t_c} \cdot \frac{z}{t_c} + A \right) \ln \left(\frac{11.25}{t_c} \cdot \frac{z}{t_c} + A \right) - 11.25 \frac{z}{t_c} \right] + \frac{11.25}{t_c} \frac{z}{t_c} + A$$

$$A = \frac{W = 10^6}{20 \pi^2 D_0^2} = 26.54$$

$$B = \frac{120(C_0 S)_{max} t_c}{D_0^2} = \begin{cases} t_{c1} = 1.057 \\ t_{c2} = 1.153 \\ t_{c3} = 1.249 \end{cases}$$

$$\frac{D_0^2 t_c^2 \pi}{\pi} = \begin{cases} t_{c1} = 21820 \\ t_{c2} = 23810 \\ t_{c3} = 25794 \end{cases}$$

$$\frac{B \pi}{2 \pi 11.25} = \begin{cases} t_{c1} = 1.107 \\ t_{c2} = 1.207 \\ t_{c3} = 1.308 \end{cases}$$

$t_{c1} = 0.38$ $C_0 = 0.78$
 $t_{c2} = 0.36$ $\gamma_c = 26.5$
 $t_{c3} = 0.39$ $C = 0.046$
 $D_0 = 28$ $\sigma = 0.533$
 $W = 200$ $h = 20,000$

1	t/t_c	0.0	0.1	0.2	0.3	0.4	0.5	0.6	0.7	0.8	0.9	1.0
2	$(t/t_c)^{1/2}$	0.0	0.464	0.585	0.669	0.736	0.794	0.843	0.888	0.928	0.965	1.0
3	$11.25 \cdot t/t_c$	0.0	1.125	2.250	3.375	4.500	5.625	6.750	7.875	9.000	10.125	11.250
4	$1 - (t/t_c)$	1.0	0.900	0.800	0.700	0.600	0.500	0.400	0.300	0.200	0.100	0.0
5	$(t/t_c)^{1/2} - z/c$	—	0.372	0.493	0.577	0.644	0.702	0.751	0.796	0.836	0.873	—
6	$(t/t_c)^{1/2} (1 - t/t_c) [(t/t_c)^{1/2} - z/c]$	0.0	0.033	0.079	0.121	0.153	0.176	0.190	0.194	0.184	0.179	0.0
7	$D_0^2 t_c^2 \pi / \pi = 6$	0.0	720	1724	2640	3382	3940	4326	4574	4704	4724	0.0
8	t_{c1}	0.0	786	1881	2881	3691	4191	4486	4616	4661	4681	0.0
9	t_{c2}	0.0	891	2037	3121	3996	4599	4942	5077	5107	5107	0.0
10	t_{c3}	—	—	—	—	—	—	—	—	—	—	—
11	$[11.25 t/t_c] + A$	—	27.67	28.79	29.92	31.04	32.17	33.29	34.42	35.54	36.67	—
12	$[(11.25 t/t_c) + A] / A$	—	1.043	1.085	1.127	1.170	1.212	1.254	1.297	1.339	1.382	—
13	$\ln [(11.25 t/t_c) + A] / A$	—	0.042	0.082	0.120	0.157	0.192	0.226	0.260	0.292	0.324	—
14	$[11.25 t/t_c] + A$	—	1.162	2.361	3.590	4.879	6.177	7.524	8.949	10.378	11.801	—
15	$(1 - t/t_c)$	—	0.937	0.111	0.218	0.315	0.413	0.512	0.611	0.710	0.810	—
16	$[B \pi / (2 \pi 11.25)] = 3$	—	0.041	0.123	0.236	0.413	0.611	0.837	1.109	1.529	1.944	—
17	t_{c1}	—	0.045	0.134	0.260	0.430	0.646	0.934	1.296	1.663	2.119	—
18	t_{c2}	—	0.048	0.148	0.281	0.488	0.722	1.012	1.408	1.802	2.297	—
19	t_{c3}	—	—	—	—	—	—	—	—	—	—	—
20	$(3 + 3)$	—	1.084	1.208	1.365	1.553	1.773	2.111	2.486	2.864	3.266	—
21	t_{c1}	—	1.088	1.219	1.387	1.620	1.878	2.188	2.593	3.002	3.501	—
22	t_{c2}	—	1.091	1.230	1.408	1.658	1.934	2.266	2.702	3.141	3.679	—
23	t_{c3}	—	—	—	—	—	—	—	—	—	—	—
24	$f(t/t_c, t_c)$	0.0	664	1427	1934	2136	2106	1861	1466	1021	518	0.0
25	t_{c1}	0.0	722	1543	2077	2278	2232	1933	1533	1033	537	0.0
26	t_{c2}	0.0	780	1636	2217	2411	2347	2043	1634	1100	554	0.0
27	t_{c3}	—	—	—	—	—	—	—	—	—	—	—

Fig. 4-44 Sample Calculation Sheet for Determining Instantaneous Canopy Volume

tory agreement, several values of t_f should be assumed and operations (4) and (5) repeated.

- (7) Compare again and if no satisfaction is reached, plot a curve showing the measured areas obtained in the preceding operations versus the assumed values of filling time. From this curve, the particular value of t_f for which the value of the curve equals the volume of the included air may be found. This value is the required filling-time.

(f) *Sample Calculation.* The preceding numerical calculation method is illustrated by the determination of the filling time of a standard flat circular type parachute canopy with a nominal diameter, D_o , of 28 ft (Type C-9). The following conditions apply:

- (1) Drag coefficient of the canopy: $C_{D_o} = 0.75$
- (2) Drag area of the canopy: $(C_{D_o} S)_{\max} = 586 \text{ ft}^2$
- (3) Canopy material: 1.1 oz. Nylon cloth, MIL-C-702C, Type I
- (4) Weight of suspended load: $W = 200$ pounds
- (5) Velocity at beginning of canopy inflation:
 $v_s = 265 \text{ fps}$
- (6) Altitude at parachute inflation:
 $h = 20,000 \text{ ft}$
- (7) Density ratio at 20,000-ft altitude:
 $\sigma = 0.533$

Step 1: Determination of volume of air included in fully inflated canopy.

$$V_{\max} = \frac{2D_o^3}{3\pi^2} = \frac{2(28)^3}{3(3.14)^2} = \frac{2(21952)}{3(9.86)} = 1484 \text{ ft}^3$$

Step 2: Determination of effective cloth porosity. Standard atmosphere tables show the density ratio for 20,000-ft altitude to be $\sigma = 0.533$. The pressure ratio at which canopy inflation begins is $\Delta p / \Delta p_{\text{crit}} = 0.0527$. The effective porosity value for the specific canopy cloth used is found to be $C = 0.046$, from Fig. 4-18.

Step 3: Determination of velocity of load-parachute configuration at beginning of canopy inflation.

Velocity given: $v_s = 265 \text{ fps}$

Step 4: Assume filling time and calculate value of integrand.

Filling time assumed: $t_f = 0.33 \text{ sec}$

Calculation of integrand is performed with the aid of calculation sheet, Fig. 4-44.

Step 5: The calculated values for the integrand are plotted versus T in Fig. 4-45. A curve is drawn through these points and the area under the curve

measured with a planimeter. This area is found to represent 1320 ft^3 and is significantly lower than the value of the included-air volume.

Step 6: Since the value of the integrand found for an assumed filling-time of 0.33 sec does not compare favorably with the value for the included-air volume, additional filling time values of 0.36 and 0.39 sec are chosen and integrands for these filling times determined. All calculations are performed on the same calculation sheet, Fig. 4-44. The calculated values for the integrand are plotted in Fig. 4-45 and the area under each individual curve derived. For a filling time of 0.36 sec, an area value representing 1407 ft^3 is found, and for $t_f = 0.39 \text{ sec}$, a value representing 1498 ft^3 . It can be seen that the value for a filling time of 0.39 sec compares favorably with the value for the included-air volume (1484 ft^3).

Step 7: In order to obtain an accurate filling-time value, the derived area-values are plotted against filling time in Fig. 4-46, and the points connected. The corresponding filling-time, t_f , for an included-air volume is determined from this relationship to be 0.386 sec.

5.1.1.2 *Opening-Shock.* The force experienced by a parachute canopy during the opening process can be found from Newton's Law

$$(4-115) \quad F = -\frac{W}{g} \frac{dv}{dt}$$

The value of dv/dt can be found from Eq 4-107

$$(4-116) \quad \frac{dv}{dt} = -\frac{v(22.5 + BTv)}{2(A + 11.25T)}$$

As defined in Eq 4-108 and 4-109, above,

$$(4-117) \quad A = \frac{W \cdot 10^6}{20 g \sigma D_o^3} \text{ and } B = \frac{120(C_{D_o} S)_{\max} t_f}{D_o^3}$$

with

$$(4-118) \quad \frac{dv}{dT} = t_f \frac{dv}{dt}$$

The force exerted upon the suspended weight during the period of canopy filling amounts to:

$$(4-119) \quad F = \frac{Wv}{2gt_f} \left(\frac{22.5 + BTv}{A + 11.25T} \right)$$

where v is the instantaneous velocity given by Eq 4-110.

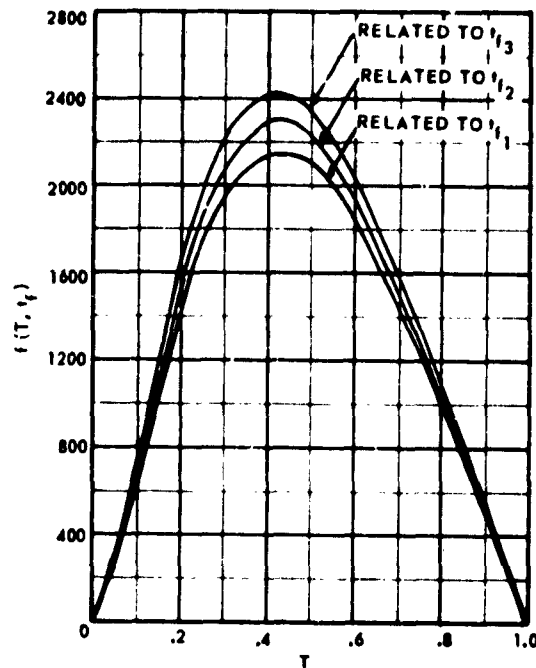


Fig. 4-45 Instantaneous Volume of the Canopy as a Function of the Dimensionless Filling Time

It is not possible to find the maximum force (the parachute opening-shock) directly from Eq 4-119. Therefore, using the value of t_f found by the analytical method described in (f) above, the value of F is calculated for T ranging from 0 to 1 in intervals of 0.1. This calculation can be made on a calculation sheet such as the one shown in Fig. 4-47. The history of force versus time of the canopy can then be plotted, and the maximum force, or opening-shock, can be determined.

(a) *Sample Calculation.* The opening-shock for the canopy for which the filling time was determined in (f), above, can now be calculated.

Step 1: Calculate the instantaneous parachute force for various values of T , using the canopy filling time of 0.386 sec calculated previously. The process and results of this calculation are shown in Fig. 4-47.

Step 2: Plot the calculated values for the instantaneous parachute force, F , versus opening time T . Draw a smooth curve through the plotted points and determine the maximum force value. For this sample calculation, the maximum force or opening-shock experienced by the canopy is 4720 lb, as shown by Fig. 4-48.

5.1.1.3 Comparison of Theoretical and Experimental Results. The determination of opening time and opening-shock of conventional canopies under finite-

mass conditions has been the subject of several experimental efforts. Ref (4-23) describes such a study in which canopies of different types were investigated with respect to launching velocity and altitude. In view of the experimental information presented in Ref (4-23), a number of similar cases have been calculated using the methods described in the preceding paragraphs. A review of these results indicates that favorable comparison exists for parachute canopies launched at low and moderate velocities at various altitudes. For velocities in excess of about 250 knots, the calculated forces are somewhat higher than the measured values, and it appears that further research, both in obtaining valid experimental data and in refining the analytical calculation, is necessary.

In general, the theoretical approach yields values for the filling time and opening-shock which are of the right order of magnitude. The principal trends of the opening phenomena, such as a decrease in inflating parachute canopy filling time and consequent increase in opening force with decreasing canopy cloth permeability, increasing altitude, and increasing velocity at the instant the canopy starts to inflate, are well explained by the theory and are in agreement with experimental results. One situation makes a comparison very difficult: the experimental results available are all related to the launching velocity, although the calculation of the filling times and opening forces begins with the instantaneous velocity of the load-parachute configuration at the instant the canopy be-

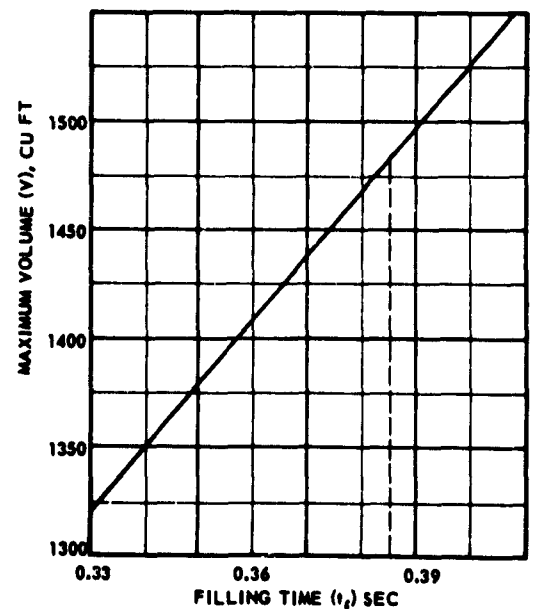


Fig. 4-46 V vs t_f , and the Determination of Proper Filling Time (see Fig. 4-42)

$$t_f = 386 \quad C_0 = .75$$

$$D_0 = 28 \quad V_c = 265$$

$$W = 200 \quad h = 20,000$$

$$\sigma = .533 \quad (C_0)_{max} = .506$$

$$F = \frac{WV}{2gt_f} \left[\frac{22.5 + BT \frac{t_f}{t_f}}{A + 11.25 \frac{t_f}{t_f}} \right]$$

$$A = \frac{W \cdot 10^6}{20 g r D_0^3} = 26.54$$

$$B = \frac{120(C_0)_{max} t_f}{D_0^3} = 1.236$$

$$V_c = \frac{B V_c}{2 + 11.25^2} \left[(11.25 \frac{t_f}{t_f} + A) \ln \frac{11.25 \frac{t_f}{t_f} + A}{A} - 11.25 \frac{t_f}{t_f} + \frac{11.25 \frac{t_f}{t_f} + A}{A} \right]$$

$$\frac{B V_c}{2 + 11.25^2} = 1.294$$

$$\frac{W}{2gt_f} = 6.046$$

1	t/t_f	0.0	0.1	0.2	0.3	0.4	0.5	0.6	0.7	0.8	0.9	1.0
2	$11.25 = ①$	0.0	1.125	2.250	3.375	4.500	5.625	6.750	7.875	9.000	10.125	11.250
3	$11.25 \frac{t_f}{t_f} + A = ② + A$	26.540	27.665	28.790	29.915	31.040	32.165	33.290	34.415	35.540	36.665	37.790
4	$[11.25 \frac{t_f}{t_f} + A] / A = ③ / A$	1.000	1.042	1.085	1.127	1.170	1.212	1.254	1.297	1.339	1.381	1.424
5	$\ln [11.25 \frac{t_f}{t_f} + A] / A = \ln ④$	0.0	0.041	0.082	0.120	0.157	0.192	0.226	0.260	0.292	0.323	0.353
6	$⑤ + ③$	0.0	1.134	2.361	3.590	4.873	6.176	7.524	8.948	10.378	11.843	13.340
7	$⑥ - ②$	0.0	0.009	0.111	0.215	0.373	0.551	0.774	1.073	1.378	1.718	2.090
8	$[B V_c / (2 + 11.25^2)] = ⑦$	0.0	0.12	0.144	0.218	0.483	0.718	1.002	1.388	1.783	2.223	2.704
9	$⑧ + ④$	1.000	1.054	1.229	1.405	1.653	1.925	2.256	2.685	3.122	3.604	4.128
10	$V_c / ⑨ = V$	265.0	251.4	218.6	188.6	160.3	137.7	117.5	98.7	84.9	73.5	64.2
11	$BT = ⑩$	327.5	310.7	266.5	233.1	198.1	170.2	145.2	122.0	104.9	90.8	79.4
12	$8r \frac{t_f}{t_f} = ⑪ + ①$	0.0	31.07	53.30	69.93	79.24	85.10	87.12	85.40	83.92	81.72	79.40
13	$r [W / 2gt_f] = W / 2gt_f = ⑫$	2132	2023	1735	1517	1290	1108	945.4	794.1	683.1	591.4	516.6
14	$22.5 + ⑫$	22.5	53.57	75.80	92.43	101.74	107.60	109.62	107.90	106.42	104.22	101.90
15	$⑭ / ③$	0.848	1.936	2.633	3.090	3.278	3.348	3.293	3.135	2.994	2.842	2.696
16	$⑮ + ⑬ = F$	1808	2917	4268	4688	4229	3706	3113	2490	2045	1681	1393

Fig. 4-47 Sample Calculation Sheet for Maximum Force vs t/t_f

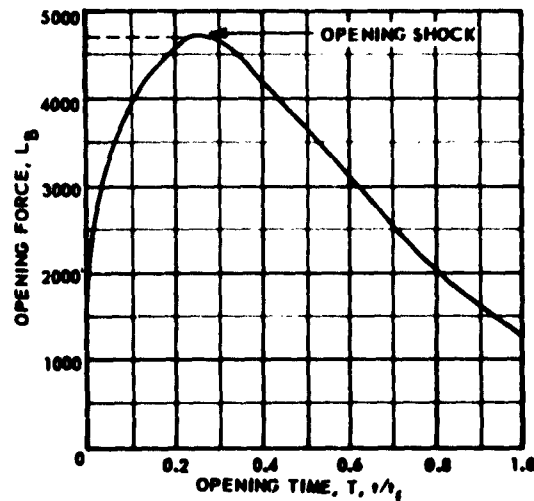


Fig. 4-48 Values of the Parachute Force and Determination of the Opening-Shock

gins to inflate. In view of the uncertainty which necessarily exists in the calculation of this instantaneous velocity from launch velocity, particularly if a non-stable body is used as the suspended load, one must consider the comparison between experimental and analytical results as not completely satisfactory.

In general, however, it appears that the method is a workable one. It must also be remembered that the analytical approach yields average rather than peak opening-shock values, and that two basic assumptions were made in developing the analytical approach, the validity of which may not be borne out by results of continuing research: (1) that the drag area of the inflating canopy increases linearly with time, and (2) that the inflow velocity of the air at the canopy mouth opening decreases linearly with time. It is anticipated that further research efforts in these areas will refine the analytical approach, leading to a more exact agreement of results. Until these results are available, the present method is suggested as a working concept; its results should be checked with experimental evidence whenever possible.

5.1.2 CANOPIES WITH INHERENT GEOMETRIC POROSITY. A strictly analytical approach to the calculation of filling times and maximum opening forces experienced in the operation of canopies with inherent geometric porosity, such as ribbon and ring-slot canopies, has not as yet been developed. Therefore, empirical values have been compiled and analyzed to determine the filling time, which can be considered acceptable for purposes of canopy design and performance prediction.

5.1.2.1 Filling Time. Measured filling-time values for canopies with inherent geometric porosity

operating at altitudes between sea level and 80,000 ft have been compiled (Ref (4-39)), resulting in the curves shown in Fig. 4-49. This graph represents the ratio of the filling time to diameter ratio (t_f/D_o) as a function of the instantaneous velocity, v_s , at the beginning of canopy inflation. Three curves have been plotted: a so-called "design" curve, a "performance" curve, and a "mean" curve, which represents the expression $t_f/D_o = 0.65 \lambda_g/v_s$. In this expression, λ_g is the geometric porosity for the canopy. The "design" and "performance" curves shown establish an operational band which illustrates possible variations from the "mean" empirical curve.

The inverse variation with velocity expressed by the curves is consistent with the simplest theoretical calculation of filling time as a function of velocity. Such considerations further indicate that the filling time of a canopy would be essentially independent of air density as long as the orifice coefficient of the material is independent of Reynolds number. As was shown in Section 3, such a dependency exists in the case of solid cloth materials; however, in the case of ribbon grids it appears that this dependency is relatively small. It can be reasoned that as the air density decreases, i.e., as the altitude of canopy operation increases, the filling time eventually must increase, since under such conditions the inertia of the canopy in extending from a folded condition to full inflation would become significant. The correlation of data, neglecting entirely any density variation, appears satisfactory when the inherent variability of filling is considered. It must be concluded that the effect of density ratio on filling time for canopies with geometric porosity is small. Data obtained during testing at higher altitudes indicate some correlation with the fifth root of the density ratio.

Until additional and more accurate data are obtained on canopy filling-time, the relationship shown in Fig. 4-49 represents a satisfactory approach. To anticipate possible variations from the "mean" curve due to variations in parachute pack-configuration, packing techniques, and inflation, which are difficult to control, design loads should be based on shorter inflation times and performance estimates should be based on the larger values.

5.1.2.2 Opening-Shock. The force experienced by the canopy can be found by the same method as presented in 5.1.1.2 above, once the filling time of the canopy has been determined.

5.2 Opening-Shock of Canopies Under Infinite-Mass Conditions. The analysis of the dynamics of parachute canopy opening for operations under infinite-mass conditions — that is, under conditions where the canopy drag-loading under sea-level terminal-velocity conditions is larger than 30 psf—is not

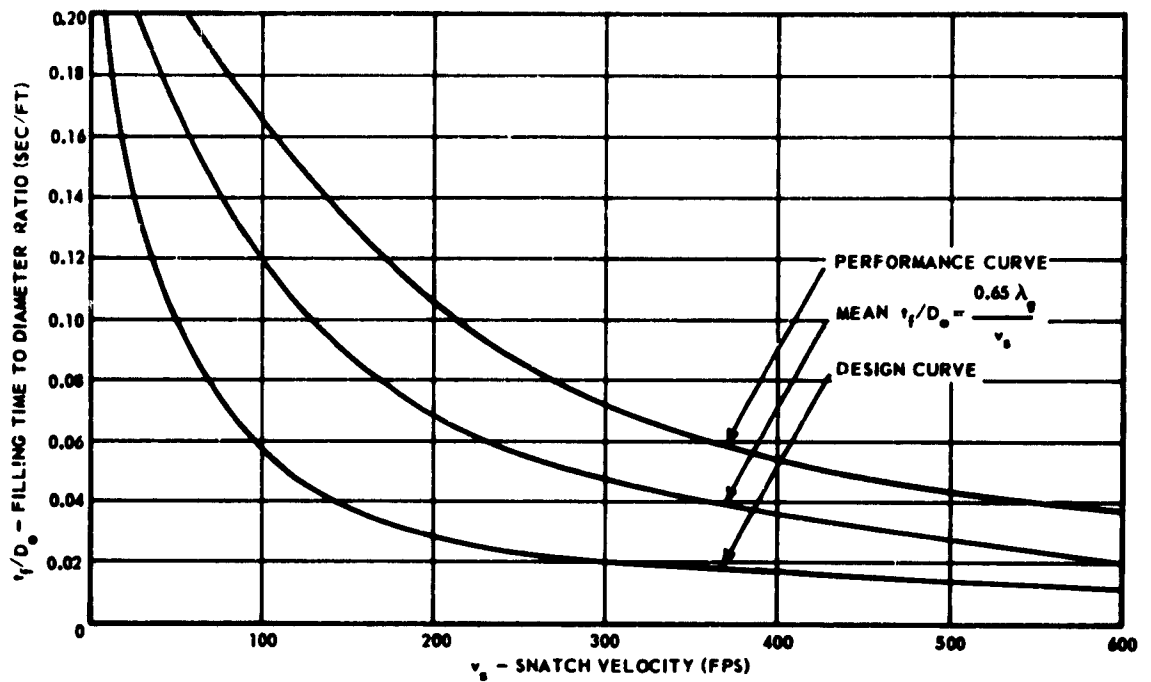


Fig. 4-49 Variation of Ratio of Filling Time to Diameter with Snatch Velocity

as complicated as for the finite-mass condition, since the velocity during the period of canopy opening does not change significantly.

5.2.1 FILLING TIME. In order to determine the filling time of canopies operating under infinite-mass conditions, the distinction between the two canopy types, canopies constructed of solid cloth material and canopies with inherent geometric porosity, must again be made.

5.2.1.1 Solid Cloth Canopies. To determine the filling time of solid cloth canopies, the basic working equation

$$(4-120) \frac{dV}{dT} = \frac{D_o^2}{\pi} t_f v \left[(1-T) T^{4/3} - 2CT(1-T) \right]$$

can be directly integrated with v constant and equal to v_s , the velocity at the beginning of inflation. Putting the above equation in integral form,

$$(4-121) \frac{t_f D_o^2 v_s}{\pi} \int_0^1 \left[T^{4/3} (1-T) - 2CT(1-T) \right] dT = \int_0^{V_{\max}} dV$$

Performing the integration and substituting

$$(4-122) V_{\max} = \frac{2D_o^3}{3\pi}$$

the final expression for the filling time is obtained as

$$(4-123) t_f = \frac{2D_o}{3\pi v_s \left(\frac{9}{70} - \frac{C}{3} \right)}$$

Knowing the nominal canopy diameter, D_o , the effective porosity value, C , and the velocity at beginning of canopy inflation, v_s , the filling time, t_f can be calculated directly.

5.2.1.2 CANOPIES WITH INHERENT GEOMETRIC POROSITY. Empirical values are used to determine the filling time of canopies with geometric porosity. Working curves are presented in Fig. 4-50 which yield satisfactory values for the filling time of parachute canopies with inherent geometric porosity under infinite mass operating conditions.

5.2.2 OPENING-SHOCK. The maximum force experienced by the canopy can be obtained from the filling time by the same method presented in 5.1.1.2 above. However, if only the opening shock is required knowledge, the calculation of the maximum force of canopies for the infinite-mass case can be very much simplified if based upon experimental values.

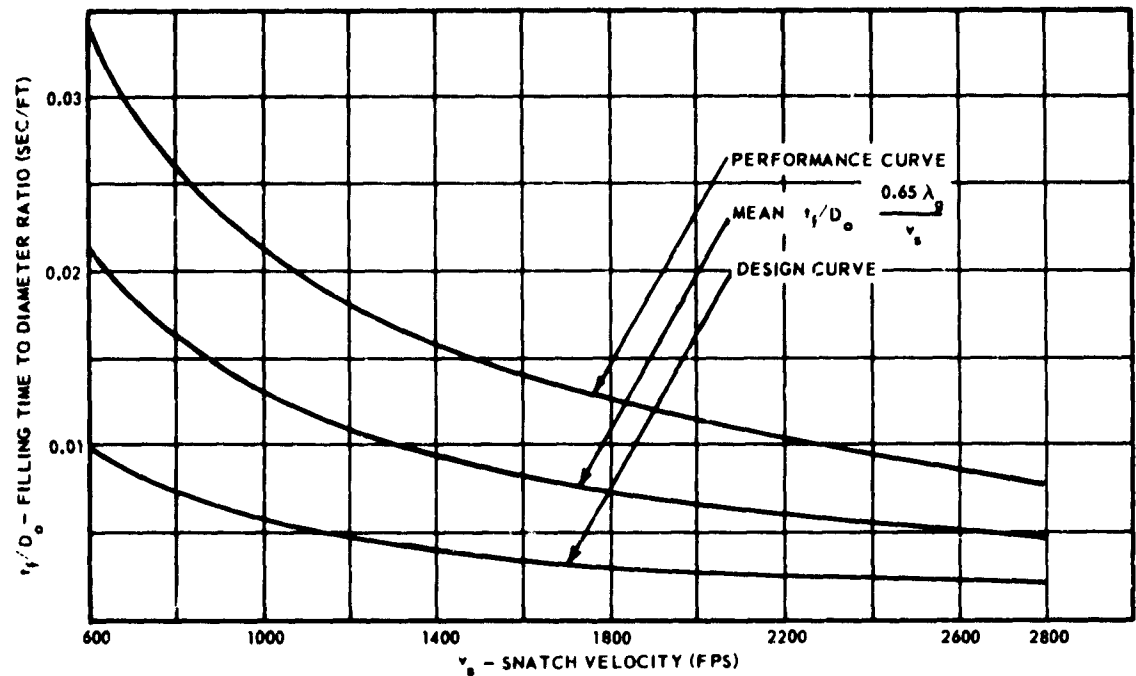


Fig. 4-50 Variation of Ratio of Filling Time to Diameter with Snatch Velocity

If F_o is used to denote the maximum opening force, and F_c the drag force obtained at constant velocity with a fully inflated canopy, expressed as

$$(4-124) \quad F_c = (C_D S)_{o,p} q_s$$

and if X is an amplification factor denoting the relationship between maximum opening force, F_o , and the constant drag force, F_c , expressed as

$$(4-125) \quad X = \frac{F_o}{F_c}$$

then the maximum opening shock or opening force is

$$(4-126) \quad F_o = (C_D S)_{o,p} q_s X$$

where X is a dimensionless factor, the value of which has been established experimentally for various types of canopies.

X -factors have been determined from subsonic tests with practically infinite load and no appreciable velocity decrease during the period of canopy opening (wind-tunnel tests, aircraft deceleration, and drop tests under conditions of very high ratios of weight to drag area). For infinite-mass conditions, the X -factor is a constant for a specific canopy type and has been found not to change with altitude of operation. For higher transonic and supersonic canopy deployment some downward variation in X -factor may be expected, due to Mach-number effects upon canopy operation.

Typical X -factor values for specific canopy types are:

- | | |
|---|--|
| (a) Solid cloth, flat circular: | $X \geq 2.0$ |
| (b) Solid cloth, extended-skirt: | $X \geq 1.8$ |
| (c) Solid cloth, guide-surface (ribbed): | $X \geq 1.1$ |
| (d) Solid cloth, guide-surface (ribless): | $X \geq 1.4$ |
| (e) Solid cloth, personnel guide-surface: | $X \geq 1.2$ |
| (f) Ribbon: | $X \geq 1.1$ |
| (g) Ringslot: | $X \geq 1.05$ |
| (h) Shaped gore and conical: | X somewhat lower than for comparable canopy designs. |

SEC. 6 AERODYNAMIC DRAG

6.1 Introduction. When a body moves along a straight line at a uniform velocity through a fluid at rest, a force is exerted on it in a direction opposite to that of the motion of the body. This force is called "resistance" or "drag" of the body.

The drag, then, is an aerodynamic force which is defined by the equation

$$(4-127) \quad D = (1/2) \rho v^2 C_D S$$

where ρ = Density of the fluid;

v = Velocity of the moving body;

S = Reference area of the body; and

C_D = Drag coefficient of the body based on reference area.

Eq 4-127 is used in calculating the total aerodynamic-drag force generated by canopies operating in the subsonic, transonic, and supersonic speed regimes. At some speeds and above the impact pressure at the stagnation point of a body the value of $(1/2) \rho v^2$ is greater, due to compressibility of the fluid. However, fluid-dynamic coefficients (in this use, drag coefficient C_D) are still based on free-stream dynamic pressure which here represents the momentum of the fluid flow (Ref (4-29)).

For canopies, except for the ribbed and ribless guide-surface canopies, the reference area is the nominal canopy area, S_o , which is the equivalent of the total area of the surface that produces drag including the vent area ($s_o < 0.01 S_o$) and the area not covered by ribbons or cloth in canopies with geometric porosity. The canopy diameter corresponding to this reference area is the nominal diameter, D_o . For ribbed and ribless guide-surface canopies, the reference area is the projected canopy area, S_p . The canopy diameter associated with the projected canopy area is the projected diameter, D_p . For these canopies, the projected diameter is equivalent to the constructed canopy diameter, D_c . The canopy drag coefficient, C_{D_o} , is related to the reference area, S_o , whereas with the reference area, S_p , the drag coefficient, C_{D_p} , is used.

6.2 Aerodynamic Drag of Canopies. For any solid body moving steadily through a fluid, drag is generated by changing the momentum of the fluid through which the body passes. In parachute canopies, however, the generation of aerodynamic drag differs from that generated by these solid bodies in two respects. First, the drag-producing surface is porous and permeable to the air streaming against it, since the drag-producing surface is usually made of cloth or

fabric with considerable air permeability or is constructed out of spaced ribbon-grids. Second, the airflow pattern around conventionally shaped canopies is usually not stable, and canopy descent is accordingly oscillating, gliding, spiral, or any combination of these. For these reasons, valid theoretical approaches for the calculation of the drag of textile canopies have as yet not been established, although a number of approaches have been advanced (Ref (4-41) through (4-43)). Therefore, drag coefficients for various canopy types have been experimentally derived, either during captive tests (wind tunnel or rocket sled) or free-flight tests (free drop or missile).

6.2.1 TANGENTIAL-FORCE COEFFICIENTS OF CANOPIES. The tangent force, T , is the force acting along the centerline or axis of symmetry of a canopy. It also represents the aerodynamic drag generated by a canopy at an angle of attack $\alpha = 0$. The tangential-force coefficients, C_T , presented in Fig. 4-51 through 4-59 are calculated from test data obtained on model canopies in a wind tunnel (Ref (4-27)) employing the conventional aerodynamic relationship, where

$$(4-128) \quad C_{T_{o,p}} = \frac{T}{q S_{o,p}}$$

where T = Tangential force;

q = Dynamic pressure; and

$S_{o,p}$ = Reference area of the canopy.

The drag coefficient, $C_{D_{o,p}}$, is represented by the tangential-force coefficient, $C_{T_{o,p}}$, at an angle of attack $\alpha = 0$. The tangential-force coefficient of a particular canopy is generally somewhat larger when determined in a wind tunnel than that determined by full-size drop test. This discrepancy between wind-tunnel and full-size drop-test results may arise partially from the fact that during wind-tunnel tests all conditions are known, and the canopy models may also be partially or fully restrained, whereas in free drop-test, uncontrolled conditions may exist. For practical applications, average drag-coefficient values listed in Chapter 3 should be utilized for design calculations.

6.2.2 EFFECTS OF CLOTH PERMEABILITY. Test results obtained on model canopies (Ref (4-27)) indicate a variation of the stable angle of attack, and therefore the tangential force coefficient, with the permeability or effective porosity of the drag-producing surface. This is true for all canopy types, although changes in the effective porosity of ribbon and ring-slot canopies have a much smaller effect than the changes for solid cloth canopies, at least in the region of incompressible flow.

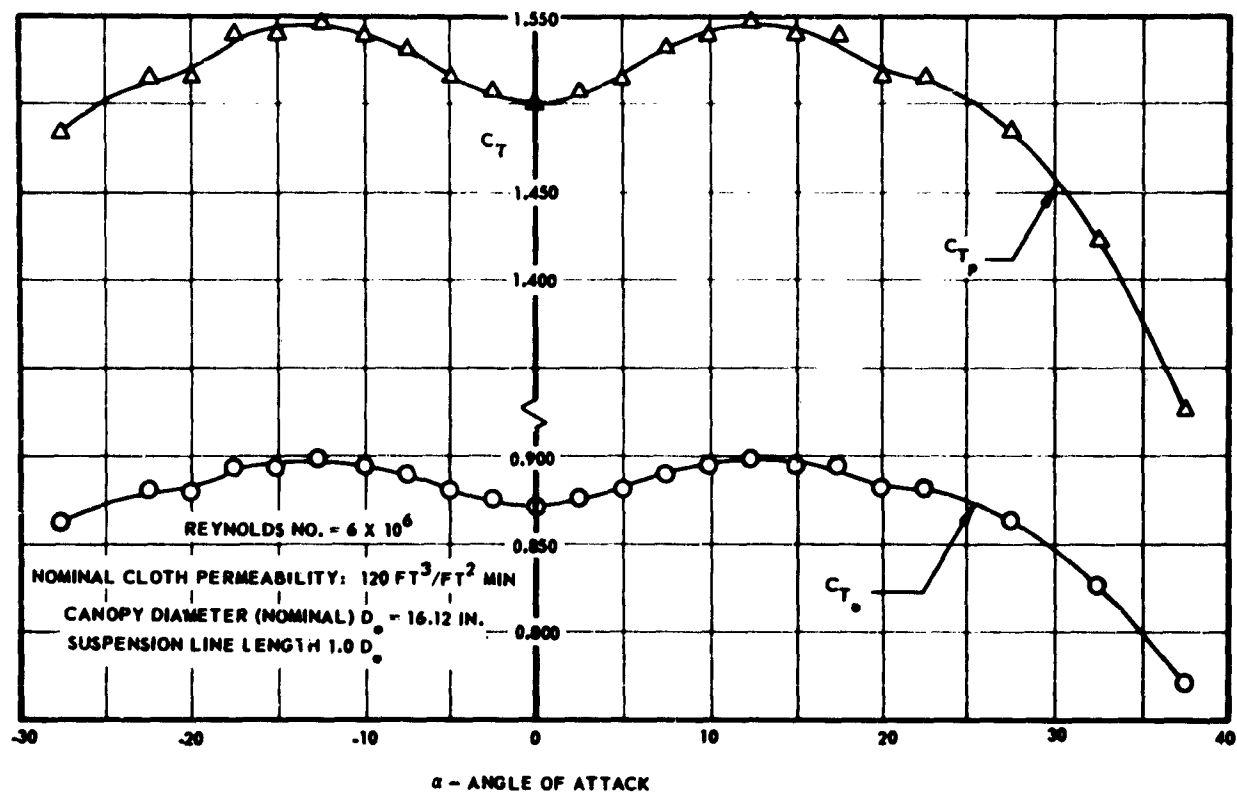


Fig. 4-51 Tangent Force Coefficient vs Angle of Attack for Circular Flat Cloth Type Canopy

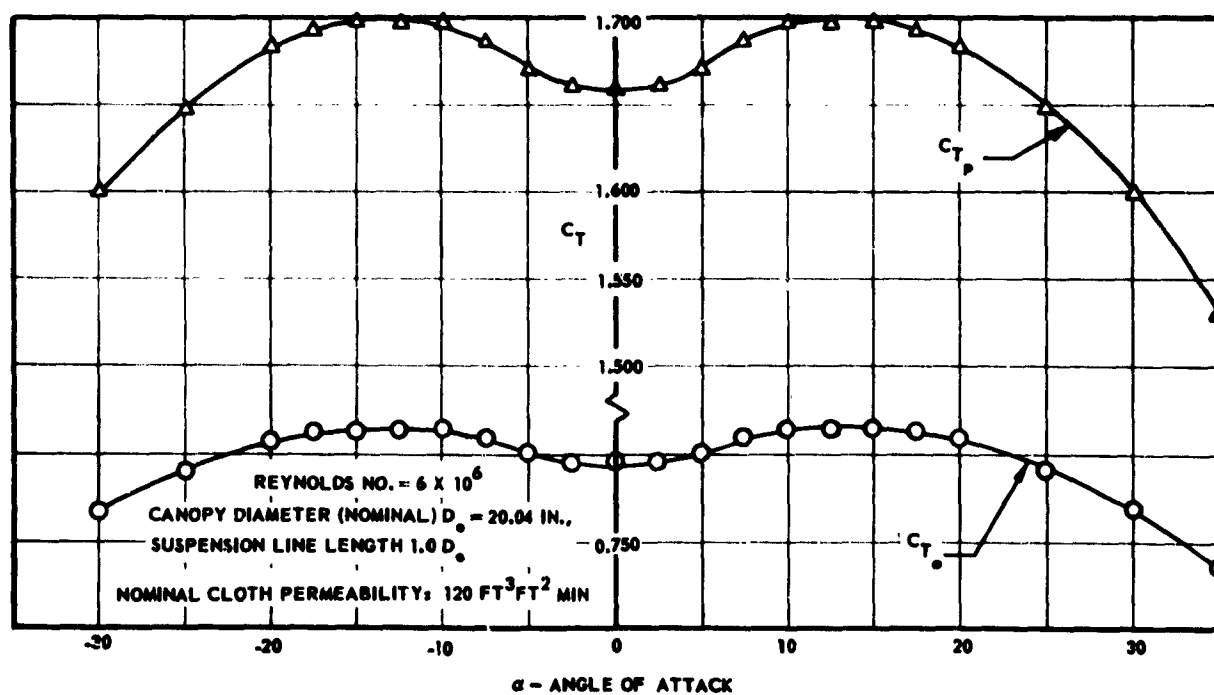


Fig. 4-52 Tangent Force Coefficient vs Angle of Attack for 10% Flat Extended Skirt Cloth Type Canopy

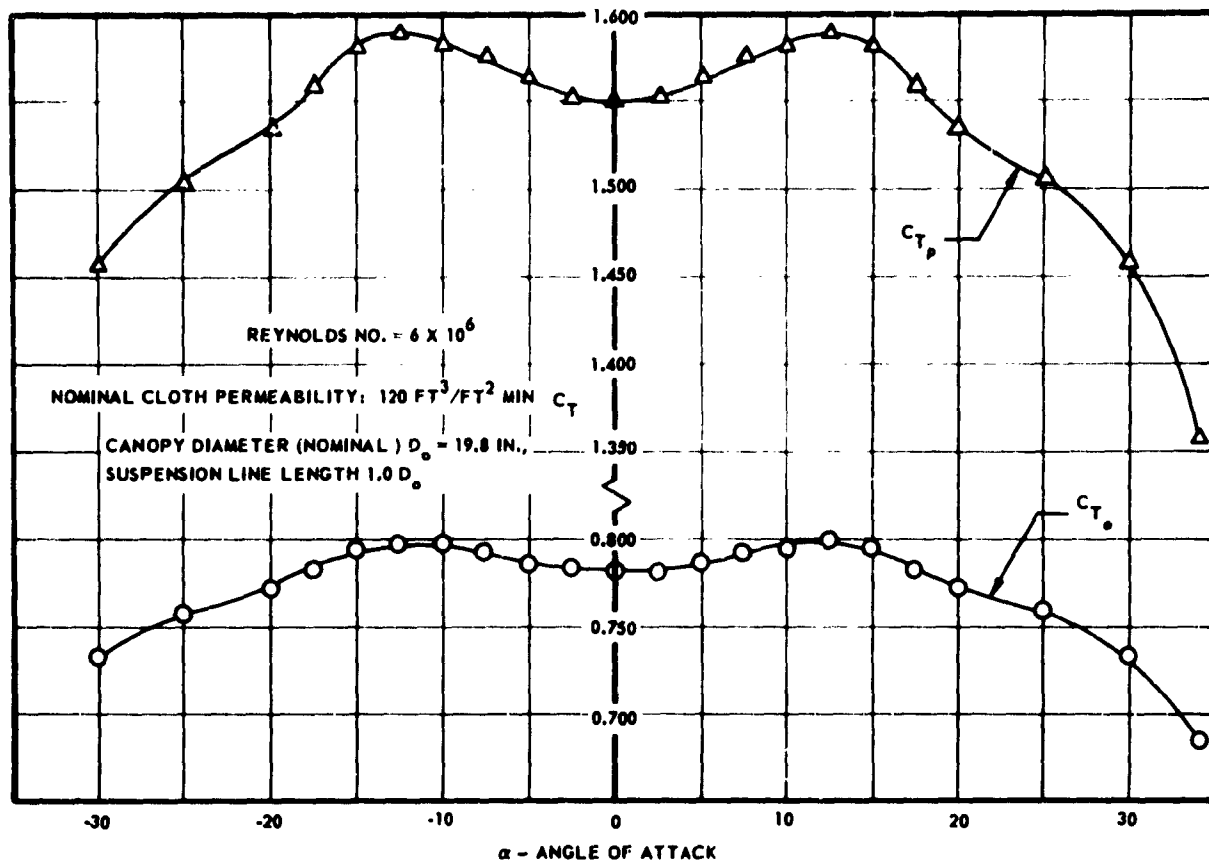


Fig. 4-53 Tangent Force Coefficient vs Angle of Attack for 14.3% Full Extended Skirt Cloth Type Canopy

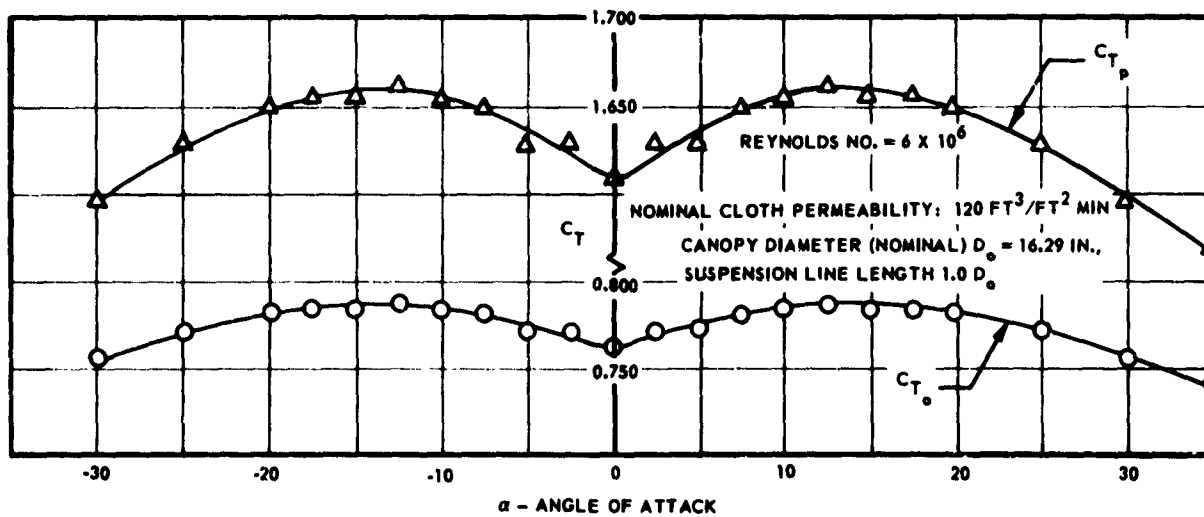


Fig. 4-54 Tangent Force Coefficient vs Angle of Attack for Conical Cloth Type Canopy

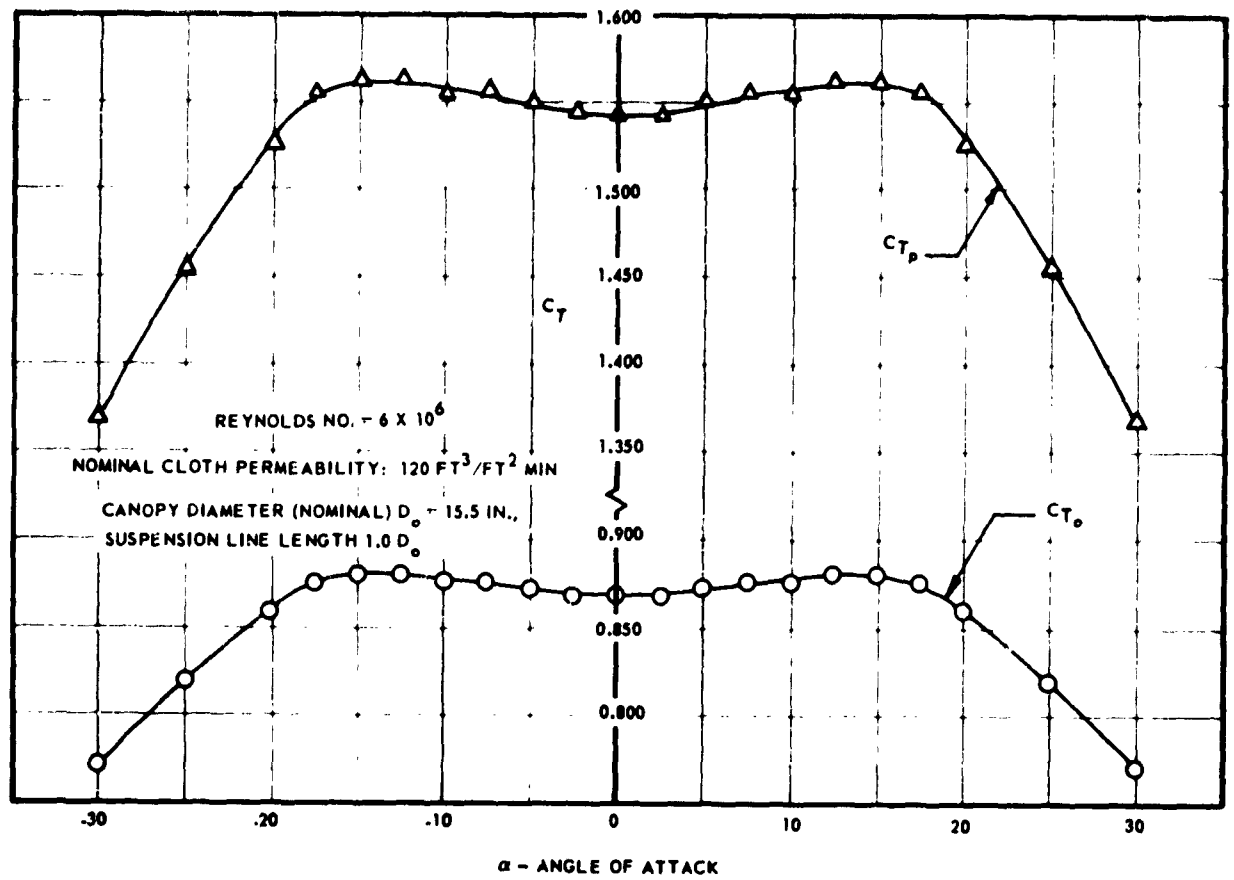


Fig. 4-55 Tangent Force Coefficient vs Angle of Attack for Personnel Guide-Surface Cloth Type Canopy

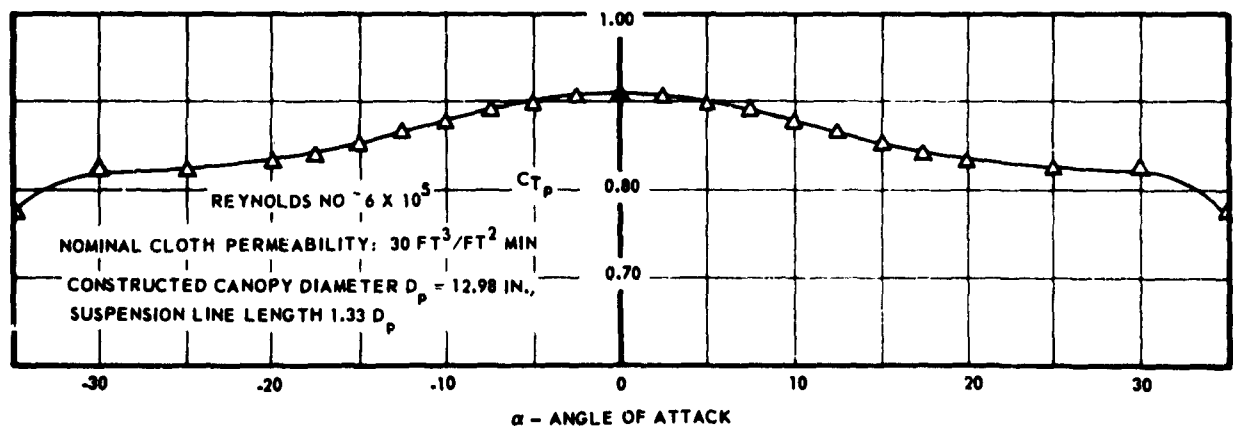


Fig. 4-56 Tangent Force Coefficient vs Angle of Attack for Ribbed Guide-Surface Cloth Type Canopy

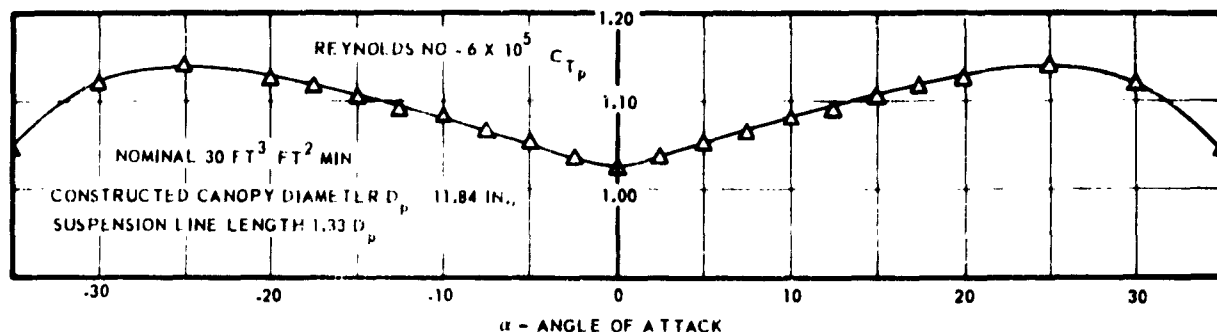


Fig. 4-57 Tangent Force Coefficient vs Angle of Attack for Fibless Guide-Surface Cloth Type Canopy

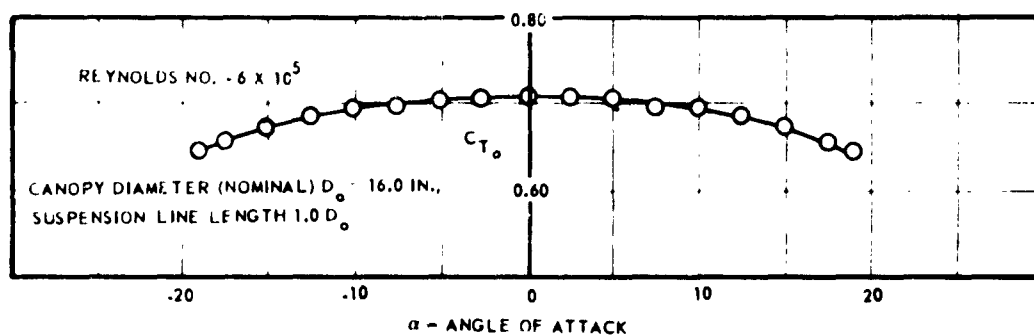


Fig. 4-58 Tangent Force Coefficient vs Angle of Attack, Ping Slot Type Canopy of 20% Geometric Porosity

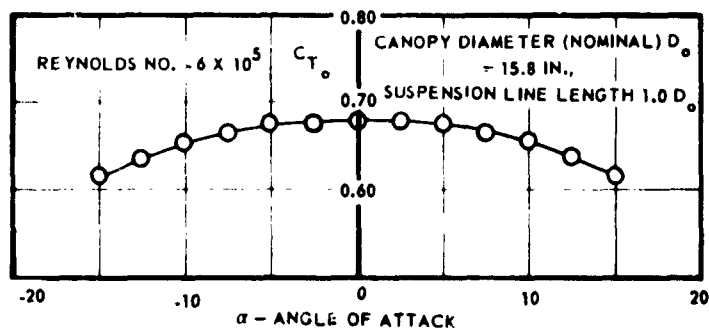


Fig. 4-59 Tangent Force Coefficient vs Angle of Attack, Ribbon Parachute of 20% Geometric Porosity

Fig. 4-60a, b and c present the tangent-force coefficients, C_T , for three types of solid cloth canopies: the flat circular, the personnel guide-surface, and the 10 per cent extended-skirt types. Models fabricated of cloth with cloth permeability values ranging between 0 and 275 cu ft per sq ft min were tested. An increase in cloth permeability or effective porosity is asso-

ciated with a general decrease of the tangential-force coefficient at the stable angle of attack, as is evident from Fig. 4-61. If the effective porosity of the cloth of the drag-producing surface for all three types of canopies is high enough to cause static stability at zero angle of attack, the tangent-force coefficient of the three quite different types of canopies assumes ap-

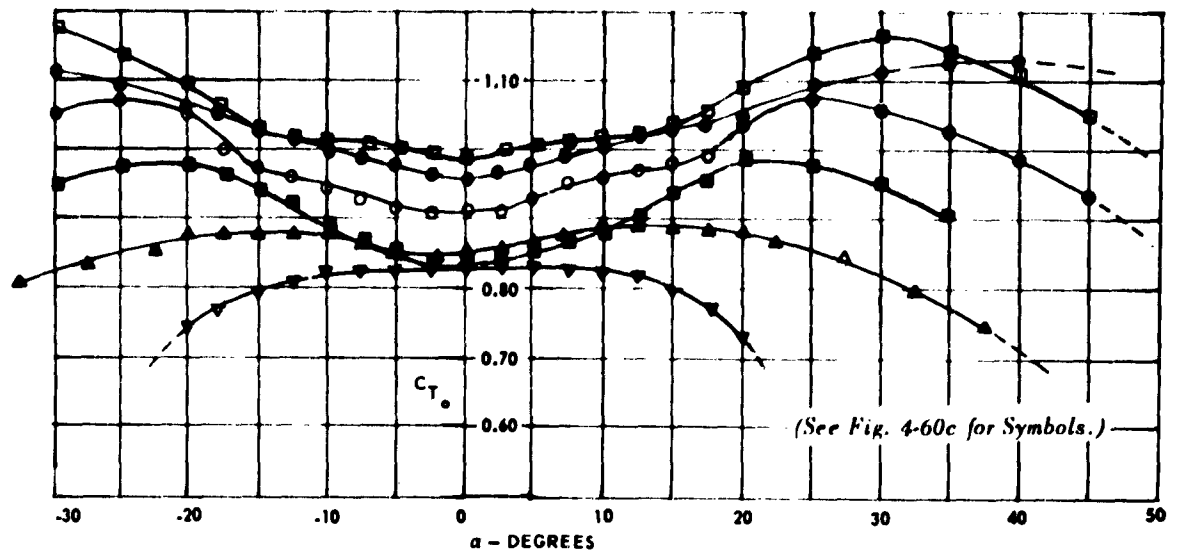


Fig. 4-60a Tangent Force Coefficient vs Angle of Attack of Various Canopies - Circular Flat

proximately the same value.

Fig. 4-62 shows the change in drag coefficient, $C_{D_{o,p}} - C_{T_o} = 0$, with effective porosity of the drag-producing surface. In the case of the flat circular, personnel guide-surface, and 10 per cent extended-skirt canopies, a general trend of decreasing drag-coefficient with increasing effective-porosity is evident. In contrast, the drag-coefficient values for the ribless guide-surface canopy, also plotted in Fig. 4-62, show a pronounced increase with increasing effective-

porosity. It can be assumed that the increasing trend in drag coefficient for this type of canopy is caused by the considerable change in inflated canopy shape that is caused by permeabilities of the cloth used in construction.

6.3 The Descending Canopy. As pointed out above, the flow pattern around conventionally shaped parachute canopies is usually unstable and the descent of the canopy is accordingly oscillating, gliding, spiral, or any combination of these. These descent

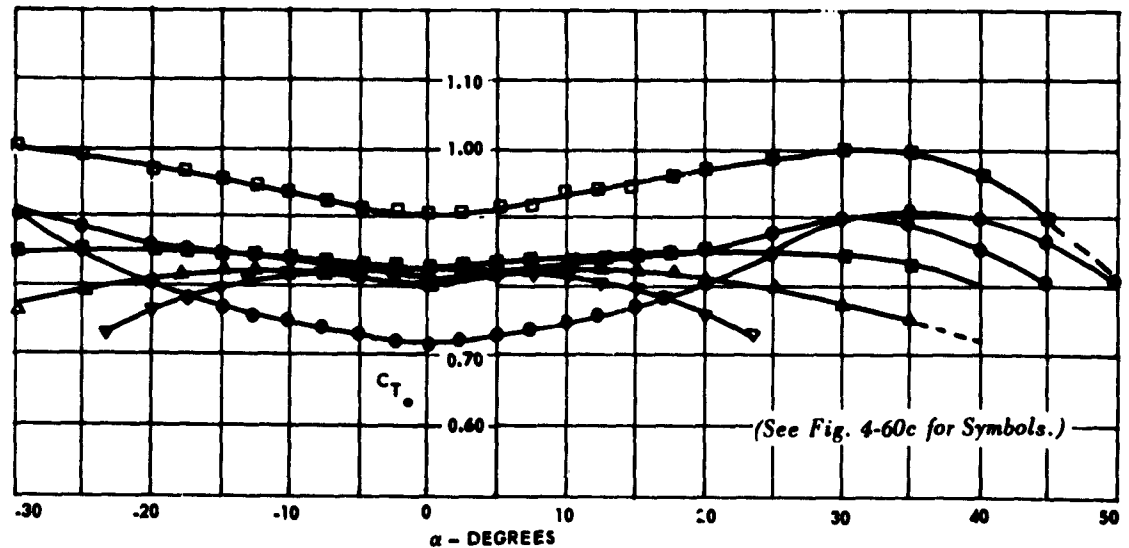


Fig. 4-60b Tangent Force Coefficient vs Angle of Attack of Various Canopies - 10% Extended Skirt

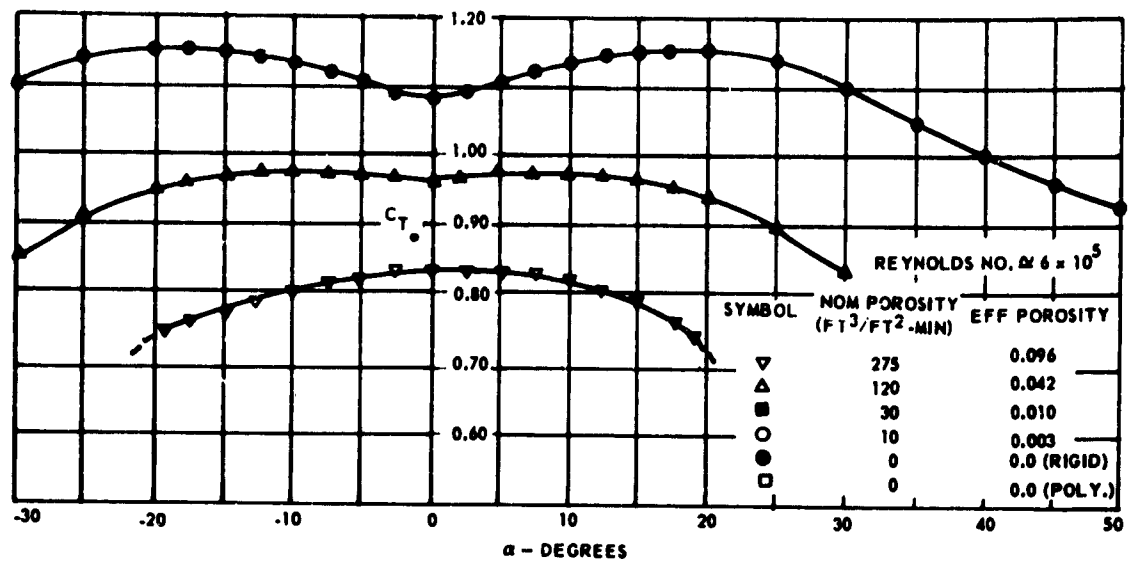


Fig. 4-60c Tangent Force Coefficient vs Angle of Attack of Various Canopies - Personnel Guide-Surface

motions are usually reflected in the value of the canopy drag-coefficient (Ref (4-44)).

In free descent, the longitudinal axis of a canopy assumes an angle to the tangent of the trajectory. This angle is the angle of attack at which the suspended load and the aerodynamic forces on the canopy are in equilibrium. In steady descent, the resultant of the lift and drag forces is in the same line with the force vector of the suspended load (Ref (4-26)). Considering this equilibrium condition (Fig. 4-63), the

total velocity of the system depends upon the coefficients of lift and drag which are functions of the angle of attack related to the stable position of the canopy. Similarly, the effective drag coefficient, $C_{D_o}(\text{eff})$, is a function of the angle of attack.

Wide variations in effective drag have been measured on textile canopies, in particular on solid cloth canopies of flat circular, extended skirt, and other conventional designs. These canopies are statically unstable about zero-degree angle of attack. Fig. 4-64

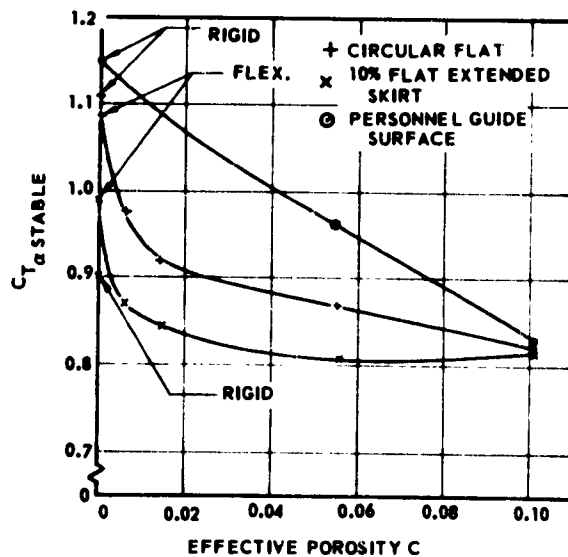


Fig. 4-61 Tangent Force Coefficient at Stable Angle of Attack as a Function of Effective Porosity for Several Canopy Types

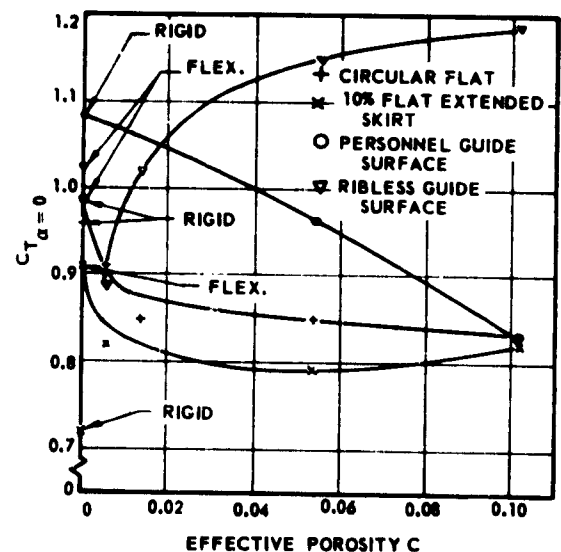


Fig. 4-62 Drag Coefficient at Zero Angle of Attack as a Function of Effective Porosity for Several Canopy Types

$$F = W$$

$$F = \sqrt{L^2 + D^2}$$

$$F = (p/2)v^2 \sqrt{C_L^2 + C_D^2}$$

$$(1)v^2 = \frac{W}{(p/2)v^2 \sqrt{C_L^2 + C_D^2}}$$

$$C_L = f_1(\alpha)$$

$$C_D = f_2(\alpha)$$

$$V_y = v \cos \alpha$$

CONSEQUENTLY

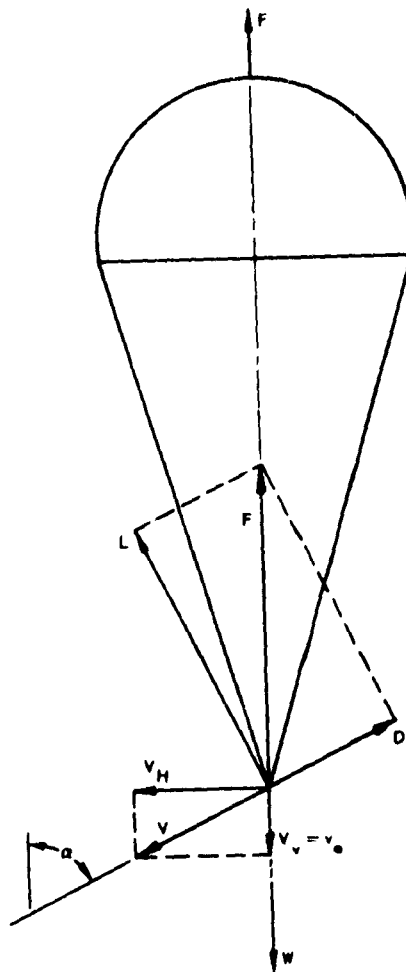
$$(2) V_v^2 = \frac{W}{(\rho/2)S} |f_3(\alpha)| \cos^2 \alpha$$

WHERE

$$I_3(\alpha) = \sqrt{\frac{1}{I_1^2(\alpha) + I_2^2(\alpha)}}$$

$$C_{D_v} = \frac{W}{V_v^2 \frac{\rho}{2} S} = f(\alpha)$$

RATE OF DESCENT AS A FUNCTION OF THE STABLE POSITION



F = W

$$(1) F = T = C_T \frac{\rho}{2} v^2 S$$

FOR STEADY DESCENT UNDER
GLIDE ANGLE α

$$C_H = 0$$

$$C_M = 0$$

RATE OF DESCENT

$$V_y = v_y = v \cos \alpha$$

WITH THE EFFECTIVE DRAG
COEFFICIENT, $C_{D_{o,p}}(eff)$

FOR THE VERTICAL DESCENT

$$(2) W = \frac{\rho}{2} V_v^2 C_{D_{o,p}} S_{o,p}$$

COMBINING (1) AND (2)

$$\frac{\rho}{2V} v^2 C_{D_{o,p(off)}} S_{o,p} = \frac{\rho}{2V} v^2 C_{T_{o,p}} S_{o,p}$$

OR

$$C_{D_{o,p}(eff)} = C_{T_{o,p}} \frac{v^2}{V_v^2} ; \text{ WITH}$$

$$\frac{v}{v} = \frac{1}{\cos \alpha}$$

$$(3) C_{D_{o,p \text{ (eff)}}} = \frac{C_{T_{o,p}}}{\cos^2 \alpha}$$

EFFECTIVE DRAG AS A FUNCTION OF THE TANGENT FORCE AND THE ANGLE OF THE STABLE POSITION

Fig. 4-63 General Equilibrium Conditions

shows the effective drag coefficient, C_{D_0} (eff), versus rate of descent for a flat circular solid cloth (C.9) canopy, with ratio of total weight to cloth area (WT/S_0 is constant) as parameter.

The variation in effective drag-coefficient could be explained if this canopy had several stable positions or if the drag and lift coefficients of this canopy varied for the same angle of attack. However, the results of wind-tunnel tests show that conventional canopies have only one statically stable position (Sec. 11).

The angle of attack at which a particular canopy is statically stable varies between 0 deg and 45 deg and depends upon type and the air permeability or effective porosity of the drag-producing surface. Therefore, the wide variation in the effective drag of canopies cannot be explained through static stability alone; the unsteady motions of a canopy in free descent must be considered also.

6.3.1 THE GLIDING PARACHUTE CANOPY. For a steady glide of a canopy, the effective drag is mere-

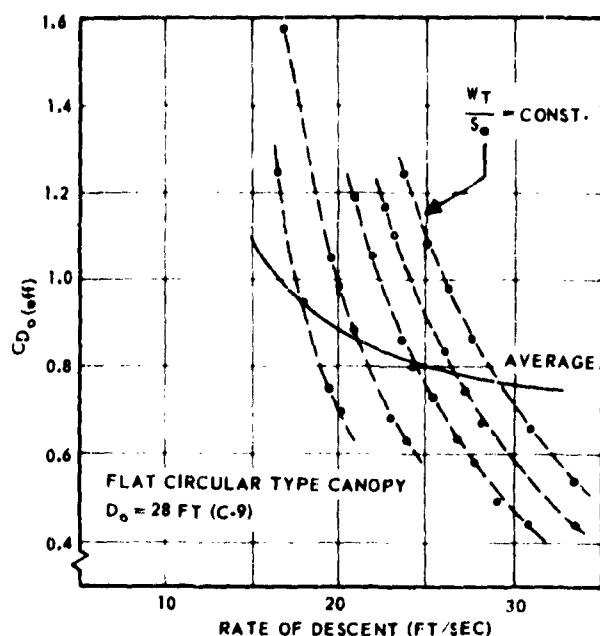


Fig. 4-64 Variation of the Coefficient of Effective Drag, $C_{D_0}(\text{eff})$, as a Function of Rate of Descent

ly a function of the tangent force, T , and the angle of the stable position, α_{stable} (Fig. 4-63). The free-moving canopy assumes this angle of attack either in a steady glide, in a motion along a helix called a "coning" or spiral motion, or in a motion resulting from combining these two. Of these three types of motion, only the steady glide is a motion with a steady aerodynamic-flow pattern. Associated with the other two motions are fields of high and low pressure which revolve on the drag-producing surface with the rhythm of the rotational motion.

The gliding canopy can be compared with a canopy model in a captive-test experiment (wind tunnel) with an adjusted angle of attack. An evaluation of the curves of the moment coefficient versus angle of attack presented in Sec. 11 and of the curves of the tangent-force coefficient versus angle of attack in this section shows that the flat circular canopy with a nominal cloth permeability of 120 cu ft per sq ft per min is stable at an angle of attack $\alpha = 20$ deg, with a tangent-force coefficient, $C_{T_0}(\alpha = 20 \text{ deg}) = 0.87$, and normal and moment coefficients, $C_N = C_M = 0$. According to these experimentally determined values, this particular type of canopy would glide under an angle of attack $\alpha = 20$ deg, and the canopy would descend with an effective-drag coefficient, $C_{D_0}(\text{eff}) = C_{T_0} / \cos^2 \alpha \approx 0.985$.

Effective-drag coefficients as high as 1.15 have

been recorded during jumps with modified canopies to obtain an extended glide. Considering that these canopies incorporated slots or open gores to increase the glide range, these experimental values show good agreement. From this comparison, it can be concluded that the high values of effective-drag coefficient in Fig. 4-64 are related to gliding canopies.

6.3.2 THE OSCILLATING PARACHUTE CANOPY.

In general, an oscillating or coning canopy adjusts itself to the same angle of attack as the gliding canopy; however, the zones of separation and attachment of the airflow on the drag-producing surface are not necessarily the same, because of the transverse motion of the canopy with respect to the airflow. Therefore, a variation of the aerodynamic coefficients, depending on the gliding or oscillating motion of the canopy, is the logical consequence. Experimental test results substantiate this conclusion and prove that oscillating or coning canopies have a lower effective drag coefficient, or effective drag, than the same canopy under gliding conditions.

In theory, the conditions under which a particular canopy will glide or oscillate are governed primarily by its dynamic stability characteristics. In actual practice, however, it is well known that the same canopy may glide under conditions of low canopy-loading ($W/(C_D S)_{0,p}$) and will usually descend with an oscillating or coning motion under conditions of high canopy-loading. The area of transition from a gliding to an oscillating descent, or vice versa, varies for different canopy types, and depends upon the static stability characteristics of the particular canopy. For example, the statically unstable flat circular cloth canopy changes its stability behavior markedly within a relatively small range of canopy-loading values. On the other hand, the statically stable guide-surface and ribbon canopies descend practically vertically, independent of canopy loading. This phenomenon is understandable since one of the requirements for dynamic parachute stability is stability under static conditions.

Because of this difference in stability behavior, statically unstable canopies change their effective drag over a considerable range, whereas statically stable canopies have an effective drag that is practically constant. To a certain extent, the type of motion during descent also depends upon the size of the canopy. This change in motion is related to a stronger damping because of the larger mass of air included by the drag-producing surface of larger canopies.

6.3.3 THE RATE OF DESCENT. The majority of conventional canopy types in use today are statically unstable. Therefore, it has become customary to state the coefficient of effective drag (based on the

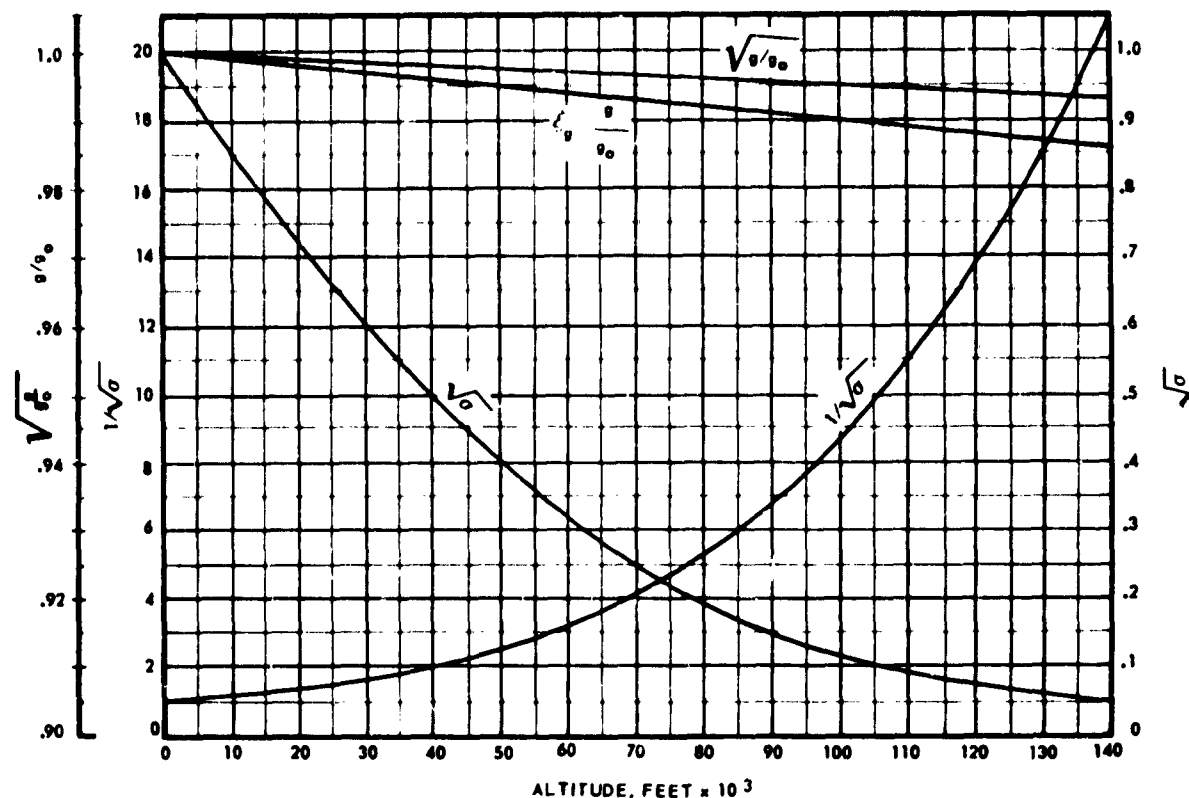


Fig. 4-65 Density and Gravity Ratios as a Function of Altitude (Ref: AFCRC-TR-59-267)

appropriate reference area) as a function of the rate of descent (also called equilibrium velocity at sea level) v_{e0} . The rate of descent, or equilibrium velocity, is merely another way of expressing canopy loading.

For sea-level conditions:

$$(4-129) \quad v_{e0} = \frac{2 \sqrt{\frac{2}{\pi \rho_0}}}{D_{o,p}} \sqrt{\frac{W_T}{C_{D_{o,p}}}} = \frac{K}{D_{o,p}} \times$$

$$\sqrt{\frac{W_T}{C_{D_{o,p}}}} = \frac{32,724}{D_{o,p}} \sqrt{\frac{W_T}{C_{D_{o,p}}}}$$

For any given altitude the equilibrium velocity of the parachute-load system of total weight, W_T , is a function of air density and gravity and, at high speeds, also a function of Mach number. Thus

$$(4-130) \quad v_e = v_{e0} \sqrt{\frac{\xi_g}{\sigma}}$$

where $\xi_g = g/g_0$ and $\sigma = \rho/\rho_0$

Graphs showing the relationship between $\sqrt{\xi_g}$ and σ and altitude are presented in Fig. 4-65.

Canopy diameter versus total load, i.e., suspended weight plus weight of the parachute system, for various rates of descent and drag coefficient can be obtained from Fig. 2-13. This graph is presented for sea-level conditions. For other altitudes, values obtained should be modified by multiplying by $1/\sqrt{\sigma}$. Values for this ratio can be obtained from Fig. 4-65.

6.4 Effects of Mach Number. In general, the average or nominal drag-coefficient of canopies shows a decreasing trend with an increase in velocity. This decrease is more pronounced at the lower values of rate of descent, between 5 and 20 fps, as illustrated by the data in Chapter 3. The reason for this change may be seen in the inflated shapes of the canopy as affected by canopy loading. Above a rate of descent of approximately 20 fps, and below the transonic-velocity regime, the drag coefficient of canopies remains approximately constant.

At transonic and supersonic velocities, one of the prime prerequisites for selection of suitable type of canopy is that the canopy has to be statically stable, since in most cases its function is also to stabilize

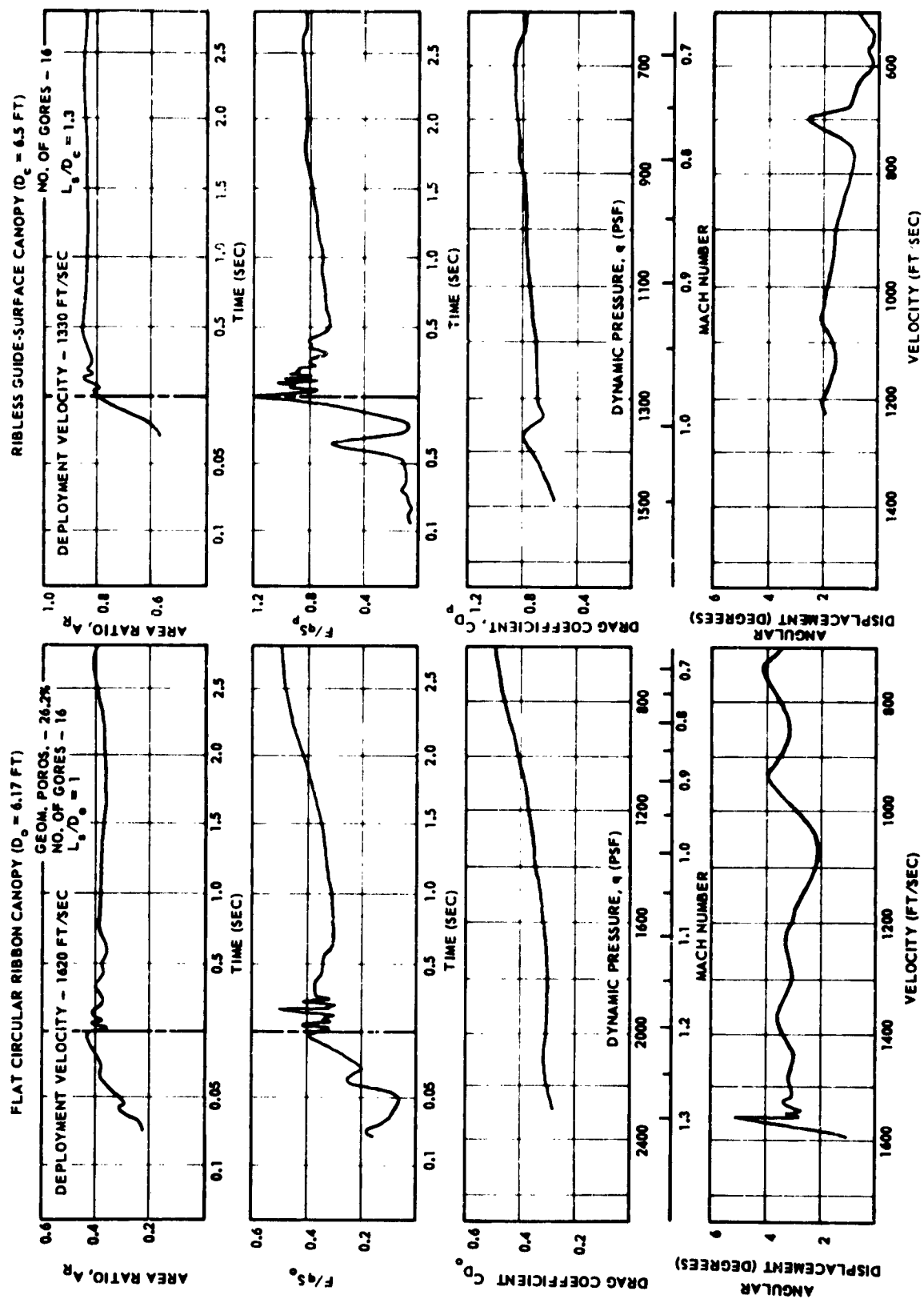


Fig. 4-66 Comparative Performance Characteristics, Captive (Rocket Sled) Tests

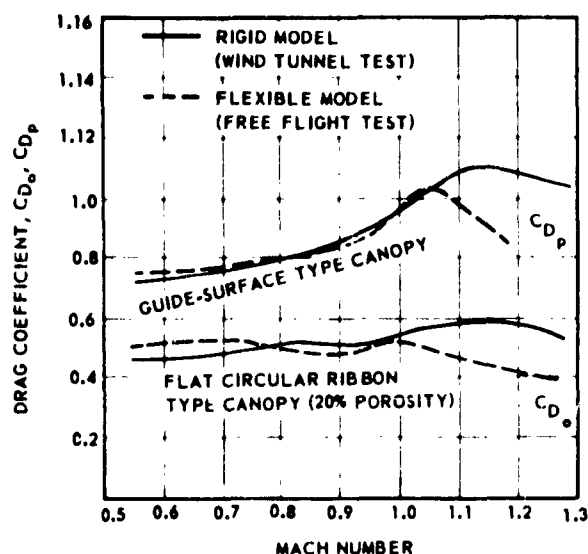


Fig. 4-67 Drag Coefficient vs Mach Number, Rigid and Flexible Type Canopies

the load or vehicle to be decelerated. Therefore, the two types which have been extensively employed in the transonic-velocity regime are both statically stable and have a relatively high drag efficiency: the ribbon and the guide-surface canopies. Comparative performance characteristics for these two types under almost identical transonic-speed deployment and infinite-mass conditions (sled test) are shown in Fig. 4-66. The transonic drag-coefficients for these two types are again plotted in Fig. 4-67. These data compare the change in canopy drag-coefficient for flexible models under free-flight (missile test) conditions (Ref (4-45)) with that for rigid models in captive (wind tunnel) test (Ref (4-46)). As is evident, the value of the drag coefficient decreases rapidly as the Mach number increases, after the characteristic rise at sonic velocity. It is noted in the drag curves for the flat circular ribbon canopy that a dip occurs at a free-stream Mach number of approximately 0.9. This deviation from a smooth drag-rise is attributed to the fact that the flow through the openings in the drag-producing surface becomes choked. So long as the flow through the openings is subsonic, the mass flow through the openings will be a function of both internal and external pressures. When choking takes place, the mass flow through the slots can be considered as a function of internal pressure only. This explains the discontinuity at the choking-pressure ratio.

At higher velocities, both the flat circular and conical ribbon as well as the guide-surface canopies exhibit erratic inflation tendencies, violent pulsing or

"breathing" of the drag-producing surface, considerably reduced drag, and failure of cloth, ribbons, and suspension lines at a fraction of their rated strength due to violent oscillation of the material. In the case of the ribbon canopy, this condition may prevail over a considerably range of geometric porosities. (Ref (4-47) and (4-48)).

Results of tests on flexible-canopy models in the wake of a primary body indicate that there is usually a strong pressure-disturbance standing in front of the mouth of the canopy, but behind the confluence point of the suspension lines. There appears to be no oblique shock associated with the suspension lines originating at the confluence, as is present on rigid models when tested in undisturbed flow. The suspension lines, however, do affect the strong shock ahead of the drag-producing surface by distorting the shock from normal in nature to a combined normal and oblique shock, or a detached, somewhat conical, shock wave.

The results of tests on rigid models of the drag-producing surface reveal much the same tendencies as those of flexible-canopy models, except that there is no distortion of the strong pressure disturbance ahead of the canopy mouth. This disturbance is clearly a normal shock, which moves closer to the canopy skirt with increasing canopy porosity. Adding suspension lines to the rigid model, converging into a cone at the confluence point, produces a distinct oblique shock emanating from the apex of this cone. These models usually experience unsteady flow similar to the "inlet buzz" phenomena of spiked inlets.

The flow picture observed on rigid models in supersonic undisturbed flow, however, cannot explain the inflation and operating instabilities of flexible canopies, since flexible canopies must be towed and the flow field surrounding the canopy is strongly influenced by the wake of the primary body. Naturally, tests on flexible-canopy models would be ideal to establish a flow picture; however, the distortion of the normal shock makes these tests extremely difficult.

Studies of the happenings inside a drag-producing surface under supersonic undisturbed-flow conditions have shed some light upon "breathing" or fluctuation phenomena observed on flexible textile canopies in supersonic flow (Ref (4-46)).

In general, the textile canopy is a device which produces aerodynamic drag by changing the momentum of the air through which it passes. In subsonic operation, the drag-producing surface captures a large amount of air which is accelerated to the terminal or descent velocity of the canopy. This system, consisting of the canopy and the "dead air", passes rather smoothly through the free-stream air. The pressure of the captured air is essentially constant within the

drag-producing surface, and no significant spillage of air or violent motion of air within the drag-producing surface results. These conditions, however, change rapidly as sonic free-stream velocity is exceeded. A canopy operating at supersonic velocities does not exhibit the characteristic collecting of "dead air" within the drag-producing surface results; rather, the canopy keeps rejecting the captured and recapturing more air because of the tremendous energy caused by supersonic flow. The filling of the canopy is associated with the development of a pressure area inside the drag-producing surface, which at the beginning is evenly distributed. This pressure area forms a fairly even high plateau which has an abrupt change across or slightly forward of the skirt of the canopy towards free stream. This normal-pressure ridge in front of the skirt of the canopy recedes with time and as a consequence, a small high-pressure area is developed at the apex of the canopy. At this time, the pressure in the skirt area is considerably lower than at the apex area, and the skirt area contracts, thereby reducing the inlet diameter and elongating the canopy. Since the pressure near the skirt of the canopy is lower than that of the surrounding flow, a movement of particles toward the drag-producing surface is initiated and is often accompanied by a pronounced pressure area moving into the drag-producing surface. This moving pressure area may be met by the pressure wave which has been reflected from the apex area and now moves forward. In general, these inward and outward moving pressure areas collide, interfere with each other, and form an infinite variety of low- and high-pressure formations inside and in the neighborhood of the drag-producing surface. Due to the inherent flexibility of the canopy, the canopy distorts because of the movement of these pressure regions, and as a result, "breathing" and "pumping" take place.

Some theoretical knowledge as to how to achieve stable flow conditions can be obtained by assuming that the geometric porosity of the drag-producing surface is low enough to give sonic flow ($M = 1.0$) through the openings (which means that the flow is choked), that a detached cone-like or near-normal shock stands in front of the drag-producing surface, that this shock is not distorted by the presence of the suspension lines, and that there is no oblique shock emanating from the confluence point of the suspension lines.

It is evident, then, that the value of the ratio of the area of the canopy mouth to the area of openings in the drag-producing surface controls the velocity of the air at the mouth as long as the flow through the drag-producing surface is choked. The detached cone-like or near-normal shock is the result of the choked flow and its position is dependent upon the ratio of the velocity of the air immediately behind the shock

to that in the mouth opening. If the velocity of the air immediately behind the shock is greater than that at the mouth, the shock will remain detached from the drag-producing surface and the streamlines behind the shock to the mouth will be divergent. This tends to hold the skirt of the drag-producing surface open by creating lift outwardly on the skirt band and lower ribbons. Should the shock wave reach the skirt of the drag-producing surface, there will be no lift on the skirt band or lower ribbons because of the change in local angle of attack. The mouth of the drag-producing surface may then tend to close.

From this it can be seen that the ratio of the area of the mouth to the area of openings in the drag-producing surface is critical. If this ratio falls below a certain value at a given Mach number, the canopy will lose its tendency to inflate or stay open.

Required theoretical values for the geometric porosity of a canopy to achieve stable flow conditions over a range of Mach numbers are shown in Fig. 4-68. This band incorporates required values for a variety of ribbon canopies, and assumes a normal shock in front of a choked canopy.

Since, however, the canopy is flexible, it is possible for the area of mouth to vary. For flat circular ribbon and conical ribbon designs, it is obvious that most of the excess material that may be subject to flutter exists at and adjacent to the skirt of the canopy. This amount of excess material decreases towards the apex area. The free length of the skirt band or the lower ribbons between adjacent suspension lines can now be compared to a flat plate positioned with its flat side normal to the airstream. Because of the instability of these "flat plates", oscillations in the individual ribbons are set up under certain conditions which also

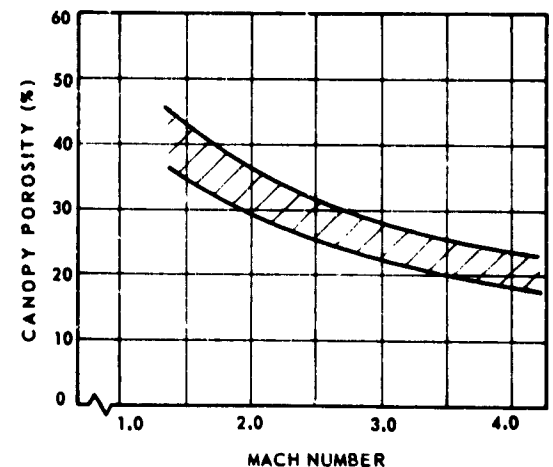


Fig. 4-68 Required Theoretical Canopy Porosity to Achieve Stable Airflow Conditions (Canopy Diameters $D_0 < 6$ ft)

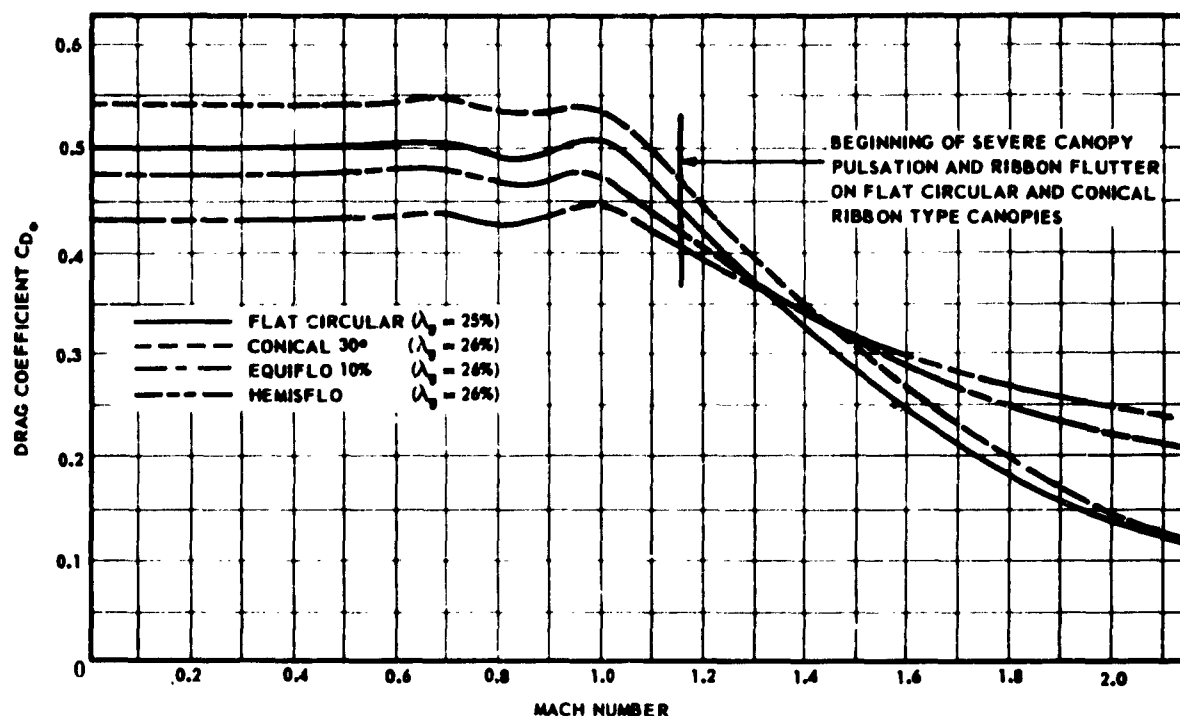


Fig. 4-69 Comparative Drag Coefficients for Various Ribbon Type Canopy Designs

cause a change in the area of the canopy mouth opening, since the ribbons will, besides "blossom out", also "flop in", at random.

These considerations led to the modification of the flat circular ribbon canopy for supersonic-speed operation. By extending the skirt along the suspension lines and extending the suspension lines to $2 D_0$ (partially to achieve optimum drag), the shape of the inflated canopy is altered. In this way, a desirable ratio of inlet area to outlet area can be achieved without sacrificing canopy inflation tendencies due to high geometric porosity, and the free length of the horizontal ribbons in the vicinity of the skirt is shortened substantially, which alleviates the problem of lower ribbon-instability.

Initially, the triangular gore of the flat circular ribbon canopy was taken as the basis and a conical extension (10 per cent of the nominal canopy area) was added. This resulted in the so-called Equiflo ribbon canopy (10 per cent extended skirt). In order to obtain a more effective shape, the gores were later shaped, resulting in the so-called Hemisflo ribbon canopy (210-deg hemispherical). Gore patterns of both of these canopy types are shown in Chapter 3. Curves showing generalized drag coefficient versus Mach number for the flat circular, Equiflo, Hemisflo, and a 30-deg conical ribbon canopy are shown in Fig. 4-69. Since most

of the performance data obtained to date are on the Hemisflo ribbon canopy, these data are available in somewhat more detail (Ref (4-49)).

All data presented were acquired on canopies with diameters (D_0) of 2.18 ft (66.5 cm) and 4.12 ft (122 cm). These canopies were deployed behind a primary body of 9-in. diameter at supersonic velocities, under free-flight conditions, and at altitudes between 50,000 and 80,000 ft. The drag coefficient, C_{D_0} , versus Mach number for this type of canopy is plotted in Fig. 4-70. Here a definite dependency of drag coefficient upon Mach number is evident. The value of C_{D_0} drops sharply after sonic velocity is exceeded. In the region above Mach 1.5, the curve seems to level out. As a comparison, drag-coefficient values obtained during wind-tunnel tests on somewhat smaller models are also shown. The subsonic drag coefficient of the Hemisflo ribbon canopy is somewhat lower than that of the flat circular ribbon canopy, due to its increased nominal area and slightly lower inflated diameter. From Fig. 4-71, which shows the dependency of area ratio (ratio of instantaneous projected canopy area, S_{p_i} , to nominal canopy area, S_0) upon Mach number, it is obvious that the reduction in the drag coefficient above Mach 1 is caused partly by the accompanying reduction in inflated-canopy area. As the Mach number approaches zero, the value of the area ratio approaches

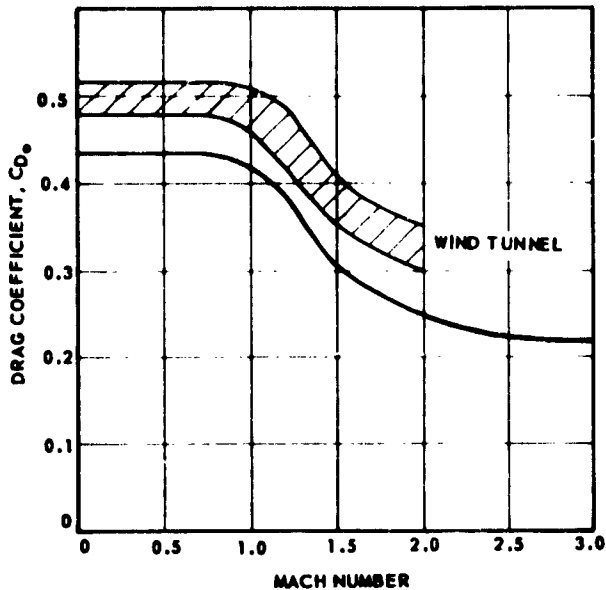


Fig. 4-70 Drag Coefficient vs Mach Number, Hemisflo Ribbon Type Canopy (Free-Flight Test)

a maximum of 0.387, the theoretical maximum area-ratio for this canopy. Plots of drag coefficient versus area ratio and versus dynamic pressure are shown in Fig. 4-72 and 4-73, respectively. When the trend of drag coefficient versus area ratio for the Hemisflo ribbon canopy is compared with that for a flat circular ribbon canopy, which is also shown in Fig. 4-72, the same trend is evident; but the Hemisflo ribbon canopy shows a much steeper rise in the sonic region. Approximate Mach number levels are indicated.

Although Hemisflo ribbon canopies have only been tested so far at dynamic pressures lower than 3800 psf, there is no reason to believe that adequately designed canopies of the ribbon type will not operate at higher dynamic pressures. On the other hand, guide-surface canopies manufactured of solid cloth and of diameters less than 6 ft have incurred extensive damage at dynamic pressures higher than 1700 psf, and it is doubtful that an extension of this limit is possible.

In general, it has been demonstrated that during supersonic operation a better behavior of the canopy is exhibited when positioned behind a relatively large-diameter forebody. This can be attributed to the favorable effects of the body wake-characteristics upon shock-wave and flow-field pattern forming ahead of the trailing canopy (Ref (4-39)).

Although textile canopies of the shaped-gore type have shown predictable performance characteristics at low supersonic velocities, their drag efficiency is relatively low, and an extension of their use into the

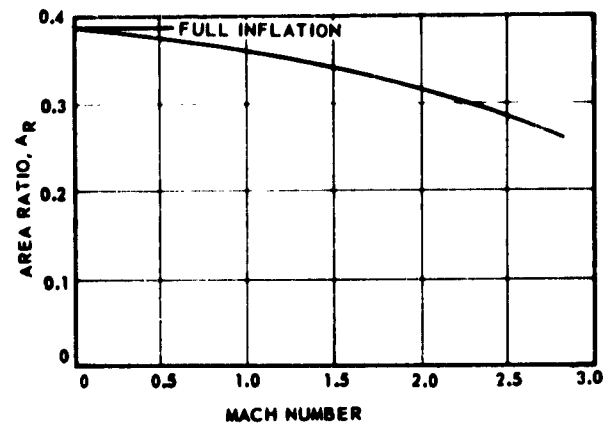


Fig. 4-71 Area Ratio vs Mach Number, Hemisflo Ribbon Type Canopy (Free-Flight Test)

higher supersonic-speed regime appears doubtful, unless there are significant modifications.

It appears difficult if not impossible to change the momentum of the air by carrying its entire mass along with the drag-producing surface. The conclusion is that to overcome these problems a means must be found to change the momentum of the air in steps, or to utilize only a portion of the available energy. These are the trends in current research efforts to evolve suitable self-inflating shapes for higher supersonic-speed operation.

6.5 Effects of Reynolds Number.

If such a strong variation in drag as shown in Fig. 4-64 and 4-70 occurs in classical aerodynamics, conditions are usually present where the Reynolds number is

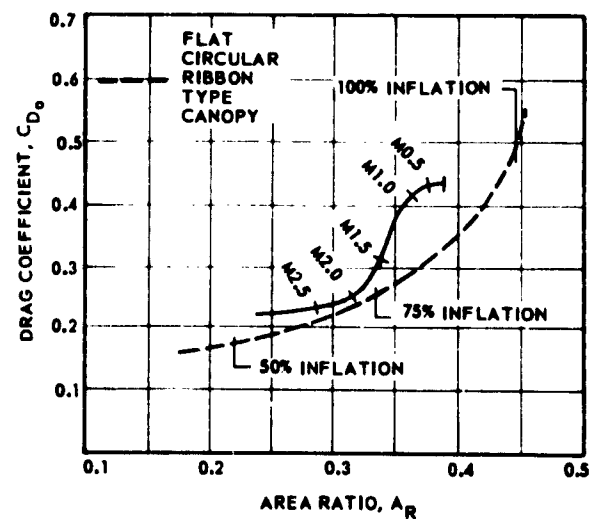


Fig. 4-72 Drag Coefficient vs Area Ratio, Hemisflo Ribbon Type Canopy (Free-Flight Test)

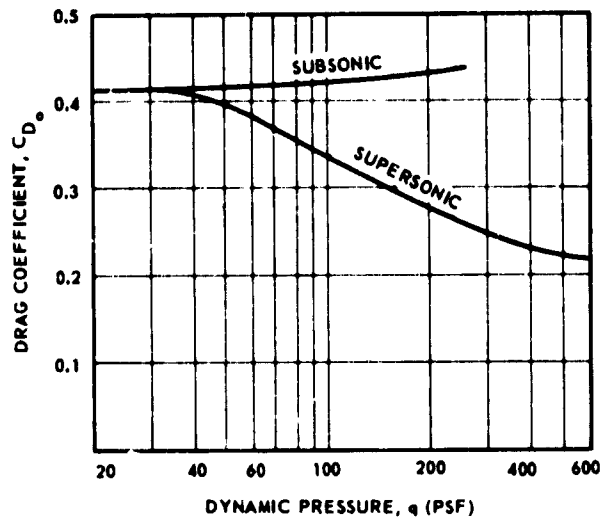


Fig. 4-73 C_D vs q , Hemisflo Ribbon Type Canopy (Free-Flight Test)

significant. Generally, Reynolds number is used as a factor indicating the type of boundary layer existing on a moving body in an airstream, whether it is laminar or turbulent. Reynolds number has its greatest significance for the aerodynamic characteristics of bodies below the *critical Reynolds number*: that region in which the flow in the boundary layer changes from laminar to turbulent. In the region of turbulent boundary-layer, Reynolds number has very little effect on the aerodynamic characteristics. Reynolds number is defined by the relationship

(4-131)

$$R = \frac{\rho v l}{\mu}$$

where ρ = Density of the air;
 v = Velocity of the canopy;
 l = "Representative length" of the canopy (see below); and
 μ = Coefficient of viscosity of air.

For calculations concerning canopies, the "representative length" is usually taken as either the projected diameter, D_p , or the nominal diameter, D_o , of the canopy. The projected diameter is more nearly a true aerodynamic reference length than is nominal diameter, but it is also more difficult to measure with accuracy. Consequently, Reynolds number is commonly calculated using the nominal canopy diameter, D_o .

In the case of textile canopies, the coefficient of effective drag of canopies of various sizes obtained at approximately the same rate of descent (about 20-25 fps) and identical stability behavior does not show a characteristic change over a wide range of Reynolds numbers. For example, the flat circular solid cloth canopy tested within a Reynolds number range between 1.5×10^5 and 1.3×10^7 exhibits drag coefficients which are relatively constant throughout the range tested (Fig. 4-74). A difference in drag-coefficient values for this type of canopy between free-descending and restrained models is evident. Here, the higher values of effective drag are associated with and generated by the unsteady motions of the canopy during descent.

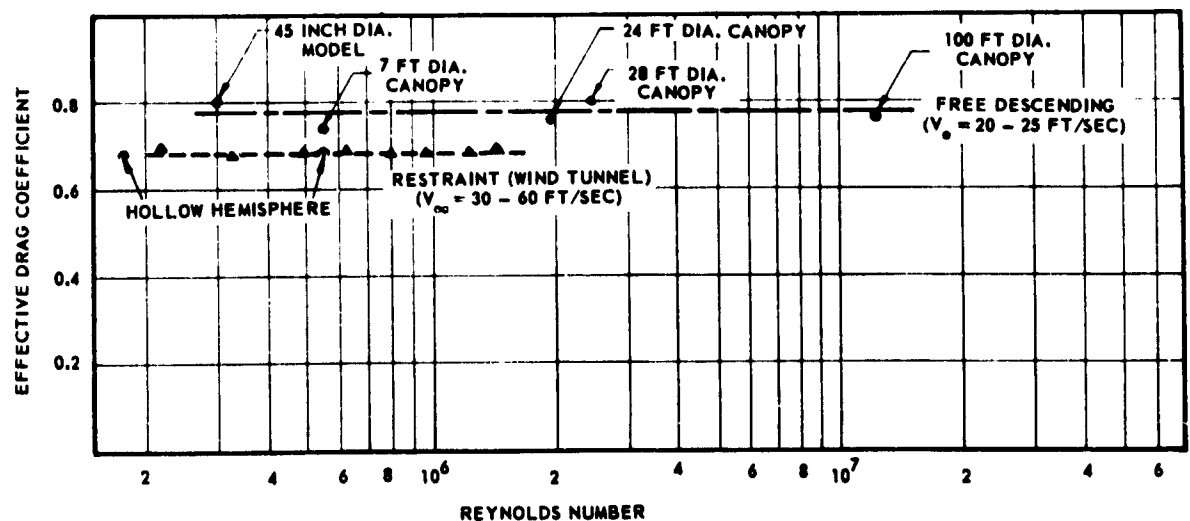


Fig. 4-74 Effective Drag Coefficient vs Reynolds Number, Flat Circular Solid Cloth Type Canopy

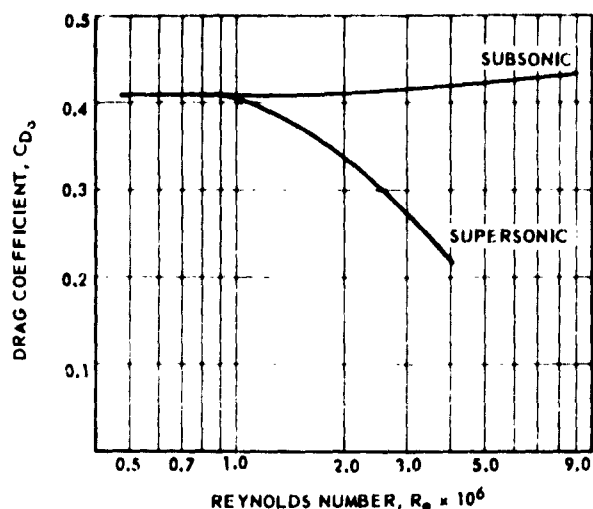


Fig. 4-75 Drag Coefficient vs Reynolds Number, Hemisflo Ribbon Type Canopy (Free-Flight Test)

As a cause for the significant change in drag coefficient for the Hemisflo ribbon canopy operating in the transonic and low-supersonic speed regimes (Fig. 4-70), Reynolds-number significance may again be suspected. However, it becomes obvious from an evaluation of Fig. 4-75 and 4-76 which are derived from test data obtained on Hemisflo ribbon canopies, that velocity effects must be the cause, since for subsonic operation with the same Reynolds-number range the ratio of drag coefficient to the area remains nearly constant.

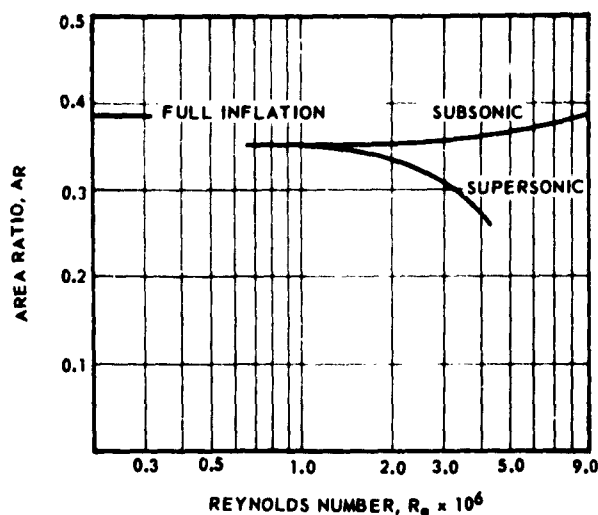


Fig. 4-76 Area Ratio vs Reynolds Number, Hemisflo Ribbon Type Canopy (Free-Flight Test)

6.6 Effects of Clustering. For the delivery or final recovery of heavy loads or vehicles, it is advisable to arrange moderately sized canopies in a cluster, rather than increase the diameter of a single canopy to the required dimension.

For solid cloth canopies, the drag efficiency of canopies arranged in a cluster configuration decreases with the number of parachute canopies used. The reason for this decrease may be seen in the altered flow field around individual canopies; this flow, on the other hand, improves static stability of the cluster configuration. A depiction of the drag coefficient versus number of canopies in a cluster is shown in Fig. 4-77.

For canopies with geometric porosity, such as ribbon or ring-slot types, the decrease in canopy drag-efficiency with number of canopies in a cluster is negligibly small. Here the flow field around the individual canopies is not significantly altered or influenced by other canopies in the cluster. In general, it can be said that statically stable canopies, when clustered, do not change their drag efficiency significantly. Statically unstable canopies, however, show a marked decrease in drag efficiency with number of canopies in a cluster. The magnitude of decrease in drag efficiency is a function of the static-stability characteristic of the individual canopy.

In supersonic flow, the performance of a cluster of canopies is similar to that of a single ribbon canopy. Typical performance characteristics of a cluster of three flat circular ribbon canopies for supersonic deployment and infinite-mass conditions (sled test) are shown in Fig. 4-78 (Ref (4-50)).

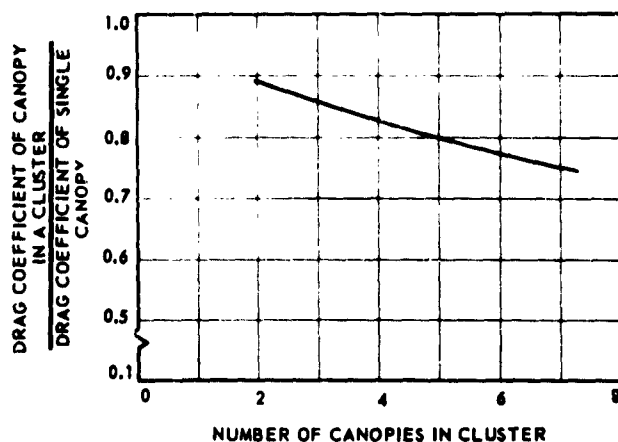


Fig. 4-77 Average Decreasing Drag Coefficient Ratio for Flat Circular Solid Cloth Type Canopies in Clustered Configurations

TYPICAL DYNAMIC CHARACTERISTICS

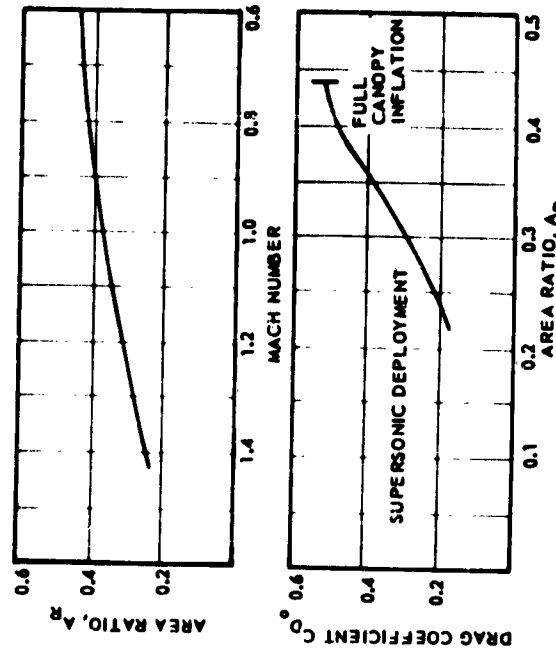
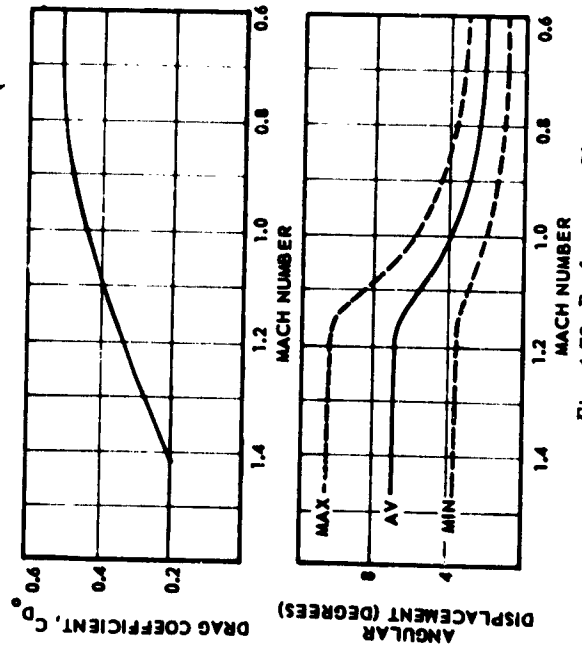
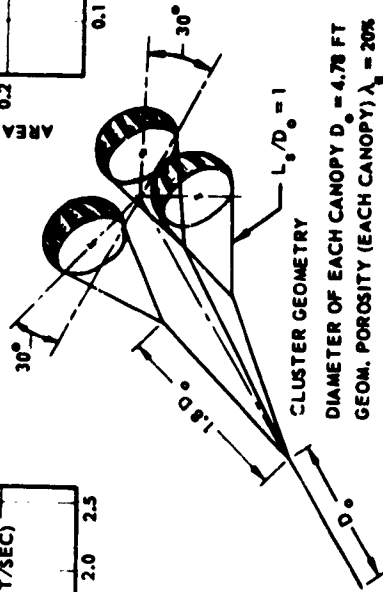
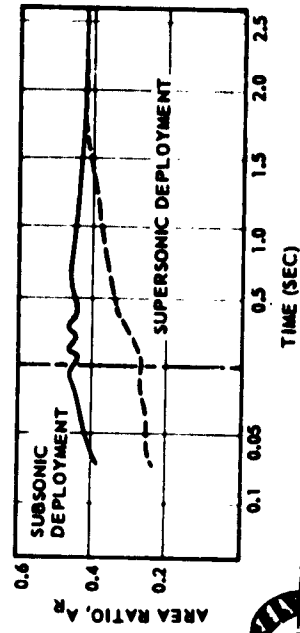
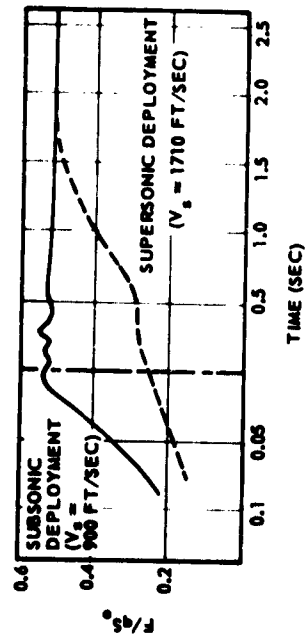


Fig. 4-78 Performance Characteristics of Flat Circular Ribbon Type Canopies in Triple Cluster Configuration.

SEC. 7 DRAG-AREA CONTROL

Under certain conditions it may become necessary to control the drag area of a parachute canopy. Canopy reefing is a method by which the projected diameter of a canopy is reduced temporarily, resulting in a reduction of the drag area of the canopy.

7.1 Application of Drag-Area Control. Reefing, as a method of drag-area control, may be applied for the following purposes:

(1) To limit canopy opening-force to a predetermined value, through successive steps of opening at predetermined intervals, called disreefing, or through controlled continuous disreefing.

(2) To attain a preliminary high rate-of-descent by extensive reefing to achieve accurate drops from high altitudes.

(3) To achieve a temporary low-drag area while still having a large landing-brake parachute for planes and gliders. Reefing also allows such parachutes to be used as dive and gliding-angle brake parachutes. After levelling off, the canopy is disreefed and becomes a powerful landing brake.

(4) To use parachutes as dive brakes, which can be retracted and extended in flight by means of reefing methods.

(5) To increase the stability of a canopy, either temporarily (for a particular application) or to adapt an available parachute to an application that requires increased stability.

7.2 Reefing Methods Used for Controlling Drag Area.

System I. Fig. 4-79 shows skirt-reefing System I, the most frequently used method. A line, called the reefing line, is placed around the skirt of the canopy. The reefing line is guided in small metal rings (reef-

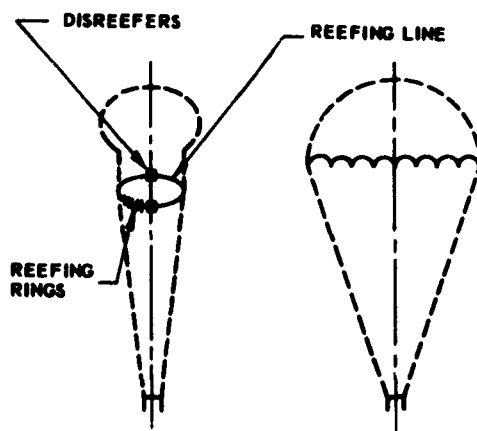


Fig. 4-79 Reefing Methods - System I

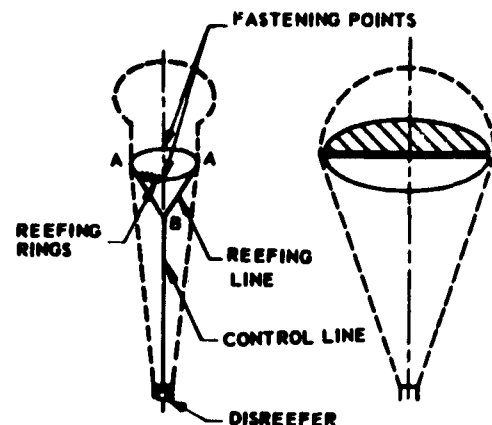


Fig. 4-80 Reefing Methods - System II

ing rings), which are fastened on the skirt on the inside of the canopy at each suspension line. The reefing line is fastened at both ends and is cut with a disreefing device after a certain delay period. At least two disreefing devices are recommended, for reliability. System I is recommended where one-step disreefing, or a short reefing-period is desired.

System II. For longer or variable periods, reefing System II, illustrated in Fig. 4-80, is advisable. The reefing line is guided through reefing rings inside the canopy skirt. It consists of two separate lines leading out from the skirt at point (A) and connected with the control line at point (B). By retraction of the control line, the canopy is reefed, and by extension of the control line, it is disreefed. Application of this system for continuous disreefing is feasible and depends primarily on the design and operation of the disreefing device. The control line is connected with the disreefing device at the suspension-line connecting point, to

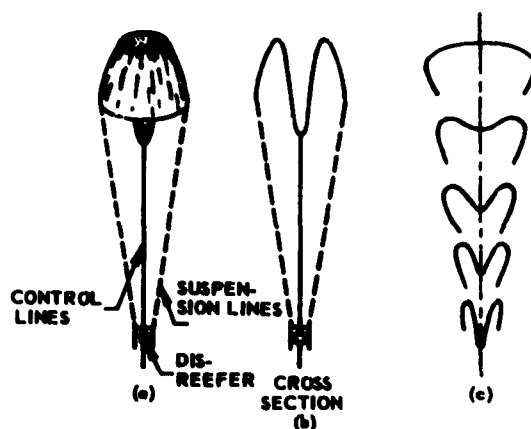


Fig. 4-81 Reefing Methods - System III

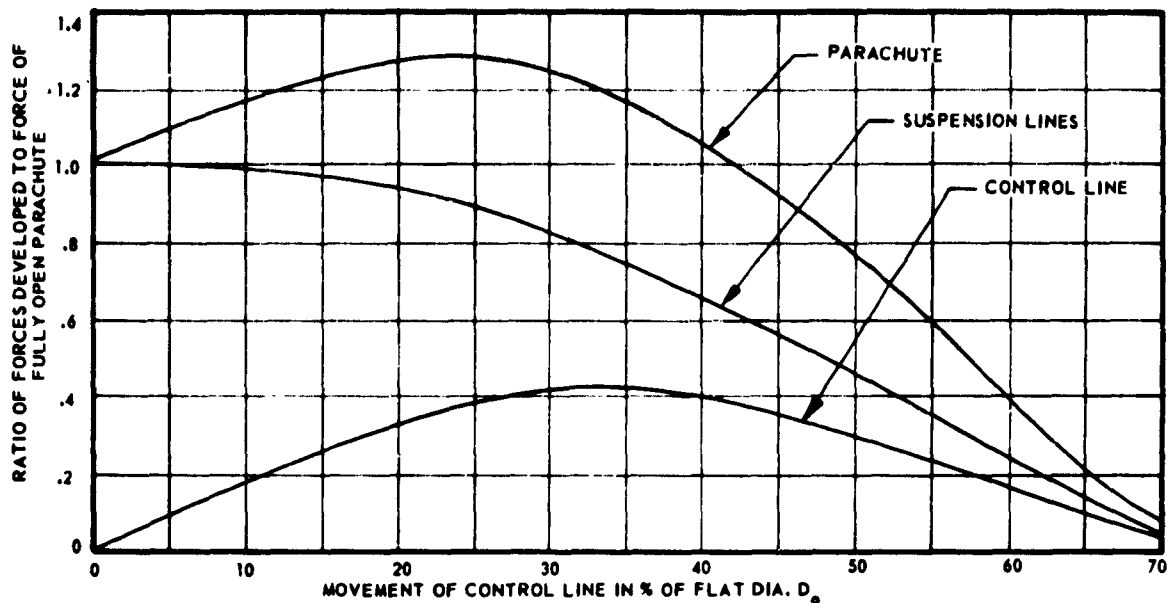


Fig. 4-82 Vent Reefing Forces in the Parachute, Suspension Lines and Control Lines

the suspended load, or in the aircraft. This method is particularly adaptable to designs in which diareefing must be a function of several variables and require a large and complicated actuating device.

System III. Fig. 4-81 (a), (b), and (c) shows the schematic outline of this reefing system. Fig. 4-81c illustrates the canopy at various stages of reefing. The canopy is reefed by pulling the vent down inside the canopy, as opposed to a skirt restriction system. The force required to pull the vent down amounts to approximately one-half the total force exerted on the canopy. As shown in Fig. 4-82, a significant increase in drag is produced by this reefing method up to a control line movement of about 40 per cent of the flat canopy diameter. At this point this method starts becoming effective for reducing the total drag force experienced by the canopy. A disadvantage of this reefing method is the high force in the control line and the large amount of reefing necessary to obtain a significant drag-reduction.

7.3 Reefing Lines. In the design of a reefed canopy, the choice of the proper reefing-line length is extremely important.

There are three methods now used for expressing the extent of reefing for a canopy: (1) drag-area ratio is the ratio of the drag area of the reefed parachute to that of the fully opened canopy; (2) reefed-diameter ratio is the ratio of the diameter of the reefed parachute skirt to that of the fully inflated parachute skirt diameter; and (3) reefing ratio, $\frac{(L/R)}{\pi D_0}$ is a ratio

of reefing line length to nominal diameter. Methods (1) and (2) were in WADC TR 55-265; method (3) is in Ref (4-51).

The reefing line must be designed to withstand maximum forces dependent upon the percentage of drag area of the canopy in the reefed condition compared with its drag area in the fully inflated condition.

The forces in the control lines of a reefing system similar to System II were measured on a flat circular

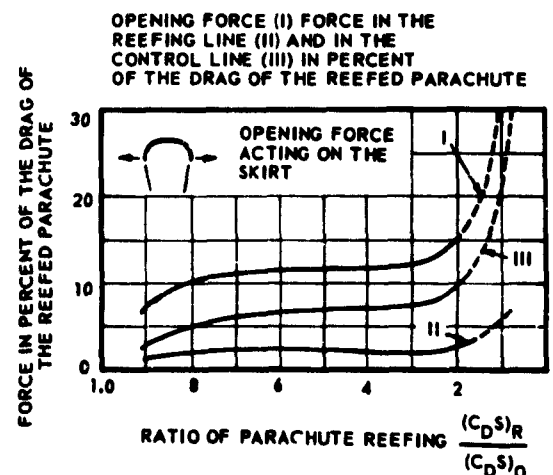


Fig. 4-83 Skirt Reefing; Reefing Line, Control Line, and Skirt Opening Forces

ribbon parachute 10 ft in diameter, towed behind an aircraft at 125 mph. The forces in the reefing line and the skirt-opening forces were calculated from the forces measured in the control line. These forces as a function of reefing ratio $(C_D S)_R / (C_D S)_O$ are shown in Fig. 4-83.

7.4 Multiple Reefing. Attempts to provide closer control of forces imposed on inflating canopies have led to the development of methods of staged reefing of parachutes. One system (Ref 4-53) utilized three stages of skirt-reefing by having one continuous reefing-line with suitable jumpers strung through reefing-line cutters with three different time-delays located along the canopy skirt. Another method incorporates reefing lines of different lengths, located at various positions on the drag-producing surface. These lines are cut at pre-selected times by the cutter located on the same circumferential line as the reefing line.

7.5 Reefed Inflation Characteristics. The drag area that should be exposed to the airstream at any given speed will depend upon the deceleration required and the strength of the individual components that make up the parachute structure. The area exposed, in turn, is controlled by the reefing-line length and the porosity of the inflated portion of the canopy. If at any stage, instability occurs at the reefed opening that results in a tendency for the canopy to squid or collapse, a loss in drag and deceleration will result, and failure of the canopy at the next disreefing stage may occur.

The reefing-line length controls the area of the opening through which air can enter the drag-producing surface, but the porosity of the canopy will determine its maximum inflated diameter. At equilibrium, the ratio of outflow area to inflow area is a characteristic of each parachute; increasing the porosity will reduce the inflated diameter, and decreasing the porosity will increase the inflated diameter for any given reefing-line length. Consequently, too much porosity will cause the inflated diameter to approach the (smaller) reefed diameter, and a point will be reached where the canopy has a tendency to elongate.

7.6 Calculations for Skirt Reefing for Flat Circular Canopies. If the opening shock of the required canopy is too high, or if a smaller drag-area is needed temporarily, the diameter of a smaller canopy, whose drag area will not cause an excessive opening shock, must be calculated. The drag coefficient undergoes a change during reefing, due to the change in canopy shape. In order to overcome this difficulty, a method is used in which the drag area of the canopy, instead of the drag coefficient, is the basis for calculations. The permissible diameter and

drag-area of a reefed canopy can be determined as the diameter of a reefing line, as in the following example:

C_{D_O} = drag coefficient based on total canopy surface area

D_O = nominal diameter of the unreefed canopy

$(C_D S)_O$ = drag area of the unreefed canopy (based on C_{D_O})

D_1 = (theoretical) diameter of the reefed canopy

$$D_1 = 2 \sqrt{\frac{(C_D S)_R}{\pi C_{D_O}}}$$

D_{R1} = skirt diameter of the reefed canopy

D_{R_O} = skirt diameter of the fully inflated canopy

$(C_D S)_R$ = drag area of the reefed canopy

Z = number of gores

C = ratio of reefing-line diameter length to flat (constructed) canopy diameter
 $= D_{R_O} / D_O$

δ = ratio of skirt diameters D_{R1} / D_{R_O}

If a canopy with a $C_{D_O} = 0.47$ of $D_O = 20$ ft, with $Z = 20$ gores, and a drag area $(C_D S) = 148$ sq ft, has a permissible drag-area reefed $(C_D S)_R = 16$ sq ft, the drag-area ratio then equals

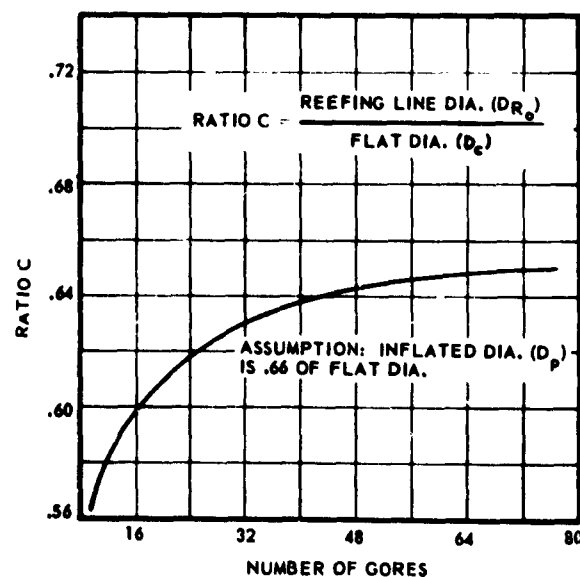


Fig. 4-84 C vs Number of Gores

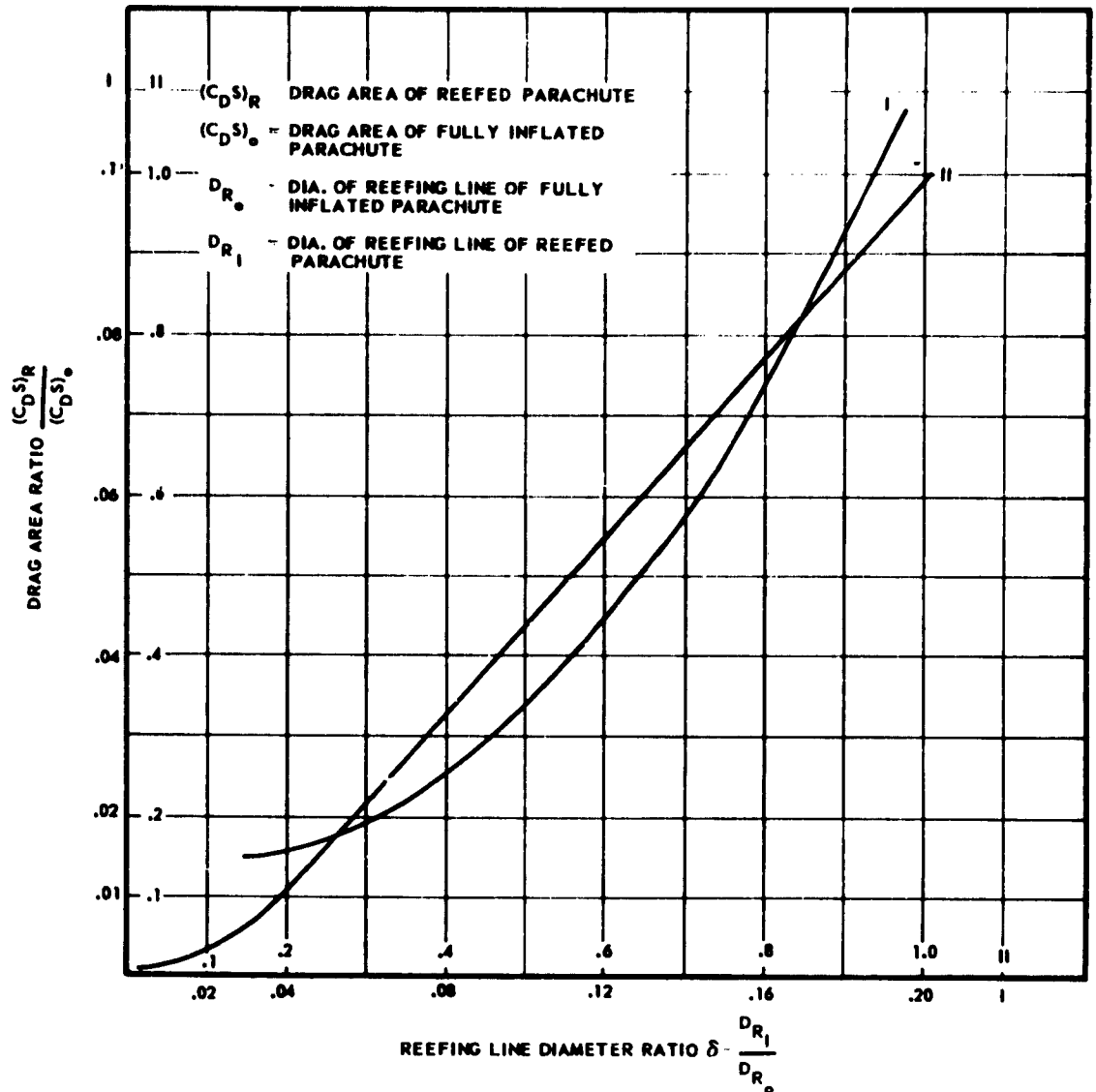


Fig. 4-85 Drag Area Ratio vs Reefing Line Diameter Ratio

$$\frac{(C_D S)_R}{(C_D S)_O} = \frac{16}{148} = 0.108$$

Therefore, for 20 gores, $C = 0.61$ (see Fig. 4-84). For a drag area ratio of 0.108, $\delta = 0.194$ (see Fig. 4-85). With this data, the diameter of the reefing-line circle may be determined:

$$D_{R1} = D_o C \delta$$

$$D_{R1} = 20 \times 0.61 \times 0.19 = 2.36 \text{ ft}$$

The theoretical diameter of the reefed canopy can

also be calculated.

$$D_1 = 2 \sqrt{\frac{16}{(\pi)(0.47)}}$$

$$= 6.6 \text{ ft}$$

The data presented in Fig. 4-84 and 4-85 have been verified by tests and apply to all types of flat circular canopies.

7.7 Skirt-Reefing of Extended-Skirt Canopies.

As noted in the preceding paragraph, the curves shown in Fig. 4-85 apply only to flat circular canopies. However, tests have been made on reefed extended-skirt

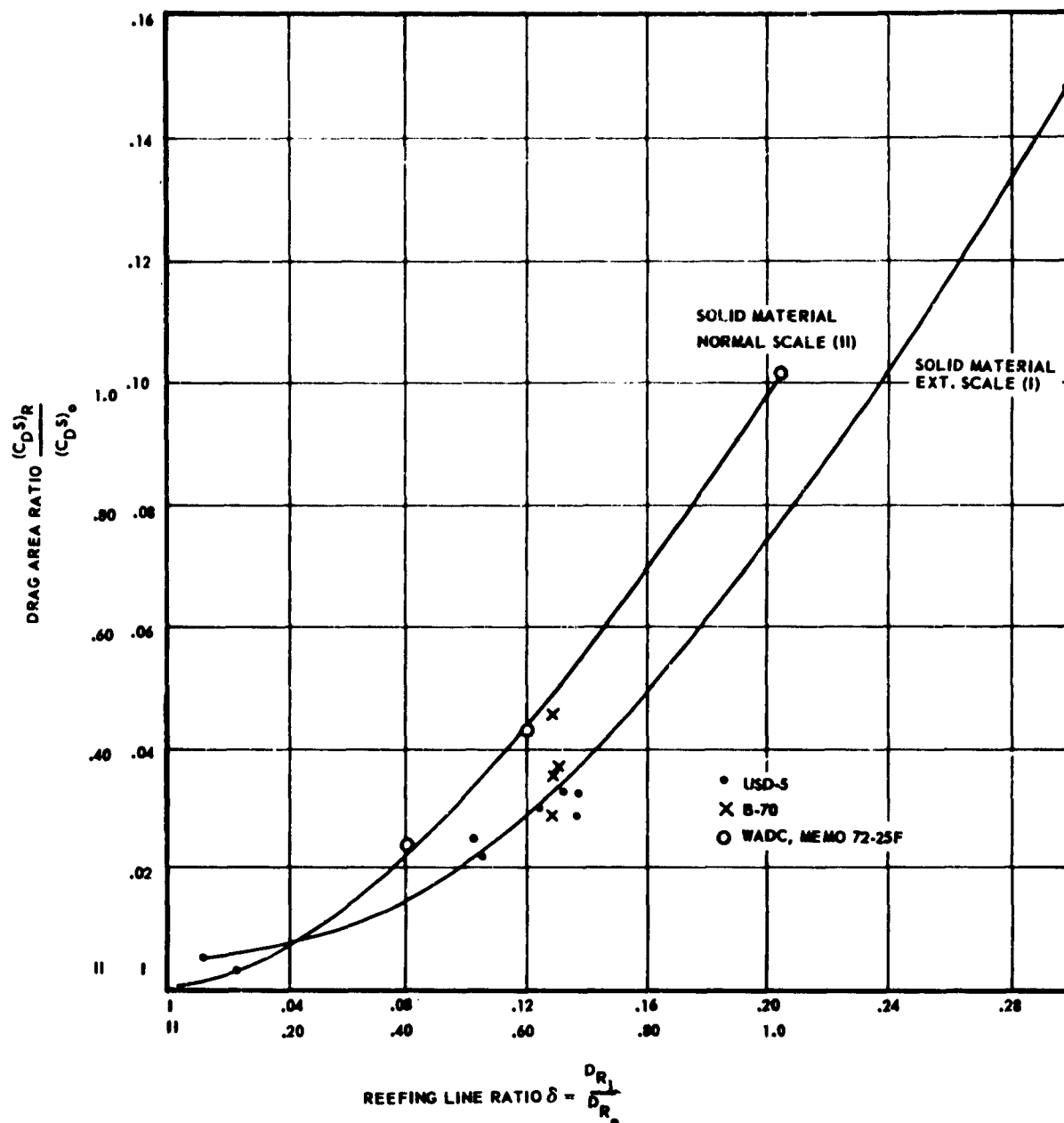


Fig. 4-86 Drag Area Ratio vs Reefing Line Diameter Ratio for Extended Skirt Canopies

canopies (Ref(4-54)) to provide sufficient data to make a similar plot of drag-area ratio versus reefing ratio for this type of canopy. These curves, plotted from empirical data, are shown in Fig. 4-86.

7.8 Reefed Supersonic Parachutes. Recovery systems for aerospace vehicles presently utilize ribbon canopies for first- and second-stage decelerators. Consideration has been given to recovery-system designs in which the second-stage decelerator is reefed to provide a drag area comparable to the drag area of

the original first-stage canopy. This would eliminate the need for an individual first-stage decelerator.

Supersonic wind-tunnel tests have been conducted with a ribbon canopy with a 10 per cent extended-skirt (Hemisflo) reefed to diameters of 0.125, 0.250, 0.333, and 0.400 of the nominal diameter of the canopy. Fig. 4-87 shows the results of these tests. The reefed drag-coefficients, based on an area equal to $\frac{(L_R)^2}{4\pi}$

(where L_R equals reefing-line length) are plotted as a

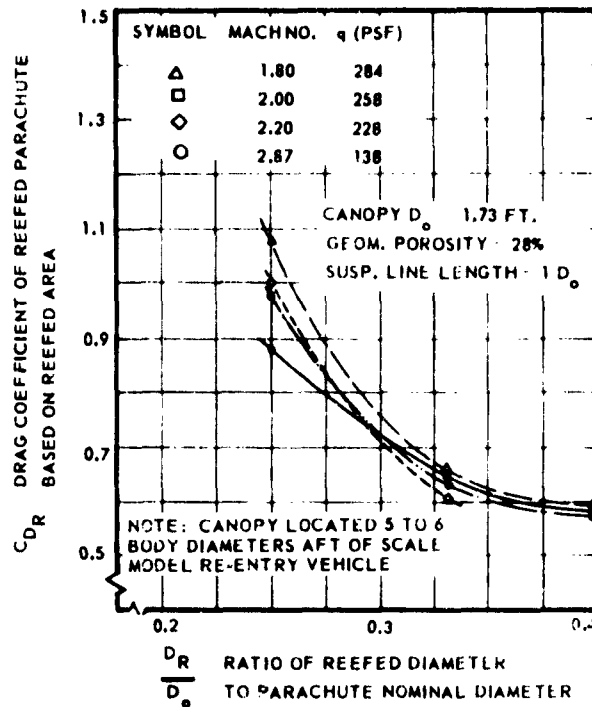


Fig. 4-87 Drag Coefficient Variation With Reefed Diameter Ratio

function of diameter ratio.

However, within the current state of the art, it is felt that the use of reefed canopies at supersonic speeds is unreliable. One of the major considerations is the availability of a disreefing device which would withstand the high g -forces which develop at the skirt of the reefed canopy when inflating at supersonic speeds. In addition, performance characteristics of reefed canopies at supersonic speeds at present are unpredictable. Therefore, the use of a multi-stage system, in lieu of reefing, is recommended as current state-of-the-art design of aerospace-vehicle recovery systems.

7.9 Reefing Rings. The use of rectangular cross-section reefing rings, as discussed in Chapter 9, is very important, since the surface area presented prevents any hinging action in the ring, which can result in binding of the reefing line between the ring and the skirt of the canopy. Use of reefing rings with round cross-section should be avoided, as failures may occur.

When using the skirt-reefing method, reefing rings are attached to the skirt of the canopy with thread or webbing. When using webbings for retaining the rings to the skirt, the stitching must be as close to the ring as possible, to avoid turning of the ring.

SEC. 8 CANOPY PRESSURE DISTRIBUTION

The knowledge of the pressure distribution over the drag-producing surface of a textile canopy is a valuable tool for the prediction of canopy inflation characteristics, and is a prerequisite for any attempt to analyze accurately the stress distribution in the canopy, particularly during the period of inflation. As the canopy starts to inflate, the airflow into and around it causes a rapidly changing pressure-distribution, which in turn causes the canopy to change shape. Consequently, stress distribution and magnitude of stress also change rapidly with the shape and change in pressure distribution.

8.1 Inflated Canopy - Pressure Distribution in Subsonic and Transonic Flow. Some experimental data are available on the pressure distribution over the surface of conventional canopies under static, fully inflated conditions. It has been commonly assumed that the internal pressure is uniformly distributed over the fully inflated canopy surface. This assumption has been verified experimentally on rigid and textile scale models by determining the internal pressure coefficients for several drag-producing surfaces. The coefficient of pressure is defined as

$$(4-132) \quad c_p = \frac{\Delta p}{q} = \frac{P_L - P_\infty}{q} = \frac{P_L - P_\infty}{\gamma P_\infty M_\infty^2} = \frac{2}{\gamma M_\infty^2} \left(\frac{P_L}{P_\infty} - 1 \right)$$

where P_L = local static pressure;

P_∞ = free-stream static pressure;

$q = (\rho/2)v^2$ = dynamic pressure;

M_∞ = free-stream Mach number; and

γ = ratio of specific heats (assumed as 1.40 for temperature range of 72-94 F during tests).

In subsonic and transonic flow, it may be expected that, inside a hollow non-porous or slightly porous object, the local pressure is approximately the isentropic stagnation pressure. In compressible flow, the stagnation pressure, P_O , can be expressed in terms of the dynamic pressure, q , by means of the relationship

$$(4-133) \quad P_O = P_\infty + q \left(1 + \frac{\gamma_\infty^2}{4} + \frac{\gamma_\infty^4}{40} + \frac{\gamma_\infty^6}{1600} + \dots \right)$$

If perfect isentropic stagnation pressure is achieved in the inside of the canopy models, then the pressure

coefficient would be (Ref (4-55))

$$(4-134) \quad c_p = \frac{\Delta p}{q} = 1 + \frac{M_\infty^2}{4} + \frac{M_\infty^4}{40} + \frac{M_\infty^6}{1600} + \dots$$

The pressure distribution over the drag-producing surface of rigid models of flat circular ribbon canopy (20 per cent geometric porosity) and a guide-surface canopy has been experimentally determined (Ref (4-56)). Models used in these experiments were constructed of stainless steel and had a maximum projected diameter of 2.5 in. Suspension lines were not included. The canopy models were rear-sting mounted at zero-degree angle of attack and the test range was at free-stream Mach numbers between 0.6 and 1.25. The Reynolds number range was from 6.99×10^5 to 9.71×10^5 , with the maximum model diameter as the characteristic dimension. The ratio of the sting diameter to maximum diameter was 0.175; the mounting point of the model to the sting corresponded in size to the vent opening of a full-sized canopy. The combined external and internal pressure coefficients are shown in Fig. 4-89 and 4-90 for the ribbon and guide-surface canopies

respectively. Vectors pointing toward the surface of the model indicate positive c_p values, while the vectors pointing away indicate negative c_p values. These data show how the pattern of pressure distribution varies with Mach number. The relationship between external pressure coefficient and free-stream Mach number for various points on the drag-producing surface is shown in Fig. 4-88 and 4-91.

Generally, pressure distribution for the ribbon canopy indicates a decrease in external pressure-coefficient and an increase in internal pressure-coefficient with increasing Mach number. The net change of pressure distribution, however, represents a decrease in the tendency of inflation of the flexible canopy. While the pattern of the external pressure distribution changes with Mach number, the internal pressure coefficient always assumes a value approximately equal to the ratio of $\Delta p/q$ of compressible flow.

Shadowgraph pictures taken during these tests show that in subsonic flow a well-defined stream of air passes through the slots between the individual ribbons. This flow is subsonic below a free-stream Mach number of approximately 0.80. Beginning at Mach 0.80, the airstream between the ribbons begins to show a

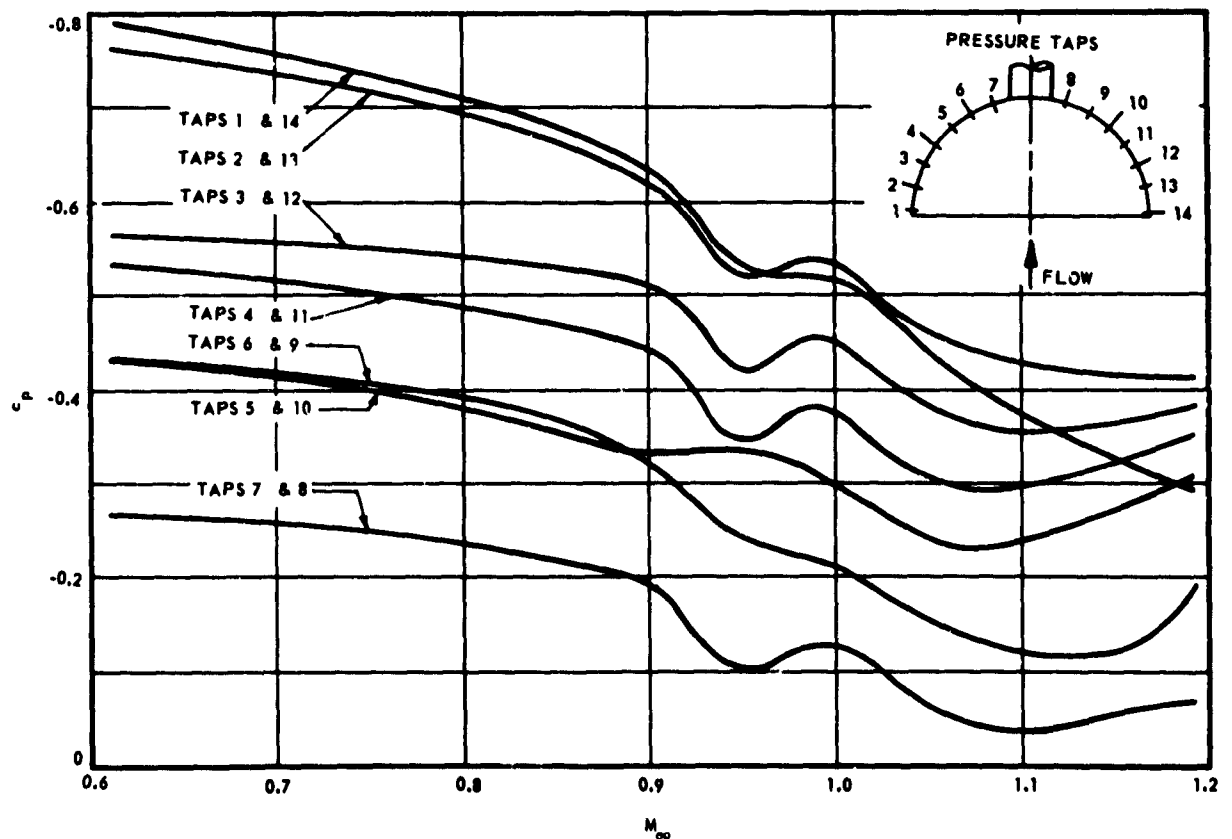


Fig. 4-88 External Pressure Coefficients vs M_∞ for Flat Circular Ribbon Type Canopies

TAPS 1 & 14 $r_1 = 0.49960$
 2 & 13 $r_2 = 0.4850$
 3 & 12 $r_3 = 0.4520$
 4 & 11 $r_4 = 0.4000$
 5 & 10 $r_5 = 0.3720$
 6 & 9 $r_6 = 0.2500$
 7 & 8 $r_7 = 0.1670$

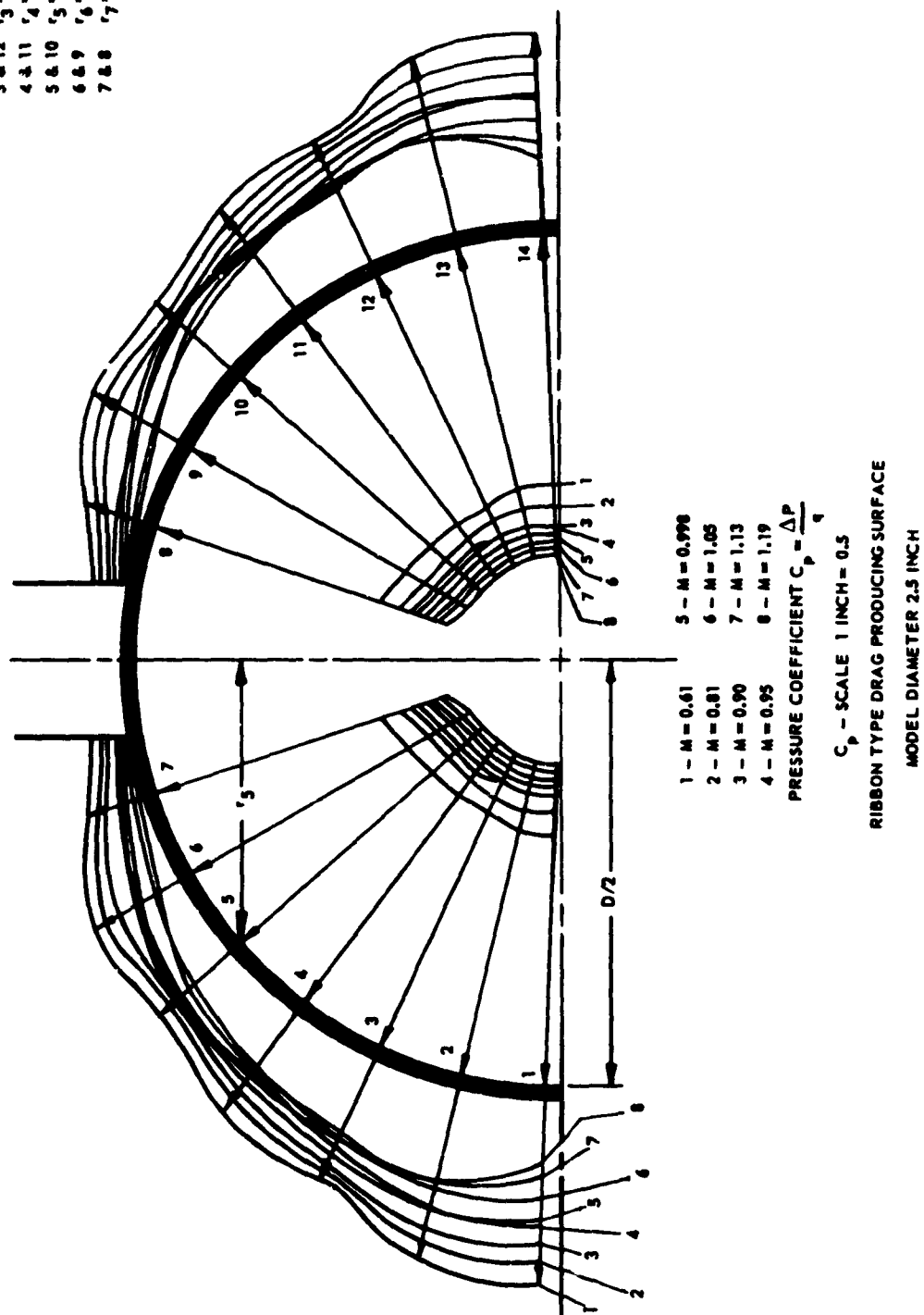


Fig. 4-89 External and Internal Pressure Distribution for Flat Circular Ribbon Type Canopies

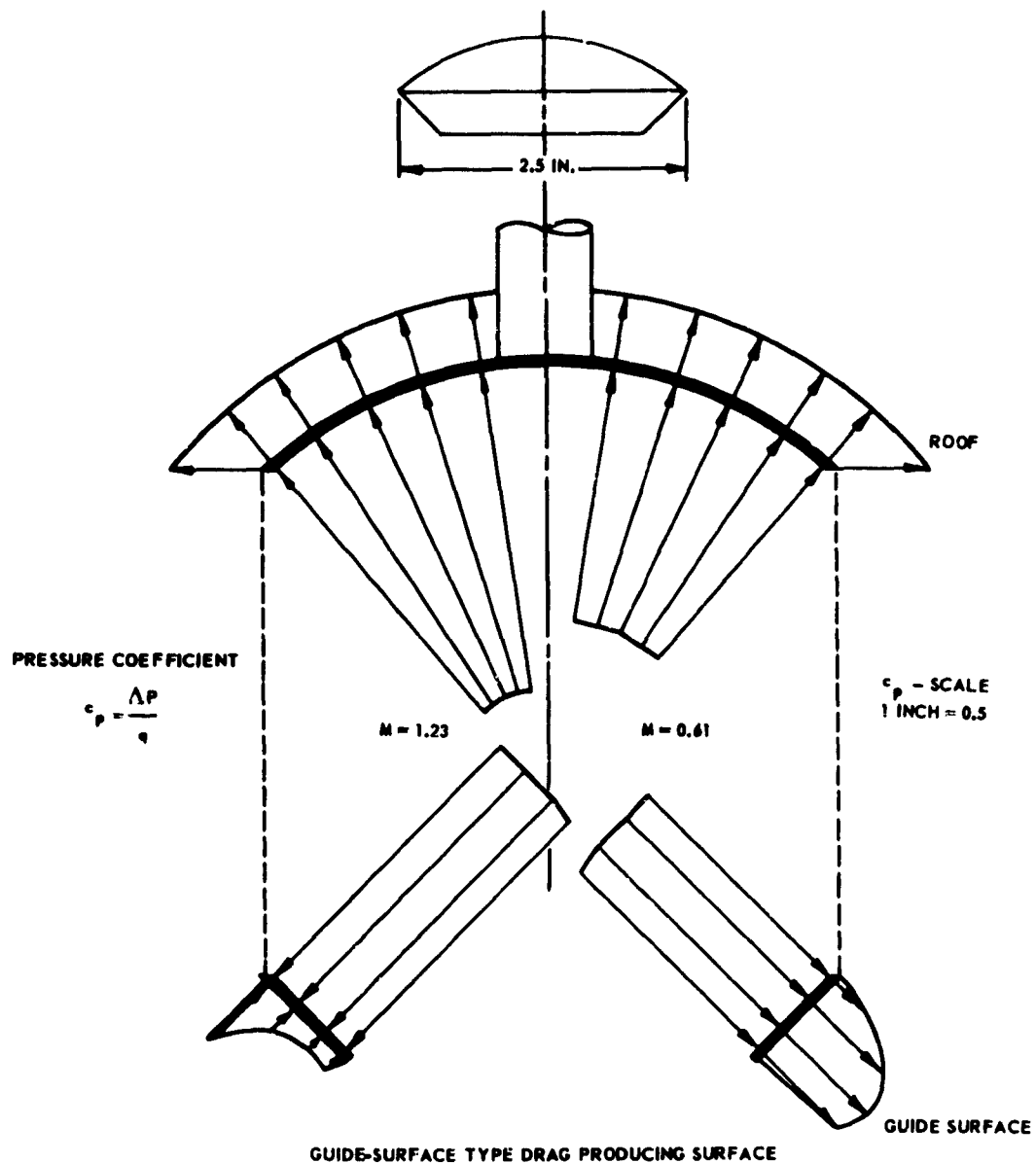


Fig. 4-90 External and Internal Pressure Distribution for Guide-Surface Type Canopies

diamond pattern which is characteristic of jet flow with sonic speed. This means that sonic flow exists in the slots even though the free-stream Mach number is still subsonic. This phenomena is caused by the reduced pressure on the outside of the drag-producing surface while almost full isentropic stagnation pressure exists inside the inflated drag-producing surface. Fig. 4-92 shows a shadowgraph picture of a circular flat ribbon canopy model (20 per cent geometric por-

osity) at free-stream Mach 0.897, in which the diamond pattern forming behind the slots can be distinguished.

The pressure distribution across the roof of the guide-surface canopy does not change appreciably, and remains nearly constant for any particular free-stream Mach number. The internal pressure distribution is also nearly constant across the drag-producing surface; its value is almost equal to the isentropic stagnation pressure. However, a significant change of the

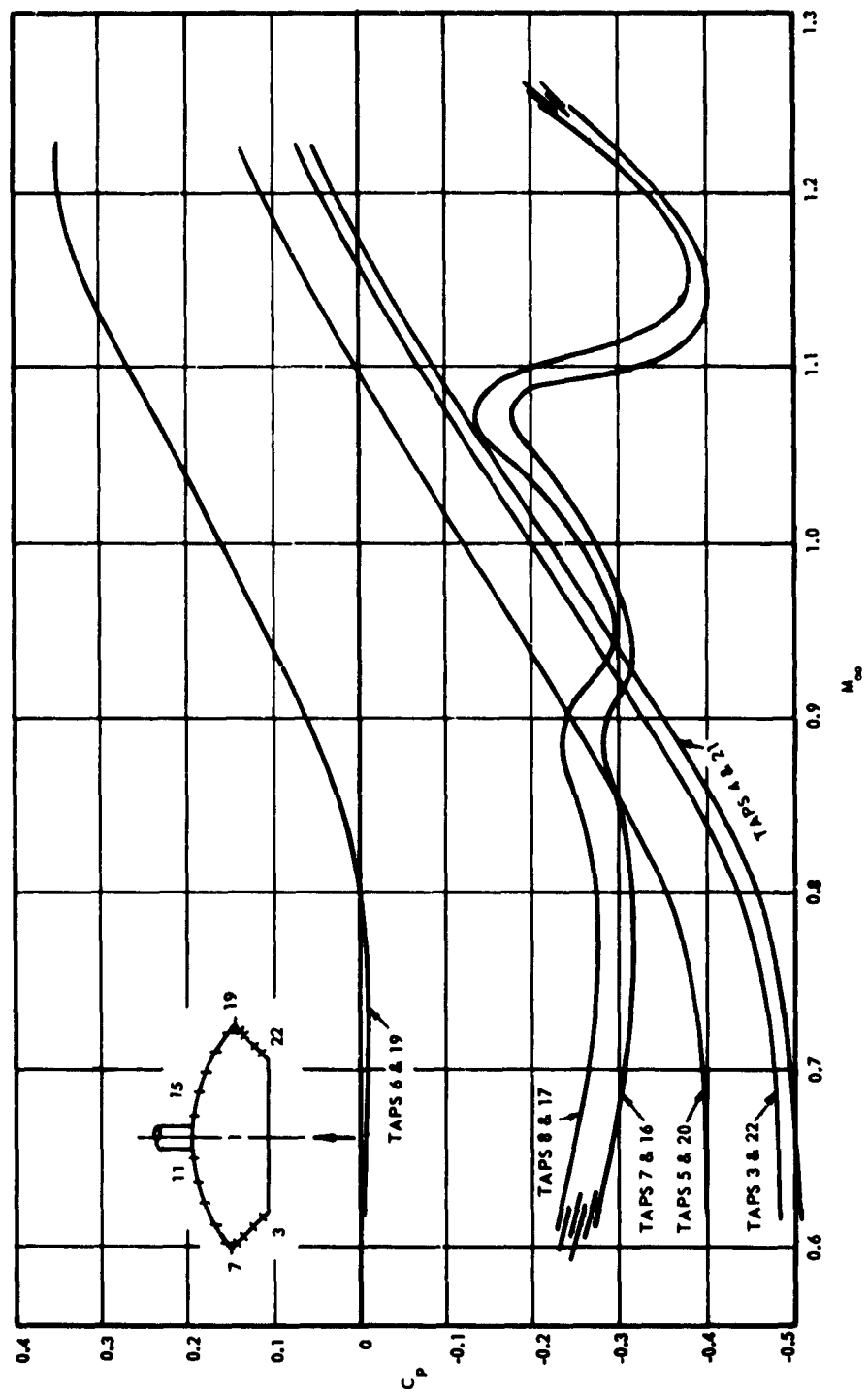


Fig. 4-91 External Pressure Coefficients vs Mach Number for Guide-Surface Type Canopies

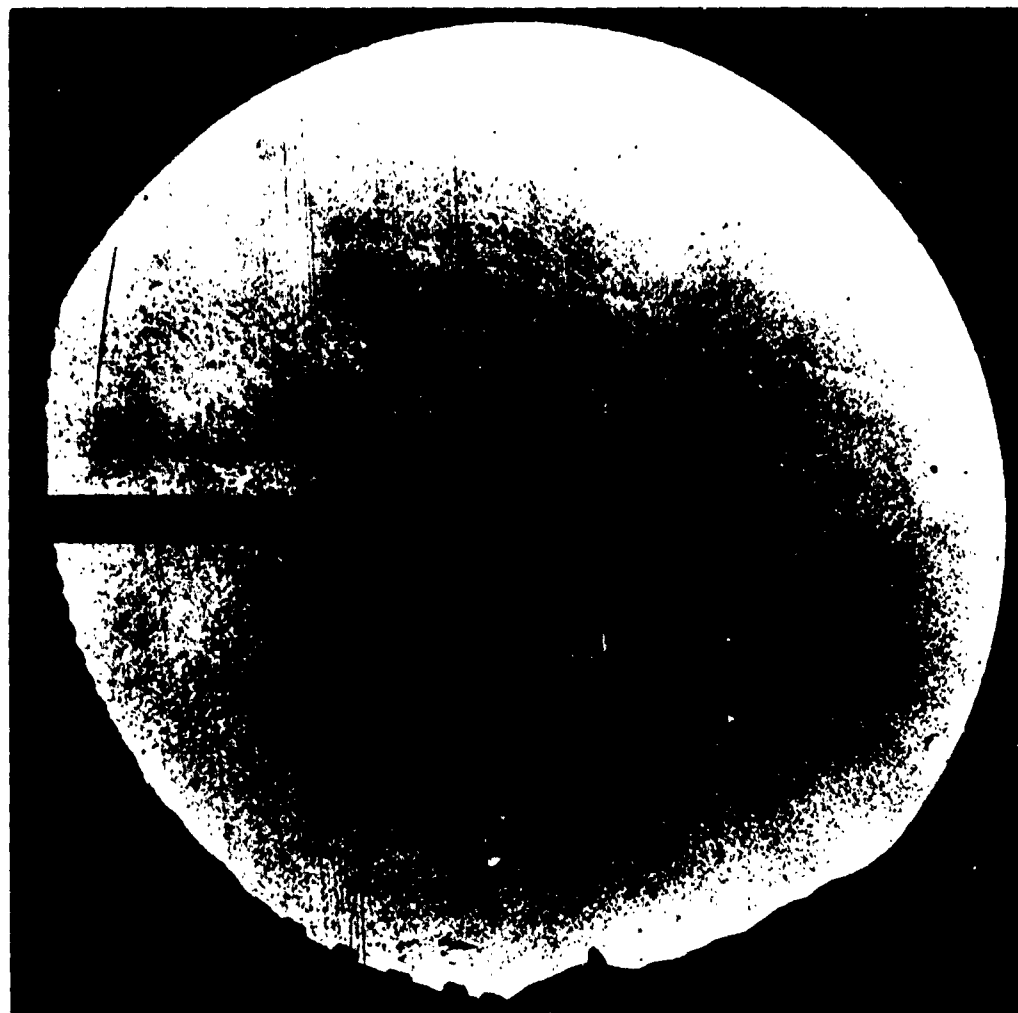


Fig. 4-92 Schlieren Picture of a Ribbon-Type Drag-Producing Surface at a Free-Stream Mach Number of 0.897

external pressure coefficient with Mach number is indicated along the guide surfaces, and the net force which keeps the canopy inflated decreases rather rapidly with Mach number. Fig. 4-91 shows that for the taps located on the guide surfaces the external pressure coefficient changes from negative values to positive values at transonic free stream velocities.

8.2 Inflated Canopy – Pressure Distribution in Supersonic Flow.

An analysis of the external and

internal pressure distribution over the drag-producing surface of a circular flat ribbon canopy in supersonic flow has been performed (Ref (4-57)). The experimental determination of the pressure distribution was conducted on rigid models of a canopy simulating the actual flying shape in high subsonic flow. The drag-producing surface had a geometric porosity of 26 per cent, and its projected diameter was 1.94 in. To determine the effects of suspension lines and primary body upon

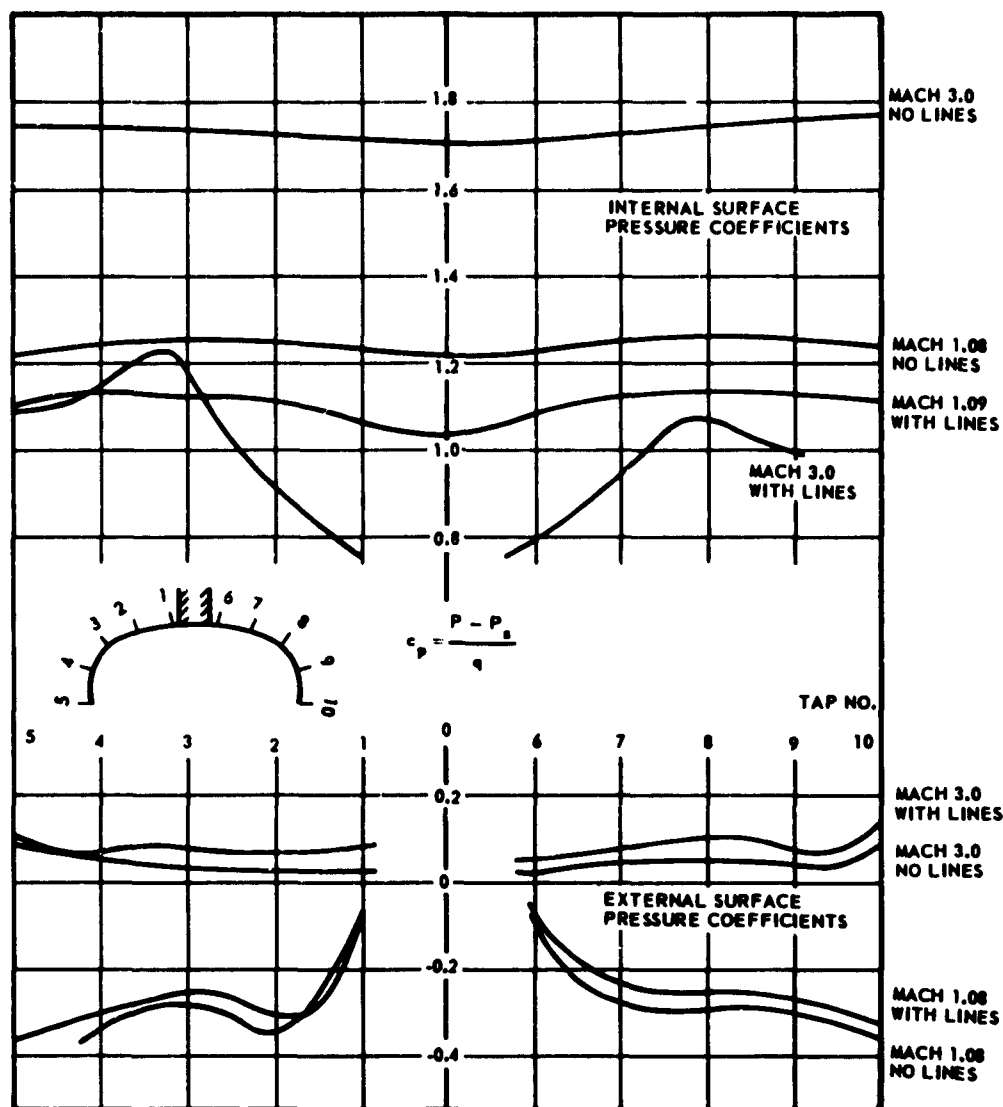


Fig. 4-93 Pressure Coefficient Distribution Curves of a 26%-Porosity Ribbon-Type Canopy Model With and Without Suspension Lines, No Forebody

canopy pressure-distribution, suspension lines of $2D_o$ lengths and a primary body of ogive cylinder shape (1.94 in. in diameter, 2.5 caliber with a fineness ratio of 4.5) were added. All models were rear-sting mounted at zero angle of attack. The external and internal pressure coefficients for the ribbon canopy drag-producing surface with and without suspension lines in free stream are shown in Fig. 4-93 for free-stream Mach numbers of 1.09 and 3.0. Comparing the pressure

coefficient values measured on the ribbon canopy drag-producing surface without lines with those presented in Fig. 4-88 for the same free-stream Mach number, slight changes in c_p values are apparent, due primarily to changes in model shape. The internal pressure distribution for the model without lines is nearly constant; the values approximately equal the ratio of $\Delta p/q$ of compressible flow. When suspension lines are added to the model, the internal pressure coeffi-

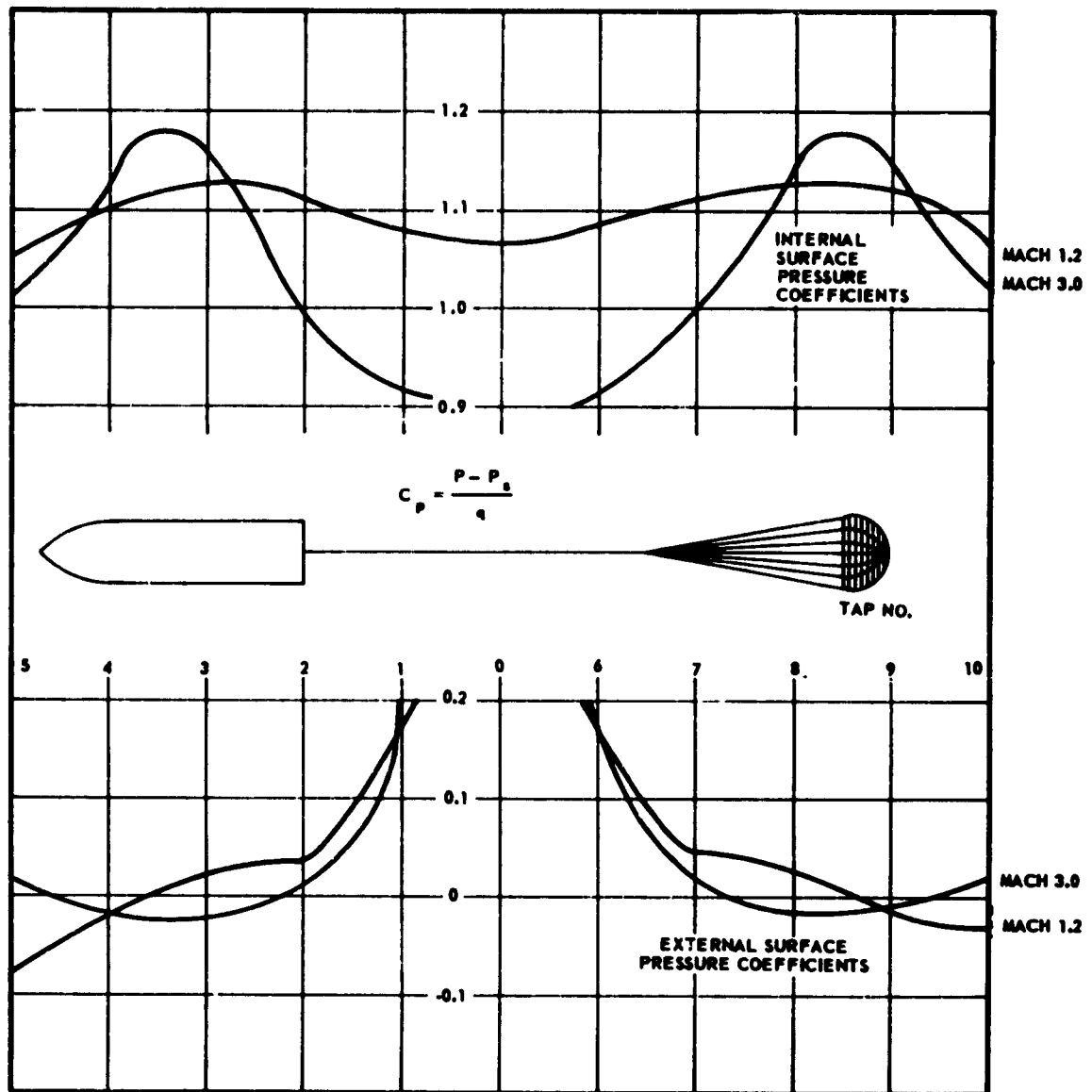
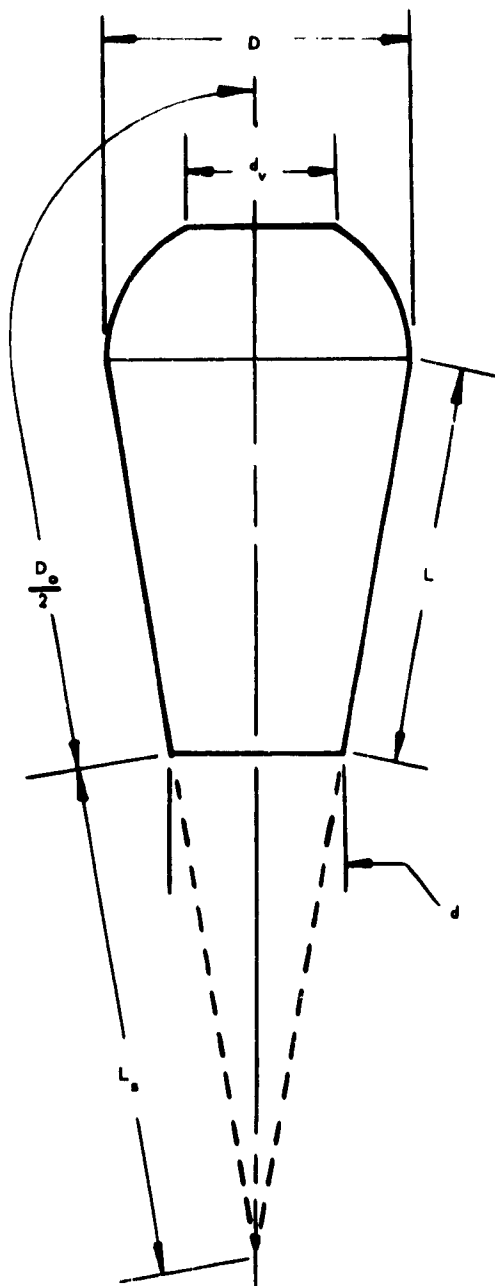


Fig. 4-94 Pressure Coefficient Distribution of a 26%-Porosity Ribbon-Type Canopy Model With Suspension Lines and Forebody



Sketch of Inflating Canopy Model

cients are changed drastically, particularly at the higher free-stream Mach number. The increase in the internal pressure coefficients in the case of the drag-producing surface without lines at the higher free-stream Mach number is due to the large pressure recovery across the well-defined shock ahead of the drag-producing surface. The effect which the suspension lines have upon the external pressure coefficients is relatively small. Values of the external pressure coefficient, however, are positive over the entire surface at a free-stream Mach number of 3.0. Placing an ogive cylinder of diameter equal to the projected diameter of the drag-producing surface eight cylinder-diameters ahead of the drag-producing surface has only a small influence upon the external pressure coefficients, as seen in Fig. 4-94. A modification of the internal-pressure distribution as compared with free-stream conditions is apparent.

8.3 Inflating Canopy - Pressure Distribution in Subsonic Flow.

Very little information is available on the change in pressure distribution during the period of canopy inflation. This lack of data is due primarily to the extreme difficulty encountered in attempts to determine internal and external pressure values experimentally under dynamic conditions.

A trend in the change in external and internal pressure-distribution during the period of canopy inflation is indicated in Fig. 4-95 thru -102 (Ref (4-58)). Pressure values shown were determined experimentally under static conditions on seven geometrically synthesized shapes of a flat circular solid-cloth canopy. Tests were conducted without suspension lines; however, the effect of the suspension lines upon the pressure distribution in low subsonic flow ($M < 0.2$) is considered to be negligible.

Model No.	D_o (in.)	d_v (in.)	D (in.)	L (in.)	d (in.)
1	16	1.6	2.55	6.00	1.85
2	16	1.6	3.82	5.00	2.91
3	16	1.6	5.09	4.00	4.07
4	16	1.6	6.37	3.00	5.36
5	16	1.6	7.64	2.00	6.79
6	16	1.6	8.91	1.00	8.39
7	16	1.6	10.02	0	10.02

Supplement to Fig. 4-95-102

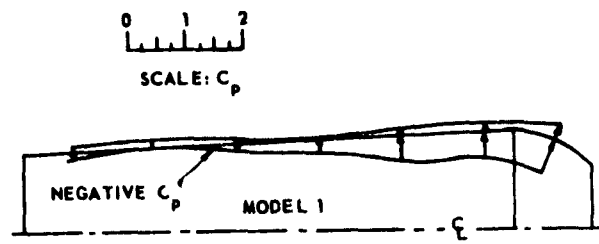


Fig. 4-95

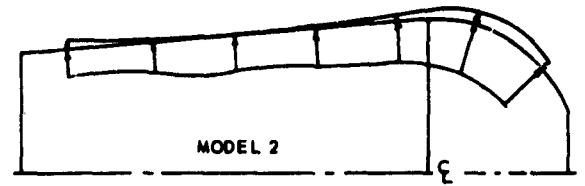


Fig. 4-96

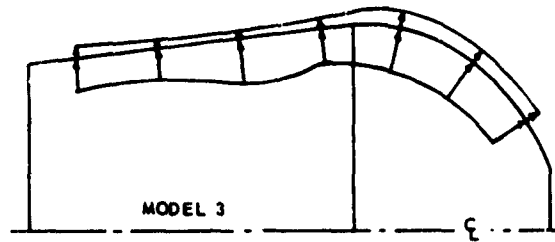


Fig. 4-97

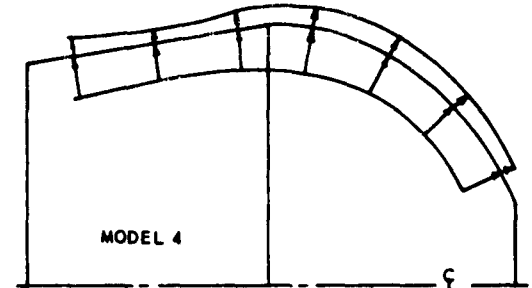


Fig. 4-98

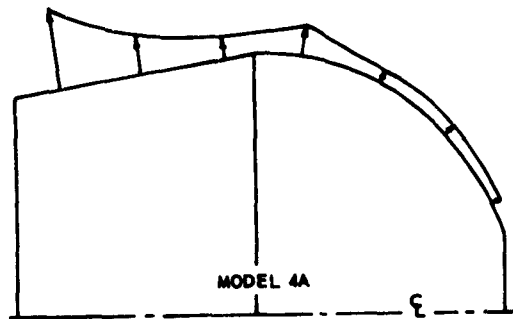


Fig. 4-99

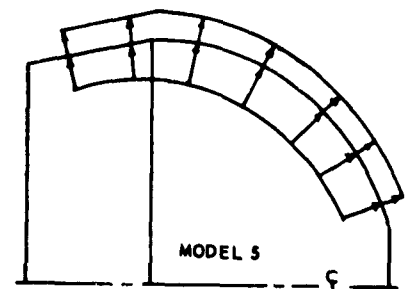


Fig. 4-100

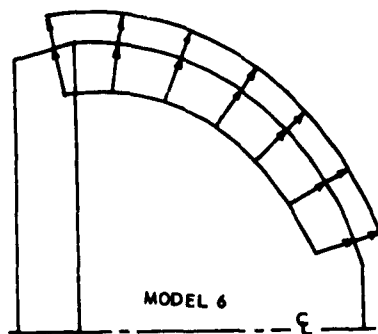


Fig. 4-101

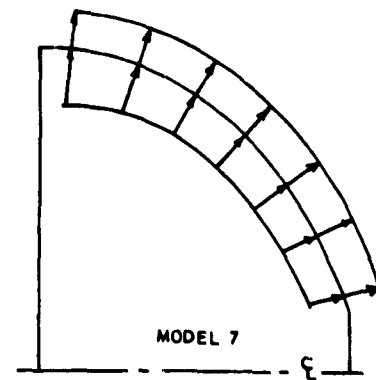


Fig. 4-102

Fig. 4-95-102 Schematic Pressure Coefficient Distribution of Models 1 through 7 in Inflating Parachute Canopy Series

SEC. 9 CANOPY STRESS DISTRIBUTION

The importance of knowing the stress distribution in canopies and its relation to canopy strength lies in the necessity for minimizing the weight of the canopy and, with it, required packing volume. In light-weight designs, where maintenance of canopy strength is an important factor, stress analysis is an indispensable element.

The stresses in a canopy are caused by aerodynamic loads acting on and between the various structural components. The stresses are both dynamic and static. Dynamic stresses usually exist for a comparatively short time, during the transition period from the moment the suspension lines are stretched and canopy filling begins to the moment a steady state is reached (i.e., the moment the canopy assumes its fully inflated shape). Although the stresses are not constant during the steady state, their variation is small compared to that encountered during the transition period. Therefore, the stresses in steady state can be considered as static.

Although the structure of a canopy differs considerably in many respects from more-common load-bearing structures, a stress analysis still requires a knowledge of three basic items: the shape and fabrication details of the structure, the manner and magnitude of application of the loads, and the characteristics of the structural material. The load-carrying elements are primarily fabric that has little stiffness and, therefore, can take no bending loads. Loads are resisted by tension in the members. Many types of fabric can be utilized, each having its own strength and elongation characteristics. Shape and construction vary with the type of canopy.

Stress analysis for a canopy is extremely complicated, since maximum stresses occur during the opening process, which is the period of rapidly changing shape and load. The determination of stresses in a canopy is essentially an aeroclastic problem, insofar as the cloth and suspension lines may be said to be elastic. Experience with structural failures in canopies, as well as measurements of snatch and opening forces, indicate that the critical stresses occur during opening-shock. Nevertheless, the steady-state problem is of interest, because the maximum stresses in the infinite-mass case, which approximates conditions of opening for such applications as first-stage deceleration, aircraft landing deceleration, and others, seem to occur when the canopy is fully, or almost fully, opened. The steady-state problem may also serve as a helpful preliminary to the more difficult and important problem of the determination of critical transient stresses during opening.

Jones (Ref (4-41)) and Topping, et al (Ref (4-59)) have attempted the calculation of stresses in parachute canopies under steady-state conditions. Both studies are based principally on the assumption that the radial stresses in a canopy may be neglected because of the magnitude of the circumferential stresses. This assumption then provides a certain profile which is known as the "Taylor shape". However, the results given in Ref (4-59) show that the actual profile of a free-flying canopy deviates significantly from that of the Taylor shape. Therefore, one may expect that the results of stress calculations based on the Taylor shape will not be the same as the stresses in actual canopies of conventional shape.

In view of this background, Heinrich and Monson (Ref (4-60)) formulated a method to calculate the stresses in a canopy whose free-flying profile and gore pattern are known. This concept also makes it possible to calculate the stresses in a canopy during the period of inflation, while the methods used in Ref (4-41) and (4-59) are restricted to the fully inflated canopy.

9.1 Definitions and Determination of Basic Working Equations for Cord-Line Profile. The important effect which the canopy shape has on the stresses in the drag-producing surface is well known. Accordingly, the starting point of the method developed in Reference (4-60) is the profile shape of an inflated canopy. This shape is most readily obtained by photographing a freely descending canopy or a wind tunnel model from the side, although any other accurate method is valid. Since a profile photograph fails to reveal the profile shape of the cord lines of the canopy, it is first necessary to derive the cord-line profile from the photographed gore-centerline profile.

Theoretically the canopy may be considered to be a thin flexible shell acted on by normal and tangential forces. To apply the equilibrium equations of a small section of this shell (Fig. 4-103), certain other assumptions must be made. These assumptions are: (1) the surface is formed by rotating a curve about an axis; and (2) the aerodynamic forces are rotationally symmetrical.

These assumptions are quite realistic and simplify the future process of analysis. The method is further based on the fact that any given gore pattern has a certain unstretched width at any given location on its surface. Upon inflation of the canopy, this gore must bulge out and assume a curved shape between adjacent cords, since their separation distance, Z , is less than the gore width. This separation distance depends only on the distance from the canopy to the central axis (Fig. 4-106). Fig. 4-107 shows a typical

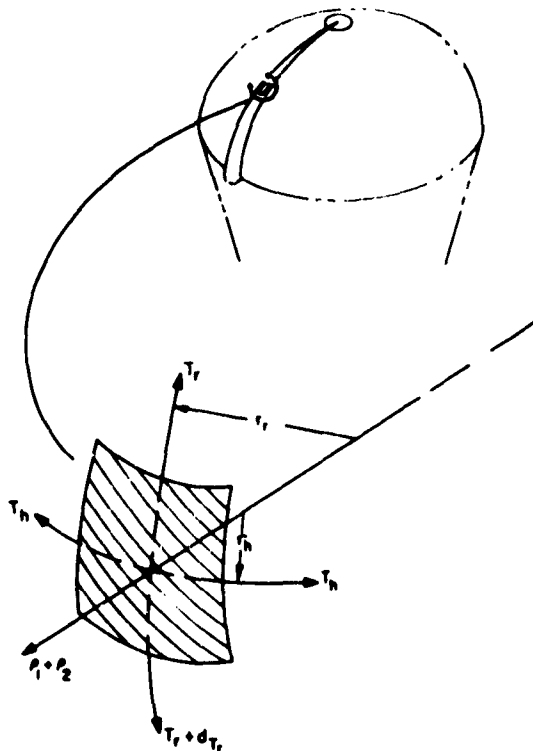


Fig. 4-103 Forces Acting on a Small Segment of a Flexible Shell in Equilibrium

gore-centerline profile. It is seen to be separated from the associated cord-line profile by the distance measured normal to the gore centerline at any point. An approximate analytical solution for the distance, b , in terms of geometric properties of the canopy will allow the graphic construction of the cord-line profile.

As a first step in obtaining the cord-line profile, the parachute cloth shall be assumed to be unextendible, which provides a relatively simple treatment. After a solution is derived, a simple correction can be introduced which accounts for the stress-strain properties of the material and the pressure distribution over the drag-producing surface. In this first step, the effect of neglecting the strain of the material is of minor importance since, for the steadily descending canopy, the strain generally amounts to less than one per cent. The situation may be entirely different, however, when applying the method to the inflation period of the canopy where much higher differential pressures occur than during steady state.

Fig. 4-105 presents a cross section of a typical inflated gore cut by a plane, P_1 , which is any plane formed by the normals erected at two points equidistant from the apex on adjacent cords and passing

through the axis of the canopy. Referring to this figure, one may write

$$(4-135) \quad Z = 2(r_o \sin \alpha_o)$$

where Z = Distance between adjacent cords;

r_o = Bulge radius of unstretched gore; and

α_o = half angle of unrestrained gore bulge.

$$(4-136) \quad Z = 2(R_g - b) \tan \beta$$

where R_g = Local radius of curvature of the locus of points resulting from the intersection of a plane P_1 with the surface of revolution formed by rotating the gore-centerline profile. This radius is approximated by the distance between the gore-centerline profile and the canopy central axis in plane P_1 (Fig. 4-105 and 4-107);

b = Distance from gore centerline to cord line measured normal to gore centerline at any point (Fig. 4-107); and

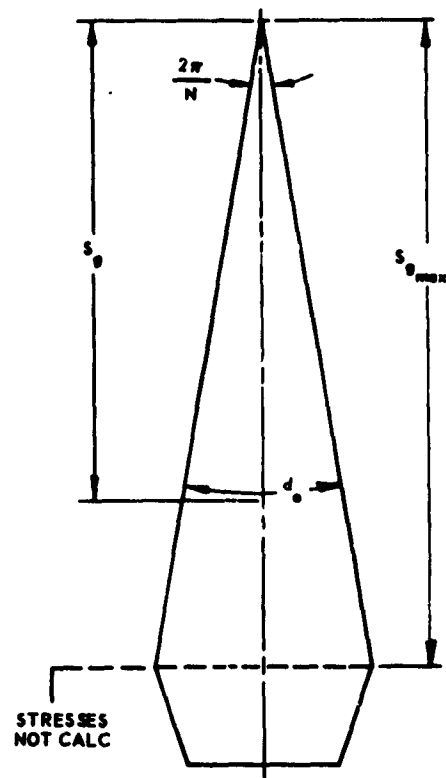


Fig. 4-104 Gore Pattern of T 10 Extended Skirt Parachute

β = Angle between gore centerline and cord measured from central axis in plane P_1 (Fig. 4-105).

$$(4-137) \quad b = r_o (1 - \cos \alpha_o)$$

$$(4-138) \quad a = 2 R_g \beta$$

where a = Length of arc resulting from intersection of plane P_1 with the surface of revolution formed by rotating the gore-centerline profile.

$$(4-139) \quad d_o = 2 r_o \alpha_o$$

where d_o = Length of arc resulting from intersection of plane P_1 with the surface of revolution formed by unextended inflated gore cloth.

While many types of canopies are "shaped" by incorporating unconventional gore patterns, canopies in their simplest form are composed of N triangular gores. Accordingly, this analysis will be limited to the simple triangular gore shape, although the concept is generally applicable to any gore shape. Considering this geometry and referring to Fig. 4-104, it is seen that

$$(4-140) \quad d_o = 2 S_g \frac{\pi}{N}$$

where S_g = Arc length measured on the gore-centerline profile.

From Fig. 4-106, it can be seen that

$$(4-141) \quad a = 2 x_g \frac{\pi}{N}$$

where x_g = Abcissa measured from the central axis of the canopy to a point on the gore-centerline profile.

Eq 4-135 through 4-141 can now be solved for b since there are seven independent relations involving the seven unknowns r_o , α_o , Z , b , β , d_o , and a .

It is most convenient to solve first for α_o and obtain

$$(4-142) \quad \sin \alpha_o = \left[\frac{\alpha_o R_g}{S_g (\pi/N)} + \cos \alpha - 1 \right] \tan \frac{x_g \pi/N}{R_g}$$

The final expression for b is

$$(4-143) \quad b = \frac{S_g (\pi/N)}{\alpha_o} \left[1 - \cos \alpha_o \right]$$

Eq 4-142 and 4-143 will be dimensionless if the terms they contain are dimensionless. Introducing the maximum inflated radius of the canopy $x_{g\max}$ the following non-dimensional terms can be written.

$$(4-144) \quad \begin{aligned} R_g^* &= R_g / x_{g\max} & S_g^* &= S_g / x_{g\max} \\ x_g^* &= x_g / x_{g\max} & b^* &= b / x_{g\max} \end{aligned}$$

Substituting these terms into Equations 4-142 and 4-143, one obtains

$$(4-145) \quad \sin \alpha_o = \left[\frac{\alpha_o R_g^*}{S_g^* (\pi/N)} + \cos \alpha_o - 1 \right] \tan \left(\frac{x_g^* \pi/N}{R_g^*} \right)$$

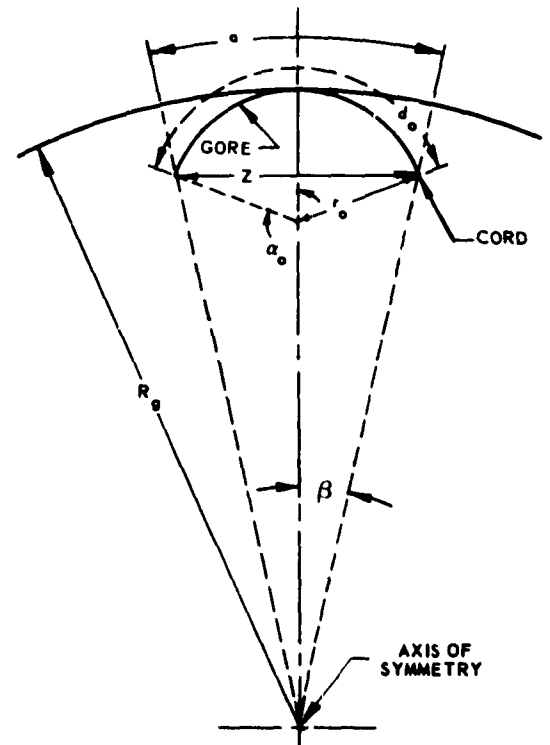


Fig. 4-105 Intersection of a Plane P_1 , with Inflated Gore

and

$$(4-146) \quad b^* = \frac{S_g^* \pi \cdot N}{\alpha_0} [1 - \cos \alpha_0]$$

In Eq 4-145 and 4-146, N is the number of gores in the canopy and S_g^* , x_g^* , and R_g^* are measured graphically from a gore-centerline profile as shown in Fig. 4-107. The profile of a cord is determined by calculating values of b^* along the gore centerline from the apex to the skirt. Mechanically, the value for b^* is found by means of an iteration process. This consists of choosing values of α_0 until the left- and right-hand sides of Eq 4-145 are equal, then substituting this value of α_0 into Eq 4-146 and solving for b^* .

With profiles of the gore centerline and the cord known, and with the assumption of circular arcs between adjacent cords, the tension in the cloth can now be calculated.

9.2 Cloth Stress as Function of the Gore Bulge and the Differential Pressure. If the meridian forces applied to the cloth are neglected, the circumferential tension in the canopy cloth can be calculated as simple hoop tension (Fig. 4-108). From the geometry of an element of the canopy surface

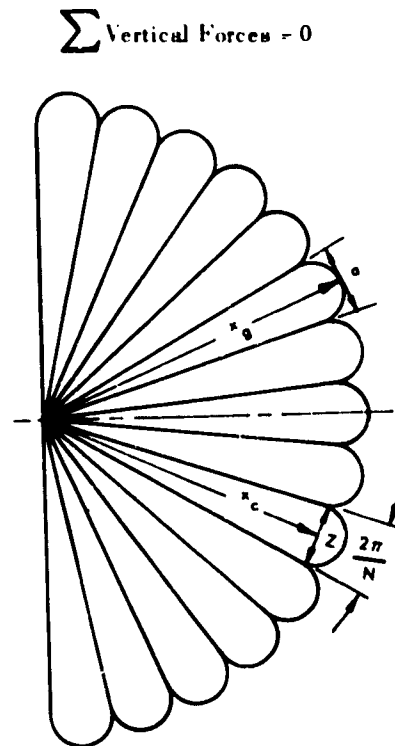


Fig. 4-106 Top View of Inflated Canopy

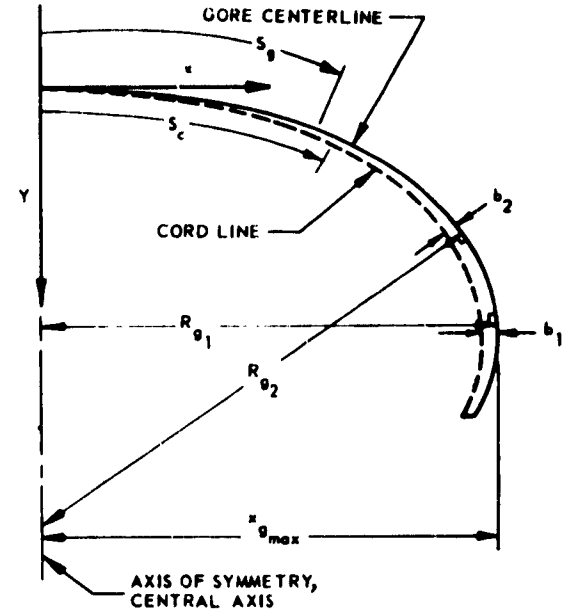


Fig. 4-107 Profile of a Canopy Formed by the Gore Centerline

$$(4-147) \quad \Delta P \cdot \Delta S_c \cdot 2r \sin \alpha - 2 T_h \cdot \Delta S_c \sin \alpha = 0$$

where ΔP = Differential pressure;

r = Bulge radius of stretch gore (Fig. 4-109);

α = Half angle of gore bulge measured in plane P_1 ; and

T_h = Stress existing in canopy cloth.

Performing simplifications, Eq 4-147 becomes

$$(4-148) \quad T_h = \Delta P(r)$$

Making the expression dimensionless, one obtains

$$(4-149) \quad T_h = \Delta P r^* x_{gmax}$$

By expressing r^* in terms of the geometric properties of the canopy and the elastic properties of the cloth, Eq 4-149 will give a solution for cloth stress.

When the strain of the cloth is considered, the inflated gore stretches from an initial width, d_0 , to a final width, d , and, as shown in Fig. 4-109, the bulge radius becomes r and the half angle of the gore bulge becomes α . From the geometry of Fig. 4-109

$$(4-150) \quad Z = 2 r \sin \alpha$$

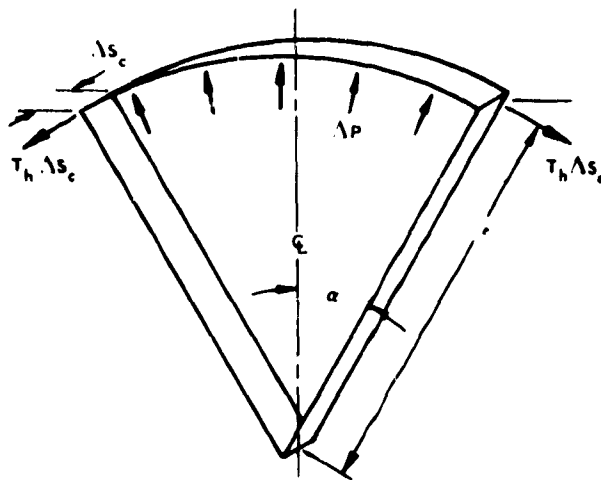


Fig. 4-108 Equilibrium of a Strip of a Canopy Gore

and

$$(4-151) \quad d = 2 r \alpha$$

From Fig. 4-106 it can be seen that

$$(4-152) \quad Z = 2 x_c \tan (\pi / N)$$

where x_c = Abcissa measured from the central axis of the canopy to a point on the cord-line profile.

Assuming perfect elasticity and considering Hooke's law, the stress in the canopy cloth may be established to be

$$(4-153) \quad T_h = E \epsilon$$

where E = Modulus of elasticity of the canopy cloth;
and

ϵ = Strain of canopy cloth.

$$(4-154) \quad d = d_o (1 + \epsilon)$$

It is well known, however, that the cloth used in the construction of canopies has a non-linear stress-strain relationship. In order that Eq 4-153 will remain valid, E may be taken in the first approximation as the ratio of the failure stress to the failure strain. If more accuracy is required, a second approximation to E may be found by dividing the stress calculated according to the first E by its strain.

Eq 4-148 and 4-150 through 4-154 may be solved for r since they make up seven independent relations in-

volving the seven unknowns d_o , T_h , r , d , α , Z , and ϵ .

$$(4-155) \quad x_c = \cot (\pi / N) r \sin \left[S_c \left(\frac{1}{r} + \frac{\Delta P}{E} \right) \tan \pi / N \right]$$

making this relationship dimensionless by again introducing the term $x_{g \max}$, the following is obtained

$$(4-156) \quad x_c^* = \cot (\pi / N) r^* \sin \left[S_c^* \left(\frac{1}{r^*} + \frac{\Delta P x_{g \max}}{E} \right) x \tan \frac{\pi}{N} \right]$$

In Eq 4-156, N is the number of gores and x_c^* and S_c^* are measured graphically from the cord-line profile as shown in Fig. 4-107. It is seen that r^* also depends upon a dimensionless parameter $\Delta P x_{g \max} / E$. For any particular value of this parameter, r^* may be found over the drag-producing surface of a canopy by means of an iteration process. Mechanically, this consists of choosing values of r^* until the left- and right-hand sides of Eq 4-156 are equal. Once r^* is known, the stress distribution can be found by means of Eq 4-149.

When the differential pressure over the drag-producing surface is assumed to be constant, the plot of bulge radius, r^* , versus location on the canopy, S_g^* , also represents a plot of the stress in the cloth versus the distance from that location along the gore

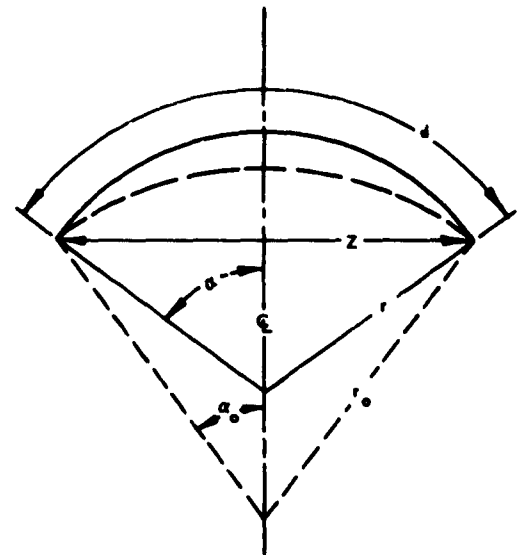
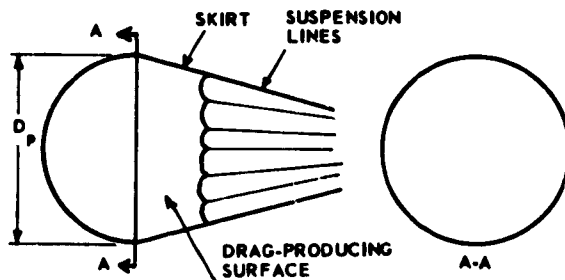


Fig. 4-109 Geometry of a Gore Section with Consideration of the Cloth Strain

centerline to the apex. If the differential pressure varies over the drag-producing surface, the value of the parameter must be calculated at each point under consideration in order to determine from the graph the correct bulge radius.

9.3 One Method of Stress Analysis. The method of stress analysis presented in the foregoing applies to a canopy which has attained a fully inflated free-flying shape. The mechanics of this method of stress analysis may be applied to the case of an inflating canopy also if sufficient empirical data is available. The data necessary include the pressure distribution over the canopy, the shape of the canopy during inflation, and a knowledge of the amount of material strain caused by the high differential-pressure experienced during the canopy-inflation period. This last parameter may be of such significance that the assumption of unextendible cloth utilized in calculating the cord-line profile may not be valid.

One method, reported in Ref (4-61), is being used to calculate the stress in the drag-producing surface of a canopy during the period of inflation, or more specifically at the time of maximum loading. This method is based upon the initial assumption of a generalized shape which the canopy tends to reach at the time of maximum loading or opening force. The generalized shape of a canopy at the time of maximum loading is shown in the following sketch.



The entire opening-shock load is now assumed to be acting upon the hemispherical portion of the drag producing surface from the vent to approximately Section A-A. The surface area of this portion of the drag producing surface will vary depending upon canopy type, canopy loading, canopy porosity, and degree of reefing, among other factors. The relationship between the constructed diameter of the canopy, D_c , and the diameter of the assumed hemisphere, D_p , may be written as

$$Y D_c = \frac{\pi D_p^2}{2}$$

$$D_p = \frac{2 Y D_c}{\pi}$$

where Y is the ratio of the length of the drag-producing surface over which the forces act to the constructed diameter of the canopy. The diameter of the hemisphere may now be solved in terms of the constructed diameter of the canopy from a closed condition ($Y = 0$) to a full open condition ($Y = 1.00$). These results are tabulated below.

Y	D_p/D_c	Y	D_p/D_c
0.01	0.00636	0.50	0.31800
0.05	0.03180	0.60	0.38200
0.10	0.06360	0.80	0.51000
0.20	0.12750	1.00	0.63600
0.40	0.25500		

With the above information, the stresses may be calculated in the hemispherical portion of the drag-producing surface for any open condition. Since this portion of the drag producing surface may be assumed to be a thin-walled hemisphere, the stress is calculated as:

$$S = \frac{P D_p}{4t}$$

where P is the pressure acting uniformly throughout the hemisphere and t is the thickness of the material. The resulting stress, S , is generally given in pounds per square inch. A common manner of terminology is to express the loading in pounds per inch of length of cloth. This gives

$$L = St = \frac{P D_p}{4}$$

where L is the load in pounds per inch.

The pressure acting inside the hemisphere is assumed to be equal to the opening-shock force, F_o , divided by the cross-sectional area of the hemisphere, resulting in the relationship

$$P = \frac{F_o}{S_p} = \frac{F_o}{\pi D_p^2/4} = \frac{4 F_o}{\pi D_p^2}$$

By substituting this equation into the previous one, the resulting relationship for the determination of the load per inch becomes

$$L = \frac{P D_p}{4} = \frac{4 F_o}{\pi D_p^2} \frac{D_p}{4} = \frac{F_o}{\pi D_p} = \frac{F_o}{2 Y D_c}$$

The load per inch may now be directly related to the flat constructed diameter of the canopy in terms of the ratio Y at the time of maximum loading. This

relationship gives the following values:

Y	$\frac{L}{F_o/D_c}$
0.01	50
0.05	10
0.10	5
0.20	2.5
0.40	1.25
0.50	1.00
0.60	0.834
0.80	0.625
1.00	0.500

The remaining step in analyzing the parachute canopy for loads is to relate the type of canopy being analyzed to the correct value of D_p at the point of maximum force. This may be obtained through photographic and force-time data of the canopy while the canopy is being deployed under actual or simulated use-conditions.

It should be pointed out that this method is considered applicable only for use in initial design of canopies. This analysis should not be considered as an established or final method for computing drag-producing surface stress during the period of inflation. Factors such as geometric and effective porosity and the elastic properties of various materials are important variables and were not considered. In addition, this method is only applicable to those canopies which inflate to a shape similar to that shown in the sketch.

SEC. 10 PRIMARY-BODY WAKE EFFECTS

The performance of aerodynamic deceleration devices is strongly dependent upon the aerodynamic flow field, since the function of the decelerator is to produce a retarding force by obstruction to or deflection of the air flow. Several additional and related factors combine to influence the flow field characteristics, including configurations of both the deceleration device and the vehicle to which it is attached; the location and position of the decelerator with respect to the suspended load; and atmospheric conditions, including pressure, density, and temperature.

In classical aerodynamics, the distribution of velocity and pressure in the wake (that region of reduced energy located downstream from an object which is moving through the air or has air moving past it) is of minor interest. Wakes must be classified

among the largely unsolved problems of fluid mechanics, particularly for supersonic free-stream conditions. One of the basic problems is the difficulty of solving the equations of fluid motion (Navier-Stokes) without the employment of gross approximations. Although approximations such as boundary-layer theory and nonviscous-flow theory have been extremely useful in fluid mechanics, wakes involve simultaneous interaction of an external viscous flow and an internal viscous flow, making the usual simplifying assumptions inapplicable. Furthermore, the case of most practical interest, the turbulent wake, involves a time-dependent transport mechanism about which very little is known.

In order to solve the problems of aerodynamic deceleration, in which a secondary body (the canopy) is deployed in the wake of a moving primary body (the suspended load) in order to reduce the velocity of both bodies through aerodynamic drag, knowledge of the general physical and aerodynamic characteristics of the wake region becomes very necessary. The turbulent wake of primary bodies moving through a fluid affects the inflation and drag-producing characteristics of the trailing or secondary body, in this case the aerodynamic decelerator. Since it is the objective of good decelerator-system design to utilize the most efficient system for the retardation of vehicles or payloads, the characteristics of the turbulent wake of the particular vehicle or payload must be known. Although an analytical approach to determine the pressure and velocity distribution in the primary-body wake, and to approximate the drag reduction of secondary bodies placed in a primary-body wake, have been developed for the subsonic free-stream case, wake characteristics, secondary-body drag-reduction, and overall primary-secondary body systems drag must be determined primarily in an empirical manner at the present time. The following discussion presents some analytical and empirical considerations of wake for subsonic, transonic, and supersonic free-stream conditions.

10.1 Subsonic Flow

10.1.1 THEORETICAL APPROACH FOR DETERMINING VELOCITY AND PRESSURE DISTRIBUTION IN WAKE OF PRIMARY BODIES OF REVOLUTION (Ref (4-62)). It is customary to present the turbulent wake as shown in Fig. 4-120 and 4-121. In considering the turbulent wake, it is necessary to distinguish between two cases: (1) one in which the undisturbed flow is at rest and the body moves with the velocity u_o , creating in its wake a turbulent flow with a varying velocity u which is less than the velocity of the moving body (Fig. 4-110), and (2) the case in which the body is at rest while the undisturbed fluid moves with the

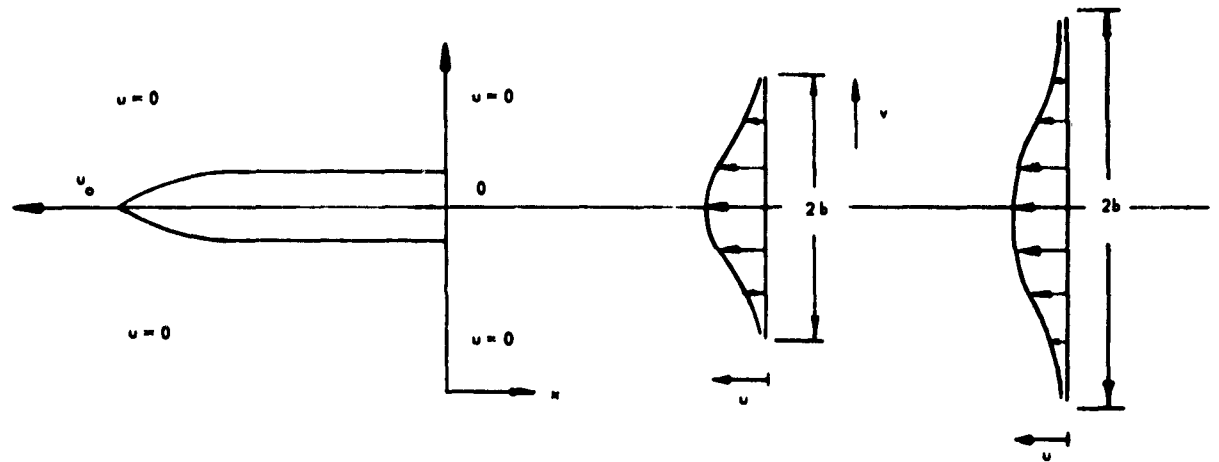


Fig. 4-110 Velocity Distribution for a Fluid at Rest and a Moving Body

velocity u_0 , with a varying velocity u' in the wake of the body (Fig. 4-111). Experience shows that as the distance behind the primary body increases, the area of the disturbed velocity increases while the difference between the free-stream and the disturbed velocity decreases.

10.1.1.1 Simplified Equation of Motion. Assume that a body of revolution is immersed in a fluid that is moving with velocity u_0 , while the body is held at rest, and a fixed longitudinal axis is arranged which coincides with the direction of the undisturbed flow (Fig. 4-110). At a given distance x behind the body, the components of the disturbed velocity in the x and y directions are $u' = u_0 - u$ and v , respectively. As is usual in boundary-layer phenomena, it may be assumed that the variation of the velocity perpendicular to the x -axis is large compared to that along the x -axis, and that the pressure gradient parallel to the x -axis may be neglected. Under these circumstances, the equation of continuity and the approximate differential equation of motion may be established as follows (Ref 4-63):

$$(4-157) \quad \frac{\partial}{\partial x} (yu) + \frac{\partial}{\partial y} (yv) = 0$$

$$(4-158) \quad (u_0 - u) \frac{\partial u}{\partial x} + v \frac{\partial u}{\partial y} = \frac{1}{y} \frac{\partial}{\partial y} \left[l^2 y \left(\frac{\partial u}{\partial y} \right)^2 \right]$$

The term

$$(4-159) \quad \rho l^2 \left(\frac{\partial u}{\partial y} \right)^2$$

is the so-called "apparent stress" or "Reynolds stress", while l in the term represents the mix-

ing distance. Using the condition of continuity and the fact that the aerodynamic drag of the body equals the loss of momentum in the turbulent wake,

$$(4-160) \quad \frac{\rho}{2} C_D S u_0^2 = 2\pi\rho \int_0^\infty (u^2 + u_0 u) y dy$$

in which the term

$$(4-161) \quad \frac{\rho}{2} C_D S u_0^2$$

is the conventional presentation of the aerodynamic drag of the body. Since the velocities u and v are small compared with u_0 , Eq 4-158 and 4-160 can be written as:

$$(4-162) \quad u_0 \frac{\partial u}{\partial x} = \frac{1}{y} \frac{\partial}{\partial y} \left[l^2 y \left(\frac{\partial u}{\partial y} \right)^2 \right]$$

and

$$(4-163) \quad \frac{\rho}{2} C_D S u_0^2 = 2\pi\rho \int_0^\infty u_0 u y dy$$

In cylindrical coordinates, Eq 4-163 is written as

$$(4-164) \quad \frac{\rho}{2} C_D S u_0^2 = 2\pi\rho \int_0^\infty u_0 u r dr$$

Replacing the term for apparent stress in conventional manner, (Ref 4-31)

$$(4-165) \quad l^2 \left(\frac{\partial u}{\partial y} \right)^2 = \kappa b (u_{\max} - u_{\min}) \frac{\partial u}{\partial y}$$

With $u_{\min} = 0$ and the derivation completed, Eq 4-162 may be written in cylindrical coordinates r and x as

$$(4-170) \quad \frac{\partial u}{\partial x} = -\frac{2}{3} \frac{A u_0}{x^{5/3}} (1 + S\eta^2) e^{S\eta^2}$$

and

Substituting these expressions into Eq 4-166 results in

and the velocity at the centerline

$$(4-172) \quad (1 + S\eta^2)(1 + 6\kappa KAS) = 0$$

which provides

$$(4-173) \quad S_1 = -\frac{1}{\eta^2}$$

and

$$(4-174) \quad S_2 = -\frac{1}{6\kappa KA}$$

Eq 4-169 may now be written as

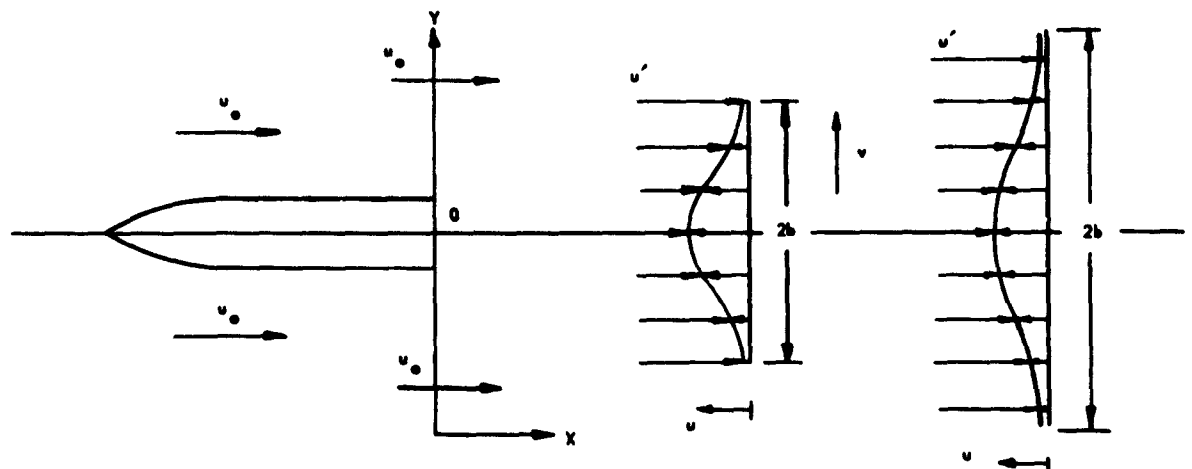


Fig. 4-111 Velocity Distribution for a Body at Rest and a Moving Fluid

$$(4-175) \quad u = \frac{A u_0}{x^{2/3}} (C_1 e^{-\frac{\eta^2}{6 \kappa K A}} + C_2 e^{-1})$$

The boundary conditions of the wake are $u = 0$ for $r = \infty$ and $u = u_{\max}$ for $r = 0$, from which the constants can be evaluated as $C_1 = 1$ and $C_2 = 0$. Therefore, the disturbing velocity amounts to

$$(4-176) \quad u = \frac{A u_0}{x^{2/3}} e^{-\frac{\eta^2}{6 \kappa K A}}$$

The velocity relationship presented in Eq 4-176 contains two unknown coefficients, A and K . For their determination only the drag equation 4-164 is available so far. The second condition may be taken from experimental data given in Ref (4-64) and those shown in Fig. 4-112. The analytical treatment by Swain (Ref 4-63) can be used to derive another condition for the determination of A and K for the purpose of comparing the validity of the entire treatment.

To make use of the experimental data, Eq 4-176 may be transformed into the form

$$(4-177) \quad \frac{u}{u_{\max}} = e^{-\frac{K(r')^2}{6 \kappa A}}$$

with the notation

$$(4-178) \quad r' = \frac{r}{K x^{1/3}} = \frac{r}{b}$$

Experiments show that the ratio of u/u_{\max} varies very little in the vicinity of the centerline, which particularly qualifies this region for numerical evaluation. Thus, the velocity ratio at a point with $r' = 0.1$ is chosen, which amounts to approximately $u/u_{\max} = 0.96$ (Ref (4-64) and Fig. 4-112). Therefore,

$$(4-179) \quad 0.96 = e^{-\frac{0.01 K}{6 \kappa A}}$$

which provides $K = 24.48 A \kappa$

Expressing the drag momentum Eq 4-164 in terms of the velocity as presented in Eq 4-177,

$$(4-180) \quad \frac{C_D S}{4\pi} = A K^2 \int_0^\infty e^{-\frac{K(r')^2}{6 \kappa A}} r' dr'$$

which after integration becomes

$$(4-181) \quad \frac{C_D S}{4\pi} = 3 A^2 K \kappa$$

Substituting the previously obtained value for K into this equation gives

$$(4-182) \quad C_D S = (12\pi) (24.48 A^3 \kappa^2)$$

$$\text{or} \quad A = 0.103 \left(\frac{C_D S}{\kappa^2} \right)^{1/3}$$

From Eq 4-179 and 4-182,

$$(4-183) \quad K = 2.52 (C_D S \kappa)^{1/3}$$

For the velocity distribution, Swain (Ref (4-63)) derived

$$(4-184) \quad \frac{u}{u_{\max}} = (\xi^{3/2} - 1)^2$$

in which $\xi = r/r_0 = r/b$, r_0 being the value of r at the edge of the wake.

The velocity ratio of the particular point at which $u = u_{\max}/2$ may now be considered, and the related coordinate called $\xi = \xi_m$.

This coordinate can be determined numerically from the relationship

$$(4-185) \quad u = \frac{u_{\max}}{2} = u_{\max} (\xi_m^{3/2} - 1)^2$$

which provides

$$(4-186) \quad \xi = 0.293^{2/3}$$

In the same manner, Eq 4-177 can be transformed by means of r_m as the coordinate at which $u = u_{\max}/2$:

$$(4-187) \quad u = \frac{u_{\max}}{2} = u_{\max} e^{-\frac{K r_m^2}{6 \kappa A}}$$

From this

$$(4-188) \quad r_m = (4.158 \frac{\kappa A}{K})^{1/2}$$

If it is assumed that both systems are correct, the values of ξ_m and r_m must be equal. Consequently,

$$(4-189) \quad (4.158 \frac{\kappa A}{K})^{1/2} = (0.293)^{2/3}$$

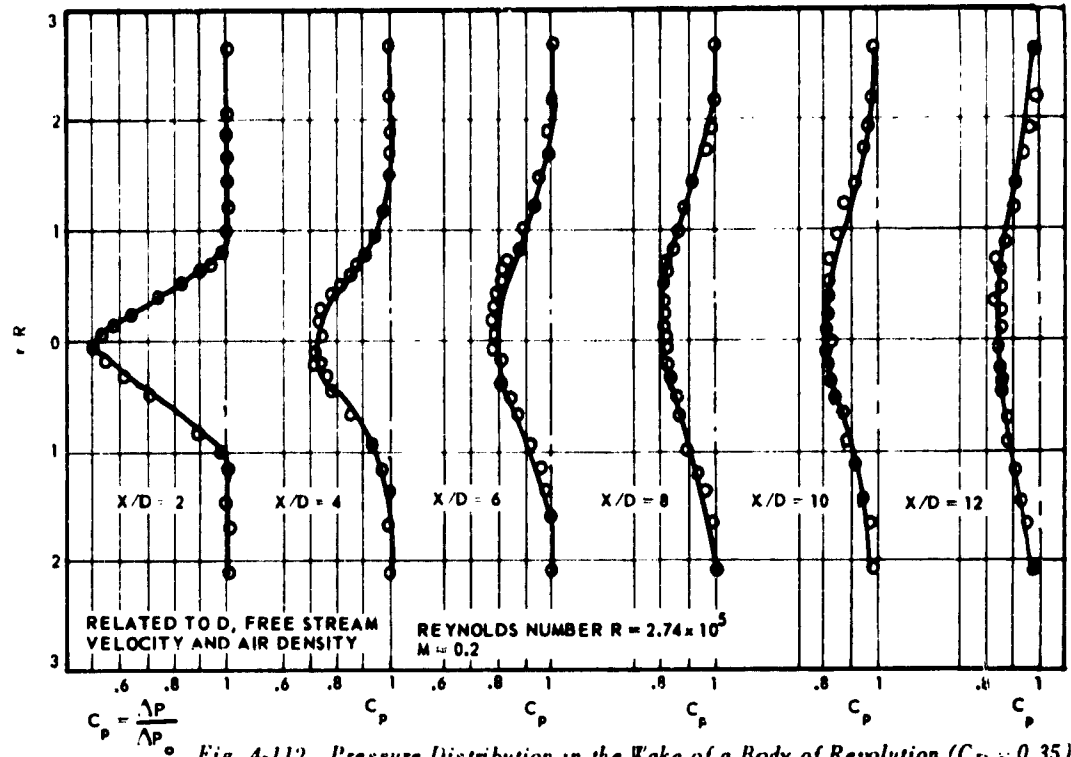
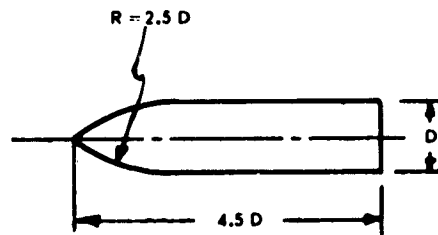


Fig. 4-112 Pressure Distribution in the Wake of a Body of Revolution ($C_D = 0.35$)



(For Fig. 4-112)

From which it follows that $A = 0.0468 K/\kappa$. Substituting 4 into Eq 4-181 provides

$$(4-190) \quad C_D S = 12 \pi (0.0468)^2 K^3 / \kappa$$

where

$$(4-191) \quad K = 2.3 (C_D S \kappa)^{1/3}$$

$$A = 0.107 (C_D S / \kappa^2)^{1/3}$$

and

The values of A and K which were obtained from experimental data (see Eq 4-182 and 4-183, and the re-

lated data derived from Swain's equation (Ref (4-63)) presented above agree very well. In view of the fact that the results from the experimental data as well as the ones derived from Swain's equation include certain assumptions, it appears to be justifiable to establish average values for A and K based on the two independent methods:

$$(4-192) \quad A = 0.105 (C_D S / \kappa^2)^{1/3}$$

$$K = 2.41 (C_D S \kappa)^{1/3}$$

These values shall be used in the further treatment of the wake problem.

The velocity equation Eq 4-176 presented, with $\eta = r/x^{1/3}$ and with expressions for A and K derived above, may now be written in the following form:

$$(4-193) \quad \frac{u}{u_0} = \frac{0.105}{x^{2/3}} (C_D S / \kappa^2)^{1/3} x - \frac{r^2}{1.525 (C_D S \kappa x)^{2/3}}$$

Eq 4-184 and 4-193 represent the local velocity in the turbulent wake. Judging from their structure, Eq 4-193 might offer an easier numerical process for solution,

and will be considered further. The first point is a comparison of the predictions of available theoretical methods with experimental results. For this purpose, the predictions represented by Eq 4-193 may be compared with those given by Swain's equation Eq 4-184, Goldstein's results obtained by means of "modified vorticity theory" (Ref (4-65)), and the mean experimental results obtained by Hall and Hislop (Ref (4-64)). For a convenient comparison, the quantity r_m or ξ_m may be introduced as defined before, and, from Eq 4-184 and 4-193

$$(4-194) \quad \frac{u}{u_{\max}} = \left[0.293 \left(\frac{\xi}{\xi_m} \right)^{3/2} - 1 \right]^2$$

and

$$(4-195) \quad \frac{u}{u_{\max}} = e^{-0.693 \left(\frac{r}{r_m} \right)^2}$$

Eq 4-194 and 4-195 represent the velocity ratio as functions of $r/r_m = \xi/\xi_m = Z$. The same process can also be applied to Goldstein's findings (Ref (4-65)) and to the experimental results of Hall and Hislop (Ref (4-64)). The results of this process are illustrated in Fig. 4-113; it can be seen that Eq 4-195 agrees better with the experimental values in the central portion, while Eq 4-194 is a better approximation in the outer portion of the wake.

In practical cases, the drag coefficient, C_D , is usually known, and the related area is generally given by $S = \pi D^2/4$, where D is the diameter of the body of revolution. In such a case, it is convenient to present Eq 4-193 in terms of C_D and D :

$$(4-196) \quad \frac{u}{u_o} = \frac{0.105}{(x/D)^{2/3}} \left(\frac{C_D \pi}{4 \kappa^2} \right)^{1/3} \times e^{-\frac{0.415 (r^*)^2}{(x/D)^{2/3} (C_D \pi \kappa)^{2/3}}}$$

where $r^* = 2r/D$.

Thus, the velocity in the wake of the body of revolution which moves with a velocity u_o through the fluid is given by Eq 4-196. If the fluid moves with the velocity u_o past the fixed body, the velocity of the fluid in the wake u' equals $u' = u_o - u$ and the ratio u'/u_o may be expressed by means of Eq 4-196 as:

$$(4-197) \quad \frac{u'}{u_o} = 1 - \frac{0.105}{(x/D)^{2/3}} \left(\frac{C_D \pi}{4 \kappa^2} \right)^{1/3} \times e^{-\frac{0.415 (r^*)^2}{(x/D)^{2/3} (C_D \pi \kappa)^{2/3}}}$$

10.1.1.3 *Determination of Pressure Distribution in the Wake.* In the calculation of the pressure distribution in the wake behind a primary body, for incompressible flow

$$(4-198) \quad \Delta P_o = P_{\text{tot}} - P_{s_o} = \frac{\rho}{2} u_o^2$$

and

$$(4-199) \quad \Delta P = P_t - P_s = \frac{\rho}{2} (u')^2$$

where P_{tot} = Total free-stream pressure;
 P_{s_o} = Free-stream static pressure;
 P_t = Total wake pressure; and
 P_s = Static pressure in the wake.

Thus,

$$(4-200) \quad C_p = \frac{P_t - P_s}{P_{\text{tot}} - P_{s_o}} = \frac{\Delta P}{\Delta P_o} = \left(\frac{u'}{u_o} \right)^2$$

or by substituting from Eq 4-197

$$(4-201) \quad \frac{\Delta P}{\Delta P_o} = \left[1 - \frac{0.105}{(x/D)^{2/3}} \left(\frac{C_D \pi}{4 \kappa^2} \right)^{1/3} \right]^2 \times e^{-\frac{0.415 (r^*)^2}{(x/D)^{2/3} (C_D \pi \kappa)^{2/3}}}$$

10.1.1.4 *Parameter κ .* Eq 4-196, 4-197, and 4-201 are expressions for the pressure and velocity distribution in the wake of the primary body; they contain the empirical parameter κ , which must be known for their solution. In order to evaluate the parameter κ , wind-tunnel tests were conducted to obtain pressure-distribution measurements at various distances in the wake of a cylindrical body with an ogive nose and a blunt tail at Mach number 0.2 (Ref (4-66)). The results are presented in Fig. 4-112. By utilizing Eq 4-201 and, for convenience, considering $\Delta P/\Delta P_o$ points on the longitudinal axis where $r^* = 0$,

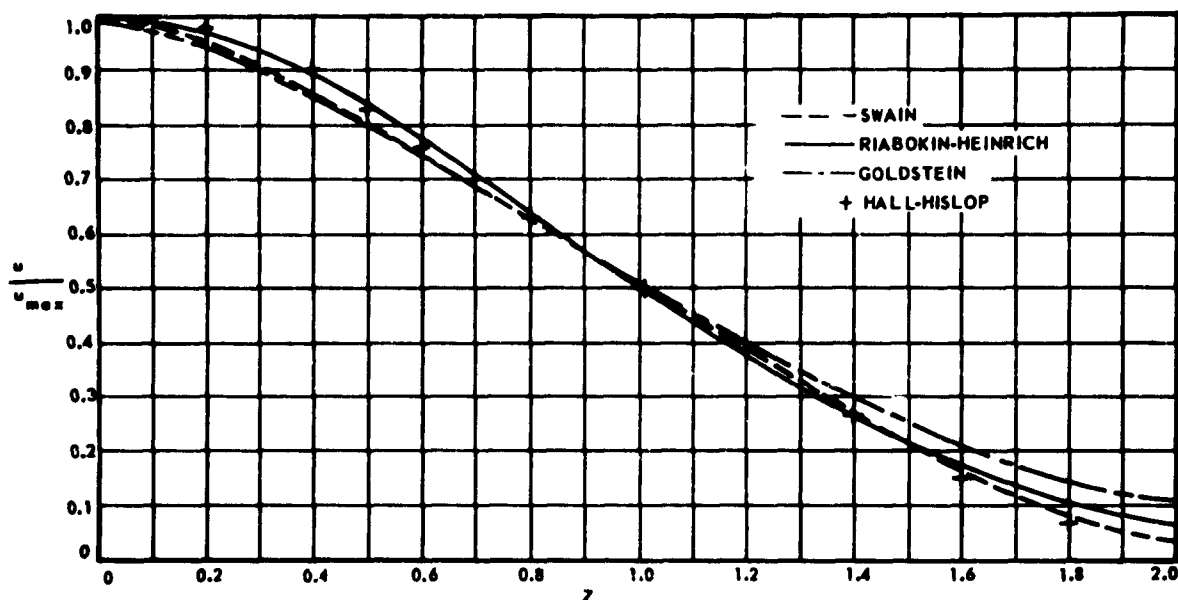


Fig. 4-113 Velocity Distribution in Accordance with Analytical and Experimental Studies

$$(4-202) \quad \frac{\Delta P}{\Delta P_o} = \left[1 - \frac{0.105}{(x/D)^{2/3}} \left(\frac{C_D \pi}{4\kappa^2} \right)^{1/3} \right]^2$$

Using the free-stream drag coefficient for the primary body of $C_D = 0.35$, and utilizing the experimental data given in Fig. 4-112, a value of κ corresponding to each value of x/D can be determined. The results of this calculation are presented in Fig. 4-114. It can be seen that the value of κ is not the same at every value of x/D , but does tend to level off at a value of 0.055 as x/D increases. Because the theory is based upon the assumption that κ is a constant, the experimental results should be compared with those predicted by the theory. This may be done by calculating the theoretical pressure-distribution at each x/D value by substituting an average value of κ in Eq 4-202. The average value of κ from Fig. 4-114 is $\kappa = 0.063$, which corresponds to $\Delta P/\Delta P_o$ at $x/D = 8$.

It can be seen from Fig. 4-115 that the pressure distribution which was calculated is in good agreement with the theoretical curves, except at the x/D stations near the primary body. This discrepancy can be explained by the fact that pressure equilibrium has not been reached in the wake near the primary body. It appears that the accuracy of a constant κ depends on how rapidly pressure equilibrium is obtained in the wake; this would make κ a function of the primary-body shape. In order to validate this conclusion, tests were conducted (Ref (4-67)) to obtain κ values for bodies of various shapes. Fig. 4-116 shows the geometrical dimensions of the bodies of revolution tested.

The results of these tests are shown in Fig. 4-117. For a certain class of bodies in the low drag-coefficient range, the value of κ remains essentially constant throughout the entire range of x/D values. On the other hand, those bodies in a higher C_D range produce κ values which are not constant until x/D values of 10 are reached. It is the goal of further research work to arrive at a parameter, such as either primary body shape or C_D , which would provide a relationship of κ to x/D for bodies of revolution.

10.1.2 DRAG REDUCTION ON A SECONDARY BODY DUE TO WAKE OF A PRIMARY BODY. According to classical hydrodynamic theory, it can be shown that, for axially symmetric primary and secondary bodies disposed along the same axis, the pressure on the secondary body depends on the flow characteristic along the line of symmetry only, provided that the wake velocity profile is assumed to be axially symmetric. This theory however, is limited by the assumptions of classical hydrodynamic theory which do not account for drag (d' Alembert's Paradox). However, since the drag is influenced largely by the pressure distribution on the first part of the body, it may be assumed that for the case where the primary and secondary bodies are fixed and the air moves past them

$$(4-203) \quad \frac{D}{D_\infty} \propto \left(\frac{u'}{u_\infty} \right)^2 = 0$$

That is the ratio of the drag in the wake to the free-stream drag is proportional to the square of the velo-

city ratio, where u' is the reduced centerline wake velocity and u_∞ the upstream undisturbed velocity. Thus the drag coefficient of the body in the wake can be expressed by

$$(4-204) \quad C_D = C_{D_\infty} \left(\frac{u'}{u_\infty} \right)^2 \quad r = 0$$

Use of this assumption however gives drag coefficients consistently too low for all L/D_1 and D_1/D_2 ratios, as shown in Fig. 4-118. Attempts at arriving at an empirical equation which would give C_D values in good agreement with experimental data have resulted in the relation

$$(4-205) \quad C_D = C_{D_\infty} \left(\frac{u'}{u_\infty} \right)^2 \quad r = 0$$

which gives reasonable agreement over a wide range of L/D_1 and D_1/D_2 ratios as shown in Fig. 4-119. The variations are greatest at low L/D_1 values, i.e., close to the primary body. For L/D_1 values between 2 and 15, the maximum variation between the experimental results and the empirical formula is about 20 per cent for a ratio of primary to secondary body-diameter of 1:3 and $L/D_1 = 2$. The variations are appreciably less for larger L/D_1 ratios. This simple formula (Eq 4-205) does not take into consideration the size of the secondary bodies relative to the size of the primary one; therefore, the formula gives results

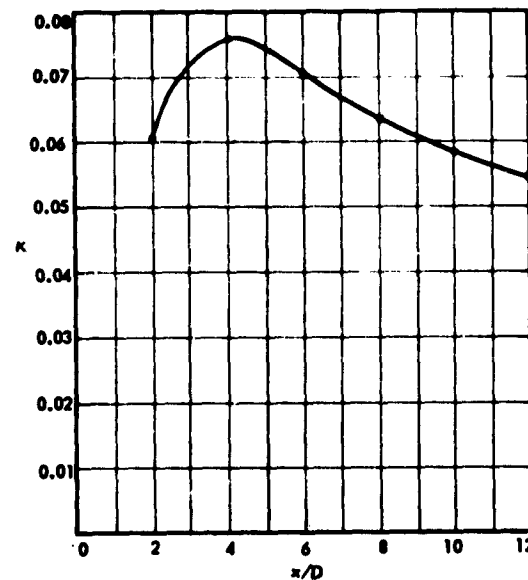


Fig. 4-114 κ vs x/D as Determined From Experimental Data

that are satisfactory for $D_1/D_2 = 1/2$ and $1/3$, but numerical values are somewhat high for $D_1/D_2 = 1$. The expression

$$(4-206) \quad C_D = C_{D_\infty} \left(\frac{u'}{u_\infty} \right)^{1.32} \quad r = 0$$

predicts the drag variation for the 1:1-ratio bodies more accurately.

In order to express Eq 4-205 as a function of L/D_1 , the expression for the velocity ratio as shown by Eq 4-193 is used. Substituting Eq 4-197 into Eq 4-206 gives

$$(4-207) \quad \frac{C_D}{C_{D_\infty}} = \left[1 - \frac{0.105}{(x/D)^{2/3}} \left(\frac{C_{D_\infty}}{4\kappa^2} \right)^{1/3} \right] \times e^{-\frac{0.415(r^*)^2}{(x/D)^{2/3} (C_{D_\infty} \kappa^2)^{2/3}}}$$

Since only the flow characteristics along the wake centerline are of interest, $r^* = 0$. Therefore,

$$(4-208) \quad \frac{C_D}{C_{D_\infty}} = \left[1 - \frac{0.105}{(x/D)^{2/3}} \left(\frac{C_{D_\infty}}{4\kappa^2} \right)^{1/3} \right]_{r=0}$$

This equation expresses the drag coefficient of a secondary body in the wake of a primary body in terms which can be determined empirically by means of available data. It should be remembered, however, that the expression may not give results comparable to experimental data if the drag coefficient of the secondary body being investigated is known to vary near the Reynolds number of the particular operation of the primary-body decelerator system.

10.2 Transonic and Supersonic Wake

10.2.1 WAKE BEHIND BODIES OF REVOLUTION.

The airflow around the base and in the wake of a body of revolution is illustrated in Fig. 4-120. At some distance aft of the base of the body, the cross-sectional area of the wake "necks down" so that a shape is formed that is approximately conical. The height of this cone appears to vary with Mach number, but is of the order of magnitude of the body-base diameter. In general, it can be said that the supersonic wake is determined by this "critical region" where the streamlines from the sides of the body converge (Ref (4-68)). The angle at which the streamlines converge is determined by a shock-wave boundary-layer type of interaction. In this interaction the streamlines assume the maximum expansion angle for which the boundary

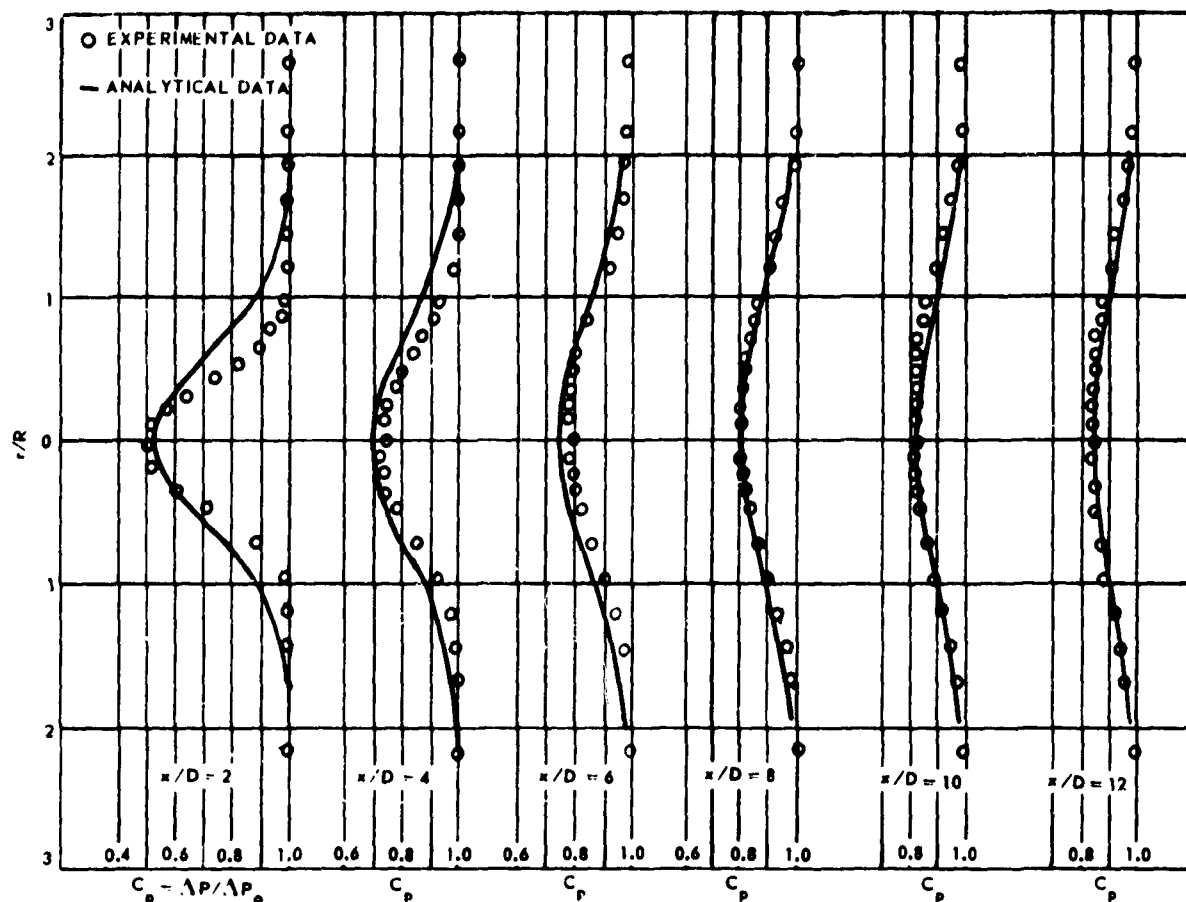
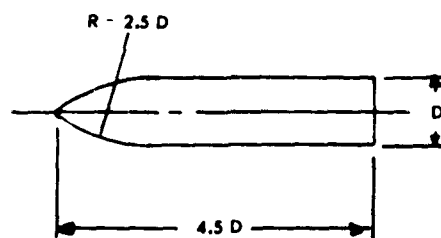


Fig. 4-115 Data for a Body of Revolution (Based on $\kappa = 0.0633$ Related to C_p at $x/D = 8$)

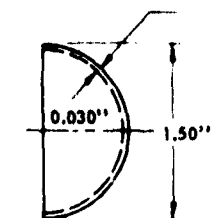


(For Fig. 4-115)

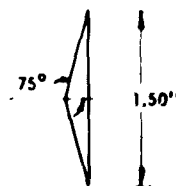
layer flow has sufficient energy to negotiate the pressure rise that results from the recompression at the convergence point.

Immediately behind the base of the body, and bounded by the converging streamlines, there is a region sometimes characterized as the still or "dead air" region. There are, however, definite indications of reverse-flow conditions in this so-called "dead air" region aft of the body base. For a two-dimensional case, it has been shown experimentally that the re-

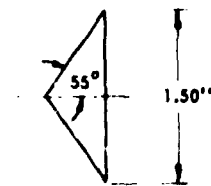
circulation velocity is very small. Behind a three-dimensional body of revolution, however, the recompression no longer takes place according to a simple function such as the Prandtl-Meyer expansion for two-dimensional flow. The boundaries of the dead-air region are thus no longer at constant pressure. A positive pressure-gradient exists in this region, allowing a subsonic reverse-flow jet for subsonic portions of the boundary-layer flow. Since only part of the boundary-layer flow is subsonic and the recompression pressure-coefficients appear to decrease with increasing Mach number (Ref (4-69)), it is suspected that the effect of the reverse flow will diminish with increasing Mach number. Indications of substantial reverse-flow in the wake of a three-dimensional body have been shown in wind-tunnel tests (Ref (4-70)). The prime significance of these experimental data is that they verify the existence of a reverse flow at low supersonic free-stream velocities. For a free-stream Mach number of 1.2, this reverse-flow region extends for approximately two body-base diameters aft of the body base.



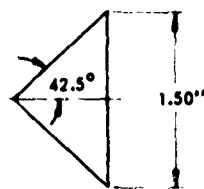
MODEL A
HOLLOW HEMISPHERE
(OPEN TO FLOW)
 $C_D = 1.40$



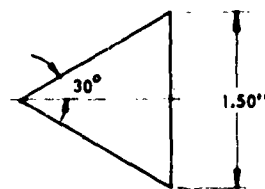
MODEL B
CONE
 $C_D = 1.03$



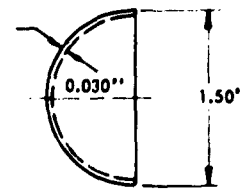
MODEL C
CONE
 $C_D = 0.836$



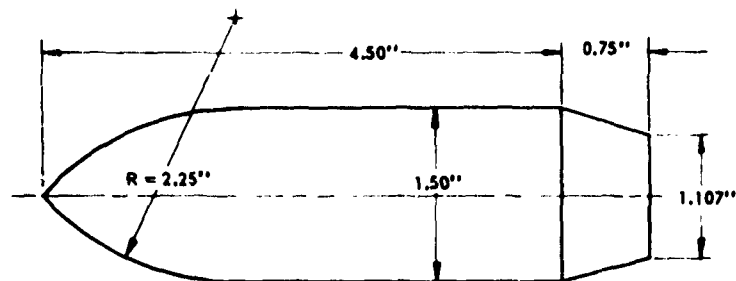
MODEL D
CONE
 $C_D = 0.743$



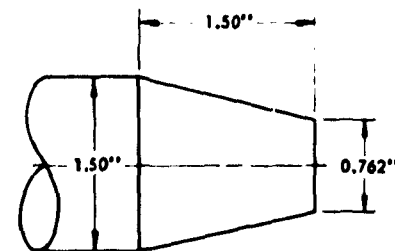
MODEL E
CONE
 $C_D = 0.577$



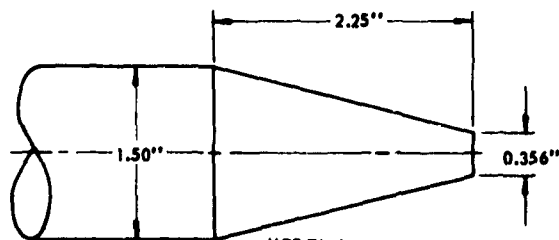
MODEL F
HOLLOW HEMISPHERE
(CLOSED TO FLOW)
 $C_D = 0.425$



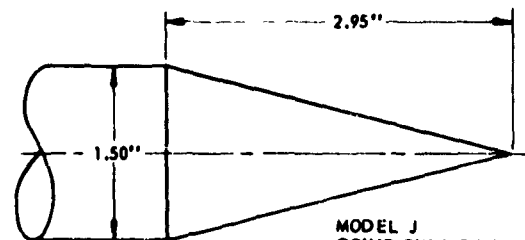
MODEL G
OGIVE CYLINDER WITH
AFTER BODY NO. 1
 $C_D = 0.230$



MODEL H
OGIVE CYLINDER WITH
AFTER BODY NO. 2
 $C_D = 0.206$



MODEL I
OGIVE CYLINDER WITH
AFTER BODY NO. 3
 $C_D = 0.197$



MODEL J
OGIVE CYLINDER WITH
AFTER BODY NO. 4
 $C_D = 0.194$

Fig. 4-116 Bodies of Revolution

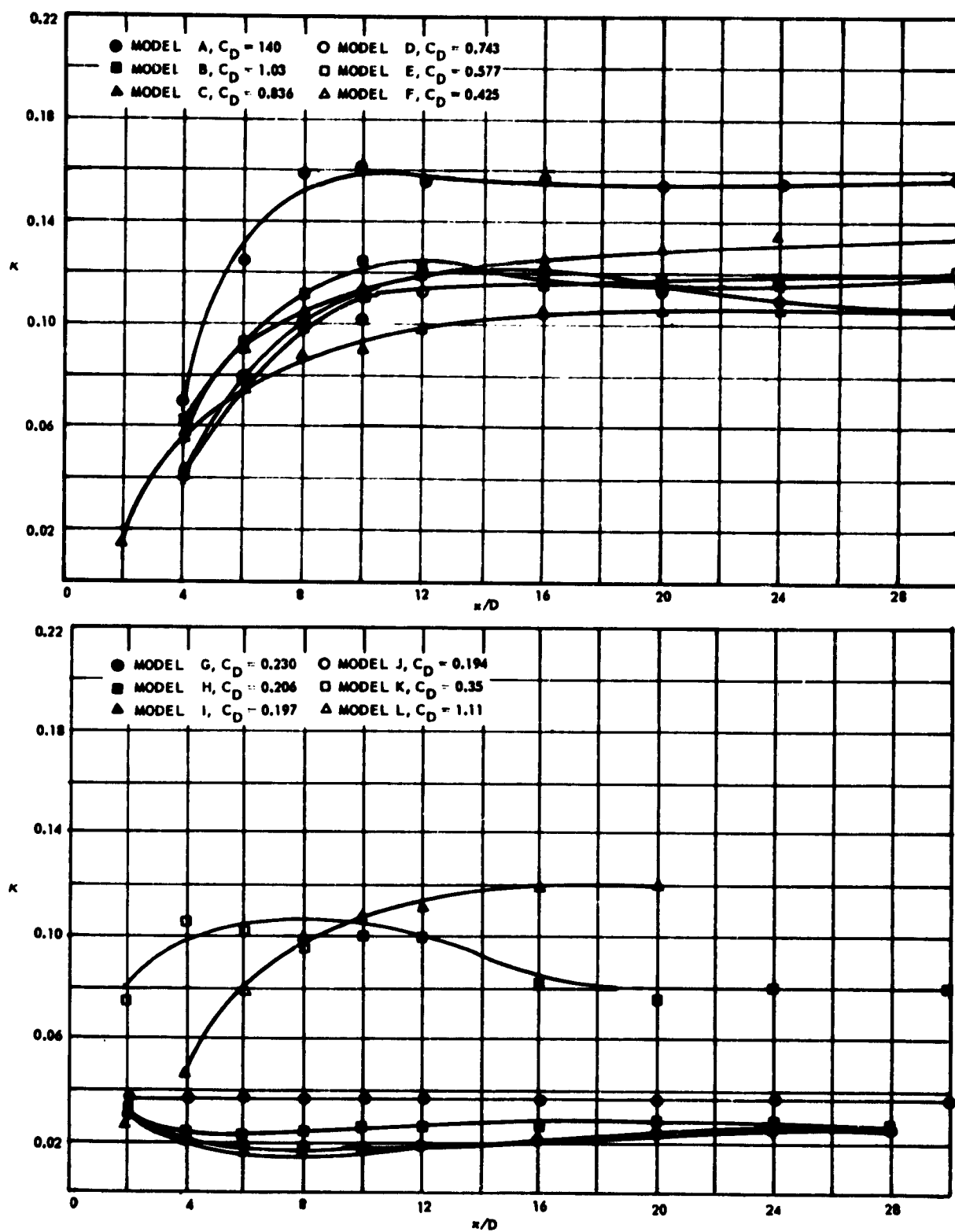


Fig. 4-117 κ vs x/D as Determined by Experiment

Behind the dead-air region, the supersonic wake spreads in a manner similar to an incompressible wake, such that the width increases approximately with distance to the one-third power. Behind the neck or throat of the wake, the wake core appears to maintain an essentially constant width except for occasional irregularities due to vortices, and is generally similar to a subsonic wake. The primary source of airflow in the wake consists of boundary-layer air, which expands from an annulus at the base of the body to fill the throat area. The main stream turns through the angle α at the vicinity of the wake throat, with resulting compression and formation of the trailing shock. This shock generally appears to form at an angle nearly equal to that of the bow shock.

10.2.2 SUPERSONIC WAKE PREDICTION. A discussion of the wake behind primary bodies in supersonic free-stream can be divided into two general regions of interest: (1) the region of recirculation, which is the region between the base of the primary body and the location in the wake where the minimum thickness of the wake core occurs (this location will be referred to as the wake-core throat; it should not be confused with the sonic-point location within the wake, which is about 1.9 body-base diameters behind the base); (2) the region aft of the wake-core throat, commonly called the "spreading downstream wake".

10.2.2.1 Recirculation Region. The magnitude of the reverse-flow subsonic jet between the base of the primary body and the wake-core throat is largely a function of the recompression pressure; hence, the determination of this quantity is of major importance. Based upon the rather limited data available (Ref (4-62), (4-69), and (4-70)), it is reasonable to assume for calculation purposes that the wake-core throat location is between 1.70 and 1.75 calibers aft of the primary-body base, and that the maximum recompression pressure occurs 0.25 caliber aft of this wake-core throat and is independent of Mach number. The value of the maximum recompression pressure-coefficient as a function of Mach number has been obtained by fitting an exponential equation to experimentally obtained pressure-coefficient data. The equation arrived at is

$$(4-209) \quad C_{p_{\max}} = e^{\left[\frac{0.335}{(M + 0.35)^{2.42}} \right] - 1}$$

where M = Free-stream Mach number.

To obtain a representation of the variation of static pressure with distance aft of the primary-body base to the wake-core throat, as a function of longitudinal

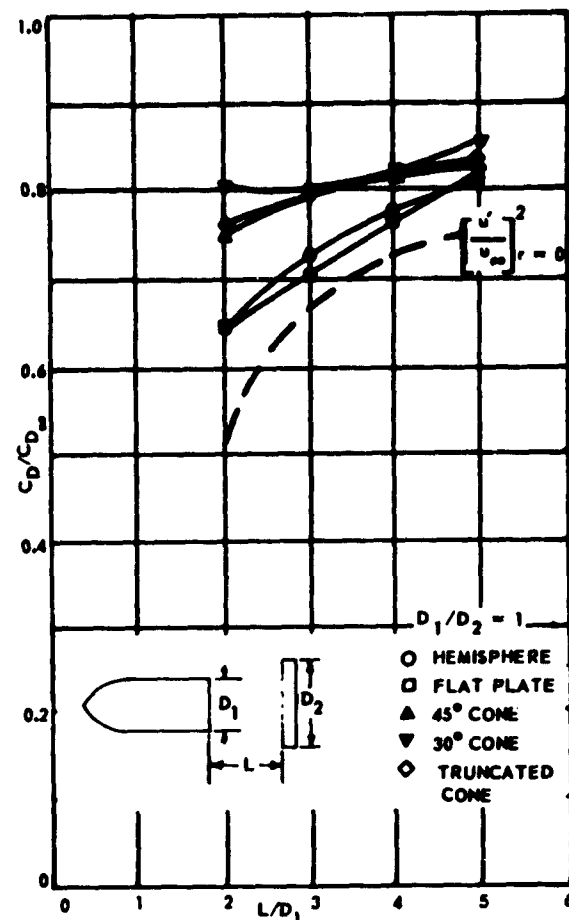


Fig. 4-118a Wake Drag Coefficient Ratio

distance and Mach number, the following general equation may be used:

$$(4-210) \quad C_{p_{\text{static}}} = \frac{\frac{x_0}{d} + A}{B\left(\frac{x_0}{d}\right)^2 + C\left(\frac{x_0}{d}\right) + D}$$

$$\text{where } \frac{x_0}{d} = \left(\frac{x}{d} - 0.5\right);$$

$\frac{x}{d}$ = Distance in calibers aft of the base of the body; and

$$C_{p_{\text{static}}} = \text{Static pressure coefficient} = \frac{(P_w - P_\infty)/q_\infty}{(P_w - P_\infty)/q_\infty}$$

To solve for the four unknowns, four equations are needed, using the following information:

(1) The value of the base pressure; i.e., the pressure at $x/d = 0$ (yields the ratio of A/D);

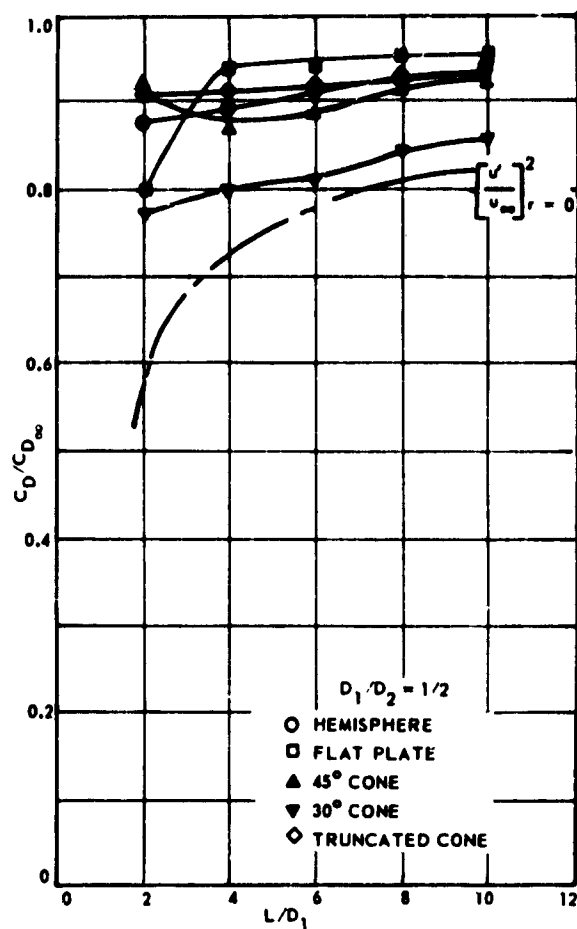


Fig. 4-118b Wake Drag Coefficient Ratio

(2) The location of zero pressure-coefficient (yields $D = A + \text{constant}$);

(3) The location of maximum recompression pressure-coefficient (yields B as a function of C by equating $\partial C_{p_{\text{static}}} / \partial (x_0/d)$ to zero); and

(4) The location and value of the maximum recompression pressure-coefficient (yields A as a function of B , C , and D).

Using the value of the maximum recompression coefficient given by Eq 4-209 and its location of 0.25 caliber aft of the wake-core throat, only (1) and (2) need be measured to determine uniquely the four constants A , B , C , and D .

10.2.2.2 The Spreading Downstream Wake. For practical purposes only the turbulent downstream wake-core need be considered, since the downstream laminar wake core becomes unsteady or turbulent at very low Reynolds numbers. Solution of the momentum equation for distances far from the body (where the velocity defect is small compared with the free-stream velocity)

results in asymptotic velocity profiles, all similar to a simple "universal" velocity profile. Further, dimensional analysis specifies the following conditions for velocity and wake-core width:

$$\begin{aligned} v_{\text{max}} &= v_{\text{centerline}} \\ (4-211) \quad v_{\text{centerline}} &= x^{-N} \\ n_0 &= x^{1-N} \end{aligned}$$

where $N = 2/3$, for three-dimensional axisymmetric flow;

$N = 1/2$, for two-dimensional flow;

v = Velocity defect in the wake;

x = Coordinate in the free-stream direction (origin is at point at which separation begins); and

n_0 = Wake width.

Using Prandtl's mixing-length theory for turbulent momentum transfer and assuming the mixing length to be constant across the width of the wake core and proportional to the width, the following expression for velocity (defect) distribution results:

$$(4-212) \quad \frac{v}{v_{\text{max}}} = \left[1 - \left(\frac{n}{n_0} \right)^{3/2} \right]^2$$

This is a rather good approximation for the wake-velocity profile, and may be readily integrated to give the average velocity defect in the axisymmetric case, letting $\mu = n/n_0$.

$$(4-213) \quad \frac{v_{\text{av}}}{v_{\text{max}}} = \frac{2\pi \int_0^1 (1 - \mu^{3/2})^2 \mu d\mu}{2\pi \int_0^1 \mu d\mu} = 0.257$$

To describe the properties of the wake core downstream of the wake-core throat, an equation describing the average velocity must be obtained by fitting it to empirical data such as those obtained by Chapman (Ref (4-71)). The generally accepted equation is:

$$(4-214) \quad \frac{v_w}{v_\infty} = \frac{1 - 0.684 \left(\frac{v_{\text{av}}}{v_{\text{max}}} \right)}{\left(\frac{x}{d} \right) - \left(\frac{x_1}{d} \right)^{2/3}}$$

where $x_L/d = x_T/d = (0.684)^{3/2}$;

v_w = Average velocity in the wake as determined by the value of μ chosen;

$v_{av} v_{max}$ = Nondimensional velocity-defect ratio dependent on value of μ

x = Axial distance from vehicle base;

x_T = Wake-throat distance from vehicle base; and

d = Diameter of primary body.

After the average velocity in the wake core is obtained as a function of distance, the average wake static temperature may be found by assuming constant enthalpy and free-stream static pressure to exist aft of the throat:

$$(4-215) \quad \frac{T_{wake}}{T_\infty} = 1 - \frac{\gamma-1}{2} M_\infty^2 - \frac{\gamma-1}{2} M_\infty^2 \left(\frac{v_w}{v_\infty} \right)^2$$

where T_{wake} = Average static temperature within the wake;

T_∞ = Free-stream static temperature;

γ = Ratio of specific heats (1.4 for air);

M_∞ = Free-stream Mach number;

v_w = Average wake velocity; and

v_∞ = Free-stream velocity.

The average wake-core Mach number, density, and dynamic pressure within the wake can then be obtained immediately:

$$(4-216) \quad M_{wake_{av}} = \frac{v_w}{v_\infty} \sqrt{\frac{T_\infty}{T_{wake}}} M_\infty$$

$$(4-217) \quad \rho_{wake} = \frac{\rho_\infty T_\infty}{T_{wake}}$$

$$(4-218) \quad q_{wake} = q_\infty \left(\frac{\rho_{wake}}{\rho_\infty} \right) \left(\frac{v_w}{v_\infty} \right)^2$$

10.2.3 DRAG REDUCTION OF SECONDARY BODIES IN THE WAKE OF PRIMARY BODIES. A body moving through the air, or with air flowing past it, generates a region of low-energy flow behind it, i.e., a total pressure less than that of free stream. It would then be expected that a body placed in this lower-energy flow field will produce less drag than it would if placed in the higher-energy free stream. Experimental investigations have been conducted to validate this prediction (Ref (4-67)). During these investigations, the stagnation pressure and drag coefficients of various aerodynamic decelerator shapes were determined in free stream and behind two different primary-body shapes, an ogive cylinder with blunt end and a skirted hemisphere-cylindrical body. The primary-body shapes

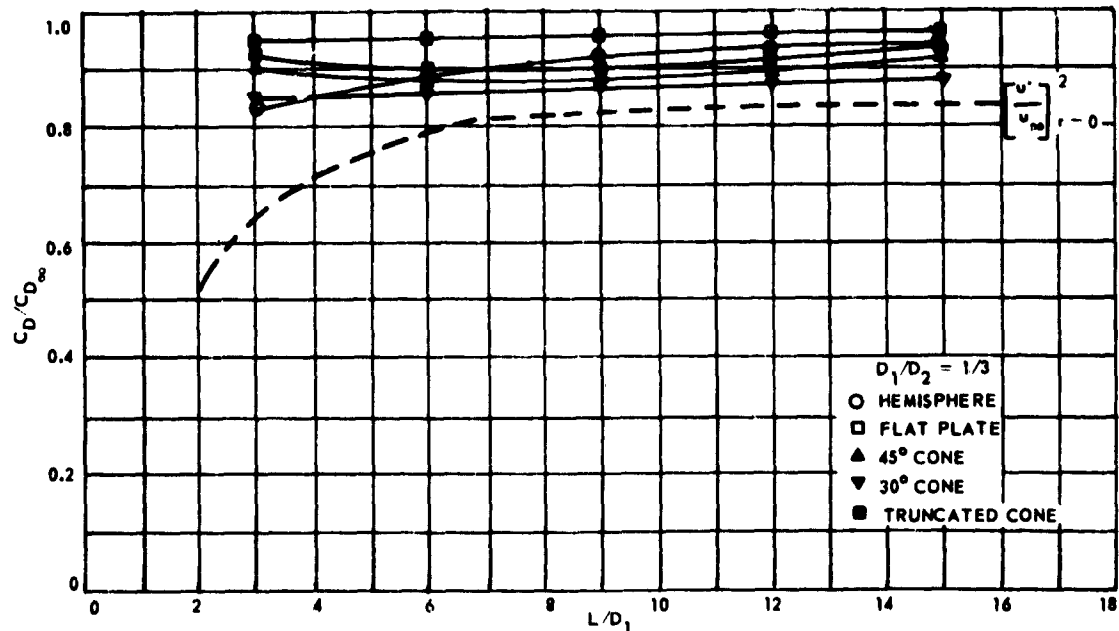


Fig. 4-118c Wake Drag Coefficient Ratio

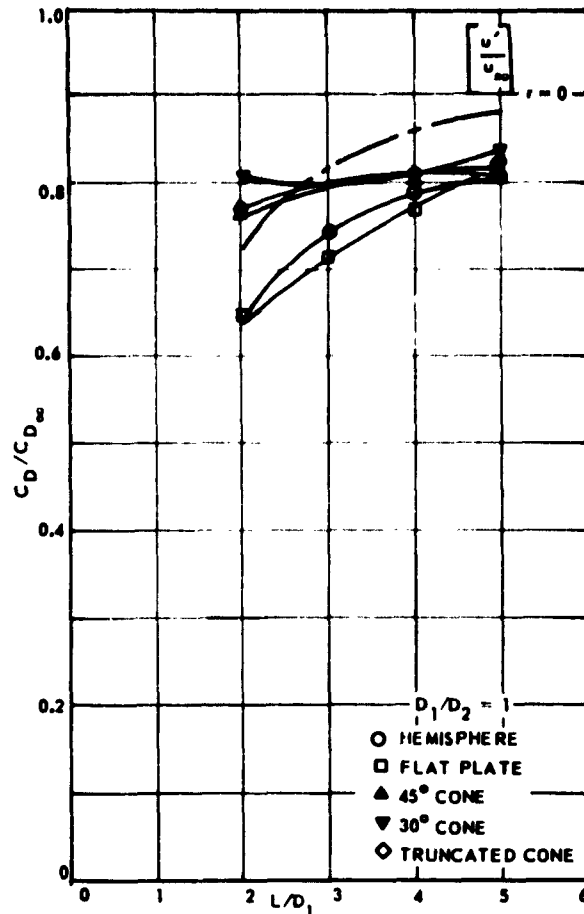


Fig. 4-119a Wake Drag Coefficient Ratio

and associated flow fields are shown in Fig. 4-121. In general, the results of this investigation substantiate the trend previously predicted.

Examples of the magnitude of stagnation pressure-coefficient reduction are indicated in Fig. 4-122 and 4-123. It is seen that for a flat plate placed close behind a cylinder, the reduction in stagnation pressure-coefficient is as much as 90 per cent. However, as the secondary body is moved further down stream where the energy of the flow increases, the stagnation pressure-coefficient increases and approaches the free-stream value. Similarly, Fig. 4-124 shows the reduction of the drag coefficient of a flat plate in the wake of an ogive cylinder. Again, it can be seen that as the body is placed further away from the primary body, the drag coefficient approaches its free-stream value. It can also be noted that for both the pressure and drag-coefficients, the larger the secondary-body diameter, the less pronounced is the effect of the wake on the secondary body. The effects shown are characteristic of the general trend of these coefficients on a body of any shape in the wake of a primary body

of any shape.

10.2.4 SYSTEM DRAG. The presence of a secondary body in the wake field of a primary body immersed in a supersonic free-stream affects the pressure distribution at the base of the primary body. This phenomenon is due to the pressure recovery associated with the flow-velocity decrease in the area of the secondary body. Since the boundary of the wake is not rigid in this area, the pressure inside the wake rises to a value equal to the external pressure in order to alleviate any pressure gradients perpendicular to the flow direction, as illustrated in Fig. 4-125. This, then, establishes a pressure gradient in the longitudinal direction in the subsonic portions of the wake core which causes a pressure and velocity feedback through this portion of the wake. The greater pressure and the direction of this velocity impart a total pressure that significantly increase the base pressure.

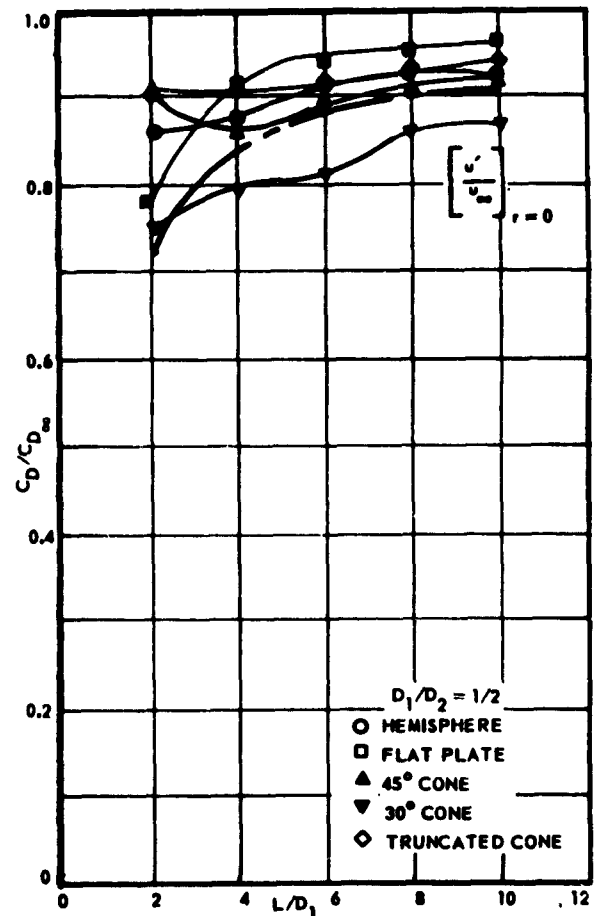


Fig. 4-119b Wake Drag Coefficient Ratio

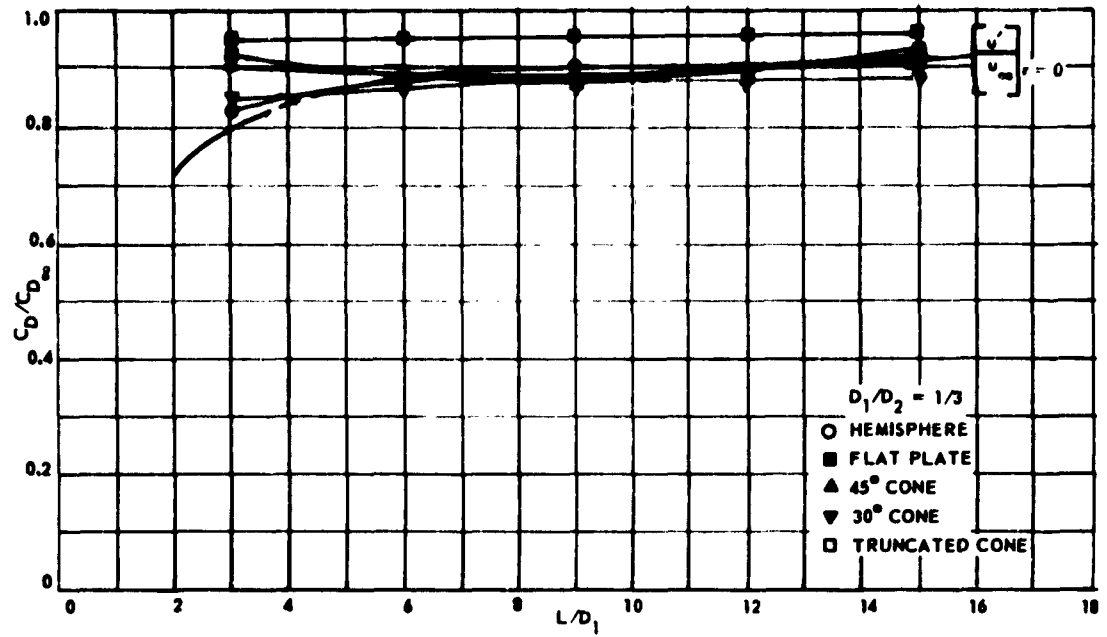


Fig. 4-119c Wake Drag Coefficient Ratio

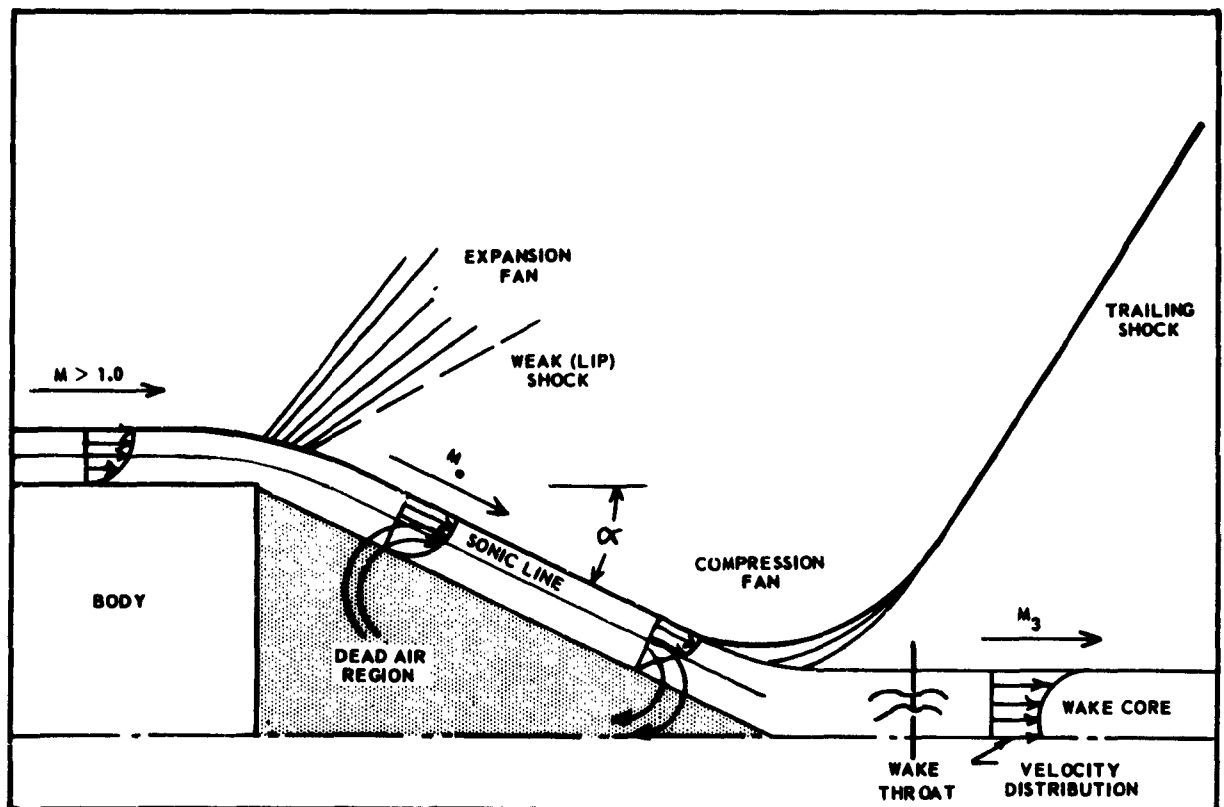
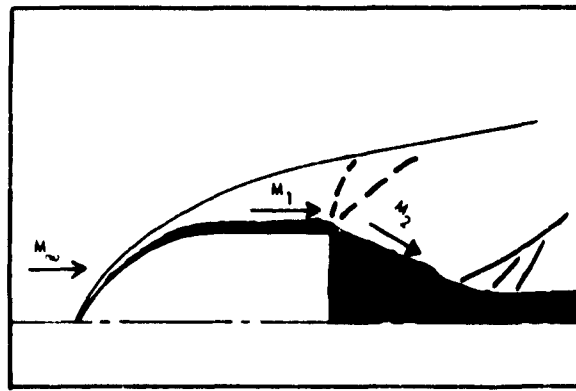
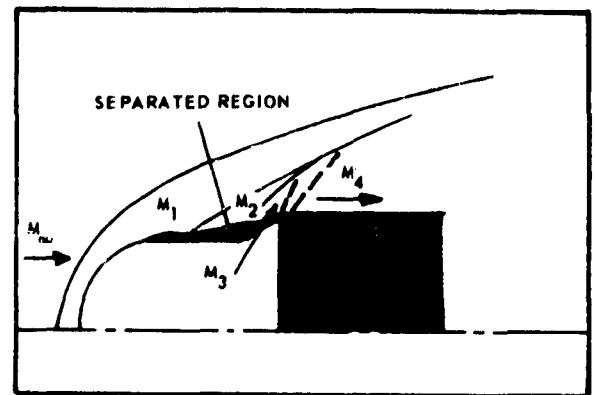


Fig. 4-120 Schematic Diagram of Wake Structure



OGIVE - CYLINDER PRIMARY BODY



SKIRTED - BLUNT PRIMARY BODY

Fig. 4-121 Sketch of Flow Patterns Around Primary Bodies Alone at Supersonic Speeds

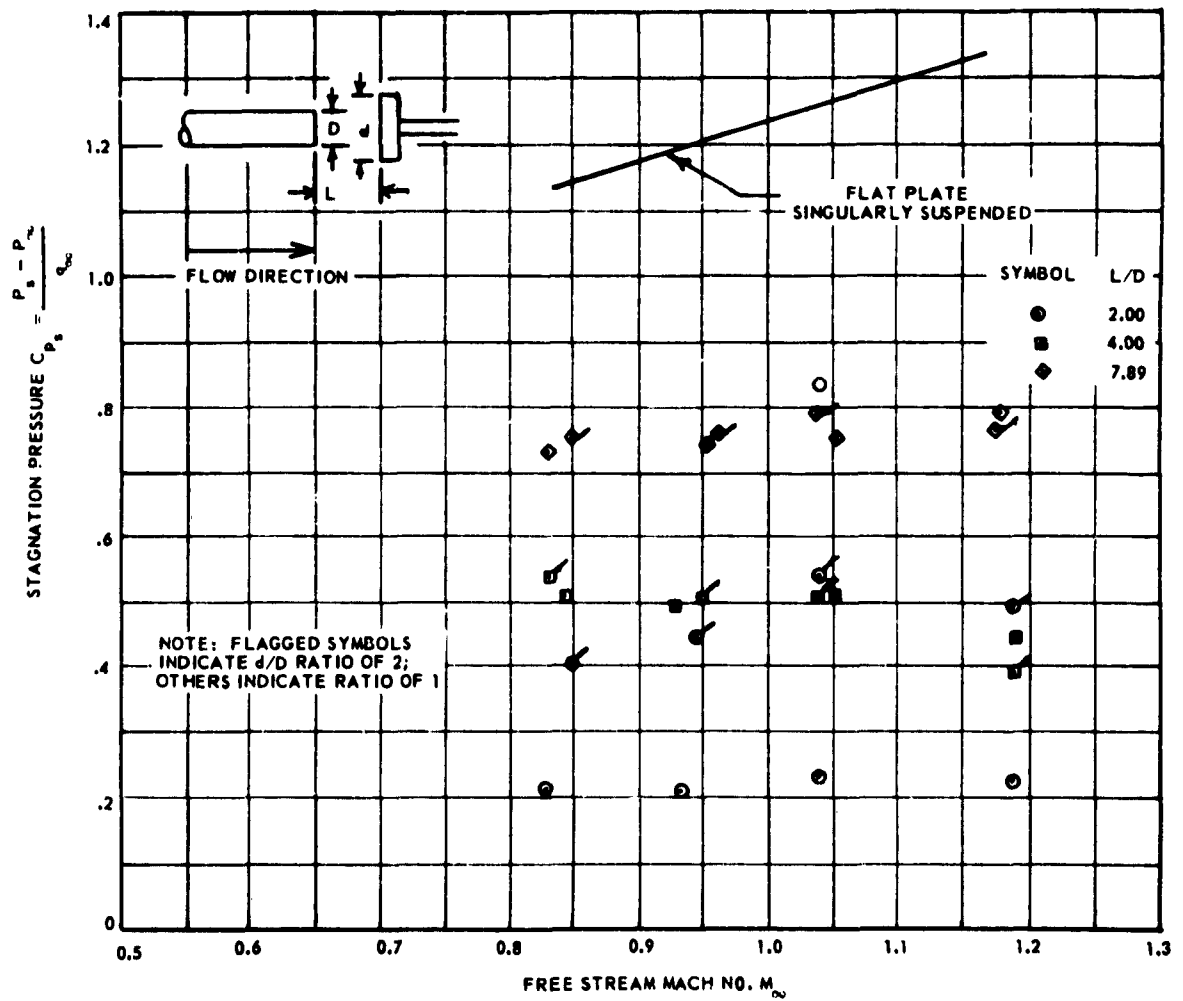


Fig. 4-122 Secondary Body Stagnation Pressure Coefficient vs M_∞ with Boundary Layer Bleed

Fig. 4-126 and 4-127 are representative test results showing the variation in base pressure-coefficients for various primary-secondary body combinations. (Ref (4-67)). These test results clearly indicate the expected base-pressure rises with decreasing distance between the secondary body and the primary body. In addition, the test results also indicate that the larger the diameter of the secondary body is in relation to that of the primary body, the greater the primary-body base pressure rise. Therefore, the distance at which

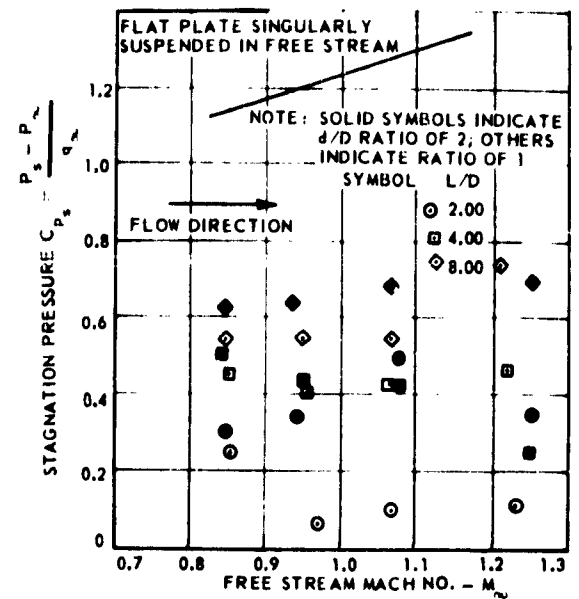
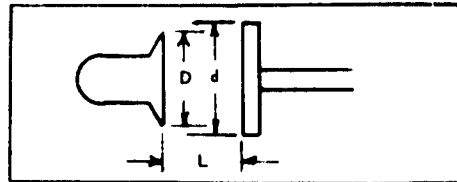


Fig. 4-123 Secondary Body Stagnation Pressure Coefficient vs Free-Stream Mach Number for a Flat Plate in the Wake of a Skirted Hemisphere

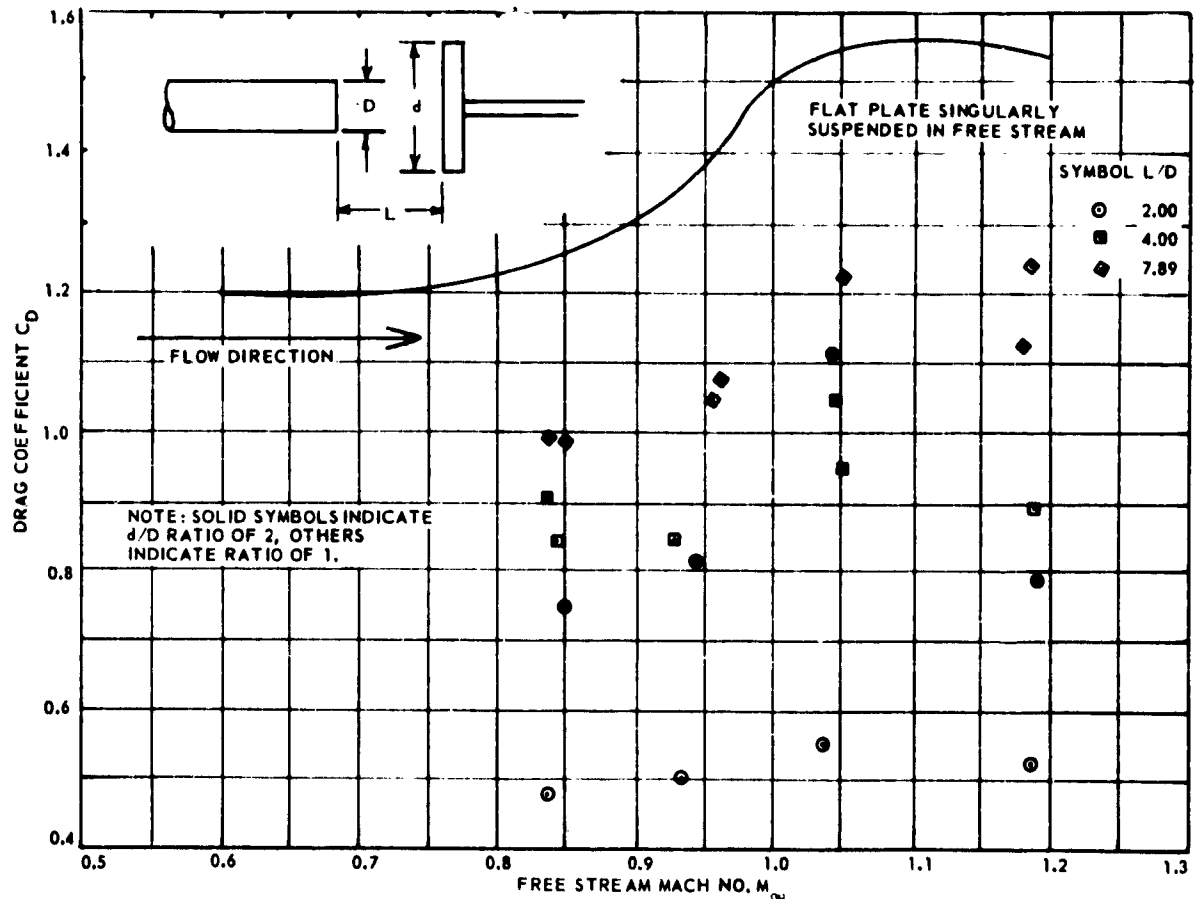


Fig. 4-124 Total Drag Coefficient vs Free-Stream Mach Number for Flat Plate in the Wake of a Semi-Infinite Cylinder with Boundary Layer Bleed

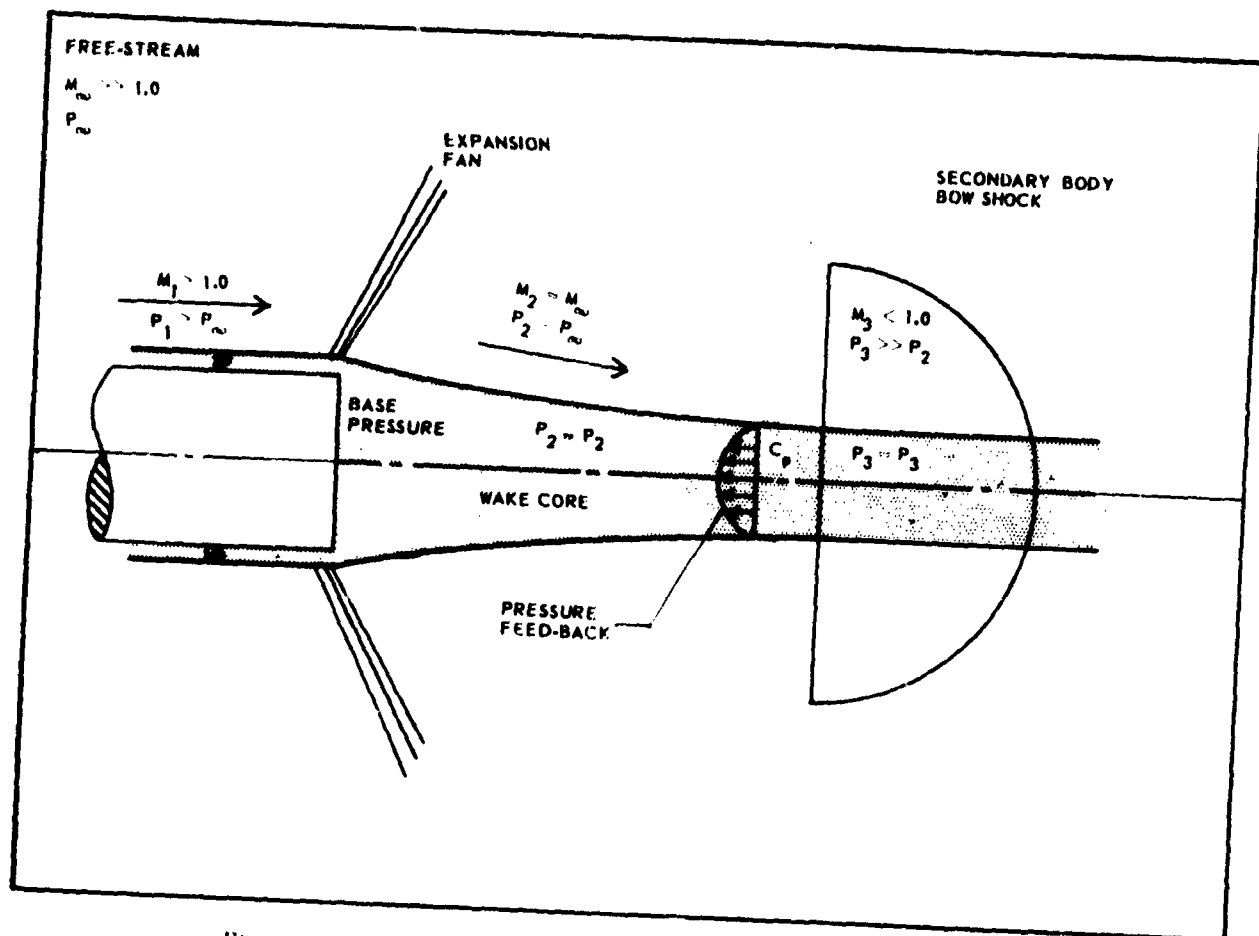


Fig. 4-125 Pressure Relations of Body Combinations in Supersonic Flow

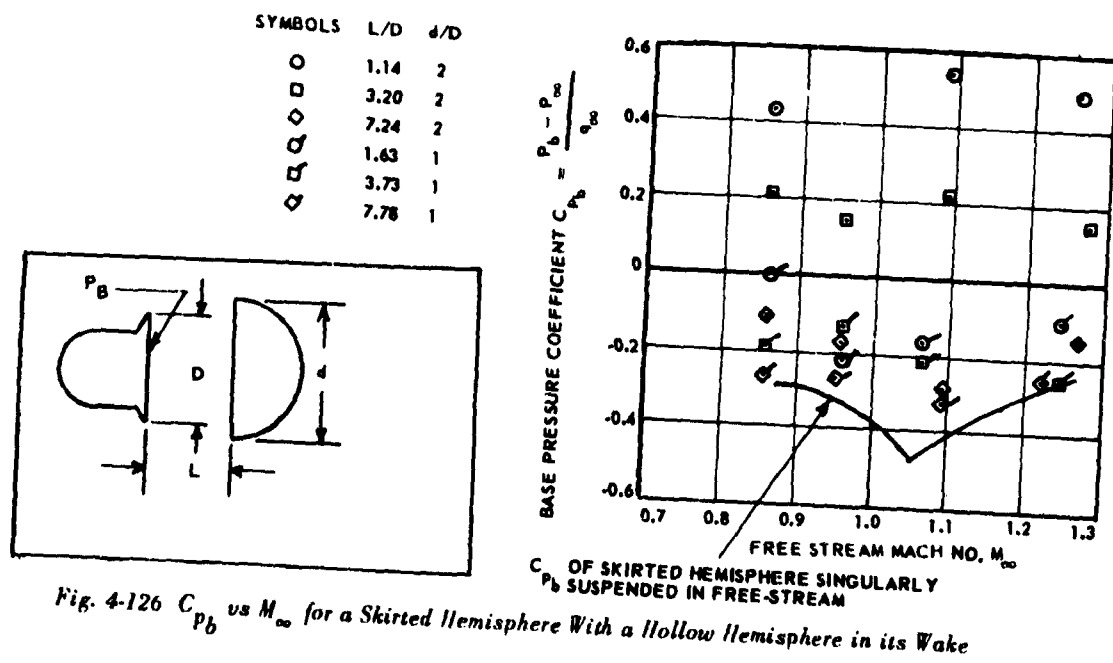


Fig. 4-126 C_{pb} vs M_∞ for a Skirted Hemisphere With a Hollow Hemisphere in its Wake

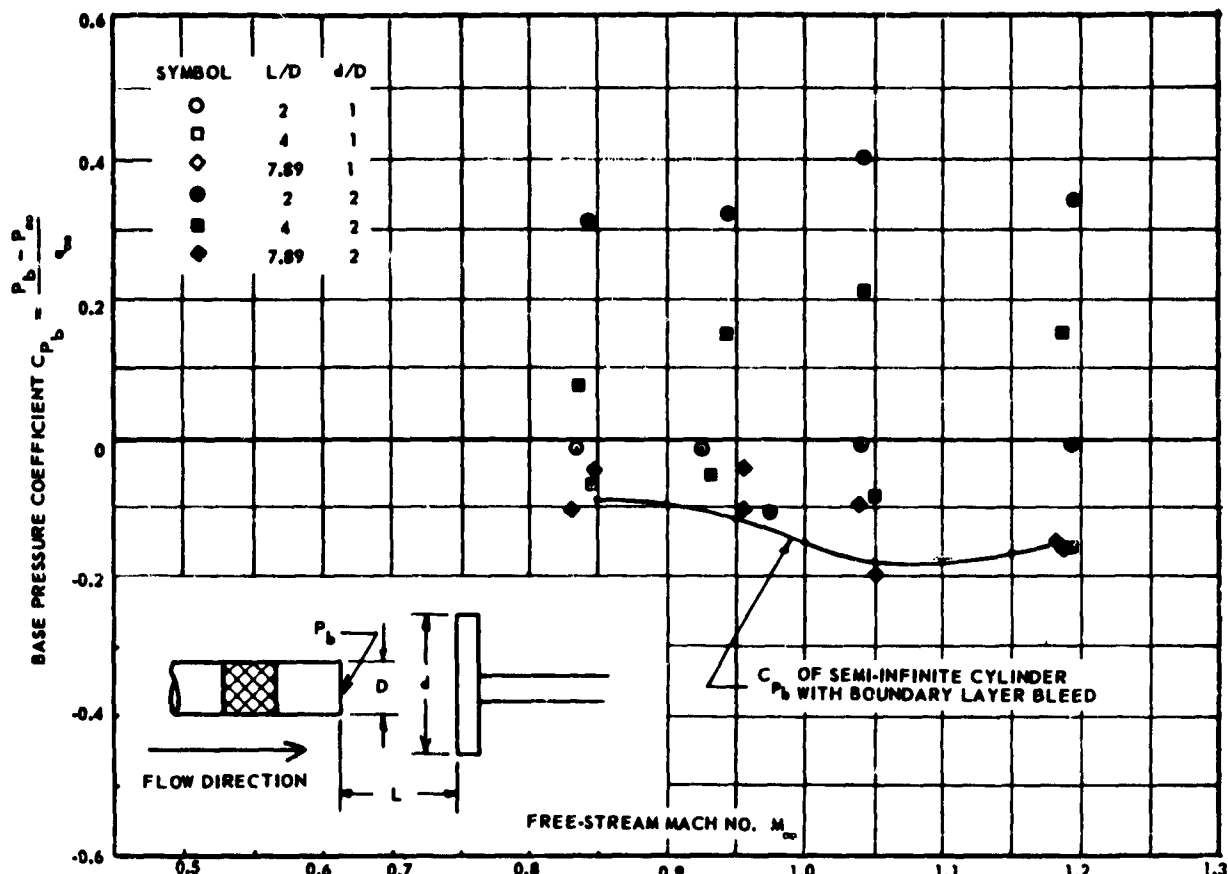


Fig. 4-127 C_{p_b} vs M_∞ for a Semi-Infinite Cylinder with Boundary Layer Bleed and a Flat Plate in its Wake

an aerodynamic decelerator is positioned behind the primary-body base becomes an important parameter for the development of overall payload-decelerator system drag. This is illustrated by the example in which a 45-deg half-angle cone is positioned in the wake of a cylinder with ogive nose and blunt end, and its total drag-coefficient determined throughout the transonic speed regime. The projected diameter, D_p , of the cone-shaped secondary body is twice the diameter, D , of the primary body. Drag coefficients versus Mach number for the secondary body when it is positioned along the centerline 1.5 and 3.2 primary-body

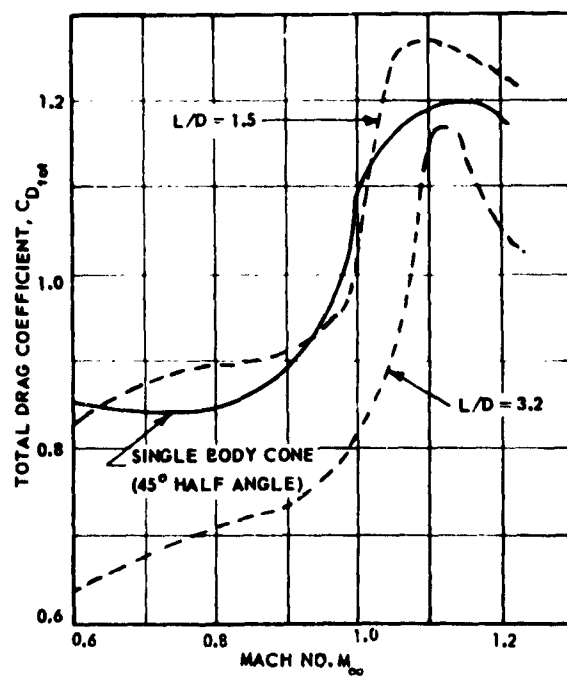
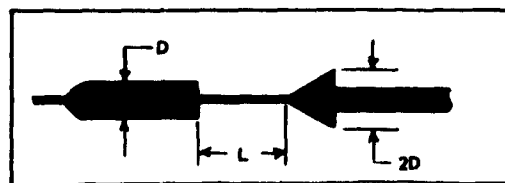


Fig. 4-128 Drag Coefficient vs Mach No.

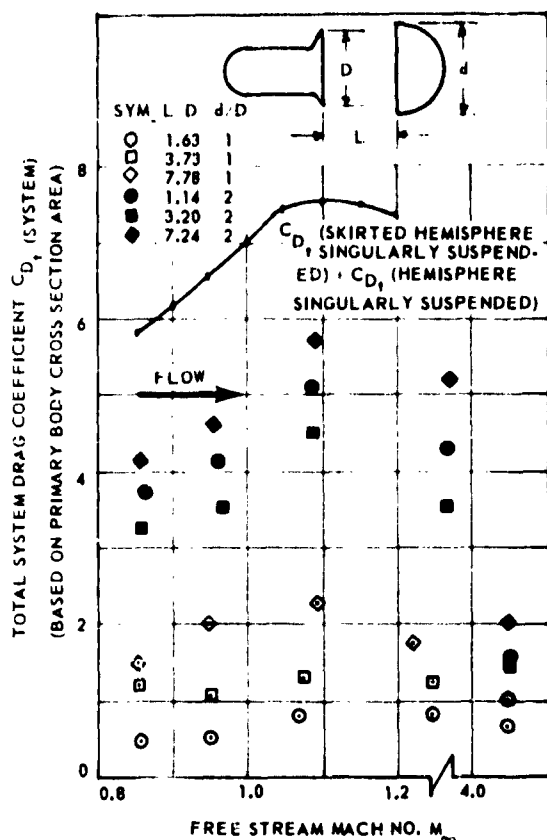


Fig. 4-129 C_D vs M_∞ for a Hollow Hemisphere in the Wake of a Skirted Hemisphere

diameters, respectively, behind the base of the primary body, are shown in Fig. 4-128. The solid curve in this plot represents the drag coefficient of the 45-deg half-angle cone as a single body. The fact that the values for the drag coefficient of the cone positioned at a distance of 1.5 primary-body diameters behind the base of the primary body are almost everywhere higher than the free-stream values for the cone appears, at first thought, to indicate that by placing an aerodynamic deceleration device in this position, increased total-drag effectiveness may be obtained. This, however, is not the case if one considers the combined vehicle-decelerator system. Although the drag coefficient of the secondary body in the wake of the primary body at this distance is higher than its free-stream value, the drag of the primary body is considerably reduced by an increased base-pressure due to interference effects by the secondary body. Therefore, it is the interaction of the two bodies which must be considered in the determination of the overall-system drag.

Two effects, then, combine to produce an overall-system drag or combined drag of the primary- and secondary-body combination: (1) the base-pressure rise

of the primary body caused by the secondary body positioned in its wake, and (2) the drag reduction of the secondary body due to its location in a lower-energy flow field. This combined drag, in transonic and supersonic free-stream, is less than the sum of the individual body-drag values. The order of magnitude of this drag reduction is illustrated in Fig. 4-129.

In general, it can be said that in order to maintain or even gain overall drag efficiency, an augmenting drag-device must be placed at a considerable distance downstream from the primary body. For supersonic applications, this distance is in the order of 8 to 10 primary-body diameters.

SEC. 11 PARACHUTE STABILITY

An analysis of the stability of a freely moving body usually requires the consideration of two different categories:

- (1) Static stability: the tendency of a moving body to develop steady-state restoring moments when disturbed from a position of equilibrium.
- (2) Dynamic stability: the tendency of a moving body to develop moments that act to damp motion.

Any given force system has either none, or one or more positions of equilibrium. Whether or not the system is statically stable at any one of these positions of equilibrium, however, depends upon the change in moment with angle of attack about the position of equilibrium; the degree of static stability depends upon the slope of the moment curve.

Moving under the influence of only drag, inertia, and gravitational forces, the combination of a weight and a canopy may be compared with a body traveling along a ballistic trajectory; i.e., without the influence of lifting forces. Consideration of the objectives of parachute drops indicates that an ideal canopy moves like a ballistic missile; because of this similarity, the methods and force system used in ballistics have been adopted for consideration of parachute performance.

In ballistics, it is customary to define a moment which tends to reduce any deflection from zero angle of attack as positive stability. Such a moment is also called stabilizing moment. Although a given canopy may have more than one position of static equilibrium, the only position of real interest in considering parachute or parachute-load system stability, is that about a zero-degree angle of attack (keeping in mind the objectives of parachute applications). Then, by similarity with the field of ballistics, a parachute canopy is statically stable about this position of equilibrium, if, for a positive change in angle of attack from such

a position of equilibrium, the change in moment is negative; i.e., when $dC_m/d\alpha < 0$. The moment coefficient, C_m , is defined as positive in the clockwise direction about the point of reference (moment center).

A canopy is dynamically stable if oscillations caused by the stabilizing moment are rapidly damped out. If the oscillations caused by the stabilizing moment tend to increase in amplitude with time, the canopy is dynamically unstable. For a canopy, static stability is a prerequisite for dynamic stability, but static stability alone does not assure dynamic stability.

11.1 Static Stability. The force system used for static-stability considerations is shown in Fig. 4-130. The coefficients of normal or side force, of tangential force, and of moment force are the aerodynamic coefficients of a canopy. Individually and collectively, these aerodynamic coefficients describe to some extent

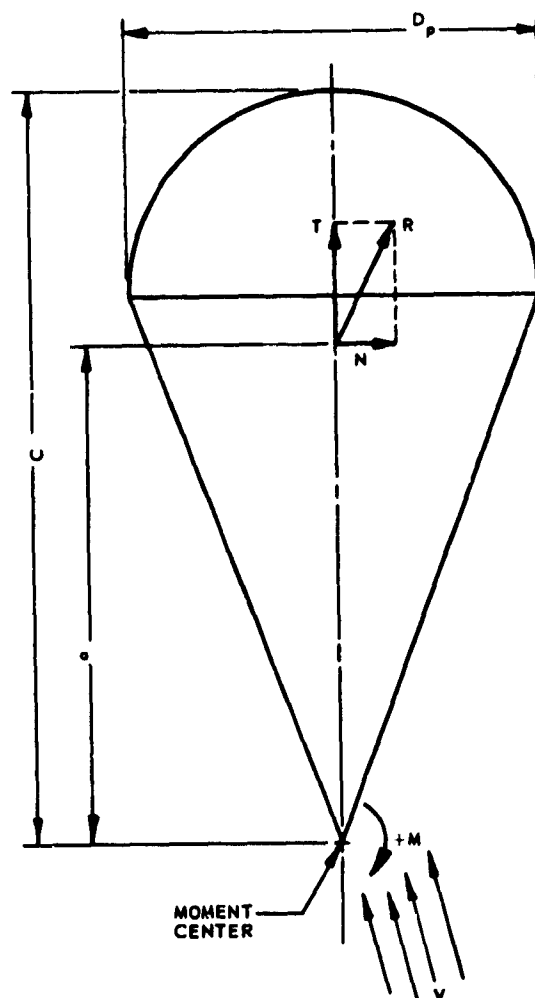


Fig. 4-130 Parachute Coordinate System

the aerodynamic and performance characteristics of a particular type of canopy, such as:

- (1) The static stability, determined from the sign of the $dC_m/d\alpha$ curve;
- (2) The degree of static stability, determined from the slope of the moment curve;
- (3) The glide angle, which is the angle at which the normal- or side-force coefficient is 0;
- (4) The drag-producing capability, which is related to the tangential-force coefficient at specific angles of attack (drag coefficient at zero angle of attack).

The static stability is expressed in the moment coefficient (Ref (4-57))

$$(4-219) \quad C_m = \frac{M}{(1/2)\rho v^2 S_{o,p} D_{o,p}} = \frac{M}{q S_{o,p} D_{o,p}}$$

where q = Dynamic pressure, psf;

$S_{o,p}$ = Characteristic canopy area, sq ft;

$D_{o,p}$ = Diameter of the characteristic canopy area, ft; and

M = Moment acting on the canopy, ft-lb.

The moment acting on the canopy is a function of the normal force and can be determined about any point of interest. For comparative purposes, the moment coefficients presented herein are based on moments acting about a point on the axis of canopy symmetry at a distance $1.0 D_o$ ($1.33 D_p$) below the skirt of the canopy, where $D_o = \sqrt{4 S_{o,p} / \pi}$. In most cases of wind-tunnel testing, the suspension point of the canopy models does not correspond exactly to the moment center as defined above. Therefore, the distance from the actual suspension point to the moment center must be added to the moment arm, a , to obtain the moment (Fig. 4-131), or

$$(4-220) \quad M = V(a + e)$$

where N = Normal force;

a = Distance from the normal force to the suspension point; and

e = Distance from the suspension point to the moment center.

The resultant force acts at the center of pressure on the canopy. This resultant force can be moved along

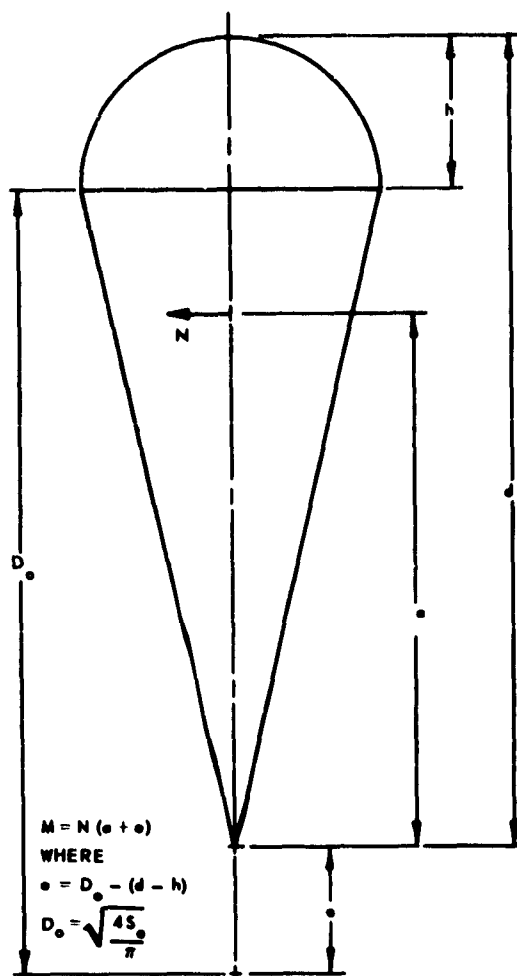


Fig. 4-131 Application of Forces on a Canopy

its line of action to the axis of symmetry of the canopy. This displacement produces no net moment to the system, but the tangent force now acts along the centerline of the canopy and provides no moment force. Since the side force is measured at the apex of the canopy in experimental testing, a method has been devised to determine the actual normal force acting on the canopy (Ref (4-57)). In this method, two different suspension-line lengths and the procedures shown in Fig. 4-132 are used to determine the aerodynamically realistic normal force. With the normal force, N , determined, the normal-force coefficient is obtained from

$$(4-221) \quad C_N = \frac{N}{(1/2) \rho v^2 S_{o,p}} = \frac{N}{q S_{o,p}}$$

The initial determination of the normal-force and moment coefficients of canopies was made on rigid shell-like bodies of revolution (Ref (4-72)). Fig. 4-133 shows the results of wind-tunnel measurements on four models which resemble the drag-producing surfaces of four typical canopies: the flat circular cloth type, a slotted high-porosity type, a horizontal-ribbon type, and a guide-surface type.

Since for steady parachute descent the resultant air force must be equal to the suspended weight, the parachute will descend with an angle of attack, or glide angle, at which the coefficients C_n and C_m are zero. Therefore, canopies A, B, and C (Fig. 4-133) would descend with a resultant angle of attack of 45 deg, 35 deg, and 15 deg, respectively. Canopy D would descend vertically. It is important to note that the curves of the moment and side force for canopies A, B, and C indicate two separate positions of equilibrium, but only one position of static stability where $dC_m/d\alpha < 0$. The angular magnitude of the position of static stability, however, is different for each type of canopy, and none of the first three canopies is statically stable about zero angle of attack. Canopy D has only one position of equilibrium; the slope of the moment curve signifies strong static stability about zero angle of attack. These comparative curves are representative of highly idealized models. When flexibility is introduced into the model, slight changes become evident as shown in Fig. 4-134. These curves show the difference in the characteristics of idealized and real canopy models: flexible and porous models have a smaller range of instability than their prototype rigid models.

11.1.1 NORMAL-FORCE AND MOMENT COEFFICIENTS OF VARIOUS CANOPY TYPES. The normal-force and moment coefficients of nine different types of conventional canopy models, for a range of angles of attack, are presented in Fig. 4-135 through 4-143. (Ref (4-57)). All cloth canopy models were fabricated of standard Nylon material (MIL-C-7020B, Type III) with a nominal cloth permeability of 120 cu ft per sq ft per min. For convenience, the aerodynamic coefficients plotted are based upon the projected as well as the total cloth area, with the exception of the guide-surface types for which the aerodynamic coefficients are based upon the projected area only.

11.1.2 EFFECTS OF CLOTH PERMEABILITY (EFFECTIVE POROSITY). The static stability of textile canopies is greatly affected by the permeability or effective porosity (see Sec. 3) of the cloth from which the drag-producing surface of the canopy is fabricated. In the case of canopies with geometric porosity, static stability is affected by the degree of porosity constructed in the drag-producing surface.

T, P₁, AND P₂ ARE MEASURED FORCES
 R = RESULTANT FORCE ON THE PARACHUTE
 C.P. = CENTER OF PRESSURE

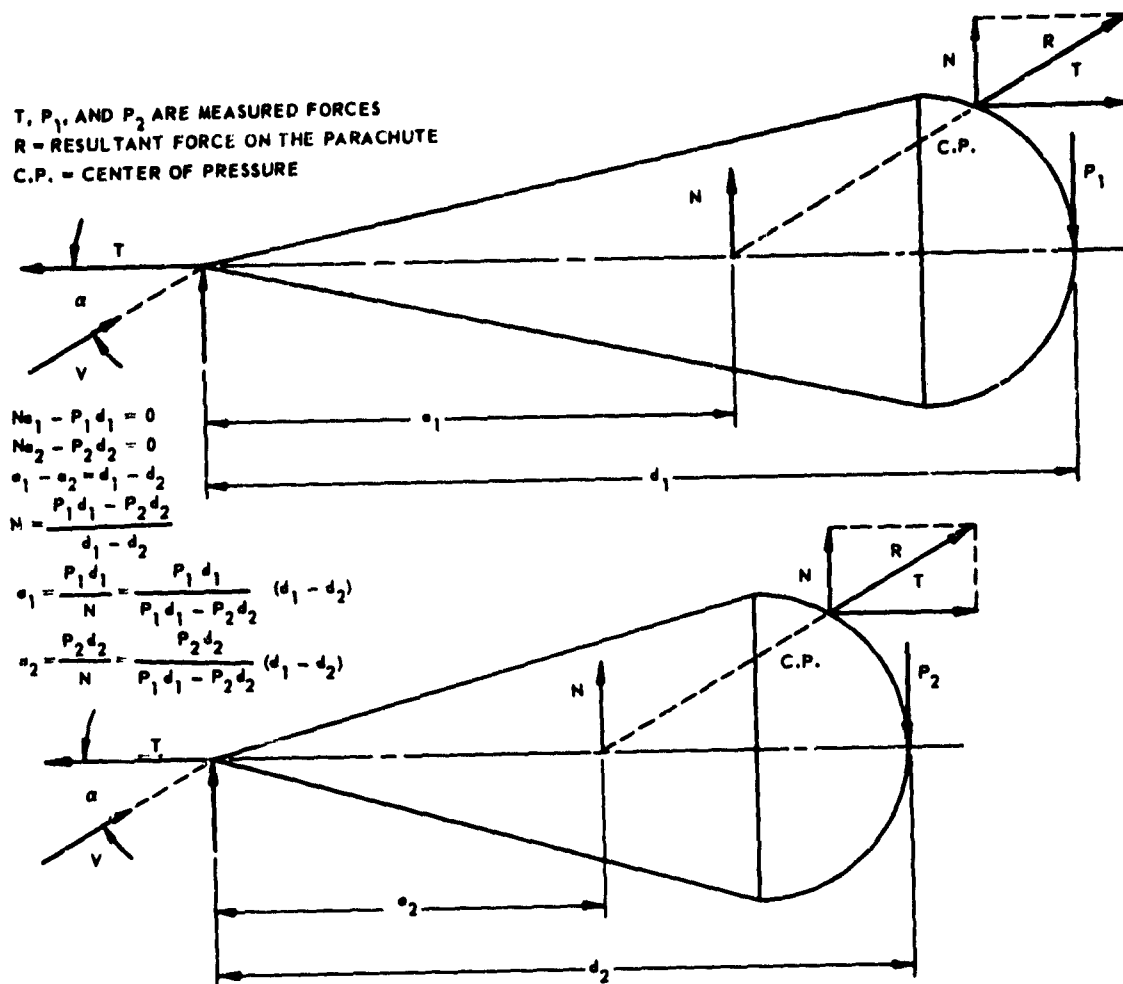


Fig. 4-132 Determination of Normal Force Acting on Canopy

In general, the static stability of canopies increases with increasing cloth permeability or grid porosity, as shown in Fig. 4-144 and 4-145, in which the normal-force and moment coefficients of three types of cloth canopies are plotted versus angle of attack with cloth permeability (effective porosity) as a parameter (Ref(4-57)). Naturally, a balance of mass airflow must be maintained in the drag-producing surface if reliable parachute opening is to be expected. Therefore, although the moment curve for the flat circular canopy with a cloth permeability of 275 cfm per sq ft shows considerably improved static canopy stability about zero angle of attack, utilization of this high-porosity cloth in the fabrication of canopies is not practical, since the inflation tendencies of the canopy will become marginal.

11.1.3 STATIC STABILITY DETERMINATION THROUGH FLOW VISUALIZATION. The relative degree of the stability of a canopy has also been determined by studying the flow field around the canopy (Ref (4-73), (4-74)). Several representative sketches of these flow studies at 15-deg angle of attack are shown in Fig. 4-146. From these sketches it can be seen that the air tends to adhere less to the side of the canopy which is deflected away from the airstream (a low-pressure area) with increasing porosity and consequently with increasing static stability. For the guide-surface canopy, however, the difference in pressure between opposite sides of the canopy in the plane of rotation is reduced by the "spoiler" or flow-separation action of the edge created by the seam between the roof and guide-surface panels, rather

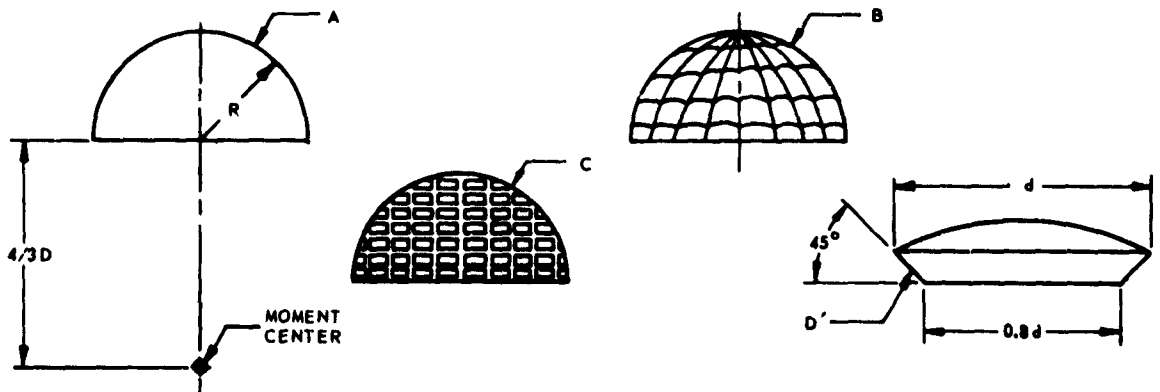
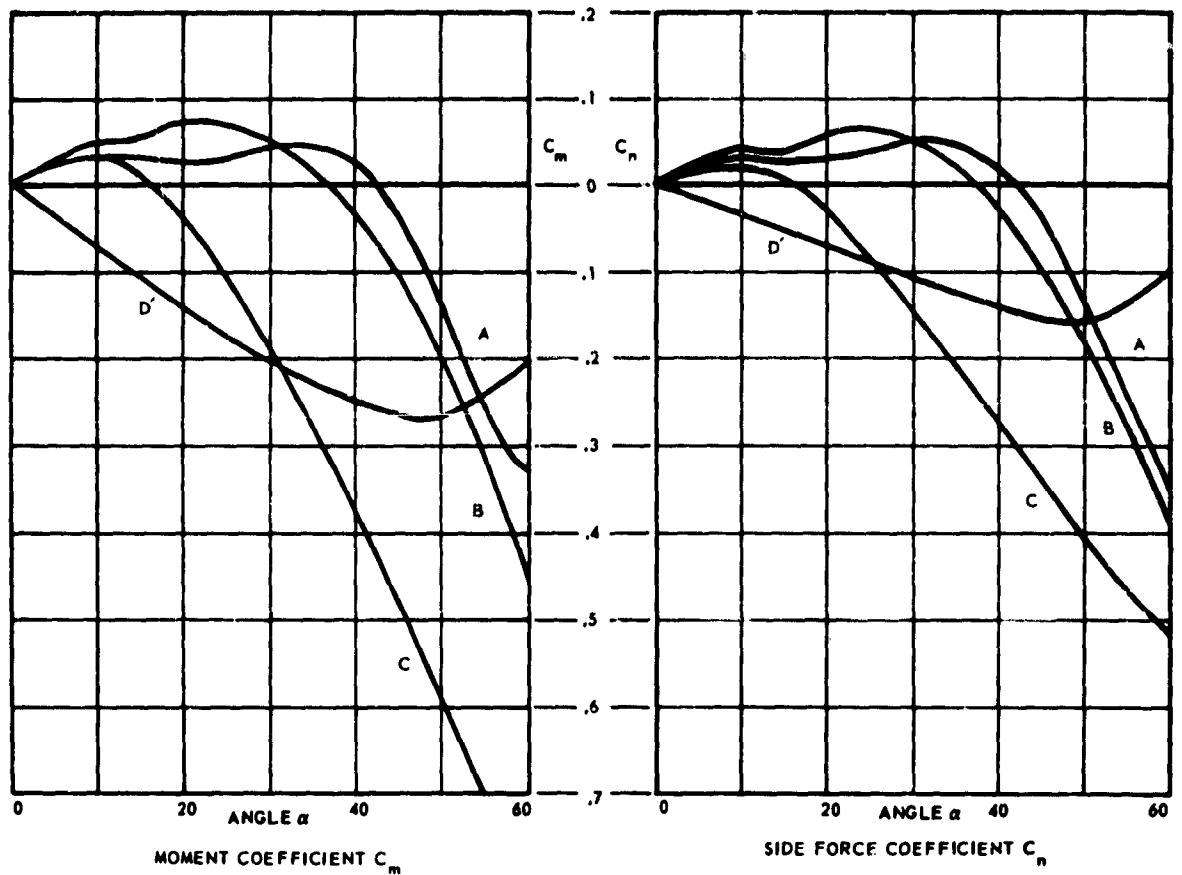


Fig. 4-133 Results of Wind Tunnel Tests on Solid Flat, Slotted High Porosity, Ribbon and Guide-Surface Type Parachute Canopies (Rigid Models)

than by an increase in canopy porosity. It is also evident from this flow picture that the side of the skirt offering the greatest resistance to the air is also creating a high-pressure area, which in turn causes a restoring moment. Analyzing these flow pictures further, it can be stated that the instability of a canopy originates in the flow about the canopy. At any mod-

erate angle of attack the streamlines tend to separate from one side and adhere to the other side. Consequently, a force and moment develop which tend to increase the angle of attack.

11.2 Dynamic Stability. The behavior of a canopy moving through the air is governed by characteristics which, in airplane design, are called dy-

dynamic stability characteristics. For aircraft and missiles, certain characteristic parameters have been established which, when known, allow the prediction of the dynamic stability of specific airplanes or missiles. Attempts have been made by various investigators to establish similar parameters for parachutes (Ref (4-75) through (4-78)). However, success has been limited, due to lack of knowledge of some of the experimental parameters.

Using a number of pertinent experimental parameters presented in recent publications, particularly on static stability and apparent mass, a new attempt was made (Ref (4-58)) to express analytically the dynamic stability of canopies with point mass.

11.2.1 EQUATION OF MOTION OF A PARACHUTE AS A RIGID BODY. The differential equations of the laterally disturbed motion of a rigid, parachute-like body are of the following form for the coordinate system shown in Fig. 4-147:

$$(4-222) \quad (\bar{m}_L + m_{Lx}) \beta' + (m_{Lx} - m_{Ly}) \alpha' -$$

$$m_{Ly} \frac{S}{r} (\alpha'' + \beta'') = \frac{\partial C_L}{\partial \alpha} \alpha + \frac{\partial C_L}{\partial \omega_z r/v} (\alpha' + \beta') - C_D \beta$$

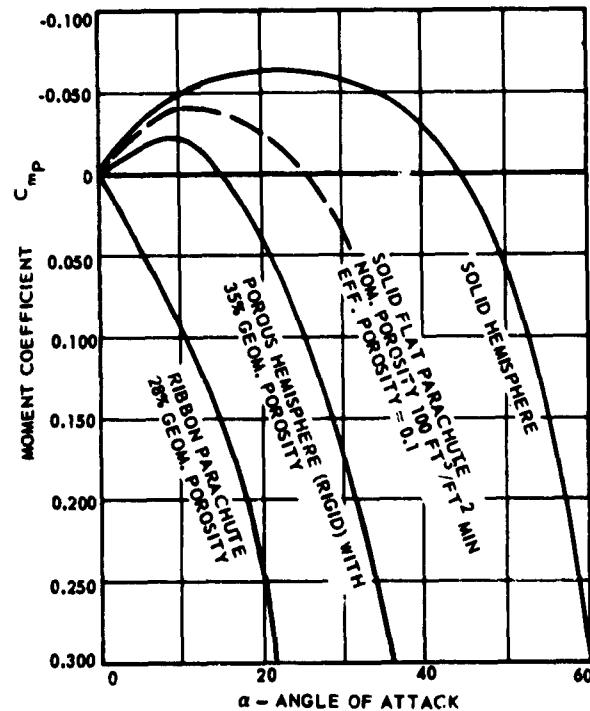


Fig. 4-134 Moment Coefficients of Canopy Models

and

$$(4-223) \quad \left[I_{Lz} + m_{Ly} \left(\frac{S}{r} \right)^2 \right] (\alpha'' + \beta'') - m_{Lx} \frac{S}{r} \beta' +$$

$$(m_{Ly} - m_{Lx}) \frac{S}{r} \alpha' = \frac{\partial C_m}{\partial \alpha} \alpha + \frac{\partial C_m}{\partial \omega_z r/v} (\alpha' + \beta')$$

where α = Angle of attack (degrees);

β = Angle between trajectory of load and vertical;

Prime (', '') indicates differentiation with respect to non-dimensional time $\tau = \frac{vt}{r}$;

ω_z = Angular velocity of the system about the z axis;

S = Distance between center of gravity of the inflated canopy and the load;

r = Radius of the inflated canopy;

C_m = Moment coefficient;

C_L = Lift coefficient;

C_D = Drag coefficient;

$\frac{\partial C_m}{\partial \alpha}$ = Slope of moment coefficient versus angle of attack;

$\frac{\partial C_L}{\partial \alpha}$ = Slope of lift coefficient versus angle of attack;

$\frac{\partial C_m}{\partial \omega_z r/v}$ = Dependence of moment coefficient on the angular velocity;

$\frac{\partial C_L}{\partial \omega_z r/v}$ = Dependence of lift coefficient on the angular velocity;

m_L = Mass of load;

\bar{m}_L = Dimensionless mass of load;

m_{Lx} = Dimensionless apparent mass in x-direction;

m_{Ly} = Dimensionless apparent mass in y-direction;

I_{Lz} = Dimensionless apparent moment of inertia of canopy rotating about an axis through the center of volume and parallel to the x-axis;

v_0 = Rate of descent;

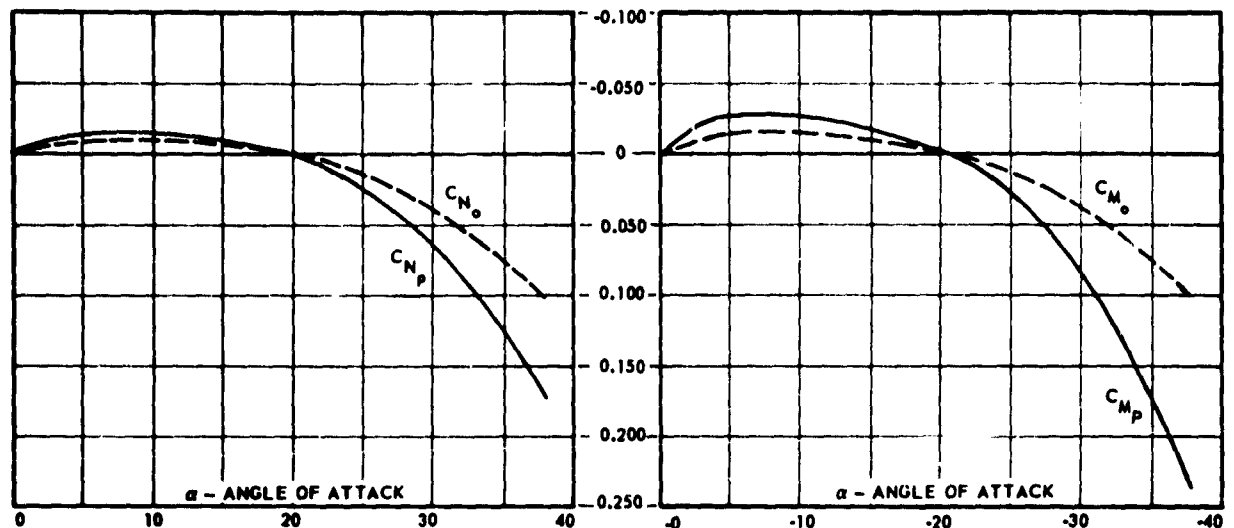


Fig. 4-135 Normal Force and Moment Coefficient vs Angle of Attack for Circular Flat Cloth Canopy

v = Resultant velocity; and

ρ = Air density.

The assumptions made in deriving the equations of motion (Eq 4-222 and 4-223) are:

- (1) The motion is restricted to one plane;
- (2) The parachute-load system constitutes a rigid body;
- (3) The load is considered a point mass;
- (4) The mass of the canopy is negligible;
- (5) The aerodynamic forces act only on the canopy;

(6) The forces and additional apparent (virtual) masses act at the center of volume of the canopy; and

(7) The additional air-mass of the load and the additional apparent moment of inertia of the load can be neglected.

11.2.2 FREQUENCY EQUATION OF THE SYSTEM OF EQUATIONS OF MOTION. To solve the system of differential equations of motion, it is assumed that

$$(4-224) \quad \alpha = Ae^{\lambda r} \quad \text{and} \quad \beta = Be^{\lambda r}$$

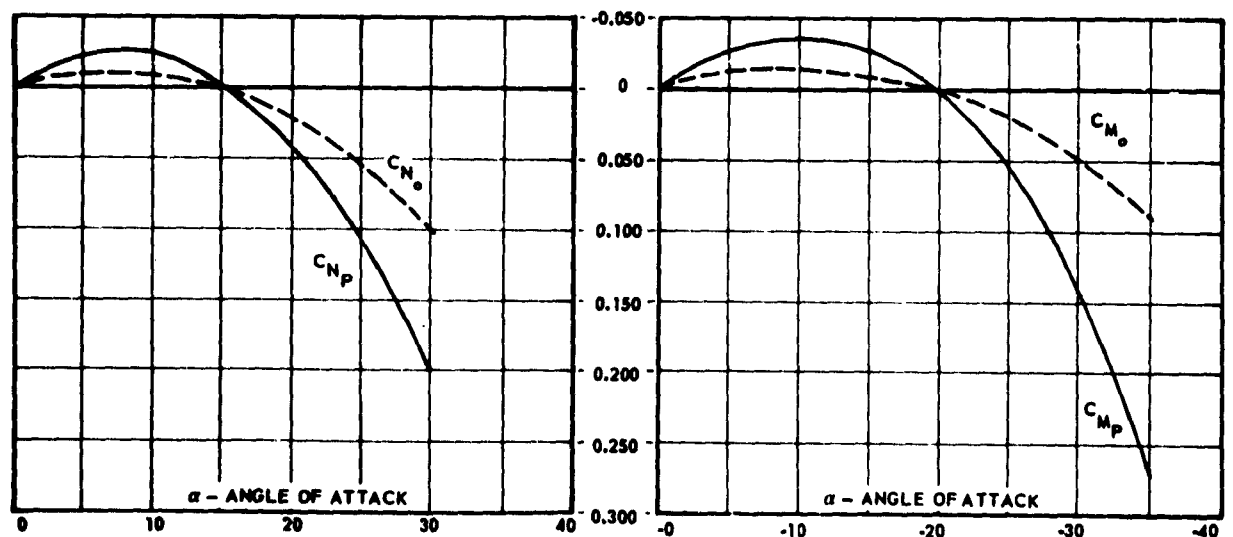


Fig. 4-136 Normal Force and Moment Coefficient vs Angle of Attack for 10% Flat Extended Skirt Cloth Canopy

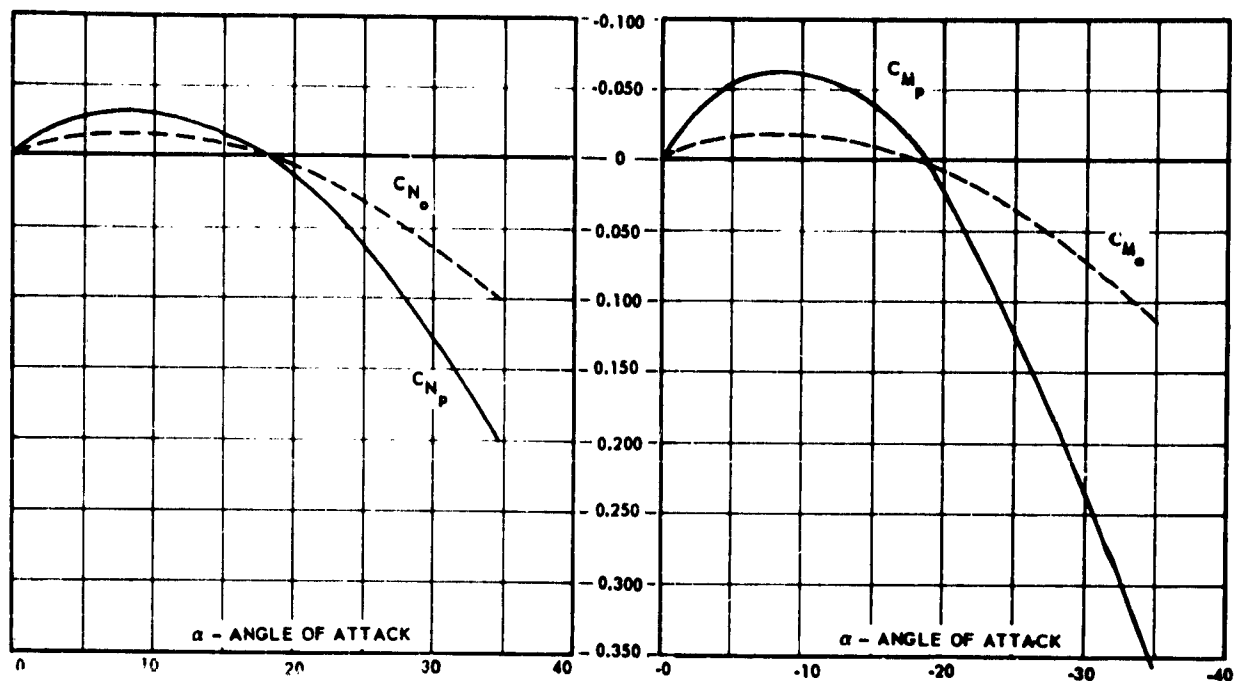


Fig. 4-137 Normal Force and Moment Coefficient vs Angle of Attack for 14.3% Full Extended Skirt Cloth Canopy

where A, B = Arbitrary constants;

$r = vt/r$; and

t = Time.

The value of λ , which may be real or complex, can be determined from the cubic equation

$$(4-225) \left[l_{vz} (\bar{m}_L + m_{vy}) + \bar{m}_L m_{vy} \left(\frac{S}{r} \right)^2 \right] \lambda^3 +$$

$$\left\{ l_{vz} + m_{vy} \left(\frac{S}{r} \right)^2 \right\} \cdot \left(\frac{\partial C_L}{\partial \alpha} + C_D \right) +$$

$$\left(\frac{\partial C_m}{\partial \alpha} - \frac{\partial C_L}{\omega_z r} \right) m_{vy} \frac{S}{r} - (\bar{m}_L + m_{vy}) \frac{\partial C_m}{\partial \frac{\omega_z r}{v}} +$$

$$(m_{vy} - m_{vx}) \bar{m}_L \frac{S}{r} \left\{ \lambda^2 - \left\{ \frac{\partial C_m}{\partial \alpha} (\bar{m}_L + m_{vx}) - \frac{\partial C_L}{\omega_z r} \right\} + \right.$$

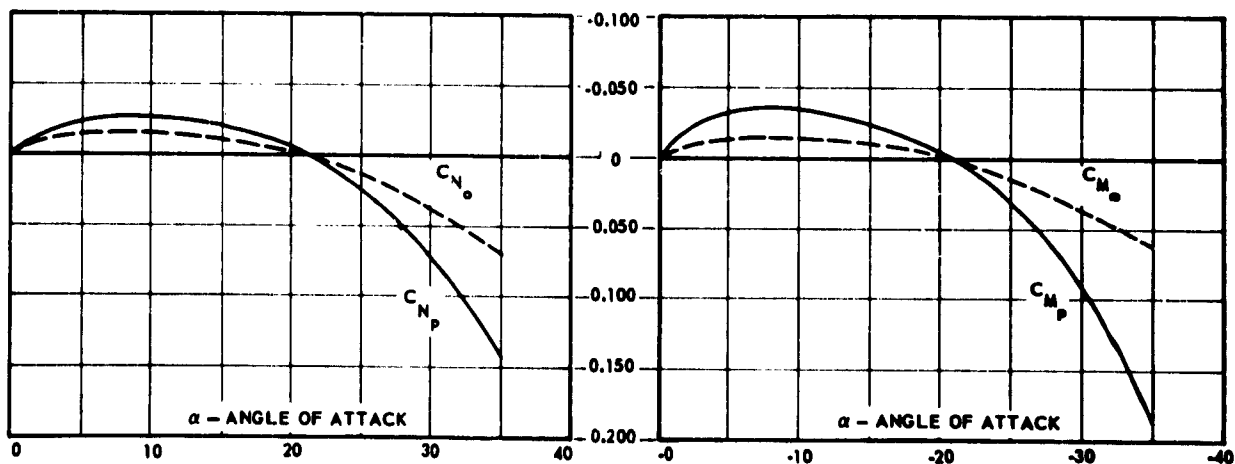


Fig. 4-138 Normal Force and Moment Coefficient vs Angle of Attack for Conical Cloth Type Parachute Canopy

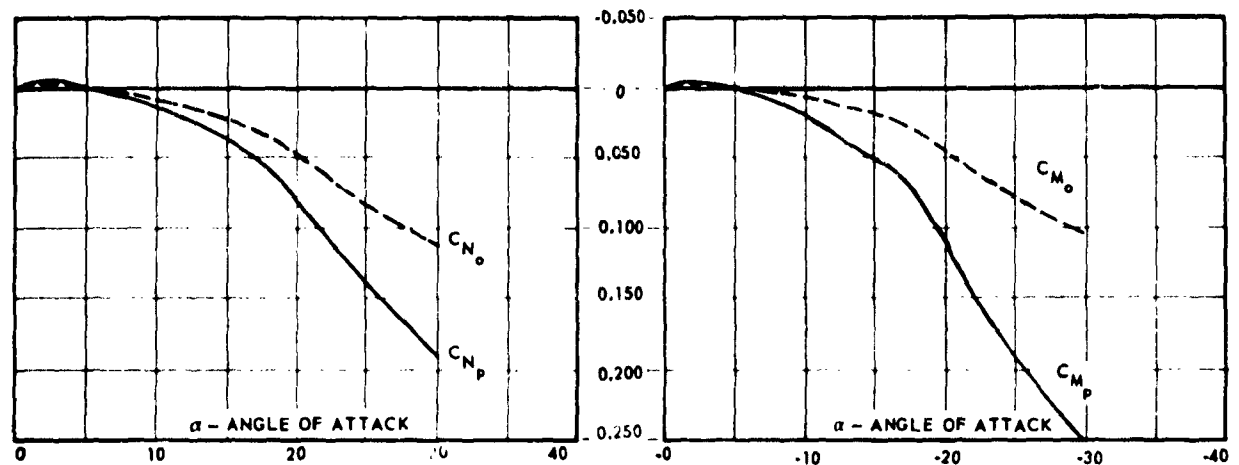


Fig. 4-139 Normal Force and Moment Coefficient vs Angle of Attack for Personnel Guide-Surface Cloth Canopy

$$\frac{\partial C_L}{\partial \alpha} \left(m_{vx} \frac{S}{r} + \frac{\partial C_m}{\partial \omega_z r} \right) - C_D \left[(m_{vy} - m_{vx}) \frac{S}{r} - \frac{\partial C_m}{\partial \omega_z r} \right] \lambda - C_D \frac{\partial C_m}{\partial \alpha} = 0$$

or

$$(4-226) \quad a \lambda^3 + b \lambda^2 + c \lambda + d = 0$$

where a , b , c , and d are the coefficients in Eq 4-225. This equation, 4-225 or 4-226, is the frequency equation of the system of equations of motion 4-222 and 4-223. To satisfy Routh's Criteria, $a > 0$, $b > 0$, $c > 0$, $d > 0$, and $bc > d$.

To apply these equations to a particular parachute, it is necessary that each value of the coefficients a , b , c , and d of Eq 4-226 be determined for the particular canopy type under consideration.

11.2.2.1 Aerodynamic Force and Moment Coefficients. Wind-tunnel tests have been conducted on a number of conventional canopy types with various cloth porosities to determine the varia-

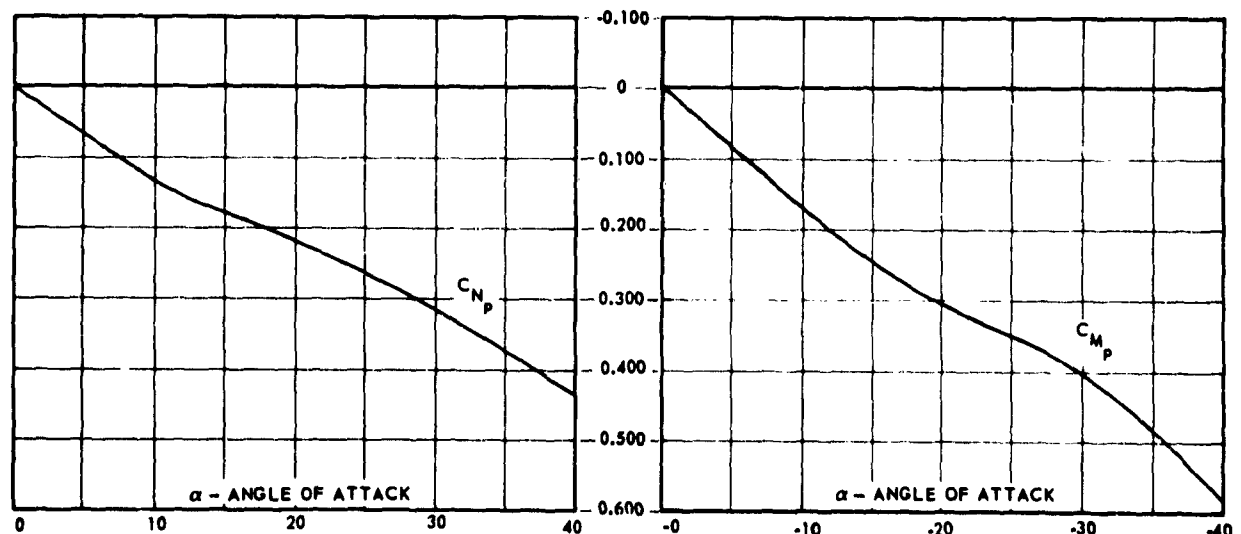


Fig. 4-140 Normal Force and Moment Coefficient vs Angle of Attack for Ribbed Guide-Surface Cloth Canopy

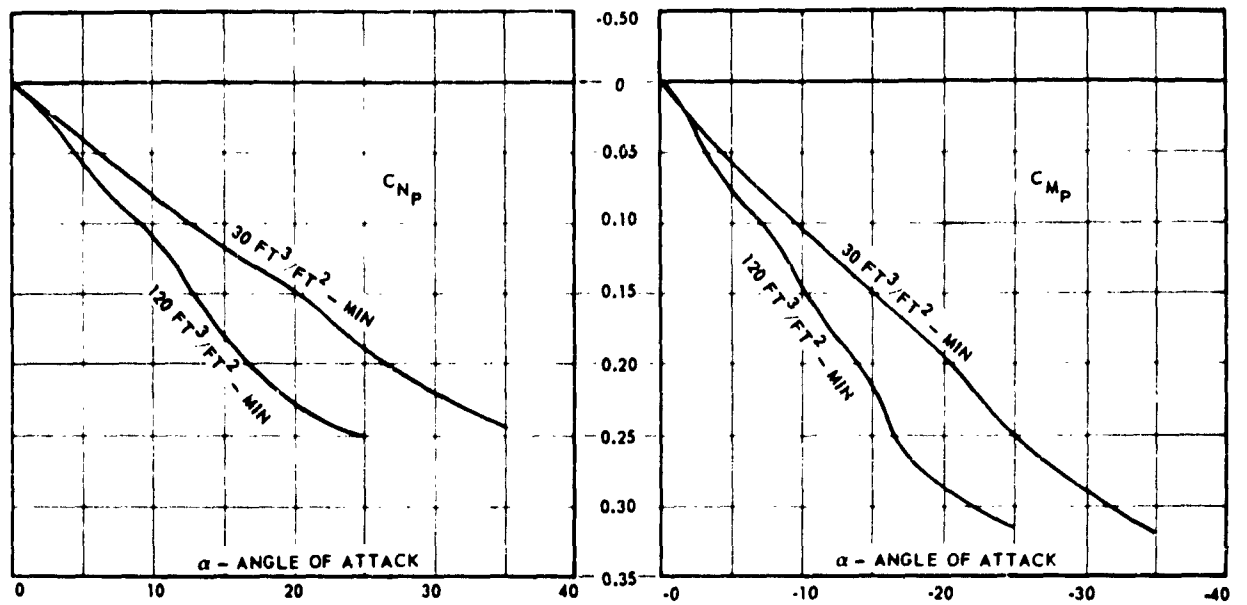


Fig. 4-141 Normal Force and Moment Coefficient vs Angle of Attack for Ribless Guide-Surface Cloth Canopy

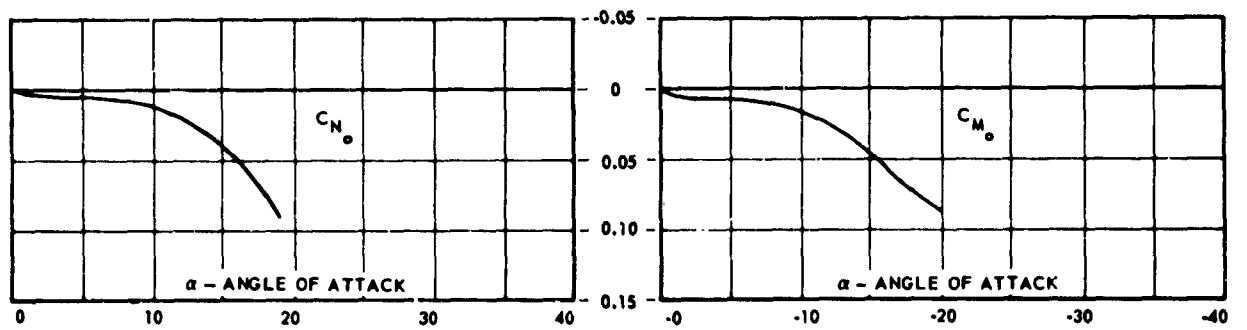


Fig. 4-142 Normal Force and Moment Coefficient vs Angle of Attack, Ring-Slot Canopy of 20% Geometric Porosity

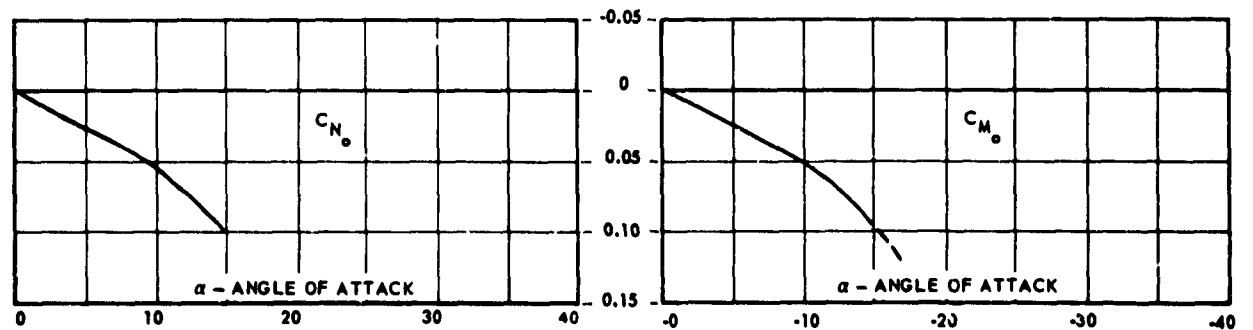


Fig. 4-143 Normal Force and Moment Coefficient vs Angle of Attack, Ribbon-Type Canopy of 20% Geometric Porosity

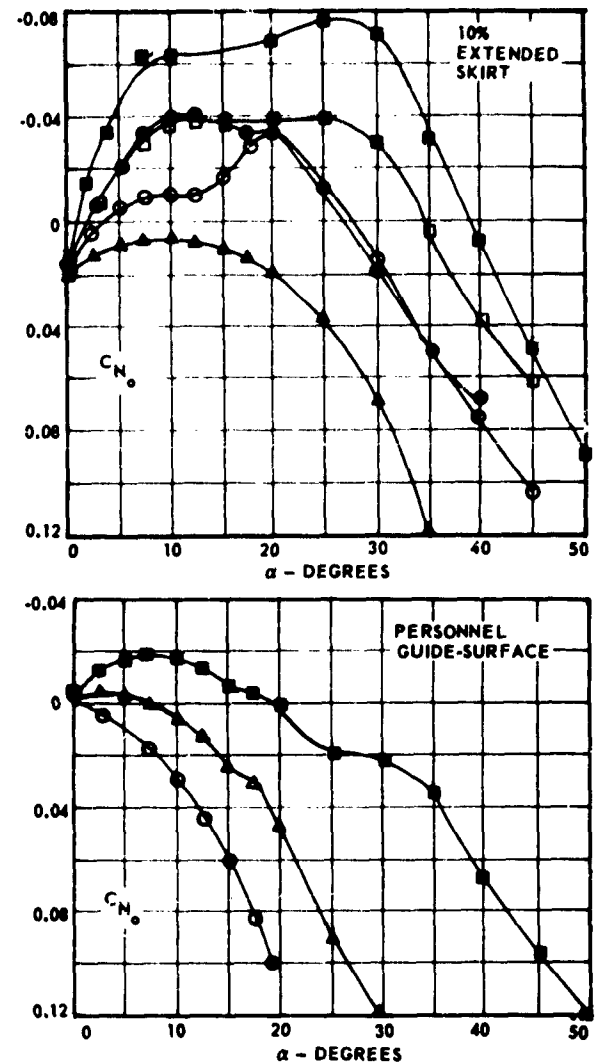
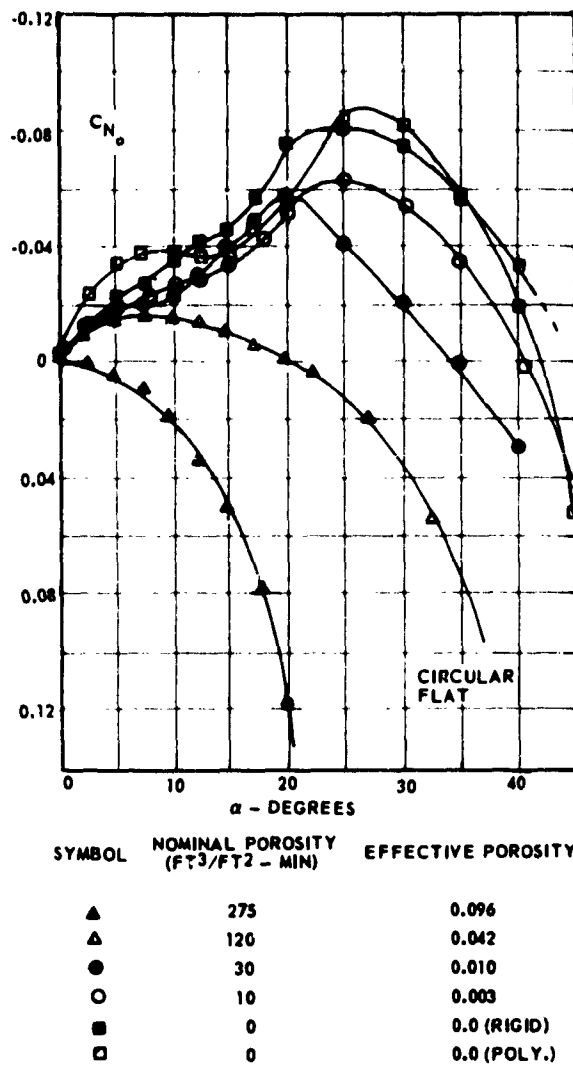


Fig. 4-144 Normal Force Coefficient vs Angle of Attack of Various Parachutes

tion of tangent force (T), normal force (N), and moment (M) with angle of attack. The results of these investigations are presented in Sec. 6 and 11 of this chapter.

To use the experimental data for the solution of the frequency equation, it is necessary to calculate values of C_L , C_D , $\partial C_L / \partial \alpha$, and $\partial C_m / \partial \alpha$ from the experimental data. Fig. 4-148 shows the relationship between the forces L and D , and the forces N and T . Simple geometric relationships give

$$(4-227) \quad L = N \cos \alpha - T \sin \alpha$$

$$C_L = C_N \cos \alpha - C_T \sin \alpha$$

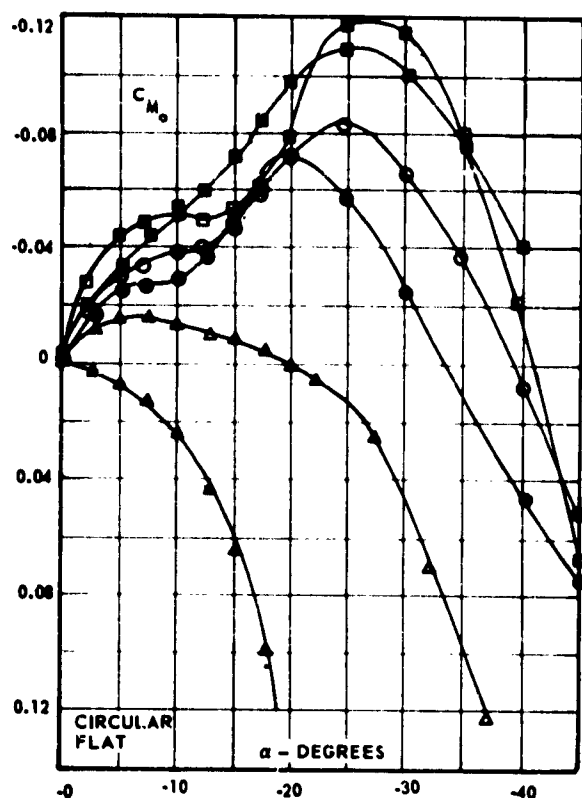
and

$$(4-228) \quad D = N \sin \alpha + T \cos \alpha$$

$$C_D = C_N \sin \alpha + C_T \cos \alpha$$

These equations can be used to calculate values for C_D and C_L as based upon experimental data. Subsequently, values for $\partial C_L / \partial \alpha$ and $\partial C_m / \partial \alpha$ can be calculated.

11.2.2.2 Influence of Angular Velocity. The influence of the angular velocity, ω_z , of the canopy about the z -axis upon the values derived above must now be considered. This velocity might have been caused by the sudden deceleration of the load as the canopy opened or by gusts of wind which may act upon the canopy during descent. Since there are no



SYMBOL	NOMINAL POROSITY (FT3/FT2-MIN)	EFFECTIVE POROSITY
▼	275	0.096
▲	120	0.042
●	30	0.010
○	10	0.003
◇	0	0.0 (RIGID)
□	0	0.0 (POLY.)

experimental data concerning the effects of the angular velocity, these effects must be estimated.

First, consider the effects of an angular velocity ω_z about an axis parallel to the z-axis and passing through the center of the volume of the canopy. The subscript k will be used to indicate the quantities analytically determined. The drag and lift are practically independent of this velocity; hence

$$(4.229) \quad \left(\frac{\partial C_D}{\partial \frac{\omega_z r}{v}} \right)_k = 0 \quad \text{and} \quad \left(\frac{\partial C_L}{\partial \frac{\omega_z r}{v}} \right)_k = 0$$

The moments produced by the rotational velocity arise from frictional forces and from an unsymmetrical pres-

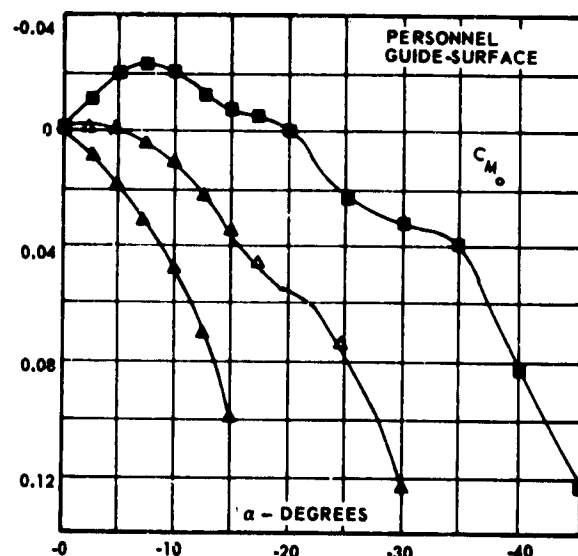
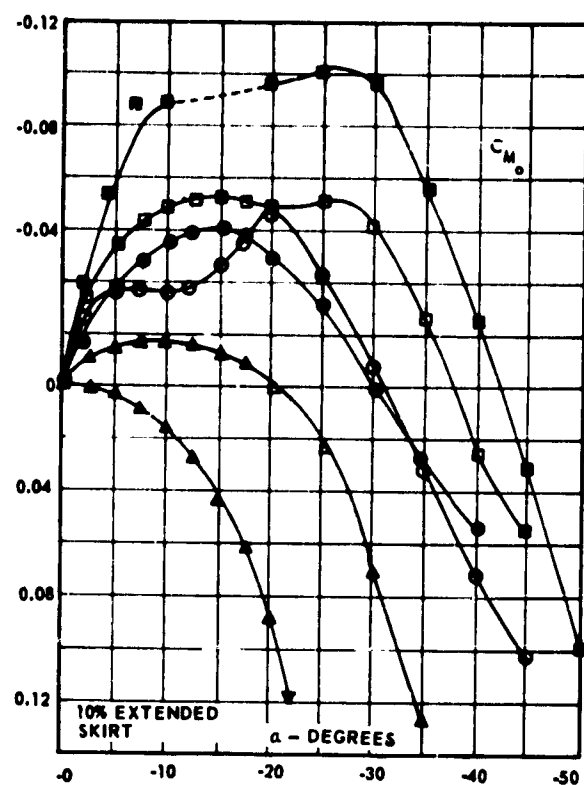


Fig. 4-145 Moment Coefficient vs Angle of Attack of Various Parachutes

sure-distribution on the canopy. The frictional forces and their moments are very small compared to those caused by the pressure distribution, and can therefore be neglected. The moment caused by the pressure



SOLID SHAPE HEMISPHERICAL



RING SLOT



GUIDE SURFACE



HORIZONTAL RIBBON

Fig. 4-146 Flow Field Around Several Canopies at 15-Degree Angle of Attack

distribution is primarily dependent upon the ratio c/r (Fig. 4-149) and must be an even function of this ratio. When c/r changes from 0 to 1, the body of revolution changes from a circular disk to a sphere. Therefore, for $c/r = 0$, the moment is equal to the

moment of a circular disk which is subjected to a flow of air perpendicular to its plane and is rotating about a diameter. For $c/r = 1$, the moment is equal to the moment of a sphere rotating about its center. In this latter case, however, the moment is zero, since

each surface element of the sphere is moved tangentially. If the drag on a unit area of the circular disk is

$$(4-230) \quad D_1 = \frac{1}{2} C_D \rho v^2$$

then the drag for a unit area of the sphere can be approximated as:

$$(4-231) \quad D = \frac{r^2 - c^2}{r^2} D_1$$

(Note that if $c = 0$, $D = D_1$; and if $c = r$, $D = 0$.)

Since the area of a hemisphere is twice that of a circular disk with the same radius, we introduce the coefficient $(r^2 + c^2)/r^2$, which is equal to 1 for a disk and 2 for a sphere. Thus, the moment element dM is given by

$$(4-232) \quad dM = \frac{r^2 - c^2}{r^2} D_1 \frac{r^2 + c^2}{r^2} dy dz$$

where D , the drag per unit area of the canopy, is

$$(4-233) \quad D = \frac{1}{2} C_D \rho v^2$$

$$(4-234) \quad D = \frac{1}{2} C_D \rho (v_o + v \omega_z)^2$$

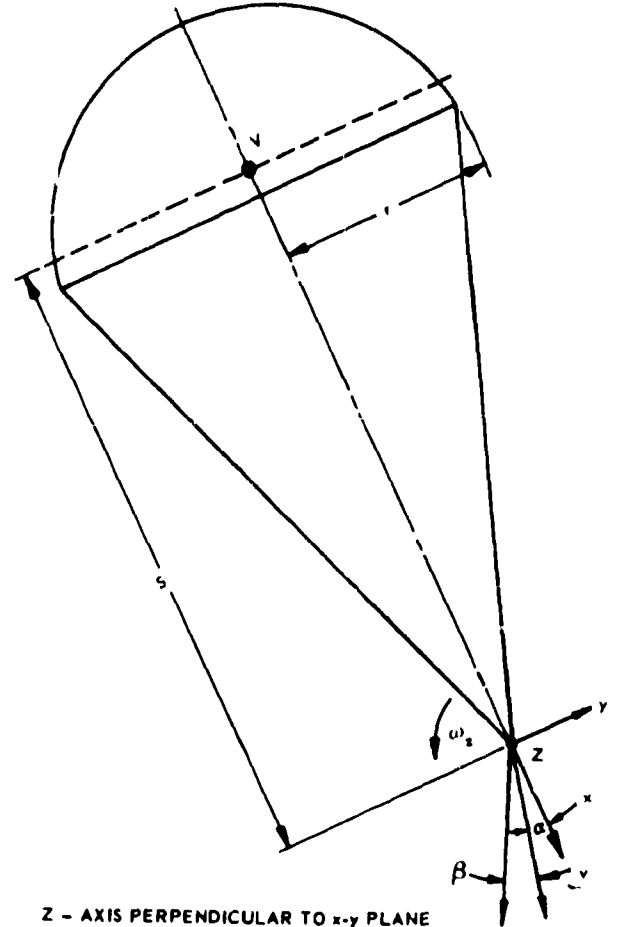
Therefore, for the canopy,

$$(4-235) \quad M = \frac{r^4 - c^4}{r^4} C_D \frac{\rho}{2} \int_{-r}^r \int_{-\sqrt{r^2 - y^2}}^{\sqrt{r^2 - y^2}} (v_o + v \omega_z)^2 y dz dy$$

or

$$(4-236) \quad C_m = \frac{M}{(\rho/2) \pi v_o^2 r^3}$$

$$= \frac{r^4 - c^4}{r^4} \frac{C_D}{\pi r^3 v_o^2} \int_{-r}^r \int_{-\sqrt{r^2 - y^2}}^{\sqrt{r^2 - y^2}} (v_o + v \omega_z)^2 y dz dy$$



Z - AXIS PERPENDICULAR TO x-y PLANE

Fig. 4-147 Parachute Canopy in Motion

Performing this integration yields

$$(4-237) \quad C_m = \frac{C_D}{\pi} \frac{r^4 - c^4}{r^4} \left(\frac{2}{3} - \frac{\pi}{4} \frac{\omega_z r}{v_o} + \frac{4}{15} \frac{\omega_z^2 r^2}{v_o^2} \right)$$

so that

$$(4-238) \quad \frac{\partial C_m}{\partial \frac{\omega_z r}{v_o}} = \frac{C_D}{\pi} \frac{r^4 - c^4}{r^4} \left(-\frac{\pi}{4} + \frac{8}{15} \frac{\omega_z r}{v_o} \right)$$

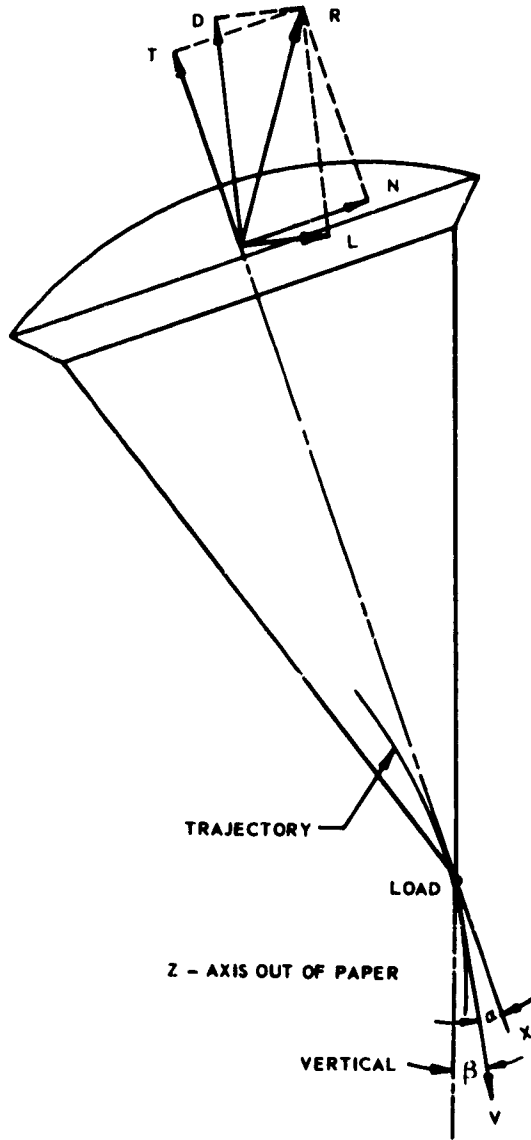


Fig. 4-148 Arrangement of Coordinates and Forces for Parachute System in Flight

For sufficiently large v_o and small ω_z

$$(4-239) \quad \left(\frac{\partial C_m}{\partial \frac{\omega_z r}{v_o}} \right)_k = -\frac{C_D}{4} \left(1 - \frac{c^4}{r^4} \right)$$

The terms

$$\frac{\partial C_L}{\partial \frac{\omega_z r}{v_o}}, \quad \frac{\partial C_m}{\partial \frac{\omega_z r}{v_o}}, \quad \text{and} \quad \frac{\partial C_m}{\partial \alpha}$$

for the total canopy with the load as moment center can now be evaluated. It is assumed that the forces and moments have arisen due to rotation of the parachute system about the z-axis which goes through the load. This rotation can be considered to be composed of a rotation of the canopy about an axis parallel to the z-axis passing through the center of the canopy volume and the simultaneous subjection of the canopy to an oblique flow of air at the angle $\Delta\alpha$. From Fig. 4-150 it can be seen that for sufficiently small $\Delta\alpha$

$$(4-240) \quad \Delta\alpha = \frac{\omega_z S}{v_o}$$

The lift coefficient, C_L , is a function of α and of ω_z . Therefore, ΔC_L can be approximated by

$$(4-241) \quad \Delta C_L = \frac{\partial C_L}{\partial \alpha} \Delta\alpha - \frac{\partial C_L}{\partial \omega_z} \Delta\omega_z$$

If $\Delta\alpha = \alpha_2 - \alpha_1$, and $\Delta\alpha$ is sufficiently small (from Eq 4-227 and 4-228):

$$(4-242) \quad \Delta C_L = -C_D \Delta\alpha$$

Thus, Eq 4-241 becomes

$$(4-243) \quad -C_D \Delta\alpha = \frac{\partial C_L}{\partial \alpha} \Delta\alpha - \frac{\partial C_L}{\partial \omega_z} \Delta\omega_z$$

Since $\Delta\alpha = \Delta\omega_z S / v_o$,

$$(4-244) \quad \Delta\alpha (C_D + \frac{\partial C_L}{\partial \alpha}) = \frac{\partial C_L}{\partial \omega_z} \Delta\alpha \frac{r}{S}$$

or

$$(4-245) \quad \frac{\partial C_L}{\partial \frac{\omega_z r}{v_o}} = \left(C_D + \frac{\partial C_L}{\partial \alpha} \right) \frac{S}{r}$$

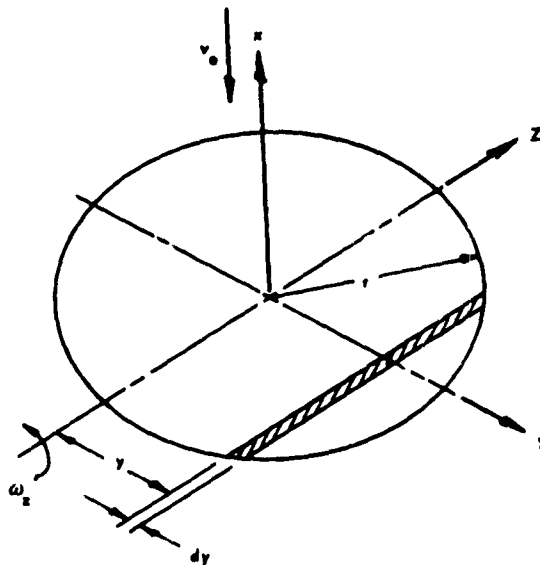


Fig. 4-149a Body of Revolution for $c/r = 0$
(Circular Disk)

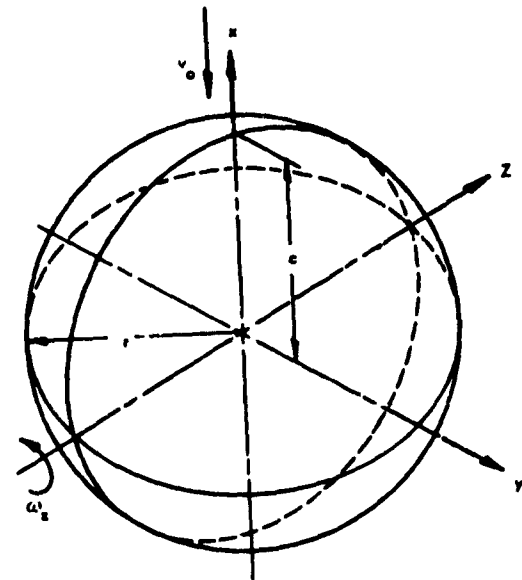


Fig. 4-149b Body of Revolution for $c/r = 1$
(Sphere)

The dependency of C_m on α has been shown through wind-tunnel tests (see 11.1). However, in these experiments the parachute system was fixed, and thus, the results do not include the influence of an angular velocity ω_z . The total change in C_m may be approximated by

$$(4-246) \quad \Delta C_m = \left(\frac{\partial C_m}{\partial \alpha} \right)_n \Delta \alpha - \frac{\partial C_N}{\partial \omega_z} \Delta \omega_z \frac{S}{r}$$

where n indicates a value determined from wind tunnel tests.

$$(4-247) \quad \frac{\Delta C_m}{\Delta \alpha} = \left(\frac{\partial C_m}{\partial \alpha} \right)_n - \frac{\partial C_N}{\partial \omega_z} \frac{\Delta \omega_z}{\Delta \alpha} \frac{S}{r}$$

Let $\omega_{z_0} = 0$; then, since $\Delta \alpha = \omega_z S / v_0$ for small $\Delta \alpha$

$$(4-248) \quad \frac{\Delta C_m}{\Delta \alpha} = \left(\frac{\partial C_m}{\partial \alpha} \right)_n - \frac{\partial C_N}{\partial \omega_z} \frac{v_0}{r} =$$

$$\left(\frac{\partial C_m}{\partial \alpha} \right)_n - \frac{\partial C_N}{\partial \frac{\omega_z r}{v_0}}$$

or

$$(2-249) \quad \frac{\partial C_m}{\partial \alpha} = \left(\frac{\partial C_m}{\partial \alpha} \right)_n - \frac{\partial C_N}{\partial \frac{\omega_z r}{v_0}}$$

For sufficiently small values of α , $C_N = C_L$.

This gives

$$(4-250) \quad \frac{\partial C_N}{\partial \frac{\omega_z r}{v_0}} = \frac{\partial C_L}{\partial \frac{\omega_z r}{v_0}} = (C_D + \frac{\partial C_L}{\partial \alpha}) \frac{S}{r}$$

Thus

$$(4-251) \quad \frac{\partial C_m}{\partial \alpha} = \left(\frac{\partial C_m}{\partial \alpha} \right)_n - (C_D + \frac{\partial C_L}{\partial \alpha}) \frac{S}{r}$$

To determine

$$\frac{\partial C_m}{\partial \frac{\omega_z r}{v_0}}$$

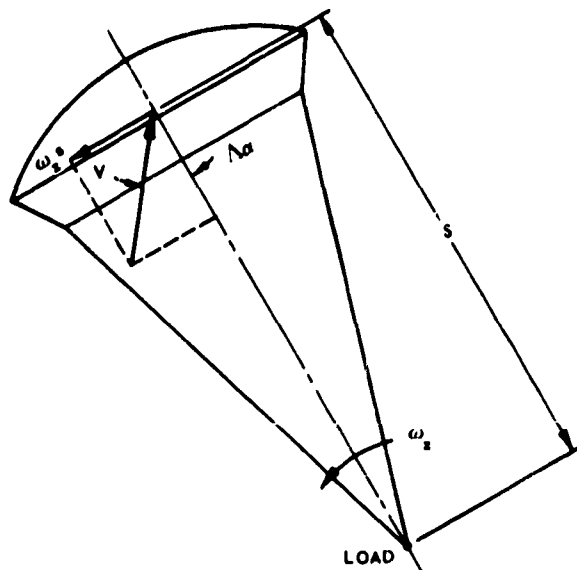


Fig. 4-150 Rotating Parachute System

it is noted that the portion of this quantity given by

$$\left(\frac{\partial C_m}{\partial \frac{\omega_z r}{v_o}} \right)_k$$

was formulated with the volume center of the canopy as moment center. The total change in C_m can be approximated by

$$(4-252) \quad \Delta C_m = \frac{\partial C_m}{\partial \alpha} \Delta \alpha + \left(\frac{\partial C_m}{\partial \omega_z} \right)_k \Delta \omega_z$$

or

$$(4-253) \quad \frac{\Delta C_m}{\Delta \omega_z} = \frac{\partial C_m}{\partial \alpha} \frac{\Delta \alpha}{\Delta \omega_z} + \left(\frac{\partial C_m}{\partial \omega_z} \right)_k$$

Again with $\omega_{z_o} = 0$, and since $\Delta \alpha = \omega_z S/v_o$

$$(4-254) \quad \frac{\partial C_m}{\partial \frac{\omega_z r}{v_o}} = \frac{\partial C_m}{\partial \alpha} \frac{S}{r} + \left(\frac{\partial C_m}{\partial \frac{\omega_z r}{v_o}} \right)_k$$

Substituting into this equation the expression for $\partial C_m/\partial \alpha$ given by Eq 4-251 gives

$$(4-255) \quad \frac{\partial C_m}{\partial \frac{\omega_z r}{v_o}} = \left(\frac{\partial C_m}{\partial \frac{\omega_z r}{v_o}} \right)_k$$

$$\left[\left(\frac{\partial C_m}{\partial \alpha} \right)_n - \left(\frac{\partial C_L}{\partial \alpha} + C_D \right) \frac{S}{r} \right] \frac{S}{r}$$

The above relationships for $\frac{\partial C_L}{\partial \alpha}$, $\frac{\partial C_m}{\partial \alpha}$, and $\frac{\partial \frac{\omega_z r}{v_o}}{\partial \alpha}$

$\frac{\partial C_m}{\partial \frac{\omega_z r}{v_o}}$ given by Eq 4-245, 4-251 and 4-255 respectively and the relationships

$$C_D = (C_D)_n \quad \frac{\partial C_L}{\partial \alpha} = \left(\frac{\partial C_L}{\partial \alpha} \right)_n$$

can be substituted into the frequency equation Eq 4-225. Therefore, by performing this substitution, the only terms in the frequency equation remaining to be evaluated are the dimensionless mass of the load, \bar{m}_L , the dimensionless apparent moment of inertia of the parachute canopy, I_{pz} , and the dimensionless virtual masses in the x and y direction, m_{vx} and m_{vy} .

The subscript n in the above relationships indicates that the value of the particular term has been experimentally determined under static conditions in the wind tunnel.

11.2.2.3 *Dimensionless Mass of the Load.* The dimensionless mass of the point load is defined as

$$(4-256) \quad \bar{m}_L = \frac{2m_L}{\pi \rho r^3}$$

11.2.2.4 *Dimensionless Apparent Moment of Inertia of the Canopy.* The dimensionless apparent moment of inertia of the canopy can be determined as follows. The kinetic energy of a rigid body due to its rotation can be expressed by

$$(4-257) \quad E_k = \frac{1}{2} \omega_x^2 I_x + \frac{1}{2} \omega_y^2 I_y + \frac{1}{2} \omega_z^2 I_z - \omega_x \omega_y I_{xy} - \omega_x \omega_z I_{xz} - \omega_y \omega_z I_{yz}$$

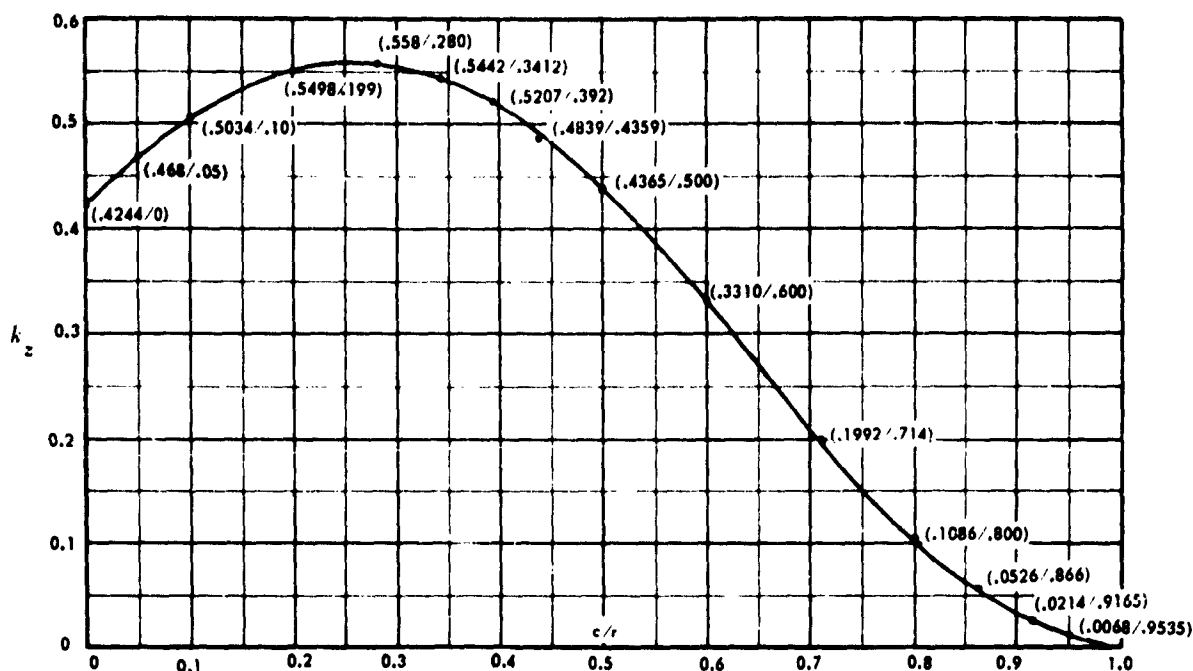


Fig. 4-151 Graphical Representation $k_z = \frac{e^4 \sqrt{1-e^2} (\gamma_0 - \alpha_0)}{2e^2 - (2-e^2)(\gamma_0 - \alpha_0)} + \frac{e^4 \sqrt{1-e^2}}{2-e^2}$ as a Function of c/r

For the simplified case, the rotational axis can be taken as coinciding with a coordinate axis x , and I_x as the moment of inertia of the body with respect to the x -axis. The equation is then

$$(4-258) \quad E_k = \frac{1}{2} \omega_x^2 I_x$$

For an ellipsoid (which, due to lack of experimental values, the canopy shape is assumed to be)

$$(4-259) \quad x^2/a^2 + y^2/b^2 + z^2/c^2 = 1$$

If the shape is immersed in a liquid and rotating with angular velocity ω , the kinetic energy of the liquid is

$$(4-260) \quad E_k = \frac{m}{5} \left[\frac{(b^2 - c^2)(\gamma_0 - \beta_0)}{2(b^2 - c^2) - (b^2 + c^2)(\gamma_0 - \beta_0)} \frac{\omega^2}{2} \right]$$

where m = mass of the displaced liquid

$$\beta_0 = abc \int_0^\infty \frac{(a^2 + \lambda)^{-1/2} (b^2 + \lambda)^{-3/2}}{(c^2 + \lambda)^{-1/2}} d\lambda$$

$$\gamma_0 = abc \int_0^\infty \frac{(a^2 + \lambda)^{-1/2} (b^2 + \lambda)^{-1/2}}{(c^2 + \lambda)^{-3/2}} d\lambda$$

(according to Ref (4-79) through (4-81)).

For the prolate ellipsoid of Eq 4-259, the additional moment of inertia is given by

$$(4-261) \quad I_{az} = \frac{m}{5} \left[\frac{(a^2 - c^2)(\gamma_0 - \alpha_0)}{2(a^2 - c^2) - (a^2 + c^2)(\gamma_0 - \alpha_0)} \right]$$

$$\alpha_0 = \beta_0 = \frac{\sqrt{1-e^2}}{e^3} \arcsin e - \frac{1-e^2}{e^2}$$

$$\gamma_0 = \frac{2}{e^2} \left(1 - \frac{\sqrt{1-e^2}}{e} \arcsin e \right)$$

$$e^2 = 1 - (c^2/a^2)$$

Eq 4-261 can now be expressed as

$$(4-262) \quad I_{az} = \frac{4}{15} \pi \rho a^2 c \left[\frac{(a^2 - c^2)(\gamma_0 - \alpha_0)}{2(a^2 - c^2) - (a^2 + c^2)(\gamma_0 - \alpha_0)} \right]$$

$$= \frac{4}{15} \pi \rho a^5 k_{az}$$

$$k_{az} = \frac{e^4 \sqrt{1-e^2} (\gamma_0 - \alpha_0)}{2e^2 - (2-e^2)(\gamma_0 - \alpha_0)}$$

When the terms for a_0 and γ_0 are substituted into the term for k_{az} ,

$$k_{az} = \frac{e^4 \sqrt{1-e^2} \left[e(3-e^2) - 3\sqrt{1-e^2} \arcsin e \right]}{2e^5 - (2-e^2) \left[e(3-e^2) - 3\sqrt{1-e^2} \arcsin e \right]}$$

It can be seen that as $e \rightarrow 0$, $k_{az} \rightarrow 0$, and as $e \rightarrow 1$, $k_{az} \rightarrow 0$. When L'Hospital's rule is applied to k_{az} ,

$$\lim_{e \rightarrow 1} k_{az} = \frac{4}{3\pi} = 0.4244$$

The included moment of inertia of a thin-shelled, liquid-filled ellipsoid of axes a , b , and c (Ref (4-79)) can be expressed as

$$I_{incl} = \frac{4}{5} \pi \rho a^2 c \frac{(a^2 - c^2)}{a^2 + c^2} = \frac{4}{15} \pi \rho a^5 k_{incl}$$

$$k_{incl} = \frac{e^4 \sqrt{1-e^2}}{2-e^2}$$

The apparent moment of inertia of a canopy, the volume of which has been transformed into an ellipsoid, will then be

$$I_z = I_{az} + I_{incl}$$

$$I_z = \frac{4}{15} \pi \rho a^5 \left[\frac{e^4 \sqrt{1-e^2} (\gamma_0 - a_0)}{2e^2 - (2-e^2) (\gamma_0 - a_0)} + \frac{e^4 \sqrt{1-e^2}}{2-e^2} \right]$$

$$I_z = \frac{4}{15} \pi \rho a^5 K_z$$

$$K_z = k_{az} + k_{incl}$$

Numerical values of K_z are plotted as a function of $c/a (= c/r)$ in Fig. 4-151.

The dimensionless apparent moment of inertia of the canopy is defined as

$$I_{vz} = \frac{2 I_z}{\pi \rho r^5}$$

or since

$$I_z = \frac{4}{15} \pi \rho r^5 K_z$$

then

$$I_{vz} = \frac{8}{15} K_z$$

11.2.2.5 Determination of the Dimensionless Virtual Mass. To determine the dimensionless virtual mass of the canopy in the x -direction (m_{vx}) and in the y -direction (m_{vy}), it is necessary to know the nominal parachute cloth porosity. The nominal cloth porosity is defined as the volume rate of airflow through a unit area of cloth under standard atmospheric conditions, with a differential pressure (Δp) across the cloth of one-half inch of water, corresponding to 2.6 psf. The velocity of the flow is then calculated as

$$v_c = \sqrt{\frac{2 \Delta p}{\rho}} \quad (\text{fps})$$

In the case of canopies with geometric porosity, the equivalent nominal porosity of the ribbon grid must be calculated. For example, in a canopy with x per cent geometric porosity, the open area in one sq ft of canopy area is $x/100$ sq ft. Hence, the volume of air which will flow through one sq ft of area in one second is

$$v_a = \frac{x}{100} v_c = Y$$

Therefore, the nominal porosity is Y cu ft per sq ft per sec or $Y \times 60$ cu ft per sq ft per min.

With the nominal cloth porosity known, the apparent mass of the canopy can be derived from experimentally determined data (Ref (4-25)), as plotted in Fig. 4-152. This plot gives the ratio of the apparent mass to the included mass of the canopy, m_{ap}/m_{incl} . By definition, the total additional mass is

$$(4-263) \quad m_{ad} = m_{ap} + m_{incl}$$

and can now be calculated.

The dimensionless virtual mass is defined as

$$m_{vx} = \frac{2m_{adx}}{\pi \rho r^3} \quad \text{and} \quad m_{vy} = \frac{2m_{ady}}{\pi \rho r^3}$$

Henn (Ref (4-37)) advises taking $m_{adx} = m_{ady}$. Therefore

$$m_{vx} = m_{vy}$$

11.2.3 SAMPLE CALCULATION FOR A STATICALLY STABLE CANOPY. The dynamic stability of a ribless guide-surface canopy and point mass are determined in this example with velocity, v_0 , equal to

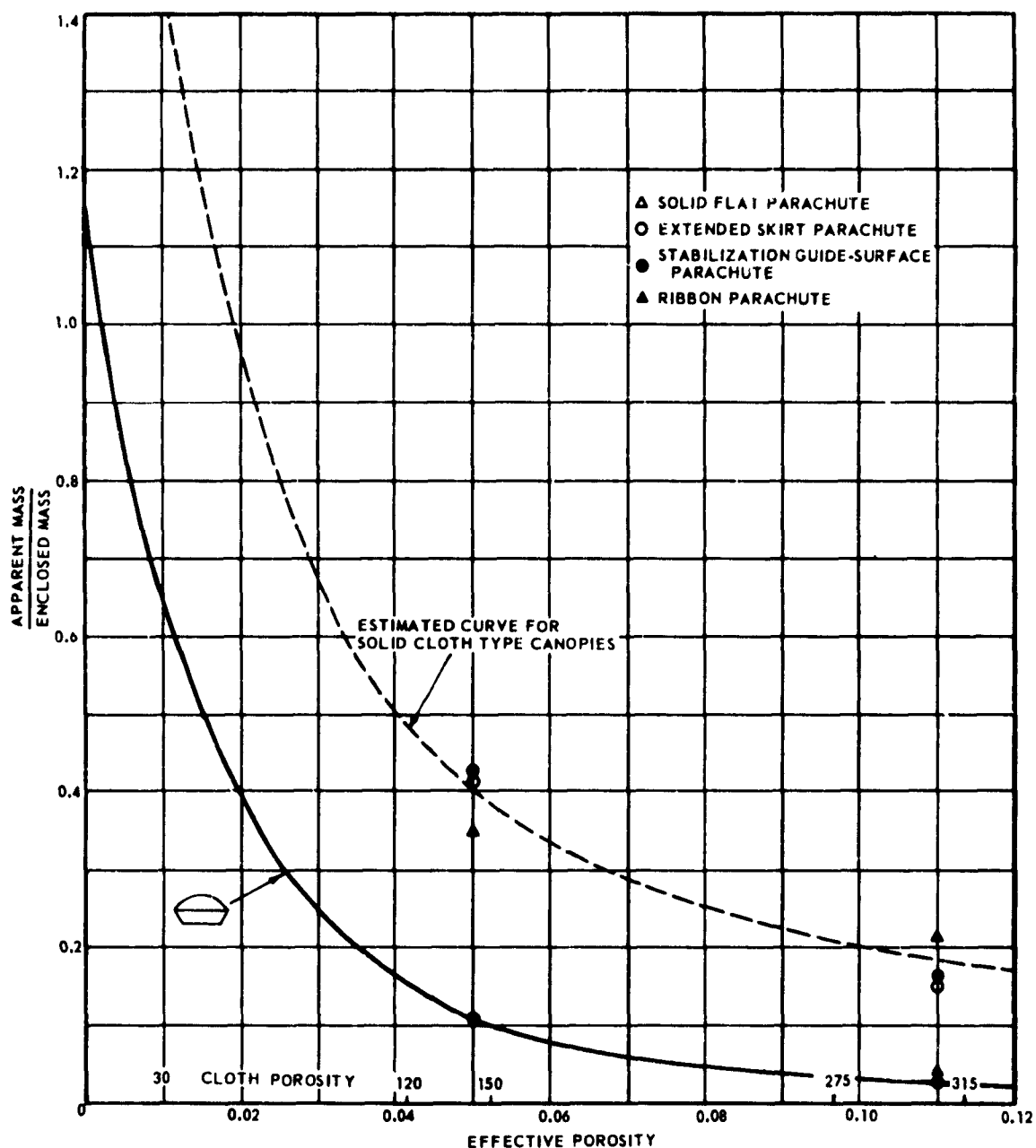


Fig. 4-152 Apparent Mass Related to Enclosed Mass vs Porosity

105 fpm.

11.2.3.1 *Physical Canopy Dimensions and Data.* For the purpose of this sample calculation, the ribless guide-surface canopy is assumed to be fabricated of Nylon material with a nominal cloth permeability of 120 cu ft per sq ft per min (MIL-C-7020B, Type III). The other defining dimensions of the canopy (Fig. 4-153) are:

R = Radius of spherical portion of the canopy = $0.75/D_p = 3.75$ ft;

$DE = 2r_1$ = Smaller diameter of the conical canopy portion = $0.7 D_p = 3.50$ ft;

h_1 = Height of the spherical canopy portion = 0.96 ft;

h_2 = Height of the conical canopy portion = 0.75 ft; and the base angle of conical canopy portion = 45° .

(1) *Canopy Volume.* The volume of the spherical portion of the canopy is

$$\begin{aligned}
 (4-264) \quad V_{\text{sph}} &= \frac{1}{3} \pi h_1^2 (3R - h_1) \\
 &= \frac{1}{3} \pi (0.96)^2 [(3 \times 3.75) - 0.96] \\
 V_{\text{sph}} &= \frac{1}{3} \pi (0.921) (10.29) = 9.93 \text{ cu ft}
 \end{aligned}$$

and the volume of the conical canopy portion is

$$\begin{aligned}
 (4-265) \quad V_{\text{con}} &= \frac{1}{3} \pi h_2 \left\{ \left(\frac{DE}{2} \right)^2 + \left[\left(\frac{D_p}{2} \right) \left(\frac{DE}{2} \right) + \left(\frac{D_p}{2} \right)^2 \right] \right\} \\
 &= \frac{1}{3} \pi 0.75 \left\{ \left(\frac{3.5}{2} \right)^2 + \left[\left(\frac{5.0}{2} \right) \left(\frac{3.5}{2} \right) + \left(\frac{5.0}{2} \right)^2 \right] \right\} \\
 &= 0.785 [3.06 + (2.5 \times 1.75) + 6.25] \\
 V_{\text{con}} &= 0.785 \times 13.69 = 10.74 \text{ cu ft}
 \end{aligned}$$

Therefore, the total volume of the canopy is

$$(4-266) \quad V_{\text{par}} = V_{\text{sph}} + V_{\text{con}} = 9.93 + 10.74 = 20.67 \text{ cu ft}$$

(2) *Location of Center of Volume.* The location of the center of volume of the spherical portion of the canopy is calculated as follows (Fig. 4-153) (measured from point O):

$$\begin{aligned}
 (4-267) \quad y_{\text{sph}_O} &= \frac{3}{4} \frac{(2R - h_1)^2}{(3R - h_1)} \\
 &= \frac{3}{4} \frac{[(2 \times 3.75) - 0.96]^2}{[(3 \times 3.75) - 0.96]} \\
 y_{\text{sph}_O} &= 0.75 \left(\frac{42.76}{10.29} \right) = 3.12 \text{ ft}
 \end{aligned}$$

or, measured from point H:

$$y_{\text{sph}} = y_{\text{sph}_O} - R + h_1 + h_2$$

$$y_{\text{sph}_H} = 3.12 - 3.75 + 0.96 + 0.75 = 1.08 \text{ ft}$$

For the conical portion, measured from point F:

$$\begin{aligned}
 (4-268) \quad y_{\text{con}} &= \frac{h_2}{4} \left[\frac{\left(\frac{D_p}{2} \right)^2 + (2 \frac{D_p}{2} \frac{DE}{2}) + 3 \left(\frac{DE}{2} \right)^2}{\left(\frac{D_p}{2} \right)^2 + \left(\frac{D_p}{2} \frac{DE}{2} \right) + \left(\frac{DE}{2} \right)^2} \right] \\
 &= \frac{0.75}{4} \left[\frac{(2.5)^2 + (2 \times 2.5 \times 1.75) + 3 (1.75)^2}{(2.5)^2 + (2.5 \times 1.75) + (1.75)^2} \right] \\
 y_{\text{con}_F} &= 0.187 \left(\frac{24.18}{13.68} \right) = 0.33 \text{ ft}
 \end{aligned}$$

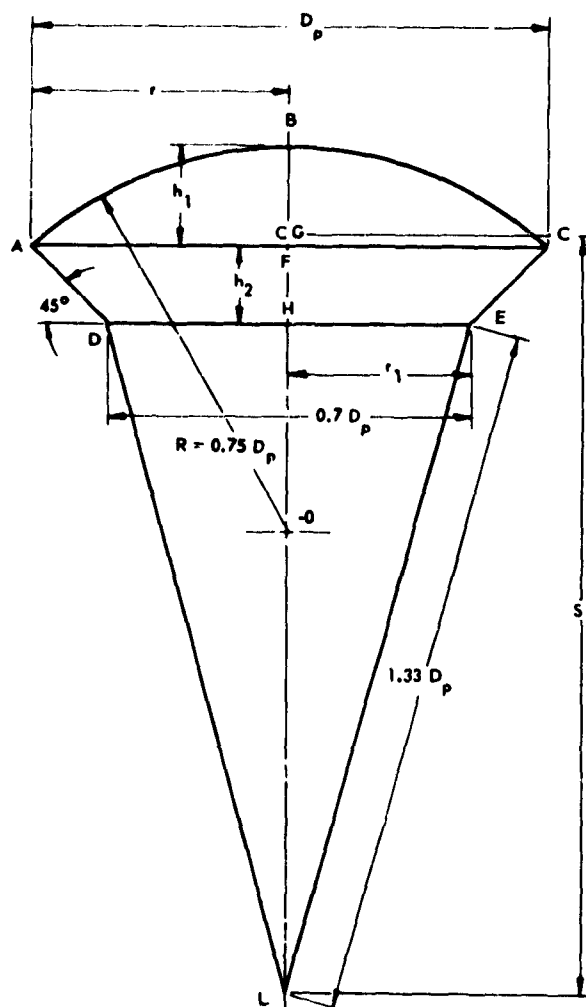


Fig. 4-153 Ribless Guide-Surface Parachute Canopy

or, measured from point *H*:

$$\begin{aligned} v_{\text{con}} &= h_2 - v_{\text{con}F} \\ (4-269) \quad v_{\text{con}H} &= 0.75 - 0.33 = 0.42 \text{ ft} \end{aligned}$$

Therefore, the center of volume of the canopy (measured from point *H*) is located at

$$\begin{aligned} v_{\text{par}H} &= \frac{I_{\text{sph}} v_{\text{sph}H} + I_{\text{con}} v_{\text{con}H}}{I_{\text{sph}} + I_{\text{con}}} \\ (4-270) \quad v_{\text{par}H} &= \frac{10.72 + 1.51}{20.67} = 0.737 \text{ ft} \end{aligned}$$

In the actual case, the center of volume of the canopy will be somewhat higher due to deformation of the conical portion by the relative airstream. Thus, let the center of volume be located at

$$(4-271) \quad v_{\text{par}H} = 0.8 \text{ ft}$$

(3) *Determination of Ratio S/r.* The distance *S* from the center of volume of the canopy to the suspended load can now be determined as (Fig. 4-153)

$$(4-272) \quad S = v_{\text{par}H} + L/H = 0.8 + 6.4 = 7.20 \text{ ft}$$

Thus, the ratio *S/r* is

$$(4-273) \quad \frac{S}{r} = \frac{7.20}{2.50} = 2.88$$

11.2.3.2 *Determination of Values for C_D , $\partial C_L/\partial \alpha$, and $\partial C_m/\partial \alpha$.* From the measured values of C_N and C_T (Sec. 11 and 6, respectively) and by means of Eq. 4-227 and 4-228, corresponding values of C_L and C_D are calculated. These values, based upon the projected canopy diameter, D_p , are tabulated in Table 4-3 along with the calculated values for $\partial C_L/\partial \alpha$ and $\partial C_m/\partial \alpha$. The values of C_L and C_m are plotted versus α in Fig. 4-154. From this plot, it can be seen that both C_L and C_m are approximately proportional to α in the region $0 \leq \alpha \leq 20^\circ$.

Therefore

$$(4-274) \quad C_L = \left(\frac{\partial C_L}{\partial \alpha} \right) \alpha$$

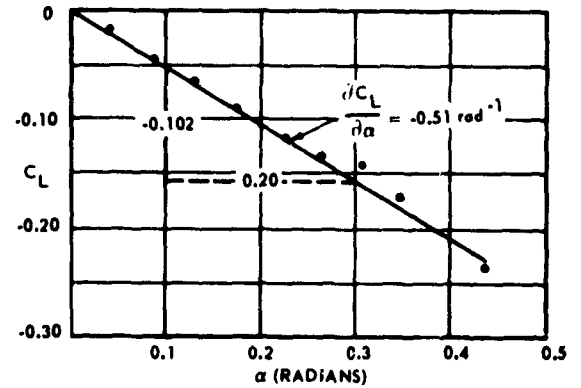
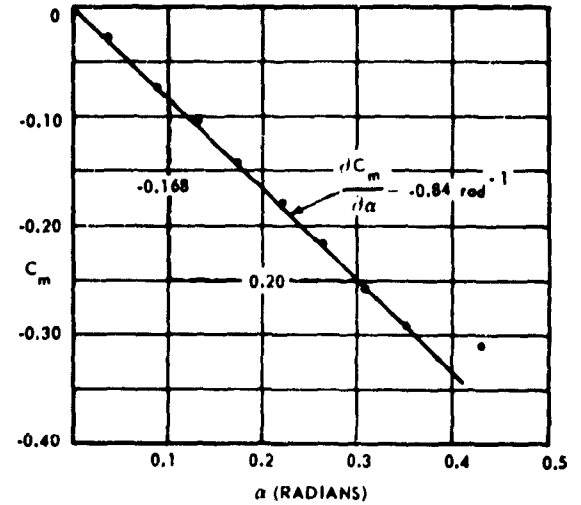


Fig. 4-154 Moment and Lift Coefficients vs Angle of Attack for Ribless Guide-Surface Canopy

and

$$(4-275) \quad C_m = \left(\frac{\partial C_m}{\partial \alpha} \right) \alpha$$

From Fig. 4-154 one finds that for the region of angle of attack considered above

$$(4-276) \quad \left(\frac{\partial C_L}{\partial \alpha} \right)_n = -0.51 \text{ rad}^{-1}$$

and

$$(4-277) \quad \left(\frac{\partial C_m}{\partial \alpha} \right)_n = -0.84 \text{ rad}^{-1}$$

The subscript *n* indicates that the quantity is measured in the wind tunnel under static conditions.

TABLE 4-3 EXPERIMENTAL DATA FOR RIBLESS GUIDE-SURFACE CANOPY MEASURED IN WIND TUNNEL AT $Re_p \approx 6 \times 10^5$ AND $v_\infty \approx 105$ FT PER SEC (NOMINAL CANOPY CLOTH POROSITY = 120 CU FT PER SQ FT PER MIN)

Angle of Attack		Measured				Calculated		
Degrees	Radians	C_T	C_Y	C_m	C_L	$\partial C_L / \partial \alpha$	C_D	$\partial C_m / \partial \alpha$
0	0	1.148	0	0	0	—	1.148	—
2.5	0.044	1.157	-0.028	-0.035	-0.022	-0.500	1.157	-0.795
5.0	0.087	1.162	-0.060	-0.074	-0.042	-0.483	1.163	-0.850
7.5	0.131	1.162	-0.085	-0.106	-0.067	-0.511	1.163	-0.810
10.0	0.174	1.157	-0.113	-0.142	-0.089	-0.512	1.159	-0.816
12.5	0.218	1.157	-0.142	-0.177	-0.112	-0.514	1.161	-0.812
15.0	0.262	1.153	-0.176	-0.220	-0.129	-0.492	1.159	-0.840
17.5	0.305	1.135	-0.210	-0.263	-0.141	-0.462	1.145	-0.863
20.0	0.349	1.118	-0.227	-0.284	-0.169	-0.485	1.129	-0.815
25.0	0.436	1.096	-0.252	-0.316	-0.234	-0.536	1.100	-0.724
30.0	0.524	0.705	-0.323	-0.405	-0.073	—	0.773	-0.774

It is also apparent from Table 4-3 that (C_D) is very nearly independent of α , and has the average value

$$(4-278) \quad (C_D)_n = 1.15$$

11.2.3.3 Determination of the Value of $\partial C_m / \partial \frac{\omega_z r}{v_o}$

To evaluate this term for the ribless guide-surface canopy, the ratio c/r must be determined. To accomplish this, the canopy must be replaced with a rotational ellipsoid having the same volume as the canopy, the same position of volume center, and major axis equal to the projected diameter, D_p , of the canopy (Fig. 4-155). The semi-minor axis, c , is then determined from

$$(4-279) \quad V_{\text{par}} = V_{\text{ell}} = \frac{4}{3} \pi r^2 c = 20.67 \text{ cu ft}$$

With $r = D_p/2 = 2.5$ ft, this equation gives

$$(4-280) \quad \frac{c}{r} = 0.32$$

From Eq 4-239, and for $c/r = 0.32$,

$$(4-281) \quad \left(\frac{\partial C_m}{\partial \frac{\omega_z r}{v_o}} \right)_k = - \frac{(C_D)_n}{4} \left[1 - \left(\frac{c}{r} \right)^4 \right] =$$

$$= - \frac{1.15}{4} \left[1 - (0.32)^4 \right]$$

$$= -0.288 (1 - 0.0105) = -0.284 \approx -0.30$$

11.2.3.4 Determination of the Value of the Dimensionless Mass of the Load. The assumed weight of the suspended point load is 200 lb. With the definition of the dimensionless mass of load (11.2.2.5), and with $\rho = 0.00238$ slugs per cu ft the value of the dimensionless mass of the load is

$$(4-282) \quad \bar{m}_L = \frac{2m_L}{\pi \rho r^3} = \frac{2 \times 200}{32.2 \times \pi \times (2.5)^3 \times 2.38 \times 10^{-3}}$$

$$\bar{m}_L = 106.5$$

11.2.3.5 Determination of the Value of the Dimensionless Apparent Moment of Inertia. The dimensionless apparent moment of inertia of the canopy is given by

$$(4-283) \quad I_{vz} = \frac{8}{15} k_z$$

For the ribless guide-surface canopy, with the ratio $c/r = 0.32$, the value of k_z is found from Fig. 4-151 to be

$$(4-284) \quad k_z = 0.54$$

Therefore, for this canopy, the dimensionless apparent moment of inertia is

$$(4-285) \quad I_{vz} = \frac{8}{15} (0.54) = 0.288$$

11.2.3.6 *Determination of Values of the Dimensionless Additional Mass.* From Fig. 4-152, for a nominal cloth porosity of 120 cu ft per sq ft per min (effective porosity 0.042), the ratio of the apparent mass to the included mass for the ribless guide-surface canopy is

$$(4-286) \quad \frac{m_{ap}}{m_{incl}} = 0.16$$

The included mass, m_{incl} , for the canopy is

$$(4-287) \quad m_{incl} = V_{par} \rho = 20.67 \rho$$

Hence

$$(4-288) \quad m_{ap} = 3.31 \rho$$

By definition, the total additional mass is

$$(4-289) \quad m_{ad} = m_{ap} + m_{incl} = 3.31 \rho + 20.67 \rho \\ = 23.98 \rho$$

Equation 4-289 then gives the value of the dimensionless apparent mass of the canopy as

$$(4-290) \quad m_{vx} = m_{vy} = \frac{2m_{ad}}{\pi \rho r^3} = \frac{2 \times 23.98 \rho}{\pi (2.5)^3 \rho} \\ = \frac{47.96 \rho}{49.06 \rho} = 0.98$$

11.2.3.7 *Solution of the Frequency Equation.* Each term in the frequency equation has now been evaluated; this equation can therefore be solved to obtain the

final solution to the differential equations 4-222 and 4-223. All values of terms evaluated are summarized below:

$$\begin{aligned} \frac{S}{r} &= 2.88 \\ (C_D)_n &= 1.15 \\ \left(\frac{\partial C_L}{\partial \alpha} \right)_n &= -0.51 \text{ rad}^{-1} \\ \left(\frac{\partial C_m}{\partial \alpha} \right)_n &= -0.84 \text{ rad}^{-1} \\ \left(\frac{\partial C_m}{\partial \frac{\omega_z r}{v_o}} \right)_k &= -0.30 \\ \bar{m}_L &= 106.5 \\ I_{vz} &= 0.288 \\ m_{vx} = m_{vy} &= 0.98 \end{aligned}$$

(1) *Routh's Criteria.* Substituting these values in the frequency equation

$$(4-291) \quad \left[I_{vz} (\bar{m}_L + m_{vx}) + \bar{m}_L m_{vy} \left(\frac{S}{r} \right)^2 \right] \lambda^3 + \\ \left\{ \left[\left(\frac{\partial C_L}{\partial \alpha} \right)_n + (C_D)_n \right] \left[I_{vz} + \bar{m}_L \left(\frac{S}{r} \right)^2 \right] - \left(\frac{\partial C_m}{\partial \alpha} \right)_n \right\} \lambda^2 + \\ \bar{m}_L \frac{S}{r} - (\bar{m}_L + m_{vx}) \left(\frac{\partial C_m}{\partial \frac{\omega_z r}{v_o}} \right)_k - (m_{vx} - m_{vy}) \bar{m}_L \frac{S}{r} \lambda^2 - \\ \left\{ \left(\frac{\partial C_m}{\partial \alpha} \right)_n (\bar{m}_L + m_{vx}) - \bar{m}_L \left(\frac{\partial C_L}{\partial \alpha} \right)_n \frac{S}{r} - (C_D)_n \right\} \lambda - \\ (\bar{m}_L + m_{vy}) \frac{S}{r} + \left(\frac{\partial C_m}{\partial \frac{\omega_z r}{v_o}} \right)_k \left[\left(\frac{\partial C_L}{\partial \alpha} \right)_n + (C_D)_n \right] \lambda - \\ (C_D)_n \left\{ \left(\frac{\partial C_m}{\partial \alpha} \right)_n - \left[\left(\frac{\partial C_L}{\partial \alpha} \right)_n + (C_D)_n \right] \frac{S}{r} \right\} = 0$$

This yields

$$(4-292) \quad \lambda^3 + 0.959 \lambda^2 + 0.316 \lambda + 0.0034 = 0$$

Necessary and sufficient conditions for dynamic stability of motion are expressed in Routh's criteria as $a > 0$, $b > 0$, $c > 0$, $d > 0$ and $bc > d$, where a , b , c , and d are the coefficients of the frequency equation. Applying these criteria to the above equation it can be seen that the motion of the ribless guide-surface canopy is dynamically stable.

The roots of Eq 4-292 define the descent characteristics of the canopy. A real root corresponds to an aperiodic sideslip motion and a complex conjugate root corresponds to an oscillation, with the real part of the complex root defining damping and the complex part defining frequency.

The values of the three roots in Eq 4-292 are

$$\begin{aligned}\lambda_1 &= -0.0111 \\ \lambda_2 &= -0.474 + 0.284i \\ \lambda_3 &= -0.474 - 0.284i\end{aligned}$$

11.2.3.8 *Solution of the Equations of Motion.* Substituting the above values of λ into Eq 4-224 gives the solution to the differential equations of motion (Eq 4-222 and 4-223) for the ribless guide-surface canopy as

$$(4-293) \quad \alpha = A_1 e^{-0.0111r} + A_2 e^{(-0.474+0.284i)r} + A_3 e^{(-0.474-0.284i)r}$$

$$(4-294) \quad \beta = B_1 e^{-0.0111r} + B_2 e^{(-0.474+0.284i)r} + B_3 e^{(-0.474-0.284i)r}$$

Since $r = v_o t / r$ and for our case $v_o = 105$ fps and $r = 2.5$ ft,

$$(4-295) \quad r = 42t$$

With this, the solution becomes

$$(4-296) \quad \alpha = A_1 e^{-0.466t} + A_2 e^{(-19.9+11.93i)t} + A_3 e^{(-19.9-11.93i)t}$$

$$(4-297) \quad \beta = B_1 e^{-0.466t} + B_2 e^{(-19.9+11.93i)t} + B_3 e^{(-19.9-11.93i)t}$$

or finally

$$(4-298) \quad \alpha = A_1 e^{-0.466t} + e^{-19.9t} (A_2 \cos 11.93t + A_3 \sin 11.93t)$$

$$(4-299) \quad \beta = B_1 e^{-0.466t} + e^{-19.9t} (B_2 \cos 11.93t + B_3 \sin 11.93t)$$

The arbitrary constants A_i and B_i ($i = 1, 2, 3$) are calculated from the initial conditions (at $t = 0$, $\alpha = \alpha_o$, $\beta = \beta_o$, and $\omega_z = \omega_{zo}$). Eq 4-222, 4-223, 4-224, and 4-245 combine to form the following equation:

$$(4-300) \quad \frac{A_i}{B_i} = [\lambda_i \{ \bar{m}_L + m_{vx} - [\left(\frac{\partial C_L}{\partial \alpha} \right)_n + (C_D)_n] \frac{S}{r} - \lambda_i^2 m_{vy} \frac{S}{r} + (C_D)_n] + [\lambda_i \{ m_{vy} - m_{vx} - [\left(\frac{\partial C_L}{\partial \alpha} \right)_n - (C_D)_n] \frac{S}{r} + \lambda_i^2 m_{vy} \frac{S}{r} + \left(\frac{\partial C_L}{\partial \alpha} \right)_n]$$

From this, the individual values of A_1/B_1 , A_2/B_2 , and A_3/B_3 can be calculated, giving

$$(4-301) \quad A_1/B_1 = 0.0457, \quad A_2/B_2 = 40.0 - 42.2i,$$

$$A_3/B_3 = 40.0 + 42.2i$$

The initial conditions are, in general, for $t = 0$, $\alpha = \alpha_o$, $\beta = \beta_o$, and $\omega_z = \omega_{zo}$ which give

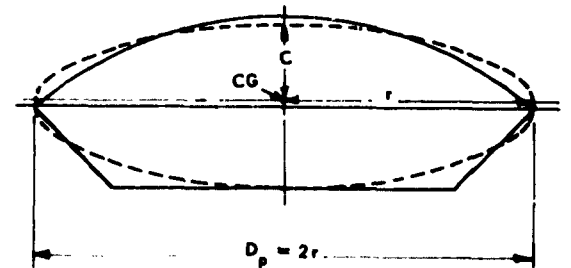


Fig. 4-155 Replacement of Ribless Guide-Surface Parachute by Rotational Ellipsoid

$$(4-302) \quad \alpha_o = A_1 + A_2 + A_3$$

$$(4-303) \quad \beta_o = B_1 + B_2 + B_3$$

$$\omega_{z_o} = (\alpha' + \beta')_o = (A_1 + B_1) \lambda_1 + (A_2 + B_2) \lambda_2 + (A_3 + B_3) \lambda_3$$

Thus, for a given set of initial conditions, Eq 4-301 through 4-303 determines the constants A_i and B_i .

With the results obtained, a number of important conclusions can be drawn concerning the static and dynamic stability of the parachute, and its motion during descent.

The derivative $\partial C_m / \partial \alpha$, represented by the next equation, is of special importance. From it a distance $s = \xi$ can be determined that locates the so-called "point of difference". This is the point about which the moment is always zero; i.e., with the suspended load positioned at this point, the parachute stability is indifferent to outside disturbances. It corresponds to the aerodynamic center of an airplane. The distance ξ is calculated as

$$\frac{\partial C_m}{\partial \alpha} = \left(\frac{\partial C_m}{\partial \alpha} \right)_n - \left[\left(\frac{\partial C_L}{\partial \alpha} \right)_n + (C_D)_n \right] \frac{\xi}{r} = 0$$

or with the values calculated previously for $(\partial C_m / \partial \alpha)_n$, $(\partial C_L / \partial \alpha)_n$ and $(C_D)_n$ and listed in 11.2.3.7, above, $\xi = 3.28$ ft.

For any distance, ξ , which satisfied the condition

$$\left(\frac{\partial C_m}{\partial \alpha} \right)_n - \left[\left(\frac{\partial C_L}{\partial \alpha} \right)_n + (C_D)_n \right] \frac{\xi}{r} < 0$$

the parachute will have weathercock stability; i.e., it will tend to turn into the wind when subjected to an oblique flow of air. For the ribless guide-surface canopy under consideration, the condition for weathercock stability is therefore $\xi > 3.28$ ft. Since the distance, s , is 7.20 ft, the parachute is stable.

Eq 4-298 and 4-299 indicate that the parachute has two inherent motions, an aperiodic motion and an oscillation. The real roots of the frequency equation were found to be negative; therefore, the aperiodic motion is non-progressive. Also, the complex root pairs have negative real parts, which means that the occurring oscillations fade out. The half-value times for the oscillation portion of the motion of the para-

chute are determined from Eq 4-298 and 4-299 as

For α_1 and β_1 , $(t_{1/2}) = 1.49$ sec

For α_2 and β_2 , $(t_{1/2}) = 0.035$ sec

For α_3 and β_3 , $(t_{1/2}) = 0.035$ sec

If the parachute is descending at a rate of 105 fps, the amplitude of any disturbance which occurs will therefore decay to one-half its original value after a descent of the order of 155 ft. The period of oscillation and the frequency of the periodic motion are calculated from the imaginary portion of Eq 4-298 and 4-299 as

$$(4-304) \quad T = \frac{2\pi}{11.93} = 0.527 \text{ sec}$$

$$f = \frac{1}{T} = 1.90 \text{ cps}$$

The selection of the initial conditions for the moving parachute is one of the most difficult problems in the solution of the equation of its motion because it is very difficult to say when the "parachute" actually becomes a functioning parachute (i.e., fully inflated) after it is released from an aircraft. Henn (Ref (4-75)) suggests considering, as a first step, one of the most common cases of disturbed motion of a parachute, the strong pendulous motion of the load about the canopy initiated by the opening-shock. The initial conditions are chosen, then, for $t = 0$, $\alpha = \alpha_o \neq 0$, $\beta = \beta_o = 0$, and $\omega_z = \omega_{z_o} = 0$. With these boundary conditions, and the set of equations 4-301 through 4-303, the coefficients A_i and B_i can be determined. Substituting the numerical values of these coefficients into Eq 4-298 and 4-299, and performing a few algebraic manipulations, the equations of motion for the ribless guide-surface canopy are

$$(4-305) \quad \begin{aligned} \alpha &= \alpha_o \left[-0.00137e^{-0.466t} + 1.77e^{-19.9t} \times \right. \\ &\quad \left. \sin(11.93t + 34.4^\circ) \right] \\ \beta &= \alpha_o \left[-0.0300e^{-0.466t} + 0.0304e^{-19.9t} \times \right. \\ &\quad \left. \sin(11.93t + 80.9^\circ) \right] \end{aligned}$$

Assuming the initial conditions $t = 0$ and $\alpha_o = 7.5^\circ = 0.1309$ radians, from Eq 4-305

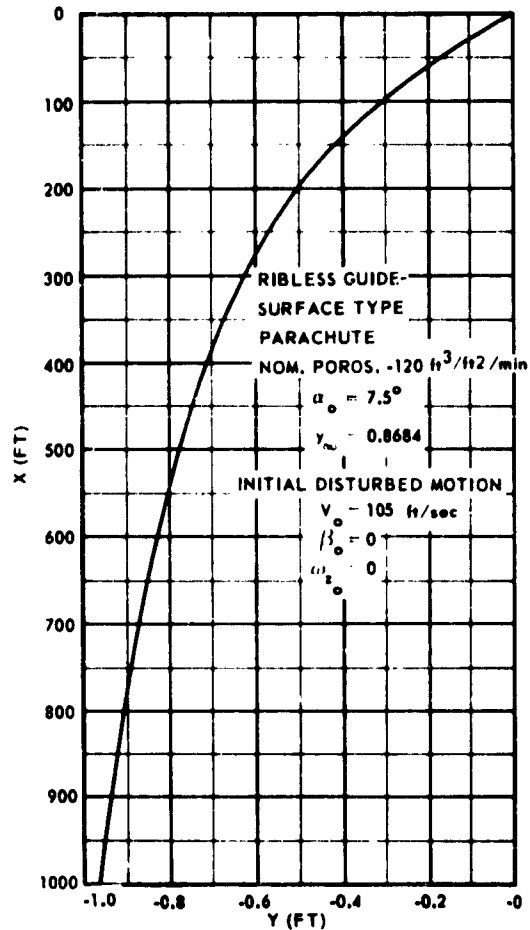


Fig. 4-156 Graphical Presentation of Motion of Parachute System During Descent

$$(4-306) \quad \alpha = -0.000179e^{-0.466t} + 0.232e^{-19.9t} \sin(11.93t + 34.4^\circ)$$

$$\beta = -0.00393e^{-0.466t} + 0.00398e^{-19.9t} \sin(11.93t + 80.9^\circ)$$

Eq 4-306 can be solved for the inclination angle, $(\alpha + \beta)$, to give

$$(4-307) \quad (\alpha + \beta) = -0.0041e^{-0.466t} + 0.236e^{-19.9t} \sin(11.93t + 35.1^\circ)$$

In order to describe the motion of the parachute, the motion of the load and the motion of the canopy are

considered separately. The motion of the load can be determined from the trajectory angle β . The vertical and horizontal coordinates (x and y , respectively) of the position of the load are

$$(4-308) \quad x = \int v \cos \beta dt \quad \text{and}$$

$$y = \int v \sin \beta dt$$

or, for β sufficiently small, v is approximately equal to v_0 and, therefore

$$(4-309) \quad x = v_0 t$$

$$(4-310) \quad y = v_0 \int \beta dt$$

Substituting the expression for β given by Eq 4-306 into Eq 4-310 and assuming that $v_0 = 105$ ft/sec, the motion of the ribless guide-surface canopy is then given by

$$(4-311) \quad x = 105 t$$

$$(4-312) \quad y = 0.885e^{-0.466t} + 0.0179e^{-19.9t} \sin(11.93t + 68.1^\circ) - 0.868$$

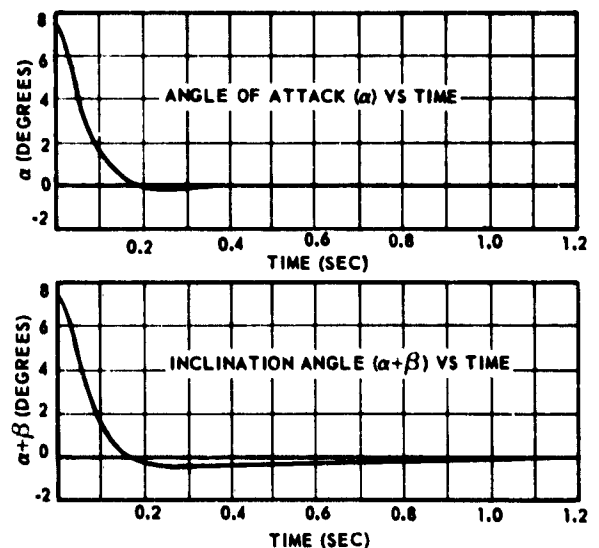


Fig. 4-157 Graphical Presentation of α and $\alpha + \beta$ vs Time

TABLE 4-4
COORDINATES OF PARACHUTE SYSTEM DURING DESCENT

t (sec)	0	0.1	0.2	0.3	0.4	0.5	0.7	1.0	1.5	2.0	3.0	5.0	10.0	20.0	30.0	100.0
x (ft)	0	10.5	21.0	31.5	47.0	60.3	73.5	105.0	157.5	210.0	345.0	525.0	1050	2100	3150	10500
y (ft)	0	-0.02	-0.06	-0.10	-0.15	-0.17	-0.23	-0.31	-0.43	-0.52	-0.65	-0.78	-0.86	-0.87	-0.87	-0.87
$\alpha + \beta$	$7^{\circ}30'$	$1^{\circ}35'$	$-0^{\circ}11'$	$-0^{\circ}15'$	$-0^{\circ}12'$	$-0^{\circ}11'$	$-0^{\circ}10'$	$-0^{\circ}09'$	$-0^{\circ}07'$	$-0^{\circ}05'$	$-0^{\circ}04'$	$-0^{\circ}01'$	0	0	0	0

TABLE 4-5
ANGLE OF ATTACK (α) AND INCLINATION ANGLE ($\alpha + \beta$)

t (sec)	0	0.01	0.02	0.03	0.04	0.05	0.06	0.07	0.08	0.09	0.10	0.125
α	$7^{\circ}30'$	$7^{\circ}10'$	$6^{\circ}37'$	$5^{\circ}58'$	$5^{\circ}16'$	$4^{\circ}34'$	$3^{\circ}52'$	$3^{\circ}15'$	$2^{\circ}42'$	$2^{\circ}05'$	$1^{\circ}47'$	$57'$
$\alpha + \beta$	$7^{\circ}30'$	$7^{\circ}08'$	$6^{\circ}34'$	$5^{\circ}53'$	$5^{\circ}08'$	$4^{\circ}26'$	$3^{\circ}44'$	$3^{\circ}05'$	$2^{\circ}31'$	$2^{\circ}00'$	$1^{\circ}35'$	$44'$
t (sec)	0.15	0.175	0.20	0.25	0.30	0.40	0.50	0.70	1.00	1.50	2.00	
α	$27'$	$11'$	$2'$	$-3'$	$-2'$	$-2'$	0	0	0	0	0	
$\alpha + \beta$	$14'$	$-2'$	$-11'$	$-15'$	$-15'$	$-12'$	$-11'$	$-10'$	$-9'$	$-7'$	$-5'$	

If the initial altitude of the parachute is approximately 10,000 ft, the time of descent will be approximately 100 seconds. In Table 4-4, x , y , and $(\alpha + \beta)$ are tabulated for various values of t between 0 and 100 seconds. The results are presented graphically in Fig. 4-156. The angles α and $(\alpha + \beta)$ are tabulated in Table 4-5 for the smaller range of t between 0 and 2 seconds. These results are presented in Fig. 4-157.

The most significant results of this stability analysis can be summarized as follows:

- (a) Fig 4-298 and 4-299 indicate that the parachute has an aperiodic motion and a periodic oscillation;
- (b) The periodic as well as the aperiodic motion is damped;
- (c) The influence of the oscillation on the resultant motion is relatively small;
- (d) The period of the oscillation and the frequency of oscillation are $T = 0.527$ sec and $f = 1.90$ cps; and
- (e) Any disturbances that occur during an equilibrium speed of 105 fps will decay to one-half the original value after a vertical descent of approximately 155 ft.

SEC. 12 AERODYNAMIC HEATING

During supersonic flight within the perceptible atmosphere, it is evident that a considerable region exists where the operation of an aerodynamic deceleration device of practical dimensions will produce little or no deceleration for a prolonged period of time. Under such conditions the deceleration device will be subject to aerodynamic heating long enough to attain a near-equilibrium temperature. The deceleration of aerospace vehicles prior to the deployment of the main recovery parachute has been successfully accomplished, by means of textile canopies, from initial speeds as high as Mach 2.45 and altitudes of the order of 60,000 ft. These conditions may be regarded as the threshold, past which aerodynamic heating may weaken or even destroy Nylon textile canopies. However, because of the rapid deceleration usually associated with aerospace-vehicle recovery operations, the dwell time in the threshold environment has not been sufficiently long to produce damaging surface temperatures. But as the application of textile canopies is extended into the higher Mach number regime, the prediction of the temperature history of a canopy along its descent trajectory will be of vital interest to the design engineer.

A method was initially proposed in Ref (4-82) and expanded in Ref (4-83) and (4-84), to calculate the

temperature-time history of a canopy during descent. Ref (4-83) presents an analysis which predicts the average instantaneous equilibrium temperature of a canopy, assuming an average heat-transfer coefficient. This method would be adequate for design purposes if the materials used in the fabrication of canopies were good thermal conductors. However, canopies constructed of fabrics are poor conductors, and since aerodynamic decelerators are, in a majority of cases, of irregular shape, large temperature gradients can develop in the material, both normal and parallel to the canopy surface. Ref (4-85) extends the analysis initially developed in Ref (4-83) and considers the case of a practical aerodynamic decelerator capable of dissipating heat by radiation from its surface and thermal diffusion to its structure.

The thermal problems encountered in designing aerodynamic deceleration devices for operation at high Mach numbers are similar to those encountered in the design of any reentry body. Many different design approaches have been considered for the control of temperature; cooling by mass transfer, ablation, radiation, and diffusion; employing temperature-resistant organic fabrics, glass cloth, and graphite cloth; and using conductive materials, such as wire mesh cloth. Using subliming coatings, blunting of the leading edge, and constructing with thicker materials are other alternatives. However, since aerodynamic decelerators should exhibit a large drag-to-weight ratio and must be stored in a small volume, materials used in the construction of parachute-like drag-producing devices must be relatively thin. These limitations generally rule out cooling by mass transfer or ablation. Diffusion in the material is effective only for relatively short exposure time (a few seconds) because of the thinness and light-weight construction of practical aerodynamic decelerators, making it of significance only if the trajectory conditions are changing rapidly. Radiative cooling is therefore the primary method by which the surface of high-temperature aerodynamic decelerators dissipates heat.

12.1 Energy Equations. When a body moves through the air at supersonic speed, its surface becomes heated to a temperature above that of the surrounding undisturbed air. This phenomenon is known as aerodynamic heating. The cause of this temperature rise is the deceleration of the air in the boundary layer located along the surfaces of the moving body and in the wake behind it; the kinetic energy is converted into thermal energy. This aerodynamic heating, together with that from solar radiation, and friction caused by one layer of air sliding over another in the sharp velocity gradient of the boundary layer, may become so severe that the surfaces or other struc-

tural components of the moving body may become severely damaged or completely destroyed.

The temperature-time history of aerodynamic deceleration devices may be studied by applying the principle of conservation of energy, which can be expressed as: the difference between the rate of energy entering and leaving a body must be equal to the rate at which energy is stored within the body. In the case of a canopy moving through the atmosphere at high speeds, there will be a flow of energy into the canopy by convection from the surrounding air, which has been heated by friction in the boundary layer and compression in the shock wave; in addition, heat will flow into the canopy from solar radiation. The only process by which the canopy may lose heat is by radiation to space and to the earth (Ref (4-83)).

12.1.1 ENERGY FLOW INTO CANOPY BY CONVECTION. The heat transfer to a canopy by convection may be calculated from the following relation:

$$(4-313) \quad Q_c = h S_1 (T_{AW} - T_W)$$

where S_1 = Surface area of body exposed to aerodynamic heating (sq ft); for hollow hemisphere = $\pi D_p^2/2$;

h = Convection heat transfer coefficient (Btu per sec $^{\circ}\text{F}$ sq ft);

T_W = Temperature at the walls ($^{\circ}\text{R}$); and

T_{AW} = Adiabatic wall temperature ($^{\circ}\text{R}$).

The adiabatic wall or recovery temperature, T_{AW} , is dependent upon the trajectory of the canopy, and will vary with air density. It can be expressed as

$$(4-314) \quad T_{AW} = T_{\infty} + \frac{n V_{\infty}^2}{2 C_p} = T_{\infty} \left[1 + n \left(\frac{\gamma-1}{2} \right) M_{\infty}^2 \right]$$

where T_{∞} = Free-stream static temperature ($^{\circ}\text{R}$);

V_{∞} = Free-stream velocity (fps);

C_p = Specific heat of fluid at constant pressure (sq ft per sec per sec $^{\circ}\text{R}$);

n = Recovery factor;

γ = Ratio of specific heats; and

M_{∞} = Free-stream Mach number.

If as a result of a solution of T_{AW} (Eq 4-314) the temperature is found to be below the maximum allowable temperature of the decelerator material, no further considerations are required, since the calculated equilibrium local instantaneous temperature will be well above the actual surface temperatures experienced while the decelerator is being heated. If, however, the maximum equilibrium temperature exceeds the design limit, it is then necessary to tackle the more complex problem of calculating the actual surface temperatures, including the heat-sink effect of the decelerator wall.

12.1.2 CONVECTIVE HEAT-TRANSFER COEFFICIENT. The greatest source of uncertainty in the energy equation (4-313) lies in the determination of the convective heat-transfer coefficient, since only limited theoretical and experimental values are available. However, some indication of the magnitude of this coefficient can be gained by analytical methods.

A ribbon-grid canopy is the most common type considered for supersonic operations. At supersonic speeds the aerodynamic conditions encountered by this canopy type, incorporating moderate geometric canopy porosity, are essentially as follows: a detached shock occurs in front of the canopy; behind this shock wave, the velocity of the air relative to that of the canopy is reduced to subsonic values. While part of this subsonic air flow spills over the skirt edge of the canopy, the other part is passing through the open spaces between the ribbons and through the porous fabric of the ribbons themselves. Thus, the canopy resembles a porous hemisphere subjected to an axially symmetrical air flow from the direction of the concave side of the hemisphere. On the downstream side, a separated flow region exists. On the upstream side (inside) of the canopy, the static pressure approaches the stagnation pressure of the air downstream of the detached shock. Even at high subsonic velocities, the pressure ratio across the canopy may become supercritical on the entire canopy. Therefore, the flow velocities through all open spaces between the ribbons will approach sonic (Ref (4-56)).

The pressure and temperature of the air inside the canopy depend on altitude and on the velocity of the canopy. Heat will be transferred from the hot air to the ribbons. The combination of the convective heat-transfer coefficient, h , the significant length, l , and the thermal conductivity of the fluid, k , in the form hl/k , is called the Nusselt modulus, or Nusselt number, Nu (Ref (4-86)). In practice, the Nusselt number is a convenient measure of the convective heat-transfer coefficient, because once its value is known, the convective heat-transfer coefficient can be calculated from the relation

$$(4-315) \quad h = Nu \frac{k}{l}$$

The Nusselt number is a function of several parameters and can be expressed by the following dimensionless relationship (Ref (4-87)):

$$(4-316) \quad \text{Nusselt number } (Nu) = f \left[\text{Prandtl } (Pr), \text{ Mach } (M_\infty), \text{ Reynolds } (Re), \text{ and Knudsen } (Kn) \text{ numbers} \right]$$

The value of the Prandtl number (Pr) under normal atmospheric pressure and temperatures up to about 6000 R is approximately 0.7. The descent Mach number (M_∞) has only an indirect influence upon the heat transfer to the ribbons, as far as it determines pressure and temperature inside the canopy and behind it. For the flow and heat transfer around the ribbons, the pressure ratio p_o/p_e is a more suitable parameter. The Reynolds number (Re) describes the flow conditions around the ribbons and is based, in this case, upon the ribbon width, l , and the average velocity and properties of the flow through the openings between the ribbons. For an approximate evaluation of the conditions during descent at various descent Mach numbers and altitudes, it is convenient to define a Reynolds number based on the velocity and flow properties in the narrowest cross-section of the jet, where for supercritical-pressure ratios, sonic velocity exists. This Reynolds number is denoted as $Re^* = l \cdot \rho^* \cdot V^*$, values versus descent Mach number, M_∞ , for various altitudes were determined in Ref (4-87) and are plotted in Fig. 4-158. The ribbon width, l , was taken to be 2.0 in. The Knudsen number (Kn) will enter as a parameter only at very low densities. It can be expressed as a relation between Mach number and Reynolds number, as for instance $M_\infty^2 = Re^*/Re$. Ref (4-88) gives as a critical value $M_\infty^2 = Re^*/Re = 10^{-3}$. Since in the case of a ribbon canopy in supersonic flow, the flow through the openings has near sonic velocity (when M would equal 1), continuum flow can be expected to exist for descent conditions at which $Re = Re^* > 1000$.

Considering the effects of various parameters upon the heat transfer of a parachute ribbon, the following relation can be expected (Ref (4-87)):

$$(4-317) \quad Nu = f(Re, p_o/p_e)$$

This relationship was determined experimentally; the results obtained are shown in Fig. 4-159 for both the upstream and downstream sides of a ribbon grid under supercritical-pressure ratios.

12.1.3 ENERGY FLOW INTO CANOPY FROM SOLAR RADIATION. The heat flow into a canopy by solar radiation may be determined from the relation

$$(4-318) \quad Q_r = I a S_2$$

where I = Solar radiation intensity; a reasonable estimate of its value is 425 Btu per hr per

sq ft;

a = Absorptivity of the canopy material; absorptivity values for various materials may be found in Chapter 6; and

S_2 = Projected area of body in a plane normal to the sun's rays (sq ft) (for hollow hemisphere: $\pi l^2 p/4$).

12.1.4 ENERGY LOSS FROM CANOPY BY RADIATION TO SPACE. The energy loss from a canopy by radiation to space is given by

$$(4-319) \quad Q_r = \sigma S_3 \epsilon (T_w^4 - T_{\text{space}}^4)$$

where σ = Modified Stefan-Boltzman constant equal to 4.80×10^{-13} Btu per sec $^{\circ}R^4$ sq ft;

ϵ = Emissivity of the canopy material; (emissivity values for various materials may be found in Chapter 6);

S_3 = Area of body radiating to space (sq ft); (for hollow hemisphere: $\pi l^2 p/2$);

T_w = Temperature at the walls ($^{\circ}R$); and

T_{space} = Temperature of space ($^{\circ}R$).

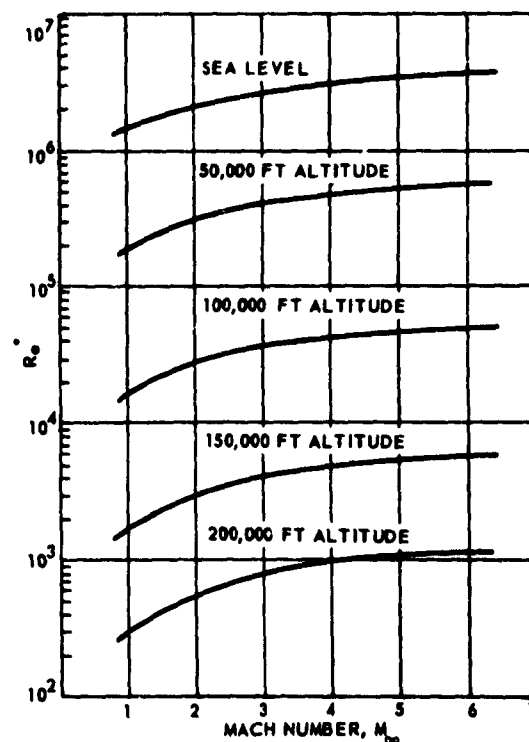


Fig. 4-158 Reynolds Numbers for Various Altitudes

1

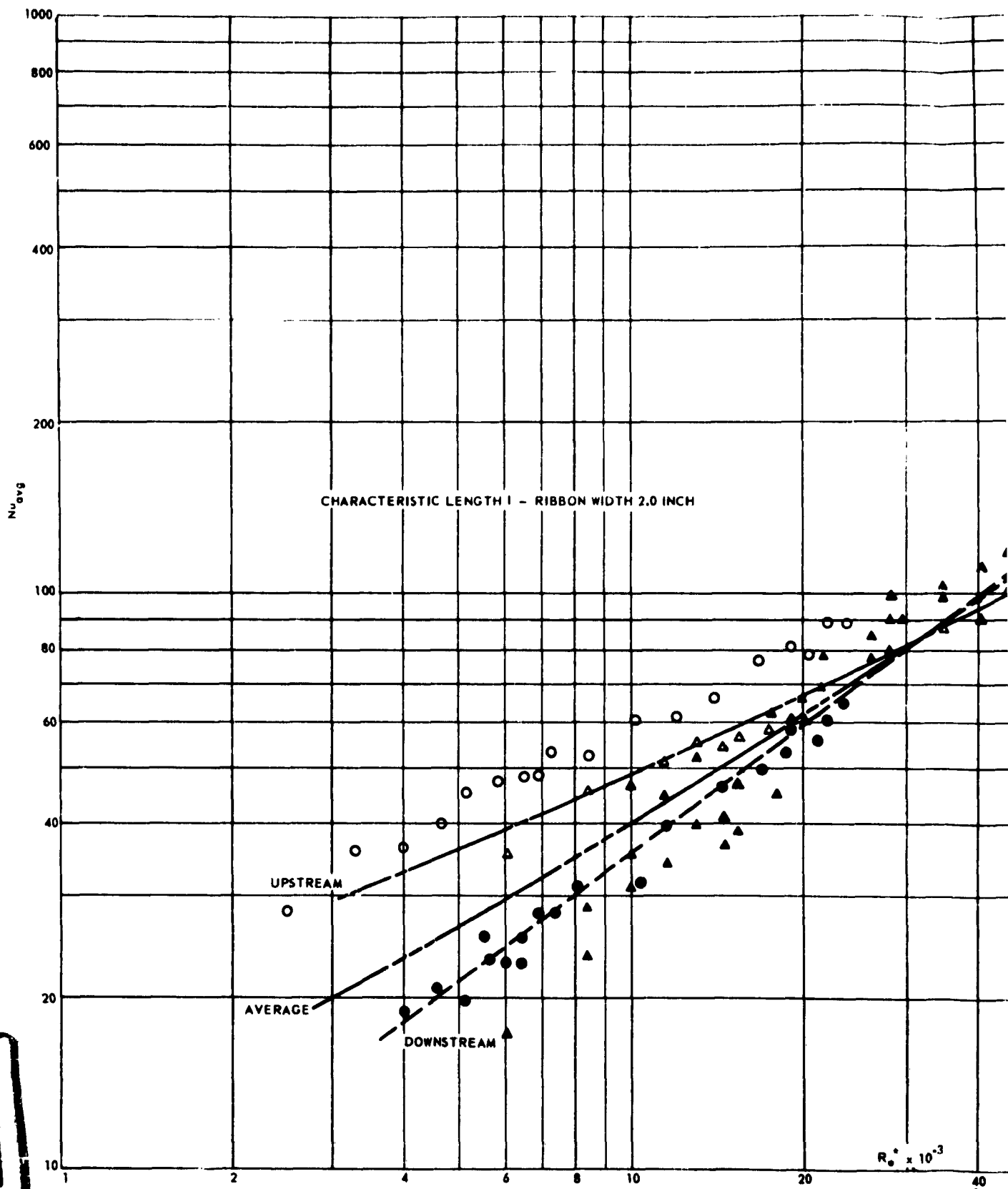
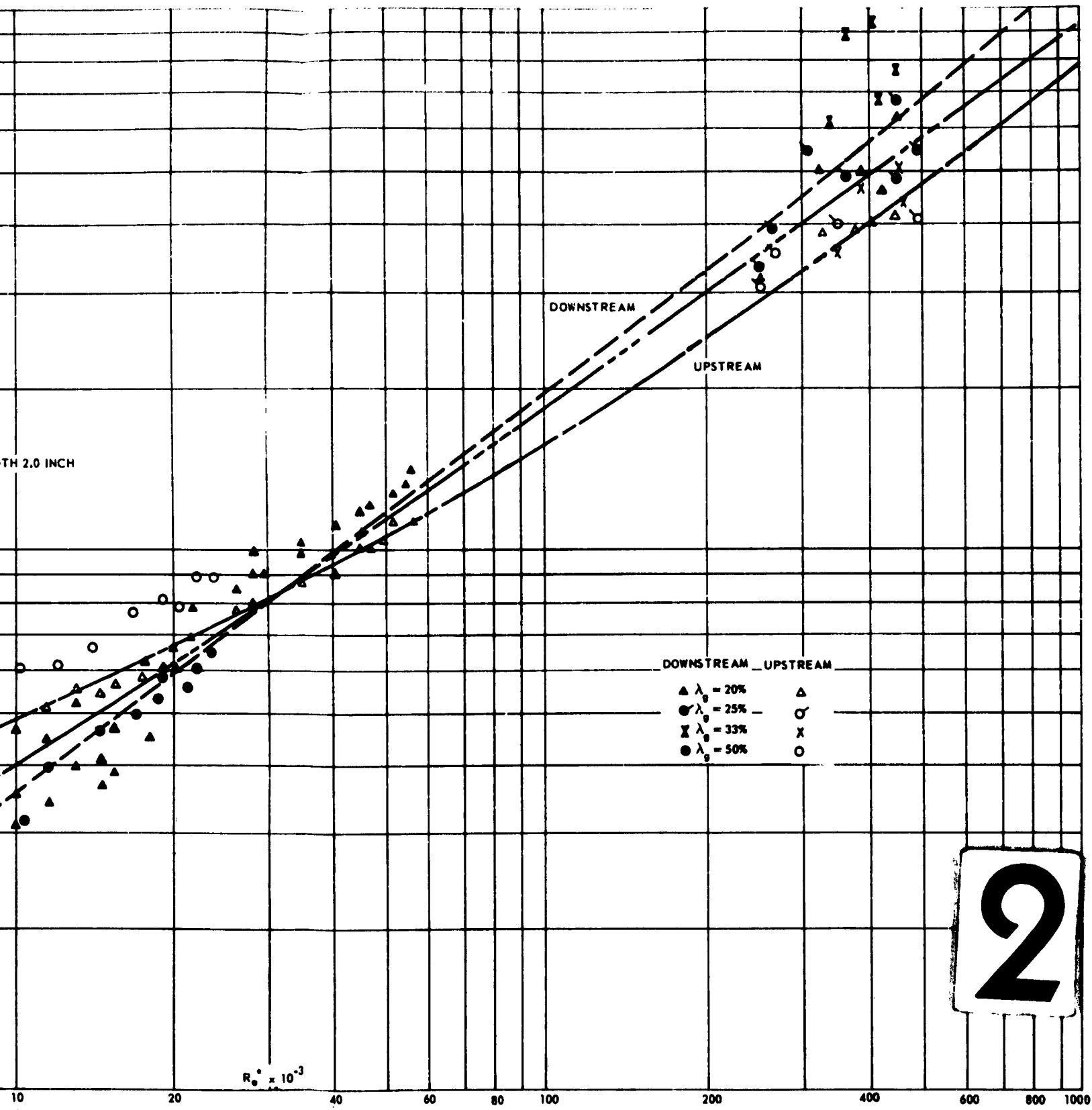


Fig. 4-159 Average Heat Transfer Coefficients on Ribbon Grid



2

Average Heat Transfer Coefficients on Ribbon Grids at Supercritical Pressure Ratios (Ref 4-87)

12.1.5 ENERGY LOSS FROM CANOPY BY RADIATION TO THE EARTH. The energy loss from a canopy to the earth is given by the relation

$$(4-320) \quad Q_r'' = \sigma F_s \epsilon S_4 (T_W^4 - T_{\text{earth}}^4)$$

where S_4 = Area of body radiating to the earth (sq ft);
(for hollow hemisphere: $\pi D^2/2$); and

F_s = Radiation shape-factor.

12.1.6 ENERGY STORED BY CANOPY. The rate at which energy is stored by a canopy is given by the relation

$$(4-321) \quad \frac{dE}{dt} = mC \frac{dT_W}{dt}$$

where m = Mass of the canopy (lb); and

C = Specific heat of the canopy material (Btu per lb °F).

12.1.7 TOTAL ENERGY BALANCE. An energy balance can now be written directly from the above equations:

Energy Stored = Energy In - Energy Out

$$(4-322) \quad mC \frac{dT_W}{dt} = hS_1 (T_{AW} - T_W) +$$

$$I a S_2 - \sigma S_3 \epsilon (T_W^4 - T_{\text{space}}^4) -$$

$$\sigma F_s \epsilon S_4 (T_W^4 - T_{\text{earth}}^4)$$

This equation can now be solved to yield a temperature-time history, once the trajectory conditions are known. In this development of the total energy balance, it is assumed that the sun is located vertically above the vertically descending canopy. In a majority of cases that consider canopy surface temperatures, the terms for energy flow into the canopy by solar radiation (Eq 4-318) and for energy loss from the canopy by radiation to the earth (Eq 4-320) can be neglected since their values generally are negligible compared to those of radiation to space or heat caused by velocity.

Then

$$(4-323) \quad mC \frac{dT_W}{dt} = hS_1 (T_{AW} - T_W) - \sigma S_3 \epsilon (T_W^4 - T_{\text{space}}^4)$$

If, furthermore, no heat is absorbed by the material of the canopy, the convective heat flux must be equal to the radiant flux. Consequently

$$(4-324) \quad Q_{\text{convected}} = Q_{\text{radiated}}$$

or

$$(4-325) \quad hS_1 (T_{AW} - T_W) = \sigma S_3 \epsilon (T_W^4 - T_{\text{space}}^4)$$

The temperature of space may also be neglected compared to equilibrium temperatures of practical interest. Therefore

$$(4-326) \quad hS_1 (T_{AW} - T_W) = \sigma S_3 \epsilon T_W^4$$

or rewritten,

$$(4-327) \quad \frac{T_W^4}{T_{AW} - T_W} = \frac{h}{\sigma \epsilon} \frac{S_1}{S_3}$$

Eq 4-327 may be solved for the equilibrium or wall temperature, T_W , by trial and error. An explicit solution of T_W from Eq 4-327, may be obtained using the following equation:

$$(4-328) \quad T_W = \frac{1}{2} \left(\sqrt{Z} + \sqrt{-Z + 2(Z^2 + 4a)^{1/2}} \right)$$

$$Z = \left(\frac{b^2}{2} + \sqrt{\frac{b^4}{4} + \frac{64a^3}{27}} \right)^{1/3} +$$

$$\left(\frac{b^2}{2} - \sqrt{\frac{b^4}{4} + \frac{64a^3}{27}} \right)^{1/3}$$

$$a = \frac{h T_{AW}}{\sigma \epsilon}$$

$$b = \frac{h}{\sigma \epsilon}$$

Thus, Eq 4-327 or 4-328 may be used to predict the maximum possible wall temperature T_W of the canopy while it is heating.

12.2 Sample Calculations. In order to demon-

strate the process of calculation, two different cases are considered.

12.2.1 CASE I. The following conditions are assumed to exist:

Projected diameter of canopy (hemisphere)	$D_p = 4.0$ ft
Velocity of canopy	$V_\infty = 2000$ fps
Altitude of canopy operation	$h = 29,000$ ft

Applying Eq 4-314, the adiabatic wall temperature may be calculated:

$$(4-329) \quad T_{AW} = T_\infty + \frac{n V_\infty^2}{2 C_p} = T_\infty \left[1 + n \frac{(\gamma-1)}{2} M_\infty^2 \right]$$

Based upon the operational conditions assumed, the following terms can be defined:

T_∞	= Free-stream static temperature = 415°R (Ref (4-1));
n	= Recovery factor = 0.85 (assumed);
C_p	= Specific heat of fluid = 6000 sq ft per sec per sec °R;
γ	= Ratio of specific heats of air = 1.4; and
M_∞	= Free-stream Mach number at given altitude = 2.0.

Inserting these values into the above equation yields

$$T_{AW} = 415 + \frac{0.85 \times 2000^2}{2 \times 6000} = 415 \left[1 + 0.85 \left(\frac{1.4-1}{2} \right) (2.0)^2 \right] = 698^\circ\text{R or } 697.2^\circ\text{R}$$

Since this temperature is well below the maximum allowable temperature for Nylon (940°R), it is immediately recognized that a Nylon canopy will not be damaged by aerodynamic heating under the operational conditions specified.

12.2.2 CASE II. The following conditions are assumed to exist:

Projected diameter of the canopy (hemisphere)	$D_p = 4.0$ ft
Geometric porosity of the canopy	$\lambda_g = 20\%$
Width of the Nylon ribbons	$l = 2$ in.
Velocity of canopy	$V_\infty = 4360$ fps
Altitude of canopy operation	$h = 150,000$ ft

Applying Eq 4-329, the adiabatic wall temperature may be calculated.

$$T_{AW} = T_\infty + \frac{n V_\infty^2}{2 C_p} = T_\infty \left[1 + n \frac{(\gamma-1)}{2} M_\infty^2 \right]$$

Based upon the operational conditions assumed, the following terms can be defined:

T_∞	= Free-stream static temperature = 502°R (Ref (4-1));
n	= Recovery factor = 0.85 (Assumed);
C_p	= Specific heat of fluid = 6000 sq ft per sec per sec °R;
γ	= Ratio of specific heats of air = 1.4; and
M_∞	= Free-stream Mach number at given altitude = 4.0.

Inserting these values into the above equation yields

$$T_{AW} = 502 + \frac{0.85 \times 4360^2}{2 \times 6000} = 502 \left[1 + 0.85 \left(\frac{1.4-1}{2} \right) (4.0)^2 \right]$$

$$T_{AW} = 1849^\circ\text{R or } 1867^\circ\text{R}$$

This temperature value is significantly above the allowable maximum temperature for Nylon material and a closer approximation of the wall temperature, T_w , is required.

Based upon the calculation of the adiabatic wall temperature, T_{AW} , above, an average value of $T_{AW} = 1858^\circ\text{R}$ is chosen.

The Reynolds number of operation for the condition specified is

$$Re_\infty = \frac{\rho_\infty V_\infty D_p}{\mu_\infty}$$

where $\rho_\infty = 3.415 \times 10^{-6}$ lb sec²/ft⁴ (Ref (4-1))

$V_\infty = 4360$ fps (Given)

$D_p = 4.0$ ft (Given)

$\mu_\infty = 3.642 \times 10^{-7}$ lb sec per sq ft (Ref (4-1))

$$Re_\infty = \frac{(3.415 \times 10^{-6}) (4.36 \times 10^3) \times 4.0}{3.64 \times 10^{-7}} = 1.635 \times 10^5$$

For the determination of the average Nusselt number, Nu_{avg} , the Reynolds number Re^* , is based upon the ribbon width, l , and the average velocity of the flow through the openings of the ribbon grid ($M = 1$). From Fig. 4-158, and for the operational conditions of $M_\infty = 4.0$ and $h = 150,000$ ft, the value of the Reynolds number, Re^* , is

$$R_e^* = 4.90 \times 10^3$$

For this Reynolds number, the average Nusselt number, Nu_{avg} , is (Fig. 4-159):

$$Nu_{avg} = 27$$

Since

$$Nu = \frac{hl}{k}$$

the convective heat transfer coefficient, h , can be calculated:

$$h = \frac{(Nu)k}{l}$$

For free-stream static temperature of 502 R, $k = 0.0125$ Btu per hr cu ft °R.

Therefore,

$$h = \frac{(27)(0.0125)}{(2.0)(0.0833)(3600)} = 5.64 \times 10^{-4}$$

The instantaneous equilibrium wall-temperature, T_w , can now be determined from Eq 4-327:

$$\frac{T_w^4}{T_{4W} - T_w} = \frac{h}{\sigma \epsilon} \frac{S_1}{S_3}$$

where ϵ = Emissivity of Nylon ribbon; chosen to be 0.85;

S_1 = Surface area of canopy exposed to aerodynamic heating; for this case it equals $\pi D_p^2/2$; and

S_3 = Area of the canopy radiating to space; for this case it equals $\pi D_p^2/2$.

Therefore,

$$\frac{T_w^4}{T_{4W} - T_w} = \frac{5.64 \times 10^{-4}}{(4.80 \times 10^{-13})(0.85)} \quad (1)$$

$$\frac{T_w^4}{T_{4W} - T_w} = 1.3824 \times 10^9 = \frac{T_w^4}{1858 - T_w}$$

Solving this equation by trial and error, the value for T_w is: $T_w = 1045^\circ\text{R}$

It is seen that the maximum possible instantaneous equilibrium wall temperature is above the maximum allowable temperature for Nylon material.

In order to determine the time-temperature history for the canopy, a trajectory calculation for the assumed operational conditions must be performed, and a solution of Eq 4-327 or 4-328 must be obtained.

SEC. 13 RELIABILITY

13.1 Reliability Requirements. Aerodynamic decelerator reliability requirements, for almost every type of application, are necessarily as high or higher than for most types of military equipment. However, in the analysis of a parachute or other decelerator design, or of the actual item of equipment during its development, it is necessary to quantify reliability requirements; the mere statement that "high" or "very high" reliability is required is not adequate to describe the performance desired from a given design. Thus, it is necessary to have some firm basis on which to measure the reliability requirements for a decelerator system, balancing the obvious desire for maximum reliability against possible penalties in weight, bulk, cost, development time, etc.

The best approach to the determination of the minimum reliability required of a decelerator system is an analysis of its mission. This can be accomplished by a study of the overall effects on the mission of failure of the decelerator system. It must consider, when applicable, the entire number of such missions likely to be run, and the balance of such factors as cost, development time, weight, bulk, etc., against the level of reliability which can be achieved for specific levels of effort in each of these directions. In this way a reliability level can be chosen within the realm of practical attainment.

It is not possible to lay down a hard-and-fast set of rules for such an analysis. Each application must be considered within the context of its own specialized conditions. As was pointed out above, all decelerator reliability requirements must be high. However, it is convenient to divide such high requirements into two groups: ultra-reliability, and very high reliability. The ultra-reliability group includes such applications as personnel parachutes, special-weapons parachutes, space-vehicle-recovery decelerator systems, and similar critical applications in which costs are extremely high, assurance of mission success must be very high, or human life is involved. In general, it may be said that such ultra-reliability requirements start with reliabilities higher than 0.999. Of course, there is no practical upper limit on reliability other than the per-

fection of 1.0. In the real world, the latter is virtually unobtainable, but requirements for many critical applications are such that it must be approached.

The very high reliability requirements are those of the more usual parachute applications other than personnel: cargo delivery, missile and drone recovery, weapons delivery, etc. Here, some of the urgency of factors requiring virtual certainty of recovery may be tempered by overriding considerations of cost, development time, personnel training, or many of the other factors which are involved in the compromises required by expediency in military development. It is difficult to draw a sharp line between ultra-reliability requirements and very high reliability requirements; however, the choice of reliability levels up to 0.999 is probably an adequate one for most purposes.

To interpret reliability generally above 0.999 in terms of failure rate is a relatively simple matter: this implies less than one failure may be expected in every thousand trials over many thousands of trials. The very high reliability case, similarly, may be regarded as that in which a level of one, or possibly somewhat more than one failure per thousand uses is acceptable, again in the long run over many thousands of uses. It must be realized that the reliability values expressed in this manner do not refer to the result of a single trial or even a few trials. There is no way of determining the reliability of a single item used once; whether the item will work properly or not can be determined only by using it and examining the results. Reliability refers to performance in the long run; when applied to a single use, all the reliability analysis can do is quote the "odds" that the usage will be successful.

13.2 Causes of Unreliability. Three major causes of unreliability in parachute operation may be recognized: (1) inadequate design; (2) materials failure due to accident; and (3) human error in parachute assembly, packing, and use. In designing for reliable performance, and in assessing the reliability of a given design, the possibility of failures from all three causes must be considered.

From the viewpoint of operational parachutes and other decelerator systems, inadequate design is generally not a major failure-factor in actual field use. Since virtually every decelerator system goes through a design, a development, and a shake-down testing period, design errors are generally eliminated in development. The exceptions are those cases in which the design can be said to be really marginal, and in which the failure rate due to the design error is so low as to be undetectable even in an adequate test program, and indistinguishable from accidental causes.

Materials failures may be divided into two classes,

failures of the fabric and static-hardware portions of parachutes, and failures of the mechanical devices which are necessary to parachute-system operation. Failures in the fabric portions of canopies are probably the most difficult to assess on a theoretical basis. First, experience indicates that fabric failures must be considered from the viewpoint of critical or non-critical applications of the fabric in the parachute. Thus, for example, in many missions the blowing out of a panel in a canopy does not necessarily mean a failure of the mission. If the decelerator function is merely to land the load without damage in a general area, and the decelerator is somewhat over-designed (as is the usual case), the loss of a panel from the canopy may not affect the reliability of the parachute in the mission at all. On the other hand, in such a mission the failure of a riser or a suspension line could very well result in major damage or destruction to the load, and thus failure in the mission.

In the cases in which both the deceleration of the load and the achievement of a reasonably precise touch-down point are vital (e.g., delivery of a special weapon) failure of a single panel might so change the trajectory of the parachute system and load that the mission would be a failure even though the deceleration function of the parachute had been accomplished successfully. Thus, mission analysis is a vital factor in determining which specific types of fabric failure cause parachute system failure.

To pinpoint the exact reason for the failure of a fabric portion of a parachute is a rather difficult engineering task. However, from a broader viewpoint, it can be realized that the fabric portions of the parachute have a definite distribution of strength in each member; if the tensile strength of a large number of samples of the fabric used for any given member of the canopy is tested under conditions reasonably simulating those of actual use, it will be found that the strength will vary over a certain range, with the actual strength values generally tending to group around a central average. (Of course, in the actual parachute design and construction, some allowance must also be made for the effects of seams, hardware attachments, etc., on the strength.)

A similar study of the stresses which are placed on the various canopy members during parachute deployment and descent will indicate that for each given portion of the parachute deployment and operation, a given range of stresses will act on each component of the canopy. Again, a series of measurements will tend to show a range of such stresses at any given point, depending on the specific conditions of each deployment, tumbling of the load, gusts, specific manner in which the canopy unfolds, etc. As in the strength

case, these values usually will group around a central average with both extremes considerably less common than the mean.

To understand the reasons for many accidental failures of fabric portions of parachutes, it is necessary to examine the relationship between the distribution of the strength of the material in each portion of the canopy and the stress on each portion of the canopy in its operation. In every application of the parachute there is some probability of very low or very high stress, but the probability of the extremes is less than the probability of a stress closer to the average. Similarly, in every choice of a specific piece of fabric for the construction of a canopy there is a possibility of getting a lower-strength piece or a higher-strength piece. Thus, it can be seen that the probability of accidental failure will depend to a considerable extent on the probability of the specific portion of the canopy which fails being constructed of a low-strength piece of material that encounters an accidentally high stress during the operation.

Of course, everything possible should be done in parachute design, construction, and operation to minimize the possibility of selecting a low-strength piece of material (e.g., testing of batches of material after they are manufactured and before they are used) and to minimize the possibility of an extremely high loading in use by limiting the speed of the aircraft at parachute release, by designing the load for reasonably good aerodynamic characteristics, etc.). Indeed, such precautions may be pointed out as the primary reason for the remarkably high record of reliability for parachutes in general. However, it must be realized that, to some extent at least, the failures which do occur may be caused by these two factors.

Failures of the mechanical devices used in various types of parachute systems are more a straightforward problem than failures in the fabric portions. That is, from the viewpoint of static hardware, items whose functions are primarily passive, the cause of failure, to a large extent, may be attributed to the distribution of strength and of the stresses placed on the components, as in the case of fabrics. However, there is another class of mechanical devices which must perform active functions during the deployment or operation of the parachute system. This class consists of reefing-line cutters, interstage disconnects, deployment-initiation devices, etc. Here the reliability problem is one of the functioning of mechanical devices in an environment which may include low temperatures, shock, vibration, acceleration, and possibly other interfering factors. In such cases, assessment of reliability is a matter of testing adequate numbers of such devices under conditions closely simulating their use environments to determine the probability of fail-

ure. Development of reliable devices is primarily a problem of good engineering design.

The third cause of parachute failure, human error, is more difficult to deal with than the purely mechanical problems. Of course, human error in the process of parachute design is part of the design problem rather than the parachute-use reliability problem. However, human error in parachute construction and use is probably one of the primary causes of failure in the operation of many of the most common types of parachutes, including man-carrying parachutes and cargo parachutes. In considering the human-error factor in parachute reliability, three major areas of possible error should be distinguished: (1) errors in manufacture not caught by inspection procedures; (2) errors in rigging the parachute to the load; and (3) errors in packing the parachute.

The human error in the manufacturing process is quite difficult to evaluate in reliability studies. Here, reliability is primarily a function of quality control by the manufacturer, and also depends on proper training of manufacturing personnel and on thorough and effective inspection. It would appear that such errors are relatively rare; in a recent study of parachute reliability (Ref (4-89)) it was not possible to isolate any such cases in examining the records of well over 5,000 parachute-uses.

A distinction is made between human error in rigging and human error in packing primarily because a functional failure due to an error in packing can be definitely detected in the parachute behavior, while a failure due to an error in rigging is probably more readily traced to the characteristics of the load rather than the parachute itself. In the study cited above, it was found that parachute rigging-errors which caused failure of the drop mission were most likely in those air-drop applications in which irregularly shaped loads were employed. This appears to be particularly true in the case of heavy vehicles loaded on drop platforms, and other types of loads having protuberances, sharp corners, and unsymmetrical shapes. In these failures, the actual failure-mechanism can usually be traced to the snagging or tangling of some portion of the deploying canopy or lines on a portion of the load.

While it is true that this latter failure causes unreliability in the mission, the advisability of considering such failures as caused by unreliability of the parachute is open to question. In general, the rigging of the parachute to the load in cargo drop, and to personnel in man-carrying applications, is not under the control of the parachute design or engineering agency. Thus, the unreliability due to rigging error can be corrected primarily by operational discipline rather than by processes which can truly be said to be under engineering control. Such problems probably should not be

considered as a part of the reliability of the parachute itself, although they are undoubtedly a portion of the reliability of the mission. Rigging problems in many other types of parachutes are not as serious from the human-error viewpoint. For such applications as missile and drone recovery, aircraft deceleration, and space-vehicle recovery, where the load and parachute have been designed as a unit, the rigging error may be considered as a portion of the packing error.

Human error in packing has been found to be one of the major failure-producing factors in some types of parachute reliability studies (Ref (4-89)). Here, two distinct portions of the packing process can be recognized from the viewpoint of error control: (1) the canopy lay-out, folding, tying, and stowing, and (2) the installation of hardware and auxiliary devices required for parachute operation. In the previously mentioned study of heavy-duty parachute reliability, survey of the records of parachute failures in normal use indicated that the majority of human-error failures in packing were not in the canopy portion of the operation, but rather in the auxiliary-device installation.

Observation of the packing process for large and complex parachute systems has indicated what is probably the basic reason behind this preponderance of error in the installation of the hardware items: quality-control measures applied to the parachute-packing process require constant inspection as each step of the packing proceeds. During the lay-out, examination, folding, and stowage of the canopy the inspection process can follow each individual packing operation quite closely, since, in general, the parts of the canopy involved are large and readily visible to the inspector.

However, when hardware, auxiliary devices, reefing-line cutters, and similar mechanical devices are installed, the parts involved are usually quite small. The operations required of the parachute packer are such that frequently his hands hide the part from the inspector. Further, after the completion of the operation, it is sometimes difficult for the inspector to see all portions of the part clearly. This is particularly true in the case of canopies which must be installed in compartments that are in integral portions of the load, and where electrical connections, etc., must often be made. Here, inspection becomes very difficult and it appears entirely possible that the inspector, no matter how diligent, might miss an error in the process which could eventually cause failure of the parachute in its mission.

Of course, examples of such errors are the exception rather than the rule. The observed rate from a study of failure records was about 14 in over 5500 packings of complex parachute systems, with an estimated 100 possible opportunities for error in each complete packing. Thus, over a half million chances for error were pos-

sible. However, in ultra-reliable systems an error rate of this magnitude may well be the major single cause of unreliability.

It would appear that more inspection and closer inspection would not be the key to eliminating entirely failures of this type. Rather, it is necessary to design the parachute systems for inspection of the results of these portions of the parachute packing operation. This requires the design engineer to consider not only the problems of the parachute operation and packing, but also the problem of the inspector who must determine whether the packing or installation of the small device has been done properly.

13.3 Reliability Assessment. The assessment of parachute reliability, either from the design prior to the start of the actual experimental development program, or from test data gathered during a developmental and test program, is a problem which must be approached in a logical step-by-step manner if meaningful results are to be obtained. Space is not adequate in this section to present detailed instructions on the complete procedure for parachute reliability assessment. Instead, the reader is urged to consult Ref (4-89), which presents a complete methodology for parachute-reliability assessment, and many of the necessary auxiliary data, including values for human-error rates observed in parachute packings, the reliability of certain mechanical devices commonly used in parachute systems, and mathematical tables which facilitate computations. The discussions presented below are a brief outline of the major points which must be considered in the assessment of parachute reliability.

13.3.1 DEFINITION OF RELIABILITY. Reliability is inversely related to the expected rate of failure; it can be measured by subtracting the expected probability of failure from unity. The important concept to note here is the use of the term "expected rate of failure". The calculated reliability of a system cannot be used to forecast, on an absolute basis, the performance of a single example of that system in a single use. It gives the "odds", but does not foretell the result of any single event. It refers to the rate of successful uses to be expected when a large number of identical systems are used, or when a given system is used a large number of times. Thus, reliability may be defined as the probability of successful operation of the parachute system under given conditions in the long run.

An examination of the definition of reliability indicates that in itself it is not adequate for the basis of assessment of any given parachute system. It is necessary, before starting the analysis, to choose the boundaries defining the system. A decision must be reached by the evaluating agency as to the exact point in the parachute use at which the consideration of reliability

will start, and the exact point at which it will end. For example, if a simple static-line-deployed system is considered, the reliability evaluation may include the fastening which holds the end of the static line to the aircraft, or may not, depending on whether the system designer or evaluator chooses to consider this a portion of the parachute system. Similarly, if a cargo parachute-system has an automatic canopy-release which separates the canopy from the load at touchdown, this may or may not be considered as part of the system from a reliability viewpoint, depending upon the objectives of the analysis.

Another factor which is important in the overall definition of the reliability to be assessed is the matter of the use-conditions under which this reliability will be considered. Therefore, it is also necessary to specify the limits of applicability of the system with respect to the deployment speed and altitude, the load, the permissible aircraft maneuvers during release, etc. Finally, as discussed previously, a definition of success or failure of the parachute mission is necessary as a yardstick upon which to base the computations of system reliability.

13.3.2 RELIABILITY DISTRIBUTIONS. In any given parachute mission, the reliability of each portion of the parachute system is determined, in effect, at a virtually instantaneous time, rather than over a period of time. For example, the maximum load on the suspension lines, and thus the maximum probability of a line breaking, comes either in the opening-shock or in the snatch force. Similarly, the reefing-line cutter is called upon to perform at a particular instant, and its success or failure in this performance is measured at that instant rather than over a time period. The other devices and components of the parachute system are also called upon to perform or to resist their maximum loads at a virtually instantaneous time.

Consequently, from a reliability viewpoint, a parachute is a "one-shot" system. When called on to perform in its mission, its reliability is not dependent on the length of time the mission will last, but rather upon success or failure in a single operation at a single time. The distribution of the probability of parachute failure can only take on a finite number of values, and is called a discrete distribution. The probability distribution best describing such a system is the Binomial Distribution, which expresses mathematically the probability ($f(x)$) that failure will occur exactly x times in N independent trials of the system, where p is the expected probability of failure:

$$(4-329) \quad f(x) = \frac{N!}{x!(N-x)!} p^x (1-p)^{N-x}$$

It should be noted that $x = 1, 2, 3, \dots, N$, and that if p is the probability of failure, then $(1-p)$ represents the probability of success.

Examination of the expression for the Binomial Distribution given in Eq 4-329 indicates that both the numerator and denominator of the fraction involved contain factorials, and that when the numbers become large, the expression is rather difficult to evaluate. For cases in which N (the number of trials) is quite large and (p) (the probability of failure) is quite small, the Poisson probability distribution is a good approximation to the binomial:

$$(4-330) \quad f(x) = \frac{n^x e^{-n}}{x!}$$

In this distribution, n is the average number of times the event (failure) occurs, or the "expectation" of x ; numerically, $n = Np$. Since only one factorial is involved, that of x , and since x must be small to apply the Poisson distribution as an approximation to the Binomial, it can be seen that numerical manipulations are considerably simplified by the approximation.

13.3.3 SINGLE-USE VERSUS MULTIPLE-USE.

One important factor governing the application of reliability methods to parachute missions must be considered before the discussion of the details of reliability assessment; the condition of the parachute at the start of the mission. Some types of parachutes (for example, those which are used to decelerate weapons and are destroyed in the process of use) must be new at the start of each mission. Others, such as the usual man-carrying parachutes, aircraft-deceleration parachutes, and cargo parachutes, may be used for a number of missions. In the single-use cases, since all the parachutes are new at start of the mission, it may be assumed that all have equal reliability. Of course, if the parachute has been subjected to severe environments in storage (high temperature, acid fumes, etc.), this assumption will not be valid. However, such situations are not legitimately a portion of a reliability investigation, since (1) they are analogous to the inadequate-design situation and are not actually related to the parachute; and (2) they are isolated instances which cannot be controlled. Thus, to make the parachute-reliability assessment feasible at all, it must be assumed that accidental damage or deterioration during storage after packing has not occurred.

In the case of the multiple-use parachute, it is necessary to establish the effect of prior use on reliability. Such factors as wear, age, damage on landing, weakening of fabric members by previous loading, and effects of exposure to sunlight during previous uses must be evaluated with respect to their effects

on overall reliability. The problem here is one of determining whether the inspection and repair process which follows the parachute-use prior to packing for the next mission returns the parachute to the equivalent of new condition. This is a matter which will be determined by the facts of the individual case. If it is found that the re-used parachute is equivalent from a reliability viewpoint to a new parachute, then the analysis proceeds as if the parachute were a single-use item. If it is found that inspection and repair does not return the parachute to its "as-new" condition, then some allowance must be made for the deteriorating effect of prior use in assessing the parachute reliability.

13.3.4 OVERALL SYSTEM RELIABILITY. The simplest case in the evaluation of the reliability of a parachute system is that of a single-canopy system which has been tested a number of times under reasonably close conditions of operation of load, altitude, velocity of release, and aircraft attitude at release. Under these conditions, the simplest estimate of parachute failure rate is the actual failure rate observed: the number of failures observed divided by the total number of drops. The reliability is this value subtracted from unity. This gives a "point estimate"; that is, a reliability value given as a single number based on the available number of trials. For some purposes, especially if only a crude estimate of reliability is required, this "best estimate" is satisfactory. It must be realized, of course, that the accuracy of such a point estimate or best estimate depends upon the number of trials which were made.

Such an estimate of reliability has several advantages: it is relatively simple to compute and can utilize any consistent data that are available. However, it must be realized that the single-number value representing the reliability gives no information about the degree of confidence that may be placed in this number as a true measure of the potential performance of the system. It is quite possible that the true reliability is either lower or higher than the given maximum-likelihood estimate, since, in theory, reliability expresses the probability of a given number of successes in *all* possible uses of the parachute system, while, for most practical cases, the test data available represent only a small fraction of all possible uses. But the point estimate does have legitimate use in reliability assessment of parachute systems, because when only limited test-data are available it is often the only assessment which can be made; even with ample data, it provides a rapid method for determining whether or not reliability requirements are being met.

To take into account the possibility that the true reliability may be either lower or higher than the maxi-

mum-likelihood (point) estimate computed from a single series of trials by the simple method, a more refined measure of reliability is needed. The basis for this type of reliability value, the confidence-interval estimate, may be understood by realizing that, roughly speaking, if an estimate of the reliability of a system is made, there is associated with that estimate a probability of it's being incorrect. The lower such an estimate of reliability (expressed as a probability of "at least" a given fraction of successes), the higher is the probability of the estimate being correct. The estimate of the reliability can be denoted in the present case by R_p ; the probability of the estimate being correct will be called the confidence coefficient (denoted by the subscript g), the interval between the reliability value given and unity is called the confidence interval. A probabilistic interpretation of these concepts is that if in many empirical trials with F failures out of a total of N trials, the reliability is estimated to be at least R_g , then the estimate will be correct on the average of at least g (per cent) of the time.

In order to compute R_g , it must be recalled that if the true reliability is R , then in a single use of the system the probability of failure is $(1-R)$ and the probability of success is R . Using the Binomial Distribution described above, the probability of F or less failures in N trials is given by:

$$(4-331) \quad \sum_{i=0}^F \frac{N!}{i!(N-i)!} (1-R)^i R^{N-i}$$

As R decreases, the values obtained from Eq 4-331 also decrease; the estimate R_g will be that value of R which causes Eq 4-331 to be equal to $1-g$, for then the probability of obtaining more than F failures in N tests will be g . If F is small while N is large (that is, if there are not many failures in a large number of parachute uses) the Poisson approximation to the Binomial may be used:

$$(4-332) \quad 1-g \approx \sum_{i=0}^F \frac{N^i (1-R)^i e^{-N(1-R)}}{i!}$$

When R_g is computed from Eq 4-332, it is possible to state that the reliability lies between R_g and 1, with the assurance of being correct given by the confidence coefficient, g .

To facilitate computations of R to a given confidence coefficient, tables have been developed and are presented in Ref (4-89). Values taken from these tables

for 90, 95, and 99 per cent confidence coefficients are plotted in Fig. 4-160. To calculate the reliability at the selected confidence-coefficient from N trials with F failures, the plot is entered at F , and the value for the computation factor read from the appropriate curve. Then, reliability with the chosen confidence coefficient, R_g , is computed from

$$(4-333) \quad R_g = 1 - \frac{\text{computation factor}}{N}$$

The choice of the confidence coefficient for use in interval reliability-analyses depends, to some extent, upon the objectives of the evaluation. Of course, any desired confidence-coefficient may be used in the calculations, although in practice the choice of a 100 per cent confidence-level will obviously result in a reliability of zero, unless the parachute under analysis is absolutely perfect and can never fail. In the choice of a confidence coefficient for calculations, it must be realized that the higher the confidence coefficient used, the lower the reliability computed for the same set of data (and the higher the failure rate), and vice versa.

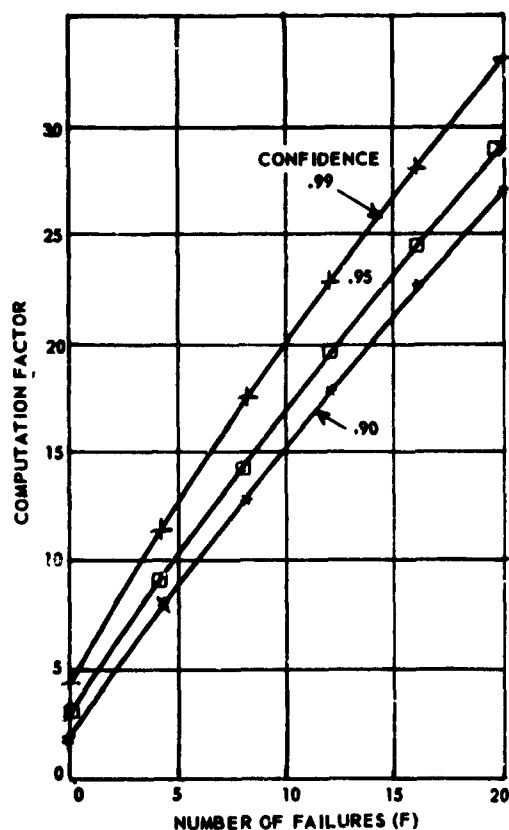


Fig. 4-160 Reliability from a Series of Trials

The choice of confidence coefficient in practical cases tends to be dictated by the amount of test data available for the evaluation. As can be seen from Fig. 4-161, the data required to demonstrate high reliability with very high confidence is quite extensive, even if no failures at all are encountered in the testing. Thus, unless the test data can be obtained from other trials of the system, made for purposes other than reliability testing, the cost of doing the testing is probably the controlling factor in the choice of confidence coefficient. Studies of the amount of testing required versus the optimum confidence-coefficient for calculation (Ref (4-89)) indicate that 90 per cent confidence is probably the best choice for most computations of reliability. By working at this level, the evaluating agency gets the greatest return for a given amount of test effort.

The major advantage of the confidence-interval estimate of reliability over the point estimate is the fact that the confidence coefficient expresses the degree of reliance which the evaluating agency may place in its results. Obviously, if the reliability-evaluation of a given parachute system is based only on a limited number of trials, there is the possibility that in the next series of trials the results will be somewhat different. The point-estimate tends to ignore this fact; the confidence-interval estimate expresses numerically the probability that the failure rate on the next series of trials may be different from that used in the computations. The disadvantages of the latter estimate, of course, are the requirement for larger amounts of data, and a somewhat more complex method of computation.

In the discussion of both point estimates and confidence-interval estimates above, the viewpoint taken was that of the single-canopy system. In many parachute applications, instead of a single canopy, multiple canopies are used, either in clusters or in sequence. Reliability data obtained on a single canopy may be applied to either type of multiple-canopy used, if due allowance is made for the effects of simultaneous or sequential use of the canopies on the reliability of the complete system.

In the case of canopies in clusters, it is necessary to determine the number of canopies which must operate successfully to decelerate the load to the velocity required for a successful drop. If it is found that all canopies which are used must operate, then the overall reliability of a system with clustered canopy system, R_m , is equivalent to the reliability of an individual canopy, R , raised to the power of the number of canopies used, N :

$$(4-334) \quad R_m = R^N$$

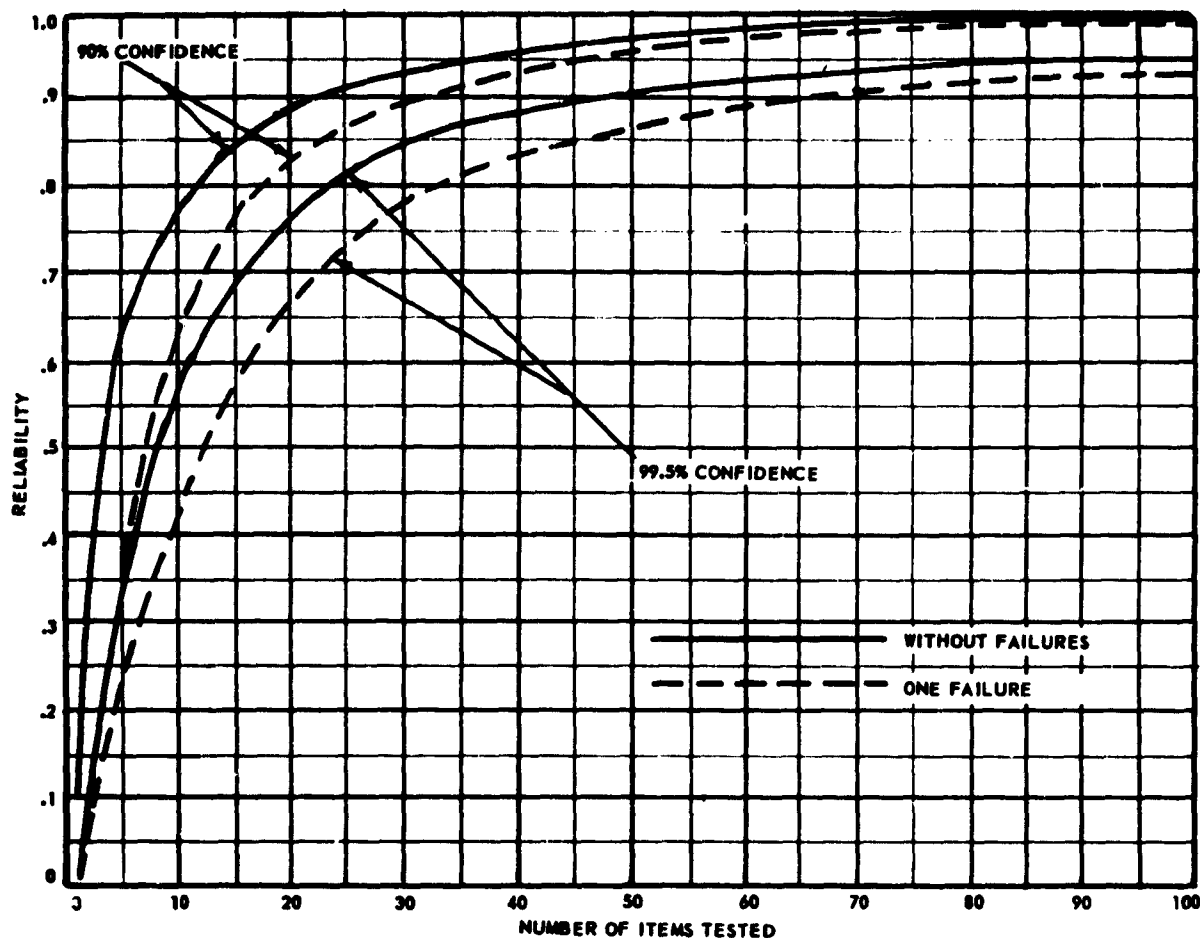


Fig. 4-161 Reliability Levels for a Series of Tests With and Without Failures

If a successful drop requires fewer than the total number of canopies used (n = number actually required), the overall reliability, R'_m , of the system may be calculated from:

$$p_d = \sum_{r=m+1}^N p_r$$

where

- p_d = Probability of failure of the entire cluster;
- p_r = Probability of failure of r identical canopies;
- N = Number of canopies in the cluster; and
- m = Maximum number of canopies that can fail without affecting the success of the mission.

Then the overall reliability of the system, R'_m (when N exceeds n), can be expressed

$$(4-335) \quad R'_m = 1 - p_d$$

In the case of multi-stage systems, in which each canopy must open sequentially to decelerate the load, the reliability of each canopy is considered as a series term in a simple product-model (see below).

13.3.5 COMPONENT RELIABILITY ANALYSIS.

The case in which there are sufficient test data on the complete parachute system to allow assessment of reliability on either a point or a confidence-interval basis is the exception rather than the rule. Of course, in the analysis of parachute designs before the system is actually built and tested, there can be no test data. In the case of systems under development, the tests are generally conducted at varying altitudes and speeds, and under varying load-conditions to establish engi-

neering parameters, so that the data are rarely collected under conditions homogeneous enough to allow good reliability estimation. Thus, it is necessary to have some other method of assessing the reliability of parachutes.

13.3.5.1 Product Rule. Since any parachute system may be resolved into a series of individual components, and since it can be demonstrated that the reliability of the overall system is equivalent to the product of the reliability of each of its individual components (Ref (4-90)), an analysis of the reliability of the components of the system allows the synthesis of a reliability value for the complete system. The basic mathematical model used in this case is simple; the system reliability (R) is equal to the product of the component reliabilities (R_c):

$$(4-336) \quad R = \pi R_c$$

This model allows the reliability evaluation to take into account all of the mechanical factors involved in the parachute operation from the start of deployment until touch-down, or during any portion of the operation desired, as the basis for the reliability evaluation. However, as pointed out at the beginning of this section, a major factor in parachute reliability is human error in the parachute-packing process. Thus, it is necessary to introduce another term in the model to take into account the probability of failure due to this human error. This term, called the operational reliability term, R_p , is used as an additional portion of the product expression:

$$(4-337) \quad R = R_p \pi R_c$$

If desired, an additional term may be included in this model, as another factor in the product, to represent the probability of an error in rigging causing system failure. As discussed previously, this is a matter of choice on the part of the evaluating agency. Generally, rigging errors, which seem to occur most often in parachutes which are used for heavy-cargo drops, are not considered part of the parachute-reliability study.

13.3.5.2 Evaluation of Component Terms. The evaluation of the terms in the model in the process of reliability analysis of a specific parachute-system may be divided into two major types of tasks: (1) the evaluation of component terms; and (2) the evaluation of the operational term. In such an evaluation, it is possible to work toward a point-estimate or a confidence-interval estimate of the system reliability, although, of course, the data requirements for an interval-esti-

mate are considerably more stringent than for a point-estimate. In general, when parachute designs are being evaluated for potential reliability prior to the actual construction of hardware, it will be quite difficult to obtain enough data of the type required to permit confidence-interval estimates, unless the parachute system uses at least some components that have been previously used in other systems, and for which performance data are available. In the case of parachute systems which are in the development or test phases, and upon which some performance data are available, confidence-interval estimates of reliability can be made in a great many cases.

For the analysis of the reliability of a parachute system using the product-rule reliability model (for either point or confidence-interval evaluations) data will be required on the performance of all critical components of the parachute system; generally, this includes the suspension lines and risers, the hardware devices which are critical to system operation, and any mechanical actuators, control components, etc., which must operate properly for the system to perform its mission successfully. (It is not necessary to have performance data on every component of the parachute system to evaluate reliability; only those components most likely to experience failures are actually studied in detail in the analysis — see below.)

The best data for use in the reliability analysis is actual-performance data obtained on the components in previous use under conditions similar to the use of the system under analysis, or in tests which closely simulate the conditions of use. In some cases, it is possible to obtain such data on virtually every component of the parachute system; this is true for those systems which are made up of components which have been used in other systems. Generally, however, for systems which are relatively new in design, such data will be available only for the standardized hardware items such as reefing-line cutters, interstage disconnects, or standard components from which such disconnects are built up, and similar components. Despite the small size of these components in relation to the major canopy, if their function is essential to the operation of the system their importance from a reliability viewpoint is as great as that of the canopy.

Where test data are available, the reliability of the part is computed in precisely the same manner as for the reliability of the overall system as discussed in 13.3.4 above. For a point-estimate, the failure rate of the observed sample is taken as the desired component-failure rate. For a confidence-interval estimation the data in Fig. 4-160 are applicable (although in actual computations the tables presented in Ref (4-89) should be used).

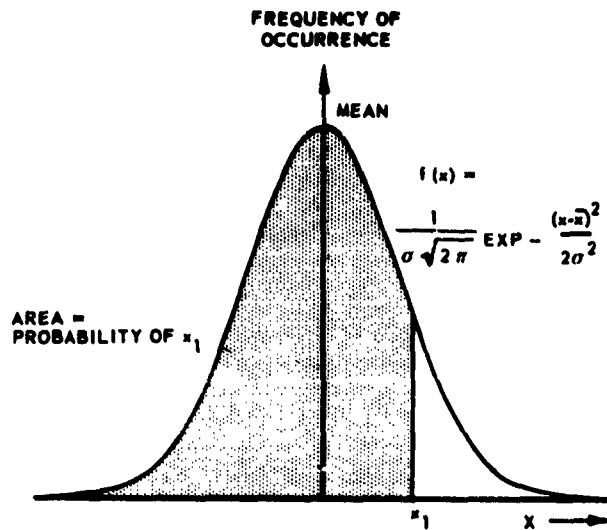


Fig. 4-162 The Normal Distribution

In many actual cases of reliability analysis of new parachutes, either in the design stage or in actual development-testing, it will be found that while reliability data can be developed for most mechanical and hardware components, the canopy and its suspension lines (and generally the risers, if any) are unique, and have not had enough use or testing to allow reliability analysis from actual performance data. In such cases, if even limited test-data are available, it is possible to use a method of analysis which compares the distribution of the loads on the suspension lines, risers, etc., as determined by test, with the distribution of the strength of the components under study determined from tests of the materials from which they are constructed and from other considerations to be discussed below. Studies of suspension-line and riser load-distributions and of the strength distributions of parachute fabrics (Ref (4-89)) indicate that both these distributions are essentially normal; that is, the spread of values obtained from a large series of tests may be described by the normal probability density function (Ref(4-91)):

$$(4-338) \quad f(x) = \frac{1}{\sigma \sqrt{2\pi}} \exp - \frac{(x - \bar{x})^2}{2\sigma^2}$$

where

σ = Standard deviation of x ; and

\bar{x} = Mean of x .

The characteristics of this probability function are such that for any given series of test results, the probability of occurrence of a specific value is equivalent to the integral from zero to the desired value, or equivalent to the area under the normal curve up to the ordinate of interest (see Fig. 4-162). Thus, if the distribution of stresses on the suspension-line or riser and the distribution of strength of the materials from which it is made are both normal and are plotted on the same set of axes, the probability of the stress exceeding the strength is equivalent to the area of intersection of the two distributions (Fig. 4-163). The probability of failure may be analyzed by studying the characteristics of the strength distribution and stress distribution for a specific canopy.

Methods for performing this analysis, and tables and graphs which facilitate computation, are presented in Ref (4-89). The data requirements are essentially a series of test results on samples of the parachutes, obtained under reasonably consistent conditions, and information on the strength distribution of the fabric materials. Test results, of course, must be obtained from a specific test-program; one is generally conducted during the parachute-development process. Data on strength of materials, including both means and standard deviations as required, are presented in Ref(4-89) for most of the commonly used parachute webbings, tapes, and cords.

It must be realized that the construction of the parachute does, to some extent, change the strength characteristics of the fabrics from which they are made. The primary problems here are the effects of sewing on fabric strength and the effects of the use of multiple layers of fabric on both strength and standard deviation of strength. Means for allowing for such factors are discussed in detail in Ref(4-89), based on the results of studies of stress on materials described in Ref (4-92) and (4-93).

Where test data from which load-distribution information can be derived are not available, it is possible to utilize engineering estimates of component reliability for those portions of the system for which no data can be obtained. This will usually be the case in reliability analyses of parachute designs prior to the start of development, and possibly in the case of items in development for which test programs have not yet been run. These estimates should be based on performance records of similar components, engineering analysis of the design, and experience with reliability prediction. Of course, it will not be possible to utilize such data in interval-type estimates, but they are adaptable to point-estimates if no other means of reliability analysis of the specific component are possible. Such estimates should be used with caution, since it must be realized that the reliability of every

component of the parachute system is important to overall reliable performance in the mission.

13.3.5.3 Evaluation of Operational Terms. The operational term in the product-reliability model, R_p , represents the probability of correct, error-free packing of the parachute into its deployment bag or other container. According to the desires of the evaluating agency, and if data are available, it may also include the probability of correct stowage of the deployment bag into a compartment on the load, such as the recovery-parachute compartment in the drone or missile, the deceleration-chute compartment in an aircraft, or the parachute compartment of a special weapon.

Implicit in this term is the assumption that if the parachute is properly stowed in its container, the deployment process will proceed successfully. This means that the reliability evaluation is assuming that the design of the deployment bag or other container is adequate for successful operation of the system. Such an assumption must be based on a program of good deployment-bag design and adequate testing to insure that the design is successful. With parachute systems in the development process this is no problem, since if the canopy does not deploy from the bag, it is obvious that further reliability testing is useless. From the viewpoint of the parachute system in the design stage, prior to construction, this means that the reliability being evaluated is "inherent" reliability; that is, the reliability which can be achieved with proper deployment-bag and stowage design.

The evaluation of the operational terms should be based on a statistical study of previous packings of similar canopies in similar systems. Data for the packing of relatively large canopies, such as might be used in cargo drops, missile and drone deceleration, aircraft deceleration, and weapons delivery have been collected and analyzed and are presented in Ref (4-89). These data are in a form that can be directly applied to most types of parachute analyses. In considering personnel parachutes, it is strongly recommended that a similar type of study be done on packing errors in personnel canopies, since here the characteristics of the canopy, and possibly of a portion of the packing process, are somewhat different.

In the analysis of multiple-canopy systems, it is necessary to include one packing-term in the reliability model for each canopy used. This creates no additional complexity, since if the canopies are of similar type, the same reliability value for the packing process can be used for each.

13.3.5.4 Computation of Reliability. The computation of system reliability, once data on all component reliabilities and on operational reliability have been obtained, is a relatively simple process. As can be seen from Eq 4-337, the overall reliability is the pro-

duct of all the component reliabilities and the operational reliability. However, for a system with a large number of components, this computation, while not complex, can be extremely laborious if one term is included for each component. The computing process can be shortened considerably by including only those terms in the model which are of numerical significance in calculating the results. Obviously, those components of the system with very high reliability will not affect the overall system reliability to any significant degree if components of lower reliability are also present. (The numerical values of reliability range from zero to unity; it is obvious that the lowest component-reliability will have the greatest effect on overall system reliability. For example, if a system is composed of three components with reliabilities of, say, 0.999, 0.999, and 0.900 respectively, the overall reliability, the product of the three numbers, will be 0.898, which differs by only 2/10 of one per cent from the value for that of the lowest component, 0.900.)

Thus, a preliminary analysis of the parachute system in which all components are divided into two major groups, those of extremely high reliability, and those which have a possibility of having lower reliability, will eliminate a considerable portion of the computations. It is not possible to write hard-and-fast rules for the classification of components in this process. The experience and judgment of the engineer evaluating this system is the key factor in making such decisions. However, it may be pointed out that, in general, failures which will affect mission success of hardware items, deployment bags, reefing lines, break cords, radial canopy-reinforcements, and other similar components appear to be so rare as to be generally negligible unless the parachute system is of unusual design. On the other hand, consideration of the failure rates of such components as risers, bridles, suspension lines, reefing-line cutters, and mechanical disconnects, will probably be required for most systems.

A preliminary qualitative analysis of a parachute system to select those components known to be very highly reliable can thus eliminate terms for these components from the model, and considerably simplify the computational process.

Once the list of components to be considered in the final reliability-computations has been compiled, it is necessary to conduct an analysis to determine whether these components are series-components or parallel-components in the reliability sense. The series-component is defined as one which must operate successfully if the parachute system is to operate successfully in its mission, and is represented by a single term in the model. One example of such a component is a riser; another, generally, is a suspension line, since experience has shown that the breaking of one

suspension line throws so great a load on the neighboring lines that they usually break also. Parallel-components (those which are designed as redundant sub-systems) have more than one component performing the same function, where the operation of any one will insure system success. An example is in reefing-line cutters, where two or even four may be used on the same canopy, and the functioning of any one will cut the reefing line. Another example of this arrangement is inter-stage disconnects, where two disconnect-mechanisms are often installed and the functioning of either will serve to separate the stages. The entire redundant system is represented by one term in the model. In such a case, the component-reliability term for the model is calculated from the redundant-reliability formula; for any number, n , of parallel components, the reliability of the parallel (redundant) system will be:

$$(4-339) \quad R_b = 1 - (1-R_{b_1})(1-R_{b_2}) \dots (1-R_{b_n})$$

If a point-estimate of reliability is made, the results of the use of Eq 4-339 are the desired value for substitution for the redundant-component term in the reliability model. If a confidence-interval analysis is made, and all the reliability values for the parallel components have been calculated to the same confidence coefficient, then this confidence coefficient is the one applicable to the term used in the model. If the redundant systems have had reliability calculated to differing confidence coefficients, the overall confidence coefficient will be that of the lowest term.

Once the final component-list for the analysis has been made up, and the redundancy problem has been settled, the calculation of a point-estimate of system reliability is a straightforward task of taking the product of the operational reliability and all necessary component-reliabilities. The computation of a confidence-interval reliability estimate requires not only the application of the product rule to the component — and operational-reliability terms, but also the computation of an overall confidence coefficient. Mathematically exact computations of an overall confidence coefficient for a system from confidence-interval reliability values for its components is an extremely complex task. However, an approximation method has been developed (see Ref (4-89)) which facilitates this computation with a minimum of mathematical complexity. Essentially, the method consists of pre-selecting the final confidence-coefficient desired, and then computing operational and all component reliability-terms to such confidence coefficients that the product of all of the individual confidence-coefficients is equal to the final desired confidence-coefficient. Details of the method, and tables which facilitate selection of the proper values of confidence coefficient, are pre-

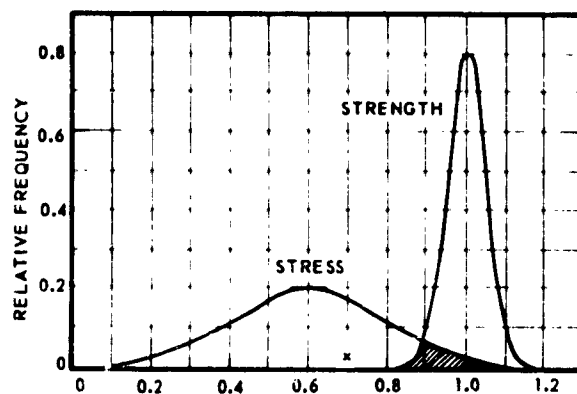


Fig. 4-163 Exaggerated Stress - Strength Distribution presented in Ref (4-89).

The only additional complexity which may arise in the reliability evaluation is that of a re-use factor, for those parachute systems which are recoverable and re-usable after the mission. As was explained in the introductory portions of this section, it is necessary to determine whether the inspection and repair process after parachute use returns the parachute to an "as-new" condition. If so, the re-use factor may be ignored. If not, it is necessary to make some sort of engineering judgment as to the effect of re-use on the strength of the parachute materials, and to adjust the stress-strength computations accordingly.

13.4 Reliability-Assessment Interpretation

The result of the computation of the reliability of a parachute system by the methods described above can be used to evaluate the long-run performance which can be expected of large numbers of such systems. It must be emphasized again that this reliability value does not reflect the absolute performance of any individual system. It merely gives the "odds" that an individual trial of the parachute will be successful. However, the process of reliability evaluation has broader and possibly more valuable applications than the single-number, overall evaluation of potential system-performance.

In the process of the evaluation of the component reliability model, the individual components of the parachute system most likely to fail are evaluated, as is the effect of the possible human error rate in manufacturing, rigging, and packing. These sub-results are really the key to the study of the potential causes of failure in a parachute system, as well as a guide to the efficient expenditure of effort in the improvement of system reliability (see below).

To produce the most efficient parachute system for a given cost, efforts should be concentrated on achieving approximately the same degree of reliability for all components and for the packing process. Effort

expended in this matter has the greatest pay-off in increasing the reliability of the system.

As was shown previously, the level of system-reliability is influenced primarily by those components with the highest expected failure-rates. Since the process of reliability analysis detailed herein detects these components explicitly, it can be of major value in locating those portions of the parachute system upon which the expenditure of further development effort will most improve system reliability.

The accuracy of the results of the reliability assessments described herein will depend to a considerable extent upon the types and sources of data available for the analysis. The interpretation of the values obtained must be made in light of the quality of the data used in the reliability assessment. This is particularly important in the case of point-estimates, since the final value of the reliability is a single number which does not reflect the amount of data nor the quality of the data which were used in its generation. In the case of a confidence-interval analysis, the confidence coefficient which accompanies the reliability value does give more information, at least from the viewpoint of data quantity, than in the point-estimate case. Here, however, the quality of the data must also be assessed. It is necessary to examine carefully all test and use records utilized to ascertain whether or not the conditions of use closely match those of the analysis. This is particularly important from the viewpoint of loads, deployment speed, and, to a lesser extent, deployment altitude.

13.5 Reliability Improvement. The results of a component-reliability analysis offer an excellent basis for a study of design changes that would improve reliability of any given system. As pointed out above, the component-by-component reliability study will indicate specifically those portions of the system where additional design effort may bring their reliability up to the average level of other components. Depending on the particular component, this may call for redesign of auxiliary devices or hardware items, or choice of other materials for fabric portions of the canopy. If the stress-strength method has been applied to canopy analysis, further detail is also available with respect to the specific fabrics used in load-bearing members. If a material with an apparently adequate mean strength is actually not adequate from the viewpoint of the stresses expected, it suggests that the standard deviation of this mean strength be examined. If it is found that the particular material chosen has a relatively high standard deviation of tensile strength (and individual samples of the same material have a large variation in strength), it may be necessary either to go to a stronger material of the same type, or to change to a material of a somewhat different type

with a lower standard deviation.

The analysis of the packing-process reliability can be used to assess the human factor in failure, both in system design and in the actual packing process. Again, such an analysis conducted for the study described in Ref (4-89) indicated that one of the primary problems in human error in the parachute-packing process is the inspection of small components for proper installation. Here, a hand or the body of the installer blocks the view of the inspector during the installation process, and, once the part has been installed, it is often difficult to determine whether the installation is correct. The detection of such cases in the course of the reliability analysis would suggest that some system redesign might be necessary to allow for better inspection procedures during the packing process.

The problem of human factors in rigging has already been discussed as one which probably should not be considered in the evaluation of the parachute-system reliability under many circumstances. However, an analysis similar to that for the packing process can be applied to the rigging process to determine whether design changes in the parachute system can result in improved reliability in human performance in parachute rigging.

One factor often ignored in reliability improvement is the matter of the maintenance of good records of performance. As is obvious from the discussion above, performance records are really the key to reliability analysis, not only on the system for which records are kept, but also for those components of that system which are used in other parachute systems. Thus, the maintenance of detailed records of use, and of inspection records, can be of major assistance in future reliability evaluations. The information which may be developed can be applied to a wide variety of hardware and mechanical items, to the analysis of common fabric-portions of parachutes, and to the development of better factors for analysis of human performance.

REFERENCES

- (4-1) Minzner, R.A., et al., The ARDC Model Atmosphere, 1959. AFRCR TR 59-267, Aug. 1959, AD 229 482.
- (4-2) Study of a Drag Brake Satellite Recovery System, AVCO-Everett Research Laboratory, Nov 1961, ASD TR 61-348.
- (4-3) King-Hele, D.G. and Walker, D.M.C., Variation of Upper Air Density with Latitude and Season: Further Evidence from Satellite Orbits. *Nature*, vol 185, pp 727-729, Mar 12, 1960.
- (4-4) Mikhnevich, V.V. et al, Some Results of the Determination of the Structural Parameters of the At-

- mosphere Using the Third Soviet Artificial Earth Satellite. *ARS Journal*, vol 30, no. 4, pp 407-413, Apr 1960.
- (4-5) Shklovskii, I.S. and Kurt, V.G., Determination of Atmospheric Density at a Height of 430 km by Means of the Diffusion of Sodium Vapors. *ARS Journal*, vol 30, no. 7, pp 662-667, July 1960.
- (4-6) King-Hele, D.G., Density of the Upper Atmosphere from Analysis of Satellite Orbits: Further Results. *Nature*, vol 184, pp 1267-1270, Oct 24, 1959.
- (4-7) Landberg, S.R., Densities of the Upper Atmosphere Derived from Discoverer Satellites. Lockheed Missiles and Space Division, Sunnyvale, Calif., Mar 1960.
- (4-8) Ewen, C.J. and Winer, D.E., Criteria for Environmental Analysis of Weapon Systems, Aug 1960, WADD TR 60-627.
- (4-9) Hyers, H.R., *General Meteorology*. McGraw-Hill, New York, 1959.
- (4-10) Faust, H. and Attmannspacher, W., Cell Structure of the Atmosphere, Deutscher Wetterdienst. Final Report, Contract No. DA 91-508-ENG-387, Oct 1959, AD 231502.
- (4-11) Dvoskin, N. and Sinscawine, N., Evaluation of AN/GMD-2 Wind Shear Data for Development of Missile Design Criteria. Apr 1958, AFCRC TN 58-259, AD 152495.
- (4-12) Garland, G.D., Gravity and Isostasy. *Encyclopedia of Physics*, vol XLVIII. Springer-Verlag, Berlin, 1956.
- (4-13) Parvin, R.H., The Earth and Inertial Space, Part II-Shape of the Earth. *Aerospace Engineering*, vol 18, no. 5, pp 33-36, May 1959.
- (4-14) Dole, S.H., The Atmosphere of Venus. Rand Paper P-978, Rand Corporation, Oct 1956.
- (4-15) Shaw, J.H. and Bobrovnikoff, N.T., Natural Environment of the Planet Venus. Ohio State University Research Foundation, TN 847-2, Feb 1959, AD 242176.
- (4-16) Kniper, G.P., The Atmospheres of the Earth and Planets. University of Chicago Press, 1947.
- (4-17) Urey, H.C., The Atmospheres of the Planets. *Encyclopedia of Physics*, vol LII, Astrophysics III, The Solar System. Springer-Verlag, Berlin, 1959.
- (4-18) Strong, J.R. and Moore, C.B., Some Observations of the Atmospheres of Venus and the Earth During the Stratola IV Balloon Flight. Paper given at the American Geophysical Union Meeting, Wash., D.C., Apr 1960.
- (4-19) de Vancouleurs, G., *Physics of the Planet Mars*. Macmillan, New York, 1954.
- (4-20) Bobrovnikoff, N.T., Natural Environment of the Planet Mars. Ohio State University Research Foundation, TN 847-1, Feb 1959, AD 242177.
- (4-21) Campen, C.F. et al (eds), *Handbook of Geophysics for Air Force Designers*. ARDC, Geophysics Research Directorate, AFCRC, 1957.
- (4-22) Hallenbeck, G.A., The Magnitude and Duration of Parachute Opening Shocks at Various Altitudes and Air Speeds. AF MR ENG 49-696-66, 1944.
- (4-23) Freeman, H.F. and Rosenberg, I., High Altitude and High Air Speed Tests of Standard Parachute Canopies. AFFTC TR 58-32, Oct 1958, AD 152286.
- (4-24) Von Karman, T., Note on Analysis of the Opening Shock of Parachutes at Various Altitudes. Army Air Corps Scientific Advisory Group, 1945.
- (4-25) Heinrich, H.G., Experimental Parameters in Parachute Opening Shock Theory. Shock and Vibration Bulletin No. 19, Research and Development Board, Dept of Defense, Feb 1953, AD 9513.
- (4-26) Heinrich, H.G., Drag and Stability of Parachutes. *IAS Engineering Review*, vol 15, pp 73-81, Jan-June 1956.
- (4-27) Heinrich, H.G. and Haak, E.L., Stability and Drag of Parachutes with Varying Effective Porosity. Apr 1962, ASD TDR-62-100.
- (4-27a) Haak, E.L., Stability and Drag of Parachutes with Varying Effective Porosity. Lecture, University of Minnesota Summer Course, July 17-28, 1961.
- (4-28) Eckert, R. and Pfluger, F., The Resistance Coefficient of Commercial Round Wire Grids. NACA TM 1003, Jan 1942.
- (4-29) Hoerner, S.F., *Fluid-Dynamic Drag*. Published by author, 1958.
- (4-30) Schubauer, G.B. et al, Aerodynamic Characteristics of Damping Screens. NACA TN 2001, Jan 1950.
- (4-31) Schlichting, H., *Boundary Layer Theory*. McGraw-Hill, New York, 1955.
- (4-32) Heinrich, H.G., Dynamic Problems of Retardation Devices. Lecture Notes, Parachute Course, University of Minnesota, 1959.
- (4-33) Theoretical Parachute Investigations. Progress Report 15, University of Minnesota, Contract AF 33 (616)-6372.
- (4-34) O'Hara, F., Notes on the Opening Behavior and Opening Forces of Parachutes. *Royal Aeronautical Society Journal*, vol 53, pp 1053-1062, London, Nov 1949.
- (4-35) Foote, J.R. and Scherberg, M.G., Dynamics of the Opening Parachute. Proceeding of the Second Midwestern Conference on Fluid Dynamics. Ohio State University, 1952.
- (4-36) Weinig, F.S., On the Dynamics of the Opening Shock of a Parachute. USAF Office of Aeronautical Research, TR 6, 1951.
- (4-37) Wilcox, B., The Calculation of Filling Time and Transient Loads for a Parachute Canopy Dur-

- ing Deployment and Opening. Sandia Corp., SC-4151 (TR), Feb 1958.
- (4-38) Milne-Thompson, L.M., *Theoretical Hydrodynamics*. Macmillan, New York, 1955.
- (4-39) Fredette, R.O., *Parachute Research Above Critical Aerodynamic Velocities*. Cook Research Laboratories, May 1961.
- (4-40) *Equations, Tables, and Charts for Compressible Flow*. NACA Report 1135, 1953.
- (4-41) Jones, R.A., *On the Aerodynamic Characteristics of Parachutes*, British ARC Report R&M No. 862, June 1923.
- (4-42) Hoerner, S., *Drag Characteristics of Parachutes*, USAF AFTR 6201, ATI 92530, October 1950.
- (4-43) Weinig, F.S., *Parachutes with Canopies Composed of Self-Supporting Ribbons*. USAF Translation of German Report F-TR-2148-ND, Oct 1947, ATI 25818.
- (4-44) Stimler, F.J. and Ross, R.S., *Drag and Stability Characteristics of 27 Different Types of 16,000-Square-Inch Model Parachutes*. AF TR 5867, Apr 1960.
- (4-45) Engstrom, B.A., *Performance of Trailing Aerodynamic Decelerators at High Dynamic Pressures, Phase IV*. WADD TR 58-284, Part IV, Feb 1961.
- (4-46) Heinrich, H.G. et al, *Quarterly Progress Reports, Contract AF 33 (616)-6372, University of Minnesota*. Jan 1961 - June 1961.
- (4-47) Meyer, R.A., *Wind Tunnel Investigation of Conventional Types of Parachute Canopies in Supersonic Flow*. WADC TR 58-532, Dec 1958.
- (4-48) Engstrom, B.A., *Performance of Trailing Aerodynamic Decelerators at High Dynamic Pressures, Phase III*. WADD TR 58-284, Part III, Dec 1960.
- (4-49) Engstrom, B.A., *Performance of Trailing Aerodynamic Decelerators at High Dynamic Pressures, Phases V and VI*. WADD TR 58-284, Part V, May 1961.
- (4-50) Pedersen, P.E., *Study of Parachute Performance at Low Supersonic Deployment Speeds: Effects of Changing Scale and Clustering*. ASD TR 61-186, July 1961.
- (4-51) Rosenlof, K.D., *Drag Coefficient of FIST Ribbon Parachutes - Reefed and Fully Inflated*. AFFTC TR 58-5, May 1958, AD 131459.
- (4-52) Knacke, T., *Reefing Methods, Parachute*. TSEPE 672-25D, Oct 1947.
- (4-53) X-7A Supersonic Ramjet Test Vehicle Parachute Recovery System, Sections I and II (Confidential Report, Unclassified Title). WADC TR 55-162, June 1955, AD 95744.
- (4-54) Knacke, T.W. and Dimmick, L.L., *Design Analysis of Final Recovery Parachute, B-70 Encapsulated Seat and USD-5 Drone*. ASD TDR 62-75, Mar 1962.
- (4-55) Liepman, H.W. and Puckett, A.E., *Introduction to Aerodynamics of a Compressible Fluid*. Galt Aeronautical Series, Wiley, New York, 1947.
- (4-56) Heinrich, H.G. et al, *Pressure Distribution in Transonic Flow of Ribbon and Guide Surface Parachute Models*. WADC 59-32, Feb 1959.
- (4-57) Heinrich, H.G. et al, *Quarterly Progress Reports, Contract AF 33(616)-6372, University of Minnesota*. Jan 1960 - June 1961.
- (4-58) Heinrich, H.G. et al, *Quarterly Progress Reports, Contract AF 33(616)-8310, University of Minnesota*. June 1961 - Oct 1961.
- (4-59) Topping, A.D. et al, *A Study of Canopy Shapes and Stresses for Parachutes in Steady Descent*. WADC TR 55-294, Oct 1955.
- (4-60) Heinrich, H.G. et al, *Quarterly Progress Reports, Contract AF 33 (616)-8310, University of Minnesota*. June 1961 - Aug 1961.
- (4-61) *A Study of Design and Materials for Development of Low Cost Aerial Delivery Parachutes*. Cook Research Laboratories, WADC TR 59-385, Sep 1959.
- (4-62) Heinrich, H.G. and Riabokin, T., *Analytical and Experimental Considerations of the Velocity Distribution in the Wake of a Body of Revolution*. WADD TR 60-257, Dec 1959.
- (4-63) Swain, L.M., *Turbulent Wake Behind a Body of Revolution*. Proceedings of the Royal Society of London, ser A, vol 125, 1929.
- (4-64) Hall, A.A. and Hislop, G.S., *Velocity and Temperature Distributions in the Turbulent Wake Behind a Heated Body of Revolution*. Proceedings of the Cambridge Philosophical Society, vol 34, pp 345-353, 1939.
- (4-65) Goldstein, S., *On the Velocity and Temperature Distribution in the Turbulent Wake Behind a Heated Body of Revolution*. Proceedings of the Cambridge Philosophical Society, vol 34, pp 48-67, 1938.
- (4-66) *Theoretical Parachute Investigations, Progress Reports, WADC Contract AF 33 (616)-3955*, Sep 1958.
- (4-67) *Theoretical Parachute Investigations, Progress Reports, WADD Contract AF 33(616)-6372*.
- (4-68) Broderick, M.A. and Turner, R.D., *Design Criteria and Techniques for Deployment of Aerodynamic Drag Devices*. ASD TR 61-188, May 1961.
- (4-69) Love, E.S., *Base Pressure at Supersonic Speeds of Two-Dimensional Airfoils and on Bodies of Revolution, With and Without Fins Having Turbulent Boundary Layers*. NACA TN 3819, Jan 1957.
- (4-70) Howarth, L. (ed), *Modern Developments in Fluid Dynamics, High Speed Flow*, vol II. Oxford at the Clarendon Press, 1953.
- (4-71) Chapman, D.R., *An Analysis of Base Pressure*

- at Supersonic Speeds, and Comparison with Experiment. NACA TN 2137, 1950.
- (4-72) Doetsch, H., Three-Component Measurements of Parachute Canopies of Different Shapes. USAF Translation of German Report FB 229, Feb 1935.
- (4-73) Heinrich, H.G. and Gerhard, R., Wind Tunnel Tests of Parachutes. USAF Translation of German Report FGZ 192, Mar 1942, ATI 23380.
- (4-74) Heinrich, H.G., Investigation of the Stability of Parachutes in the Development of a Stable Parachute Manufactured of Permeable Material. USAF Translation of German Report No. 300, Mar 1943, ATI 42978.
- (4-75) Henn, Descent Characteristics of Parachutes. USAF Translation of German Report ZWB WM/6202, Oct 1944.
- (4-76) Brown, W.D., Parachutes. Pitman, New York, First Edition, 1957.
- (4-77) Reagan, J.F. and Stimler, F.J., The Development of an Analytical Method for Investigating Parachute Stability. Guggenheim Airship Institute Report DGAI 134, Oct 1945.
- (4-78) Ashley, H., Dynamic Stability of a Body Moving Through the Air. MIT Parachute Technology Notes, June 1955.
- (4-79) Milne-Thompson, L.M., Theoretical Hydrodynamics. Macmillan, New York, Third Edition, 1955.
- (4-80) Lamb, H., Hydrodynamics. Dover, New York, Sixth Edition, 1932.
- (4-81) Ketschin, Kibel and Rose, Theoretische Hydro-mechanik. Akademie Verlag, Berlin, 1954.
- (4-82) Eckert, E., Calculation of the Temperature which a Parachute Canopy Attains at High Altitude. AMC TR F-TR-2133-WD, Dec 1946.
- (4-83) Eckert, E. et al, Transient Temperatures of Parachutes During Descent. WADC TN 57-320, Aug 1957.
- (4-84) Ruoff, A.L. et al, Aerodynamic Heating of Parachutes. WADC TR 57-157, Dec 1957.
- (4-85) Engholm, G. et al, Instantaneous Local Temperatures of Aerodynamic Decelerators, Part I - Method of Predicting, WADD TR 60-670, Sep 1960.
- (4-86) Kreith, F., Principles of Heat Transfer. International Textbook Co., Scranton, Pa., 1958.
- (4-87) Schoeck, P.A. et al, Experimental Studies for Determining Heat Transfer on Ribbons of FIST Type Parachutes. WADC TN 59-345, Feb 1960.
- (4-88) Herman, R., Problems of Hypersonic Flight at the Re-Entry of Satellite Vehicles. Proceedings of the 9th Annual Congress of the IAF, Amsterdam, 1958.
- (4-89) Jailer, R.W., Freilich, G. and Norden, M.L., Analysis of Heavy Duty Parachute Reliability. American Power Jet Co., WADD TR 60-200, June 1960, AD 246490.
- (4-90) Chorafas, D.M., Statistical Processes and Reliability Engineering. Van Nostrand, Princeton, 1960.
- (4-91) Dixon, W.J. and Massey, F.J., Introduction to Statistical Analysis. McGraw-Hill, New York, 1951.
- (4-92) Coplan, M.J. and Bloch, M.G., A Study of Parachute Seam Design Criteria, Part I - Investigation of the Strength of Nylon and Rayon Cloth Seams. Fabric Research Laboratories, WADC TR 56-313 Part I, June 1956, AD 110406.
- (4-93) Miller, C.R., A Study of Parachute Seam Design Criteria, Part II - Investigation of the Strength of Nylon Webbing Joints. Pioneer Parachute Co., WADC TR 56-313 Part II, June 1956, AD 110407.

CHAPTER 5 APPLICATIONS

Table of Contents

<i>Section</i>	<i>Page</i>
1 GENERAL	280
2 AIR DROP	280
2.1 Aircraft Systems	282
2.1.1 Aircraft Types	282
2.1.2 Method of Ejection	284
2.1.3 Restraining Systems	284
2.2 Design Criteria	284
2.2.1 Objectives	284
2.2.2 General Considerations for Design of an Air-Drop System	284
2.2.3 Other Design Considerations	288
2.3 Parachute Canopies	288
2.3.1 General	288
2.3.2 Extraction Canopies	288
2.3.3 Types of Cargo Parachutes	288
2.4 Cargo Platforms	288
2.5 Deceleration and Anti-Toppling Devices	290
2.5.1 General	290
2.6 Reefing	290
2.7 Skirt Hesitator	290
2.8 Deployment Methods	292
2.8.1 General	292
2.8.2 Deployment-System Design	292
2.9 Canopy Ground-Release System	293
3 STABILIZATION	293
3.1 General	293
3.2 Fuel-Tank Stabilization	293
3.2.1 Considerations	293
3.2.2 Fuel-Tank Stabilization-System Requirements	293
3.2.3 Fuel-Tank Stabilization-System Design	293
3.3 Bomb Stabilization	293
3.3.1 General	293
3.3.2 Bomb-Stabilization System Requirements	293
3.3.3 Bomb-Stabilization System Design	294
3.4 Droppable-Wheel Recovery	294
3.4.1 General	294
3.4.2 Requirements for a Droppable-Wheel Recovery System	295

<i>Section</i>	<i>Page</i>
3 STABILIZATION (Cont'd)	
3.4.3 Droppable-Wheel Recovery-System Design	295
3.5 Ejection-Seat and Emergency-Escape-Capsule Stabilization	295
3.5.1 General	295
3.5.2 Requirements for Ejection-Seat and Emergency-Escape-Capsule Stabilization by Parachute	295
3.5.3 Ejection-Seat and Emergency-Escape-Capsule Stabilization-System Design	295
3.6 Anti-Spin Parachutes	295
4 AEROSPACE-VEHICLE RECOVERY	297
4.1 General	297
4.2 Overall Design	297
4.2.1 Principles	297
4.2.2 Atmospheric Re-Entry and Hypersonic-Speed Deceleration	297
4.2.3 Supersonic-Speed Deceleration	300
4.2.4 Final Recovery	300
4.3 General Design Considerations	301
4.3.1 Initiation	301
4.3.2 Recovery Sequence	301
4.3.3 Maximum Deceleration	301
4.3.4 Parachute Compartment	302
4.3.5 Deployment	303
4.4 Release and Control Sub-Systems	304
4.4.1 Compartment-Door Release	304
4.4.2 Controls	304
4.4.3 Sequencing	304
4.4.4 Canopy Disconnect	305
4.4.5 Pyrotechnic Devices	305
4.5 Landing-Impact Shock-Absorption	305
4.6 Flotation and Retrieval	305
5 AIRCRAFT DECELERATION	305
5.1 General	305
5.1.1 Brief History	305
5.1.2 Jet Applications	306
5.2 Aircraft Landing-Deceleration Parachute (Drag Parachute)	307
5.2.1 General	307
5.2.2 Operational Sequence	307
5.2.3 Overall Design	307
5.2.4 Design Considerations	310
5.2.5 Calculation of Aircraft Landing-Roll	311
5.3 Aircraft Inflight Control Parachute (Landing-Approach Parachute)	313
5.3.1 General	313
5.3.2 Overall Design	313
5.3.3 Design Considerations	313
5.4 Deceleration-Parachute Control System	316
6 SPECIAL WEAPONS	317
6.1 General	317

<i>Section</i>	<i>Page</i>
6 SPECIAL WEAPONS (Cont'd)	
6.2 Design Objectives	317
6.3 Design Considerations	317
6.3.1 Delivery Requirements	317
6.3.2 Reliability	318
6.3.3 Volume and Weight	318
6.3.4 Environment	318
6.3.5 Trajectory Control	318
6.3.6 Types of Parachute Retardation Systems	318
6.4 Deployment Methods	318
6.4.1 Static-Line Deployment	318
6.4.2 Automatic Deployment	318
6.4.3 Forced Ejection	319
6.5 Parachute-System Components	319
6.5.1 Canopy Types	319
6.5.2 Deployment Bags	319
7 PERSONNEL PARACHUTES	319
7.1 General	319
7.1.1 Requirements	319
7.1.2 Personnel-Parachute Components	321
7.1.3 Canopy Deployment	331
8 TARGET	331
8.1 Early History	331
8.2 Applications	331
8.3 Requirements	334
8.4 System	334
8.5 Radar Targets	334
8.6 Simulation	335
<i>References</i>	335
<i>Bibliography</i>	336

Illustrations

<i>Number</i>		
5-1	Air-Drop of Heavy Cargo	281
5-2	Gravity Ejection System	282
5-3	Extraction-Parachute System	283
5-4	Extraction System Using Skid-Type Platform	283
5-5	Overhead Monorail Extraction System	284
5-6	Effect of Variation of Extraction Force	285
5-7	Comparison of Various Air-Drop Parachutes	286

Illustrations (Cont'd)

Number		Page
5-8	Typical Force vs Time Histories of Air-Drop Canopies	287
5-9	Deployment and Opening of a 150-ft Air-Drop Canopy	289
5-10	Dual-Rail Modular Side-Rail Restraint Platform	290
5-11	Typical Pendulum Ejection System	291
5-12	G-12 Parachute	292
5-13	G-13 Parachute	292
5-14	Droppable Fuel Tank Parachute Stabilization System	293
5-15	Geodetic Suspension System	294
5-16	Stabilization and Recovery System Sequence	296
5-17	Ballistic Coefficient vs Maximum Deceleration and Stagnation Point Surface Temperature	298
5-18	Possible Operational Sequence for Multiple-Stage Parachute Recovery System	302
5-19	Limits of Human Tolerance	302
5-20	Diagram of Deployment System	303
5-21	Minimum Required Ejection Velocity vs Parent Vehicle Deceleration	304
5-22	Minimum Required Ejection Velocity vs Vehicle Base Diameter	304
5-23	Minimum Required Pack Ejection Velocity vs Vehicle Mach Number	304
5-24	Minimum Required Pack Ejection Velocity vs Pack Weight	305
5-25	Landing Deceleration Parachute	308
5-26	Landing Roll vs Parachute Diameter and μ Factor	308
5-27	Schematic Arrangement of Aircraft Decelerator Parachute	309
5-28	Force vs Time of a 32-ft Ribbon Landing-Deceleration Parachute	309
5-29	Force vs Time of a 16-ft Ring-Slot Landing Deceleration Parachute	310
5-30	Approach Parachute on B-47 Aircraft	313
5-31	Typical Climb-Performance Curves for a Medium Bomber Using Landing-Approach Parachutes with Different Drag Areas	314
5-32	Typical Force vs Time Diagram of 12-ft Ring-Slot Parachute Behind Medium Bomber Aircraft	315
5-33	Location of Parachute Attachment Point	316
5-34	Special Weapons Parachute	317
5-35	Flat Circular Canopy	320
5-36	Flat Extended-Skirt Canopy	322
5-37	Personnel Guide-Surface Canopy	323

Illustrations (Cont'd)

<i>Number</i>	<i>Page</i>
5-38 Opening Force vs Aircraft Release Velocity for Type C-9, MC-1, and C-11 Canopies	325
5-39 Force vs Time Histories of Canopy Inflation of C-9, MC-1, and C-11 Canopies	326
5-40 Type F-1 Steerable Parachute	327
5-41 Type MC-2 Steerable Parachute	327
5-42 Halo (Modified MC-1) Canopy	328
5-43a Hart Type Steerable Parachute	328
5-43b MC-1 With Tilted Extensions	328
5-44 Parachute Assembly, Automatic, Back	329
5-45 Maximum Force Percentages on a Parachute Harness During Canopy Inflation	330
5-46 Correlation of Static-Line Force to State of Deployment of a Type A/P 28S-2 Parachute	332
5-47 Typical Trajectory for a Target Parachute System	333
5-48 Radar Cross-Section of 220-Degree Spherical Canopy	334
5-49 Radar Cross-Section of Ring-Slot Canopy	335

Tables

5-1 Drag Forces Developed by Standard Cargo Extraction Canopies	291
5-2 Variation of Factors with L/D Ratios	299
5-3 Aircraft-Deceleration Parachutes	306
5-4 Parachute Characteristics	324

CHAPTER 5 APPLICATIONS

Aerodynamic decelerators are used in a broad spectrum of applications ranging from the air-drop of equipment to the recovery of re-entry vehicles. Decelerators are used for air-drop, to stabilize fuel tanks and bombs, aircraft anti-spin, and to recover droppable wheels, ejection seats, and emergency escape capsules. Aerospace vehicle recovery continues to grow as a major decelerator application. Other important uses include the deceleration of aircraft and special weapons, and the recovery of personnel and targets. Each type has a specific developing scope of design considerations and technology. Each mission requires appropriate consideration of speed and altitude effects, stabilization and drag. The decelerator must not be considered separately from the system as a whole.

SEC. 1 GENERAL

The aerodynamic decelerator provides a vital link in the safe recovery of a variety of aerospace vehicles. Future applications will not be limited to earth-bound recovery; the decelerator must also be considered for application to planets other than Earth. Work directed to these new uses are paralleled by continuing improvement and refinement of designs for established applications. These include:

- (a) Airdrops of equipment;
- (b) Emergency escape;
- (c) Paratroopers;
- (d) Stabilization and deceleration of bombs, mines, and torpedos;
- (e) Trajectory control;
- (f) Missile and drone recovery;
- (g) Aircraft deceleration and aircraft-spin recovery;
- (h) Radiosonde; and
- (i) Special purposes (aerial pick-up, etc.).

Decelerators may be selected on the basis of mission requirements. A compromise between drag, strength, deployment speed and altitude, stability, repeatability of application, and cost of production must be made to obtain the most satisfactory design for meeting the operational requirements.

There are three basic types of decelerators: the self-inflating, the pressure-inflated, and the mechanically actuated, each having its advantage for a particular application. The self-inflating parachutes are utilized to meet the majority of current mission requirements in both the subsonic and supersonic flight regimes. The pressure-inflated devices, either spherical, conical, or segments thereof, are considered for high-altitude, high Mach-number application where self-inflating parachutes may not inflate well, due to

insufficient dynamic pressure. The mechanically actuated types, currently the rotor-blade decelerators, have the advantage of providing a flare-out capability to obtain a near-zero touch-down velocity.

For a majority of cases, decelerators must be designed for a specific application to meet the criteria of deployment speed, deployment altitude, desirable stability characteristics during descent, rate of descent, and weight to be recovered. These conditions will establish the number of drag stages required during the region of deceleration and recovery and will establish the size of the decelerator used in each stage based on a certain drag coefficient applicable to each design. Consequently, modifications of existing designs or new aerodynamic decelerator designs must be manufactured and tested to demonstrate system performance under simulated or actual operational conditions.

SEC. 2 AIR DROP

Air-drop concepts require the use of parachutes for aerial delivery of vital supplies and equipment in an operational condition in support of combat operations and in supply missions. Present standard air-drop systems are designed for unit cargo loads weighing up to 21,500 lb. Air-drop systems are now under development for delivery of unit loads weighing 35,000 lb. The primary objective of the air-drop system is to achieve the capability of delivering a variety of vehicles, weapons, heavy cargo, and miscellaneous supplies to any strategic locality in such a manner that they will be usable within a minimum amount of time and with minimum hazard to personnel involved. The present standard air-drop system is scheduled to be phased out in late 1962. The dual-rail system (see 2.4) then will be the only standard method of aerial delivery of palletized

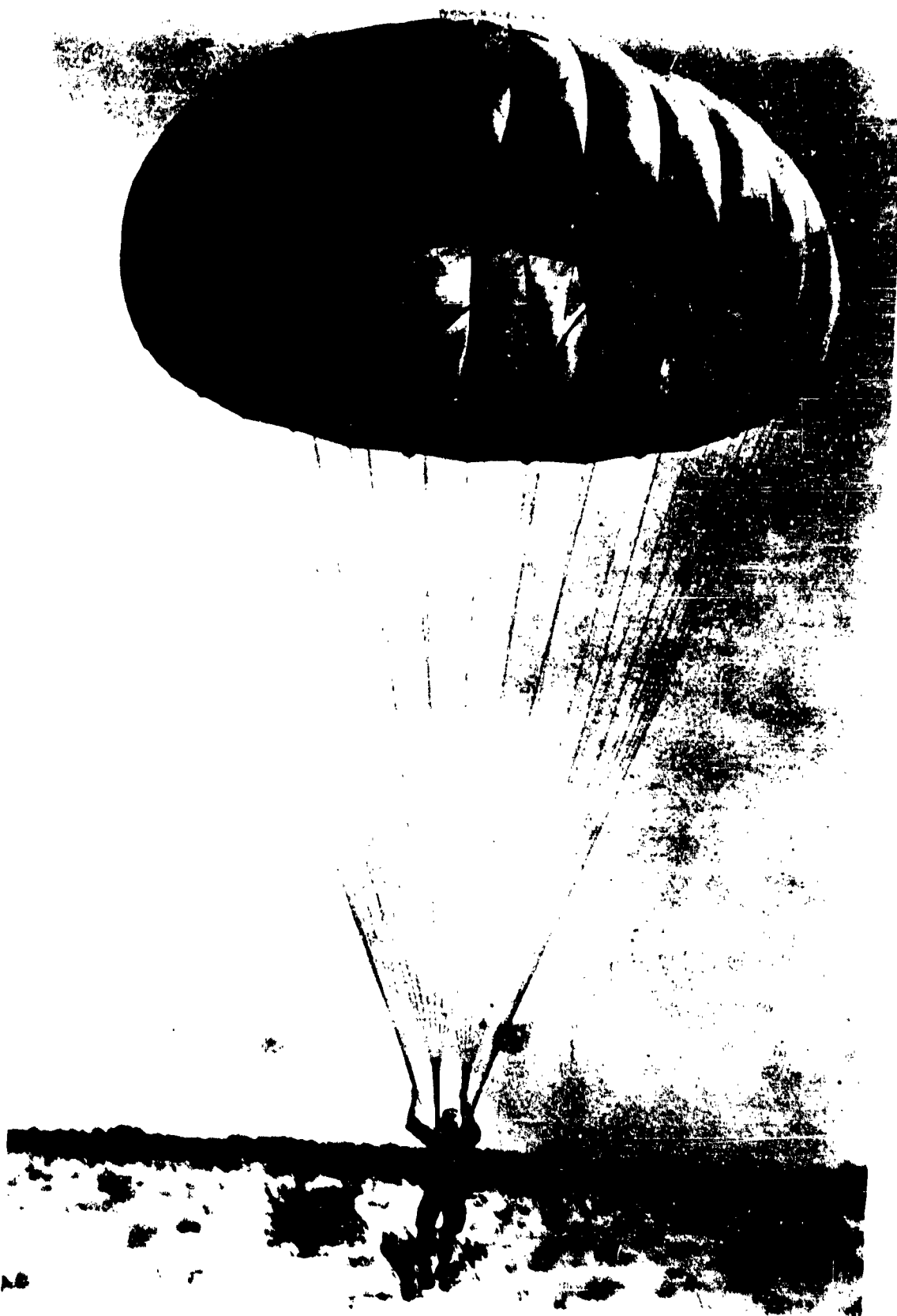


Fig. 5-1 Air-Drop of Heavy Cargo

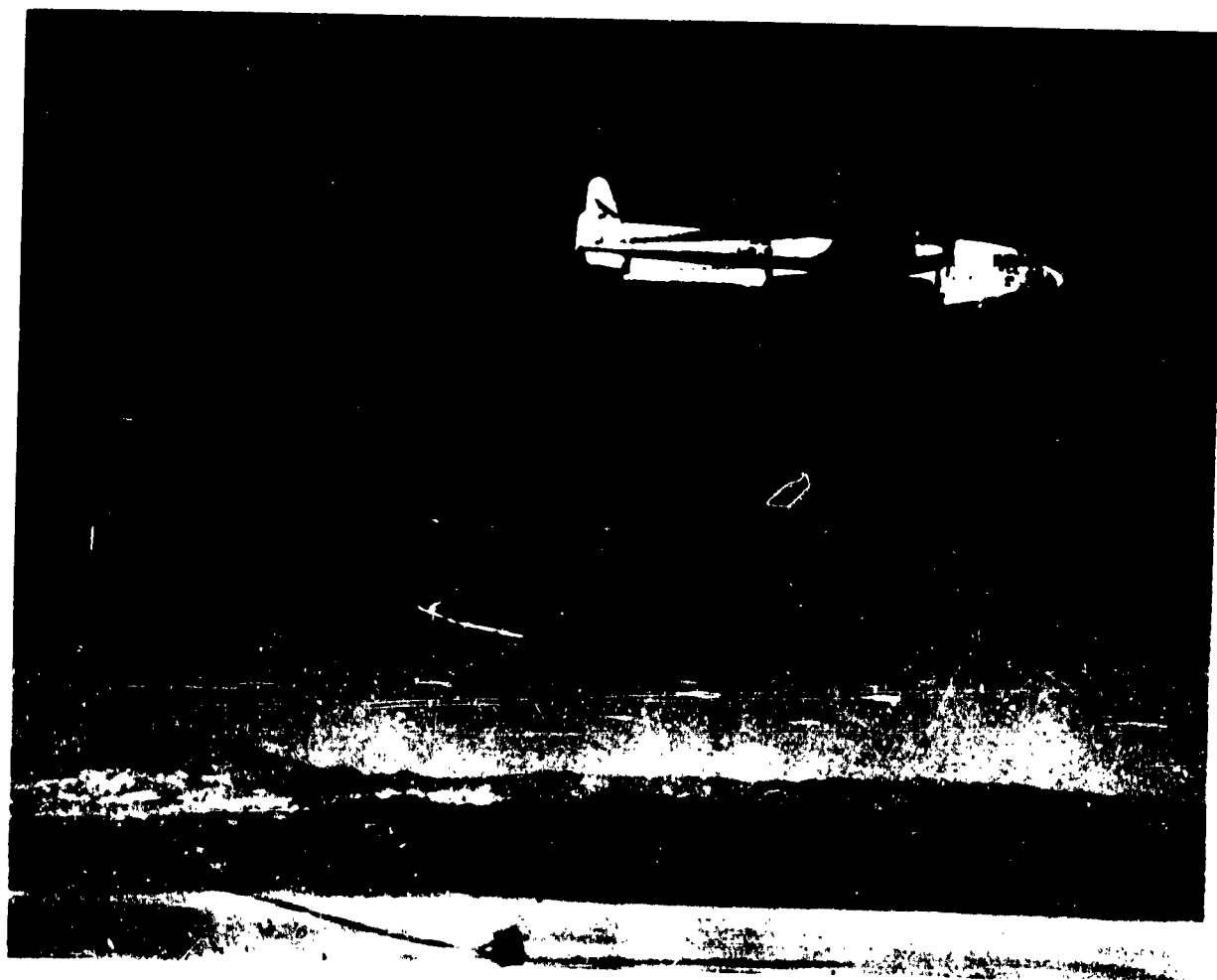


Fig. 5-2 Gravity Ejection System

equipment.

An air-drop system must include the restraining, releasing, and moving of compatible pallets or platforms safely and positively out of an aircraft in flight at the pilot's command. The system generally consists of: a platform or pallets to hold the cargo; guide rails, automatic restraint and release and roller conveyors to transport the equipment out of the aircraft; an extraction parachute capable of producing the cargo-extraction force required; a parachute system capable of producing the proper rate of descent, and a ground shock-attenuation system designed to soften the impact of the equipment to preclude any damage. A canopy ground-release is provided to prevent load turnover or the dragging of parachuted supplies during high ground-wind conditions. An air-drop sequence of a tank is shown in Fig. 5-1.

2.1 Aircraft Systems

2.1.1 AIRCRAFT TYPES. At the present time, the following cargo aircraft are considered suitable for air-drop purposes: the C-119, C-123, C-124, and C-130. The C-119 and the C-130 are designed to permit equipment extraction from the aft end of the cargo compartment using extraction-type parachutes. The C-119 aircraft is also equipped for overhead monorail delivery for dropping small containers. All current cargo aircraft are propeller-driven and allow dropping of cargo at relatively low speeds, in the range between 110 and 150 knots. In the next few years it may become necessary to devise air-drop systems for use at high speeds with faster cargo-aircraft. At the present time, however, most air-drop systems are designed for launching at aircraft speeds up to 130 knots. Future



Fig. 5-3 Extraction-Parachute System

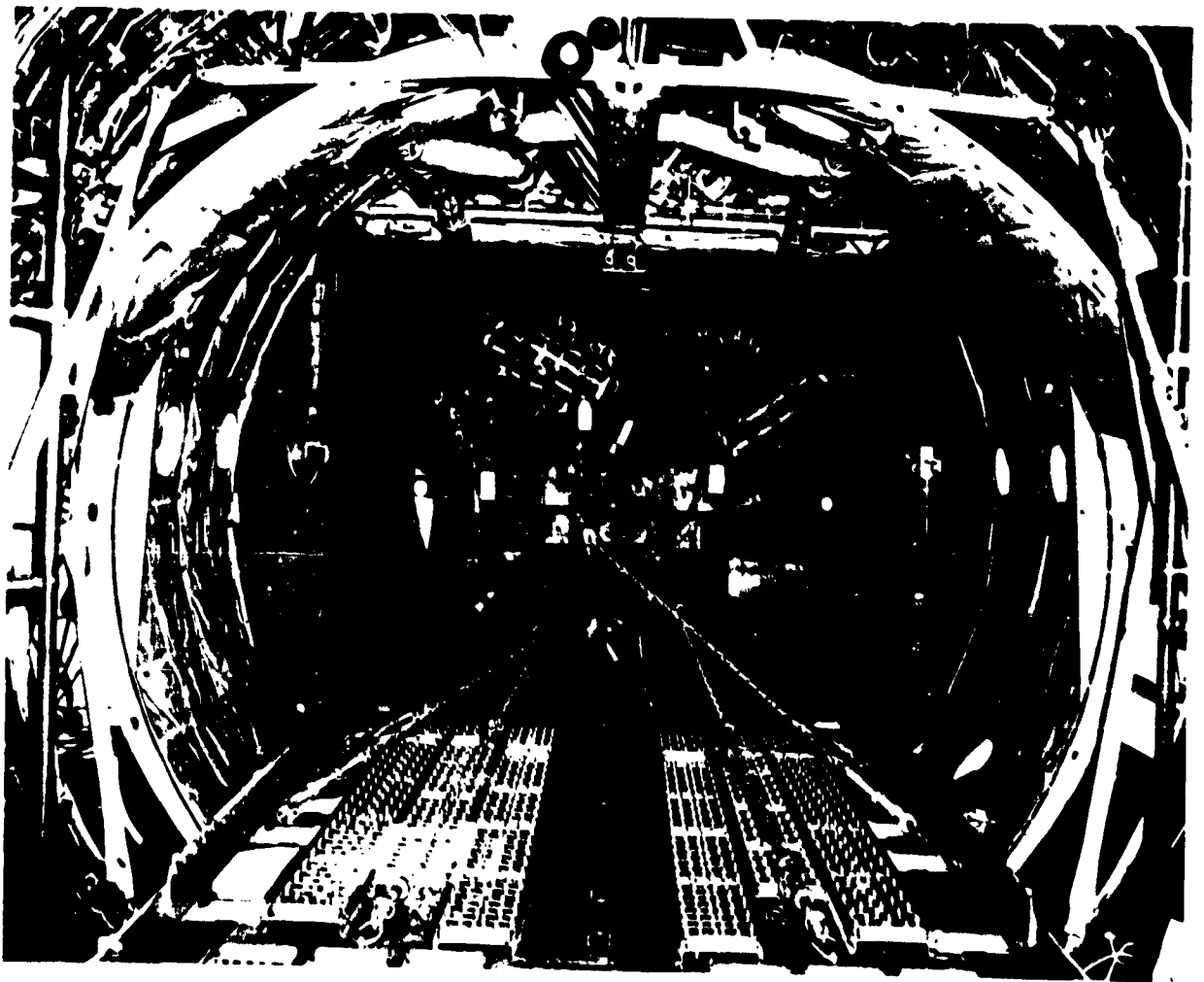


Fig. 5-4 Extraction System Using Skid-Type Platform

air-drop missions may be made from altitudes of 100 ft and below and speeds as high as 200 knots.

2.1.2 METHOD OF EJECTION. Three general methods of cargo ejection are applicable for use in today's cargo aircraft.

2.1.2.1 Gravity System. In this method (Fig. 5-2) the cargo rolls (only by gravity) from the aircraft when released by the pilot. It utilizes a floor-secured roller system. The roller conveyor is sloped by change of attitude of the aircraft to facilitate positive disposal of the cargo from the aircraft. This technique is the least preferred method of ejection, because of gravity shift within the aircraft; low load-exit velocity; and time-variations of ejection which result in inaccurate impact predictions.

2.1.2.2 Extraction-Parachute System. The most common method of load ejection from aft-loading cargo aircraft is by means of a parachute large enough to provide the force necessary for extraction of the palletized load from the aircraft in flight (Fig. 5-3). The extraction parachute is activated by the pilot through an electrically operated system.

2.1.2.3 Power Ejection. Another system for releasing the cargo from the aircraft is the power-ejection method. This type uses an overhead monorail and numerous trolleys suspending individual containers each up to 500 lb in gross weight. The trolleys are moved along the overhead monorail by a motor-driven cable. When the trolley reaches the release point, a trigger operates a latch to release the load. In this system, up to twenty 500-lb packages can be released in a period of 7 to 8 sec. Only the C-119 aircraft is equipped with this monorail system.

2.1.3 RESTRAINING SYSTEMS. The design of the aircraft restraining-system must be based on aircraft design load-factors, as given in specification MIL-A-8865, "Airplane Strength and Rigidity, Miscellaneous Loads," which outlines general ultimate *g*-values. When skid-type platforms are used, the primary restraints are applied and removed manually by releasing the tie-downs shortly before the drop (see Fig. 5-4). Platforms used with the dual-rail system are automatically released from the restraint by action of the extraction parachute. On the overhead monorail system, Fig. 5-5, the cable controls the fore and aft movement. Lateral container movement is restricted by side curtains or similar means.

2.2 Design Criteria

2.2.1 OBJECTIVES. In most instances, the design of an air-drop system is based on getting the cargo to the ground in the least possible time without damage to the aircraft or to the cargo, by applying the most economical and practical methods. The least



Fig. 5-5 Overhead Monorail Extraction System

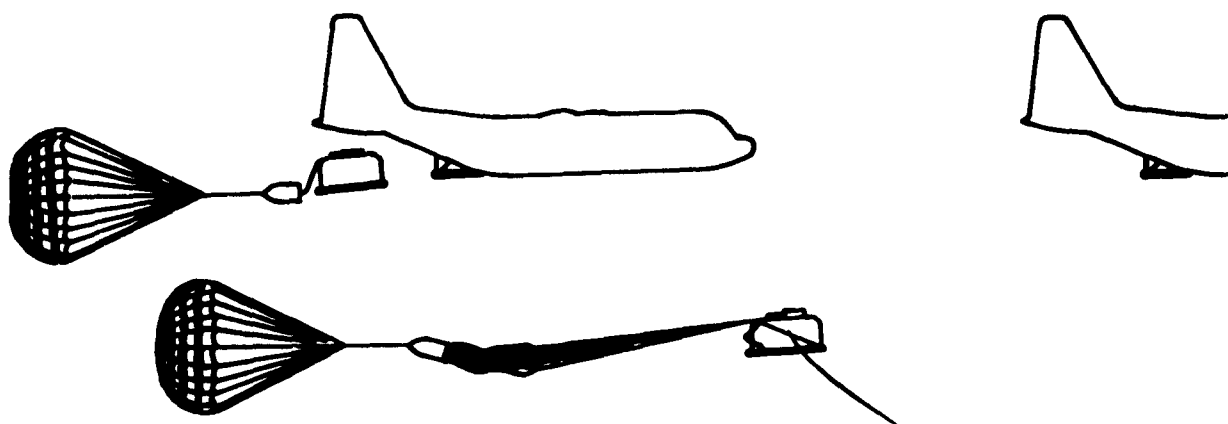
possible drop-time is desirable for maximum drop-accuracy, minimum dispersion of drop loads, and minimum effect of wind drift. Theoretically, the ideal system would let the equipment free-fall, not employing any type of deceleration device, but would absorb landing shock to prevent damage to cargo. Practically, however, size, weight, and cost of the shock-absorbing devices that would be required prohibit their use, particularly for bulky or heavy objects. Shock-absorbing devices on platforms and containers, in conjunction with parachutes, have great advantages. The stabilizing effect of the canopy permits the cargo to absorb impact-shocks in essentially only one direction. Air-drop systems strive, in general, to achieve the best possible compromise between a system for landing-impact absorption and a rate of descent low enough to hold the design of the shock-absorbing devices to reasonable size, weight, and cost and in proportion to the fragility of a specific item.

2.2.2 GENERAL CONSIDERATIONS FOR DESIGN OF AN AIR-DROP SYSTEM.

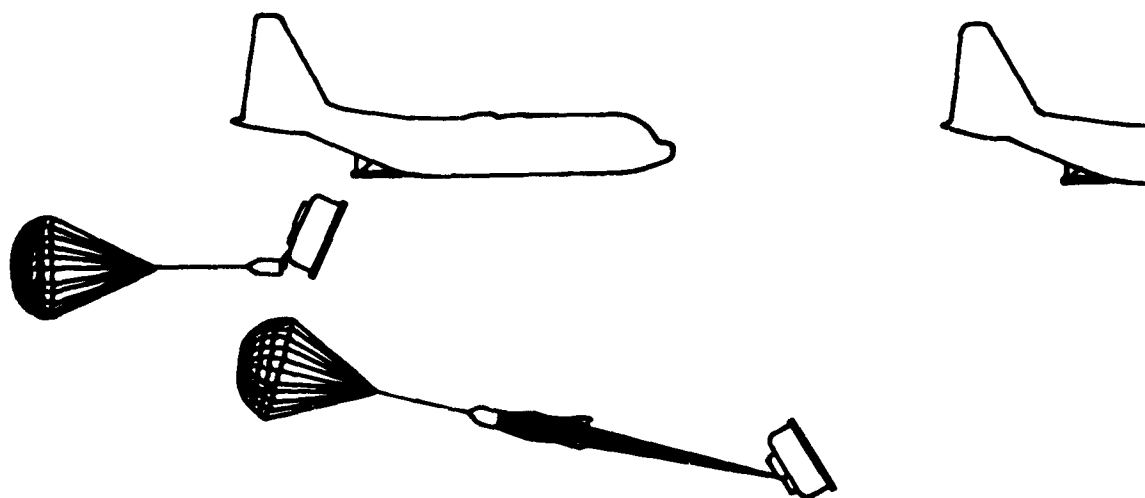
2.2.2.1 Durability. Many air drops take place in an area where it is possible to recover the parachute for re-use. It is therefore desirable to employ parachutes and hardware that will resist damage under ordinary, anticipated conditions.

2.2.2.2 Ease of Manufacture and Low Cost. Wherever possible, parachute design should be simple, for ease of manufacture. Low-cost designs adapt themselves to a high rate of production.

2.2.2.3 Critical Materials. At the present time,



A. TOO-HIGH EXTRACTION SPEED CAUSES CARGO TO REMAIN IN NEARLY LEVEL POSITION. INTERFERENCE MAY TAKE PLACE BETWEEN CARGO AND DEPLOYING SUSPENSION SYSTEM. UNEVEN AND EXCESSIVE LOADS MAY BE PLACED ON PARTS OF THE SUSPENSION SYSTEM



B. TOO LOW AN EXTRACTION SPEED CAUSES CARGO TO ROTATE AND TUMBLE

C. SEE FIG. 5-1 AND FIG. 5-3 FOR AN EXAMPLE OF CARGO EXTRACTION USING PROPER SIZE EXTRACTION CHUTE

Fig. 5-6 Effect of Variation of Extraction Force

Rate of Descent 25 fps					
Weight (lb)	Approx. Bulk (cu ft)	Load Capability (lb)	130 Knots Opening Time (sec)	Flat Circular	Remarks
620	30	12,000	23	200 ft dia. (Experimental)	Fig. 5-12
325	20	8,000	19	150 ft. dia. (Experimental)	
240	11	3,500	10	100 ft dia. (G-11A)	
120	5	2,200	7.2	64 ft dia. (G-12)	
16	0.3	100	-	12 ft dia. (G-7)	
45	2.3	500	5	Shaped hemispherical (G-13)	Fig. 5-13
11	0.25	200	1 sec at 115 knots	8 ft dia. (G-8)	

Fig. 5-7 Comparison of Various Air-Drop Parachutes

cargo canopies utilize Nylon, rayon, and cotton muslin. Rayon is used in the 24-ft diam. G-1A, 12-ft diam. G-7, and 8-ft diam. G-8 parachutes. Cotton muslin cloth is used in the G-13 hemispherical parachute. Nylon materials are used in the construction of the 64-ft diam. G-12 and the 100-ft diam. G-11A parachutes, and for all cargo-extraction parachutes.

2.2.2.4 Reliability of Inflation. Air-drop canopies do not have to meet the high reliability requirements of personnel canopies. However, for accurate dropping, they must be dependable, must have predictable inflation-characteristics, and must be consistent in performance.

2.2.2.5 Ease of Maintenance. Ease of maintenance is principally a result of design simplicity. Air-drop canopies are subject to damage not only by ground-and-object contact but also by lack of atten-

tion after completion of drop, or through mishandling by inexperienced personnel.

2.2.2.6 Rate of Descent. In general, a rate of descent of 25 ft per sec should be strived for. However, higher rates of descent may be used for cargoes that can resist damage at higher impact-shocks and for special air-drop application.

2.2.2.7 Stability. An oscillation of ± 10 deg is permissible for most cargo-container drops. A higher degree of stability, such as achieved with clusters of canopies (Sec. 11, Chap. 4), is required for air-drop systems equipped with pneumatic shock-absorbers.

2.2.2.8 Opening-Shock. For most air-drop systems, opening-shock is not of primary concern, except that it should be low enough so that it is within the design limitations of the parachute system.

2.2.2.9 Bulk and Weight. Bulk and weight are of

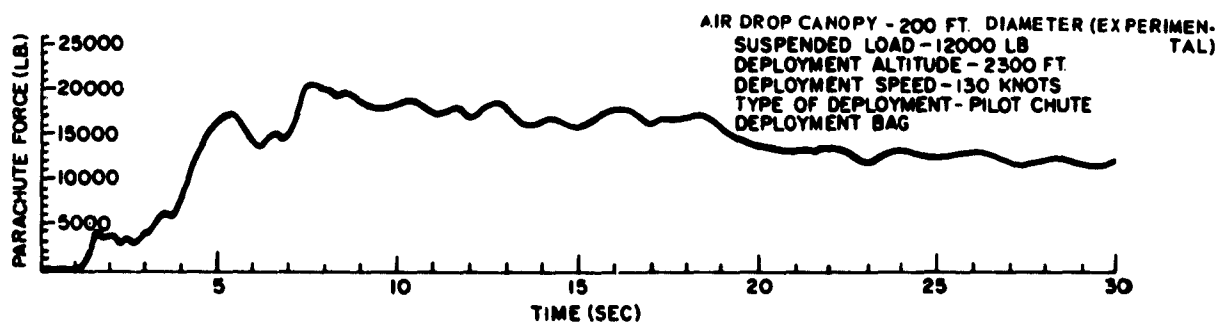
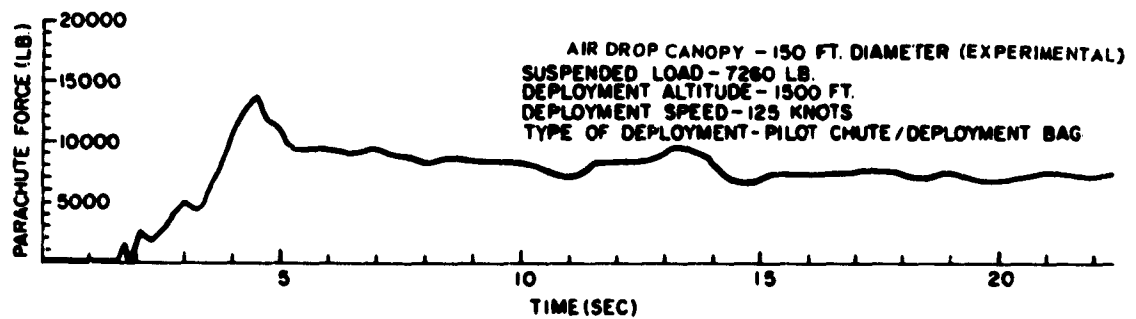
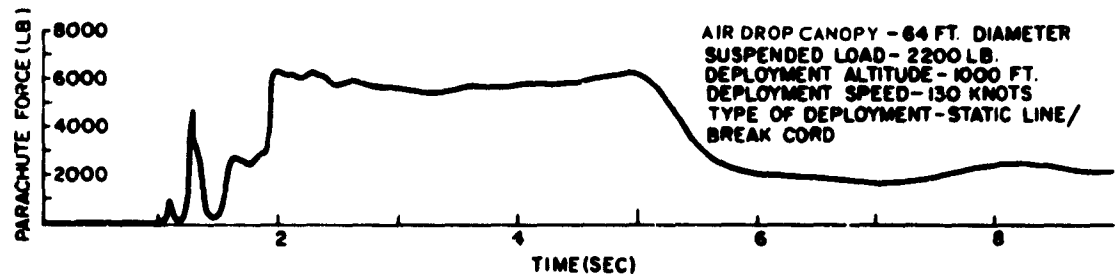
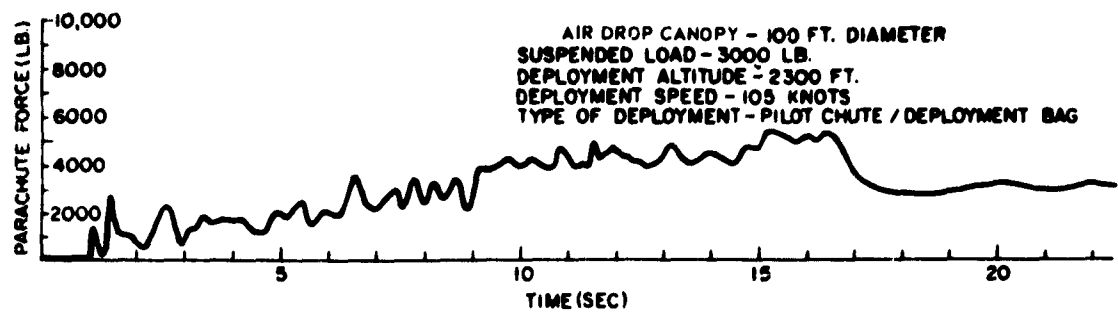


Fig. 5-8 Typical Force vs Time Histories of Air-Drop Canopies

particular importance for ease of handling by ground personnel. In most cases, however, the bulk of the parachute is not critical because of the space available in the aircraft. Of course, a light-weight, small-bulk system is desirable if both system economy and design criteria can be met.

2.2.2.10 Environment. Air-drop canopies are often packed and stored for a considerable time in areas of high humidity, relatively high temperatures, or extreme cold. When the environmental conditions for a specific design are expected to be unusual, it will be necessary to select the proper material or make provision for special protective packing, or both.

2.2.3 OTHER DESIGN CONSIDERATIONS.

(a) The maximum tolerable shock loads during deployment and the direction of these shock loads in relation to the cargo.

(b) The maximum vertical-fall distance permissible before terminal velocity is reached.

(c) The specific stability requirements for the particular cargo being dropped.

(d) The rate of descent desirable during any stage or reefed-canopy condition.

(e) Suspension design in relation to center of gravity of the load and its attitude for landing.

(f) Conformation to available space in aircraft prior to and during exit.

(g) The anticipated range of launching speed and altitude for drop.

(h) The anticipated aircraft to be utilized and its characteristics and capabilities in regard to load extraction or ejection.

(i) The minimum weight possible for the system, including platforms or containers, and parachutes.

(j) The determination of whether to use expendable or reusable containers or platforms.

(k) The maintaining of the center of gravity of the aircraft within controllable limits.

(l) The provision for rapid exit to keep the drop-dispersion area to a minimum.

(m) The point of attachment to the structure of the platform or cargo for the absorption of opening-shock.

(n) A deployment system so designed that the load does not get a chance to overturn completely after exit.

(o) The attitude of the load prior to main-canopy deployment.

(p) Reliable deployment without a complicated deployment system.

(q) Selection of proper material in relation to cost and strength.

(r) Ease of packing and handling.

(s) Low cost of maintenance.

2.3 Parachute Canopies

2.3.1 GENERAL. Single canopies or canopy clusters may be used either for extraction or for vertical descent. In general, it is desirable to have canopies with a high drag-coefficient, which has a direct bearing on the weight and bulk of the system.

2.3.2 EXTRACTION CANOPIES. Extraction canopies must have a design that is simple and must be dependable (see Fig. 5-3). An important requirement is that they perform reliably in the wake of the aircraft. Another requirement is good stability. The ring-slot canopy is generally used for extraction purposes. The size of the extraction canopy is determined by the force necessary to remove the load from the aircraft compartment. An extraction force equal to one g is recommended for initial-extraction canopy selection. Drag forces produced by standard extraction canopies for aircraft release velocities from 110 to 150 knots are shown in Table 5-1. Too high an extraction speed prevents the load from rotating sufficiently to permit smooth canopy deployment from the top of the cargo. Too low an extraction speed may permit the cargo to overturn (see Fig. 5-6). To insure proper inflation, risers must be of sufficient length to minimize the aircraft-wake effect. The system must be designed to insure that the canopy is so placed during and after inflation that it does not interfere with the aircraft structure.

2.3.3 TYPES OF CARGO PARACHUTES. There are two main types of parachute canopies used for air-drop systems: the standard circular flat, and the hemispherical, or "baseball". Some of their characteristics are shown in Fig. 5-7. Typical force-versus-time histories of air-drop canopies with various diameters are shown in Fig. 5-8. A correlation of canopy shape and force developed during canopy deployment and opening of a 150-ft-diam experimental air-drop canopy is presented in Fig. 5-9.

2.4 Cargo Platforms. Cargo platforms support the load or serve as a base for rigging a load. Loadings on the largest bearing area of the cargo, skid, or platform shall not be less than 35 pcf. This applies to all cargo loads. Wooden platforms can be salvageable or expendable, depending on design and use. They serve as a base for the load while the load is in the aircraft. After deployment, the parachute system is connected directly to the load and the platform is reduced to a base or container for ground shock-absorption materials. A platform also serves as a base and support for the load while it is in the aircraft, during descent, and upon landing. Recently the dual-rail Modular side-rail restraint platform was standardized and designated as aerial unloading Kit AF/A32H-1 (Fig. 5-10).

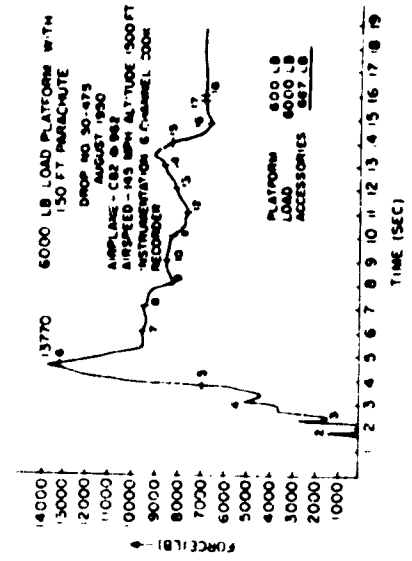
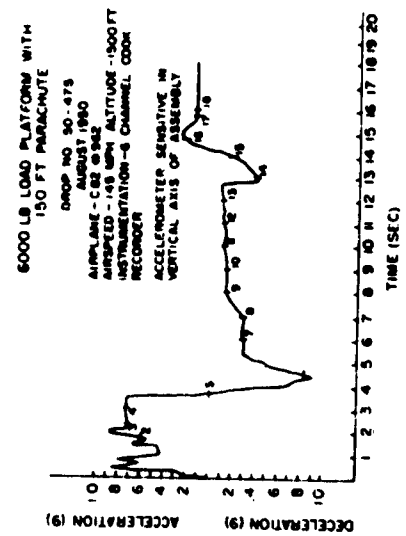


Fig. 5-9 Deployment and Opening of a 150-ft Air-Drop Canopy



Fig. 5-10 Dual-Rail Modular Side-Rail Restraint Platform

2.5 Deceleration and Anti-Toppling Devices.

2.5.1 GENERAL. Most air-drop systems have been designed to achieve a rate of descent in the neighborhood of 25 fps. The intended rate of descent may be varied according to the fragility of the cargo, the tactical situation, the accuracy of drop desired, and the efficiency of the ground-impact absorption system. The importance of the impact-absorption system cannot be overrated. Ground-impact forces of up to 100 *g*'s have been measured on platforms descending at approximately 30 fps. Currently, air-drop systems utilize paperboard honeycomb material to provide necessary energy dissipation upon ground impact. Design criteria and application for ground-impact shock-absorption devices are discussed in detail in 4.5 of Chap. 9.

2.6 Reefing. Reefing is not generally used in most air-cargo parachute operation, because canopies are designed to withstand opening-shock forces at normal deployment velocities. At present,

reefing is confined mostly to clusters of large parachute canopies, where the reefing insures that all canopies reach the same stage of inflation at the same time. Disreefing of the canopies then results in an even deployment and minimizes canopy damage. On high-altitude drops, utilizing any substantial size of air-drop canopy, prolonged reefing may be employed to achieve better accuracy of drop. In such cases, stage-reefing may be desirable. In a majority of cases where reefing is presently employed, a 2-sec reefing time will serve the purpose. An increase in reefing time automatically raises the minimum altitude at which the drop may be accomplished successfully. Reefing-system design and fabrication must be simple, to permit local installation.

2.7 Skirt Hesitator. Skirt hesitators can be employed on air-drop canopies to prevent inflation before line stretch is complete. This is particularly desirable in cases where snatch-force would exceed the opening-shock force.

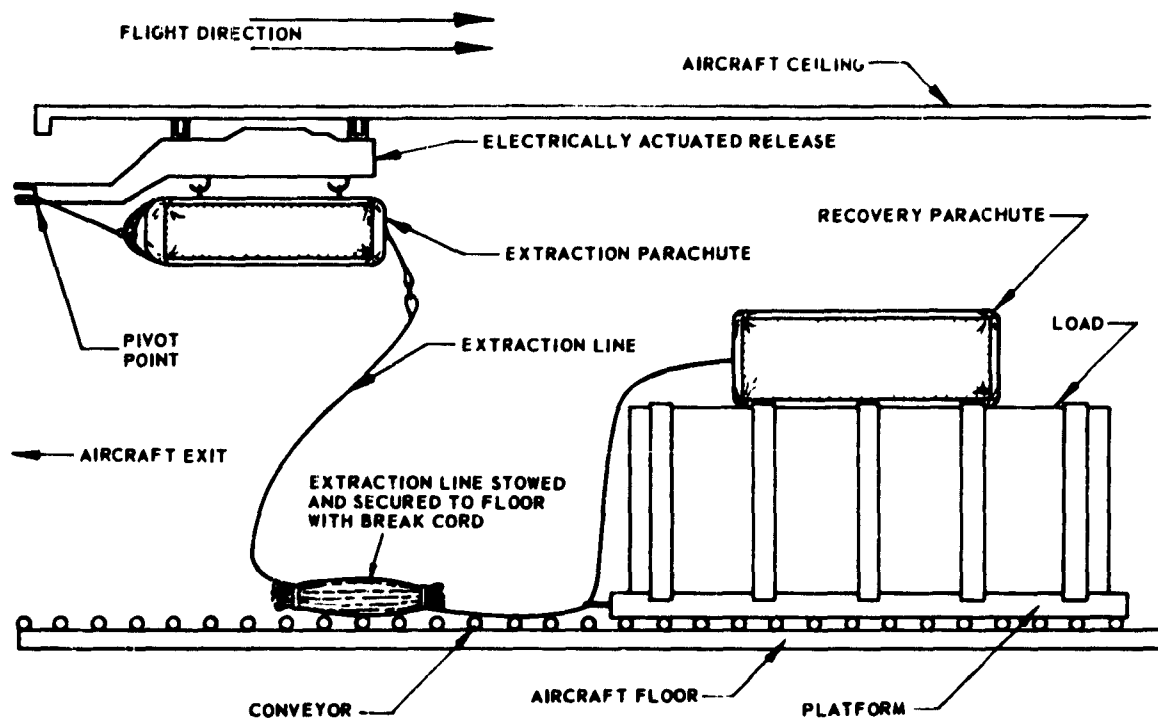


Fig. 5-11 Typical Pendulum Ejection System

TABLE 5-1
DRAG FORCES DEVELOPED BY STANDARD
CARGO-EXTRACTION CANOPIES

Aircraft Release Velocity Knots IAS	15' Ring-Slot (Reefed To Size Representing 10' D_o Canopy)	15' Ring-Slot (Reefed To Size Representing 12' D_o Canopy)	15' Ring-Slot	22' Ring-Slot	28' Ring-Slot	35' Ring-Slot
110	1,690	2,430	3,800	8,200	13,300	20,800
120	2,010	2,900	4,500	9,700	15,500	24,600
130	2,430	3,380	5,400	11,400	19,500	28,600
140	2,720	3,950	6,100	13,300	23,200	33,700
150	3,140	4,520	7,050	15,200	26,200	38,600

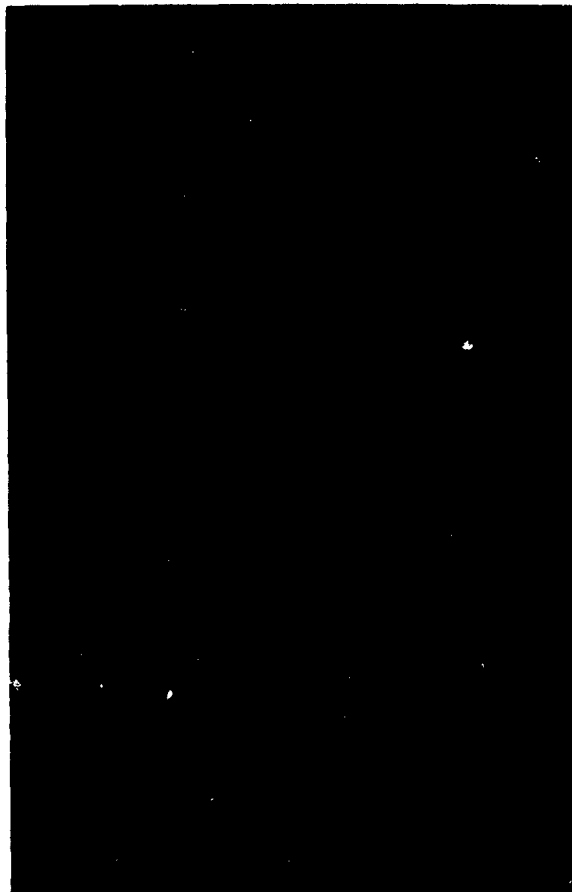


Fig. 5-12 G-12 Parachute

2.8 Deployment Methods

2.8.1 GENERAL. Deployment of air-drop parachutes may be by pilot chute or by static-line. Complicated deployment systems are not desirable, since they increase cost, maintenance, and rigging time.

A common method which has been used successfully to initiate deployment of an extraction parachute for cargo delivery is the pendulum system. (See Fig. 5-11.) In the present stage of development, a notched arm or pendulum bar and an electrically activated release are mounted as a unit in the top aft portion of the cargo compartment. The parachute is retained in a horizontal position by the release, engaging V-rings secured to the deployment bag. A short pendulum line runs horizontally from the deployment bag to the notch in the pendulum bar. Upon actuation of the release by either the pilot or an alternate crew member, the parachute falls as a pendulum in an arc around the end of the pendulum bar until a satisfactory release-attitude is reached for deployment. At this

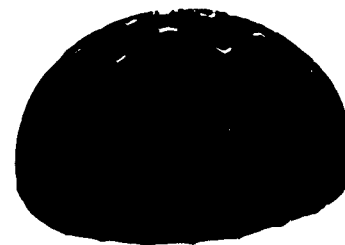


Fig. 5-13 G-13 Parachute

point, the loop in the pendulum line slips from the notch and the parachute is then free to be carried aft through the cargo door and is subsequently deployed by the airstream.

2.8.2 DEPLOYMENT-SYSTEM DESIGN. The deployment system must be kept as simple as possible. Small loads generally can be dropped from the aircraft using a simple static-line to open the parachute.

Cargo canopies for 100- to 500-lb loads are packed in the standard envelope pack. This pack is attached to the load and does not assist deployment. The static-line is attached directly to the apex of the canopy with a break cord of predetermined size placed between the apex and the free end of the static-line (loop). Reliability is not as good as that of many other systems, but low cost and simplicity warrant extensive use of this system. The G-13 and the T-7 (as converted for cargo) parachutes are most often used with this system.

For cargo loads between 700 and 2200 lb, utilizing an A-22 container and a G-12 parachute, a Nylon deployment bag is used. Deployment is initiated by a 68-in. octagonal pilot chute, which is deployed by a static-line attached to the aircraft. For cargo loads between 2,200 and 35,000 lb, clusters of the G-12 or

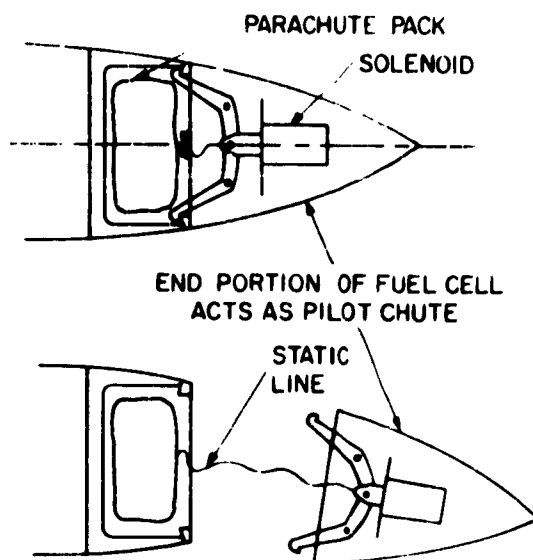


Fig. 5-14 Droppable Fuel Tank Parachute Stabilization System

G-11A parachutes are used. Both of these parachutes are deployed by the bag-type deployment method.

2.9 Canopy Ground-Release System. Unless the parachute is released immediately upon ground impact of the cargo, surface wind may cause the canopy to drag, topple, or otherwise damage the cargo. Both mechanically and electrically operated release devices have been developed for air-drop systems. A description of these devices may be found in Sec. 3 of Chap. 9.

SEC. 3 STABILIZATION

3.1 General. Parachutes offer certain definite advantages for stabilizing free-falling bodies. They provide a relatively large stabilizing force at a considerable distance from the center of gravity of the object to be stabilized without exacting an undue premium in weight or bulk. They have a particular advantage over fin-type stabilized objects, which are carried externally on an aircraft, in that they do not contribute to the object's drag until after the drag can no longer affect the aircraft's performance.

3.2 Fuel-Tank Stabilization

3.2.1 CONSIDERATIONS. The use of external droppable tanks on high-performance aircraft necessitates investigation of the aerodynamic characteristics of these tanks. The trend of modern droppable

fuel-tank design is toward an elongated cylinder with streamlining fore and aft. When mounted on the wingtip, its angle of incidence is generally the same as that of the wing. When mounted inboard and under the wing, it is generally hung from streamlined supports in a manner that produces about zero degrees angle of attack at the normal cruising speed of the aircraft. It has been found advisable to stabilize tanks mounted inboard of the wingtip. Any slight positive angle of attack tends to pitch up the nose of the tank upon release. On full tanks, the weight involved overrides the aerodynamic lift and the tanks drop free and clear; on empty or near-empty tanks, pitching of the tank can endanger the aircraft structure. It is possible to devise fins that will stabilize the tank, but the additional drag caused by the fins will be high. Stabilization by parachute has proven satisfactory, and the bulk and weight of the system is relatively small.

3.2.2 FUEL-TANK STABILIZATION-SYSTEM REQUIREMENTS.

- Immediate stability upon release of fuel tank.
- Minimum bulk to decrease fuel-capacity penalty.
- Reliable deployment system.
- Sufficient drag to insure separation of the tank from the aircraft.

(e) Low opening-shock or a suitable mechanical arrangement to insure that the tank will not be released before the canopy is inflated and therefore capable of producing the required stabilization.

(f) A provision to drop full tanks (such as at take-off) without the canopy imposing a considerable load on the aircraft for an appreciable time interval.

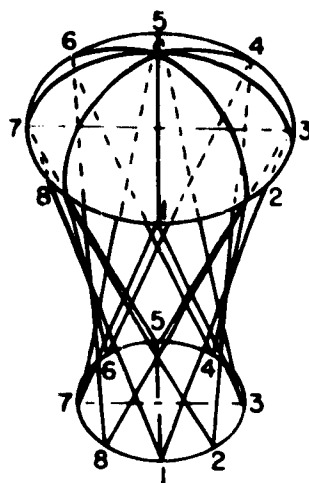
3.2.3 FUEL-TANK STABILIZATION-SYSTEM DESIGN. Fuel-tank stabilization systems generally use a portion of the rear cone of the drop tank as a pilot chute. (See Fig. 5-14.) As the forces on the rear cone may be negative, the cone must be spring-loaded for positive ejection. The tail-cone section then pulls out the main canopy. The fuel-tank stabilization system used on the B-47 aircraft utilizes an 8-ft flat circular ribbon canopy reefed to 7-1/2 ft in diameter.

3.3 Bomb Stabilization

3.3.1 GENERAL. The use of parachutes for bomb, mine, or torpedo stabilization permits stowage of a greater payload within a compartment than would be possible if the bombs were fitted with fixed fins capable of producing the same stabilizing effect.

3.3.2 BOMB-STABILIZATION SYSTEM REQUIREMENTS.

- Rapid stabilization upon deployment of the parachute.
- Constant or predictable drag-coefficient for



CONNECT POINT	TO POINTS
1	7, 3
2	8, 4
3	1, 5
4	2, 6
5	3, 7
6	4, 8
7	5, 1
8	6, 2
ON SKIRT	ON BOTTOM

8 PANEL PARACHUTE

SUSPENSION LINE ADJUSTMENT IS ACHIEVED BY PLACING ONE DISC IN THE MOUTH OF THE PARACHUTE (SIMULATING THE INFLATED PARACHUTE) AND A SECOND DISC AT THE FREE END OF THE SUSPENSION LINES. THE LOWER DISC MUST BE WEIGHTED AND THE TWO DISCS MUST BE PARALLEL.

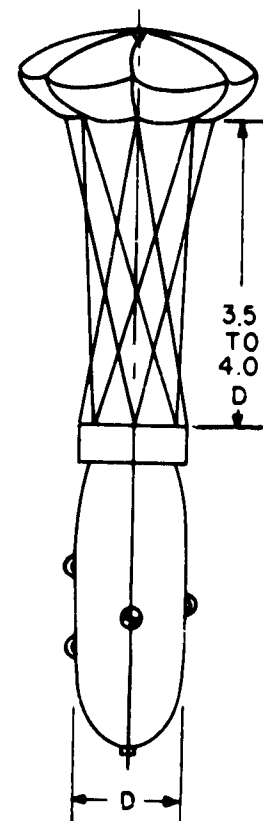


Fig. 5-15 Geodetic Suspension System

accurate computation of flight path.

(c) Ability to withstand opening-shock without damaging distortion at highest altitude and airspeed anticipated for drop.

(d) Stability, at highest velocity, of ± 2 deg.

3.3.3 BOMB-STABILIZATION SYSTEM DESIGN.

Bomb-stabilization systems usually employ ribless guide-surface parachutes. To decrease oscillation, the forces on the canopy are transmitted directly to the body of the bomb by means of a geodetic suspension system (see Fig. 5-15). At subsonic speeds, distance between the bomb and the parachute skirt varies between 3.5 and 4.0 times the diameter of the bomb at its widest portion (generally at the designed center of gravity). The shorter distance is preferable for rigidity of the suspension system, but the wake effect of some bombs makes the longer distance necessary. For stabilization at supersonic speeds the distance between bomb and parachute should be increased to a minimum of five times the diameter of the bomb. Deployment of the parachute is accomplished by static-

line. Since bomb accuracy is adversely affected by decrease in speed, it is desirable to use the smallest parachute that will achieve the required degree of stabilization. When a properly designed adapter-housing is used, the parachute system adds very little to the overall bomb length. Systems have achieved a decrease in bomb length over the standard fin assembly bomb of better than 20 per cent in addition to a considerable saving in weight.

3.4 Droppable-Wheel Recovery

3.4.1 GENERAL. Installation of extra-long-range fuel tanks or heavier-than-normal armament may bring the take off weight of an aircraft above the normal wheel-loading of the aircraft. It is therefore desirable to supplement the normal landing-gear with additional wheels and tires. This can be accomplished by the use of auxiliary wheels, which support a portion of the load during takeoff. Immediately after takeoff, such wheels must be dropped because of lack of provision for carrying them in the retracted position and also because they will not be necessary once the

fuel or armament is expended. Such wheels also can permit takeoffs from semi-prepared or light-duty runways. Recovery of the wheels may be accomplished by a small parachute. The parachute serves to decrease rapidly the speed and distance the wheels travel after drop.

3.4.2 REQUIREMENTS FOR A DROPPABLE-WHEEL RECOVERY SYSTEM.

- (a) Rapid-opening canopy.
- (b) Simple single-parachute system.
- (c) Positive deployment system.
- (d) Provision on the auxiliary wheel for housing the parachute.

3.4.3 DROPPABLE-WHEEL RECOVERY-SYSTEM DESIGN. In this system, the degree of stabilization is not of primary concern. The octagonal canopy has proved quite adequate. Accelerated opening should be strived for, and may be achieved by canopy selection and use of pocket bands. Deployment should be accomplished by use of a simple static-line system from the strut to the droppable wheel that is designed to break at the strut.

3.5 Ejection-Seat and Emergency-Escape-Capsule Stabilization

3.5.1 GENERAL. Seat ejection at high subsonic and supersonic speeds poses a stabilization problem. Aerodynamic forces can cause such abrupt and rapid tumbling of the seat that a man's physical and mental control may be lost. Many avenues of research are being taken to overcome this problem, including aerodynamically stabilized capsules or compartments, parachute-stabilized capsules or compartments, and parachute-stabilized ejection seats.

3.5.2 REQUIREMENTS FOR EJECTION-SEAT AND EMERGENCY-ESCAPE-CAPSULE STABILIZATION BY PARACHUTE.

- (a) Extremely rapid deployment of stabilization parachute to avoid canopy fouling on gyrating seat or capsule.
- (b) Rapid and reliable opening at subsonic and supersonic airspeeds.
- (c) Positive parachute deployment; forced ejection to deploy parachute in a region not appreciably affected by the wake of the seat or capsule.
- (d) Sufficient drag to control seat or capsule tumbling before parachute system is fouled.
- (e) Manual control must be possible for any individual operation during the sequence prior to the deployment of the recovery parachute. If manual control is not used, automatic control must take over.
- (f) Adequate clearance of aircraft structure must be

assured.

- (g) Accelerations must be kept within acceptable human tolerances.

3.5.3 EJECTION-SEAT AND EMERGENCY-ESCAPE-CAPSULE STABILIZATION-SYSTEM DESIGN. Because deployment may take place at supersonic airspeeds, and very rapid canopy-opening characteristics are required, the canopy selected must be able to withstand high opening-shock. However, the opening-shock of the canopy must not exceed human tolerances. Gravitational forces imposed upon the seat or capsule by the canopy must not exceed 20 g for a period of one second, and the rate of application of force must not exceed 200 g per sec. Canopy deployment must be rapid and positive, and must be accomplished in a region not blanketed by the seat or capsule. Normally, positive deployment requires forcible ejection of the parachute by means of ejector guns, blast bags, or other pyrotechnic systems. The bridle must be designed for quick stabilization of the seat or capsule without creating excessive snap or overcorrection. Deployable aerodynamic decelerators considered for stabilization of emergency-escape capsules that separate from aircraft at supersonic speeds have ribbon canopies and spherical or conical pressure-inflated devices. Recovery parachutes for final-stage descent are based on cargo or missile-recovery parachute designs. Some ejection-seat designs allow for altitude-controlled separation of person and seat, while with others, the person remains in the seat all the way to the ground. For the latter type, a main recovery-parachute must be packed and carried on the seat. Stabilization-parachute designs, basically, are the same as those used for first-stage missile and drone recoveries. A schematic diagram of possible stabilization-parachute system-operation for a pilot-ejection seat or escape capsule is shown in Fig. 5-16.

3.6 Anti-Spin Parachutes. A spin-recovery parachute is used as an emergency device on airplanes during flight spin-demonstration in order to restore normal flying attitude if conventional control methods applied by the pilot fail. Spinning is a condition in flight where the entire aircraft rotates around an inclined or vertical axis until stopped by control-manipulations of the pilot. Under some conditions, the pilot is unable to restore normal flying attitude. In such cases the pilot releases an anti-spin parachute. The retardation force of such a parachute usually recovers the aircraft within 1-1/2 to 3 spins, depending upon the size of the parachute used. The size of the parachute, however, is limited by the structural-design criteria of the particular aircraft. In recent years, ribbon or ring-slot canopies have been selected for anti-spin

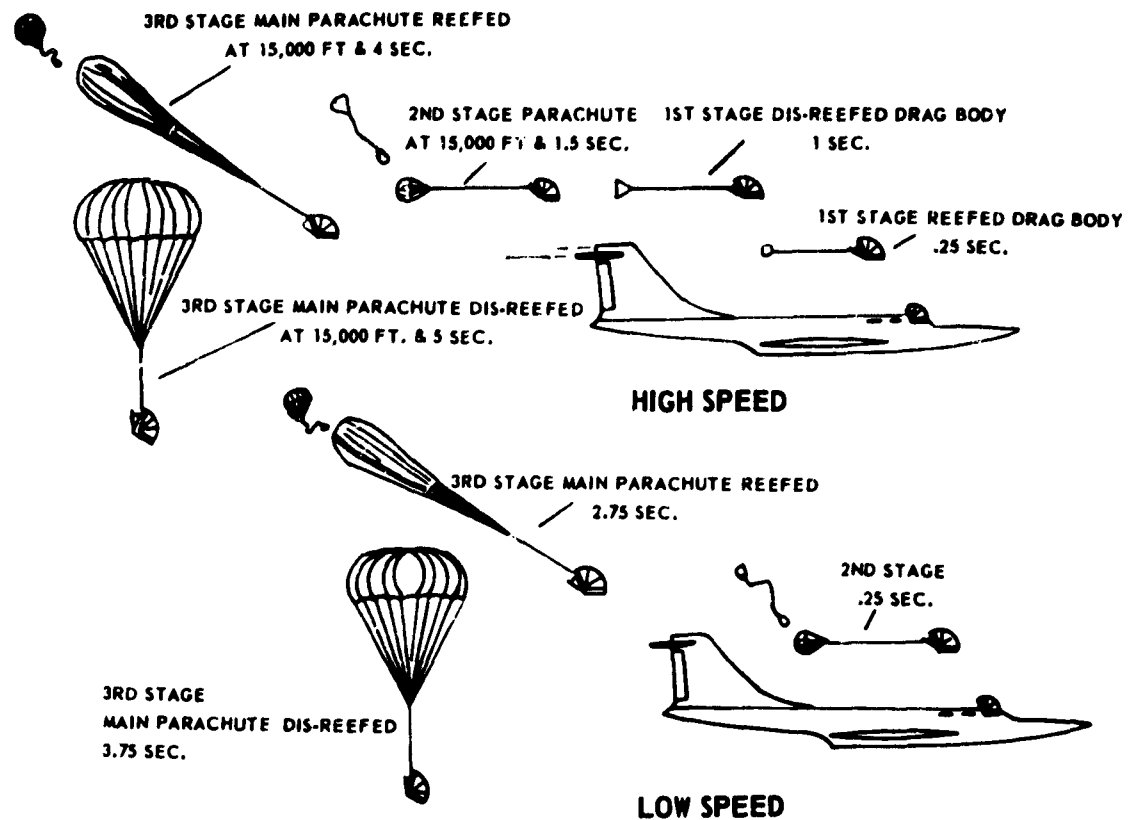


Fig. 5-16 Stabilization and Recovery System Sequence

application. They provide good stability and their opening-shock factor is only slightly above the steady effective-drag force. When there is a need for a spin-recovery parachute, wind-tunnel tests of scale-model canopies are conducted to establish the necessary design criteria, size, stability, riser length, etc., for fabrication of a full-size parachute.

Anti-spin parachutes are designed with a safety factor of three, whenever possible. The geometrical porosity of the canopy is held to approximately 16 per cent to insure quick and proper inflation. The riser (or tow-line) length, the distance between the aircraft attachment and the suspension-line confluence point, may vary from 30 ft to 50 ft.

A typical anti-spin parachute is inclosed in a specially designed parachute pack for installation on the outside of the tail section. These packs are closed by a two- or three-pin ripcord cable. A pilot chute of a standard coil-spring type, 2 or 3 ft in diameter, is

stored inside the pack. The ripcord cable is extended through the fuselage to the pilot cabin, terminating in a control handle easily reached by the pilot. In an emergency, the handle will be operated for disengaging the ripcord pins, allowing the pilot chute to escape and subsequently deploying the anti-spin parachute. Installation of the pack outside the aircraft is considered adequate in most instances since the aircraft speed during spin-demonstration is kept considerably below the maximum flying speed of the aircraft.

This method of parachute deployment is satisfactory for speeds up to 160 knots. However, a sequenced-deployment method using deployment bags should be applied for speeds above 160 knots. Applying a controlled-deployment method reduces snatch forces and also provides a more even canopy-deployment. In some cases, especially in high-speed missions, the anti-spin parachute is stored in the deceleration-parachute compartment. The volume available in such compart-

ments is usually sufficient for storage of an anti-spin parachute.

In some instances a dual-parachute system has been utilized, which is sequenced so that if one system should fail to function the reserve parachute can be released. In a series of actual flights, this system proved to be very effective and is recommended for installation where the controllability of the aircraft during the initial phase of testing represents a difficult problem.

Most spin-demonstration tests are accomplished at high altitudes, so that there is ample time for recovery maneuvers and sufficient time for the pilot to escape if all control methods applied should fail.

SEC. 4. AEROSPACE-VEHICLE RECOVERY

4.1 General Parachute systems for the recovery of missiles, drones, or other aerospace vehicles must be designed to recover such vehicles under the most critical conditions anticipated. This capability is a substantial aid in the development of a reliable weapon-system, since it allows examination of missile systems and components and subsequent determination of the cause of any failure due to the malfunction of a specific missile element. These recovery systems must be individually designed to obtain the desired performance applicable to a specific vehicle, a specific flight, and a specific performance desired. Problems in devising a satisfactory vehicle-recovery system can be grouped in four major categories:

- (1) Overall design consideration based on the anticipated flight conditions and environments;
- (2) Detailed design layout based on number of deceleration stages and components required;
- (3) Requirement for repeated use of recovered items; and
- (4) Fabrication of the recovery system and free-flight testing under simulated or actual recovery conditions.

The development and testing of aerodynamic decelerators for this application has been sponsored largely by the military services. Theoretical considerations and design criteria in this field are sufficiently fluid to permit the introduction of new ideas, designs, and procedures, provided they are proven by test. It is recommended that recovery-system designers maintain close liaison with governmental agencies that are responsible for research, design, and development of aerodynamic decelerators in order to profit from the latent experience in this field.

4.2 Overall Design

4.2.1 PRINCIPLES. The basic purpose in designing any recovery system is to decelerate the recoverable body from the speed and altitude at which it is traveling prior to recovery to a low vertical speed at a low altitude, at which ground impact shall cause no or only minimum damage.

The designer must study the recovery system and, if applicable to the body to be recovered, devise a system complete with a number of stages, parachute types and sizes, parachute-compartment location and configuration, deployment system and procedure, release and control system, and landing shock-absorbing or flotation methods.

Before any one stage or component of a recovery system can be designed, it is necessary for the designer to give consideration to the overall requirements and conditions imposed by the vehicle design and the flight regime in which it is to operate. The final design of an aerodynamic decelerator recovery-system must reflect the best possible compromise between decelerator size and cost, damage factor, and effect on the performance of the vehicle caused by weight and bulk of the recovery system.

Recovery of vehicles from atmospheric and space flight consists of all or some of the following phases:

- (a) Atmospheric re-entry and hypersonic deceleration;
- (b) Supersonic deceleration and stabilization;
- (c) Final recovery;
- (d) Ground or water impact; and
- (e) Location and retrieving.

Overall design considerations for aerodynamic decelerators utilized in recovery systems will be discussed as they relate to the flight regimes listed under (a), (b), and (c) above.

4.2.2 ATMOSPHERIC RE-ENTRY AND HYPERSONIC-SPEED DECELERATION. Aerospace vehicles in the outer fringe of the atmosphere introduce new phenomena and concepts which must be considered in the design philosophy to be used for such vehicles. Considering that returning space-vehicles will be encountering the perceptible atmosphere almost as fast as meteors do, the feasibility of safe atmospheric deceleration is by no means obvious at first glance. The terminal phase of an orbiting vehicle (when the vehicle encounters the perceptible atmosphere) can be the most critical phase of a satellite's flight. The major aspects of the re-entry problem are aerodynamic heating, vehicle maneuverability, and deceleration. The lowest heating rates and smallest decelerations are obtained for tangential (very shallow) re-entries, but the total heat absorbed during a shallow re-entry is greater than during a steep one. The heating rate and decelerations can be controlled by any method

that increases the re-entry time; i.e., by use of lift, the re-entry angle can be held to a relatively low angle, or by having large surfaces whereby significant aerodynamic drag forces can be generated at high altitudes. In the case of a constant-drag device, the optimum ballistic coefficient ($W/C_D A$) is approximately 10 (Ref (5-1), (5-2)). For re-entry angles less than or equal to -3 deg, the peak decelerations with a $W/C_D A$ of 10 are below $8 g$'s, ($g = D/W$) (Fig. 5-17). Kemp and Riddell have shown that for hyperbolic flight the approximate heat-transfer rate can be obtained from the following expression:

$$q_s = \frac{17,600}{\sqrt{R_N}} \sqrt{\rho/\rho_0} (V/V_c)$$

The temperature in degrees Rankine can be obtained by the following expression:

$$T_s = \sqrt[4]{q_s / \epsilon E}$$

where q_s = Stagnation heating rate Btu/sec sq ft ;
 R_N = Nose radius;
 ρ/ρ_0 = Local-to-sea-level density ratio;
 V/V_c = Local-to-circular orbital-velocity ratio;

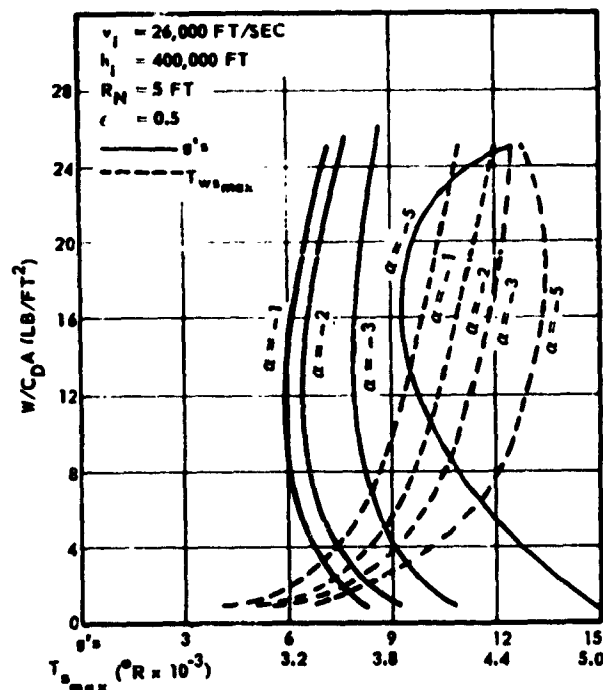


Fig. 5-17 Ballistic Coefficient vs Maximum Deceleration and Stagnation Point Surface Temperature

ϵ = Emissivity (dependent on material) between 0.7 and 0.9; and
 E = Stefan-Boltzman constant (0.476×10^{-12} Btu/ft²-sec-°R⁴).

Analytical calculations and shock-tube tunnel tests have shown that when for various drag shapes, the drag, heating, and static stability are compared, the 70-deg cone is the optimum configuration. The C_D of the 70-deg cone, with a length-to-diameter ratio of 0.3 and a ratio of drag device to capsule area of 50, is approximately 1.5 at Mach 8.

In the development of an exploratory test-model, the structural problems and complexity of a system often make it necessary to deviate from the optimum aerodynamic shape. For the sake of model structural simplicity, numerous wind-tunnel tests and free-flight tests have been conducted on an inflatable spherical balloon (Ref (5-3)). Wind-tunnel tests on spherical balloons have been conducted up to Mach 3.5 and free-flight tests above Mach 2 at an altitude of 150,000 ft. The results of both the wind-tunnel and free-flight tests indicate that an inflatable sphere, utilizing readily available material and present-day manufacturing methods, is feasible and is a practical method of decelerating and stabilizing a recoverable pay load from high-altitude and high-speed flight regimes. In the low subsonic-speed regime it was found necessary to use an inflatable torus around the sphere as a boundary-layer trip to obtain static stability. The supersonic C_D of a sphere is slightly less than unity (0.93 C_D).

The optimum or conical, flexible, inflatable shape has undergone wind-tunnel tests up to Mach 10 and shows compatible C_D with data obtained from solid models. The questionable part of a cone-shape performance is the stability of the cone when cone angles greater than 70 deg are considered. The shock-tube tunnel tests and the tests on the inflatable cone both show static stability for cone angles up to 70 deg.

The pace or speed that aerospace vehicles were being developed forced deviation from an analytical step-progression to orbital velocities. On a competitive basis with retro-rockets, heat-sink, and parachute final-recovery, a mechanically expandable re-entry vehicle with light, flexible, foldable skin, and low $W/C_D A$ was investigated. This high-drag device became known as the AVCO drag-brake. In low-altitude orbits (150 n.m.) or lower, the drag-brake had sufficient area to produce a drag force large enough to circularize or make in-plane orbit corrections and de-orbit. The drag-brake is radiation-cooled with temperature remaining below 1300 F at all times and at all points (Ref (5-4)). It does not require any additional drag-producing body for final recovery over

TABLE 5-2 VARIATION OF FACTORS WITH L/D RATIOS

L/D Ratio	Relative Wt for Equal Payload	Heating-Rate Ratio	Total Heat Ratio	Peak Decel. for Entry at -30°	Gross Range	Structure
0	1	1.0	1.0	8	0	Mechanically Expandable
0.5	1.5	0.44	1.85	3.3	135	Rigid ↓
1.0	1.6	0.32	2.60	2.25	540	
1.5	1.7	0.26	3.10	1.85	1200	
2.0	1.8	0.22	3.50	1.70	2140	
2.5	1.9	0.20	3.85	1.60	3340	

water. The multiple use of the drag-brake aerodynamic surfaces eliminates the requirement for a retro-rocket, an attitude-control system, or a final-recovery parachute-system and results in a significant weight saving (Ref (5-5)). In comparison with rigid re-entry bodies the expandable-structure decelerator will be between 25 per cent and 50 per cent lighter. It should be noted that the missions possible with the drag-brake are limited to orbital-plane re-entries and orbital altitudes below 150 n.m. In comparing the drag-brake with rigid vehicles having a constant lift-to-drag ratio (see Table 5-2), it can be seen that the drag-brake has a much lower total heat ratio. It can also be seen that the maximum benefit of lift in controlling deceleration and heating-rate is obtained from lift-to-drag ratios between zero and one-half. The control of deceleration and heating rate is not greatly improved for vehicles with higher L/D ratios, but the altitude-range and the horizontal-travel capability (cross-range capability) increases proportionally with the square of the L/D ratio.

The base for the above comparison is an expandable-structure zero-lift decelerator. It can be seen from Table 5-2 that lift, in addition to permitting cross-range maneuverability, also decreases the heating rate and peak deceleration.

It has been shown that both the lightweight expandable structure with zero lift and rigid vehicles with lift each have desirable features not obtainable by the other. It can, therefore, be concluded that the desirable re-entry decelerator should possess the desirable qualities of both non-lifting and lifting re-entry bodies. The desirable features of an expandable non-lifting decelerator are high weight-efficiency (relative weight for the same payload), compact launch-

vehicle, low ballistic-coefficient ($W/C_D A$), high operational-altitude (above 200,000 ft), high emissivity, low total-heat, and reduced communication-problem through the ionized flow. The lifting vehicle has as desirable features maneuverability, lower heating, rates, lower deceleration, and confidence in design and fabrication gained from years of aircraft experience. A composite vehicle in which as many desirable features of both expandable non-lifting decelerators and lifting vehicles are combined is the decelerator now being explored by analytical and environmental tests. The applications of the composite vehicle for three general missions are being explored (Ref (5-6)): (1) re-entry and recovery in the plane of orbit for a low-altitude earth-orbit (less than 150 n.m.); (2) the maximum cross-range achievable from that type of orbit; and (3) super-orbital re-entries considering both a parking orbit and a straight-in or single-orbit re-entry. The indications to date are that both of the earth-orbiting missions can be accomplished and that the maximum range obtainable is approximately one-half the distance between orbital passes. The limiting temperature of the material for this study was established to be 1800 F. In the achievement of the 600 n.m. cross-range capability, the temperature limit imposes a payload limit which will be established in this study. The super-orbital application is far from feasible due to limitations on an expandable structure caused by temperature. The radiative heating can be lessened with a low- $W/C_D A$ high-altitude decelerator design.

The major areas to be further explored before practicable wide-scale application of a composite vehicle can be realized lie in the method of achieving attitude-control forces and expandable structure for flexibility

and higher-temperature service. The design and fabrication methods will also require much attention, but will depend greatly upon the characteristics of the expandable or cloth-like skin structure. Even though many improvements in expandable structures are required, meaningful exploratory test-assemblies can now be fabricated and tested.

4.2.3 SUPERSONIC-SPEED DECELERATION.

Aerodynamic decelerators are essential for the initial deceleration and stabilization of aerospace vehicles to reduce their velocity for the safe initiation of final recovery by a large parachute (Ref (5-7), (5-8)). In addition, aerodynamic deceleration devices are required for the initial deceleration or stabilization (or both) of missiles and drones, boosters, space and data capsules, and a variety of re-entry vehicles.

To fulfill these requirements, a number of decelerator concepts are being investigated.

For applications in the transonic and supersonic-flight regimes, self-inflating trailing aerodynamic decelerators are considered to be the most suitable because of their relative simplicity of design and operation.

Two of the most common types of trailing aerodynamic decelerators which have been employed extensively for these applications use the guide-surface and the ribbon-type canopies. The guide-surface parachute has been successfully deployed at transonic speeds (up to $M = 1.4$) and sea-level conditions (Ref (5-9)) and the Hemisflo (ribbon) parachute has been successfully tested at $M = 2.45$ and 60,000 ft altitude (Ref (5-10)). The latter device represents the extent of the present state-of-the-art of supersonic-speed self-inflating aerodynamic decelerators.

4.2.3.1 Design Considerations. Although the above configurations were successfully tested, phenomena detrimental to their use as effective supersonic-speed decelerators became evident. In the case of high-altitude and high Mach-number applications, the immediate consideration was that of dynamic pressure. If this pressure is too low, the parachute may not fully inflate, and twisting of the lines may result, thereby preventing full inflation at a later time (even if the dynamic pressure increases). Assuming that the parachute inflates satisfactorily after deployment at these conditions, additional problems may arise. One problem encountered is that of "canopy breathing", i.e., the canopy will extend from over-inflation to complete collapse (or any degree between these limits), pulsing at a very rapid frequency. This can be reduced by choosing either proper geometric-porosity distribution or a suitable canopy shape, or both. An additional problem (also related to the first one) is that of para-

chute instability about the attachment point due to the fluctuation of the canopy bow-shock wave. This fluctuation is the change of direction, force, and shape of the shock wave brought about by the spilling and recapturing of air within the canopy (Chap. 4, Sec. 6), the interactions with the wake and suspension-line boundary-layers, and any other small disturbance in the flow field ahead of the canopy. Again, proper canopy shape and the magnitude and distribution of porosity, along with any prevention of induced-flow field-disturbances, will reduce this effect. A third problem is that of aerodynamic heating (Chap. 4, Sec. 12), which may require parachute material other than Nylon or Dacron (Chapter 6) if the expected parachute temperature exceeds the maximum allowable for these materials. Time of exposure under these temperatures, naturally, has a large effect. Consideration must be given to the problem of aerodynamic flutter; flutter is especially pronounced on ribbon parachutes where the individual ribbons experience high-frequency oscillations. This can cause canopy instability about its own center of gravity as well as about the attachment point and can cause early material deterioration through the transformation of kinetic energy to heat. Flutter may be reduced by eliminating any excess material and arranging ribbons to yield the least amount of flat-plate lift (considering the ribbon as a flat plate at an angle of attack to the flow).

For the case of parachutes operating at high Mach-numbers and high dynamic pressures (such as at sea level), another problem (in addition to those previously discussed) must be given consideration. This is the fact that the parachute must be capable of withstanding large structural-loading. Further, these heavy loads can contribute to or aggravate the other design considerations or make them more critical. These large canopy loadings necessitate judicious design and fabrication of the canopy including the selection of the type of fabric, the location of heaviest construction ("beefing-up" of expected high-load and high-temperature areas), and choice of canopy-component junctions.

4.2.3.2 Other Approaches. Concepts other than conventional parachute configurations (as mentioned in the Introduction) are being considered for applications in this speed regime to eliminate or reduce some of the problems, or to provide a choice of methods for completing a given mission in the most effective and efficient manner.

4.2.4 FINAL RECOVERY. After the vehicle has been decelerated to an equilibrium condition, the final parachute will be deployed. It is desirable to keep the deployment altitude of this parachute below

15,000 ft in order to limit the opening forces and restrict the drift of the system during final descent. The final parachute should provide a large drag-area and should limit oscillation to ± 10 deg. To obtain these characteristics, clustering of final-stage recovery parachutes has been used successfully in some instances. Allowable terminal-velocities depend on the vehicle or human g -limitations.

In general, rates of descent for proper load recovery are less than 20 fps if no shock-absorption devices are used, 25-30 fps with shock-absorption devices, and about 50 fps with nose spikes or for over-water recovery.

Usually, the canopy selected for final-stage recovery will be one, or a cluster, of the following:

- (a) Extended-skirt canopy;
- (b) Solid flat circular canopy (generally used in clusters of three or more to achieve the desired stability);
- (c) Ring-slot canopy;
- (d) Flat circular ribbon canopy; or
- (e) Ring-sail canopy.

4.3 General Design Considerations. The following is a list of considerations in the design of missile, drone, or space-vehicle recovery systems:

- (a) Possible range of speed at initial deployment;
- (b) Possible range of altitude at initial deployment;
- (c) Type of recovery desired, such as (1) rapid, stabilized descent, (2) delayed descent, and (3) free descent, in which final impact is the only consideration;
- (d) Allowable weight and space available for deployable aerodynamic decelerator and impact-attenuation system;
- (e) Location of decelerator or decelerators, which may affect the insulation required and type of deployment, such as (1) pilot chute, (2) static-line, or (3) forced-ejection equipment;
- (f) Ride design, which includes (1) desirable angle for vehicle support, (2) center of gravity of vehicle at time of deployment and descent, and (3) force-limitations of vehicle at load connections;
- (g) Maximum g -tolerances of vehicle and direction of g 's. In the case of manned vehicles, maximum human g -tolerances and rate of g -onset;
- (h) Desirable stability and angle of descent at final impact;
- (i) Shock-attenuation system to be used for final impact;
- (j) Geographical and physiographical area in which vehicle is expected to operate;
- (k) Weight of vehicle at anticipated recovery time;
- (l) Position of first-stage parachute at inflation, as influenced by (1) motor-blast heat and pressure,

and (2) wake effect;

- (m) Aerodynamic heating; and
- (n) Vehicle configuration (stable or unstable in descent).

4.3.1 INITIATION. Deployment of a recovery system can be initiated by ground command; by flight conditions such as engine failure, loss of control signal, or loss of braking signal; or in the case of emergency escape, by an altitude-velocity sensor which is armed by a timer at a predetermined interval (usually 0.5 sec) after separation of escape-capsule from aircraft.

4.3.2 RECOVERY SEQUENCE. Recovery normally consists of, but is not limited to, two or more stages involving parachutes or other drag-producing devices to accomplish the deceleration and subsequent descent to the ground. Fig. 5-18 shows a plot of altitude and flight-path speed for a typical five-stage recovery system. The number of stages and the design of the decelerator for each stage is determined by the following recovery conditions:

(a) *Deployment Speed and Altitude.* The requirements for the first-stage decelerator design are determined by the speed and altitude at which it is to be deployed. The values selected shall be the most critical (maximum and minimum) that can reasonably be expected during uncontrolled tests or operational flights of the vehicle.

(b) *Recovery Weight.* The recovery weight is the weight of the missile, the drone, the escape-capsule with occupant, the aerospace vehicle, or their components, to be recovered. This value can vary because of changing conditions or fuel load. Therefore, it should be the maximum weight under which recovery is to be made. Consideration must be given to reducing this value by dumping fuel or jettisoning parts of the body that are to be recovered.

4.3.3 MAXIMUM DECELERATION. Knowledge of the magnitude and, in the case of emergency escape, the rate of application, of the g 's imposed on a vehicle or its occupant is required to determine the number of stages required, the decelerator sizes, and the timing of the recovery sequence. Not only must the limit of the vehicle structure be considered in determining the allowable g 's, but also the powerplant, instruments, control system, and other accessories. Fig. 5-19 illustrates human tolerance to accelerations. This chart is extracted from USAF Specification MIL-C-25969A. The graph depicts zones of allowable accelerations in both the transverse and longitudinal directions. Further limitations must be established as to the magnitude of the longitudinal and transverse accelerations that can be imposed when both are acting concurrently on a human. In addition to consideration of translational accelerations, in some instances it may be

15,000 ft in order to limit the opening forces and restrict the drift of the system during final descent. The final parachute should provide a large drag-area and should limit oscillation to ± 10 deg. To obtain these characteristics, clustering of final-stage recovery parachutes has been used successfully in some instances. Allowable terminal-velocities depend on the vehicle or human g -limitations.

In general, rates of descent for proper load recovery are less than 20 fps if no shock-absorption devices are used, 25-30 fps with shock-absorption devices, and about 50 fps with nose spikes or for over-water recovery.

Usually, the canopy selected for final-stage recovery will be one, or a cluster, of the following:

- (a) Extended-skirt canopy;
- (b) Solid flat circular canopy (generally used in clusters of three or more to achieve the desired stability);
- (c) Ring-slot canopy;
- (d) Flat circular ribbon canopy; or
- (e) Ring-sail canopy.

4.3 General Design Considerations. The following is a list of considerations in the design of missile, drone, or space-vehicle recovery systems:

- (a) Possible range of speed at initial deployment;
- (b) Possible range of altitude at initial deployment;
- (c) Type of recovery desired, such as (1) rapid, stabilized descent, (2) delayed descent, and (3) free descent, in which final impact is the only consideration;
- (d) Allowable weight and space available for deployable aerodynamic decelerator and impact-attenuation system;
- (e) Location of decelerator or decelerators, which may affect the insulation required and type of deployment, such as (1) pilot chute, (2) static-line, or (3) forced-ejection equipment;
- (f) Riddle design, which includes (1) desirable angle for vehicle support, (2) center of gravity of vehicle at time of deployment and descent, and (3) force-limitations of vehicle at load connections;
- (g) Maximum g -tolerances of vehicle and direction of g 's. In the case of manned vehicles, maximum human g -tolerances and rate of g -onset;
- (h) Desirable stability and angle of descent at final impact;
- (i) Shock-attenuation system to be used for final impact;
- (j) Geographical and physiographical area in which vehicle is expected to operate;
- (k) Weight of vehicle at anticipated recovery time;
- (l) Position of first-stage parachute at inflation, as influenced by (1) motor-blast heat and pressure,

and (2) wake effect;

(m) Aerodynamic heating; and

(n) Vehicle configuration (stable or unstable in descent).

4.3.1 INITIATION. Deployment of a recovery system can be initiated by ground command; by flight conditions such as engine failure, loss of control signal, or loss of braking signal; or in the case of emergency escape, by an altitude-velocity sensor which is armed by a timer at a predetermined interval (usually 0.5 sec) after separation of escape-capsule from aircraft.

4.3.2 RECOVERY SEQUENCE. Recovery normally consists of, but is not limited to, two or more stages involving parachutes or other drag-producing devices to accomplish the deceleration and subsequent descent to the ground. Fig. 5-18 shows a plot of altitude and flight-path speed for a typical five-stage recovery system. The number of stages and the design of the decelerator for each stage is determined by the following recovery conditions:

(a) *Deployment Speed and Altitude.* The requirements for the first-stage decelerator design are determined by the speed and altitude at which it is to be deployed. The values selected shall be the most critical (maximum and minimum) that can reasonably be expected during uncontrolled tests or operational flights of the vehicle.

(b) *Recovery Weight.* The recovery weight is the weight of the missile, the drone, the escape-capsule with occupant, the aerospace vehicle, or their components, to be recovered. This value can vary because of changing conditions or fuel load. Therefore, it should be the maximum weight under which recovery is to be made. Consideration must be given to reducing this value by dumping fuel or jettisoning parts of the body that are to be recovered.

4.3.3 MAXIMUM DECELERATION. Knowledge of the magnitude and, in the case of emergency escape, the rate of application, of the g 's imposed on a vehicle or its occupant is required to determine the number of stages required, the decelerator sizes, and the timing of the recovery sequence. Not only must the limit of the vehicle structure be considered in determining the allowable g 's, but also the powerplant, instruments, control system, and other accessories. Fig. 5-19 illustrates human tolerance to accelerations. This chart is extracted from USAF Specification MIL-C-25969A. The graph depicts zones of allowable accelerations in both the transverse and longitudinal directions. Further limitations must be established as to the magnitude of the longitudinal and transverse accelerations that can be imposed when both are acting concurrently on a human. In addition to consideration of translational accelerations, in some instances it may be

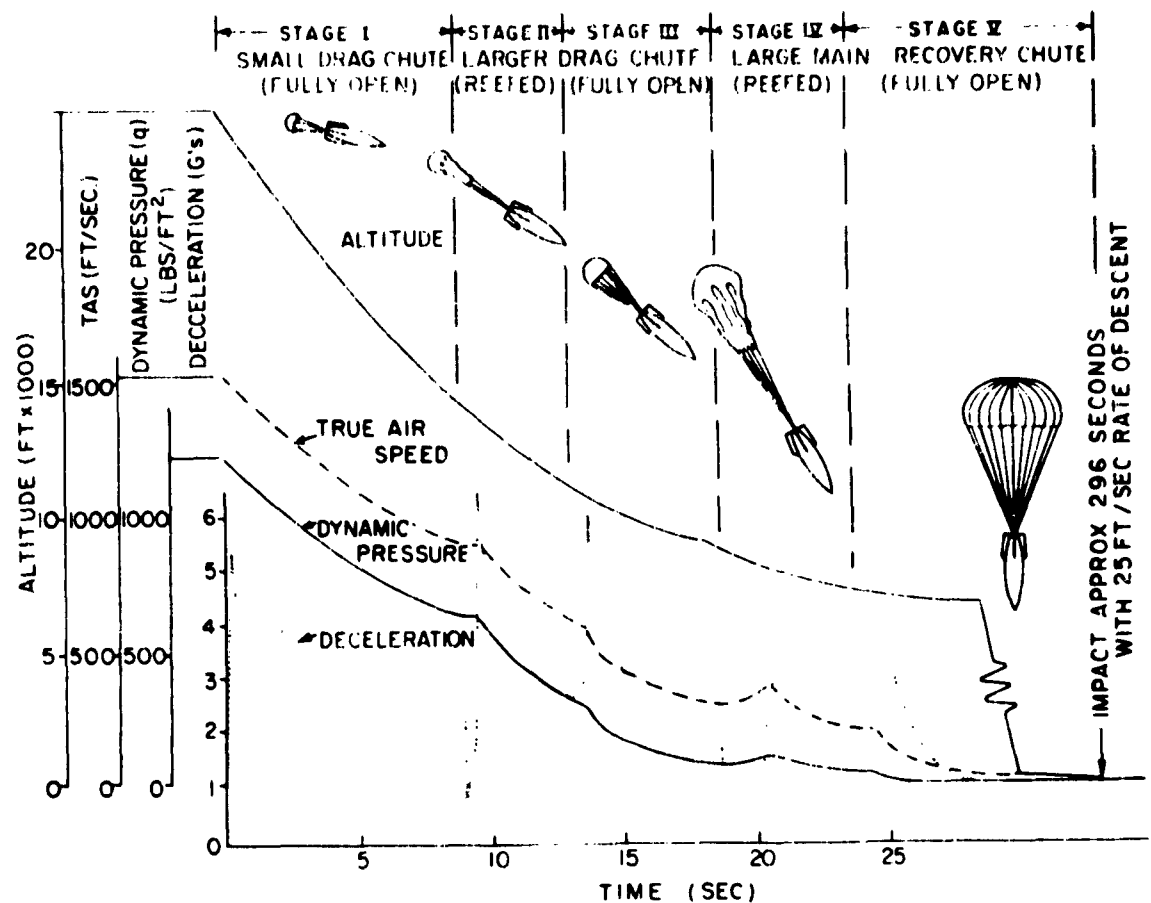


Fig. 5-18 Possible Operational Sequence for Multiple-Stage Parachute Recovery System

necessary to consider the rotational accelerations which are being imposed on the human in combination with the translational accelerations.

4.3.4 PARACHUTE COMPARTMENT. Reliable recovery operations depend upon a minimum of interference with the deployable aerodynamic decelerator during the deployment procedure. There should be no projections or sharp edges in the way of the deploying decelerator. The compartment must be located so that the deployment path passes between any protrusions such as tail surfaces. If possible, the aft wall of the compartment should have a considerable slope to aid in extracting the packed parachute. The outer edges of the compartment should be rounded, so that nothing can snag or tear the bag in which the decelerator is packed.

In general, the motion of the deploying aerodynamic decelerator will be straight aft in relation to the flight path of the body. The best location for the compart-

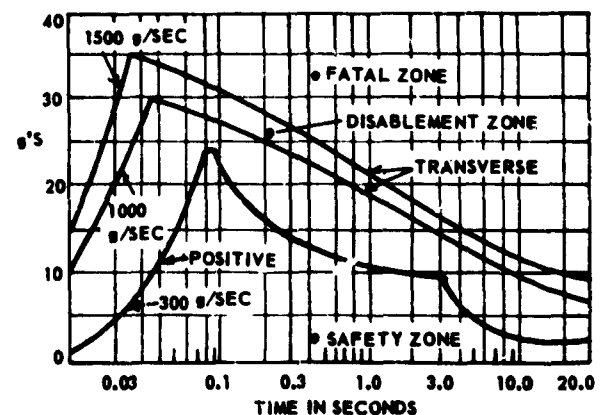


Fig. 5-19 Limits of Human Tolerance

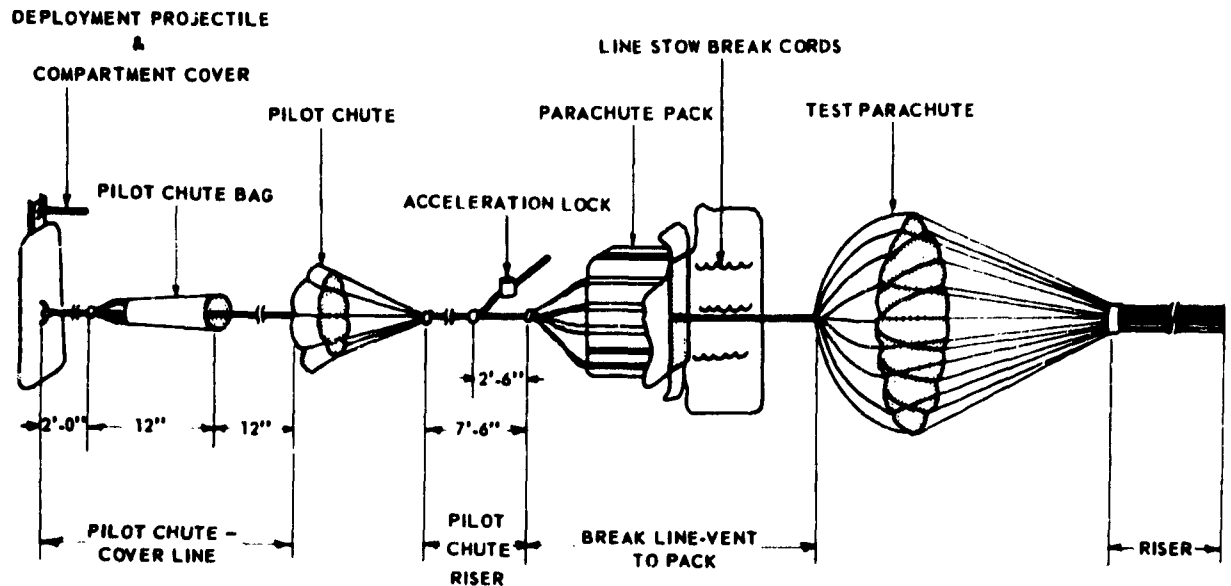


Fig. 5-20 Diagram of Deployment System

ment is, therefore, in the extreme tail of the vehicle. In many cases, however, the temperature of this location is excessive, because of its proximity to the power plant. In such cases, the possibility of insulating or cooling the compartment must be considered. If this is not practical, the compartment must be located in an area where excessive heat will not be encountered.

In cases where a missile is expected to be tumbling at the time of deployment, the aft position will not necessarily be the best. The decelerator compartment will then have to be located to accommodate such special deployment methods.

4.3.5 DEPLOYMENT. This process must be orderly and, insofar as possible, there should be no slack in the connecting line between the decelerator and the vehicle being recovered. For deployment of first-stage decelerators at speeds greater than sonic, some means of forceful ejection must be utilized. Current techniques for providing ejection impulses are as follows:

- (a) Drogue gun and pilot chute;
- (b) Cartridge-actuated ejection piston; or
- (c) Parachute mortar.

A deployment system for first- or second-stage application is schematically shown in Fig. 5-20. A projectile removes the compartment cover by its initial rearward movement in the gun barrel. Continued rearward move-

ment by the projectile and cover pulls the pilot-chute bag away from the adverse pressure region immediately behind the parachute compartment and into the airstream aft of the vehicle. When the rearward travel stops, the inertia of the cover assembly removes the bag from the pilot chute, allowing the parachute to inflate. At the same time, an acceleration lock attached to the pilot-chute riser is released from the harness assembly holding the second-stage parachute in the compartment. The pilot-chute riser, now attached to the parachute pack through a bridle of heavy webbing, pulls the second-stage parachute pack from the compartment. To assure an orderly lines-first deployment, the vent of the second-stage parachute is secured to the inside of the parachute pack by a break line attached to the vent lines of the parachute and to the pack-bridle confluence point. Minimum velocities required for pack ejection to insure deployment of the first-stage decelerator through the adverse wake of a vehicle are presented in Fig. 5-21 through 5-24 as functions of vehicle deceleration, base diameter, Mach number and pack weight, respectively (Ref (5-11)).

Emergency-escape systems which must operate through a large range of velocities and altitudes may employ dual pilot-chutes to insure reliable deployment. The size of the two chutes would be such as to develop approximately the same force when deployed in the individual speed-regimes in which they are to

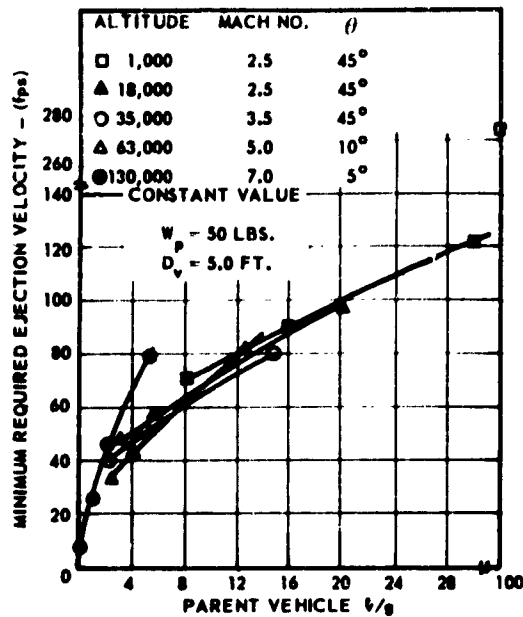


Fig. 5-21 Minimum Required Ejection Velocity vs Parent Vehicle Deceleration

operate. At high-speed deployments, the large, low-speed chute will shred, enabling the smaller chute to execute the deployment.

4.4 Release and Control Sub-Systems

4.4.1 COMPARTMENT-DOOR RELEASE. The re-

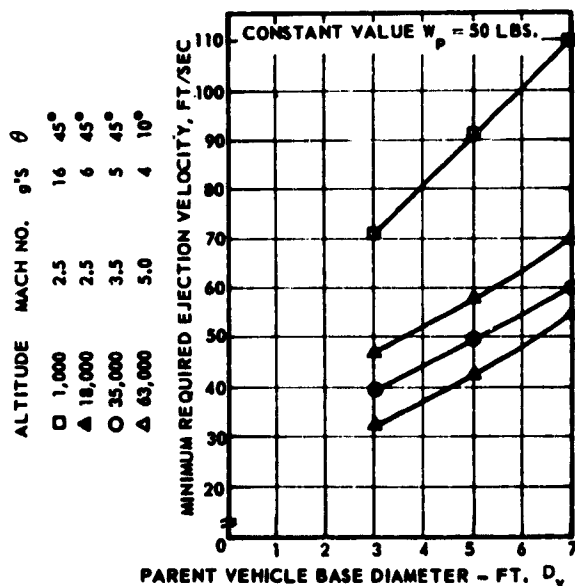


Fig. 5-22 Minimum Required Ejection Velocity vs Vehicle Base Diameter

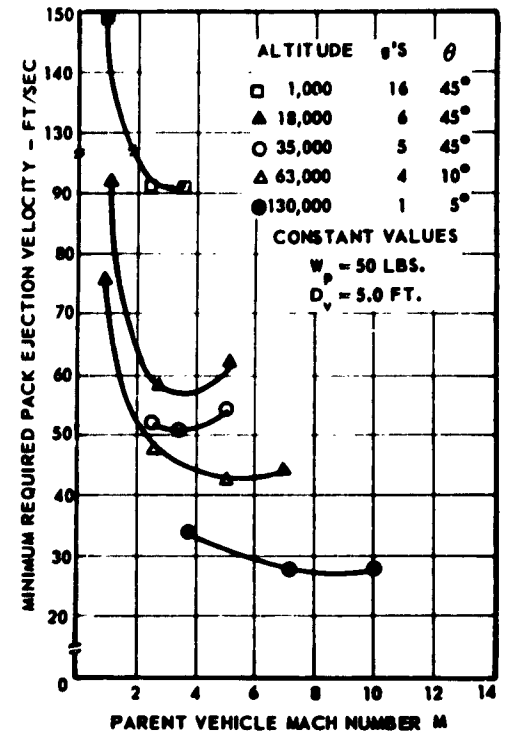


Fig. 5-23 Minimum Required Pack Ejection Velocity vs Vehicle Mach Number

liable opening of a decelerator compartment-door, or release of the whole door, at high speeds is essential in a successful aerospace-vehicle recovery operation. The problem is usually not as simple as it appears. The unlatching mechanism must function under various environmental extremes, such as low temperature (-65 F), high altitude, high acceleration (positive and negative), and extreme vibrations. The mechanism must not have an adverse effect on the performance of the missile. Two of the most common devices utilized as mechanisms are explosive bolts and Primacord. These and other devices are discussed in detail in Chapter 9.

4.4.2 CONTROLS. The functioning of the recovery system must be controlled by time, altitude, or pressure, or a combination of these, arranged in order to deploy the different aerodynamic decelerators as desired. These devices may perform their function either by direct mechanical linkage or through electrical circuits. Where electrical circuits are utilized, two independent parallel circuits, complete with timers or other controls and batteries, must be provided. They must be so arranged that the failure of one circuit will not prevent the proper functioning of the recovery system as a whole.

4.4.3 SEQUENCING. Sequencing is usually accomplished by means of timers started with or prior

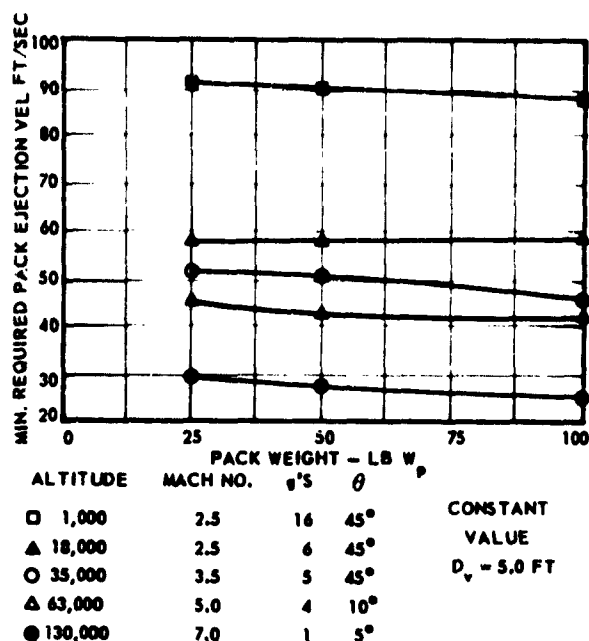


Fig. 5-24 Minimum Required Pack Ejection Velocity vs Pack Weight

to the initiation of recovery. Mechanical, electrical, or pyrotechnical (powder-train) timers may be used if they are adaptable to the system, and provided that they meet the environmental requirements of the recoverable body.

Altitude or ram-pressure switches, or both, may be used for sequencing the operation of the recovery system, provided that a safety timer system is also incorporated. A suitable altitude control must be placed in series with the release system on the final-recovery stage so that this stage will not be actuated higher than 15,000 ft above mean sea level.

4.4.4 CANOPY DISCONNECT. All canopy disconnects must be mechanical, and they must be actuated either by springs or by pyrotechnic devices. A suitable device must be incorporated for releasing the final-stage canopy from the recoverable body after ground or water impact to prevent the final-stage canopy from dragging the missile as a result of surface winds.

4.4.5 PYROTECHNIC DEVICES. The use of pyrotechnics for powering releases, explosive bolts, and other devices is acceptable, provided that two independent powder charges are used, either one of which will accomplish the action. In such devices, individual powder charges are ignited either by an electrical igniter or by a percussion cap. (See Chap. 9, 2.4.2.)

4.5 Landing-Impact Shock-Absorption. In order to permit a higher rate of descent with the final-stage parachute, thus reducing to a great extent the weight

and volume of the entire system, the use of devices to absorb landing shock must be considered. Devices currently used to provide impact shock-absorption are penetration spikes, air bags, or crushable portions of the recoverable body itself, such as paper-honeycomb platforms. Current design requirements and applications of these three shock-absorption devices are presented in Chapter 9, Sec. 4. Investigations have shown that retro-rockets may become effective as impact-attenuators when considered for systems of heavy load which require low-impact decelerations.

4.6 Flotation and Retrieval. To accomplish over-water recovery, reliable flotation equipment is essential. Two methods have been utilized to provide vehicle flotation. Both utilize flotation balloons, the difference in the two systems being that in one the balloon inflates during vehicle descent while in the other the balloon inflates underwater (Ref (5-10), (5-12), (5-13)). The latter method appears to be a more reliable method for flotation and retrieval for the following reasons:

(a) The vehicle could still be recovered even if it impacted at a high rate of descent due to failure of the final-recovery aerodynamic decelerator.

(b) The method eliminates the possibility of the balloon entangling with the suspension system of the final-recovery aerodynamic decelerator.

Typical components, other than a flotation balloon, of a flotation system are a compressed-air storage bottle (if forced inflation is used), radio transmitter and light beacon, marker dye, and shark-repellent. A typical over-water recovery sequence is as follows: The operational sequence is initiated on impact by water-activated batteries, which produce sufficient energy to open the air valve between the balloon and a compressed-air bottle, allowing the high-pressure air to pass through a short rubber hose to the balloon. The balloon inflates to full size while held snugly to the side of the vehicle by tethering lines. This keeps the vehicle very close to the surface of the water.

A radio transmitter is put into operation upon water entry, using the internal power supply of the transmitter. The transmitter is secured to the top of the balloon, in order to place the antenna and the light at maximum heights above the water. The shark repellent and marker dye are dispersed in the water to complete the sequence.

SEC. 5 AIRCRAFT DECELERATION

5.1 General

5.1.1 BRIEF HISTORY. The use of a parachute

TABLE 5-3 AIRCRAFT-DECELERATION PARACHUTES

Type	Aircraft	Diameter, ft	Type*	No. of Gores	Deployment Velocity, knots
MB-1	B-47 Approach	16	RS	20	195
MB-2	F-94	16	RS	20	170
MB-4	F-86	16	RS	20	190
MB-5	F-100	16	RS	20	190
MB-6	F-101	15.5	RS	20	200
MB-7	F-104	16	RS	20	200
MB-8	F-105	20	RS	24	200
MB-10	F-102	14.5	RS	20	220
MB-13	F-84	16	RS	20	200
MB-15	B-66	28	RS	28	175
D-1	B-47	32	FCR	36	160
D-2	B-52	44	FCR	48	170
	B-58	24	RS	28	190
A-28A-1	F-106	14.5	RS	20	220

*RS = Ring-Slot
FCR = Flat circular ribbon

as an auxiliary brake has proved to be very efficient for decelerating an aircraft during landing approach, touch-down, and ground roll. The first known test using a parachute as a landing brake was made as early as 1923 at McCook Field, now called Wright-Patterson Air Force Base, at Dayton, Ohio. A conventional man-carrying parachute was used to reduce the landing-roll distance of a de Havilland biplane. Around 1933 systematic investigations were conducted in Germany for the purpose of improving existing parachutes or developing new types of parachutes of improved characteristics specifically intended as an aircraft-deceleration device. As a result of these investigations the ribbon parachute was developed and successfully tested on a Junkers W-34 airplane as a landing brake. The tests proved that this parachute is adequately stable, opens reliably and uniformly, produces a minimum opening-shock, does not interfere with the controllability of the airplane, and provides supplemental deceleration for aircraft.

5.1.2 JET APPLICATIONS. The most important application for deceleration parachutes came with the development of high-speed jet aircraft. High aircraft wing-loadings resulted in high landing-speeds and

long landing-rolls, and a means had to be developed to reduce the landing-roll distance. The answer to this problem was the aircraft deceleration parachute. Many improvements have been made over original designs and various types of aircraft have been equipped with parachutes. The B-47 jet bomber is a good example of the efficient and useful operation of the parachute as an auxiliary device for decreasing landing-roll. The landing-roll of the B-47 is decreased 35 to 45 per cent. There are two types of aircraft-deceleration parachutes: one is used for aircraft landing-deceleration (drag parachute) and is a specially designed drag-producing device that is used to reduce the landing roll of aircraft, especially jet aircraft. The aircraft inflight control-parachute (approach parachute) is just what the name implies. It is a parachute that is deployed prior to landing to produce added drag, which in turn allows a steeper approach angle, which permits clearing higher obstacles, and more engine power to be maintained, which improves control of the aircraft. The advantage is that safer and more accurate landings can be executed. Currently, only the B-47 aircraft employs an approach parachute. General requirements for aircraft deceleration parachute systems

are described in the specification MIL-D-9056. Table 5-3 lists current aircraft with their respective aircraft-deceleration and approach parachute systems.

5.2 Aircraft Landing-Deceleration Parachute (Drag Parachute)

5.2.1 GENERAL. Drag parachutes of the ribbon and ring-slot types are today being used for aircraft landing-deceleration. They have proved successful for a number of conditions under which the aircraft brakes, although functioning properly, would normally be inadequate. The drag parachute has proven to be a big asset because it produces the highest deceleration force at the touchdown speed of the aircraft, where the brakes are relatively inefficient. During landings on icy or wet runways, a large percentage of the braking is accomplished by the deceleration parachute.

There are other advantages besides a reduction in landing roll obtainable with the utilization of a drag parachute. For example, the F-101 has pitch-up and spin characteristics in landing that have been overcome by deploying the deceleration parachute to maintain control. Another major advantage is the increased flight safety under emergency conditions such as landings with inoperative brakes, or aborted take-offs, certain emergency landings, and landings over obstacles or on short runways. Under some emergency conditions, it is even conceivable that the parachute could be used for rapid descent. Moreover, a monetary savings in tires and brakes is quite apparent. Using the parachute and the normal applications of brakes, the number of uses per tire can be increased five or six times over that obtainable when landing repeatedly without a parachute. No exact figures relating to the actual savings on brakes are available; however, it is known that brake maintenance and replacement are considerably reduced when a deceleration parachute is used.

5.2.2 OPERATIONAL SEQUENCE. In operation, the pilot makes a normal approach and landing. At touchdown, or very shortly thereafter, the drag parachute is deployed by movement of a control handle in the cockpit. Fig. 5-25 shows a landing deceleration parachute in action. Brakes may or may not be used to supplement deceleration. In normal operation, the aircraft is permitted to continue rolling to the runway "turnoff" at a speed sufficient to keep the canopy inflated. This speed, with a moderate into-wind condition, is usually below the maximum safe turnoff speed of the aircraft. If the canopy will not stay inflated, the pilot may apply brakes and maintain inflation of the canopy by increasing the engine thrust. After turnoff, the pilot maintains canopy inflation until he reaches a designated parachute release-point.

The parachute is released and then ground personnel retrieve it. The parachute should never be detached from the aircraft while it is on the runway or on the taxiway, where it might jeopardize other aircraft during landing. Drag parachutes are used for the deceleration of fighter and bomber aircraft. The relationship between landing-roll distance and canopy diameter for various friction coefficient factors is shown for a medium-bomber aircraft in Fig. 5-26.

5.2.3 OVERALL DESIGN. Aircraft landing-deceleration parachutes should be designed to have the following characteristics. These are not necessarily listed in the order of importance.

- (1) High degree of stability;
- (2) High degree of reliability;
- (3) Adequate strength for repeated usage;
- (4) Low opening force;
- (5) High drag, low weight, low bulk;
- (6) Not affected by environmental conditions within the limits of use;
- (7) Ease of maintenance; and
- (8) Low cost.

To understand why these characteristics are important, (1) through (5) will be analyzed below. The others are self-explanatory.

(1) *Stability.* One of the most important requirements for a landing-deceleration or approach parachute is that it is stable. The word "stable" applied to aircraft-deceleration parachutes is intended to mean that the parachute should not oscillate through an angle greater ± 5 deg. Pilots consider a parachute stable when it in no way effects controllability of the aircraft and does not require a trim change.

Stability of ribbon and ring-slot canopies depends to a large extent on the canopy's total porosity. The total porosity required for a stable deceleration parachute varies with canopy diameter and there is an upper limit on porosity which, if exceeded, can cause inflation difficulties. Tests have proven, however, that parachutes can be designed to be in the safe range of porosity (from the standpoint of reliable inflation) and also be adequately stable.

(2) *Reliability.* Parachutes to be useful as in-flight and landing aids must be reliable. A high degree of reliability can best be obtained by designing a system of proven components, using a properly designed pilot chute that adequately regulates the deployment of the deceleration parachute from a properly designed deployment bag. This will result in a uniform, trouble-free deployment and opening of the parachute. The deployment bag which contains the pilot chute and the deceleration parachute with riser is made to conform to the shape of the compartment in



Fig. 5-25 Landing Deceleration Parachute

the aircraft. The function of the bag is to cause orderly deployment of the parachute, combined with a low opening-shock, and to protect the deceleration system during handling on the ground and extraction. A pilot chute deploys the deceleration parachute. The characteristics of the pilot chute are such that it inflates quickly when the compartment doors open, resulting in an immediate deployment of the deceleration parachute. The usual sequence of deployment of the para-

chute system from the deployment bag is riser first, then suspension lines, and then canopy, which component is stored in a separate section of the bag. In the deployed position, the components of the deceleration parachute appear as shown in Fig. 5-27. If the aircraft-decelerator compartment is located in the forward portion of the fuselage, and consequently nearer to the ground level, it may be more feasible to reverse this sequence of deployment. However, the method may

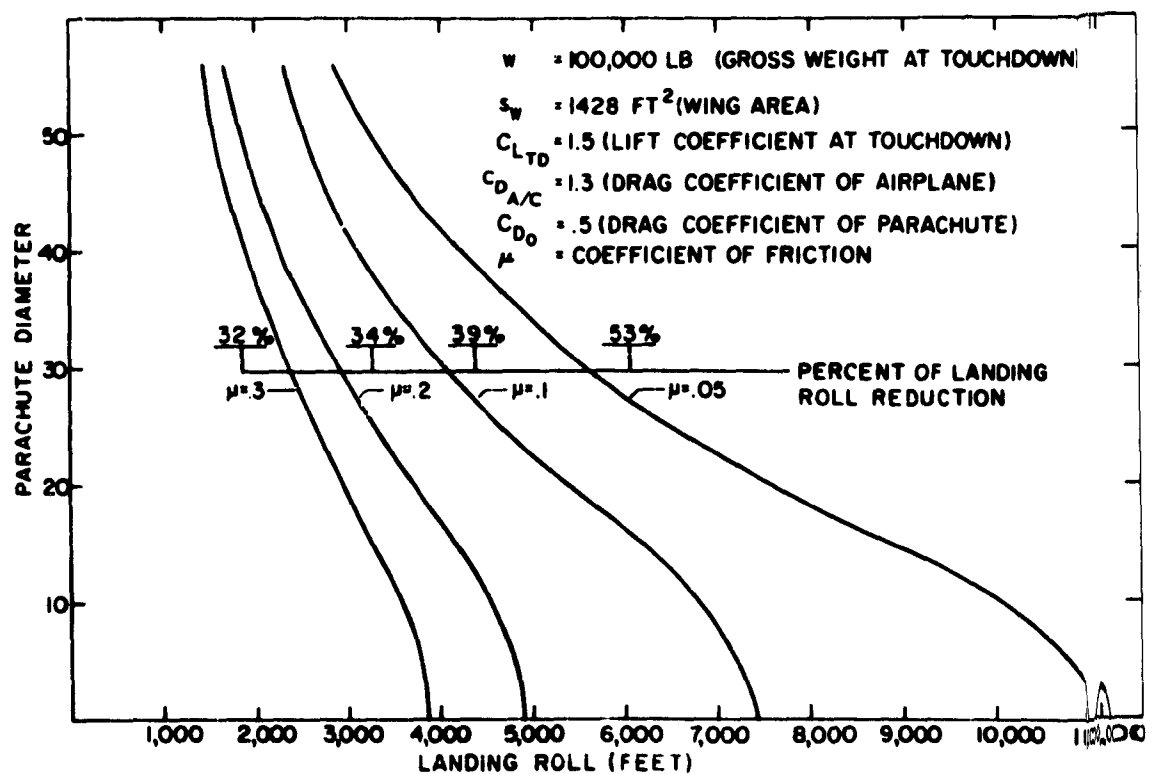


Fig. 5-26 Landing Roll vs Parachute Diameter and μ Factor

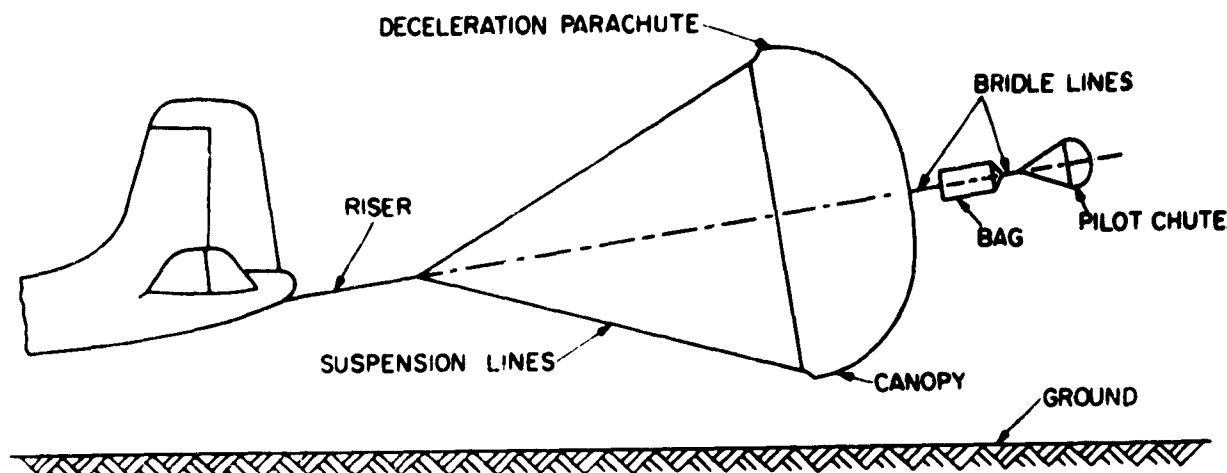


Fig. 5-27 Schematic Arrangement of Aircraft Decelerator Parachute

result in a slight increase of the opening-force. Any ground contact of the parachute system during the deployment sequence may result in damage and must be avoided.

During parachute deployment and operation, the aircraft must remain under full control of the pilot at all times. The parachute must not interfere with the normal landing attitude of the aircraft. It must not effect the longitudinal control of the aircraft. Provision must be made for immediate release of the parachute, in case of emergency. There must be no possibility of contact between the deploying or inflated parachute and the control surfaces or any other part of the aircraft.

To insure that landing-deceleration parachute

systems perform adequately and reliably, a limited test-program is conducted on each new system. There are certain test vehicles and methods that are utilized for testing such a system. Since it is standard practice to equip most military jet aircraft with deceleration parachutes, the parachute system and parachute should be tested with the designated aircraft under actual operating conditions. Only in this manner can the performance capabilities and reliability of the system and parachute be determined accurately. The reason is that the wake behind the different aircraft varies with each aircraft.

(3) *Strength.* The design strength of deceleration parachutes is based upon the anticipated opening shock at the highest speed at which the parachute is

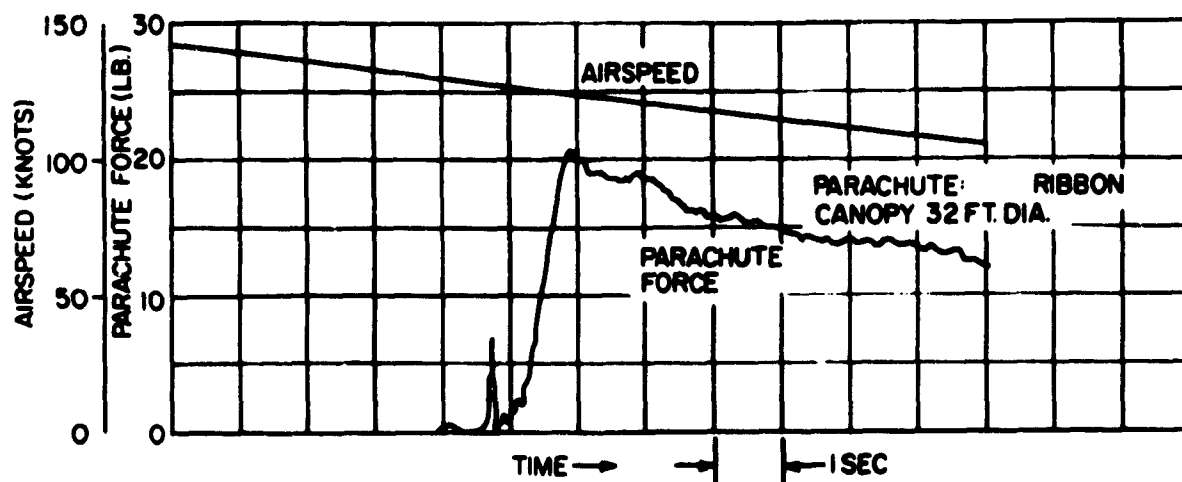


Fig. 5-28 Force vs Time of a 32-ft Ribbon Landing-Deceleration Parachute

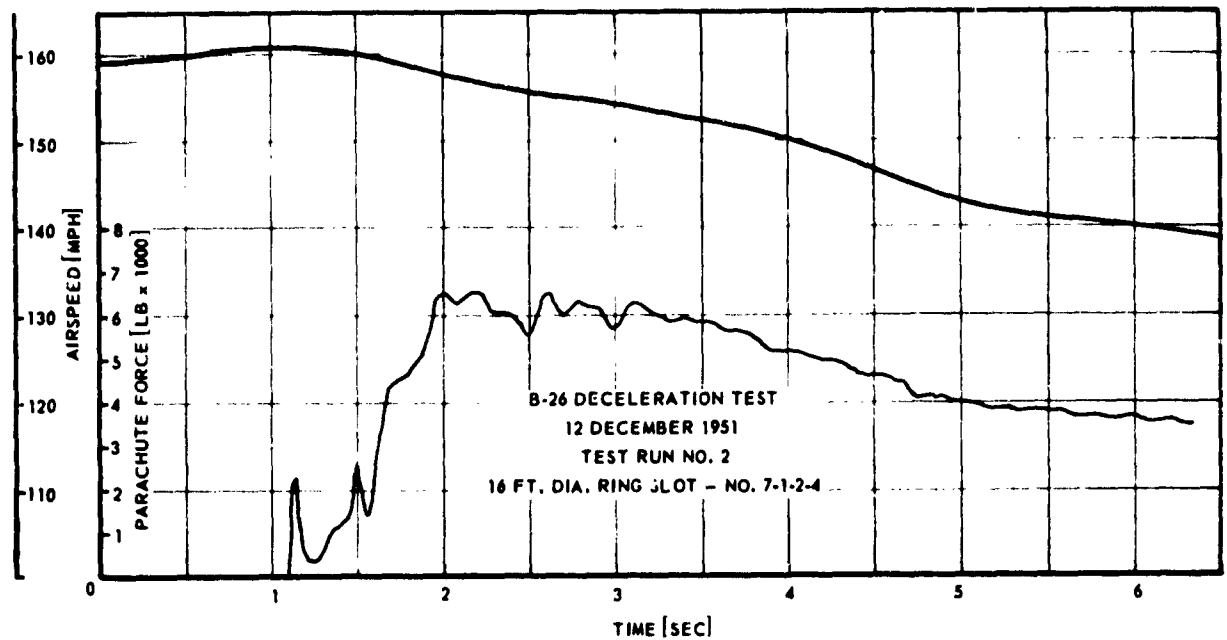


Fig. 5-29 Force vs Time of a 16-ft Ring-Slot Landing Deceleration Parachute

designed to be deployed. For the landing-deceleration parachute, this speed is the maximum speed of the aircraft with maximum gross take-off weight under these conditions, which will not permit take-off. A minimum design factor of 2.3 is employed in the selection of the canopy and suspension-line material. This design factor includes the standard safety factor of 1.5 and additional compensation for losses in strength due to sewing, etc. For further details, see Chapter 7.

To prevent undue stresses on the aircraft structure, parachutes with low opening-shock are required. The parachutes that are presently being used for deceleration meet this requirement. The opening-shock is determined from the equation $F_o = (C_{D_o}) (S_o) (q) (X)$ where C_{D_o} is the drag coefficient based on surface area of the canopy; S_o is the surface of the canopy; q is the dynamic pressure; and X is the opening-shock factor for the particular canopy.

(4) *Opening-Force.* The low opening-shock of the ribbon and ring-slot drag parachutes can be attributed to the relatively long inflation-time of the canopies compared to other types. The time of inflation, in turn, is basically a function of the total porosity of the parachute. Fig. 5-28 and 5-29 show representative curves of force versus time of 15 ft. diameter ring slot and 32 ft. diameter ribbon landing deceleration parachutes.

(5) *Drag, Weight, and Bulk.* There is a continual striving for landing-deceleration parachutes that

produce higher drag and at the same time have less weight and bulk, without sacrificing other performance characteristics. The landing-deceleration parachutes that are presently in use have been selected as the optimum in design efficiency from a ratio of drag to weight and bulk. Future improvements in materials and construction will undoubtedly improve efficiency.

5.2.4 DESIGN CONSIDERATIONS.

5.2.4.1 *Drag Requirement.* The drag requirement is generally determined by the aircraft manufacturer. The parachute system must be considered as supplementary to the available deceleration components with which the aircraft is equipped, such as flaps and brakes.

5.2.4.2 *Canopy Selection.* Ring-slot and ribbon canopies have been found most suitable for drag-parachute application. The ring-slot canopy is preferred for deceleration because of its lower cost and ease of production and maintenance.

5.2.4.3 *Size of Canopy.* The size of the canopy will be determined by the drag requirement. Wake effects behind the aircraft tend to decrease the drag coefficient, C_{D_o} , which may make it necessary to use a larger canopy than would otherwise be required. Longer risers tend to reduce wake losses, but they increase the bulk and weight of the system and may contribute to the dragging of the canopy on the runway during deployment. The drag coefficient C_{D_o} with

regard to constructed canopy area for the flat circular ribbon and ring-slot canopies ranges from 0.45 to 0.6, depending upon the air flow behind the aircraft. For design purposes, a drag coefficient $(C_D)_0$ of 0.55 for ring-slot canopies and 0.5 for flat circular ribbon canopies is generally used.

5.2.4.4 Riser and Suspension-Line Length. Long risers tend to reduce aircraft-wake effects upon the parachute canopy. Practical experience, however, has indicated that the riser length should be kept to from 1.0 to 1.5 times the constructed (flat) diameter (D_c) of the canopy. Length of suspension lines should be 1.0 times the constructed (flat) diameter (D_c) of the canopy. The most important consideration in determining riser length is that the location of the force-line relative to the aircraft should coincide with the line projected from the center of gravity of the aircraft through the parachute attachment-point. When this is not the case, the drag force tends to raise or lower the nose of the aircraft, depending on whether the canopy force-line, when extended, goes above or below the aircraft center of gravity. Such a condition can have serious consequences if the parachute is deployed while the airplane still has flying speed high enough to climb. Even at lower speeds it can cause damage to the nose gear, by exerting excessive pressure.

5.2.4.5 Parachute-Compartment Location. The best location for the parachute compartment is at the very end and top of the fuselage, aft of the empennage. Such a location is not always possible, because of space limitations, heat problems, or interference with installed equipment. The required location of the parachute attachment-point may also have some bearing on compartment location. In some instances, it is not possible to have the parachute attachment-point within the compartment because the canopy force-line must pass through the center of gravity of the airplane. Parachute-compartment locations at the bottom of the fuselage are particularly undesirable because the deployment bag or canopy might drag on the runway surface during deployment. Parachute-compartment interiors must be smooth, with no protrusions or sharp edges that might catch or damage any portion of the parachute. The compartment should not be located in any section where such corrosive materials as acid or battery-acid fumes can penetrate. The temperature in the compartment should at no time exceed 250 F for Nylon parachutes and 325 F for Dacron parachutes. Compartment temperature should not exceed 600 F for parachutes manufactured from HT-1 material.

5.2.4.7 Reefing. Temporary reefing is not recommended for aircraft deceleration parachutes because the increased complexity can reduce parachute-system reliability.

5.2.4.8 Clusters. The use of canopies in clusters is recommended if, when a single canopy would be used, it would be larger than 44 ft in diameter. Larger-diameter canopies are likely to be heavy and bulky, and present difficult problems in maintenance, packing, and installation, along with the need for expanded field facilities.

5.2.5 CALCULATION OF AIRCRAFT LANDING-ROLL. The problem of calculating landing roll is essentially a problem of velocity, acceleration, and time. Therefore, starting with the basic equations:

$$dS = v dt = \frac{v}{a} dv$$

Integration gives

$$(5-1) \quad S_L = \int_0^{v_c} \frac{v}{a} dv = \frac{1}{2} \int_0^{v_c} \frac{1}{a} d(v)^2$$

where S_L = Landing-roll distance; and

v_c = Velocity of aircraft at instant of ground contact.

Eq. (5-1) can be rewritten as follows:

$$(5-2) \quad S_L = \frac{1}{2g} \int_0^{v_c} \frac{W}{F} d(v)^2$$

where W = Total aircraft weight; and

F = Total retarding force.

To continue, an assumption as to how the retarding force (F) varies during landing roll must be made. Assuming that $1/F$ varies linearly with v^2 , Eq 5-2 can now be integrated as follows:

$$(5-3) \quad S_L = \frac{W v_c^2}{2g (F_c' - F_o')} \ln \frac{F_c'}{F_o'}$$

where F_c' = Retarding force at the instant aircraft contacts ground; and

F_o' = Retarding force at the instant of aircraft stop.

Eq 5-3 can be used when brakes are applied either during the landing roll or at the instant of ground-contact. If the brakes are applied at some time during the landing roll, a more descriptive equation is:

$$(5-4) \quad S_L = \frac{W v_b^2}{2g (F_{b2} - F_o')} \ln \frac{F_{b2}}{F_o'}$$

$$+ \frac{W (V_c^2 - V_b^2)}{2g (F_c - F_{b1})} \ln \frac{F_c}{F_{b1}}$$

where V_b = Velocity of aircraft at the instant brakes are applied;

F_{b1} = Retarding force immediately before brakes are applied; and

F_{b2} = Retarding force immediately after brakes are applied.

To calculate the retarding force, consider the air and ground forces and engine thrust acting on the aircraft.

$$(5-5) \quad F = D + F_f - T$$

where T = Engine thrust (when applicable);

F_f = Aircraft frictional force; and

D = Drag produced by aircraft and parachute when deployed.

$$(5-6) \quad F_f = \mu (W - L)$$

where μ = Coefficient of friction; and

L = Aerodynamic lift developed by aircraft.

Eq 5-6 can be written

$$(5-7) \quad F = D + \mu (W - L) - T$$

$$\text{or} \quad F = \frac{1}{2} \rho C_D S_w V^2 + \mu W - \mu \frac{1}{2} \rho C_L S_w V^2 - T$$

$$(5-8) \quad F = \mu W + \rho \frac{V^2}{2} S_w (C_D - \mu C_L) - T$$

where S_w = Wing area.

The forces F_c , F_{b1} , F_{b2} , and F_o can now be calculated by use of Eq 5-8 and substituted in Eq 5-4 to obtain a landing-roll distance.

Sample Calculation

Assume:

$$W = 100,000 \text{ lb}$$

$$\mu = 0.02 \text{ without brakes}$$

$$= 0.3 \text{ with brakes}$$

$$V_c = 145 \text{ knots}$$

$$V_b = 115 \text{ knots}$$

$$S_w = 1428 \text{ sq ft}$$

T = Thrust developed by engines idling = 500 lb per engine (6 engines)

$$C_L = 1.5$$

$$C_D (\text{aircraft}) = 0.126$$

$$C_{D_o} (\text{parachute}) = 0.5$$

$$D_o (\text{parachute}) = 32 \text{ ft}$$

Retarding force, F_c , equals

$$F_c = \frac{1}{2} \rho V_c^2 C_D (a/c) S_w - T_{\text{idle}}$$

$$= \frac{(0.126) (246)^2}{841} (1428) - 500 (6)$$

$$= 12950 - 3000 = 9,150 \text{ lb}$$

Immediately upon ground contact, a deceleration parachute is deployed. When aircraft velocity has dropped to 115 knots the brakes are applied.

Then,

$$F_{b1} = \mu W + \frac{\rho V_b^2}{2} S_w (C_D (\text{total}) - \mu C_L)$$

$$- T_{\text{idle}}$$

where $C_D (\text{total}) = C_D (\text{aircraft}) +$

$$C_{D_o} (\text{parachute}) \frac{S_o}{S_w}$$

$$= 0.126 + 0.5 \frac{804}{1428}$$

$$= 0.126 + 0.282 = 0.408$$

$$F_{b1} = 0.02(100,000) + \frac{(195)^2}{841} 1428 [0.408 -$$

$$(0.02) (1.5)] - 500 (6)$$

$$= 2,000 + 24,350 - 3000 = 23,350$$

Now

$$F_{b2} = 0.3 (100,000) + \frac{(195)^2}{841} (1428) [(0.408 -$$

$$(.3) (1.5)] - 500 (6)$$

$$= 30,000 - 2710 - 3000 = 24,290$$

The retarding force at the instant the aircraft has stopped is

$$F_o = \mu W - T_{idle}$$

$$= 0.3 (100,000) - 500 (6) = 27,000 \text{ lb}$$

Solving for landing-roll distance by use of Eq 5-4 gives

$$S_L = \frac{(100,000) (195)^2}{2 (32.2) (24,291 - 27,000)} \ln \frac{24,291}{27,000} +$$

$$\frac{(100,000) [(246)^2 - (195)^2]}{2 (32.2) (9,950 - 23,350)} \ln \frac{9,950}{23,350}$$

$$= 21,750 \ln 0.9 - 2,495 \ln 0.426$$

$$= 21,750 (0.1052) - 2,495 (-0.852)$$

$$= 2,290 + 2,120 = 4,410 \text{ ft}$$

5.3 Aircraft Inflight Control Parachute (Landing-Approach Parachute)

5.3.1 GENERAL. This parachute is utilized for better control of the inflight characteristics of certain types of jet aircraft, particularly during landing approach. High rates and steep angles of descent may be desirable for jet aircraft, as jet aircraft should operate at high altitudes, where their flight is much more economical than at low altitudes. In order not to exceed speed limitations, jet aircraft must begin descents from high cruising altitudes when still a

considerable distance away from the airbase. The same jet aircraft can start its descent relatively close to the airbase when using a landing-approach parachute. Use of a landing-approach parachute facilitates instrument-controlled letdowns, particularly GCA, as the additional drag permits a rapid deceleration, steepens the glide path, and also prevents overcontrol. The higher throttle-setting, which may be used during approach because of the added drag, also permits a more rapid response of the aircraft in the event of emergency, or "go-around". The B-47 is one aircraft for which a landing-approach parachute system was adopted. The approach parachute on the B-47 aircraft is shown in operation in Fig. 5-30.

5.3.2 OVERALL DESIGN. The design of any inflight-control or landing-approach parachute system must meet the requirements in 5.2.4 for drag parachutes.

5.3.3 DESIGN CONSIDERATIONS. At the present time, landing-approach parachutes are standard on the B-47 aircraft. Some of the considerations given hereafter are applicable particularly to that type of aircraft. Designs for other type of aircraft may require further consideration.

5.3.3.1 Drag Requirement. The drag requirement for the landing-approach parachute system will have to be established by the prime contractor of the whole system. For the B-47 aircraft, the drag of the approach parachute is of such a value that the aircraft, in landing configuration, is able to achieve a rate of climb, in case it is needed, for a "go-around", of at least 500 fpm at the optimum designed landing gross-

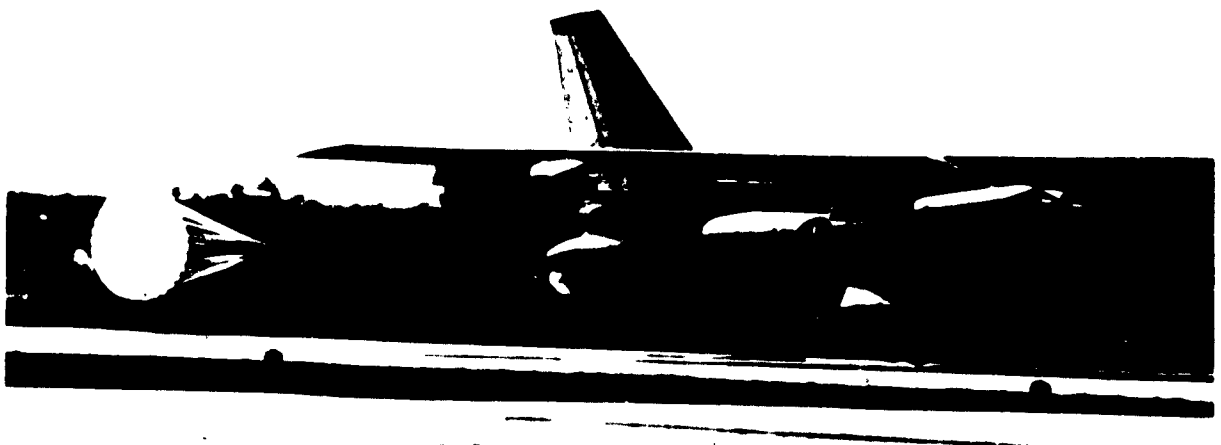


Fig. 5-30 Approach Parachute on B-47 Aircraft

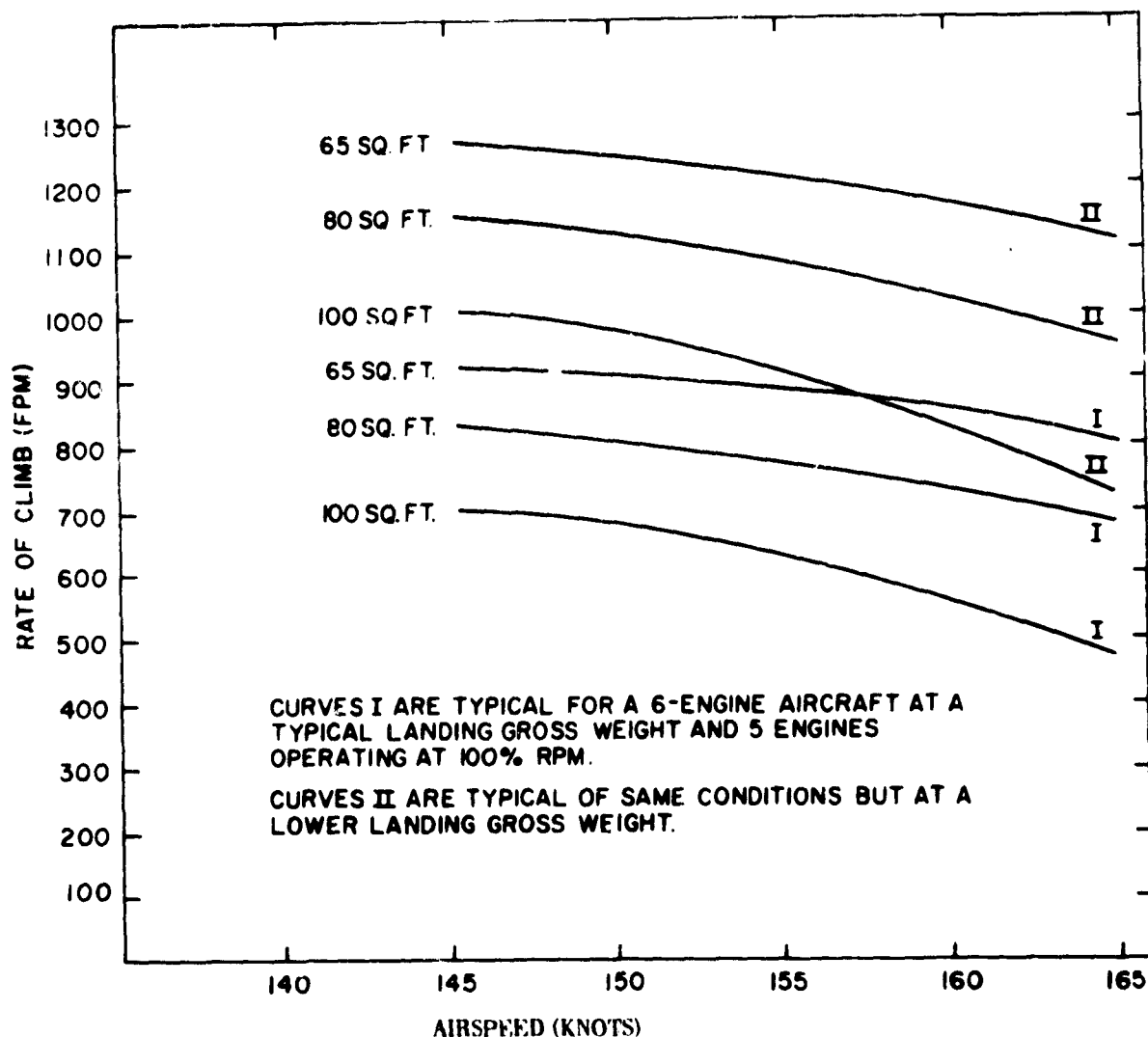


Fig. 5-31 Typical Climb-Performance Curves for a Medium Bomber Using Landing-Approach Parachutes with Different Drag Areas

weight at sea level. Fig. 5-31 shows typical climb-performance curves for a medium-bomber aircraft using landing-approach parachutes with different drag areas.

5.3.3.2 Canopy Selection. The ring-slot canopy should receive primary consideration in any aircraft landing-approach parachute system. Tests have indicated that it satisfies desired stability requirements. Its cost and ease of production and repair give it a decided advantage over the ribbon canopy. The ribbon canopy should be considered for applications in which the deployment speed requirement is higher than the design limits of the ring-slot canopy. Many other types of canopies are ruled out because of their characteristics of stability, cost, bulk, or strength-factor.

5.3.3.3 Size of Canopy. The size of the canopy is determined by the drag requirement. The drag coefficient, CD_o , for the ribbon and ring-slot canopies ranges from 0.4 to 0.6, depending upon the air-flow behind the aircraft. For design purposes, a drag coefficient CD_o of 0.55 for ring-slot canopies and 0.5 for ribbon canopies is generally used. A typical force-time diagram obtained during the deployment and steady drag of a 12-ft-diameter ring-slot parachute behind a medium-bomber aircraft is shown in Fig. 5-32.

5.3.3.4 Riser and Suspension-Line Length. If both inflight control (landing-approach) and landing-deceleration (drag) parachutes are used, the position of the skirt of the landing-deceleration parachute is

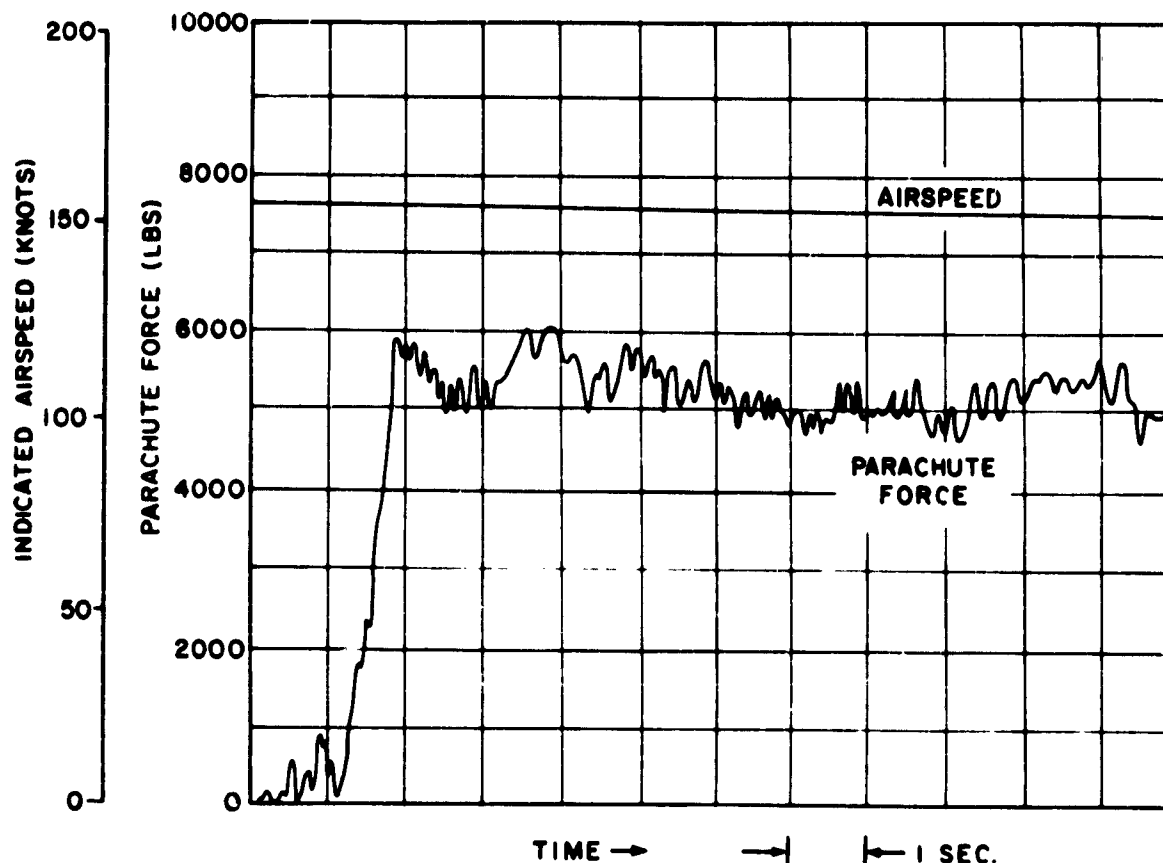


Fig. 5-32 Typical Force vs Time Diagram of 12-ft Ring-Slot Parachute Behind Medium Bomber Aircraft

the determining factor for the riser length of the landing approach parachute, as the skirt of each canopy must be equidistant from the aircraft. If a landing-approach parachute only is used, the length of the riser should in general be 1.0 to 1.5 times the constructed (flat) diameter (D_c) of the canopy. Suspension-line length should be equal to the constructed (flat) diameter (D_c) of the canopy.

5.3.3.5 Location of Parachute Compartment. The compartment for the landing-approach parachute may be located on the top, side, or bottom of the aft end of the aircraft. The location of the parachute attachment-point is an important factor in determining the compartment location (Fig. 5-33). Tests conducted with the B-47 aircraft have indicated that a location of the attachment point as much as 2 ft to either side of the aircraft centerline did not appreciably affect the longitudinal control. On aircraft with a relatively short fuselage section, side attachment requires further investigation. In some cases, the attachment point must be located in an area away from the com-

partment. There is little likelihood that the canopy will be burned by the jet exhaust, although riser and suspension lines may be exposed to excessive temperatures that may damage and eventually cause failure of the parachute. This condition may be overcome by the use of steel-cable risers, if the limited bending radius of steel cable does not create a stowage problem. For protection of Nylon risers, a short distance of the riser may be covered with flexible Neoprene-treated materials having high heat-resistance. All compartments should be designed to permit parachute deployment rearward along a line parallel to the flight path. Compartment interiors must be smooth, with no protrusions or sharp edges which might catch or damage any portion of the parachute. The compartment should not be located in any section where battery acid or battery-acid fumes can penetrate. Bottom compartments may use an elevator to lower the parachute directly into the airstream. The temperature in the compartment should at no time exceed 250 F for Nylon parachutes and 325 F for Dacron parachutes. Compartment temperature for

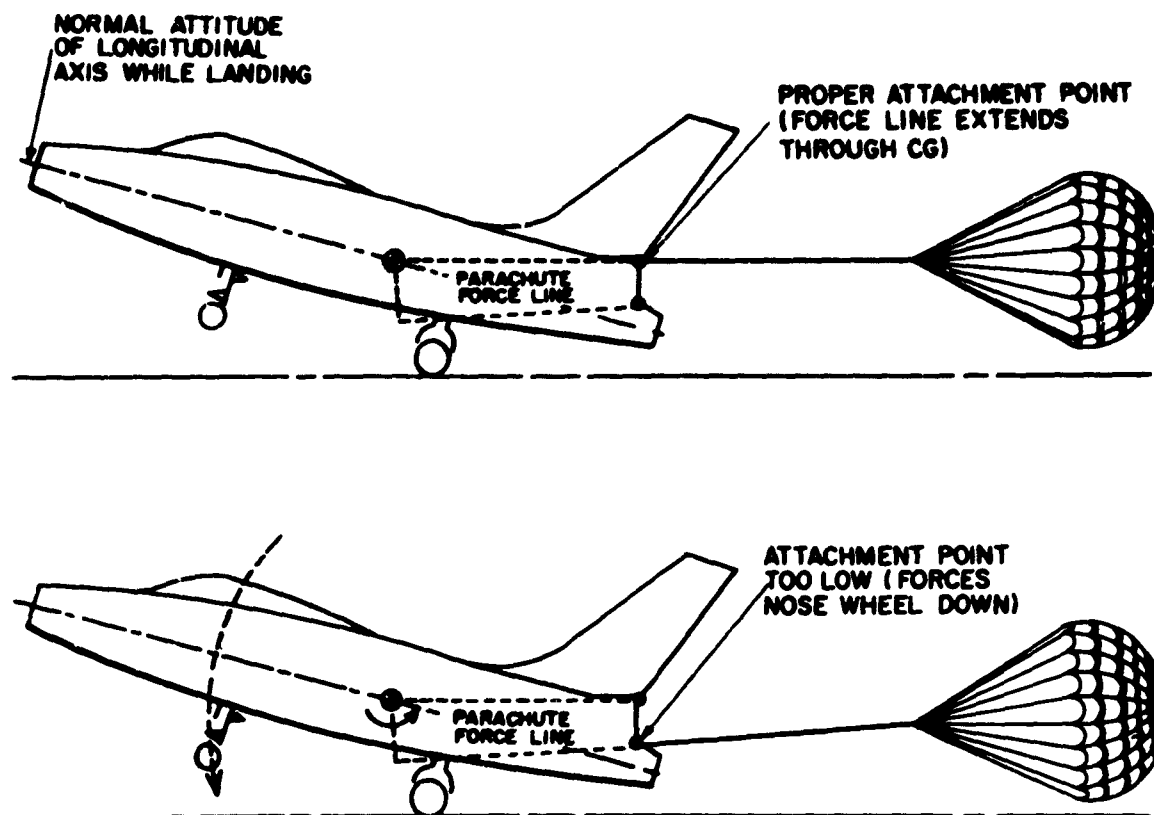


Fig. 5-33 Location of Parachute Attachment Point

parachutes manufactured from HT-1 material can approach 600 F.

5.3.3.6 Deployment. In all installations, deployment bags and spring-loaded pilot chutes should be used to facilitate the maintenance and installation of the parachutes in the aircraft and to insure orderly deployment. Riser-first deployment should be used whenever practical.

5.3.3.7 Reefing. Generally, reefing is not recommended for aircraft inflight-control parachutes. However, a permanent reefing line may be installed to achieve greater stability or to reduce the drag area of an existing canopy, which when unreefed creates only slightly higher drag than is desired for the particular application. For instance, the standard landing-approach parachute for the B-47 aircraft incorporates a 15.5-ft-diameter ring-slot canopy which is slightly reefed by means of a 27.5 ft reefing line. This reefing line is permanently installed at the skirt of the canopy. Thus, drag area is decreased slightly and a higher degree of stability is obtained.

5.4 Deceleration-Parachute Control System.

The control system for aircraft-deceleration parachutes must be designed to reliably and repeatedly perform a number of functions. Two of these functions are performed in sequence in one operation. When deployment of the parachute is initiated by pulling the control handle in the pilot's cockpit: (1) the mechanism must lock the riser attachment to the attachment point on the aircraft; and (2) then, after positively locking the parachute, it must open the compartment door. The attachment hook shall remain open as long as the control handle is in stowed position. This is a safety measure to allow the parachute to drop free if the compartment door is accidentally opened by means other than actuation of the control handle while the aircraft is in flight. The parachute may be jettisoned by using either a separate control cable, or the same control cable with the handle moved into a different position. Experience has indicated the desirability of using a two-cable system for bomber aircraft and a single-cable system for fighter aircraft. A mechanical

system is preferred because of simplicity and positive operation. One disadvantage of a mechanical system is the difficulty of routing the control cable in such a manner that it does not interfere with crew or equipment, yet will operate with a minimum of friction and without reliability loss because of detrimental effects of environment. In installations where a mechanical system is impractical, a hydraulic, electric, or pneumatic system may be utilized.

SEC. 6 SPECIAL WEAPONS

6.1 General. The basic reason for the development of parachute retardation-systems for special weapons is to control the trajectory of the weapon. Because of the high dynamic pressures frequently encountered during deployment, special-weapons parachutes are usually of very heavy-duty construction. Parachutes for each special weapon usually have to be "tailor-made" to specific requirements, which generally precludes the use of off-the-shelf components from other special-weapons retardation-systems. The general design and construction technique can be found in MIL-P-25716A, Parachute System, Heavy Duty, General Specification for.

6.2 Design Objectives. The main design objective is to produce a parachute system that will meet the delivery requirements, have a high degree of reliability, and still be as light as possible. Fig. 5-34 shows a typical parachute for special-weapons retardation in operation. Naturally, it must also be designed to fit the storage volume in the weapon.

6.3 Design Considerations

6.3.1 DELIVERY REQUIREMENTS. Of prime importance to the design engineer are the delivery requirements which the parachute retardation-system must meet. These requirements include velocity and altitude of delivery, weight of the weapon, stability required, and impact conditions (which include impact angle and velocity), time of fall, range, delivery mode, etc. A stringent requirement for stability introduces unforeseen problems for the design engineer. Parachute retardation-systems should not induce a roll of the weapon either during deployment or during descent. Stability requirements vary from no restriction on oscillation to ± 10 deg. Where precise stability is not a requirement, the less-stable parachutes, such as those with a solid flat canopy, may be used. However, a high-porosity ribbon or ring-slot parachute or a cluster of three parachutes may be the only solution to stay

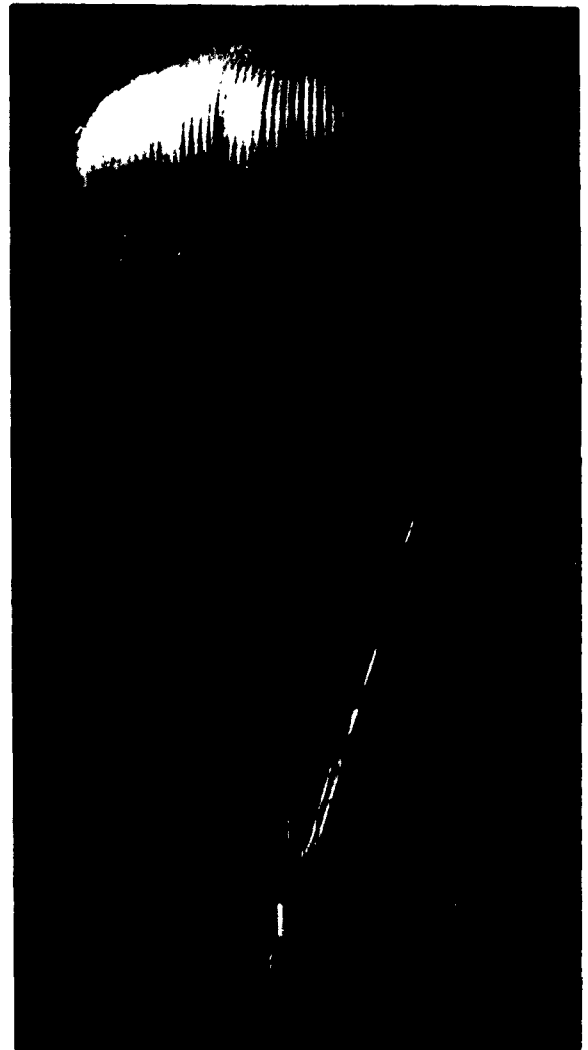


Fig. 5-34 Special Weapons Parachute

below the maximum oscillation. Impact requirements are usually given as some angle measured between the longitudinal axis of the weapon and the horizontal and some maximum vertical velocity. In some applications a minimum and a maximum impact-velocity may be imposed. Prior to actual drop-testing, computer studies are normally run to determine as nearly as possible the proper configuration of the parachute system to meet all the delivery requirements. The drop-testing program directly follows the computer studies and is used to determine the effect of the variables that are impossible to predict and thus cannot be programmed in the computer studies. The test program also permits refinements in the design of the various components (deployment bags, bridles, lan-

yards, etc.) of the system, so that the result should be the best possible design when everything is considered.

6.3.2 RELIABILITY. In order to meet the reliability requirement, each parachute retardation-system must be designed so that it will successfully retard the weapon when delivered at a dynamic pressure in excess of that expected under the normal drop-conditions. In the past, 110 to 125 per cent of the expected maximum dynamic pressure has been used in tests. It is believed that if the parachute retardation-system functions properly during the overtest then it could be expected to perform without fail during normal conditions. Penalties required in a parachute that passes such overtests are probably much less expensive, and require less time, than a test program of sufficient length to prove reliability.

6.3.3 VOLUME AND WEIGHT. Canopy weights may be predicted to within 3 per cent of the actual weight by detailed calculations. The other components of the parachute retardation-system may be accurately estimated from past experience so that the weight of the total system may be predicted with an accuracy of approximately 5 per cent. From this information, the volume needed for the retardation system in the weapon may be determined.

6.3.4 ENVIRONMENT. Storage environment is quite important to the parachute retardation-system. Nylon tends to adhere to itself if it becomes damp for any reason; hence the design engineer must insure that adequate precautions are taken to protect the system from rain, snow, humidity, etc., while it is in storage.

6.3.5 TRAJECTORY CONTROL. The reasons for controlling the trajectory of the weapon are several: to provide escape for the delivering aircraft, to allow precise control to the impact area, to retard the weapon sufficiently so that it may survive the impact, and to stabilize the weapon. In doing any or all of these things the retardation system must produce a trajectory that may be accurately reproduced.

6.3.6 TYPES OF PARACHUTE RETARDATION SYSTEMS. Parachute retardation-systems are used in several configurations: single-stage, multi-stage, reefed, or unreefed. A single-stage parachute system is one in which only one parachute or cluster of parachutes provides the retardation. A single-stage system may be reefed, either permanently or for some specific time, or unreefed. Reefing, its uses and its types, is adequately discussed elsewhere and hence will not be discussed here. A light single-stage or cluster system normally contains a pilot chute and one or more main parachutes. A heavier single-stage system, either a single parachute or a cluster of para-

chutes, usually incorporates an extraction parachute in addition to the pilot chute because the pilot chute can not generate sufficient force to properly deploy the main parachute or parachutes. Extraction parachutes usually have small ribbon-canopies measuring from 10 to 16 ft in diameter. A multi-stage system has components similar to those in single-stage systems using an extraction parachute. Multi-stage systems could conceivably be made up of any number of stages, each stage acting independently in sequence to stabilize and retard the weapon. The attachment of the extraction parachute in a multi-stage system is to the weapon as well as to the second-stage parachute or parachutes. When the extraction parachute, or (more properly) the first-stage parachute, is deployed, it does not immediately extract the main canopy or canopies, but instead retards the weapon to a predetermined velocity where the main parachute or parachutes can be safely deployed. Using this sequence of deploying the second-stage parachute, the main canopy or canopies may be of light-weight construction, whereby a considerable saving in weight may be realized. A multi-stage system invariably requires more altitude to accomplish the same results as a single-stage system, however.

6.4 Deployment Methods. Three methods of parachute deployment are common: static-line, automatic, and forced-ejection.

6.4.1 STATIC-LINE DEPLOYMENT. A static-line, provided the free end of the line is adequately connected to the aircraft, will always initiate deployment at the same time and place relative to the delivering aircraft. When the weapon has fallen the distance equal to the length of the static-line, the pilot chute is deployed by the static-line and deployment of all remaining parachutes follows in the desired order. The use of a static-line is limited because it fixes the length of free-fall before any drag-producing surface begins opening and creates the problem of a loose, flailing line on the carrier aircraft.

6.4.2 AUTOMATIC DEPLOYMENT. Automatic deployment is required when the weapon is carried externally on the aircraft or when any amount of free-fall is desired prior to deployment of the parachutes. The sequence of an automatic deployment is as follows: (1) after release from the aircraft the weapon falls free for some specific length of time, after which the weapon's tail or the parachute-compartment cover is removed, usually by explosives; (2) the pilot chute, connected to the tail cover, is deployed as the cover moves away; (3) once the pilot chute reaches the air stream, deployment of the remaining components is identical to static-line deployment.

6.4.3 FORCED EJECTION. Forced ejection is a method of deploying a canopy where other methods may not work or may be too erratic if they do work. Forced ejection is usually used on smaller parachutes (pilot chutes or small ribbon and ring-slot canopies) and is accomplished by packing the parachute around a tube filled with a propellant. As the propellant burns the tube pulls or pushes the parachute out. (See Chap. 9.)

6.5 Parachute-System Components. There are two main types of components in any parachute retardation-system: the canopy and the deployment bag in which the canopy is packed. Other components of lesser importance and almost infinite variety are lanyards and bridles.

6.5.1 CANOPY TYPES. There are only four different types of canopies used in retardation systems for special weapons. They are the solid flat, ribbon, ring-slot, and guide-surface. The first three are used primarily as retardation devices, while the fourth is used almost exclusively as a pilot chute. These four types of parachutes are adequately discussed elsewhere in this book remembering that their construction is stronger than similar canopies employed in air drop and aircraft deceleration applications.

6.5.2 DEPLOYMENT BAGS. Deployment bags are tailor-made to provide an enclosure for the canopy in the proper shape so that the parachute will fit in the space provided in the weapon. Liberal use is made of webbings having up to 10,000-lb strength and pack cloth of 7.25 oz per sq yd. The deployment bag must be strong enough to withstand the shock of accelerating the packed parachute.

In most parachute retardation systems for special weapons, pressure packing in one form or another is used. Sometimes this takes the form of a localized high-pressure and sometimes this pressure is applied by large hydraulic presses capable of 80 tons total force. Pressure packing must be used to achieve the high pack-densities required so that the retardation system can be made to fit in the space provided in the weapon.

SEC. 7 PERSONNEL PARACHUTES

7.1 General. Personnel parachutes may be used for premeditated jumps or emergency escape. This section considers as personnel parachutes only those which lower an individual directly. Parachutes for lowering a capsule, platform, or other devices containing personnel may be designed and constructed as discussed under Air Drop, Aerospace-Vehicle Re-

covery, or Aircraft Deceleration; however, reliability requirements must meet those discussed here. General design and construction techniques for personnel canopies can be found in MIL-P-6645D(2), "Parachutes, Personnel, General Specification for."

7.1.1 REQUIREMENTS

7.1.1.1 Mandatory. All personnel parachutes must meet the requirements below. With the exception of reliability, this list is not necessarily in the order of importance.

(a) Absolute reliability, both in deployment and opening, whether automatic or manual;

(b) Rapid opening;

(c) Rate of descent of no more than 25 fps for a 300-lb jumper (usually achieved by high drag-coefficient to keep bulk to a minimum). Rate of descent of escape-capsules is dependent upon weapon-systems requirements and design attenuation of ground-impact loads;

(d) Low bulk and weight (refer to (c) above);

(e) Comfortable, light, and properly designed harness;

(f) Provision for fast release of canopy from harness or person;

(g) Tolerable snatch and opening forces at anticipated maximum speed and altitude of deployment; and

(h) Stability within ± 20 deg for emergency use and ± 10 for premeditated jump.

Requirements (d), (e), and (f) are only applicable in part to emergency-escape parachute systems.

7.1.1.2 Desirable. Additional desirable requirements and features for personnel parachute-systems are:

(a) A pack without corners or protuberances, which is properly positioned in order not to be subject to damage or snagging preceding or during deployment;

(b) Adaptability to automatic operation;

(c) Resistance to damage during use and recovery;

(d) Ease of repair;

(e) Ease of packing; and

(f) Low initial cost.

7.1.1.3 Considerations. The designer of personnel parachutes must consider many design requisites. He must know these facts:

(a) Rate of descent desired;

(b) Allotted load limits;

(c) Amount of desirable stability;

(d) Primary use: emergency escape, troop-dropping, or air-rescue;

(e) Bulk and weight requirements;

(f) Speed range;

(g) Altitude range;



Fig. 5-35 Flat Circular Canopy

(h) Opening method.

In most cases, knowledge of (a) through (f) is sufficient to make a quick and easy determination of type and size of canopy. However, if (g) and (h) impose unusual conditions, it will be necessary to consider additional factors.

7.1.2 PERSONNEL-PARACHUTE COMPONENTS

7.1.2.1 *Canopies.* Selection of one of three canopy styles (the flat circular, the flat extended-skirt, or the guide-surface personnel) meets, or can be developed to meet, the majority of needs for deployment at subsonic speeds. Where the characteristics of these canopies do not meet a specific requirement, it will be necessary to consider the data available on other types, as given in Chapter 3. For emergency escape at speeds in the transonic and supersonic range, it will be necessary to use a capsule or other protective device, since present research indicates the probability of injury from wind blast or deceleration effects at those speeds. For such high-speed emergency-escape applications, the canopy types covered under Aerospace-Vehicle Recovery should be considered for first and final stage.

(1) *Flat Circular Canopy.* (See Fig. 5-35.) This type has a high coefficient of drag, is relatively simple to produce, is sufficiently stable for most personnel applications, is reliable at speeds up to 400 knots (with a 15-ft static-line and a pilot chute), is relatively simple to pack and repair, and is light and compact. It may be deployed by ripcord or static line or a combination of both. Its chief disadvantage is the limitation of deployment speed and insufficient stability for certain other applications. The flat solid circular canopy, Type C-9 which has a nominal diameter of 28 ft, is in standard use at the present time. It is the canopy for the standard Parachute Assembly Back Style.

(2) *Flat Extended-Skirt Canopy.* (See Fig. 5-36.) This type of canopy may be deployed at higher speeds than the flat circular type and has better stability. It is relatively simple to produce, pack, and repair. The 35-ft nominal diameter, 10 per cent flat extended-skirt canopy, Type MC-1, is standard at the present time. It is an integral part of the Type A/P28S-2 parachute.

(3) *Personnel Guide-Surface Canopy.* (See Fig. 5-37.) This 30-ft nominal-diameter canopy (Type C-11) seems to offer the most promise for a high deployment-speed personnel parachute. Present designs utilize a shaped (for example, conical) canopy similar to the flat circular type, but with four gores removed. The guide surfaces are created by extending alternate roof panels. This canopy has excellent stability for personnel applications. Opening-shock is somewhat less

than that for the flat circular type due to its slower opening time. This slower opening time necessitates its deployment at altitudes higher than those required by the flat circular or extended-skirt canopies.

A comparison of average opening-force versus aircraft release-velocity for the C-9, MC-1, and C-11 canopies is presented in Fig. 5-38. Typical force-versus-time histories of canopy inflation for these types are shown in Fig. 5-39. Various characteristics for parachutes, which have the three types of canopies discussed above, are presented in Table 5-4.

(4) *Steerable Parachute Canopies.* Steerable-parachutes are used primarily for the delivery of rescue, fire-fighting, and other specialized personnel requiring precise entry into limited or unprepared target areas. They are not used as personnel emergency parachutes because (a) they have a longer opening time; (b) they can be deployed successfully only at limited speeds; and (c) they can be used to advantage only by experienced parachutists. They are not used by paratroopers primarily due to the hazards of mid-air collision resulting from loss or misuse of control during mass jumps.

Practically all steerable parachutes let entrapped air to escape through slots or orifices in the canopy. This "jet thrust" generally results in a glide velocity on the order of 5 knots. Rotational control is achieved by warping the canopy or vents to deflect the jet and impart a turning moment. All require the use of full bags, partial bags, or sleeves, to contain the canopy during deployment and to reduce inflation malfunctions.

Early steerable parachutes had modifications of flat circular canopies; however, the relative instability of flat circular canopies introduced an unacceptable landing injury rate and resulted in a change to use of the more stable extended-skirt canopy.

(4a) *Derry Slot.* The Type F-1 parachute (Fig. 5-40) is steerable by two strategically located slots. These "Derry" slots are positioned symmetrically aft of the canopy lateral axis and on each side of the fore and aft centerline. The slot design causes air to jet inboard and to the rear. Control lines are attached to the lower edge of the slots and when either line is shortened the slot is deformed which results in a reversal of the jet thrust from the deformed slot. Derry slots can be used in either flat circular or shaped canopies. The basic disadvantage of Derry-slotted canopies is the necessity of using control lines of greater length than the canopy suspension-lines. The additional longer-length lines introduce line-deployment problems during inflation.

(4b) *Slit Skirt (Type MC-2) (See Fig. 5-41.)* The MC-1 becomes steerable with incorporation of a V-slot approximately 6 ft long in the rear-most gore.



**A. Extraction Pack Falls
Into Free Stream**



**B. Extraction Parachute
Deployed**



**C. Extraction Parachute
Removing Load**



**D. Extraction Force Shifted
To Recovery Parachute
Packs**



**E. Recovery System Being
Deployed**



**F. Recovery System After
Deployment**

Fig. 5-36 Flat Extended-Skirt Canopy



Fig. 5-37 Personnel Guide-Surface Canopy

TABLE 5-4 PARACHUTE CHARACTERISTICS

Components	Parachute Assembly, Back-Style Assembly No. 50C-7024-20 Assembly No. 50C-7024-18	Parachute Assembly Type A/P 28S-2	Parachute Assembly Type A/P-28S-10
	Emergency escape	Paratrooper	Air rescue-service
Harness Assembly Material Release	Nylon webbing Type XIII & XXII J-1 canopy release	Cotton or Nylon webbing 3-prong, quick, Type B-2A & J-1 canopy release	Nylon webbing Type XIII J-1 canopy release & B-2A harness release
Fittings	Quick-adjustable V-rings & snaps	Quick-adjustable legatrap adapters, D-ring for reserve parachute	Quick-adjustable V-rings & snaps Quick-adjustable V-rings & snaps
Main Parachute Pack Dimensions Material	26" x 15" x 5" Nylon cloth, plied yarn	20" x 12" x 6" 10 oz cotton duck	25-1/2" x 16" x 6" Nylon cloth, plied yarn
Main Canopy	Type C-9	Type MC-1	Type MC-1 with elliptical orifice
Diameter	28' (Flat circular)	35' (nominal)	35' (nominal)
Material	1.1-oz Nylon cloth, orange & white	1.1-oz camouflaged ripstop-Nylon	1.1-oz ripstop-Nylon orange & white
Suspension lines	14—each 75.3' length, running continuously from connector to connector (550 lb T.S.)	30—each 25.5' (375 lb T.S.)	30—each 25.5' (375 lb T.S.)
No. of gores	28	30 (shaped)	30 (shaped)
Connection links	Separable connector links	4-Replaceable	4-Replaceable
Deployment Bag Dimensions	None	18" x 12" x 5" (full bag)	18" x 12" x 5" (Full bag)
Material	Nylon	8.5-oz Cotton twill	Nylon cloth, plied yarn
Static line	None	15" Nylon webbing Type XIII	15" Nylon webbing Type XIII
Stow loops	Fabric	2 Rows (11 loops each)	2 Rows (11 loops each)
Reserve Canopy	None	24' (Flat circular)	24' (Flat circular)
Diameter		1.1-oz camouflaged ripstop-Nylon	1.1-oz camouflaged ripstop-Nylon
Material		24—each 20' (550 lb T.S.)	24—each 20' (550 lb T.S.)
Suspension lines		24	24
No. of gores			
Ripcord Assembly	Flexible steel cable with grip and locking pin	Steel-wire handle with 6.75" metal cable	Steel-wire handle with 6.75" metal cable
Automatic Release	None Type F-1B	None	None
Wt of Parachute	26 lb 29 lb	39 lb	40 lb

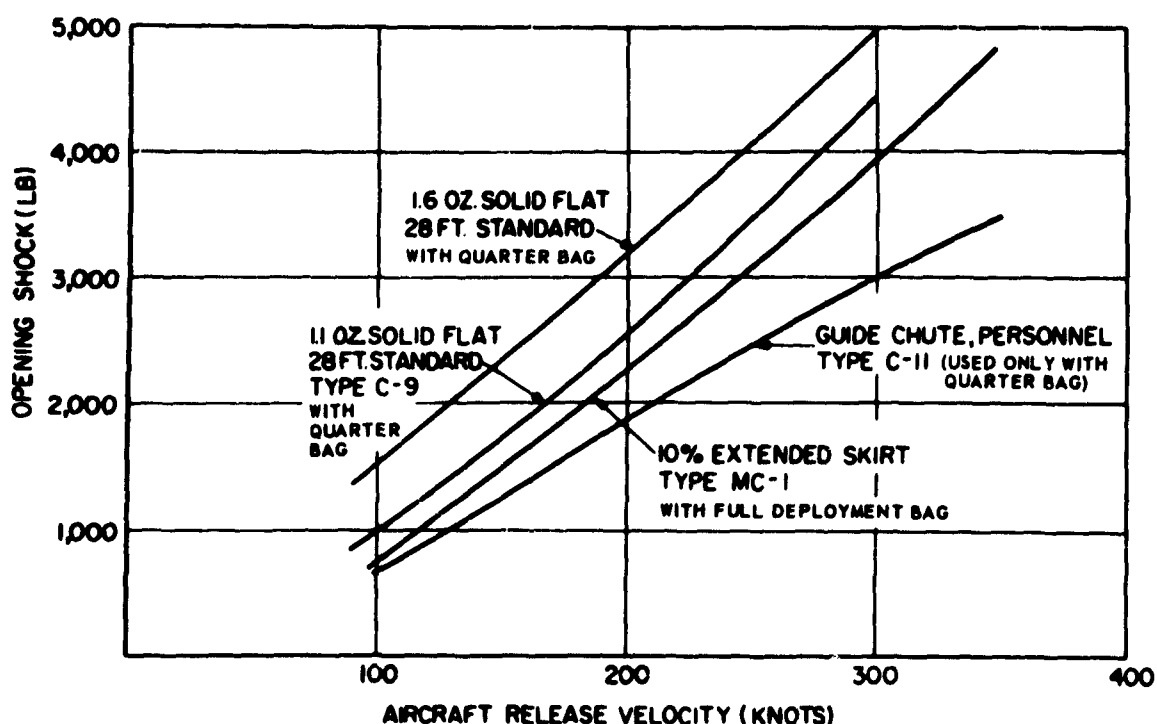


Fig. 5-38 Opening Force vs Aircraft Release Velocity for Type C-9, MC-1, and C-11 Canopies

The skirt hem does not cross the open slot. Reinforcement at the apex of the slot is necessary. When the aft risers are pulled on the side toward which it is desired to turn, the skirt on that side is forced to a lower position than the skirt on the other side of the slot. The resulting direction of jet flow causes the canopy to rotate. This canopy has proved to have stability, rate of descent, and opening-shock comparable to that of the conventional MC-1. Slit-skirt parachutes encounter an extremely high inversion-rate if the skirt is not contained during the deployment process. The use of a quarter-deployment bag or skirt-heminator provides for acceptable deployment and inflation. Control of the slit skirt also requires the attachment of an additional suspension line to each cutedge and the line length differential involved inflicts the deployment penalties noted for the Type E-1 parachute.

(4c) *Single Orifice.* The Type A/P28S-3 and A/P28S-10 parachutes (Fig. 5-42) use a basic MC-1 canopy that has been modified by locating a polygonal orifice symmetrically on the fore and aft centerline in the rear quadrant of the canopy. The main-seam radial tapes are left intact to provide structural and shape integrity. Canopy deformation and result-

ant directional change in jet thrust is obtained through the use of "slip risers". Slip risers are similar to conventional risers, except that the midpoint is not restricted and shortening one riser results in an equal lengthening of the opposite riser. The single-orifice modification is adaptable to free-fall and static-line-actuated parachutes and does not seriously compromise the stability or descent-rate requirements of troop parachutes. The canopy is contained by a full deployment bag during deployment. This design is considered to be the most effective for military applications.

(4d) *Other Types.* There are a number of other steerable parachutes that have been tested. With few exceptions all parachutes tested rely upon a canopy vent with various shapes and areas to effect steerability. A notable exception is the Hoffman triangular canopy which attains the necessary thrust through shape rather than venting. Examples of other steerable canopies are shown in Fig. 5-43a and b.

The recent revival of sports parachuting has resulted in the appearance of numerous steerable-canopy designs and principles of canopy venting and sleeve deployment are used almost exclusively. Some practitioners have mated venting with permeability

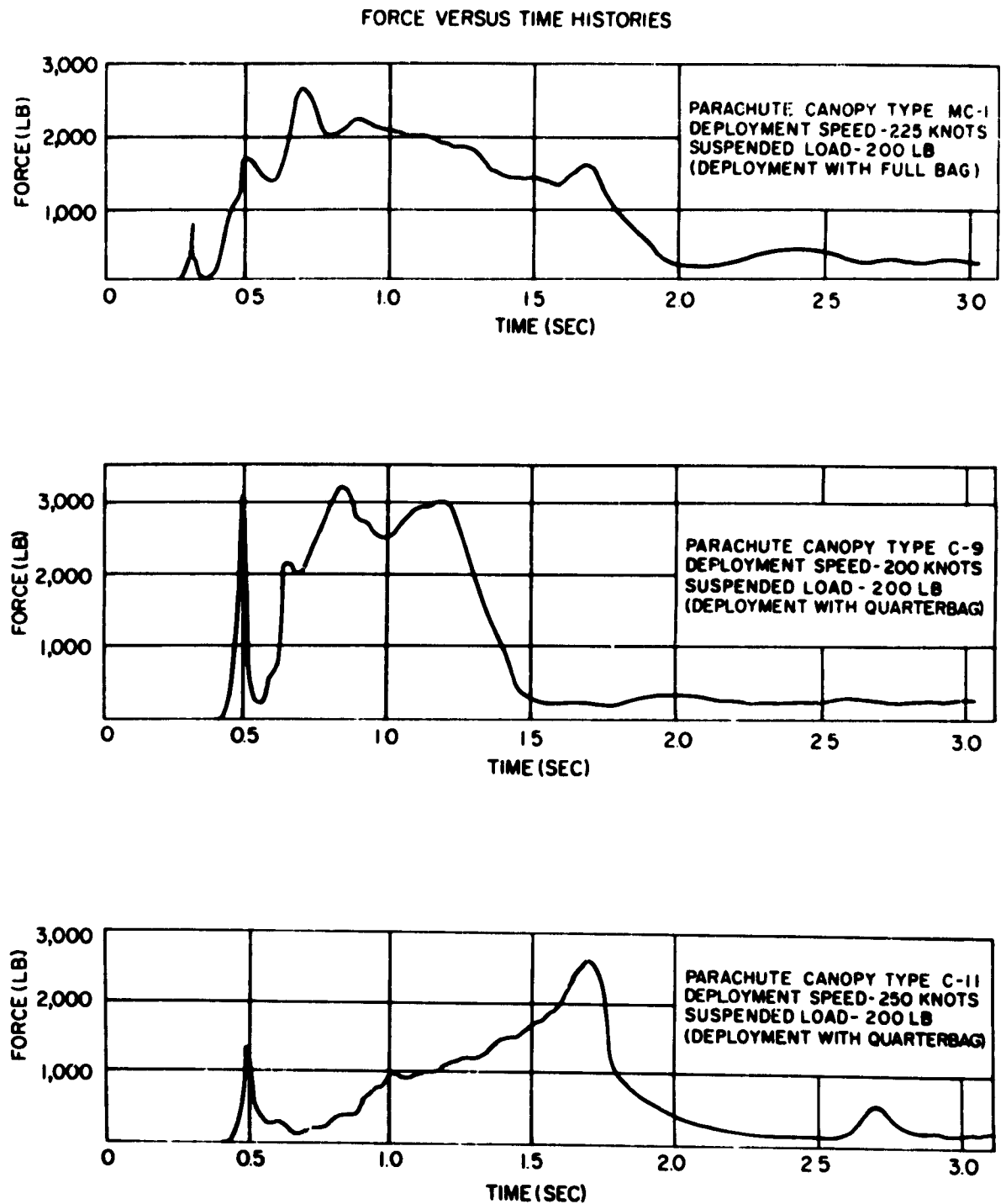


Fig. 5-39 Force vs Time Histories of Canopy Inflation of C-9, MC-1, and C-11 Canopies

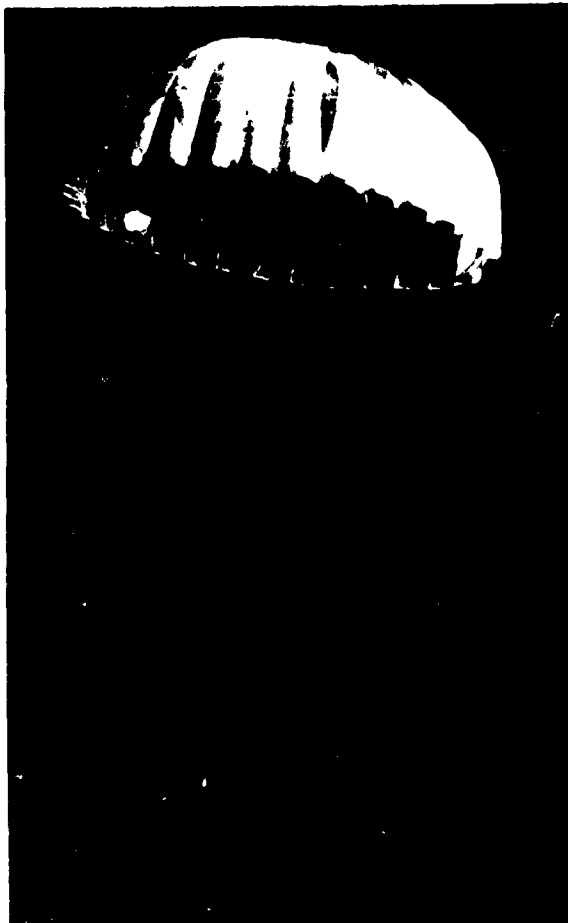


Fig. 5-40 Type E-1 Steerable Parachute



Fig. 5-41 Type MC-2 Steerable Parachute

control to attain effective steerability. The relative merits of the various configurations of steerable canopies existent in sports parachuting today are argumentative, as precise engineering data to support performance claims has not been made available.

7.1.2.2 Automatic-Opening Parachutes. With the exception of parachutes used in certain types of aircraft, such as liaison airplanes, helicopters, and some transport aircraft, all personnel parachutes should be designed for the installation of an automatic ripcord release. The release should be mounted inside the parachute pack, so that:

- (a) Comfort of the parachute wearer is not affected;
- (b) The release is easily accessible for inspection, servicing, and installation;
- (c) Automatic actuation of the ripcord is reliable; and
- (d) The arming knob or handle of the release is suitably mounted and accessible to either hand.

The automatic parachute enables the wearer to escape above a preset altitude, arm his automatic release, and parachute deployment is initiated automatically at a safe and predetermined level above the terrain. If the wearer escapes from the aircraft below an altitude equivalent of the preset altitude value of the automatic release, parachute deployment should be initiated automatically after a predetermined delay-time to allow for sufficient speed decay and avoid high or excessive opening-shock forces. Different views of the parachute assembly (automatic, back), incorporating an automatic ripcord release, oxygen bottle, C-9 canopy, and harness are shown in Fig. 5-44.

7.1.2.3 Parachute Pack. The parachute pack shall suitably house, protect, and mount the canopy on the person. It is mandatory that the pack open with absolute reliability, both automatically and manually, at the time the ripcord is actuated and per-



Fig. 5-42 Halo (Modified MC-1) Canopy

mit uninterrupted deployment of the canopy. Such operation must take place under the extremes of environmental and handling conditions imposed in service. The use of metal ribs or stiffeners in the pack design should be minimized to reduce weight and maintain wearing comfort. The pack should mount firmly and form-fit the body to minimize fouling on aircraft equipment and seats. The integration of the pack with other personal equipment the person may be required to wear is highly important and will influence the design and configuration of the pack.

7.1.2.4 Harness

(4a) *General.* The parachute harness worn by the jumper is employed first to transmit the parachute opening-forces to the wearer in such a manner that he is not injured, and second to support the wearer satisfactorily during the descent. The harness, consisting primarily of webbings and associated hardware, may be connected directly to the suspension lines by use of links. It is preferred that risers be employed to connect the suspension lines to the harness. The support during descent should be such that the wearer's vertical axis is approximately perpendicular to the earth's surface.

On personnel emergency-parachutes, packs and

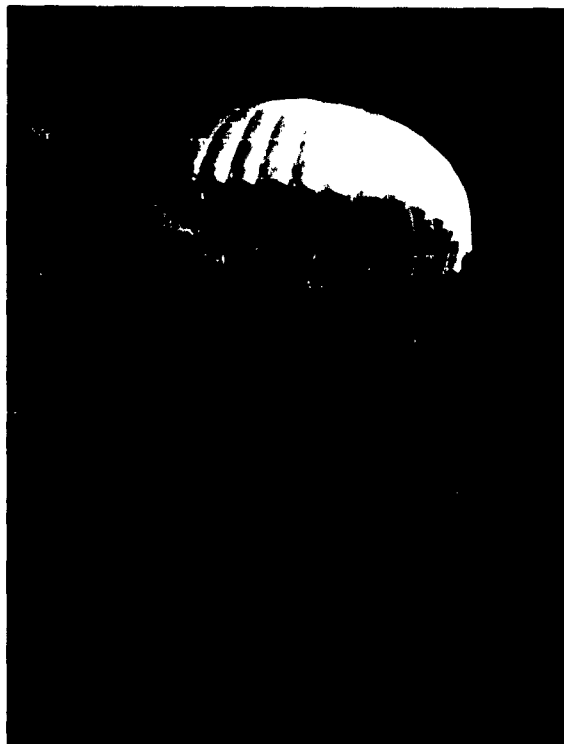


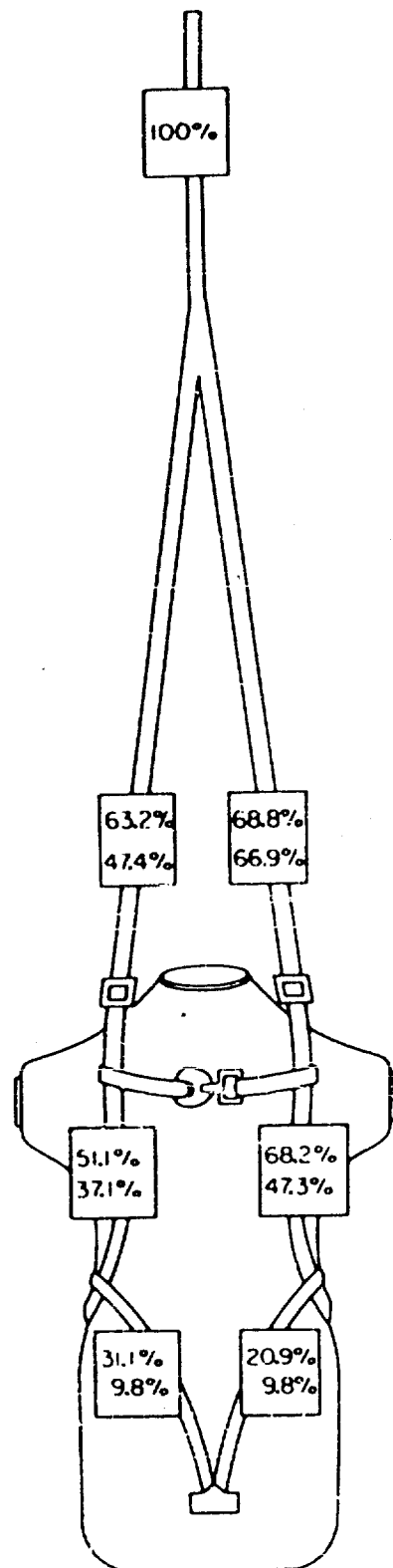
Fig. 5-43a Hart Type Steerable Parachute



Fig. 5-43b MC-1 With Tilted Extensions



Fig. 5-44 Parachute Assembly, Automatic, Back



harnesses are usually maintained as one unit. The wearer carries the parachute, harness, and certain attached personal equipment when on the ground. Another arrangement is the separation of the harness from the pack and other attached personal equipment while on the ground. The parachute and attached personal equipment is kept in the aircraft. The aircrew member wears only the harness until he enters the aircraft, when he attaches the parachute and personal equipment to the harness. This system can be so arranged that the straps attaching the parachute pack to the harness also serve as the aircraft safety-straps. The portion of the parachute system remaining in the cockpit at all times can be hooked up for automatic disconnection from the seat during an emergency ejection. Survival kits and other personal equipment can also be attached to that portion remaining in the aircraft. A series of drop tests have given an indication of the maximum percentage of total force that may be exerted at various points in conventional personnel harnesses (Ref (5-14). Fig. 5-45 lists these forces and locations for both cotton and Nylon harnesses.

Many attempts have been made to improve basic harness design. One is the use of netting with low-strength intertwining strands. A big drawback to such a system is the difficulty of providing adjustment to desirable limits, and of designing to prevent extreme elongation.

(4b) General Considerations for Harness Design.

(1) Harnesses must be constructed so that adjustment can be made by the user and repairs can

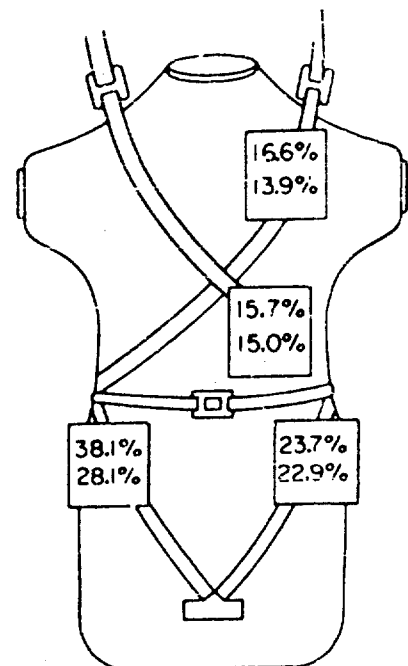


Fig. 5-45 Maximum Force Percentages on a Parachute Harness During Canopy Inflation

easily be made by personnel of operating units and overhaul bases.

(2) A safety factor of 1.5 (minimum) must be maintained throughout all portions of the harness. Technical Memorandum Report WCLF-53-292 gives guidance on the relative strength of the various straps and fittings of the harness necessary to meet requirements.

(3) Design should be such that only a minimum of temporary sewing or tacking is necessary.

(4) The harness must encompass the body in such a manner that its basic function of retaining the body at the lower end of the parachute suspension-system is absolutely and inherently secure.

(5) The suspension straps and harness must not interfere with normal vision or seriously hamper movement required for canopy manipulation during descent or at ground impact.

(6) The harness must incorporate a suitable connection for a canopy. On present designs, four risers are attached to the harness to provide proper suspension and suitable transmission of the maximum canopy opening-force. The connection of the riser straps and the harness should be located 1 to 2 in. below the collarbone of the wearer.

(7) The harness should be simple in design, with an absolute minimum of parts that may become entangled, twisted, or interposed with one another, which would force the wearer to realign the parts in order to put the harness on.

(8) The harness should be so designed that an individual may put on and adjust the assembly while in a standing or seated position.

(9) The harness must incorporate a method whereby the wearer can remove the harness quickly and easily by operating each connector with one hand.

(10) The number of adjustment points required to make the harness fit should be kept to a minimum. The adjustment points should be accessible, preferably visible, to the wearer when seated.

(11) The adjustment points must not hamper or prevent actuation of the ripcord or automatic parachute arming-knob on the accessible front area of the harness when worn.

(12) The harness must be so designed that even after faulty or careless adjustment it will resist falling from the wearer's shoulders during canopy deployment or opening.

(13) The harness must be quickly and easily adjustable without roping or jamming of the webbings in the adjustment fittings. The size of the harness should be indicated by a visible marking, so that the size to which the harness should be adjusted will be readily seen at a glance.

(14) Unless individually sized, the harness must be readily and quickly adjustable to a suitable fit for individual personnel sizes varying from 5 ft. 2 in. to 6 ft 6 in. in height and 110 to 250 lb in weight, with or without standard Air Force winter flight-clothing.

(15) The harness must not cause discomfort to the wearer resulting from limited-area body-contact and pressure points, or cause uncomfortable restriction from bulky protrusions, which may invite snagging on other personal equipment or the aircraft seat.

(16) There must be no strap adjusters, connectors, or metal fittings directly against the wearer's back when the harness is worn. Metal fittings must not contact the wearer's face or head during opening or descent of the canopy.

7.1.3 CANOPY DEPLOYMENT. Two basic deployment methods are used with personnel parachutes:

(a) Free-type deployment; or

(b) Static-line deployment.

The free-type deployment method has been used for many years for personnel emergency-parachutes. The static-line deployment is still used for air rescue-service, Army paratroopers, and other premeditated jumping. See Chapter 7 for further information on deployment systems. Fig. 5-46 shows the deployment of a Type A/P 28S-2 parachute and a correlation of static-line force to state of deployment. Note the deployment bag and the smooth, straight deployment of the suspension lines.

The free-type deployment method incorporates a pilot chute which, when released into the air-stream, produces enough drag to deploy the main canopy. The static-line deployment method incorporates a direct connection between the aircraft and the main parachute to cause deployment.

SEC. 8 TARGET

8.1 Early History. The use of parachutes for targets is one of the latest applications in the parachute field today. Although crude and without reflective fabric, the first parachutes used in 1949 proved feasible as targets for anti-aircraft missile tests. For these first target parachutes, standard flat canopies were modified by gluing strips of aluminum metal foil to the gores. This greatly reduced the porosity of the canopy and caused a high degree of instability. Improvements have been made so that reflective canopy material is now produced commercially.

8.2 Applications. Target parachutes are used primarily when a relatively large number of scheduled anti-aircraft missile firings are to take place. In

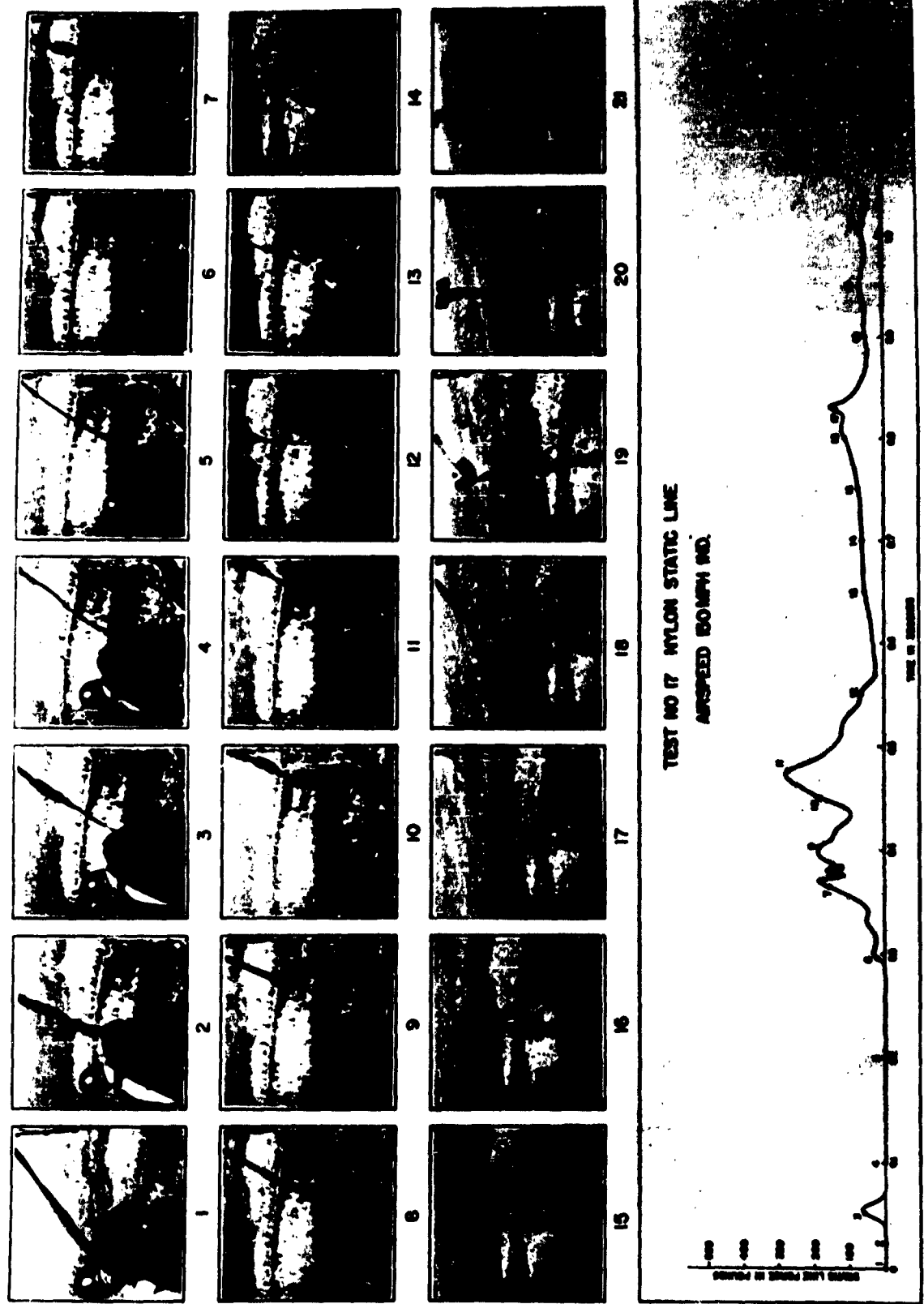


Fig. 5-46 Correlation of Static-Line Force to State of Deployment of a Type A/P 28S-2 Parachute

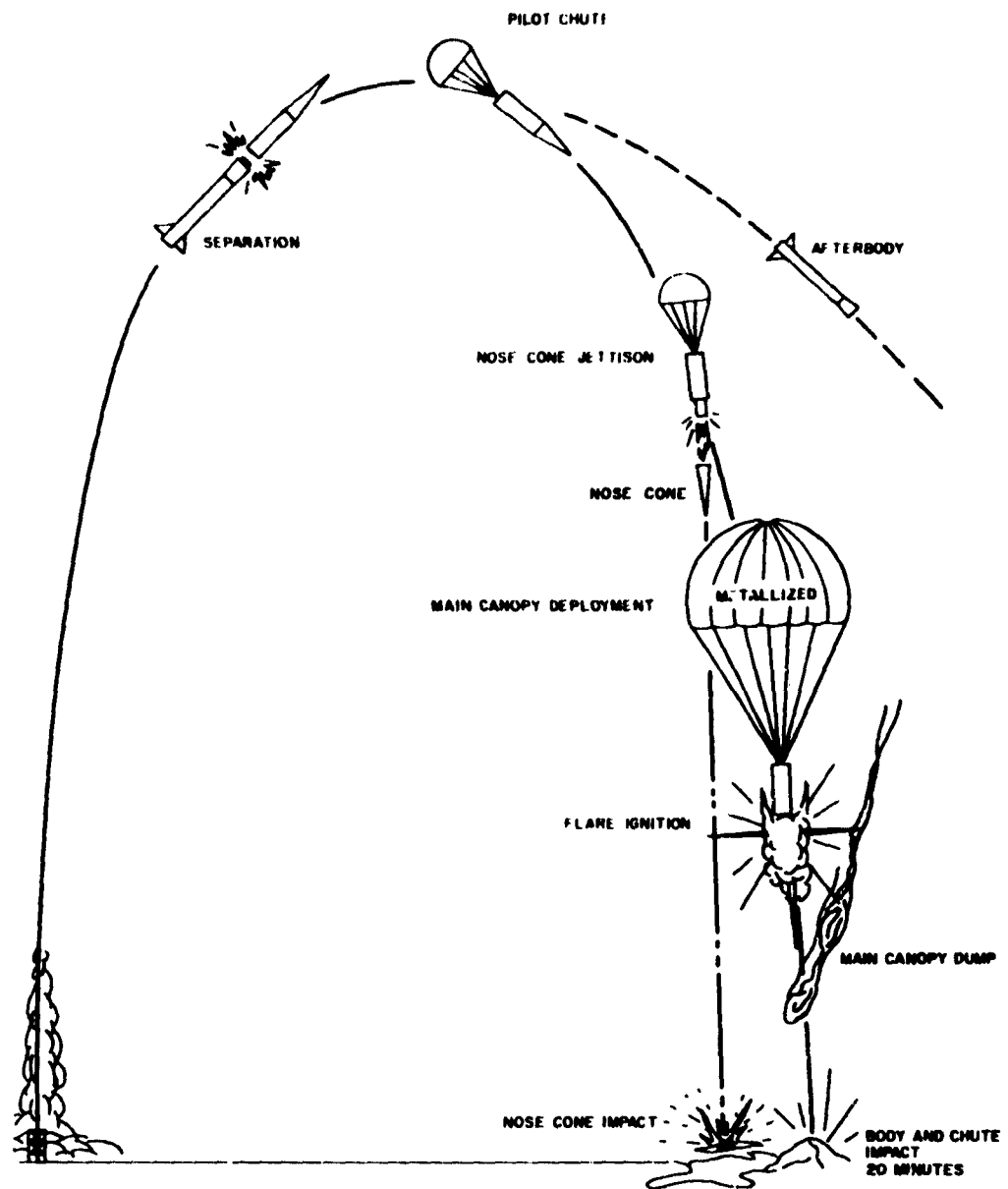


Fig. 5-47 Typical Trajectory for a Target Parachute System

such instances, the number and cost of drone aircraft required for testing become excessive. The target parachutes can generally be reused several times, thus increasing their economy. They may be dropped from aircraft at desired altitudes or deployed by ground-launched rockets at desired altitudes, depending on the nature of the test to be conducted. Fig. 5-47 shows a typical rocket-launch trajectory of a target parachute.

8.3 Requirements. The major requirement for a target parachute is that it be "stationary" at the pre-determined target altitude. Stationary means a maximum descent velocity of 10 fps for approximately 5 min. After the anti-aircraft missile test is completed, the target parachute should descend as quickly as possible (75 to 100 fps) so that it will not drift off-range and be lost. However, in order to protect the suspended instrumentation and photo equipment, the target parachute descent should be reduced to a minimum speed near the ground to allow for safe impact. These conditions have been obtained by the application of vent reefing; by disconnecting the target canopy and deploying a recovery parachute at a pre-selected altitude; or, in the case where there is almost negligible suspended weight, a significant number of the suspension lines may be severed to partially spill the canopy and still achieve a satisfactory impact velocity.

Another important requirement is that the target parachute have the same reflectivity as a particular target, such as a specific airplane or missile, in order to activate the automatic guidance system of the anti-aircraft missile. The method presently being applied to make the parachute material reflective is impregnation of the material with silver. This process, which is accomplished commercially, does not appreciably harm the material, nor change its characteristics significantly. Various coating-patterns have been utilized to effect better simulation of aircraft. One pattern, in which alternate panels of the canopy are coated, has been effective in simulating the "noise" or interference effects of modern jet-aircraft on target-detection systems.

8.4 System. A target-parachute system includes the target parachute, pilot chute or chutes, instruments, and cameras. In cases where the system is dropped from aircraft these items are packed in a case, such as a bomb-shaped container which is suspended either internally or externally from the bomb shackle of the drop aircraft. This container should be made from material non-reflective to radar, as the target-parachute reflection-picture could be easily distorted by container reflectivity. In some cases, when the canopy is deployed, a smoke grenade is

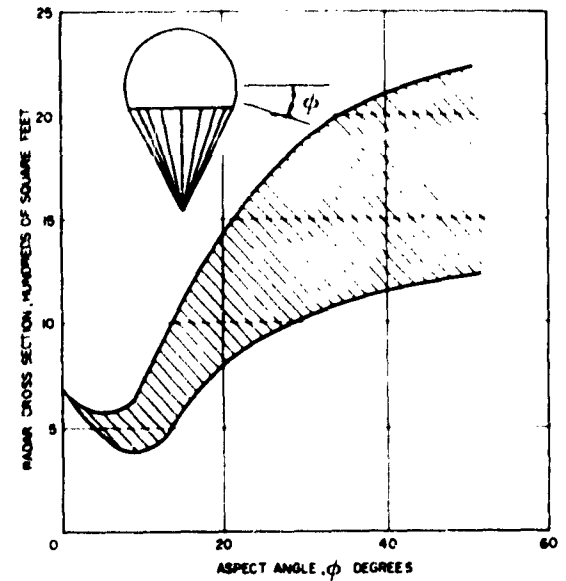


Fig. 5-48 Radar Cross-Section of 220-Degree Spherical Canopy

ignited and burns to aid in visual location of the target. This also provides more time for the drop aircraft to clear the danger area, since the target system is normally dropped about three minutes before missile-launch.

8.5 Radar Targets. When an object is hit by beam of electromagnetic radiation, the reflected radiation is scattered. The direction of this scattering depends on the orientation of the various surfaces of the object; only that reflection towards the radar set or incoming missile is useful. The "effective radar cross-section" of an object is the area which reflects radiation back to the receiver. It depends on the size, curvature, and direction of motion of the target. Effective radar cross-section can be measured by the ratio of the amount of energy that is reflected toward the radar set to the amount of energy that is transmitted towards the target by the radar set. The larger the effective radar cross-section of a target, the larger the percentage of the illuminating radiation is returned to the original source of the radiation. Thus, a flat plate perpendicular to the axis of illumination is the most efficient radar target. It is noted that radar cross-section measurements are not precise, so several runs must be made and the average cross-section determined. In Fig. 5-48, ten measurements were taken of a 220-deg spherical canopy to determine the radar cross-section. Two boundary-curves were obtained with the shaded area between the two curves being caused by oscillation of the parachute. Fig. 5-49 re-

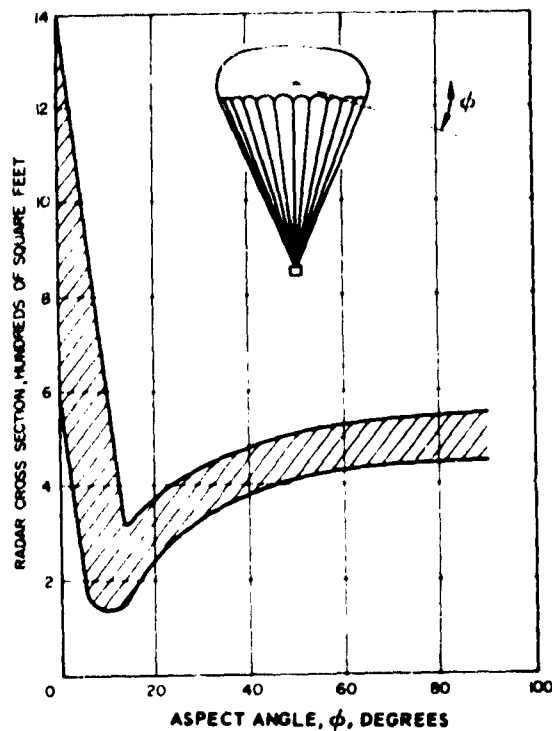


Fig. 5-49 Radar Cross-Section of Ring-Slot Canopy

presents the radar cross-section of a ring-slot parachute.

8.6 Simulation. The problem of simulation or producing a radar target of a specified "effective radar cross-section" is difficult, since this "effective" area is governed by the attitude of the parachute relative to the intercept missile. A radar target which represents one type of aircraft to an air-to-air missile would not represent the same aircraft for a ground-to-air missile. Although the use of a metalized sphere would alleviate the problem of relative attitude between the target and missile, the sphere is a very inefficient target when considering the amount of incident radiation it returns to the original source. The most common type of missile target in use today is the hemispherical or "shaped" canopy. In addition to providing a desired effective radar cross-section, the use of parachutes allows the storage of a potentially large reflective surface in a relatively small volume.

Although target parachutes can never replace fast-moving drone aircraft, the savings realized by their use during a major portion of an anti-aircraft missile-

development stage warrants their use.

REFERENCES

- (5-1) Champney, W.B. and Engel, B., A Study of Hypersonic Aerodynamic Drag Devices, Interim Technical Report (Unclassified Title), WADC TR 59-324 (CONFIDENTIAL REPORT), April 1960.
- (5-2) Champney, W.B., Athans, J.B., and Mayerson, C.D., A Study of Hypersonic Aerodynamic Drag Devices, WADC TR 59-324, Part II, June 1961.
- (5-3) Nebiker, F.R., Feasibility Study of an Inflatable Type Stabilization and Deceleration System for High-Altitude and High-Speed Recovery, WADD TR 60-182, Dec. 1961.
- (5-4) Study of a Drag Brake Satellite Recovery System, Results of Phase I, WADD TR 60-775, Jan. '61.
- (5-5) Hayes, J.E., Rose, P.H., Vander Velde, W.E., Analytical Study of a Drag Brake Control System for Hypersonic Vehicles, WADD TR 60-267, Jan. 1960.
- (5-6) Investigation of Landing Point Control of Re-entry Vehicles Utilizing Variable Area Aerodynamic Decelerators Incorporating Lift, ASD - TR 62-287, April 1962.
- (5-7) Wells, John A., Design Study of the Capsule-Escape Vehicle Parachute Recovery System Hardware, ASD TR 61-178, Vol. I, Oct. 1961.
- (5-8) Newquist, E.A., Cassidy, M.D.; Lindblom, C.W. and Sullivan, P.J., "Development of an Ejectable Nose Escape Capsule," WADC TR 59-493, June 1959.
- (5-9) Pedersen, P.E., "Study of Parachute Performance at Low Supersonic Deployment Speeds; Effects of Changing Scale and Clustering", ASD TR 61-186, July 1961.
- (5-10) Engstrom, B.A., "Performance of Trailing Aerodynamic Decelerators at High Dynamic Pressures", ASD TR 58-284, Part V.
- (5-11) Broderick, M.A., Turner, R.D., "Design Criteria and Techniques for Deployment and Inflation of Aerodynamic Drag Devices", ASD TR 61-188, Nov. 1961.
- (5-12) Engstrom, B.A., "Performance of Trailing Aerodynamic Decelerators at High Dynamic Pressures", WADD TR 58-284 Part II, Jan. 1960.
- (5-13) Engstrom, B.A. and Lang, R.P., "Performance of Trailing Aerodynamic Decelerators at High Dynamic Pressures", WADD TR 58-284, Part IV, June 1961.
- (5-14) Berndt, R.J., Force Distribution in a Parachute Harness, TMR WCLE-53-292, Nov. 1953.
- (5-15) Epple, H.K., "Missile Target Systems, Pogo-

Hi, Hughes Aircraft Company Report Nr. TM-603,
Volume 4, 15 January 1960.

- (5-16) Moore, R. Gilbert, "Radar Reflectivity of
Metalized Parachutes", Paper presented at Para-
chute Engineering Short Course at Purdue Univer-
sity, June 1956.

BIBLIOGRAPHY

Milhouan, F.M., Vorachek, J.J., D'Allura, J., "Investi-
gation of Escape Capsule Systems for Multi-Place
Aircraft, Parts I and II," WADD TR 57-329, Dec.
1961.

CHAPTER 6

MATERIALS FOR DEPLOYABLE AERODYNAMIC DECELERATORS

Table of Contents

<i>Section</i>	<i>Page</i>
1 PARACHUTE TEXTILES	339
2 MECHANICAL PROPERTIES OF DEPLOYABLE AERODYNAMIC DECELERATOR MATERIALS	339
2.1 Standard Materials	339
2.2 New and Experimental Materials	342
2.2.1 High Temperature Materials	342
2.2.2 Lightweight Materials	343
2.2.3 Low-Cost Expendable Materials	344
3 TABULATION OF PARACHUTE MATERIALS	345
3.1 Webbing	345
3.1.1 Webbing, Textile, Woven Nylon, MIL-W-4088D (USAF); Webbing, Textile, Woven Nylon, Impregnated, MIL-W-27265	345
3.1.2 Webbing, Textile, Nylon, Tubular, MIL-W-005625C	346
3.1.3 Webbing, Textile, Cotton Warp, MIL-W-5665D	346
3.1.4 Webbing, Textile, Nylon, Multiple Tubular, MIL-W-5666A	347
3.1.5 Webbing, Textile, Nylon, Heavy Duty, MIL-W-5787C	347
3.1.6 Webbing, Textile, Nylon, Locking Loop, MIL-W-9049B	347
3.1.7 Webbing, Textile, Polyester, MIL-W-25339A (ASG)	347
3.1.8 Webbing, Textile, Dacron, Low Elongation, MIL-W-25361 (USAF)	348
3.1.9 Webbing, Textile, Woven Nylon, Impregnated, MIL-W-27265 (USAF)	348
3.2 Tapes	348
3.2.1 Tape and Webbing, Textile, Reinforcing, Nylon, MIL-T-5638C	348
3.2.2 Tape, Textile, Nylon, Parachute Canopy, MIL-T-5608E (ASG)	349
3.2.3 Tape and Webbing, Textile, Cotton, Reinforcing, Woven, MIL-T-5661B	350
3.2.4 Tape, Textile (Parachute Construction), MIL-T-5663A	350
3.2.5 Tape, Textile, Nylon, Parachute Construction, MIL-T-6134B	350
3.2.6 Tape and Webbing, Textile, Woven, Nylon, MIL-T-8363A	350
3.3 Cords	351
3.3.1 Cord, Rayon, Without Core, Braided, MIL-C-4232A (USAF)	351
3.3.2 Cord, Nylon, MIL-C-5040B (ASG)	351
3.3.3 Cord, Nylon, Coreless, MIL-C-7515B (USAF)	351
3.4 Threads	351
3.4.1 Thread, Cotton, High-Tenacity, MIL-T-5660A (ASG)	351
3.4.2 Thread, Nylon, MIL-T-7807B	352
3.4.3 Thread, Polyester, MIL-T-40040A	353
3.5 Cloths (Canopy)	353
3.5.1 Cloth, Cotton, Muslin, MIL-C-4279A (USAF)	353
3.5.2 Cloth, Nylon, Parachute, MIL-C-7020D	354

3.5 Cloths (Canopy) (Cont'd)	
3.5.3 Cloth, Nylon, Parachute, Cargo, MIL-C-7350C (ASG)	354
3.5.4 Cloth, Rayon, Parachute (Nonpersonnel), MIL-C-8006A (ASG)	354
3.5.5 Cloth, Nylon, Parachute, Drag, MIL-C-8021B (ASG)	355
3.5.6 Cloth, Dacron, Drag Parachute, MIL-C-25174 (USAF)	355
3.5.7 Cloth, Dacron, Parachute, MIL-C-25312 (USAF)	355
3.6 Cloths (Parachute Pack)	356
3.6.1 Cloth, Cotton, Duck, Unbleached, Plied Yarns (Army & Numbered), CCC-C-419	356
3.6.2 Cloth, Nylon, Duck, Plied Yarns, for Parachute Packs, MIL-C-7219B	356
References	357
Bibliography	357

Tables

Number	
6-1	Effects of Environments on Natural and Man-Made Textiles 340
6-2	Radiation Properties of Parachute Cloth 343
6-3	Webbing, Textile, Woven Nylon, for Decelerators, MIL-W-27657 (USAF) 344

CHAPTER 6

MATERIALS FOR DEPLOYABLE AERODYNAMIC DECELERATORS

The selection of materials for the fabric portions of deployable aerodynamic decelerator systems requires that the designer consider textiles from a structural engineering viewpoint. The range of standard cloths, webbings, cords, tapes, etc., covered by current military specifications meets most of the requirements for conventional personnel, cargo, recovery, deceleration, and stabilization decelerators designed for use in the subsonic range. More advanced systems, involving greater canopy loading, higher temperatures, lower bulk and weight, etc., will require modifications of such materials, or the design of completely new textiles. The characteristics of current parachute materials, requirements for more advanced systems, and trends in research and development of parachute textiles are described in this chapter.

SEC. 1 PARACHUTE TEXTILES

The use of textiles as engineering materials requires consideration not only of strength, elongation, flexibility, and response to environments, but also of porosity, sewability, and other factors not usually vital to the use of more conventional structural materials.

Textiles are used in parachute applications in the form of cloths, webbings, tapes, ribbons, and cords for the construction of both the aerodynamic portions of the system, and for such auxiliary devices as packs, deployment bags, and harnesses. Newer aerodynamic decelerators now under development may use other types of materials, such as metal sheets, and plastic films (see Chapter 3).

The textile fibers most common in present-day parachute canopy and load-bearing member applications are Nylon and Dacron, although some use is made also of textiles woven of rayon fibers in a limited range of applications. Cotton and silk, although used extensively in the past, are no longer in general use as canopy materials. Cotton cloths, webbings, and tapes, however, do find application in deployment bags, packs, ties, and related devices. Materials used experimentally, and for limited special-purpose applications, include Fiberglas, Orlon, paper, polyethylene, polypropylene, Mylar, and other plastics. Some experimental work has been conducted with metal fibers, wire cloths, and ceramic fibers, and with special heat-resistant synthetic organic fibers, but no fabrics woven of these materials are available for routine use as yet.

SEC. 2 MECHANICAL PROPERTIES OF DEPLOYABLE AERODYNAMIC DECELERATOR MATERIALS

The specific properties of textiles of interest to the parachute-system designer will vary somewhat with the portion of the system under consideration. However, the effects of environmental exposure, especially heat, aging, sunlight, weather, and chemicals and their fumes, are of importance in virtually every application (see Table 6-1). In load-bearing applications, especially in the design of suspension lines, risers, etc., the strength of the fabrics, and their elongation, elastic-recovery, and energy-absorption properties are of primary concern in materials selection and application. For canopy designs, fabric porosity and tear resistance are of major interest, especially in the case of solid textile types. Friction, abrasion, and wear characteristics, electrostatic properties, inflammability, fungus resistance, and the effects of fungicides, lubricants, and other fabric treatments on mechanical performance also must be considered in specific applications.

The use of textiles as engineering materials, of course, requires sewing to effect joints between two or more layers of the same or different materials. Thus, sewability (see Chapter 8) and the other fabric properties such as stiffness, flexibility, handle, and drape also must be considered in materials selection and system design.

2.1 Standard Materials. There is no single source of data on all of the above-mentioned properties for

TABLE 6-1. EFFECTS OF ENVIRONMENTS ON NATURAL AND MAN-MADE TEXTILES

Environment	Cotton	Silk	Viscose Rayon	Fortisan	Nylon
Heat	Highly resistant to dry heat; yellows at 248 F; decomposes at 302 F; burns readily	Begins to decompose at 270 F; rapid disintegration above 300 F; burns readily	Loses strength above 300 F; decomposes at 350 F to 400 F; burns readily	Scorches in ironing at about 20 C higher than cotton, otherwise like cotton, viscose rayon	Yellows slightly at 300 F when exposed for 5 hr; melts at 482 F
Age	Little or none	Slight yellowing and loss of tensile strength	Slight	Little or none	Virtually none
Sunlight	Loses strength; formation of oxycellulose; tendency to yellowing	Loses tensile strength; affected more than cotton	Loses tensile strength after prolonged exposure; very little discoloration	Loses strength; tends to color	Loses strength on prolonged exposure; no discoloration; bright yarn more resistant than semi-dull
Chemicals	Disintegrated by hot dilute acids or cold conc. acids. Shells (mercerization) in caustics, damaged by prolonged exposure in presence of air. Bleached by hypochlorites and peroxides, oxidized into oxycellulose by strong oxidizing agents.	Fairly resistant to weak acids; dissolved by strong acids except nitric. Insensitive to dilute alkali unless hot; dissolves in strong alkalis. Above pH11 and below pH3 stability decreases rapidly	Strong alkali causes swelling and reduces strength. Attacked by strong oxidizing agents; not damaged by hypochlorite or peroxide bleaches	Disintegrates in hot dilute or cold concentrated acids. Strong caustic shrinks, as in mercerizing. Resistant to bleaches, phenols, and dyehouse reagents	Boiling in 5% HCl ultimately causes disintegration; dissolves in cold conc. sulfuric or nitric acids. Substantially inert to alkali. Generally good resistance to other chemicals
Organic Solvents	Resistant	Resistant	Generally insoluble; soluble in cuprammonium	Unaffected	Insoluble except in some phenolic compounds and conc. formic acid
Moths	Not attacked	Attacked slightly	Not attacked	Not attacked	Not attacked
Mildew	Poor resistance unless bleached or acetylated	Attacked	Attacked	Same as for cotton	Good resistance

- Continued on next page -

TABLE 6 -1, Continued

Environment	Orlon	Dacron	Glass Fiber	Polyethylene	Mylar
Heat	Sticks at 455 F; slight loss in strength after 32 days in air at 257 F; melts at 480 F	Highly resistant to degradation and discoloration; melts at 480 F	Will not burn; strength loss starts at 600 F, continues to limiting temp. of 1000-1500 F softens at 1500 F	5% shrinkage at 165 F; softens at 225 to 235 F; melts at 230 to 250 F; slow burning	Strength reduced above 200 F, useful to 300 F, melts 482 F
Age	Virtually none	Virtually none	None	Virtually none under normal conditions	Virtually none
Sunlight	Very resistant to degradation by ultraviolet light and atmosphere	Loses strength on prolonged exposure; no discoloration	None	Prolonged exposure decreases tensile strength	Moderate resistance
Chemicals	Good to excellent resistance to mineral acids. Fair to good resistance to weak alkalis. Not harmed by oils, greases, neutral salts, and some acid salts	Good resistance to mineral acids except concentrated sulfuric. Good resistance to weak alkali, moderate to strong alkali at room temp.; dissolves in hot strong alkali. General good resistance to other chemicals; excellent to bleaches and oxidizing agents.	Good resistance to all but hot strong acids. Attacked by hot solutions of weak alkalis and cold solutions of strong alkalis. Generally good resistance.	Very resistant to acids. Generally good resistance to caustics and other chemicals.	Good resistance to cold dilute acids and alkalis. Becomes brittle in hot mineral acids and alkalis. Generally resistant to common chemicals
Organic Solvents	Unaffected by common solvents	Generally insoluble; soluble in some phenolic compounds	Insoluble	Insoluble, but swells in chlorinated hydrocarbons, aromatics	Insoluble; degraded by phenols and cresols
Moths	Not attacked	Not attacked	Not attacked	Not attacked	Not attacked
Mildew	Good resistance (coating may be attacked)	Good resistance	Wholly resistant (binder may be attacked)	Good resistance	Good resistance

all fabric and fiber types of interest to the parachute engineer. The mechanical structure, strength, weight, volume, dimensions, air permeability (where applicable), and (for some textiles) elongation of standard Nylon, Dacron, cotton, and rayon materials are described in the appropriate military specifications (see Chapter 13; the bulk of these data are summarized in the tables of Section 3). Further background data on these and other materials are summarized in two USAF Handbooks (Ref 6-1 and 6-2). Other pertinent documents containing detailed information also are listed as References at the end of this chapter.

In general, current Nylon and Dacron parachute fabrics are suitable for most applications in the subsonic speed range, and to some extent in supersonic applications. The major problems arise in those cases in which high temperatures are encountered (aerodynamic heating in high-speed deployment, friction-generated heat during deployment, and storage under elevated temperatures), and in which canopy bulk or weight are problems (see 2.2.2 below).

Dacron textiles are more resistant to high temperatures than Nylon materials, retaining their strength and elastic recovery properties somewhat better. The limit of useful application is 300 to 350 F, as compared with a maximum temperature point for Nylon of 250 to 280 F. For systems which must withstand higher temperatures, new materials must be developed (see 2.2.1 below).

2.2 New and Experimental Materials. Research and development effort in textile materials for parachute applications is being directed toward increasing environmental resistance (especially high temperature), improving mechanical properties (including air permeability -- see Chap. 4), producing narrow fabrics with minimum bulk for specified strength, and developing low-cost materials for use in expendable parachutes.

2.2.1. HIGH TEMPERATURE MATERIALS. The increasing use of parachutes for recovery of equipment from high-speed missiles and returning space vehicles will intensify the problem of selecting materials which can withstand the temperatures generated by aerodynamic heating. The temperature of the canopy fabric in such an application depends upon a balance between the convective and radiative heat transfer from aerodynamic and solar heating respectively, and the radiation of heat by the canopy fabric to its surroundings.

The prediction of such temperatures requires data on the absorption coefficients for solar radiation, the emission coefficient for long-wave radiation, and the thermal diffusivity of the canopy fabric. Values for the first two parameters for several types of Nylon and

Dacron parachute fabrics are given in Table 6-2 (Ref 6-3). Thermal diffusion may be determined from the fabric's specific heat, weight per unit area, thickness, and thermal conductivity. Methods, data, and experimental results are discussed in References 6-4 and 6-5. A basis for the calculation of aerodynamic heating rates for parachutes at high speeds and altitudes is presented in Ref 6-6; the results of studies of heat transfer rates are discussed in Ref. 6-7. The problems of aerodynamic heating of decelerators are discussed in detail in Chap. 4, Sec. 12.

Approaches to the development of high-temperature fabrics include research on high-melting organic polymers (Ref 6-8); the use of protective coatings for heat resistance and cooling by mass transfer (Ref 6-9); designs in which partial destruction of the canopy by heat can be tolerated after initial deployment (Ref 6-10); and fabrics woven of fine metallic wires, high-melting glasses, coated refractory metals, metal and metal oxide whiskers, and ceramic fibers (Ref 6-11, 6-12, 6-13, 6-14).

The most promising of the conventional fabric materials at present is HT-1, a temperature-resistant synthetic organic fiber with a melting point of 840 F, which extends the useful range of fibrous materials for parachute application to about 600 F. At this temperature HT-1 retains over 50 per cent of its original strength; after 8 hr at 400 F, it has approximately 550 per cent more strength than nylon. It does not melt, drip, or fuse together as nylon does when exposed to flame, and it has good resistance to commonly used solvents and chemicals (Ref 6-8).

Experimental work with a coated wire-mesh fabric woven of 1.6 mil, 200 x 200 mesh, Rene 41 high-nickel, super-alloy steel wire indicates that such fabrics may be applicable to decelerator construction for higher temperature use in such devices as space vehicle drag brakes. The requirements here are for a material strong enough to carry the aerodynamic pressure loading, foldable into the launch configuration of the vehicle, and resistant to the space environment during orbit and the thermal environment during re-entry.

The severe thermal environment requires a structure which is nonporous, so that the relatively cool boundary layer is not bled off with consequent increase in heat transfer to the material. In addition, the emissivity of the metal mesh fabric must be high, so that re-entry heating can be rejected by radiation as efficiently as possible. To meet this combination of environmental factors, it has been found necessary to utilize silicone rubber, glass frit, high temperature paint, or other coatings on the wire mesh fabric.

Temperature resistance of the experimental fabrics

has been found to be generally good. The coated material retained over 80 per cent of its room-temperature tensile strength at 1000 F, and from 39 per cent to 57 per cent at 1500 F. Tests of foldability, resistance to tearing, porosity at high temperatures, thermal emissivity, and resistance to space environments indicate a favorable prognosis for the development of this type of material for space vehicle decelerator applications. (Ref 6-15)

2.2.2 LIGHTWEIGHT MATERIALS. Problems of excess bulk and weight in parachute systems arise because parachute textile specifications for webbings, tapes, and cords are so written that materials produced in accordance with their provisions usually have actual breaking strengths considerably in ex-

cess of the minimum specified (Ref 6-16). Since the designer has no choice but to use the specification minimum strength as his design point, the result is generally an over-designed system with more weight and bulk than is necessary to meet minimum requirements. This can cause problems in decelerator systems designed to fit minimum-size stowage compartments in aircraft, missiles, weapons, etc.

To help alleviate this situation, a series of nylon webbings have been designed with average breaking strengths close to the specification minimum. These webbings, with minimum weight and thickness for the specified strength, and at least 80 per cent seam efficiency, allow the decelerator system designer to choose a realistic safety factor, and at the same time

TABLE 6-2. RADIATION PROPERTIES OF PARACHUTE CLOTH (Ref 6-3)

	Normal Incident Solar Radiation			Normal Incident Black Body Radiation 350 F		
	Reflectivity	Transmissivity	Absorptivity	Reflectivity	Transmissivity	Absorptivity*
Dacron - 100 lb	0.35	0.60	0.05	0.08	0.17	0.75
Dacron - 300 lb	0.54	0.35	0.11	0.07	0.14	0.79
Dacron - 600 lb	0.61	0.27	0.12	0.07	0.07	0.86
Dacron - 800 lb	0.62	0.19	0.19	0.07	0.03	0.90
Nylon Rip-Stop 1.1 oz/yd ² (orange) MIL - C - 7020B Type I	0.23	0.64	0.13	0.05	0.19	0.76
Nylon Rip-Stop 1.1 oz/yd ² (white) MIL - C - 7020	0.27	0.65	0.08	0.06	0.21	0.73
Nylon Rip-Stop 1.6 oz/yd ² (white) MIL - C - 7020B Type III	0.22	0.72	0.06	0.07	0.21	0.72
Nylon Cloth 2.25 oz/yd ² MIL - C - 7350B Type I	0.36	0.59	0.05	0.07	0.05	0.88
Nylon Cloth 4.30 oz/yd ² MIL - C - 8021 Type I	0.44	0.48	0.08	0.07	0.06	0.87
Nylon Cloth 7.0 oz/yd ² MIL - C - 8021 Type II	0.46	0.41	0.13	0.10	0.05	0.85
Nylon Cloth 14.0 oz/yd ² MIL - C - 8021 Type III	0.62	0.27	0.11	0.10	0.04	0.86

* This value is equal to the emissivity of the material at 350 F when the monochromatic absorptivity is considered to be independent of temperature.

achieve the lowest possible weight and volume in his system. These materials have now been standardized in specification form, and are currently available for use as a Military Specification. The characteristics of each of the six types of webbing are summarized in Table 6-3.

2.2.3 LOW-COST EXPENDABLE MATERIALS. Materials which have been studied for application to low-cost expendable aerial-delivery parachutes include nylon papers, both plain and scrim-reinforced, Dacron paper, polypropylene film, "Scotchpak" film, reinforced polyethylene film, and printed cotton fabrics. Suspension-line materials used include braided

polyethylene line, braided nylon line, and braided fine and coarse filament polypropylene lines. Fortisan-reinforced polyethylene tape has been used for radial reinforcements.

The plastic films and braids perform better when the canopies are fabricated by heat sealing or cementing, rather than by sewing. Seam efficiencies close to 100 per cent have been achieved with some materials by a heat seal and adhesive process.

Air drops of experimental solid flat circular and ring slot canopies fabricated of the above materials have been made successfully with loads ranging from 300 to 1500 pounds (Ref 6-13 and 6-14).

TABLE 6-3 WEBBING, TEXTILE, WOVEN NYLON, FOR DECELERATORS
(REF 6-17) MIL-W-27657 (USAF)

Type	Break Strength, lb (min)*	Wt in oz/yd (max)	Width in.	Thickness in.
I	3000	0.90	$3/4 \pm 1/16$	0.080 - 0.095
II	4000	1.25	$1 \pm 1/16$	0.090 - 0.110
III	6000	1.65	$1 \pm 1/16$	0.100 - 0.120
IV	8700	2.40	$1 \frac{23}{32} \pm 1/16$	0.080 - 0.100
V	9000	2.40	$1 \pm 1/16$	0.175 - 0.195
VI	10000	2.70	$1 \frac{3}{4} \pm 1/16$	0.115 - 0.135

* The minimum breaking strength shall be the average of five breaking tests made on each sample.

SEC. 3 TABULATION OF PARACHUTE MATERIALS

3.1 Webbing

3.1.1 WEBBING, TEXTILE, WOVEN NYLON; MIL.-W-4088D (USAF),
15 JAN 1960; AMENDMENT 1, 27 MAY 1960
WEBBING, TEXTILE, WOVEN NYLON, IMPREGNATED; MIL.-W-
MIL.-W-27265 (USAF), 1 JAN 1960; AMENDMENT 1, 11 MAY 1960*

Type	Wt in oz/yd (max)	Width in.	Thickness in.	Break Strength lb (min)
I	0.28	$9/16 \pm 1/32$	0.025 - 0.04	500
II	0.42	$1 \pm 1/32$	0.025 - 0.04	600
III	0.52	$1\ 1/4 \pm 1/32$	0.025 - 0.04	800
IV	1.20	$3 \pm 1/8$	0.025 - 0.04	1800
VI	1.15	$1\ 23/32 \pm 1/16$	0.030 - 0.050	2500
VII	2.35	$1\ 23/32 \pm 1/16$	0.060 - 0.10	5500
VIII	1.60	$1\ 23/32 \pm 1/16$	0.040 - 0.07	3600
IX	4.00	$3 \pm 3/32$	0.065 - 0.10	9000
X	3.70	$1\ 23/32 \pm 3/32$	0.110 - 0.14	8700
XII	0.85	$1\ 23/32 \pm 1/16$	0.025 - 0.04	1200
XIII	2.90	$1\ 23/32 \pm 1/32$	0.080 - 0.12	6500
XIV	0.80	$1/2 \pm 1/32$	0.070 - 0.10	1200
XV	1.25	$2 \pm 1/16$	0.035 - 0.05	1500
XVI	2.00	$1\ 23/32 \pm 1/16$	0.045 - 0.080	4500
XVII	1.15	$1 \pm 1/32$	0.045 - 0.07	2500
XVIII	2.05	$1 \pm 1/16$	0.100 - 0.16	6000
XIX	4.10	$1\ 3/4 \pm 3/32$	0.105 - 0.13	10,000
XX	3.25	$1 \pm 3/32$	0.19 - 0.235	9000
XXI	1.70	$1\ 1/4 \pm 1/16$	0.065 - 0.085	3600
XXII	3.50	$1\ 23/32 \pm 3/32$	0.09 - 0.12	7300
XXIII	3.70	$1\ 1/8 \pm 1/32$	0.20 - 0.30	12,000
XXIV	2.25	$1\ 15/16 \pm 3/32$	0.055 - 0.075	5500
XXV	1.50	$1 \pm 1/16$	0.090 - 0.125	4500

* MIL.-W-27265 base webbings are woven to MIL.-W-4088D specifications.

Impregnated Webbing Classes: R = Resin Impregnated

L = Latex Impregnated

Additional tolerances for impregnated webbings: + 10% in weight
- 12% in thickness

Types V and XI deleted

Colors: White, olive drab, green, yellow, gray

Use: Parachutes and accessories

**3.1.2 WEBBING, TEXTILE, NYLON, TUBULAR;
MIL.-W-005625C (USAF), 12 AUG 1958**

Wt in oz./yd (max)	Width in. $\pm 1/16$	Thickness in. (max)	Break Strength lb (min)
0.50	1/2	0.090	1000
0.60	9/16	0.090	1500
0.70	5/8	0.090	1850
0.95	3/4	0.095	2300
1.30	1	0.120	3500

Color: Natural; for dyed webbing a 10% increase in maximum weight is permitted.

Identification: 1/2, 3/4 and 1" - black yarn center one side; 9/16" - black yarn center both sides; 5/8" - 2 black separated by 3 white yarns.

Use: Parachute construction

**3.1.3 WEBBING, TEXTILE, COTTON WARP; MIL.-W-5665D, 6 DEC 1956;
AMENDMENT 2, 4 FEB 1959**

Type	Wt in oz./yd (max)	Width in.	Thickness in.	Break Strength* lb (min)
I	0.40	9/16 $\pm 1/16$	0.040 - 0.050	350
II	0.75	1 $\pm 1/16$	0.040 - 0.050	575
III	0.90	1 1/4 $\pm 1/16$	0.040 - 0.050	750
IV	4.30	3 $\pm 1/8$	0.050 - 0.100	1900
V	4.30	5 $\pm 1/8$	0.050 - 0.100	3100
VI	2.10	1 3/4 $\pm 1/16$	0.070 - 0.090	1800
VII	3.00	1 3/4 $\pm 1/16$	0.140 - 0.170	2600
VIII	3.00	1 3/4 $\pm 1/16$	0.075 - 0.095	2900
IX	4.65	3 $\pm 1/8$	0.090 - 0.115	4500
X	3.50	1 3/4 $\pm 1/16$	0.130 - 0.150	5000
XII	1.25	1 3/4 $\pm 1/16$	0.040 - 0.050	1000
XIII	3.40	1 3/4 $\pm 1/16$	0.100 - 0.130	3400
XIV	4.95	3 $\pm 1/8$	0.090 - 0.120	5200
XV	3.50	1 3/4 $\pm 1/16$	0.130 - 0.150	4500
XVI	2.60	1 3/4 $\pm 1/16$	0.095 - 0.115	2700
XVII	1.25	1 $\pm 1/16$	0.075 - 0.095	1000
XVIII	1.40	2 1/2 $\pm 1/16$	0.050 - 0.060	1250

* Breaking strength of full-width webbing except for Type V; Type XI deleted.

Furnished in following classes:

Class 1A - Undyed & not fungus-proofed; Class 1B - Dyed & fungus-proofed;

Class 2A - Dyed & not fungus-proofed; Class 2B - Dyed & fungus-proofed;

Class 3 - Resin-dyed & fungus-proofed during dyeing.

Identification:

Type VII - 2 black threads at selvage; Type VIII - 2 black threads in center;

Type XV - 2 red threads at selvage; Type XVI - 2 yellow threads in center.

Color: Olive drab

Use: Parachute harness and packs

3.1.4 WEBBING, TEXTILE, NYLON, MULTIPLE
TUBULAR; MIL-W-5666A, 25 JUNE 1959

Wt in oz/yd (max)	Width in.	Thickness in.	Break Strength lb (min)	Ultimate Elong. % (min)
0.40	1 5/6 ± 1/16	0.020 to 0.025	500	20

Color: Green

Use: Parachute packs

3.1.6 WEBBING, TEXTILE, NYLON, LOCKING
LOOP; MIL-W-9049B (ASG), 22 MAR 1961

Wt in oz/yd (max)	Width in.	Break Strength lb (min)	Elong. % (min)	Length of Loop in.	Loop Strength* lb (min)
0.22	1/4 ± 1/16	400	20	1/4 ± 1/16	185

* No break below minimum specified.

Webbing in cut lengths:

Class 1 - 2 5/8 to 2 7/8

Class 2 - 3 5/8 to 3 7/8

Class 3 - 5 7/8 to 6 1/8

Color: Natural

Use: Locking & reinforcing parachute packs

3.1.5 WEBBING, TEXTILE, NYLON, HEAVY
DUTY; MIL-W-5787C, 4 APR 1957

Type	Wt in oz/yd (max)	Width ± 1/16 in.	Thickness in. (max)	Break Strength lb (min)
I	9	1 3/4	0.375	20,000
II	18	3 1/8	0.480	40,000

Use: Cargo parachute harness

Color: Natural

3.1.7 WEBBING, TEXTILE, POLYESTER*;
MIL-W-25339A (ASG), 8 FEB 1961

Type	Wt in oz/yd (max)	Width in.	Thickness in.	Break Strength** lb (min)
I	1.30	1 23/32 ± 1/16	0.040 to 0.050	1800
II	1.80	1 ± 1/32	0.110 to 0.140	3000
III	3.75	1 23/32 ± 1/16	0.125 to 0.145	8700
IV	4.35	2 ± 1/16	0.110 to 0.130	9700

* Dacron

** No break below minimum specified

Identification: Type I - 2 red threads in center of
warp. Type III - 2 green threads in center of warp

Color: Natural

Use: Parachutes for high temperature resistance

**3.1.8 WEBBING, TEXTILE, DACRON, LOW ELONGATION; MIL.-W-25361 (USAF), 28 MAR 1956;
AMENDMENT 3, 26 JUNE 1959**

Type	Wt in oz/yd (max)	Width in.	Thickness in.	Break Strength lb (min)	Elongation % (max) at		
					2500 lb	3000 lb	90% of break
I	1.65	1 23/32 ± 1/16	0.040 - 0.065	3600	18	--	----
II	2.10	1 23/32 ± 1/16	0.060 - 0.080	6000	---	13	17.5
III	2.50	1 23/32 ± 1/16	0.075 - 0.090	7000	---	12	17.5
IV	3.50	3 ± 1/8	0.065 - 0.085	8700	---	12	18.5

Color: Natural

Use: Safety belts, harnesses

**3.1.9 WEBBING, TEXTILE, WOVEN NYLON, IMPREGNATED; MIL.-W-27265 (USAF), 15 JAN 1960,
AMENDMENT 1, 11 MAY 1960.**

Types and physical characteristics identical with MIL.-W-4088D (see 3.1.1 above).

3.2 Tapes

**3.2.1 TAPE AND WEBBING, TEXTILE, REINFORCING, NYLON;
MIL.-T-5038C, 6 JAN 1960**

Type	Wt in oz/yd (max)	Width in. (± 1/32)	Thickness in.	Break Strength lb (min)	Ultimate Elongation % (min)
II Tape	0.40	1	0.025 - 0.035	900	18
	0.60	1 1/2	0.025 - 0.035	1300	18
	0.80	2	0.025 - 0.035	1700	18
III Tape	0.12	3/8	0.015 - 0.025	200	18
	0.15	1/2	0.015 - 0.025	250	18
	0.20	3/4	0.015 - 0.025	400	18
	0.30	1	0.015 - 0.025	525	18
	0.40	1 1/2	0.015 - 0.025	900	18
IV Web- bing	0.35	1/2	0.030 - 0.040	550	18
	0.40	5/8	0.030 - 0.040	625	18
	0.50	1	0.030 - 0.040	1000	18
	0.60	1 1/8	0.030 - 0.040	1100	18
	0.75	1 1/2	0.040 - 0.040	1500	18
V Tape	0.20	9/16	0.020 - 0.030	500	18
VI Tape	0.020	3/4	0.020 - 0.030	425	18

Color: Types II, III, IV and V - Natural

Type I deleted

Use: Binding and reinforcing parachute packs

3.2.2 TAPE, TEXTILE, NYLON, PARACHUTE CANOPY; MIL.-T-5608E (ASG), 8 JAN 1958;
AMENDMENT 2. 9 JUNE 1959

Class	Type	(min) No. of yd/lb	Width in.	Break Strength lb (min)	Elongation % (min)	Air Permea- bility** cfm/ft ²
A	I	1,300	0.250 ± 0.0156	13	18	--
	II	875	0.375 ± 0.0156	18	18	--
	III	440	0.625 ± 0.0312	43	18	--
	IV	260	1.250 ± 0.0625	65	18	--
	V	165	2.000 ± 0.0625	96	18	150 ± 30
B	I	970	0.250 ± 0.0156	22	18	--
	II	650	0.375 ± 0.0156	33	18	--
	III	360	0.625 ± 0.0312	70	18	--
	IV	210	1.250 ± 0.0625	120	18	--
	V	120	2.000 ± 0.0625	200	18	150 ± 30
	VI	50	5.000 ± 0.1875	100*	18	150 ± 30
C	I	770	0.250 ± 0.0156	39	22	--
	II	520	0.375 ± 0.0156	58	22	--
	III	335	0.625 ± 0.0312	90	22	--
	IV	160	1.250 ± 0.0625	185	22	--
	V	100	2.000 ± 0.0625	300	22	150 ± 30
D	I	80	1.250 ± 0.0625	280	18	--
	II	45	2.000 ± 0.0625	460	18	--
E	I	50	1.250 ± 0.0625	650	18	--
	II	30	2.000 ± 0.0625	1000	18	--
	III	22	2.000 ± 0.0625	1500	--	--
	IV	17	2.000 ± 0.0625	2000	--	--
	V	13	2.000 ± 0.0625	3000	--	--
	VI	11	2.000 ± 0.0625	4000	--	--

* lb/in. of width

** Applicable to dyed and undyed ribbon

Class: A - Extra light weight

B - Light weight

C - Medium weight

D - Heavy weight

E - Extra heavy weight

Color: Natural

Class B Type VI -

Orange

Class C Type V -

Yellow

Use: Fabrication of ribbon parachutes

3.2.3 TAPE AND WEBBING, TEXTILE, COTTON,
REINFORCING, WOVEN; MIL-T-5661B,
22 MAY 1956

Type	Wt in oz/yd (max)	Width in. $\pm 1/32$	Weave	Strength* lb (min)
I	0.11	1 4	Plain	80
	0.15	3 8		120
	0.22	1 2		150
	0.28	5 8		170
	0.33	3 4		200
	0.47	1		250
II	0.15	1 2	Double Herring- bone	110
	0.22	3 4		165
	0.29	1		220
	0.36	1 1/4		275
	0.43	1 1/2		330
	0.50	1 3/4		375
III	0.10	1 2	Twill	45
	0.12	5 8		55
	0.14	3 4		75
IV	0.30	3 4	Double	115
	0.40	1		150
	0.45	1 1/8		165
	1.20	1 1/4		590
	0.60	1 1/2		215
V	0.65	1	Plain (Trans- verse cord)	350
	1.30	2		650

* Full Width

Color: Unbleached (natural)

Use: Type I - Reinforcing tape on fabric; Type II,
III, IV, V - binding and reinforcing parachute
packs.

3.2.4 TAPE, TEXTILE (PARACHUTE CON-
STRUCTION); MIL-T-5663A, 12 NOV 1952;
AMENDMENT 1, 26 JAN 1953

No. of yd/lb		Width in.		Thickness in.		Strength lb (min)	Elong. % (min)
min	max	min	max	min	max		
110	130	15/16	1-1/16	0.010	0.030	300	14

Color: Natural

Use: Reinforcing bands

3.2.5 TAPE, TEXTILE, NYLON, PARACHUTE
CONSTRUCTION; MIL-T-6134B, 20
APR 1960

Type	Wt in oz/yd (max)	Width in. $\pm 1/16$	Thickness in.	Break Strength lb	Elong. % (min)
I	0.40	1	0.025 to 0.045	525	16
II	0.145	1	0.010 to 0.030	300	14

Color: Natural

Use: Type I - Skirt bands

Type II - Reinforcing bands

3.2.6 TAPE AND WEBBING, TEXTILE, WOVEN,
NYLON; MIL-T-8363A, 14 APR 1958;
AMENDMENT 1, 17 MAY 1960

Type	Wt in oz/yd	Width in.	Thickness in.	Break Strength lb (min)
I	0.08 (min)	5/16 $\pm 1/32$	0.030 to 0.040	350
II	0.09 (min)	7/16 $\pm 1/32$	0.020 to 0.030	290
III	0.50 (max)	3/4 $\pm 1/16$	0.050 to 0.060	400
IV	1.05 (max)	3/4 $\pm 1/16$	0.070 to 0.085	2600
V	0.70 (max)	25/32 $\pm 2/32$	0.050 to 0.060	1000

Type I and II - Tape

Type III, IV and V - Webbing

Color: Green

3.3 Cords

3.3.1 CORD, RAYON, WITHOUT CORE, BRAIDED; MIL.-C-4232A (USAF), 29 JULY 1954

Type	No. of yd/lb (min)	Break Strength lb (min)	Elongation % (min)
I	42	400	14
II	20	1000	12
III	13	1500	—

Color: Natural, orange, or as specified
Use: Cargo parachute suspension lines

3.3.2 CORD, NYLON; MIL.-C-5040B (ASG), 6 FEB 1958

Type	No. of yd/lb (min)	Break Strength lb (min)	Elongation % (min)
I	350	100	30
IA	350	100	30
II	105	375	30
III	75	550	30
IV	55	750	30

Type II—One black yarn

Age: Max, 2 years from manufacture to delivery

Color: Natural, or olive drab

Use: Parachute suspension lines

3.3.3 CORD, NYLON, CORELESS; MIL.-C-7515B (USAF), 1 MAY 1959; AMENDMENT 1, 29 JUNE 1960

Type	No. of yd/lb (min)	Break Strength lb (min)	Elongation % (min)
I	110	400	20
II	85	550	20
III	50	750	20
IV	40	1000	—
V	25	1500	—
VI	20	2000	—
VII	15	2400	—
VIII	12	3000	—
IX	9	4000	—
X	7.5	5000	—
XI	160	300	20
XII	4.0	10000	—
XIIa	4.0	10000	—

Color: Olive drab (except XI—natural white),
and black

Use: Personnel and cargo parachutes

3.4 Threads

3.4.1 THREAD, COTTON, HIGH-TENACITY; MIL.-T-5660A (ASG), 20 NOV 1953; AMENDMENT 1, 12 NOV 1954

Style	Size	Break Strength lb (min)		No. of yd/lb (min)	
		Type I	Type II	Type I	Type II
A	3	15.0	16.0	1850	1775
	4	20.0	21.0	1250	1200
	5	30.0	31.0	900	860
	6	36.0	37.0	750	720
	7	40.0	41.0	650	625
	8	44.0	45.0	550	525
	9	51.0	57.0	530	500
	10	58.0	62.0	500	480
	25	12		2400	
	30	10		2800	
B	35	8 1/2		3300	
	40	7 1/2		3800	
	50	6		4750	

(See notes on next page)

(Notes for 3.4.1)

Type I—soft finish

Type II—polished finished

Twist: Left-hand or "Z" twist

Style: A—Lockstitch twist thread

B—Stitching thread

Color: As specified

Use: Parachute harness

3.4.2 THREAD, NYLON; MIL-T-7807B,
4 DEC 1958; AMENDMENT 1, 11 SEP 1959

Type	Thread/ Cord Size	No. of yd/lb (min)	Break Strength lb (min)	Elongation at Break % (max)	
				Class 1	Class 2
I	0000	45,200	0.85	22	33
	000	29,500	1.30	22	33
	00	25,800	1.85	22	33
	A	16,900	2.75	22	33
	B	8,200	5.50	22	33
	E	5,600	8.50	22	33
	F	3,750	11.00	22	33
	FF-1	3,500	14.00	22	33
	FF	2,725	16.00	22	33
	FFF	2,900	17.00	22	40
	No. 3	1,800	24.0	22	40
	No. 4	1,300	32.0	22	40
	No. 5	1,000	40.0	22	40
	No. 6	850	50.0	22	40
	No. 7	725	60.0	22	40
	No. 8	625	68.0	22	40
	No. 9	550	80.0	22	40
	No. 10	450	90.0	22	40
II	0000	40,000	0.85	22	33
	000	26,000	1.30	22	33
	00	23,000	1.85	22	33
	A	15,000	2.75	22	33
	B	7,375	5.50	22	33
	E	5,000	8.50	22	33
	F	3,350	11.00	22	33
	FF-1	3,150	14.00	22	33
	FF	2,450	16.00	22	33
	No. 3	1,600	24.0	22	40
	No. 4	1,200	32.0	22	40
	No. 5	950	40.0	22	40
	No. 6	775	50.0	22	40
	No. 7	650	60.0	22	40
	No. 8	575	68.0	22	40
	No. 9	500	80.0	22	40
	No. 10	450	90.0	22	40

Type	Thread/ Cord Size	No. of yd/lb (min)	Break Strength lb (min)	Elongation at Break % (max)	
				Class 1	Class 2
III	0000	49,000	0.85		40
	000	34,400	1.30		40
	00	23,900	1.85		40
	A	16,350	2.75		40
	AA	13,300	3.40		40
	B	8,000	5.50		40
	E	5,200	8.50		40
	F	3,850	11.00		40
	FF-1	3,500	14.00		40
	FF	2,500	16.00		40
	No. 3	1,700	24.0		40
	No. 4	1,300	32.0		40
	No. 5	1,000	40.0		40
	No. 6	850	50.0		40
IV	No. 7	725	60.0		40
	No. 8	625	68.0		40
	No. 9	600	80.0		40
	No. 10	510	90.0		40
V	A	13,000	3.50		40
	C	8,900	5.75		40
	E	4,300	11.00		40
V	6	2,320	20.00		40
	8	2,920	16.00		(max)
	10	3,310	14.00		
	12	4,180	11.20		

Type I—Machine twist

Type II—Twisted bonded multicord

Type III—Bonded monocord (not for use in flight
safety equipment)

Type IV—Waxed hand sewing twist (not for use in
flight safety equipment)

Type V—Buttonhole twist (not for use in flight
safety equipment)

Color: Conform to standard

Use: Sewing nylon materials

3.4.3 THREAD, POLYESTER*; MIL-T-40040A,
31 MAR 1960; AMENDMENT 1, 28 SEPT 1960

Class	Letter/ Number Size	Final Ply	No. of yd/lb (min)	Break Strength lb (min)	Elong- ation %(max)	Class	Letter/ Number Size	Final Ply	No. of yd/lb (min)	Break Strength lb (min)	Elong- ation %(max)
							3	3	1,620	24	15
							4	3	1,230	32	15
							5	3	1,010	40	15
							6	3	810	48	15
							7	3	700	54	15
							8	3	630	60	15
							8	5	630	60	15
							9	3	590	65	15
							10	6	550	70	15
1	00	2	26,500	1.4	25						
	A	3	17,600	2.0	25						
	AA	2	13,200	3.0	25						
	B	3	8,500	4.3	25						
	B	2	8,500	4.3	25						
	SB 2/	2	9,000	6.0	20						
	E	3	5,700	8.0	20						
	F	4	4,200	10.6	20						
	FF	3	2,600	16.0	20						
	3	3	1,800	24	15						
	4	3	1,370	32	15						
	5	3	1,120	40	15						
	6	3	900	48	15						
	7	3	780	54	15						
	8	3	680	60	15						
	8	5	680	60	15						
	9	3	660	65	15						
	10	3	590	70	15						
	10	6	590	70	15						
						3	00	2	21,200	1.25	15
							A	3	13,650	1.90	35
							B	3	7,000	3.80	
							E	3	4,550	6.80	
							F	3	3,500	7.60	
							3	3	1,450	20.40	15
							4	3	910	27.25	35
							5	3	700	34.00	
							6	3	600	41.00	
							7	3	515	47.70	
2	00	2	23,800	1.5	25						
	A	3	15,800	2.3	25						
	AA	2	11,900	3.0	25						
	B	3	7,600	4.5	25						
	B	2	7,600	4.5	25						
	E	3	5,100	8.0	25						
	F	4	3,800	10.0	25						
	FF	3	2,300	16.0	25						

* Dacron

Finish:

Class 1 - Soft Finish

Class 2 - Bonded Finish

Class 3 - Heat Stable - Soft finish

Color: Conform to shade standard

Use: Class 1 and 2 - Machine sewing of clothing,
tentage, equipage, etc.

Class 3 - Parachutes

3.5 Cloths (Canopy)

3.5.1 CLOTH, COTTON, MUSLIN; MIL-C-4279A (USAF), 21 JULY 1953

Type	Wt in oz/yd ²	Width in.	Strength (min)				Air Perme- ability cfm/ft ²	Seam Eff % (min)
			Break, lb/in.		Tear, lb			
			Warp	Fill	Warp	Fill		
I	5.0-6.0	37	50	55	6	3	125 ± 35	--
II	3.7-4.6	37	48	42	4	2 1/2	200 ± 30	90

Weave: Plain

Use: Cargo Canopies

3.5.2 CLOTH, NYLON, PARACHUTE; MIL-C-7020D, 19 SEPT 1960

Type	Wt in oz/yd ² (max)	Thickness in. (max)	Strength, lb (min)				Elongation (both directions) % (min)	Air Perme- ability ₂ cfm ft ²	Weave
			Break (Ravel Strip)		Tear (Tongue				
			Warp	Fill	Warp	Fill			
I	1.1	0.0032	42	42	5	5	20	100 ± 20	Ripstop
II	1.6	0.0042	50	50	4	4	20	130 ± 30	Twill
III	1.6	0.0042	50	50	4	4	20	130 ± 30	Ripstop

Color: Natural, white, olive green, orange, sand

Width: 36.5 ± 0.5 in.

Use: Canopies

3.5.3 CLOTH, NYLON, PARACHUTE, CARGO; MIL-C-7350C (ASG), 10 OCT 1957; AMENDMENT 1, AUG 1958

Type	Wt in oz/yd ² (max)	Thickness in. (max)	Strength (min)				Ultimate Elongation % (min)		Air Permeability cfm/ft ²	
			Break, lb/in.		Tear, lb		Warp	Fill	Warp	Fill
			Warp	Fill	Warp	Fill				
I	2.25	0.0060	90	90	10	10	25	25	100	150
II	3.50	0.014	135	125	30	30	25	25	150	200

Bolt Width: 36 1/2 ± 1/2 in.

Color: Natural

Use: Cargo Parachute Canopies

3.5.4 CLOTH, RAYON, PARACHUTE (NONPERSONNEL); MIL-C-8006A (ASG), 20 SEPT 1955

Type	Wt in oz/yd ² (max)	Strength (min)				Elongation % (min)	Air Permeability cfm/ft ²
		Break, lb/in.		Tear, lb			
		Warp	Fill	Warp	Fill		
I							
II	4.25	85	80	10	10	15	150 ± 30
III	4.50	80	80	10	10	15	150 ± 30
Class 1	8	145	135	30	30	18	180 ± 40
Class 2	4.50	75	70	10	10	15	150 ± 30
Class 3	1.50	25	25	2	2	18	200 ± 40

Color: As specified

Type I—High tenacity

Type II—Semi-high tenacity

Type III—Regular tenacity

Use: Type I, II, III

Class 1 and 2—Aerial delivery parachutes

Type III

Class 2—Parachutes for radio equipment

Not for personnel parachute

3.5.5 CLOTH, NYLON, PARACHUTE, DRAG; MIL-C-8021B (ASG), 6 FEB 1958; AMENDMENT 1, 17 APR 1959

Type	Wt in oz/yd ² (max)	Thickness in. (min)	Strength (min)				Elongation % (min)		Air Perme- ability cfm/ft ² (1/2" H ₂ O)
			Break, lb/in. (Ravel Strip)		Tear, lbs (Tongue)		Warp	Fill	
			Warp	Fill	Warp	Fill			
I	4.75	0.020	200	200	15	15	25	25	50 – 90
II	7.00	0.024	300	300	20	20	25	25	50 – 90
IIa	10.5	0.025	500	500	75	75	35	35	50 – 90
III	14.00	0.035	600	600	75	75	25	25	15 – 55

Air permeability (At)

cfm/ft², 20" H₂O:

Type I - 450-650

Type II - 450-650

Type IIa - 650-750

Type III - 250-450

Width: 36 1/2 ± 1/2 in.

Color: Natural white Use: Drag, brake and cargo parachutes

3 5.6 CLOTH, DACRON, DRAG PARACHUTE; MIL-C-25174 (USAF), 29 JUNE 1956

Type	Wt in oz/yd ² (max)	Break, lb/in. (Ravel Strip)		Tear, lb (Tongue)		Elongation % (min)		Air Permeability cfm/ft ²	Shrinkage % (max)	
		Warp	Fill	Warp	Fill	Warp	Fill		Warp	Fill
I	1.80	45	45	5	5	20	20	100-160	2.0	2.0
II	2.90	100	100	7.5	7.5	20	20	100-160	2.0	2.0
III	3.00	85	85	10	10	20	20	100-160	2.0	2.0
IV	3.90	135	135	15	15	25	25	140-190	2.0	2.0

Weave: Type I - 2 up, 1 down, right hand twill; others plain

Aging: Break not less than 95% of original. Tearing not less than table values. Permeability not more than 15% of unaged

Color: Natural Width: 36 1/2 ± 1/2 in. Use: Drag parachutes

3.5.7 CLOTH, DACRON, PARACHUTE; MIL-C-25312 (USAF), 19 SEPT 1956

Wt in oz/yd ² (max)	Width in. ± 1/2	Thickness in. (max)	Strength (min)				Elongation % (min)		Air Perme- ability cfm/ft ²
			Break, lb/in. (Ravel Strip)		Tear, lb (Tongue)				
			Warp	Fill	Warp	Fill	Warp	Fill	
5.0	36 1/2	0.015	190	190	14	14	30	30	50-80

Weave: 2-up, 2-down right-hand twill

Aging: Break not less than 95% of original. Tear not less than table values. Permeability not more than 15% of unaged

Color: Natural Use: Canopies

3.6 Cloths (Parachute Pack)

3.6.1 CLOTH, COTTON, DUCK, UNBLEACHED, PLIED YARNS (ARMY & NUMBERED); CCC-C-419, 30 JULY 1956; AMENDMENT 1, 4 APRIL 1957

Type	Texture	Number/ Comm Design- ation	Wt in oz/yd ² (min)	Break Strength lb (min)		Air Permeability cfm/ft ² (max)
				Warp	Fill	
I	Hard	12/0	48.00	800	430	—
		8/0	40.00	800	665	—
		2/0	31.90	465	435	—
		1/0	30.31	450	405	—
		1	28.71	440	370	2
		2	27.12	420	345	—
		3	25.53	390	330	2
		4	23.93	375	300	2
		5	22.33	345	285	—
		6	20.74	335	250	2
		8	17.55	285	210	2
		10	14.35	245	160	4
		11	12.75	240	140	—
		12	11.16	195	120	4
	Medium	1	28.71	425	345	—
		2	27.12	410	320	—
		3	25.53	370	315	—
		4	23.93	350	290	—
		5	22.33	315	285	—
		6	20.74	305	250	—
III			8.25	125	120	—
			9.85	160	110	—
			12.29	210	130	4
			14.77	235	175	—
			15.90	245	200	—
			18.48	315	200	—

Type I — Numbered Duck Type III — Army Duck

3.6.2 CLOTH, NYLON, DUCK, PLIED YARNS, FOR PARACHUTE PACKS; MIL-C-7219B, 19 MAR 1958; AMENDMENT 1, 11 APRIL 1960

Type	Wt in oz/yd ² (max)	Strength (min)				Air Perme- ability cfm/ft ² (max)	Shrinkage % (max)	
		Break, lb/in. (Ravel Strip)		Tear, lb (Tongue)			Warp	Fill
		Warp	Fill	Warp	Fill			
I	9.50	400	300	35	45	5.0	2.5	2.0
II*	8.75	400	150	35	20	5.0	2.5	2.0
III	7.25	325	275	20	20	8.0	2.0	2.0

* Not applicable for Air Force procurement

Color: Type III — Sage Green Use: Parachute packs

REFERENCES

- (6-1) Mileaf, H. (ed), Handbook of Fibrous Materials. WADD TR 60-584, Oct 1960, AD 249782.
- (6-2) McCarthy, J. (ed), Handbook of Parachute Textile Materials and Properties. WADC TR 55-264, Feb 1956, AD 89171.
- (6-3) Hartnett, J.P., et al., Values of the Emissivity and Absorptivity of Parachute Fabrics. WADC TN 57-433, Dec 1957, AD 151072.
- (6-4) Engholm, E., et al, Instantaneous Local Temperatures of Aerodynamic Decelerators, Part I. WADD TR 60-670, Part I, Feb 1961.
- (6-5) Engholm, E., et al., Instantaneous Local Temperatures of Aerodynamic Decelerators, Part II. WADD TR 60-670, Part II, Feb 1961.
- (6-6) Ruoff, A.L., et al., Aerodynamic Heating of Parachutes. WADC TR 57-157, Dec 1957, AD 142261.
- (6-7) Schoeck, P.A., Experimental Studies for Determining Heat Transfer on the Ribbons of FIST Type Parachutes. WADC TN 59-345, Feb 1960, AD 235922.
- (6-8) Little, C.O., Jr., Thermal and Gamma Radiation Behavior of a New High Temperature Organic Fiber. WADD TN 60-299, Dec 1960.
- (6-9) Cornish, R.H., et al., Mass Transfer Cooling of Parachute Materials. WADC TR 58-684, Sep 1959, AD 229441.
- (6-10) Coplan, M. J., A Possible Application of Organic Fibers in High Temperature Environment. WADD TR 60-9, June 1960, AD 243905.
- (6-11) Johnson, D. E., et al., Candidate Materials for High Temperature Fabrics. WADC TR 59-155, Sep 1959, AD 232975.
- (6-12) Lamberton, W. A., et al., Continuous Filament Ceramic Fibers. WADD TR 60-244, June 1960.
- (6-13) Ruprecht, F. A., et al., A Study of Design and Materials for Development of Low Cost Aerial Delivery Parachutes. WADC TR 59-385, Sep 1959, AD 237460.
- (6-14) Ruprecht, F. A. and Prima, C. D., A Study of Design and Materials for Low Cost Aerial Delivery Parachutes. Technical Report II. Cook Research Laboratories, Contract AF 33(616)-6009, Parachute Section, Crew Equipment Branch, ASD, Apr 1961.
- (6-15) Study of a Drag Brake Satellite Recovery System, Results of Phase I. WADD TR 60-775, Jan 1961, AD 254673.
- (6-16) Jailer, R. W., et al., Analysis of Heavy Duty Parachute Reliability. WADD TR 60-200, June 1960, AD 246490.
- (6-17) McGrath, J. C., Fibrous Materials for Decelerators and Structures. ASD TN 61-59, May 1961.

BIBLIOGRAPHY

- Baker, A. and Swallow, J. E., Impact Testing of Textile Yarns, Part I, Experiments with a Falling Weight Method. Tech Note Chem 1355, Royal Aircraft Establishment (Great Britain), Nov 1959, AD 232617.
- Bickford, H. J., Development of 0.9-oz. Nylon Parachute Cloth. WADC TR 53-351, Sep 1953, AD 26850.
- Bickford, H. J., et al., Development of Dacron Parachute Materials. WADC TR 55-432, Feb 1956.
- Bickford, H. J., et al., The Development of High Strength Nylon Parachute Fabrics. WADC TR 55-465, May 1956, AD 101948.
- Block, L. C., Aerodynamic Heating of Parachute Ribbons. WADC TR 54-572, Nov 1955, AD 91772.
- Block, L.C., Evaluation of Fabric Finishes for High Temperature Operation of Parachute Ribbons. WADC TR 54-571, Nov 1955, AD 91084.
- Brandt, H. H. and Linden, L., Effects of Picks per Inch and Finishing Procedures on the Properties of 1.1-ounce Nylon Ripstop Parachute Fabric. Textile Series Report No. 113, Quartermaster Research and Engineering Command, June 1960, AD 241246.
- Cates, D. M., A Study of the Effects of Chemicals on the Properties of Parachute Fabrics. WADC TR 55-340, Supplement 1, Nov 1956, AD 110524.
- Cates, D. M., A Study of the Effects of Chemicals on the Strengths of Nylon and Dacron Parachute Fabrics. WADC TR 56-288, Nov 1956, AD 110558.
- Chu, C. C., et al., Development of High Tenacity Heat Stable Dacron Parachute Items. WADC TR 57-765, May 1958, AD 155511.
- Chu, C. C., et al., Development of Improved Nylon Webbing. WADC TR 58-509, Apr 1959, AD 211911.
- Chu, C. C., et al., Investigation of the High Speed Impact Behavior of Fibrous Materials, Part I, Design and Apparatus. WADD TR 60-511, Part I, Sep 1960, AD 247493.
- Coplan, M. J., A Study of the Effect of Temperature on Textile Materials. WADC TR 53-21, Part 1, May 1953.
- Coplan, M. J. and Block, M. G., A Study of Parachute Seam Design Criteria, Part I, Investigation of the Strength of Nylon and Rayon Cloth Seams. WADC TR 56-313, Part I, June 1956, AD 110407.
- Coplan, M. J. and Singer, E., A Study of the Effect of Temperature on Textile Materials. TR 53-21, Part 2, July 1953.
- Coskrew, R. J. and Constantine, T. T., Development of High Tenacity-Heat Stable Dacron Yarns. WADC TR 55-297, Sep 1956, AD 97242.
- Eckert, E. R. G., et al., Transient Temperatures of Parachutes During Descent. WADC TN 57-320, Aug 1957, AD 142300.
- Eirich, F. R. and Saad, I., Improvement of Thermal

Stability of Textile Fibers. Progress Report No. 8, Annual Summary, Contract N140(132)577513, Polytechnic Institute of Brooklyn for U. S. Navy Supply Research and Development Facility, July 1957 - 30 June 1958, AD 213554.

Kaswell, E. R. and Coplan, M. J., Development of Dacron Parachute Fabrics. WADC TR 55-135, Sep 1956, AD 97241.

Klein, W. G., et al., Development of Design Data on the Mechanics of Air Flow Through Parachute Fabrics. WADC TR 56-576, Sep 1957, AD 131055.

Klein, W. G., et al., Research Program for the Development of a Design Procedure to Engineer Parachute Fabrics. WADC TR 58-65, May 1958, AD 155517.

Krizik, J. G., et al., Design Data on Biaxial Forces Developed in Parachute Fabrics. WADC TR 57-443, Dec 1957, AD 142208.

Landis, M. B. and Fraim, F. W., Development of Coreless Type Braids for Use in Personnel Parachute Suspension Lines. WADC TR 58-410, Dec 1958, AD 206891.

Lavrakas, V., The Effect of Fabric Structure on the Frictional Fusion of Parachute Materials. WADC TR 54-570, Aug 1955, AD 90859.

Lavrakas, V. and Katz, A., The Effect of Surface Finishes on Friction and Fusion of Parachute Cloth and Line. WADC TR 54-323, Part 1, Dec 1955, AD 91910.

Lavrakas, V. and Katz, A., The Effect of Surface Finishes on Friction and Fusion of Parachute Cloth and Line. WADC TR 54-323, Part 2, Oct 1955, AD 91873.

Lith, J. T., et al., Evaluation of Textile Components of Overage T-7A Reserve Parachutes. Textile Engineering Laboratory Report No. 245, Quartermaster Research and Engineering Command, May 1959.

Little, C. O., Jr., Amount of Deterioration Present in Parachutes Manufactured Over 15 Years Ago. WADC TN 59-30, Feb 1959.

Little, E. F., An Evaluation of Fungicidal Treatments in Cotton Cargo Parachute Webbing Stored at College, Alaska. WADC TR 56-384, Part II, Aug 1958, AD 155857.

McGrath, J. C., Symposium on Parachute Textiles. WADC TR 54-49, July 1954, AD 4978.

McGrath, J. and Johnson, R. H., The Effects of Gamma Radiation on Textile Materials. WADC TR 56-15, Feb 1956, AD 92044.

Miller, C. R., A Study of Parachute Seam Design Criteria, Part II, Investigation of the Strength of Nylon Webbing Joints. WADC TR 56-313, Part II, June 1956, AD 110406.

Muse, J. W., Jr., A Study of the Effect of Temperature on Parachute Textile Materials. WADC TR 54-117, July 1954, AD 55667.

Neff, R. J., The Development of Current Nylon Webbing Utilizing 840 Denier Yarns in Lieu of Now-Specified 210 Denier Yarns. WADC TR 55-494, May 1956, AD 102826.

Neff, R. J., Development and Evaluation of Webbing Made From Nylon 6. WADC TR 57-538, Mar 1958, AD 151090.

Serbin, J. and Becker, H., The Design and Evaluation of Heat Stabilized Tapes and Webs. WADC TR 60-252, Oct 1960, AD 249409.

Seshadri, C. V., et al., Air Flow Characteristics of Parachute Fabrics at Simulated High Altitudes. WADC TR 59-374, Mar 1960.

Sublette, R. A., The Effect of Five Synthetic Lubricants on USAF Fabrics. WADC TR 55-379, May 1956, AD 100696.

Sweeney, J. W., Evaluation of Antistatic Agents on Nylon Parachute Cloth. WADC TR 54-513, Sep 1955, AD 90581.

Templeton, J. G., A Study of the Effects of Chemicals on the Properties of Parachute Fabrics. WADC TR 55-340, Sep 1956, AD 97243.

Thomson, G., et al., Research and Development of Abrasion Resistant Treatments for Nylon Webbing. WADC TR 56-151, Jun 1956, AD 103961.

Thomson, G., et al., Research and Development of Abrasion Resistant Treatments for Dacron Webbing. WADC TR 55-313, July 1956, AD 97103.

Walcox, W. S., Deterioration of Textile Materials by Ultraviolet Light. WADC TR 60-510, Oct 1960, AD 249237.

Williams, R. B. and Benjamin, R. J., Analysis of Webbing Impact Data and Determination of Optimum Instrumentation to be Used in Conjunction with the Impacting of Webbing. WADC TR 59-694, Mar 1960.

Impact Behavior of Textile Materials. Final Report MIT-DSR No. 5-7426, Textile Division, Mechanical Engineering Department, MIT, Aug 1957, AD 139272.

Materials for Parachutes and Retardation Devices. Notes on Special Summer Program. MIT, 20-31 July 1959.

CHAPTER 7

DESIGN OF DEPLOYABLE AERODYNAMIC DECELERATORS AND DEPLOYABLE AERODYNAMIC DECELERATOR SYSTEMS

Table of Contents

<i>Section</i>	<i>Page</i>
1 OPERATIONAL CONSIDERATIONS	363
2 AERODYNAMIC DECELERATOR SYSTEM DESIGN CONSIDERATIONS	363
2.1 System Performance Considerations	363
2.1.1 Drag Loading	363
2.1.2 Trajectory Control	365
2.1.3 Stability	365
2.1.4 Reliability	365
2.2 Parachute Canopy Performance Considerations	366
2.2.1 Canopy Drag	366
2.2.2 Canopy Stability	367
2.2.3 Critical Canopy-Opening Conditions	367
2.2.4 Canopy Geometry	368
2.2.5 Canopy Porosity	369
2.2.6 Canopy Strength	369
2.2.7 Canopy Drag Efficiency	369
2.2.8 Canopy Weight and Volume	370
2.3 Parachute Canopy Deployment and Opening	370
2.3.1 Deployment Methods	371
2.3.2 Forced Canopy-Opening	372
2.4 Deployment Bags, Packs, Pressure Packing	372
2.4.1 Deployment Bags	372
2.4.2 Packs	372
2.4.3 Pressure Packing	372
3 AERODYNAMIC DECELERATOR SYSTEM DESIGN DETAILS	374
3.1 Parachute Canopy	374
3.1.1 Drag-Producing Surface	374
3.1.2 Gore Design	377
3.1.3 Suspension Lines	377
3.1.4 Canopy Design Factors	378
3.1.5 Flat Circular Canopy	379
3.1.6 Guide-Surface Type Canopies	379
3.1.7 Extended-Skirt Type Canopy	381
3.1.8 Ribbon Canopy	381
3.1.9 Conical Ribbon Canopy	382
3.1.10 Ring-Slot Canopy	384
3.1.11 Shaped-Gore Canopies	385
3.2 Pocket Bands	386

<i>Section</i>	<i>Page</i>
3 AERODYNAMIC DECELERATOR SYSTEM DESIGN DETAILS (<i>Cont'd</i>)	
3.3 Risers	386
3.4 Keeper	389
3.5 Deployment Bags	389
3.5.1 Deployment Bag Design	390
3.6 Pilot Chutes	392
<i>References</i>	393
<i>Bibliography</i>	394

Illustrations

<i>Number</i>		<i>Page</i>
7-1	Rate of Descent vs Canopy Loading for Terminal Velocity Conditions	364
7-2	Boundary Curves for Horizontal Ribbon Strength of a Flat Circular Ribbon-Type Canopy	365
7-3	Inflated Profile of Typical Circular Canopy	366
7-4	Parachute Pack Density vs Pack Pressure	373
7-5	Inflated Profile of Flat Circular Canopy	376
7-6	Effect of Suspension Line Length on Projected Diameter for Flat Circular Canopy and on Drag Coefficient for Various Canopy Types	378
7-7	Flat Circular Canopy	379
7-8	Personnel Guide-Surface Canopy	380
7-9	Ribbed Guide-Surface Canopy	380
7-10	Layout for Roof Panel, Guide-Surface Panel, and Rib for Stabilization Ribbed Guide-Surface Canopy	381
7-11	Ribless Guide-Surface Canopy	381
7-12a	Pattern-Dimension Factors for Ribless Guide-Surface Canopy	382
7-12b	Pattern-Dimension Factors for Ribless Guide-Surface Canopy (Ratios)	383
7-13	Pattern-Dimension Factors for Modified Ribless Guide-Surface Canopy	384
7-14	Extended-Skirt Canopy	385
7-15	Flat Circular Ribbon Canopy	385
7-16	Gore Construction of Flat Circular Ribbon Canopy	385
7-17	Total Porosity vs Canopy Diameter for Flat Circular Ribbon Canopies	386
7-18	Typical Geometry and Inflated Profile of Conical Ribbon Canopy	387
7-19	Ring-Slot Canopy	387
7-20	Gore Construction of Ring-Slot Canopy	387

Illustrations (Cont'd)

Number		Page
7-21	Total Porosity vs Canopy Diameter of Ring-Slot Canopies	388
7-22	Shaped Gore Canopy Layout	388
7-23	Pocket-Band Design for Flat Canopy	388
7-24	Effect of Bolt Diameter on Efficiency of 3000-lb Webbing Loops	389
7-25	Typical Keeper Design	389
7-26	Deployment Bag, Aerospace Vehicle Recovery	390
7-27	Deployment Bag with Laced Gusset for Pressure-Packed Canopy	391
7-28	Deployment Bag and Line Stowage Flaps	392
7-29	Pilot Chute Type MA-1	392

Tables

7-1	Canopy Design Factors	370
7-2	Constants a and b for Various Canopy Types and Canopy Materials	371
7-3	Comparison of Pack-Density Values with Canopy Packing Methods	374
7-4	Comparison of Pressure Packing Methods	375
7-5	Ribbon-Parachute Material Strength Requirements	376
7-6	Material-Strength Requirements for Other than Ribbon Parachutes	376
7-7	Pilot Chute Data	393
7-8	Ratios of Pilot Chute to Main Canopy Area	393

CHAPTER 7

DESIGN OF DEPLOYABLE AERODYNAMIC DECELERATORS AND DEPLOYABLE AERODYNAMIC DECELERATOR SYSTEMS

Operational requirements for deployable aerodynamic decelerator systems are continually expanding, necessitating a concurrent advancement of the state-of-the-art in decelerator design. New and complex deployable aerodynamic decelerator performance parameters are encountered with almost every new application. It is the task of the designer, utilizing both proven and theoretical design criteria, to provide a design which appears analytically to have the best chance of attaining the necessary performance requirements. However, deployable aerodynamic decelerator performance parameters are subject to conditions of application which, in the end, may be so diverse that the determination of the success with which the design is carried out usually becomes a matter for statistical evaluation over a considerable period of time. Thus, after an aerodynamic decelerator design has been completed and the drag device and associated components manufactured, tests should be conducted to verify their performance and design characteristics. This chapter presents the most important design criteria for textile parachutes, together with a variety of design details applicable to their fabrication.

SEC. 1 OPERATIONAL CONSIDERATIONS

For each parachute application, performance requirements of the parachute-load system must be defined quantitatively in terms of maxima and minima. Generally, the knowledge of (1) Gross load range, (2) Deployment speed range, and (3) Deployment altitude range will be necessary to determine the strength characteristics required of the parachute. Reliable performance of the aerodynamic decelerator may be defined loosely, with respect to these parameters, as the percentage by which the maxima and minima specified may be exceeded without resulting failure. In addition to the operational conditions above, the limits of a number of other operational characteristics must be known to allow determination of decelerator type and size, and system variation possibilities:

- (a) Rate of descent;
- (b) Oscillation;
- (c) Allowable g -force on load;
- (d) Allowable weight of aerodynamic decelerator;
- (e) Allowable volume of aerodynamic decelerator.

SEC. 2 AERODYNAMIC DECELERATOR SYSTEM DESIGN CONSIDERATIONS

The major design considerations involved in the selection of any deployable aerodynamic decelerator include:

- (a) Characteristics of the aerodynamic decelerator itself; drag coefficient and stability and their change with velocity and wake; rapidity of canopy or drag device inflation; squidding and critical opening speed; opening shock; maximum deployment speed.
- (b) Limitation of space, shape, and weight, as determined by the application.
- (c) Method of deployment and snatch force.
- (d) Component reliability in light of overall system reliability.
- (e) Initial cost.
- (f) Maintenance cost.
- (g) System variation possibilities, including: ground shock absorption devices to permit an increase in rate of descent by supplying required load impact attenuation; reefing control for opening shock reduction or drag variation; aerodynamic decelerator clustering or staging; automatic timers, disconnects and other special devices; and the effect, if any, of load configuration on aerodynamic decelerator behavior during deployment or descent.

2.1 System Performance Considerations.

2.1.1 DRAG LOADING. Aerodynamic decelerator drag or canopy loading is defined as the ratio of drag force to the drag area of the decelerator. The canopy loading under terminal-velocity conditions is the ratio of total weight (F equals W) to the drag area ($C_D S$)_{o.p.} Under terminal-velocity conditions, a given canopy

loading will always result in the same rate of descent, independent of canopy size or weight involved:

$$(7-1) \quad v_c = \sqrt{\frac{2W_t}{(C_D S)_{o,p}}} = \sqrt{\frac{W_t}{(C_D S)_{o,p}}} \sqrt{\frac{2}{\sigma \rho_o}} \\ = \sqrt{\text{Canopy Loading}} \sqrt{\frac{2}{\sigma \rho_o}}$$

Typical canopy loadings versus rate of descent are plotted in Fig. 7-1 for a wide range of parachute applications. The aircraft-approach and landing-deceleration curves in the figure are of theoretical value only; however, the plot indicates that parachute applications resulting in a terminal velocity over 150 ft/sec may be considered as infinite-mass cases in the calculation of canopy opening forces. Personnel,

air drop, and final-stage aerospace-vehicle recovery canopies have final rates of descent from 16 to 50 ft/sec and a canopy loading ($W/C_D S$) from 0.3 to 3.0 psf. Parachutes with canopy loadings between 3.0 and 25 psf are used in ordnance applications for stabilization or deceleration purposes. For all other applications, canopy loadings are higher and may be treated as infinite-mass cases. While differences in canopy loadings under terminal-velocity conditions must be considered in canopy design because they establish limits on canopy porosity, construction, and stability, design strength of parachute canopies under high canopy-loading conditions is largely governed by the instantaneous canopy loading, the ratio of opening shock force (F_o) to canopy drag area $(C_D S)_{o,p}$. For flat circular ribbon canopies, the required strength of the ribbons for a given gore base width and instantaneous canopy loading is fairly well known. (See

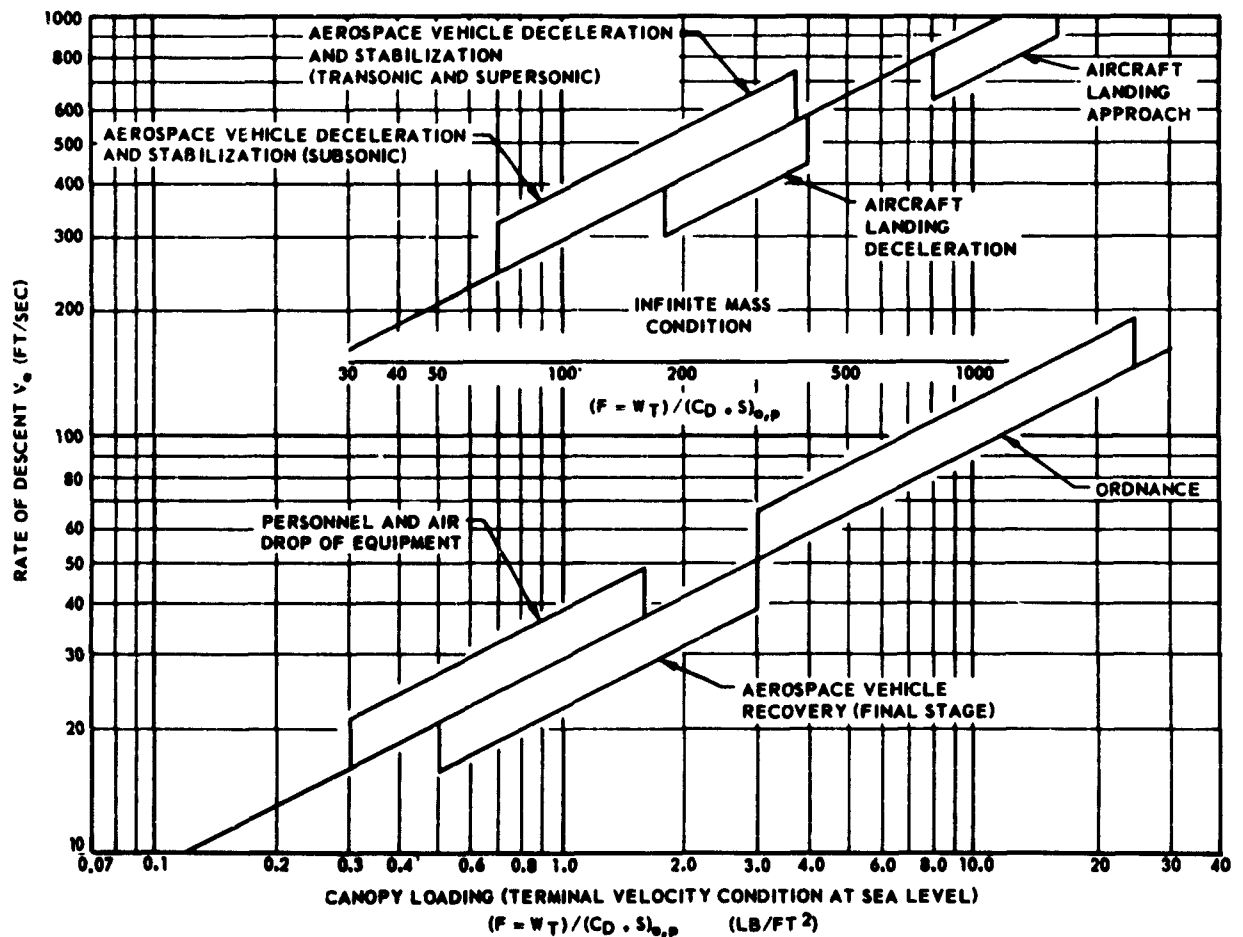


Fig. 7-1 Rate of Descent Versus Canopy Loading for Terminal Velocity Conditions

Fig. 7-2). For solid cloth canopies stress distributions may be calculated following the method presented in Chapter 4 and selecting suitable cloth material as dictated by the stresses expected.

2.1.2 TRAJECTORY CONTROL. Trajectory control of aerodynamic decelerator load systems is, and will continue to be, an important consideration in the design of personnel, air drop, aero-space vehicle recovery, and special-weapon parachute systems. Trajectory control is required in order to accomplish:

- (1) Impact or landing at pre-selected location;
- (2) Temperature minimization;
- (3) g -load limitation;
- (4) Impact velocity and angle control, and
- (5) Accurate computation of flight path (for unstable primary body).

Methods of obtaining trajectory control by means of deployable aerodynamic decelerators include:

- (1) Drag area control;
- (2) Drag device staging; or
- (3) Canopy control during deployment.

Special construction and packing techniques, and auxiliary equipment such as automatic timers, must usually be incorporated in the design of aerodynamic decelerator systems to be employed for trajectory con-

trol. Methods of system-operation variation and control, and the utilization of special-system components, are discussed in detail in Chapters 4, 5, 9 and in subsequent sections of this chapter.

2.1.3 STABILITY. Good stability of a parachute-load system is generally obtained at the price of reduced drag efficiency.

During the design phase, it is therefore important to assess carefully the requirements of each particular application in terms of the ratio of stability gains versus efficiency losses. A near approach to absolute dynamic stability is generally necessary only for such applications as bomb stabilization. Undamped oscillations or erratic gliding during descent may not be objectionable for some applications. For the great majority of first-stage aerospace-vehicle recovery or deceleration applications, undamped oscillations up to ± 2 deg can be tolerated; for other cases, a range of oscillation of up to ± 5 deg is considered tolerable. The objective in the design of deployable aerodynamic decelerator systems for air drop, final-stage aerospace-vehicle recovery and personnel applications is the reduction of the incidence of damage and injury caused by swinging impact with the ground; stability ranges of between ± 5 and ± 20 deg are adequate, in the majority of these cases, for these applications.

2.1.4 RELIABILITY. The reliability requirements for any aerodynamic decelerator system are necessarily high. To achieve the required reliability in the face of weight and space limitations and the consequent necessity to avoid extreme overdesign, the parachute designer must consider every aspect of the strength of the materials which he uses, the actual canopy, deployment bag, and other component construction procedures, and the details of the planned deployment process.

A recent study of the reliability of parachute systems (Ref 7-1) has indicated that there are two major types of reliability considerations in the design of parachute systems. It is necessary to consider both component reliability for every part of the system, and the operational reliability: that is, the reliability of the deployment and opening process itself.

The major consideration in component reliability is that each component function properly under the expected loads. Since the maximum loads in parachute operation are generally those of snatch force and opening shock, these are the primary factors in the design of the load-bearing members of the system. However, for some components, such as static lines and deployment bags and parachute packs, the maximum loads may be due to other forces. Thus, the operation of the system must be considered in detail in the study of load requirements for reliable design.

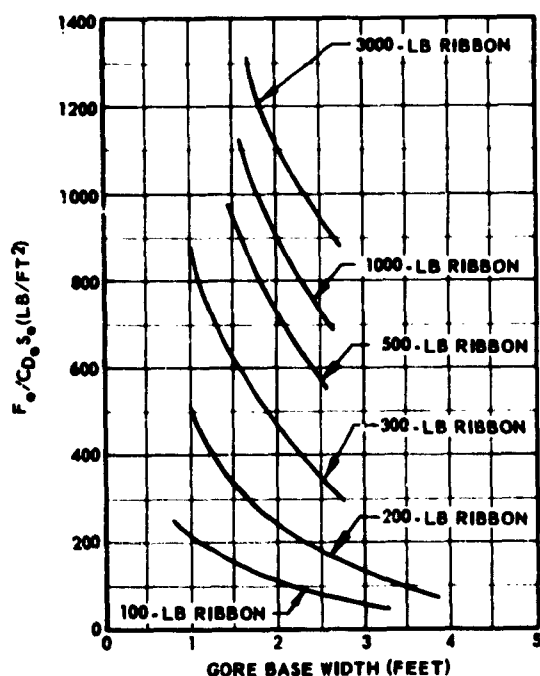


Fig. 7-2 Boundary Curves for Horizontal Ribbon Strength of a Flat Circular Ribbon-Type Canopy

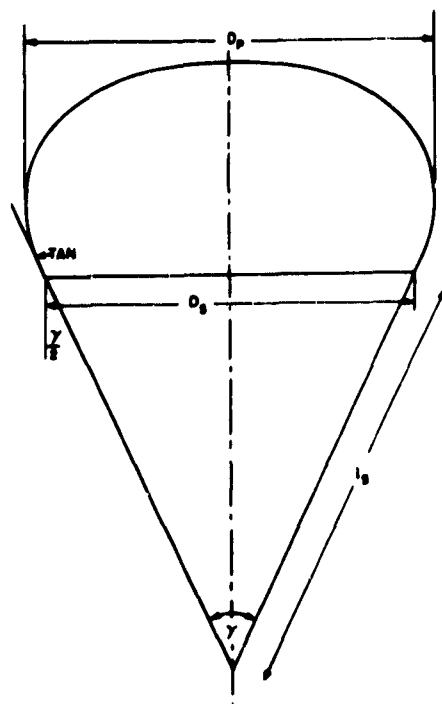


Fig. 7-3 Inflated Profile of Typical Circular Canopy

The reliability of the load-bearing members of the parachute system, including both fabric and hardware items, is a function of the load itself, the strength of the materials from which the components are made (including the strength of seams of the fabrics), and the variation of the strength of the materials permissible under the specification requirements and design conditions. Auxiliary mechanical devices, such as reefing-line cutters, stage disconnects, and timing systems, must function with high reliability under conditions of system operation, including high shock and acceleration forces developed during deployment and canopy opening.

The environments which the decelerator system will be exposed to, both in storage and in operation, are prime considerations in design for reliable operation. In general, temperature and other factors which affect fabric and metal strength and the operation of mechanical devices are of extreme importance in assessing the reliability of the system design.

The operational reliability of an aerodynamic decelerator system is the probability of the successful sequence of the necessary operations in the deployment of the system. Thus, it is a function of adequate design of the deployment bags, packs, and other con-

tainers, and of the actual packing process itself. The details of the design of the decelerator containers are covered in Sec. 3 of this chapter. The problem of correct packing of the decelerator in the container so that deployment occurs in the required manner is a matter of human performance. While this is generally not under the control of the parachute designer, nevertheless his design should be such that the inspection of the packing process is readily facilitated. Thus, critical connections, ties, and parts placement should be such that they are visible to the inspector both during the packing process, and, wherever possible, after the process is completed so that he may insure the correctness of the operation.

The actual determination of the reliability of an aerodynamic decelerator system is discussed in Sec. 13 of Chapter 4. The details of the method of reliability calculation, and examples of applications, are presented in Ref (7-1).

2.2 Parachute Canopy Performance Considerations. Parachute canopy selection is always a compromise in some respects: highest drag and maximum stability cannot be achieved in the same canopy; high strength means increased weight and bulk. In general, the selection and design of any parachute canopy type must be based on the particular application. Since there are a large number of applications and canopy types, there is a decided advantage to being able to narrow consideration for any one application to two or three canopy types before detailed design computations are started. The comparison of the desired or required performance characteristics for a specified mission with the performance characteristics of the possible canopy types can usually narrow the choice to a practical number.

2.2.1 CANOPY DRAG. The drag of a body such as an inflated parachute canopy may be written as:

$$(7-2) \quad D = C_D S q$$

where $C_D S$ = drag area; and

$$q = 0.5 \rho v^2 = \text{dynamic pressure.}$$

Thus, drag depends upon the reference area S , the dynamic pressure q , and the canopy shape, which essentially determines the value of the drag coefficient C_D .

Two areas are generally used as reference areas, the area of inflated drag-producing surface projected in axial direction, S_p , and the developed or "nominal" area of the material forming the drag-producing surface, S_n . In one case the drag coefficient C_{Dp} , based on the projected canopy area, is used for rib-

bed and ribless guide-surface canopies only, while the coefficient C_{D_o} , based on the "nominal" cloth area, is used for all other types of canopies.

The value of the drag coefficient depends primarily upon the shape of the inflated parachute canopy and total porosity of the drag-producing surface. The shape is a complex function of the canopy design, depending on such parameters as the gore shape, porosity or permeability of the drag-producing surface, suspension-line length, size of the canopy, number of gores, and canopy drag-loading. The porosity not only affects the drag directly, but also has an important influence upon the dynamic behavior (flow pattern) of the canopy. Oscillating or gliding parachute canopies have considerably higher drag coefficients than the more stable types.

Experimental values of the drag coefficients are listed in Chapter 3. For preliminary calculations, the following values for drag coefficients may be used:

Type Parachute Canopy	Drag Coefficient
Flat Circular, Solid Cloth	$C_{D_o} = 0.75$
Extended Skirt, Solid Cloth	$C_{D_o} = 0.70$
Guide Surface (Stabilization)	$C_{D_p} = 0.95$
Guide Surface (Ribless)	$C_{D_p} = 0.80$
Guide Surface (Personnel)	$C_{D_o} = 0.72$
Rotafoil	$C_{D_o} = 0.78$
Shaped	$C_{D_o} = 0.80$
Flat Circular Ribbon	$C_{D_o} = 0.50$
Ring Slot	$C_{D_o} = 0.55$

2.2.2 CANOPY STABILITY. In Chapter 4 static-stability coefficients and dynamic-stability equations for canopies were presented. These provide a theoretical means of predicting the stability of a canopy design prior to full-scale free-flight tests. The discussion of parachute stability presented in Chapter 4 is primarily analytical; the following discussion is more practical in nature and considers the various parameters which influence parachute canopy stability.

2.2.2.1 Porosity Effect. In general, an increase in porosity increases the stability and filling time of a canopy, but simultaneously decreases the drag efficiency and critical opening velocity. In addition,

there is evidence that the distribution of porosity is also an important consideration; better stability characteristics may be obtained by increasing the porosity in the region of the canopy skirt.

2.2.2.2 Suspension-Line-Length Effect. Reduction of suspension-line length, within the recommended range, provides an increase in the damping of parachute motion. However, if suspension-line length is reduced beyond a practical value in order to gain stability, the projected diameter of the canopy will be decreased, with a corresponding decrease in drag.

2.2.2.3 Shaped-Canopy Effect. The stability characteristics of canopies can be improved by shaping the gores so that the length of the conical portion of the inflated canopy which is tangent to the suspension lines is increased. This produces an inflated canopy profile resembling a combination of a hemispherical segment and a truncated cone, a shape known to be more stable than a hemispherical one. However, an increase in the length of the conical segment results in a reduction of drag efficiency. Thus, stability gain must be measured against drag-efficiency losses in the design of shaped-gore canopies.

2.2.3 CRITICAL CANOPY-OPENING CONDITIONS. Two critical conditions exist for any self-inflating porous parachute canopy: the maximum or critical opening velocity and the minimum opening dynamic pressure. The maximum opening velocity is defined as the lowest speed at which the canopy does not fully develop. For speeds above the critical opening speed a parachute opens only to a squid state; it will not open fully unless the speed is reduced.

O'Hara (Ref (7-2)) presents an analytical method for determining the critical opening speed. However, on the basis of experimental observation (Ref (7-3)), the critical opening velocity can be estimated by assuming that the drag of a squidding canopy is at least one-sixteenth the drag of the fully inflated canopy at the same velocity, so that:

$$(7-3) \quad \frac{F_{sq}}{W_t} > \frac{v^2}{16 v_c^2}$$

where F_{sq} = steady drag of squidded parachute canopy.

This then means that if a canopy is selected with a critical opening velocity not less than four times the equilibrium descent velocity, then F_{sq}/W_t is greater than 1, and the parachute is deployed at a velocity greater than its critical opening velocity, the steady drag of the squidded canopy will be greater than the weight of the load (steady-state drag of fully inflated

canopy), and the load will be continually retarded until the parachute canopy reaches the critical opening velocity and it opens fully.

With respect to critical opening velocity, the governing design parameters for a parachute canopy are:

- (1) Total porosity or permeability of the canopy;
- (2) Distribution of canopy porosity; and
- (3) Shape of the canopy mouth opening.

Generally, the shape of the canopy mouth opening during inflation is influenced by various geometrical factors, such as the shape of the gore pattern and the length of the suspension lines. Since a certain amount of slackness exists between the skirt and the suspension lines prior to canopy inflation, it is difficult either to control canopy mouth shape or to predict the effect of such inflation-promoting devices as pocket bands (see Glossary, Chap. 1, Sec. 2, and 3.2 of this chapter). Pocket bands are, however, effective in getting canopy inflation started by limiting the inward fold of the slack skirt material. If canopy inflation has started, it will continue to a state either where equilibrium is attained between the volume of air flowing into the canopy through its mouth and that flowing out through the fabric pores or other openings, or where equilibrium is reached between internal pressure and structural tension.

Several methods of improving opening characteristics of parachute canopies have been tried in the past, with varying degrees of success. Among these are: (1) adding pocket bands at the canopy skirt between adjacent skirt sections across suspension lines; (2) lengthening suspension lines; (3) using canopy-crown material with low-porosity fabric; or (4) adding external air-pockets to the skirt. The opening characteristics of large canopies may be improved by the proper placement of a small secondary canopy near the skirt of the primary canopy (Ref 7-4). In the case of the guide-surface and other shaped-gore canopies, opening characteristics are, to a certain extent, a function of gore shape. Primarily, however, opening characteristics are dependent upon porosity. Solid-cloth canopies with inverted conical or inward curving skirts, and those geometrically porous canopies of the ribbon family in which the total porosity required for stability is close to the critical limit, without inflation aids, are sensitive to variations in total porosity. A small increase in porosity, due either to opening-shock damage or to variations in textile weave, can reduce the critical opening velocity below a safe level.

The inflation of parachutes in the upper atmosphere, above 150,000 ft, where the density is low, is governed by the pressure differential developed between the internal and external surfaces of the canopy. The magnitude of this pressure differential depends upon

the dynamic pressure. The minimum dynamic pressure to sustain canopy inflation has been determined from drop tests and wind-tunnel tests to be approximately 0.3 to 0.7 lb/sq ft. Parachutes may open partially or fully at high altitudes due to inertia forces of the ejected canopies, or due to induced rotation of the canopy. At extremely low density and very high speeds, even lower dynamic pressures than those above may be sufficient to open the canopy. However, in all these cases the pressure inside the canopy is not sufficient to maintain a definite inflation, to counteract squidding, twisting, and entanglement of the canopy, or to prevent interference and entanglement of parachute and load. Therefore, for reliable assurance of canopy inflation at high altitudes, it is suggested that the canopy be deployed at dynamic pressures greater than 1 lb/sq ft.

2.2.4 CANOPY GEOMETRY. When considering the effect of canopy geometry upon performance, attention should be paid to the fact that canopies of large diameter are neither geometrically nor mechanically similar to canopies of small diameter, even though they may be of the same basic design. This may be explained by means of two factors associated with the scale effect: the variation in the number of gores with canopy diameter, and the variation in the weight and flexibility of the materials. This consideration serves to point out again that, even if the geometry of a parachute canopy has been found suitable by constructing and testing smaller-scale models, full-size parachute canopies should also be drop-tested as long as definite relationships of performance data to physical design parameters (similarity laws) have not been established.

The inflated profile of a typical circular canopy is shown in Fig. 7-3. This profile is that of the radial seam, or rib; no attempt has been made to indicate the profile of the panel bulges between ribs. Because of the panel bulges, the profile shown represents the limiting shape with an infinite number of gores. However, a canopy designed as a surface of revolution usually does not pull-in appreciably at the skirt because of the gore shape, and so shows the least variation in profile with number of gores.

The skirt lip of the canopy will be tangent to the suspension lines if it is assumed that no bending stresses are present. Under this assumption, the canopy skirt assumes a negative angle of incidence equivalent to half the angle enclosed by the suspension lines. The negative angle of incidence of the skirt and, more important, the length of the conical surface to the tangency point, have a strong influence upon several important characteristics. As the length of the conical surface is increased, (1) the critical open-

ing-velocity is reduced, (2) canopy-filling time is increased, (3) opening shock is reduced, (4) the average angle of oscillation is decreased, (5) the damping characteristics are improved, and (6) the ratio of D_p to D_s (see Fig. 7-3) is increased. These effects appear in varying degrees in the performance of the extended-skirt and guide-surface canopies. In general, the smaller the relative canopy mouth, the lower the allowable porosity of the canopy, if the critical opening-velocity is to be maintained at a safe value. Because of the scale effect, this trend becomes more pronounced as the diameter is increased, but beyond a certain point the area of conical surface extensions required for stability and other desirable performance characteristics diminishes, approaching zero for very large parachute canopies. Experience indicates that this limit is reached when the diameter approaches 80 ft.

Other geometric shape-factors associated with the skirt of circular canopies can be observed to a marked degree in the performance of ribbed and ribless guide-surface canopies. Here, the pronounced bulges or lobes, as well as the high rate at which the crown profile breaks away from the tangency point on the conical surface (thus producing a flattened top), determine to a large degree the performance characteristics of this type of canopy. In these canopies the separation line between crown and conical surface can be considered a flow separation edge which creates the same effect as that obtained through the use of high-porosity fabric.

2.2.5 CANOPY POROSITY. The porosity of a canopy arises from two types of openings in the canopy through which air can flow: (1) the air permeability of the canopy fabric itself; and (2) openings deliberately constructed in the canopy. The air permeability of canopy fabric is commonly expressed as the volume of air flowing through a unit area in a unit time (ft³/min/ft²) at a specified constant pressure-differential. This mass flow of air through the fabric has its major effect on canopy opening. Positive canopy inflation in the case of solid fabric canopies is obtained by maintaining a balance between air flow into the canopy and air loss due to fabric porosity and any vent openings.

The value of porosity or air-mass flow is dependent on air pressure and density. For purposes of performance calculations, a dimensionless term, effective porosity (C), has been established for filling time determination of solid cloth canopies. (See Chap. 4, Sec. 3, *Effective Porosity*).

Geometric openings, in addition to the vent, are built into some types of canopies. These canopies derive their performance characteristics from careful

selection and spacing of these openings. For these types, porosity is defined as geometric porosity,

$$(7.4) \quad \lambda_g = 100 \frac{S_{T_o}}{S_o} \%$$

where S_{T_o} = total area of openings in canopy; and

S_o = nominal surface area of canopy.

At the present time, a relationship between geometric porosity of ribbon grids and the effective porosity term as applicable to solid cloth canopies has not been established. This conversion is most difficult to achieve for those canopies operating at transonic and supersonic speeds, where the ribbon grid undergoes unknown structural deformation. Such deformation makes the calculated geometric porosity an almost meaningless value.

2.2.6 CANOPY STRENGTH. The overall strength requirements for a parachute canopy and other components are presently established by applying a design factor (Table 7-1) to the allowable maximum opening shock. This factor is commonly specified in relation to a particular application. At present, destructive tensile-tests of structural samples combined with drop-tests of the complete assembly are relied upon to demonstrate that a margin of safety exists for the given design conditions. However, experimental and analytical programs are in progress to provide data on the load distribution in both the suspension lines and the drag-producing surface during the deployment and inflation of canopies. Such data may result in the revision of present parachute design strength factors. Insofar as the suspended load alone is concerned, an additional margin of safety is provided by the ability of a parachute to sustain extensive damage and still function properly.

2.2.7 CANOPY DRAG EFFICIENCY. Drag efficiency of a parachute canopy is defined by considering canopy weight to be the critical design consideration:

$$(7.5) \quad \text{Weight-Drag: } \eta_w = \frac{C_D S_{o,p}}{W_p}$$

where W_p = Total weight of parachute canopy including swivel, if required.

In order to establish a basis of comparison for different canopy types, it is advisable to assume the same structural margin of safety relative to the opening shock under identical deployment conditions. It can then be seen that a parachute canopy with a good drag coefficient and a high opening-shock character-

TABLE 7-1 CANOPY DESIGN FACTORS

Application	Safety Factors		Strength Factors						Overall Factor $\frac{j \times c}{u \cdot o \cdot e \cdot k}$ (Nylon)
	j	c $(L_s = D_o)$	u	o			e	k	
				Nylon	Silk	Rayon			
Paratroop Use	2.0	1.055	0.8	0.95	0.8	N/A	0.95	0.95	3.075
Personnel Emergency Escape	2.0	1.055	0.8	0.95	0.8	N/A	0.95	0.95	3.075
Air-Drop of Cargo	1.5	1.055	0.8	0.95	0.8	0.5	1.00	0.95	2.195
A/C Landing Deceleration & Approach	1.5	1.055	0.8	0.95	0.8	N/A	0.95	0.95	2.305
Aerospace-Vehicle Recovery, Deceleration Stages	1.9	1.055	0.8	0.95	0.8	N/A	0.95	0.95	2.91
Aerospace-Vehicle Recovery, Final Stage	1.5	1.055	0.8	0.95	0.8	N/A	0.95	0.95	2.305
Special Weapon Use	1.5	1.055	0.8	N/A	N/A	N/A	N/A	N/A	2.0

N/A - Not applicable.

istic may have a poor drag efficiency because of the greater strength of materials required. This method may facilitate the selection of a canopy type by determining which of several different canopies designed for the same purpose provide the required drag performance for the least material weight.

The fact that otherwise equivalent canopies differ greatly in drag efficiency may be attributed largely to their differences in canopy geometry. This difference in canopy geometry, which changes the total cloth area without proportionally affecting the drag coefficient, may be made for the purpose of effecting improvements in canopy performance; e.g., to increase stability, reduce opening shock, reduce local fabric stresses, or gain better controllability.

2.2.8 CANOPY WEIGHT AND VOLUME. The weight and packed volume of parachute canopies can be calculated from the dimensions of a given canopy design, provided the weight and volume of the material used in canopy fabrication are also known. In order to obtain an approximate weight value for a specific canopy type, a simple mathematical expression may be utilized. This expression has the form:

$$(7-6) \quad W_p = a D_o^2 p + b D_{o,p}$$

where W_p = Weight of the parachute canopy;

$D_{o,p}$ = Diameter of the canopy (nominal or projected); and

a, b = Constants.

Solution of this equation provides a valid approximation for the weight of parachute canopies which have a suspension-line strength to canopy-material or ribbon strength (as listed in 3.1.1.1 of this chapter), which have a suspension-line length equal to the diameter of the canopy, and where the number of gores is approximately equal to the value of the nominal or constructed canopy diameter. The values of the constants a and b depend upon the canopy type and the material or ribbon strength used in the fabrication of the parachute canopy and are listed in Table 7-2. Knowing the weight of the canopy, its packed volume may be obtained by multiplying the weight by the average pack-density value listed in Table 7-3 for compressed or uncompressed packing.

2.3 Parachute Canopy Deployment and Opening. Opening characteristics of a parachute may be loosely defined to include all the consecutive motions

of parachute system operation, from the instant of initiation of canopy deployment until complete canopy inflation. Deployment is defined as covering the extension of the drag-producing surface and suspension lines from the stowed position. The prime requirement for a deployment system is reliability. Deployment systems should provide for the controlled movement of the deploying canopy to prevent side loads on the skirt area before completion of suspension line stretch, and to allow orderly deployment of the canopy along the path of primary vehicle travel.

In addition, the deployment system should provide for the reduction of snatch force. The magnitude of snatch force is directly proportional to the effective drag area of the pilot chute and main canopy. For example, a partially open canopy with a drag area of 20 sq ft will impose a considerably higher snatch force on a suspended load than a deployed but uninflated canopy with a drag area of 2 sq ft. Canopies which are free to inflate during deployment impose a pseudo-opening-shock snatch force. Good high-speed deployment must, therefore, present the smallest system drag area that is consistent with orderly deployment, until line stretch is complete. Thereafter, the deployment system must provide completely reliable release of the canopy for inflation. Low bulk and weight of the

deployment system are also desirable for reduction of snatch force.

2.3.1 DEPLOYMENT METHODS. The three most common canopy deployment methods presently in use are (1) static-line deployment, (2) pilot-chute deployment, and (3) forced ejection.

2.3.1.1 *Static-Line Deployment.* Most small air-drop parachutes and troop main-parachutes are opened and deployed by a static-line assembly, consisting of (1) static-line snap, (2) static line, and (3) break cord. The static-line snap is firmly attached to a body whose differential velocity and mass will be sufficient to break a pack open, or to withdraw the ripcord pins. The static line, upon full extension, begins to deploy the parachute canopy, which is attached to the static line by means of a break cord. The apex of the canopy is held until sufficient drag is exerted on the deploying canopy to break the cord attaching the apex to the static line. Unfortunately, the rate of deployment of the parachute often exceeds the speed of the dropped load. This permits a "sail" to develop, during which inversions and semi-inversions can readily form. The extent and duration of the sail is governed primarily by the strength of the break cord. Strong break-cords tend to straighten the sail. If break cords are too weak, canopies are not withdrawn from the pack sufficiently

TABLE 7-2
CONSTANTS a AND b FOR VARIOUS CANOPY TYPES AND CANOPY MATERIALS

Canopy Type		1.1 oz	1.6 oz	2.25 oz	3.5 oz	4.75 oz	14 oz	1.1,1.6, 2.25 oz	300 lb	1000 lb
Flat Circular	a	0.018345	0.02526	0.03885	0.0612					
	b	-0.0113	-0.0104	-0.03185	-0.0221					
Extended Skirt	a	0.01435	0.02043					0.02951		
	b	-0.00993	-0.01017					-0.02420		
Personnel Guide	a	0.011963	0.01734							
	b	-0.008290	-0.01038							
Ribbed & Ribless Guide	a					0.09	0.36			
	b					0.60	1.02			
Ribbon	a								0.0585	0.3849
	b								-0.1445	-0.4521
Ringslot	a			0.05424	0.1496					
	b			-0.16050	-0.4090					

for orderly deployment, and further deployment depends only upon the drag area of the exposed canopy. Static-line deployment of an exposed and uncontrolled canopy is not reliable or desirable at high speeds or with large canopies.

2.3.1.2 Pilot-Parachute Deployment. The use of pilot parachutes to withdraw the main canopy from a pack or deployment bag and guide it for positive and proper inflation is common with most ripcord-operated and deployment-bag-packed systems. The pilot-parachute deployment system consists of a small canopy, its individual bag or sleeve if required, and its suspension system. In some cases the pilot chute is spring-loaded for positive ejection. The pilot parachute is attached to the apex of the main canopy in systems which are deployed "canopy-first" and to the bag housing the main canopy in systems deployed "lines-first".

For certain applications in aerospace-vehicle and drone recovery and high-speed tests utilizing bomb shapes, jettisonable objects such as decelerator compartment covers or tail plates are used to replace the pilot chute. These jettisonable objects, upon separation from the primary vehicle, develop sufficient drag to withdraw parachute packs from the decelerator compartment and deploy the parachute canopy.

2.3.1.3 Forced Ejection. Deployment initiation by means of forceful ejection is finding wide application because this method provides for good control of the rearward movement of the pilot chute, and in the case of transonic and supersonic deployment, propels the pilot chute out of the adverse wake pressure-distribution behind the primary vehicle. Forced ejection of the pilot chute from the decelerator compartment is accomplished by means of an ejection gun, blast bag, or similar propulsive device (see Chapter 9).

2.3.2 FORCED CANOPY-OPENING. Requirements for low-air-speed low-altitude (less than 500 ft) emergency escape of personnel from aerial vehicles have led to investigations of parachute system designs incorporating propulsive devices to accomplish both forceful ejection of the canopy from the pack and forced spreading of canopy skirt to insure fast opening. One system which was evaluated utilized forceably ejected slugs attached to the canopy suspension lines to accomplish spreading of the canopy skirt (Ref. 7-4).

2.4 Deployment Bags, Packs, Pressure Packing.

2.4.1 DEPLOYMENT BAGS. The use of deployment bags to enclose the drag-producing surface of the canopy during deployment provides for a reliable and efficient method of deployment. This method has

a number of advantages: (1) snatch forces are reduced, since it restricts the drag area of the deploying mass; (2) malfunctions are reduced considerably because of the correct placement of the canopy in relation to the suspended load before opening; and (3) damage to the canopy from friction or from protrusions is reduced because of the protection afforded by the bag. One disadvantage is the possible occurrence of friction burns during exceptionally high-speed removal of the canopy from the bag. In certain instances this can be overcome by use of a protective sleeve, which can be pulled inside-out by the deploying canopy to reduce friction.

2.4.2 PACKS. Packs protect the canopy, pilot chute, or other deployment device from disarrangement and damage during handling as well as operation. In some installations, packs are integral with the suspended load, have flush openings, and may incorporate ejection devices to initiate or aid deployment. Requirements for satisfactory packs include:

- (1) A non-restricting opening, or an opening that is not exceeded by any internal cross-sectional area perpendicular to the direction of deployment;
- (2) A simple design, without sharp corners, recesses, or sides that taper inward toward the area open for deployment;
- (3) A smooth, low-friction interior, free from protrusions, snags, or obstructions to canopy or lines;
- (4) Provision for attachment and storage of pilot chutes, if used, and for pilot-chute bridle cords;
- (5) Provision for deployment bag or sleeve;
- (6) Provision for incremental retention of canopy and lines in proper arrangement without shifting until deployed;
- (7) Rapid and complete opening to prevent damage to the canopy during first phases of deployment;
- (8) Positioning of the pack to preclude snagging on any portion of the suspended load during deployment;
- (9) Provision either for passage of the suspension lines or risers through the pack to the main harness (which can be accomplished through the base or sides of the pack), or for placement of main fittings within the pack, and shielding these fittings to prevent snagging or tangling with canopy or suspension lines; and
- (10) Metal packs, if used, must be smooth and provided with beaded or bevelled edges at the area open for deployment. For certain applications, metal packs, so constructed, are satisfactory.

2.4.3 PRESSURE PACKING. The application of pressure or vacuum on a parachute canopy is a method used to reduce the packed volume of the canopy to a practical minimum. This method of packed-parachute

volume-reduction has proved to be very beneficial to the advancement of decelerator application, especially in the areas of special weapons and aerospace-vehicle recovery. There are three basic methods of pressure packing: (1) press packing - this method of pressure application consists of a mechanical press, utilizing a hydraulically operated piston, to obtain optimum volume reduction; (2) vacuum packing - a vacuum is applied to the system and the atmospheric pressure of the surrounding air is used as the pressurizing force; and (3) lace packing - a mechanical-advantage lever ("grasshopper") is used to tighten the laces. The significant reduction in volume is due to the large circumferential stress applied to the pack.

The basic parameter of major importance in all parachute pressure- or vacuum-packing techniques is termed pack density. Pack density is defined as the ratio of the packed weight of the system to the packed volume of the system, and serves as a guide in de-

termining optimum volume-reduction. Values of pack density versus applied pressure are approximately equal for different types of canopies. Therefore, the curve shown in Fig. 7-4 is applicable for any type of canopy.

As can be seen from Fig. 7-4, the greatest pack-density increase can be achieved in the pressure range of 0 to 80 psi. Only minor increase in pack density is obtained with a considerable increase in pressure. The range of pack densities attainable by the three methods of pressure packing are tabulated in Table 7-3.

The shape into which the canopy is to be packed has a significant effect on the attainable pack density. Pack densities of 35 to 46 lb/ft³ are attainable for cylindrical shapes. Pack densities not exceeding 30 to 35 lb/ft³ are recommended for irregular or rectangular shapes.

Each of the three methods (press, vacuum, and lace

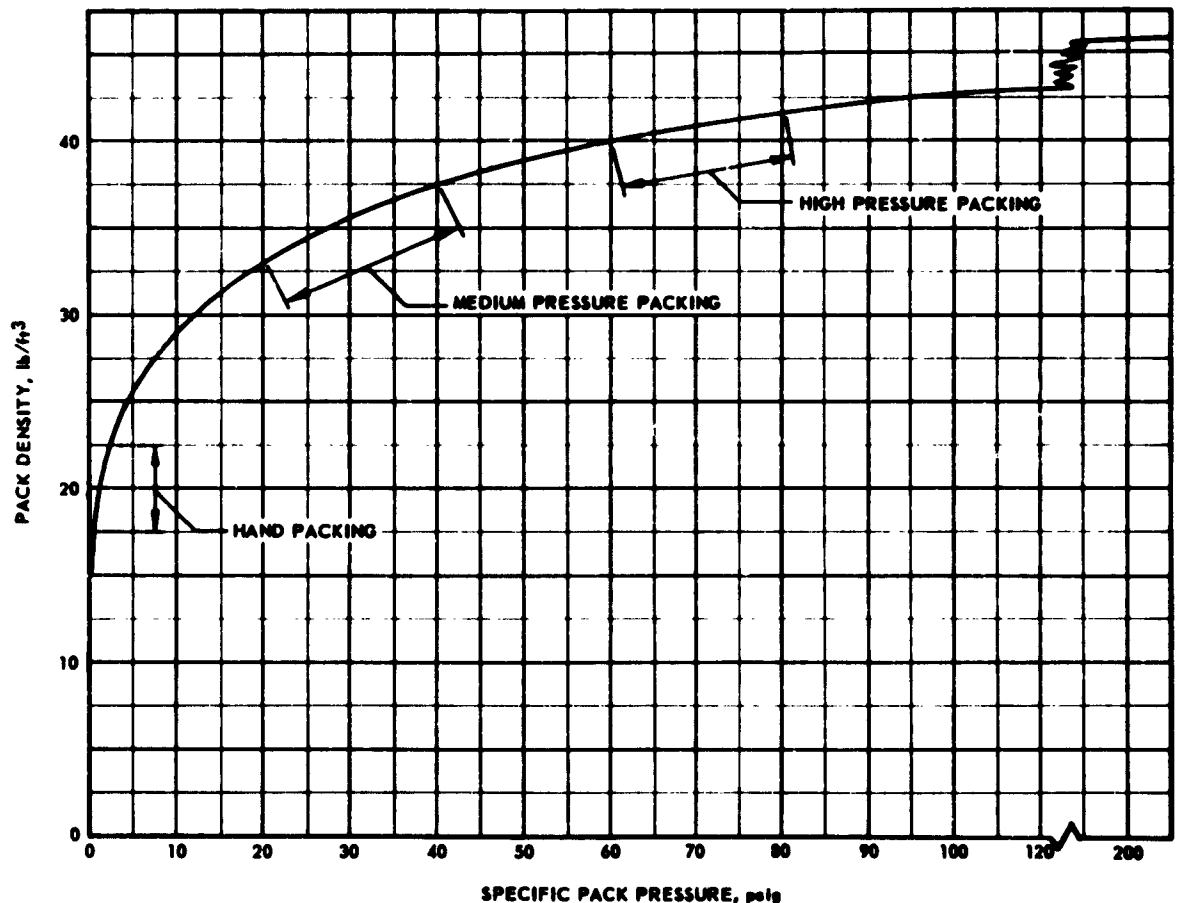


Fig. 7-4 Parachute Pack Density vs Pack Pressure

TABLE 7-3 COMPARISON OF PACK-DENSITY VALUES WITH CANOPY PACKING METHODS

Method	Applied Pressure Range (psig)	Max % Volume Reduction	Max Pack Density lb/ft ³	Aver Pack Density lb/ft ³
Hand Pack (Uncompressed)	1-2.5	0	21-23	20
Mechanical (Compressed)	0-200	50	42-46	41
Vacuum (Compressed)	0-15	25-30	30-33	30
Lace (Compressed)	0-40	30-40	33-39	34

packing) has its limitations and disadvantages; however, each is also unique in its advantages (see Table 7-4). Availability of the three methods makes the application of packed-parachute volume-reduction feasible for a majority of system requirements.

Press packing, for example, is limited by the inability to lace the pack while pressure is being applied; but this method gives higher pack densities with greater packed volume-reduction than other methods. Vacuum packing is limited because significant volume reduction cannot be achieved; however, this method shows great promise in packing irregular shapes and is definitely very useful when the packed parachutes are to be stored for any length of time and shape retention is necessary. Lace packing is limited to cylindrical shapes, but considerable volume reductions can be obtained by experienced packers using the "grasshopper".

SEC. 3 AERODYNAMIC DECELERATOR SYSTEM DESIGN DETAILS

Physical differences between the various parachute types are primarily those of construction and detail geometry. For all parachutes, materials and fabrication methods are more or less uniform. A few parachute types employ special members, devices, or auxiliary mechanisms, which affect the performance characteristics, method of control, and installation requirements.

3.1 Parachute Canopy. A parachute canopy, by definition, consists of the drag-producing surface (cloth area) and the suspension lines. The most common types of drag-producing surfaces are divided in-

to identical gores, which are in turn divided into sections. The shape of the gores determines both the constructed and the inflated shape of the drag-producing surface. The gores may be constructed of solid fabric, or of some geometric pattern of fabric strips or ribbon. The gores are joined by a radial seam running from the vent to the skirt. Because the suspension lines are attached to the skirt at the radial seams in a majority of cases, additional strength along these seams is required. This strength is generally obtained by seam reinforcement with webbing or tape. In cases where this strength cannot practically be obtained in this manner, the suspension lines are extended across the drag-producing area. In some cases it is also necessary to add reinforcements to critically stressed portions of the drag-producing surface. The most common form of reinforcement consists of bands along the skirt and the vent. Additional circumferential reinforcement bands are sometimes needed at intermediate locations on the drag-producing surface.

3.1.1 DRAG-PRODUCING SURFACE. The constructed shape of the drag-producing surface varies widely among canopy types. This difference is effected chiefly in the layout of the gore pattern. For rotationally symmetrical surfaces, the width of the gore in relation to its radial dimensions determines whether the assembled envelope will tend to restrict the diameter or allow the surface to assume a free inflated shape.

In conventional parachute canopies, the included angle of the gore determines whether the drag-producing surface will be flat or conical. The tendency of an inflated elastic envelope to assume a curvature of uniform surface-tension ensures that the maximum

included gore-angle (projected) will always be equal to $360/n$ degrees (n = number of gores). Of course, variations from this basic pattern of radial elements can cause the drag-producing surface to assume any shape desired. The flat circular type of drag-producing surface, which is made in the form of a regular polygon built up from a number of triangular gores, is a special case in that no pre-shaped structural limitations are placed on the free development of the surface. Assuming that the length of the suspension line is great enough to have only a negligible effect on the inflated profile, the skirt will tend to pull inward to an equilibrium position where each gore bulge has a semi-circular cross-section. This canopy profile is shown in Fig. 7-5. If the number of gores in a flat circular drag-producing surface is large, the ratio of the projected diameter (measured between opposite gore bulges) to the constructed diameter is approximately 0.7. The ratio $D_p/D_c = 0.7$ represents a good average value for preliminary design purposes.

The free inflated shape of the drag-producing surface is not readily predicted from the shape of the gore, except for those pattern types that define surfaces known to fall entirely within the envelope of aeroelastic equilibrium. Therefore, in designing a new

canopy for a desired inflated shape, it is usually necessary to estimate the gore pattern on the basis of experience and then modify it after building and testing the first experimental model. The other approach, which is the more common one, is to base the gore pattern on some easily defined or aerodynamically desirable geometric shape, such as the sphere or cone, and evaluate the performance of whatever inflated shape might result from it. This method, however, also may not produce a desired shape or certain performance characteristics during the first attempt, and may require modification.

3.1.1.1 Strength Requirements. At the present time, no widely applicable system exists for determination of the strength required to prevent failures in the drag-producing surface. One possible method for determining analytically the forces acting in the plane of the fabric in the drag-producing surface is presented in Sec. 9 of Chapter 4. A second and strictly empirical method for the determination of the approximate strength requirements for a drag-producing surface is based on the strength of the suspension lines correlated with the strength of the drag-producing surface, assuming a number of gores equal to $D_o + (3$ or

TABLE 7-4 COMPARISON OF PRESSURE PACKING METHODS

Press	Vacuum	Lace
<p><i>Advantages</i></p> <ol style="list-style-type: none"> 1. Maximum volume-reduction 2. Good shape-retention 	<p><i>Advantages</i></p> <ol style="list-style-type: none"> 1. Good shape-retention 2. Good for irregular shapes 3. Excellent storage ability 	<p><i>Advantages</i></p> <ol style="list-style-type: none"> 1. Limited specialized equipment
<p><i>Disadvantages</i></p> <ol style="list-style-type: none"> 1. Special equipment required 2. Lace limitations 	<p><i>Disadvantages</i></p> <ol style="list-style-type: none"> 1. Packing force limited to atmospheric pressure 2. Special non-permeable pack needed 3. Problems in tying-off bag without losing vacuum 4. Special pumps, gages, etc., required 	<p><i>Disadvantages</i></p> <ol style="list-style-type: none"> 1. Shape limitations 2. Requires experienced packers 3. Heavily reinforced deployment bags needed 4. Time-consuming

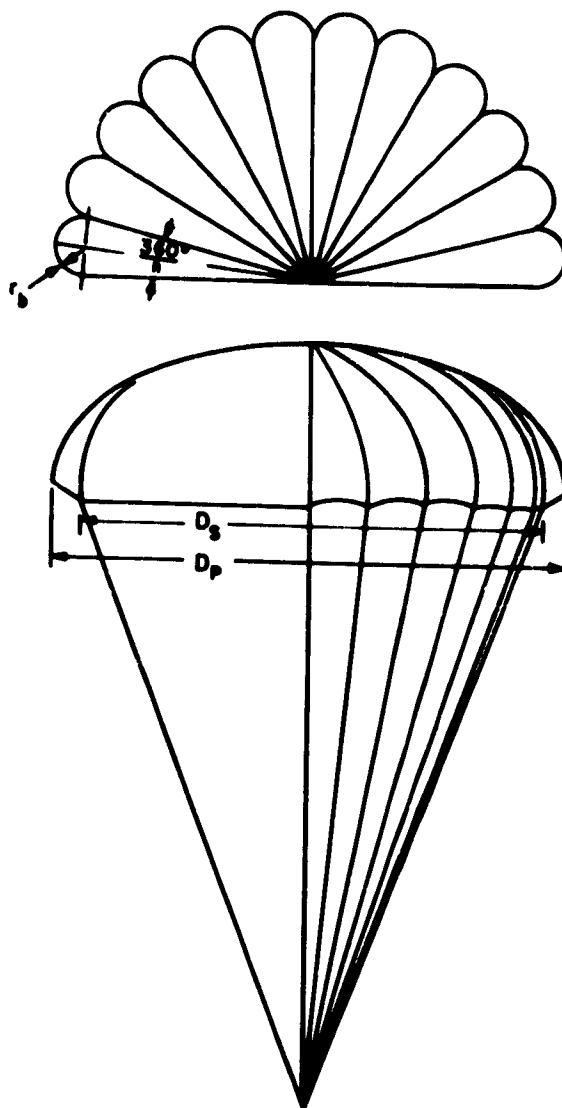


Fig. 7-5 Inflated Profile of Flat Circular Canopy

4), resulting in an even number of gores, and that a fairly constant ratio of suspension-line to canopy-fabric strength is chosen. For ribbon canopies, operating under infinite-mass conditions, a balanced relationship between suspension line and surface material may be taken to be as in Table 7-5.

For all other types of parachute canopies, the relationship may be assumed to be that in Table 7-6.

Assuming that canopies are constructed in accordance with the classes outlined above, and that a fairly constant ratio of suspension-line strength to fabric strength is assured, the following assumptions can be made:

TABLE 7-5 RIBBON-PARACHUTE MATERIAL STRENGTH REQUIREMENTS

Class	Suspension-Line Material (T.S., lb, Nylon)	Ribbon Material (T.S., lb, Nylon)
I	375	100
II	550	200
III	1500	300
IV	2300	500
V	4000	1000
VI	6000	1500
VII	9000	2000
VIII	12000	3000

TABLE 7-6 MATERIAL-STRENGTH REQUIREMENTS FOR OTHER THAN RIBBON PARACHUTES

Class	Suspension-Line Material (T.S., lb, Nylon)	Surface Material (oz, Nylon)
I	375	1.1
II	550	1.6
III	1500	2.25
IV	2300	3.5
V	4000	4.75
VI	6000	7.0
VII	9000	14.0
VIII	12000	14.0

(1) Losses of strength in suspension lines due to sewing and attachment of fittings and reinforcements generally amount to between 20 and 35 per cent of the original strength, depending upon the type of line (webbing, braided cord, etc.) and the method of stitching being used.

(2) Parachute deployment and inflation sequences cannot, at present, be considered so perfect as to allow assumption of ideal and equal distribution of load throughout the parachute canopy during the opening process; some portions of the canopy receive loads disproportionately high in comparison with the loads imposed on other portions. In order to compensate for uneven load distribution, a safety factor (Table 7-1) should be applied.

For flat circular ribbon canopies, test data provide a more accurate method for determining the required strength of the horizontal ribbons for a given ratio of opening shock (F_0) to drag area ($CD_0 S_q$) to skirt gore width. This relationship is shown in Fig. 7-2. If the required strength is above the curve limit,

the next higher ribbon-strength should be used, or, in some cases, reinforcement should be used with the horizontal ribbons. Tests show that graduating the ribbon strength — placing ribbons with lower strength at the skirt area and ribbons with the higher strength near the vent where the stresses in the canopy are greatest — does not affect the reliable inflation and descent characteristics of the canopy. A canopy constructed in this manner will have a higher volume and weight efficiency than a canopy which utilizes the same-strength ribbon material over the entire drag-producing surface.

Flat circular drag-producing surfaces show increasing fabric tension along the gore surface, moving inward from skirt to vent. Although various construction techniques are employed to provide fabric fullness in the vent area, it is well established that opening-shock damage usually appears first in the area around the vent.

3.1.2 GORE DESIGN. In the past, gores designed by attempting to derive gore coordinates analytically have not been too successful in predicting the performance of the resulting canopy. This may be attributed mainly to the large number of variables involved in the physical process of canopy functioning. Experience has shown that descriptive geometry remains the most direct and satisfactory method of gore designing, particularly when it is supported by test observation.

If the shape of a drag-producing surface is to be designed, rather than adopting some approximate geometrical construction, a number of considerations are applicable. It may first be assumed that the primary design objective is to obtain maximum drag efficiency in combination with a defined degree of stability. The attainment of a good drag efficiency implies a low opening-shock characteristic and adequate distribution of fabric stresses so that minimum weight materials may be used. The attainment of a good degree of stability may require an inverted conical skirt, both conical skirt and a flattened roof, geometric porosity, or both a conical skirt and limited geometric porosity. On the other hand, the attainment of a good drag efficiency also requires that the projected area relative to total surface area (S_p/S_o) be a maximum, and that the total porosity be a minimum.

3.1.3 SUSPENSION LINES. Depending upon the purpose and choice of the designer, the length of suspension lines (L_s) to be used with different types of drag-producing surfaces may vary. For nearly all known canopy types, suspension-line lengths range between 0.7 and 1.3 D_o . One parameter which may influence the proper choice of suspension-line length is the effect of primary-body wake. As shown in Chap-

ter 4, canopies should be inflated a minimum of three vehicle-diameters behind the primary body in subsonic flow and eight vehicle-diameters in supersonic flow. Tests show (Ref (7-5)) that the influence of suspension-line length on the inflated shape of the drag-producing surface and its performance generally is greatest up to a ratio of $L_s/D_o = 1.0$, with minor changes in drag coefficient and stability still observed up to a ratio of $L_s/D_o = 2.0$ (Ref (7-6)).

For purposes of comparative evaluation, a ratio of $L_s/D_o = 1.0$ (Ref (7-6)) is commonly used; however, shorter and longer suspension-line lengths have been used in service. The effect of suspension-line length on projected diameter for a flat circular canopy and on the drag coefficient for various types of canopies is illustrated in Fig. 7-6. Since some variation of effect occurs from type to type, it is good practice to determine and specify the optimum length of suspension line to be used with each type of drag-producing surface in relation to the specific function which it is to perform.

The suspension-line system can be considered as a group of tension members which extend from the skirt of the drag-producing surface to the riser connection point. Prior to line stretch, the lines are extended by the drag of the drag-producing surface and assume many shapes other than straight. As the drag load is increased to a maximum, the lines are so straightened that the only load considered is the one transmitted from the drag-producing surface to the riser. Assuming that the load is uniformly distributed among number (Z) of lines, the load per line is determined by the geometrical configuration of the structure:

$$(7.7) \quad \frac{\text{load}}{\text{line}} = \frac{\text{drag}}{Z \cos (\gamma/2)}$$

This is true at any time during the descent period so long as the lines are assumed to be straight. In service, the maximum line load may occur at a drag value less than the maximum, since it is possible that the maximum drag, F_o , and the maximum confluence angle, γ , do not occur at the same time. The most severe line-loading condition would result from a maximum drag and maximum confluence angle. The maximum possible angle is that based on an unextended suspension line and the mouth diameter in the fully distended position. This distension beyond a steady-state position is common in many types of canopies (e.g., flat circular), while in others (e.g., guide-surface) it is not as severe. The distension is commonly disregarded and the confluence angle is

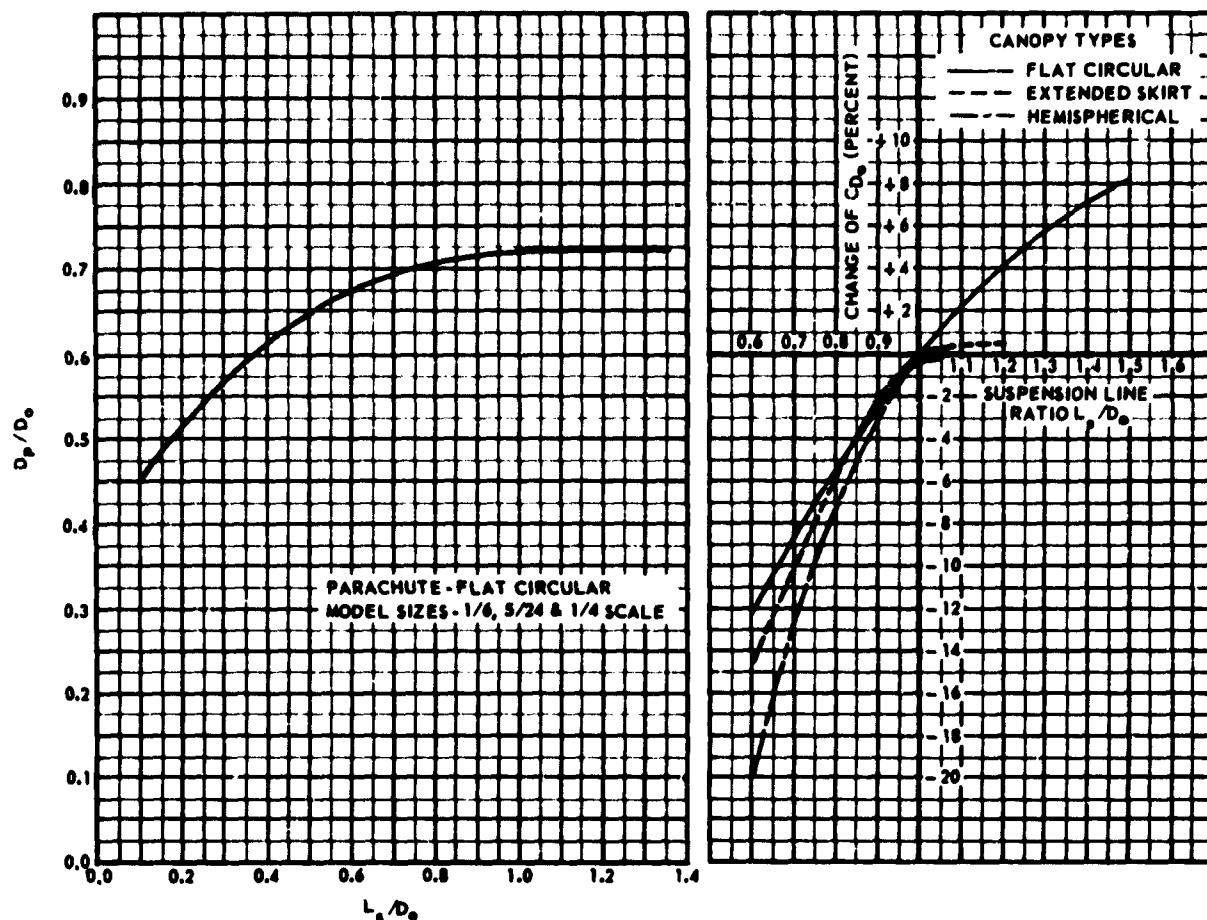


Fig. 7-6 Effect of Suspension Line Length on Projected Diameter for Flat Circular Canopy and on Drag Coefficient for Various Canopy Types

based on the unstretched line length and the skirt diameter D_s , or the inflated projected diameter D_p , in the steady-state condition.

Because of the extreme variation in opening characteristics, the ideal case, in which it is assumed that the total load is uniformly distributed among the lines, is seldom achieved. For all practical purposes however, the load to be expected in the lines can be predicted, and a suitable textile material can be selected. The method of attaching the suspension line to the drag-producing surface greatly affects the strength available. The two major attachment points are the juncture of the suspension line and the skirt of the drag-producing surface, and the juncture of the suspension line and riser. These attachment points are discussed in detail in Sec. 3 of this chapter.

3.1.4 CANOPY DESIGN FACTORS. Design factors for parachute canopies may vary for different appli-

cations. Since every effort should be made to design a balanced canopy, identical design factors apply to both the suspension lines and the drag-producing surface. The suspension line is selected on the basis of its static breaking strength. Although the actual breaking strength of the material is often greater than the minimum value in the specification (see Chapter 6), the strength is commonly based on the latter value. The breaking strength of each suspension line may be expressed by the equation

$$(7-8) \quad \text{Strength} = \frac{F_o \cdot j \cdot c}{Z \cdot u \cdot o \cdot e \cdot k}$$

where F_o = Maximum opening force;
 j = Safety factor;
 Z = Number of suspension lines;

- c = Factor related to suspension line convergence angle;
- u = Factor involving the strength loss at the connection of suspension line and drag-producing surface or riser respectively;
- o = Factor related to strength loss in material from water and water vapor absorption;
- e = Factor related to strength loss by abrasion; and
- k = Factor related to strength loss by fatigue.

The value of these factors varies for different canopy applications, as tabulated in Table 7-1. The factor c , which is related to suspension-line convergence angle, will change with suspension line length. For $L_s = D_o$, the factor c is approximately 1.055.

3.1.5 FLAT CIRCULAR CANOPY. The flat circular canopy may be generally described as a regular polygon of five or more sides. The drag-producing surface is made up of a number of triangular gores stitched together. The joints form the radial, or main seams. The central vent, which facilitates ease of construction of the drag-producing surface, has an area of less than one per cent of the total cloth area (S_o). The skirt and vent hems are reinforced by rolling a tape or webbing inside the hem. Each gore may be made of a single piece of cloth (block cut) or of several sections cut on the bias and joined selvage to selvage, forming a star pattern of diagonal seams in the finished assembly. Bias construction is preferred because of its higher structural strength. Fig. 7-7 shows the planform, shape, and gore of a typical flat circular canopy. The suspension lines are generally sewn to the skirt at the main seams and so are equal in number to the number of gores. After passing through the channel formed by the main seam, the suspension lines are again fastened at the vent, pass across the vent of the drag-producing surface, and follow inside the channel formed by the opposite seam; two suspension lines are thus formed by a single continuous length of material. Generally, the radial length of the line when it crosses the canopy is made approximately 5 per cent less than the radius of the drag-producing surface, providing fabric fullness to relieve radial stresses in the gores. When the number of gores is less than approximately twenty-four, the total cloth or design surface area may be more accurately determined from the formula

$$(7-9) \quad S_o = \frac{\pi D_o^2}{4}$$

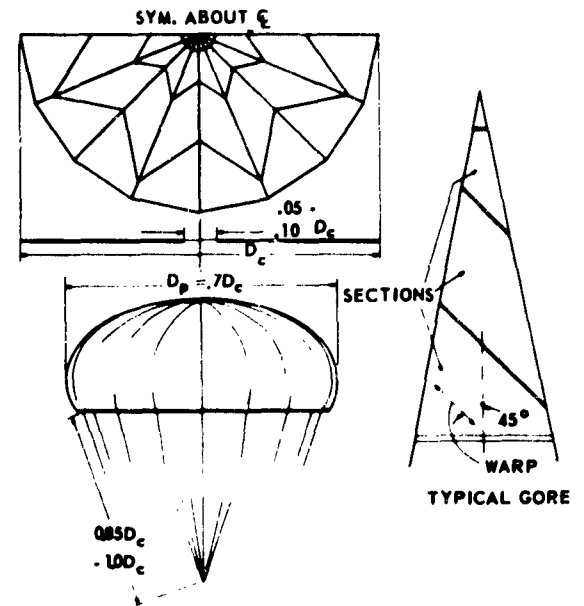


Fig. 7-7 Flat Circular Canopy

where π_o = Polygon shape factor for number of sides; and

D_o = Nominal diameter of the canopy.

Values for the polygon shape-factor as related to the number of gores in a flat circular drag-producing surface are tabulated below.

Number of Gores	π_o
5	2.378
6	2.598
8	2.828
10	2.939
12	3.000
16	3.062
20	3.090
24	3.106
<	3.140

3.1.6 GUIDE-SURFACE TYPE CANOPIES.

3.1.6.1 Personnel Guide-Surface Canopy. The personnel guide-surface canopy was developed for drag efficiency equivalent to that of the flat circular canopy, with improved stability and lower opening-shock characteristics. This design goal was achieved by improving the aerodynamic stability through shaping of the extensions to form guide surfaces. The canopy was used as the standard personnel escape canopy

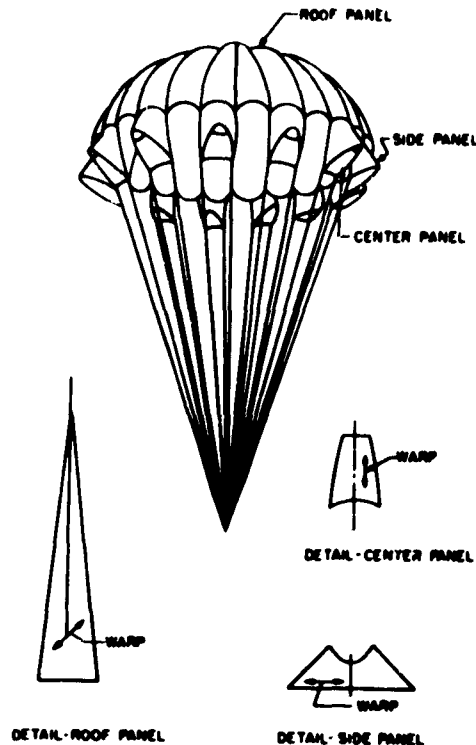


Fig. 7-8 Personnel Guide-Surface Canopy

until the requirement for "on the deck" operation generated a need for canopies with opening times less than those which could be obtained with the personnel guide-surface type. The present personnel guide-surface canopy, Type C-10, was developed from flat circular drag-producing surface 28 feet in diameter, and contains 24 gores. The solid portion of the drag-producing surface is made slightly conical by removing four of the original 28 gores. Twenty per cent interference extensions are added to each alternate gore. At present, the percentage of skirt extension cannot be calculated and must be experimentally determined for each particular application. The inflated shape and gore layout of this canopy type are shown in Fig. 7-8.

3.1.6.2 Ribbed Guide-Surface Canopy. This canopy is made of solid cloth with a relatively flat roof section and an inwardly sloped conical shaped surface extending downward from the roof along the suspension lines. In order that the drag-producing surface might form the guide-surface and flow-separation edge required for stabilization, ribs are placed between the roof and guide surface sections and the suspension lines. The roof and guide-surface panels are made of low-porosity cloth cut on the bias at an angle of 45 deg to the central axis of the gore. Little or no

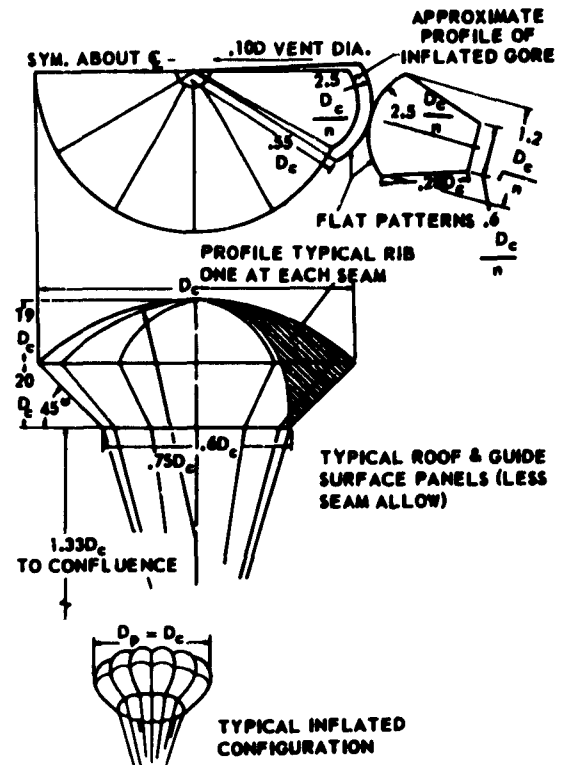


Fig. 7-9 Ribbed Guide-Surface Canopy

vent opening is provided. The planform and shape of the typical ribbed guide-surface canopy is shown in Fig. 7-9. Layouts for the roof panel, guide-surface panel, and rib for a stabilization-type ribbed guide-surface canopy are illustrated in Fig. 7-10.

3.1.6.3 Ribless Guide-Surface Canopy. The ribless guide-surface canopy is a refinement of the ribbed guide-surface canopy and is designed, as the name implies, without ribs. The planform, shape, and gore of a typical ribless guide-surface canopy are shown in Fig. 7-11. Dimensions for roof and guide-surface panels depend upon both diameter and gore number of the drag-producing surface. Dimensional factors utilized in the design of the roof and guide-surface panels for ribless guide-surface canopies with 6, 8, 10, 12, 14, 16, and 20 gores are shown in Fig. 7-12. In other respects, the design of this canopy parallels that of the ribbed guide-surface canopy.

3.1.6.4 Modified Ribless Guide-Surface Canopy. The modified ribless guide-surface canopy is similar in constructed shape to the ribless guide-surface type, differing only in that the gores are constructed from one pattern rather than two. This single pattern design allows for ease in construction, but reduces to some extent the desirable performance characteristics of the two-pattern ribless guide-surface design. The

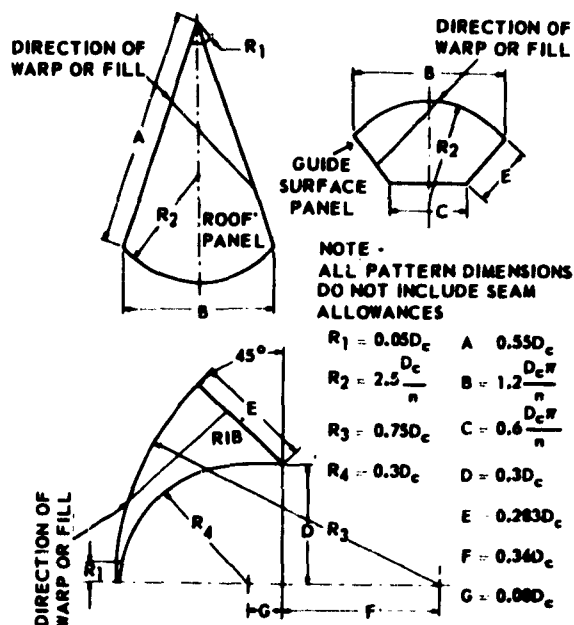


Fig. 7-10 Layout for Roof Panel, Guide-Surface Panel, and Rib for Stabilization Ribbed Guide-Surface Canopy

single pattern design produces a relatively smooth junction of the roof and guide panels of the canopy when compared with the two-pattern design. This eliminates the well-defined flow-separation edge and reduces the projected diameter, thus detracting from the drag-producing and stability characteristics of the ribless design. A typical gore planform, along with dimensional factors utilized in the design for a modified ribless guide-surface canopy with 6, 8, 10, and 12 gores is shown in Fig. 7-13.

3.1.7 EXTENDED-SKIRT CANOPY. Originally, the extended-skirt parachute canopy was made by modifying a flat circular canopy with a restricted extended section attached to the skirt hem in such a manner as to decrease slightly the normal convergence angle of the suspension lines at the extension hem. In present designs, the gore is created by the construction of a "joined gore" which consists of a triangular portion and an added trapezoid. The geometry of the skirt extension varies slightly with different types of extended-skirt parachutes. In one case, it is geometrically similar to the lower portion of the triangular section, while in the other case, the slant height of the trapezoid follows the direction of imaginary lines which would connect the end points of the triangular section of the gore with the confluence point of the suspension lines. In the former case, the base angle of the triangular section and those of the

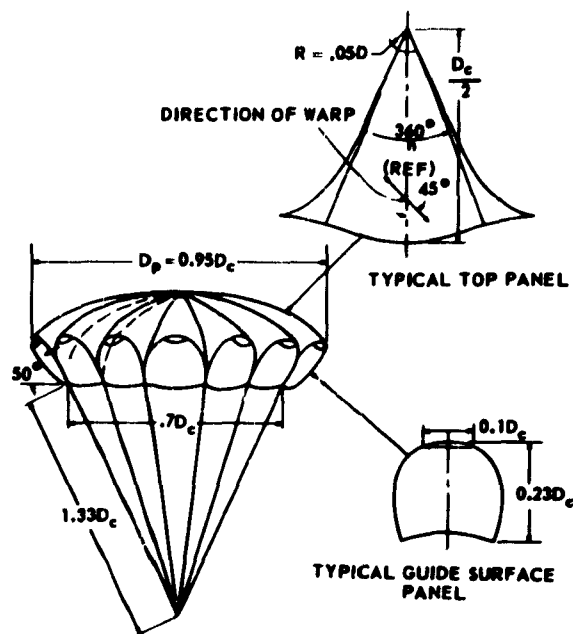


Fig. 7-11 Ribless Guide-Surface Canopy

trapezoid are identical. Canopies built with these gores are sometimes referred to as Flat Extended-Skirt Canopies. In the latter case, the base angles of the triangular and trapezoidal sections are not equal and canopies of this design are referred to as Full Extended-Skirt Canopies. Extended-skirt lengths vary from 10 to 15% of the major flat diameter of the drag-producing surface. The planform, shape, and gore of a typical extended-skirt canopy are shown in Fig. 7-14. In other respects, the design of this canopy type parallels that of the flat circular canopy. For most efficient canopy operation and performance, a suspension line length of $l_s = 0.95D_0$ is recommended.

3.1.8 RIBBON CANOPY. The ribbon canopy (flat circular type) is composed of concentric ribbons supported by a number of radial ribbons, which transmit the loads to the suspension lines (Ref (7-10)). The planform and shape of a typical flat circular ribbon canopy are illustrated in Fig. 7-15. As in the conventional flat circular canopy, the gores of a flat circular ribbon canopy are constructed as flat triangles - the gore construction is illustrated in Fig. 7-16. The gores consist of wide ribbons running parallel to the skirt (horizontal ribbons), and of narrow tapes sewed perpendicular to the skirt and the horizontal ribbons (vertical tapes). The horizontal ribbons are the main drag generators; the narrow vertical tapes serve only to space and control the horizontal

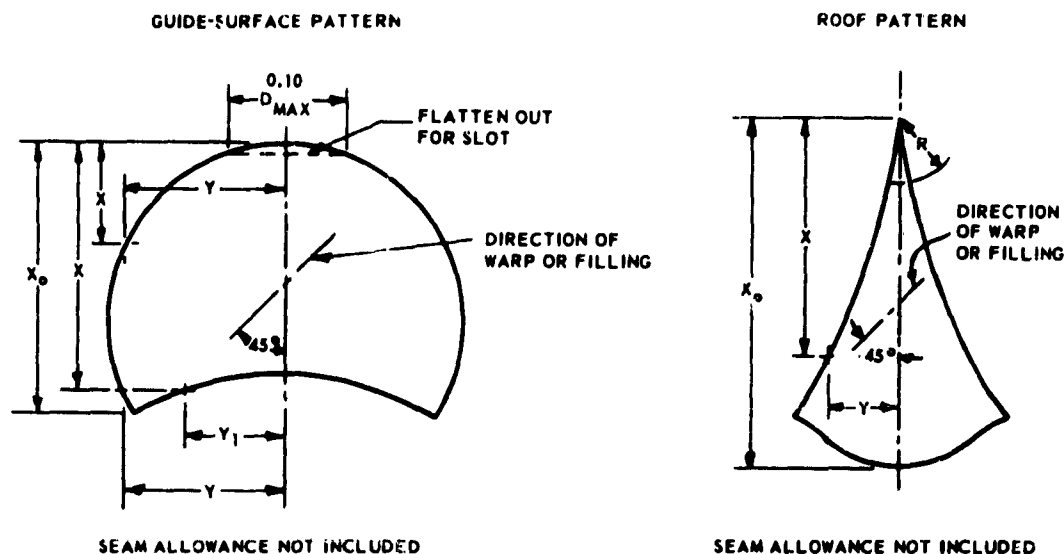


Fig. 7-12a Pattern-Dimension Factors for Ribless Guide-Surface Canopy

ribbons. The gores are interconnected by radial ribbons which extend from vent to skirt and overlap the horizontal ribbons of two adjoining gores.

The filling time of this canopy may be extended by increasing the spacing of the vertical tapes; this also reduces the opening shock appreciably. Variation in spacing of the horizontal ribbons affects total porosity of the drag-producing surface and, consequently, stability. Total porosity includes both geometrical and fabric porosity, the former being produced by ribbon-spacing and the latter by weave and composition of the ribbon itself. Varying total porosities are required for ribbon canopies of varying diameter, and for different applications. In general, as the diameter increases, the total porosity must decrease in order to achieve a constant drag coefficient, constant stability, and relatively constant opening characteristics. Fig. 7-17 shows the relationship between total porosity, λ_t , and canopy diameter for various applications.

The width of horizontal ribbons is generally 2 in. for canopies with nominal diameters larger than 4 ft. The number of horizontal ribbons in canopies is determined by ribbon width and geometric porosity.

Distance between the vertical tapes is generally determined by the filling time required for the canopy to obtain a certain opening shock, or a certain minimum loss of altitude during inflation, or both. The following vertical tape spacings are recommended:

- (1) 5-6 in., without center vertical tape for canopies for low-speed applications (finite-mass cases).
- (2) 4-5 in., for canopies used for aircraft-approach and aircraft-deceleration applications.
- (3) 2-4 in., for canopies required to open rapidly

and for applications at high dynamic pressures.

In porosity calculations, the influence of ribbon permeability (mechanical porosity) must be taken into consideration, if porous ribbons are used. The total porosity of the drag-producing surface, λ_t , is expressed as per cent and is determined from the ratio of the porous area (including ribbon permeability) to the total drag-producing surface area. It has been empirically established, that a ribbon permeability of 27.4 cu ft per sq ft per min is equivalent to a geometric porosity of one per cent. The total porosity of a canopy may then be expressed in per cent, as:

$$(7-10) \quad \lambda_t = \lambda_g + \frac{\lambda_m}{27.4}$$

A method of calculation of geometric porosity has been established; its application is illustrated in Chapter 12.

3.1.9 CONICAL RIBBON CANOPY. Experimental tests with flat circular ribbon canopies at high dynamic pressures and under high canopy loading ($W/C_D S$) conditions have indicated the desirability of effecting better load distribution in the canopy. One solution (Ref (7-11), (7-12), (7-13)) is the development of a shaped or conical design. Such a design was first realized by removing a certain number of gores from a flat circular design. This provides more efficient strength distribution than the flat circular canopy for certain applications, such as special-weapon deceleration. A gore design evolved that produced the desired conical inflated shape of the canopy as shown in Fig. 7-18. The gore design for the conical ribbon

GUIDE SURFACE PATTERN

		Number of Panels					ROOF PATTERN									
		6	8	10	12	14	16	20	Number of Panels							
X/X_o	Y/X	Y/X	Y/X	Y/X	Y/X	Y/X	Y/X	Y/X	X/X_o	6	8	10	12	14	16	20
.05	5.56	5.52	4.83	4.33	4.12	3.85	3.535	3.535	.10	.605	.532	.465	.394	.346	.303	.260
.10	3.85	3.81	3.52	3.21	3.01	2.77	2.42	2.42	.15	.605	.520	.464	.394	.344	.3045	.257
.15	3.08	2.96	2.76	2.58	2.37	2.18	1.90	1.90	.20	.605	.516	.461	.394	.348	.305	.258
.20	2.54	2.43	2.285	2.13	1.975	1.82	1.606	1.606	.30	.605	.514	.462	.407	.352	.307	.259
.30	1.93	1.80	1.69	1.58	1.48	1.37	1.215	1.215	.40	.605	.511	.459	.410	.354	.311	.263
.40	1.56	1.42	1.335	1.25	1.18	1.075	.953	.953	.50	.605	.511	.463	.416	.362	.317	.275
.50	1.314	1.17	1.10	1.03	.965	.882	.772	.772	.60	.605	.509	.469	.428	.378	.336	.294
.60	1.138	.977	.919	.86	.80	.729	.636	.636	.70	.613	.525	.481	.441	.403	.366	.328
.70	1.01	.823	.769	.722	.672	.615	.528	.528	.80	.676	.588	.545	.495	.464	.434	.402
.80	.89	.705	.655	.61	.568	.517	.440	.440	.832	.725	.713					
.885	.808								.866							
.90	.000								.875			.696	.676		.622	.590
.919	.796	.603	.558	.515	.472	.43	.3665	.3665	.882							
.922	.278	.586	.000						.888							
.93		.000	.540						.896	.428	.496	.512	.527	.538	.554	.569
.937			.000						.90	.280	.261	.261	.261	.261	.261	.261
.944									.95	.193	.1625	.1625	.1625	.1625	.1625	.1625
.95	.757	.559	.515	.472	.432	.394	.334	.334	.975	0	0	0	0	0	0	0
.954	.613	.305	.261	.226	.161	.0896	.328	.328	1.0	0	0	0	0	0	0	0
1.0	.72	.517	.474	.430	.393	.358	.3025	.3025								

NOTE:

1. For 6 Panel Design, $X_o = .27 D_{max}$

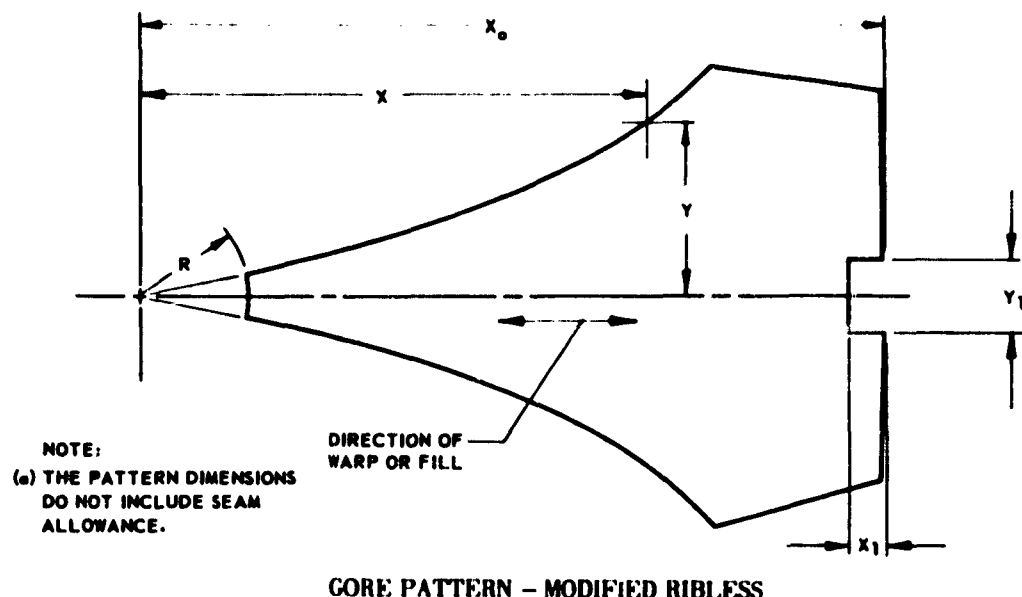
2. For 8, 10, 12, 14, 16, and 20 Panel Design, $X_o = 0.5 D_{max}$

3. $R = .05 D_{max}$ to $.075 D_{max}$ (Varies with number of panels)

NOTE: 1. For 6 Panel Design, $X_o = 0.6 D_{max}$
 2. For 8, 10, 12, 14, 16, and 20 Panel Designs, $X_o = 0.5 D_{max}$
 3. $R = .05 D_{max}$ to $.075 D_{max}$ (Varies with number of panels)

NOTE: 1. For 6 Panel Design, $X_o = .27 D_{max}$
 2. For 8, 10, 12, 14, 16, and 20 Panel Design, $X_o = .23 D_{max}$

Fig. 7-12b Pattern-Dimension Factors for Ribless Guide-Surface Canopy (Ratios)



Panels	X/X_0	.1	.2	.3	.4	.5	.6	.65	.7	.711	.75	.792	.796	.8	.9	.988	1.0
6	Y/X	.592	.594	.596	.599	.602	.628		.694	.717	.673			.625	.542	.482	
8	Y/X	.492	.495	.500	.500	.501	.512	.543	.585		.657		.713	.710	.611		.534
10	Y/X	.456	.461	.465	.467	.469	.473	.496	.532		.617	.686		.674	.587		.515
12	Y/X	.402	.406	.408	.410	.419	.434		.477	.549		.658	.657	.571			.504

NOTE: (1) For 6-panel design, $X_0 = 0.70 D_{\max}$ (2) For 8-, 10-, and 12-panel designs, $X_0 = 0.55 D_{\max}$
(3) For 6-, 8-, 10-, and 12-panel designs, the following applies:

$$Y_1 = \frac{D_{\max}}{N} \text{ where } N = \text{number of gores}$$

$$X_1 = 0.50 Y_1 \quad R = 0.1 D_{\max}$$

Fig. 7-13 Pattern-Dimension Factors for Modified Ribless Guide-Surface Canopy

canopy is obtained from the porosity calculation as illustrated in Chapter 12. Tests conducted under infinite-mass conditions show a slight decrease in drag coefficient with increasing cone angle (Ref (7-14)).

3.1.10 RING-SLOT CANOPY. The drag-producing surface of a ring-slot canopy consists of polygonal cloth rings joined together by radial tapes to provide open spaces or slots between rings. The planform and inflated shape of a typical ring-slot canopy are shown in Fig. 7-19. A typical gore of a four-slotted ring-slot canopy is shown in Fig. 7-20, with the principal component parts and dimensions indicated. The selection of total porosity of the drag-producing surface is, as for the ribbon canopy, dependent on the stability and opening characteristics required. The range of recom-

mended total porosity for the drag-producing surface is shown in Fig. 7-21. Geometric porosity, the major component of total porosity, is the ratio of total slot and vent areas to the total canopy area. Even distribution of the geometric porosity is an important factor. Tests show that slots equally spaced between vent and skirt produce the most satisfactory results. The total slot area of the drag-producing surface may be determined from:

$$(7-11) \quad S_{\lambda} = \lambda_g S_o - s_o$$

where S_{λ} = Total slot area in square feet; and
 λ_g = Geometric porosity expressed as a decimal

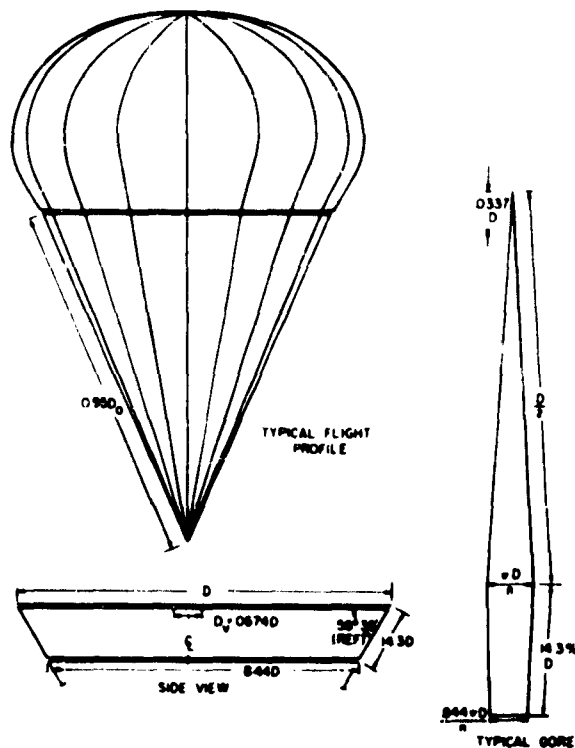


Fig. 7-14 Extended-Skirt Canopy

Dividing this total slot area by the number of gores results in the slot area required for each gore. The design problem then requires balancing the number and height of the cloth sections and the slot width to obtain the required diameters and slot area. The cloth sections are cut in the form of trapezoids, with the warp of the cloth parallel to the parallel sides. Although the section height may be any value desired, the cloth yardage is most efficiently used if cut into quarters, thirds, halves, or used in full width. Vertical ribbons, sometimes called vertical tapes, are usually placed from the vent to the skirt, down the center of each gore.

3.1.11 SHAPED-GORE CANOPIES. The shaped-gore type of drag-producing surface was designed to achieve maximum drag efficiency, as described in 3.1.2 of this chapter. Once the desired inflated profile of this canopy type has been defined, several specific considerations become pertinent to the determination of the gore coordinates. The drag-producing surface may first be treated as a surface of revolution generated by the desired profile as illustrated in Fig. 7-22. When a suitable number of gores has been assigned, the gore width at any radius is defined as the length of the arc

$$(7-12) \quad a = (2\pi r) / n$$

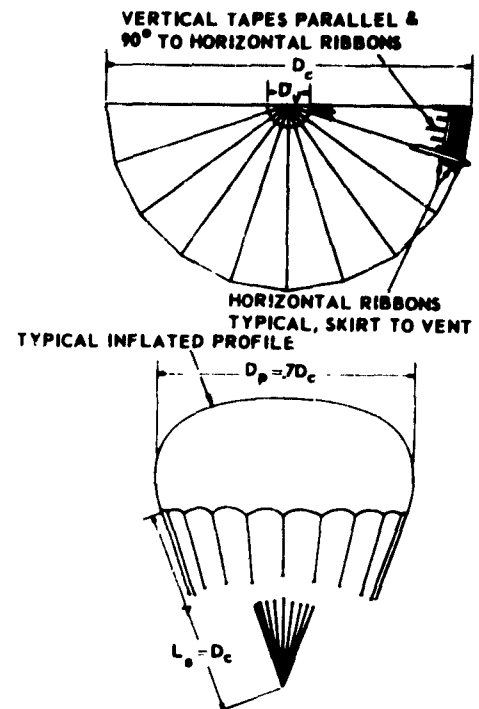


Fig. 7-15 Flat Circular Ribbon Canopy

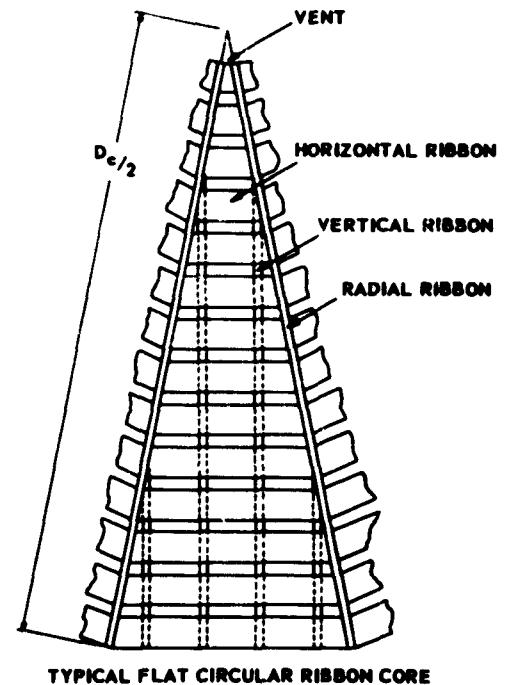


Fig. 7-16 Gore Construction of Flat Circular Ribbon Canopy

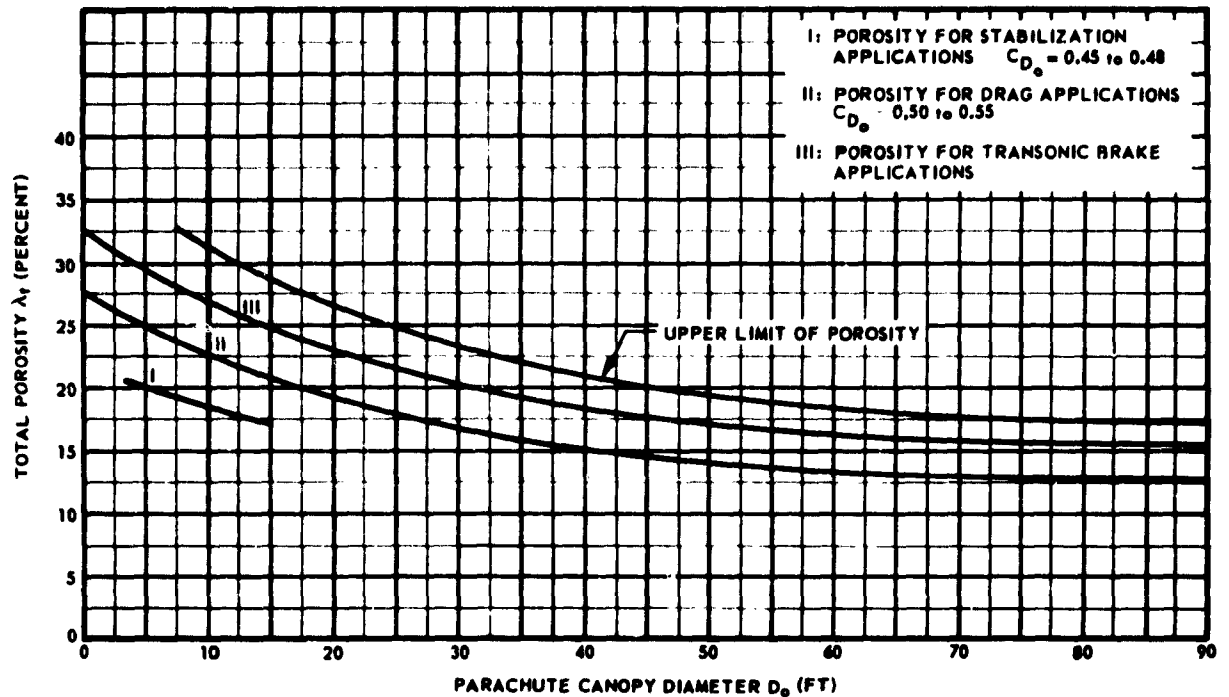


Fig. 7-17 Total Porosity vs Canopy Diameter for Flat Circular Ribbon Canopies

and the ordinate at distance S is

$$(7-13) \quad v = a/2 = \pi r/n$$

If additional fullness is desired between the main seams, a bulge radius, r_b , may be defined to establish the slightly greater gore width, d , of the lobed surface. This bulge radius must be established with due allowance for the elasticity of the fabric and the further effect of shortened suspension lines over the drag-producing surface. A lobe may be produced at the periphery by a local widening of the gore in the region of a_{\max} (see Fig. 7-22); however, the effect on the inflated shape cannot be predicted with any certainty and model tests must be conducted so that suitable adjustments of the gore pattern may be determined by measurement.

The design of shaped-gore canopies has become increasingly important when operation at supersonic speeds is required. At supersonic speeds conventional flat circular ribbon designs produce a reduced inflated canopy diameter when compared with the inflated diameter in subsonic flow, and exhibit violent pulsation of the drag-producing surface and higher horizontal ribbon flutter (Ref (7-15)). A shaped-gore canopy design, the ribbon Hemisflo, alleviates these undesirable performance characteristics by altering

the shape of the inflated canopy to approximate the shape which the flat circular canopy tends to assume in supersonic flow, and shortens the free length of horizontal ribbons in the vicinity of the skirt. The design of the ribbon Hemisflo is presented in Chapter 12.

3.2 Pocket Bands. The use of pocket bands is recommended to assist in the inflation of ribbon and ring-slot canopies. Pocket bands provide for a more rapid inflation rate, and allow the canopy to be deployed at speeds below its minimum, non-pocket-band-design opening-velocity. Use of pocket bands, in effect, reduces the design porosity of the canopy between 8 and 10 per cent. Fig. 7-23 shows the general configuration of pocket bands and values for the free length, L_a , of the pocket band for any given number of suspension lines. Strength of the pocket bands should always be at least 50 per cent of that of the suspension lines used.

3.3 Risers. The riser system is commonly composed of one or more members of heavy webbing, which extend between the lower end of the suspension-line system and the load, and of any metal interconnection fittings that may be required. Since the individual webbing members are considered parallel while under load, the maximum load is simply the drag load, which is usually considered as the opening-shock load. The general equation for the load on each riser is then

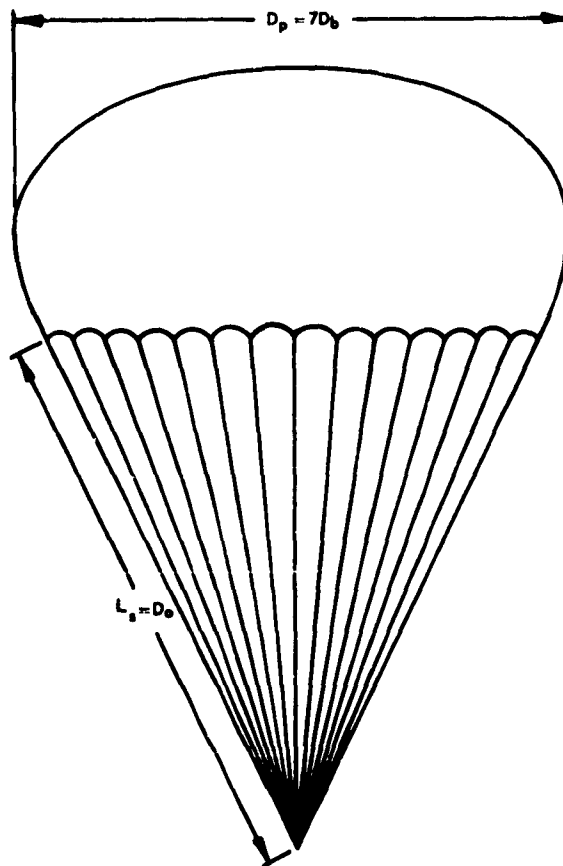
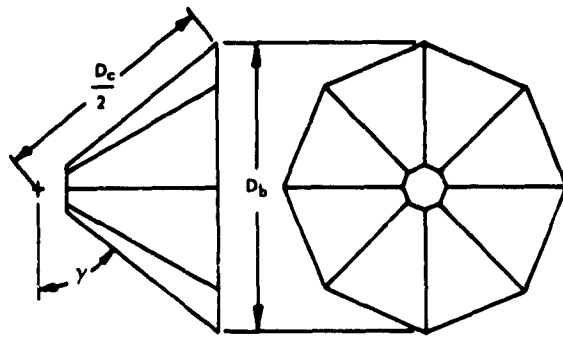


Fig. 7-18 Typical Geometry and Inflated Profile of Conical Ribbon Canopy.

$$(7-14) \quad F_R = \frac{F_o \cdot j}{Z_R \cdot u \cdot o \cdot e \cdot k}$$

where F_o = Maximum opening force;
 j = Safety factor;

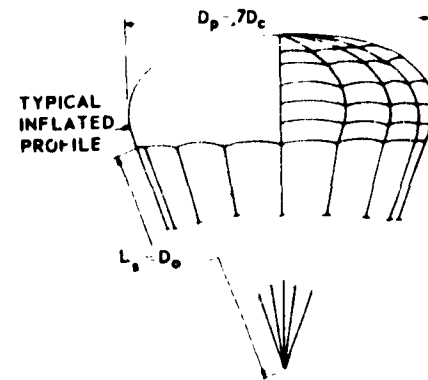
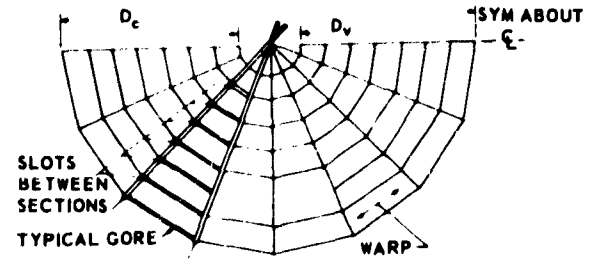


Fig. 7-19 Ring-Slot Canopy

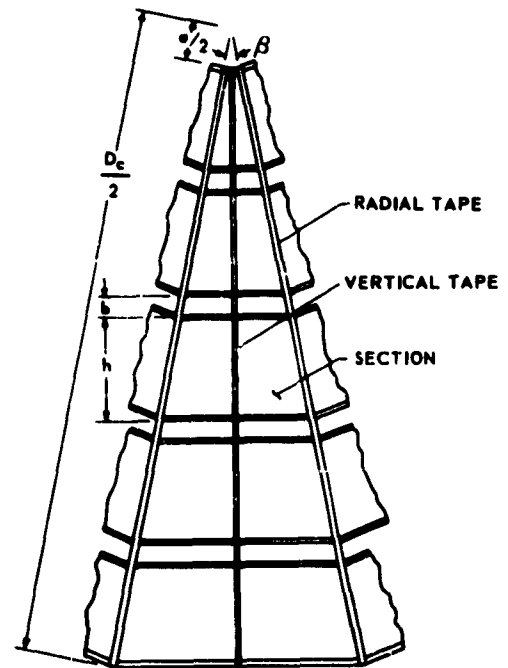


Fig. 7-20 Gore Construction of Ring-Slot Canopy

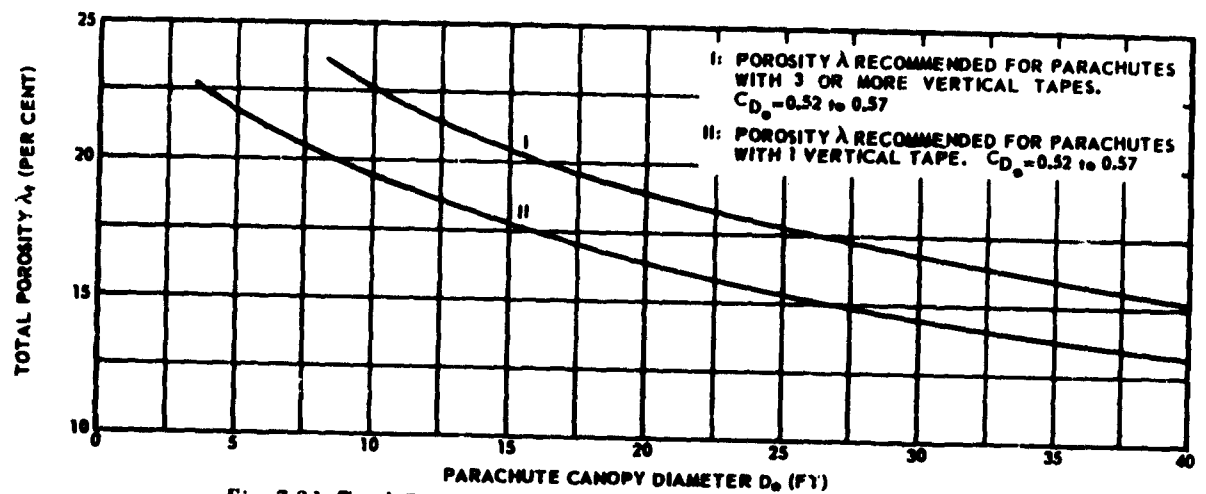


Fig. 7-21 Total Porosity vs Canopy Diameter of Ring-Slot Canopies

- Z_R = Number of individual webbings;
 a = Factor involving the strength loss at the connection loops;
 o = Factor related to strength loss in material from water and water vapor absorption;
 c = Factor related to strength loss by abra-

FLAT DEVELOPMENTS FOR
a. SURFACE OF REVOLUTION
b. FLUTED SURFACE
c. PERIPHERAL LOBE

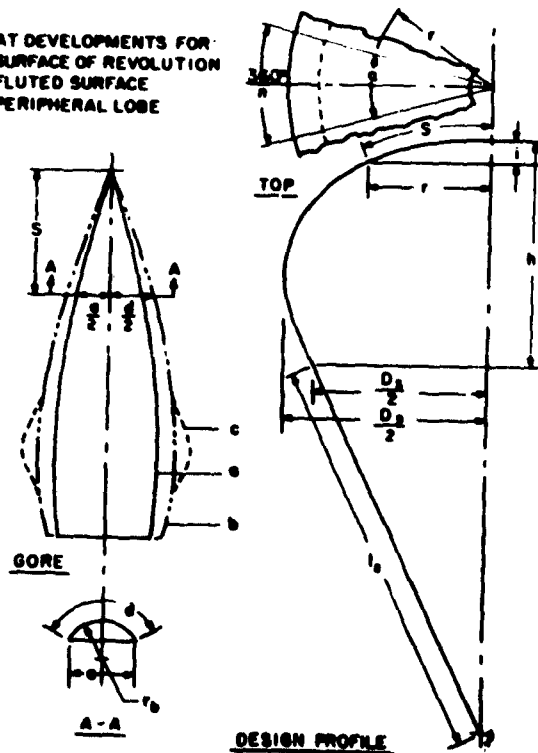


Fig. 7-22 Shaped Gore Canopy Layout

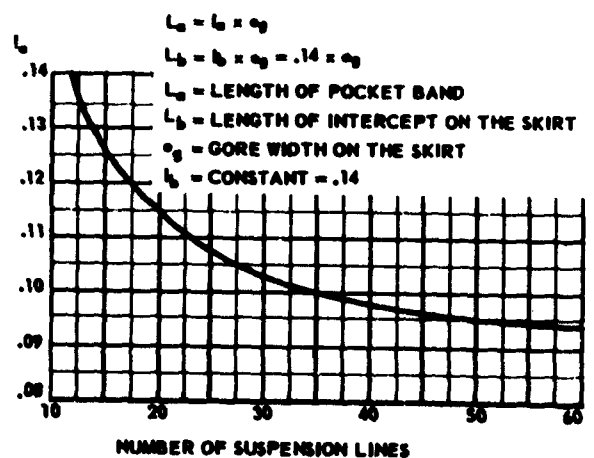
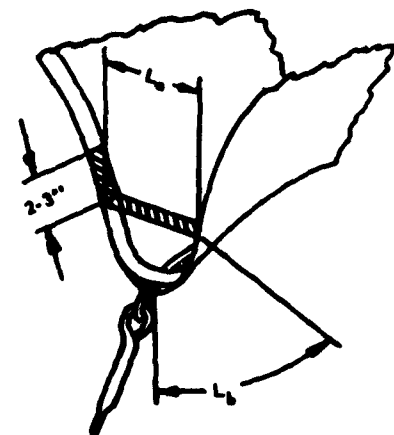


Fig. 7-23 Pocket-Band Design for Flat Canopy

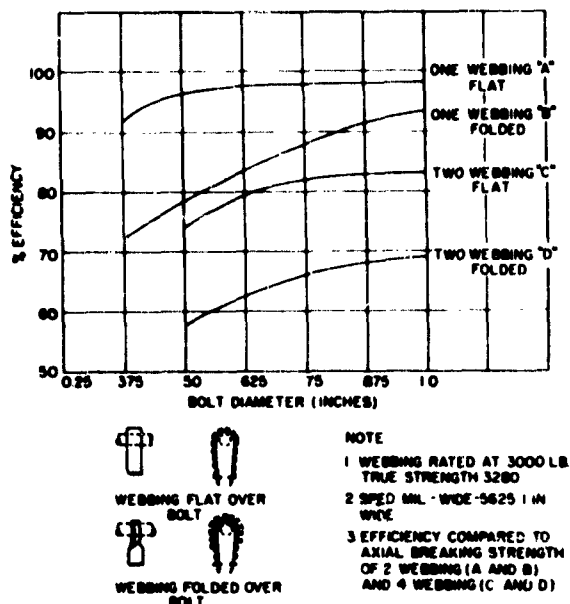


Fig. 7-24 Effect of Bolt Diameter on Efficiency of 3000-lb Webbing Loops

sion; and

k = Factor related to strength loss by fatigue.

Actual values for these factors may be obtained from Table 7-1.

The weakest point in the riser system is generally not the webbing itself, but the junctions with other parts of the assembly. The most common type of joint in use is one in which the webbing is looped around a circular bar of some form of hardware and sewed to itself. The diameter of the metal link has been found to have an effect on the efficiency of the joint; the efficiency generally decreases as the bolt diameter decreases. The efficiency of various 3,000-lb webbing loops as affected by the bolt diameter is presented graphically in Figure 7-24.

3.4 Keeper. The keeper in the suspension-line or riser system is an integral unit which maintains the desired ratio of suspension-line length to diameter (L_s/D_o) for optimum parachute performance, and reinforces the line confluence point. The keeper is generally fabricated of the same type of material as the riser, although usually of a lower rated strength, depending upon the construction and application of the riser. For the majority of applications, a keeper material having approximately 30 per cent of the rated strength of the individual riser webbings is considered sufficient.

The keeper is constructed by wrapping webbing

around the riser webbings at least $2\frac{1}{2}$ turns and then stitching it to the riser proper. For first-stage aerospace-vehicle recovery applications, and other applications in which the suspension lines are extended beyond the confluence point to form the riser, a different type of keeper is required. A typical keeper for first-stage aerospace-vehicle recovery applications is shown in Fig. 7-25. This arrangement of keeper and suspension lines provides for a generally equalized distribution of the loads transferred from the drag-producing surface through the lines, and minimizes elongation differences due to unsymmetrical canopy loading. Most significant, perhaps, is the total elimination of relative motion between keeper and lines, which has often been found to be the initial cause of line failure due to subsequent friction-heating and material crystallization.

3.5 Deployment Bags. Since a multitude of different types are known to exist, and since there are limitless variations within types, no general description of deployment bags in terms of size or shape can be attempted. Deployment bags may, however, be de-

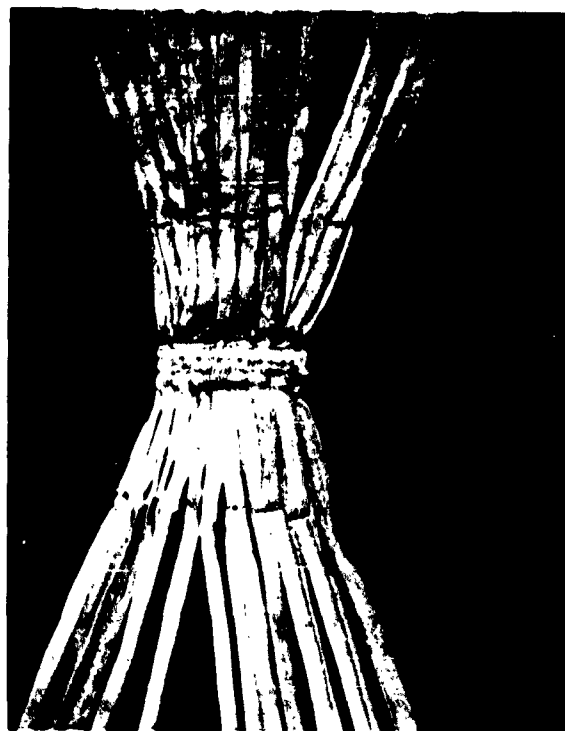


Fig. 7-25 Typical Keeper Design



Fig. 7-26 Deployment Bag, Aerospace Vehicle Recovery

scribed in terms of function:

(1) Deployment bags contain primarily the drag-producing surface of a canopy; they may or may not provide stowage positions for the suspension lines.

(2) Deployment bags control the sequential operations of deployment by means of a closure or control method which locks the canopy in the bag, and which may depend for operation upon line deployment, pilot-chute drag, snatch force, or operation of a mechanical device.

In general, little difficulty will be encountered in shaping a deployment bag to the space available. Space, however, definitely affects the line placement and closure methods used.

3.5.1 DEPLOYMENT BAG DESIGN. Deployment bag design problems may be divided into two general groups: methods used for storage and placement of suspension lines, and methods used for control and operation of canopy mouth closure. Major considerations in the design of bags are (1) bag strength, (2) smooth inner working surfaces, (3) allowance for the most efficient use of space available, and, (4) if

pressure packing is to be employed, a practical means of maintaining the packed shape after the pressure is removed. Deployment bags must be able to contain and control the canopy throughout the two most difficult conditions of deployment: (1) lift-off or ejection of the deployment bag by a static line, pilot chute, or ejection device, and (2) the opening of the bag for release of the canopy. Smooth working surfaces are required in all areas of the bag adjacent to the drag-producing surface during deployment, and in the area adjacent to the suspension lines. The basic enclosure for the canopy, whatever its shape, should, if possible, be sufficiently tight to prevent movement of the canopy within the bag during high accelerations encountered during lift-off or ejection. A well designed bag will allow the canopy to be extracted manually with very little effort once the bag closure is opened.

Normal layout and cutting methods are used in the construction of bags (Ref (7-17)). The basic container is usually formed in a cylindrical, trapezohedronal, or cubical shape (or may be in the shape of a segment of a circle, with uniform thickness, in instances when

canopies are clustered), in a manner to obtain maximum strength from the material along the longitudinal axis of the bag. Wherever possible, seams should be faced away from the areas adjacent to the canopy.

Most reinforcing webbings should be added to the basic container before sewing the container into its final shape. In general, two basic systems of webbing reinforcement are used, depending upon the forces involved in the use of the bag. For personnel and light air-drop parachute applications, straight-through reinforcement is normally used, with lateral webs usually of fairly light materials. On bags for very high-speed equipment it may be necessary to provide additional lateral webs to prevent bursting of the basic container. On heavy bags for large canopies X or W longitudinal web designs may be used, since much strength is added to the assembly by such construction. In addition, lateral webs should be considerably increased in strength to prevent bursting of the basic container. Locking loops should be reinforced heavily, since the full weight of the accelerated canopy bears on the locking loop flap, and failure of material at this point seriously affects bag performance. Fig. 7-26 shows a typical heavy bag for aerospace-vehicle recovery application.

Deployment bags for systems which require the use of pressure packing to reduce their pack volume are of necessity unique in their design. Provision must be made for restricting the bag during packing, and then loosening the bag at the proper time during deployment to allow relatively easy removal of the canopy from the bag. One method of accomplishing this is by incorporating an additional width of cloth (called a gusset) along the longitudinal axis of the bag and a row of grommets along the axis where the gusset material is attached to heavier bag material so that the bag can be laced down to its pressure-packed shape (Fig. 7-27). The lacings on the bag are strung through several cut-knives attached to a nylon-webbing

lanyard fastened securely at one end to the load. As the bag moves aft of the load at the start of deployment, the knives cut the lacings, allowing the bag to expand and the canopy to be removed from the bag freely and with little danger of friction burns.

Bags designed for use at high speeds, or for the handling of heavy canopies, are constructed of fairly strong materials. Heavier cotton ducks are suitable for this purpose, but are usually so rough that canopies are badly burned due to friction during withdrawal. It is considered good practice to line such bags with cotton material of lighter weight and smoother finish, particularly if the construction and reinforcement of the basic bag result in a rough interior. Generally, linings are assembled to the bag after the basic container has been cut and longitudinal webs added.

Bridles are either integral or detachable, depending upon conditions of use. Bags subjected to severe operating conditions or to constant service, particularly if small and cheap, are equipped with integral bridles which are normally extensions of the main longitudinal reinforcing webs on the bag. Detachable bridles are designed to attach directly to main longitudinal reinforcing-webs by suitable hardware. Bridles for large or heavy bags normally provide an effective length, from bag to common connection to the pilot-chute bridle-line, of at least 75 per cent, and preferably 100 per cent of the largest dimension of the bulkhead of the bag. Line locking-loops and permanent retaining-loops are usually constructed of cotton materials, or of nylon faced with cotton if high strength is required. Since locking loops are subject to high forces, it is usual to attach them to main longitudinal reinforcing-webs. Locking loops are usually formed with the same webbing used to provide retaining loops, or loops to which breakable line retaining-tapes may be tied. Webs provided for tying breakable line-retaining tapes are formed in much the same manner as permanent line-loops.

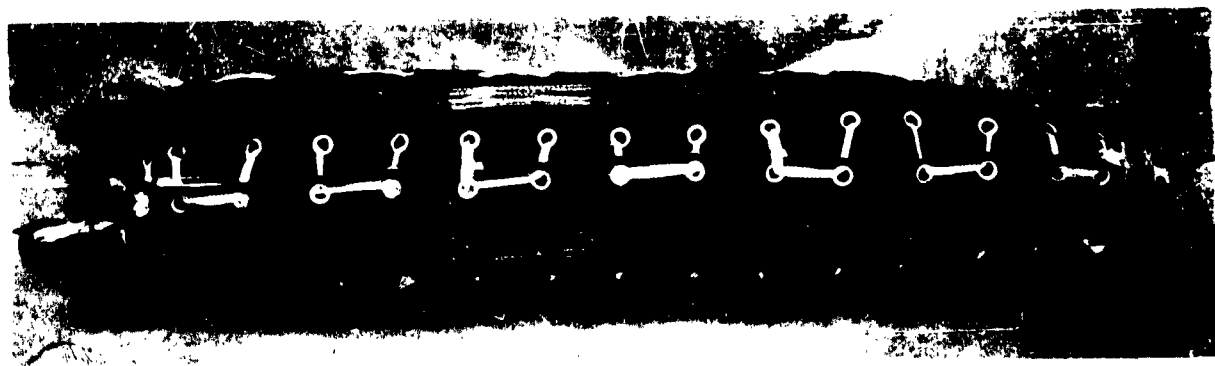


Fig. 7-27 Deployment Bag with Laced Gusset for Pressure-Packed Canopy

Covers for line stowage areas may be formed very simply on the top or side of a deployment bag, as shown in Fig. 7-28. If necessary, line stowage areas may be lined with soft cotton fabric. If large risers and heavy hardware must be stowed in the bag, additional space may be provided by forming a large pocket on the line cover itself.

Line flaps, when placed at the mouth of the bag, are usually extensions of the bag side, and are constructed in much the same manner as a normal closure flap, as illustrated in Fig. 7-28. Line retention-loops may be added to stowage flaps in the same manner as permanent line-loops; longitudinal reinforcements are extended down stowage flaps to provide strength for line retention.

3.6 Pilot Chutes. Pilot chutes are necessary to activate positive and proper deployment for all parachute applications except for those systems deployed by static line. A number of pilot-chute types have been used experimentally, including flat octagon, flat square, "baseball", and hemispherical types. The flat octagon type is equipped with a spring to insure im-



Fig. 7-28 Deployment Bag and Line Stowage Flaps



Fig. 7-29 Pilot Chute Type MA-1

mediate opening upon pilot-chute release. The standard pilot chute now used for personnel, air drop, aircraft deceleration, and other applications, was derived primarily from the flat octagon type of pilot chute, with vanes added to obtain the following advantages:

- (1) The vanes prevent the lines from entangling inside the parachute pack;
- (2) Should the pilot chute strike some object, the vanes tend to slide past it rather than wrap about it, or permit the object to pass between the lines;
- (3) The vanes cause the airflow to be directed into the pilot chute and act as a sail to aid in the deployment of the pilot chute from the pack; and
- (4) The addition of vanes decreases the possibility of pilot-chute canopy-inversion.

A typical pilot chute, Type MA-1, is shown in Fig. 7-29. Basically, pilot chutes used for personnel, air-drop, and aircraft-deceleration applications have a hemispherical canopy and are constructed with a conical coil spring and vanes. In general, the canopy and the vanes of the pilot chute are constructed of the same material.

Any of the conventional canopy designs can be used as a pilot chute; however, a balance must be achieved between the required stability and drag, and to a cer-

tain extent, weight and volume. For example, a guide-surface pilot-parachute canopy will have excellent stability but, due to its lower drag efficiency, will require a larger canopy for a given force than if the stability of a ring slot or flat circular canopy were acceptable. On the other hand, however, a slight increase in volume and weight must be tolerated. Drag coefficient and opening-shock factor data for the most commonly used types of pilot chutes are listed in Table 7-7.

TABLE 7-7 PILOT CHUTE DATA

Type	Drag Coefficient	Opening-Shock Factor (Infinite-Mass)
Vane	$C_{D_o} = 0.55$	2.5
Flat Circular	$C_{D_o} = 0.75$	2.5
Ring-Slot	$C_{D_o} = 0.65$	1.5
Flat Circular Ribbon	$C_{D_o} = 0.55$	1.5
Ribless Guide-Surface	$C_{D_p} = 0.80$	2.0
Ribbed Guide-Surface	$C_{D_p} = 0.95$	2.0

The size of the pilot chute is of the utmost importance for positive and orderly deployment of the main canopy. No definite method has as yet been established to determine the required pilot-chute size for any particular application; however, experience has shown that certain ratios of pilot-chute drag area to main-canopy drag area perform best (see Table 7-8).

TABLE 7-8 RATIOS OF PILOT CHUTE TO MAIN CANOPY AREA

Deployment Speed (Indicated Air Speed)	$C_{D_p} S$ Ratios	Ratio Pilot Chute to Main Canopy
Up to 200 knots	≈ 0.03	$\approx 3\%$
200 to 300 knots	≈ 0.02	$\approx 2\%$
Over 300 knots	≈ 0.01	$\approx 1\%$

These data are only approximate, and may require modification for the particular parachute application. For high-speed aerospace-vehicle recovery application, for example, in which it is necessary to extract the main canopies out of tight compartments, and so

that orderly deployment sequences of the main canopies is insured, pilot chutes of higher drag-area ratios than those listed in Table 7-8 have been used. For the determination of correct sizes of pilot chutes, several other considerations, such as deployment-speed ranges, wake effects, and breaking strength of ties, must be taken into account. It should be remembered, however, that a certain energy is required to fulfill all the functions of a successful parachute deployment.

For high-speed applications, pilot chutes of the guide-surface type or ribbon type are commonly used. In such designs, these pilot chutes should be packed in separate deployment bags in order to separate snatch and opening forces of the pilot chute.

The bridle between the pilot chute and the main canopy bag, or the apex of the main canopy, must be of sufficient length to prevent the suspended load from blanketing the action of pilot chute. On the other hand, if the bridle is too long, the maximum snatch force or opening force exerted by the pilot chute will increase greatly, and the opening shock factor will be greater than that given in Table 7-7. In general, the bridle used should be of such length that the skirt of the inflated pilot chute will be five to six diameters of the suspended load behind the load. The actual strength design of the bridle depends upon the maximum pilot-chute force and the efficiency of the bridle connection. Strength calculations for bridles are discussed in 3.3 of this chapter.

Fabrication methods for pilot chutes are identical to those employed for other types of canopies.

REFERENCES

- (7-1) Jailer, R. W., et al., Analysis of Heavy-Duty Parachute Reliability. WADD TR 60-200, Jun 1960, AD 246 490.
- (7-2) O'Hara, F., Notes on the Opening Behavior and the Opening Forces of Parachutes. Journal of the Royal Aeronautical Society, Vol. 53, No. 467, pp 1053 - 1062, Nov 1949.
- (7-3) Johns, T. F., Parachute Design. British RAE Technical Note No. ARM 365, R&M 2404, Dec 1946, ATI 254 15.
- (7-4) Heinrich, H. G. and Niccum, R. S., A Method to Reduce Parachute Inflation Time with a Minor Increase of Opening Force. WADD TR 60-761, Oct 1960.
- (7-5) Murray, E. J., Ultra-fast Opening Personnel Parachute Type XMP-2. WADD TR 60-485, Apr 1961.
- (7-6) Downing, J. R., et al., Recovery Systems for Missiles and Target Aircraft, Part III, High Sub-

- sonic and Transonic Track Borne Parachute Tests, AF TR 5853 Part III, WADC, Dec 1956, AD 122 635.
- (7-7) Heinrich, H.G., Aerodynamics, Performance, and Design of Personnel Guide Parachute, WCTFE-672-145-A-9-1, 21 Nov 1951.
- (7-8) Heinrich, H. G., Parachutes, Guide Surface; MCREXF-672-25F; Feb 1948.
- (7-9) Heinrich, H. G., and Scipio, L. A., Performance Characteristics of Extended Skirt Parachutes. WADC TR 59-562, Oct 1959, AD 232 149.
- (7-10) Knacke, T., Design, Use, and Construction of FIST Type Parachute. MCREXF-672-191.1., Jun 1948.
- (7-11) X-7A Supersonic Ramjet Test Vehicle Parachute Recovery System, Sections I and II. WADC TR 55-162, Jun 1955, AD 95743, AD 95744, Confidential Reports, Unclassified Titles.
- (7-12) Culver, I. H., et al., Notes on the Aeroelastic Stability of Reefed Ribbon Parachutes. Lockheed Rpt. No. 8544, Aug 1952.
- (7-13) Jaeger, J. A., et al., Study of the Load Distribution in a Conical Ribbon Type Parachute. Lockheed Rpt. No. 8541, Aug 1952.
- (7-14) Pedersen, P. E., Study of Parachute Performance at Low Supersonic Deployment Speeds; Effects of Changing Scale and Clustering. ASD TR 61-186, May 1961.
- (7-15) Meyer, R. A., Wind Tunnel Investigation of Conventional Types of Parachute Canopies in Supersonic Flow. WADC TR 58-532, Dec 1958, AD 202 856.
- (7-16) Berndt, R. J., Supersonic Parachute Research, ASD Technical Documentary Rpt. No. 62-236, Mar 1962.
- (7-17) Barnes, R. W., Deployment Bags, Parachute, General Development of, Memorandum Report MCREXF-672-23-1., Sept 1949.
- (7-18) Calhoun, J. A., Pilot Parachutes, Study of, MCREXF-672-19-FFF, Mar 1951.
- (7-19) Coy, R. G., Investigation of the Relative Efficiency of Pilot Parachutes, WADC TR 56-147, Mar 1956, AD 89 095.

BIBLIOGRAPHY

Jacobsen, C.R., et al., A Study to Establish a Parachute Research and Development Program, Vol. III, Summary and Analysis of Existing Knowledge. WADC TR 53-78, Aug 1953, AD 110 453.

CHAPTER 8 DEPLOYABLE AERODYNAMIC DECELERATOR SYSTEM CONSTRUCTION DETAILS

Table of Contents

<i>Section</i>	<i>Page</i>
1 LAYOUT AND CUTTING	396
2 SEWING AND STITCHING	396
3 STRUCTURAL JOINTS	397
4 STRENGTH OF JOINTS AND SEAMS	402
4.1 Type of Stitch	402
4.2 Type of Thread	402
4.3 Number of Stitches per Inch and Stitching Pattern	402
4.4 Seams and Seam Construction	402
4.5 Strength of Suspension-Line Seams	403
<i>References</i>	403

Illustrations

<i>Number</i>	<i>Page</i>
8-1 Typical Flat Fabric Seams	397
8-2 Skirt and Vent Construction, Ribless Guide-Surface Type Canopy	397
8-3 Typical Joint Construction of Roof Panels, Ribless Guide-Surface Canopy	398
8-4 Suspension Line Connection to Skirt, Flat Circular Ribbon Canopy	398
8-5 Suspension Line Connection to Skirt Loop Attachment	398
8-6 Joint Reinforcement, Butterfly Type	398
8-7 Installation of Reefing Ring as Seen from Inside of Ribbon Canopy	399
8-8 Cross-Section of Typical Heavy-Duty Ribbon Canopy Gore	400
8-9 Radial Ribbon – Horizontal Ribbon Spliced Joint	400
8-10 Dependence of Seam Efficiency on Stitches per Inch	401
8-11 Illustration of Orthogonal and Bias Orientation of Fabric with Seam	402

CHAPTER 8

DEPLOYABLE AERODYNAMIC DECELERATOR SYSTEM CONSTRUCTION DETAILS

The methods by which the parachute may be assembled from its component parts are limited in number and variety, both by available equipment (principally sewing-machines), and by the physical properties of applicable materials. While these restrictions are of major importance in the economics of parachute manufacturing, fabrication methods also have considerable influence on the strength, elasticity, and flexibility of the structure. These constitute design criteria relating mainly to details of assembly at seams, joints, and hems, the types of which depend on their location and function.

SEC. 1 LAYOUT AND CUTTING

The large number of pieces of material that must be handled and assembled to form a canopy makes it mandatory that layout markings and indexing points be held to a minimum. Since section edges can be cut accurately enough to serve as mating points as well as seam and hem bases, layout marks are not usually required on the fabric in the construction of large canopies. Some dimensional variations will result from lack of uniformity in the lay of successive layers of fabric during the cutting operation. The flexibility of the weave pattern makes this a difficult factor to control, unless some form of temporary filler or sizing can be applied to the fabric.

Webbings and tapes are measured and marked under sufficient tension to assure uniformity. Weights from 5 to 40 lb are used, depending on the strength of the material being measured, to achieve the necessary tensile force. In constructions where the suspension lines pass over the drag-producing surface, the skirt and vent edge-intersection points are marked on the lines. Since the lines are stitched to the cloth surface only at the skirt and vent, the intervening fullness of fabric represents no problem. In all types of construction requiring the continuous attachment of tapes, webbings, and circumferential bands to the exterior surface of the cloth, uniform distribution of cloth fullness along the seam is difficult to achieve. It is frequently necessary to provide numerous intermediate indexing marks on both tape and cloth surfaces to guide the sewing, and tacking or basting may also be required. The main seams provide indexing marks for circumferential bands so that only the tape need be marked for each intersection. Radial dimension marks, however, are needed on the drag-producing surface for reinforcing bands at intermediate locations between skirt and vent. The problem of distributing

fullness along a seam arises, even though the measured lengths of cloth and tape are the same, because of the great difference in elasticity, but this difference diminishes with increasing weight of fabric.

SEC. 2 SEWING AND STITCHING

Stitching with thread by any one of a variety of sewing machines, and sometimes by hand, is the traditional method for joining textiles. Strong, efficient joints result when the correct number, spacing, and pattern of stitchings are employed. The strongest type of stitch is the two-thread link stitch formed by most sewing-machines when the proper tension is applied. Zigzag stitching, both single- and double-throw, is valuable in parachute manufacturing, primarily because seams and joints so joined are capable of great elongation without creating excessive tensile stress in the thread itself.

Several difficulties of varying importance arise in the stitching together of parachute components. These difficulties must be considered carefully. The tightness of the stitching resulting from excessive thread tension has two effects which may be undesirable in certain types of seam: the finished length of the seam is shorter than the cut length of the material, because of gathering between each needle penetration; and the binding together of the material creates friction, which reduces the flexibility and elasticity of the joint. In machine-sewing, differential feed can occur between the upper and lower pieces of material being joined, thus causing end mating-points to pull out of register as the seam is sewn. Yarn filaments can be broken by needle penetration, thereby weakening the basic fabric. The thread itself may be weakened or broken in thick joints and at seam intersections as a result of increased friction of penetration attending the superimposition of successive rows of stitches. High-speed sewing may weaken Nylon materials by

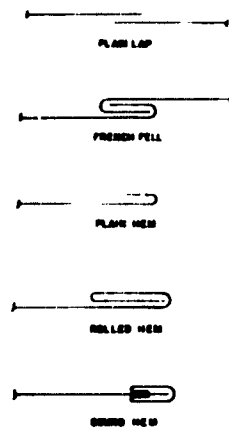


Fig. 8-1 Typical Flat Fabric Seams

frictional overheating.

When differential feed or "creep" of materials cannot be overcome to the extent required by the dimensional tolerances of the structure, basting may become

necessary. Basting is the temporary holding of two or more pieces of fabric together until they are permanently assembled. This is usually accomplished by temporary sewing. Cement is also utilized, but only in certain instances, such as model-canopy construction, since it is considered undesirable because of possible deleterious effects on fabric, particularly at elevated temperatures. Where the use of cement is permissible for basting, the quantity of cement applied to one point must be carefully metered so that the area of fabric affected has a minimal diameter (generally, approximately 0.1 in.). All of the thicknesses of material at the seam or joint should be joined by one application on the centerline or midpoint. The cement must set quickly and remain flexible with age. Successive cement spots on the same seam must be as widely spaced as practicable.

SEC. 3 STRUCTURAL JOINTS

The many types of hems and seams employed in the construction of canopies have certain geometrical properties in common. Fig. 8-1 depicts several typical flat fabric hems and seams. The width of an integral reinforcing tape, and the number of rows and spacing of stitching, is determined by strength and other

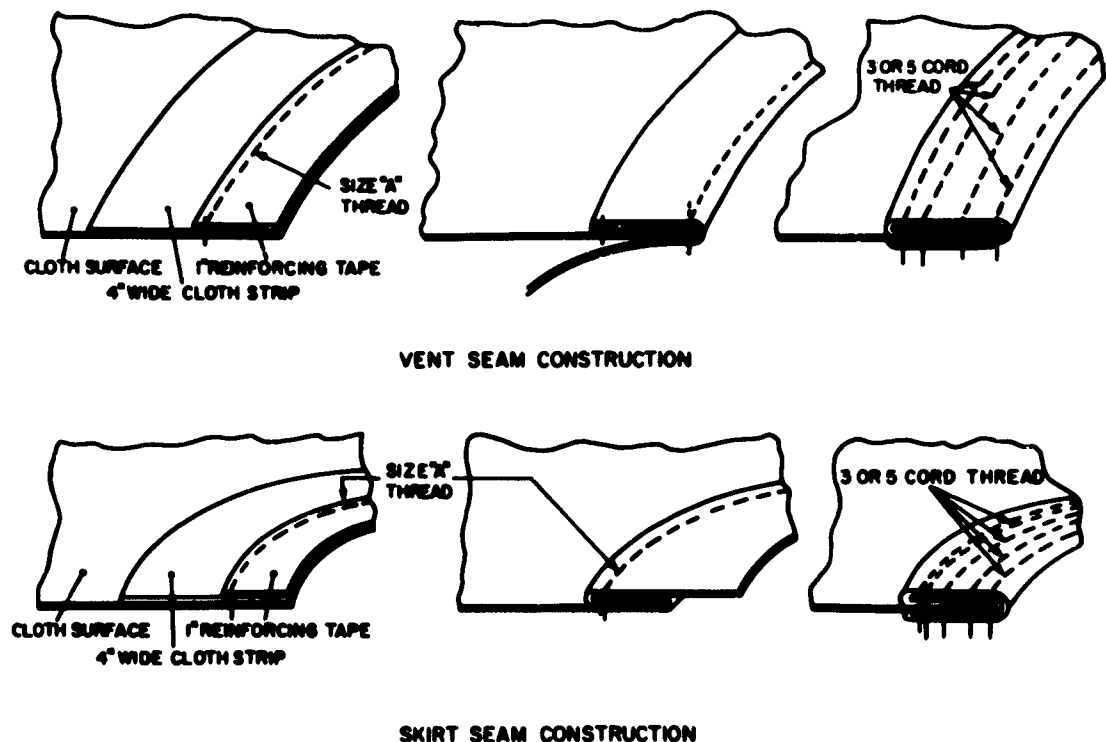


Fig. 8-2 Skirt and Vent Construction, Ribless Guide-Surface Type Canopy

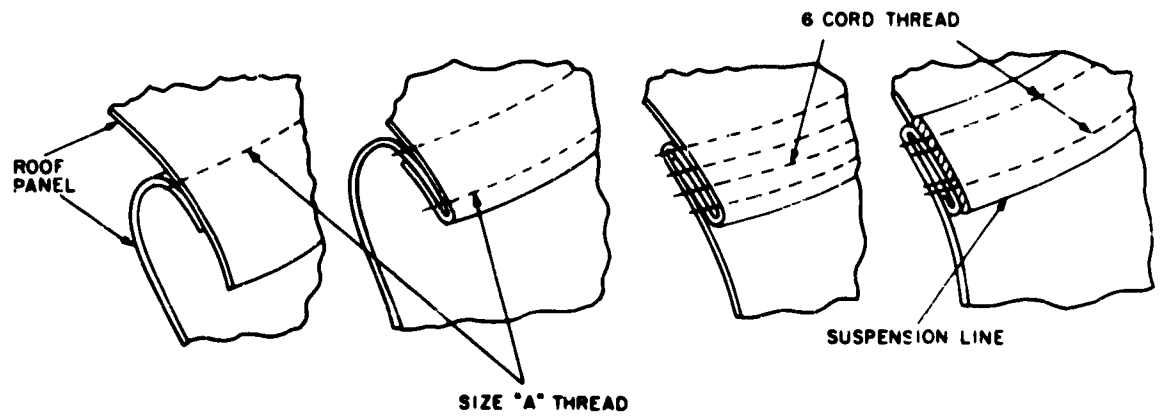


Fig. 8-3 Typical Joint Construction of Roof Panels, Ribless Guide-Surface Canopy

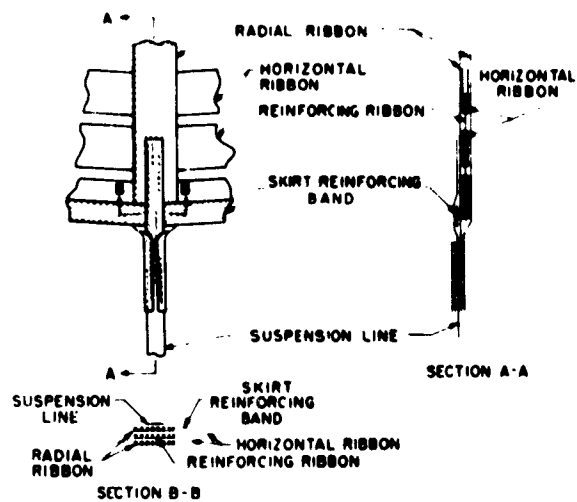


Fig. 8-4 Suspension Line Connection to Skirt, Flat Circular Ribbon Canopy

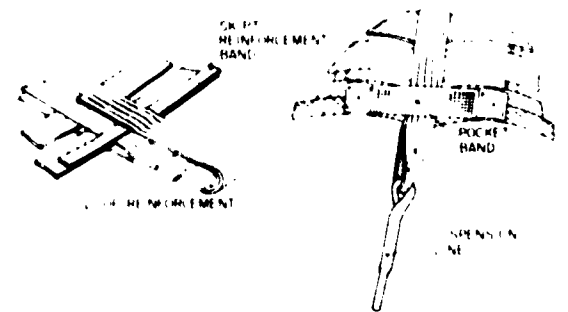


Fig. 8-5 Suspension Line Connection to Skirt Loop Attachment

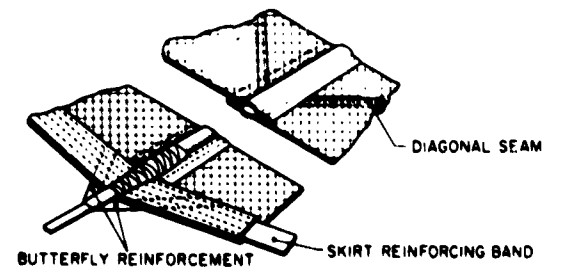


Fig. 8-6 Joint Reinforcement, Butterfly Type

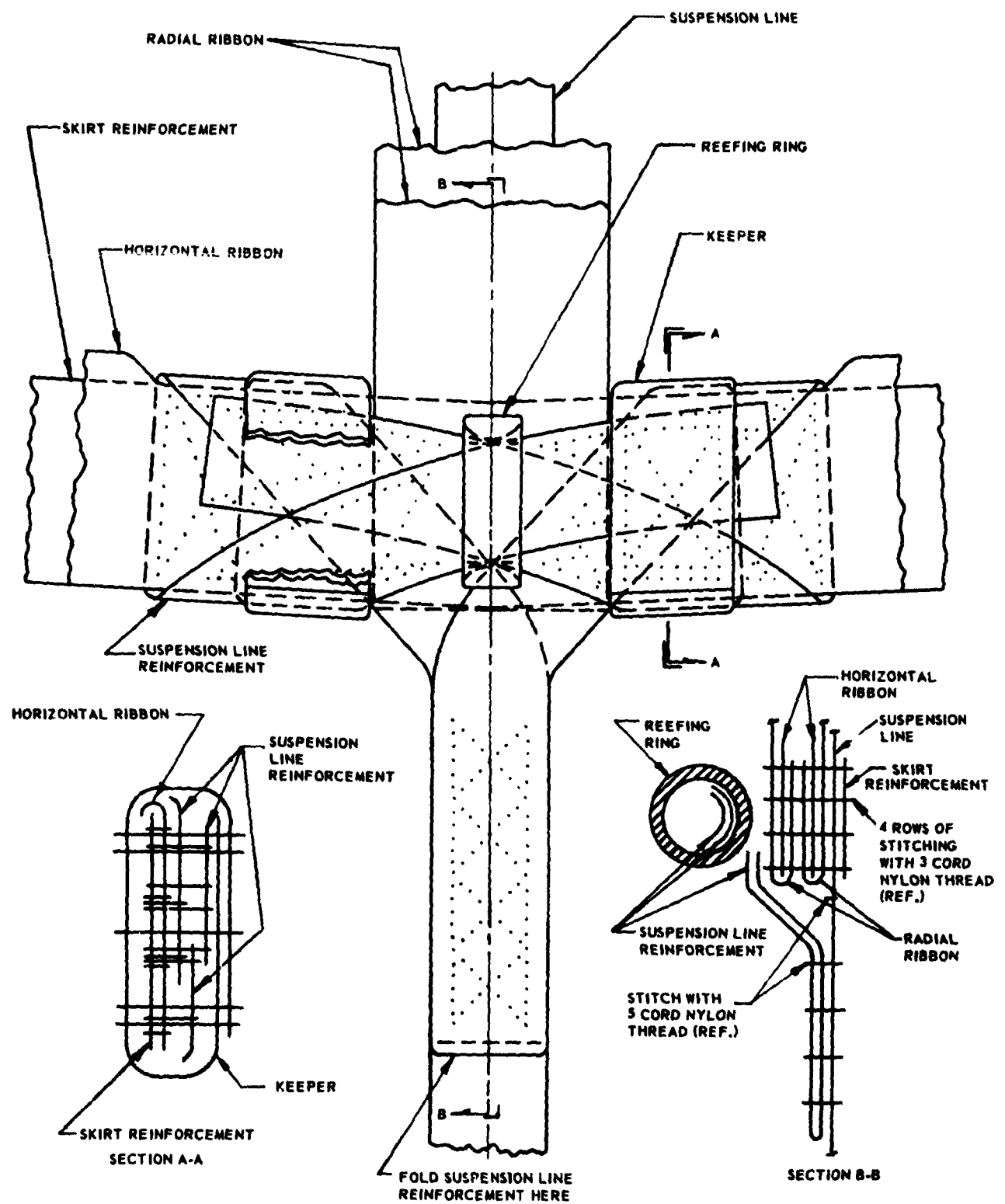


Fig. 8-7 Installation of Reefing Ring as Seen From Inside of Ribbon Canopy

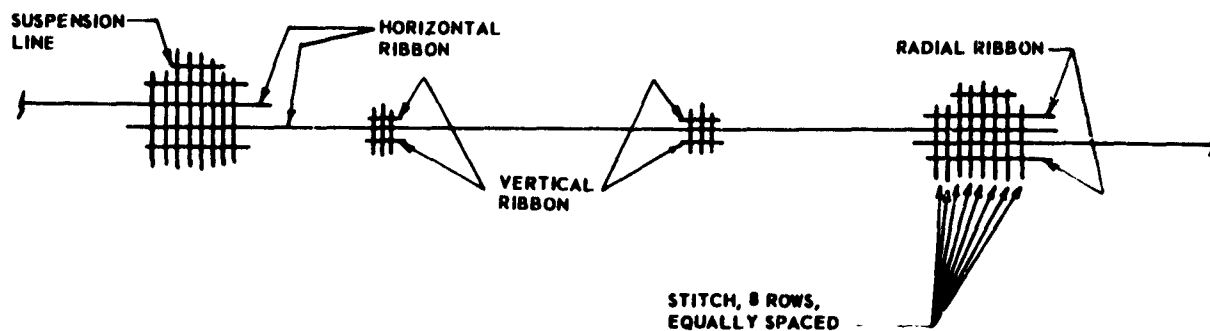


Fig. 8-8 Cross-Section of Typical Heavy-Duty Ribbon Canopy Gore

functional requirements. The width of hem or seam allowance is governed by its type. The simplest types of hem and seam are generally used where the fraying of an exposed cut edge is not objectionable. Otherwise, an additional turn of fabric is required to place the cut edge inside. The rolled-hem and French-fell seam are commonly employed for this reason, as well as for their slightly greater strength. A bound hem is used occasionally, such as on the skirt and vent of the ribless guide surface canopy (Fig. 8-2). There, a narrow strip of fabric or webbing is applied to the cut edge and rolled under on each side. An integral reinforcing-tape may also be bound into the hem at the same time by this means. A typical joint of roof panels of a ribless guide-surface canopy is shown in Fig. 8-3.

Canopies with geometric porosity have many addi-

tional free edges that must be hemmed, except where selvages are strong enough alone, as in the ribbon-type canopies. Such factors materially affect the economy of fabrication. In addition to the common practice of sewing the suspension lines to the drag-producing surface at skirt and vent with double-throw zigzag stitches, there are such practices as:

- (1) Lines lapped over and stitched to the ends of main radial-ribbons or reinforcement tapes at the skirt. This arrangement is shown in Fig. 8-4.
- (2) Lines tied to loops formed at the end of each main radial-ribbon as shown in Fig. 8-5.
- (3) Lines formed as continuous extensions of main radial-ribbons, made of narrow webbing.
- (4) Continuous suspension lines sewn from the skirt to the vent with four rows of stitching.

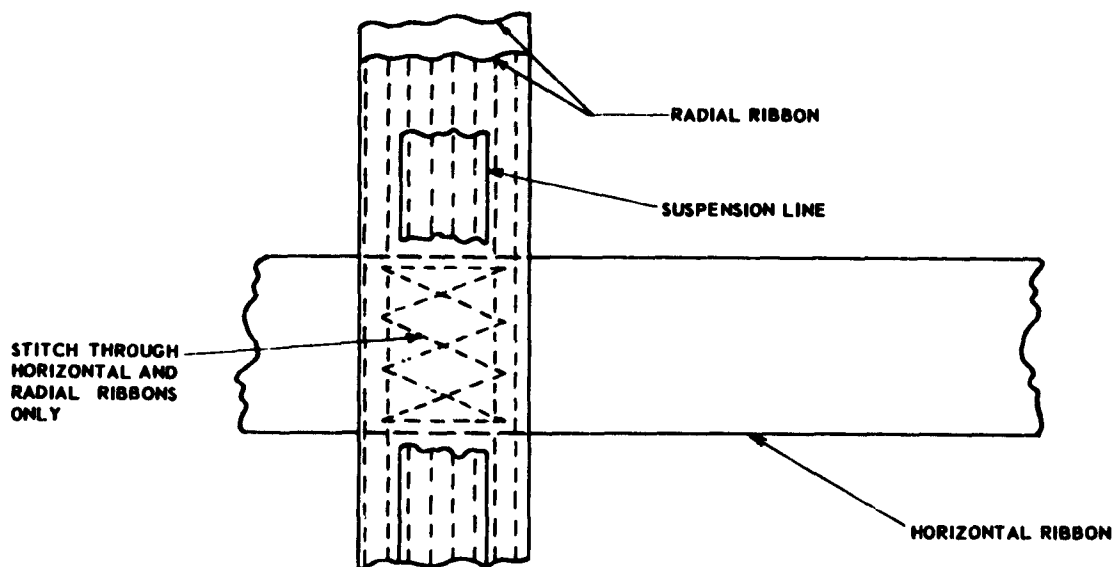


Fig. 8-9 Radial Ribbon - Horizontal Ribbon Spliced Joint

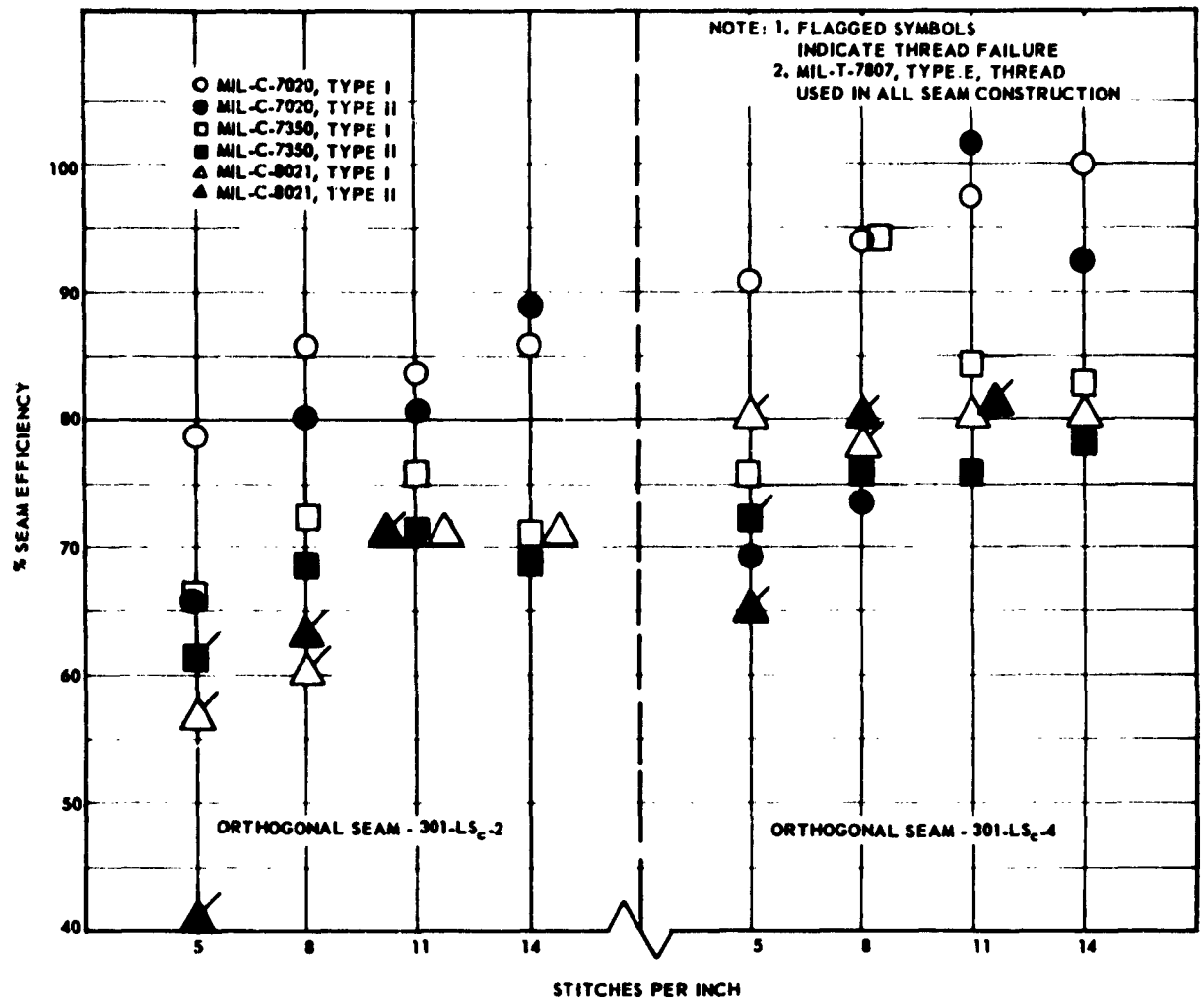


Fig. 8-10 Dependence of Seam Efficiency on Stitches per Inch

Joint reinforcements at the skirt, made of short lengths of tape or webbing, include the following arrangements:

- (1) The common "butterfly" type shown in Fig. 8-6.
- (2) A single-lapped doubler.
- (3) Two-piece doublers, inside and out, and combinations of doublers, butterflies, and looped rib-extensions.
- (4) A single piece of webbing which provides for suspension-line reinforcement and attachment of the reefing ring to the skirt, as shown in Fig. 8-7.

The major load-carrying members of a heavy-duty ribbon canopy are the horizontal ribbons and the suspension lines. A typical cross-section of a heavy-duty ribbon-type gore is shown in Fig. 8-8. The sectional

view shows the continuous suspension-line sewn on the radial ribbon with four rows of stitching. In the continuous-suspension-line design, the radial ribbons are used for ease of production and are not required for structural purposes. The eight rows of radial stitching are required to splice the horizontal ribbons. This spliced joint will hold ribbons up to 2000 lb. When heavier ribbons are used, a four-point cross-stitch pattern is required in addition to the eight rows of stitching as shown in Fig. 8-9. To improve the horizontal-ribbon efficiency and to reduce the canopy bulk and the number of stitching patterns, a continuous-ribbon construction may be used.

The design objective, with respect to economy of fabrication, is to obtain optimum joint efficiency and

serviceability with maximum simplicity of construction. The number of parts and operations must be the fewest possible consistent with functional requirements, and preference is given to operations that can be performed to advantage on high-speed machines.

SEC. 4 STRENGTH OF JOINTS AND SEAMS

When joining fabric components into one complete structure, it is important to make junctions in such a manner that the strength of the joint is not below that of the components being joined. This ideal is not always realized. A relationship can be set up between the material and joint (joint-efficiency factor), which is defined as

$$\eta = (\text{Strength of joint}) \div (\text{Strength of material being joined})$$

Failure can occur in either or both of two ways. The first is by failure of the stitching thread, and the second, by failure of the materials being joined. Thread failures should normally occur in the efficiency-factor range of up to 100 per cent. When the joint-efficiency factor approaches the upper limit, failure is generally a fabric failure. The fabric may fail at the joint at a lower strength-value than if the failure were in the unobstructed fabric. The probable cause for this is the weakening of the material by cutting, or damaging of the yarns as the needle passes through the fabric, or a local reduction of the elasticity because of friction between the layers caused by the tightness of the stitching. The strength of a sewn joint depends on factors covered in the paragraph below.

4.1 Type of Stitch. There are many different types of stitches practicable, all described in the Federal Specifications for Stitches, Seams, and Stitching, DDD-S-751. The most frequently used are Type 301, which is formed by two threads, and Type 304, which is similar but in a zigzag pattern (single-throw).

4.2 Type of Thread. Usually, the thread material is the same as the fabric being joined. Nylon and cotton threads are extensively used and are covered by Military Specifications. The use of heavier thread improves the seam strength, even though its use requires a larger needle, which may mean greater yarn damage in sewing (Ref. 8-1)).

4.3 Number of Stitches per Inch and Stitching Pattern. The stitching pattern depends on the materials being joined. The flat fabric seams use parallel rows of zigzag stitching. Formed fabrics, such as lines and webbings, employ patterns that are combinations of straight, cross, and zigzag stitching. The number of stitches per inch used depends on the

strength required and the type of material, but is restricted by the working range of a given sewing-machine. Both the number of stitches per inch and the pattern (number of rows) are varied to achieve the desired strength. It would be expected that an increase in either or both would increase the strength, up to some point where the closeness of the penetrations might possibly cause a decrease in strength. As the breaking strength of the fabric is surely not increased as the number of rows or stitches per inch is increased, it can be assumed that the thread failures, not the cloth strength, are contributing factors. However, if the strength of the cloth is reached, the addition of more stitches cannot make the seam any stronger. The dependence of seam efficiency on stitches per inch for various canopy cloth materials and rows of stitches is graphically illustrated in Fig. 8-10.

4.4 Seams and Seam Construction. A seam is defined as a series of stitches which join two or more plies of cloth. A complete seam-designation contains the type of stitch, the seam class, the type within the class, and the number of rows of stitching. For example, 301-I,Sc-2 means: Type 301 stitch, LS class, c type of that class, with two rows of stitching. Seam strength varies with the orientation of the fabric to the seam. Results from strength tests of orthogonal and 45-deg bias seams (see Fig. 8-11) show

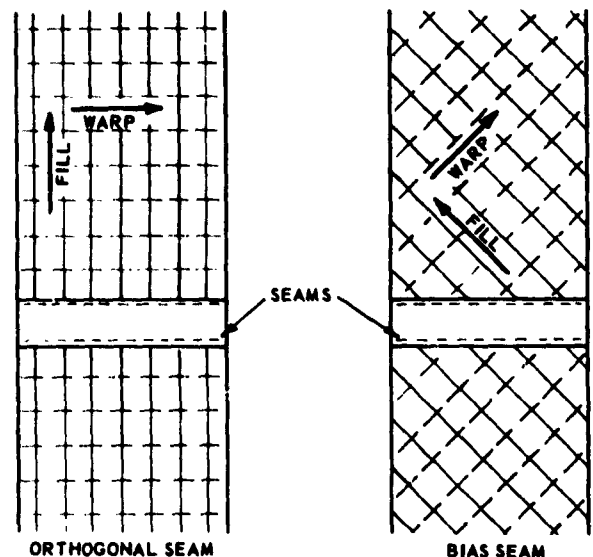


Fig. 8-11 Illustration of Orthogonal and Bias Orientation of Fabric with Seam

that the latter seam-orientation produces the greater seam efficiency.

4.5 Strength of Suspension-Line Seams. There are three different types of joints in the suspension-line system: the line-to-skirt type, the line-to-riser type, and the line-to-line type. In the suspension-line-to-skirt joints, the suspension line joins the skirt periphery at a point where the main radial-seam joins the skirt hem. The suspension line can be either a continuation of all or part of the members that make up the radial seam or it can be a separate member that is attached to the skirt. The former is always sewed to the canopy in the skirt band area, with reinforcements if required. The latter can be of two general types, a loop connection or an entirely sewed connection. In general, the looped joint is more efficient than the entirely sewed joint, with a joint-efficiency factor of approximately 90 per cent, compared to 80 per cent for the entirely sewed type. The method of construction of the joint is partially suggested by the size of

the members being joined. Other than this, a type is selected which has proved satisfactory in the past. Exceptions to this selection method are canopies constructed completely according to specifications, such as the flat circular ribbon and ring-slot types.

In the suspension-line-to-riser joint, two basic types are used: an entirely sewed joint; and a combination loop-and-sewed joint, which can include a metal link. Use of a metal link in the latter is the more common. The line is tied to the link and the free end attached to the line by various means.

The suspension-line-to-line joint, in its most common form, is a stitched lap joint.

REFERENCES

- (8-1) Coplan, M.S. and Bloch, M.G., "A Study of Parachute Seam Design Criteria, Part I-Investigation of the Strength of Nylon and Rayon Cloth Seams", WADC TR 56-313, Part I, AD No. 110407, June 1956.

CHAPTER 9 PARACHUTE HARDWARE AND AUXILIARY DEVICES

Table of Contents

<i>Section</i>	<i>Page</i>
1 PARACHUTE HARDWARE	408
1.1 General	408
1.2 Connector Links	408
1.3 Adapters	408
1.4 Rings	408
1.5 Snaphooks	410
1.6 Cut Knives	410
1.7 Reefing Rings	410
1.8 Clevises	410
1.9 Other Hardware	411
2 ACTUATING DEVICES	411
2.1 Canopy Releases and Disconnects	411
2.1.1 Personnel-Parachute Releases	411
2.1.2 Deceleration and Drone-Recovery Releases	411
2.1.3 Air-Drop Releases	413
2.1.4 Other Releases	414
2.2 Reefing Line Cutters	414
2.2.1 Operating Principles	414
2.2.2 Design Principles	416
2.2.3 Standard Reefing-Line Cutters	416
2.2.4 New Reefing-Line Cutters	417
2.2.5 Experimental Reefing-Line Cutters	418
2.3 Automatic Parachute Ripcord Release	418
2.4 Parachute Compartment Door Release	419
2.4.1 Explosive Bolt, Shear-Pin Type	419
2.4.2 Explosive Bolt, Frangible Type	419
2.4.3 Pin Puller	419
2.4.4 Primacord	419
2.5 Parachute Ejection Devices	420
2.5.1 Deployment Gun	420
2.5.2 Deployment Mortar	421
2.5.3 Blast Bag	421
3 CONTROL DEVICES	421
3.1 Timing Devices	421
3.1.1 Resistance-Capacitance Timers (R-C Circuit)	421

<i>Section</i>	<i>Page</i>
3 CONTROL DEVICES (Cont'd)	
3.1.2 Thermal Timers	422
3.1.3 Pyrotechnic Timer	422
3.1.4 Mechanical Timing Motors	423
3.1.5 Electrical Timing Motors	425
3.2 g-Switches	426
3.3 Pressure Switches	426
3.3.1 Static-Pressure Switches	427
3.3.2 Dynamic-Pressure Switches	427
3.4 Force Sensors	428
4 GROUND-IMPACT SHOCK-ATTENUATION DEVICES	428
4.1 Shock Attenuation by Ground Penetration	429
4.2 Non-Penetrating Methods	429
4.2.1 Inflatable Bags	430
4.2.2 Paper Honeycomb	433
4.2.3 Foamed Plastic	435
4.3 Pre-Contact Retardation	435
<i>References</i>	436
<i>Bibliography</i>	436

Illustrations

<i>Figure</i>	<i>Page</i>
9-1 Typical Items of Air-Drop Parachute Hardware	409
9-2 Cut Knives, Harness Release	410
9-3 A P 28S-2 Personnel Harness Release	411
9-4 Standard Personnel Canopy Release	411
9-5 Parachute Canopy Release Assembly, Spring-Actuated Hook Type	412
9-6 Parachute Canopy Release Assembly, Latch Type	412
9-7 Parachute Canopy Release Assembly, Hook Type	413
9-8 Disconnect Swivel, Squib Operated	413
9-9a Parachute Canopy Ground Disconnect, Mechanical, Air-Drop Parachute System	414
9-9b Parachute Canopy Ground Disconnect, Mechanical, Air-Drop Parachute System (Interior)	414
9-10 Experimental Pyrotechnic Time Delay Disconnects	415
9-11a Reefing Line Cutter, Type M-2	416
9-11b Reefing Line Cutter, Type M-2 (Disassembled)	417
9-12 Reefing Line Cutter, Heavy Duty, Type MC-1	418
9-13a Reefing Line Cutter, Type XM-9	419

Illustrations (Cont'd)

<i>Figure</i>	<i>Page</i>
9-13b Reefing Line Cutter, Type XM-9 (Disassembled)	420
9-14 Automatic Parachute Ripcord Release, Type F-1B, Cover Removed	421
9-15 Automatic Parachute Ripcord Release, Type F-1B, Major Components	421
9-16 Explosive Bolt, Shear Pin Type	423
9-17 Explosive Bolt, Frangible Type	424
9-18 Pin Puller	424
9-19 Parachute Deployment Gun	425
9-20 Blast Bag Ejection Velocity	425
9-21 Parachute Pack Trajectories, Lateral Ejection	426
9-22 R-C Time Delay Circuit	426
9-23 Thermal Time Delay Circuit	426
9-24 Effect of Voltage Variation on Timer Speed	427
9-25 Simple g-Switch Circuit	427
9-26 Static Pressure Actuated Switches	428
9-27 Ground-Impact Shock-Attenuation Device	428
9-28 Parallel Paper Honeycomb, Plastic Foam and Air Bag Force vs Deflection Characteristics	429
9-29 Landing Bag	429
9-30 Bag Diameter vs Burst Pressure	431
9-31 Factor K vs Rate of Descent	433
9-32 $\frac{P_{max}}{P_{burst}}$ vs Rate of Descent	433
9-33 Orifice Area/Bag Radius vs Burst Pressure	434
9-34 Service Test of the Combat Expendable-Platform System	435

CHAPTER 9 PARACHUTE HARDWARE AND AUXILIARY DEVICES

The major non-textile components of parachute systems are hardware, actuating devices, control devices, and ground shock absorbing devices. The hardware items are used as connectors and links between various textile components, and as knives to cut ties and webbings at the appropriate time during the deployment of decelerator systems. Actuating devices initiate specific portions of the decelerator deployment sequence. Some types (for example, reefing line cutters, ground disconnects, and compartment-door releases) operate from self-generated or aircraft-system signals; others depend upon the various types of separate control devices for the initiating signal. Ground-impact shock-absorbing devices are often provided to reduce the possibility of landing damage to missiles and drones, and to cargo loads when the decelerator system is such that the rate of descent at touchdown is high.

SEC. 1 PARACHUTE HARDWARE

All metal parts and assemblies used on a parachute are, broadly speaking, parachute hardware. The simpler mechanical attachments will be considered in this section; more complex actuating and control devices and shock absorbers are covered in the three sections following.

1.1 General. Over the course of parachute development, a number of hardware items have become standardized for use in a range of designs for more or less conventional decelerators. In the case of unusual decelerators, especially those systems which must fit limited storage compartments or which must withstand high loads, it is sometimes necessary to design special hardware.

The broad requirements for parachute hardware are outlined in Military Specification MIL-H-7195 (see Chap. 13). Metals which come in contact with textiles must not produce oxides or other corrosion products which will affect the properties of the textile materials in any manner. The hardware items must be finished smoothly, without protrusions which could cause snagging, or injury or damage to fabrics. Weight should be kept to a minimum consistent with required strength and safety factors. While cost is a consideration for items to be used in quantity, the ability of the device to perform its function with maximum reliability is of primary importance.

The most common items of parachute hardware are links, adapters, rings, snaphooks, clevises, cut knives, and reefing rings (see Fig. 9-1). In general, only the first four are used on personnel parachutes, while any of the list may be used on aerial delivery and heavy-load parachute types, depending on the specific design of the decelerator system.

1.2 Connector Links. Connector links are rectangular frames used to fasten two lengths of webbing together; each webbing is provided with an end loop which bears on a link member of circular cross-section. Some links used in personnel-parachute harnesses are of fixed construction; most, however, are separable to facilitate replacement of webbings without the necessity for sewing. In personnel-parachute design, connector links (harness links) are used to connect the harness straps (risers) to the suspension lines of the canopy. In air-drop and heavy-load decelerator systems, links are used for a variety of functions, such as connecting parachute suspension lines to suspension webbings, connecting deployment bags together when canopies are used in clusters, and connecting container webbings when there is a requirement for assembly and disassembly of fixed lengths of webbing.

1.3 Adapters. Adapters are rectangular metal frames, usually with sliding friction bars to allow adjustment of webbing length. They are used to connect lengths of webbing together when routine disconnection is not required, but when adjustment of length may be necessary. Adapters are commonly used to connect harness straps which may require adjustment in personnel parachutes, and on container webbings which must be adjusted to varying container dimensions in air-drop applications.

1.4 Rings. Parachute harness and webbing rings are usually triangular or D-shaped, often with two parallel arms closing the wide end of the D or V. They are used primarily at the joining points and closing ends of personnel harnesses and container webbings, and usually mate with snaphooks. D-or V-rings are also used at the attachment points on per-

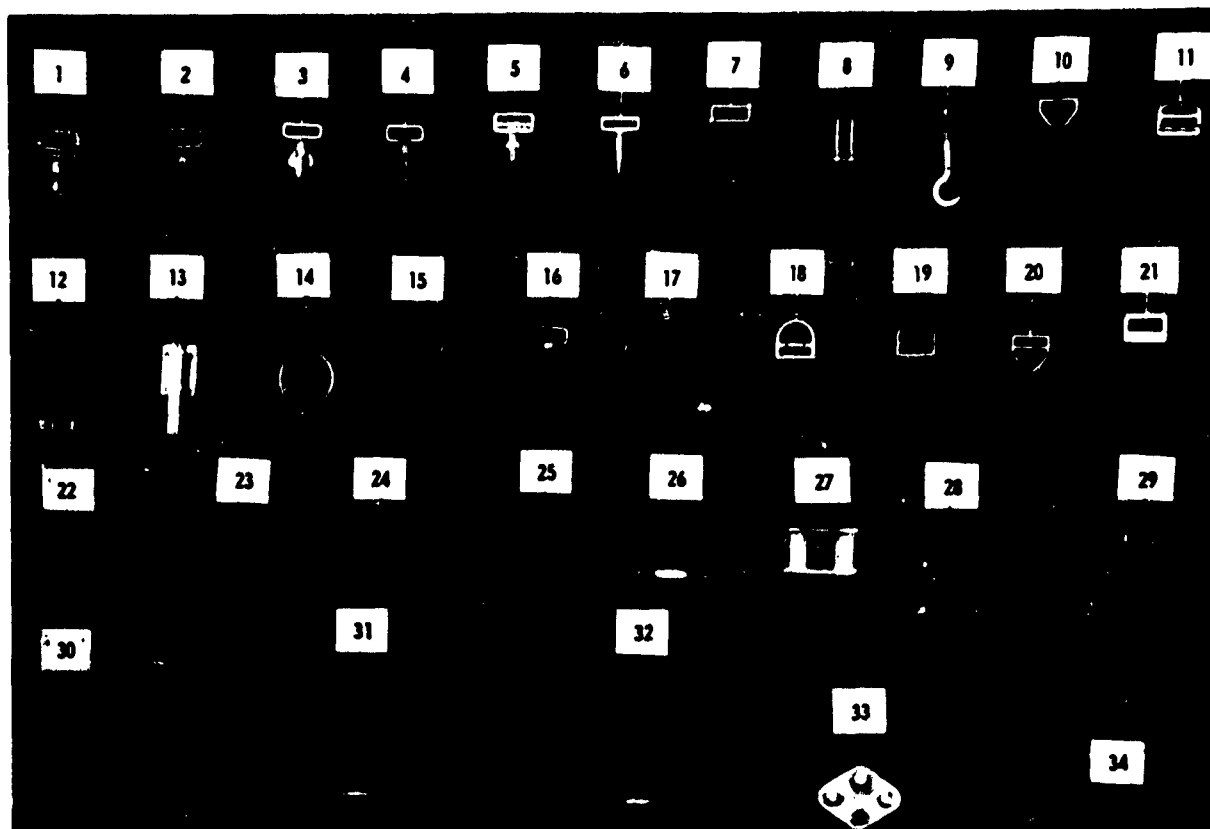


Fig. 9-1 Typical Items of Air-Drop Parachute Hardware

1. Snap and friction adapter, quick fit, parachute harness, proof load 2,500 lbs. Used for tie-down, equipment
2. Snap assembly with flanges, parachute connector, proof load 5,000 lbs. Part No. 47D3138
3. Snap assembly with flange, proof load 5,000 lbs.
4. Snap assembly, general purpose, proof load 5,000 lbs.
5. Snap assembly, parachute connector
6. Snap assembly, general purpose, proof load 2,500 lbs.
7. Link assembly connector, replaceable parachute. Part No. 50B6869
8. Link assembly connector, replaceable parachute. Part No. 52B6660-1
9. Scuff board hook and screw, side buffer assembly. Part No. 51B6595
10. Ring, parachute accessory attaching. Part No. 44A9361
11. Ring, V, quick fit. Part No. 48B7055
12. Load, set weblock assembly
13. Cutter, reefing line
14. Ring, C-119 tie-down
15. Ring, C-119 tie-down. Part No. 4150528
16. Ring, shear web tie-down, C-119 aircraft
17. Clamp assembly, conveyor
18. Ring, parachute, D-drilled. Part No. 43A26411
19. Ring, parachute, D. Part No. 43B21549
20. Knife, shear web, modified V ring
21. Adapter, harness, quick fit
22. Clevis, static line, cargo parachute. Part No. 51B6719
23. Clevis, static line, cargo parachute
24. Clevis, small. Part No. 49B7459. Used W/C-1 aerial delivery kit
25. Clevis, M, not standard
26. Clevis, parachute aerial delivery kit. Part No. 51B6086
27. Connector Link, Extraction Line, Aerial Delivery Kit
28. Link assembly, C-1 aerial delivery kit, single. Part No. 50B7456
29. Line assembly, aerial delivery kit, dual cluster. Part No. 50B7457

Fig. 9-1 Identifications (Continued)

- 30. Clevis, aerial delivery. Part No. 51B6245
- 31. Clevis, aerial delivery. Part No. 49B7460
- 32. Clevis, large square

- 33. Plate, link platform aerial delivery. Part No. X51B6301 and X51B6330
- 34. Diaphragm, Air bag

1.4 (Continued)

sonnel harnesses for a reserve parachute or accessory equipment.

1.5 Snaphooks. Snaphooks are used in both personnel-parachute harnesses and aerial-delivery parachute systems as the releasable joining members used to connect webbing ends to attachment points having V- or D-rings. They are also used for connecting reserve parachutes and accessories to personnel harnesses, and for attaching static lines to aircraft in both troop and air-drop parachute applications. Common types of snaphooks are operated or opened by depressing a hinged guard which allows the ring to disengage from the hook. Special types of snaphooks employ safety locks on the guard, or ejecting-type guards, which facilitate disengagement of the hook from the ring.

1.6 Cut Knives. Cut knives are used in the rigging of air-drop parachutes to allow the cutting, in proper sequence, of retainer webbings securing the load to the aircraft, and in the packing of multiple-canopy decelerator systems to release ties and holding tapes and webbings at the appropriate point in the deployment process. The cut knives used for air-drop cargo-release are usually modified V-rings, sharpened on the inside of the V-shaped members. A series of four sizes of special cut knives (see Fig. 9-2) has been designed for use in the packing of heavy-duty, multiple-canopy systems to allow

controlled sequential deployment. Each has a central circular hole sharpened around the inside edge for cutting the tape or webbing, a slot at one end for attachment of the webbing which provides the pull for the cutting action, and three small holes to allow sewing the knife in place during the packing process to avoid shifting during subsequent handling.

1.7 Reefing Rings. Reefing rings are used on reefed canopies at suspension-line attachment points on the inside of the canopy skirt-band to secure the reefing line in position axially, while allowing it to move freely circumferentially during canopy opening and disreefing. A series of sizes are available for use with various weights of webbing. The rings are of polished steel, with a rectangular cross section. This provides sufficient surface area at the attachment point to prevent any hinging action of the ring, which could cause binding of the reefing line between the ring and the skirt of the parachute. The use of reefing rings having round cross-sections should be avoided, because the above type of failure may occur with their use. Methods of attaching reefing rings to the skirt of the canopy are discussed in Chapter 8.

1.8 Clevises. Clevises are used primarily for the attachment of parachutes to loads. They are generally U-shaped, incorporating a bolt through the open end for attachment purposes. Various clevis sizes are available for load attachments; capacities for

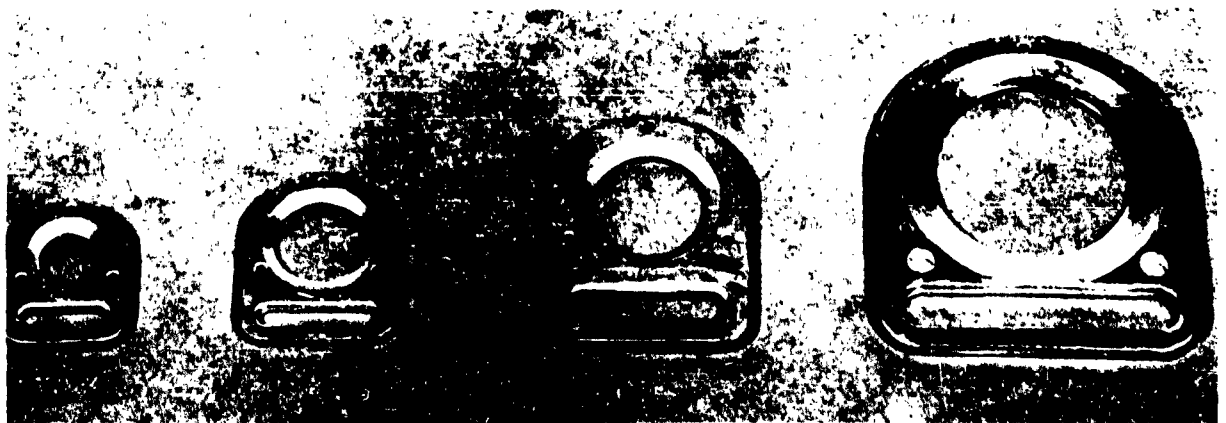


Fig. 9-2 Cut Knives, Harness Release

withstanding opening forces for suspended loads run up to 25,000 lb.

1.9 Other Hardware. Other types of parachute hardware, generally associated with personnel-parachute packs, include such familiar devices as ripcord handles, housings, stiffeners, mounting plates, zippers, grommets, and springs.

SEC. 2 ACTUATING DEVICES

Actuating devices of one sort or another are used in nearly all aerodynamic decelerator applications to set in motion a specific function within the desired operational sequence upon the command of a control signal. Some types of actuating devices require a control signal from an outside source to initiate the action; others have self-contained control devices (usually timers or pressure sensors) to activate the device at the desired point in the operational sequence. Compartment-door releases, decelerator-ejection devices, and some types of canopy disconnects and releases are examples of the first type. Automatic ripcord releases, reefing-line cutters, and some canopy disconnects fall in the second group.

2.1 Canopy Releases and Disconnects. Most types of aerial-delivery, final-stage recovery, and personnel parachutes remain inflated under moderate wind velocities (10 knots or more), and tend to drag or overturn the load or jumper after touchdown. Disconnects are used primarily to separate the parachute canopy from the load or man after ground contact, reducing the chances of damage or injury. Personnel-

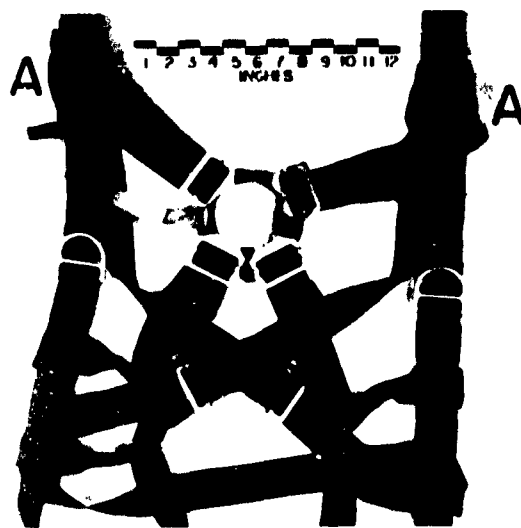


Fig. 9-3 A/P 28S-2 Personnel Harness Release

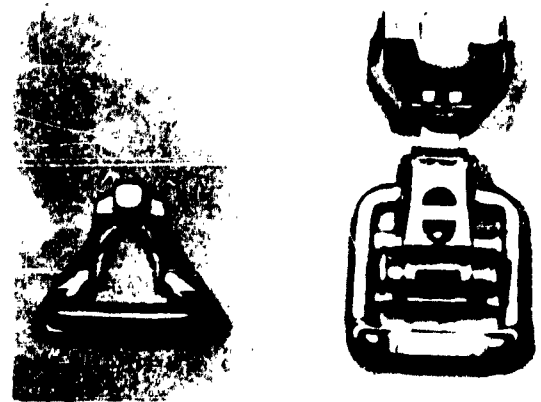


Fig. 9-4 Standard Personnel Canopy Release

parachute disconnects are operated by the jumper; aerial-delivery and final-stage recovery disconnects operate automatically. Disconnects are used on all personnel and aircraft-deceleration parachutes, on most types of air-drop, missile and drone final-stage recovery canopies (and as interstage releases in recovery systems), and in heavy-duty multi-stage systems.

2.1.1 PERSONNEL - PARACHUTE RELEASES. Personnel-parachute releases are used to jettison the canopy after touchdown to prevent injury to the jumper from dragging. They are of two types, usually manually activated: harness releases and canopy releases. The A/P 28S-2 harness release (Fig. 9-3) is used to collect and attach the restraining straps of the parachute harness to a central point on the body of the wearer. Manual actuation of the device simultaneously releases several straps, freeing the harness and canopy from the body. The canopy release (Fig. 9-4) is used to separate the canopy from the harness, which remains on the wearer. Two such releases are required for a canopy, one connecting each canopy riser to the appropriate point on the harness. Release activation is manual; each must be opened separately to free the jumper of the canopy (Ref 9-1, 9-2, 9-3, 9-4).

2.1.2 DECELERATION AND DRONE-RECOVERY RELEASES. Aircraft-deceleration and drone-recovery parachute systems use canopy-release devices to separate the canopy from the vehicle after the landing deceleration or recovery mission has been accomplished. A variety of release devices have been tested and used for such applications; the most common are described below.

2.1.2.1 Spring-Actuated Hook Type. Fig. 9-5 shows a spring-actuated hook release that has been used in

drone recovery. While the drone is in flight, the spring *S* pushes ring *R* against pin *P*, holding the pin in place. As the parachute is deployed, a load is placed on the ring, and the ring and spring move to the position shown in Fig. 9-5, at the same time relieving the friction between the ring and pin. The pin is designed to fall free of the cylinder, when in a vertical position, approximately 10 sec after release of the friction of the ring. When the vehicle touches the ground and the load is partially relaxed, the spring forces the ring off the then unobstructed hook, disconnecting the parachute canopy. Disadvantages of this design are that foreign matter in the cylinder may cause improper operation of the pin, and that the reduction of imposed stress caused by air currents may result in mid-air separation of the load and parachute canopy.

2.1.2.2 Explosive - Squib Types. The following three ground releases are actuated by electrically ignited explosive squibs. This is considered the most positive means of accomplishing the release action; however, an additional device is introduced into the operation. In order to fire the squibs, an electrical

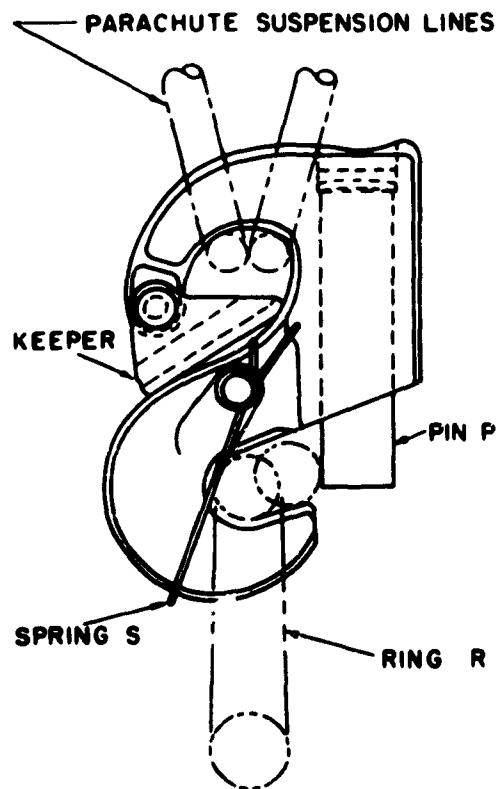


Fig. 9-5 Parachute Canopy Release Assembly, Spring-Actuated Hook Type

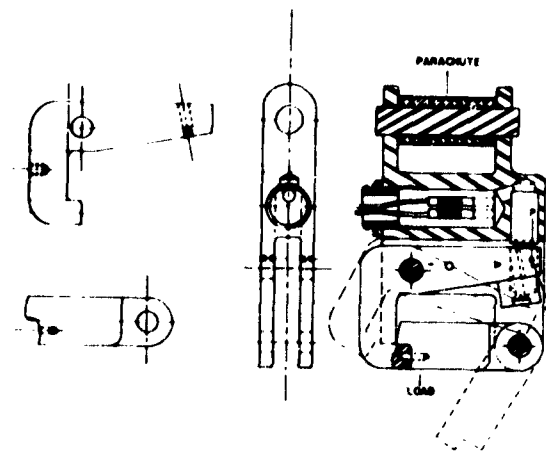


Fig. 9-6 Parachute Canopy Release Assembly, Latch Type

circuit must be closed when the vehicle strikes the ground. To date, this has been accomplished in the most satisfactory manner by actuating a switch through the action of a feeler wire, which projects 3 to 6 in. beyond the bottom of the vehicle.

- a. Latch Type. Fig. 9-6 shows a squib-actuated latch-type canopy-release assembly. The parachute canopy is attached to the end link; the load is suspended from the latch. Actuation may be accomplished by a timer switch completing the squib circuit, by an impact switch, by a normally closed switch that is kept open by the load, by a feeler wire switch, or by such other switch arrangement as may be required for the particular application. Firing of either one of the squibs forces pin *P* to move the arm that rotates about *O*, breaking shear pin *S* and releasing the latch.
- b. Hook Type. Fig. 9-7 shows a squib-operated hook-type release. When the squib fires, the high-pressure gases produced, exit through holes (1), travel down the air gap (2), and reenter holes (3), forcing the piston (4) up against the spring. The latch *L* is then released, permitting ring *R* to fall free.
- c. Disconnect Swivel. Fig. 9-8 shows a squib-operated disconnect swivel. The left half of the drawing shows the plunger *P* in the unfired position, with the shear pin *S* in place. In this condition the load is transmitted from the cage *C* through the ball bearings *B* to the outer race *R*. When the squib fires, the plunger breaks the shear pin and moves to the positions shown on

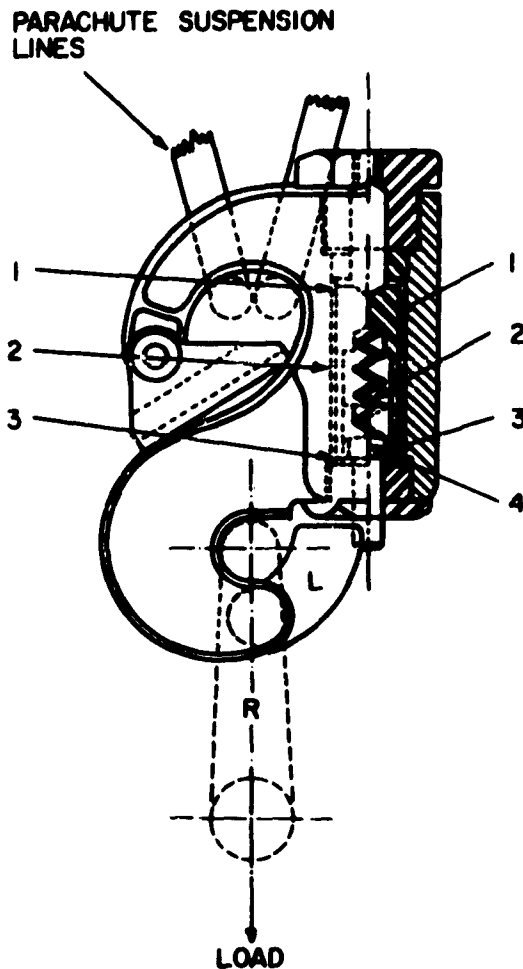


Fig. 9-7 Parachute Canopy Release Assembly, Hook Type

the right half of the drawing. This allows the balls to move inward, and the cage slips out of the outer race, thus disconnecting the parachute canopy.

2.1.2.3 Other Types. Development work has been performed on mechanically operated jaw-type releases for aircraft-deceleration parachutes with load capacities of 30,000 and 100,000 lb (Ref 9-5).

2.1.3 AIR-DROP RELEASES. In air-drop systems, standard disconnects are of mechanical and explosive-actuated release types. The avoidance of premature mid-air release during canopy deployment and descent, as well as a high degree of reliability of release at ground impact, are of prime importance for any disconnect design. Integral time-delay devices have been found effective in eliminating

premature load-release during canopy deployment and descent. Standard mechanical disconnects depend upon the principle of load-stress reduction to separate the parachute canopy from the load after ground impact.

The standard ground-disconnect device used by the Air Force is mechanically actuated, with 500-lb capacity which operates on the principle of load-stress reduction (Fig. 9-9). It separates the canopy from aerial-delivery containers after ground impact. For heavier aerial-delivery loads, two standard U. S. Army release assemblies are available, a Single-Release Assembly (FSN 1670-360-0463) and a Multiple-Release Assembly (FSN 1375-694-2004). These are installed between the cargo suspension slings and the parachute risers. In general, the Single-Release Assembly is used for loads requiring not more than two parachutes, while the Multiple-Release Assembly is used with three or more parachutes (Ref 9-6). Both assemblies use M2 Reefing-Line Cutters (see 2.2.3 below) as time-delay devices to prevent premature release of the load during deployment; they operate on a load-stress reduction principle to release the canopy after

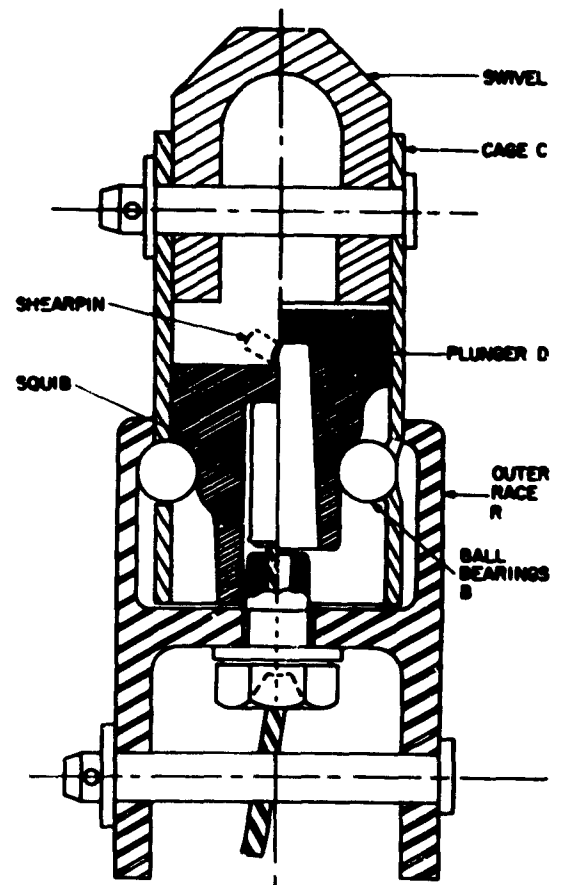


Fig. 9-8 Disconnect Swivel, Squib Operated



Fig. 9-9a Parachute Canopy Ground Disconnect, Mechanical, Air-Drop Parachute System

ground impact. Two cutters are used on the Single-Release Assembly, one on the Multiple-Release device. In both types the cutter pyrotechnic delay-trains are initiated by lanyards attached to the firing wires at the start of deployment. After the 10-sec delay, the cutters fire, severing holding cords and allowing the cutter bodies to drop out of their sockets, thereby freeing the release arms of the disconnects. The loads are held in place by their own weight, exerted on the attachment to the release. As this force is relaxed at touchdown, the cargo suspension-sling attachments are freed from the release assembly, separating the canopies from the load.

A number of experimental cargo-parachute releases have been developed, based on the load stress-relaxation principle. Most of these have used some form of pyrotechnic delay-device to prevent premature release during deployment (Fig. 9-10). To facilitate recovery, some models release all but one group of suspension lines on ground impact, retaining the parachute in the vicinity of the load after disconnect (Ref 9-7, 9-8, 9-9, 9-10).

2.1.4 OTHER RELEASES. Interstage disconnects in systems using multi-stage decelerators are generally designed specifically for the system, during its development. Mechanical releases actuated by timers or pressure switches, and electrically operated primacord loops for cutting first-stage canopy risers, have been used in various designs.

2.2 Reefing Line Cutters. The need for reduction of the opening shock of conventional aerodynamic decelerators and for the control of drag area led to the development of reefed canopies. So that reefed canopies could be used, devices were required which would initiate the disreefing sequence.

2.2.1 OPERATING PRINCIPLES. Most reefing-line cutters in use today operate in the same basic manner. At the time during the deployment process at which the suspension lines are fully stretched, and the force on the particular line to which the arming wire is attached builds up to approximately 25 lb, the arming wire is withdrawn from the cutter. This releases a firing pin, which strikes a primer cap, which in turn initiates a powder-train time-delay designed to burn for a predetermined number of seconds. After the delay interval, the final propellant is ignited, driving the piston-shaped cutter knife down the barrel, and severing the reefing line threaded through the holes near the end of the barrel.



Fig. 9-9b Parachute Canopy Ground Disconnect, Mechanical, Air-Drop Parachute System (Interior)

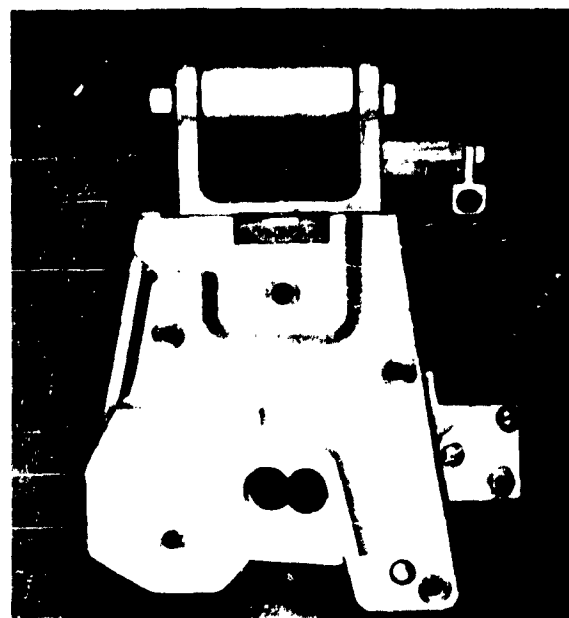
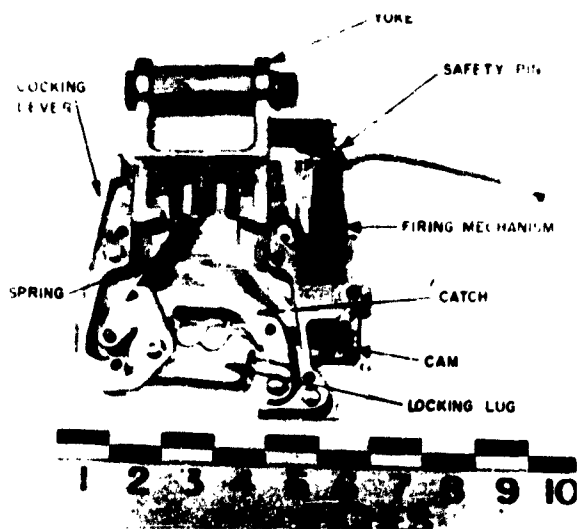


Fig. 9-10 Experimental Pyrotechnic Time Delay Disconnects

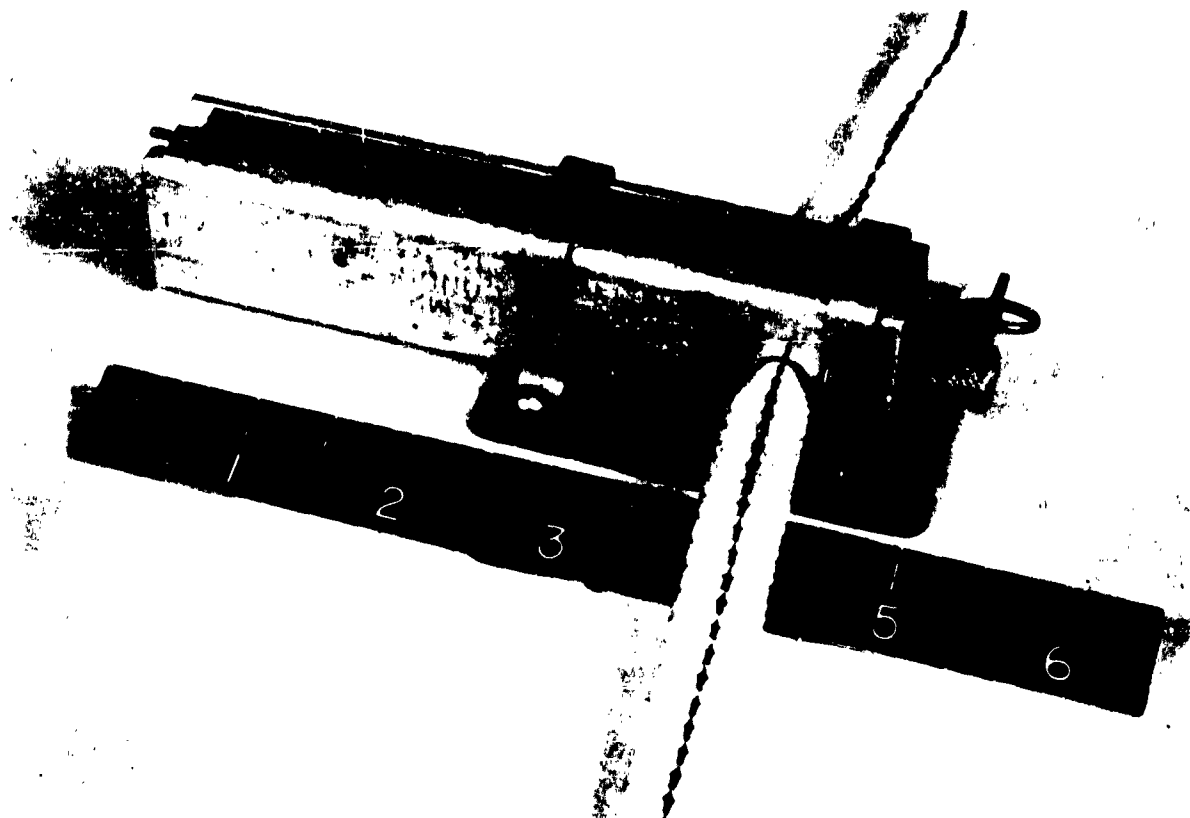


Fig. 9-11a Reefing Line Cutter, Type M-2

2.2.2 DESIGN PRINCIPLES. In designing a reefing line cutter, particular attention should be paid to certain details:

(1) The piston-shaped knife of the device must be longer than the diameter of the reefing line hole to prevent the high-pressure propellant-generated gases from escaping prematurely. Accurate fit of the cutter piston in the barrel is also important for the same reason.

(2) Sufficient space must be provided beyond the reefing line hole for a full stroke of the cutter piston, so that the plug cut out of the reefing line can clear the ends of the line.

(3) The powder charge must be well blocked-off from the firing mechanism.

(4) The snatch force of the decelerator, which occurs at the time the arming wire is withdrawn and the firing pin strikes the primer cap, can impose a force opposite to the direction of movement of the firing pin, possibly causing so light a strike that the cap does not detonate. In some cases a stronger firing-pin spring may solve this difficulty. However, consideration should also be given to designing the

cutter so that the snatch force will operate in the same direction as the movement of the firing pin, assisting rather than opposing the striking force.

2.2.3 STANDARD REEFING-LINE CUTTERS. The current standard method of disreefing a parachute canopy, when skirt reefing is used, is to cut the reefing line threaded through reefing rings around the skirt of the canopy. In general, pyrotechnic reefing-line cutters are employed for this purpose.

The Reefing-Line Cutter, Type M-2 (MIL-C-10362), is the primary standard model used in AF applications (Fig. 9-11). Removal of the arming wire (7) allows the firing pin (5) to initiate the time delay powder train (4) by means of a percussion cap. A powder charge is ignited by the powder train, causing the piston (3) to move. The reefing line is inserted into the housing (1) through the reefing line holes. A mounting plate (9) with clamps (10) is provided to facilitate installation of the device on the parachute canopy. The arming wire (7) is connected to a suspension line. When the parachute is deployed, this arming wire is removed, starting the cutting sequence. In order to prevent premature release, the arming wire is de-

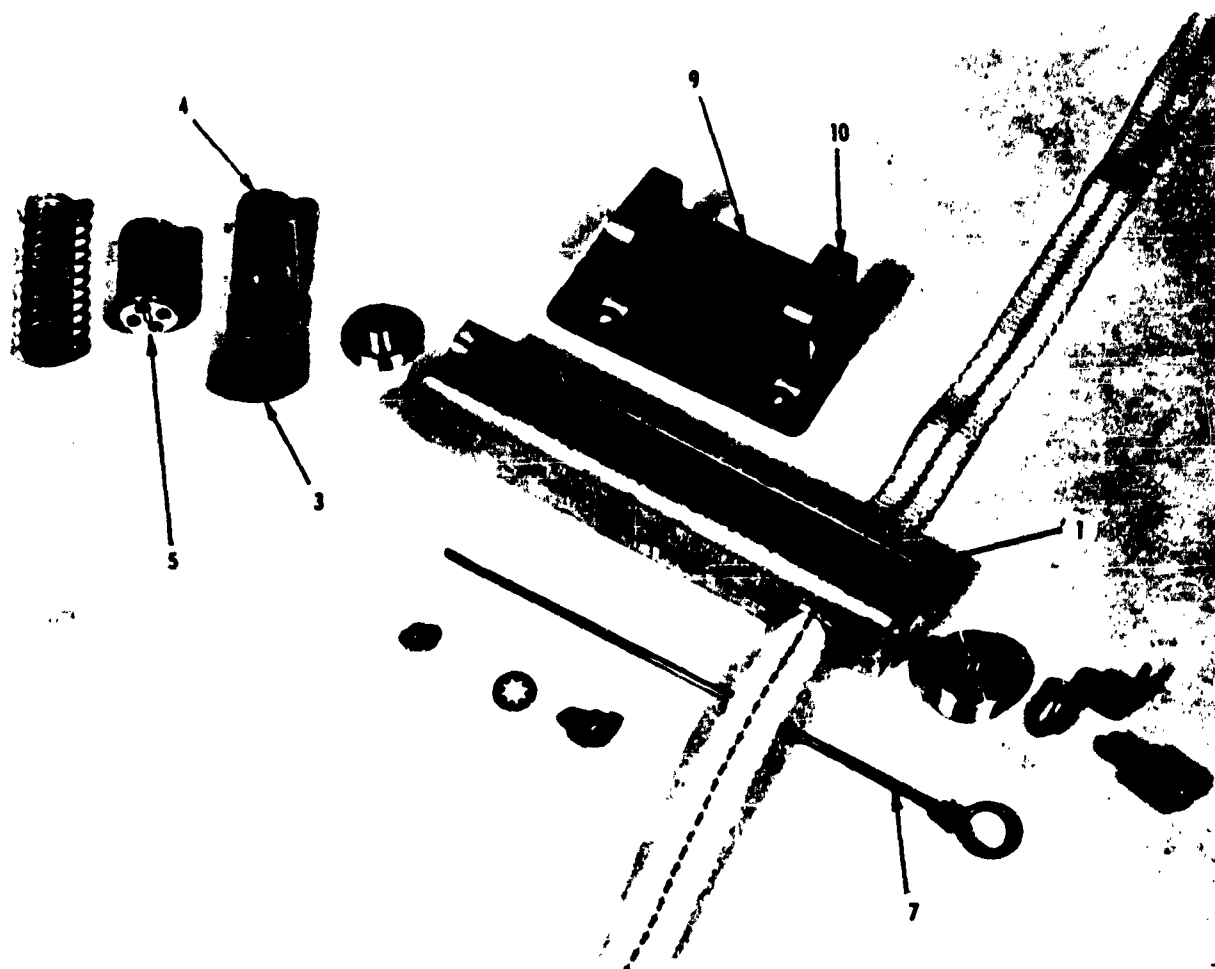


Fig. 9-11b Reefing Line Cutter, Type M-2 (Disassembled)

signed with a safety device requiring the application of 25 lb of tension prior to release, and also for some free travel before the firing pin actuates the device. This disreefing device is designed to cut lines of up to 1,000 lb tensile strength. Time delays are available for intervals of 2, 4, 6, 8 or 10 sec. This device can be used only once, and therefore must be considered expendable. The Reefing-Line Cutter Type M2A1 was developed from the Type M2 (Ref 9-11). This cutter is used as a standard in U. S. Army applications, and to a limited extent by the Air Force. Actuation and mounting of the cutter are identical with the methods described for the M2 above.

The Reefing-Line Cutter Type MC-1 (Fig. 9-12) is a heavy-duty device which has been standardized for operation in that systems utilizing heavy reefing lines with a tensile strength of up to 14,000 lb. A

Type T-2 explosive actuator and a delay powder-train are used to actuate and govern the cutting sequence. Cutting of the reefing line is accomplished by means of a knife propelled by the powder charge. Actuation of the device is accomplished by the removal of an arming wire. This device can be reused simply by changing the time delay powder train; however, the barrel of the cutter should be cleaned of all residue before reuse, to insure free travel of the knife. Time delays for intervals of 0.75, 1, 2, 4, 6, 8, and 10 sec are available.

2.2.4 NEW REEFING-LINE CUTTERS. Effort to improve the action and reliability of reefing-line cutters for cargo delivery systems and drone parachute-recovery systems has resulted in the development of the XM-9 through XM-13 series cutters. These are designed to operate during the higher opening-shock

forces encountered in high-speed deployment. The XM-9 series reefing-line cutter (Fig. 9-13) has passed qualification tests during which it was subjected to forces similar to those occurring during parachute opening, being successfully fired during 750g shock and 500g sustained-acceleration tests. The new series of cutters will be available with time delay intervals of 2 sec (XM-9), 4 sec (XM-10), 6 sec (XM-11), 8 sec (XM-12), and 10 sec (XM-13). The cutters, with the standard Mounting Plate, Drawing 52186658, as part of the assembly, will mount in standard reefing-line-cutter pockets. The XM-9 series cutter is capable of severing two 1000-lb. tubular reefing lines.

A typical cutter of the XM series (Fig. 9-13) is mounted in the pocket on the mounting plate (8) by two semicircular brackets (7), Drawing X61135241. The extraction cable (1) is connected to the parachute riser line; when the parachute is deployed, and approximately 38 lb of force acts in the line, the cable (1) is extracted from the housing. This action draws the firing pin (3) back against the firing spring (2) and then releases the pin. It strikes the time-delay cartridge (4), initiating the time-delay pyrotechnic train. After a predetermined time, the cutting blade (4-A) is propelled forward through the cutter housing (5), severing the reefing lines and stopping against the end plug (6). The XM series cutters were designed for a one-time use.

2.2.5 EXPERIMENTAL REEFING - LINE CUTTERS. A number of disreefing devices actuated by electrical impulses and by clockwork and other mechanical means have been used in the past, or are

under development, in an attempt to provide delay timing which is accurate under widely varying temperatures. The major difficulty encountered with these devices, especially those using mechanical timers, is the effect of the high-g shock on the timing-system operation during deployment.

2.3 Automatic Parachute Ripcord Release.

The operation of aircraft at high altitudes and supersonic speeds has created a requirement for automatic devices to actuate emergency-escape personnel-parachute systems. The Type F-1B Automatic Parachute Ripcord Release (Fig. 9-14) automatically pulls the parachute ripcord after the arming cable of the unit has been pulled (Ref 9-12; MIL-R-25565A). The release operates only after the lapse of a pre-set time interval and below a pre-set altitude pressure after timer actuation. The automatic ripcord release can be set to operate after a time delay of from 1 to 13 sec and for altitudes between 5,000 and 20,000 ft. As shown in Figure 9-15, the release consists of a power source in the form of a main spring (25), a timer mechanism (5) and an aneroid leak indicator which also indicates altitude. Except for the arming and power cables, the entire release is enclosed in a rainproof case approximately 2½ by 2½ by 4½ in., with a removable cover to allow winding and setting of the mechanism. To operate the release the following operations must be performed:

- Wind the main spring (25) fully.
- Lift timer knob (19), pull the power cable (21) from the case, and set the desired time delay.
- Set the desired altitude by turning the aneroid

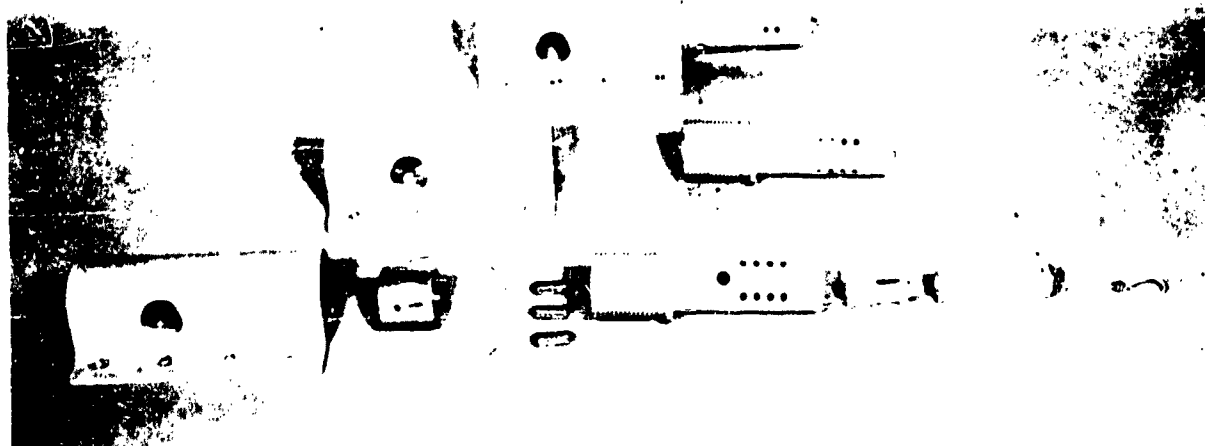


Fig. 9-12 Reefing Line Cutter, Heavy Duty, Type MC-1

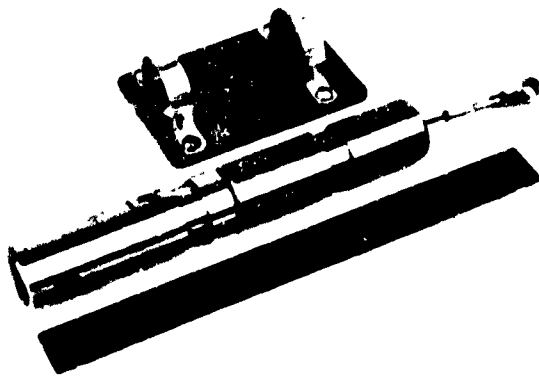


Fig. 9-13a Reefing Line Cutter, Type XM-9

setting pointer (11).

d. Replace the cover on the case and tighten the cover screw securely.

e. Pull the arming cable out of the case.

The escapement mechanism begins to operate after the predetermined altitude has been reached. The time is accurately measured and the main spring (25) unwinds at a uniform rate for the duration of the time set. After the pre-selected time has elapsed, the remaining (major) portion of the mainspring energy retracts the power cable (21), which pulls the parachute ripcord.

2.4 Parachute Compartment Door Release. The opening of the parachute compartment door, or release of the whole door, at high aircraft speeds is essential in aircraft deceleration and for successful missile or drone recovery. The problem is usually not as simple as it appears. The unlatching mechanism must function reliably under environmental extremes, such as low temperatures (around -65 F), high altitude, high acceleration, and severe vibration. The mechanism must not have an adverse effect on the performance of the aircraft or missile, such as adding extra drag. Generally, the space allotted inside the vehicle for this device is small. For aircraft deceleration, actuating devices based on mechanical or solenoid principles are commonly used. For missile applications, explosive bolts have been used successfully. These bolts have various configurations, depending on the particular application, and have been put to other uses, such as opening landing-bag hatches on missiles, or releasing wing tanks on piloted aircraft. One feature which is common to all explosive-bolt functioning is that it is actuated by one or more electrically ignited explosive squibs. Several of the principles which have proven successful during actual

operation are explained below.

2.4.1 EXPLOSIVE BOLT, SHEAR-PIN TYPE. Fig. 9-16 shows how an explosive bolt may be used to separate a tail cone, containing a parachute, from the rest of the vehicle. The bolt installation is shown in Detail A of the drawing, and is also shown disassembled. The barrel, the squib, and the plug, which is held in place by the rivet, are attached to the airframe. The screw is inserted through a hole in the cone, then screwed into the plug. With this type of installation, the head of the bolt is flush with the skin of the fuselage. When the squib fires, the plug shears the rivet, and the plug and screw are ejected, thus releasing the parachute and cone.

2.4.2 EXPLOSIVE BOLT, FRANGIBLE TYPE. Fig. 9-17 shows this bolt, both assembled and disassembled. When the squib explodes, the internal pressure causes the bolt to fracture and break away at the section that has been weakened by undercutting, releasing the compartment door or other device. This design of bolt uses one squib, which is considered good design practice only if reliability is demonstrated by a large number of functional tests; therefore, the figure is intended only to illustrate a principle of operation.

2.4.3 PIN PULLER. The basic operating principle of this type of device is illustrated in Fig. 9-18. It consists of a cylinder, containing a piston that is attached to the retaining pin of the compartment door or to a device with a function similar to a retaining pin. Prior to actuation, the piston, with the retaining pin attached, is held in place in the assembly by a shear pin. The actuating force is provided by two explosive squibs, which give higher reliability than one does. When either or both of the squibs fire, the internal pressure produced causes the shear pin to break, and the piston to move in the cylinder (to the left in Fig. 9-18), pulling the retaining pin out of the mechanism to be actuated. A vent is required to prevent compression of the air ahead of the piston from interfering with the piston's motion.

2.4.4 PRIMACORD. Primacord (PETN Explosive-filled Detonating Cord) has been used with highly reliable results in the design of "brute force" methods of opening decelerator compartment-doors. The Primacord, which resembles a thin braided rope, is stored in a channel running lengthwise in the center of the compartment cover. Both sides of the cover are hinged to the edges of the compartment opening, and may be spring-loaded. Two electrical actuators are used for the ignition of the Primacord. Upon detonation, the compartment cover is ruptured along the Primacord channel and forced open. The decelerator must be so packed and stowed in the compartment that

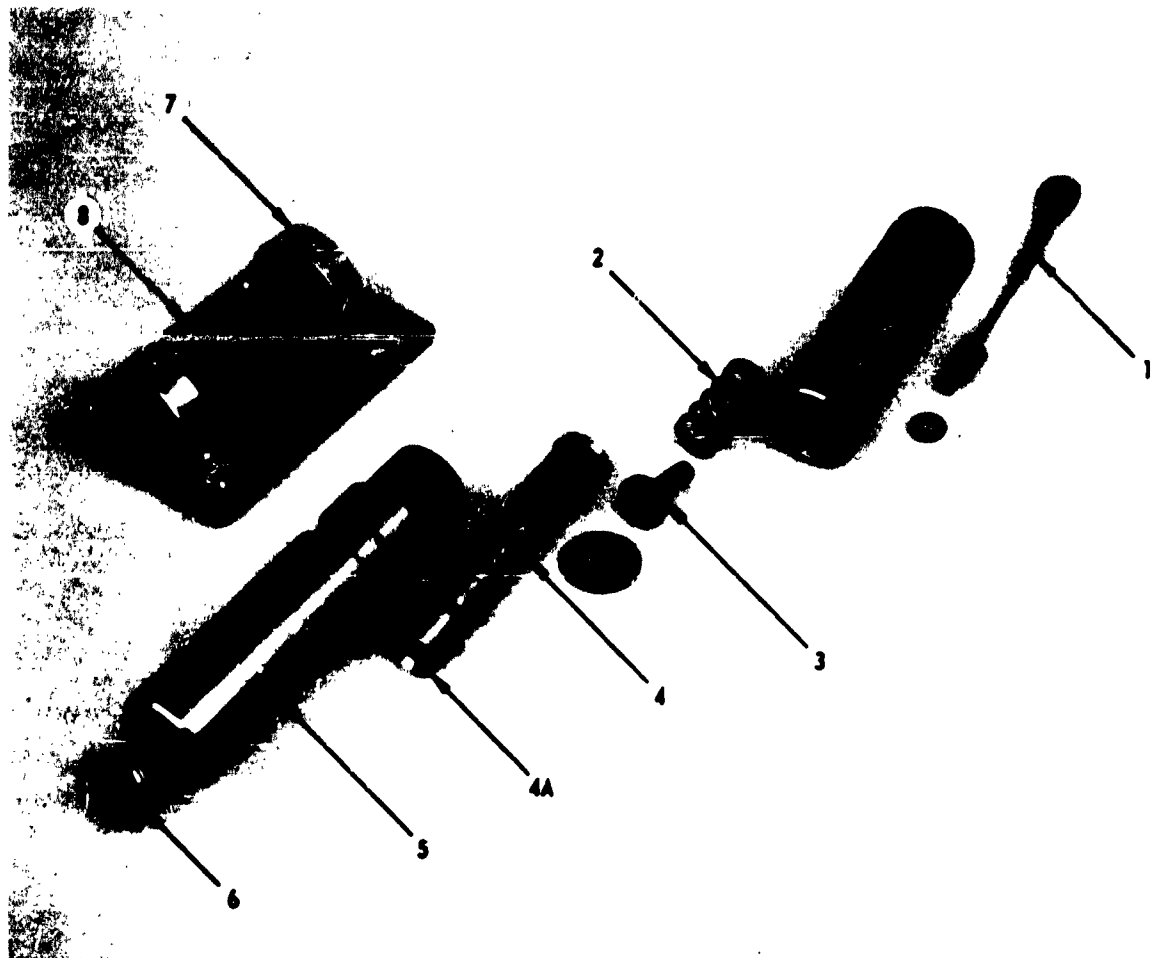


Fig. 9-13b Reefing Line Cutter, Type XM-9 (Disassembled)

it is protected from the effects of the Primacord explosion.

2.5 Parachute Ejection Devices. The entire success of the operation of an aerodynamic decelerator system depends upon the effectiveness with which the decelerator is deployed. Thus, the ejection device constitutes an integral part of any decelerator system. For the majority of systems which are designed to operate only at relatively low speeds, a simple, spring-loaded pilot parachute will perform the function of deploying the decelerator. However, for systems which will be required to deploy behind tumbling or blunt bodies, or which are to be deployed at high speeds, more force for the ejection of the aerodynamic decelerator is required. Three types of devices have been developed for ejection: deployment guns (ejector guns), which use projectiles; mortars, which exert force directly on a deployment bag; and blast bags, which are fabric bags used to confine an explosion.

2.5.1 DEPLOYMENT GUN. These devices have been used in a number of applications (Ref 9-13, 9-14, 9-15, 9-16) as deployment aids for first-stage aerodynamic decelerators. In a typical deployment-gun design (Fig. 9-19), a projectile weighing approximately 2 lb is driven out of a barrel by pressure generated when a powder charge is ignited electrically, or by a firing pin and primer cup. A balsa-wood pad or coil-spring arrangement absorbs the recoil when the gun is fired. The kinetic energy of the projectile, acting through a wire rope or nylon webbing, pulls the pilot parachute out of its stowage compartment into the airstream behind the vehicle.

The same system may also be used to remove the compartment door or cover, and then deploy the parachute. In such a system, the projectile only pulls the cover from the compartment. The cover then acts as a drag plate in the air stream, and by means of a bridle pulls the bag-packed pilot chute from the compartment, initiating the decelerator deployment sequence.

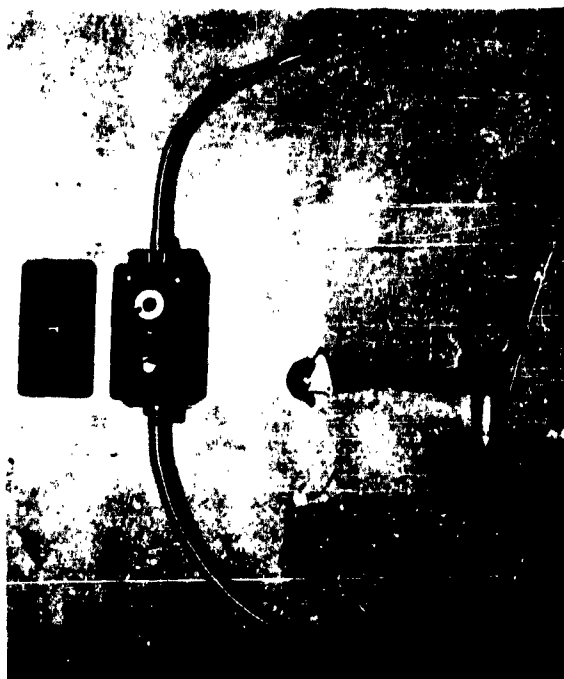


Fig. 9-14 Automatic Parachute Ripcord Release, Type F-1B, Cover Removed

quence.

2.5.2 DEPLOYMENT MORTAR. Mortar-type ejection methods are particularly effective for rearward ejection of decelerators from vehicles. A canvas deployment bag, with a double-ply canvas base, is ejected from the stowage compartment by the explosion of a powder charge acting directly on the bag. Rearward deployments of aerodynamic decelerators weighing about 25 lb have been successfully accomplished with 30- to 40-gram charges of black powder ignited electrically.

2.5.3 BLAST BAG. A blast bag, or bladder, has been used in some aerodynamic decelerator systems for the ejection of the decelerator from its stowage compartment. In this system the blast bag, constructed of nylon cloth or canvas, is used to confine the explosion of the propellant powder, protecting the decelerator pack from burn damage. This type of deployment is particularly advantageous if the decelerator must be ejected in a direction perpendicular to the air stream, requiring a higher ejection velocity than rearward deployment, and hence a larger powder charge. The results of tests of the variation of ejection velocity with FFFg black powder charge weight for a 25-lb pack is shown in Fig. 9-20. Theoretical trajectories for a decelerator pack ejected perpendicular to the airstream under the conditions noted are shown in Fig. 9-21.

SEC. 3 CONTROL DEVICES

The purpose of the control device is, as the name implies, the control of a specific function within the sequence of decelerator system operation. This control component, when employed as an independent device, will in most cases furnish electrical impulses to the actuating device to initiate its function. The most frequently used devices to control sequence functions are various types of timers; other control devices include μ -switches, dynamic- and static-pressure sensors, and force sensors.

3.1 Timing Devices.

3.1.1 RESISTANCE-CAPACITANCE TIMERS (R-C CIRCUIT). Simple resistance-capacitance timing circuits may be constructed from a capacitor of sufficient size and design to hold its electrical charge for a given period of time, and a suitable resistor through

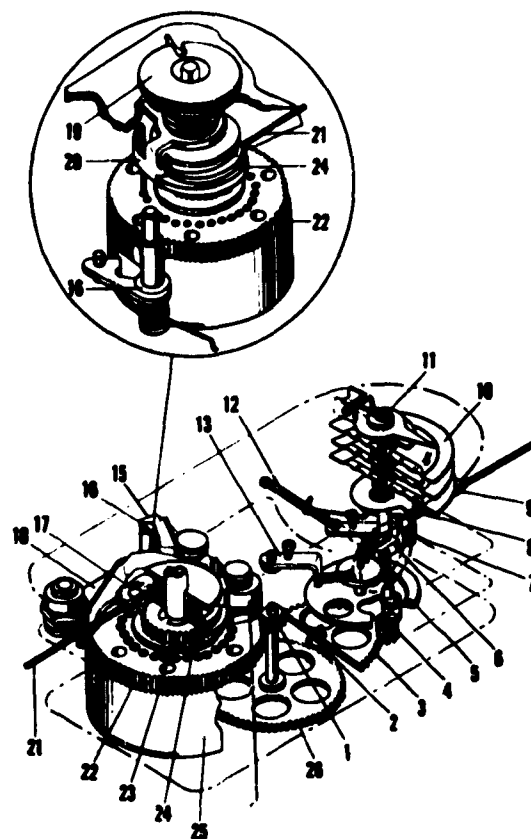


Fig. 9-15 Automatic Parachute Ripcord Release, Type F-1B, Major Components

Identifications (Continued on next page)

Identifications for 9-15

- | | |
|-----------------------------------|-----------------------------|
| 1. Intermediate drive gear pinion | 13. Spring adjustment lever |
| 2. Roller drive gear pinion | 14. Safety latch pawl |
| 3. Actuating pinion drive gear | 15. Safety latch |
| 4. Pinion and roller | 16. Safety lever and shaft |
| 5. Escapement | 17. Stop plate pinion |
| 6. Cam contact arm | 18. Stop plate rack |
| 7. Arming lever | 19. Timer knob |
| 8. Aneroid cam | 20. Stop plate pawl trip |
| 9. Arming cable | 21. Power cable |
| 10. Aneroid | 22. Drive gear |
| 11. Altitude setting pointer | 23. Stop plate gear |
| 12. Rocker arm | 24. Power cable spool |
| | 25. Main spring |
| | 26. Intermediate gear |

which it can discharge at a given rate to control the time element. Of course, the timing accuracy obtained is not very good with so crude an arrangement, since variations in component tolerances and environmental conditions imposed upon the system will change the condenser discharge time. However with the addition of a few simple components, a timer can be built which has no moving parts to be adversely affected by vibration or acceleration forces, and which can be isolated from adverse temperature and pressure environments by its packaging. Since it can be constructed with small physical size, weight, and volume, this method of timing has wide potential application in aerodynamic decelerator systems.

A typical circuit diagram of an R-C timer is shown in Fig. 9-22. When the switch S_1 is in position a , the capacitors C_1 and C_2 will be kept close to the breakdown voltage of the regulating diode D_1 by battery B . At the same time, a short will be maintained across the pyrotechnic initiating switch S_2 and diode D_2 . If switch S_1 is then moved to position b , the capacitor C_2 will discharge its stored electrical energy through resistor R_2 . The time of discharge will depend upon the resistance of R_2 . The voltage across capacitor C_2 will drop until it has reached a value equal to the difference between the voltage across capacitor C_1 and the breakdown voltage of diode D_2 . At this point, the diode D_2 permits current flow, and the resulting surge of current into capacitor C_2 will initiate the pyrotechnic switch S_2 .

The single-pole, double-throw action of switch S_1 can be incorporated in a variety of primary sequence-initiating devices, including latching relays operated by radio-frequency receivers, g-switches,

pressure switches, arming lanyard switches, and others. The component shown as switch S_2 can be either a pyrotechnic switch, which is commercially available and can be obtained in various open- and closed-contact configurations, or a sensitive relay coil. If the latter is used, a separate power source to initiate the actuating component will be required. This method of timing is particularly well suited for incorporation in a combined control-and-actuation device. In this case, the switch S_2 would be replaced by the actuating component, generally an electrically ignited squib.

Because of its design and performance characteristics, this device can be located almost anywhere in a given vehicle. It can be completely self-contained, using miniature batteries of extremely long shelf-life; provisions for checking the operational functioning of the timing circuitry can be included in the design.

3.1.2 THERMAL TIMERS. This type of timing device depends upon a bimetallic strip that closes a set of contact points after a predetermined time-interval, when it bends on being heated at a known rate by an electrical resistance coil. In most such devices, the closing of the contact points of the delay timer actuates a relay installed in the same hermetically sealed case. The relay, in turn, closes a set of switch points in the actuating device circuit and de-energizes the thermal delay heater coil. Since this type of device is electrically activated, it can be located almost anywhere within the vehicle or suspended load. The device itself is relatively light in weight, and is not bulky. However, since the electric-current requirements for the operation of the thermal delay-timer are generally quite high, a fairly substantial primary power-source is required.

A schematic circuit diagram for a thermal time-delay relay is shown in Fig. 9-23. When the timer initiation voltage is applied, resistance element A heats bimetallic strip B at a controlled rate. At the end of the pre-set interval, B contacts C , closing the circuit between the initiation-voltage source and relay coil D . Contact 3 closes, completing the circuit to the actuation device; at the same time contact 1 opens, de-energizing the thermal delay heater, and contact 2 closes, keeping the relay coil attached to the initiation voltage source. The accuracy of the timing cycle depends largely upon the accuracy of the electrical voltage fed into the thermal delay; however, extremes of ambient temperature can also affect the timing accuracy. Both relays and the thermal switch are also vulnerable to the dynamic environments of vibration, acceleration, and shock.

3.1.3 PYROTECHNIC TIMER. Pyrotechnic delay

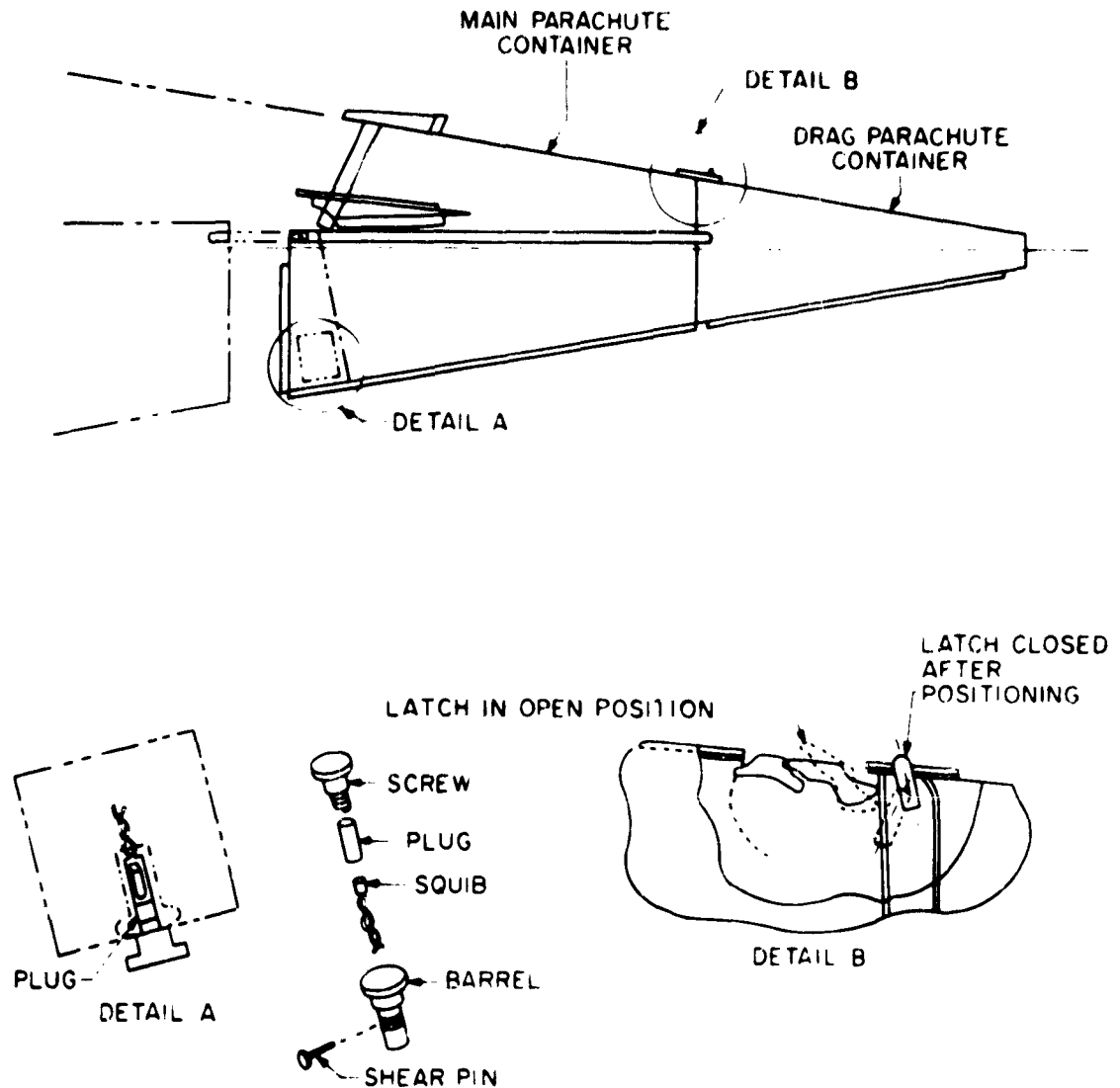


Fig. 9-16 Explosive Bolt, Shear Pin Type

elements are used for timing purposes primarily in reefing-line cutters, and as time-override devices for system control functions based upon phenomena other than time lapse. A pyrotechnic delay element consists of a primer, a delay train, and an igniter which fires the main charge. For any given delay time, this type of element will probably have the lowest bulk and weight of any timing method, and is particularly well suited for direct incorporation into actuation devices. At present, however, timing accuracies vary considerably with temperature, and are not adequate to allow utilization of this timing method for other than, primarily, override functions, and in

those applications where tolerances are broad. Timing accuracies of better than ± 10 per cent of the rated delay-time are difficult to obtain. Initiation of the timing cycle may be accomplished either by electrical or mechanical-pyrotechnic means.

3.1.4 MECHANICAL TIMING MOTORS. The mechanical timing motor, in the form of a clock-type escapement mechanism, has been used with good reliability in sequence control applications, although satisfactory operation at constant acceleration above 50g becomes doubtful. For most applications a cam or series of cams is mounted on the drive shaft of the mechanical timing motor. These cams open or

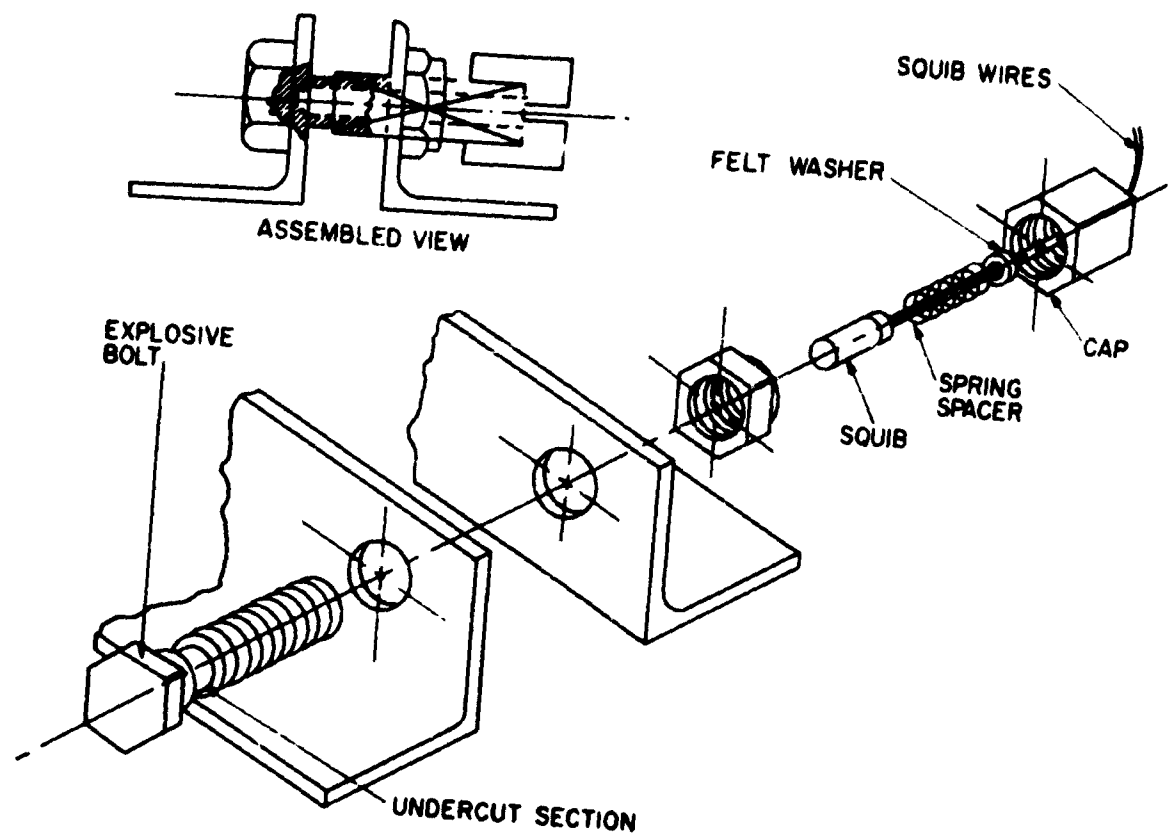


Fig. 9-17 Explosive Bolt, Frangible Type

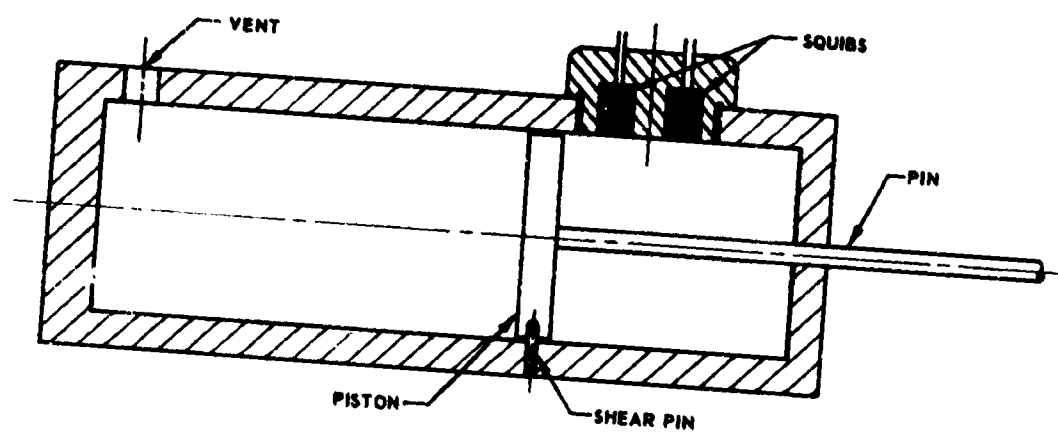


Fig. 9-18 Pin Puller

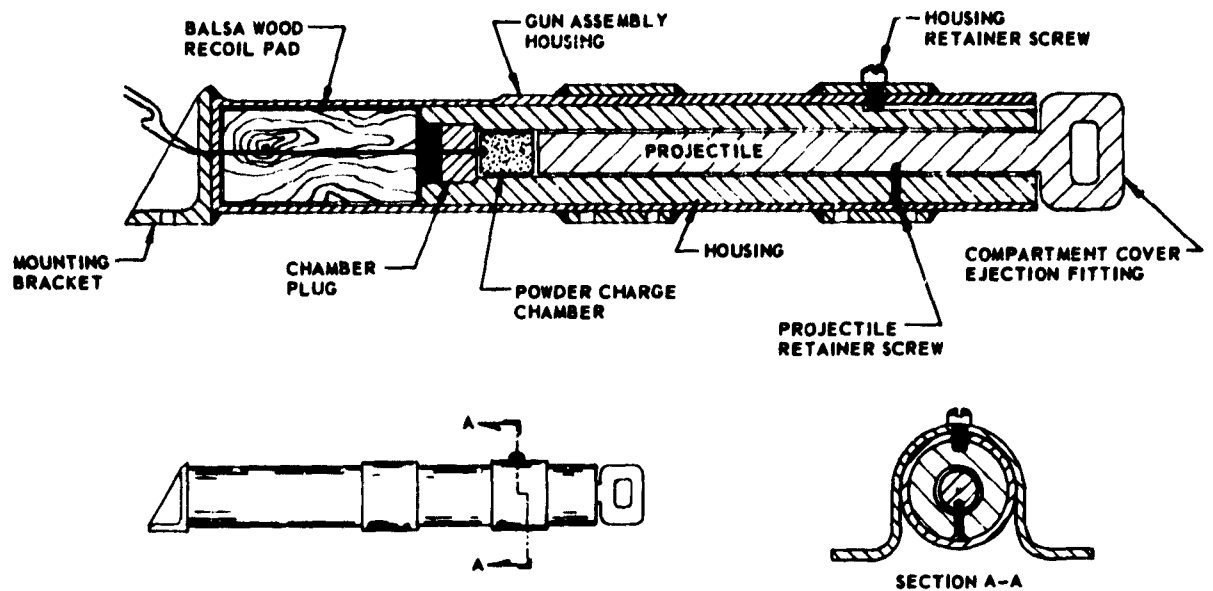


Fig. 9-19 Parachute Deployment Gun

close Microswitches connected to the actuating device in a predetermined sequence.

Other types of mechanical timing-motors have been constructed using a Neg'ator (constant-force spring) type motor and a centrifugal-friction governor with

a balance motor designed to make its performance independent of accelerations to which the device may be subjected. The Neg'ator (Ref 9-17) is a strip of flat spring material which has been given a curvature by continuous heavy forming at a constant radius. In its relaxed condition the Neg'ator is a tightly wound spiral; by reverse-winding the free end of the spring around a drum larger than the relaxed spiral diameter, the tendency of the spring to recur to its pre-set curvature can be utilized to make a mechanical motor with nearly constant output torque. A majority of the commercially available mechanical timing motors are activated by withdrawing a lanyard. This activation method, of course, severely restricts the location of the timing device within the vehicle. Mechanical timing devices are now available which wind and activate themselves by electrical impulses.

3.1.5 ELECTRICAL TIMING MOTORS. Electrical timing motors are perhaps the most widely used devices for time-sequence functions. In most applications, low-voltage d-c motors are used, with the rotor shaft connected through suitable reduction gears to a cam shaft. The cams open or close electrical contacts in a predetermined sequence during shaft rotation. This timing method has certain disadvantages; for example, in some types of electrical timing motors, resonance of the motor brushes at an excitation frequency of approximately 85 cps has been observed, making satisfactory operation questionable where vibration is present, and indicating a requirement for extensive environmental testing before use. The

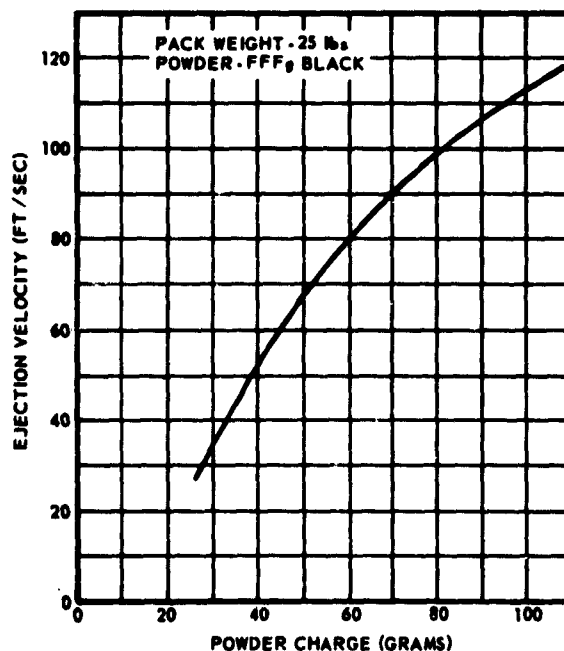


Fig. 9-20 Blast Bag Ejection Velocity

most serious disadvantage, however, is the fact that voltage variation will to some extent affect the duration of the timing cycle, and in most cases a well regulated primary-power supply will be required. Fig. 9-24 is a plot of voltage variation against time for one revolution of the cam shaft for one particular electrical timing motor tested.

Compared with other timing methods, electrical motor timers are relatively heavy devices. Their major advantage is that the timing device may be located almost anywhere within the vehicle.

3.2 g-Switches. The use of g-switches (inertia-activated switches) allows control of actuation functions to be initiated when a pre-set level of acceleration or deceleration is reached. The operation of almost all inertia switches is based on a mass-spring system, as shown in the simple case of Fig. 9-25. Here, a weighted contact arm 4, which is an integral part of a d-c relay BB' , is utilized as the sensory component. Acceleration forces acting upon the mass will bend the contact arm C until contact is made with D , thus energizing both coils of the electrical relay by completing the circuit through negative terminal 1. Coil B then closes contacts $E-F$, completing the circuit to the actuating device, and also holding $C-D$ closed after the accelerating force is removed.

In general, the construction of the inertia switch is such that it is sensitive to g-forces in one direction only, although it will also respond to forward components of accelerations in other directions. Types of g-switches have been designed which operate only when subjected to decelerations above a pre-set magnitude and sustained for a definite minimum time-duration. These switches are insensitive to g-forces of considerably greater magnitude if the time duration is

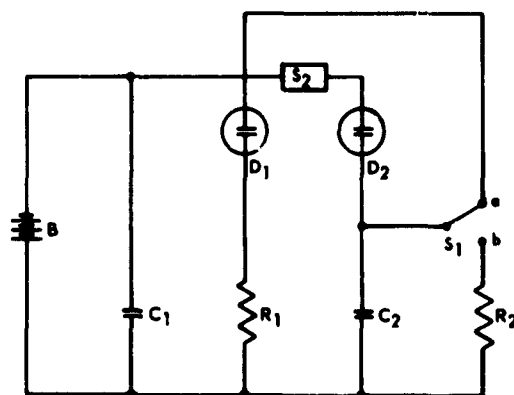


Fig. 9-22 R-C Time Delay Circuit

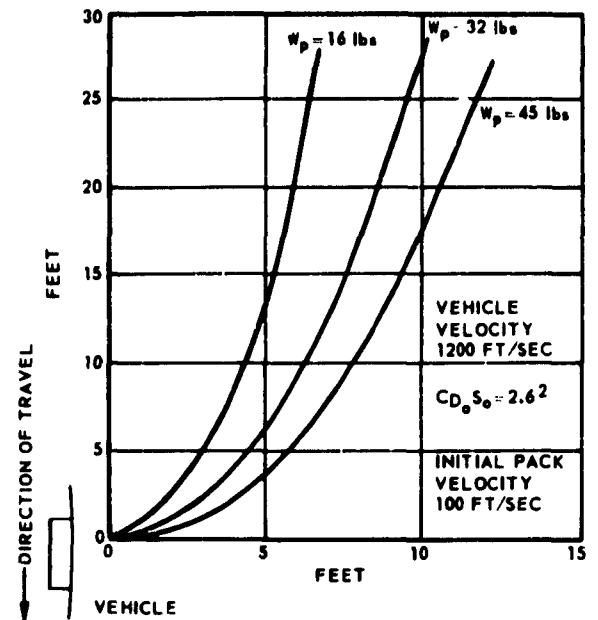


Fig. 9-21 Parachute Pack Trajectories, Lateral Ejection

too short, and are commonly used to control the actuation of disconnects upon ground impact of the vehicle; they have also been used for the initiation of time sequencing-devices in missile-recovery systems.

3.3 Pressure Switches. Pressure-actuated switches, which control actuating devices when a pre-set pressure level or pressure rate-of-change has been reached, generally depend on bellows-type aneroids which expand or contract with changing pres-

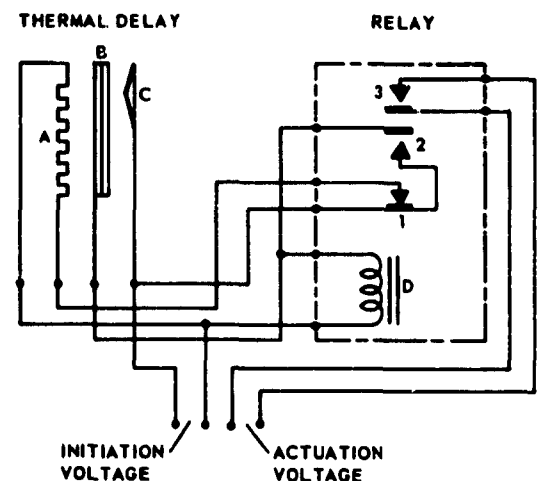


Fig. 9-23 Thermal Time Delay Circuit

suren. After the bellows have moved a predetermined distance, which occurs at a specific pressure-level or rate-of-pressure change, a switch is actuated, connecting the electrical power source with the controlled device. Two types of pressure-actuated control devices have been constructed, static- (or absolute-) pressure sensors and dynamic- (or differential-) pressure sensors.

3.3.1 STATIC - PRESSURE SWITCHES. Static-pressure-actuated switches (barometric switches) are frequently used to initiate the deployment of first- or final-stage aerodynamic decelerators in multi-stage deceleration systems. A variety of aneroid switches in various configurations are commercially available for this purpose, a few of which are shown in Fig. 9-26. The simplest principle of operation is the utilization of the expanding bellows to make or break a set of electrical contacts. Although a fairly high degree of reliability and accuracy can be achieved with this method, intermittent operation may be caused by contact chatter in a strong dynamic environment. Reliability of the control device may be increased by substituting a snap-action switch for the electrical contacts, but accuracy probably will not be high because of additional frictional forces and tolerances introduced in operating the switch. Sensitivity and

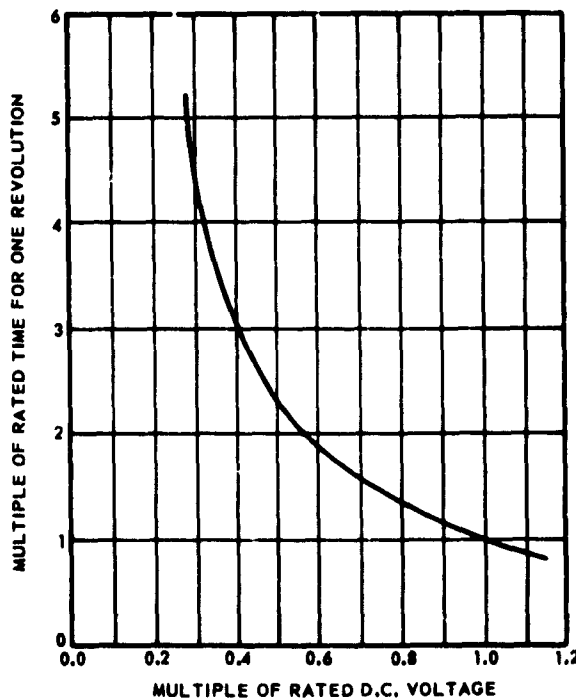


Fig. 9-24 Effect of Voltage Variation on Timer Speed

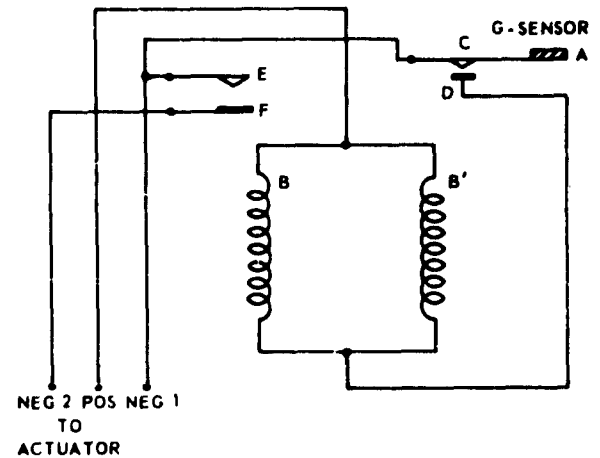


Fig. 9-25 Simple G-Switch Circuit

accuracy of the barometric switch can generally be increased by utilizing two or more bellows, internally interconnected. Tests have shown, however, that in a vibratory environment multiple bellows will decrease the reliability of the device. Probably the highest reliability and accuracy can be obtained by locating the electrical contacts inside the bellows; with this arrangement, contact closure is obtained below the set altitude with a minimum of components. This arrangement has minimum sensitivity to shock and vibration applied along the critical axis perpendicular to the plane of the bellows. The location of the bellows-controlled device in the vehicle is of major importance if operation at precise pressure levels is required.

3.3.2 DYNAMIC-PRESSURE SWITCHES. Because of the complexity required for accurate and reliable functioning under adverse environmental conditions, dynamic-pressure (or differential-pressure) sensors that would be routinely adaptable to decelerator system applications have not reached an advanced state of development. Devices have been designed which consist essentially of two independent bellows, one to sense static pressure and the other for ram pressure. The physical arrangement of the bellows is such that the movement of a pivoted lever is blocked until the resultant expansion of the two sensors allows the movement of the lever, and actuation of a Microswitch. It is also possible to utilize a strain-gage differential-pressure transducer as a sensor and let the resulting diagonal bridge current, which is a function of the applied differential pressure, actuate a sensitive current relay or vacuum switch. In order to obtain a high degree of accuracy, however, the applied bridge voltage must be maintained constant, since the bridge output current is also a function of the input voltage.

3.4 Force Sensors. Control devices in which the principle of force-sensing is employed are not very common at present, primarily because of the limited number of applications for this type of device. Force-sensing devices are used chiefly for control of the point of disconnect of aerodynamic-deceleration stages from the load, either prior to deployment of a succeeding stage or upon ground contact. Here again, a variety of principles may be used. Some force-sensing devices employ springs, and operate on the stress-relaxation principle; others utilize hydraulic pressure acting upon a diaphragm, which, when deflected a predetermined distance, actuates a Microswitch. Force sensors may also be built with a strain-gage link, using bridge output-currents directly for switching or actuating purposes.

SEC. 4 GROUND-IMPACT SHOCK-ATTENUATION DEVICES

Generally, designers of aerospace-vehicle recovery and air-drop systems strive to achieve a rate of descent of 25-30 fps. However, there are advantages in designing for the highest rate of descent at which a drop can be accomplished successfully without undue damage to the load. Hence, most systems which require a limitation on imposed impact forces are designed for the best possible compromise between the rate of descent and the ground-impact shock-attenuation systems. In some cases, the resistance to damage of the dropped object at the acceptable rate of descent is sufficient to make the use of an impact shock attenuation system unnecessary.



Fig. 9-27 Ground-Impact Shock-Attenuation Device

There are three general methods by which ground-impact shock forces imposed on the load can be reduced: (1) shock attenuation by ground penetration; (2) shock attenuation without penetration; and (3) pre-contact retardation. Although the three methods employ distinctly different devices, they all satisfy the main objective of a shock-attenuation system: to provide an opposing force in the direction of the velocity of the object to be recovered until its momentum is reduced to zero. At the same time, depending on the fragility of the load, these devices must also con-

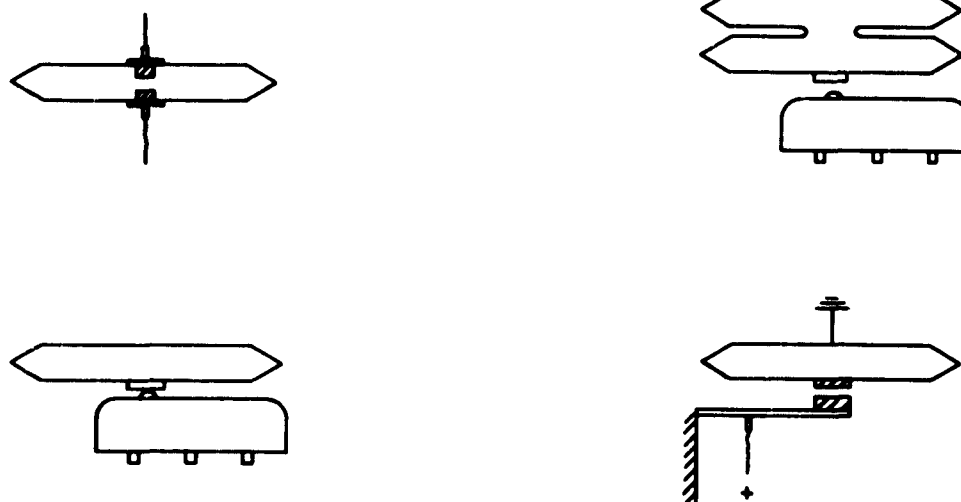


Fig. 9-26 Static Pressure Actuated Switches

trol the rise time and the magnitude of the imposed force during deceleration. An added requirement for the landing-deceleration system is the prevention of toppling of the load during or after the deceleration phase.

4.1 Shock Attenuation by Ground Penetration.

The ground-penetration method is most commonly used for the recovery of missiles. In this method, a spike rigidly attached to the missile nose section is employed (Fig. 9-27). The main attraction of this method is its simplicity. Its use is advantageous when the volume in the missile does not permit the stowage of a large parachute or of air-bag decelerators. Its disadvantage is that the effectiveness of the spike depends largely upon the type and hardness of the terrain on which impact occurs. The use of this method of landing shock attenuation requires high rates of load descent (50-60 fps) so that the spike will penetrate the ground to a depth that will prevent toppling of the vehicle. As a result of the required high rate of impact, the missile structure must be designed to withstand the high decelerative forces in the direction imposed by the spike.

4.2 Non-Penetrating Methods. This general class of shock-attenuation devices is relatively indifferent to terrain conditions. Performance depends upon placement of the shock-attenuation device be-

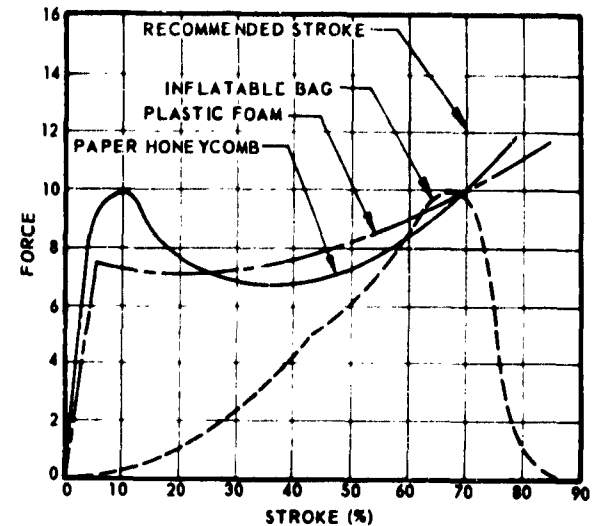


Fig. 9-28 Parallel Paper Honeycomb, Plastic Foam and Air Bag Force vs. Deflection Characteristics

tween the load and the ground before impact. Some of the devices used for the method of shock attenuation are inflatable bags, paper honeycomb cushion, and foamed plastics. Representative deceleration force versus stroke diagrams for the three shock attenuation devices are shown in Figure 9-28.



Fig. 9-29 Landing Bag

4.2.1 INFLATABLE BAGS. The inflatable-bag system (Fig. 9-29) may consist of one or more bags which are fabricated of strong, impermeable fabric. Initially, the bags are stored in a collapsed state in compartments provided for on the load and are inflated prior to ground contact. The geometrical configuration, mass, and strength distribution of the vehicle or load to be decelerated determine the size, shape, and location of the bags.

Three different types of inflatable bags are currently used in recovery or landing shock-attenuation systems (Ref 9-18). One type fills with air as gravity extends the bag vertically below the load during descent. Air may enter the bag at the bottom or through ports covered with one-way flap valves. Exhaust orifices, covered with burst diaphragms to prevent the air from escaping during descent, are usually spaced around the periphery of the bag or at the top of the bag. On impact, the compressed air escapes through the fixed-diameter orifices after diaphragm burst-pressure is reached and as landing energy is absorbed. A second type of bag inflates to a relatively high pressure (12 psig) from a compressed-air source carried by the load or vehicle. On impact, the air again exhausts through fixed-diameter orifices after diaphragm burst-pressure is reached. The third type of bag inflates to a relatively low pressure (½ psig), and at impact exhausts air through variable orifices, thereby increasing energy-absorption efficiency.

The critical parameter in the design of inflatable bags is the release rate of the air through the exhaust orifices so as to expend the available energy simultaneous with load or vehicle ground contact without excessive "bottoming" or toppling of the load. The ideal orifice design would allow air to escape at a rate which would maintain constant deceleration until the end of the stroke.

In designing an inflatable-bag shock-attenuation system, the goal is a bag configuration satisfying the requirements of the particular problem. The geometry and the dynamic characteristics of the vehicle or load will generally dictate a basic bag shape. Toppling problems will usually be present and their solution will generally require care in the bag arrangement.

Extensive analysis to establish criteria for the efficient design of inflatable bags of spherical shape have been conducted (Ref 9-18). These criteria are applicable to all inflatable-bag types provided that the relationship of bag volume, stroke, and footprint area is known.

A cross plot interrelating various parameters to determine bag diameter and burst pressure for a number of conditions is shown in Fig. 9-30. These and

the following curves are for inflatable bags of spherical shape exhibiting an 18 percent elastic deformation at the design burst-pressure with the load applied by a vehicle having a flat bearing surface. The parameters A and B represent

$$(9-1) \quad A = \frac{W V_v^2}{F_v \cdot W} K \quad \frac{V_v^2}{a_{\max}} K$$

and

$$(9-2) \quad B = \sqrt[3]{\frac{W V_v^2 F_v}{4(F_v \cdot W)}} K = \sqrt[3]{\frac{V_v^2 F_v}{4 a_{\max}}} K$$

Where

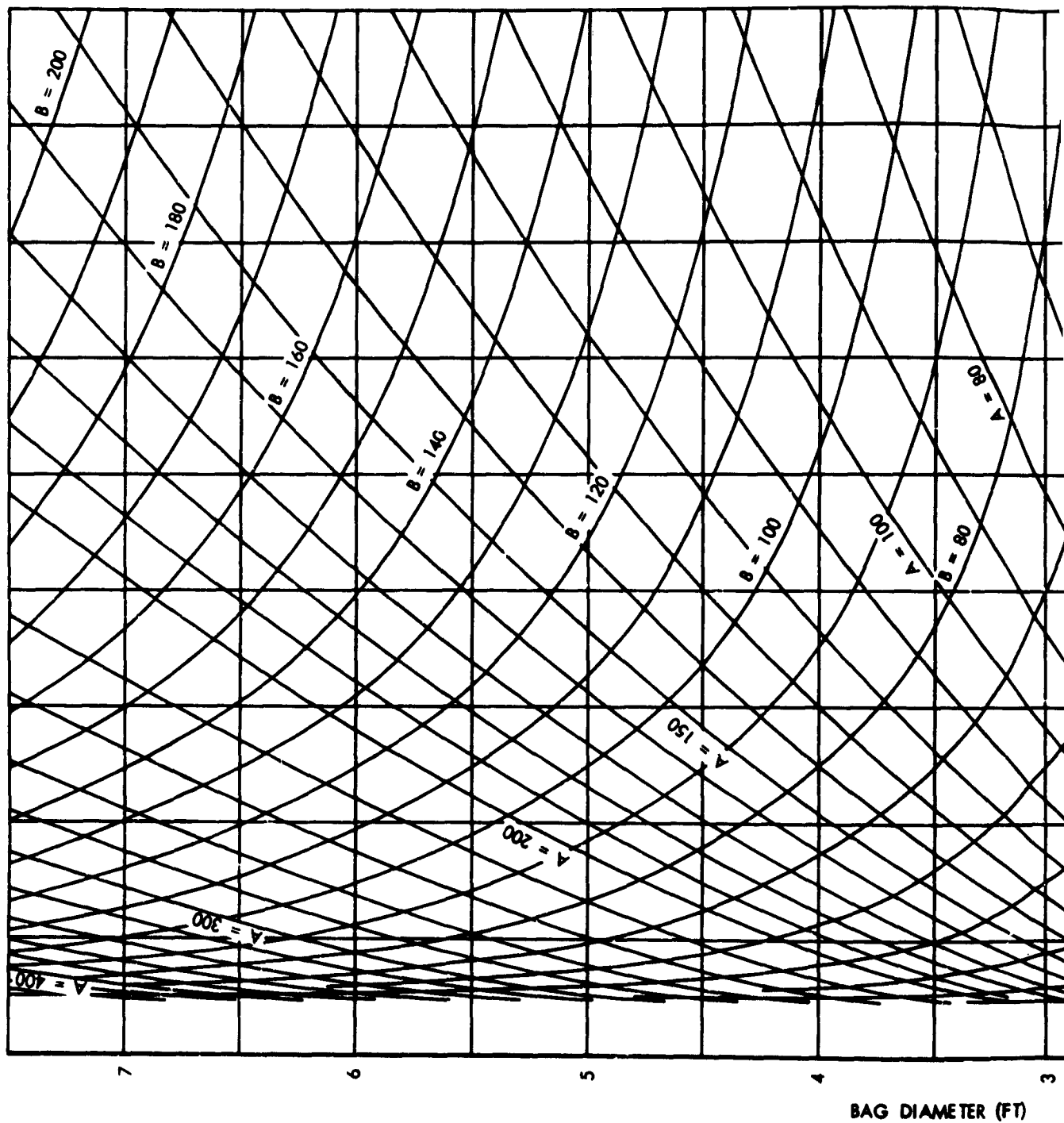
- W = Weight of load or vehicle (lb);
- V_v = Vertical descent velocity (ft/sec);
- F_v = Vertical force exerted on the suspension lines and risers (lb);
- a_{\max} = Allowable deceleration rate (g); and
- K = Factor related to orifice efficiency.

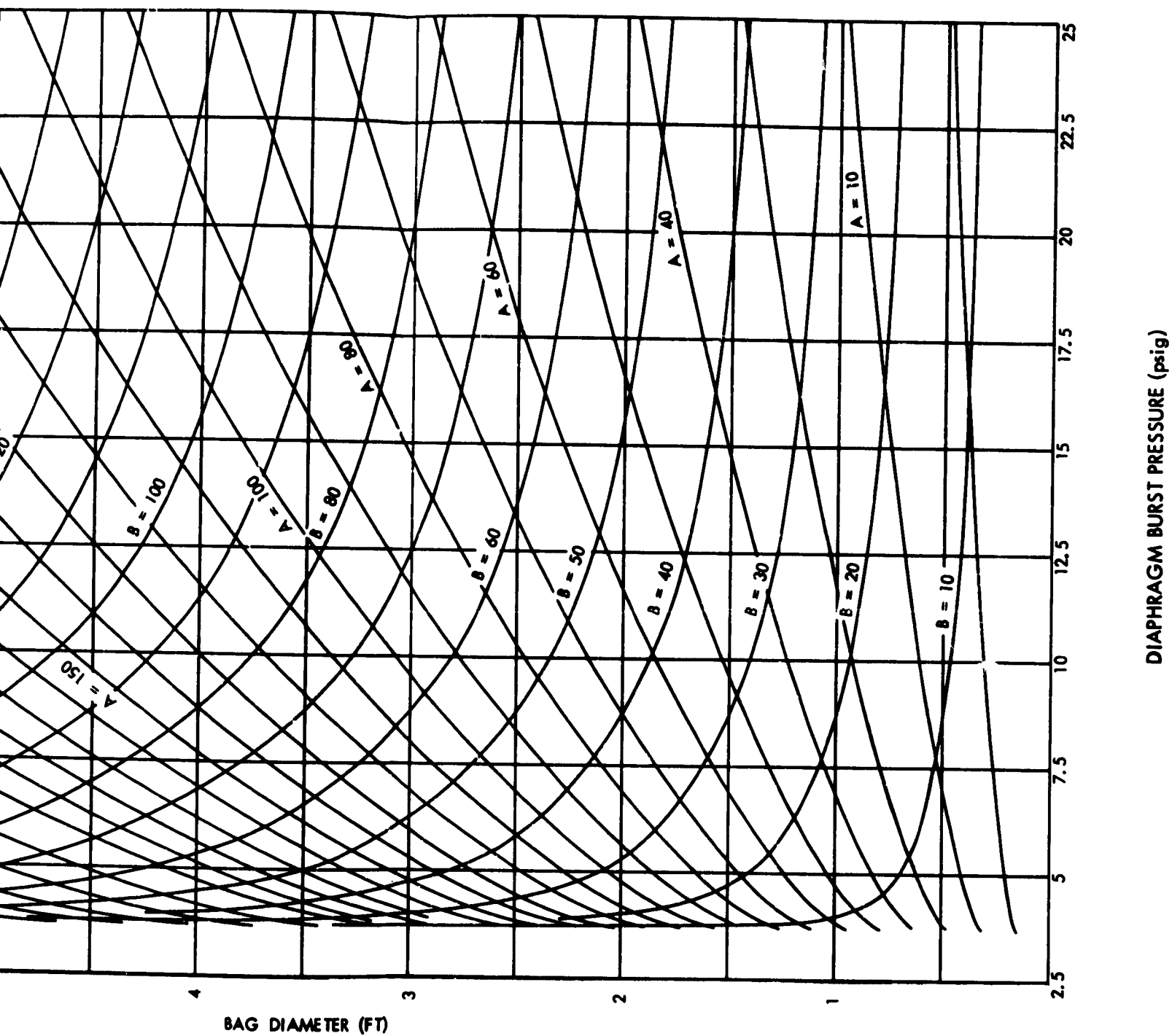
For an "ideal" orifice, a value of 1.0 for K may be applied for all impact velocities. For the conventional fixed-area orifice, K -factors have been determined experimentally and are plotted against rate of descent in Fig. 9-31. The variation of the ratio of maximum bag pressure, P_{\max} , to diaphragm burst-pressure, P_{burst} , with impact velocity for fixed-area orifices and two different initial bag-inflation pressures are shown in Fig. 9-32. These data allow the determination of the peak internal pressure to be taken into consideration for the stress analysis of the bag. The curves plotted in Fig. 9-33 interrelate impact velocity, bag radius, orifice area, and diaphragm burst-pressure.

When considering the design of inflatable bags in conjunction with a particular vehicle or load, problems of pitching or toppling of the load must be taken into account. Suggested methods for increasing the anti-toppling characteristics of the load to be decelerated by two or more air-filled bags are:

- (1) Vary the distance between the bags;
- (2) Provide a means for changing the force-stroke relationship of one or more of the bags as compared to the other(s) as a function of impact angle or horizontal velocity or both;
- (3) Provide a means for reducing friction between the ground and the bag(s); or

1





2

Fig. 9-30 Bag Diameter vs Burst Pressure

(4) Limit the landing conditions to those which will not result in toppling.

These suggested methods are arranged in order of increasing complexity for any given vehicle configuration. The four methods should, therefore, be considered in the order listed.

Materials used in the construction of inflatable bags are largely selected from available commercial stock or materials developed for military applications other than inflatable-bag construction. The basic yarns used are usually of the synthetic fiber family, such as nylon or Dacron. Important factors to consider in selection of inflatable-bag material are low elasticity, high ratio of strength to weight, tear resistance, temperature limitations, and adaptability to construction techniques. Basic materials are normally coated with synthetic rubber, which produces little or no effect on their strength.

In the selection of an inflation system for inflatable bags, parameters of weight, bulk, reliability, and cost must be carefully weighed against the requirements of the vehicle or load to be decelerated. Weight and bulk are normally of the greatest importance, and these parameters are strongly influenced by the inflation pressure and time allowed for inflation. The following table presents an order of merit for representative systems without regard to penalties imposed on the system by unusual installation or environmental problems. The ratings *A*, *B*, and *C* are in order of desirability.

System	Weight	Bulk	Reliability	Cost	Limitations
Blower (Fan)	A	A	C	C	Low Pressure-Low Altitude
Pressure Vessel	C	C	A	A	Completely Sealed Systems
Aspirator	B	B	B	B	Low Inflation-Pressure Low Altitude Completely Sealed Systems

Data from water-impact tests with spherical airbags indicate that pressure and deceleration rates are approximately 65 per cent as great for water impact as compared to land impact with the same system. Bag diameters, therefore, may be reduced about 15 per cent from the size required for land impact.

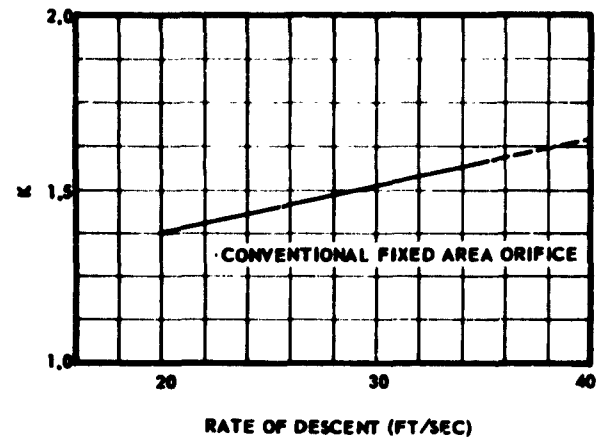


Fig. 9-31 Factor K Versus Rate of Descent

A landing-bag system designed for impact on either water or land should have its dimensions established by the land-impact conditions.

4.2.2 PAPER HONEYCOMB. Vertical-cell paper honeycomb has, in some cases, replaced shock pads and inflatable bags as the method of energy dissipation used for air drops of equipment and supplies (Ref 9-19 and 9-20). The development of paper honeycomb has produced an efficient, inelastic, and low-cost cushioning material. The standard type of paper honeycomb presently in use, Military Specification MIL-H-9084, is fabricated in sheets 3 ft wide, 8 ft long, and 3 in. thick. Blocks of various sizes can be easily cut from the sheet with a saw or knife. The blocks are stacked on the air-delivery platform so that the inelastic parts of the vehicle frame and crossmembers

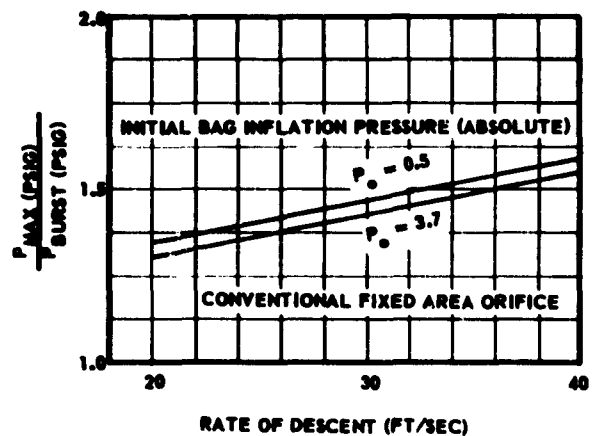


Fig. 9-32 $\frac{P_{max}}{P_{burst}}$ Versus Rate of Descent

will rent on the honeycomb. The total crushing area of the honeycomb for a desired deceleration value may be calculated from the following equation:

$$(9-3) \quad A = \frac{W(G+1)}{S_a}$$

where

A = Area (ft²);

W = Weight (lb);

$G = a/g$ (a = deceleration in ft/sec²; $g = 32.2$ ft/sec²);
and

S_a = Average crushing stress of paper honeycomb.

The maximum required thickness of each stack can be calculated from equation:

$$(9-4) \quad t = \frac{V^2}{2gGE}$$

where

t = Thickness (ft);

V = Impact velocity (ft/sec); and

E = Thickness efficiency = 0.7 for paper honeycomb.

The use of these equations to arrive at a paper-honeycomb energy-dissipator configuration for com-

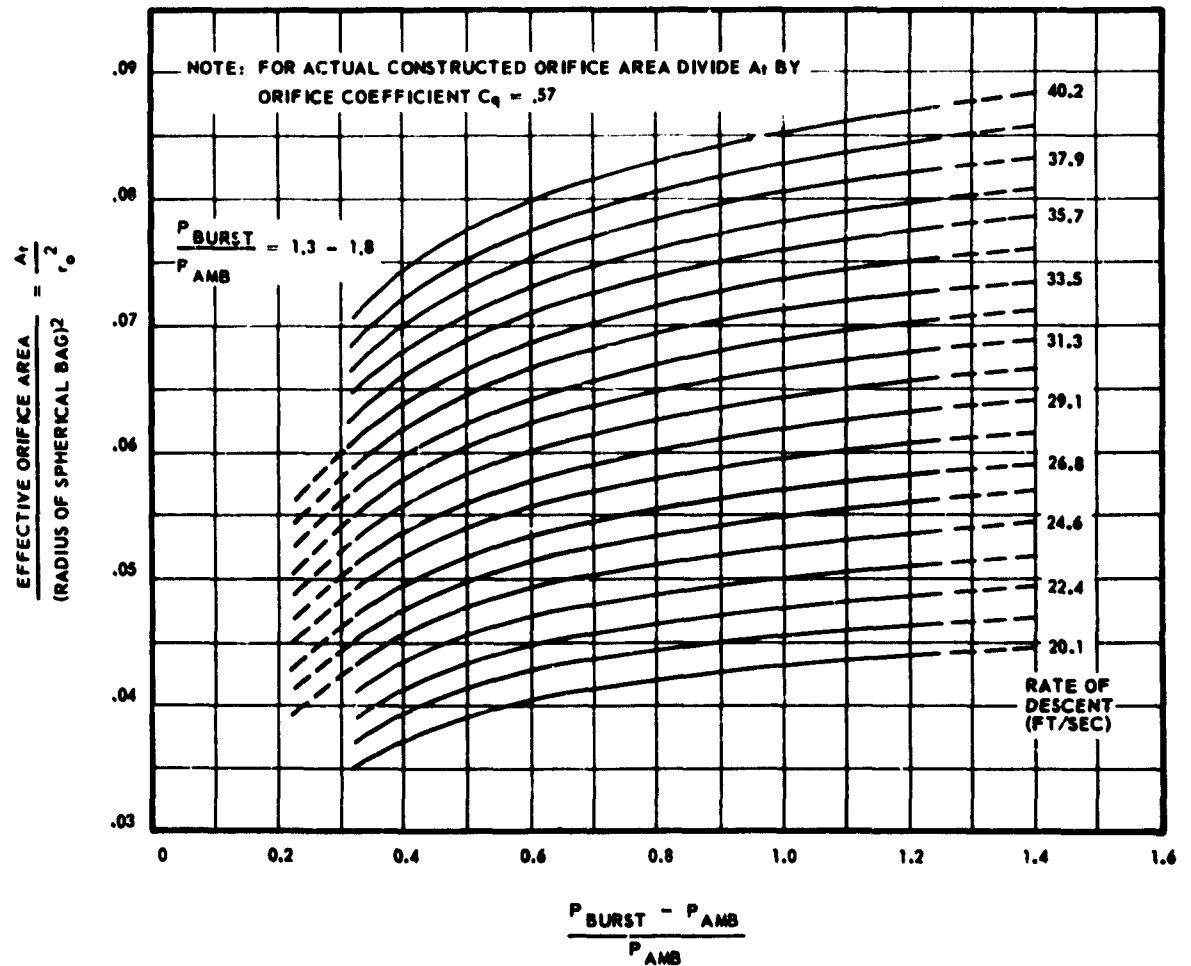


Fig. 9-33 Orifice Area/Bag Radius Versus Burst Pressure

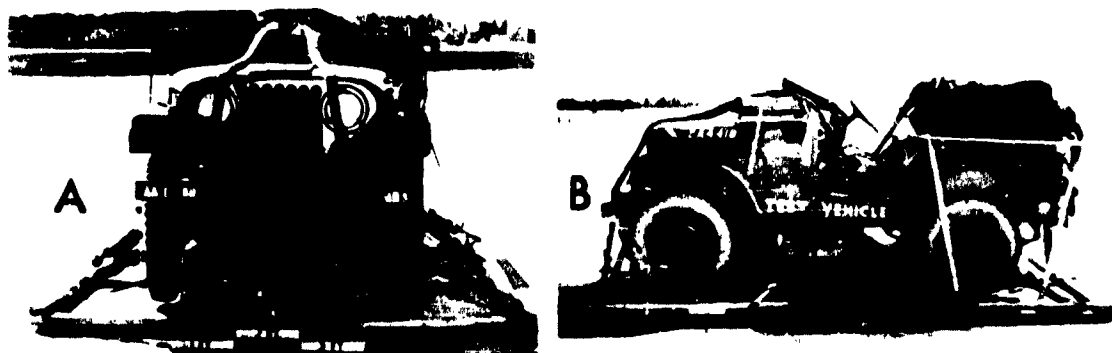


Fig. 9-34 Service Test of the Combat Expendable-Platform System

TRUCK, $\frac{1}{4}$ T, M38A1, RIGGED FOR PARACHUTE DELIVERY ON THE 12-FT COMBAT EXPENDABLE PLATFORM

A - TRUCK, $\frac{1}{4}$ T, RIGGED ON 12-FT PLATFORM (FRONT VIEW)

B - TRUCK, $\frac{1}{4}$ T, RIGGED ON 12-FT PLATFORM (SIDE VIEW)

plex loads (Fig. 9-34) requires information which presently can only be obtained experimentally. Such unknown factors as number of g's the vehicle can withstand, the number of combinations possible for arranging the stacks beneath the vehicle, distribution of total cushioning area among the number of stacks positioned under the vehicle, and knowledge of weight supported by individual stacks make impact testing of various system-configurations necessary before selection of final design.

The amount of rebound energy created by paper honeycomb is approximately 8 per cent of the impact energy, provided the honeycomb is not crushed to more than 70 per cent of its original thickness.

An indication of the ability of a paper honeycomb stack to resist toppling when transverse motions are imparted to the stack is the ratio of the thickness of the stack to the length of the shortest side. Experience has shown that generally a ratio not much higher than one will provide sufficient stack stability.

4.2.3 FOAMED PLASTIC. Foamed plastic is a light-weight expanded cellular structure produced by combining a liquid plastisol with a foaming agent (Ref (9-21) and (9-22)). Nearly any combination of foam density and rigidity may be produced by using various combinations of plastisols and foaming agents. Certain foamed polystyrene plastics have stress-strain characteristics similar to paper honeycomb, and the cost per foot-pound of energy absorbed is comparable. Problems connected with the storage of these materials in unexpanded liquid form and their ready expansion in the field have so far precluded the

use of foamed plastics for air delivery of equipment.

A rapidly expandable plastic could be used to form a landing shock attenuator and could expand while in flight. The plastisol and foaming agent could be carried under the air-delivery platform prior to air drop, and combined and foamed during descent to form the plastic structure. However, presently known quick-foaming plastics require thorough mixing to insure a homogeneous foam, and a minimum curing time greater than the normal descent time of air delivery items.

4.3 Pre-Contact Retardation. Pre-contact retardation techniques decelerate the load prior to contact with the ground by applying a force opposite to the direction of motion. Energy is added to the system by impulse-generating units which operate to counter-

act the momentum of the load. The use of retro-rockets falls under this general class of landing decelerators. Disadvantages, such as actuation, timing, and reliability problems; high cost; and the close quality-control required if more than one rocket is used, have restricted their application as practical landing decelerators. However, investigations have shown that for impact attenuation of heavy loads (greater than 10,000 lb) which require a low-impact loading, a system incorporating retro-rockets may have a significant advantage, from an overall system-weight standpoint, over a recovery system utilizing parachutes alone or parachutes with inflatable bags. At this point, the designer is confronted with the trade-off between desired recovery-systems performance and reliability, and permissible recovery-system weight.

REFERENCES

- (9-1) Ward, J. A., Canopy Spiller for Troop Personnel Assembly, Type T-10. WADC TR 59-245, May 1959, AD 233016.
- (9-2) Jablonsky, H. J., Service Test of the Capewell Canopy Release Assembly and the Capewell Canopy Release Assembly (Modified) for Use with Troop Type T-10 Personnel Parachute Assembly. Report of Project Nr. AF 2158, HQ U. S. Army Airborne and Electronics Board, Jan 1959, AD 209600.
- (9-3) Roberts, J. F., Confirmatory Test of Modified Capewell Canopy Release Assemblies for Use with Troop Type T-10 Personnel Parachute Assemblies. Letter Report of Project Nr. AB 2859, HQ U. S. Army Airborne and Electronics Board, Jan 1960, AD 231536.
- (9-4) Townsend, D. E., Service Test Modified Troop Type T-10 Personnel Parachute Harness Incorporating Modified Capewell Canopy Release Assembly. Project Nr. ATB 3-280, U. S. Army Arctic Test Board, Apr 1960, AD 236476.
- (9-5) Aron, W. K., Study and Development of Parachutes and Systems for In-Flight and Landing Deceleration of Aircraft, Part III, Design of Assisting and Control Devices. WADC TR 57-566, Part III, Jan 1959, AD 155708.
- (9-6) Aerial Delivery of Supplies and Equipment, General. T.O. 13C7-1-5, TM 10-500, D A and D AF, May 1958, and Changes 1-5, 1958-1961.
- (9-7) Roberts, J. F., Service Test of Release, Automatic, Cargo Parachute, 5000-Pound Capacity, and Load Coupler. Report of Project Nr. AB 2658, HQ U. S. Army Airborne and Electronics Board, July 1959, AD 226773.
- (9-8) Angel, J. F., Cargo Parachute Release. WADD TV 60-292, Dec 1960, AD 251835.
- (9-9) Beckwith, W. L., Jr., et al., Cargo Parachute Release Device. Final Report, Contract No. DA-19-129-QM-1188, Universal Winding Company, June 1959, AD 219278.
- (9-10) Tager, R. F., Parachute Ground Disconnect. WADC TR 59-455, July 1959, AD 227349.
- (9-11) Johnson, J. H., M2F1 Reefing Line Cutter. Summary Report, Contract DAI-28-017-501-ORD-(P)-1822, Ordnance Division, Minneapolis-Honeywell Regulator Co., May 1956, AD 93988.
- (9-12) Automatic Parachute Ripcord Release Type F-1B. T.O. 14D2-2-23, Technical Manual, Overhaul, D. AF, 15 May 1959.
- (9-13) Downing, J. R., et al., Recovery Systems for Missiles and Target Aircraft, Part I, Subsonic Sled Test Phase. AF Technical Report 5853, Part I, WADC, Mar 1954, AD 112981.
- (9-14) Downing, J. R., et al., Recovery Systems for

- Missiles and Target Aircraft, Part II, Subsonic Free-Flight Validation Test Phase. AF Technical Report 5853, Part II, WADC Mar 1955, AD 114101.
- (9-15) Downing, J. R., et al., Recovery Systems for Missiles and Target Aircraft, Part III, High Subsonic and Transonic Track Borne Parachute Tests. AF Technical Report 5853, Part III, WADC, Dec 1956, AD 122635.
- (9-16) Knacke, T. W., et al., Study of Soft Recovery. Technical Report AFOSR-104, Air Force Office of Scientific Research, Mar 1961, AD 255766.
- (9-17) Mankonen, H. E., Constant Force Springs. Tool and Manufacturing Engineering, pp. 117-120, Nov 1960.
- (9-18) Simonson, J. R., Study of Design Criteria for Landing Shock Absorption Devices for Recoverable Flight Vehicles. ASD TR 61-583.
- (9-19) Bixby, H. W., Development of a Paperboard Honeycomb Decelerator for Use with Large Platforms in Aerial Delivery Systems. WADC TR 59-776, May 1959.
- (9-20) Sabbagh, E. N., Performance Characteristics of Paper Honeycomb Cushioning Materials Impacted under a Heavy Weight High Impact Shock Machine. WADC TR 55-343, AD 91460, Jan 1956.
- (9-21) Amidon, R. W., Studies Toward Development of Expandable Plastics. Sixth Quarterly Report, Contr. No. DA-44-009 ENG-j740, Proj. 8-93-13-001, AD 50091, Sep 1957.
- (9-22) Chakoumakos, Charles, Development of an Inorganic Foamed-in-Place Material. Progress Rpt III, Contr. No. 53-040-C, AD 9120, Feb 1953.

BIBLIOGRAPHY

- Krakover, Stewart M., 1 Lt. USAF and Olevitch, A., Investigation of Design Criteria for Cushioning Materials. WADC TR 58-639, AD 201227, Mar 1959.
- Martin, R. C., Low Level Aerial Delivery Feasibility Study. WADC TR 57-517, AD 14202, Nov 1957.
- Tomesak, S. L., Decelerator Bag Study. WADC TR 59-775, June 1960.
- Idomis, Kenneth, TM-76 Mace Landing Mat Design. Aero Space Engineering, Glenn L. Martin Company, Baltimore 3, Maryland, Feb 1960.
- Scheele, W. and Fuller, F. E., Preliminary Design of XQ-4A Landing Bags. TFM-74, Radioplane, A Division of Northrop Corp., Van Nuys, Calif. 5 June 1957.
- Varland, W. B., Lower, J. B., Yates, J. E., and Blackburn, R. R., Study of Guided Missile Structural Design Criteria. WADD TR-140, Volume I, AD 155888, Feb 1959.

CHAPTER 10 PARACHUTE SUPPORT EQUIPMENT AND FACILITIES

Table of Contents

<i>Section</i>	<i>Page</i>
1 DRYING FACILITIES	438
1.1 Drying Tower	438
1.2 Drying Cabinet	438
2 PACKING & INSPECTION FACILITIES	439
2.1 Packing Tables	440
2.2 Inspection Tables	440
2.3 Bins	441
2.4 Storage Facilities	441
2.5 Packing Tools	441
2.6 Packing Presses	442
2.7 Sewing Machines	442

Illustrations

<i>Number</i>		<i>Page</i>
10-1	Parachute Drying Tower	438
10-2a	Parachute Drying Cabinet, Portable, Interior View (Racks Removed)	439
10-2b	Parachute Drying Cabinet, Portable, Interior View	440
10-3	Parachute Packing Tools	440
10-4	Parachute Packing Press	441

CHAPTER 10

PARACHUTE SUPPORT EQUIPMENT AND FACILITIES

Before parachutes are re-used they are cleaned and dried, inspected for possible damage, repaired if necessary, and then packed for immediate re-use or storage until they are needed. The specialized equipment necessary to insure the proper maintenance, handling, and packing of parachutes is discussed in the following sections.

SEC. 1 DRYING FACILITIES

1.1 Drying Tower. Parachute drying-towers are used to ventilate and dry parachute canopies. They provide a place to allow creases in the canopy to soften, and to permit shaking out dust, dirt, and the like. Availability of a parachute drying-tower is a requisite for the maintenance of personnel parachutes.

A drying tower (Fig. 10-1) is an oversized room, sufficiently high for a canopy suspended from the apex to hang without touching the floor. To draw the canopy to the ceiling, hooks and pulleys must be provided. Canopy suspension hooks are generally spaced approximately 3 ft apart, but this distance may be varied if the canopies usually hung in the facility require more room to hang clear of each other. Areas likely to come in contact with the canopy should be smooth and free of nails. Walls should be covered with polished hardboard or equivalent material. Warm, filtered, forced air should be provided, and dehumidification is desirable. The area should not be subject to exhaust, solvent, or acid fumes.

1.2 Drying Cabinet. Parachute drying-cabinets are used for the accelerated drying of all types of parachutes. Drying cabinets were first developed as a result of shortages of drying-tower facilities at bases where there was frequent use of aircraft-deceleration parachutes in large numbers. Because of conditions inherent in their use, aircraft-deceleration parachutes tend to become wet and collect dust, tar, and other contaminants, and they should not be hung in a drying tower adjacent to personnel parachutes. Thus, the drying cabinet is now used primarily for rapid drying of aircraft-deceleration parachutes, and does not replace the drying tower but supplements it.

The drying cabinet (Fig. 10-2) is an all-metal cabinet capable of being transported by air. It measures 6 ft by 6 ft by 8 ft in the erected state. The cabinet is designed so that it can be assembled or disas-

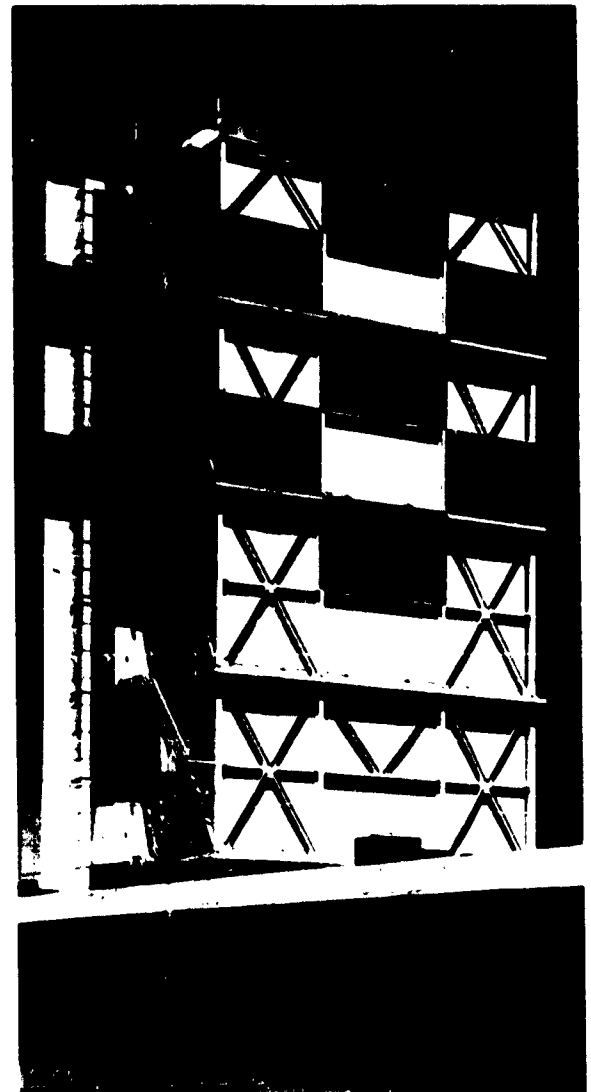


Fig. 10-1 Parachute Drying Tower

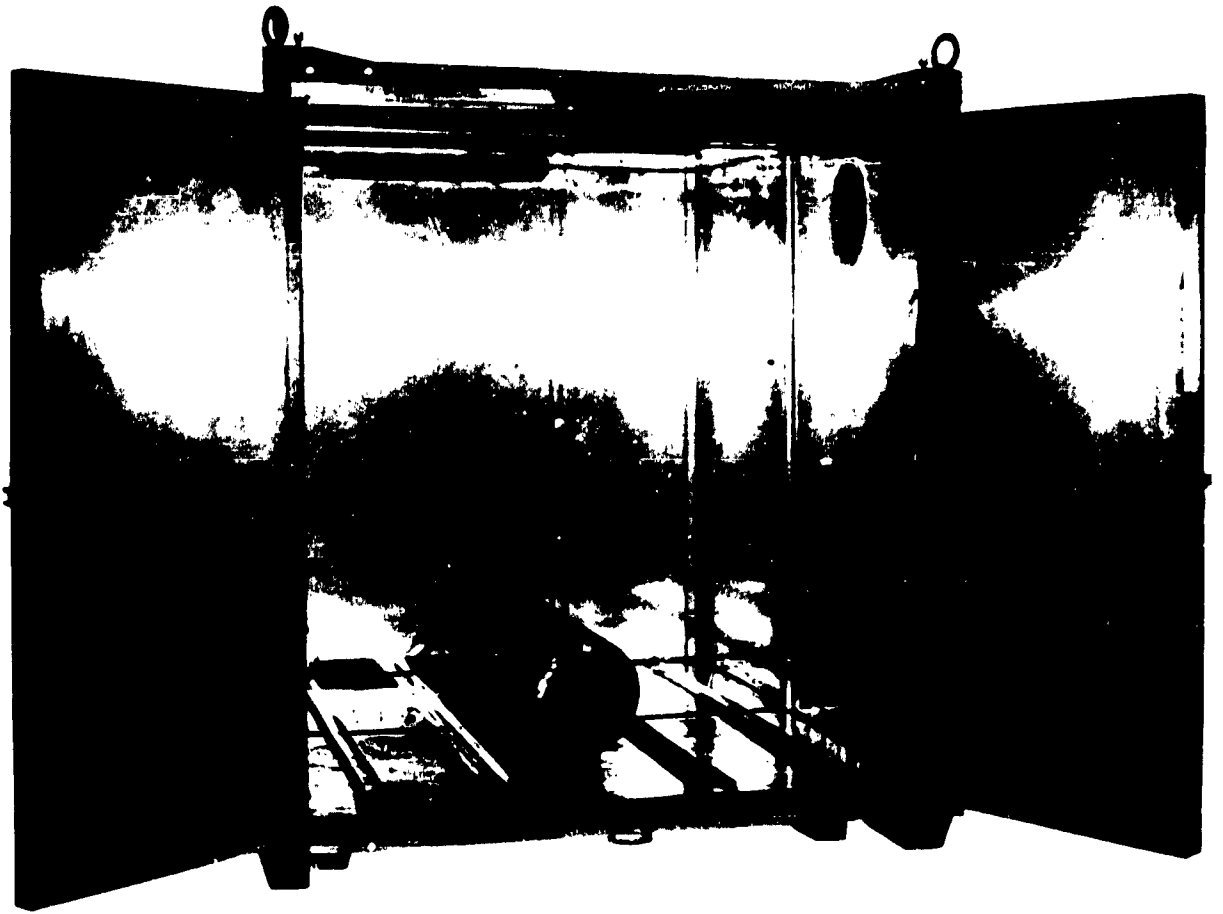


Fig. 10-2a Parachute Drying Cabinet, Portable, Interior View (Racks Removed)

sembled in the field by two men using standard tools. The heating source for the cabinet is a heater equivalent to a Herman Nelson BT-400, capable of delivering 400,000 Btu's per hr at an ambient temperature of -65 F. The heat is transferred from the heater to the cabinet through a 12-in.-diameter duct, 15 ft long. Temperature within the cabinet is automatically maintained at a level of 200 F. The inside of the cabinet is smooth and without protrusions. Dual racks, provided with easily removable and replaceable caster wheels, hold the canopy in place during the drying cycle. The cabinet can dry two thoroughly wet 44-ft-diameter ribbon canopies or their equivalent in 3 hr.

SEC. 2 PACKING & INSPECTION FACILITIES

The requirements for a packing and inspection facility are relatively simple. The building itself must be sufficiently large to permit free movement around the packing and inspection tables. Lighting in the vicinity of the working areas, both daylight and artificial, must be very good. Washing facilities for canopies are desirable. A drying tower (and cabinets, as required) must be part of the building, or be attached to it. Special furnishings include bins, issuing counters, and storage facilities.



Fig. 10-2b Parachute Drying Cabinet, Portable, Interior View

2.1 Packing Tables. Parachute packing tables may be of local manufacture. They should stand about 30 in. high and be of sufficient length to accommodate the full length of the canopy and the suspension lines. A width of 3 ft is sufficient for personnel parachutes, and 6 ft for cargo parachute canopies larger than 28 ft in diameter. The top of the table should be of polished hardboard or similar material. The top and other areas likely to come in contact with material should be free of anything that might snag or pull the material. The table should be equipped with a suitable device to place the suspension lines and canopy under an evenly distributed tension when the parachute is folded.

2.2 Inspection Tables. Inspection tables may be manufactured locally. They may be ironing-board shaped, approximately 18 ft long, 3 ft high, and tapering in width from 3 to 2 ft. A light is inset in the

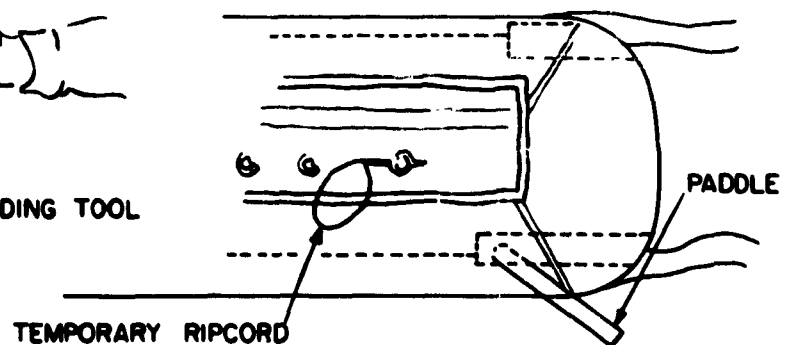
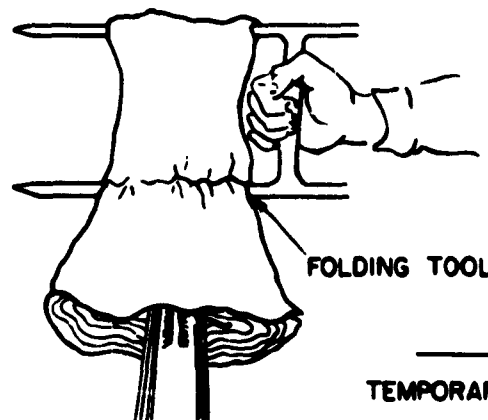
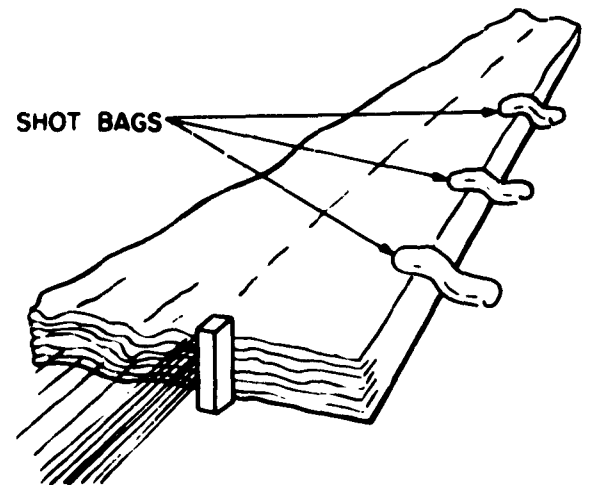
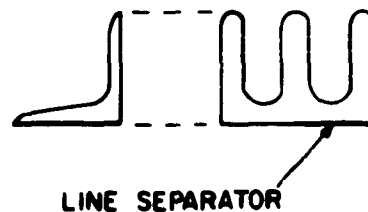


Fig. 10-3 Parachute Packing Tools

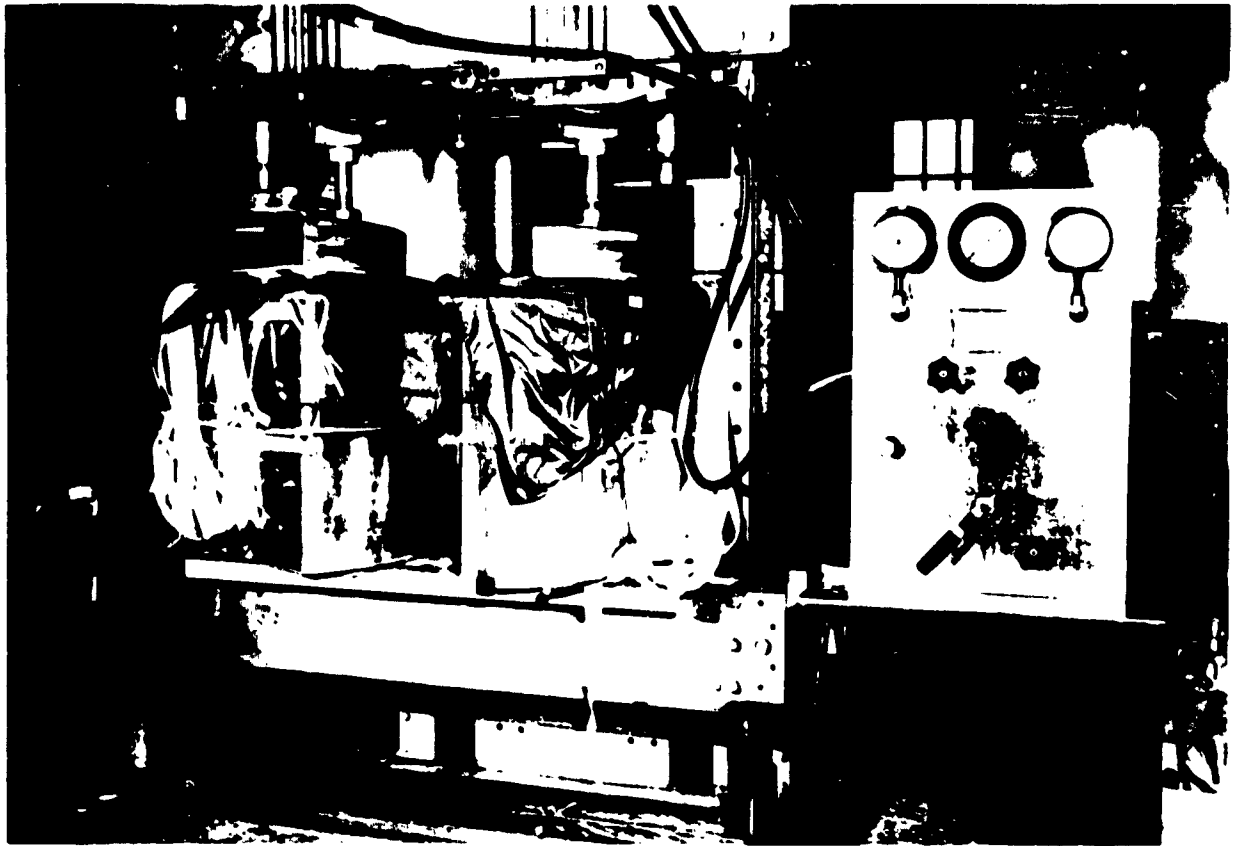


Fig. 10-4 Parachute Packing Press

center of the table and extends the full length. The face of the light should be smooth plate-glass set flush with the table surface. During inspection, the light passes through the canopy, revealing the condition of the yarn, radial and diagonal seam edges, suspension lines in channels, and the threading between surfaces of the material. A hand-held ultra-violet light is used to detect stains in the material. All portions of the table that might come in contact with material must be free of anything that could snag or pull the material.

2.3 Bins. Bins should be located convenient to the packing and inspection tables. They must be able to accommodate unpacked parachutes. The bin surfaces must be smooth and free of cracks, nails, or other objects that might snag or pull the material.

2.4 Storage Facilities. Storage facility requirements vary with the contemplated length of time of storage, climatic conditions, and the type of building

construction. Some fabrics are particularly susceptible to mildew damage in a warm, humid climate. (See Chap. 6.) Parachutes should be dried thoroughly before packing and then stored in a dry place protected from the sun. They should not be stored in direct contact with concrete floors; wooden racks are desirable. Cleanliness is important: grease, oil, or other contaminants must not be kept in, or used on the surfaces of, the storage area.

2.5 Packing Tools. The following tools are generally considered necessary for packing and inspection (Fig. 10-3):

Line Separator: A small, slotted stand used to hold the suspension lines in their respective group for packing.

Shot Bags: Cloth sacks, approximately 18 in. by 4 in., filled with about 4 lb of shot, used to hold material or lines in temporary placement. They are particularly useful for holding the folded half of a canopy while the other half is being folded.

Folding Tool: A device used to fold the canopy to the correct width or length so that it will fit the pack properly.

Temporary Ripcord: A short ripcord with pins, inserted into the locking cones or loops of the pack to hold the side flaps in place, so that the end flaps may be placed in position to insert the permanent ripcord.

Seal Press: A hand-operated device used to secure the seal applied by the packer or inspector to seal the packed parachute against tampering.

Assortment of Small Tools: Long-nosed pliers; knife; 6-in. shears; 10-in. shears; needles: sharp, blunt, and curved; hammer; packing paddle; 6-in. steel tape; hook; palm.

2.6 Packing Presses. Increased demands for space conservation in aircraft and aerospace systems using textile aerodynamic decelerators have led to

the development of pressure-packing techniques. The hydraulic press is the most common means of achieving reduction in the packed volume of textile aerodynamic decelerators. Fig. 10-4 shows one type of small hydraulic press now in use. A larger model, designed for a capacity of 100 tons, with 100 in. between vertical supports and 80 in. between horizontal beams, is also used for the pressure-packing of large canopies.

2.7 Sewing Machines. Machines suitable for parachute repair and production are covered in Federal Specification 00-S-256a, "Sewing Machines, Industrial Type for Textiles", and Federal Specification GG-S-225. There are many sewing machine attachments and accessories used to facilitate parachute production and repair, such as needle coolers and thread lubricants to reduce needle heat.

CHAPTER 11 DEPLOYABLE AERODYNAMIC DECELERATOR TESTING

Table of Contents

<i>Section</i>	<i>Page</i>
1 TEST METHODS	446
1.1 Introduction	446
1.2 Free Flight Testing (Non-Restraints)	450
1.2.1 Gravity Drop-Tests	452
1.2.2 Powered-Missile Tests	459
1.3 Captive or Tow Testing (Restraint)	463
1.3.1 Aircraft Tow	463
1.3.2 Rocket-Sled Tow	465
1.3.3 Water Tow	465
1.3.4 Wind-Tunnel Testing	471
1.3.5 Laboratory Testing	471
1.3.6 Landing-Condition Simulation	477
2 TEST-VEHICLES	478
2.1 Introduction	478
2.1.1 Gravity-Drop Test-Vehicles	478
2.1.2 Rocket-Boosted Free-Flight Test Vehicles	483
2.1.3 Rocket-Sled Test-Vehicles	488
3 TEST INSTRUMENTATION	490
3.1 Introduction	490
3.2 Sensing Elements (Transducers)	490
3.2.1 Measurement of Displacement and Position	490
3.2.2 Measurement of Strain	491
3.2.3 Measurement of Pressure	492
3.2.4 Measurement of Fluid Flow	492
3.2.5 Criteria for Transducer Selection	492
3.3 Self-Contained Recording Instruments (Drop Test)	492
3.3.1 Measurement and Recording of Direct Forces	492
3.3.2 Measurement and Recording of Gravitational Forces	495
3.4 Recording-Instrument Systems (Drop Test)	496
3.4.1 Magnetic-Tape Data Recording Systems	496
3.4.2 Telemetry Systems	497
References	499

Illustrations

<i>Number</i>		<i>Page</i>
11-1	Altitude vs Mach Number Regimes for Deployable Aerodynamic Decelerator Applications	449
11-2	Joint Parachute Test Facility, Auxiliary Landing Field, El Centro, California	453
11-3	White Sands Missile Range, New Mexico	456
11-4	Air Proving Ground Center Missile Range, Florida	457
11-5	Drop Test in Large Airship Dock	458
11-6	Aircraft Drop Test	458
11-7	Helium-Filled Balloon Used as Launch Platform	459
11-8	Generalized Carrier Balloon Performance Chart	460
11-9	Parachute Whirl Tower Test Facility	460
11-10	Nacelle with Provisions for 230-lb Dummy	461
11-11	General Purpose Test Vehicle for Test Loads from 200 to 500-lb	461
11-12	Skokie Aircraft Drop, Powered	462
11-13	Cree Cluster Aircraft Drop, Powered	462
11-14	Cree Ground Launch	463
11-15	General Performance Capabilities for Aerodynamic Decelerator Tests for Various Solid Fuel Rocket Booster Combinations (Ground Launch)	464
11-16	B-66 Taxi Testing	465
11-17	B-47 Inflight Testing	465
11-18	LOX/Alcohol Sled with Parachute	466
11-19	Tomahawk Sled with Parachute	467
11-20	Water Flow Channel	468
11-21	Water Tow Channel	469
11-22	Schematic Diagram of Impact Testing Machine	476
11-23	Inclined Test Facility	477
11-24	Weight Bomb Test Vehicle	478
11-25	Cylindrical Test Vehicle	483
11-26	Transonic Vehicle, Type III	484
11-27	Rocket Boosted Bomb	484
11-28	Cree Cluster at Separation	485
11-29	Supersonic Vehicle, Type II	486
11-30	Supersonic Vehicle, Type III	487

Illustrations (Cont'd)

Number		Page
11-31	Tomahawk Sled Test Vehicle	488
11-32	Mach 3 Sled Test Vehicle	489
11-33	Liquid Fuel Rocket Propelled Sled Test-Vehicle	489
11-34	Embossing Stylus Tensiometer	493
11-35	Photographic Type Tensiometer	494

Tables

11-1	Test Conditions and Applicable Test Methods	447
11-2	Characteristics of Various Aerodynamic-Decelerator Test Methods	450
11-3	Aerodynamic Decelerator Test-Site Characteristics	454
11-4	Shallow Water Surface-Wave Analogy	470
11-5	Wind Tunnel Test Facilities Which Have Been Utilized for Testing of Deployable Aerodynamic Decelerators	472
11-6	Recovery Systems Test Vehicle Chart	479
11-7	Performance Regimes, Cree Missile	485
11-8	Desired Test Capability Requirements	488
11-9	Nomenclature for Transducers	491
11-10	Subcarrier Bands for Selected Measurements	498

CHAPTER 11

DEPLOYABLE AERODYNAMIC DECELERATOR TESTING

Deployable aerodynamic decelerators of various types are being employed or are being considered for a multitude of applications. In order to be effective, particular types of aerodynamic decelerators have to operate efficiently in specific portions of the flight spectrum. Sufficient basic technical data concerning the particular type of aerodynamic decelerator must be known upon which to base its design, and to predict its performance.

Since valid scaling and model laws for aerodynamic-decelerator design and performance have as yet not been developed, the aerodynamic decelerator must be tested under closely simulated operational and environmental conditions to verify its performance characteristics, and to obtain a degree of confidence in its functional reliability. This applies in particular to types of aerodynamic decelerators which are of other than standard design or which have to operate under high speed, extremely low or high dynamic pressures, or under environmental conditions not normally encountered during operation of standard aerodynamic decelerators.

It has become increasingly evident that not only the availability of reliable and accurate testing methods and testing equipment is a necessity during the exploratory and experimental research-and-development phases, but also that economic aspects and the close simulation of environmental and operational conditions must be seriously considered in the choice of a test method and equipment. While aerodynamic-decelerator performance-trends in relation to design parameters may be obtained during wind-tunnel test programs, and design and performance characteristics of the aerodynamic decelerator may be verified by means of other existing test methods that use available test equipment and commercially available instrumentation, actual systems-testing should be done with the actual or closely simulated flight-vehicle. This is advisable since the dynamic and wake characteristics of the flight vehicle tend to influence, and sometimes lower, the performance characteristics of deployable aerodynamic decelerators as compared to those in undisturbed flow.

Test methods, test equipment, and instrumentation developed, or which have become available, during the last decade have been prime factors in establishing the design and performance characteristics of textile parachutes for a variety of applications. These same methods and test equipment, perhaps with minor modifications, will undoubtedly play a major part in the search for new concepts and the development of other types of aerodynamic decelerators. It has been shown that the use of proper test methods and equipment makes possible the quick comparison and evaluation of new concepts, establishment of performance and design trends, fast development and evaluation of new developments, the most expeditious correction of design deficiencies, and the economical transition to the stage of actual application.

In the following sections, experimental methods for aerodynamic-decelerator testing, experimental vehicles for aerodynamic-decelerator testing and specialized instruments and systems for aerodynamic decelerator performance data acquisition are described. This description presents a comprehensive picture of available and proven experimental methods and equipment for testing and their specific capabilities, characteristics, and limitations.

SEC. 1 TEST METHODS

1.1 Introduction. In recent years the use of

deployable aerodynamic decelerators has extended into many new areas other than the prime purpose of the conventional textile parachute: that of providing a means of escape from airborne vehicles under either

premeditated or emergency conditions. While the conventional textile parachute is still used for this purpose, the field of use for deployable aerodynamic decelerators has continuously expanded and other types of aerodynamic decelerators have come into being. In addition, the environment in which some decelerators are required to function has become increasingly severe. Fig. 11-1 presents an overall picture of the regimes of velocity, altitude, and dynamic pressure in which deployable aerodynamic decelerators will be required to operate. Table 11-1 lists the test methods which are available for aerodynamic decelerator testing in specific altitude-velocity regimes to determine the comparative performance characteristics of an aerodynamic deceleration device as its design parameters are varied.

The experimental testing methods for deployable aerodynamic decelerators which are available can be divided into the following categories:

(I) *Free-flight testing (non-restraint):*

- (1) Gravity drop-tests:
 - (a) In enclosed shelters;

- (b) From aircraft;
- (c) From stratospheric-altitude balloons;
- (d) From parachute whirl-tower;
- (2) Powered-missile tests:
 - (a) Aircraft-launched;
 - (b) Balloon-launched;
 - (c) Ground-launched;

(II) *Captive or tow testing (restraint):*

- (1) Aircraft tow:
 - (a) Inflight;
 - (b) Runway taxi;
- (2) Rocket-aid tow
- (3) Water tow:
 - (a) Shallow water;
 - (b) Deep water;

(III) *Wind-tunnel testing (restraint);*

(IV) *Laboratory testing;*

(V) *Simulated landing-condition testing.*

Aside from the testing of a model, or in some cases, of a full-scale canopy in wind tunnels, the majority of exploratory or experimental test programs of de-

TABLE 11-1 TEST CONDITIONS AND APPLICABLE TEST METHODS

(X indicates complete capability; N/A means Not Applicable)

FREE-FLIGHT TESTING									CAPTIVE OR TOW TESTING
Mach No.	Altitude, 10 ³ ft	Gravity Drop				Powered Missile			Aircraft Tow
		Shelter Drop	Acft Drop	Balloon Drop	Whirl-Tower Drop	Acft Launch	Balloon Launch	Ground Launch	Inflight Tow
0-1.0	Under 10	Models Low Sub- sonic	X	N/A*	0.6 max (sea-level density)	N/A	N/A	N/A	0.8 max
	10-50	—	X	X	—	X	X	X	X
	50-100	—	—	X	—	X	X	X	—
	100-250	—	—	—	—	—	X	X	—
1.0-5.0	Under 10	—	2.0 max	Trans	—	3.0 max	Limited Cap.	3.0 max	—
	10-50	—	2.0 max	Trans	—	3.0 max	X	X	—
	50-100	—	2.0 max	Trans	—	Limited Cap.	Limited Cap.	X	—
	100-250	—	—	—	—	—	Limited Cap.	X	—
Above 5.0	50-100	—	—	—	—	—	Limited Cap.	X	—
	100-250	—	—	—	—	—	Limited	X	—

TABLE 11-1 (Cont'd)
CAPTIVE OR TOW TESTING

Mach No.	Simulated Altitude 10 ³ ft	Aircraft Tow Runway Taxi	Rocket Sled Tow	Water Tow		Wind Tunnel Test
				Shallow	Deep	
0-1.0	Under 10	0.2 max	X	2-Dim. Models	0.8 max	X
	10-50	—	—	—	—	X
	50-100	—	—	—	—	Limited Cap.
	150-250	—	—	—	—	—
1.0-5.0	Under 10	—	3.0 max	2-Dim. 2.0 max	—	X
	10-50	—	—	—	—	Limited Cap.
	50-100	—	—	—	—	X
	100-250	—	—	—	—	Limited Cap.
Above 5.0	50-100	—	—	—	—	X
	100-250	—	—	—	—	X

Numbers in the table, other than those indicated as meaning altitude or dimension, are Mach numbers.

Complete Capability — All Mach number—altitude combinations can be obtained;

Limited Capability — The majority of the Mach number—altitude combinations can generally be obtained;

Trans — Maximum Limitations: transonic Mach numbers.

* Not generally used in this altitude range.

ployable aerodynamic decelerators, in particular those with textile canopies, have been and are being conducted under free-flight conditions utilizing various types of aircraft from which the load with the attached parachute is ejected. Although this method does provide for the testing of deployable aerodynamic decelerators under actual operational and environmental conditions, the accomplishment of repeated tests under identical conditions is difficult and sometimes impossible. In addition, aerodynamic-decelerator testing by means of the aircraft gravity-drop test is limited by the speed and altitude ceilings of current aircraft available. Naturally, comparative and specific performance data on various types of deployable aerodynamic decelerators have been and are being obtained in wind tunnels under controlled conditions and with great accuracy and reasonable economy. These tests, however, are generally performed on scale models and under infinite-mass operating conditions. Although it is recognized that testing with scale-model aerodynamic decelerators provides a relatively inexpensive means of obtaining performance data, primarily, trends are established in aerodynamic

decelerator performance with changing design parameters.

Determination of decelerator performance under desired values of Reynolds number is sometimes difficult to achieve in a wind tunnel or during scale-model drop testing; the aerodynamic coefficients measured, in particular the drag coefficient, will generally not be of the same value as those of their full-scale counterparts. However, any change in aerodynamic decelerator design which shows a drag-coefficient change during scale-model testing will generally achieve a change in the same direction on a larger-scale device that is so modified. The same holds true for design changes affecting stability and, to a certain degree, opening-characteristics.

Results obtained during tests performed under infinite-mass operating conditions cannot, in general, be directly transferred to aerodynamic-decelerator operations under finite-mass operating conditions, or to operations with deceleration devices of significantly different scale or under appreciably different velocity and air-density conditions. For this reason, a variety of methods for testing deployable aerodyna-

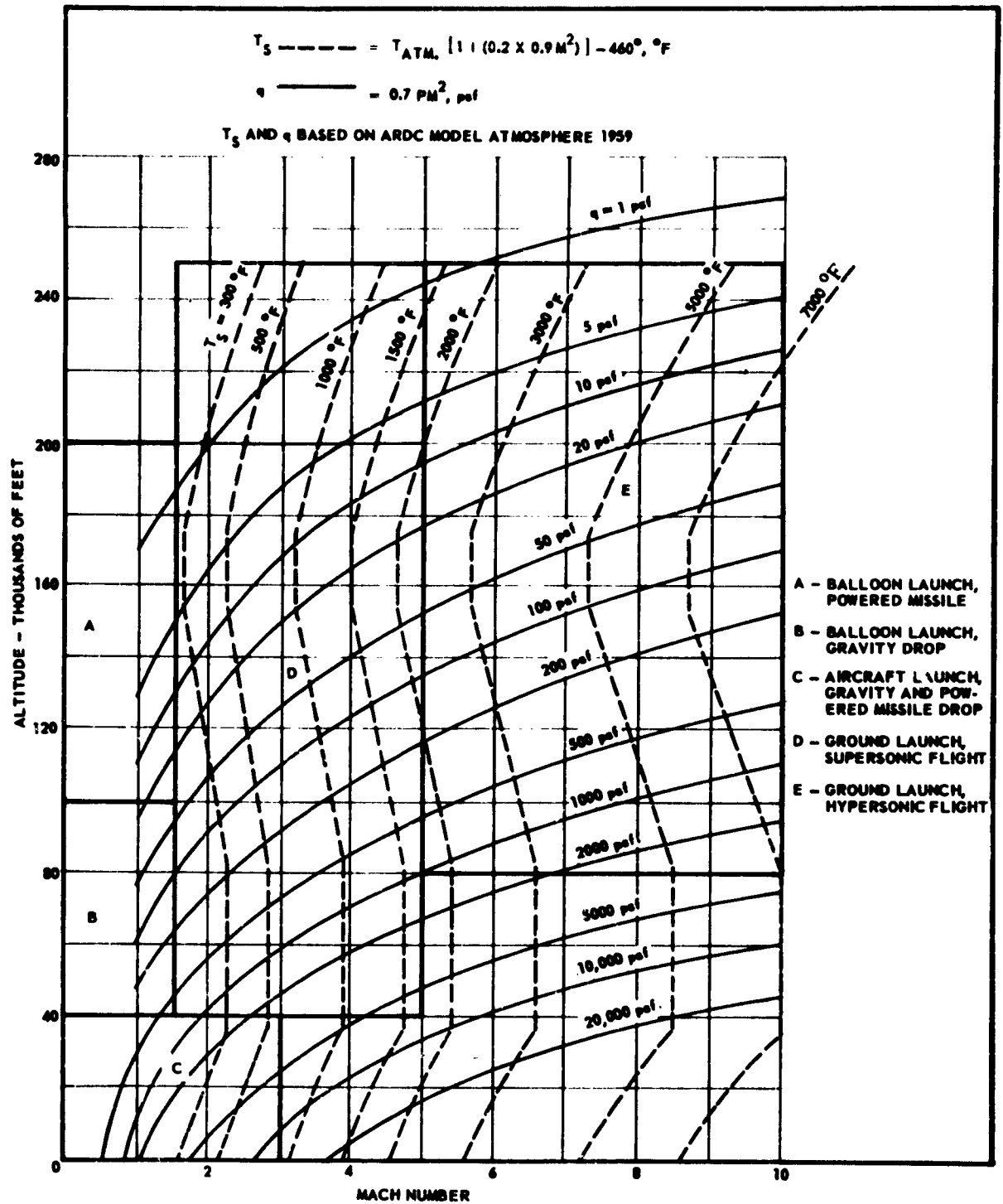


Fig. 11-1 Altitude vs Mach Number Regimes for Deployable Aerodynamic Decelerator Applications

mic decelerators have been made available.

Each of these test methods has its own particular advantages and disadvantages. Ability to perform tests under controlled conditions, availability and accuracy of test data, economics of testing, and achievement of specific operational and environmental conditions are among the factors governing the selection and choice of a particular test method. In some instances, the only worthwhile testing will be by means of actual free-flight tests. In other instances, utilization of other types of test methods will produce substantial savings in cost, much more rapid testing, more precise control of desired test-conditions, and more accurate and complete acquisition of performance data.

Some of the limitations of various methods for testing aerodynamic decelerators are compiled in Table

11-2, based upon experience gained during exploratory and experimental parachute test-programs.

1.2 Free-Flight Testing (Non-Restraint). The area of free-flight testing of deployable aerodynamic decelerators can be divided into two general categories: (1) gravity drop-tests, in which the payload or test vehicle with its packed and attached test-item is released from a stationary or moving platform and free-falls under the influence of gravity until the desired test speed or altitude is reached, at which point the test item is deployed for performance evaluation; and (2) powered-missile tests, in which the test vehicle with its packed and attached test item is launched from the ground or from a stationary or moving aerial platform and boosted by suitable rocket engines to desired speeds and altitudes, at which time the test item is deployed for subsequent free-flight evaluation.

TABLE 11-2 CHARACTERISTICS OF VARIOUS AERODYNAMIC-DECELERATOR TEST METHODS

Test Method		Advantages	Disadvantages
Free-Flight Test (Non-Restraint)	Gravity Drop	<ul style="list-style-type: none"> (1) Achievement of full range of test conditions possible (2) Dynamic simulation of vehicle effects during test-item deployment and operation (3) Absence of restraint on the motion of the test item. (4) Actual simulation of complete system performance. 	<ul style="list-style-type: none"> (1) Recovery of vehicle must be provided to allow inspection of test item. (2) In general, control and measurements of test conditions as well as observation of the dynamics of test item operation are difficult.
	Whirl Tower	<ul style="list-style-type: none"> (1) Low cost of testing. (2) Rapid test-programming and conductance. (3) Good control of test conditions. (4) Close duplication of test conditions. 	<ul style="list-style-type: none"> (1) Limited test velocities. (2) Limited to ground-level air density. (3) Limited size and weight of test item and payload. (4) Evaluation of final (terminal) descent not possible.
	Powered Missile	<ul style="list-style-type: none"> (1) Achievement of full range of test conditions possible (2) Dynamic simulation of vehicle effects during test-item deployment and operation (3) Absence of restraint on the motion of the test item. (4) Actual simulation of complete system performance. 	<ul style="list-style-type: none"> (1) Complexity of test equipment and relatively high cost of test.

TABLE 11-2 (Cont'd)

Captive Test (Restraint)	Test Method	Advantages	Disadvantages
	Aircraft Tow	(1) Extreme accuracy in control of initial test conditions. (2) Recoverable and reusable test-vehicle. (3) Measurements of maximum precision.	(1) Testing is under infinite-mass operating conditions. (2) Limited freedom of motion during tests.
	Rocket Sled	(1) Testing of relatively large-test-items. (2) Deceleration of vehicle-decelerator system can be realized. (3) High dynamic pressures permitting tests which can establish structural safety factors. (4) Reduced problems associated with flow-field interference.	(1) Testing limited to ground-level air density. (2) Test duration short (limited by track length). (3) Primary body symmetric in no more than two dimensions. (4) High propulsion costs associated with testing at extreme test conditions.
	Wind Tunnel	(1) High frequency of testing. (2) Determination of flow & shock (3) Measurement with maximum precision.	(1) Limited range of dynamic pressures. (2) Limited model size. (3) Uncertain effects of wall interference.
	Water Tow	(1) High frequency of testing. (2) Low cost of testing. (3) Study of internal aerodynamics possible. (4) High dynamic pressures permit tests which can establish structural safety factors.	(1) Limitation in test velocities: (a) Two-dimensional models: limitation of analogy. (b) three-dimensional models: cavitation begins at approx. 0.8 Mach. (2) Difficult correlation of cloth permeability influences.

The greatest single advantage of the free-flight test method is the absence of any restraint (except atmospheric) on the motion of the aerodynamic decelerator-load system. This allows for the dynamic simulation of vehicle effects on the aerodynamic decelerator after deployment and the testing under changing dynamic conditions and changing air density. The full range of test conditions is achievable by this method and the actual simulation of complete system functions may be accomplished. Observation and measurements of system stability, flight trajectory, rate of descent, drift tendencies, and other

phenomena are also attainable during tests. There are, however, disadvantages to the free-flight test method. Among the major disadvantages are: (1) with the exception of gravity drop-tests in enclosed shelters and from the whirl tower, control and measurement of test conditions as well as observation of the motion of the test items are difficult; (2) the test vehicle must be recovered to perform first-hand inspection of the test article; and (3) the extreme complexity of test equipment and high costs of a test program especially for high-speed and high-altitude test programs is sometimes unavoidable.

In the selection of a suitable test-site or range, a number of factors must be taken into consideration. The most important of these are:

- (a) Range size;
- (b) Launch facilities;
- (c) Tracking capability and data gathering;
- (d) Retrieval;
- (e) Data processing; and
- (f) Availability.

General characteristics of sites at which the majority of free-flight testing of aerodynamic decelerators are currently being carried out are summarized in Table 11-3. General maps of these three test ranges are shown in Fig. 11-2, 11-3, and 11-4 (Ref (11-1)).

1.2.1 GRAVITY DROP-TESTS. Gravity drop-testing is generally limited to the subsonic-speed regime, although testing may be extended into the transonic—or even low supersonic speed regime by launching streamlined, unpowered, aerodynamically clean test-missiles from fighter-type aircraft or from high-altitude balloon-borne platforms.

1.2.1.1 Drop-Testing in Enclosed Shelters. Scale-model aerodynamic decelerator tests provide a relatively inexpensive means of determining trends in performance and design. This is particularly true if the testing can be done under precisely controlled conditions and free of random atmospheric influences. Such a test capability, which allows testing under finite-mass operating conditions, is provided in large enclosed shelters. Actually, scale-model parachute drop-test programs conducted in enclosed shelters such as airship docks (Fig. 11-5) and parachute drying towers have been the most productive as far as acquiring accurate quantitative data is concerned. Depending upon the size and height of the shelter, both scale-model and some full-scale canopies may be drop-tested. Such performance characteristics as drag coefficient, amplitude and frequency of load-parachute oscillation, drift rates, and comparative opening-time and opening-shock values can be accurately determined. Instrumentation requirements for this test method involve primarily photographic equipment; however, a simple force-measuring strain-gage type tensiometer with associated recording instrumentation will provide valuable additional data.

1.2.1.2 Drop-Testing from Aircraft. The most widely used method for the free-flight testing of deployable aerodynamic deceleration devices is undoubtedly that which utilizes cargo, bomber, or fighter aircraft as the launch platform for a gravity drop-test vehicle. In general, two types of tests are performed utilizing the aircraft drop-test method (Fig. 11-6): functional tests and performance tests. The purpose of the functional drop-test is to determine whether a specific

type of deployable aerodynamic decelerator or system will function as predicted when subjected to a known set of test conditions. This type of drop test is usually the simplest to conduct since it will require very little instrumentation in the test vehicle. The performance test is made for the purpose of evaluating the various aerodynamic, opening, and other performance characteristics of aerodynamic decelerators of various types or configurations and over a wide range of operating conditions.

Depending upon the weight and configuration of the test vehicle, gravity drop-testing of deployable aerodynamic deceleration devices may be conducted at speeds up to low supersonic, and at altitudes that can be attained by the particular test aircraft utilized.

Test-vehicle weights of up to 50,000 lb have been dropped from bomber aircraft, and cargo air-drop tests have been conducted with a total test-load weight of up to 35,000 lb extracted from cargo-type aircraft. Gravity drop-tests of deployable aerodynamic decelerators at low supersonic speeds can be accomplished by releasing or, preferably, ejecting an aerodynamically clean and stable test-vehicle from a wing pylon or ejector rack of fighter aircraft. Test-vehicle weights of up to 2,500 lb (on wing pylon) and 3,500 lb (on fuselage centerline) have been successfully dropped utilizing this method. Aerodynamic decelerator testing utilizing the gravity drop method from aircraft is being performed primarily at the Joint Parachute Test Facility, ALF, El Centro, Calif.

1.2.1.3 Drop-Testing from High-Altitude Carrier Balloons. For the purpose of testing and determining the performance characteristics of deployable aerodynamic decelerators at subsonic or transonic speeds and at altitudes above the ceiling altitude of conventional test aircraft, helium-filled high-altitude polyethylene balloons are widely used to provide a launch platform from which the test vehicle is released for a programmed descent (Fig. 11-7). Generalized load-carrying characteristics of high-altitude polyethylene carrier balloons are shown in Fig. 11-8. Test-item deployment in the subsonic-, transonic-, and low supersonic-speed regimes can be achieved. Attainable test-conditions are determined primarily by the drag characteristics of the test vehicle in conjunction with the vehicle free-fall distance. Vehicle-recovery parachutes in the deployed state should be incorporated into the balloon-load train to avoid loss of the test vehicle should the balloon burst during ascent. Balloon launches for the testing of deployable aerodynamic decelerators are generally performed at the Air Force Missile Development Center, Holloman Air Force Base, Alamogordo, N.M. (utilizing the White Sands Missile Range).

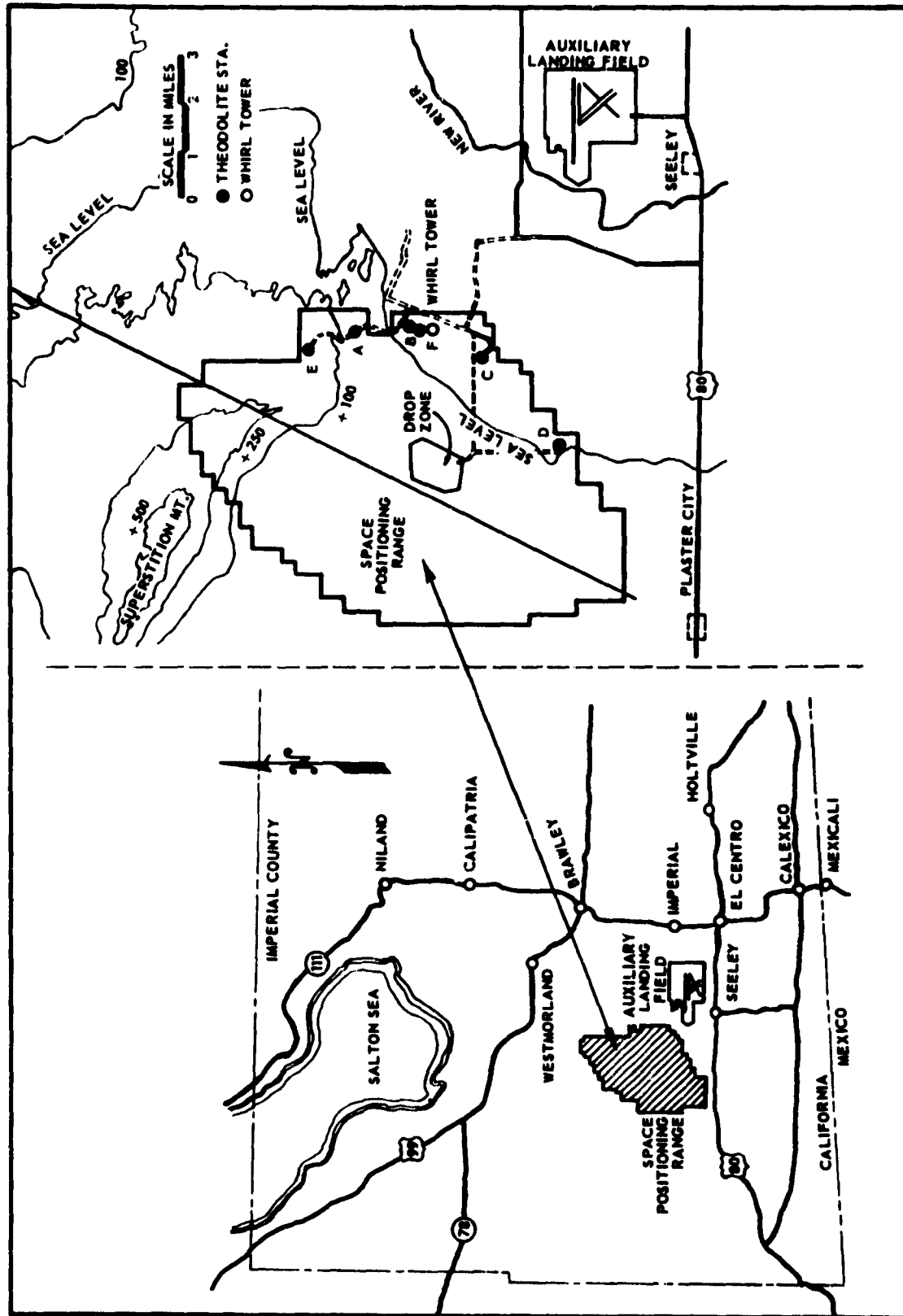


Fig. 11-2 Joint Parachute Test Facility, Auxiliary Landing Field, El Centro, California

TABLE 11-3 AERODYNAMIC-DECELERATOR TEST-SITE CHARACTERISTICS

Test Range	Useful Range	Launch Facilities	Tracking and Data Gathering
Air Proving Ground Center Eglin AFB, Florida	500 + mi long Azimuth 130° to 180° (Gulf of Mexico)	(1) Excellent ground handling equipment (2) Three useable launchers plus integrated blockhouse (3) Trained explosive-handling personnel (4) Limited assembly & storage areas	Optical and Photographic (1) Cinetheodolites (2) Tracking telescopes (3) Ballistic cameras Electronic (1) C & S band radars (2) Dovap (3) FM-FM telemetry
White Sands Missile Range Holloman AFB, New Mexico	100 mi long	(1) Six launch areas with total of 36 launch pads (2) Ground handling-equipment available (3) Well established explosives-handling techniques (4) Excellent work areas (5) Balloon launch facility	Optical and Photographic (1) 35, 70, 170 mm inter-motion ribbon frame & 35 mm rotating prism cameras (2) Cinetheodolite (3) Tracking telescopes (4) Ballistic cameras Electronic Radar, Dovap, Velocimeter, NOL, miss distance, FM-FM & PDM-FM telemetry
Joint Parachute Test Facility Auxiliary Landing Field, El Centro, California	3 ranges available. Largest 22 mi long x 10 mi wide	(1) Aircraft-launch facilities: fighter, bomber, cargo (2) Whirl-tower test facility (3) Ground handling-equipment available (4) Good work areas (5) No existing launchers or blockhouse (6) Limited experienced personnel for handling missiles and rockets	Optical and Photographic (1) Cameras (2) Cinetheodolite Electronic (1) Radar (2) FM-FM telemetry

TABLE 11-3 (Cont'd)

Retrieval	Data Processing	Remarks
(1) Trained boat crews, skin divers & boats available; Navy deep-sea divers also available (2) Normal support includes search aircraft with helicopters on hand (3) Search receivers on boat & aircraft	(1) All necessary facilities available; Good capability (2) Normal schedule 3-4 weeks	No destruct system required if safe impacts can be predicted to minimum of 3-sigma factors of safety. Maximum elevation angles 88° to 89°. Average yearly test cancellation 10%. Estimated test cancellation during hurricane season 30-35% (Aug-Oct). Peak work load June-Sept
(1) Ground vehicles, (cranes, etc.) (2) Search aircraft, and helicopters	(1) Excellent facilities (2) Efficient operation 7-1/2 day schedule	Destruct capability may be required on 3-stage vehicles; excellent weather conditions; excellent instrumentation calibration facilities
(1) Ground vehicles, cranes, etc. (2) Search aircraft, and helicopters	(1) Photo-processing (2) Limited data-reduction	Excellent year-round weather

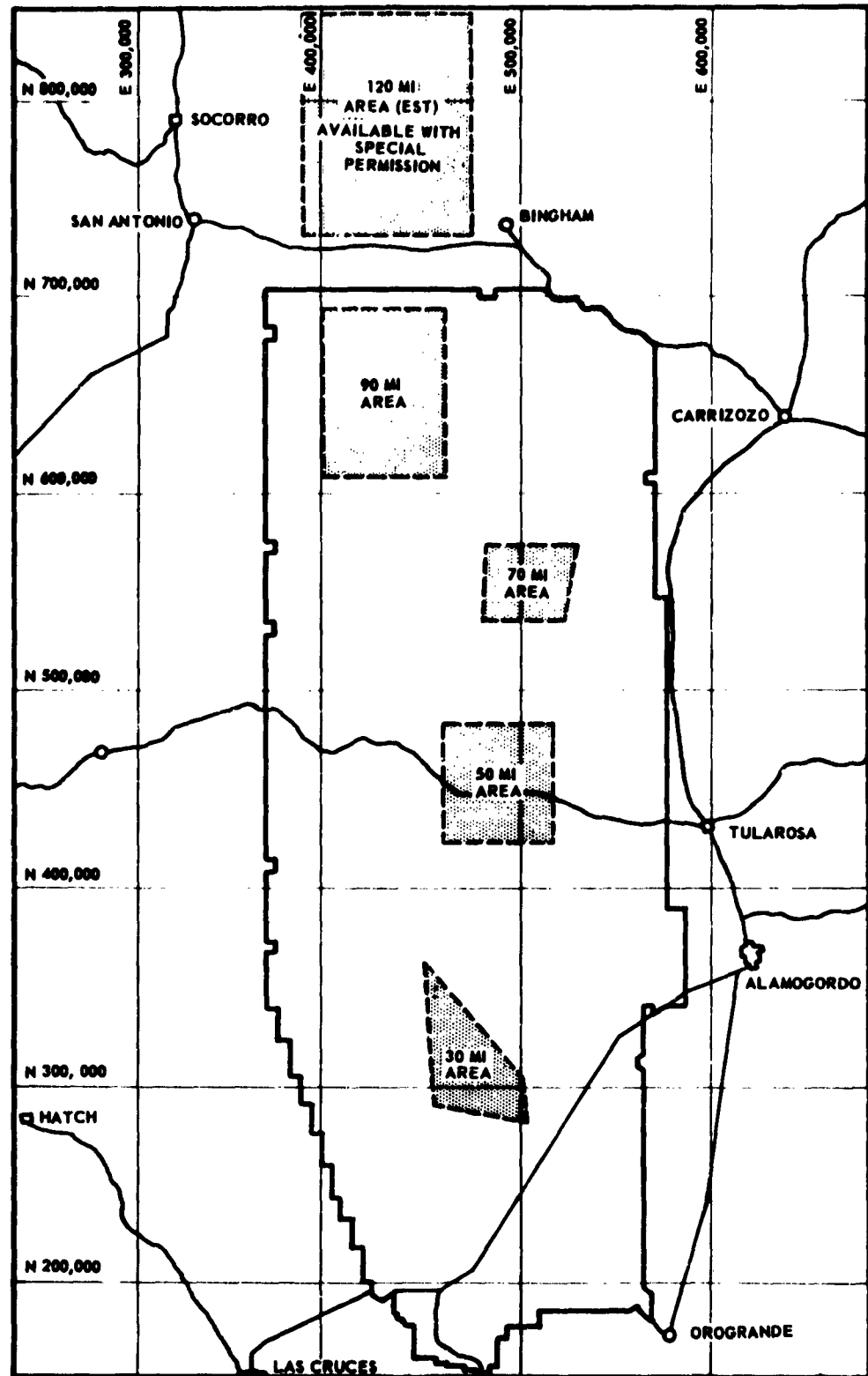


Fig. 11-3 White Sands Missile Range, New Mexico

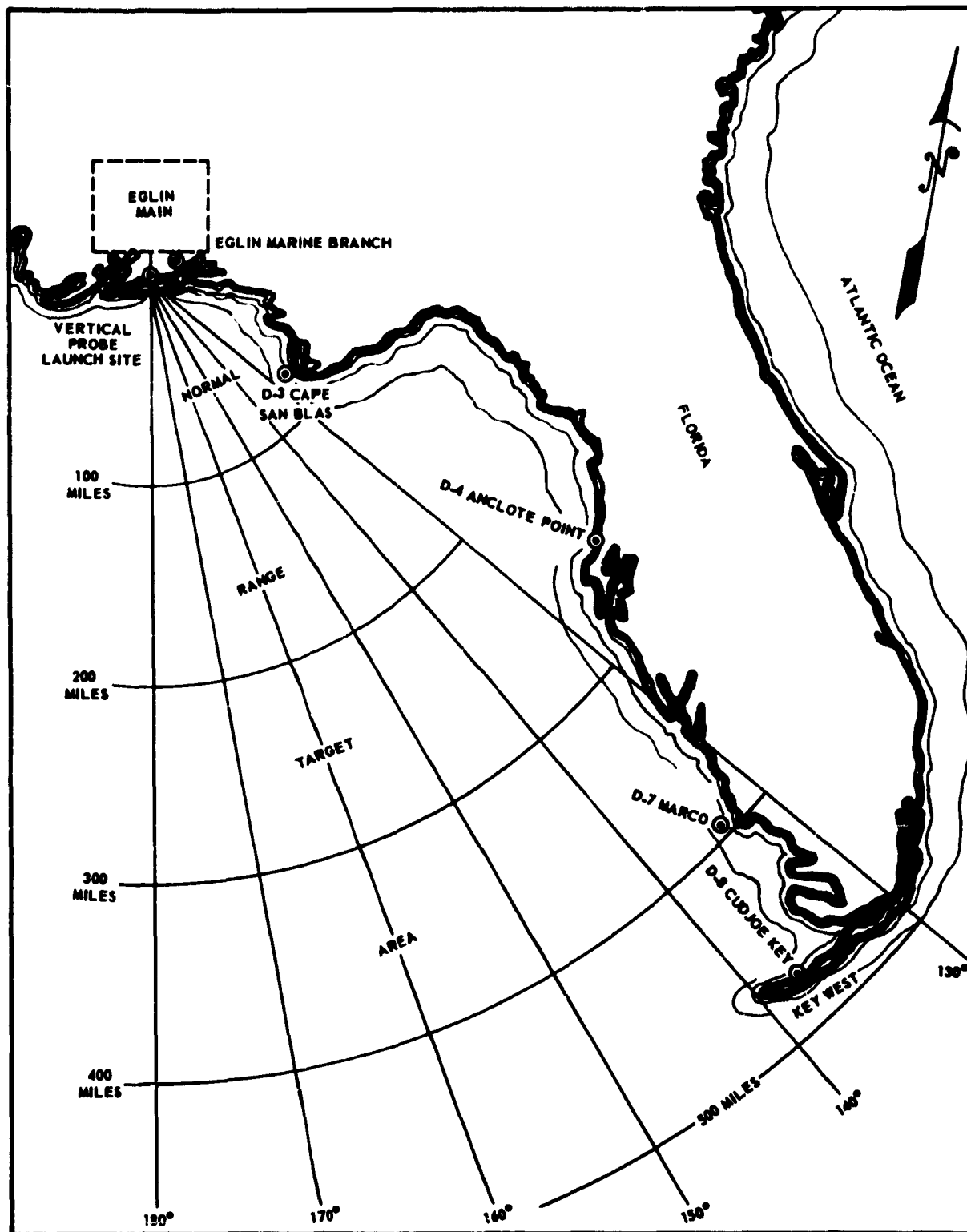


Fig. 11-4 Air Proving Ground Center Missile Range, Florida

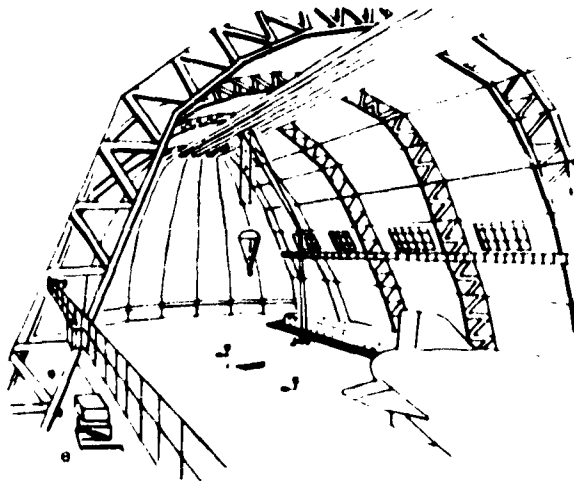


Fig. 11-5 Drop Test in Large Airship Dock

1.2.1.4 *Drop-Testing from Whirl Tower.* The problems of conducting and observing controlled experiments with large- or full-scale models under normal or near-normal operating conditions led to the development of the Parachute Whirl-Tower Test Facility (Fig. 11-9) located at the Joint Parachute Test Facility, ALE, El Centro, Calif. In addition to providing precise speed controls and predictable flight-path data, the whirl tower provides free-fall test data and evaluation of large-scale parachutes by permitting

release of the parachute-load system from all restraints during the test. This is made possible by mounting the test vehicle with a parachute pack on a release device inside a streamlined nacelle suspended from the whirling arm of the tower. Parachute deployment is effected immediately after release from the whirling nacelle by means of a short static-line. Since the action of centripetal force ceases at the instant of release, the free-flying parachute-load system follows a predetermined course similar to the trajectory encountered in normal drops from aircraft. The height of the release point generally is sufficient to enable the canopy to reach the stabilized, fully inflated condition of normal operation for a brief interval prior to touchdown of the suspended load. Because the flight trajectory is short and its direction reproducible within narrow limits, very complete fixed instrumentation coverage is possible.

Structurally, the parachute whirl-tower consists of a truncated steel tripod erected to support a vertical central drive-shaft. At a point 120 ft above the ground, a counterbalanced boom is secured to the central drive-shaft. From the arm of the boom, 56 ft outboard of the central drive shaft, a 114-ft flexible steel cable is suspended. The cable supports a streamlined missile which incorporates equipment to carry and release test vehicles and the parachutes to be tested. The whirl tower has a maximum working radius of 172 ft and is powered by a 2800-hp motor. Two test vehicles are presently in use for whirl-tower testing: (1) a nacelle with provisions for mounting a 230-lb

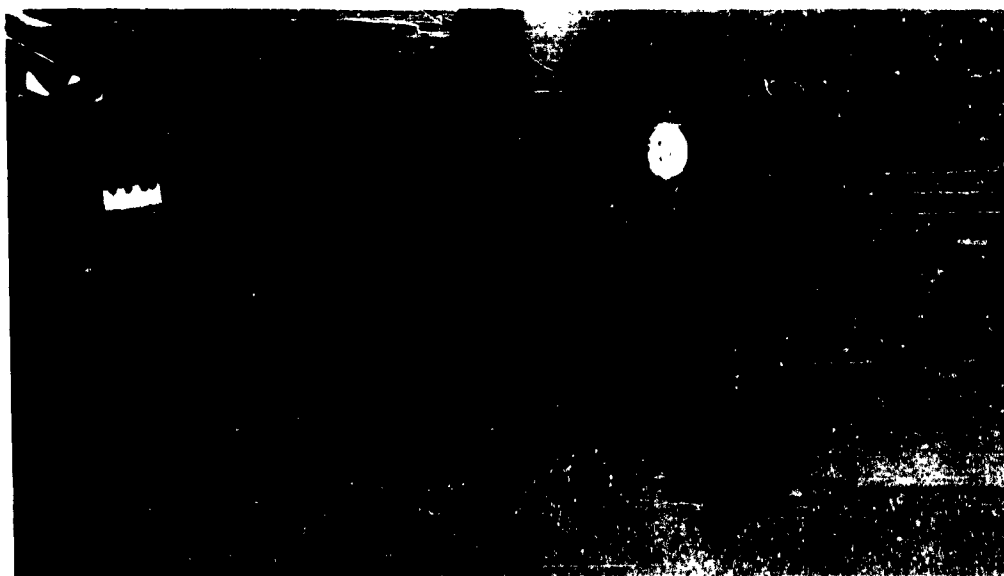


Fig. 11-6 Aircraft Drop Test

dummy (Fig. 11-10); and (2) a general-purpose test vehicle for test loads from 200 to 550 lb (Fig. 11-11).

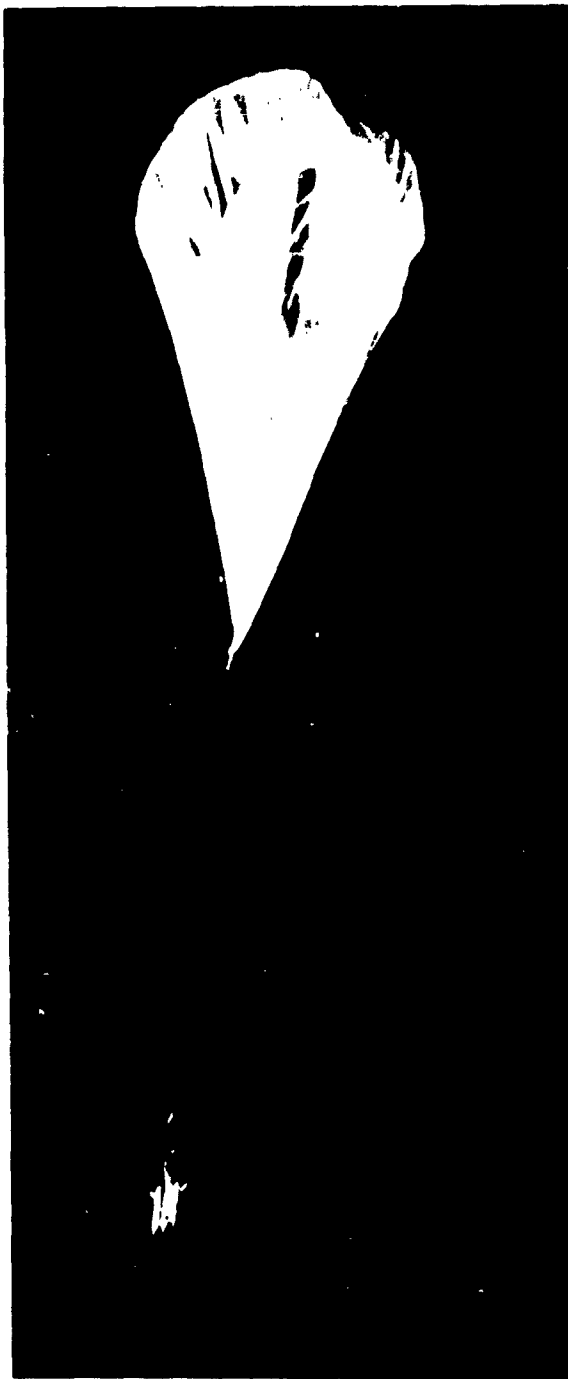


Fig. 11-7 Helium-filled Balloon Used as Launch Platform

In the nacelle tests, the dummy can be released from the nacelle at speeds up to 435 knots. The nacelle in this case provides a streamlined shape to support a stable, high-speed test run. In the use of the general-purpose test-vehicle, the test vehicle is released and serves as the streamlined missile as well as the test load. With the general-purpose test-vehicle, test speeds up to 400 knots have been attained. A compartment of 13 in. diameter and 30 in. length is available for stowage of the test item.

The types of tests which may be conducted on this test facility can be defined as:

(a) Reliability tests: the consistency and uniformity of deployment and opening processes over a large number of tests.

(b) Functional tests: general behavior during deployment and inflation

(c) Performance evaluation tests: the determination of characteristic performance data.

(d) Strength-evaluation tests: the evaluation of strength characteristics by means of destruction tests.

(e) Applied-research tests: validation testing in support of theoretical studies.

The whirl tower never can be adequate for a complete study of the behavior of a parachute or other aerodynamic decelerator, because the maximum drop-altitude is fixed at 120 ft by the tower's height. In its present state, the facility is not suitable for performance of tests that require deployment speeds above 435 knots, suspended-load weights of more than 500 lb, or canopies larger than 32 ft in diameter. It appears to be possible to undertake and accomplish a running average of six drop tests an hour. Obviously, this number will be reduced by occasional, normal delays, and also will be less for more complicated tests employing special instruments or unusual test procedures. Normal instrumentation at the site consists of telemetering systems or self-recording instruments installed in the test or suspended load, and of photographic instrumentation placed at strategic locations around the test facility.

Besides the evaluation of deployable aerodynamic decelerators of various types and designs, and for different applications, accessories such as harnesses, fittings, deployment bags, static lines, pilot chutes, extraction parachutes, and devices associated with decelerator deployment may be thoroughly tested. The behavior of parachutes in the reefed condition may also be observed and measured.

1.2.2 POWERED-MISSILE TESTS. The extension of deployable aerodynamic decelerator operation into supersonic speeds, and into high-altitude flight regimes, has required the development and acquisition of new decelerator test-methods. To achieve the de-

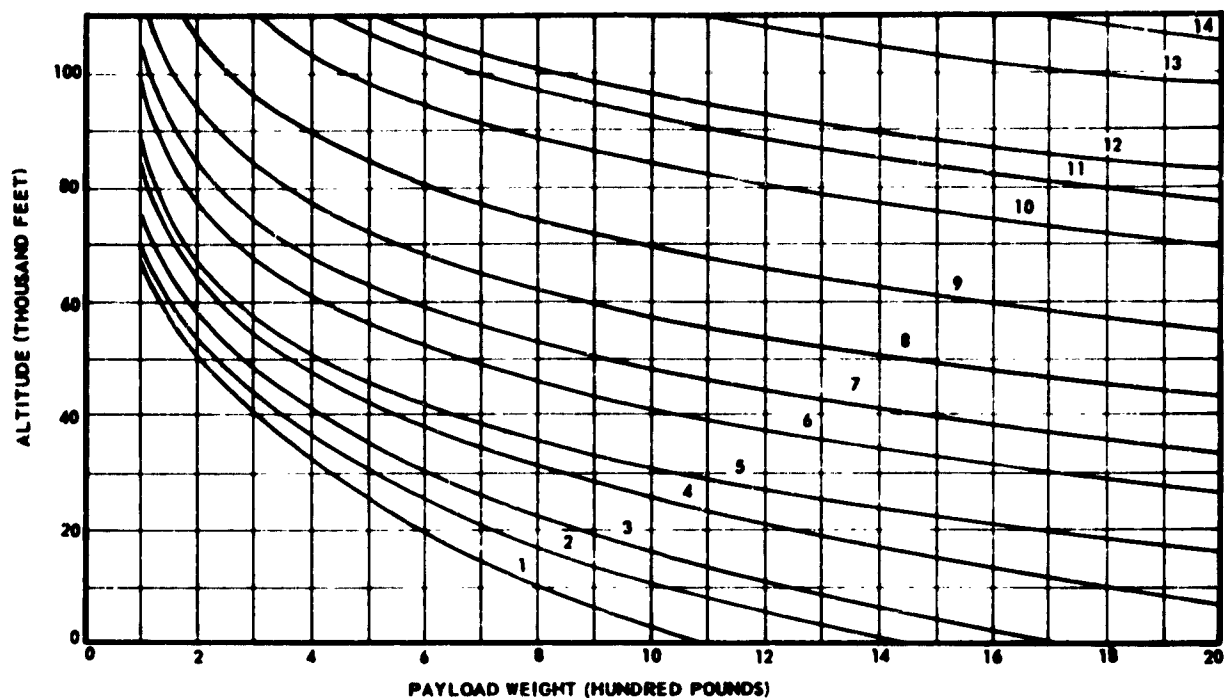


Fig. 11-8 Generalized Carrier Balloon Performance Chart

sired deployment conditions for the aerodynamic decelerators in terms of speed and altitude, solid-fuel rocket-boosted, low-drag test-vehicles are being employed. To obtain economy of test operations, test missiles are launched from aircraft, from stratospheric-altitude balloons, or from the ground, depending upon the particular test point to be achieved.

The use of powered free-flight test-vehicles has required increased data-acquisition, safety, recovery, and reliability over those used before. Basically, data-acquisition systems incorporated in powered free-flight test-vehicles consist of photographic subsystems to record dynamic phenomena during aerodynamic decelerator deployment, and operation, and electronic subsystems (usually telemetry links) to sense and transmit desired performance characteristics throughout the period of flight. Radar tracking beacons and booster or test-vehicle destruction systems are usually re-

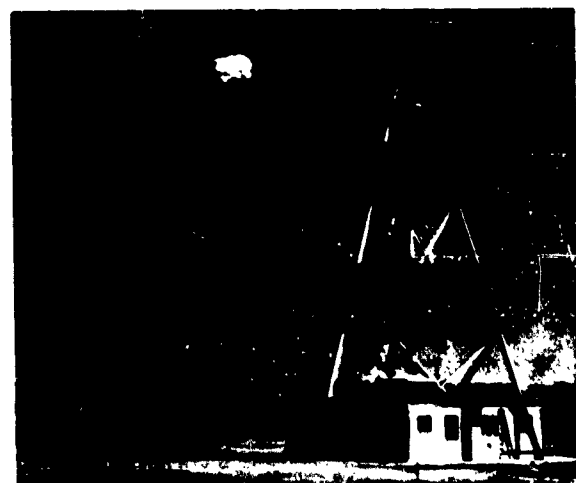


Fig. 11-9 Parachute Whirl-Tower Test Facility



Fig. 11-10 Nacelle with Provisions for 230-lb Dummy

quired by the test center.

1.2.2.1 Test-Missile Launch from Aircraft. To achieve supersonic test-points at altitudes below 40,000 ft, the launching of rocket-booster test-vehicles from fighter or bomber aircraft is most economical. Single (Fig. 11-12) and clustered (Fig. 11-13) aerodynamic decelerator test-missiles boosted by single, clustered, or staged solid-fuel rockets may be launched from aircraft. The solid-fuel rocket is usually ignited after a sufficiently long period of vehicle free-fall from the carrier aircraft to allow for sufficient escape-time of the launching aircraft for flight safety. In order to avoid accidental ignition of solid-fuel rockets or other pyrotechnic devices, it is the practice at some test centers to use squibs, ignitors, etc., which do not fire unless more than a one-watt and a one-ampere signal is applied, or which are shielded against electro-magnetic radiation.

1.2.2.2 Test-Missile Launch from High-Altitude Carrier Balloons. Powered test-missiles may be launched from platforms suspended from stratospheric-

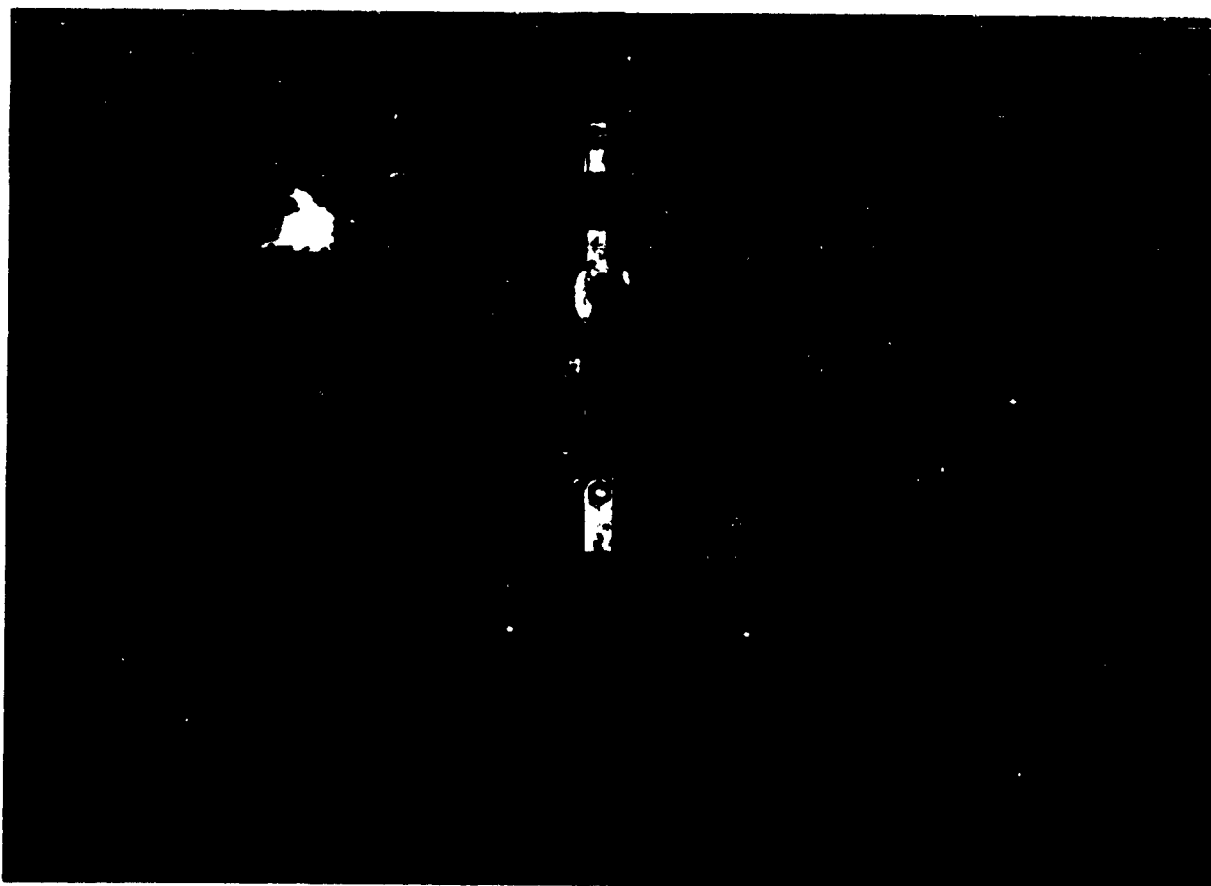


Fig. 11-11 General-Purpose Test Vehicle for Test Loads from 200 to 500-lb.



Fig. 11-12 Skokie Aircraft Drop, Powered

altitude balloons to achieve supersonic decelerator test-points at altitudes above those obtainable with aircraft launches. The choice of whether to launch from a balloon or from the ground to obtain a specified test-point is largely governed by the economic and safety aspects of each particular mission. Test missiles may be launched through the apex of the balloon or at an angle from the vertical, by-passing the carrier balloon. In the latter case, a capability for directional control of the test-missile launch at balloon floating-altitude will be required. This can be achieved by

means of "sun-seekers" coupled with pulse jets to rotate the balloon-missile system at floating altitude into the desired launch-direction. Generalized performance curves for stratospheric-altitude carrier balloons are shown in Fig. 11-8.

1.2.2.3 *Test-Missile Launch from Ground.* The most common method of launching powered missiles for an aerodynamic decelerator test is the ground-launch method (Fig. 11-14). Short rail-launchers guide the test vehicle during its initial period of acceleration.

Selection of the propulsion units and staging for

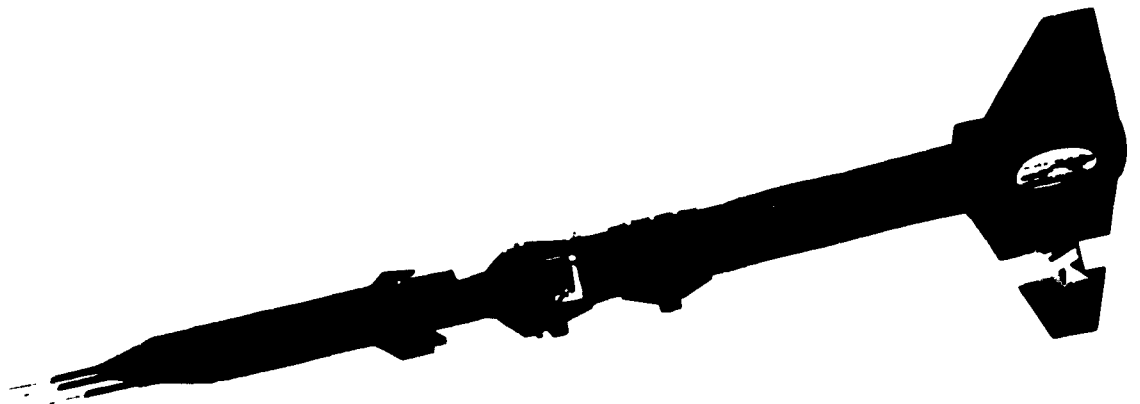


Fig. 11-13 Cree-Cluster Aircraft Drop, Powered



Fig. 11-14 Cree Ground Launch

launching of test vehicles must be predicated on an analysis of several considerations, among which are performance, range safety, aerodynamics, reliability, structure and thermal effects. The primary consideration in determining rocket-motor staging is reliability in attaining the desired velocity-altitude conditions in the test. Selection of the booster units for the various stages should include consideration of relative booster size to achieve near-optimum mass-ratios for the stages, efficiency, cost, reliability, and previous record of performance. Selection of the initial stage is also influenced by thermal and inertial loading considerations. To minimize aerodynamic heating and the g-load effects during boost, the initial stage should have a relatively long burning time. Generalized performance capabilities for test vehicles ($W = 250, 500$ and 800 lb) for aerodynamic decelerators for various solid-fuel rocket-booster combinations (Ref (11-1)) are shown in Fig. 11-15. The trajectories shown are not necessarily optimum from the standpoint of aerodynamic-heating and range considerations. This is especially true for the higher velocities. For such cases, the range and aerodynamic-heating considerations can have a strong influence on the design of the vehicle system, the initial launch-altitude of the vehicle, and staging operations.

1.3 Captive or Tow Testing (Restraint). In the area of captive or tow testing of deployable aerodynamic decelerators, four different test methods have been developed and are being utilized extensively:

(1) aircraft tow-tests, in which the aerodynamic decelerator is deployed behind the test aircraft either in free-flight or during the landing roll; (2) rocket-aided testing, in which the test vehicle is propelled by suitable rocket-propulsion units along a railed track and the aerodynamic decelerator deployed after a desired velocity has been reached; (3) water-tow testing in which two-dimensional or three-dimensional test models are towed in water or other similar fluids; and (4) wind-tunnel testing.

The advantages of captive or tow testing are the extreme accuracy in control of initial test-conditions, the highly accurate and precise measurement of performance parameters, the use of recoverable and reusable test-vehicles, and the high frequency of testing obtainable. In some cases, the cost of testing is significantly lower than that obtainable with other test methods. There are, however, disadvantages to captive or tow testing, the major ones being that in all cases the test item is restrained and only limited freedom of motion during test is obtained, and that all testing is conducted under infinite-mass operating conditions, meaning that the velocity decay during test-item inflation is extremely small.

1.3.1 AIRCRAFT TOW. Towing parachutes behind aircraft has proven to be a satisfactory method of testing, particularly if the parachute is intended to be used in aircraft inflight and landing deceleration. Since it is standard practice to equip jet fighters and bombers with deceleration parachutes, the parachute system designed for a particular aircraft should be tested behind that aircraft. By doing this, the performance characteristics of the parachute system can be accurately determined under actual operating conditions. This is especially valuable where wake effects are encountered.

1.3.1.1 Runway Tow. A B-66 taxi-test vehicle is being utilized at the Aeronautical Systems Division, W-P AFB, Ohio, to obtain performance data on various parachute designs and to evaluate the performance of parachute systems for aircraft landing deceleration (Fig. 11-16). Parachute deployment, drag, and to some extent, stability characteristics can be determined at speeds up to 130 knots on a 12,000 ft runway. Canopies of diameters up to 35 ft may be tested. Instrumentation to measure and record parachute forces, ground speed, and various other data on a common time-base is installed in the test vehicle.

1.3.1.2 Inflight Tow. To determine specific parachute performance characteristics at higher deployment speeds and higher altitudes, and to evaluate the performance of parachute systems for inflight applications, a B-47 aircraft has been used successfully as a test vehicle (Fig. 11-17.) Canopies with diameters up to

- (1) N-500 LB (TEST VEHICLE WEIGHT)
 (2) H.J.-500 LB, N-250 LB
 (3) N-N-800 LB
 (4) N-N-500 LB
 (5) G-G-G-800 LB
 (6) N-N-250 LB
 (7) G-G-250 LB
 (8) H.J.-N-800 LB
 (9) N-N-N-800 LB
 (10) G-G-G-500 LB, $T_w = 490$ F
 (11) N-N-N-500 LB
 (12) H.J.-N-500 LB
 (13) H.J.-N-N-800 LB
 (14) H.J.-N-250 LB
 (15) G-G-G-250 LB, N-N-N-250 LB
 (16) H.J.-N-N-900 LB, $T_w = 400$ F
 (17) T-N-G-800 LB
 (18) H.J.-G-250 LB
 (19) H.J.-N-L-800 LB
 (20) H.J.-N-N-250 LB, $T_w = 350$ F
 (21) H.J.-N-L-500 LB
 (22) X-800 LB
 (23) H.J.-N-G-250 LB
 (24) X-500 LB
 (25) H.J.-N-L-250 LB, $T_w = 330$ F
 (26) T-N-G-250 LB
 (27) T-N-L-250 LB
 (28) H.J.-L-L-250 LB, $T_w = 500$ F
 (29) X-C-C-250 LB
 (30) X-R-250 LB
 (31) T-N-800 LB
 (32) T-N-500 LB
 (33) T-N-250 LB

SYMBOL CODE

H.J. - HONEST JOHN ROCKET
 N - NIKE ROCKET
 L - LANCE ROCKET
 X - XM20 ROCKET
 T_w - WALL TEMPERATURE
 q - DYNAMIC PRESSURE psf
 C - CAJUN ROCKET
 T - TALOS ROCKET
 R - RECRUIT ROCKET
 G - GENIE ROCKET

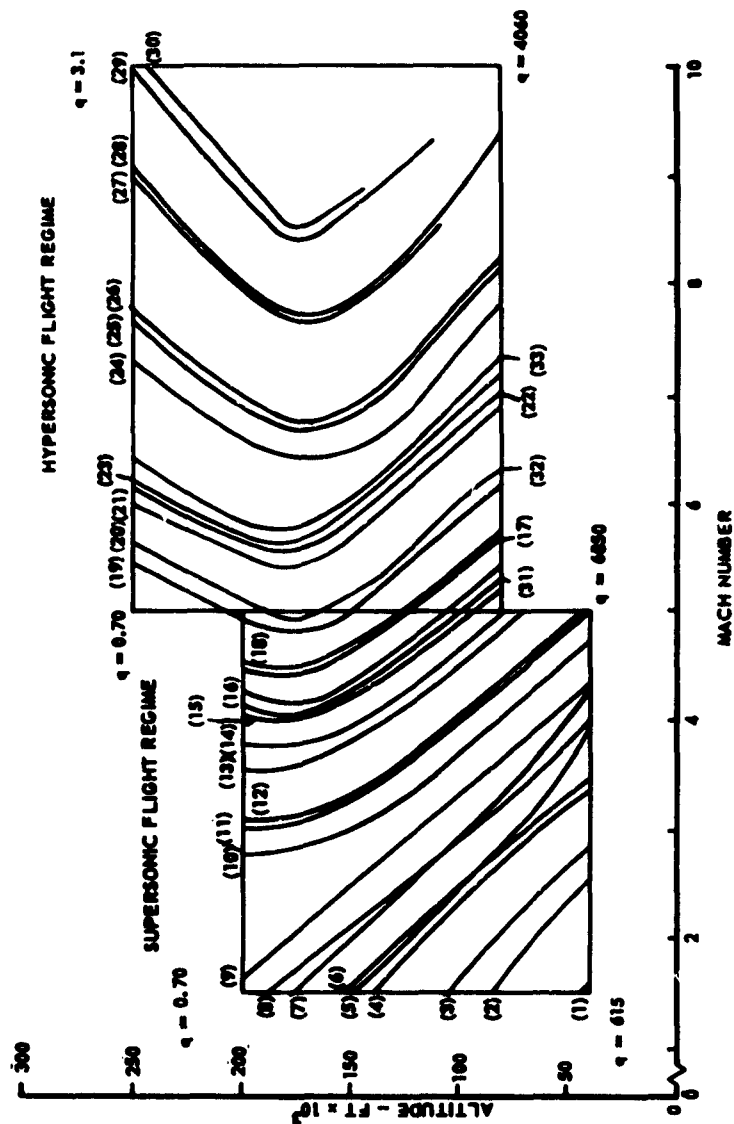


Fig. 11-15 General Performance Capabilities for Aerodynamic Decelerator Tests for Various Solid Fuel Rocket Booster Combinations (Ground Launch)

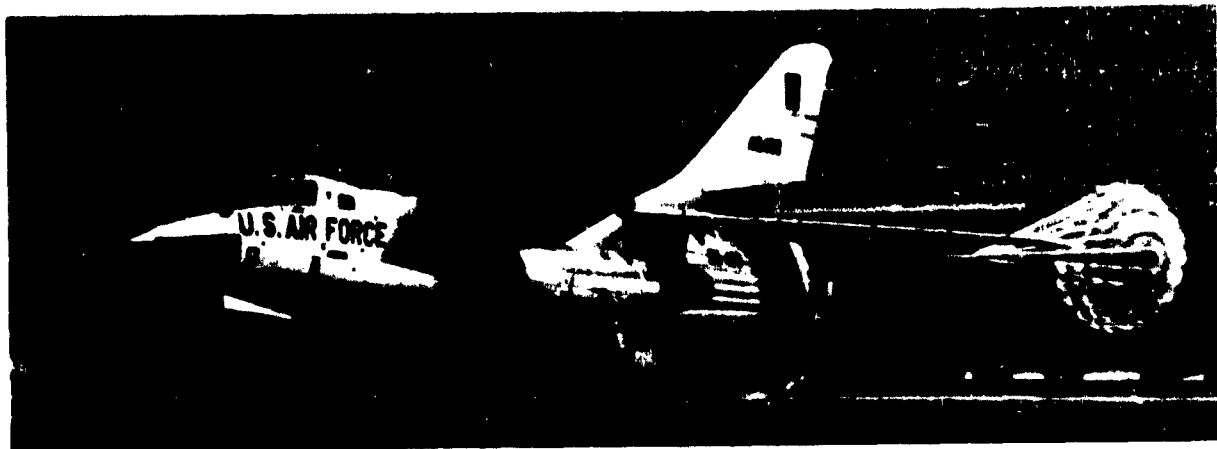


Fig. 11-16 B-66 Taxi-Testing

16 ft may be deployed at speeds of up to 195 knots without impairing the safety of flight. The B-47 aircraft is equipped with instrumentation to measure and record parachute forces, aircraft speed, and other operational data versus time.

1.3.2 ROCKET-SLED TOW. "Free-air" test facilities are being used successfully for determining deployment and aerodynamic characteristics as well as general performance characteristics of parachutes and other aerodynamic decelerator systems at subsonic, transonic, and supersonic speeds. Basically, a free-air test facility consists of a straight, precisely aligned, dual-rail track along which powered test sleds can move. The canopy or system to be tested initially is stowed on the test sled and remains attached after deployment (Fig. 11-18 and 11-19). The free-air test facilities have a number of advantages over other test methods, among which are most important (1) large-size models or even full-scale parachutes or other aerodynamic decelerators may be tested; thus, the effect of dimensional scale-factors need not be considered; (2) high dynamic pressures, which are

attainable, permit testing that can establish structural safety factors; and (3) problems associated with flow-field interference are reduced compared with other test methods. Disadvantages of this test method include the fact that testing is limited to one atmosphere density, and usable test-periods are of short duration since the test period is limited by the track length and by the length of time during which the sled can be maintained at required test velocities; also, propulsion costs may be high, especially for testing at higher velocities.

The free-air test facility currently used for testing deployable aerodynamic decelerators is located at and operated by the Air Force Missile Development Center, Holloman Air Force Base, N.M. The facility consists of dual-rail track 35,000 ft long, and is located at the edge of the White Sands Missile Range. The track uses two crane rails spaced 7 ft apart. The rail foundation is designed to resist vertical down loads of 70,000 lb per slipper, vertical up loads of 25,000 lb per slipper, and lateral loads of 40,000 lb per slipper on any two slippers. To decelerate and stop the test sled at the conclusion of the test run, a water trough 60 in. by 14 in. is located between the rails. For every 10 ft 10 in. interval, for the entire length of the track, there is a holding fixture into which a frangible dam can be inserted. This, together with a scoop or "water brake" mounted on the sled, can provide means for test-vehicle deceleration.

1.3.3 WATER TOW. A very inexpensive means of testing aerodynamic deceleration devices is available in the water-tow test method. This test is particularly well-suited for the study of the internal and external aerodynamic characteristics during supersonic operation of flexible aerodynamic deceleration



Fig. 11-17 B-47 Inflight-Testing

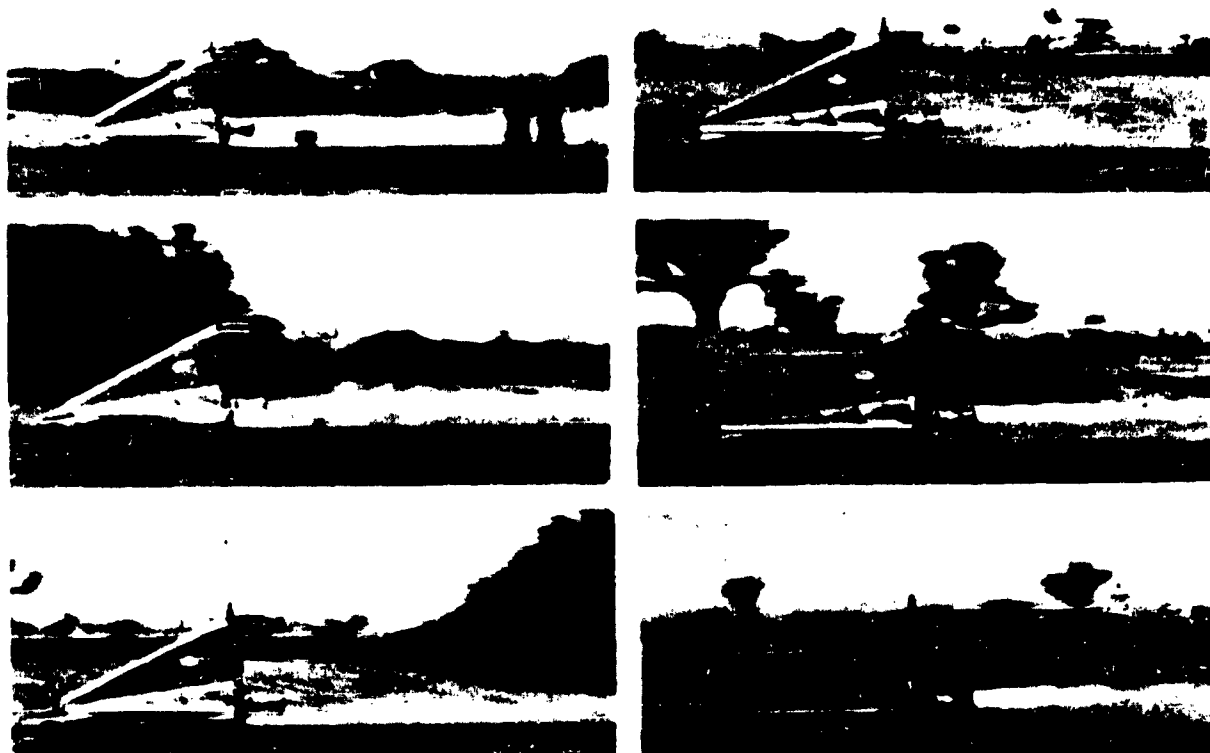


Fig. 11-18 LOX/Alcohol Sled with Parachute

devices and primary-secondary body combinations, as well as for the strength-testing of deceleration devices under high dynamic pressures. Naturally, there are limitations to this method of testing with respect to the velocity that can be simulated. For two-dimensional model testing, this limit is given by bounds of validity of the water surface-wave analogy, whereas for "deep-water" tow the limit is reached at an equivalent Mach number of 0.8, when cavitation around the test item usually develops.

1.3.3.1 Shallow-Water Test. The shallow-water test is especially advantageous in studying the external and internal aerodynamic characteristics of flexible aerodynamic decelerators and primary-secondary body combinations at supersonic speeds, employing the water surface-wave analogy. Two types of facilities are the most commonly employed. The first uses a fixed model with the water flowing past the model (water-flow channel, Fig. 11-20). Here, the velocity of fluid flow and depth of the fluid are controlled and maintained through a reservoir and sluice-gate arrangement and by changing the slope of the

table. The second is basically a trough containing fluid of a specified depth, through which a two-dimensional model is towed at constant velocity or at a velocity with predetermined variation (water-tow channel, Fig. 11-21). The analogy of the flow of a liquid with a free surface in a gravity field to the two-dimensional flow of a compressible gas has been known for some time (Ref (11-2), -3), -4), and -5)). The analogy explains the phenomena that occur when a body moves through a fluid with a free surface; that is, it predicts the "hydraulic jump" or standing wave that forms ahead of the moving body. In the case of a two-dimensional aerodynamic decelerator model, this wave is analogous to the wave visualized by Schlieren and Shadowgraph photographic methods on three-dimensional bodies in supersonic air-streams.

A summary of the water surface-wave analogy is presented in Table 11-4. As can be readily seen, there are limitations to the application of this analogy to model testing at simulated supersonic velocities. Some of these are: (1) the analogy applies to a hypothetical gas having $\gamma = 2.0$. Thus, changes in flow

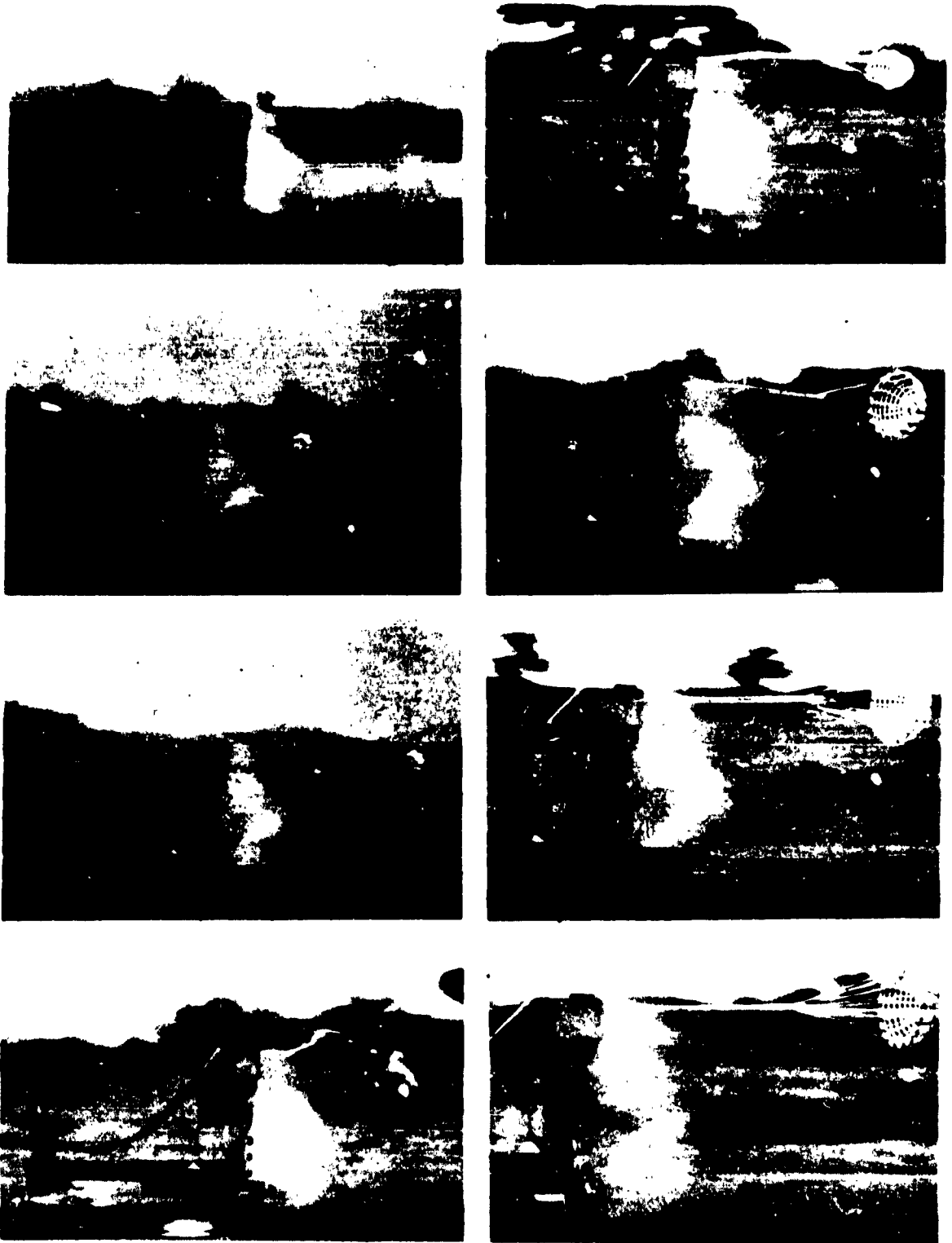


Fig. 11-19 Tomahawk Sled with Parachute

characteristics resulting from the difference between the actual and hypothetical values must be kept in mind; (2) since in the analogy the water depth represents the density, only two other dimensions remain for the geometric representation of the flow field; hence, only two-dimensional shapes or bodies can be geometrically represented; (3) the actual velocity of the wave propagation is not given exactly by the equation:

$$C = \sqrt{g \delta_w} \quad \text{or (Water Wave Velocity)}$$

$$= \sqrt{(\text{Force of Gravity} \times \text{Water Depth})},$$

as assumed, but more accurately by the equation

$$C = \frac{g\lambda}{2\pi} + \frac{2\pi\sigma}{\rho\lambda} \tanh \frac{2\pi\delta_w}{\lambda}$$

where

λ = Wavelength; and

σ = Surface tension.

After expanding the term for the hyperbolic tangent:

$$C = \sqrt{g\delta_w} \left[1 + \frac{4\pi^2\sigma}{g\rho\lambda^2} + \text{terms of } \frac{\delta_w^2}{\lambda^2} \right. \\ \left. \text{or higher} \right]^{1/2}$$

Thus, the actual velocity of wave propagation depends not only on the depth of the liquid, δ_w , but also on its surface tension, σ , and the wavelength, λ ; and (4) the disturbance wavelength in shallow water is

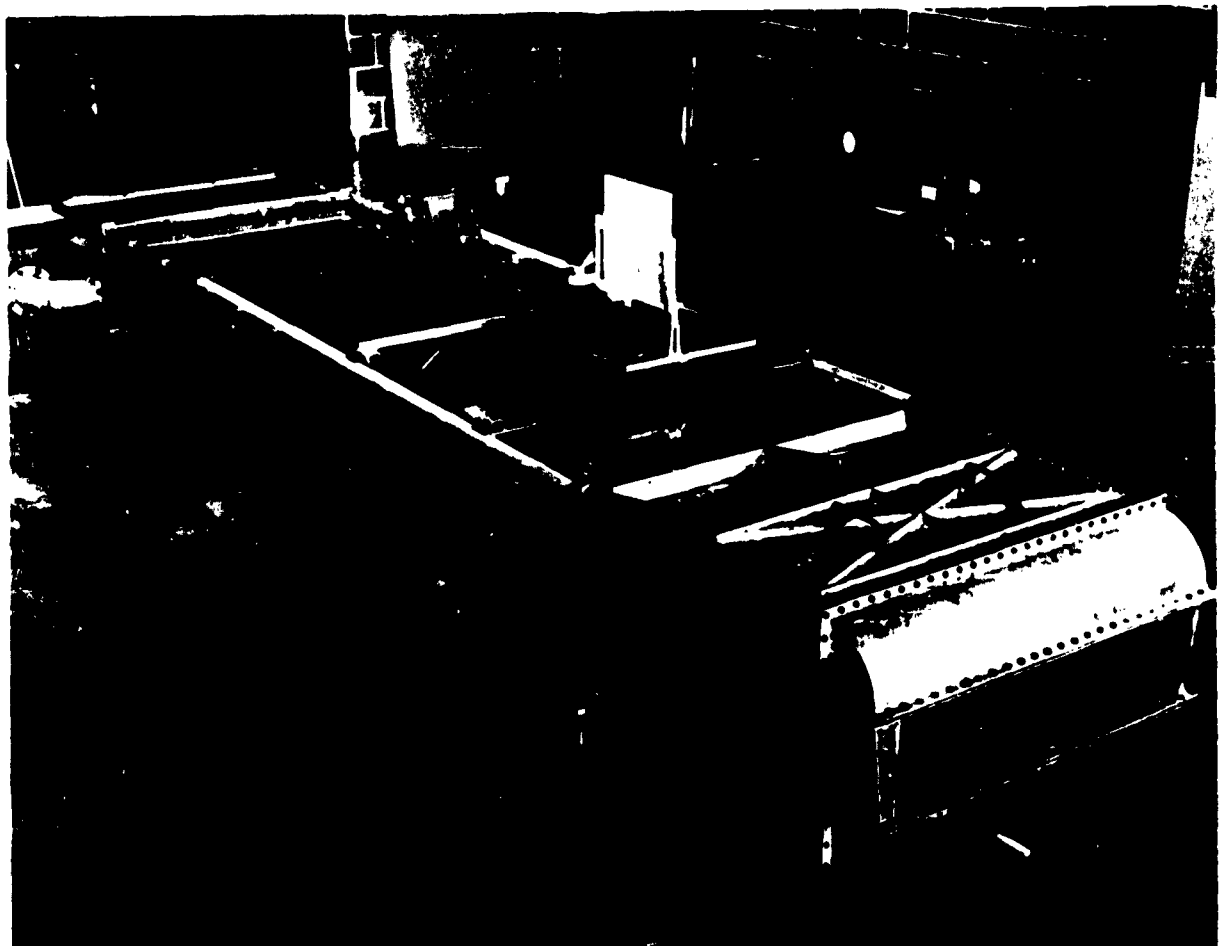


Fig. 11-20 Water Flow-Channel

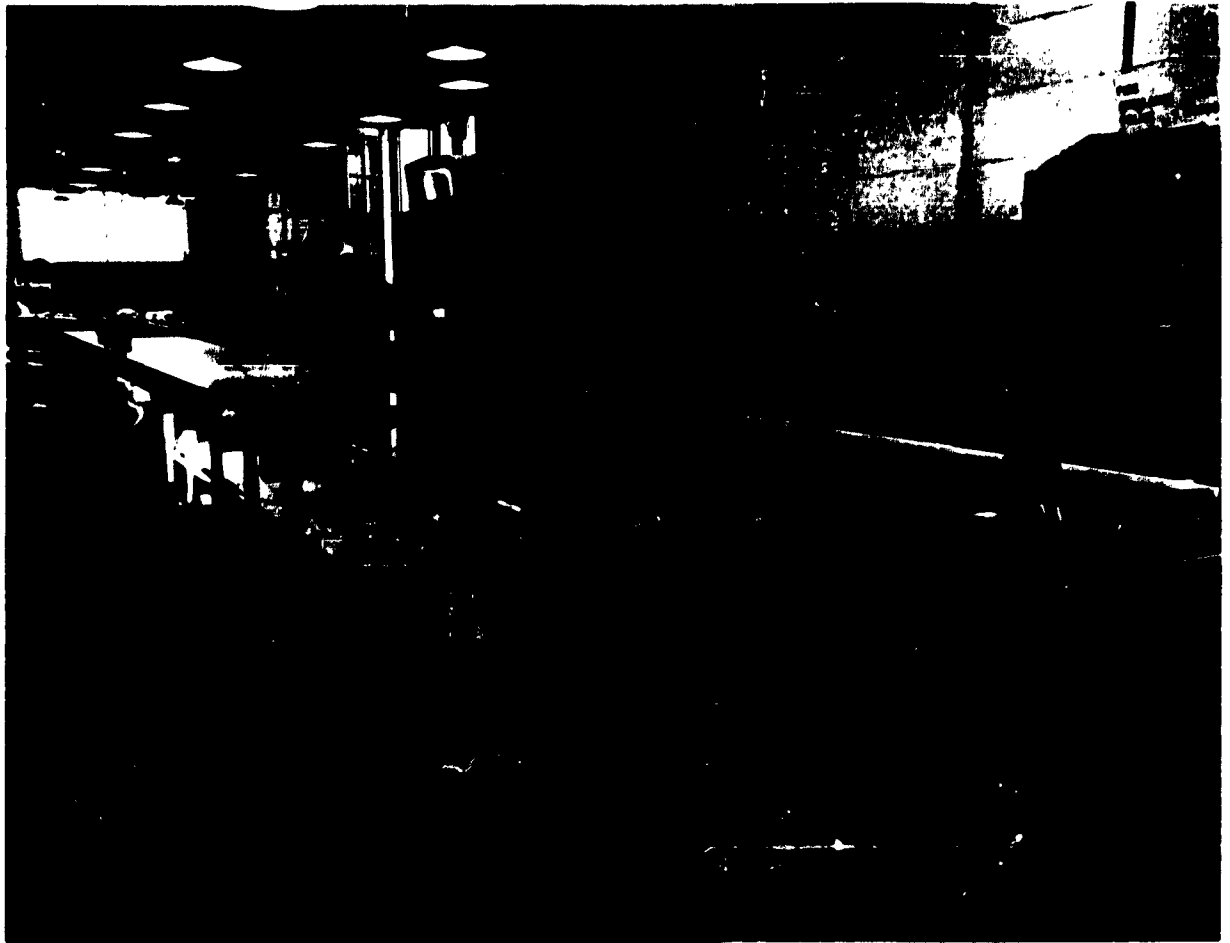


Fig. 11-21 Water Tow-Channel

proportional to the model size; hence, relatively large models should be used during tests to reduce the capillary ripples.

While both the shallow-water flow and shallow-water tow methods have advantages of inexpensive and accurate supersonic flow simulation and provide a rapid qualitative analysis of fluid-flow phenomena, there are inherent disadvantages, as in any type of testing. For the shallow-water flow test, some of the disadvantages are: (1) non-uniform velocity distribution and turbulence in free-stream; (2) transonic speed cannot be simulated to provide accurate and reliable data; (3) varying and accelerating free-stream velocity are virtually impossible to achieve; (4) due to choking, the size of the model is critically limited; and (5) vertical accelerations can become quite large. For the shallow-water tow test, disadvantages are: (1) test time is relatively short and is limited by the

length of the tow channel; (2) pressure (water-depth) measurements are difficult to obtain during the transient part of the test run; and (3) movement of the test model increases the difficulty of measuring and recording desired parameters.

1.3.3.2 Deep-Water Test. The testing of strength, even to destruction, of canopies, as well as the determination of their opening-characteristics in subsonic flow at relatively high dynamic-pressures, may be accomplished most expeditiously and economically by means of towing canopies in deep water. Because of the higher density of water, which is approximately 800 times that of air, high dynamic-pressure-conditions can be satisfied in water at relatively low towing-speeds.

Testing may be conducted in open water, with a boat or ship as the towing means, or in existing water

TABLE 11-4 SHALLOW-WATER SURFACE-WAVE ANALOGY

Two-Dimensional Compressible-Gas Flow

Flow Medium:

Hypothetical gas with

$$c_p/c_v = \gamma = 2$$

Field Geometry:

Two-dimensional field, model and side boundaries geometrically similar

Corresponding Quantities:

Velocity ratio $(V/V_{\max})_4$ Temperature ratio T/T_0 Density ratio ρ/ρ_0 Pressure ratio P/P_0 Velocity of sound $a = \sqrt{\gamma p/\rho}$ Mach number V/a

Subsonic flow

Supersonic flow

Shock wave

Liquid Flow With Free Surface in Gravity Field

Flow Medium:

Incompressible liquid

Field Geometry:

Shallow water with horizontal bottom and free top surface. Model and sides geometrically similar.

Corresponding Quantities:

Velocity ratio $(V/V_{\max})_w$ Water depth ratio δ_w/δ_{w0} Water depth ratio δ_w/δ_{w0} Square of water depth ratio $(\delta_w/\delta_{w0})^2$ Wave velocity $C = \sqrt{g \delta_w}$ Mach number $V_w/\sqrt{g \delta_w}$

Streaming flow

Shooting flow

Hydraulic jump

tow-channels, such as the ones at the David Taylor Model Basin, Bureau of Naval Weapons, Carderock, Md. (Ref (11-6)). Tests are conducted by towing a model or even a full-scale canopy in water over a relatively large distance at a known constant speed. The test canopy is initially packed in a stowage container (Ref (11-7)), and the boat or ship (in open-water testing), or the tow carriage (in water-tow channel testing), is accelerated to the desired velocity. At this time, the test canopy is deployed by remote control, exposing it to the flow. Visual observations, motion pictures of the parachute's dynamic behavior, as well as continuous force-measurements are possible. Quantitative as well as qualitative analyses of parachute performance may be made, with consideration of cloth permeabilities as affected by air and water (Ref (11-8)).

This testing method has several distinct advantages over other testing methods in which high dynamic pressure conditions are required. Testing can be conducted at relatively low towing speeds compared with air speeds necessary to obtain equivalent dynamic pressure conditions. Significantly lower test-costs are realized due to the utilization of less-sophisti-

cated test equipment. The canopies can be subjected to high dynamic pressures for a long period of time, making possible an accurate determination of canopy steady-state characteristics. Transient characteristics such as opening time, opening-shock loads, and oscillations can be easily determined over a wide range of dynamic pressures.

However, testing of parachutes in deep water can be conducted only up to speeds where cavitation occurs. Cavitation takes place when a fluid flows into a region where its absolute pressure is reduced to its vapor pressure; thus it boils and vapor pockets develop in the fluid. The vapor bubbles are carried along with the fluid until a region of higher pressure is reached where the vapor bubbles rapidly collapse. Obviously, after the inception of cavitation, the flow around parachutes in water is not similar to the flow around parachutes in air. Experience has shown that with parachutes towed at a water depth of 8 ft, cavitation begins to develop at a towing speed of 20.8 knots (Mach 0.8 equivalent air speed). Model size is limited in channel testing to avoid wall effects. For a correct analogy of dynamic pressures care must be taken to conduct tests below the "critical" speed.

The critical speed is that velocity where a shock wave is formed ahead of the body, and is analogous to the speed of sound in air.

Based upon test results, the following comparison may be made between parachute performance characteristics in water and in air under equivalent velocity and dynamic pressure conditions: (1) The opening-shock factor associated with a particular canopy type is larger in air than it is for the same type in water. This is because of the difference in the rate of loading by the air and water masses. (2) The drag area of a solid cloth canopy towed in water is higher than that of the same canopy tested in air, because of effective-porosity differences. (3) Wake effects are somewhat different in water than in air. Although in subsonic flow the drag of a canopy increases as its distance behind a primary body is lengthened, this trend is reversed in water. It is believed that in water there exists a "super-velocity" region in that portion of the wake to which the aerodynamic decelerator is exposed, diminishing with distance behind the forebody. This accounts for the fact that the drag of a canopy placed behind a primary body in water is highest "close-in" and decreases as the canopy is moved downstream.

1.3.4 WIND-TUNNEL TESTING. The use of wind tunnels for the measurement of aerodynamic characteristics and the acquisition of performance data for the design of aerodynamic deceleration devices has proved to be one of the most productive test methods. Results from wind-tunnel tests have contributed significantly to the advancement of aerodynamic decelerator technology. Although wind-tunnel testing is not well suited for the study and determination of all of the aerodynamic and performance characteristics of deployable aerodynamic decelerators, this test method nevertheless presents advantages that balance out the shortcomings of some of the data which may be obtained. The main advantages of using the wind tunnel, compared with other test methods, are: (1) the test conditions are subject to close control; (2) measurements of maximum precision may be made; (3) much data can be obtained within a relatively short period of time; (4) flow visualization around aerodynamic decelerators is possible; and (5) within certain limits, comparative relationships and trends determined during wind-tunnel testing usually correlate with full-scale free-flight performance.

Disadvantages arise mainly from the limitation of size of models which can be investigated, from the restraint on the freedom of motion of the system in the wind tunnel, and from the limitation of the maximum dynamic pressure which may be obtained. A number of test problems are encountered during wind-tunnel tests, of which the most difficult are: (1) wind-tunnel

blocking and wall effects; (2) testing below critical Reynolds numbers; (3) direct measurement of canopy side loads, and (4) mounting of models to minimize separation effects.

Blocking effects arise when the ratio of the model projected area to the test-section area is large. For subsonic testing, the maximum ratio of model area to test section area should not be larger than approximately 15 per cent if blocking effects are to be minimized. This area ratio applies primarily to opening-shock measurements of canopies. For the determination of aerodynamic coefficients, smaller models should be utilized. In general, for best results, the projected area of the inflated aerodynamic decelerator model should not exceed 10 to 15 per cent of the test section area.

Wind-tunnel tests are generally conducted above the critical Reynolds number in order to avoid scale effects. As in aircraft work, an attempt is made to achieve Reynolds numbers equivalent to actual full-scale test or operational conditions; however, this has seldom been feasible because of the large diameters of canopies.

The system for mounting the model in the wind tunnel should be sufficiently rigid to prevent vibration from causing excessive angles of attack of the model.

The extension of wind-tunnel testing into the regimes of transonic, supersonic, and hypersonic speeds has opened up an entire new field of research in the area of deployable aerodynamic decelerators. Naturally, there are also problems connected with testing in such higher Mach-number speed regimes, particularly with respect to choice of model size and model placement in the test section.

Some wind-tunnel test facilities which have been used for the testing of deployable aerodynamic decelerators are listed in Table 11-5.

1.3.5 LABORATORY TESTING. Laboratory tests are made on components rather than on the complete aerodynamic decelerator assembly. The primary area of investigation of fabrics involves permeability, strength, and elasticity. Subsidiary tests, such as the results of chemical analysis, determining weathering qualities, or determining the friction coefficient of a material, are made with reference to their effect on the primary characteristics. Since required characteristics for textiles in other fields are somewhat similar, the testing equipment for aerodynamic decelerator textiles has been borrowed or adapted from these other fields. However, characteristics such as permeability, and elongation because of load, are more thoroughly investigated. The methods described in the following paragraphs are primarily for textile testing. Some testing is done on aerodynamic decelerator hardware, but this follows the same pattern as any metal

TABLE 11-5 WIND-TUNNEL TEST-FACILITIES WHICH HAVE BEEN UTILIZED FOR TESTING OF DEPLOYABLE AERODYNAMIC DECELERATORS								
Name and Location	Owner Operator	Test Section Dimensions and Features	Speed Range	Intermittent or Continuous	Stagnation Pressure (Atmos)	Stagnation Temp (°R)	Reynolds No. ft	Dynamic Pressure psi
8x10-ft Subsonic Wind Tunnel No. 1, Aerodynamics Laboratory, David Taylor Model Basin, Washington 7, D.C.	BUWEPS DTMB	8x10x14 ft: Single return, closed circuit; atmospheric test-section; provision for simulating both propeller and jet power.	Subsonic Wind-Tunnels					
			0-160 knots	Continuous	1	576 (with external cooling)	$0-1.77 \times 10^6$	0 - 90
8x10-ft Subsonic Wind Tunnel No. 2, Aerodynamics Laboratory, David Taylor Model Basin, Washington 7, D.C.	BUWEPS DTMB	Same as above	0-135 knots	Continuous	1	Same as above	$0-1.54 \times 10^6$	0 - 70
20-ft Free-Spinning Tunnel, AeroSpace Mechanics Division, NASA Langley Research Center, Langley Field, Va.	NASA NASA	20-ft diam, 12-sided	0-50 knots	Continuous	1	Ambient	$0-0.60 \times 10^6$	0 - 10
300-mph, 7x10-ft Tunnel, Full-Scale Research Division, NASA Langley Research Center, Langley Field, Va.	NASA NASA	7x10 ft and 15.75 x 17 ft	0-250 knots 0-58 knots	Continuous	1	Ambient +20 Ambient +20	$0-2 \times 10^6$ $0-0.83 \times 10^6$	0 - 200 0 - 12
12-ft Vertical Tunnel, Aeronautical Systems Division, Wright-Patterson Air Force Base, Ohio	Air Force ASD	12 ft diam, 12-sided	0-80 knots	Continuous	1	Ambient	$0-0.83 \times 10^6$	0 - 20

TABLE 11-5 (Cont)

Name and Location	Owner Operator	Test Section Dimensions and Features	Speed Range	Intermittent or Continuous	Stagnation Pressure (Atmos)	Stagnation Temp (°R)	Reynolds No./ft	Dynamic Pressure psi
Transonic Model Tunnel, Propulsion Wind-Tunnel, Arnold Engineering Development Center, Arnold Air Force Station, Tenn.	Air Force ARO, Inc	12x12x 37.5 in.	<i>Small, Transonic Wind-Tunnels</i>		1.37	120 above ambient	3.5×10^6 - 4.6×10^6	425-1240
			Mach 0.55-1.5	Continuous				
7x10-ft Transonic Wind-Tunnel, Aerodynamics Laboratory, David Taylor Model Basin, Washington 7, D.C.	BUWEPS DTMB	7x10x18 ft	<i>Large, Transonic Wind-Tunnels</i>		0.019-1.9	610	1×10^6 - 6×10^6	50-950
			Mach 0.3-1.17	Continuous				
Transonic Circuit Tunnel, Propulsion Wind-Tunnel, Arnold Engineering Development Center, Arnold Air Force Station, Tenn.	Air Force ARO, Inc.	16x16x40 ft	Mach 0.5-1.6	Continuous	0.019-1.9	620	5.5×10^4 - 8.3×10^6	6-1650
16-ft Transonic Tunnel, Full-Scale Research Division, NASA Langley Research Center, Langley Field, Va.	NASA NASA	Octagonal, 15.5 ft across	Mach 0.2-1.3	Continuous	1	635	1.2×10^6 - 4.15×10^6	57-905

TABLE D-5 (Cont)

Name and Location	Owner Operator	Test Section Dimensions and Features	Speed Range	Intermittent or Continuous	Stagnation Pressure (Atmos)	Stagnation Temp, (°R)	Reynolds No. ft	Dynamic Pressure psi
Tunnel E-1, Von Karman Gas Dynamics Facility, Arnold Engineering Development Center, Arnold Air Force Station, Tenn.	Air Force ARO, Inc.	<i>Small, Supersonic Wind-Tunnels</i>		Intermittent	0.055-4.00	510-560	$0.25 \times 10^6 - 18.7 \times 10^6$	27-2600
		12x12 in., variable-geometry flexible nozzle	Mach 1.5-5					
2-ft Supersonic Wind-Tunnel, Gas Dynamics Facility, Aeronautical Systems Division, Wright-Patterson Air Force Base, Ohio	Air Force ASD	<i>Large Supersonic Wind-Tunnels</i>		Continuous	0.02-2.5	630	$7.0 \times 10^4 - 7.5 \times 10^6$	15-1300
		2x2 ft, fixed nozzles	Mach 1.5-5					
Supersonic Circuit, Propulsion Wind-Tunnel, Arnold Air Force Station, Tenn.	Air Force ARO, Inc.	16x16x40 ft	Mach 1.5-4	Continuous	0.019-0.95	1110	$2.3 \times 10^4 - 3.2 \times 10^6$	3-730
Tunnel A, Von Karman Gas Dynamics Facility, Arnold Engineering Development Center, Arnold Air Force Station, Tenn.	Air Force ARO, Inc.	40x40 in., variable-geometry flexible nozzle	Mach 1.5-6	Continuous	0.07-13.6	760	$0.5 \times 10^6 - 8.5 \times 10^6$	45-1780
Unitary Plan Wind Tunnel, NASA Langley Research Center, Langley Field, Va.	NASA NASA	4x4x7 ft	Mach 1.5-2.81	Continuous	0.14-4	760	$0.3 \times 10^6 - 15 \times 10^6$	100-3500

TABLE 11-5 (Cont)

Name and Location	Owner/Operator	Test Section Dimensions and Features	Speed Range	Intermittent or Continuous	Stagnation Pressure (Atmos)	Stagnation Temp ($^{\circ}$ R)	Reynolds No. ft	Dynamic Pressure psi
Tunnel E-2, Von Karman Gas Dynamics Facility, Arnold Engineering Development Center, Arnold Air Force Station, Tenn.	Air Force ARO, Inc.	12x12 in.	<i>Small, Hypersonic Wind-Tunnels</i>					
			Mach 5-8	Intermittent	27-87	1375	0.9×10^6 - 20.4×10^6	1-2850
Low-Density Hypersonic Gas Dynamics Facility, Aeronautical Systems Division, Wright-Patterson Air Force Base, Ohio ⁴	Air Force ASD	2x2 ft. two-dimensional	<i>Large, Hypersonic Wind-Tunnels</i>					
			2500-3500 fps	Intermittent	0.05-1	750	0.9×10^3 - 1×10^6	3.5-70
Tunnel B, Von Karman Gas Dynamics Facility, Arnold Engineering Development Center, Arnold Air Force Station, Tenn.	Air Force ARO, Inc.	50-in. diam. circular, axisymmetric contoured nozzle	<i>Large, Hypersonic Wind-Tunnels</i>					
			Mach 8	Continuous	6.7-53.3	1360	0.4×10^6 - 3.3×10^6	67-520
Tunnel C (Same as above)	Air Force ARO, Inc.	Same as above	<i>Large, Hypersonic Wind-Tunnels</i>					
			Mach 10 Mach 12	Continuous	11.7-160 11.7-160	1960 2460	0.3×10^6 1.25×10^6	

¹Entrance cone used as low-speed test-section for V-STOL research.²Can accommodate airbreathing and rocket engines.³Can accommodate airbreathing and rocket engines.⁴Being modified to give higher-temperature air and higher Mach-numbers, and finally to a low-density arc plasma-generator.

testing — such as bending and hardness testing, and spectrographic and chemical analysis. A number of instruments are commercially available for all of these tests.

1.3.5.1 Air Permeability. Through its control of the air mass inside the canopy and the flow over it, the air permeability of the fabric is an important factor in determining parachute performance characteristics such as critical opening-velocity, opening-shock, and stability. Air permeability is measured by clamping a fabric specimen tightly over an orifice. The air flow is either drawn or blown through the fabric specimen. The standard method has been to measure flow in terms of cubic feet per minute per square foot of area with 0.5 in. of water pressure-drop across the fabric specimen.

1.3.5.2 Strength. The strength of a textile material is usually measured by clamping a specimen between a fixed and a movable set of grips or jaws and subjecting it to tension. The loading can be imposed to the point of rupture or to any lesser value. The elongation and energy-absorption can be determined and, in some instances, pencil-graphed directly from the instrument. Tensile strength is usually expressed in terms of pounds, kilograms, or grams: per width of the specimen for webbings, tapes, and ribbons; per specimen shaped-area with fibers, yarns, threads, and cords; and per inch width in the case of canopy fabric. Strength factors are measured under many different conditions, depending upon the study being made. But normally, they are expressed in terms of standard dry-specimen conditions at $70\text{ F} \pm 2^{\circ}$ and 65 per cent \pm one per cent relative humidity. The proper grip or clamp is as important as the tensile-testing instrument. If the specimen is not held correctly, errors will result. A specimen undergoing a tensile test must have the load applied uniformly across the specimen, or a tearing action will result, regardless of the type of instrument used.

1.3.5.3 High-Speed Impact Loading. Failure of

suspension lines of parachutes deployed at high speeds have occurred under total load conditions which were less than 50 per cent of the total rated strength of the lines. And failures have resulted in the investigation of the properties and behaviors of textile materials under impact loading. Impact testing at high rates of loading differs from static testing primarily in the emphasis on the phenomenon of stress-wave propagation in both the test specimen and the attachments. In static testing, the force applied to extend the specimen is uniform throughout the entire length of the test piece. At impact velocities there is a non-uniform change in load along the test specimen, which is a consequence of the stress wave, i.e., the applied force on one end of the specimen is not instantly measurable at the restrained or clamped end.

In textile material, this stress wave-phenomenon manifests itself at impact velocities in excess of 100 fps. The resistance offered by the internal inertia of the test specimen to an applied impact produces stress waves which are reflected from end to end until the breaking stress of the specimen is reached. In order to collect data such as breaking strength, curves for elongation by load versus time, times to rupture, impact velocities, and rupture energies for webbings and for various seams, splices, and joints fabricated from webbings subjected to conditions of high-rate loading, an impact test machine was developed (Ref (11-9)). This machine has the capability of rupturing specimens with static strengths up to 10,000 lb at impact velocities ranging from 200 to 750 fps. Necessary instrumentation for determining required data parameters is available. The impact test machine is schematically shown in Fig. 11-22. A gas gun propels a small specially designed impacting missile (weights range from 1/2 lb to 10 lb) at a desired velocity and with sufficient energy to rupture the test specimen mounted on pendulum No. 1. This first pendulum is used primarily as a low-frequency specimen-mounting device. However, if its mass is known and its displacement after impact is measured, the velocity and energy of the missile can be calculated. The missile ruptures the test specimen, at the apex of the V-shaped configuration and continues on, lodging itself in pendulum No. 2. This pendulum permits calculation of missile velocity and residual energy after rupturing the test specimen and also serves as a low-frequency shock mount for stopping and containing the missile. The multi-flash light source aids the camera in recording impact data. Results from tests conducted with various webbings, and seam and joint configurations are presented in Ref (11-10).

1.3.5.4 Tear Resistance. Tear resistance is considered an essential characteristic of parachute textile fabric and is a physical requirement outlined

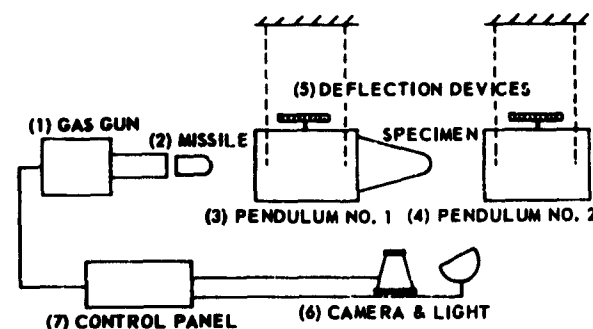


Fig. 11-22 Schematic Diagram of Impact-Testing Machine

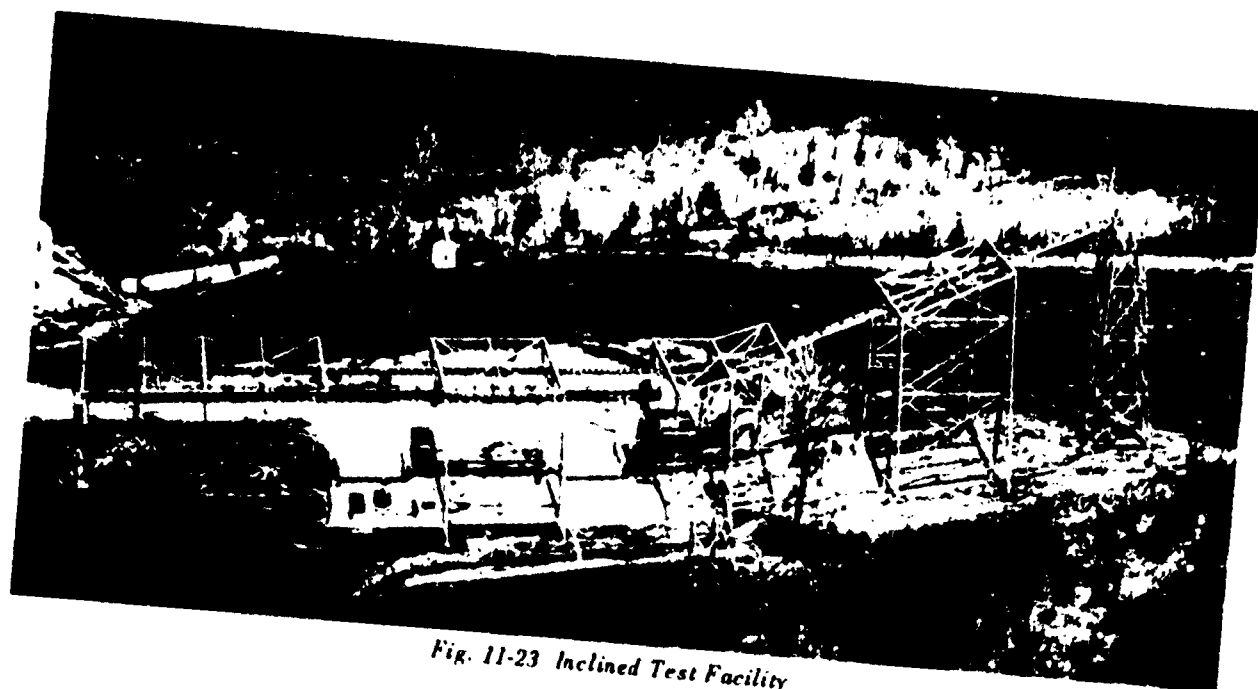


Fig. 11-23 Inclined Test Facility

in parachute fabric specifications. The usual tensile-testing instruments are used. Two methods are used for determining tear resistance: the "tongue" method and the "trapezoid" method. The tongue method is used to determine the tearing strength of woven fabrics that have approximately the same tearing strengths in both warp and filling directions. The trapezoid method is used for fabrics that have unequal warp or filling strengths.

1.3.5.5 Heat and Friction. Because of present high-speed applications, heat resistance has become an important property of aerodynamic decelerator textiles. The generation of heat by friction has also made it important to know the coefficient of friction of the fabric. For determining the static coefficient of sliding friction, the inclined-plane type of apparatus is the simplest in construction, operation, and calibration. The distance of the inclined plane to the horizontal is gradually increased and the angle is measured at the instant when a block begins to slide down the plane. The tangent of this critical angle is numerically equal to the coefficient of static friction of whatever material is on the block and plane surfaces. The tangent is measured by means of a vertical scale fixed behind the inclined plane at a known distance from the hinge of the plane. In addition to the tests described, a variety of miscellaneous tests are made on parachute cloth. These material tests are described in Federal Specification CCC-T191B.

1.3.6 LANDING-CONDITION SIMULATION. To simulate the ground landing conditions that occur dur-

ing the impact phase of parachute-retarded equipment, supplies, and various types of vehicles, an Inclined Test Facility (Fig. 11-23) was erected at the Aeronautical Systems Division, Wright-Patterson Air Force Base, Ohio, as a joint Army-Air Force test facility. The facility is capable of providing a means for obtaining technical data for the study and analysis of ground-impact of a parachute-retarded load under closely controlled conditions.

The Inclined Test Facility consists of structural-steel members, columns, and beams mounted on reinforced-concrete footings. Structural-steel cross-members support dual rails that extend over the complete length of the facility, approximately 380 ft. One end of the structure is inclined at an angle of 22 deg to the horizontal. This end rises to a height of approximately 110 ft above the impact-area surface. The dual rails on the incline are joined with the horizontal rails by a section that describes an arc with a radius of 112 ft. Load release for free-fall occurs at the end of the dual-rail arc.

Mounted on the rail system is a hoist mechanism and "free-wheeling" load carrying trolley. The hoist mechanism lifts and supports the test load during test preparations. It also is used to move the prepared test-load along the dual rails to any predetermined location. The free-wheeling load-carrying trolley serves as the support for a test load after rigging and during the initial movement on the inclined rail. The trolley contains a mechanism that carries the test load and then releases the load at the release point.

Adjustable spring-loaded brake-shoes, mounted internally in the trolley, brake the trolley travel on the horizontal dual rail section.

The normal drop zone or impact area is 50 ft wide and 100 ft long. It has a 6-in. surface of sand spread over a basic bed of crushed rock. The total available zone is divided into three distinct areas. The areas and their use are: (1) a 25 ft by 25 ft concrete pad, that is used primarily for loading and rigging of test vehicles and for vertical drop-testing on concrete surfaces; (2) a 20 ft by 20 ft "sandbox" for vertical drop-testing on a sandy surface or, if necessary, any other soil condition that may be required; and (3) the normal impact area, which is used for all tests when testing under combined horizontal and vertical velocities at ground impact is required.

The Inclined Test Facility is instrumented so that such data as test-load impact-velocities, gravitational forces, pressure forces, stress forces, and general performance of the test items at ground impact may be accurately measured and recorded. Data recording and facility operation are controlled from the Facility Control House, the necessary equipment being located there. Overall operation of the facility during a test is controlled by a rotating sequencing drum.

Two 16-channel Century Static and Dynamic Strain Recording Systems record impact-test data obtained from sensing elements placed on board the test item. Additional data from tests is obtained by high- and low-speed motion-picture cameras and by sequenced still-cameras located in the test impact area. The combined data (from oscillograph tracings and movie film) give a complete history of an impact sequence during a drop test.

The Facility is designed to provide a means for drop-testing parachute-retarded equipment under closely controlled conditions. Velocities of parachute-delivered equipment at ground contact are closely duplicated at the Facility. It is possible to simulate ver-

tical descent velocities up to 40 fps and horizontal wind-drift velocities up to 60 fps. Almost any condition of descent and drift may be simulated by combining the velocity capabilities available and applying these to a test item.

Many types of equipment for testing can be accommodated, provided the rigged weight does not exceed 25,000 lb. The minimum weight for a test item is approximately 500 lb if testing under combined horizontal and vertical velocities is required. Geometric configurations of the test load generally have no bearing on the Facility's capability. However, test items with a physical length in excess of 35 ft cannot be drop-tested in the lateral or broadside direction.

SEC. 2 TEST-VEHICLES

2.1 Introduction. Numerous test-vehicles have been developed and are being utilized to test experimental deployable aerodynamic decelerators and deployable aerodynamic decelerator systems under velocity-altitude conditions that simulate those encountered in ultimate use. Current test-vehicles (see Table 11-6) can be grouped into three categories:

- (1) Gravity-drop test-vehicles;
- (2) Rocket-boosted free-flight test-vehicles; and
- (3) Rocket-sled test-vehicles.

2.1.1 GRAVITY-DROP TEST-VEHICLES. (Ref (11-11)) Gravity-drop test-vehicles are test-vehicles which are released from an aircraft or balloon and achieve, through free-fall, the necessary test deployment conditions. These vehicles have bomb-like or similar ogive-cylinder configurations. Fig. 11-24 shows a weight-bomb test-vehicle used for parachute testing in the low subsonic-speed range. Bomb casings ranging in weight from 500 to 4,000 lb have been modified by welding a flat steel plate to them. The plate distributes the load and facilitates the handling of the test vehicle. A bomb-to-parachute adaptor plate is attached to the end of the bomb casing with maximum allowable design forces as indicated in Table 11-6. This class of test vehicles provides a test weight-range of 200 to 10,000 lb. There are no parachute compartments attached to the test vehicle. The parachute is tied to the bomb as shown in Fig. 11-24. The usual carrying aircraft is a cargo type with a rear door, the C-130 being utilized most extensively. This particular test-vehicle is principally used for rate of descent tests. A 300-ft drop-line, attached to the nose of the vehicle, is released by a timed cutter to determine rate of descent of the test vehicle and deployed parachute. Another class of test

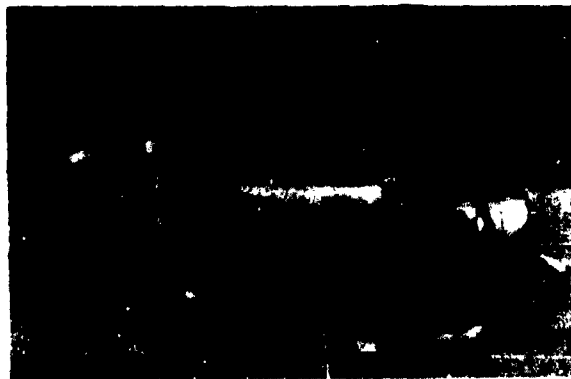


Fig. 11-24 Weight-Bomb Test-Vehicle

TABLE 11-6 RECOVERY-SYSTEMS




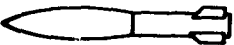
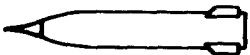




	Basic Structure	Weight Range (lb)		Max "g" Load	Max Speed (Knots or Mach No.)	Diameter (in.)	Volume of Parachute Compartment (cu ft)	Maximum Size Type of Para
		Min	Max					
Weight-Bomb Test-Vehicles	GP 500	200	1000	15	150	14	None	Not applicab.
 General Purpose and Light Case	GP 1000	500	3000	10	150	18-1/2	None	Not applicabl
	GP 2000	2500	5000	8	150	23	None	Not applicabl
	LC 4000	4000	10000	5	150	35	None	Not applicabl
Cylindrical Test Vehicles	GP 500	400	750	20	500	14	3.85	1 T-10 (35-ft
 General Purpose and Light Case	GP 1000	650	2400	20	500	18-1/2	9.32	1 67-ft extend
	GP 2000	1500	4000	15	500	23	17.75	1 G-11A (100-
	LC 4000	4000	10000	10	500	35	53.30	3 24-ft heavy- 1 G-11A and 1
 T-10	T-10	7000	36000	7	B-47 290 B-66 570	37-1/2	Approx 60.00	3 G-11A
Transonic Test Vehicles	Mark 83	800	1500	25	1.1 M	14	2.30	1 16-ft ribbon
 Mark 83  Transonic III	Transonic III	2000	6000	1st Stage 10 2nd Stage 17	1.0 M	24-1/2	1st Stage 7.0 2nd Stage 2.5	1st stage: 1 9-ft ribbon 2nd stage: 1 36-ft ribbo

TABLE 11-6 RECOVERY-SYSTEMS TEST-VEHICLE CHART

Max Speed (Knots or ftach No.)	Diameter (in.)	Volume of Parachute Compartment (cu ft)	Maximum Size, Quantity, and Type of Parachutes Used to Date	Parachute Attachment	Methods of Deployment	Instrumen- tation	Suspen- sion Lug Spacing (in.)	No. Avail- able for Immediate Testing
150	14	None	Not applicable	Adapter ring	Static line	Tensiometer or dropline	Not applicable	5
150	18-1/2	None	Not applicable	Adapter ring	Static line	Tensiometer or dropline	Not applicable	9
150	23	None	Not applicable	Adapter ring	Static line	Tensiometer or dropline	Not applicable	3
150	35	None	Not applicable	Adapter ring	Static line	Tensiometer or dropline	Not applicable	1
500	14	3.85	1 T-10 (35-ft flat circular)	Premature release	Static line or T-2 ejec. gun	Tensiometer or telemeter- ing	14	7
500	18-1/2	9.32	1 67-ft extended skirt or 3 T-10	Premature release	Static line or T-2 ejec. gun	Tensiometer or telemeter- ing	14	7
500	23	17.75	1 G-11A (100-ft flat circular)	Premature release	Static line or T-2 ejec. gun	Tensiometer or telemeter- ing	30	9
500	35	53.30	3 24-ft heavy-duty ribbon or 1 G-11A and 1 22-ft ring slot	Premature release	Static line or T-2 ejec. gun	Tensiometer or telemeter- ing	30	1
B-47 XO B-66 570	37-1/2	Approx 60.00	3 G-11A	Premature release	Static line or T-2 ejec. gun	Telemetering	30 or sling	2
1.1 M	14	2.30	1 16-ft ribbon	Premature release	T-2 Ejection Gun	Tensiometer	14	0
1.0 M	24-1/2	1st Stage 7.0 2nd Stage 2.5	1st stage: 1 9-ft ribbon 2nd stage: 1 36-ft ribbon	Premature release	Internal programming timer	Telemetering	30	3*

TABLE 11-6 (Co

	Basic Structure	Weight Range (lb)		Max "g" Load	Max Speed (Knots or Mach No.)	Diameter (in.)	Volume of Parachute Compartment (cu ft)	Maximum Size, Qua. Type of Parachutes
		Min	Max					
Supersonic Test Vehicles								
 Rocket-Boosted Bomb	Rocket Boosted bomb	2250**	2350**	10	1.5 M	Aft end 22.2 x 32.4 Forward section 14		Test 1st stage: 1 4.5-ft ribbon 2nd stage: 1 7.3-ft ribbon Recovery Forward section: 1 16-ft ribbon Aft section: 1 40-ft conical
 Cree Missile	Cree missile (composed of 3 missiles)	2390**	2350**	60	2.0 M	Booster: 12 Missile: 9		Test: 1 6.26-ft ribbon, 1 4' and 1 2.02-ft ribbon Recovery 3 8-ft ribbon (one e To be determined a
 Supersonic II	Supersonic II*	2200**	3200**	Test 30 Recov 60	2.0 M	18	Test: 1.0 Test Recov: 1.0 Recovery 3.0	
 Supersonic III	Supersonic III***	2000	6000	25	3.0 M	25	Test: 4.0 Recovery 3-4.5	Test Test parachute Recovery 1st stage: 1 11-ft 2nd stage: 2 38-ft

* These vehicles are undergoing acceptance tests.

** The weight indicated is total launch weight.

*** Supersonic III test vehicle is in the preliminary design stage.

TABLE 11-6 (Cont'd)

Max Speed (Knots or Mach No.)	Diameter (in.)	Volume of Parachute Compartment (cu ft)	Maximum Size, Quantity, and Type of Parachutes Used to Date	Parachute Attachment	Methods of Deployment	Instrumen- tation	Suspension Lug Spacing (in.)	No. Avail- able for Immediate Testing
1.5 M	Aft end 22.2 x 32.4 Forward section 14		Test 1st stage: 1 4.5-ft ribbon 2nd stage: 1 7.3-ft ribbon Recovery Forward section: 1 16-ft ribbon Aft section: 1 40-ft conical	Premature release	Internal programming timer	Telemetering	14	0
2.0 M	Booster: 12 Missile: 9		Test: 1 6.26-ft ribbon, 1 4.12-ft ribbon, and 1 2.02-ft ribbon Recovery: 3 8-ft ribbon (one each missile)	Premature release	Internal programming timer	Telemetering	30	0
2.0 M	18	Test: 1.0 Test Recov: 1.0 Recovery 3.0	To be determined at a later date.	— — — —	Internal programming timer	Telemetering	30	2*
3.0 M	25	Test: 4.0 Recovery 3.4.5	Test Test parachute Recovery: 1st stage: 1 11-ft ring slot 2nd stage: 2 38-ft ring slot	— — — —	internal programming timer	Telemetering	30	0

ceptance tests.
ch weight.
ie preliminary design stage.

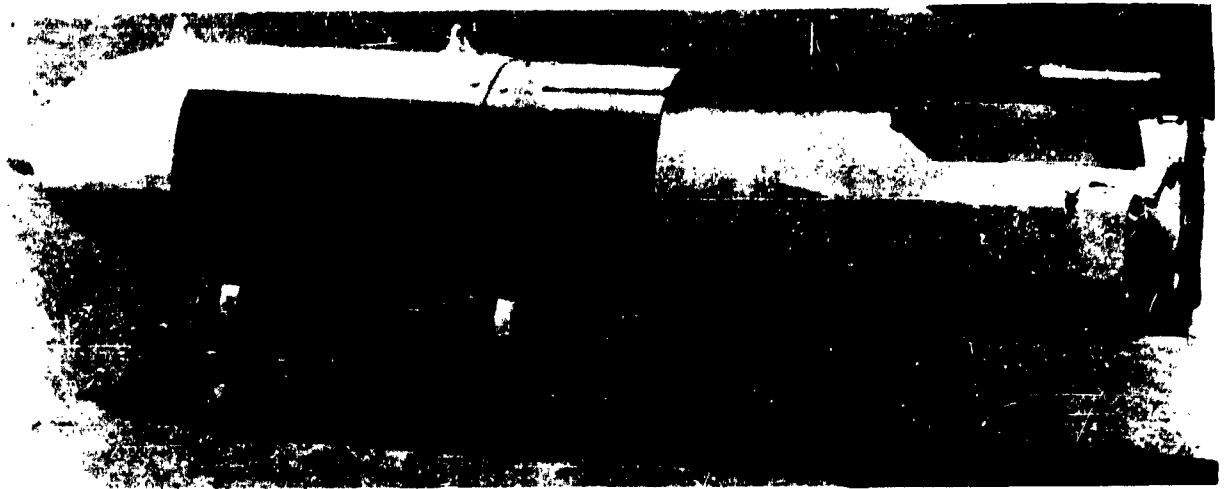


Fig. 11-25 Cylindrical Test-Vehicle

vehicles, the so-called "cylindrical" type, in the weight range of 400 to 36,000 lb, is utilized for parachute testing in the medium-subsonic-speed range. Like the weight-bomb test-vehicles, the cylindrical test-vehicles are made by modifying bomb-casings. A bomb plate assembly is attached to the end of the bomb (Fig. 11-25) with maximum allowable design forces as indicated in Table 11-6. A premature release, which is a device providing an automatic release of the parachute system from the test vehicle in the event of a premature parachute release, is made a part of the parachute bomb plate-assembly. This protects the carrier aircraft from drag loads and is required whenever the test vehicle is carried on externally mounted bomb-suspension equipment. An open-end cylindrical container is attached to the aft part of the bomb casing to house the instrumentation and the main recovery-parachutes. The instrumentation which can be used in the cylindrical test-vehicle includes a choice of camera equipment, tensiometers, and telemetry equipment to sense and record opening-forces, indicated air-speed, dynamic pressure, altitude, and time sequence of the recovery. With the cylindrical test-vehicle, deployment can be initiated by either static-line or explosive charges. The parachute container is closed with a canvas cover in the case of static-line deployment and with a plywood cover in the case of deployment initiated by the T-2 ejection gun. The ejection of the parachute-container cover can also be initiated by starting two timers simultaneously at the instant of release from the aircraft. At a preset time, these timers close an electrical circuit to fire squibs in the specially designed gun-chamber. When telemetry is employed in a cylindrical test-vehicle, an antenna

is attached to the bomb and provision is made for housing a power source (batteries) and the telemetry equipment.

The final class of vehicles which are still applicable to the gravity-drop category are the Mark 83 and Transonic III test-vehicles. These vehicles are capable of attaining speeds of Mach 1.0 during free-fall. The Mark 83 test vehicle is essentially a Mark 83 bomb-casing with modifications similar to those of the cylindrical test-vehicles. This vehicle is used mostly for testing single-stage parachutes.

The Transonic III test-vehicle (Fig. 11-26) is a double-stage parachute-test vehicle which has an ejectable test-parachute compartment held in place by four latches, which are released on command of the control system to jettison the test parachute and compartment and to deploy the vehicle-recovery parachute. This test-vehicle is designed for maximum parachute loads of approximately 60,000 lb. The vehicle is 24.5 in. in diameter, and is approximately 175 in. long with the landing spike retracted. The landing spike can be extended to a maximum of 50 in. The gross weight of the vehicle without parachute can be adjusted from 2000 to 6000 lb in increments of approximately 100 lb. Four removable fins, each 12 in. high, are provided for aerodynamic stability. With the fins attached, the vertical height of the vehicle is approximately 34.2 in. and the fin span is 48.5 in. The vehicle is designed for suspension from 30-in. Air Force S-4 bomb shackles.

2.1.2 ROCKET-BOOSTED FREE-FLIGHT TEST VEHICLES. Free-flight testing of deployable aerodynamic decelerators at speeds greater than transonic has necessitated a departure from the gravity-drop



Fig. 11-26 Transonic Vehicle, Type III

test method. Test missiles were developed that could be powered by means of rocket boosters to the desired test velocities and altitudes. One such test-vehicle, specifically designed for testing the parachutes for the Q-4 supersonic drone, is the rocket-boosted bomb (see Fig. 11-27). The vehicle was made by using the nose section of a Mark 83 bomb casing and attaching a nose spike and a tail can with an elliptical cross-section. The nose spike houses the pitot static tube and telemetering antenna. The nose section contains the ballast weights and the nose-recovery parachute (a 16-ft ribbon-type canopy). The tail section contains the telemetry package, timers, a conical 40-ft ribbon recovery parachute, a GSAP camera, two test parachutes, and two rocket boosters (11,000 lb thrust for 2.2 sec). This test missile is launched from aircraft.

Many other aircraft-launched parachute test-missiles have been used in recent years. The most successful of these is the Cree missile (Ref (11-12)). This vehicle is a very versatile unit capable of attaining a wide range of test conditions due to its adaptability to launching from aircraft, balloon, and the ground. The Cree test missile has three configurations of 170, 200, and 800 lb. These three missiles are employed for the purpose of testing deployable aerodynamic decelerators under drag loadings of 10 through 150 psf under conditions of speeds and altitudes indicated in Table 11-7. The three missiles have basic instrumentation and recovery sections which are identical. The only difference in the three missiles is the nose ballast-section which is varied to achieve the individual weight requirements. Because the indi-

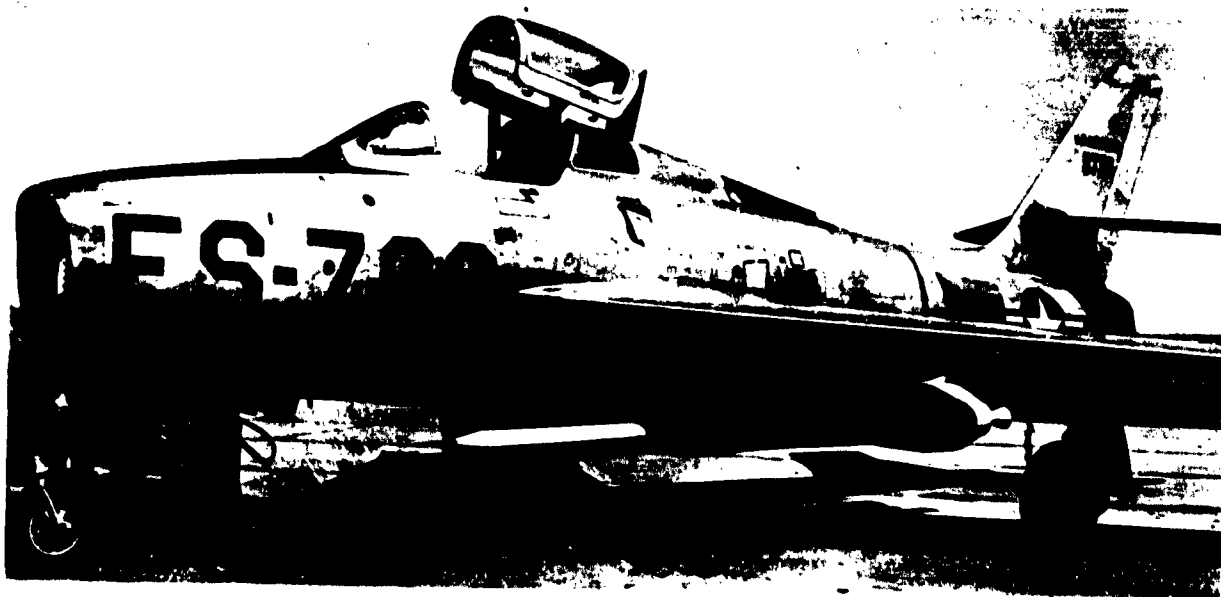


Fig. 11-27 Rocket-Boosted Bomb

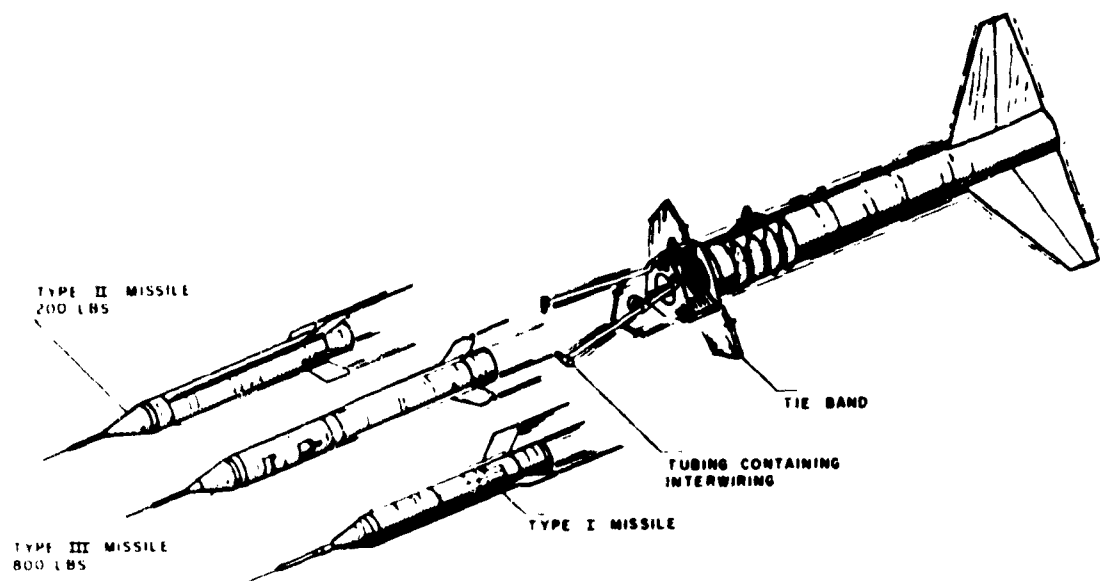


Fig. 11-28 Cree Cluster at Separation

vidual missiles are identical in operation and construction, provisions have been made to allow the units to be assembled into a cluster of three (see Fig. 11-28). This clustering of the missiles results in economy in testing.

TABLE 11-7 PERFORMANCE REGIMES, CREE MISSILE

Mach No.	Altitudes x 1000 ft
0.5	15 to 30
0.75	15 to 30
1.5	15 to 30 30 to 70 70 to 100
2.0	15 to 30 30 to 70 70 to 100

The Cree missile has a parachute compartment 8 in. in diameter and 13 in. long. Each Cree missile has a complete four-channel telemetry system to record and transmit data. The data collected and transmitted consists of ram or total pressure, static pressure, drag force, and shock force. A high-speed camera photographs the test decelerator during and after deployment.

Timing marks are impressed upon both the photographic film and one of the telemetry channels, so that proper correlation of data is possible. Several higher-performance test missiles are currently under development. These are the Supersonic II (Fig. 11-29), the Supersonic III (Fig. 11-30), and the Arapaho test vehicles. The first two vehicles are being developed under the guidance of the AFFTC, 6511th Test Group (Parachute), Auxiliary Landing Field, El Centro, Calif.

The Supersonic II is designed to provide the capability of testing two-stage deceleration parachute systems up to Mach 2.0 at 40,000-ft altitude with a test weight of 2000 lb. The vehicle is 18 in. in diameter and 25 ft 3-1/2 in. long in its largest configuration (with booster and long nose-spike installed). It contains two test-parachute compartments, each with a volume of 1 cu ft, and a 3-cu-ft compartment for a missile-recovery parachute. A single-point strain-gage link attachment, capable of 60,000-lb working load, is provided for the two test parachutes. Forces, speeds, altitudes, dynamic pressures, and event times are telemetered. Two GSAP movie cameras are provided to photograph the parachute functions. The vehicle is built to fit the adapter of a number of standard rocket boosters. This permits programming tests for different test conditions. The Nike booster is used to obtain performance characteristics under maximum conditions. Lacrosse or Regulus boosters are used to obtain performance at lower speeds, altitudes, and weights. In a boosted test, the vehicle is dropped from the modi-

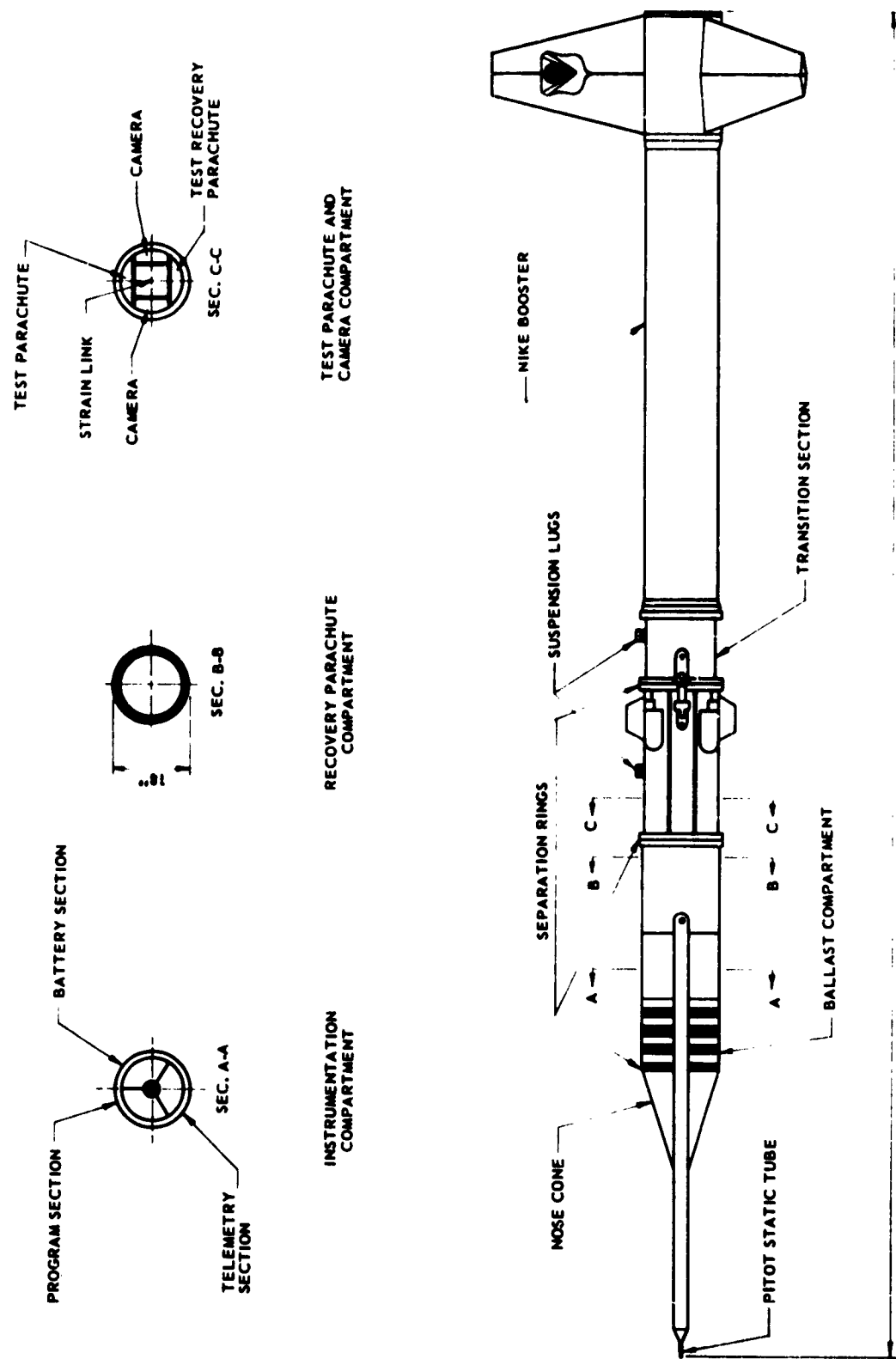


Fig. 11-29 Supersonic Vehicle, Type II

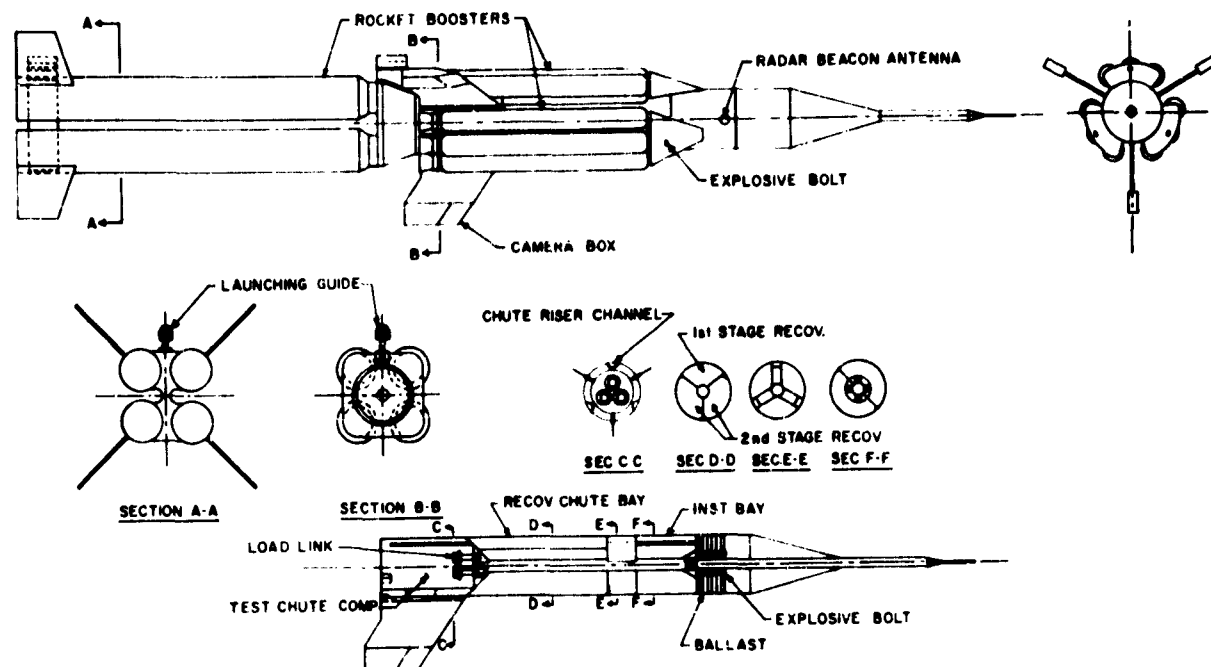


Fig. 11-30 Supersonic Vehicle, Type III

fied wing-pylon of a B-66 aircraft. The booster accelerates the vehicle to the speed and altitude required by the test. At booster burnout, a frangible mating-ring is broken by Primacord detonation and the booster separates. The first test parachute is deployed by a blast bag. After a pre-determined operating time, the first test parachute is freed and the second test parachute is deployed by another blast bag. At the end of the test flight, the aft section, which houses the test-parachute compartments and cameras, is separated from the nose section by breaking the mating ring with Primacord detonation and is recovered by the second-stage test-parachute. The nose section, containing telemetry equipment, ballast, and programming equipment, is decelerated by the recovery parachute and impacts on the landing spike.

The Supersonic III is currently in the design stage. Studies of feasible designs will consider ground launch as well as air launch of the test-vehicle. Briefly, the system requirements are:

- (a) To test under the following test conditions:
 - (1) Velocity between Mach 1.5 and 3.0;
 - (2) Altitude range from 5,000 to 80,000 ft; and
 - (3) Test weights of 2000 to 5000 lb in 100-lb increments.
- (b) To have a flow disturbance no greater than that resulting from a body with an effective cross-sectional

area of 500 sq in.

(c) To record decelerator characteristics and forces by means of photographic and electronic equipment.

(d) To recover the vehicle for re-use, by a parachute recovery-system.

(e) To sustain working loads of 125,000 lb.

The acceleration of the Supersonic III test vehicle to the desired speed and altitude from launch is accomplished by a series or cluster of boosters. The boosters planned for use are the Terrier and Javelin. The parachute compartment, 4 cu ft in volume, is the aft end of the vehicle. Three compartments of 4.5 cu ft each are located symmetrically around the fuselage for recovery systems or other systems as desired. The instrumentation section, programmer section, and ballast compartment are located in the forward portion of the vehicle. The vehicle is equipped with a 45-in. combined impact-spike and antenna. The cameras are mounted on the tips of the stabilizing fins.

A supersonic-hypersonic test-vehicle, the Arapaho, is presently being studied by Aeronautical Systems Division, W-PAFB, Ohio (Ref (11-1)). The Arapaho test-vehicles are intended to permit testing deceleration devices over a range of drag-loadings at various altitude-velocity test-points. The required drag loading and the wide altitude-velocity range for specified test-vehicle weights are shown in Table 11-8. The

TABLE 11-8 DESIRED TEST-CAPABILITY REQUIREMENTS

Capability	Weight, lb	Diameter, in.	Velocity, Mach No.	Comparable Altitude Range, x 1000 ft	Anticipated Test Drag Loading, W/C _D A, psf
A	2000	12 min	Transonic to 3.0	2 to 5	100 min
B	250 500 800	12 max	1.5 to 5.0	40 to 200	10 to 200
C	250	12 max	5.0 to 10.0	80 to 250	1.0 to 10

data-acquisition system to be incorporated in the Arapaho will consist of a telemetry system capable of sensing, converting, and transmitting such performance data as shock force, drag force, test-vehicle acceleration, ram pressure, static pressure, atmospheric temperature, dynamic pressure, and timing marks. For Test Capability C, a backup on-board tape recorder, on which all sensed data are stored for subsequent recovery and playback, or a delayed-telemetry capability, may be required in the test-vehicle. In addition to the telemetry system, two cameras will be used with the test vehicle. All instrumentation should be capable of withstanding a force of 100 g's.

The vehicle for Test Capability A has a test-item compartment with a volume of at least 5 cu ft, and the vehicle for Test Capabilities B and C has a test-item compartment of at least 1-1/2 cu ft.

The Arapaho test vehicle will be ground launched from existing test sites, using standard booster rockets.

2.1.3 ROCKET-SLED TEST-VEHICLES. Two different types of rocket-powered sled test-vehicles are presently being used for the testing of deployable aerodynamic deceleration devices and systems.

2.1.3.1 Solid-Fuel Rocket-Sleds. Fig. 11-31 shows the configuration and dimensions of the Tomahawk low-supersonic-speed test-sled. This sled is powered by eight JATO units, each having 11,000-lb thrust for 2.2 sec, for a maximum (total) thrust of 88,000 lb. This is sufficient to develop a final velocity of Mach 1.2. With the addition of a first-stage pusher, containing 14 additional boosters, it is possible for the sled to attain a maximum velocity of Mach 1.65. The vehicle weighs approximately 3,300 lb and is structurally strong enough to withstand parachute loads up to 100,000 lb. The Tomahawk sled supports the test item to be tested approximately 10-1/2 ft above the level of the track. The largest decelerator that can be tested without undue ground interference is about 12 ft in diameter. The Tomahawk

sled has been operated on the 10,000-ft track of the Free-Air Test Facility at Edwards Air Force Base.

At present, a sled test-vehicle is being developed that will be able to attain velocities up to Mach 3 (Fig. 11-32). It is expected to be available for test runs on the Holloman Air Force Base 35,000-ft track by the summer of 1963. The sled is designed to use, interchangeably, up to five Nike or Genie solid-propellant rocket motors. The maximum velocity of Mach 3 can be obtained with the combination of five Nikes, or with five Genie motors, in the sled, and a first-stage pusher-vehicle with 13 Genie motors.

The weight of the sled, exclusive of rocket motors, is approximately 2800 lb. The test vehicle will be structurally capable of sustaining loads applied at the test-item attachment-point of up to 200,000 and 15,000 lb in the longitudinal and lateral directions respectively. The test-item attachment-point is approximately 84 in. above the track. A rectangular compartment with a volume of 2.5 cu ft is provided for the test item.

2.1.3.2 Liquid-Fuel Rocket Sled. Fig. 11-35 shows the overall dimensions and configuration of this test vehicle. The main structural member of the sled is the high-pressure tank for nitrogen, which is 10 in. in diameter. Box-frame cross-members are welded



Fig. 11-31 Tomahawk Sled Test-Vehicle

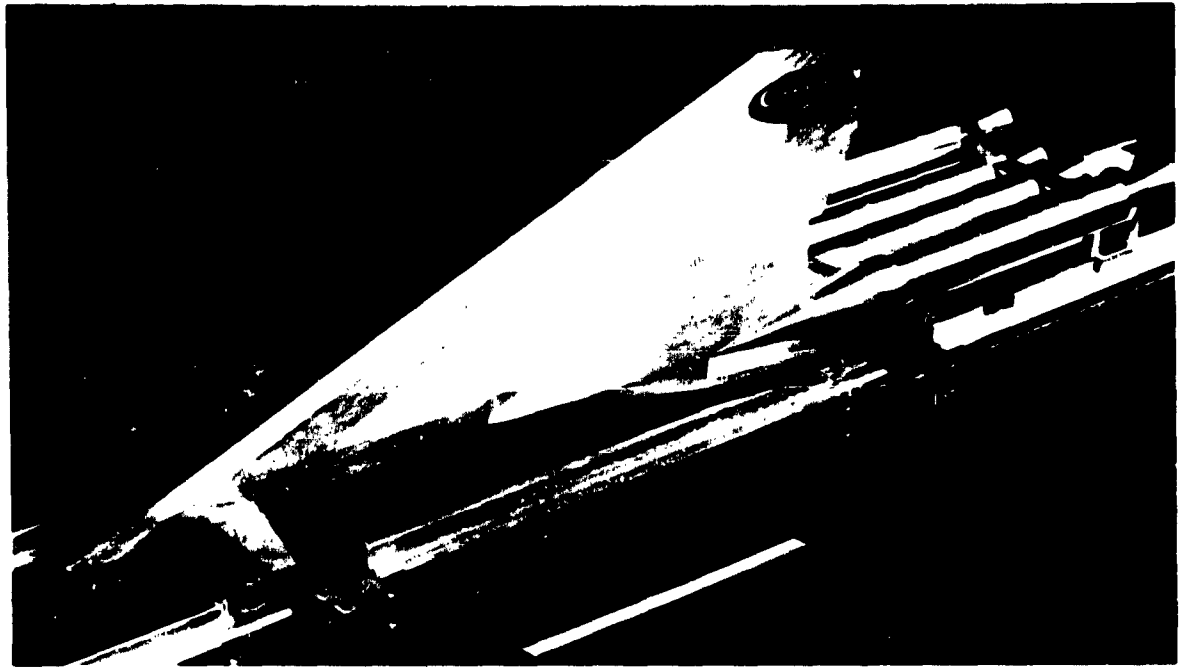


Fig. 11-32 Mach 3 Sled Test-Vehicle

to each end of the nitrogen tank. The alcohol and liquid-oxygen propellant tanks are 12 in. in diameter, and are attached to either side of the nitrogen tank, with fixed supports at the rear. The front supports permit longitudinal movement to accommodate growth or shrinkage of the tanks. The tubular diagonal sup-

port between the front of the sled and the decelerator attachment-point also acts as an auxiliary source of high-pressure nitrogen for the engine-control system. The sled is powered by a gas-pressurized, liquid-fuel, rocket motor. The fuel for this motor is a mixture of 75 per cent ethyl alcohol and 25 per cent water. The

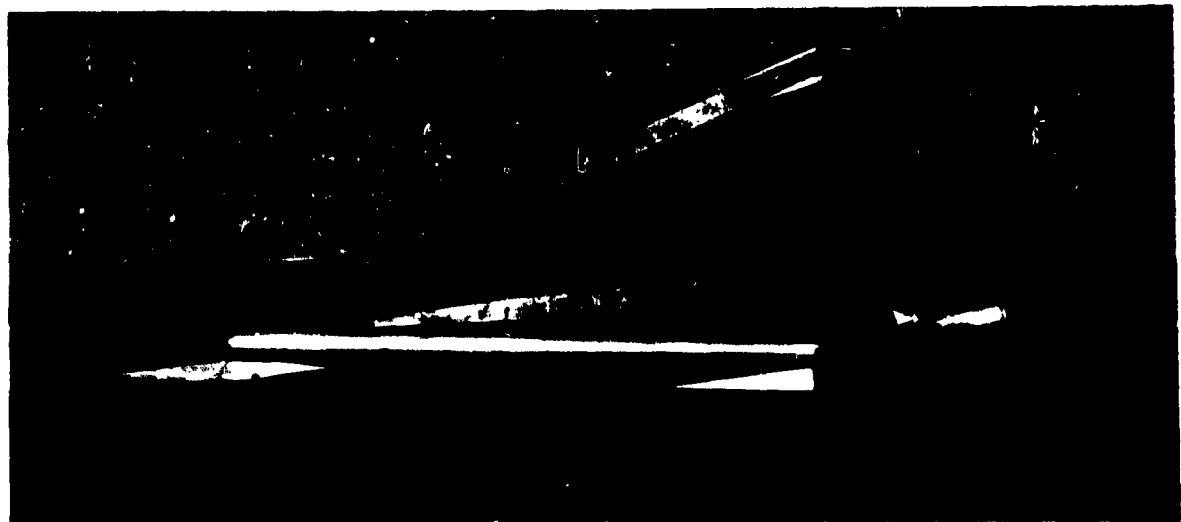


Fig. 11-33 Liquid-Fuel Rocket-Propelled Sled Test-Vehicle

oxidizer is liquid oxygen. A gaseous mixture of nitro- and helium is used for pressurizing the fuel system. The thrust is adjustable from 30,000 to 50,000 lb. The maximum duration at 50,000-lb thrust is approximately 4.5 sec. The weight of this sled is approximately 4,000 lb, and the maximum speed attainable is approximately 750 knots. The thrust chamber of the engine is of conventional design, with a ratio of chamber area to throat area of 2 to 1 and an expansion ratio of 3.65 to 1. The injector is of the triplet impinging type. Ignition is obtained with two integral alcohol-oxygen igniters which are fired by aircraft spark plugs. All valves are pneumatically controlled by 750-psi nitrogen supplied through solenoid-actuated valves. Here, as in the case of the solid-fuel rocket sled, separate slippers that ride on the rails are mounted on the ends of the front and rear cross-members. A compartment containing the parachute is mounted on the top of the sled structure, providing a decelerator attachment point 108 in. above the rails. Instrumentation, consisting of a multi-channel-tape recording system, is in a separate compartment located on the side of the sled. Braking is done with techniques similar to those described in 1.3.2.

2.1.3.3 Test-Sled Data Acquisition. The decelerator sled test-vehicles discussed above carry on-board instrumentation consisting of load cells to measure decelerator drag-loads, a pitot tube to measure ram air-pressure, accelerometers to measure axial accelerations, and high-speed and low-speed cameras to record behavior of tested decelerators. Both the Tomahawk and the liquid-fuel rocket-sled record data, other than photographic, on magnetic tape. The Mach 3 sled incorporates a telemetry system to sense, convert, and transmit decelerator performance information. In addition, one channel will be reserved to permit multiple-point measurement of temperatures on the test-decelerator surface.

SEC. 3 TEST INSTRUMENTATION

3.1 Introduction. The successful accomplishment of applied research and engineering development in the area of deployable aerodynamic decelerators requires specialized instruments or systems for acquiring performance data. Since the design of new decelerators and the improvement of existing ones is largely dependent upon the knowledge of performance characteristics of different types of conventional decelerators, the availability and utilization of accurate and reliable data-recording instruments or systems cannot be overemphasized. For a majority of data-gathering missions, particularly during the early ex-

perimental stages, only exploratory information on performance of decelerator or system is required. Therefore, for this test phase, an instrument should be used which will be economical but still capable of recording results with satisfactory accuracy. For this type of data-gathering mission, an over-all accuracy of ± 5.8 per cent in data acquisition and reduction is usually acceptable. Self-contained recording instruments can be placed in this category. If a deployable aerodynamic decelerator or system has proved a certain degree of reliability during the experimental testing phase of test, and more accurate or different types of performance data are desired, multi-channel instrumentation systems (such as telemetry or magnetic-tape data-recording systems) are used. The choice depends upon economy of test and accuracy of data required. Accuracy of data with a variance of one to two per cent is obtainable. During the initial stages of research and development on aerodynamic decelerators, static test-facilities, such as wind tunnels, are used to a large extent. Here, various instrumentation systems are available to measure and record performance characteristics, and physical phenomena that are required, with a high degree of accuracy. The following is a summation of general information on sensing elements, recording instruments, and recording systems which are commercially available and which are being employed during data-gathering missions in the field of aerodynamic decelerator technology. No attempt is made to furnish a complete listing of all instruments that may be used. Only those instruments are mentioned, and their performance characteristics listed, that have been developed especially for applications in the field of aerodynamic decelerator technology or have proven their suitability during a large number of aerodynamic decelerator tests.

3.2 Sensing Elements (Transducers). The transducer is a device which measures a physical quantity and converts it into an electrical signal, it is defined by the Inter-Range Instrumentation Group (IRIG) as "a device which responds to a phenomenon and produces a signal which is a function of one or more characteristics of the phenomenon" (Ref(11-13)). Standard nomenclature for transducers has not yet been agreed upon by manufacturers and users. However, a tentative listing of transducer types used in aerodynamic decelerator technology has been prepared in Table 11-9.

3.2.1 MEASUREMENT OF DISPLACEMENT AND POSITION. The more frequently used transducers are those acted upon by the measurand (which is a generic term designating any physical quantity which can be measured, detected, or sensed, or can be controlled by using these means to cause rectilinear or

TABLE 11-9 NOMENCLATURE FOR TRANSDUCERS

<i>Main Noun</i>
Transducer
<i>First Modifier (Measured)</i>
Acceleration
Angle of attack
Attitude
Displacement
Flow
Force
Pressure
Radiant-heat flux
Speed
Strain
Temperature
Velocity
Vibration
<i>Second Modifier (Restricts Measured)</i>
Absolute
Angular
Differential
Dual
Gage
Linear
Mass
Surface
Triaxial
Volumetric
<i>Third Modifier (Transduction Principle)</i>
Electric element
Float
Force balance
Gyro type
Bonded strain-gage
Unbonded strain-gage
Capacitance
Inductance
Ionization
Differential transformer
Photo-electric
Piezoelectric
Potentiometer
Reluctance
Resistance
Thermocouple
Thermistor
Variable frequency
<i>Range</i>
As applicable
<i>Units</i>
g

rad/sec
 °/s
 lb/min
 inch
 degree
 inch/sec
 rpm
 psi
 (etc)

angular displacement of one of its integral parts). The magnitude of displacement corresponding to the maximum permissible measurand value may be minute or large. For instance, displacement of the moving mass of a force-balanced accelerometer is hardly discernible, yet a displacement must exist in order to obtain a signal proportional to acceleration. Relatively large displacements are encountered in pressure elements such as the bellows and Bourdon tube. Very large displacements occur in transducers which are used for measuring position. The conversion of physical displacement to electrical signals may be accomplished by taking advantage of such effects as the change in electrical capacitance between two metal plates due to change in distance between the plates; the change in electrical resistance produced by a movable contact, as in the potentiometer or rheostat; the change in self-inductance or mutual inductance produced by a movable magnetic element; the voltage produced by force applied to a piezoelectric crystal; and the variation in electrical resistance of wire because of mechanical strain.

3.2.2 MEASUREMENT OF STRAIN. In almost all cases, strain is measured by electrical strain-gages. The strain gage has importance as a transducer for two reasons. First, it is a basic transducer itself for measurements of strain. Second, numerous other transducers, notably the pressure transducer and accelerometer, often employ a strain gage as the electrical pick-off. Strain gages are applied to the surface of materials in order to sense the strain of the material. The strain gage is sensitive to elongation; that is, the electrical properties change in proportion to the elongation of the gage. Strain elongation is usually small as long as the applied stress does not exceed the elastic limit for a material. The most common form of strain gage consists of a short length of small-diameter (approximately 0.001 in.) wire of high electrical resistance. To apply the gage, it can be cemented to the member to be tested; this is a bonded resistance-wire strain-gage.

Recently, the semiconductor or "solid-state" strain gage has come into being. This operates on the same piezoelectric effect which applies to previous metal

strain-gages: the change in electrical resistivity of a material because of applied stress. With germanium and silicon semiconductors, the ratio between the unit strain and the unit resistance change can be up to 175 as compared to 2 to 5 for metallic wires.

3.2.3 MEASUREMENT OF PRESSURE. Force is equal to the product of pressure and the area over which pressure is exerted. In the sensing and transducing of pressure (and vacuum), certain mechanical elements are usually used to convert the applied force into a displacement; however, the displacement is not always a linear function of the force or the pressure. These mechanical elements are often referred to as force continuous-recording devices. Those which are most commonly used for translating pressure into displacement are diaphragms (flat, corrugated, and capsule), Bourdon tubes (circular, twisted), bellows, and straight tubes. Force-peak recording devices provide a displacement as a result of input pressure, and it is necessary that this be converted to an electrical parameter which can be fed to, or sensed by, any electronic input circuitry; the methods of measuring displacement have been discussed in 3.2.1, above.

3.2.4 MEASUREMENT OF FLUID FLOW. To measure volumetric flow values, three basic types of transducers are generally employed. These are displacement meters, velocity meters, and differential-pressure meters. A great variety of each type exists, the selection being dependent upon density, viscosity, flow rate, and corrosiveness of the fluid to be measured. Meter flow-range, pressure loss, monitoring technique, size, accuracy, reliability, and cost must also be considered. A displacement meter is usually in the form of a fluid pump that is run in reverse by the flowing fluid. In velocity meters, the volumetric flow is inferred as being equal to the velocity multiplied by the cross-sectional area of the flow. The moving element is usually a helix, fan, or turbine rotor. Differential-pressure meters consist either of a probe or a constriction in a conduit. There is no limit to the size of these meters, and they can handle corrosive fluids containing large amounts of suspended matter. A flowing fluid has a total (ram or stagnation) pressure which is the sum of its static and dynamic pressures. These terms are often referred to as total, static, and dynamic (velocity) head, respectively, when the pressure is expressed in feet or inches of the working fluid. Fluid-flow rate is directly proportional to fluid velocity and, therefore, to the square root of the differential pressure.

3.2.5 CRITERIA FOR TRANSDUCER SELECTION. The selection of a specific transducer for a particular application remains more of an art than a science be-

cause the choice between available alternatives nearly always represents a compromise between desirable and undesirable characteristics. A catalog of commercially available transducers together with their physical and operating characteristics is given in Ref (11-14). Although this catalog lists transducers for telemetering applications, the majority of the transducers can also be employed in other instrumentation systems, such as direct recording and magnetic-tape data recording.

3.3 Self-Contained Recording Instruments (Drop Test). Self-contained recording instruments can sense physical phenomena, measure their quantities, and mechanically or electrically translate those quantities into displacements or electrical signals recorded on a suitable medium versus a known time base. In the majority of cases, the self-contained recording instruments are capable of sensing and recording only one particular datum. These instruments are designed to contain the sensing, translating, and data-recording components, as well as sources of mechanical or electrical power and other required components within a single housing.

3.3.1 MEASUREMENT AND RECORDING OF DIRECT FORCES. The knowledge of the magnitude and duration of forces acting on an aerodynamic decelerator during its deployment and during steady descent of the decelerator-load combination is of the utmost value in aerodynamic decelerator research and development. An early method of measuring and recording direct forces acting between the aerodynamic decelerator and the suspended load consisted of determining the amount a small copper column would be compressed after being subjected to compression forces. This compression could then be evaluated in terms of direct load in pounds. Obviously, this measurement will only yield maximum force values, and with doubtful accuracy (particularly at the higher rates of force application). To evaluate some of the more significant performance characteristics of aerodynamic decelerators, especially of canopies, a history of force versus time, covering at least the time interval equal to that of the inflation or opening period must be obtained. For the quantitative analysis of canopy opening, a mechanical recording-tensiometer has proven to be more advantageous than any electronic sensing and recording device used. Two types of tensiometers have been developed and are being used extensively during exploratory and experimental parachute test-programs.

3.3.1.1 Embossing-Stylus Type. The magnitude and duration of forces, as well as a time scale, are recorded on a moving strip of polished aluminum foil

by embossing styli. The force stylus follows the movement occurring when the force transmitted through the instrument deforms the individual units of a column of radially tapered disk springs. The assembly is shown in Fig. 11-34. The suspended load is attached to the lower clevis with an appropriate harness, while the upper clevis is attached to the parachute suspension-point or riser. Operation is initiated by a pull-cord. The component parts of the instrument can be grouped into four operating units:

- (a) A round aluminum casing to which two clevises are attached;
- (b) A column of steel disk springs on a pull rod supporting the force stylus;
- (c) The chart drive mechanism, consisting of the recorder assembly and the chart drum assembly; and
- (d) The time marker mechanism, consisting of the oscillator and the time marker.

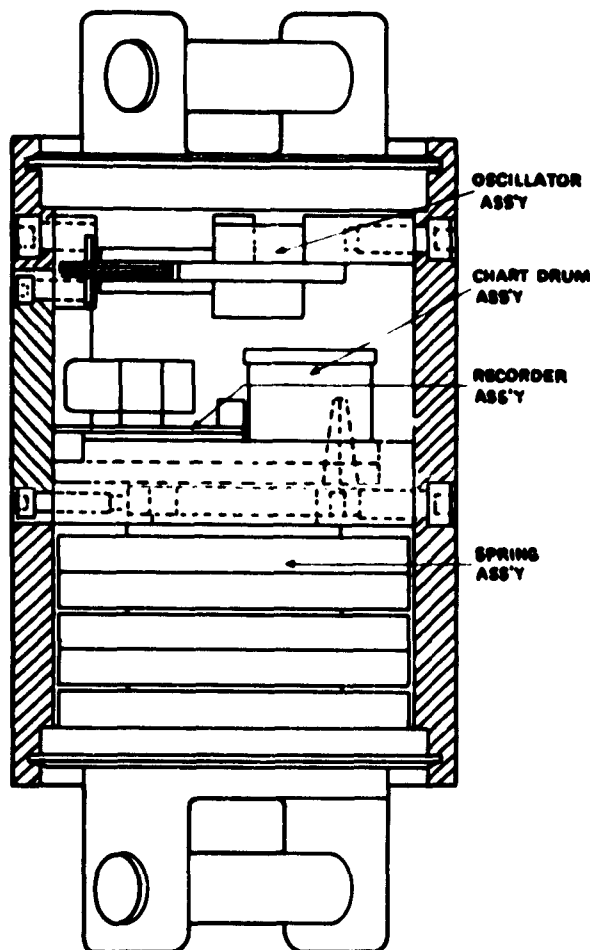


Fig. 11-34 Embossing-Stylus Tensiometer

The casing for the instrument is made out of round-stock aluminum capable of supporting a radial load of 18,000 lb. The upper and lower clevises are attached to the casing and pull rod. An access window in the casing is provided for easy removal of the recording unit. Tension applied to the instrument is transmitted through the casing and the pull-rod from the clevises.

A column of radially tapered steel disk springs, mounted on the pull-rod is housed in the lower portion of the instrument. When compressed, these springs have a nearly linear deflection up to maximum rated load. To prevent any looseness in the spring assembly, which would disturb the zero-line, a load is pre-imposed on the spring system. A bar, supporting the force stylus, is screwed in place in a slot across the head of the pull rod. The projecting ends of the bar are used as guides to prevent any rotation of the pull rod due to an angular acceleration acting upon the instrument. The force stylus is mounted in two cantilever springs, which are soldered into slots near the end of the bar. The stylus must be deflected slightly when the chart drum is placed in position; thus, its location is important, since the stylus must always act with only a slight force against the recording medium. The natural frequency of this force-recording system is approximately 700 cps.

The recorder assembly consists of the escapement-mechanism and the chart-drum assembly. The construction of the escapement mechanism is more rigid and shockproof than that commonly used in spring-powered clocks. The escapement is started by the movement of a slider bar, which is actuated by a pull cord. Battery current to the oscillator is connected by the same motion. After one complete turn of the drive shaft, the escapement is stopped and the battery current disconnected. The edges of the recorder base plate are beveled to fit into the dovetails milled into the guide plate of the instrument. The moment of inertia of the rotating system is sufficiently low when compared with that of the torque spring. This is essential to prevent any slowing down of the clock as a result of angular accelerations which might be imposed on the system externally. The chart drum is designed to hold the recording medium in a true cylindrical shape. The recording medium is a polished aluminum foil approximately 0.003-in. thick. It is pre-formed to a cylindrical shape slightly smaller in radius than the drum surface and firmly held in position on the chart drum.

The function of the oscillator is to interrupt the battery current periodically to cause the time-marker to record the desired time intervals on the recording medium. The oscillator is of electromechanical design and should be given particular attention to ensure that it is free of inertia and acceleration effects. The frequency of oscillation depends upon the moment of

inertia of the two soft-iron disks, each mounted on pivot bearings to rotate about its own axis, and the value of the restoring torque of the straight-wire springs connecting the two disks. The nominal frequency of the oscillator is 20 cps. The time-marker is a simple solenoid magnet carrying a pivoted armature. On one end of this armature is a spring-loaded stylus. The time-marker solenoid is connected in series with the oscillator solenoid. Thus, each oscillation of the oscillator disk causes the time-marker armature to move up and down. The time-marker stylus is located slightly above the force stylus inside the instrument case. The force-sensing system is calibrated by subjecting the instrument to known forces and recording the position of the stylus on the recording medium. The deflection of the spring column when subjected to a load of 1000 lb is approximately 0.014 in.

For the purpose of evaluating the recorded information, it is necessary to magnify the recorded trace. A toolmaker's microscope is satisfactory to evaluate individual force-values. To obtain histories of force versus time, other conventional reproducing devices may be used.

The overall length of the instrument is 8.5 in., and the diameter of the instrument case is 4 in. The weight of the instrument is 11.2 lb.

Advantages of this instrument are:

- (a) The record of the forces recorded may be read even if the recording medium is the only item to survive destruction of the instrument unharmed; and
- (b) Relatively inexperienced personnel may be used for installation, loading, and unloading of the instrument

Disadvantages are:

- (a) The adjustment of the force stylus is critical, to produce a visible record and avoid gouging; and
- (b) The frequency response of this instrument is relatively low and, therefore, the application of the instrument is limited.

The following types have been developed and are available:

Type I - Capacity 7,500 lb, 10 sec recording time;
 Type II - Capacity 7,500 lb, 20 sec recording time;
 Type III - Capacity 15,000 lb, 20 sec recording time.

This self-recording tensiometer was developed by Ex-line Engineering Co., Tulsa, Okla., and was assigned the Model No. B-194.

3.3.1.2 Photographic Type. The magnitude and duration of forces, as well as a time scale, are recorded on a moving strip of 35-mm photo-sensitive film by means of light-beam recording. The assembly is shown in Fig. 11-35. The use of this instrument and the start-

ing procedure of the recording cycle are identical to those described for the previous instrument. The force sensing and recording system operates as follows: An annular-disk spring is deflected slightly under load, and this deflection causes an angular rotation of a small mirror. The image of an illuminated slit is focused on a narrow aperture in front of a moving strip of photo-sensitive film after reflection from the rotating mirror. As this mirror rotates, the image is caused to move lengthwise along the aperture, so that the developed film shows the displacement of the image as a curved line. A fixed mirror, adjacent to the rotating mirror, provides a stationary image near one end of the aperture and produces a straight reference-line on the developed film. The natural frequency of the force sensing and recording system is approximately 1200 cps.

The recorder assembly contains commercially available 35-mm film and is fastened light-tight to the instrument-case window. When the recorder is inserted

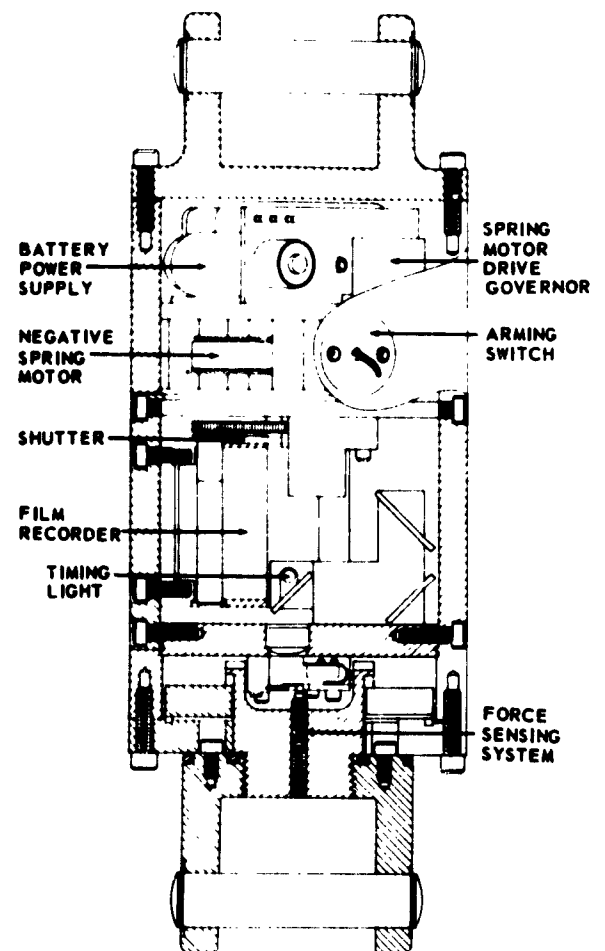


Fig. 11-35 Photographic Type Tensiometer

in the instrument, a gear on the takeup reel of the recorder meshes with the drive gear of the spring motor and the instrument is ready for operation.

The drive motor for the recorder is a Neg'ator-type spring-motor of sufficient torque to pull the recording medium past the aperture with constant speed for a minimum period of 20 sec. Recording time may be changed by adjusting the governor on the spring motor.

A small neon bulb, located near the aperture, is caused to flash with a constant frequency from a vacuum-tube oscillator. Each flash illuminates the aperture. The developed film then shows a series of lines across the film, the distance between any two successive lines representing a time interval of .04 sec.

The force-sensing system is calibrated by subjecting the instrument to known forces and recording the position of the deflected light beam on the film strip. An applied maximum rated load to the force-sensing system of the instrument corresponds to a light-beam deflection on the record medium of approximately 0.75 in.

The recording may be reproduced for evaluation by means of a photographic reproduction device, which prints the recorded traces and a calibration grid on a standard-size sheet of photographic paper.

The overall length of the instrument is 11 in., and the diameter of the instrument case is 4 in. The weight of the instrument is 11.45 lb.

This tensiometer allows the recording of forces of very short duration with great accuracy. While it does not require highly skilled personnel to maintain the instrument, the recording accuracy that may be obtained is substantially higher than that of the embossing-stylus tensiometer. This instrument was also developed by the Exline Engineering Co., Tulsa, Okla., and is designated Model No. BX-101. The following types are available:

- Type I - Capacity 4,000 lb, 10 sec recording time;
- Type II - Capacity 7,500 lb, 10 sec recording time;
- Type III - Capacity 7,500 lb, 20 sec recording time;
- Type IV - Capacity 15,000 lb, 20 sec recording time;
- Type V - Capacity 30,000 lb, 20 sec recording time;
- Type VI - Capacity 50,000 lb, 20 sec recording time.

3.3.2 MEASUREMENT AND RECORDING OF GRAVITATIONAL FORCES. A self-recording accelerometer was developed by Gulton Mfg. Co., Metuchen, N.J., for the purpose of measuring and recording gravitational forces during exploratory parachute drop-tests. It was developed for installation in the center of a parachute dummy. This self-recording accelerometer is designated Glenite Tape Recording System KAT-1. This system has been designed to permit the instantaneous recording of gravitational forces in moving devices when neither wire nor radio-signal connection between transducer and recording system is fea-

sible. The system consists of two basic devices; a self-contained, self-recording accelerometer, which provides a coded record of acceleration versus time on magnetic tape, and a playback unit, which can drive conventional permanent recording devices, such as those using a light-beam galvanometer. In application, the tape record is made within the accelerometer. This is followed by removal of the tape, which is then played back in the play-back system.

The self-recording accelerometer consists of the seismic transducer, the electronic circuitry, and the tape transport-mechanism. The self-recording accelerometer provides a 30-sec continuous tape-record of shock and acceleration phenomena. It is packaged within a housing 4-1/2 in. in diameter and 3 in. high, and weighs 3 lb complete. This accelerometer can be mounted in relatively inaccessible locations in moving objects. The unit is completely self-contained, and only the pull of a cord or the action of a contact pair is necessary to start the recording action.

The seismic transducer in this instrument is a differential transformer device utilizing a spring suspension. The undamped natural (resonant) frequency of the transducer is about 500 cps. Fluid damping ensures flat frequency-response from 0 to 300 cps. The seismic transducer is mounted to the inside of the top plate of the accelerometer and produces a carrier-modulated output proportional to the instantaneous acceleration.

The entire electronic circuit, cast in resin for extreme ruggedness, is fastened to the inside of the cover plate and is transistorized. A phase-modulation technique is employed and both reference and information signals are recorded on a single track of tape. While both are used to decode the data in the playback system, the reference signal may also be used as a timing signal on the final playback record.

The tape transport-mechanism, electrically driven by a self-contained battery, is designed to drive the magnetic tape at a speed of 15 ips. This provides a useful running time of 30 sec, using 500 in. of magnetic tape (1/4 in. wide). The tape transport-mechanism is normally supplied with a pull-wire starting-switch designed to energize the complete accelerometer with 10-lb tension. Other starting devices may be used, such as relays or acceleration switches.

A playback system to process the phase-modulated tape-recording is required to obtain a signal containing the required acceleration-time characteristics. This unit consists of two components mounted in a single rack, approximately 22 x 18 x 28 in. The instantaneous filtered output of the playback unit is fed to standard recording devices, such as those used with galvanometers, oscilloscopes, or meters, or direct-writing recorders.

3.4 Recording-Instrument Systems (Drop Test).

These instrument systems are used for the measuring and recording of a number of aerodynamic decelerator phenomena versus a common time base. The instrument systems available fall into two general categories, magnetic-tape data-recording systems, and telemetry systems.

3.4.1 MAGNETIC-TAPE DATA-RECORDING SYSTEMS. The magnetic-tape data-recording system used in aerodynamic decelerator drop-testing was developed and constructed by Cook Research Laboratories, Morton Grove, Ill. The purpose of the data-recording system is to take amplitude-modulated signals, either alternating current or direct current, from various types of sensing elements; convert them into frequency-modulated audio range signals between 3000 and 4000 cps; and record the resulting signals on magnetic tape. The magnetic-tape data-recording system provides a means of recording simultaneously the data supplied by a number of sensing elements. A fixed frequency of 4000 cps from a reference-frequency oscillator is also recorded on one channel on the magnetic tape for the purpose of compensating for error and control of tape speed in the play-back system. The components of the equipment generally consist of sensing elements, signal converters, a reference-frequency oscillator, a magnetic-tape recorder, and a motor-alternator power supply. Signal converters are electronic circuits used to convert the signals obtained from various types of sensing elements to variable frequencies within the audio range. The audio-frequency shift obtained is proportional to the output received from the sensing element.

3.4.1.1 Six-Channel Magnetic-Tape Recording System (Single Unit). This system, which is used particularly for heavy-cargo drop-tests, contains all components within one unit. The overall dimensions of this unit are 24 in. long, 18 in. wide, and 12 in. high. Six data-channels, power supplies, and a reference-frequency channel are included in this system. A 24-volt, d-c power source is used to power the electronic components and the tape recorder. A calibration unit is included so that it is possible to simulate full-scale deflection on sensing elements by switching precision resistors into the sensing-element input circuits. The tape recorder in this system can record under sustained gravitational forces of up to 75 g 's. The overall running-time of this recorder is three minutes and the average tape speed is 30 ips.

3.4.1.2 Miniature Tape-Recording System. Two miniature tape-recording systems were developed for installation in the internal tubes of a parachute dummy. One system consists of three data-channels

and one reference-frequency channel, while the other consists of six data-channels and one reference-frequency channel. The overall dimensions of this system are approximately 5 in. in diameter and 23 in. long. The auxiliary equipment required for the operation of this system consists of a power-switching unit, a calibration unit, and a power supply. The power-switching unit may be installed in the right-arm tube of a parachute dummy and has as its function the switching from externally to internally applied d-c power. The left-arm tube of the dummy contains the calibration unit, which can simulate full-scale sensing-element deflection by switching a known resistance into the input circuits of the data-signal converters. The two leg tubes of the parachute dummy contain a 24-volt, d-c power supply for the operation of the system. Tests have been conducted on this system at altitudes up to 100,000 ft and temperatures down to -65 F. The tape recorders in both systems are miniaturized and have a recording time of three minutes with an average tape speed of 11 in. per sec. For the three-channel system, 1/2-in. magnetic tape is used, while 1-in. tape is used for the six-channel system.

3.4.1.3 Magnetic-Tape Playback System. The magnetic-tape playback-system converts the frequency-modulated signals recorded previously on magnetic tape into analog voltages through discriminator action. The recording is a frequency-modulated signal with a full-scale swing of 500 cycles about a signal frequency of 3.5 kc. The tape transport-mechanism drives the tape past a pickup head. After amplification, the signal is clipped and shaped into pulses suitable for triggering a mono-stable-multi-vibrator-pulse-rate counter. The resulting pulses are passed to a low-pass filter circuit, which has a cutoff frequency of 200 cps. The d-c voltages at the filter output are then sent to an amplifier, which furnishes the power amplification necessary to drive a galvanometer or light-beam oscillograph. Since the speed of recording may not be constant, playback at constant speed would not result in faithful reproduction of data. Therefore, a variable-speed tape-transport is used for playback. This tape transport receives its control signal from the reference-frequency channel on the recorded tape. A 4000-cps fixed-frequency is recorded on this channel. Tape "flutter" and "wow" appear as a frequency modulation of the 4000-cps carrier-frequency. This signal is detected in a manner similar to that used in the data discriminator. The signal is amplified and used to control the capstan-drive speed, where it removes the long-term speed-variation problem. The large inertia of the system prevents instantaneous action. Therefore, this reference signal is also used to control the bias on the pulse height-limiting diode of the data-

discriminator circuits. The result is a cancellation of the noise at the output of the data discriminator. This action achieves a faithful analog reproduction of the digital-input data. The six-channel playback system is completely contained in a 70-in. relay-rack cabinet. Auxiliary equipment for this magnetic-tape playback-system consists of either a six-channel direct-writing recorder or a six-channel light-beam oscillograph, which converts the output signals of the data recon-verters into permanent records.

3.4.2 TELEMETRY SYSTEMS (REF (11-14)). Telemetry is defined as a system that takes measurements at a remote location and reproduces them at a convenient location in a form suitable for display, recording, or insertion into data-reducing equipment. To perform its basic functions, a telemetry system has a remote terminal for collecting and transmitting its measurement data, a connecting link, and a receiving terminal for collecting and disseminating the data. A sensor located at the remote terminal produces an electrical signal which is processed and applied to a transmitter. The transmitter output is carried by the connecting (radio) link to the receiving terminal, where it is processed for the combined use of display, storage, and later computer analysis and display, or is fed directly into a computer.

Although other types of telemetry systems are in use, the FM/FM system is currently the most widely used in the acquisition of performance data for an aerodynamic decelerator. Wide use of this technique results from signal-to-noise ratio improvement for increase in bandwidth occupancy, reduction in crosstalk, and higher efficiency transmitters. A disadvantage is the greater radio frequency bandwidth which is required to improve the ratio of signal to noise. Frequency modulation (FM) is by definition that type of modulation in which the instantaneous frequency is equal to the constant frequency of the carrier plus a time-varying component that is proportional to the magnitude of the modulating wave. In FM/FM telemetry systems, the quantity (variable) to be measured is converted by a transducer to an equivalent electrical signal. This signal is used to frequency-modulate a subcarrier oscillator in one of the standard subcarrier bands. The outputs of the subcarrier oscillators are mixed and used to frequency-modulate the transmitter. After transmission by an air link, the FM/FM output is received by a suitable receiver. The composite signal is then broken down into various subcarriers by band-pass filters. Finally, the electrical equivalent signal is recovered by FM discriminators for recording, processing, and display.

In a multi-channel FM/FM system, there are basically two systems: continuous reading, and sequential

sampling.

In the continuous-reading system, each subcarrier is assigned a single quantity to be measured. The sequential sampling system accommodates a number of different measurements by sampling the quantities in a recurring sequence. This greatly increases the number of measurements which can be carried over a single radio-frequency carrier. Although sampling has the advantage of increasing the number of data channels, the penalty for this is a reduction in the change of rate of intelligence that can be accurately transmitted. To recover the intelligence, each subcarrier is separated by a band-pass filter and converted into bursts of amplitude modulated direct current. These bursts are then separated by decommutation before recording.

3.4.2.1 Subcarrier Oscillators. Subcarrier oscillators commonly used in FM/FM systems fall into four general classifications. They are voltage-controlled; resistance bridge; inductance-controlled; and saturable reactive oscillators. Each type is used for a specific purpose, and, in general, the four are not interchangeable.

Voltage-controlled oscillators (VCO) are widely used to measure a-c or d-c voltages. These voltages may be the output of appropriate transducers or may be voltages of the quantity being measured. The input impedance is usually one megohm. Most of the voltage-controlled oscillators are available as plug-in units and are pretuned at the factory. Prepackaged plug-in filters for harmonic suppression in the 22-kc to 40-kc bands are also available.

The resistance-bridge oscillator consists of a phase-shift oscillator employing a resistance bridge as a part of the phase-shift network. A change in the resistance of any one of the four bridge elements will produce a proportional change in the oscillator frequency. Use of two or more active arms in the bridge increases the sensitivity of the oscillator-bridge combination. This type of oscillator is designed for transducers employing strain-gage elements and is recommended for use in one or more arms of a four-arm 120-ohm resistance bridge. Subcarrier bands from 1.7 kc to 14.5 kc are used with this oscillator.

Inductance-controlled oscillators are used primarily with variable-inductance transducers. The oscillator circuit is basically a Hartley LC with the transducer constituting the inductive portion of the tank circuit. As the transducer inductance is changed by the action of the quantity to be measured, the frequency of the oscillator is varied, thus producing a frequency-modulated subcarrier signal proportional to the applied stimulus. In general, the inductance oscillators are rugged, stable, physically small, and light in weight.

They are available in all of the subcarrier bands from 1.7 kc to 14.5 kc.

Reactance oscillators employ saturable reactors which are current-controlled pickups. Coils of the reactor are used as inductance elements to modulate the oscillator. This type of oscillator is used for measuring current, small voltages, or temperature, and operates in the 1.7-kc to 14.5-kc range of subcarrier bands.

3.4.2.2 Data Commutation. Because of the limitation on channel capacity in the FM/FM system and the relatively slow changes of certain measured quantities, it is sometimes advantageous to sample rather than monitor the quantity continuously. This process is known as commutation. In a practical use of commutation, the various intelligence channels are sampled sequentially. An important consideration in commutation is the rate at which the input function must be sampled. For optical interpolation, it has been determined that the sampling rate should be 5.7 times the highest frequency of the measured quantity for a maximum error of ± 2 per cent. When automatic channel-separation is used, the sampling rate can be reduced by a factor of approximately two. Common methods of commutation include the customary recording of input and output and refer primarily to the subcarrier oscillator.

3.4.2.3 Transducers. An important consideration in the use of FM/FM system is the mating of transducer outputs with the optimum subcarrier channel. The choice of transducers will, in general, be determined by the frequency response of the measured quantity. Once the transducer has been selected, it is necessary to choose the subcarrier which has a maximum intelligence-frequency equal to, or slightly greater than, the required system-response. The list, given in Table 11-10, can serve as a guide in selecting subcarrier bands for certain measurands.

3.4.2.4 Transmitter. The transmitter employs conventional techniques. Thus, for FM systems, the transmitter is frequency-modulated with the appropriate modulating signal.

3.4.2.5 Transmission Link. In current and future applications, the mostly used connecting-link is radio. At the present time, telemetry bands for military use are 225 to 260 mc and 2350 mc (IRIG).

3.4.2.6 Receiver. The receiver, like the transmitter, employs conventional equipment.

3.4.2.7 Receiving Terminal. It is the function of the receiving-terminal processor to recover the transmitted information and make it available for one or all of the following: display, storage, or computation. For the FM/FM technique, the processor consists of filtering, discrimination, and decommutation, and finally, recording.

TABLE 11-10 SUBCARRIER BANDS FOR SELECTED MEASURANDS

Subcarrier Frequency, kc	Intelligence Frequency, cps	Suggested Measurands
1.3	20	1. Linear and constant acceleration
1.7	25	2. Equipment supply voltages
2.3	35	3. Slow-varying positions
3.0	45	4. Static and slow-varying forces
3.9	60	5. Static and slow-varying pressures
		6. Coordinated temperatures
5.4	80	1. Low-frequency vibration
7.35	110	2. Servo-system measurements
10.5	160	1. Pressure surges and shocks
14.5	220	2. Radiated temperatures
22	660	1. Vibration
40	1200	2. Snatch forces
70	2100	3. Monitoring of affecting voltages
		4. Rapid motion

REFERENCES

- (11-1) ASD Technical Report 61-600, Feasibility Study of Hypersonic Parachute Free Flight Test Capability, Phase I; Cook Research Laboratories, November, 1961.
- (11-2) Streeter, Victor, Fluid Mechanics; 2nd Ed., McGraw-Hill Book Co.
- (11-3) Heinrich, H.G., and Ibrahim, S., WADC Technical Report 59-457, Application of the Weber Surface Wave Analogy in Visualizing the Wave Pattern of a Number of Primary and Secondary Body Configurations in Supersonic Flow; University of Minnesota, 1959.
- (11-4) Preiswerk, E., NACA Technical Memoranda 934 and 935, Application of the Methods of Gas Dynamics to Water Flow With Free Surface, Parts I and II.
- (11-5) Harleman, D., AF Technical Report 5985, Part 4, Studies on the Validity of the Hydraulic Analogy to Supersonic Flow; MIT.
- (11-6) Miller, Lt. A.P., The David Taylor Model Basin; Dept. of the Navy.
- (11-7) Whicker, E., and Lum, F., Stability, Strength, and Opening Characteristics of Parachutes in Water; David Taylor Model Basin, Dept. of the Navy.
- (11-8) Royal Aircraft Establishment (Great Britain) Technical Note No. M.E. 319, A Comparison of the Performance of Small Parachutes in Air and Water.
- (11-9) Caskren, R.J., et al., WADD Technical Report 60-511, Investigation of the High Speed Impact Behavior of Fibrous Materials, Part I: Design and Apparatus, Sept., 1960.
- (11-10) Caskren, R.J., and Chu, C.C., ASD Technical Report 60-511, Investigation of the High Speed Impact Behavior of Fibrous Materials, Part II: Impact Characteristics of Parachute Materials, Feb. 1962.
- (11-11) Dirian D. and Lang, C.K., Testing Equipment for Missile, Drone and Escape Capsule Recovery Systems; 6511th Test Group (Parachute), ALF EL Centro, Calif., June 1960.
- (11-12) Engstrom, B.A., WADC Technical Report 58-284, Performance of Trailing Aerodynamic Decelerators at High Dynamic Pressures, Part I: Development of Test Method and Test Equipment, June 1958.
- (11-13) WADD Technical Report 61-67, Telemetry Transducer Handbook, Vol. I; Radiation, Inc., July 1961.
- (11-14) WADD Technical Report 61-67, Telemetry Transducer Handbook, Vol. II, Catalog; Radiation, Inc., April 1961.

CHAPTER 12

SAMPLE CALCULATION FOR A DEPLOYABLE AERODYNAMIC DECELERATOR SYSTEM

Table of Contents

<i>Section</i>	<i>Page</i>
1 MISSION CRITERIA	503
2 SELECTION OF DEPLOYABLE AERODYNAMIC DECELERATORS	503
2.1 Parachute Canopy for Terminal Deceleration	503
2.2 Parachute Canopy for Intermediate Deceleration	503
2.3 Parachute Canopy for First-Stage Deceleration	504
3 TRAJECTORY CALCULATIONS	504
3.1 Required Cone-Ejection Velocity	504
3.2 Cone Deployment Time and Required Drag	504
3.3 Calculation of Hemisflo Deployment Time and Snatch Force	505
3.4 Calculation of Hemisflo Filling Time and Opening Shock	506
3.5 Intermediate Parachute Deployment Time and Snatch Force	507
3.6 Intermediate-Canopy Filling Time and Opening Shock	511
3.7 Calculation of Final-Recovery Canopy-Filling Time and Opening Shock	511
4 DESIGN CRITERIA	514
4.1 Canopy and Suspension-Line Characteristics	514
4.2 Reefing-Line Length—(16-ft Canopy)	516
4.3 Porosity Calculation	526
4.4 Construction Specifications	526
4.5 Packing Volume (Pressure Packing)	527
<i>References</i>	527

Illustrations

<i>Number</i>		<i>Page</i>
12-1	(C _D S) vs Time	513
12-2	Velocity vs T for the Filling-Time Values $t_f = 5.2$ Sec.	514
12-3	Opening-Shock Force vs Ratio of T for 100-ft-Diameter Canopy	514
12-4	Gore Pattern of Canopy with Skirt Extension	518

<i>Number</i>	Illustrations (Cont'd)	<i>Page</i>
12-5	Dimensions Measured on Hemispherical Canopy	519
12-6	Dimensions Measured on Hemispherical Ribbon Canopy	519
12-7	Diagram of Half-Gore	523
12-8	Vertical Ribbon Placement on Half-Gore	524

Tables

12-1	Calculation of Deployment Time of 6-ft Hemisflo Canopy	506
12-2	Trajectory Calculation	508
12-3	Calculation of Deployment Time—16' Conical Ribbon Canopy	513
12-4	Calculation of Opening-Shock Force— $W = 2883.5$	515
12-5	Construction Details of 6-ft Hemisflo Parachute	526
12-6	Construction Details of 16-ft Conical Ribbon Parachute	526
12-7	Construction Details of 100-ft Flat Circular Parachute	527
12-8	Pack Density	527

CHAPTER 12

SAMPLE CALCULATION FOR A DEPLOYABLE AERODYNAMIC DECELERATOR SYSTEM

In order to provide a mathematical guide for the calculations used to select and design a deployable aerodynamic deceleration system for a particular application, the following sample calculation is included. The initial and terminal conditions of the mission as well as the staging of the aerodynamic decelerators are hypothetical. This Chapter incorporates as many individual calculation considerations as possible. However, the placement of these individual calculations within the Chapter does not reflect an exact sequence of steps to be followed in decelerator system design.

SEC. 1 MISSION CRITERIA

For the purpose of this sample calculation, the following problem is selected, for which a multi-stage deployable aerodynamic-decelerator system is required: A vehicle of combined ogive-cylinder shape with blunt end with a maximum diameter of 20 in. is released from an aircraft in horizontal flight at an altitude of 40,000 ft at a velocity of 2,130 ft/sec. (Mach 2.2). The total weight of the vehicle at time of release from the aircraft is 3000 lb. The vehicle is to be decelerated and stabilized throughout the supersonic and transonic speed regime with terminal deceleration by means of a recovery parachute to impact at sea level with a rate of descent not higher than 22 ft/sec (limits of system); oscillation during the final descent portion of the mission shall be within ± 20 deg. The maximum loading imposed upon the vehicle during the period of aerodynamic decelerator operations shall not exceed 12 g's. The analysis shall terminate with pre-impact conditions and shall not include the attenuation of ground impact shocks.

SEC. 2 SELECTION OF DEPLOYABLE AERODYNAMIC DECELERATORS

2.1 Parachute Canopy for Terminal Deceleration.

Since the terminal velocity is specified to be approximately 22 ft/sec and total weight of the descending system is approximately 3000 lb, the drag area, $(C_D S_o)$, required for this parachute canopy, can be obtained from Chapter 2 (Fig. 2-13) to be approximately 5200 sq ft. Assuming that a solid cloth flat circular canopy can be utilized as the final recovery parachute establishes a drag coefficient, (C_{D_o}) which permits calculation of the size of canopy required. Selecting a C_{D_o} of 0.75 given

$$C_D S_o = \frac{(0.75) (\pi) D_o^2}{4} = 5,200$$

$$D_o^2 = 8,831$$

$$D_o = 94 \text{ ft}$$

Because it is a standard canopy and readily available, and since its stability characteristics are within required limits (± 20 deg), a 100-ft diameter (D_o) solid flat circular canopy is initially selected to accomplish final recovery of the vehicle.

Having selected the type and size of the final recovery canopy, the terminal conditions for the preceding or intermediate aerodynamic-decelerator can be approximated. Although canopies of this type and size have been deployed under more severe conditions, deployment conditions for the terminal descent canopy are chosen to be at a velocity of 175 ft/sec and at an altitude of 5000 ft. This selection insures reliable deployment and opening, avoidance of excessive drifts, and eliminates the necessity for canopy reefing.

2.2 Parachute Canopy for Intermediate Deceleration. Considering among other factors the inflation characteristics, drag coefficient, stability, and stress distribution of ribbon parachute canopies of various designs, a conical ribbon parachute canopy is selected to decelerate the vehicle to a velocity of 175 ft/sec at an altitude of 5,000 ft. Again referring to Chapter 2 (Fig. 2-13), the required drag area $(C_D S_o)$, for the intermediate deceleration parachute canopy is 94.5 sq ft to give an equilibrium velocity of 175 ft/sec. Assuming a drag coefficient, C_{D_o} of 0.5, the nominal diameter of the canopy, D_o will be 15.5 ft. To insure that the desired equilibrium velocity is attained and the stated deployment conditions for the terminal descent canopy are not exceeded, a canopy with a nominal diameter of 16 ft is selected. The deployment initiation speed for the intermediate-stage parachute was selected as Mach 1.3. For this deployment condition, and considering the size of the canopy, the canopy will incorporate a cone angle of 20 deg and a geometric porosity of approximately 27 per cent.

2.3 Parachute Canopy for First-Stage Deceleration. The requirements for selection of the first-stage canopy are reliable deployment and inflation at Mach 2.2 and an altitude of 40,000 ft. After inflation the canopy is to insure stability of the vehicle and decelerate it to a speed of Mach 1.3. For this calculation a 6-ft-diam Hemisflo will be employed with a total porosity of approximately 21.5 per cent. (A 2.18-ft Hemisflo has been successfully deployed at speeds greater than Mach 2 (Ref (12-1)).

SEC. 3 TRAJECTORY CALCULATIONS

Upon release from the aircraft, the ogive-cylinder vehicle is allowed to free-fall for a period of 0.35 sec before deployment initiation of the decelerator system. This deployment delay is considered necessary to insure separation of vehicle from the aircraft and to allow deployment of the decelerator system away from any adverse wake conditions generated by the aircraft. It is assumed that during the free-fall period the vehicle experiences no change in velocity, altitudes, and attitude. To insure that deployment of the first-stage canopy is accomplished, a 30-deg half-angle cone with a base diameter of 6 in. and a weight of 3 lb will be deployed through the wake of the vehicle and will serve as the extraction device for the first-stage chute. This device was selected because it has predictable aerodynamic characteristics. An ejection mechanism is employed to give an impulse to the cone, sufficient to propel it through the wake of the vehicle a distance of five vehicle diameters. This distance is considered sufficient to allow essentially free-stream dynamic pressure to act on the cone.

3.1 Required Cone-Ejection Velocity. Ref (12-2) presents curves of required ejection velocities versus primary-vehicle deceleration, primary-body base diameter, primary-vehicle Mach number, and pack weight. (See Fig. 5-21 through 5-24 of Chapter 5.) The Mach-number-altitude flight regime in this sample calculation does not fit those in the above-referenced curves. However, it is observed from Fig. 5-21 of Chapter 5 that at a given altitude-Mach number condition, as the primary-body deceleration (\dot{v}/g) is decreased, the required ejection velocity is also decreased. The deceleration of the primary vehicle in this sample calculation is

$$a = \frac{F}{m} = \frac{(\text{Drag}) g}{W_t}$$

or

$$\frac{\dot{v}}{g} = \frac{\text{Drag}}{W_t} = \frac{1/2 (5.8512 \times 10^{-4}) (2129.6)^2 (0.35) (\pi) (20)^2}{(144) (4) (3000)}$$

$$= 0.337.$$

This deceleration is low and should require only a low ejection velocity to achieve separation of the cone from the vehicle.

By utilizing the data presented in Fig. 5-21 through 5-24 of Chapter 5 a minimum ejection velocity of 30 ft/sec was selected.

3.2 Cone Deployment Time and Required Drag.

Due to the lack of data available on supersonic wake characteristics, several assumptions will have to be made to determine the time for the cone to travel a relative distance of five calibers aft of the primary vehicle. It will be assumed that the velocity of the primary body does not decrease during the deployment time, since it has such a low deceleration. It can also be assumed that the cone produces negligible drag during its initial movement of a relative distance equal to two primary-body diameters. These are fairly good assumptions, the latter because in the wake region behind the primary body subsonic flow exists (see Sec. 10, Chap. 4). In addition, results from wind-tunnel tests with a 30-deg half-angle cone stationed at various distance behind a primary body showed that the drag coefficient of the cone in this region based on free-stream dynamic pressure was small (Ref (12-3)). Therefore, using the relationship

$$(12-1) \quad S = v_0 t + 1/2 a t^2$$

and the above assumptions, the time for the cone to travel a relative distance of two calibers is

$$S = \frac{2}{5} (8.33) = 30 t$$

$$(12-2) \quad t = \frac{3.33}{30} = 0.111 \text{ sec}$$

Utilizing drag-coefficient data from the above-mentioned tests, an average drag-coefficient for the cone at distances behind the primary body from two to five calibers was selected. This value was $C_D = 0.375$. Next, the average acceleration of the cone during this distance was computed as follows:

$$(12-3) \quad a = \frac{D}{m} = \frac{1}{2} \frac{(5.8512 \times 10^{-4}) (2129.6)^2 (0.375) (\pi) (6)^2}{3/32.05 \times 4 \times 144}$$

$$= 1050 \text{ ft/sec}^2$$

Solving for the time for the cone to travel a relative distance equal to three calibers,

$$S = \frac{3}{5} (8.33) = (30) t + \frac{1}{2} (1050) t^2$$

or

$$t = \frac{-30 \pm \sqrt{900 - (4)(525)(-5)}}{2(525)}$$

$$= \frac{-30 \pm \sqrt{900 + 10500}}{1050}$$

$$= \frac{-30 + 106.9}{1050} = \frac{76.9}{1050} = 0.0732 \text{ sec}$$

Therefore, total deployment time for the cone equals

$$t_{\text{tot}} = 0.111 + 0.0732 = 0.1842 \text{ sec}$$

After deployment the cone must produce sufficient drag to overcome the inertia of a 6-ft Hemisflo pack and to break the pack retaining straps. The drag of the cone after deployment is

$$D = \frac{1}{2} \frac{(5.8512 \times 10^{-4}) (2129.6)^2 (0.75) (\pi) (6)^2}{(4) (144)} = 195.6 \text{ lb}$$

The inertia of the 6-ft Hemisflo pack, which has a weight of 10 lb, is

(12-4)

$$\text{Inertia Force} = (\text{Wt}) (\text{No. of } g\text{'s}) = 10 (0.34) = 3.4 \text{ lb}$$

Using four strands of MIL-R-5608, Class A, Type II, Nylon Ribbon, which has a breaking strength per strand of 18 lb, requires that a minimum force of

$$\text{Force} = 3.4 + 18 (4) = 75.4 \text{ lb}$$

by applied to the Hemisflo pack. With the drag produced by the cone,

$$(12-5) \text{ Margin of Safety} = \frac{195.6 - 75.4}{75.4} = 1.6$$

is realized.

3.3 Calculation of Hemisflo Deployment Time and Snatch Force. The Hemisflo first-stage parachute has 2-D₀ - length suspension lines. Therefore, using Eq 4-46 in Chap. 4,

(12-6)

$$L_s = 12' = \frac{1}{J_b} \ln (1 + J_b v_d t_2) - \frac{1}{J_c} \ln (1 + J_c v_d t_2)$$

where

$$J_b = \frac{\rho (C_D S)_b}{2 m_b} = \frac{(5.8512 \times 10^{-4}) (0.35) (\pi) (20)^2}{2 \left(\frac{2987}{32.05} \right) (144) (4)}$$

$$= 2.39 \times 10^{-6}$$

$$J_c = \rho (C_D S)_c / 2 m_{\text{tot}}$$

The drag area, $(C_D S)_c$, is the drag area of the cone and uninflated Hemisflo canopy. It is assumed that the total drag area of the cone and uninflated canopy is only slightly larger than the drag area of the cone which is $(C_D S)_{\text{cone}} = 0.147$. Therefore, $(C_D S)_c$ is taken to be 0.16.

The term, m_{tot} , is the sum of the mass of the cone, the deployment bag for first-stage canopy, and the first-stage canopy without lines. These are as follows:

$$m_{\text{cone}} = \frac{3.0}{32.05} = 0.094$$

$$m_{\text{bag}} = \frac{2.8}{32.05} = 0.087$$

$$m_{\text{drag-producing surface}} = \frac{\text{Wt of Canopy} - \text{Wt of lines}}{g}$$

$$= \frac{7.2 - 5.2}{32.05} = 0.062$$

$$\text{Then, } m_{\text{tot}} = 0.094 + 0.087 + 0.062 = 0.243.$$

Substituting these values of $(C_D S)_c$ and m_{tot} into the equation for J_c gives

$$J_c = \frac{(5.8512 \times 10^{-4}) (0.16)}{(2) (0.243)} = 1.92 \times 10^{-4}$$

It was assumed that the velocity of the primary vehicle did not change during deployment of the cone. Therefore, the velocity, v_d , equals 2129.6 ft/sec. A trial-and-error solution (as discussed in 4.2.2., Chap. 4) for t_2 , is now performed utilizing Eq 4-46 of Chap. 4. This calculation is shown in Table 12-1.

From Table 12-1, t_2 is 0.18 sec. This value is substituted into Eq 4-47 and 4-48 of Chap. 4 to solve for the velocities of the primary and secondary bodies at suspension-line extension.

TABLE 12-1 CALCULATION OF DEPLOYMENT TIME OF 6-FT HEMISFLO CANOPY

(1)	(2)	(3)	(4)	(5)	(6)	(7)	(8)	(9)	L_s
t_2	$J_b v_d t_2$	$J_c v_d t_2$	1 + (2)	1 + (3)	ln (4)	ln (5)	$\frac{1}{J_b}$ (6)	$\frac{1}{J_c}$ (7)	(8)-(9)
	$5.091 \times 10^{-3} t_2$	$0.409 t_2$							
0.3	1.527×10^{-3}	0.1227	1.001527	1.1227	0.001527	0.1156	640	603	37
0.2	1.018×10^{-3}	0.0818	1.001018	1.0818	0.001018	0.0786	426	410	16
0.18	0.916×10^{-3}	0.0736	1.000916	1.0736	0.000916	0.0710	383	371	12

$$V_{I, 2} = \frac{v_d}{J_b v_d t_2 + 1} = \frac{2129.6}{(2.39 \times 10^{-6})(2129.6)(0.18) + 1}$$

$$= 2128 \text{ ft/sec}$$

$$V_{II, 2} = \frac{v_d}{J_c v_d t_2 + 1} = \frac{2129.6}{(1.92 \times 10^{-4})(2129.6)(0.18) + 1}$$

$$= 1985 \text{ ft/sec}$$

Then

$$V_{II, 2}(\text{rel}) = \Delta V = V_{I, 2} - V_{II, 2} = 2128 - 1985$$

$$= 143 \text{ ft/sec}$$

Utilizing Eq 4-26 of Chap. 4, the snatch force can now be calculated.

$$P = \sqrt{\frac{m_c (V_{II, 2}(\text{rel}))^2 Z P'}{L_s \xi'}}$$

where Z = Number of suspension lines = 20;

P' = Suspension-line breaking-strength
= 2300 lb;

ξ' = Percentage of elongation of suspension line under force equal to P' . This value is 22.5 per cent and

m_c = Mass of canopy drag-producing surface only.

Therefore,

$$P = \sqrt{\frac{(0.0624)(143)^2(20)(2300)}{(12)(0.225)}} = 4610 \text{ lb}$$

It is assumed that drag produced by uninflated Hemisflo is negligible, and therefore is not added to the force (P).

3.4 Calculation of Hemisflo Filling Time and Opening Shock. The 6-ft Hemisflo inflates under infinite-mass conditions. Therefore the filling time is calculated as discussed in 5.1.2.1 of Chap. 4.

$$t_f/D_o = \frac{0.65 \lambda g}{V_s}$$

The velocity, V_s , is equal to the velocity, $V_{I, 2}$ calculated in the preceding paragraph (see Eq 4-49 of Chap. 4). Then

$$t_f = \frac{(0.65)(21.5)(6)}{2128} = 0.0394 \text{ sec}$$

The opening-shock equation for infinite-mass condition is

$$F_o = C_{D_o} S_o qX$$

where X = the dynamic opening shock factor = 1.3 for Hemisflo canopy (Ref (12-3)); and

C_{D_o} = 0.25 for Hemisflo canopy deployed at Mach 2.2 (Ref (12-1)).

Substituting,

$$F_o = (0.25)(28.3)(1327)(1.3) = 12,190 \text{ lb}$$

The Hemisflo canopy decelerates the vehicle to a speed of Mach 1.3. A trajectory calculation is made to establish the altitude, trajectory angle, horizontal displacement, and time elapsed until the point where Mach 1.3 is reached. The method utilized for this

computation is discussed in detail in Ref (12-4). The basic equations utilized are derived as follows.

The force equilibrium tangential and perpendicular to the flight path yield the following equations respectively:

$$\frac{W}{g} \frac{dv}{dt} + Kv^2 + W \sin \alpha - T = 0$$

$$W \cos \alpha - \frac{W}{g} \omega^2 r = 0$$

$$\text{With } v = \omega r$$

$$\text{and } \omega = -da/dt$$

where W = Weight;
 $K = \rho C_D S / 2$
 v = Instantaneous velocity;
 Kv^2 = Aerodynamic drag;
 T = Thrust;
 g = Acceleration due to gravity;
 ω = Angular velocity; and
 t = Time.

The above equation yields

$$\frac{da}{dt} = -\frac{g}{v} \cos \alpha$$

Introducing

$$\frac{dv}{dt} = \frac{dv}{da} \frac{da}{dt}$$

and substituting this into the first equation one obtains

$$W \sin \alpha + Kv^2 - T = W \cos \alpha \frac{1}{v} \frac{dv}{da}$$

or

$$dv = \left(\tan \alpha + \frac{Kv^2}{W \cos \alpha} - \frac{T}{W \cos \alpha} \right) v da$$

Derivations as functions of α yields:

$$dx = -\frac{1}{g} v^2 d\alpha; dy = -\frac{1}{g} v^2 \tan \alpha d\alpha$$

$$dt = -\frac{1}{g} \frac{v}{\cos \alpha} d\alpha$$

If finite increments of angle α are taken for constant values of v , these equations can be written as:

$$\Delta x_{n+1} = -\frac{1}{g} v_n^2 \Delta \alpha_{n+1}; \Delta y_{n+1} = -\frac{1}{g} v_n^2 \tan \alpha \Delta \alpha_{n+1}$$

$$\Delta t_{n+1} = -\frac{1}{g} \frac{v_n}{\cos \alpha_n} \Delta \alpha_{n+1}$$

Time can then be calculated by a step-by-step numerical method.

The preceding trajectory equation can be solved by means of analogue or digital computers. For a limited number of solutions of a trajectory problem, however, it might be more economical and less time-consuming to calculate the trajectory by a step-by-step numerical method. For such an approach, the equation may be written for finite increments (with $T = 0$) of n in the following form:

$$\Delta v_{n+1} = \left[\tan \alpha_n + \frac{C_D S}{2W} \frac{v_n^2}{\cos \alpha_n} \rho \right] v_n \cdot \Delta \alpha_{n+1}$$

where the subscripts $n, n+1, \dots$ represent the increments.

The initial portion of these trajectory calculations are shown in Table 12-2. The final results of this calculation are as follows:

Altitude: 37,000 ft

Trajectory angle: $15^\circ 10'$

Time elapsed from release: 14.354 sec

Velocity: 1254 ft/sec

3.5 Intermediate Parachute Deployment Time and Snatch Force. Initial snatch-force calculations in which the 6-ft Hemisflo was used to extract the 16-ft conical ribbon canopy resulted in a force exceeding the 12-g limitation (see Sec. 1). Therefore, a deployment system was designed whereby the Hemisflo canopy is utilized only to extract the conical ribbon canopy from the vehicle, at which time it is disengaged from the conical ribbon canopy by means of a knife-lanyard arrangement and the conical ribbon canopy continues deployment due to its own drag. An extended riser between the Hemisflo canopy and conical ribbon deployment bag provides for the removal of the bag from the conical ribbon canopy at line stretch. The conical ribbon canopy has suspension lines 20 ft long. It is assumed the canopy deploys a relative distance of 18 ft after the Hemisflo canopy is cut away. Thus, by utilizing the same equations as in 3.3 of this Chapter, the deployment time and snatch force can be calculated.

$$L_s = 18' = \frac{1}{J_b} \ln(1 + K_b v_d t_2) - \frac{1}{J_c} \ln(1 + J_c v_d t_2)$$

TABLE 12-2 TRAJECTORY CALCULATION

(1)	(2)	(3)	(4)	(5)	(6)	(7)	(8)
t_n	Δt_n (1) - (1) _{n-1}	v_{n-1}	α_{n-1} (Radians)	$\cos \alpha_{n-1}$	$\Delta \alpha_n$ $= \frac{-K(5)_n(2)_n}{(3)_n}$	α_n (4) + (6) (Radians)	α_n (Degrees)
0.000	-	-	-	-	-	- 0.00000	- 0° 0' 0''
0.100	0.100	2130.00000	- 0.00000	1.00000	- 0.00150	- 0.00150	- 0° 5' 11''
0.200	0.100	2128.91888	- 0.00150	1.00000	- 0.00150	- 0.00300	- 0° 10' 19''
0.300	0.100	2127.84421	- 0.00300	.99999	- 0.00150	- 0.00450	- 0° 15' 29''
0.400	0.100	2126.77596	- 0.00450	.99998	- 0.00150	- 0.00600	- 0° 20' 38''
0.500	0.100	2125.71408	- 0.00600	.99997	- 0.00150	- 0.00750	- 0° 25' 27''
0.600	0.100	2124.65860	- 0.00750	.99997	- 0.00150	- 0.00900	- 0° 30' 56''
0.700	0.100	2123.60948	- 0.00900	.99996	- 0.00151	- 0.01051	- 0° 36' 9''
0.714	0.014	2122.55975	- 0.01051	.99995	- 0.00021	- 0.01072	- 0° 36' 52''
0.724	0.010	2122.41465	- 0.01072	.99994	- 0.00015	- 0.01087	- 0° 37' 23''
0.734	0.010	2122.31110	- 0.01087	.99994	- 0.00015	- 0.01102	- 0° 37' 54''
0.744	0.010	2121.96018	- 0.01102	.99993	- 0.00015	- 0.01117	- 0° 38' 25''
0.754	0.010	2121.36046	- 0.01117	.99993	- 0.00015	- 0.01132	- 0° 38' 56''
0.764	0.010	2120.51401	- 0.01132	.99993	- 0.00015		

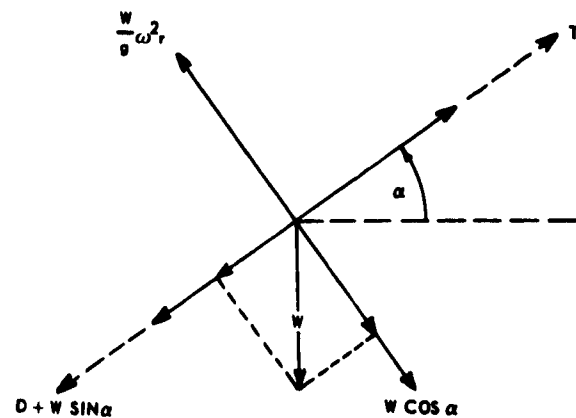
(9)	(10)	(11)	(12)	(13)	(14)	(15)	(16)
$\tan \alpha_n$	$\cos \alpha_n$	$(C_D S)_n$	$\frac{K/W}{6000}$ $(11)_n \rho_n \times 10^{+7}$	$\frac{K/W \cos \alpha_n}{(x 10^{+7})}$ $(12)/(10)$	v_n	$v_n^2 \times 10^{-6}$	$\left(\frac{K}{W \cos^2 \alpha_n}\right) \times$ $(13)_n \times (15)_n$
- 0.00000	1.00000	.762	.74583	.74583	2130.00000	4.53690	0.33838
- 0.00150	1.00000	.762	.74583	.74583	2128.91888	4.53230	0.33803
- 0.00300	.99999	.762	.74583	.74584	2127.84421	4.52770	0.33769
- 0.00450	.99998	.762	.74583	.74584	2126.77596	4.52318	0.33736
- 0.00600	.99997	.762	.74583	.74585	2125.71408	4.51866	0.33702
- 0.00750	.99997	.762	.74583	.74585	2124.65860	4.51417	0.33669
- 0.00900	.99996	.762	.74583	.74586	2123.60948	4.50972	0.33636
- 0.01051	.99995	.762	.74583	.74587	2122.55975	4.50526	0.33604
- 0.01072	.99994	.762	.74583	.74587	2122.41465	4.50464	0.33598
- 0.01087	.99994	2.525	2.47142	2.47157	2122.31110	4.50420	1.11318
- 0.01102	.99993	4.300	4.20875	4.20904	2121.96018	4.50272	1.89520
- 0.01117	.99993	6.065	5.93630	5.93588	2121.36046	4.50017	2.67126
- 0.01132	.99993	7.837	7.67070	7.67016	2120.51401	4.49658	3.44896

(Continued on next page)

TABLE 12-2 (Cont'd)

(17)	(18)	(19)	(20)	(21)	(22)	(23)	(24)
$\left(\frac{\Delta \tan \alpha_n}{v_n \cos \alpha_n}\right)^2$ $(9)_n + (16)_n$	$(17)_n \times v_n$ $(17)_n \times (14)_n$	$\Delta \alpha_{n+1}$ (Radians)	Δv_{n+1} $(18)_n \times (19)_n$	v_{n+1} $(14)_n + (20)_n$	$v_n^2 \times \tan \alpha_n$ $(15) \times (9)$	$\Delta v_R (22)$ $(22)_n + (22)_{n-1}$ 2	$(23) \times \Delta \alpha_{n+1}$ $(23) \times (19)$
0.33838	720.74940	- 0.00150	- 1.08112	2128.91888	- 0.00	-	-
0.33653	716.44507	- 0.00150	- 1.07467	2127.84421	- 6798.45	- 3399.23	5.09885
0.33469	712.16818	- 0.00150	- 1.06825	2126.77596	- 13583.10	- 10190.78	15.28617
0.33286	707.91865	- 0.00150	- 1.06188	2125.71408	- 20354.31	- 16968.71	25.45307
0.33102	703.65387	- 0.00150	- 1.05548	2124.65860	- 27111.96	- 23733.14	35.59971
0.32919	699.41636	- 0.00150	- 1.04912	2123.60948	- 33856.28	- 30484.12	45.72618
0.32736	695.18480	- 0.00151	- 1.04973	2122.55975	- 40587.48	- 37221.88	55.83282
0.32553	690.95688	- 0.00021	- 0.14510	2122.41465	- 47350.28	- 43969.38	65.95407
0.32526	690.33659	- 0.00015	- 0.10355	2122.31110	- 48289.74	- 47820.01	71.73002
1.10231	2339.44475	- 0.00015	- 0.35092	2121.96018	- 48960.65	- 48625.20	72.93780
1.88418	3998.15493	- 0.00015	- 0.35092	2121.36046	- 49619.97	- 49290.31	73.93547
2.66009	5643.00975	- 0.00015	- 0.59972	2120.51401	- 50266.90	- 49943.44	74.91516
3.43764	7289.56378	- 0.00015	- 0.84645	2119.42058	- 50901.29	- 50584.10	75.87615

(25)	(26)	(27)
Δv_n $(24)_n / -g$	$v = \sum_{k=1}^n \Delta v_k$ $\sum_{k=1}^n (25)_k$	h_v $40,000 + (26)$
-	- 0.00000	40000.00000
- 0.15908	- 0.15908	39999.84092
- 0.47693	- 0.63601	39999.36399
- 0.79414	- 1.43015	39998.56985
- 1.11072	- 2.54087	39997.45913
- 1.42666	- 3.96753	39996.03247
- 1.74199	- 5.70952	39994.29048
- 2.05778	- 7.76730	39992.23270
- 2.23799	-10.00529	39989.99471
- 2.27567	-12.28096	39987.71904
- 2.30680	-14.58776	39985.41224
- 2.33737	-16.92513	39983.07487
- 2.36735	-19.29248	39980.70752



where $v_d = 1254$ ft/sec

ρ at 37,000 ft = 6.71×10^{-4}

Assume C_D of the ogive cylinder at Mach 1.3 is 0.385.

W_b = Wt of vehicle at release minus Wt of cone minus
Wt of first-stage canopy and bag minus Wt of
second-stage canopy and bag
= $3000 - 3.0 - 10.0 = 103.5$
= 2883.5

$$m_b = \frac{W_b}{g} = \frac{2883.5}{32.06} = 90.0$$

Substituting:

$$J_b = \frac{(6.71 \times 10^{-4}) (0.385) (\pi) (20)^2}{(2) (90.0) (4) (144)} = 3.14 \times 10^{-6}$$

$$J_c = \frac{\rho (C_D S)_c}{2m_{tot}}$$

where

$$m_{tot} = \frac{Wt \text{ Canopy} - Wt \text{ Susp. Lines} + Wt \text{ Deploy. Bag}}{g}$$

From test data (Ref (12-5)), the uninflated drag area of a 16-ft conical ribbon canopy is assumed to be $(C_D S)_c = 3.15 \text{ ft}^2$.

$$m_{tot} = \frac{90 - 13 + 13.5}{32.06} = 2.805$$

Substituting in values,

$$J_c = \frac{(6.71 \times 10^{-4}) (3.15)}{(2) (2.805)} = 3.77 \times 10^{-4}$$

Deployment time t_2 can now be calculated by the trial and error method. This calculation is shown in Table 12-3. With the value of deployment time determined, 0.25 sec, the velocities $V_{1,2}$ and $V_{II,2}$ are now found.

$$V_{1,2} = \frac{v_d}{J_b v_d t_2 + 1} = \frac{1254}{(3.14 \times 10^{-6}) (1254) (.25) + 1}$$

= 1252.7 ft/sec

$$V_{II,2} = \frac{v_d}{J_c v_d t_2 + 1} = \frac{1254}{(3.77 \times 10^{-4}) (1254) (.25) + 1}$$

$$= 1122 \text{ ft/sec}$$

$$V_{II,2 \text{ rel}} = \Delta V = V_{1,2} - V_{II,2} = 1252.7 - 1122 = 130.7$$

$$P = \sqrt{\frac{(m_c) (V_{II,2 \text{ rel}})^2 Z P'}{L_s \xi'}}$$

$$\text{where } m_c = \frac{Wt \text{ of drag-producing surface}}{g}$$

$$= \frac{77}{32.06} = 2.40;$$

Z = No. of suspension lines = 32;

P' = breaking strength of lines = 3000 lb;

L_s = Suspension-line length = 20 ft; and

ξ' = Elongation of suspension line under load of 3000 lb = 40 per cent.

Substituting:

$$P = \sqrt{\frac{(2.40) (130.7)^2 (32) 3000}{20 (0.4)}} = \sqrt{\frac{391 \times 10^7}{8}}$$

$$= 22,100 \text{ lb}$$

To obtain total snatch-force, the drag of the uninflated 16-ft conical ribbon canopy is added to the above value. (See Eq 4-51 of Chap. 4.)

$$F_c = \frac{1}{2} \rho (C_D S) \left[\frac{V_{II,2}^2}{2} + \frac{V_{I,2}^2}{2} \right]$$

$$= \frac{1}{2} (6.71 \times 10^{-4}) (3.15) \left[\frac{(1122)^2}{2} + \frac{(1252.7)^2}{2} \right]$$

$$= 1492 \text{ lb}$$

Therefore, total snatch-force equals

$$F_s = P + F_c = 22,100 + 1,492 = 23,592 \text{ lb}$$

It should be noted that the filling-time and snatch-force equations utilized in the preceding calculation are based on the assumption of horizontal flight. Since the trajectory angle ($15^\circ 10'$) at deployment of the 16-ft conical ribbon canopy is small, these calculations are valid approximations.

3.6 Intermediate-Canopy Filling Time and Opening Shock. To maintain the 12-g limitation for the vehicle, this chute has to be reefed. The following calculation is made to determine the amount of reefing required.

$$12 g's = \frac{1}{2} \rho v_s^2 (C_D S)_{\text{(reefed)}} X$$

X = Opening-shock factor = 1.05 for conical ribbon parachute

$$\begin{aligned} (C_D S)_{\text{reefed}} &= \frac{24 g's}{\rho v_s^2 X} = \frac{(24) (2987)}{(6.71 \times 10^{-4}) (1252.7)^2 (1.05)} \\ &= 64.9 \text{ ft}^2 \end{aligned}$$

$$(C_D S)_{\text{fully opened}} = 100 \text{ ft}^2$$

Therefore, the 16-ft conical ribbon parachute is reefed to provide a 50 per cent reduction in drag area.

To approximate the reefed opening-shock, it is assumed that the reefed chute is a fully opened chute of nominal diameter (D_o) which produces a drag area of 50 ft².

$$\begin{aligned} \frac{C_D \pi D_o^2}{4} &= 50 \\ D_o &= \sqrt{\frac{200}{0.5 \pi}} = 11.28 \text{ ft} \end{aligned}$$

This canopy is also inflating under infinite-mass conditions, so to calculate t_f :

$$\begin{aligned} t_f / D_o &= \frac{0.65 \lambda g}{v_s} \\ t_f &= \frac{(0.65) (27.0) (11.28)}{1252.7} = 0.158 \text{ sec} \end{aligned}$$

The opening force is

$$F_o = \frac{1}{2} v^2 \rho C_D S X = \frac{1}{2} (6.7 \times 10^{-4}) (1252.7)^2 (50) (1.05)$$

$$F_o = 27,700$$

The conical ribbon canopy remains in the reefed condition for 10 sec. The canopy is then disreefed. Accompanying the disreefing of a parachute canopy is a disreefing force. In this case the velocity of the system has decreased significantly (1252.7 fps to 434.1 fps), as calculated by an extension of the method shown in Table 12.2. Therefore, this force is negligible compared to the reefed opening-shock, and it is not calculated. However, the time to disreef has to be determined for use in a trajectory calculation.

Since there is no prescribed method for calculating this duration, the following procedure is used.

The volume of the 16-ft drag-producing surface fully opened is 276.0 ft³. The volume, reefed, is 154.5 ft³. The difference is 121.5 ft³. A drag-producing surface with this volume has a D_o of 12.15 ft.

Disreefing time can then be calculated to be

$$t_f = \frac{(0.65) (27.0) (12.15)}{434.1} = 0.49 \text{ sec}$$

The 16-ft canopy is required to decelerate the vehicle to a velocity of 175 fps at an altitude of 5000 ft. With knowledge of the relationship of $C_D S$ vs time of the deceleration system up to disreefing of the 16-ft conical ribbon canopy, a trajectory calculation can be conducted by computer to check the force calculations previously made and to determine if the required deployment conditions for the final-recovery canopy are achieved. The $C_D S$ vs time relationships are shown in Fig. 12-1. Initial velocity, attitude, and vehicle attitude and weight conditions are the parameters necessary for computer calculation. Results have shown that forces as calculated in this sample calculation agreed with those computed. In addition, the following trajectory conditions existed at an altitude of 5000 ft:

Velocity = 170 fps; and
Trajectory angle = 90 deg.

3.7 Calculation of Final-Recovery Canopy-Filling Time and Opening Shock. The derivation of the force equations in Chap. 4, Sec. 5, for the finite-case assumed horizontal-deployment conditions. Results from the computer run show that deployment of the final-stage canopy will occur under vertical-flight conditions. Therefore, these equations must be re-derived. The snatch force will be small compared to opening-shock force, so its calculation is neglected.

Rewriting Eq 4-93 of Chapter 4 to include the vehicle weight term gives:

$$(12-9) \quad \frac{d}{dt} \left[\left(\frac{W}{g} + m_i + m_a \right) v \right] = - \frac{\rho}{2} C_D S v^2 + W$$

$$\left(\frac{W}{g} + m_i + m_a \right) \frac{dv}{dt} + \left(\frac{dm_i}{dt} + \frac{dm_a}{dt} \right) v = - \frac{\rho}{2} C_D S v^2 + W$$

Substituting from Chapter 4:

$$\begin{aligned} & \left\{ \frac{W}{g} + 99.1 \times 10^{-6} \sigma D_o^3 \left[1.71 - \left(\frac{t}{t_f} - 1.31 \right)^2 \right] + \right. \\ & \left[60.075 \times 10^{-6} \sigma D_o^3 \left(\frac{t}{t_f} \right)^5 \right] \left\{ \frac{dv}{dt} + \right. \\ & \left. \left\{ \left[-198.2 \times 10^{-6} \frac{\sigma D_o^3}{t_f} \right] \left(\frac{t}{t_f} - 1.31 \right) + \right. \right. \\ & \left. \left. \left[150.2 \times 10^{-6} \frac{\sigma D_o^3}{t_f} \left(t/t_f \right)^{3/2} \right] \right\} v \right. \\ & \left. = - \frac{\sigma \rho_o}{2} (C_D S)_{\max} (t/t_f) v^2 + W \right\} \end{aligned}$$

Rounding off numbers, and substituting $dt = t_f dT$ and $T = \frac{t}{t_f}$:

$$2 \left\{ \frac{W \cdot 10^6}{g \sigma D_o^3 20} + 5 \left[1.71 - (T - 1.31)^2 \right] + 3 (T)^{5/2} \right\}$$

$$\frac{dv}{dT} + 5v \left[3 (T)^{3/2} - 4 (T - 1.31) \right]$$

$$= - \frac{120 t_f}{D_o^3} (C_D S)_{\max} T v^2 + \frac{W \cdot 10^5 t_f}{\sigma D_o^3}$$

From Chapter 4

$$3(t/t_f)^{5/2} + 5 \left[1.71 - \left(\frac{t}{t_f} - 1.31 \right)^2 \right] = 11.25 T$$

$$3(t/t_f)^{3/2} - 4 \left(\frac{t}{t_f} - 1.31 \right) = 4.5$$

Substituting

$$2 \left[\frac{W \cdot 10^6}{20 g \sigma D_o^3} + 11.25 T \right] \frac{dv}{dT} + 22.5 v =$$

$$- \frac{120 t_f (C_D S)_{\max} T v^2}{D_o^3} + \frac{W \cdot 10^5 t_f}{\sigma D_o^3}$$

$$(12-10) \quad \frac{dv}{dT} = - \frac{22.5 v}{A' + 22.5 T} - \frac{B' t_f T v^2}{A' + 22.5 T} + \frac{C' t_f}{A' + 22.5 T}$$

$$\text{where } A' = \frac{W \cdot 10^5}{\sigma g D_o^3}$$

$$B' = \frac{120 (C_D S)_{\max}}{D_o^3}$$

$$C' = A' \times g$$

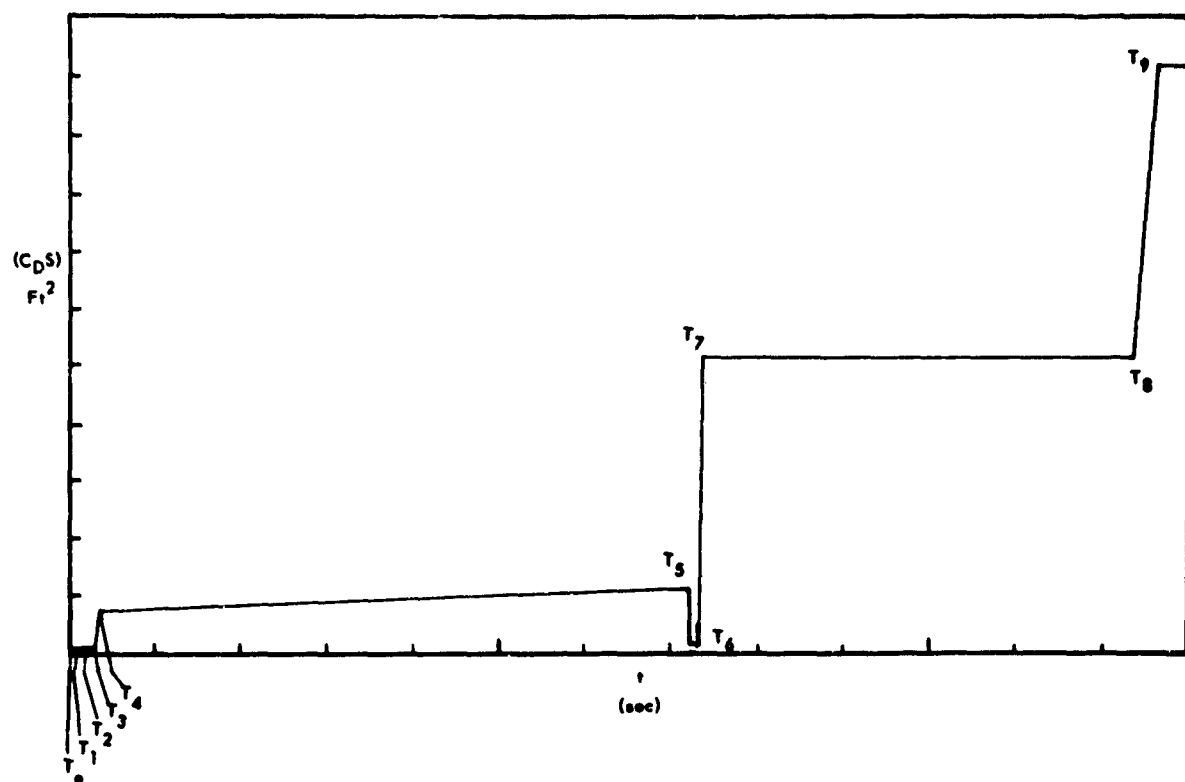
Eq 12-10 cannot be directly integrated to obtain a solution for the instantaneous velocity v . However, rewriting Eq 4-74 of Chapter 4,

$$\frac{dV}{dT} = \frac{D_o^2}{\pi} t_f v \left[(1-T) T^{4/3} - 2cT (1-T) \right]$$

or

$$(12-11) \quad \int_0^{V_{\max}} \frac{D_o^2}{\pi} t_f \int_0^1 \left[(1-T) T^{4/3} - 2cT (1-T) \right] v \left\{ dT \right.$$

By utilizing Eq 12-10 and 12-11 a filling time can be calculated by trial-and-error methods. By selecting a value for t_f , values of instantaneous velocity, v , can be obtained by solving Eq 12-10 for values of T from 0 to 1. Using the values of v from Eq 12-10, substituting these into Eq 12-11, values can be calculated for the right-hand side of Eq 12-11 for T varying from



Running Time	Δt	$C_D S (FT^2)$	Event	Running Time	Δt	$C_D S (FT^2)$	Event
$T_0 = 0.000$	0	0.762	INITIAL DROP	$T_7 = 14.762$	0.158	50.84	TIME TO OPEN (REEF)
$T_1 = 0.350$	0.35	0.762	END OF INIT. DROP	$T_8 = 24.762$	10.000	50.84	TRAJ. (REEFED 16 FT)
$T_2 = 0.534$	0.784	0.762	CONE DEPLOY	$T_9 = 25.252$	0.49	100.84	TIME TO DISREEF
$T_3 = 0.714$	0.180	0.762	TIME TO SNATCH	T_{10} - CONTINUE RUN UNTIL ALTITUDE OF 5000 FT IS REACHED.			
$T_4 = 0.734$	0.040	7.837	TIME TO FILL 6 FT	NOTE: CHANGE IN $(C_D S)$ 'S ARE LINEAR CHANGES WITH TIME.			
$T_5 = 14.354$	13.60	10.74	TRAJ. WITH 6 FT				
$T_6 = 14.604$	0.250	0.84	TIME TO SNATCH 16 FT				

Fig. 12-1 $(C_D S)$ vs Time

TABLE 12-3 CALCULATION OF DEPLOYMENT TIME - 16' CONICAL RIBBON CANOPY

(1)	(2)	(3)	(4)	(5)	(6)	(7)	(8)	(9)	(10)
$J_b v_d t_2 = J_c v_d t_2 =$									
t_2	$3.94 \times 10^{-3} t_2$	$0.473 t_2$	$1 + (2)$	$1 + (3)$	$\ln (4)$	$\ln (5)$	$\frac{1}{J_b} (6)$	$\frac{1}{J_c} (7)$	$L_s = (8)-(9)$
0.2	7.88×10^{-4}	0.0946	1.000788	1.0946	0.000788	0.0904	251.5	240	11.5
0.25	9.85×10^{-4}	0.1185	1.000985	1.1185	0.000985	0.112	314	296	18

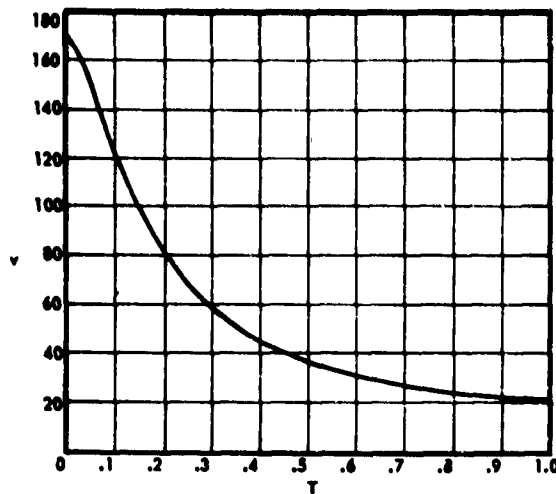


Fig. 12-2 Velocity vs T for the Filling-Time Values $t_f = 5.2$ Sec

0 to 1. These values are plotted versus T , and the area is measured under the curve. If the correct t_f was assumed, this area should equal the volume of the inflated canopy that is the solution of the integral of the left-hand side of Eq 12-11. If these values are not equal, another t_f must be assumed and complete calculation must be done again. Since this is a lengthy procedure, solution for t_f was obtained by a computer utilizing Eq 12-10 and 12-11. The solution is presented in Fig. 12-2 as a plot of velocity versus T for the filling-time value $t_f = 5.2$ sec, which fit Eq 12-11.

To solve for opening-shock force for the case of vertical descent:

$$(12-12) \quad F = -\frac{W}{\kappa} \frac{dv}{dt} = -\frac{W}{g t_f} \frac{dv}{dT}$$

where

$$F = F_o - W.$$

Eq 12-10 is substituted in Eq 12-12 to give

$$(12-13) \quad F = \frac{W}{t_f g} \left(\frac{1}{A' + 22.5 T} \right) (C' t_f - B' t_f T v^2 - 22.5 v)$$

By knowing the instantaneous velocities, v , for any value of T (obtained from Fig. 12-2), Eq 12-13 can be solved for opening-shock force. This calculation is shown in Table 12-4 and a graph of instantaneous force versus T is shown in Fig. 12-3. The peak value of force from this curve, 11,813.5 lb, represents the opening shock.

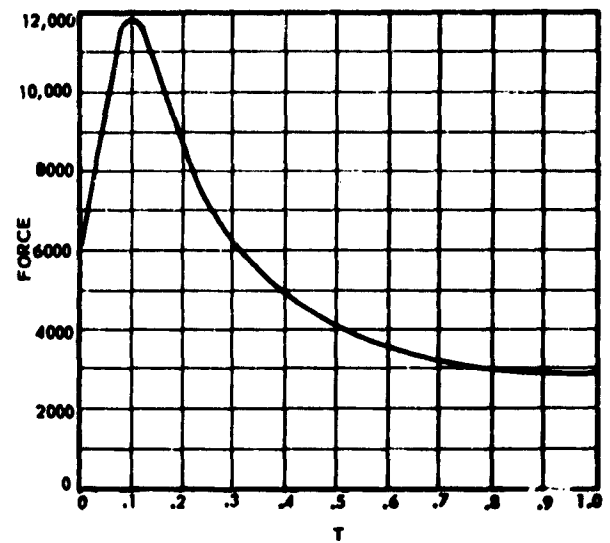


Fig. 12-3 Opening-Shock Force vs Ratio of T for 100-ft-Diameter Canopy

SEC. 4 DESIGN CRITERIA

4.1 Canopy and Suspension-Line Characteristics. In the snatch-force and opening-shock calculations, the canopy and suspension-line characteristics are assumed. Now with snatch and opening calculations complete, the suspension-line strength, reefing-line length, and porosity calculations can be made.

Required Suspension-Line Strength.

Design strength of suspension lines = $F_o \times$ Design Factor. From Table 7-1, the Design Factor = 2.91 for the first and intermediate chutes, and 2.305 for the final-recovery chute.

6-ft Hemisflo—

$$\text{Design Strength} = 12,190 \times 2.91 = 35,470 \text{ lb}$$

$$\text{Design Strength per line} = \frac{\text{Design Strength}}{\text{Number of Lines}} = \frac{35,470}{20} = 1,774 \text{ lb}$$

2300-lb lines are used for this canopy.

16-ft Conical Ribbon—

$$\text{Design Strength} = 27,700 \times 2.91 = 80,607 \text{ lb}$$

$$\text{Design Strength per line} = \frac{80,607}{32} = 2,519 \text{ lb}$$

3000-lb lines are used for this chute.

100-ft Flat Solid Circular

$$\text{Design Strength} = 11,813.5 \times 2.305 = 27,230 \text{ lb}$$

TABLE 12-4 CALCULATION OF OPENING-SHOCK FORCE $\bar{W} = 2883.5$

(1) T	0.0	0.1	0.2	0.3	0.4	0.5	0.6	0.7	0.8	0.9	1.0
(2) $22.5 T$ $x(1)$	0.0	2.25	4.50	6.75	9.00	11.25	13.50	15.75	18.00	20.25	22.50
(3) $A' + 22.5 T$ $+ (2)$	10.813	13.063	15.313	17.563	19.813	22.063	24.313	26.563	28.813	31.063	33.313
(4) v ft/sec	170	126	82.5	58.0	44.0	36.2	31.2	27.5	25.0	23.4	22.0
(5) $-22.5 v$ $x(4)$	-3825	-2838	-1855	-1306	-990	-815	-702	-618	-56.3	-52.6	-49.5
(6) v^2 $(4)^2$	28,900	15,880	6,810	3,365	1,938	1,310	974	756	625	547	484
(7) $T v^2$ $(6)x(1)$	0,000	1,588	1,362	1,009.5	775.2	655	584.4	529.2	500.0	492.3	484
(8) $-B' t_f T v^2$ $-3.67x(7)$	0,000	-5,725	-5,000	-3,700	-2,842	-2,402	-2,140	-1,941	-1,835	-1,806	-1,774
(9) $-22.5 v$ $-B' t_f T v^2$ $+ C' t_f$	-3825	-8,563	-6,855	-5,006	-3,832	-3,217	-2,842	-2,003	-1,891	-1,859	-1,823
(10) $-22.5 v$ $-B' t_f T v^2$ $+ C' t_f$	-2015	-6,753	-5,045	-3,196	-2,022	-1,407	-1,032	-193	-81	-49	-13
(11) $(10)/A'$ $+ 22.5 T$	-136.2	-516.8	-329.1	-182.0	-102.1	-63.6	-42.5	-7.29	-2.81	-1.58	-.39
(12) $F = \frac{W}{g t_f^2}(11), -17.25x(11)$	3210	8930	5680	3140	1760	1100	733	126	48.5	27.3	6.72
(13) $F_o = F + \bar{W}, \bar{W} + (12)$	6093.5	11,813.5	8,563.5	6023.5	4,643.5	3,963.5	3616.5	3009.5	2932.0	2910.8	2890.22

$$\text{Design Strength per line} = \frac{27,230}{120} = 227 \text{ lb}$$

375-lb lines are used for this chute.

4.2 Reefing-Line Length - (16-ft Canopy).

D_o = Nominal diameter of unreefed canopy = 16 ft;

D_{R1} = Diameter of reefing line of the reefed canopy;

$(C_D S)_R$ = Drag area of the reefed canopy = 50 ft²;

$(C_D S)_o$ = Drag area of the unreefed fully inflated canopy
= 100 ft²;

C = Ratio of reefing-line diameter to nominal canopy
diameter = D_{R1}/D_o ;

δ = Ratio of reefing-line diameters D_{R1}/D_o to
various drag area ratios $(C_D S)_R/(C_D S)_o$;

$$\frac{(C_D S)_R}{(C_D S)_o} = \frac{50}{100} = 0.5$$

This chute has 32 gores; therefore, referring to Fig. 12-1 in Sec. 3, $C = 0.631$. For a drag-area ratio of 0.5 (see 3.6) $\delta = 0.55$.

The values of C and δ utilized in this reefing-line length calculation were established for flat circular canopies. The lack of sufficient data to establish these parameters for a conical canopy necessitates the use of values of C and δ above in this calculation. It is felt that any error introduced by their use is small and therefore can be neglected.

With this data, the diameter of the reefing-line circle is

$$D_{R1} = D_o \delta C = (16) (0.55) (0.631)$$

$$D_{R1} = 5.56 \text{ ft}$$

So reefing-line length equals

$$\pi D_{R1} = \pi (5.56) = 17.48 \text{ ft}$$

**SAMPLE CALCULATIONS:
DESIGN EQUATIONS FOR HEMISPHERICAL CANOPIES**

(a) List of Symbols:

a	Percentage of D skirt extension (use as a decimal $\frac{a}{100}$ in equations)
A_o	Open area of a gore including vent area
A_{oH}	Open area between horizontal ribbons of one gore
b	The length of suspension lines divided by diameter D
B_{HR}	Horizontal-ribbon width
B_{RR}	Radial-ribbon width
B_{VL}	Vent-line width
B_{VR}	Vertical-ribbon width
D	Circumferential distance of the hemispherical portion only (skirt extension is not included) measured along the radial seams from skirt to skirt over the apex
e_g	Gore width
e_{gb}	Gore width at skirt of hemispherical portion
e_{gcs_n}	The distance between radial ribbon centerlines measured along the centerline of the n th open space
e_{goll}	The average width of each open space between horizontal ribbons after the width of the vertical (a) and one radial ribbon have been subtracted
e_{gv}	Gore width at the vent
e_{g2}	Gore width at the skirt of the extension
Δe_g	A varying increment added to the length of the horizontal ribbons for fullness
h	Distance along the centerline of a gore starting at the skirt of the hemispherical portion and measuring to the apex
h_{cs_n}	Distance from skirt of hemispherical portion to the centerline of the n th open space between horizontal ribbons
h_{cs_1}	Distance measured from the skirt of the hemispherical portion to the centerline of the space between the vent ribbon and the adjacent horizontal ribbon
h_e	Height of the skirt extension measured along gore centerline
h_{max}	Maximum height of a gore of the hemispherical part
h_n	Distance from the apex to the centerline of the n th space
L_v	Length of vent line divided by two
n	Number of gores
n_{HR}	Number of horizontal ribbons
n_{VL}	Number of vent lines
R_s	Height of space between horizontal ribbons
r	Radius of hemisphere
S_o	Total enclosed surface area including all open spaces between ribbons
s_o	Total vent area

S_{o1}	Area of the hemispherical portion of the canopy
S_{o2}	Area of the skirt extension
U_{RS}	Usable ribbon space
α	An angle varying from 0 deg to 90 deg (see Fig. 12-5)
γ	The included angle between adjacent suspension lines
λ_g	Geometric porosity

Note: The following equations are useful in designing a solid hemispherical canopy without a skirt extension:
Eq 12-1, 2, 3, 17, 18, 19, 20, 28, 42.

(b) Factors and Equations:

Total cloth area (S_o) = 4069.44 sq in

Number of gores (N) = 20

Skirt extension (a) = 0.10

Suspension line length divided by $D = (b) = 2.0$

$$D = \sqrt{\frac{2}{\pi^2} \sin \frac{180}{n} \times \cos \frac{180}{n} + \frac{a}{\pi} \left[\frac{a+2b}{a+b} \right] \sin \frac{180}{n} \cos \frac{\gamma}{2}}$$

Numbers standing alone in parentheses refer to the value obtained as a result of that numbered step in the calculation, and substitution of the actual value follows

- (1) $\frac{S_o}{n} = 203.47$
- (2) $\sin \frac{180}{n} = 0.156$
- (3) $\cos \frac{180}{n} = 0.9877$
- (4) $(a + 2b) = 4.10$
- (5) $\pi (a + b) = 6.59$
- (6) $a (a + 2b) = a (4) = 0.410$
- (7) $\frac{\sin \frac{180}{n}}{\pi (a + b)} = \frac{(2)}{(5)} = \frac{0.156}{6.59} = 0.0237$
- (8) $\frac{\gamma}{2} = \sin^{-1} (7) = \sin^{-1} 0.0237 = 1.36 \text{ deg}$
- (9) $\cos \frac{\gamma}{2} = \cos (8) = \cos 1.36 \text{ deg} = 0.999$
- (10) $\frac{2}{\pi^2} = 0.2028$
- (11) $(10) (2) (3) = 0.203 \times 0.156 \times 0.988 = 0.0314$
- (12) $\frac{(6)}{(5)} = \frac{0.410}{6.59} = 0.0623$
- (13) $(12) (2) (9) = 0.0623 \times 0.156 \times 0.999 = 0.0097$
- (14) $(11) + (13) = 0.0314 + 0.0097 = 0.0411$
- (15) $\frac{(1)}{(14)} = \frac{203.47}{0.0411} = 4960$
- (16) $D = \sqrt{(15)} = \sqrt{4960} = 70.5$

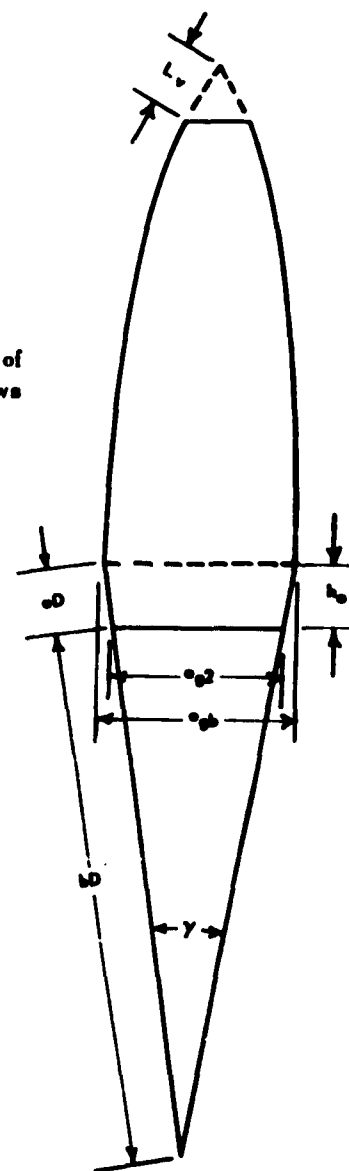


Fig. 12-4 Gore Pattern of Canopy with Skirt Extension

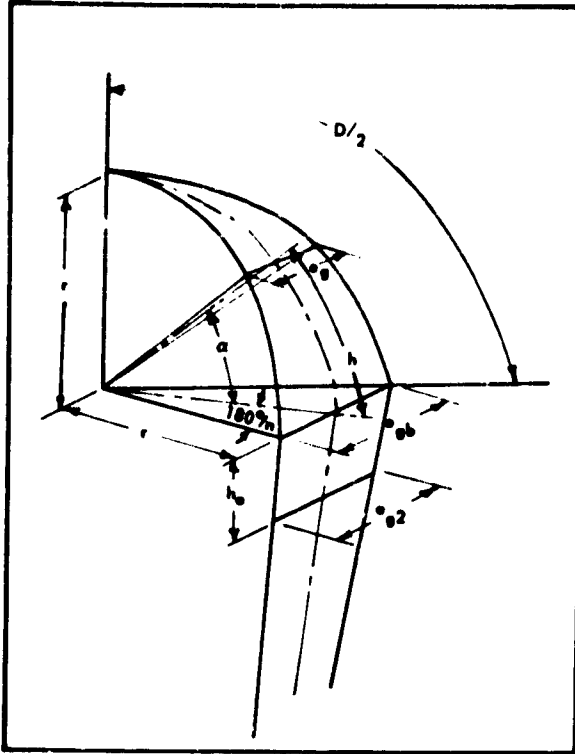


Fig. 12-5 Dimensions measured on Hemispherical Canopy

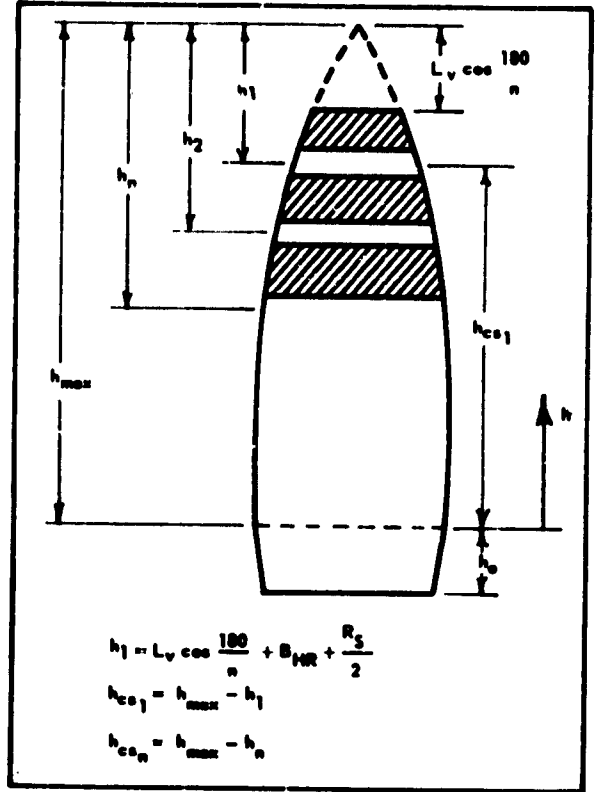


Fig. 12-6 Dimensions measured on Hemispherical Ribbon Canopy

$$(17) \quad r = \frac{D}{\pi} = \frac{(16)}{\pi} = \frac{70.5}{\pi} = 22.5$$

$$(18) \quad e_g = 2r \sin \frac{180}{n} \cos \alpha = 2(17)(2) \cos \alpha = 2 \times 22.5 \times 0.156 \times \cos \alpha = 7.0 \cos \alpha$$

$$(19) \quad h = r \alpha \cos \frac{180}{n} = (17)(3) \alpha = 22.5 \times 0.988 \alpha = 22.2 \alpha \quad \text{where } 0 \leq \alpha \leq \frac{\pi}{2}$$

$$(20) \quad h_{max} = r \frac{\pi}{2} \cos \frac{180}{n} = (17)(3) \frac{\pi}{2} = 22.5 \times 0.988 \times \frac{\pi}{2} = 34.9$$

The area per half-gore is calculated by integrating the half-gore width ($e_g/2$) over the full height (h) or from $\alpha = 0$ to $\alpha = \frac{\pi}{2}$

$$(21) \quad \frac{S_{o1}}{2n} = \int_0^{h_{max}} \frac{e_g}{2} dh = \int_0^{\pi/2} (r \sin \frac{180}{n} \cos \alpha) (r \cos \frac{180}{n}) d\alpha = r^2 \sin \frac{180}{n} \cos \frac{180}{n}$$

$$= (17)(17)(2)(3) = 22.5 \times 22.5 \times 0.156 \times 0.988 = 77.8$$

$$(22) \quad S_{o1} = 2n(21) = 2 \times 20 \times 77.8 = 3112$$

$$(23) \quad e_{gb} = 2r \sin \frac{180}{n} = 2(17)(2) = 2 \times 22.5 \times 0.156 = 7.0$$

$$(24) e_{g2} = 2b \sin \frac{\gamma}{2} = 2b (16) (7) = 2 \times 2 \times 70.5 \times 0.0237 = 6.67$$

$$(25) h_e = a \cos \frac{\gamma}{2} = a (16) (9) = 0.10 \times 70.5 \times 0.999 = 7.05$$

$$(26) S_{o2} = \frac{1}{2} n (e_{gb} + e_{g2}) h_e = \frac{1}{2} n [(23) + (24)] (25) = \frac{1}{2} \times 20 [7.0 + 6.67] \times 7.05 = 963$$

$$(27) S_o = S_{o1} + S_{o2} = (22) + (26) = 3112 + 963 = 4075$$

$$(28) L_v = \frac{\sqrt{\frac{s_o n}{\tan 180/n}}}{\cos 180/n} \cdot \sqrt{\frac{s_o n}{\sin 180/n \cos 180/n}}$$

where $s_o = 1\% S_o$

$$L_v = \sqrt{\frac{0.01 (1)}{(2) (3)}} = \sqrt{\frac{2.04}{0.154}} = \sqrt{13.247} = 3.63$$

A vent area of one per cent of the total canopy surface area is the standard value selected for this computation. However, a check should be made to insure that use of this area permits sufficient vent circumferential distance so the radial ribbons do not overlap near the vent. This check can be made as follows:

$$\text{Required circumferential distance} = R_{RR} (n) = 1\frac{1}{4} (20) = 25 \text{ in.}$$

$$\text{Available circumferential distance} = 2L_v \sin \frac{180}{n} (n) = 2 (3.63) (0.156) (20) = 22.65 \text{ in.}$$

Therefore, in this case, the radial ribbons would overlap and the vent line length (L_v) must be increased. The calculation of the minimum vent line length (L_v) required to insure that the radials do not overlap is as follows:

$$25'' = 2 (L_v) \sin \frac{180}{n} (n) = 2 L_v (0.156) (20)$$

$$L_v = \frac{25}{40 (0.156)} = 4 \text{ in.}$$

$$(29) U_{RS} = h_{max} + h_e - L_v \cos \frac{180}{n} = (20) + (25) - (28) (3) = 34.9 + 7.05 - 4.00 \times 0.988 = 38.0$$

$$(30) R_S = \frac{U_{RS} - (R_{RR}) (n_{RR})}{(n_{RR} - 1)} = \frac{(29) - (R_{RR}) (n_{RR})}{(n_{RR} - 1)} = \frac{38 - (2 \times 13)}{12} = 1.0 \text{ in.}$$

The geometric porosity is determined by finding the sum of the open area of a gore and dividing by the total area of the gore. This is easily done in tabular form as follows:

(31) SUMMATION OF THE AVERAGE WIDTH OF THE OPEN SPACE
BETWEEN THE RADIALS

Space No.	h_{cs}	α (rad)	α (deg)	$\cos \alpha$	e_{gcs}	e_{goll}
1	28.45	1.28	73.5	0.287	2.009	0.26
2	25.45	1.145	65.6	0.410	2.870	1.12
3	22.45	1.01	58.0	.532	3.724	1.97
4	19.45	0.875	50.1	.640	4.480	2.73

(31) Continued

Space No.	h_{cs}	α (rad)	α (deg)	$\cos \alpha$	e_{gcs}	e_{goll}
5	16.45	0.74	42.5	.738	5.166	3.41
6	13.45	0.605	34.7	.820	5.740	3.99
7	10.45	0.470	27.0	.891	6.237	4.49
8	7.45	0.336	19.3	.942	6.494	4.74
9	4.45	0.20	11.5	.980	6.860	5.11
10	1.45	.065	3.7	.998	6.986	5.23
11					6.94	5.19
12					6.82	5.07

$$\sum_{n=1}^{n=n_s} e_{goll} = 43.31$$

Note: For higher number of spaces, calculation is carried on in the same manner.

$$\begin{aligned} e_{gcs12} &= 2(bD \cos \frac{\gamma}{2} + B_{H/R} + \frac{R_s}{2}) \tan \frac{\gamma}{2} \\ &= 2 \left[2.0 \times 70.5 \times 0.999 + 2.0 + 0.5 \right] 0.02374 \\ &= 2 \times 143.5 \times 0.02374 \\ &= 6.82 \end{aligned}$$

$$\begin{aligned} e_{gcs11} &= 2(bD \cos \frac{\gamma}{2} + 2B_{H/R} + R_s) \tan \frac{\gamma}{2} \\ &= 2 \times \left[2 \times (70.5) \times 0.999 + 4.0 + 1.0 \right] 0.02374 = 6.94 \end{aligned}$$

(32) Example for finding the h_n 's:

$$h_1 = L_v \cos \frac{180}{n} + B_{H/R} + \frac{R_s}{2} = (28)(3) + B_{H/R} + \frac{(30)}{2} = 4.0 \times 0.988 + 2.0 + \frac{1.0}{2} = 6.45$$

$$(33) h_{csn} = h_{\max} - h_n = (20) - h_n = 34.9 - 6.45 = 28.45$$

$$(34) \alpha = \frac{h_{cs}}{r \cos \frac{180}{n}} = \frac{(33)}{(17)(3)} = \frac{28.45}{22.5 \times 0.988} = 1.28$$

$$(35) e_{gcs} = 2r \sin \frac{180}{n} \cos \alpha = 2(17)(2) \cos \alpha = 2 \times 22.5 \times 0.156 \times 0.287 = 2.01$$

$$(36) e_{goll} = e_{gcs} - B_{RR} - B_{VR_1} - B_{VR_2} \dots - B_{VR_n} = 2.01 - 1.25 - 0.25 - 0.25 = 0.26$$

$$(37) A_{oll} = R_s \sum_{n=1}^{n=n_s} e_{goll} = (30)(31) = 1.0 \times 43.31 = 43.31$$

$$(38) \text{ Vent closed Area (per gore)} = 2 \left[\frac{B_{VL}}{2} L_v - \frac{(B_{VL})^2}{8 \tan \frac{180}{n}} \right] = 2 \left[\frac{0.75}{2} (4.0) - \frac{(.75)^2}{8(0.158)} \right] = 2.11$$

$$(39) \text{ Vent open area (per gore)} = s_o - \text{Vent closed area}$$

$$= L_v^2 \sin \frac{180}{n} \cos \frac{180}{n} - (38) = (4)^2 (0.156)(0.988) - 2.11 = 2.47 - 2.11 = 0.36$$

$$(40) A_o = A_{oH} + \text{Vent open area (per gore)} = (37) + (39) = 43.31 + 0.36 = 43.67$$

$$(41) \lambda_g = \frac{A_o}{S_o/n} \times 100 = \frac{(40)}{(1)} \times 100 = \frac{43.67}{203.47} \times 100 = 21.5\%$$

$$(42) \Delta e_g = 12.5\% \text{ fullness} \left[\frac{(e_{gv})^h}{(h_{\max} - L_v \cos \frac{180}{n})} \right] = 12.5\% \left[\frac{2(28)(2)(19)}{(20 - (28)(3))} \right]$$

$$= 0.125 \times \left[\frac{2 \times 4.0 \times 0.156 \times 22.2 \text{ in}}{34.9 - 4.0 \times 0.988} \right] = 0.11 \text{ in}$$

The gore coordinates for layout are given in tabular form.

α (deg)	α (rad)	$\cos \alpha$	h	e_g	Δe_g	$e_g + \Delta e_g$	$\frac{\pm (e_g + \Delta e_g)}{2}$
90	1.5708	0.0	34.9	0	—	—	—
80	1.3963	0.1736	31.1	1.22	0.155	1.375	0.688
70	1.2217	0.3420	27.1	2.40	0.135	2.535	1.268
60	1.0472	0.5000	23.3	3.50	0.116	3.616	1.808
50	0.8727	0.6428	19.35	4.50	0.097	4.597	2.298
40	0.6981	0.7660	15.50	5.36	0.078	5.438	2.719
30	0.5236	0.8660	11.60	6.07	0.058	6.128	3.064
20	0.3491	0.9397	7.75	6.58	0.038	6.618	3.309
10	0.1745	0.9848	3.88	6.90	0.019	6.919	3.459
0	0	1.00	0	7.00	0	7.00	3.50
e_{g2}			7.05				3.34

The coordinates of the skirt extension are obtained from trigonometric relations (Fig. 12-4).

Plot h as the centerline of the gore against $\frac{\pm (e_g + \Delta e_g)}{2}$

16-Ft Conical Ribbon POROSITY CALCULATION FOR RIBBON CANOPIES

(a) List of Symbols

B_{HR}	Horizontal-ribbon width	(inch)	L_o	Length of gore	(inch)
B_{RR}	Radial-ribbon width	(inch)	n	Number of gores	
B_{VR}	Vertical-ribbon width	(inch)	n_{HR}	Number of horizontal ribbons	
R_{VL}	Vent-line width	(inch)	s_o	Area of vent	(inch ²)
D_o	Nominal canopy diameter $\sqrt{\frac{S_o}{\pi}}$	(ft)	S_G	Area of gore	(inch ²)
e_g	Base width of gore	(inch)	S_{HR}	Area covered by horizontal ribbons	(inch ²)
e_{gv}	Gore width at vent	(inch)	S_o	Total surface area of canopy, including slots and vent (vent not included if larger than $0.01 S_o$)	(ft ²)
h_a	Actual constructed height of gore	(inch)	S_{RB}	Area of reinforcing bands	(inch ²)
h_g	Height of gore	(inch)			

S_{RR}	Area covered by radial ribbons	(inch ²)	α	Cone angle for conical canopies	(degree)
S_{TC}	Total closed canopy area	(inch ²)	β	Apex angle of gore	(degree)
S_{TO}	Total open canopy area	(inch ²)	λ_g	Geometric canopy porosity	(per cent)
S_{VR}	Area covered by vertical ribbons (not including area overlapped by horizontal ribbons)	(inch ²)			

(b) Factors and Equations.

Nominal diameter D_o 16 ft

Number of gores (n) = 32

Conical angle (α) = 20 deg

I. Gore Dimensions:

$$(1) S_G = 144 \times \frac{\pi}{4} \frac{D_o^2}{n} = 36\pi \frac{16^2}{32} = 904 \text{ in.}^2$$

$$(2) (\cos \alpha) \sin \frac{180}{n} = (\cos 20) (\sin 5.63) = 0.9387 \times 0.0981 = 0.0922$$

$$(3) \frac{\beta}{2} = \sin^{-1} (\cos \alpha) \sin \frac{180}{n} = \sin^{-1} (2) = \sin^{-1} (0.0922) = 5.29^\circ$$

$$(4) \cos \frac{\beta}{2} = \cos (3) = \cos 5.29 = 0.9957$$

$$(5) \tan \frac{\beta}{2} = \tan (3) = \tan 5.29^\circ = 0.0926$$

$$(6) L_o = \sqrt{\frac{S_G}{\sin \frac{\beta}{2} \cos \frac{\beta}{2}}} = \sqrt{\frac{(1)}{(2)(4)}} = \sqrt{\frac{904}{0.0922 \times 0.9957}} = \sqrt{9850} = 99.30 \text{ in.}$$

$$(7) \frac{e_g}{2} = L_o \sin \frac{\beta}{2} = (6) (2) = 9.15 \text{ in.}$$

$$(8) h_g = (L_o) \times (\cos \frac{\beta}{2}) = (6) (4) = 99.30 \times 0.9957 = 99 \text{ in.}$$

$$(9) s_{og} = \frac{1}{100} S_G = 1\% (1) = 0.01 \times 904 = 9.04 \text{ in.}^2$$

$$(10) h_v = \sqrt{\frac{s_{og}}{\tan \frac{\beta}{2}}} = \sqrt{\frac{(9)}{(5)}} = \sqrt{\frac{9.04}{0.0926}} = \sqrt{97.6} = 9.88 \text{ in.}$$

$$(11) \frac{e_{gv}}{2} = h_v \tan \frac{\beta}{2} = (10) (5) = 9.88 \times 0.0926 = 0.914 \text{ in.}$$

$$(12) h_a = h_g - h_v = (8) - (10) = 99 - 9.88 = 89.12 \text{ in.}$$

$$(13) l_v = \frac{h_v}{\cos \beta/2} = \frac{(10)}{(4)} = \frac{9.88}{0.9957} = 9.92 \text{ in.}$$

II. Calculation of Closed Area:

$$(14) \frac{\text{Radial ribbon width } (B_{RR})}{2} = \frac{2}{2} = 1 \text{ in.}$$

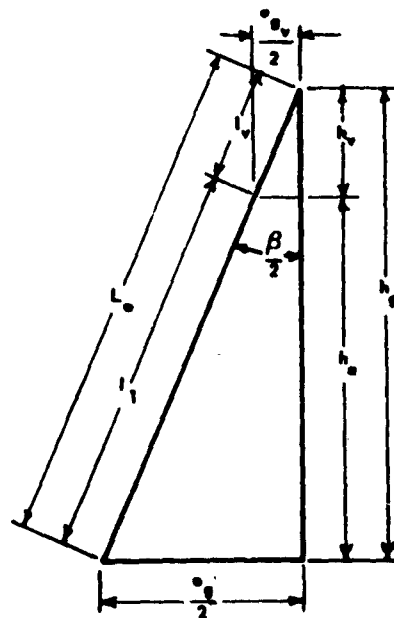


Fig. 12-7 Diagram of Half-Gore

$$(15) \frac{e_g}{2} - \frac{1/2 B_{RR}}{\cos \frac{\beta}{2}} = (7) - \frac{(14)}{(4)} = 9.15 - \frac{1}{0.9957} = 9.15 - 1.002 = 8.148 \text{ in.}$$

$$(16) \frac{e_v}{2} - \frac{1/2 B_{RR}}{\cos \frac{\beta}{2}} = (11) - \frac{(14)}{(4)} = 0.914 - \frac{1}{0.9957} = 0.914 - 1.002 = -0.088 \text{ in.} \approx 0$$

$$(17) h_{g1} = \frac{\frac{e_g}{2}}{\tan \frac{\beta}{2}} = \frac{(15)}{(5)} = \frac{8.148}{0.0926} = 87.95 \text{ in.}$$

$$(18) \frac{1}{\tan \frac{\beta}{2}} = \frac{1}{(5)} = \frac{1}{0.0926} = 10.80$$

Four vertical ribbons per gore are utilized.

- * $X_1 = (18 \times e_1) = 10.80 \times 2.806 = 30.31 \text{ in.}$
- * $X_2 = (18 \times e_2) = 10.80 \times 6.369 = 68.70 \text{ in.}$
- * $X_3 = (18 \times e_3) = \dots \times \dots = \dots$
- * $X_4 = (18 \times e_4) = \dots \times \dots = \dots$
- * $X_5 = (18 \times e_5) = \dots \times \dots = \dots$
- * $X_6 = h_a$

NOTE: all dimensions are from centerline to centerline of vertical ribbons.

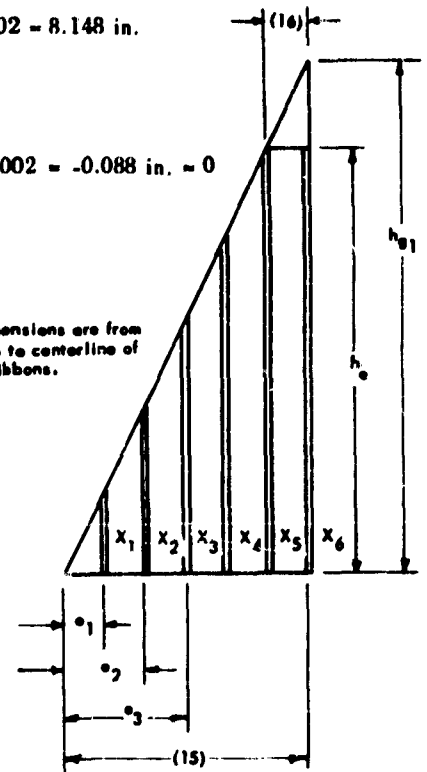


Fig. 12-8 Vertical Ribbon Placement on Half-Gore

- * If an even number of ribbons is used in the full gore, disregard calculations of X_6 or its equivalent. (Number of lengths to be found dependent on number of ribbons used in 1/2 gore.)

$$(19) \text{Area of radial ribbon } (S_{RR}) = [(6) - (13)] (14) = [99.3 - 9.92] \times 1 = 89.38 \times 1 = 89.38 \text{ in.}^2$$

$$(20) \text{Number of horizontal ribbons } (n_{HR}) = 26$$

$$(21) \text{Horizontal ribbon width } (B_{HR}) = 2 \text{ in.}$$

$$(22) \text{Average horizontal ribbon length} = \frac{(15) + (16)}{2} = \frac{8.148 + (0)}{2} = 4.074 \text{ in.}$$

$$(23) \text{Horizontal ribbon area } (S_{HR}) = (22) (21) (20) = 4.074 \times 2 \times 26 = 212 \text{ in.}^2$$

$$(24) \text{Total spacing} = (12) - (20) (21) = 89.12 - (26 \times 2) = 89.12 - 52 = 37.12 \text{ in.}$$

$$(25) \frac{(24)}{(20) - 1} = \frac{37.12}{26 - 1} = \frac{37.12}{25} = 1.482 \text{ in. per space}$$

$$(26) (25) + (21) = 1.482 + 2 = 3.482 \text{ in.}$$

$$(27) \text{Vertical ribbon width } B_{VR} = 0.5625 \text{ in.}$$

$$\text{Spaces covered by } X_1 = \frac{X_1}{(26)} = \frac{30.31}{3.482} = 9.0 (sc_1) *$$

$$\text{Spaces covered by } X_2 = \frac{X_2}{(26)} = \frac{68.70}{3.482} = 20.0 (sc_2) *$$

$$\text{Spaces covered by } X_3 = \frac{X_3}{(26)} = \frac{\dots}{3.482} = \dots (sc_3) *$$

$$\text{Spaces covered by } X_4 = \frac{X_4}{(26)} = \frac{\dots}{3.482} = \dots (sc_4) *$$

$$\text{Spaces covered by } X_5 = \frac{X_5}{(26)} = \frac{\dots}{3.482} = \dots (sc_5) *$$

$$\text{Spaces covered by } X_6 = \frac{X_6}{(26)} = \frac{\dots}{3.482} = \dots (sc_6) *$$

* Use nearest whole number.

$$\text{Exposed area covered by } X_1 = (sc_1) (27) (25) = 9.0 \times 0.5625 \times 1.482 = 7.5 \text{ in.}^2 (Sv_1)$$

$$\text{Exposed area covered by } X_2 = (sc_2) (27) (25) = 20.0 \times 0.5625 \times 1.482 = 16.68 \text{ in.}^2 (Sv_2)$$

$$\text{Exposed area covered by } X_3 = (sc_3) (27) (25) = \dots \times \dots \times \dots = \dots \text{ in.}^2 (Sv_3)$$

$$\text{Exposed area covered by } X_4 = (sc_4) (27) (25) = \dots \times \dots \times \dots = \dots \text{ in.}^2 (Sv_4)$$

$$\text{Exposed area covered by } X_5 = (sc_5) (27) (25) = \dots \times \dots \times \dots = \dots \text{ in.}^2 (Sv_5)$$

$$\text{Exposed area covered by } X_6 = (sc_6) \frac{(27)}{2} (25) = \dots \times \dots \times \dots = \dots \text{ in.}^2 (Sv_6)$$

$$(28) \text{ Total } 24.18 \text{ in.}^2 = S_{VR} \quad * \text{ Divide by 2 only if odd number of ribbons are used.}$$

$$(29) \text{ Vent closed area} = \frac{(B_{VL})}{2} (13) - \frac{(B_{VL})^2}{8 (5)} = .375 \times 9.92 - \frac{(.75)^2}{8 \times 0.0926} = 3.72 - 0.076 = 3.644.$$

III. Porosity

$$\begin{aligned} (30) \text{ Total closed area } (S_{TC}) &= (19) \ 89.38 \\ &+ (23) \ 212.00 \\ &+ (28) \ 24.18 \\ &+ (29) \ 3.644 \\ \hline &\text{Total } 329.204 \text{ in.}^2 \end{aligned}$$

$$(31) \text{ Total open area } (S_{TO}) = \frac{(1)}{2} - (30) = 452 - 329.204 = 122.796 \text{ in.}^2$$

$$(32) \text{ Geometric porosity } (\lambda_g) = \frac{2 (31)}{(1)} \times 100 = 2 \frac{100 \times 122.796}{904} = 27\%$$

4.3 Porosity Calculation. Porosity has to be calculated for ribbon parachutes. The calculation for the 6-ft Hemisflo canopy is an example of the method used for a curved-gore parachute, and the calculation for the porosity of the 16-ft conical ribbon canopy is an example of the method used for a straight-gore type. The porosity of the solid flat circular parachute is a characteristic of the cloth chosen for the canopy, and need not be calculated, since it is usually already known. The final recovery parachute uses 1.1-oz-Nylon cloth. The porosity (in terms of permeability) of this cloth is 80 to 120 cfm per sq ft at 1/2 in. of water.

The calculations for the porosity of the two ribbon parachutes are presented on standard calculation

sheets.

4.4 Construction Specifications. Based on the results of these calculations, construction details of the three parachutes used are given in the tables below.

The first-stage stabilization parachute has a 6-ft Hemisflo ribbon canopy. Table 12-5 lists the construction details for this parachute.

The second-stage parachute has a 16-ft conical ribbon canopy. Table 12-6 lists the construction details of this parachute.

The final-recovery chute has a 100-ft solid, flat, circular canopy. Table 12-7 lists the construction details of this chute.

TABLE 12-5 CONSTRUCTION DETAILS OF 6-FT HEMISFLO PARACHUTE

Item	Name	Ply	Width, in.	Break Strength, lb	Specification
1	Horizontal ribbon	1	2	460	Mil-T-5608E, Class D, Type II
2	Radial ribbon	2	1 1/4	185	Mil-T-5608E, Class C, Type IV
3	Vertical ribbon	2	1/4	22	Mil-T-5608E, Class B, Type I
4	Skirt reinforcing band	1	1	1000	Mil-T-5038 Type IV
5	Vent reinforcing band	2	1	3500	Mil-W-5625
6	Vent line	1	3/4	2300	Mil-W-5625
7	Suspension line	1	3/4	2300	Mil-W-5625
8	Pocket band	—	—	—	—

TABLE 12-6 CONSTRUCTION DETAILS OF 16-FT CONICAL RIBBON PARACHUTE

Item	Name	Ply	Width, in.	Strength, lb	Specification
1	Horizontal ribbon No. 1-18	1	2	1000	Mil-T-5608 Class E Type II
2	Horizontal ribbon No. 18-26	1	2	460	Mil-T-5608 Class D Type II
3	Radial ribbon	2	2	1000	Mil-T-5608 Class E Type II
4	Vertical ribbon	2	9/16	500	Mil-T-5038 Type V
5	Radial seam reinforcing webbing	1	3/4	3000	Mil-W-27657 Type I
6	Skirt reinforcing band	1	1-23/32	3600	Mil-W-4088D Type VIII
7	Vent reinforcing band	2	1-23/32	3600	Mil-W-4088D Type VIII
8	Vent line	1	3/4	3000	Mil-W-27657 Type I
9	Suspension line	1	3/4	3000	Mil-W-27657 Type I
10	Reefing line	1	1	6000	Mil-W-4088D Type XVIII
11	Pocket bands	1	1-23/32	3600	Mil-W-4088D Type VIII

TABLE 12-7 CONSTRUCTION DETAILS OF 100-FT FLAT CIRCULAR PARACHUTE

Item	Name	Ply	Break Strength, lb	Width, in.	Specification
1	Cloth surface	1			Mil-C-7020D (Type I)
2	Skirt reinforcing bands	1	3500	1	Mil-W-5625
3	Vent reinforcing bands	1	8700	1	Mil-W-4088D (Type X)
4	Vent line	1	375		Mil-C-5040B (Type II)
5	Suspension line	1	375		Mil-C-5040B (Type II)
6	Pocket bands	1	1000	1	Mil-T-5038B (Type IV)

4.5 Packing Volume (Pressure Packing).

Knowledge of the weight of each parachute along with the pressure used in the packing of the parachutes permits computation of the parachute-compartment volume required.

The dimensions of the available cylindrical space for packing the decelerator system are: Diameter = 20 in. Length = 4.0 ft. Therefore the available packing volume is

$$\text{Volume} = \frac{\pi D^2 h}{4} = \frac{(\pi) (20)^2}{(144) (4)} (4.0)$$

$$= 8.74 \text{ cu ft}$$

The total weight of the canopies is: 7.2 + 90.0 + 210.0

= 307.2 lb. Referring to Fig. 7-4 of Chapter 7, an average pack density of 20 lb per cu ft for hand packing is selected to determine if this method of packing is sufficient.

$$\text{Volume} = \frac{307.2 \text{ lb}}{20 \text{ lb per cu ft}} = 15.36 \text{ ft}^3$$

This calculation indicates pressure packing will be needed to pack the decelerator system in the space available. Referring again to Fig. 7-4 of Chapter 7; and assuming a pressure of 80 psi will be utilized in the packing of the canopies, a corresponding pack density of 42 lb per cu ft is obtained. This value of pack density is used to calculate the pack volume of the canopies as shown in Table 12-8.

TABLE 12-8 PACK DENSITY

Parachute	Pack Density lb/ft ³	Wt, lb	Volume, cu ft
6' Hemisflo	42	7.2	0.17
16' Conical	42	90.0	2.14
100' Flat Circular	42	210.0	5.00
Total		307.2	7.31

REFERENCES

- (12-1) Fagstrom, B.A.: "Performance of Trailing Aerodynamic Decelerators at High Dynamic Pressures, Phase V and VI," ASD TR 58-284 Part V.
 (12-2) Broderick, M.A., Turner, R.D. "Design Criteria and Techniques for Deployment and Inflation of

Aerodynamic Drag Devices", ASD TR 61 - 188, Nov. 1961.

- (12-3) Bimonthly Technical Progress Report No. 5, "Study, Design, and Fabrication of a Supersonic Parachute Sled Test Vehicle", Contract No. AF 33 (616)-7407, 27 April 1961.
 (12-4) Heinrich, H.G., and Rust, L.W., Jr. Lecture

notes from University of Minnesota Parachute Engineering and Retardation, Summer Course, July 17-28, 1961, Chap. II: Trajectory Calculations.

(12-5) Final Data Report, WADD Heavy-Duty Parachute Test Program, Contract No. AF 33 (616)-3261, Dec. 1960 (Unpublished)

CHAPTER 13 SPECIFICATIONS

- MIL.-A-8118B Aerial Delivery Kit Assembly, Cargo, General Specification for
- MIL.-A-8865 Airplane Strength and Rigidity, Miscellaneous Loads
- CCC.-C-419 Cloth, Cotton, Duck, Unbleached, Plied Yarns (Army and Numbered)
- MIL.-C-4232A (USAF) Cord Rayon, Without Core, Braided
- MIL.-C-4279A (USAF) Cloth, Cotton, Muslin
- MIL.-C-5040B (ASG) Cord, Nylon
- MIL.-C-6346A Container Kit, Aerial Delivery, Type A-22
- MIL.-C-6596C Container, Aerial Delivery, Rescue Radio and Accessories, Metal, Type A-20
- MIL.-C-6635B (1) Canopy, Parachute, FIST Ribbon, General Specification for Construction of
- MIL.-C-7020D Cloth, Nylon, Parachute
- MIL.-C-7219B Cloth, Nylon, Duck, Plied Yarns, For Parachute Packs
- MIL.-C-7350C (ASG) Cloth, Nylon, Parachute, Cargo
- MIL.-C-7515B (USAF) Cord, Nylon, Coreless
- MIL.-C-7554 (1) Container Kits, Aerial Delivery
- MIL.-C-8006A (ASG) Cloth, Rayon, Parachute (Non-Personnel)
- MIL.-C-8021B (ASG) Cloth, Nylon, Parachute, Drag
- MIL.-C-8121 Canopy Tower Parachute Free Fall, Type J-1 (Supersedes 40713-A)
- MIL.-C-8137 Canopy Tower Parachute, Controlled Fall Type J-2 (Supersedes 40745)
- MIL.-C-9401A Canopy, Parachute, Ring Slot, General Specification for Construction of
- MIL.-C-10362 Cutter, Reefing Line, M2
- MIL.-C-10967 Cutter, Reefing Line, M2, Metal Parts for
- MIL.-C-25174 (USAF) Cloth, Dacron, Drag Parachute
- MIL.-C-25312 (USAF) Cloth, Dacron, Parachute
- MIL.-D-7626 (1) Drop Kit Components, Heavy, Packaging, Packing and Marking for Shipment of
- MIL.-D-9056 (2) Deceleration Parachute Systems, Aircraft, General Requirements for
- MIL.-E-5926B (2) Extraction Kit, Aerial Delivery, Cargo, Type A-1A
- MIL.-H-7195 (1) Hardware, Parachute, General Requirements for
- MIL.-H-7750 (1) Housing, Parachute, Ripcord
- MIL.-H-9884 Honeycomb, Material, Cushioning, paper
- MIL.-I-6903A (1) Ink, Marking (For Parachutes and Other Textile Items)
- MIL.-I-8063 Ink, Marking
- GG.-P-115 Parachute, Meteorological
- MIL.-P-5374A Parachute, Cargo, Type G-8
- MIL.-P-5610B Parachutes and Parachute Component Parts, Packaging and Packing for Domestic and Overseas Shipment of
- MIL.-P-5905A Parachute, Ribbed Guide Surface, General Specifications for Construction of
- MIL.-P-5915C Parachute, Cargo, 100 ft dia, Type G-11A
- MIL.-P-6031 Parachute, Experimental, Inspection and Testing of
- MIL.-P-6364A Parachute, Aerial Cargo Delivery, Type G-1A
- MIL.-P-6634B(1) Parachute, Cargo, 500-lb Capacity, Type G-13
- MIL.-P-6645D(2) Parachutes, Personnel, General Specification for
- MIL.-P-7567(1) Parachutes, Personnel, Detail Manufacturing Instructions for
- MIL.-P-7620A(2) Parachutes, Cargo, General Specifications for
- MIL.-P-8322 Parachutes, Personnel, Assembly and Rigging Instructions
- MIL.-P-9727 Parachute, Meteorological MIL.-524-DMQ
- MIL.-P-10595A Parachute Assembly, For Shell, 81-MM, Illuminating, M301
- MIL.-P-11126A Parachute MIL.-132

MIL-P-12855	Parachute, Cargo (Parachute PG-109) (7AB)	matic, Cargo Parachute, 500-Pound Capacity Type MA-1)
MIL-P-13342B	Parachute and Container, Bomb, 10 lb, M1	DDD-S-751 Stitches, Seams, and Stitching
MIL-P-17942(1)	Parachutes and Parachute Components, Personnel, General Specifications for	MIL-T-5038C Tape and Webbing, Textile, Reinforcing Nylon
MIL-P-18545	Parachutes, Paper, for Pyrotechnic Signals	MIL-T-5608E (ASG) Tape, Textile, Nylon, Parachute Canopy
MIL-P-20374	Parachute Units, M6 and M7, for G.P. Bombs	MIL-T-5660A (ASG) Thread, Cotton, High-Tenacity
MIL-P-20408	Parachute Units for Bombs	MIL-T-5661B Tape and Webbing, Textile, Cotton Reinforcing, Woven
MIL-P-20516	Parachutes for Bombs	MIL-T-5663A Tape, Textile (Parachute Construction)
MIL-P-21904	Parachutes for Underwater Mines, General Specification for	MIL-T-6134B Tape, Textile, Nylon, Parachute Construction
MIL-P-25062A	Parachute Recovery Systems, Missile and Drone, General Requirements for Development of	MIL-T-7807B Thread, Nylon
MIL-P-25373	Parachute Assembly, Meteorological Balloon MX-1704-DMQ (Supersedes MIL-P-25108)	MIL-T-8363A (USAF) Tape and Webbing, Textile, Woven, Nylon
MIL-P-25387	Parachute, Cargo, 28 ft, Diameter, 350 Pound Capacity Type MA-2	MIL-T-40040A Thread, Polyester
MIL-P-25716A	Parachute System Heavy Duty, General Specification for	MIL-W-4088D (USAF) Webbing, Textile, Woven Nylon
MIL-R-5335E(1)	Release, Parachute Ripcord, Automatic Type F-1A	MIL-W-005625C (USAF) Webbing, Textile, Nylon Tubular
MIL-R-5897A(1)	Release, Parachute Harness, Quick, Type R-2A (Supersedes 40940)	MIL-W-5665D Webbing, Textile, Cotton Warp
MIL-R-6361(1)	Release Kit Assembly, Aerial Delivery Container, Type A-1 (Supersedes MIL-R-6459)	MIL-W-5666A Webbing, Textile, Nylon, Multiple Tubular
MIL-R-21468	Release, Parachute Ripcord, Automatic	MIL-W-5787C Webbing, Textile, Nylon, Heavy Duty
MIL-R-25565A(1)	Release, Parachute Ripcord, Automatic Type F-1B	MIL-W-9049B (ASG) Webbing, Textile, Nylon, Locking Loop
MIL-R-27211A	Release, Cargo, Parachute, 500-Pound Capacity, Type MA-1 (Release, Auto-	MIL-W-25339A (ASG) Webbing, Textile, Polyester
		MIL-W-25361 (USAF) Webbing, Textile, "Dacron", Low Elongation
		MIL-W-27265 (USAF) Webbing, Textile, Woven Nylon, Impregnated
		MIL-W-27657 (USAF) Webbing, Textile, Woven Nylon, for Decelerators
		MS-22008 Release - Parachute Canopy Quick Disconnect

INDEX

- Accelerometers, 495
- Actuating devices, 411-421
- Adapters, 408
- Aerospace vehicle recovery, 297-305
 - Low dynamic pressure regime, 300
 - High dynamic pressure regime, 300
- Aircraft
 - In-flight tow testing, 463
 - Landing approach, 313
 - Landing deceleration, 307
 - Landing roll, calculation of, 311-313
 - Runway tow testing, 463
 - Used for air-drop, 282
- Air-drop, 280-293
- Air-drop parachutes
 - Canopies, 288
 - Extraction parachutes, 288
 - Deployment, 292
 - Design requirements, 284-288
- Airfoil canopy, 99
- Angular velocity, 234-240
- Anti-spin parachute, 295-297
- Anti-toppling devices, 290
- Applications for aerodynamic decelerators, 275-336
 - Aerospace vehicle recovery, 297-305
 - Aircraft deceleration, 305-316
 - Air-drop, 280-293
 - Personnel, 319-331
 - Special weapons, 317-319
 - Stabilization, 293-297
 - Target, 331-335
- Atmosphere
 - Earth, 122-129
 - Mars, 130-131
 - Venus, 129
- Balloon, carrier, 452
- Ballute, 101
- Bands, pocket, 386
- Barnes, Richard, 8
- Bins, 441
- Blanchard, Jean Pierre, 3
- Bourget, 5
- Cabinet, drying, 438
- Canopy,
 - Aerodynamic heating, 252-259
 - Apparent mass, 153
 - Applications, 63-112, 275-336
 - Construction, 395-403
 - Design, 359-394
 - Deployment, 370-372
 - Drag coefficient, 66-67
 - Filling time, 150-163
 - Geometry, 368-369
 - Gliding, 172-173
 - Idealized shape, 150-151
 - Included mass, 153
 - Layout, 396
 - Loading, 363-365
 - Materials, 337-358
 - Opening force, 159, 162-164
 - Opening shock factor, 164
 - Oscillation, 66-67
 - Reliability, 259-271
 - Snatch force, 141-149
 - Stability, 224-252
 - Stress analysis, 198-204
 - Total mass, 153
 - Types, 66 ff
 - Volume, 370
 - Weight, 370
- Cayley, Sir George, 4
- Clevises, 410
- Cloth material, 353-356
- Cloth permeability, 353-356, 369
- Clustering effects, 181
- Coefficients
 - Drag, 66-67, 367
 - Moment, 226, 230-233, 235
 - Normal force, 226, 230-234
 - Orifice, 430
 - Tangential force, 165
- Cocking, Robert, 4

- Compartment, parachute, 302-303
- Compartment door release, 419
- Component testing, laboratory, 471, 476-477
- Conical ribbon canopy, 87, 382
- Conical solid cloth canopy, 70
- Connector links, 408
- Control systems, 304-305, 421-428
- Conversion factors, 34
- Cord line profile, 198-201
- Cord material, 351
- Cut knives, 410
- Cutting of canopy material, 396
- da Vinci, Leonardo, 2, 4
- Decelerators, aerodynamic, 63-112
 - Inflatable, conical, 101
 - Inflatable, spherical, 99
 - Parachute canopies, 68-99
 - Rotor blade type, 106
 - Spherical segment type, 104
- Deployment
 - Bags, 372, 389-392
 - Of canopies, 370-372
 - Of pilot chutes, 372
 - Speed limitations, 68-99, 367
- Descent
 - Characteristics of canopies, 170-174
 - Rate of, 173-174
- Displacement, measurement of, 490
- Drag
 - Aerodynamic, 165-182
 - Area of canopies, 366
 - Area control, 183-188
 - Coefficient, 367
 - Coefficient of canopies, 66-67
 - Efficiency, 369-370
 - Mach number effects on, 174-179
 - Of squidded canopy, 367
 - Of system, 218-224
 - Reynolds number effects on, 179-181
 - Wake effects on, 216, 217
- Drag producing surface
 - Construction of, 374-377, 395-403
 - Strength of, 375-377
- Drying
 - Cabinet, 438-439
 - Tower, 438
- Dynamic pressure, 165, 368
- Effective drag coefficient, 170-174
- Effective porosity, 131-141
- Ejection
 - Hardware for, 420-421
 - Methods for air-drop, 284
 - Seat stabilization, 295
- Emergency escape capsule stabilization, 295
- Environment, effect of, on materials, 340-343
- Equiflo canopy, 39
- Expendable materials, 344
- Extended skirt canopies, 74, 381
- Extraction parachutes, 288, 291
- Filling time, 150-163
- Final-stage recovery parachutes, 300-301
- Finite mass operating conditions, 149-162
- Flat circular ribbon canopy, 85, 381
- Flat circular solid cloth canopy, 68, 379
- Flat non-circular canopies, 99
- Flotation, 305
- Flow, measurement of, 492
- Force
 - Opening shock, 159, 162-164
 - Snatch, 141-149
- Garnerie, Andrew Jacques, 3-4
- Gliding canopy, 172-173
- Gore
 - Centerline profile, 198-201
 - Design, 377
- Ground impact
 - Shock absorption, 305
 - Shock attenuation devices, 428-435
- g-Switches, 426
- "Guardian Angel" parachute, 6
- Guide-surface canopies
 - Personnel, 81, 379
 - Ribbed, 79, 380
 - Ribless, 77, 380
 - Ribless, modified, 83, 380
- Hardware
 - Actuating devices, 411-421
 - Adapters, 408
 - Clevises, 410
 - Compartment door release, 415-420
 - Connector links, 408
 - Control devices, 421-428
 - Cut knives, 410
 - Disconnects, 411-414
 - Display board of, for air-drop, 409

- Ejection devices, 420-421
- g-Switches, 426
- Ground-impact shock-attenuation devices, 428-435
- Pressure switches, 426-428
- Reefing line cutters, 414-418
- Reefing rings, 410
- Releasers, 411-414, 418-419
- Rings, 408
- Snaphooks, 410
- Timing devices, 421-426
- Harness, personnel parachute, 328, 330-331
- Heating, aerodynamic, 252-259
- Heincke Sack parachute, 6
- Heinrich, Helmut G., 8
- Hemisflo canopy, 89
- Hems, 397-402
- Hengler, Lorenz, 4
- High temperature materials, 342
- Infinite-mass operating conditions, 162
- Inflatable decelerators, 99-106, 298-299
- In-flight deceleration parachute, 313-316
- Inspection
 - Facilities, 439-442
 - Tables, 440-441
- Instrumentation for testing, 490-498
- Instruments, recording, self-contained, 492-495
- Joints, strength of, 402-403
- Keepers, 389
- Knacke, Theodore, 8
- Knives, cut, 410
- Kuparento, Tordaki, 4
- Landing, simulation of conditions, 477
- Landing deceleration, aircraft, 307
- Landing-impact shock-absorption, 305, 428-435
- Layout, canopy, 396
- Mach number effects on drag, 174-179
- Madelung, G., 8
- Magnetic tape data recording, 496-497
- Marking, for canopy construction, 396
- Mass
 - Apparent, 153
 - Included, 153
- Materials
 - Cord, 351
 - Hardware, 408-411
 - High temperature, 342
 - Light weight, 343
 - Tape, 348-350
 - Thread, 351-353
 - Webbing, 345-348
- McComb, William, 8
- Modular system for air-drop, 288
- Moment coefficients, 226, 230-233, 235
- Moment of inertia, apparent, 240-242
- Montgolfier, Joseph, 3
- Normal force coefficients, 226, 230-234
- Opening
 - Critical conditions for, 367-368
 - Forces, 141-164
 - Shock factors, 164
- Opening force, calculation, 159-161
- Pack
 - Design, 372
 - Material, 356
 - Personnel parachutes, 327-328
- Packing
 - Facilities, 439-442
 - Presses, 442
 - Pressure, 372
 - Tables, 440
 - Tools, 440, 441-442
- Paratroops, 7
- Permeability
 - Cloth, 353-356, 369
 - Measurement of, 492
- Personnel guide-surface canopy, 81, 379
- Personnel parachutes
 - Canopies, 321-327
 - Deployment, 331
 - Design requirements, 319
 - Harness, 328, 330-331
 - Pack, 327-328
- Photographic recording instruments, 494-495
- Pilot chute
 - Deployment, 372
 - Performance, 392-393
- Pino, 5
- Platforms for air drop, 284, 288
- Porosity
 - Effective, 131-141
 - Geometric, 369
 - Mechanical, 27
 - Nominal, 131-132
 - Total, 27

- Porosity, effective
 - Calculation, 140-141
 - Effects on drag, 165-170
 - Effects on stability, 226
 - Measurement of, 133-140
- Presser, packing, 442
- Pressure
 - Measurement of, 492
 - Packing, 372
- Pressure distribution, canopy
 - Full open, subsonic and transonic flow, 188-193
 - Full open, supersonic flow, 193-196
 - Inflating, subsonic flow, 196
- Pressure packing, 372
- Pressure switches, 426-428
- Recovery of aerospace vehicles, 297-305
- Reefing, 183-188
 - Calculation, 185-186
 - Lines, 184-185
 - Line cutters, 414-418
 - Multiple, 185
 - Supersonic applications, 187-188
 - Rings, 188
- Release devices, 411-414, 418-420
- Release systems, 304
- Reliability, 259-271, 365
 - Assessment, 262-270
 - Component, 266-270
 - Improvement of, 271
 - Overall system, 264-266
 - Requirements, 259-260
- Restraining systems, air-drop, 284
- Retrieval, 305
- Reynolds number effects on drag, 179-181
- Ribbed guide-surface canopy, 79, 380
- Ribbon canopies
 - Conical, 87, 382
 - Equiflo, 89
 - Flat circular, 85, 379
 - Hemisflo, 89
 - Ringsail, 93
 - Ringslot, 90, 384
 - Wako, 99
- Ribless guide-surface canopy, 77, 380
- Ribless guide-surface canopy, modified, 83, 380
- Rings, 408
- Ring slot canopy, 90, 384
- Ring sail canopy, 93
- Risers, 386
- Rocket sleds, parachute test, 465, 488-490
- Rotafold canopy, 95
- Rotating canopies, 95-97
- Rotor blade decelerators, 106
- Seams, 397-403
 - Designation of, 402-403
 - Strength of, 402-403
- Sewing, 396
- Sewing machines, 442
- Shaped gore canopies, 72, 89, 385
- Shepardson, W.P., 8
- Silver, for target parachutes, 334
- Slits, for air-drop, 284, 288
- Skirt hesitator, 290
- Snaphooks, 410
- Snatch force
 - Calculation, 146-148
 - Reduction of, 148-149
- Special weapons deceleration parachutes
 - Canopies, 319
 - Design, 317-318
 - Deployment, 318-319
 - Deployment bags, 319
- Spherical decelerator, 99-101
- Spherical segment decelerator, 104-106
- Spin recovery parachute, 295-297
- Squidding canopy, 367
- Stability, 224-252
 - Dynamic, 228-252
 - Static, 225-228
- Stability of canopies, 66-67
- Stabilization in air-drop, 293-297
 - Bomb, 293-294
 - Droppable-wheel recovery, 294-295
 - Fuel tanks, 293
- Static line deployment, 371
- Steerable canopies, 99, 321
- Stitching, 402
- Strain, measurement of, 491
- Stress
 - Cloth, 201-203
 - Distribution calculation, 198-204
- Suspension lines, 377-378
 - Effect of length, 367

- Tangential force coefficients, 165
- Tape, textile, 348-350
- Target parascutes, 331-335
- Telemetry systems, 497-498
- Tensionometer, 492-495
- Test instrumentation, 490-498
- Test vehicles, 478-490
- Testing
 - Aircraft tow, 463-465
 - Gravity drop, 452-459
 - Inclined test facility, 477
 - Rocket boosted free flight, 459-463
 - Rocket boosted sled, 465
 - Water tow, 465-471
 - Wind tunnel, 471
- Thread, 351-353
- Time
 - Filling, 149-159, 162
 - Opening, 30
- Timing devices, 421-426
- Tools, packing, 441
- Trajectory
 - Calculation, 504-514
 - Control, 365
 - Curves, parametric, 35-53
- Transducers, 490-492
- Veranzio, Fausto, 3
- Vortex ring canopy, 97
- Wake effects, primary body, 204-224
 - Subsonic flow, 204-211
 - Transonic and supersonic flow, 211-224
- Wake canopy, 99
- Water tow testing
 - Deep water, 469-471
 - Shallow water, 466-469
- Webbings, 345-348
- Wheeler, Richard, 8
- Whirl tower testing, 458-459
- Wind tunnel testing, 471